FAA CENTER OF EXCELLENCE FOR ALTERNATIVE JET FUELS & ENVIRONMENT

Annual Technical Report

2021

For the period

October 1, 2020 – September 30, 2021

Boston University
Georgia Institute of Technology
Massachusetts Institute of Technology
Missouri University of Science and Technology
Oregon State University
Pennsylvania State University
Purdue University
Stanford University
University of Dayton
University of Hawaii
University of Illinois
University of North Carolina
University of Pennsylvania
University of Tennessee
University of Washington
Washington State University

This work was funded by the US Federal Aviation Administration (FAA) Office of Environment and Energy as a part of ASCENT Project AJFE under FAA Award Number 13-C. Any opinions, findings, and conclusions or recommendations expressed in this material are those of the authors and do not necessarily reflect the views of the FAA or other ASCENT Sponsors.

Table of Contents

Overview

This report covers the period October 1, 2020, through September 30, 2021. The Center was established by the authority of FAA solicitation 13-C-AJFE-Solicitation. During that time the ASCENT team launched a new website, which can be viewed at ascent.aero. The next meeting will be held April 5-7, 2022, in Alexandria, VA.

Over the last year, the ASCENT team has made great strides in research, outreach, and education. The team's success includes the following:

- **64 active research projects.**

The projects are divided into five main categories: tools, operations, noise, emissions, and alternative fuels, with cross-cutting research in aircraft technology innovation and supersonics. See the project category descriptions for more detail on each category and a summary of the projects. Funding for these projects comes from the FAA in partnership with Transport Canada. Note that projects 001, 059 and 065 include several separately funded projects within a single project number. An individual report section is provided for each of these funded "sub-projects" and are titled Projects 001A-001E, 059A-059E, and 65A-B.

- **117 publications, reports, and presentations by the ASCENT team.**

Each project report includes a list of publications, reports, and presentations. A comprehensive list of the publications, reports, and presentations for all projects is available in the publications index.

- **202 students participated in aviation research with the ASCENT team.**

ASCENT research projects were supported by 179 graduate students and 23 undergraduate students.
Each project report includes the names and roles of the graduate and undergraduate students in the investigator's research. Students are selected by the investigators to participate in this research.

- **62 industry partners involved in ASCENT.**

ASCENT's industry partners play an important role in the Center. Five new industry partners joined the Advisory Board in 2021. Advisory Board members provide insight into the view of stakeholders, advice on the activities and priorities of the Center's co-directors, and ensure research will have practical application. The committee does not influence FAA policy. Industry partners also play a direct role in some of the research projects, providing matching funds, resources and expertise to the project investigators.

Leadership

Dr. Michael Wolcott
Center Director and Technical Lead for Alternative Jet Fuels Research
Washington State University
(509) 335-6392
wolcott@wsu.edu

Dr. R. John Hansman
Center Co-Director and Technical Lead for Environmental Research
Massachusetts Institute of Technology
(617) 253-2271
rjhans@mit.edu

Dr. Jonathan Male
Federal Research Laboratories and Agency Liaison
Jonathan.male@pnnl.gov

Dr. James Hileman
Chief Scientific and Technical Advisor for Environment and Energy
Office of Environment and Energy
Federal Aviation Administration
james.hileman@faa.gov

Research Topics

Research projects within ASCENT are divided into five categories: alternative fuels, emissions, noise, operations, tools, aircraft technology innovation and supersonics. The list below includes all ASCENT funded research projects. This report includes research on active projects only. Reports for projects marked as COMPLETE are available on the ASCENT website at: https://ascent.aero/project/.

Alternative Fuels

The development of alternative jet fuels (AJFs) -- or sustainable aviation fuels (SAF) -- is of great interest to an array of aviation stakeholders, including aircraft and engine manufacturers and airlines. Alternative fuels that are produced from bio-based materials provide sustainable jet fuel alternatives that not only help alleviate environmental impacts from aviation emissions but can also create jobs in rural areas and lessen our reliance on foreign petroleum supplies.

Effective research and development, co-funded by the federal government and industry, enables SAF development by reducing the costs of producing renewable fuel. ASCENT research provides the scientific expertise and data to evaluate the environmental benefits associated with these sustainable fuels. ASCENT's collaborative R&D activities focuses on evaluating promising sustainable aviation fuel pathways to ensure environmental and social benefits, reduce technical uncertainties, inform aviation emission policies, and promote private sector investment in production.

Projects include:

- 001A-F - Alternative Jet Fuel Supply Chain Analysis
- 025 - National Jet Fuels Combustion Program – Area #1: Chemical Kinetics Combustion Experiments
- 026 - (COMPLETE) - National Jet Fuels Combustion Program – Area #2: Chemical Kinetics Model Development and Evaluation
- 027 - (COMPLETE) National Jet Fuels Combustion Program – Area #3: Advanced Combustion Tests
- 028 - (COMPLETE) National Jet Fuels Combustion Program – Area #4: Combustion Model Development and Evaluation
- 029A - National Jet Fuels Combustion Program – Area #5: Atomization Tests and Models
- 030 - (COMPLETE) National Jet Fuels Combustion Program – Area #6: Referee Swirl-Stabilized Combustor Evaluation/Support
- 031 - Alternative Jet Fuels Test and Evaluation
- 032 – (COMPLETE) - Worldwide LCA of GHG Emissions from Petroleum Jet
- 033 - Alternative Fuels Test Database Library
- 034 - National Jet Fuels Combustion Program – Area #7: Overall Program Integration and Analysis
- 052 - Comparative Assessment of Electrification Strategies for Aviation
- 065 - Fuel Testing Approaches for Rapid Jet Fuel Prescreening
- 066 - Evaluation of High Thermal Stability Fuels
- 067 - Impact of Fuel Heating on Combustion and Emissions
- 073 - Combustor Durability with Alternative Fuel Use

Emissions

The demand for passenger and cargo air transportation has grown rapidly over the last several decades. According to the International Air Transport Association (IATA), in 2016 there were 3.8 billion air travelers, a number it predicts will rise to 7.2 billion passengers by 2035—a near doubling of current levels. This staggering growth is accompanied by airport expansions and increases in emissions from aircraft, ground services equipment, and vehicle traffic on and near airports. The increases in these activity-based emissions impact the air quality around airports, cumulatively contribute to global climate change, and can negatively affect human health.

ASCENT researchers are analyzing data and improving predictive models to understand the effects of aircraft and ground vehicle emissions, create and refine emission-based analytical techniques at both airport-specific and global scales, and assess how policy changes affect emissions and its impacts.

Projects include:

- 002 - Ambient Conditions Corrections for Non-Volatile PM Emissions Measurements
- 013 - (COMPLETE) - Micro-Physical Modeling & Analysis of ACCESS 2 Aviation Exhaust Observations
- 014 - (COMPLETE) - Analysis to Support the Development of an Aircraft CO2 Standard

- 018 - Community Measurement of Aviation Emission Contribution of Ambient Air Quality
- 019 - Development of Improved Aviation Emissions Dispersion Capabilities for AEDT
- 020 - (COMPLETE) - Development of NAS wide and Global Rapid Aviation Air Quality
- 021 - (COMPLETE) - Improving Climate Policy Analysis Tools
- 022 - Evaluation of FAA Climate Tools
- 024 - (COMPLETE) - Emissions Data Analysis for CLEEN, ACCESS, and Other Recent Tests
- 039 – (COMPLETE) - Naphthalene Removal Assessment
- 047 - Clean Sheet Supersonic Aircraft Engine Design and Performance
- 048 - Analysis to Support the Development of an Engine nvPM Emissions Standard
- 051 - Combustion Concepts for Next-Generation Aircraft Engines
- 052 - Comparative Assessment of Electrification Strategies for Aviation
- 058 - Improving Policy Analysis Tools to Evaluate Higher-Altitude Aircraft Operations
- 064 - Alternative Design Configurations to Meet Future Demand
- 067 - Impact of Fuel Heating on Combustion and Emissions
- 068 - Combustor Wall Cooling Concepts for Dirt Mitigation
- 069 - Transitioning a Research nvPM Mass Calibration Procedure to Operations
- 070 - Reduction of nvPM emissions via innovation in aero-engine fuel injector design
- 071 - Predictive Simulation of nvPM Emissions in Aircraft Combustors
- 074 - Low Emissions Pre-Mixed Combustion Technology for Supersonic Civil Transport

Noise

ASCENT researchers work to understand all aspects of the aircraft operations that contribute to aviation's noise impact. They are working on understanding how aircraft and rotorcraft performance and operation affect noise generation and how they could be modified for mitigation measures. Research is also under way to look how noise propagates from the source to the ground and how it affects human health, wellbeing, and quality of life. This research will improve the modeling tools used to estimate the noise impacts from aviation operations and provide data to inform policy development as well as public engagement and education.

Projects include:

- 003 - Cardiovascular Disease and Aircraft Noise Exposure
- 004 - (COMPLETE) - Estimate of Noise Level Reduction
- 005 - (COMPLETE) - Noise Emission and Propagation Modeling
- 007 - (COMPLETE) - Civil, Supersonic Over Flight, Sonic Boom (Noise) Standards Development
- 008 – (COMPLETE) - Noise Outreach
- 009 - Geospatially Driven Noise Estimation Module
- 017 – (COMPLETE) -Pilot Study on Aircraft Noise and Sleep Disturbance
- 038 – Rotorcraft Noise Abatement Procedures Development
- 040 – Quantifying Uncertainties in Predicting Aircraft Noise in Real-world Situations
- 041 – Identification of Noise Acceptance Onset for Noise Certification Standards of Supersonic Airplane
- 042 – (COMPLETE) Acoustical Mode of Mach Cut-off
- 043 – Noise Power Distance Re-Evaluation
- 044 - Aircraft Noise Abatement Procedure Modeling and Validation
- 049 - Urban Air Mobility Noise Reduction Modeling
- 050 - Over-Wing Engine Placement Evaluation
- 053 - Validation of Low Exposure Noise Modeling by Open Source Data Management and Visualization Systems Integrated with AEDT
- 055 - Noise Generation and Propagation from Advanced Combustors
- 057 - Support for Supersonic Aircraft En-route Noise Efforts in ICAO CAEP
- 059A-E - Modeling and Measurements of Supersonic Civil Transport Jet Noise
- 061 – Noise Certification Streamlining
- 062 - Noise Model Validation for AEDT
- 063 - Parametric Noise Modeling for Boundary Layer Ingesting Propulsors
- 072 - Aircraft noise exposure and market outcomes in the US
- 075 - Improved Engine Fan Broadband Noise Prediction Capabilities
- 076 - Improved Open Rotor Noise Prediction Capabilities

Operations

Aviation operations result in fuel burn, emissions, and noise impacts. The nature and scale of these effects depends on a number of related factors, including:

- Aircraft flight paths and profiles,
- Schedule and frequency of operations, and
- Aircraft fleet mix.

ASCENT research focuses on identifying and accelerating the implementation of operational concepts that will reduce aviation environmental impacts and/or improve energy efficiency while maintaining the efficiency of the National Airspace System. The research spans multiple phases of flights and targets all environmental impact areas.

Projects include:

- 006 - (COMPLETE) - Rotorcraft Noise Abatement Operating Conditions Modeling
- 015 - (COMPLETE) - Cruise Altitude and Speed Optimization
- 016 - (COMPLETE) - Airport Surface Movement Optimization
- 023 - Analytical Approach for Quantifying Noise from Advanced Operational Procedures
- 038 - Rotorcraft Noise Abatement Procedures Development
- 044 - Aircraft Noise Abatement Procedure Modeling and Validation
- 053 - Validation of Low Exposure Noise Modeling by Open Source Data Management and Visualization Systems Integrated with AEDT
- 077 - Measurements to Support Noise Certification for UAS/UAM Vehicles and Identify Noise Reduction Opportunities

Tools

The aviation system operation involves complex interactions between many different components when aircraft are on the ground, taking off, in the air, and when landing. Aviation system operations also require the understanding of how to optimize aviation activities, which is best done by implementing advanced modeling tools.

The Federal Aviation Administration's suite of modeling tools have been developed to characterize and quantify the interdependences of aviation-related noise and emissions, impacts on human health and welfare, and the costs and market impacts to industry and consumers under varying policies, technologies, operations and market scenarios.

The ASCENT researchers are further developing and expanding the capabilities of these modeling tools in a variety of ways, from improving the way basic physical properties are represented and effectively modeled to how new technologies will enter the aircraft fleet and identifying the benefits of such technologies.

Projects include:

- 009 - Geospatially Driven Noise Estimation Module
- 010 - Aircraft Technology Modeling and Assessment
- 011 - (COMPLETE) - Rapid Fleet-wide Environmental Assessment Capability
- 012 - (COMPLETE) - Aircraft Design and Performance Assessment Tool Enhancement
- 035 - (COMPLETE) - Airline Flight Data Examination to Improve flight Performance Modeling
- 036 - (COMPLETE) - Parametric Uncertainty Assessment for AEDT2b
- 037 – CLEEN II Technology Modeling and Assessment
- 040 - (COMPLETE) - Quantifying Uncertainties in Predicting Aircraft Noise in Real-world Situations
- 043 - Noise Power Distance Re-Evaluation (NPD+C) to Include Airframe Noise in AEDT
- 045 – (COMPLETE) Takeoff/Climb Analysis to Support AEDT APM Development
- 046 – Surface Analysis to Support AEDT APM Development
- 049 - Urban Air Mobility Noise Reduction Modeling
- 053 - Validation of Low Exposure Noise Modeling by Open Source Data Management and Visualization Systems Integrated with AEDT
- 054 - AEDT Evaluation and Development Support
- 058 - Improving Policy Analysis Tools to Evaluate Higher-Altitude Aircraft Operations
- 060 - Analytical Methods for Expanding the AEDT Aircraft Fleet Database

- 062 - Noise Model Validation for AEDT
- 064 - Alternative Design Configurations to meet Future Demand

Aircraft Technology Innovation

The evolution of airframes and engines has resulted in modern designs that significantly reduce aviation fuel use, emissions and noise on a per-flight basis. ASCENT researchers conduct the analyses, modeling and testing required to demonstrate the viability of innovative airframe, engine and flight management technologies that reduce noise, emissions, and fuel burn. Future innovations will drive further improvements and the ASCENT research helps accelerate technology development.

Projects include:

- 010- Aircraft Technology Modeling and Assessment
- 037 - CLEEN II System Level Assessment
- 047 - Clean Sheet Supersonic Aircraft Engine Design and Performance
- 050 - Over-Wing Engine Placement Evaluation
- 051 - Combustion Concepts for Next-Generation Aircraft Engines
- 052 - Comparative Assessment of Electrification Strategies for Aviation
- 055 - Noise Generation and Propagation from Advanced Combustors
- 056 - Turbine Cooling through Additive Manufacturing
- 059 - Modeling and Measurements of Supersonic Civil Transport Jet Noise
- 063 - Parametric Noise Modeling for Boundary Layer Ingesting Propulsors
- 064 - Alternative Design Configurations to Meet Future Demand
- 066 - Evaluation of High Thermal Stability Fuels
- 067 - Impact of Fuel Heating on Combustion and Emissions
- 068 - Combustor Wall Cooling with Dirt Mitigation
- 070 - Reduction of nvPM emissions via innovation in aero-engine fuel injector design
- 071 - Predictive Simulation of Soot Emission in Aircraft combustors
- 074 - Low Emissions Pre-Mixed Combustion Technology for Supersonic Civil Transport
- 075 - Improved Engine Fan Broadband Noise Prediction Capabilities
- 076 - Improved Open Rotor Noise Prediction Capabilities
- 077 - Measurements to Support Noise Certification for UAS/UAM Vehicles and Identify Noise Reduction Opportunities

Supersonics

ASCENT supersonics research supports implementation of new technologies by advancing the understanding of the perception of sonic boom noise over a range of sonic boom levels, assessing Mach cut-off levels that will allow supersonic flight over land and furthering development of supersonic aircraft noise certification standards.

Projects include:

- 007 (COMPLETE) - Civil, Supersonic Over Flight, Sonic Boom (Noise) Standards Development
- 010- Aircraft Technology Modeling and Assessment
- 022 - Evaluation of FAA Climate Tools
- 041 - Identification of Noise Acceptance Onset for Noise Certification Standards of Supersonic Airplanes
- 042 - (COMPLETE) Acoustical Model of Mach Cut-off
- 047 - Clean Sheet Supersonic Aircraft Engine Design and Performance
- 057 - Support for Supersonic Aircraft Noise Efforts in ICAO CAEP
- 058 - Improving Policy Analysis Tools to Evaluate Aircraft Operations in the Stratosphere
- 059 - Jet Noise Modeling to Support Low Noise Supersonic Aircraft Technology Development
- 074 - Low Emissions Pre-Mixed Combustion Technology for Supersonic Civil Transport

Project 001(A) Alternative Jet Fuel Supply Chain Analysis

Washington State University

Project Lead Investigator

Michael P. Wolcott
Regents Professor
Department of Civil & Environmental Engineering
Washington State University
PO Box 642910
Pullman, WA 99164-2910
509-335-6392
wolcott@wsu.edu

University Participants

Washington State University

- PI(s): Michael P. Wolcott, Regents Professor; Christina Sanders, Acting Director, DGSS; Manuel Garcia-Perez, Professor; Xiao Zhang, Associate Professor; and Ji Yun Lee, Assistant Professor
- FAA Award Number: 13-C-AJFE-WaSU-023, 026
- Period of Performance: February 5, 2020 to September 30, 2021
- Task(s):
    1. WSU 1. Design cases. Garcia-Perez, Zhang
    2. WSU 2. Evaluate the most promising biorefinery concepts for alternative jet fuel (AJF) production. Garcia-Perez, Zhang
    3. WSU 3. Supplement and maintain the current inventory of biorefinery infrastructures that are useful for the production of AJF, as identified in the conversion design cases. Wolcott
    4. WSU 4. Perform a community social asset assessment. Gaffney
    5. WSU 5. Refine and deploy facility siting tools to determine regional demand and to identify potential conversion sites to be used in regional analyses. Wolcott
    6. WSU 6. Perform a refinery-to-wing stakeholder assessment. Gaffney
    7. WSU 7. Conduct a supply chain analysis. Wolcott, Garcia-Perez
    8. WSU 8. Provide analytical support for regional Commercial Aviation Alternative Fuels Initiative (CAAFI) and U.S. Department of Agriculture (USDA) jet fuel projects. Wolcott

Project Funding Level

$1,091,455 in FAA funding and $1,091,455 in matching funds. State-committed graduate school contributions for four PhD students. Faculty time for Michael Wolcott, Manuel Garcia-Perez, and Xiao Zhang contributes to the cost share.

Investigation Team

- Michael Wolcott, WSU, Project Director/PI
- Christina Sanders, WSU, Co-Project Director/Co-PI
- Season Hoard, WSU, Co-Project Director/Co-PI
- Manuel Garcia-Perez, WSU, Co-Project Director/Co-PI
- Xiao Zhang, WSU, Co-Project Director/Co-PI
- Ji Yun Lee, WSU, Co-Project Director/Co-PI
- Michael Gaffney, WSU, Faculty
- Kristin Brandt, WSU, Staff Engineer
- Dane Camenzind, WSU, Staff Engineer
- Lina Pilar Martinez Valencia, WSU, Graduate Student

- Tanzil Abid Hossain, WSU, Graduate Student
- Anamaria Paiva, WSU, Graduate Student
- Daniel Mueller, WSU, Graduate Student
- Kelly Nguyen, WSU, Graduate Student
- Jie Zhao, WSU, Graduate Student
- Fangjiao Ma, WSU, Graduate Student

Collaborating Researchers

- Burton English, University of Tennessee
- Greg Latta, University of Idaho
- Kristin C. Lewis, Volpe

Project Overview

As part of an effort to realize an "aviation system in which air traffic will move safely, swiftly, efficiently, and seamlessly around the globe," the FAA has set a series of goals and supporting outcomes, strategies, and performance metrics (Hileman et al., 2013). The goal entitled "Sustaining our Future" outlines several strategies collectively aimed at reducing the environmental and energy impacts of the aviation system. To achieve this goal, the FAA set an aspirational goal for the aviation industry to utilize 1 billion gallons of AJF by the year 2018. This goal was created according to economic, emissions, and overall feasibility perspectives (Richard, 2010; Staples et al., 2014).

Current approaches to the supply chain analysis for AJF optimize the feedstock-to-refinery and refinery-to-wing transportation logistics (Bond et al., 2014). One of the greatest barriers to large-scale AJF production is the high capital of greenfield facilities, which translates to risk in the investment community (Huber et al., 2007). The cost of cellulosic ethanol plants ranges from $10 to $13 per gallon capacity (Hileman and Stratton, 2014); moreover, the additional processing steps required to convert the intermediate to a drop-in AJF could increase this cost to more than $25 per gallon capacity (Hileman, 2014).

Motivated by the realities of converting these initial commercialization efforts into second-generation AJF, researchers have considered alternative conversion scenarios, including the transitioning of existing facilities (Brown, 2013). Currently, Gevo is using retrofitting strategies for corn ethanol plants to produce isobutanol, a potential intermediate for the alcohol-to-jet (ATJ) process of producing iso-paraffinic kerosene (Pearlson, 2011; Pearlson et al., 2013). Research on approaches for achieving the FAA's aspirational goal of AJF consumption has relied on "switching" scenarios, in which the existing and planned capacity are used to produce drop-in fuel (Malina, 2012). These approaches require the identification of existing industrial assets that can be targeted for future AJF production. Thus, siting becomes not only an exercise for optimizing feedstock transportation but also a necessary task for aligning this critical factor with the existing infrastructure, markets within regions, and the appropriate social capital for developing this new industry (Henrich et al., 2007; Seber et al., 2014).

To date, all published AJF supply chain analyses have been limited to stand-alone jet fuel production technologies that do not generate bio-products. Hence, the potential techno-economic and environmental benefits of using the existing industrial infrastructure and the production of coproducts with respect to the development of jet fuel production scenarios must be considered in future studies.

Design cases of stand-alone AJF production facilities will be used in supply chain evaluations. Social asset modeling is not well developed, and efforts are likely to be hampered by difficulties in quantifying social assets when compared to improved environmental performance or reductions in AJF costs, which may be better observed by optimizing economic and environmental constraints. However, the community characteristics of a potential site must be considered when determining preferred locations for a new biorefinery. Community resistance or enthusiasm for the AJF industry can strongly influence the success or failure of a facility (Martinkus et al., 2014; Rijkhoff et al., 2017). Thus, community social asset modeling efforts conducted within this project, such as those based on the Community Asset and Attribute Model (CAAM), will inform disciplinary applications and advances. Clearly, social factors can have substantial effects, either positive or negative, on project adoption and implementation, particularly in high-technology or energy-related projects (Lewis et al., 2012; Martinkus et al., 2012; Mueller et al., 2020). The consideration of social factors in site selection and implementation decisions can maximize positive social support and minimize opposition and social negatives, thereby substantially promoting the success of a project. In this regard, the CAAM originally piloted in the Northwest Advanced Renewables Alliance (NARA) project was designed to provide a quantitative rating of select social factors at the county level (Martinkus et al., 2014).

Focusing on regional supply chains, this research aims to identify the key barriers that must be overcome to produce one billion gallons of AJF. We will address this overall goal by developing tools to support the AJF supply chain assessment performed at the Volpe Center. Our effort will provide facility siting analyses that assess conversion design cases combined with regional supply chain assets and social capacity assessments for communities to act collectively toward development goals. Finally, a refinery-to-wing stakeholder assessment will support modeling and accounting of AJF distribution for downstream fuel logistics.

References

Bond, J.Q., Upadhye, A.A., Olcay, H., Tompsett, G.A., Jae, J., Xing, R., Alonso, D.M., Wang, D., Zhang, T., Kumar, R., Foster, A., Sen, S.M., Maravalias, C.T., 13, R., Barret, S.R., Lobo, R., Wayman, C.E., Dumesic, J.A., & Huber, G.W. (2014). Production of renewable jet fuel range alkanes and commodity chemicals from integrated catalytic processing of biomass. Energy Environ. Sci, 7:1500.

Brown, N. (2013). FAA Alternative Jet Fuel Activities. Overview. Presented to: CLEEN Consortium, November 20, 2013.

Henrich, E. (2007). The status of FZK concept of biomass gasification. 2nd European Summer School on Renewable Motor Fuels. Warsaw, Poland 29-31, August 2007.

Hileman, J.I., De la Rosa-Blanco, E., Bonnefoy, P.A., & Carter, N.A. (2013). The carbon dioxide challenge facing aviation. Progress in Aerospace Sciences. 63:84-95.

Hileman, J. I., & Stratton, R. W. (2014). "Alternative jet fuel feasibility." Transport Policy, 34:52-62.

Hileman, J. (2013). Overview of FAA alternative jet fuel activities. Presentation to the Biomass R&D Technical Advisory Committee, Washington DC, August 14, 2013.

Huber, G.W. & Corma, A. (2007). Synergies between bio- and oil refineries for the production of fuels from biomass. Angewandte Chemie. 46(38):7184-7201.

Lewis, K., Mitra, S., Xu, S., Tripp, L., Lau, M., Epstein, A., Fleming, G., & Roof, C. (2012). Alternative jet fuel scenario analysis report. No. DOT/FAA/AEE/2011-05. (http://ntl.bts.gov/lib/46000/46500/46597/DOT-VNTSC-FAA-12-01.pdf) (Retrieved on 2014-07)

Malina, R. (2012). HEFA and F-T jet fuel cost analyses. Laboratory for Aviation and the Environment. MIT, Nov 27, 2012.

Martinkus, N., Kulkarni, A., Lovrich, N., Smith, P., Shi, W., Pierce, J., & Brown, S. (2012). An Innovative Approach to Identify Regional Bioenergy Infrastructure Sites. Proceedings of the 55th International Convention of Society of Wood Science and Technology, Beijing, China.

Martinkus, N., Shi, W., Lovrich, N., Pierce, J., Smith, P., & Wolcott, M. (2014). Integrating biogeophysical and social assets into biomass-to-alternative jet fuel supply chain siting decisions. Biomass and Bioenergy, 66:410-418.

Mueller, D., Hoard, S., Roemer, K., Sanders, C., & Rijkhoff, S. (2020). Quantifying the Community Capitals Framework: Strategic Application of the Community Assets and Attributes Model. Community Development.

Pearlson, M.N. (2011). A techno-economic and environmental assessment of hydroprocessed renewable distillate fuels. MSc Thesis in Technology and Policy, MIT.

Pearlson, M., Wollersheim, C., & Hileman, J. (2013). A techno-economic review of hydroprocessed renewable esters and fatty acids for jet fuel production. Alternative jet fuels, Bioproducts and Biorefining, 7(1):89-96.

Rijkhoff, S., Hoard, S., Gaffney, M., Smith, P, & Wolcott, M. (2017). Communities Ready for Takeoff: Integrating Social Assets for Biofuel Site-Selection Modeling. Politics and Life Sciences, 36; 14-26.

Richard, T.L. (2010). Challenges in scaling up alternative jet fuels infrastructure. Science, 329:793.

Seber, G., Malina, R., Pearlson, M.N., Olcay, H., Hileman, J.I., & Barret, S.R.H. (2014). Environmental and economic assessment of producing hydroprocessed jet and diesel fuel from waste oil and tallow. Biomass and Bioenergy 67:108-118.

Staples, M.D., Malina, R., Olcay, H., Pearlson, M.N., Hileman, J.I., Boies, A., & Barrett, S.R.H. (2014). Lifecycle greenhouse gas footprint and minimum selling price of renewable diesel and jet fuel from fermentation and advanced fermentation technologies. Energy & Environmental Science, 7:1545.

Task 1 - Design Cases

Washington State University

Objective(s)

In previous years, our team has worked toward completing the reviews and final reports of design cases for six stand-alone AJF technologies (Table 1) and four relevant industries (sugarcane, pulp and paper, corn ethanol, and petroleum refineries). The status of each stand-alone AJF techno-economic analysis (TEA) and report is shown in Table 1. The results on pyrolysis

and ATJ pathways have been published in the referenced peer-reviewed journals. The work conducted from October 1, 2019 to September 30, 2020 focused on the following tasks:

1. Conduct a detailed analysis of a "catalytic hydrothermolysis pathway for jet fuel production"
2. Conduct a detailed analysis of a new AJF pathway for hydrothermal liquefaction (HTL) processing
3. Conduct TEA analyses on the integration of lignin coproduct technologies in the ATJ pathway to determine the potential for reducing fuel costs
4. Develop a new case report, focusing on a technology review and an evaluation of lipid conversion processes (HEFA, CH, SBI, Forge, Tyton, and decarboxylation) and new technologies for the production of alternative lipids (HTL and sugar-to-lipid)
5. Prepare manuscripts for publication

Table 1. Evaluated stand-alone AJF technologies.

	Literature review and design report date	Publications	TEA model
Pyrolysis	Literature review based on a design report, 138 pages (2017)	*Energy Fuel 33*, 4683, 2019; *Fuel Process Technology 195*, 106140, 2019	A standardized TEA is complete and available for use by university partners.
Alcohol-to-jet (ATJ)	Literature review based on a design report, 28 pages (2015)	*ChemSusChem 11*, 3728, 2018	A standardized TEA is complete and available for use by partners.
Synthetic kerosene and synthetic aromatic kerosene (SK-SKA)	Literature review based on a design report, 36 pages (2015)	Manuscript based on the case design report in preparation	This work was based on a Sasol process, on which we have not found any significant development since 2016. Because of a lack of adequate process information/data on SK-SKA production from renewable feedstock, we are not able to build a reliable TEA.
Direct sugar-to-hydrocarbon (DSHC)	Literature review based on a design report, 88 pages (2017)	Manuscript that includes DSHC submitted and under review by *Biomass and Bioenergy*	A standardized TEA is complete and available for use by partners.
Virent BioForming process	Literature review based on a design report, 46 pages (2015)	Manuscript that includes Virent submitted and under review by *Biomass and Bioenergy*	A standardized TEA is complete and available for use by partners.
Catalytic hydrothermolysis (CH)	Literature review based on a design report, 35 pages (2018)	Manuscript submitted for journal publication	A standardized TEA is complete.
Gasification Fischer Tropsch (GFT)	No literature review conducted	Manuscript that includes GFT submitted and under review by *Biomass and Bioenergy*	A standardized TEA is complete and available for use by partners.
Microchannel gasification Fischer Tropsch (microGFT)	No exhaustive literature review written; capital costs found in the open literature for microchannel FT deemed unreliable	Capital cost results deemed unreliable	A standardized microGFT TEA was completed; however, the cost information is considered unreliable.
Hydroprocessed esters and fatty acids (HEFA)	No written literature review conducted	Manuscript that includes HEFA submitted and under review by *Biomass and Bioenergy*	A standardized TEA is complete and available for use by partners.

Research Approach

Background

We have conducted a detailed literature review and prepared design case reports on six AJF pathways, including pyrolysis, ATJ, synthetic kerosene and synthetic aromatic kerosene, direct sugar-to-hydrocarbon (DSHC), Virent BioForming, and catalytic hydrothermolysis (CH). We have also collected data from the literature to conduct techno-economic analyses (TEAs) for these pathways. The results from these design cases are being applied in the development of supply chains and the

identification of synergisms that may eventually lead to the construction of integrated AJF production systems that take advantage of the infrastructure in a given region. An analysis of the locations of existing infrastructure demonstrated that the United States can be divided into regions according to the dominant biomass. Thus, we believe that the generation of advanced biorefinery concepts focused on petroleum refineries, pulp and paper mills, sugarcane mills, and corn ethanol mills is a viable approach for evaluating the synergism among AJF pathways, existing infrastructure, and coproducts. We can then compare the biorefinery concepts developed for each technology to identify the most promising approach, which will then be used in supply chain analyses.

Stand-alone design case reports were generated by conducting reviews of relevant research in the academic literature and public information provided by commercial entities developing the corresponding technology. The published papers were subjected to an industrial expert review. The reports provide details regarding the processes involved in each conversion pathway and outline the technology readiness and particular barriers to implementation. Publicly available information regarding the commercial processes and research literature will provide a foundation of information to be used in modeling efforts. In cases lacking detailed process engineering information, new models will be built to estimate the parameters needed to complete assessments such as techno-economic modeling and supply chain modeling. Aspen Plus is primarily used to generate process models and details, including mass balances, energy balances, energy requirements, and equipment size and cost. These results will also provide the basis for a comparative analysis of design cases, which will identify the key advantages and markets for each technology.

Each design case has the following components:

1. Feedstock requirements
2. Companies developing/commercializing the technology
3. Current locations of units in the United States and worldwide
4. Block and flow diagram of the technology
5. Unit operations and process conditions (reactor type, separation unit type, catalysts, product yield, and jet fuel yield)
6. Properties of the produced jet fuel
7. Identification of potential intermediates
8. Current and potential uses of wastes and effluents
9. Developed coproducts
10. Potential methods for coprocessing intermediates, wastes, and coproducts by using existing infrastructure (e.g., petroleum refineries, or pulp and paper mills)
11. Preliminary TEA
12. Technological challenges and gaps

We have submitted technical reports and supplementary Microsoft Excel files with mass and energy balances and TEAs for the pathways listed below. Furthermore, we have conducted a strategic analysis to identify the overall weaknesses of the technologies under study. All files are available on shared drives for the Project 01 team members. Where indicated, the TEAs are still undergoing internal review.

- Pyrolysis-bio-oil hydro-treatment concept (hydro-treated depolymerized cellulosic jet): The TEA is complete.
- ATJ: A manuscript with information on the mass and energy balances and the TEA has been published.
- Gasification Fischer Tropsch (GFT): Two design cases have been prepared for biomass gasification. The first case focuses on microreactors, and the second design case is applicable to technology based on larger, standard reactors (reviews on the TEAs for GFT and microGFT have been completed). However, the limited reliability of the microreactor capital costs hinders the value of the practical impact of our microreactor TEA study. The TEAs are available for use by partners.
- HEFA: A stochastic TEA was created in MATLAB and was confirmed to match the completed, deterministic TEA when the assumptions and costs match (deterministic TEA review completed). The TEA is now available for use.
- CH: The TEA is complete.

We have submitted a manuscript to *Biomass and Bioenergy* comparing the economic and environmental performance of the AJF technologies discussed above and the overall weaknesses of the technologies studied. This manuscript presents a strategic analysis of the yield increases needed to achieve a minimum selling price (MSP) comparable to those of current commercial fuels. Over the past year, we have also made progress in design cases for existing industries (corn ethanol and sugarcane mills) that could be used to reduce the production cost of AJFs. The analyses are complete.

Major progress has been made on the analysis of corn ethanol, sugarcane, and petroleum refinery infrastructure that could support jet fuel production. A manuscript on the conversion of corn ethanol mills is under review by *Biomass and Bioenergy*. Two additional manuscripts using either sugarcane mills or petroleum refineries to reduce AJF production costs are under internal review.

We have worked with the Pacific Northwest National Laboratory (PNNL) and completed a case design report on HTL for AJF conversion.

A summary report on several lipid conversion pathways, including SBI, Forge, Tyton, decarboxylation, and coprocessing, has been prepared. A manuscript entitled "Techno-economic Analysis of the CH Pathway for Jet Fuel Production" was reviewed by Agrisoma (now NuSeed) and the FAA, before submission for journal publication in September 2020.

Milestone(s)

A Microsoft Excel file with TEAs for all AJF technologies has been completed, and design cases for the corn ethanol and sugarcane industries are still being reviewed by the standardization team. A detailed analysis entitled "Catalytic Hydrothermolysis Pathway for Jet Fuel Production" has been completed, and a design case report entitled "Jet Fuel Design Case: Hydrothermal Liquefaction Case Design Report" has been completed. A summary report entitled "Lipid and Bio-processing Technologies: Process Intensification and Continuous Flow-Through Reaction (PICFTR), Lipid-to-Hydrocarbon (LTH), Tyton, Decarboxylation and Co-processing" has been produced, and manuscripts have been prepared for publication.

Major Accomplishments

A manuscript entitled "Comparison of Techno-economic and Environmental Performance of Alternative Jet Fuel Production Technologies" has been prepared and reviewed. Another manuscript entitled "Economic Analysis of Catalytic Hydrothermolysis Pathway for Jet Fuel Production" has been submitted for journal publication. "Hydrothermal Liquefaction Case Design Report" has been updated in preparation for FAA review. We intend to submit these manuscripts to the FAA for review within the next four months. We are working on the construction of a TEA for lignin extraction and utilization in a biorefinery process (National Renewable Energy Laboratory [NREL] biochemical conversion, https://www.nrel.gov/docs/fy19osti/71949.pdf).

An article detailing the impact of coproducts on the financial viability of a forest-residue-based ATJ process was published in *Biofuel, Bioproducts and Biorefining*. A companion manuscript that details the combined effect of siting and repurposing industrial facilities with multiple levels of capital cost avoidance on the economic viability of AJF is being written, and submission for internal review is expected in late 2020.

We have assisted the International Civil Aviation Organization (ICAO), Committee on Aviation Environmental Protection (CAEP) through participation in the Fuel Task Group (FTG). The ASCENT HEFA, ATJ, and GFT TEAs have been revised, streamlined, and generalized for use by scientists and non-scientists worldwide. The TEAs can be modified to reflect local costs and feedstocks. The TEAs were used to develop a "Rules of Thumb" or a heuristic approach for estimating capital requirements and relative fuel costs from these technologies. This output is compiled in both a Microsoft Word document and Microsoft Excel spreadsheet formats. These documents illustrate the influence of key variables in AJF costs: yield, capital expenditure (CAPEX), feedstock price, and conversion technology maturity.

Data generated from the design cases have been made available to A01 partners to assist with supply chain analysis and techno-economic modeling by improving the conversion and cost figure database values. Evaluations of the effects of process variations on the chemical properties of the generated products are being used to provide insight into the challenges that will be faced when AJFs are blended into commercial jet fuel.

Publications

Peer-reviewed journal publications

Brandt, K.L., Wooley, R.J., Geleynse, S.C., Gao, J., Zhu, J., Cavalieri, R.P., Wolcott, M.P. (2020). Impact of co-product selection on techno-economic analyses of alternative jet fuel produced with forest harvest residuals. BioFPR, 14(4):764-775.

Geleynse, S., Jiang, Z., Brandt, K., Garcia-Perez, M., Wolcott, M., Zhang, X. (2020). Fuel Processing Technology 201:106338

Tanzil, A.H., X. Zhang, M. Wolcott and M. Garcia-Perez, Strategic Assessment of Sustainable Aviation Fuel Production Technologies: Yield Improvement and Cost Reduction Opportunities (*Submitted to Biomass and Bioenergy, 2020*)

Outreach Efforts

During the preparation of design case reports, we have closely interacted with industrial companies, including Gevo, LanzaTech, and Agrisoma (now NuSeed). These companies have also helped us review reports and draft manuscripts. Our results have been presented to the FAA, the Washington State Academy of Science, and specialized conferences (TCS 2020). We have also made several presentations to graduate and undergraduate students.

Malina, R., Wolcott, M., Brandt, K. Update on TEA tool development. CAEP/12 Fuels Task Group, TPP subgroup. 20 May 2020.

Awards

None

Student Involvement

Several graduate students (Senthil Subramaniam, Sudha Eswaran, Kelly Nguyen, Tanzil Hossain, Anamaria Paiva, and Lina Martinez) and one undergraduate student (Kitana Kaiphanliam) participated in the creation, editing, and updating of the design cases for stand-alone AJF technologies, relevant existing infrastructure, and lignin coproducts.

Plans for Next Period

We intend to submit three to five manuscripts on the lignin coproduct analyses and other manuscripts on the AJF analyses. The following are the proposed manuscripts to be completed this project year:

1. Methodology of Quantifying the Impact of Repurposing Existing Manufacturing Facilities: Case Study using Pulp and Paper Facilities for SPORL Sustainable Aviation Fuel Facility
2. Lipid and Bio-processing Technologies: Process Intensification and Continuous Flow-Through Reaction (PICFTR), Lipid-to-Hydrocarbon (LTH), Tyton, Decarboxylation and Co-processing
3. Economic Analysis of Catalytic Hydrothermolysis Pathway for Jet Fuel Production
4. The Potential of SK-SKA for Production of Sustainable Aviation Fuel
5. The Opportunity for Lignin Co-Products to Improve the Economics of Sustainable Aviation Fuel Production

Task 2 - Evaluation of the Most Promising Biorefinery Concepts for AJF Production

Washington State University

Objective(s)

Continuation from previous years

During the upcoming year, we will complete our evaluation of biorefinery scenarios for AJF production using corn ethanol, sugarcane, pulp and paper mills, and petroleum refineries. Over the past year, we have advanced our analyses for corn ethanol and pulp and paper mills, and in the coming year, we aim to complete our analyses for sugarcane and petroleum refineries.

We will conduct detailed TEAs on the integration of lignin coproduct technologies and the ATJ pathway to determine the potential for reducing fuel costs.

Research Approach

Background

In this task, we will utilize the design cases for existing infrastructure, AJF production technology, and identified coproducts to generate new biorefinery concepts for petroleum refineries, pulp and paper mills, sugarcane mills, and corn ethanol mills. The results from this effort will allow us to identify and select the most commercially feasible biorefinery concepts. Major technical gaps or barriers to the commercialization of each biorefinery concept will also be determined from the results of this study.

The integration of process technologies will be assessed with an approach similar to that for the stand-alone design cases. The integration concepts will be developed by pairing stand-alone cases with these concepts to evaluate the economic and environmental advantages of the integration approaches. Over this period, we have conducted detailed analyses of ATJ conversion and integration with pulp mill operations. We have also investigated the potential contribution of lignin coproducts to the overall process economy.

A dry-grind corn ethanol mill (DGCEM) with a capacity of 80 million gallons of ethanol per year was studied to evaluate potential biorefinery scenarios for AJF production. Similarly, we used a sugarcane mill with a sugarcane processing capacity of 12,444 million tons per day (MTD) that produces raw sugar, molasses, surplus bagasse, and surplus electricity. The petroleum refinery used as the base case processes 120,000 barrels per day of crude oil. Five AJF technologies were studied: Virent's BioForming, ATJ, DSHC, fast pyrolysis, and GFT. A standardized methodology was adopted to compare the biorefinery concepts DGCEM, sugarcane mill, and petroleum refinery in several integration scenarios with six jet fuel production scenarios. For all cases, we estimated the minimum fuel selling price and greenhouse gas emissions.

A manuscript on the integration of ATJ technologies in the pulp mill infrastructure was published. Three new manuscripts will be published with the results for corn ethanol mills, sugarcane mills, and petroleum refineries.

Major Accomplishments

Building on the ATJ pathway analyses, we have analyzed the integration of the ATJ process in a pulp mill infrastructure. A manuscript entitled "Pulp Mill Integration with Alcohol-to-Jet Conversion Technology" has been published in *Fuel Processing Technology*. Economic models and life cycle assessments have been applied to select the most promising biorefinery concepts for corn ethanol, sugarcane, pulp and paper, and petroleum refineries. The manuscript on corn ethanol was submitted to *Biomass and Bioenergy*. The other two manuscripts (on sugarcane and petroleum refineries) are under internal review.

Publications

Written reports under peer review

Brandt, K.L., Wooley, R.J., Geleynse, S.C., Gao, J., Zhu, J., Cavalieri, R.P., Wolcott, M.P. (2020). Impact of co-product selection on techno-economic analyses of alternative jet fuel produced with forest harvest residuals. BioFPR, 14(4):764-775

Geleynse, S., Jiang, Z., Brandt, K., Garcia-Perez, M., Wolcott, M., Zhang, X. (2020). Fuel Processing Technology 201:106338

Tanzil, A.H., Zhang, X., Wolcott, M., Garcia-Perez, M. Evaluation of Biorefinery Alternatives for the Production of Sustainable Aviation Fuels in a Dry Grind Corn Ethanol Mill (*Submitted to Biomass and Bioenergy*)

Tanzil, A.H., Zhang, X., Wolcott, M., Garcia-Perez, M. Evaluation of Biorefinery Alternatives for the Production of Sustainable Aviation Fuels in a Sugarcane Mill (*Internal review*)

Tanzil, A.H., Zhang, X., Wolcott, M., Garcia-Perez, M. Evaluation of Biorefinery Alternatives for the Production of Sustainable Aviation Fuels in a Petroleum Refinery (*Internal review*)

Outreach Efforts

None

Awards

None

Student Involvement

Graduate students (Senthil Subramaniam, Kelly Nguyen, Abid Tanzil Hossain, Lina Martinez Valencia, and Anamaria Paiva) have received training in this project. An undergraduate student, Kitana Kaiphanliam, funded under a National Science Foundation Research Experience for Undergraduates (NSF-REU) grant, assisted in building techno-economic models for coproduct production scenarios.

Senthil Subramaniam, who has been supported by this project, has graduated with a PhD degree from WSU (December 2020).

Kelly Nguyen, who has been supported by this grant, has graduated with a Master's degree from WSU (May 2020).

Abid Tanzil submitted and defended a PhD dissertation during the fall 2020 semester.

Plans for Next Period
During the next period, Dr. Garcia-Perez's team will focus on publications.

Task 3 - Supplement and Maintain the Current Inventory of Biorefinery Infrastructures that are Useful for AJF Production, as Identified in the Conversion Design Cases
Washington State University

Objective
This task requires periodic evaluation of the databases to add new facilities or update the status of closed facilities in each category to ensure that the geospatially specific assets are current.

Research Approach
The use of existing infrastructure assets is a key component of retrofit approaches for advances in this industry. To differentiate between the relative values of various options, the specific assets must be valued with respect to their potential use within a conversion pathway. Regional databases of industrial assets that might be utilized by a developing AJF industry have been assessed on the national level. These baseline databases are compiled from a variety of sources, including industry associations, universities, and news outlets. These databases will be expanded, refined, and validated as the conversion design cases indicate additional needs for the regional analyses.

Milestone(s)
National databases have been compiled, geolocated, validated, and shared for biodiesel, corn ethanol, energy pellet, pulp and paper, and sugar mill production. We evaluated the databases as necessary to add new facilities or change the status of closed facilities in each category, to ensure that the geospatially specific assets are current.

The geospatial infrastructure data were converted for use in the supply chain resiliency models. Tools were updated for transportation cost modeling, which should lead to future improvements.

Major Accomplishments
National databases have been compiled, validated, and shared with the A01 teams. All metadata are available for use in regional analyses.

Publications
None

Outreach Efforts
N/A

Awards
None

Student Involvement
None

Plans for Next Period
N/A

Task 4 - Continue Work on Social Asset Decision Tools Developed in Phase 1 for Plant Siting (CAAM), Including Additional Validation and Incorporation of Multi-decision-making Tools; Extend Applications to Another U.S. Region in Coordination with Other Team Members (Inland Northwest, Appalachian Region); Prepare for National Extension and Replication in Select Countries

Washington State University

Objective(s)

The objective of this task is to update CAAM with available data and strategically apply it to additional U.S. regions.

Research Approach

Based on key measures of social, cultural, human, and political capital, WSU finalized the CAAM for strategic application to communities to determine appropriate outreach to aid in project development and implementation. The first tool with only three community assets—social, human, and cultural—was initially applied to the NARA region in the Pacific Northwest, and a refined tool that added more complete measures of social, cultural, and human capital was deployed in two subregions of NARA. The model was updated in 2019 to include political capital and was further refined through factor analysis to capture more parsimonious measures of each capital by using factor analysis. The 2019 updated model was strategically applied to case studies of biorefineries in the Pacific Northwest and Montana to provide community engagement recommendations and increase the likelihood of project success. The case study analysis was used to validate the strategic application model, which has been published online in *Community Development*. Additional efforts to apply the final CAAM in the Bioenergy Alliance Network of the Rockies (BANR) region and the Inland Northwest are ongoing.

Milestone(s)

The CAAM dataset and codebook are available and were shared with FAA ASCENT colleagues in Tennessee. CAAM benchmark measures have been developed for two additional regions: BANR and the Inland Northwest.

Major Accomplishments

A strategic application model has been created by using completed CAAM measures and supplementary data to provide engagement recommendations for improving the likelihood of success when making initial contacts with communities. A manuscript that explains the development of the new CAAM and applies the model to case studies in the Pacific Northwest and Montana has been published online with *Community Development*. The manuscript will be available in an upcoming issue of *Community Development* in 2020. Two additional manuscripts for the BANR on an application of the CAAM in Colorado and Wyoming are still underway.

Publications

Written report under peer review

Mueller, D., Hoard, S., Roemer, K., Rijkhoff, S., Sanders, C. (2020). Quantifying the Community Capitals Framework: Strategic Application of the Community Assets and Attributes Model. Community Development. DOI: 10.1080/15575330.2020.1801785

Outreach Efforts

None

Awards

None

Student Involvement

None

Plans for Next Period
We plan to update the model with new data (where available) and complete the application to the BANR and Inland Northwest regions.

Task 5 - Refine and Deploy Facility Siting Tools to Determine Regional Demand and Potential Conversion Sites to be Used in Regional Analyses
Washington State University

Objective
This task's objective is to develop tools to site potential conversion facilities. Two primary needs exist: a generalized tool to site initial locations that meet the needs of a specific conversion facility type and a second tool to select optimal conversion facility sites from the initial set of locations.

Research Approach
The geospatial siting pre-selection tool (GSP) began development in early 2019. It is a Python-based script that automates ArcGIS to produce points representing locations that suit the needs of a conversion facility. The GSP uses a combination of buffer and cost datasets. Buffer datasets ensure that a candidate is sited in proximity to the necessary infrastructure, such as roads, rails, and natural gas pipelines. Because the set of candidates generated by using only buffers would be very large, cost datasets have been added to distinguish candidates from each other. Cost datasets represent geospatially variable costs including electricity, natural gas, and transportation. An additional script has been developed to model the input transportation costs for the GSP by taking a feedstock point dataset and using it to develop an equation relating feedstock density to the average cost to supply a set amount of feedstock to that location. In early 2020, a graphic user interface was added to the GSP to make it more user friendly.

The Many Step Transshipment Solver (MASTRS) is another Python-based script that models large supply chains across multiple levels by building and solving mixed integer linear programming problems. The model starts with feedstock spread across many locations and then models the distribution and conversion of feedstock into biofuels and other coproducts through multiple levels of intermediate facilities that may include temporary storage, pre-treatment, and fuel production, before sending the new products to their destinations. Intermediate facilities may include existing facilities or new candidate facilities that are generated by the GSP. Output from MASTRS shows the flow of materials throughout the supply chain and the most cost-efficient capacities and locations of new facilities.

The modeling combination of GSP and MASTRS scripts has been implemented on several regional supply chains. MASTRS was first implemented with the Pacific Northwest oilseed-to-jet-fuel supply chain in 2018. Since 2019, GSP and MASTRS scripts have been used together for two supply chain models for both the production of jet fuel from forest residuals and lumber production byproducts in the Pacific Northwest. The first uses single-stage conversion at integrated biorefineries, and the second is a multi-stage model with distributed pre-processing facilities.

Milestone(s)
GSP and MASTRS have undergone continual progress to become much more practical tools. Along with the expansion of tool capabilities, substantial improvements have been made to tool accessibility for new potential users.

Major Accomplishments
None

Publications
None

Outreach Efforts
None

Awards
None

Student Involvement
None

Plans for Next Period
We plan to begin the process to publish papers that define GSP and MASTRS. We will continue implementation of GSP and MASTRS in regional supply chain analyses and will complete the BANR supply chain analysis.

Task 6 - Refinery-to-Wing Stakeholder
Washington State University
The report is provided in Award No. 13-C-AJFE-PSU-002.

Objective(s)
We will extend the stakeholder assessment to a limited sample of informed stakeholders in the remaining sections of the country to provide insight into market and industry dynamics, with the aim of optimizing successful outcomes.

Research Approach
In 2019, the team collected primary data via surveys to better understand the awareness, opinions, and perspectives of key aviation fuel supply chain stakeholders regarding the potential impacts and key factors for an economically viable biojet fuel production industry in the United States. These aviation fuel supply chain stakeholders include airport management, fixed base operators (FBOs), aviation fuel handlers, relevant airlines, and CAAFI personnel. Data were collected to assess the opinions, awareness, and perceptions of aviation fuel supply chain stakeholders regarding factors impacting the adoption and diffusion of AJF. A national survey of aviation management and FBOs was distributed to several hundred stakeholders across the United States and was completed in the summer of 2019.

Milestone(s)
Data have been assessed for potential manuscripts due to low response rates and potential publication identified.

Major Accomplishments
None

Publications
None

Outreach Efforts
N/A

Awards
None

Student Involvement
None

Plans for Next Period
We plan to complete an updated publication based on national results.

Task 7 - Supply Chain Analysis

Washington State University-Volpe

Objective(s)

Washington State University and Volpe have each developed modeling tools that apply trans-shipment optimization to model the geospatial layout of developing supply chains. A comparison of these tools would be useful to identify the strengths and weaknesses of each.

We have developed a framework for assessing the resilience of a sustainable aviation fuel (SAF) supply chain subjected to multiple uncertain hazards and conditions, and we have modified the Freight and fuel Transportation Optimization Tool (FTOT) for extensive utilization in a continuous re-optimization process. The team has applied the proposed resilience assessment framework to a forest-residue-based SAF supply chain in the Pacific Northwest (PNW) region to demonstrate its feasibility.

Research Approach

Focusing on the use of woody-biomass-to-jet-fuel conversion via fast pyrolysis and the upgrading of a supply chain centered in the Northern Rockies, a series of comparison studies was conducted by using optimization tools from Volpe and Washington State University. Each modeling approach was required to determine sites for new pyrolysis depots and upgrading refineries. Forest production data were provided by the LURA model from the University of Idaho. Pyrolysis depot locations were selected by candidate generation tools included in each approach, and existing petroleum refineries were used as candidates for upgrading refineries. Cities, ports, and airport hubs throughout the U.S. West Coast and Rocky Mountain regions were used as markets for road transportation fuel, bunker fuel, and jet fuel.

Resilience

A supply chain can be exposed to multiple unpredictable events and conditions over the medium- to long-term horizon. These events and conditions include natural (e.g., earthquakes, hurricanes, floods, wildfires, or tsunamis) and man-made (e.g., terrorist attacks, cyber-attacks, or industrial accidents) hazards, climate change, technology development, evolving customer preferences, dynamic changes in government regulation, and political circumstances, etc., which may have negative or positive impacts on supply chain performance. Although supply chain resilience assessments should address the combined effects of multiple negative and positive events and conditions that may occur over the planning horizon, most existing studies have focused on the negative consequences induced by a single type of natural hazard, which often leads to the under- or over-estimation of potential risks. Moreover, previous studies have assessed supply chain resilience in a qualitative manner through either conceptual or empirical analysis. To address these deficiencies in the existing literature, the proposed framework quantitatively assesses the effects of both negative and positive events and conditions on the performance of a supply chain and supports resilience-enhancing strategies that minimize negative impacts while capitalizing on opportunities. Furthermore, in contrast to conventional resilience assessments, which focus on a single type of hazard and provide a snapshot of the resilience index immediately following a hazardous event, the proposed resilience assessment considers the medium- to long-term performance of a supply chain, thereby providing the resilience index as a function of time over the planning horizon. In this way, the time-dependent performance-based supply chain resilience index enables the quantification of multiple components of resilience.

In the previous period of performance (October 2018–September 2019), we developed a multi-component resilience assessment framework for a supply chain system subjected to multiple uncertain hazards and conditions. During this period (October 2019–September 2020), our task consisted of two parts: (a) the modification and utilization of FTOT and (b) the application of the resilience assessment framework to a forest-residue-based SAF supply chain system in the PNW region. We have investigated the utilization of FTOT in solving re-routing problems following a major disruption and computing time-dependent supply chain system performance. First, we studied the FTOT Python package and scenarios thoroughly to identify the implicit assumptions and methodologies adopted in FTOT. Then, we communicated with the Volpe FTOT team from March to August of 2020 through bi-weekly meetings and FTOT GitHub to incorporate the risk and resilience assessment process into the current FTOT framework. We have made major modifications to FTOT, including the following: (a) a separate Python package that simulates multiple risk factors, (b) modifications of the main objective function and constraints, and (c) a new iterative structure embedded in the existing codes to enable the continual evaluation of system performance over the planning horizon.

To facilitate the Volpe team's understanding of the incorporation of risk and resilience assessment into the current FTOT framework, we have utilized a simple supply chain system. Specifically, quick scenario 2 from the FTOT package was used for communication purposes. Subsequently, the newly added modules and modified FTOT codes were validated with this example. After the initial validation was completed, we utilized a more realistic forest-residue-based SAF supply chain system distributed over the PNW region to identify any challenges that might arise from the application of the modified and/or newly added modules to a larger-scale supply chain system and demonstrate the feasibility and practicability of the proposed framework. We have identified multiple risk factors that may potentially affect the supply chain system. Among them, seismic hazards may induce the greatest negative impact on the system performance, because some parts of the system are located in high-seismic-hazard zones. While seismic risk assessment of civil infrastructure and regional transportation system has been well investigated in the past decades, their concern has focused on a city- or county-scale risk assessment. However, the supply chain system is distributed over a much larger geographical region, including three states (Washington, Idaho, and Oregon), and a new approach has been developed to generate a finite set of stochastic seismic events for the study region that can appropriately represent all possible events. An importance sampling technique has been used to sample large-magnitude seismic events while improving computational efficiency. In the next quarter, all risk factors will be combined to assess their effects on supply chain system performance and resilience to complete the case study.

Milestone(s)

The team has developed risk and resilience modules that are compatible with the FTOT to incorporate the resilience assessment framework into the current FTOT package.

The proposed assessment framework has been illustrated with a forest-residue-based SAF supply chain system distributed over the PNW region, to demonstrate its feasibility and practicability.

Major Accomplishments

The WSU MASTRS and Volpe FTOT were compared for siting analyses in the BANR region. Similar and differing modeling assumptions were identified, and the appropriate model for a given objective was determined.

The team has developed a theoretical framework for multi-component resilience assessment. The Python-based risk and resilience modules and the supporting documentation have been shared with the Volpe FTOT team. A manuscript describing the resilience assessment framework and its illustration with a forest-residue-based SAF supply chain system has been prepared and will be submitted to *Transportation Research Part E: Logistics and Transportation Review*. A conference abstract on this topic (but with a case study of transportation system) has been accepted, and we have been invited to submit a full paper to the *13th International Conference on Structural Safety & Reliability*.

We have performed a preliminary study on wildfire risk assessment of a supply chain system to investigate the potential effects of wildfire on a forest-residue-based SAF supply chain system.

Publications

None

Outreach Efforts

N/A

Awards

None

Student Involvement

Dane Camenzind, MS Environmental Engineering, Washington State University, graduated in September 2019 and is currently employed by WSU as an operations research engineer.

Jie Zhao, PhD candidate, Civil Engineering, Washington State University

Plans for Next Period

We will utilize regional supply chain tools to assess forest residuals for SAF using pyrolysis methods, as described in Task 8 below.

The team will submit a manuscript on a multi-component resilience assessment framework for a supply chain system in January 2021 and another manuscript on wildfire risk assessment of a forest residual-based SAF supply chain system in December 2020. During the upcoming year, we will extend this study to determine the most resilient supply chain layout among alternatives and support cost-effective resilience-enhancing activities. Moreover, we will also investigate various negative effects of wildfires on supply chain performance, including forced closedown of several facilities; delayed delivery schedules due to health risk; and closures of essential transit routes due to landslides, rock falls, etc.

In the following year, the research team will incorporate the proposed resilience assessment framework into FTOT to (a) assess the integrated effects of multiple types of hazards/conditions on long-term supply chain performance and (b) quantify the overall resilience of a supply chain system under a wide range of plausible future scenarios. To make FTOT compatible with the proposed resilience assessment framework, several modifications of the FTOT Python file package are required. For example, the framework has an iterative structure to measure supply chain performance at each time step, which generates a set of future scenarios. This structure is necessary to capture the dynamic nature of supply chain performance over a planning horizon under diverse scenarios and thus should be included in FTOT. Moreover, FTOT needs to be modified to incorporate the restoration costs and processes following a hazard event to quantify the restorative capacity of a supply chain, which is one of the three resilience components. In addition to the modifications to the FTOT simulation structure and procedure, minor modifications to variables and constraints in FTOT will be required. Although the unmet-demand ratio in FTOT can be either 0 or a positive value, the resilience assessment framework considers the positive effects of risk factors on supply chain performance and allows for redundancy of the system. Accordingly, the lower bound of the unmet-demand ratio should be changed from 0 to negative infinity. Furthermore, additional Python files need to be developed for generating the realizations of each type of risk factor and integrating the factors in supply chain analysis. To maintain the consistency between the proposed framework and FTOT, this work will involve active collaboration with the U.S. Department of Transportation Volpe Center. The incorporation of resilience assessment into FTOT will provide supply chain managers and stakeholders with information on (a) the key risk factors that should be mitigated to enhance supply chain resilience and (b) which supply chain design is the most resilient among alternative designs in the future. Such information could be further used to determine cost-effective resilience-enhancing solutions.

Task 8 - Analytical Support for Regional CAAFI and USDA Jet Fuel Project

Washington State University

Objective(s)

We will develop a readiness-level tool to assess the status of regional SAF production projects and will use supply chain and stand-alone design cases to support the USDA BANR project in TEA and supply chain analysis. This regional CAP project focuses on the use of softwood forest salvage feedstock for fuels via a catalyzed pyrolysis conversion pathway.

We will assess the regional feedstock, conversion pathways and the fuel MSP for SAF manufactured in the Northwest United States. The focus of this work requested by the Port of Seattle is to determine whether the Seattle-Tacoma International Airport can attain its 10% SAF goal by using SAF manufactured in the region from regional feedstock.

Research Approach

We will develop readiness-level tools for regional projects to assess the status of developing fuel projects and to identify critical missing components. This tool will be similar in form to the CAAFI Feedstock and Fuel Readiness Levels and will be used to assist CAAFI in understanding the stage of development for projects of interest and to assess critical gaps. In addition, we will assist the regional USDA BANR team in deploying TEA and supply chain analysis for their project. This effort will focus on the use of softwood forest salvage feedstock in a thermochemical conversion process to produce fuels and coproducts.

The facility siting tools discussed in Task 5, GSP and MASTRS, have been implemented on the BANR supply chain and Port of Seattle project. The most recent model runs included feedstock and markets in an 11-state region including the West Coast and intermountain regions. Feedstocks include forest residue from logging operations and mill residues from lumber

production. A future expansion will also include beetle-killed timber. The model run results generated by MASTRS will help determine the relationships between facility location, fuel MSP, and conversion facility revenue.

The Port of Seattle project required a detailed feedstock survey for forest residuals, municipal solid waste (MSW) and lipids. Forest residuals were quantified with the LURA model for Oregon, Washington, Idaho, and Montana. Regional landfills were identified and located, scales were determined, and the remaining lifetime was assessed to determine the most viable biorefinery location. The composition of MSW in the region was determined, as was a method and the related costs of sorting the material to match the SAF conversion pathway. Lipids were separated into two major categories: (a) waste fats, oils, and greases and (b) vegetable oil. Each feedstock was quantified and then paired with a compatible SAF conversion pathway to determine SAF MSP by using ASCENT-developed TEAs.

Milestone(s)

We are making progress in the use of supply chain and stand-alone design cases to support the USDA BANR project in TEA and supply chain analysis. Additionally, we have supported the BANR team in creating TEAs for the technologies under consideration.

The Port of Seattle analysis and report have been completed, submitted, and presented.

Major Accomplishments

We have collaborated with the USDA BANR project and attended their annual meeting to coordinate analysis. We currently await their completion of dead wood estimates to complete the supply chain analysis. Moreover, analyses with previous forest-residue data have been successfully modeled.

The Port of Seattle feedstock and SAF assessment was completed, presented to the Port of Seattle, and released to the public.

Publications

Public Reports

Potential Northwest Regional Feedstock and Production of Sustainable Aviation Fuel: 2019 Report form the Port of Seattle and Washington State University. Prepared February 2020. https://www.portseattle.org/sites/default/files/2020-08/PofSeattleWSU2019updated_appendix.pdf

Outreach Efforts

Wolcott, M., Holladay, J. Supply chains for sustainable aviation fuels: Why, What, Who? CleanTech Alliance Breakfast. 11 December 2019. Seattle, WA.

Wolcott, M., Brandt, K., Camenzind, D. Potential Northwest Regional Feedstock and Production of Sustainable Aviation Fuel. Energy and Sustainability Committee – WSU Briefing. 12 February 2020. Seattle, WA.

Wolcott, M., Brandt, K., Camenzind, D., Meyn, S._Potential Northwest Regional Feedstock and Production of Sustainable Aviation Fuel: Port of Seattle. ASCENT Spring Meeting. 31 March 2020.

Wolcott, M.P., K. Brandt, and D. Camenzind. Potential Northwest Regional Feedstock and Production of Sustainable Aviation Fuel: Port of Seattle. Washington State Aviation Biofuels Work Group. Virtual Meeting held on June 3, 2020.

Wolcott, M. Potential Northwest Regional Feedstock and Production of Sustainable Aviation Fuel: Port of Seattle. Washington Clean Fuel Forum: 2021 Industry and Policy Forecast. 22 October 2020.

Awards

None

Student Involvement

Dane Camenzind, MS Environmental Engineering, Washington State University, graduated in September 2019 and is currently employed by WSU as an operations research engineer.

Lina Martinez, PhD candidate, Biosystems Engineering, Washington State University

Plans for Next Period

Analysis of the BANR region is underway and will be completed in 2021.

The Port of Seattle report will be adapted for peer-reviewed publication.

Project 001(B) Alternative Jet Fuel Supply Chain Analysis

University of Hawaii

Project Lead Investigator

Scott Q. Turn
Researcher
Hawaii Natural Energy Institute
University of Hawaii
1680 East-West Rd., POST 109; Honolulu, HI 96822
(808)-956-2346
sturn@hawaii.edu

University Participants

University of Hawaii
- PI: Scott Q. Turn, Researcher
- FAA Award Number: 13-C-AJFE-UH, Amendment 005
- Period of Performance: October 1, 2015, to August 4, 2021
- Tasks:
    1. Informing regional supply chains
    2. Identifying supply chain barriers in the Hawaiian Islands

University of Hawaii
- PI: Scott Q. Turn, Researcher
- FAA Award Number: 13-C-AJFE-UH, Amendment 007
- Period of Performance: October 1, 2016, to August 4, 2021
- Tasks:
    1. Informing regional supply chains
    2. Supporting Indonesian alternative jet fuel supply initiatives

University of Hawaii
- PI: Scott Q. Turn, Researcher
- FAA Award Number: 13-C-AJFE-UH, Amendment 008
- Period of Performance: August 1, 2017 to August 4, 2021
- Tasks:
    1. National lipid supply availability analysis
    2. Hawaii regional project

University of Hawaii
- PI: Scott Q. Turn, Researcher
- FAA Award Number: 13-C-AJFE-UH, Amendment 011
- Period of Performance: May 31, 2019 to August 4, 2021
- Task:
    1. Hawaii regional project

University of Hawaii
- PI: Scott Q. Turn, Researcher
- FAA Award Number: 13-C-AJFE-UH, Amendment 013
- Period of Performance: June 5, 2020 to August 4, 2021
- Task:
    1. Hawaii regional project

University of Hawaii
- PI: Scott Q. Turn, Researcher
- FAA Award Number: 13-C-AJFE-UH, Amendment 017

- Period of Performance: October 1, 2021, to September 30, 2022
- Task:
    1. Hawaii regional project

Project Funding Level

Under **FAA Award Number 13-C-AJFE-UH, Amendment 005**, the Alternative Jet Fuel Supply Chain Analysis-Tropical Region Analysis project received $75,000 in funding from the FAA and cost share funding of $75,000 from the State of Hawaii.

Under **FAA Award Number 13-C-AJFE-UH, Amendment 007**, the Alternative Jet Fuel Supply Chain Analysis-Tropical Region Analysis project received $100,000 in funding from the FAA, cost share funding of $75,000 from the State of Hawaii, and $25,000 of in-kind cost match in the form of salary support for Scott Turn from the University of Hawaii.

Under **FAA Award Number 13-C-AJFE-UH, Amendment 008**, the Alternative Jet Fuel Supply Chain Analysis-Tropical Region Analysis project received $125,000 in funding from the FAA and cost share funding of $125,000 from the State of Hawaii.

Under **FAA Award Number 13-C-AJFE-UH, Amendment 011**, the Alternative Jet Fuel Supply Chain Analysis-Tropical Region Analysis project received $200,000 in funding from the FAA and cost share funding of $200,000 from the State of Hawaii.

Under **FAA Award Number 13-C-AJFE-UH, Amendment 013**, the Alternative Jet Fuel Supply Chain Analysis-Tropical Region Analysis project received $200,000 in funding from the FAA and cost share funding of $200,000 from the State of Hawaii.

Under **FAA Award Number 13-C-AJFE-UH, Amendment 017**, the Alternative Jet Fuel Supply Chain Analysis-Tropical Region Analysis project received $100,000 in funding from the FAA and cost share funding of $100,000 from the State of Hawaii.

Investigation Team

Lead
Scott Turn, University of Hawaii, PI

Other Lead Personnel
Tim Rials, professor, and Burt English, professor (University of Tennessee co-PIs)
Manuel Garcia-Perez, professor (Washington State University [WSU] co-PI)
Kristin Lewis, principal technical advisor (Volpe National Transportation Systems Center PI)
Michael Wolcott, professor (WSU PI)
Lara Fowler, professor (The Pennsylvania State University PI)

UH Investigation Team
Under **FAA Award Number 13-C-AJFE-UH, Amendment 005**, Task 1 and Task 2 include
Dr. Scott Turn, researcher, Hawaii Natural Energy Institute, University of Hawaii (UH)
Dr. Trevor Morgan, assistant researcher, Hawaii Natural Energy Institute, UH
Dr. Richard Ogoshi, assistant researcher, Department of Tropical Plant and Soil Sciences, UH
Dr. Adel H. Youkhana, junior researcher, Department of Tropical Plant and Soil Sciences, UH

Under **FAA Award Number 13-C-AJFE-UH, Amendment 007**, Task 1 and Task 2 include
Dr. Scott Turn, researcher, Hawaii Natural Energy Institute, UH
Dr. Trevor Morgan, assistant researcher, Hawaii Natural Energy Institute, UH
Dr. Richard Ogoshi, assistant researcher, Department of Tropical Plant and Soil Sciences, UH
Dr. Adel H. Youkhana, junior researcher, Department of Tropical Plant and Soil Sciences, UH
Dr. Curtis Daehler, professor, Department of Botany, UH
Ms. Sharon Chan, junior researcher, Hawaii Natural Energy Institute, UH
Mr. Gabriel Allen, undergraduate student, Biochemistry Department, UH

Under **FAA Award Number 13-C-AJFE-UH, Amendment 008**, Task 1 and Task 2 include
Dr. Scott Turn, researcher, Hawaii Natural Energy Institute, UH
Dr. Trevor Morgan, assistant researcher, Hawaii Natural Energy Institute, UH
Dr. Jinxia Fu, assistant researcher, Hawaii Natural Energy Institute, UH

Dr. Quang Vu Bach, postdoctoral fellow, Hawaii Natural Energy Institute, UH
Ms. Sabrina Summers, undergraduate student, Bioengineering Department, UH
Ms. Sarah Weber, undergraduate student, Molecular Biosciences and Biotechnology, UH
Mr. Taha Elwir, undergraduate student, Chemistry Department, UH

Under **FAA Award Number 13-C-AJFE-UH, Amendment 011**, Task 1 includes
Dr. Scott Turn, researcher, Hawaii Natural Energy Institute, UH
Dr. Quang Vu Bach, postdoctoral fellow, Hawaii Natural Energy Institute, UH

Under **FAA Award Number 13-C-AJFE-UH, Amendment 013**, Task 1and Task 2 includes
Dr. Scott Turn, researcher, Hawaii Natural Energy Institute, UH
Ms. Sharon Chan, Hawaii Natural Energy Institute, UH
TBD, Hawaii Natural Energy Institute, UH

Under **FAA Award Number 13-C-AJFE-UH, Amendment 017**, Task 1 includes
Dr. Scott Turn, researcher, Hawaii Natural Energy Institute, UH
TBD, Hawaii Natural Energy Institute, UH

Project Overview

Under **FAA Award Number 13-C-AJFE-UH, Amendment 005**, the research effort has two objectives. The first objective is to develop information on regional supply chains for use in creating scenarios of future alternative jet fuel (AJF) production in tropical regions. Outputs from this project may be used as inputs to regional supply chain analyses being developed by the FAA and Volpe Center. The second objective is to identify the key barriers in regional supply chains that must be overcome to produce significant quantities of sustainable aviation fuels (SAF) in the Hawaiian Islands and similar tropical regions.

The **FAA Award Number 13-C-AJFE-UH, Amendment 005** project goals are to:

- Review and summarize
  - the available literature on biomass feedstocks for the tropics
  - the available literature on pretreatment and conversion technologies for tropical biomass feedstocks
  - the available literature on geographic information systems (GIS) datasets available for assessment of AJF production systems in the tropics.
- Identify AJF supply chain barriers in the Hawaiian Islands.

Under **FAA Award Number 13-C-AJFE-UH, Amendment 007**, the research effort has two objectives. The first objective is to develop information on regional supply chains for use in creating scenarios of future SAF production in tropical regions. Outputs from this project may be used as inputs to regional supply chain analyses being developed by the FAA and Volpe Center. Included in this objective is the development of fundamental property data for tropical biomass resources to support supply chain analysis. The second objective is to support the memorandum of understanding between the FAA and Indonesian Directorate General of Civil Aviation (DGCA) to promote development and use of sustainable, alternative aviation fuels.

The **FAA Award Number 13-C-AJFE-UH, Amendment 007** project goals are to:

- Support the Volpe Center and Commercial Aviation Alternative Fuels Initiative (CAAFI) Farm to Fly 2.0 supply chain analysis
- Use GIS-based estimates of fiber crop production potential to develop preliminary technical production estimates of jet fuel in Hawaii
- Develop fundamental property data for tropical biomass resources
- Transmit data and analysis results to other ASCENT Project 1 researchers to support improvement of existing tools and best practices
- Support Indonesian SAF supply initiatives

Under **FAA Award Number 13-C-AJFE-UH, Amendment 008**, the research effort has two objectives. The first objective is to support a national lipid supply availability analysis that will inform industry development and guide policy. The second objective is to conduct a targeted supply chain analysis for a SAF production facility based on the Hawaii regional project.
The **FAA Award Number 13-C-AJFE-UH, Amendment 008** project goals are to:

- Support ASCENT partners conducting the national lipid supply availability analysis by contributing information on tropical oilseed availability
- Evaluate supply chains for targeted waste streams and purpose-grown crops in Hawaii to a location in the principal industrial park on the island of Oahu

Under **FAA Award Number 13-C-AJFE-UH, Amendment 011**, the main objective of the research effort is to conduct bench-scale testing of tropical feedstocks for use in targeted supply chain analysis for a SAF production facility based on the Hawaii regional project initiated under Amendment 008.

The **FAA Award Number 13-C-AJFE-UH, Amendment 011** project goals are to:

- Survey bench-scale systems available for relevant SAF conversion technology options
- Down-select from the available bench-scale systems to no more than two systems capable of conducting feedstock testing and quantify product yields and contaminant concentrations
- Conduct bench-scale feedstock tests and quantify product yields and quality and contaminant concentrations

The **FAA Award Number 13-C-AJFE-UH, Amendment 013** project goals are to:

- Conduct tropical oil to SAF supply chain analysis
- Develop management strategies for elements present in construction and demolition waste that impact use in thermochemical conversion–based SAF production pathways

The **FAA Award Number 13-C-AJFE-UH, Amendment 017** project goals are to

- Explore the impacts of HB2386 on waste management in Hawaii and potential for waste-based SAF production systems

Task 0.1 - Informing Regional Supply Chains

University of Hawaii

Objectives

This task included two activities: (1) a review of the archival literature on existing tropical crops and potential new crops that could provide feedstocks for SAF production, and (2) a review of relevant pretreatment and conversion technology options and experience with feedstocks identified in (1).

Research Approach

Activity 1: The archival literature will be reviewed to construct an updated database of relevant citations for tropical crops; new potential energy crops will be identified and added to the database. Available information on agronomic practices, crop rotations, and harvest techniques will be included. The database will be shared with and serve as a resource for the ASCENT Project 1 team and Volpe Center analyses of regional supply chains.

Activity 2: A database of relevant pretreatment and conversion technology options and experience with potential tropical feedstock materials will be assembled from the archival literature and from existing Project 1 team shared resources. Of particular interest are inventories of material and energy flows associated with the pretreatment and conversion unit operations fundamental to the design of sustainable systems and the underlying analysis. Pairings of pretreatment and conversion technology options provide the starting point for evaluation of tropical biorefineries that can be integrated into ASCENT Project 1 team and Volpe Center activities.

Milestones

Task 1, Activity 1: Identify target list of databases to search for relevant literature
Task 1, Activity 1: Interim report summarizing progress on literature search
Task 1, Activity 2: Identify target list of databases to search for relevant literature
Task 1, Activity 2: Interim report summarizing progress on literature search

Major Accomplishments
This work is completed. A report was produced for each of the two activities, and the two reports were combined to form a manuscript published in the journal *Energy & Fuels*.

Publications
Peer-reviewed journal publication
Morgan, T. M., Youkhana, A., Ogoshi, R., Turn, S., & Garcia-Perez, M. (2019). Review of biomass resources and conversion technologies for alternative jet fuel production in Hawai'i and tropical regions. *Energy & Fuels, 33,4,* 2699–2762. https://doi.org/10.1021/acs.energyfuels.8b03001

Outreach Efforts
On February 21, 2018, the PI participated in a ThinkTech Hawaii broadcast focused on SAFs with collaborators from WSU and CAAFI (https://www.youtube.com/watch?v=Ci4oWITPRKQ&feature=youtu.be).

Awards
None

Student Involvement
None

Plans for Next Period
Not applicable

Task 0.2 - Identification of Supply Chain Barriers in the Hawaiian Islands
University of Hawaii

Objective
The objective of this task was to identify the key barriers in regional supply chains that must be overcome to produce significant quantities of SAF in the Hawaiian Islands and similar tropical regions.

Research Approach
UH developed the Hawaii Bioenergy Master Plan for the State of Hawaii (https://www.hnei.hawaii.edu/sites/www.hnei.hawaii.edu/files/Hawaii%20Bioenergy%20Master%20Plan.pdf), which was completed in 2009. In that plan, UH was tasked with determining whether Hawaii had the capability to produce 20% of land transportation fuels and 20% of electricity from bio-based resources. To this end, the plan included assessments of (1) land and water resources that could support biomass feedstock production, (2) potential biomass resources and their availabilities, (3) technology requirements, (4) infrastructure requirements to support logistics, (5) economic impacts, (6) environmental impacts, (7) availability of human capital, (8) permitting requirements, and (9) limitations to developing complete value chains for biomass-based energy systems. In keeping with the stakeholder-driven development of the Hawaii Bioenergy Master Plan, barriers to development of regional supply chains for ASCENT will be identified by interacting with key stakeholder groups. Green Initiative for Fuels Transition Pacific (GIFTPAC) meetings are held quarterly and attended by biofuel development interests in Hawaii, including representatives of large landowners, producers of first-generation biofuels, petroleum refiners, electric utilities, the State Energy Office, U.S. Pacific Command, biofuel entrepreneurs, county government officials, and UH. Additional stakeholders are invited as necessary to fill information and value chain gaps. These meetings are excellent opportunities to receive stakeholder input, identify barriers to supply chain development, and organize data collection efforts that span supply chain participants.

Milestones
Task 2: Introduce activities at next regularly scheduled GIFTPAC meeting after contract executed
Task 2: Prepare interim report outlining two tropical supply chain scenarios developed in consultation with Project 1 team and with input from GIFTPAC participants

Major Accomplishments

This task has been completed. A stakeholder meeting was held and documented in a report submitted to the FAA. The stakeholders identified barriers to SAF production in Hawaii and ranked the barriers in order of importance as indicated below:

- Economic constraints (e.g., high costs of entry for production factors such as land) throughout the whole production chain
- Issues associated with access to capital, including high initial risks and uncertain return on investment
- Insufficient government support in the form of incentives and favorable policies to encourage long-term private investment
- Cost, availability, and competition for water
- SAF production technologies (emerging but have not yet demonstrated full commercial viability)
- Insufficient or inadequate infrastructure (e.g., harbors, roads, fuel distribution infrastructure, irrigation systems) to support the whole production chain

Several of the barriers are held in common with other locations in the continental United States, but those related to water and infrastructure are unique characteristics of an island state.

Publications

Not applicable

Outreach Efforts

This activity engaged stakeholders to identify barriers to SAF production in Hawaii. Preparation included reviewing stakeholder lists from previous activities. Facilitators appropriate to the stakeholder group were retained. The stakeholder meeting included a presentation about the scope and goals of the larger ASCENT program and other aspects of the UH ASCENT project.

Awards

None

Student Involvement

None

Plans for Next Period

This task is complete, but stakeholder outreach activities will continue under other tasks outlined below.

Task 0.3 - Informing Regional Supply Chains

University of Hawaii

Objectives

Building on FY16 activities, additional supporting analysis will be conducted for proposed supply chains in Hawaii, including:

0.3.1 Support Volpe Center and CAAFI Farm to Fly 2.0 supply chain analysis
0.3.2 Use GIS-based estimates of fiber crop production potential to develop preliminary technical production estimates of jet fuel in Hawaii
0.3.3 Develop fundamental property data for tropical biomass resources
0.3.4 Transmit data and analysis results to support improvement of existing tools (e.g., POLYSYS; https://bioenergykdf.net/content/polysys)

Research Approach

Activity 0.3.2 has been conducted using GIS data to identify areas suitable for purpose-grown crop production of feedstocks for SAF production in Hawaii. The approach has been to use GIS layers for land capability class (LCC), slope, and zoning as preliminary screens for suitability. Lands are classified by the Natural Resources Conservation Service (NRCS) with ratings from 1 to 6. LCCs from 1 to 3 are generally suitable for agricultural production; LCC of 4 can be productive with proper

management; and LCCs of 5 or 6 can support less-intensive production and could be suitable for forestry. The slopes of terrains affect aspects of production, including mechanization and erodibility. An elevation GIS layer was used to derive a slope layer. Zoning layers were acquired from state and county GIS offices. Only agricultural zoning was deemed suitable for this analysis.

The EcoCrop model was used to develop yield models for the crops selected in Task 0.1 based on annual rainfall and mean minimum monthly temperature data. EcoCrop includes model parameters on sugarcane, bana grass, five species of eucalyptus, gliricidia, leucaena, pongamia, jatropha, and sorghum. The parameters for sugarcane have been used to provide a base case assessment for comparison with historical sugarcane acreage and yield. Using sensitivity analysis, the model can be tuned to account for the differences between parameters developed from global sugar production and a century of production experience in Hawaii that was refined through plant breeding to adapt sugarcane varieties to a wide variety of agro-ecosystems. Analysis has purposely avoided land-use conflict with food production by limiting suitability to areas capable of sustaining AJF feedstocks under rain-fed conditions. Areas suitable for SAF production that do not conflict with current agricultural land use (i.e., fallow land) have also been identified.

Pongamia (*Millettia pinnata*) was the initial focus of Activity 0.3.3. Pongamia is an oilseed-bearing, leguminous tree that has production potential in Hawaii and Florida. The tree produces pods containing oil-bearing seeds. Pods, oilseed cake, and oil were evaluated from a number of trees growing on the island of Oahu. Fundamental measurements of chemical composition will be conducted and reported. Torrefaction of pods as a coproduct to oil production has been conducted. Investigation of pretreatment methods to improve pod feedstock properties for thermochemical conversion applications are currently underway.

Milestones

- Identify target opportunities to augment POLYSYS, Alternative Fuel Transportation Optimization Tool (AFTOT; https://trid.trb.org/view/1376122), and conversion modules
- Review previously developed GIS information layers for tropical fiber crops and identify updating requirements
- Conduct preliminary estimates of SAF technical potential in Hawaii based on previously developed GIS information layers

Major Accomplishments

The GIS-based analysis of SAF production potential is ongoing. The assessment of potential lands meeting requirements for LCC, slope, and land-use zoning is complete. The EcoCrop model is being implemented to predict yield as a function of minimum mean monthly temperature and annual rainfall. This will allow prescription of potential SAF feedstock crops on land areas capable of supporting their production under both rain-fed and irrigated conditions. This analysis will provide information necessary in determining cropping patterns and assessing transport costs to processing facility locations. The EcoCrop model's prediction of sugarcane potential was determined and the results were compared with historical sugarcane acreage, both rain-fed and irrigated. EcoCrop's upper and lower values for temperature and rainfall that support optimal sugarcane production were varied to calibrate the prediction against historical acreage. The difference between the EcoCrop values and those representative of Hawaii conditions can be attributed to improvements due to plant breeding and unique combinations of environmental conditions. An example of the latter is the relatively young volcanic soils present in high-rainfall areas on the island of Hawaii that allow for high drainage rates and accommodate sugar production.

Calibration of the EcoCrop model using historical sugarcane planted acreages was completed in 2018. This effort used a confusion matrix approach to validation (resulting in a kappa value >0.4) and demonstrated that mean annual temperature was a better indicator of environmental capability than the minimum mean monthly temperature recommended by the EcoCrop developers. This effort highlights the need to adapt models to local conditions. Model predictions for suitable cropping are being compared with current land uses to provide another indicator of agreement.

The GIS analysis of SAF feedstock production potential has been completed to include statewide working maps for each of the species summarized in a draft report currently undergoing internal review. This report will serve as the basis for a publication targeted for the upcoming, ASCENT-organized special issue of *Frontiers in Energy Research*.

Dr. Curtis Daehler (University of Hawaii, Department of Botany) completed a report assessing the invasiveness of pongamia. Retrospective analyses show that predictive weed risk assessment systems correctly identify many major pest plants, but such predictions are not 100% accurate. The purpose of this study was to make field observations of pongamia planted

around Oahu to look for direct evidence that pongamia is escaping from plantings and becoming an invasive weed. Seven field sites were visited in varying environments across Oahu. Although some pongamia seedlings were found in the vicinity of some pongamia plantings, particularly in wetter, partly shaded environments, almost all observed seedlings were restricted to areas directly beneath the canopy of mother trees. This finding suggests a lack of effective seed dispersal away from pongamia plantings. Based on its current behavior in the field, pongamia is not invasive or established outside of cultivation on Oahu. Because of its limited seed dispersal and low rates of seedling establishment beyond the canopy, the risk of pongamia becoming invasive can be mitigated through monitoring and targeted control of any rare escapes in the vicinity of plantings. Seeds and seed pods are water dispersed, so future risks of pongamia escape and unwanted spread would be minimized by avoiding planting at sites near flowing water, near areas exposed to tides, or on or near steep slopes. Vegetative spread by root suckers was not observed around plantings on Oahu but, based on reports from elsewhere, monitoring for vegetative spread around plantations is recommended; unwanted vegetative spread might become a concern in the future that could be addressed with localized mechanical or chemical control.

Pods, oilseed cake, and oil were evaluated from a number of trees growing on the island of Oahu. TerViva, a company pursuing pongamia commercialization, has provided material from orchards on Oahu. Fundamental measurements of chemical composition were made for seeds, pods, extracted oil, and post-extraction seed material. Measured values included C, H, N, and S elemental composition; energy content; volatile matter, fixed carbon and ash content; and trace element composition. Oils were characterized for peroxide value, iodine value, fatty acid profile, free fatty acid content, flash point, density, viscosity, and phase transition temperatures. Chemical composition and fuel properties of the oilseed cake and the pod material have been characterized. A manuscript summarizing the results of this effort was published in the journal *ACS Omega*.

Coproduct evaluation of pongamia pods feedstock for thermochemical conversion has been conducted. Evaluation included both untreated pods and those pretreated by a torrefaction process to improve their properties. Torrefaction produces a material that has better grindability, reduced oxygen content, improved storage stability, and reduced microbial availability. The effects of process conditions on feedstock properties relevant to thermochemical conversion technologies, proximate and ultimate composition, heating value, and Hardgrove grindability index (HGI), were measured. The chemical structure, reactivity, and changes in elemental composition of the torrefied materials were also investigated. A manuscript summarizing the results of this effort was published in the journal *Fuel*.

Pongamia seedpods are recognized as a potential feedstock for SAF production due to the relatively high oil content of the seeds. Pongamia pods are byproduct residues available after seed separation. Pods have high chlorine and potassium content that may be problematic in thermochemical energy conversion systems. Leaching experiments were performed to remove inorganic constituents of pods and thereby reduce the potential for fouling, slagging, and agglomeration. A manuscript summarizing the results of this effort was published in the journal *Fuel*.

Publications

Written report

Chan, S., Ogoshi, R. & Turn, S. Feedstocks for sustainable jet fuel production: An assessment of land suitability in Hawaii. A draft report has been prepared and a draft manuscript is under preparation for the journal *Frontiers in Energy Research*.

Peer-reviewed publications

Fu, J., Allen, G., Weber, S., Turn, S. Q., & Kusch, W. (2021). Water leaching for improving fuel properties of pongamia pod: Informing process design. *Fuel, 305,* 121480. https://doi.org/10.1016/j.fuel.2021.121480

Fu, J., Summers, S., Turn, S. Q., & Kusch, W. (2021). Upgraded pongamia pod via torrefaction for the production of bioenergy. *Fuel, 291,* 120260. https://doi.org/10.1016/j.fuel.2021.120260

Fu, J., Summers, S., Morgan, T. J., Turn, S. Q., & Kusch, W. (2021). Fuel properties of pongamia (*Milletia pinnata*) seeds and pods grown in Hawaii. *ACS Omega, 6,* 9222–9233. https://doi.org/10.1021/acsomega.1c00635

Outreach Efforts

Outreach in this task has focused on interactions with TerViva, a startup company that has identified pongamia germplasm production and marketing as the central focus of their business plan.

A poster titled "Feedstocks for Sustainable Jet Fuel Production: An Assessment of Land Suitability in Hawaii" was presented at the European Biomass Conference and Exhibition held virtually July 6–9, 2020.

"Upgraded *Milletia Pinnata* Pod via Torrefaction for the Production of Bioenergy in Hawaii" was presented orally at the 2020 Thermal & Catalytic Sciences Virtual Symposium.

Information from this task was included in the "Regional Supply Chain Analysis for Alternative Jet Fuel Production in the Tropics" presentation at the Hawaii Aviation and Climate Action Summit, December 3, 2019, at the Hawaii State Capitol.

"Water Leaching for Improving Fuel Properties of Pongamia Pods" was presented orally and virtually at the 2021 Fall National Meeting of the American Chemical Society in Atlanta, Georgia, August 22-26, 2021.

"Upgraded *Milletia Pinnata* Pod via Torrefaction for the Production of Bioenergy in Hawaii" was presented virtually and orally at the 2021 Spring National Meeting of the American Chemical Society, April 5-16, 2021.

Awards
The poster titled "Feedstocks for Sustainable Jet Fuel Production: An Assessment of Land Suitability in Hawaii," presented at the European Biomass Conference and Exhibition held virtually July 6-9, 2020, received the Best Visual Presentation Award.

Student Involvement
Three undergraduate students are involved in the project, with primary responsibility for processing and analyzing samples of biomass materials selected for evaluation as potential SAF feedstocks. The pongamia torrefaction work was the focus of an Undergraduate Research Opportunity Program project for Sabrina Summers, a bioengineering and chemistry double major. The results of her work were presented at the fall 2019 American Chemical Society meeting in San Diego, California. The pongamia pod leaching work was the focus of an Undergraduate Research Opportunity Program project for Gabriel Allen, a biochemistry major.

Plans for Next Period
The report summarizing the analysis of the GIS analysis of SAF feedstock production potential and the manuscript for the upcoming, ASCENT-organized special issue of *Frontiers in Energy Research* will be completed.

Statewide working maps for each of the feedstock species will be used as the basis for ongoing discussions with targeted stakeholder groups, including landowners and NRCS staff. Funding for planting and evaluating the more promising feedstock plants on UH experiment station land will be pursued in collaboration with stakeholders (e.g., TerViva).

Task 0.4 - Support of Indonesian Alternative Jet Fuel Supply Initiatives
University of Hawaii

Objective
This task supports the memorandum of understanding between the FAA and the Indonesian DGCA to promote development and use of sustainable, alternative aviation fuels. Under the coordination of the FAA, efforts to establish points of contact and coordinate with Indonesian counterparts are ongoing.

Research Approach
This task will support the memorandum of understanding between the FAA and Indonesian DGCA to promote development and use of sustainable, alternative aviation fuels. This will begin with working with the FAA to establish points of contact to coordinate efforts with Indonesian counterparts. The Indonesian Aviation Biofuels and Renewable Energy Task Force (ABRETF) membership includes Universitas Indonesia, Institut Teknologi Bandung, and Universitas Padjadjaran. A prioritized list of tasks will be developed in consultation with Indonesian counterparts, and data required to inform sustainability and supply analyses and potential sources of information will be identified. This could include data collection on Indonesian jet fuel use and resources for SAF production, airport locations, and annual and monthly jet fuel consumption patterns. Characterization of sustainable biomass resources with potential for use in producing SAF supplies could include developing preliminary GIS mapping information of their locations and distributions and preliminary estimates of their technical potentials.

Milestones

- Identify points of contact at Indonesian universities participating in ABRETF
- Identify research needs and develop project plan
- Develop data on potential project

Major Accomplishments

The PI traveled to Jakarta in the first week of August 2017 and met with the following individuals:

- Cesar Velarde Catolfi-Salvoni (International Civil Aviation Organization)
- Dr. Wendy Aritenang (International Civil Aviation Organization)
- Dr. Ridwan Rachmat (head of Research Collaboration, Indonesian Agency for Agricultural Research and Development)
- Sylvia Ayu Bethari (head of Aviation Fuel Physical & Chemical Laboratory, Research and Development Centre for Oil and Gas Technology)
- Dr. Ina Winarni (Forest Product Research and Development Center, Ministry of Environment and Forestry)
- Dr. SD Sumbogo Murti (Center of Technology Energy Resources and Chemical Industry, Agency for the Assessment and Application of Technology)

The activities of the tropical supply chain analysis effort were presented to the group, followed by a general discussion. The conclusion from this introductory meeting was that the Indonesian counterparts would seek agreement on how to move forward with future cooperation.

The PI traveled to Jakarta and met with Dr. Wendy Aritenang of the International Civil Aviation Organization Jakarta office. The same trip included meetings with renewable energy researchers at Universitas Indonesia. Following the meeting, Dr. Aritenang suggested points of contact for future engagement: Frisda Panjaitan from the Palm Oil Research Institute and three researchers from the Bandung Institute of Technology: Tatang Soerawidjaja, Tirto Prakoso Brodjonegoro, and Imam Reksowardojo.

A source of funds external to ASCENT has been identified to hold a post-pandemic workshop on AJF production in Indonesia. Scott Turn requested and received encouragement from FAA ASCENT program management. FAA will provide guidance on personnel, participation, and workshop content when planning begins in earnest. This portion of the activity will be resumed when COVID-19 restrictions allow.

Publications

Not applicable

Outreach Efforts

Outreach efforts by the PI are described in the Major Accomplishments section above.

Awards

None

Student Involvement

None

Plans for Next Period

The PI will continue to develop the cooperative research agenda between UH and Indonesian universities through continued dialogue with FAA, the International Civil Aviation Organization, and the Indonesian DGCA. Travel to Southeast Asia for other projects is anticipated in 2022, and meetings with the researchers at Indonesian institutions (delayed by the pandemic in 2020 and 2021) suggested by Dr. Aritenang will be pursued. Planning for a workshop on SAF will move forward as the situation returns to normal.

Task 2.2 - National Lipid Supply Availability Analysis

University of Hawaii

Objective

Activities under this task will support ASCENT partners working on a national lipid supply availability analysis by sharing data on tropical oilseed availability developed under previous years' activities.

Research Approach

Activities under this task will support ASCENT partners working on a national lipid supply availability analysis by sharing data on tropical oilseed availability developed under previous years' activities. This support will include estimates of pongamia production capability in the state, in addition to assessments of waste cooking oil and tallow.

Milestones

Milestones will coincide with the schedule of the lead institution (WSU) for the national lipid supply analysis.

Major Accomplishments

Additional seeds and pods were collected from the pongamia tree on the UH campus, Foster Botanical Garden, and the Ke'ehi Lagoon Beach Park. Large quantities (tens of kilograms) of material were acquired from TerViva's plantings on Oahu's north shore for use in oil evaluation. Two oilseed presses were acquired and safety documents developed. Pods, oilseed cake, and oil were evaluated from a number of trees growing on the island of Oahu. Fundamental measurements of chemical composition were made for seeds, pods, extracted oil, and post-extraction seed material. Measured values included C, H, N, and S elemental composition; energy content; volatile matter, fixed carbon and ash contents; and trace element composition. Oils were characterized for peroxide value, iodine value, fatty acid profile, free fatty acid content, flash point, density, viscosity, and phase transition temperatures. Development of coproducts from the pods and oilseed cake will be explored.

Areas in Hawaii with agricultural zoning suitable for rain-fed production of pongamia have been identified. Conflicts with current agricultural land use have been identified.

Waste oil resources in Hawaii are estimated to be on the order of 2 to 3 million gallons per year based on de facto population and are directed to biodiesel production.

Publications

Fu, J., Summers, S., Morgan, T. J., Turn, S. Q., & Kusch, W. (2021). Fuel properties of pongamia (*Milletia pinnata*) seeds and pods grown in Hawaii. *ACS Omega, 6,* 9222–9233. https://doi.org/10.1021/acsomega.1c00635

Outreach Efforts

Data were presented at the April 2019 ASCENT review meeting in Atlanta, Georgia.

Awards

None.

Student Involvement

Three undergraduate students—Sabrina Summers, Sarah Weber, and Taha Elwir—are involved in the project, with primary responsibility for processing and analyzing samples of biomass materials selected for evaluation as potential SAF feedstocks.

Plans for Next Period

Characteristics and suitable production areas for additional oilseed crops in Hawaii will be assessed as needed. Information will be provided to the lead institution (WSU).

Task 3.2 - Hawaii Regional Project

University of Hawaii

Objectives

A supply chain based on fiber feedstocks transported to a conversion facility located at Campbell Industrial Park (CIP) on Oahu will be evaluated (Figure 1). CIP is the current site of two oil refineries. Construction and demolition (C&D) wood waste from the PVT Land Company's landfill could be the primary source of feedstock. Other sources will be evaluated from elsewhere on Oahu and from outer islands, including municipal solid waste (MSW) stream from outer islands and mining of current stocks of waste-in-place. Waste streams and purpose-grown crops form the basis for a hub-and-spoke supply system, with the hub located on Oahu. Pipelines for jet fuel transport are in place from CIP to Daniel K. Inouye International Airport and the adjacent Joint Base Pearl Harbor/Hickam. Other coproduct off-takers for alternative diesel fuel include the Hawaiian Electric Co. and several military bases, including Schofield Barracks (~50 MW alternative fuel-capable power plant under development) and Kaneohe Marine Corps Base. Hawaii Gas (a local gas utility) is also seeking alternative sources of methane if methane or feedstock suitable for methane production is available as a coproduct. Hawaii Gas currently off-takes feedstock (naphtha) from the refinery.

Figure 1. Possible locations of value chain participants for a fiber-based alternative jet fuel production facility located at Campbell Industrial Park, Oahu.

Research Approach

Task 3.2.G1. Analysis of feedstock-conversion pathway efficiency, product slate (including coproducts), maturation
Building on activities from previous years, additional supporting analysis will be conducted for proposed supply chains in Hawaii, as follows:

- 3.2.G1.1 Assess feedstock suitability for conversion processes (e.g., characterization, conversion efficiencies, contaminants). [UH and WSU (Manuel Garcia-Perez)]
- 3.2.G1.2 Acquire data on feedstock size reduction, particle size of materials, bulk densities. [UH, WSU (Manuel Garcia-Perez)]
- 3.2.G1.3 Evaluate coproducts at every step of the supply chain. [ASCENT Project 1 team]

Task 3.2.G2. Scoping of techno-economic analysis (TEA) issues
This task will determine the current TEA status of targeted SAF production technologies that use fiber feedstocks as production inputs. [UH, WSU (Manuel Garcia-Perez), Purdue University (Wally Tyner)]

Task 3.2.G3. Screening-level greenhouse gas (GHG) life-cycle assessment (LCA)
This task will conduct screening-level GHG LCA on the proposed target supply chains and SAF conversion technologies.

Subtasks:

- 3.2.G3.1 Assess Massachusetts Institute of Technology (MIT) waste-based GHG LCA tools in context of Hawaii application. [MIT (Mark Staples)]
- 3.2.G3.2 Assess requirements to link previously completed eucalyptus energy and GHG analysis to the edge of the plantation with available GHG LCA information for conversion technology options. [MIT (Mark Staples), UH]
- 3.2.G3.3 Identify and fill information/data gaps.

Task 3.2.G4. Identification of supply chain participants/partners
Subtasks:

- 3.2.G4.1 Define C&D landfill case.
- 3.2.G4.2 Identify eucalyptus in existing plantations: landowners, leaseholder/feedstock producer, harvesting contractor, trucking, etc. [UH]
- 3.2.G4.3 Define other feedstock systems as identified. [ASCENT Project 01 Team]

Task 3.2.G5. Develop appropriate stakeholder engagement plan
Subtasks:

- 3.2.G5.1 Review stakeholder engagement methods and plans from past work to establish baseline methods. [UH, WSU (Season Hoard)]
- 3.2.G5.2 Identify and update engagement strategies based on updated Community Social Asset Modeling (CSAM) /Outreach support tool. [UH, WSU (Season Hoard)]

Task 3.2.G6. Identify and engage stakeholders
Subtasks:

- 3.2.G6.1 Identify stakeholders along the value chain and create database based on value chain location. [UH]
- 3.2.G6.2 Conduct stakeholder meeting using instruments developed in Task 3.2.G5. [UH, WSU (Season Hoard)]
- 3.2.G6.3 Analyze stakeholder response and feedback to process. [UH, WSU (Season Hoard)]

Task 3.2.G7. Acquire transportation network and other regional data needed for Freight and Fuel Transportation Optimization Tool (FTOT) and other modeling efforts
Subtasks:

- 3.2.G7.1 Acquire necessary data to evaluate harbor capacities and current usage. [UH, Volpe (Kristin Lewis), WSU (Mike Wolcott)]
- 3.2.G7.2 Acquire data on interisland transport practices. [UH, Volpe (Kristin Lewis), WSU (Mike Wolcott)]

Task 3.2.G8. Evaluate infrastructure availability
Subtasks:

- 3.2.G8.1 Evaluate interisland shipping options and applicable regulation. [UH, Volpe (Kristin Lewis), WSU (Mike Wolcott)]
- 3.2.G8.2 Evaluate transport or conveyance options from conversion location to end user and applicable regulation.

[UH, Volpe (Kristin Lewis), WSU (Mike Wolcott)]

Task 3.2.G9. Evaluate feedstock availability
Subtasks:
- 3.2.G9.1 Refine/ground truth prior evaluations of options for purpose-grown feedstock supply. [UH]
- 3.2.G9.2 Conduct projections of C&D waste supply moving forward and mining of waste-in-place on Oahu, MSW, and mining of waste-in-place on other islands. [UH]

Task 3.2.G10. Develop regional proposal
This task will use the information collected in Tasks 3.2.G1 through 3.2.G9 to develop a regional project proposal.

Milestone
One milestone is associated with each of the subtask activities identified in the Research Approach section above.

Major Accomplishments
Characteristics of the feedstock generated at the landfill have been determined and summarized in a draft publication.

Elemental compositions of the feedstock materials have been used as the basis for equilibrium analysis of gasification systems using oxygen, steam, and steam-oxygen mixtures.

Material flows relevant to the screening-level GHG analysis of C&D waste as SAF feedstock have been assembled. Preliminary discussions on GHG analysis of C&D-based SAF systems with landfill operators have been initiated.

Solid waste management plans from all counties in Hawaii have been used to provide a broader picture of the waste stream composition, diversion and recycling practices, and planned uses.

Publications
Bach, Q. V., Fu, J., & Turn, S. (2021). Fuel characterization of construction and demolition wastes as a potential feedstock for sustainable aviation fuels. *Frontiers in Energy Research, 9,* 711808.

Bach, Q. V. & Turn, S. Fate of arsenic and other inorganic elements during gasification of construction and demolition wastes – thermochemical equilibrium calculations. Draft manuscript in process.

Outreach Efforts
Results of the fuel sampling, fuel analyses, and gasification equilibrium analyses were presented at the October 2019 Thermochemical Biomass 2019 Conference in Chicago, Illinois.

Information from this task was included in the talk, "Regional Supply Chain Analysis for Alternative Jet Fuel Production in the Tropics," presented at the Hawaii Aviation and Climate Action Summit, December 3, 2019, at the Hawaii State Capitol.

Data acquired under this task were presented to the management of PVT Land Company and their consultants from Simonpietri Enterprises and T. R. Miles Technical Consultants Inc.

"Construction and Demolition Waste as an Alternative Energy Source: Fuel Characterization and Ash Fusion Properties" was presented as a poster at the 2020 Thermal & Catalytic Sciences Virtual Symposium.

As suggested by FAA management, UH worked with the Servicios y Estudios para la Navegación Aérea y la Seguridad Aeronáutica (SENASA) to identify a counterpart university in the Canary Islands, Spain. Universidad de la Laguna (ULL) was selected and a memorandum of understanding was signed between the UH and ULL. A nondisclosure agreement was subsequently signed between SENASA, ULL, UH, and the Spanish company Abengoa Energía, S.A.

Discussion with Dr. Kristin Lewis and Volpe Center staff on the addition of Hawaii transportation infrastructure to the *Freight and Fuel Transportation Optimization Tool* was initiated and deferred until a clearer definition of the system emerges.

Awards
None

Student Involvement
Three undergraduate students—Sabrina Summers, Sarah Weber, and Taha Elwir—have been involved in sample preparation and in operating the laboratory analytical equipment used for sample analysis.

Plans for Next Period
Manuscripts covering prediction of gasification product streams including contaminant concentrations will be completed and submitted.

Work on the GHG analysis of C&D waste use for SAF production will be extended from the landfill to a point of use (to be determined) and interfaced to the system TEAs described by WSU.

Outreach to interested industries will be continued.

Task 4 - Hawaii Regional Project
University of Hawaii

Objective
This task builds upon the results from the previous years' work under the Hawaii regional project. The focus is the data and analysis necessary to plan a project that uses C&D waste as feedstock for SAF production. Using previous years' C&D feedstock characterization data and thermochemical equilibrium analysis, the Task 4 objective is to conduct bench-scale gasification tests and quantify the product gas yield and composition and contaminant concentrations. These results will be compared with equilibrium prediction used to identify contaminants that must be addressed before end use and provide the basis for contaminant control system design.

Research Approach
Using samples of C&D wastes characterized in the earlier tasks, bench-scale gasification tests will be conducted to measure product yields, identify contaminants, and investigate element partitioning between product phases.

Information gained from the tests will be used to identify opportunities to improve TEA, identify coproducts, inform supply chain participants and stakeholders, and identify needed infrastructure improvements.

Milestones
- Identify and evaluate capabilities of experimental bench-scale facilities to gasifier tests
- Specify system performance parameters to be measured
- Specify techniques to sample and analyze contaminants
- Select and engage experimental bench-scale facility for testing
- Prepare and ship feedstock from Hawaii to experimental test facility
- Conduct tests, reduce data, and prepare summary report of results

Major Accomplishments
Operational measurements to be conducted as part of bench-scale tests were summarized and a test plan was developed. These were used as the basis for entertaining proposals for test services.

Through a competitively structured proposal process, Thermochem Recovery International Inc. was engaged to provide bench-scale test services for C&D waste feedstock and other opportunity fuels of relevance to Hawaii and the tropics.

Publications
Not applicable

Outreach Efforts
Not applicable

Awards
None

Student Involvement
None

Plans for Next Period
During the next period, activities identified in the Research Approach section above will continue. The primary focus will be to conduct the bench-scale gasification tests, collect and analyze samples from the tests, and prepare reports and publications summarizing the results. The sequence of milestones identified above provides a roadmap of necessary subtasks.

Task 5 - Hawaii Regional Project
University of Hawaii

Objective
Task 5 includes two subtasks:

Subtask 5.1: Tropical oil to SAF supply chain analysis
Subtask 5.2: Contaminants in gasification of C&D wastes

The goal of subtask 5.1 is to develop a model for tropical oil supply chains for AJF and associated coproducts. Hawaii will be used as the initial focus, but the modeling tools will be developed for wider use in island settings.

The goal of subtask 5.2 is to develop management strategies for elements present in C&D waste that impact its use as a feedstock for thermochemical conversion.

Research Approach
Subtask 5.1: Prior ASCENT EcoCrop GIS modeling activities identified growing locations for pongamia, kamani, croton, and jatropha, based on suitable environmental conditions, geography, and zoning. Where unavailable, primary data were also developed for chemical and physical characteristics of these tropical oils and their coproducts (e.g., pods/shell, oilseed cake). The project will use these earlier results as the basis for developing supply chain models for AJF production. Model results will identify feedstock production areas and locations and scales of primary processing sites for shell and pod separation, oil extraction from seeds, and oil conversion to SAF. Potential sources of hydrogen from oilseed coproducts, other renewable resources, and fossil sources will be analyzed and included in the model. Options for points of production, SAF production technologies (ARA, SBI, or Forge, etc.), transportation strategies, and blend ratios at airports (or for specific end users, e.g., military) across Hawaii will affect model outcomes and will be evaluated. Options for coproducts such as animal feeds and higher valued materials will be evaluated and incorporated into the model decision-making. Criteria used to drive the model solution might include minimizing SAF production costs while meeting a minimum total production benchmark or minimum blending rate for annual state jet fuel consumption. Other criteria such as system resiliency to extreme weather events and climate change, provision of environmental services, and stakeholder acceptability will also be of importance and will be used to evaluate model solutions.

Subtask 5.2: Thermochemical gasification of biorenewable resources is the initial conversion process for two entry points to AJF production: (1) synthesis gas (syngas) used in direct production of Fischer-Tropsch (FT) liquids, and/or (2) green/renewable hydrogen used in biorefineries for hydrotreating lipids or in existing petroleum refining activities for the production of hybrid jet fuel. Urban wood waste from C&D activities provides a reliable source of biorenewable material and requires a tipping fee for disposal, characteristics that enhance its attractiveness as feedstock. Negative aspects of C&D feedstock are its physical and chemical inhomogeneity. In the latter case, inorganic elements present in the feedstock can negatively impact the gasification process (e.g., corrosion of or accumulation on reactor working surfaces, bed material agglomeration, catalyst deactivation, pollutant emissions). Using data generated from previous ASCENT Project 01 tasks, this project will assess methods for managing contaminants in C&D feedstocks. This project will be based around gasification

systems proposed for production of syngas-FT liquids and green hydrogen. Technology options for contaminant removal or conversion to benign forms will be assessed at each step in the conversion process; that is, presorting at the waste generation site, sorting/diversion at the C&D waste intake facility, removal by physical/chemical/other methods before gasification, in situ reactor control methods, and gas clean-up. Technology options from existing process industries and from the scientific literature will be considered. Lab-scale testing of removal techniques will be conducted to provide preliminary assessment of selected, promising technology options. Integrated gasification process options and contaminant control options will be evaluated as complete systems to guide system design and allow system comparisons. Risks associated with the technology options will also be assessed to guide implementation and risk mitigation of the system as a whole. Impacts of processing scale (e.g., Mg waste/day) on selection of technology options will also be assessed.

Milestone
Subtask 5.1: Establish model framework for oil seed, based SAF supply chain in an island setting, using Hawaii scenario

Subtask 5.2: Complete review of options to manage contaminants along the supply chain; conduct bench-scale tests to confirm the efficacy of options

Major Accomplishments
Not applicable. Activities on this task, including recruitment of personnel, have been delayed due to COVID-19.

Publications
Not applicable

Outreach Efforts
Not applicable

Awards
None

Student Involvement
None

Plans for Next Period
Subtask 5.1: GIS data for oilseed crop production areas and petroleum jet fuel use data at Hawaii airports will be used as the starting points for building SAF model scenarios.

Subtask 5.2: A review of options to manage contaminants along the supply chain will be conducted. Results of the review and contaminant measurements from the bench-scale gasification tests in Task 4 will be used to target bench-scale contaminant control tests.

Task 6 - Hawaii Regional Project
University of Hawaii

Objective
Task activities in Year 6 will explore the impacts of Hawaii State Legislative Bill HB2386 on waste management and potential for waste-based SAF production systems. HB2386 requires 0.5 mile buffer zones around waste and disposal facilities (including landfills) and restricts facilities from land with conservation-district zoning.

Research Approach
The goal of this task is to assess and evaluate impacts of HB2386 on waste management strategies in Hawaii. HB2386 was disruptive to disposal practices for C&D waste on the island of Oahu, having impacts that currently are not fully understood. Task 6 seeks to collect updated waste generation data and understand how HB2386 will impact current management strategies and develop scenarios for waste-based SAF production scenarios under the new regulatory environment. Impacts of HB2386 on the capacity to perform landfill mining will also be considered. Preliminary assessment of restricted and

unrestricted sites for waste and disposal facilities will be reviewed and refined as necessary. Preliminary impacts on GHGs and SAF technology choices will be explored.

Milestone
Impacts of removing or reducing the role of an active C&D landfill as a supply chain participant will also be evaluated.

Major Accomplishments
Funding for this task was received recently and the task is in the planning stage.

Publications
Not applicable

Outreach Efforts
Not applicable

Awards
None

Student Involvement
None

Plans for Next Period
A postdoctoral fellow will be recruited to work on this task and analysis will begin.

Project 001(C) Alternative Jet Fuel Supply Chain Analysis

Purdue University

Project Lead Investigator

Farzad Taheripour
Research Associate Professor
Department of Agricultural Economics
Purdue University
403 West State Street
West Lafayette, IN 47907-2056
765-494-4612
tfarzad@purdue.edu

University Participants

Purdue University

- PI: Farzad Taheripour, Research Associate Professor
- FAA Award Number: 13-C-AJFE-PU, Amendments 25, 29, 34, 36, 41
- Period of Performance: October 1, 2020 to September 30, 2021
- Task(s):

1. Develop techno-economic models for relevant pathways and identify key stochastic variables to model for assessing risk in conversion pathways, which work will lead to our capability to compare pathways, their expected economic cost, and the inherent uncertainty in each pathway (lead: Farzad Taheripour; supported by Chepeliev and Stevenson)
2. Perform a life cycle analysis (LCA) of alternative jet fuel pathways in coordination with the International Civil Aviation Organization's Committee on Environmental Protection Fuels Task Group (ICAO CAEP FTG); work with the CAEP FTG life cycle assessment group on issues such as system boundaries, induced land use change (ILUC), LCA methodology, and pathway greenhouse gas emissions assessments (lead: Taheripour; supported by Sajedinia, Aguiar, and Malina [Hasselt University])
3. Develop estimates of land use change (LUC)-associated emissions for alternative jet fuels for the ICAO CAEP FTG, in close relation to Task #2 (lead: Taheripour; supported by Sajedinia, Debadrita, Aguiar, and Chepeliev)
4. Provide support for other ASCENT universities on alternative jet fuel policy analysis (lead: Taheripour)

Project Funding Level

- Amendment 3: $250,000
- Amendment 6: $110,000
- Amendment 10: $230,000
- Amendment 15: $373,750
- Amendment 19: $400,000
- Amendment 29: $400,000
- Amendment 36, 41: $523,000

Current cost sharing for this project year was provided by Sami Jauhiainen from Neste US, Inc.

Investigation Team

Farzad Taheripour (PI), research professor
EhsanReza Sajedinia, PhD student, Purdue University: Stochastic techno-economic analysis (TEA) and Global Trade Analysis Project (GTAP) ILUC analysis
Xin Zhao, former PhD student, Purdue University: Stochastic TEA and GTAP ILUC analysis (graduated and left Purdue but still voluntarily contributes to the project)

Omid Karami, postdoctoral fellow (joined the research team in August 2021)
Kundu Debadrita, PhD student, Purdue University: GTAP ILUC emissions analysis (collaborating part time with the project)
Maksym Chepeliev, PhD, research associate, GTAP Center (collaborating part time with the project)
Angel H. Aguiar, PhD, research associate, GTAP Center (collaborating part time with the project)

Project Overview

This project has five main components. The first component is focused on advancing TEA for aviation biofuel pathways, and the second centers on life cycle and production potential analysis of alternative jet fuel pathways in coordination with the ICAO CAEP FTG. The third component also coordinates with the FTG, with a specific focus on estimating LUC-associated emissions for alternative jet fuels. The fourth component aims to provide support for the policy subgroup of the FTG by providing policy guidelines to facilitate expansions in using sustainable aviation fuels (SAFs). This task includes bridging existing TEAs for alternative jet fuels with partial and general equilibrium economic models to develop alternative scenarios for alternative jet fuels in the fuel mix used by the industry. The fifth component supported "Farm to Fly 2.0" (F2F2) which was a collaboration between government and industry to enable commercially viable, sustainable alternative jet fuel supply chains in the United States, at state and regional levels, to support the goal of one billion gallons of alternative jet fuel production capacity and use by 2018. Purdue provided the analytical support necessary for this effort.

Task 1 - Develop Techno-economic Models for Relevant Pathways and Identify Key Stochastic Variables for Assessing Risk in Conversion Pathways

Purdue University

Objective

This task aimed to develop TEAs for relevant pathways and identify key factors to model for assessing the feasibility of conversion pathways. This work will lead to our capability to compare pathways, their expected economic cost, and the inherent uncertainty in each pathway. This activity will help us to include new pathways in the GTAP-BIO model to assess their LUC impacts.

Research Approach

For each fuel pathway under evaluation, we collected the required data and developed the required analyses for both TEA and LCA to determine the cost structure of new pathways to be included in the GTAP-BIO model to support FTG tasks.

Milestone(s)

Over this period, we continued to work on various analyses for ethanol-to-jet (ETJ) and hydroprocessed ester and fatty acid (HEFA) pathways. This research has been fully and successfully conducted. We will continue to publish the results of our case studies.

Major Accomplishments

The following TEAs have been developed to support the inclusion of several new pathways in the GTAP-BIO database:

- Miscanthus ETJ, E.U. and U.S. cases;
- Switchgrass ETJ, U.S. case;
- Carinata oil HEFA, Brazil and U.S. cases;
- Camelina oil HEFA, Brazil and U.S. cases;
- Jatropha oil HEFA, India case; and
- Corn alcohol-to-jet (ATJ), Brazil case.

Publications

Taheripour, F., Scott, D., Hurt, C. A., & Tyner, W. E. (2021). Technological progress in US agriculture: Implications for biofuel production. Sustainable Agriculture Research, *10*(1), 61. https://doi.org/10.5539/sar.v10n1p61

Taheripour, F., Sajedinia, E., & Karami, O. (2021). Oilseed cover crops for sustainable aviation fuels production and reduction in greenhouse gas emissions through land use savings. Manuscript submitted for publication.

Outreach Efforts
Taheripour presented a paper at the National Biodiesel Board Sustainability Workshop, Virtual Meeting, 2021.

Awards
None.

Student Involvement
EhsanReza Sajedinia, PhD student, Purdue University

Plans for Next Period
We will work on publishing the results of our TEA for producing alternative jet fuels to support FTG analyses.

Task 2 - LCA of Alternative Jet Fuel Pathways in Coordination with ICAO Alternative Fuels Task Force (AFTF) FTG
Purdue University

Objectives
- Provide required data and analysis to support the low-LUC-risk practices adopted by CAEP
- Provide required data and analysis to support the core LCA group with respect to ILUC for coprocessing of esters and fatty acids in petroleum refineries and other tasks as needed

Research Approach
This task incorporates many varied assignments and components. We followed standard approaches to support FTG subgroups including the core LCA, Technology Production Policy (TPP), Emission Reductions Accounting (ERA), and Sustainability subgroups. Using the GTAP-BIO model, we collected data and provided appropriate analyses to accomplish this task.

Taheripour is co-chair of the FTG ILUC group.

Taheripour collaborates with the LCA, TPP, ERA, and Sustainability subgroups of ICAO CAEP FTG.

Milestone(s)
Taheripour participated in the FTG6, FTG7, FTG8, FTG9, and FTG10 meetings and was involved in many of the tasks and document preparation activities for these meetings. He also responded to other subgroup requests for help and collaboration. He has led efforts in ILUC modeling and ILUC-related tasks associated with other subgroups. He developed a framework to examine regional and global ILUC values for each SAF and participated in developing a methodology to calculate Direct Land Use Change (DLUC) to support FTG activities.

Major Accomplishments
A methodology has been developed to calculate DLUC for use within the Carbon Offsetting and Reduction Scheme for International Aviation (CORSIA) sustainability systems to evaluate the land use emissions of individual projects that will be launched by economic operators for SAFs. The methodology has been tested for several case studies. For each case study, an Excel file has been developed to be used by Sustainability Certification Schemes (SCS) in the future.

Publications
Prussi, M., Lee, U., Wang, M., Malina, R., Valin, V., Taheripour, F., Velarde, C., Staples, M. D., Lonza, L., & Hileman, J. L. (2021). CORSIA: The first internationally adopted approach to calculate life-cycle GHG emissions for aviation fuels. *Renewable and Sustainable Energy Reviews, 150*, 111398.

Outreach Efforts

Taheripour attended a Coordinating Research Council (CRC) meeting and gave a presentation on updates to the GTAP database: CRC Life Cycle Analysis Workshop, Virtual Meeting, 2021.

Taheripour attended virtual ASCENT Advisory Group meetings in April 2021 and October 2021 and presented the following papers:

- Estimating induced land use change emissions for sustainable aviation biofuel pathways, Alternative Jet Fuel Supply Chain Analysis - CORSIA Fuel Support.
- Oilseed cover crops for sustainable aviation fuel production and reduction in greenhouse gas emissions through land use savings, Alternative Jet Fuel Supply Chain Analysis - CORSIA Fuel Support.

Taheripour serves as a member of the Committee on Current Methods for Life Cycle Analyses of Low-Carbon Transportation Fuels in the United States of the National Academy of Sciences, Engineering, and Medicine.

Awards

None

Student Involvement

EhsanReza Sajedinia, PhD student, Purdue University
Kundu Debadrita, PhD student, Purdue University

Plans for Next Period

We will continue to support FTG subgroups, including the core LCA, TPP, and ERA subgroups, to accomplish the required LCAs for new SAF pathways. In addition, we will continue to develop required TEAs to include the cost structure of new SAF pathways in the GTAP-BIO database.

Task 3 - Develop Estimates of LUC-Associated Emissions for Alternative Jet Fuels for the ICAO FTG

Purdue University

Objectives

- Compute ILUC emissions of alternative jet fuels for use in CORSIA
- Improve the GTAP-BIO model and its database and make appropriate modifications to the agro-ecological zone emission factor model
- Define and implement a method to determine regional ILUC values and rank countries according to their LUC determinants

Research Approach

We modify, update, and use the GTAP-BIO model to produce ILUC estimates for the FTG. We also collaborate with the International Institute for Applied Systems Analysis and Hugo Valin to evaluate the outcomes of GTAP-BIO and GLOBIOM models. We collect data and develop new approaches to assess issues related to ILUC emissions due to the production of alternative jet fuels.

Milestone(s)

We added several new pathways to the GTAP-BIO model and examined new regional ILUC values. We also developed a methodology for estimating global ILUC values and assessed ILUC values for numerous SAF pathways.

Major Accomplishments

The primary accomplishments in this task are based on the work progress of ICAO CAEP FTG. Some of the working papers and information papers that we have produced over this period are listed in this section and in the overall publication list at the end of this report.

Publications

Several working papers and information papers have been produced based on our work for the AFTF/FTG. Working and information papers presented at FTG meetings include:

- CAEP/12-FTG/06-WP/06 – "Update on ILUC default values modelling for SAF pathways", November 2020, Virtual.
- CAEP/12-FTG/06-WP/08 – "Revised guidance on Direct Land Use Change calculation", November 2020, Virtual.
- CAEP/12-FTG/06-FL/04 – "Comparison of Proposed Methodology for Global ILUC", November 2020, Virtual.
- CAEP/12-FTG/08-WP/07 – "Update on ILUC default values modelling for SAF pathways", March 2021, Virtual.
- CAEP/12-FTG/08-WP/08 – "Methodology proposal on Direct Land Use Change calculation", March 2021, Virtual.
- CAEP/12-FTG/08-WP/04 – "Pilot application of the methodology on Low Land Use Change (LUC) Risk Practices", March 2021, Virtual.
- CAEP/12-FTG/09-WP/09 – "Methodology proposal on Direct Land Use Change calculation", May 2021, Virtual.
- CAEP/12-FTG/09-IP/02 – "ILUC Modelling Assumptions on Soil Organic Carbon Accounting", May 2021, Virtual.
- CAEP/12-FTG/09-WP/08 – "Update on ILUC modelling and low LUC risk", May 2021, Virtual.
- CAEP/12-FTG/10-WP/06 – "Methodology proposal on Direct Land Use Change calculation", July 2021, Virtual.
- CAEP/12-FTG/10-WP/07 – "Revisions to methodology on Low Land Use Change (LUC) Risk Practices based on pilot applications", July 2021, Virtual.
- CAEP/12-FTG/10-WP/05 – "Update on modelling of ILUC default values", July 2021, Virtual.

Zhao, X., Taheripour, F., Malina, R., Staples, M. D., & Tyner, W. E. (2021). Estimating induced land use change emissions for sustainable aviation biofuel pathways. *Science of The Total Environment, 779*(20), 146238.

Gao, Y., Zhang, X., Davidson, E., & Taheripour, F. (2021). The increasing global environmental consequences of a weakening US–China crop trade relationship. *Nature Food, 2* (8), 578-586.

Outreach Efforts

Taheripour attended several meetings to present research outcomes on ILUC values, including:

- GTAP 24th Annual Conference on Global Economic Analysis, Virtual June 2021,
- AAEA Annual Meeting, Virtual, August 2021, and
- EAAE Annual Meeting, Virtual, July 2021.

Awards

None.

Student Involvement

EhsanReza Sajedinia, PhD student, Purdue University
Kundu Debadrita, PhD student, Purdue University

Plans for Next Period

We will continue working with ICAO on ILUC emission estimates. In particular, the current model uses a database that represents the 2011 world economy. A new benchmark database that represents the 2014 world economy has been developed. We plan to use this database for ILUC assessment, which represents a major task and new development.

Task 4 - Provide Support for Other ASCENT Universities on Alternative Jet Fuels Policy Analysis

Purdue University

Objective

Provide support for the other ASCENT universities on alternative jet fuels policy analysis

Research Approach

See Task #1

Milestone(s)
See Task #1

Major Accomplishments
See Task #1

Publications
None

Outreach Efforts
None

Awards
None

Student Involvement
Jeremiah Stevens, MS student, Purdue University

Plans for Next Period
We will continue to collaborate with ASCENT as needed.

Task 5 - Provide Support for the Farm-to-Fly Initiative as Needed
Purdue University

Objective
Provide support for the Farm-to-Fly initiative as needed

Research Approach
This task provides general support for other initiatives. Our main role is to consult with other projects and activities and provide assistance as needed.

Milestone(s)
There has been little activity under this task during this reporting period.

Major Accomplishments
None

Publications
None

Outreach Efforts
None

Awards
None

Student Involvement
None

Plans for Next Period
Support for this effort has concluded.

Project 001(D) Alternative Jet Fuel Supply Chain Analysis

The Pennsylvania State University

Project Lead Investigator

Saurabh Bansal
Associate Professor of Supply Chain Management
Department of Supply Chain and Information Systems
The Pennsylvania State University
405 Business
University Park, PA 16802
814-863-3727
sub32@psu.edu

University Participants

The Pennsylvania State University (Penn State)

- PI: Saurabh Bansal, Associate Professor of Supply Chain Management
- PI: Lara Fowler, Senior Lecturer, Penn State Law School; Assistant Director, Penn State Institutes of Energy and the Environment
- PI: Ekrem Korkut, Penn State Law School
- FAA Grant Number: 13-C-AJFE-PSU, RISK-INFORMED ALTERNATIVE JET FUEL (AJF)
- Period of Performance: 08/01/17- 01/31/2022

Washington State University (WSU)

- Kristin Brandt, Staff Engineer

University of Tennessee

- Tim Rials, Associate Dean of Agricultural Research
- Burt English, Professor of Agricultural and Resource Economics

Project Funding Level

FAA Funding: $200,000
Matching, Penn State: $200,000
Total Funding: $400,000

Investigation Team

Task 1.3.1 (Bansal; supported by Brandt and English): Risk–reward profit-sharing modeling for first facilities
Task 1.3.2 (Bansal; supported by Brandt and English): Additional quantification of risk and uncertainties in supply chains (foundational part of Task 1.3.1)
Task 1.3.3 (Bansal; supported by Brandt and English): Supply chain risk analysis tools for farmer adoption
Task 1.4.1 (Fowler; supported by Korkut): National survey of current and proposed state and federal programs that monetize ecosystem services
Task 1.4.3 (Fowler; supported by Korkut): Support of stakeholder engagement efforts

Project Overview

This project focuses on developing a qualitative and quantitative understanding of factors that can help establish biofuel supply chains for alternative jet fuels. Although efforts are being made to establish these supply chains, many face challenges due to a lack of clarity regarding the incentives that stakeholders would require to engage in these supply chains and devote their resources to invest in the facilities required for these supply chains. To this end, this project has two goals:

1. Develop pro forma cash flows that represent the financial status of various participants in biofuel supply chains for alternative jet fuels to inform a transparent risk-sharing tool, and
2. Understand the policy landscape in various parts of the United States to encourage alternative jet fuel supply chains and identify additional policy initiatives that may be needed.

Task 1.3.1 – Risk-reward Profit-sharing Modeling for First Facilities

The Pennsylvania State University

Objective

Develop a transparent risk-sharing tool to provide all partners with an understanding of the cash flows and risks faced by all supply chain partners.

Research Approach

We first collected a large number of risk-sharing tools that have been proposed in the supply chain literature. Subsequently, we narrowed this list down to 9–12 mechanisms. We created an Excel-based framework in which the cash flows of all supply chain partners are modeled based on data from the techno-economic analyses developed by WSU. This framework incorporates the risk-sharing mechanisms.

Milestone

We developed Excel models for four realistic configurations by using data from techno-economic analysis models developed by WSU.

Major Accomplishments

We developed an Excel-based framework showing the cash flows of four key stakeholders in alternative jet fuel supply chains: farmers, preprocessors, refineries, and airlines. The framework shows various risk-sharing contracts that each of the stakeholders can extend to others, as well as the financial burden or opportunities associated with these mechanisms. The framework also shows the government's financial burden of supporting these mechanisms. The framework was developed for four levels of refinery capacity. Overall, this framework can be used as a decision support tool by various stakeholders to determine whether to engage in alternative jet biofuel supply chains and negotiate with each other.

Publications

We anticipate publishing a paper based on combined work from last year and the coming year. The paper would make the important point that: no single risk-sharing approach or policy instrument is likely to be sufficient for creating a sustainable supply chain. Rather, a portfolio of instruments is needed. This perspective has not been previously presented in the literature.

Outreach Efforts

Our tool has been presented and discussed at three ASCENT advisory committee meetings.

Awards

None

Student Involvement

None

Plans for Next Period

We intended to conduct laboratory studies with graduate students. However, the behavioral research lab was closed at Penn State due to COVID-19. We will perform these studies when students are back on campus. We can conduct these studies only when students are able to interact with each other in a simulated negotiation environment. We will provide the tool and training on its use to the project sponsor.

Task 1.3.2 – Additional Quantification of Risk and Uncertainties in Supply Chains (Foundational Part of Task 1.3.1)

The Pennsylvania State University

Objective

Develop methods to rely on expert judgments to quantify uncertainties associated with biofuel supply chains.

Research Approach

We developed a new econometric approach to quantify probability distributions of uncertain quantities such as yield or demand when an expert panel provides judgments regarding the most likely values. This approach exploits the well-known theory of generalized least squares in statistics for the context in which historical data are available to calibrate expert judgments or when these data are not available.

Milestones

We have described this method in two manuscripts. In the first manuscript, *Using Subjective Probability Distributions to Support Supply Chain Decisions for Innovative Agribusiness Products*, we developed a two-stage procedure to calibrate expert judgments for the distribution of biofuel uncertainties, such as the uncertain yield of new varieties of oil seeds, demand, or selling price. In the first step of the procedure, we calibrate the expert judgments by using historical data. Specifically, we use prior judgments provided by experts and compare them with actual realizations (such as predicted yield versus actual yield) to determine the frequency with which each expert over- or underestimated the uncertainty, e.g., Expert 1 underestimated the yield 60% of the time, but Expert 2 underestimated the yield 90% of the time. In the second manuscript, *Optimal Aggregation of Individual Judgmental Forecasts to Support Decision Making in a R&D Program*, we use this information to determine the optimal approach for aggregating the experts' judgments to determine the mean and standard deviation of the probability distributions. In this manuscript, we develop a new optimization protocol for determining the optimal acreage for growing specific crops by considering the estimated mean and standard deviation as well as incorporating the variability in these estimates. This manuscript won an award at a professional conference (INFORMS 2021) in November 2021.

Major Accomplishments

Theoretical development and a numerical study have demonstrated the promise of this approach.

Publications

Bansal, S., & Gutierrez, G. J. (2020). Estimating uncertainties using judgmental forecasts with expert heterogeneity. *Operations Research*, *68*(2), 363-380. https://pubsonline.informs.org/doi/abs/10.1287/opre.2019.1938

The second manuscript has been written and will be submitted for publication during this period.

Outreach Efforts

None

Awards

2021 Decision Analysis Practice Award, INFORMS. November 2021.

Student Involvement

None

Plans for Next Period

The second paper has been submitted to the sponsor for review. It will be submitted for publication during this period.

Task 1.3.3 – Supply Chain Risk Analysis Tools for Farmer Adoption

The Pennsylvania State University

Objectives

Understand farmers' risk preferences over a long duration and how these preferences affect their decisions to grow crops that can support alternative jet fuel supply chains

Research Approach

We surveyed farmers to understand their risk preferences over extended durations. Specifically, we presented farmers with sample yield ranges over extended periods and asked them to estimate the lowest equivalent guaranteed yield that they would be willing to accept given the uncertain yields. We used these responses for statistical analyses.

Milestones

We have completed the survey and have written a manuscript based on the survey.

Major Accomplishments

We compiled data from 43 farmers in central Pennsylvania regarding their preferences given uncertain yields from their land. The results quantify the loss of value that farmers attribute to an uncertain yield. Results are reported for both 1-year and 10-year horizons. For the 10-year horizon, we also report results for an initial yield build-up, which often arises with most biofuel crops. The key takeaways from this study are as follows: (a) farmer valuations of a new crop decrease acutely as the uncertainty in yield increases and (b) the initial build-up period of low yields can be a large deterrent that inhibits farmers from adopting new crops for the purpose of supporting biofuels.

Publications

A paper detailing this work has been written and provided to the sponsor.

Outreach Efforts

None

Awards

None

Student Involvement

None

Plans for Next Period

The results in the first version of the paper revealed something interesting: when faced with uncertain yields, say from x to y, farmers were willing to swap their output for a consistent output at levels that were lower than x. This finding was initially surprising. However, the research team has recently found prior research in economics documenting similar behavior. More data collection will reinforce these findings. We plan on collecting additional data from another 50 farmers during the spring of 2021.

Task 1.4.1 – National Survey of Current and Proposed State and Federal Programs that Monetize Ecosystem Services

The Pennsylvania State University

Objective

Conduct a survey and summarize current and proposed state and federal programs to monetize ecosystem services.

Research Approach

This task builds on and continues the work performed under ASCENT Project 01, Task 8.1, which focused on the biomass and water quality benefits to the Chesapeake Bay watershed. In previous years, we examined the biofuel law and policy landscape of the Pacific Northwest and Southeast regions, as well as the state of Hawaii. This year, we have focused on federal biofuel law and policy and how it has been affected by international drivers.

Milestones

Our research has previously been circulated in three region-specific white papers. In addition, we developed a federal-level white paper to the list of tasks, which was subsequently turned into a published paper (see below).

Copies of these documents are available online:

- Western U.S. policy paper (with a focus on Washington state, last updated in 2019): https://pennstateoffice365.sharepoint.com/:w:/s/Biomasslawandpolicy/EVLle-CR5aBCjlYCrXhY3RgB7WgGPAaqjFEkl8b5JDvWEg?e=ZAGT1V

- Southeast policy paper (with a focus on Tennessee): https://pennstateoffice365.sharepoint.com/:w:/s/Biomasslawandpolicy/EVyAOEktS9xFlmBgvKslEM8B_OyGngJ_J6oMRqojDcNy7A?e=OVg7FF

- Hawaii policy paper: https://pennstateoffice365.sharepoint.com/:w:/s/Biomasslawandpolicy/EXmtXyHdCgdAs56DdQvJbq0B0SxOPlAhdplwJjLbMdax_Q?e=m6bYJb

- Federal-level white paper: https://pennstateoffice365.sharepoint.com/:w:/s/Biomasslawandpolicy/EUauzGRg2adBgUHildnKjqcB6Yg9ppAsP3ga0mYghB6AEA?e=6xiT9K

Major Accomplishments

In addition to developing the white papers described above, we adapted the federal-level white paper for publication (see below). We also presented our work as a poster during the Penn State Energy Days, provided updates during bi-weekly ASCENT 01 team meetings, and provided a briefing and poster during the ASCENT fall meeting. Additionally, PI Lara Fowler is involved in another USDA National Institute of Food and Agriculture (NIFA-funded project entitled "Consortium for Cultivating Human and Naturally Regenerative Enterprises" (USDA-NIFA Sustainable Agricultural Systems Award 2020-68012-31824), dubbed the "C-CHANGE" project. She has built upon her work in this ASCENT project to link to the regenerative agriculture work being pursued in C-CHANGE, including providing a briefing on 2nd generation biofuel law and policy.

In September 2021, both Lara Fowler and Ekrem Korkut participated in the September 16, 2021 SAF Grand Challenge Roadmap Workshop with the sustainable aviation fuel research community.

Publications

Our federal-level white paper has been submitted and published in a special edition of *Frontiers in Energy*:

Korkut, E. & Fowler, L. B. (2021). Regulatory and policy analysis of production, development and use of sustainable aviation fuels in the United States." *Frontiers in Energy Research*, 732.
https://www.frontiersin.org/articles/10.3389/fenrg.2021.750514/full

Outreach Efforts

Posters

- Fowler, L. B., & Korkut, E. (2020, September). Biofuel law & policy: Regulatory and policy analysis of production, development and use of sustainable aviation fuels in the United States. Poster presented at the ASCENT Annual Meeting.
- Fowler, L. B., & Korkut, E. (2021, May). Regulatory and policy analysis of production, development and use of sustainable aviation fuels in the United States. Poster presented at the Penn State Energy Days. https://iee.psu.edu/events/energy-days/posters

Presentations

- Fowler, L. B. (2020, December). U.S. biofuel law and policy: A quick overview on U.S. law and policy affecting second generation biofuels." Paper presented at the USDA NIFA C-CHANGE.
- Fowler, L. B., Korkut, E. (2021, June). National and regional law and policy drivers for alternative jet fuel. Paper presented at the ASCENT 01 team meeting.
- Fowler, L. B., & Lewis, K. (2021, October). Sustainable aviation fuel development: Law, policy and the blender's tax credit." Paper presented at the ASCENT Annual Meeting.

Awards
None

Student Involvement
Ekrem Korkut graduated from the Penn State School of International Affairs in May 2021 and transitioned to working as a postdoctoral associate on this project (50% of his time, with the other 50% funded by another project).

Plans for Next Period
As noted above, we will continue adapting the existing white papers for publication, with the next step being a focus again on regional efforts. In addition, we are working on law and policy research questions identified by other ASCENT team members, including how landfill regulations shape opportunities in Hawaii and other related topics. As needed, we will provide support to working groups under the SAF Grand Challenge.

Task 1.4.3 – Help Support Stakeholder Engagement Efforts
The Pennsylvania State University

Objective
Facilitate dialogue among producers, industry, government, and other affected stakeholders.

Research Approach
Our work under this objective has focused on stakeholder engagement and facilitation of effective dialogue to help bridge gaps between producers, industry, government, and other affected stakeholders. This role supports the needs of other team members.

Milestone
These efforts have supported stakeholder engagement efforts led by other teams, including but not limited to the regional partners identified in ASCENT Project 01, Tasks 3.1, 3.2, and 3.3.

Major Accomplishments
This set of tasks has been more limited, with no major accomplishments to date. We have continued to participate in discussions and calls related to potential stakeholder engagement needs.

Publications
None

Outreach Efforts
None

Awards
None

Student Involvement
None

Plans for Next Period

Future work under this objective will include presenting to the project partners on facilitation skills and tactics. Additional support for regional projects will be offered as needed for facilitation and stakeholder engagement sessions as the regional projects move to the deployment stage. As needed, we will provide support to working groups under the SAF Grand Challenge.

Project 001(E) Alternative Jet Fuel Supply Chain Analysis

University of Tennessee

Project Lead Investigator

Timothy Rials
Professor and Director
Center for Renewable Carbon
University of Tennessee
2506 Jacob Dr., Knoxville, TN 37996
865-946-1130
trials@utk.edu

University Participants

University of Tennessee

- P.I.(s): Burton English, Professor
- FAA Award Number: 13-C-AJFE-UTenn, Amendments 09, 11, 13, 15
- Period of Performance: October 1, 2020, to September 30, 2021
- Tasks:
    1. Assess and inventory regional forest and agricultural biomass feedstock options
    2. Develop national lipid analysis
    3. Lay the groundwork for lipid and/or biomass in Tennessee and the Southeastern United States
    4. Biorefinery infrastructure and siting (supporting role)
- Journal manuscripts will be prepared based on the biochar survey data, oilseed techno-economic analysis (TEA), agricultural residue availability and supply potential, and national oilseed analysis.
- McKenzie Thomas will complete her master's thesis using survey data.
- Jim Larson will complete his analysis on farmers' willingness to pay with a journal article and a department research manuscript.

Project Funding Level

Total 6-year funding/This year funding
Total Estimated Project Funding: $1,175,000/$600,000
Total Federal and Non-Federal Funds: $1,175,000/$1,175,000
The University of Tennessee Institute of Agriculture, in support of the project, provided faculty salary. Additional non-federal support derived from contributions from the stakeholder group.

Investigation Team

- Tim Rials – project director/principal investigator (PD/PI)
- Burton English – co-principal investigator (co-PD/PI)
- Kim Jensen – faculty
- Jim Larson – faculty
- Carlos Trejo-Pech – faculty
- Ed Yu – faculty
- David Hughes – faculty
- Jada Thompson – faculty
- Luis Vizcaya – master's graduate student
- A. Latif Patwary – master's student

Project Overview

The University of Tennessee (UT) will lead the feedstock production (Task 1) component of the project. This component targets the need to assess and inventory regional forest and agricultural biomass feedstock options and delineate the sustainability impacts associated with various feedstock choices, including land-use effects. The UT will lead the national lipid supply availability analysis, using POLYSYS to develop information on the potential impacts and feasibility of using lipids to supply aviation fuel. The team at UT will facilitate regional deployment/production of jet fuel by laying the groundwork and developing a regional proposal for deployment. Additionally, UT will support activities in Task 3 with information and insights on feedstocks, along with potential regional demand centers for aviation fuels and coproducts, along with information on current supply chain infrastructure, as required.

Major goals included the following:

1. Develop a rotation-based oilseed crop scenario and evaluate potential with POLYSYS
2. Reevaluate the production potential of biomass feedstocks and evaluate potential with POLYSYS
3. Develop database on infrastructure and needs for the Southeast U.S.
4. Continue monthly meetings with Central Appalachia stakeholders
5. Initiate aviation fuel supply chain studies in the Southeast using pine and oilseeds
6. Continue with sustainability work for both goals 1 and 4

Task 1 - Assess and Inventory Regional Forest and Agricultural Biomass Feedstock Options

University of Tennessee

Task 1 Goals (support/continue ongoing work from previous year)

- Complete the economic viability analysis on switchgrass, short-rotation woody crops, crop residues, forest residues, and cover crops
- Assist Risk-Reward Profit Sharing modeling by providing information from past work on cellulosic supply chains to Pennsylvania State University (PSU)
- Provide measures of economic impacts through the development of renewable fuel.

Objectives

A. Develop new supply curves for both lignocellulosic and oilseed feedstock for sustainable aviation fuel (SAF). As the markets for lignocellulosic biomass (LCB) feedstock, i.e., grasses, short-rotation woody crops, and agricultural residues, are currently not well established, it is important to evaluate the feasibility of supplying those LCB feedstocks. The production, harvest, and storage cost of the feedstocks are included in the assessment. A variety of potential crop and biomass sources will be considered in the feedstock path, including the following:

Oilseed crops: potentials include pennycress (*Thlaspi arvense*), camelina (*Camelina sativa*), and carinata (*Brassica carinata*) as "cover crops"

Perennial grasses: switchgrass (*Panicum virgatum*), miscanthus (*Miscanthus sinensis*), and energy cane (*Saccharum complex*)

Short-rotation woody crops: poplar (*Populus* species), willow (*Salix* species), loblolly pine (*Pinus taeda*), and sweetgum (*Liquidambar styraciflua*)

Agricultural residue: wheat straw, corn stover, and other agricultural residues

Forest residue: forest residue

B. Evaluate the potential economic impact of a mature SAF industry on regional, state, and national economies.

Research Approach

POLYSYS was used to estimate and assess the supply and availability of these feedstock options at the regional and national levels and different feedstock farm-gate prices. County-level estimates of all-live total woody biomass, as well as average annual growth, removals, and mortality, were obtained from the Forest Inventory and Analysis Database (FIADB). Mill residue data are not incorporated because that material already has a market, for the most part. The Forest Sustainable and Economic

Analysis Model (ForSEAM) will be used to estimate and predict forest residues. Forest residue encompasses removal of logging residues, thinnings and unmerchantable trees. Forest residues exclude any logs from areas defined as supplying sawtimber but does include the logging residues that occur from sawtimber harvest. ForSEAM uses U.S. Forest Service Forest Inventory and Analysis data to project timber supply based on the U.S. Global Forest Product Model module of the Global Forest Product Model (USFPM/GFPM) demand projections. Specific tasks related to this objective are outlined below. Estimates from 2020 through 2047 are made. The potential supply analysis is based on 2045 projections, although there is little difference in the national numbers between 2025 and 2045.

Two sets of POLYSYS scenarios were analyzed.

- The initial set examined the quantity of agricultural residues coming from traditional plantings from corn, sorghum, oats, barley, wheat, soybeans, cotton, and rice, along with the contributions of dedicated herbaceous energy crops and short-rotation woody crops (SRWCs) at farm-gate prices of $30 to $80 per ton in $5 increments. Currently the analysis has focused on $40, $60, and $80 per ton. Analysis has been extended to $90, $100, and $110 per ton.
- A second scenario focused on oilseeds as "cover crops." This analysis allowed for areas where corn and/or cotton and soybeans were grown historically to add a crop between the row crop and soybeans. The analysis assumed a 6.5% decrease in soybean yield if the region switched from corn (or cotton)/soybeans to corn (or cotton)/cover crop/soybean rotations. The data generated in these runs provided results for Task 2.

The UT Department of Agricultural & Resource Economics models supply chains for liquid and/or electricity-generating technologies currently in use or forthcoming for the bio/renewable energy industry using the input-output model IMPLAN. The approach for ethanol, biodiesel, and liquid fuels includes the establishment and production of the feedstock, the transportation of the feedstock to the plant gate, and the one-time investment and annual operating of the facility that converts the feedstock to a biofuel. This modeling approach may also include the preprocessing and storage of feedstocks at depots. Also included in the supply chain analyses are the labor/salary requirements for these activities, renewable identification numbers (RINs) values and credits attributable to the conversion facility, along with land-use changes for growing the feedstock. Recent modeling emphasis has centered on the supply chain for liquid fuels using the 179 economic areas of the Bureau of Economic Analysis (BEA) as modeling regions (Figure 1). The data layers necessary to estimate the economic impacts are contained in the Renewable Energy Economic Analysis Layers (REEAL) modeling system.

IMPLAN (version 3.0, using basic data for 2018) contains an input-output model based on county-level data that can be used to estimate the supply chain economic impacts of the bio/renewable energy industry. Data are aggregated to BEA economic areas and then converted to BEA input-output models to measure changes in economic activity. As with all input-output models, IMPLAN describes the buying and selling of products and resulting transfer of money between different industries and institutions within a BEA. Output from the model provides descriptive measures of the economy, including total industry output (the value of all sales), employment, labor income, value-added, and state/local taxes for 546 industries in each BEA.[1] Each BEA IMPLAN model provides estimates of multiplier-based impacts (e.g., how siting a conversion facility will impact the rest of the BEA economy). In analysis of the impacts of the supply chain activities, the indirect multiplier effect (i.e., the impact on the supply chain part of the economy in this case) is also included. Multipliers operate on the assumption that as consumers and institutions increase expenditures, demand increases for products made by local industries, who in turn make new purchases from other local industries and so forth. Stated another way, the multipliers in the model will measure the response of the entire BEA economy to a set of changes in production for liquid fuel technologies currently located within the region and/or forthcoming for the bio/renewable energy industry. The analysis uses IMPLAN's available local purchase percentage (LPP) option, which affects the direct impact value applied to the multipliers. Instead of a 100% direct expenditure value (i.e., electricity, water, construction, manufacturing, waste management) applied to the BEA multipliers, the value which reflects the BEA's actual purchases. The analysis is achieved by using Analysis by Parts (ABP) methodology. ABP is conducted by splitting the inputs purchased into the industries that receive the purchase and their corresponding impacts. The total impact is the aggregation of all the parts. Each part represents an industry that provides input into the industry under consideration. In addition, labor impacts and the impacts of changes in proprietor income are included.

[1] Total industry output is defined as the annual dollar value of goods and services that an industry produces. Employment represents total wage and salary employees, as well as self-employed jobs in a region, for both full- and part-time workers. Labor income consists of employee compensation and proprietor income. Total value added is defined as all income to workers paid by employers (employee compensation); self-employed income (proprietor income); interests, rents, royalties, dividends, and profit payments; and excise and sales taxes paid by individuals to businesses. State/local taxes comprise sales tax, property taxes, motor vehicle licenses taxes, and other taxes.

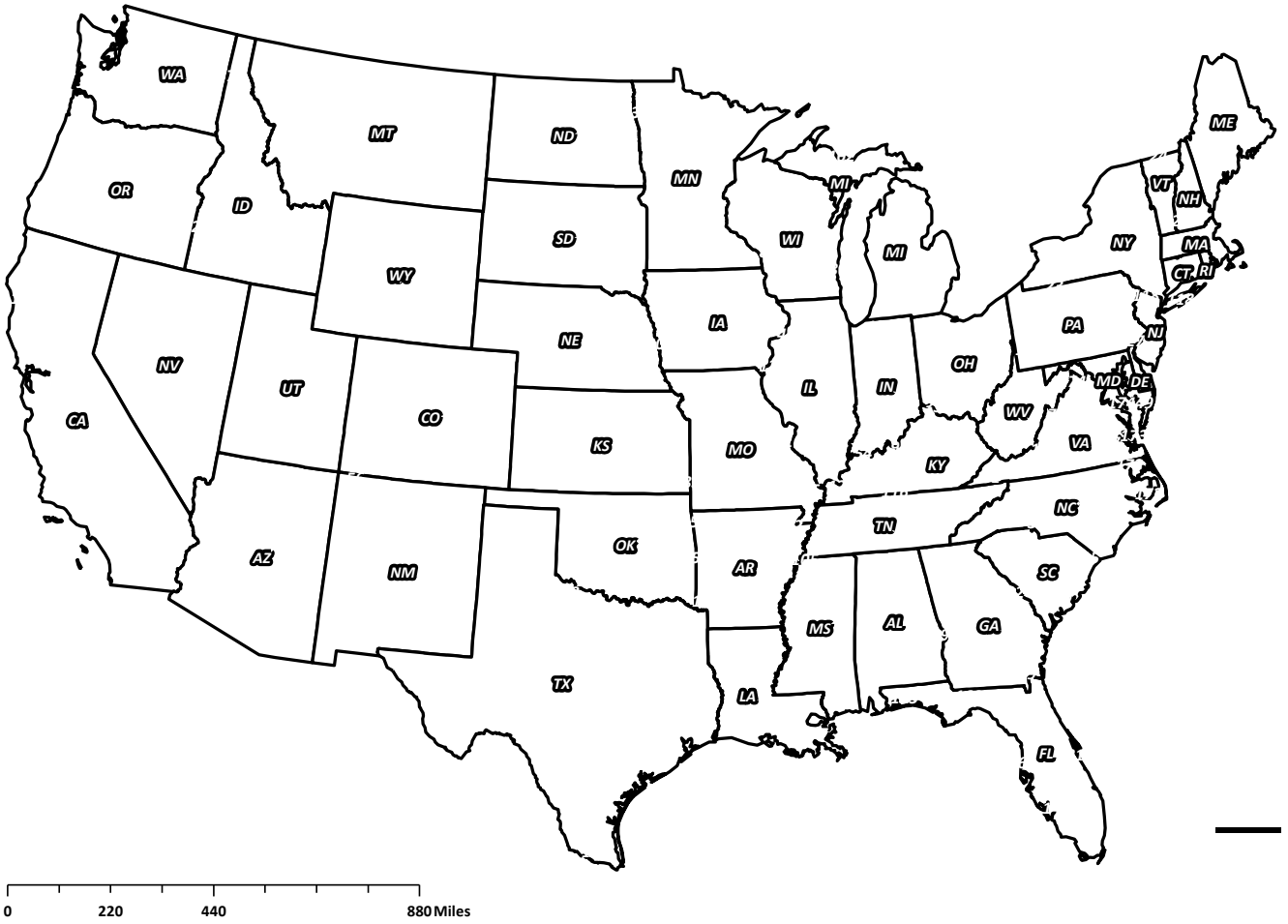

Figure 1. Bureau of Economic Analysis economic areas for input-output analysis modeling.

An example scenario is presented to show modeling capabilities. The conversion technology is a gasification Fischer-Tropsch (GFT) biorefinery with feedstock input of 545,000 tons per year of forest residue in Central Appalachia. Distance for a logging road for the feedstock is less than 1 mile. The biorefinery is expected to produce SAF, diesel, and naphtha. An estimated 1.1 million tons of forest residue is required at 10% moisture content. Working 330 days per year and 10 hours per day, an estimated 16-17 trucks must be emptied every hour (or one truck every four minutes) if truckloads are 20 tons of chips (longer trailers could haul 22.5 tons of chips and could unload 14-15 trucks per hour). Based on TEA information, for the Central Appalachia region, three biorefineries could be sited, each producing 545,000 dry short tons or 495,000 dry metric tons per year. Each biorefinery could produce 12.6 million gallons of SAF, 10.7 million gallons of diesel, and 6.2 million gallons of naphtha. Gross revenues for fuel are estimated at $425.0 million with RINs contributing an additional $52.0 million. Breakeven plant-gate fuel prices when assuming RINs and 12.2% return on investment are $4.90 per gallon for SAF, $5.05 per gallon for diesel, and $4.26 per gallon for naphtha. In addition, a blender's fee of $1 to $2 per gallon for SAF fuel might be available, reducing the costs even more. Current legislation includes a blender's fee for biodiesel of $2 per gallon and for gasoline of $1 per gallon.

Based on IMPLAN estimated economic impacts, the annual economic impact to Central Appalachia if three biorefineries are established is $1.2 billion, based on an investment of $1.7 billion. Leakages occur as investment dollars leave the region based on the regional local purchase coefficients (i.e., LPPs), which totals $500 million. This results in $2.1 billion in

economic activity with a multiplier of 1.7. In other words, for every 1 million dollars spent, an additional $0.7 million in economic activity is generated in the regional economy. Gross regional product is estimated at $1.0 billion, and nearly 14,000 jobs are created during the construction period of the biorefineries, which results in $700 million in labor income with multiplier effects.

Milestones

- Generated data passed on to the ASCENT 1 database for hardwood and softwood forest residues in the Southeast U.S. for two sustainability scenarios
- Developed a pine pathway for the Southeast U.S. and conducted an evaluation of the potential that exists within the region using an ASCENT cellulosic pathway
- Delivered pennycress and crush facility spreadsheet to PSU for use in Risk-Reward Profit Sharing modeling
- Developed economic multipliers for FT-SPK using forest residues as the feedstock. producing SAF and naphtha

Major Accomplishments

Information to develop supply curves has been generated and the $40, $60, and $80 per ton scenario solutions have been mapped in draft form. Figures 2 (forest residues), 3 (agricultural residues), 4 (switchgrass), and 5 (miscanthus) for the $80/ton solution are shown below. These data are at the county level.

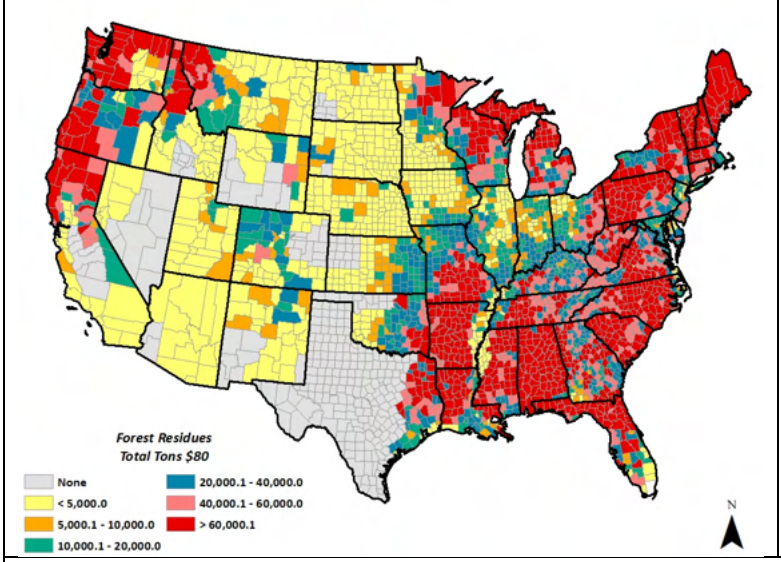

Type of wood	National quantity (tons)
Softwood	92,146,520
Hardwood	43,876,644
Total	136,023,164

Figure 2. Forest residues at $80 per ton chipped, in the truck and at the landing.

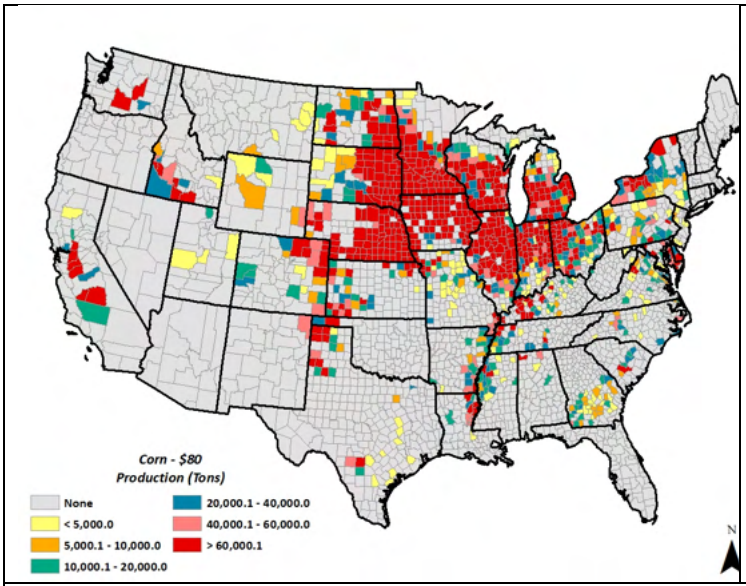

Crop	Residue harvested (acres)	Production (tons)
Barley	619,220	724,226
Corn	65,106,280	206,303,326
Cotton	171,391	57,539
Oats	167,792	176,289
Sorghum	975,592	1,205,416
Soybeans	2,428,491	2,321,166
Wheat	17,983,566	21,475,999
Total	87,452,332	232,263,961

Figure 3. Location of corn stover and information on other residues at a farm-gate price of $80 per ton.

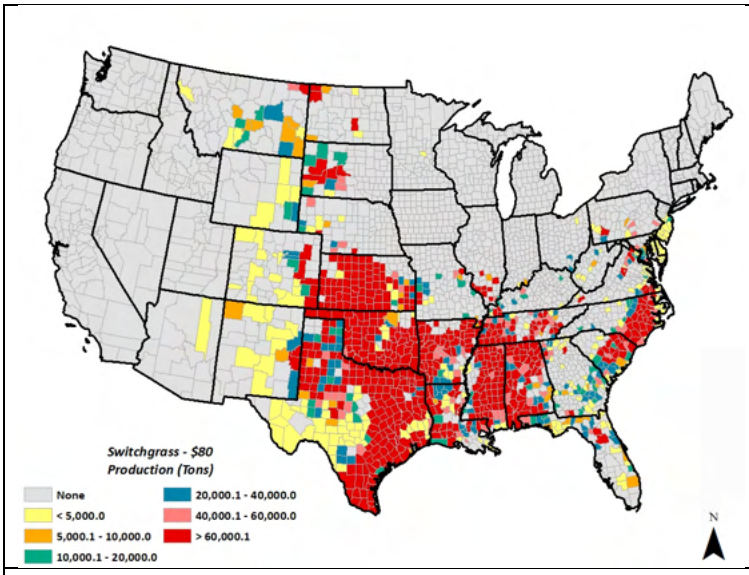

Dedicated energy crop	Acres harvested	Production (tons)
Switchgrass	30,645,632	137,206,759
Poplar	479,679	13,508,568
Willow	658,219	17,648,695
Sweet sorghum	1,243,876	10,494,139
Miscanthus	38,844,871	242,585,459
Energy cane	60	500
	71,872,337	421,444,119

Figure 4. Location of switchgrass production and information on other dedicated energy crops at a farm-gate price of $80 per ton.

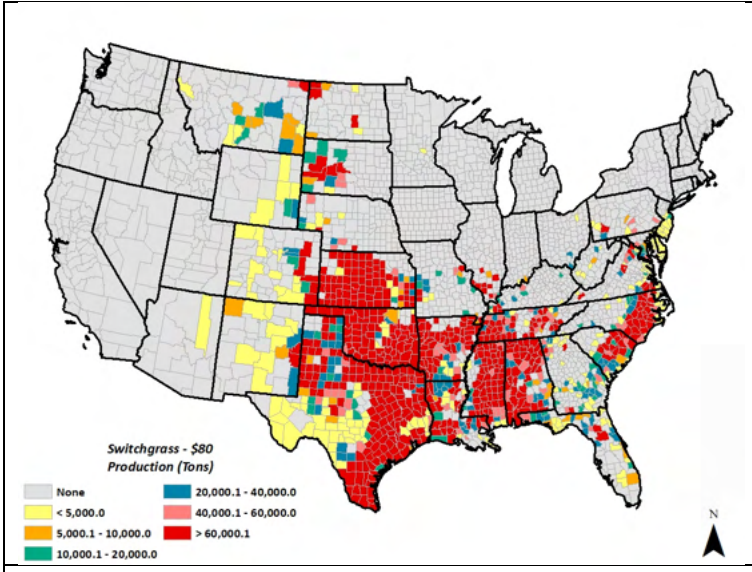

Dedicated energy crop	Acres harvested	Production (tons)
Switchgrass	30,645,632	137,206,759
Poplar	479,679	13,508,568
Willow	658,219	17,648,695
Sweet sorghum	1,243,876	10,494,139
Miscanthus	**38,844,871**	**242,585,459**
Energy cane	60	500
	71,872,337	421,444,119

Figure 5. Location of miscanthus production and information on other dedicated energy crops at a farm-gate price of $80 per ton.

A thesis titled "The Effects of Inputs on Poultry Production Output," completed this year by Ty Wolaver, under the guidance of Dr. Jada Thompson, compared the nutritional content of camelina meal to soybean meal used in a poultry broiler diet. Using poultry nutritional requirements, a minimum cost diet using linear programming was developed. Decreasing the price of camelina meal relative to soybean meal allowed the model to provide estimated meal demand curves. Prices were reduced in intervals, and 5,000 stochastic simulations were run at each price point.

The price point intervals included (1) 80 to 99% of soybean meal, (2) 60 to 80% decrease from soybean meal, and (3) 30 to 60% decrease from soybean meal prices. When the price of camelina meal varied between 99% and 80% of the price of soybean meal, camelina meal demand average ranged from 62.53 to 68.38 kg of the 200 kg of dry meal requirement in a 1,000-kg feed ration. soybean meal was replaced from 31.3% to 34.2%. Based on the quantity of soybean meal demanded for broiler finisher feed, there would be a demand of 5.61 million kg to 6.13 million kg for broiler finisher feed in Tennessee creating gross sales of $19.81 million to $19.69 million per year. When the price of camelina meal is 70% of the price of soybean meal, camelina meal demand averages 74.23kg of the 200kg of dry meal necessary in a 1000kg feed ration or 37.1% of the dry meal necessary. This amounts to a demand for camelina meal of 6.65 million kg for broiler finisher feed in Tennessee. This would create a gross sale of $16.63 million. Finally, when the price of camelina meal is 30% to 60% of the price of soybean meal, camelina meal demand averages from 83.71 million kg to 86.34 million kg of the 200 kg of dry meal necessary in a 1,000-kg feed ration or 41.9% to 43.2% of the dry meal necessary. This would create gross sales of $8.21 million to $16.57 million.

Camelina has been shown to have potential substitutability, at least in theory, for soybean meal in broiler finisher rations if the camelina meal is priced at a discount to soybean meal. An increasing quantity of camelina meal is selected as the price lowers with respect to soybean meal prices. However, the quantity demanded does not change much once camelina meal is priced at 60% to 70% of the soybean meal price.

If feasible, the broiler industry could save on feed cost and decrease risks from price volatility in the soybean market on broiler feed cost. By having camelina meal as an option, broiler feed mills would not be totally dependent on the current price of soybeans as more camelina meal can be introduced into broiler finisher feed as the price of soybean meal rises.

Publications

1. Thomas, M., Jensen, K. L., Lambert, D. M., English, B. C., Clark, C. D., & Walker, F. R. (2021). Consumer preferences and willingness to pay for potting mix with biochar. Energies *14*(12), 3432. https://doi.org/10.3390/en14123432
2. Burton, C., English, R., Menard, J., & Wilson, B. (2021). The economic impacts of a renewable biofuels/energy industry supply chain using the Renewable Energy Economic Analysis Layers (REEAL) modeling system [Manuscript submitted for publication].
3. Trejo-Pech, C. J., Larson, J. A., English, B. C., & Yu, T. E. (in press). Biofuel discount rates and stochastic techno-economic analysis for a prospective Pennycress (Thlaspi arvense L.) sustainable aviation fuel supply chain. Frontiers in Energy Research.
4. Zhou, X. V., Jensen, K. L., Larson, J. A., & English, B. C. (2021). Farmer interest in and willingness to grow pennycress as an energy feedstock. Energies, *14*(8), 2066. https://doi.org/10.3390/en14082066
5. Wolaver, T. M. (2021). The effect of inputs on poultry production output. [Master's Thesis, University of Tennessee]. https://trace.tennessee.edu/utk_gradthes/6191
6. Vizcaya, L. A. Effect of harvesting schemes on forest residue supply chain for biofuel production: A case study in tennessee. [Master's Thesis, University of Tennessee].

Outreach Efforts

The UT Institute of Agriculture (UTIA) and the Commercial Aviation Alternative Fuels Initiative (CAAFI) have partnered to identify sites with optimal woody biomass and essential supply chain infrastructure, as these factors present challenges for processors with limited resources to conduct site assessments with enough detail to attract investment capital. The initial attempt will highlight the availability of woody biomass in the region, and thereby extend its potential utilization. Analysis has been initiated for DRAX and USAENERGY.

Awards

None

Student Involvement

Luis Vizcaya completed a forest harvesting model and biorefinery siting given forest residue availability. Vizcaya was included in the project to analyze the optimal harvest pattern of forestry residues that will be the derived supply for biorefineries.

Ty Wolaver completed and defended his thesis and we are working to publish a paper on oilseed meal.

Latif Patwary was included in the project to examine the potential environmental benefits.

Plans for Next Period

- Complete blend study
- Develop Forest Harvest model
- Complete several manuscripts
- Continue our work on the forest sector
- Develop a stochastic analysis focusing on pennycress, carinata, and camelina feasibility in the Southeast U.S.
- Continue to work on Memphis airport region analysis using camelina and pennycress as feedstocks
- Work on feedstock sustainability issues
- Continue working with stakeholders

Task 2 - Develop National Lipid Analysis

University of Tennessee

Objective

The UT team will complete the national lipid supply availability analysis using POLYSYS to develop information on the potential impacts and feasibility of using lipids to supply aviation fuel.

Research Approach

POLYSYS was used to estimate and assess the supply and availability of these feedstock options at the regional and national levels. This U.S. agricultural sector model forecasts changes in commodity prices and net farm income over time. Analysis requires consistency among the crops. Budgets have been reevaluated for pennycress, camelina, and carinata for consistent assumptions where possible. These budgets have been uploaded into the Penn State BOX platform, sent to Washington State University, and are available at https://arec.tennessee.edu/. Yields have been compared with literature sources and are presented in Figures 6, 7, and 8 and are available at https://arec.tennessee.edu/.

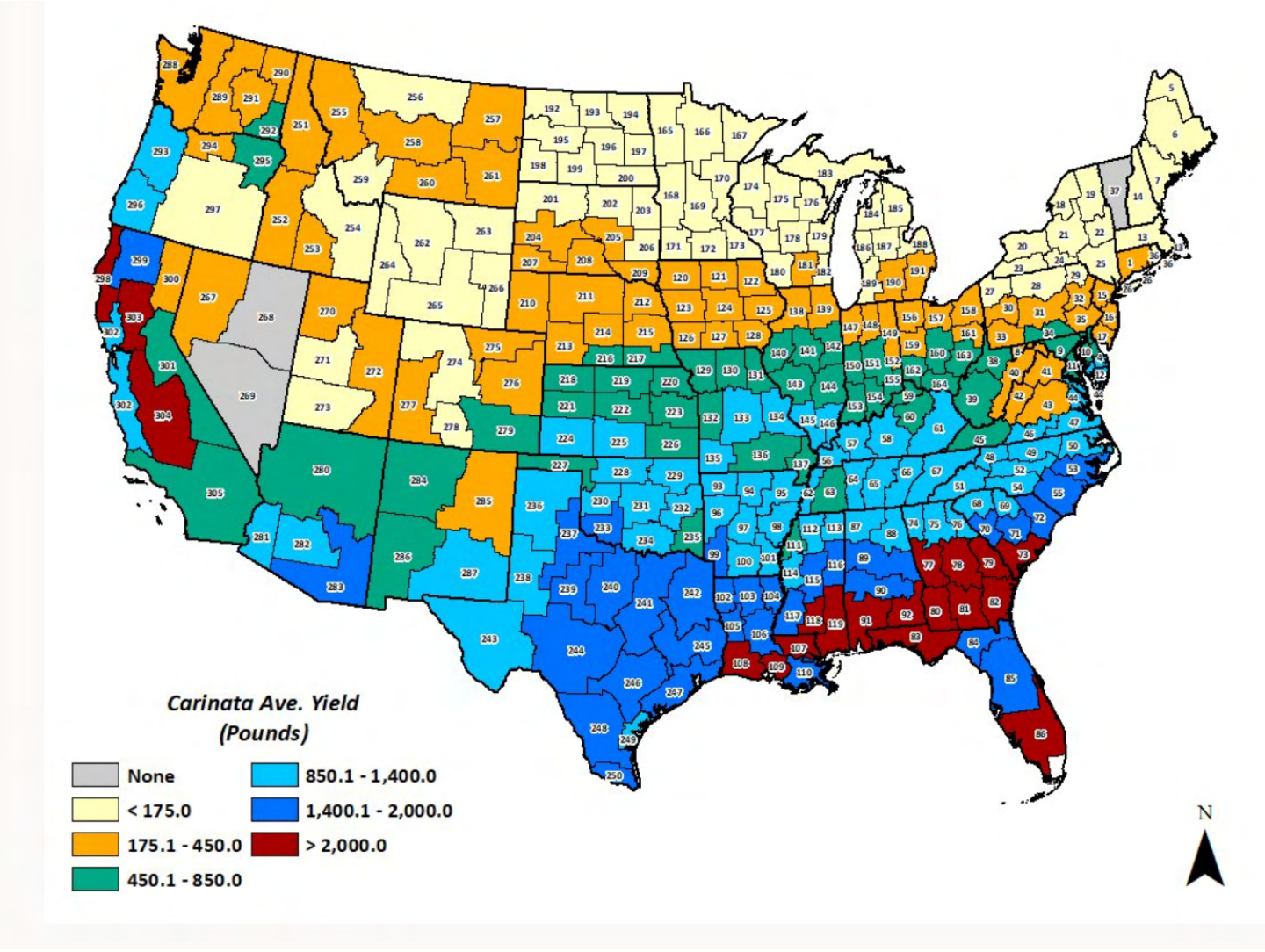

Figure 6. Yield map for carinata.

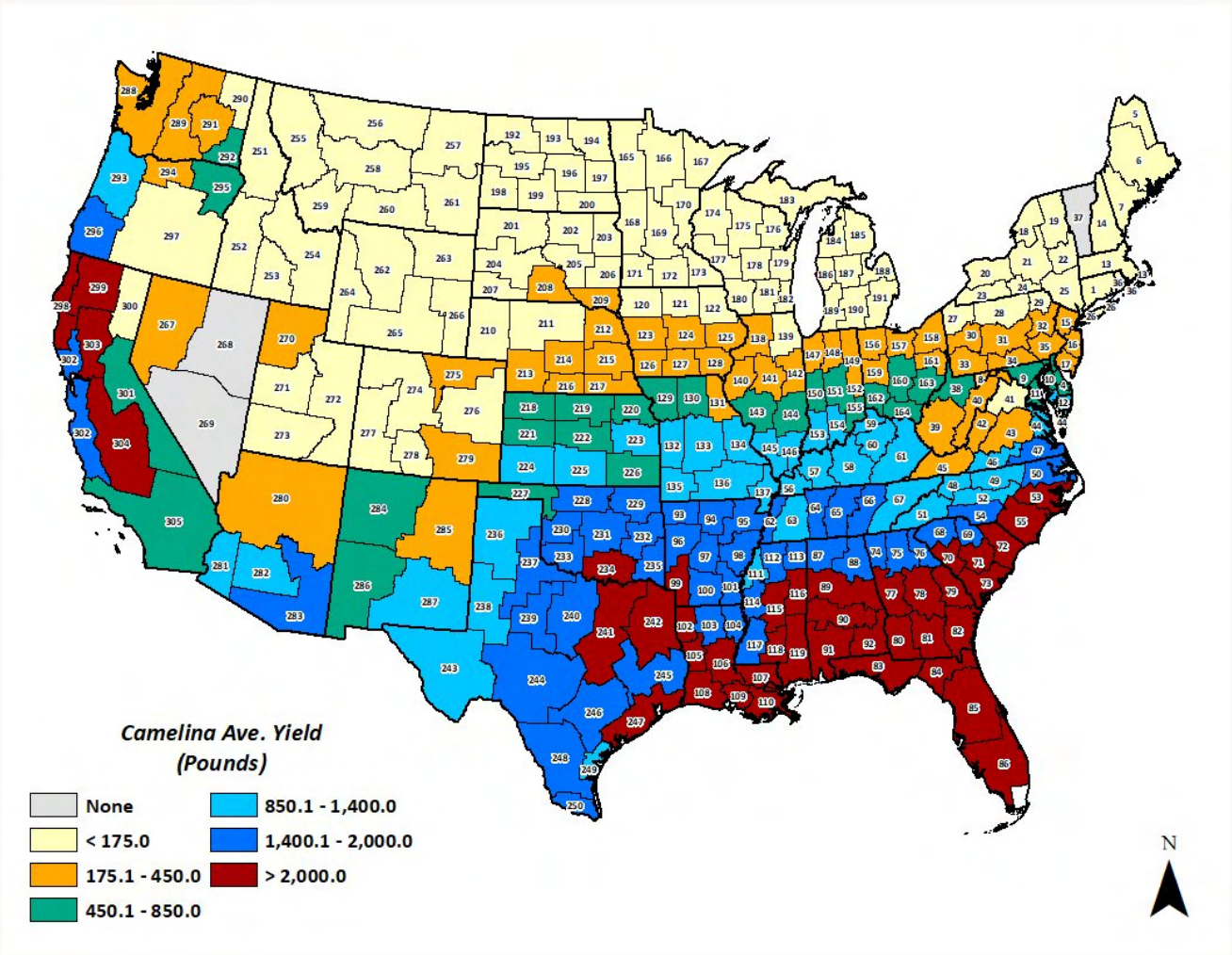

Figure 7. Yield map for camelina.

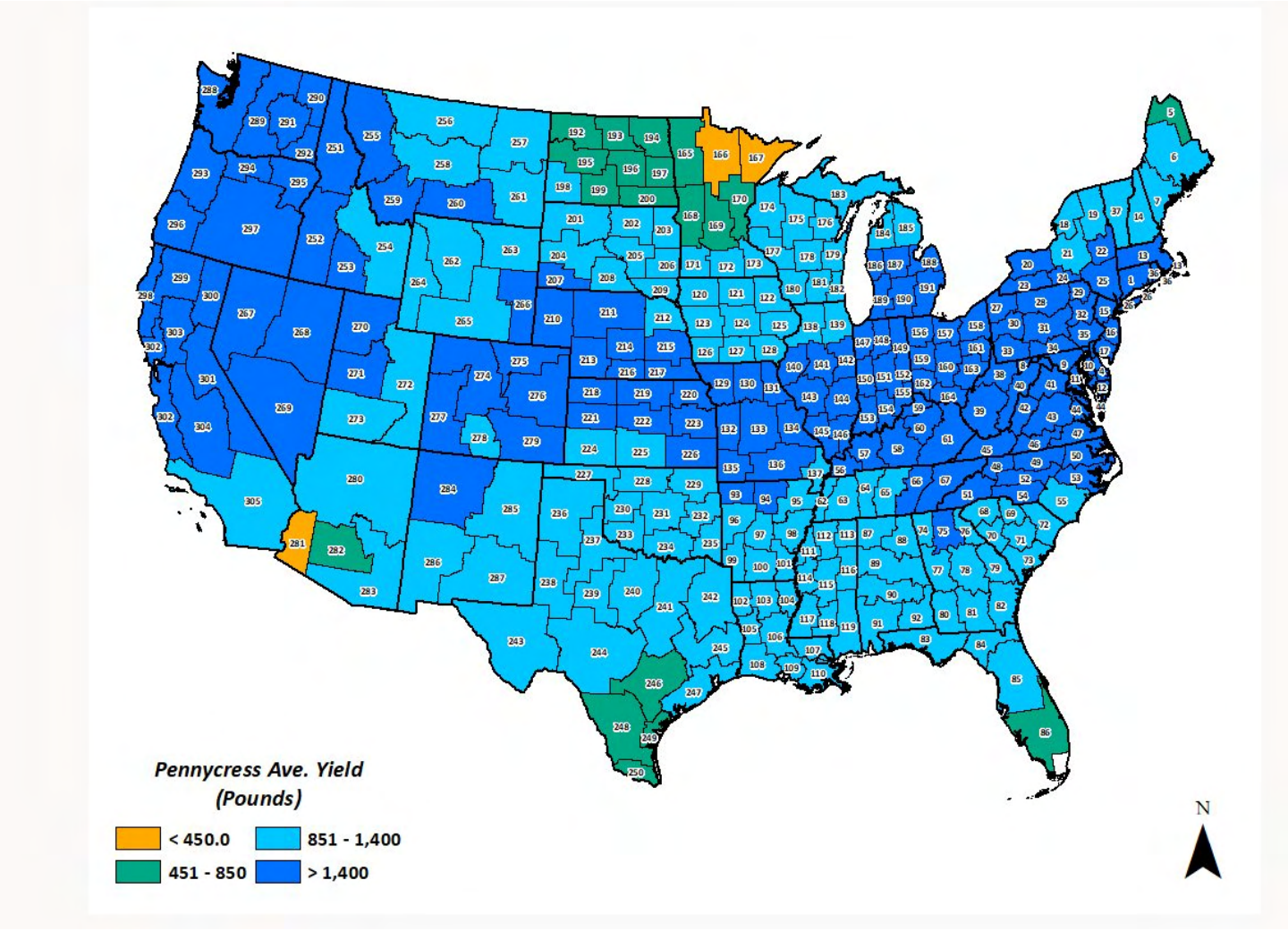

Figure 8. Yield map for pennycress.

Milestones

This project is behind because COVID-19 limited my access to POLYSYS. Although the planned article is not yet written, it is hoped that it will be included in a special issue of *Frontiers in Energy* that will feature the work of ASCENT Project 001. The article will address both feedstock and economic sustainability regarding oilseed cover crops.

Major Accomplishments

1. Consistent assumptions regarding prices of inputs were reviewed and budgets updated. POLYSIS was updated with the changes.
2. Completed the carinata spreadsheet incorporating risk into the analysis. The spreadsheet is still under review.
3. Compared the assumptions between the three oilseed crops and attempted to develop spreadsheets that contain similar price data and other assumptions.
4. Analysis has been run in POLYSYS assuming on-farm prices of $0.05 to $0.20 per pound. Supplies of the oilseed are estimated and impacts to the national and rural economies are being estimated.

Analysis indicates that without expanding to non-cropped lands, 93 million acres could be planted in a “three crop every two year” system (Table 1). This would produce 67 billion pounds of oilseed ranging from 0.32% to 0.4% oil. Assuming a

hydroprocessed esters and fatty acids (HEFA) processing technology, this would result in 23,450,000,000 pounds of oil or10 million metric tons of oil per year. Using ASCENT technology spreadsheets, this would provide sufficient feedstock for 11 biorefineries to produce 1.58 billion gallons of SAF along with 632 million, 228 million, and 466 million gallons of diesel, naphtha, and propane, respectively, assuming an average oil content of 35%.

Table 1. Projected Oilseed Production at Farm-Gate Prices of $0.05 to $0.20 per Pound.

Farm-Gate Price ($/pound)	Acres	Production	Yield on 1/2 acre
0.05	34,242,819	25,223,413,311	736.6045
0.08	49,066,461	36,049,776,550	734.7132
0.11	69,156,754	50,008,883,134	723.1236
0.14	80,617,744	58,105,888,041	720.7581
0.17	87,921,175	63,546,048,466	722.7616
0.2	93,451,551	67,476,879,966	722.052

An initial draft of this study's findings is nearing completion.

Publications
See Task 1 above for publications.

Outreach Efforts
None.

Awards
None.

Student Involvement
Alan Robertson – examined the impact of fertilizer on switchgrass yield and ash content and evaluated at what level the biorefinery would like fertilizer application to occur.

Plans for Next Period
Complete national oilseed analysis

Task 3 - Lay the Groundwork for Lipid and/or Biomass in Tennessee and the Southeast United States
University of Tennessee

Objective(s)
The team at UT will facilitate regional deployment/production of renewable jet fuel by completing the groundwork phase of the regional oilseed feedstock to biofuel pathway and developing a proposal for regional deployment in the Southeastern U.S. and in Central Appalachia, leading to the development of SAF Regional Deployment Plans for the Southeast and Appalachia.

Research Approach
- Same as Task 1 but focused on small areas such as Central Appalachia, Memphis, and Nashville regions
- Softwood analysis is focused on the Southeast, and findings were provided in last year's report
- Developed seed trial for oilseed cover crops using funding from UT seed money; will incorporate findings in this report for the first year under sub-project 2

Central Appalachia – second year of a several-year project
The project was initiated when COVID-19 hit; the project was rearranged to reflect laboratory closures and travel restrictions.

The research approach was modified somewhat to reflect these changes. A hardwood forest residue layer was developed for BioFLAME and Freight and Fuel Transportation Optimization Tool (FTOT) (Figures 7 and 8). Initial FTOT analysis has been run and adjustments to the analysis are underway.

A stakeholders group has been formed and has met multiple times. Typically, the meeting occurs on the second Thursday of each month.

The following represents a summary of the work accomplishments under the subcontract with the Center for Natural Capital to assist in the Central Appalachia area. Item 8 has been canceled because of the funding decrease for 2021-2022. In addition, the Center continues to play an active and vital role in the stakeholders' meetings even though the funding for the project covered the initial year, and future years were not funded. Initial year funding was extended for a second year through a no-cost extension.

1. Form expert advisory board
    a. Develop invitee list of potential advisory board members
    b. Hold Zoom calls and get input on stakeholder invitees
2. Group formed
    a. Monthly calls held
3. Monthly calls
    a. Advise the expert advisory board regarding the needs of the airline industry
    b. Identify and engage consultant with significant experience in airline industry fuels
4. A stakeholder cabinet will be assembled.
5. Assist UT in identifying potential brown and green field locations
6. Review and comment on UT's determination of the ability and willingness of forest landowners, agricultural producers, and reclaimed mine landowners to make land available for feedstock production
7. Procure and deliver to UT 50-60 different hybrid poplar samples in chipped form from Powell Project Travel to Powell River Project with Virginia Tech assistance and collect samples. Cut pieces of hybrid poplar and return them to Rapidan, Virginia, for processing into chips. Samples acquired, processed, and delivered to UT.
    a. Procure and deliver 110 pounds of hybrid poplar tree trunks only (without stems and leaves) from Powell Project Travel to Powell River Project with Virginia Tech assistance and collect samples.
    b. Cut boles of hybrid poplar and return them to Rapidan, Virginia.
    c. Samples acquired, processed, and delivered to UT.
8. Assist Don Hodges and his students in procuring hardwood forest residue samples from ongoing logging activities in the region by identifying current logging operations.
9. Some participants of the group have formed a task force to prepare proposals to fund follow-on work. A group of energy-related companies has been compiled and contacts are being made to solicit interest in building a biorefinery in the region. One company has prepared a high-level proposal to install wood pyrolysis systems to break down feedstock and deliver it to a biorefinery.
10. Considerable effort has been made to reach out to other related projects in the region. The most notable is the MASBIO project based at West Virginia University. The MASBIO leadership took the lead on a proposal to the U.S. Department of Commerce.

The hybrid poplar samples were evaluated by the UT BEST lab headed by Niki Labbe. In concert with a hardwood National Institute for Food and Agriculture (NIFA) project, the lab was to characterize feedstock performance and conversion potential of Central Appalachia region hardwood forest thinnings, harvest residuals, and SRWCs from university experimental plots and reclaimed surface mine lands, and the invasive species that have colonized formerly mined lands and define their locations and costs. This was accomplished by collecting hardwood residue biomass from various locations and preprocessing (drying and size reduction) for near-infrared data collection and wet chemistry analysis.

In total, 71 chipped hybrid poplar biomass samples were collected from two sites at the Powell River Project plantings on reclaimed mine land in Appalachian regions with GPS locations at 37.01557/−82.6606, and 37.00776/−82.6942. After milling the biomass materials, quality data were assessed by measuring their ash content. The ash content ranged from

1.53% to 4.41% with a mean of 2.4% (± 0.6) on an oven dry basis (Figure 9). In addition, near-infrared (NIR) spectroscopy was used to obtain a chemical fingerprint of the materials, and a model for ash was constructed by correlating the NIR spectral data with the ash content using partial least squares regression. Table 2 shows the model performance metrics for ash with a correlation of 0.67.

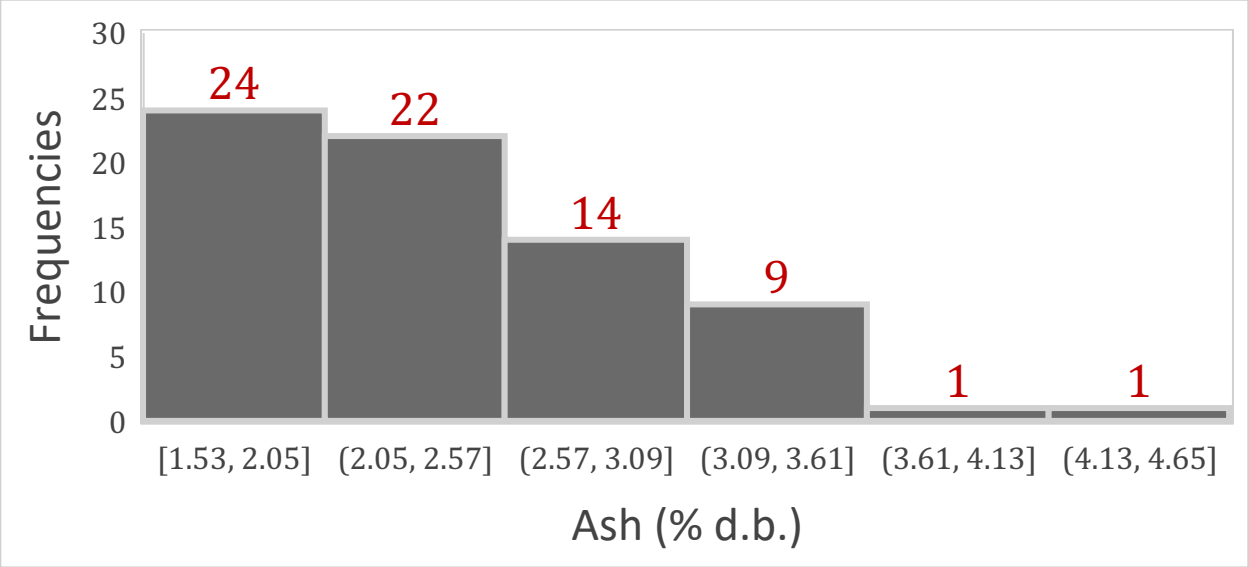

Figure 9. Percent ash (dried basis) distribution for 71 ASCENT samples.

Table 2. Near-infrared model performance metrics for 71 ASCENT samples (on dry basis).

Model	N	Range (%)	Factors	$RMSE_{Cal}$ (%)	R^2_{Cal}	$RMSEC_{Val}$ (%)	R^2_{Val}
Ash	71	1.53-4.41	3	0.31	0.75	0.33	0.72

N = number of samples included in the models.
$RMSE_{Cal}$ = root mean square error of calibration.
R^2_{Cal} =Coefficient of variation
$RMSEC_{Val}$ = root mean square error of cross validation.
R^2_{Val} = Coefficient of variation

To improve the ash model, we selected 200 hardwood residue samples from our biomass library and reconstructed the NIR model for ash (Figure 10). The biomass materials were collected from commercial sites located in Alabama, Florida, Georgia, South Carolina, Tennessee, and Virginia, primarily collected for analysis required by an Agriculture and Food Research Initiative (AFRI) project. In addition to ash, inorganics (alkali and alkaline earth metals combined [Na, K, Mg, and Ca]; AAEM) and higher heating values (HHV) models were constructed by correlating these characteristics to the corresponding NIR spectral data using partial least squares regression. Table 3 summarizes the performance of the developed models. The AAEM and HHV data for the ASCENT samples will be included in the models as soon as the data become available. The robustness of these models will be improved by including the ASCENT samples, which will expand the range of the properties of interest.

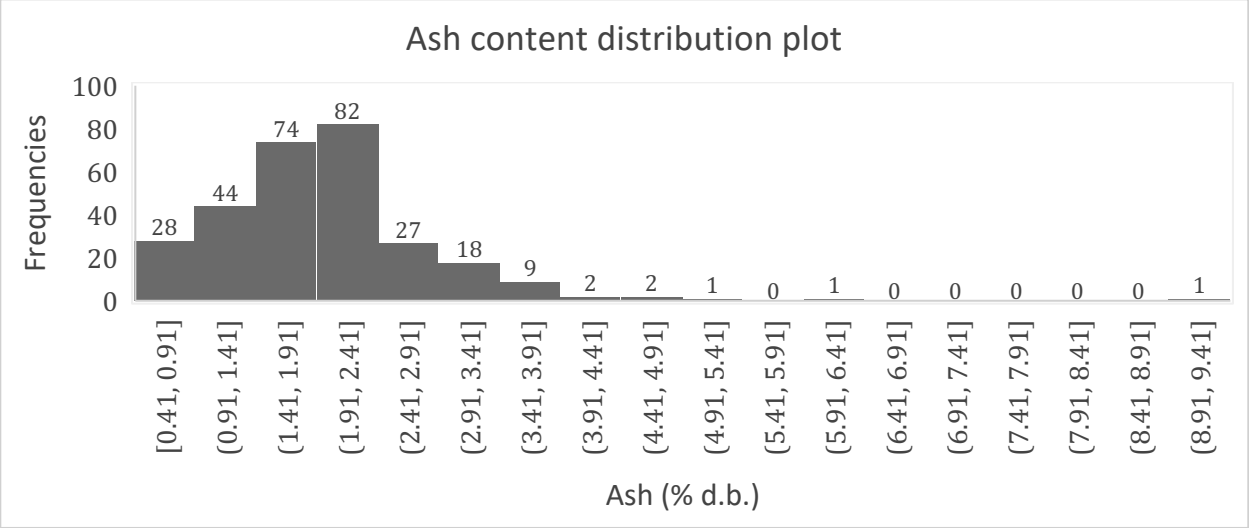

Figure 10. Distribution plot for 289 hardwood samples collected from the Southeast United States.

Table 3. Near-infrared model performance metrics for all hardwood residues from the Southeast United States.

Model	N	Range	Factors	$RMSE_{Cal}$	R^2_{Cal}	$RMSEC_{Val}$	R^2_{Val}
Ash (%)	268	0.41–4.75	6	0.34	0.79	0.37	0.75
AAEM (mg/kg)	185	1,594–18,062	9	1,052	0.89	1,185	0.86
HHV (MJ/kg)	179	19.04–20.29	8	0.10	0.81	0.11	0.77

N = number of samples included in the models.
AAEM = alkali and alkaline earth metals combined (Na, K, Mg, and Ca).
HHV = higher heating value.
$RMSE_{Cal}$ = root mean square error of calibration.
$RMSEC_{Val}$ = root mean square error of cross validation.

Major Accomplishments

- The Nashville modeling work using cover crop oilseeds is completed. The next step will be to develop a regional deployment plan once risk and uncertainty are evaluated.
- The Memphis modeling work is initiated but analysis has not begun. Analysis will be initiated during the second quarter of 2022.
- The Central Appalachian Project has a regular stakeholders group meeting and will have its initial workshop on state and national incentives to SAF development in the region. This workshop will be online.

Publications

None.

Outreach Efforts

None.

Awards

None.

Student Involvement
None.

Plans for Next Period (Year)
- Complete Central Appalachian Regional Deployment Plan
- Complete Nashville Regional Deployment Plan
- Continue working on Southeast Regional Deployment Plan
- Continue working on Memphis Regional Deployment Plan

Task 4 - Biorefinery Infrastructure and Siting (Supporting Role)
University of Tennessee

Objective
Provide feedstock support to other members of ASCENT as requested.

Research Approach
Provide necessary input through research efforts using feedstock tools developed before or as part of this project. Approach will differ as questions surface from other universities. We have had two requests, which were met this year: a request from Penn State on the cost of feedstock production and from FTOT asking for information on feedstock availability in the Central Appalachian region. We also discussed the potential of assisting the University of Hawaii with economic analysis of Hawaii feedstock and conversion effort.

Milestone
Delivered the feedstock spreadsheets on oilseeds.

Major Accomplishments
See Tasks 1 and 3 above.

Publications
None.

Outreach Efforts
None.

Awards
None.

Student Involvement
None.

Plans for Next Period (Year)
- Complete FTOT-BioFLAME comparison findings
- Enhance economic indicator analysis

Project 001(F) Alternative Jet Fuel Supply Chain Analysis

Massachusetts Institute of Technology

Project Lead Investigator

PI: Steven R. H. Barrett
Professor of Aeronautics and Astronautics
Director, Laboratory for Aviation and the Environment
Massachusetts Institute of Technology
77 Massachusetts Ave, Building 33-322, Cambridge, MA 02139
+1 (617) 253-2727
sbarrett@mit.edu

Co-PI: Dr. Raymond L. Speth
Principal Research Scientist
Laboratory for Aviation and the Environment
Massachusetts Institute of Technology
77 Massachusetts Ave, Building 33-322, Cambridge, MA 02139
+1 (617) 253-1516
speth@mit.edu

Co-PI: Dr. Florian Allroggen
Research Scientist
Laboratory for Aviation and the Environment
Massachusetts Institute of Technology
77 Massachusetts Ave, Building 33-115A, Cambridge, MA 02139
+1 (617) 715-4472
fallrogg@mit.edu

University Participants

Massachusetts Institute of Technology (MIT)

- PI: Professor Steven R. H. Barrett
- FAA Award Number: 13-C-AJFE-MIT, Amendment Nos. 003, 012, 016, 028, 033, 040, 048, 055, 058, 067, 082, and 088
- Period of Performance: August 1, 2014 to September 30, 2022
- Tasks (those listed here are for the reporting period September 1, 2020 to August 30, 2021):
    1. Support U.S. participation in the International Civil Aviation Organization Committee on Aviation Environmental Protection (ICAO CAEP) to enable appropriate crediting of the use of sustainable aviation fuels (SAF) under the Carbon Offsetting and Reduction Scheme for International Aviation (CORSIA).
    2. Support U.S. participation in the ICAO CAEP by performing core life cycle analysis (CLCA) to establish default values for use under CORSIA.
    3. Contribute to the development of the fuel production assessment for CORSIA-eligible fuels, especially as it relates to fuels produced from waste CO_2 and atmospheric CO_2.
    4. Develop methods for probabilistic life-cycle analyses and techno-economic analyses in the context of assessing U.S.-based SAF production until 2035.
    5. Support knowledge-sharing and coordination across all ASCENT Project 01 universities working on SAF supply-chain analyses.

Hasselt University (UHasselt, through subaward from MIT)

- PI: Robert Malina
- Period of Performance: September 1, 2016 to August 31, 2022

- Tasks (those listed below are for the reporting period September 1, 2020 to August 30, 2021):
    1. Support and provide leadership for U.S. participation in the ICAO CAEP to enable appropriate crediting of the use of SAF under CORSIA, especially as it relates to feedstock classification and pathway definitions.
    2. Support U.S. participation in ICAO CAEP by carrying out CLCA to establish default values for use under CORSIA.
    3. Contribute to the development of the fuel production assessment for CORSIA-eligible fuels out to the year 2035
    4. *Omitted; Task led by MIT.*
    5. *Omitted; Task led by MIT.*

Project Funding Level

$3,585,000 FAA funding and $3,585,000 matching funds. Sources of matching funds include approximately $546,000 from MIT as well as third-party in-kind contributions of $809,000 from Byogy Renewables, Inc.; $1,038,000 from Oliver Wyman Group; and $791,000 from NuFuels LLC; and $401,000 from Savion Aerospace Corp.

Investigation Team

Principal Investigator:	Prof. Steven Barrett (MIT) (all MIT tasks)
Principal Investigator (UHasselt Subaward):	Prof. Robert Malina (UHasselt) (all UHasselt tasks)
Co-Principal Investigator:	Dr. Florian Allroggen (MIT) (all MIT tasks)
	Dr. Raymond Speth (MIT) (Task 4)
Postdoctoral Associates:	Christoph Falter (MIT) (Tasks 1, 2 and 3)
	Freddy Navarro Pineda (UHasselt) (all UHasselt tasks)
	Gonca Seber (UHasselt) (Task 2)
	Parisa Raffiani (UHasselt) (Task 2)
	Katrijn Gijbel (UHasselt) (Task 2)
Research Specialist:	Matthew Pearlson (MIT) (Tasks 2 and 4)
	Charlotte Adrianssen (UHasselt) (Task 3)
Graduate Research Assistants:	Tae Joong Park (MIT) (Task 1and 2)
	Walter Kelso (MIT) (Tasks 1 and 4)
	lias Mokas (UHasselt) (Task 3)

Project Overview

The overall objectives of ASCENT Project 01 (A01) are to (i) derive information on regional supply chains to explore scenarios for future sustainable aviation fuel (SAF) production and (ii) identify supply chain-related obstacles to commercial-scale production in the near term and larger-scale adoption in the longer term.

For the assessment year (AY) 2020/21, the MIT/UHasselt team contributed to these goals by: (1) providing leadership in the International Civil Aviation Organization Committee for Aviation Environmental Protection (ICAO CAEP) core life cycle analysis (CLCA) task group of the Fuels Task Group (FTG), which is mandated to calculate lifecycle greenhouse gas (GHG) emissions associated with the use of SAF; (2) performing CLCA to enable the inclusion of additional SAF pathways under CORSIA or verify CLCA values calculated by other institutions; (3) contributing to the analysis of SAF availability in 2050; (4) analyzing the availability of U.S.-produced SAFs in 2035 and their associated lifecycle emissions and costs using a stochastic model; and (5) contributing to knowledge transfer in the ASCENT 01 team.

Task 1 – Support and provide leadership for U.S. participation in ICAO CAEP to enable appropriate crediting of the use of SAF under CORSIA, especially as it relates to feedstock classification and pathway definitions.

Massachusetts Institute of Technology
Hasselt University

Objectives

The overall objective of this task is to provide leadership for and support to the FAA in their engagement with the ICAO CAEP FTG (during CAEP/12). The specific focus of the work during this reporting period was to (1) refine pathway definitions; (2) support discussions toward the development of a CLCA method for lower-carbon aviation fuels (LCAF); and (3) provide guidance on the inclusion of Power-to-Liquid (PtL) fuels.

Research Approach

To achieve the goals outlined above, the team continued to co-lead the CLCA Task Group of FTG. Prof. Malina acted as a co-lead. This role ensures that Prof. Malina remains a focal point of CLCA research, so that specific research tasks can be guided efficiently and effectively. The following research has been conducted in support of the leadership role:

Pathway definitions

Under the leadership of the CLCA task lead, Professor Malina, we reviewed the assumptions made in the development of default CLCA values. This review aimed to understand if Sustainable Certification Schemes (SCS) require additional guidance on the applicability of a certain default value. The results of this assessment were discussed at the FTG/6 meeting, and definitions will be brought forward at the CAEP/13 meeting. These definitions pertain to sustainable residue removal rates, standalone vs. integrated conversion designs for alcohol-to-jet (ATJ) pathways, and closed-pond palm oil hydroprocessed esters and fatty acids (HEFA) systems.

Leadership for the development of the LCAF methods

The MIT and UHasselt team were actively involved in the development of a draft methodology for including LCAF in the CORSIA package via both quantitative analysis and regulatory proposals. This draft methodology addresses both LCAF eligibility considerations as well as LCAF crediting considerations.

Guidance on including Power-to-Liquid (PtL) Fuels

During FTG/08, the CLCA subgroup was tasked to begin working on CLCA values for SAF produced through PtL pathways. The MIT team led the development of a coherent definition of PtL pathways. MIT proposed creating this definition based on a classification of SAF pathways, which relies on their (1) hydrogen source, (2) carbon source, and (3) conversion process. PtL fuels are fuels which rely on electricity as a main input to produce hydrogen and, potentially, carbon. PtL pathways include, but are not limited to, Fischer-Tropsch pathways that leverage low-carbon hydrogen sources and either waste CO_2 or direct air capture. Non-traditional PtL pathways, such as gas fermentation to ethanol followed by ATJ, could use low-carbon hydrogen and carbon-containing feedstock derived similarly to other PtL pathways.

Given the broad range of potential PtL pathways, MIT and other FTG experts recommended including PtL pathways through actual values while the most practical pathways are still emerging.

Milestones

The work described above has been documented in numerous Working Papers and Information Papers submitted to FTG. UHasselt and MIT experts participated in and contributed to numerous FTG meetings, including FTG/06 (November 2020), FTG/07 (February 2021), FTG/08 (March 2021), FTG/09 (May 2021), and FTG/10 (July 2021).

Major Accomplishments

The MIT and UHasselt team accomplished the following under this task:

1. As co-lead of the FTG-CLCA Task Group, Prof. Malina drafted CLCA progress reports to FTG meetings, where CLCA topics were discussed during the current reporting period. In addition, Prof. Malina co-led several Task Group meetings.
2. The MIT team led the development of the definition of PtL pathways for consideration under CORSIA.

Publications

CAEP/12-FTG/06-WP/02. Summary of the progress of the CLCA Subgroup since FTG/03. November 2020.
CAEP/12-FTG/08-WP/04. Summary of the progress of the CLCA Subgroup since FTG/07. March 2021.
CAEP/12-FTG/10-WP/03. Summary of the progress of the CLCA Subgroup since FTG/09. July 2021.
CAEP/12-FTG/10-IP02: Life cycle analysis methodology for lower carbon aviation fuels
CAEP/12-FTG/10-IP/03: Option for Addressing Eligibility and Crediting of LCAF in CORSIA Life Cycle Analysis Framework

Zhao, X., Taheripour, F., Malina, R., Staples, M. D., & Tyner, W. E. (2021). Estimating induced land use change emissions for sustainable aviation biofuel pathways. Science of the Total Environment, *779*, 146238.

Outreach Efforts

Progress on these tasks was communicated during weekly briefing calls with the FAA and other U.S. delegation members to FTG, as well as during numerous FTG teleconferences between meetings. In addition, UHasselt and MIT experts participated in and contributed to numerous FTG meetings, including FTG/06 (November 2020), FTG/07 (February 2021), FTG/08 (March 2021), FTG/09 (May 2021), and FTG/10 (July 2021).

Awards

None.

Student Involvement

During this reporting period, the MIT graduate student involved in this task was TJ Park, who received his S.M. degree in the summer of 2021.

Plans for Next Period

In the coming year, the MIT ASCENT Project 01 team will continue its work in FTG. Default core LCA values will be calculated and proposed for additional pathways, and Prof. Malina will continue to lead the core LCA Task Group. A particular focus will be to shape the agenda for the CAEP/13 cycle.

Task 2 – Support U.S. Participation in ICAO CAEP by Performing CLCA to Establish Default Values for Use Under CORSIA

Massachusetts Institute of Technology
Hasselt University

Objective

During the CAEP/11 cycle, the MIT ASCENT Project 1 team took leadership in applying the agreed-upon CLCA method to establish default CLCA values for 26 unique pathways. However, the list of 26 pathways is not exhaustive, and further CLCA analysis is required to enable inclusion of SAF technologies that are nearing commercialization. During the current reporting period, the team supported (1) the calculation of default CLCA values for fuels produced from co-processing biogenic and fossil feedstocks in conventional refineries; (2) the calculation of default CLCA values for the Jatropha HEFA pathway; and (3) the verification of the waste gas ethanol-to-jet pathway using updated ethanol-to-jet life-cycle inventories.

Research Approach

Co-processing

Co-processed fuels are produced by upgrading biogenic feedstocks to jet fuel alongside petroleum feedstock in existing refineries. In their current specification (ASTM D1655-20, A.1.2.2 [ASTM International, 2020]), ASTM allows co-processed jet fuels to be produced by co-processing monoglycerides, diglycerides, triglycerides, free fatty acids, and fatty acid esters as biogenic feedstocks at up to 5% inputs by volume through either hydrocracking or hydrotreating and fractionation. For our initial analyses, we limited the scope of the pathways we investigated to hydroprocessing via either a hydrotreater or hydrocracker, depending on the biogenic feedstocks and petroleum-derived distillates used. Figure 1 shows a simplified refinery configuration example using middle distillates and a hydrotreater.

The initial list of feedstocks (Table 1) follows the HEFA SAF feedstocks for which CLCA values have been published (ICAO, 2019). Co-processing is not limited to these feedstocks, and the analysis can be expanded to include other feedstocks.

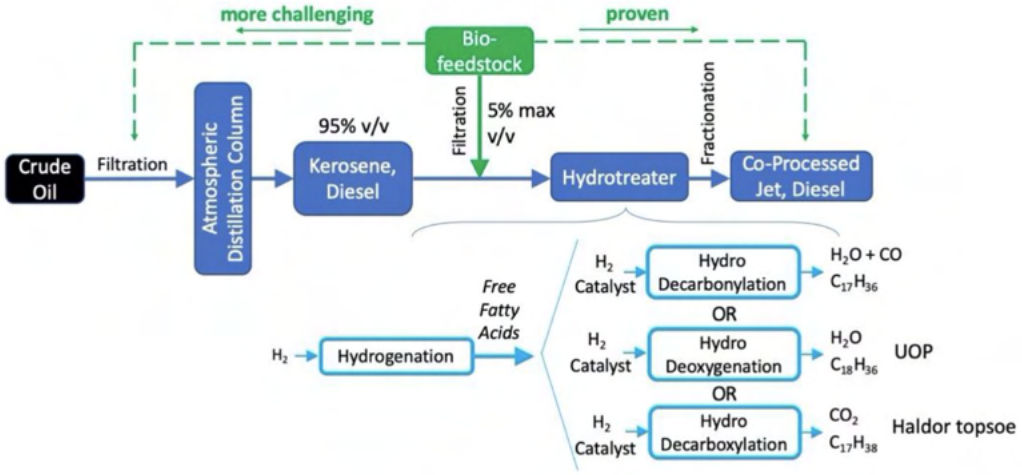

Figure 1. Illustration of co-processing of HEFA bio-feedstock with middle distillates.

Table 1. List of HEFA feedstocks to be considered for co-processing.

Feedstock	Type	Details
Used cooking oil (UCO)	Waste	Cooked vegetable oil
Tallow	By-product	Fats from cattle slaughtering
Palm fatty acid distillate		Stripped from crude palm oil during refined palm oil production
Corn oil		Extracted from distillers dry grains/solubles
Oil crops	Main	Soybean, canola/rapeseed, camelina
Palm oil		Closed (w/methane capture) or open pond (w/o methane capture)
Brassica carinata		Primary summer crop in U.S./Canada

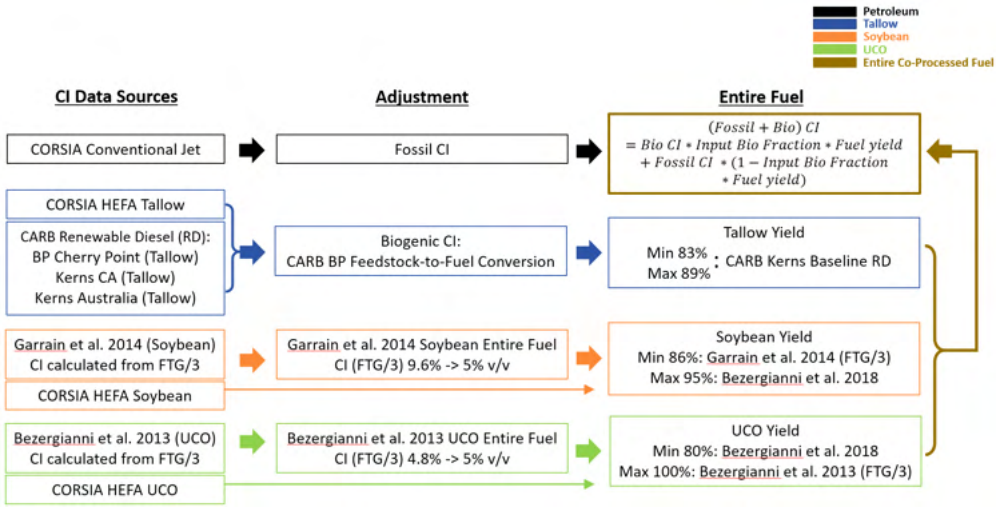

Figure 2. Data sources and adjustments made for carbon intensity (CI) calculation.

For the LCA, the MIT team used a top-down approach that incorporates values from the literature into each step of the well-to-tank LCA and considers three biogenic feedstocks: tallow, used cooking oil (UCO), and soybean oil. The purpose of the top-down approach was to validate the results from the bottom-up LCA led by the Argonne National Laboratory (ANL). Figure 3 shows results of the top-down approach for the biogenic portion of the fuel using adapted data from the academic literature (Garrain et al. [2014], Bezergianni et al. [2013]) and public industry data from renewable diesel production at the refineries in Cherry Point, WA (CARB, 2019) and Kerns in Bakersfield, CA (CARB, 2020). The ranges we obtained generally agreed with the LCA results from the bottom-up approach.

In addition, the MIT team participated in discussions led by the Argonne National Laboratory to perform linear programming modeling of a refinery with and without co-processing, including feedstock choice, feedstock chemical characterization, refinery configuration, and case combination selection. The MIT team also contributed to the marginal allocation method that was ultimately used for the bottom-up approach.

Finally, MIT contributed to the development of the equations to be used for calculating the CI of the entire co-processed fuel, including the petroleum-derived portion, to be considered under CORSIA.

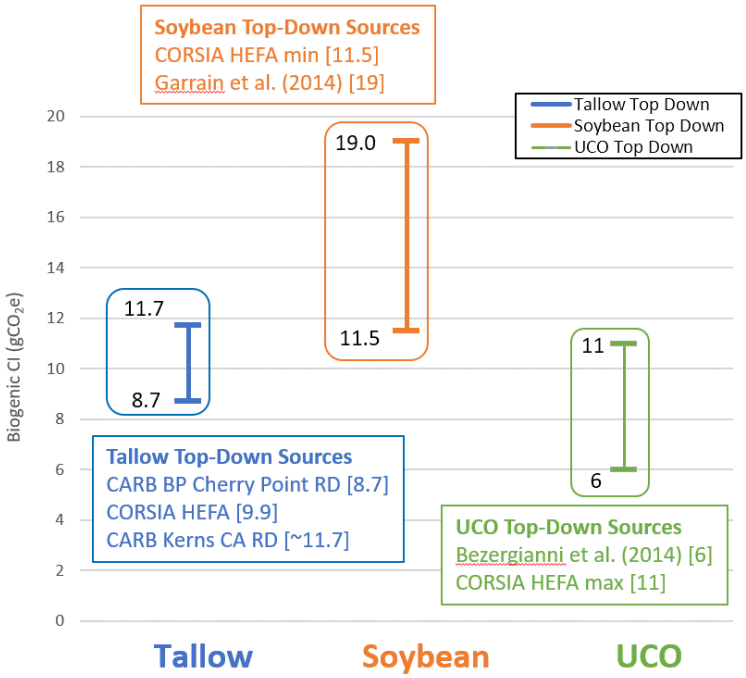

Figure 3. Top-down LCA ranges.

Jatropha HEFA pathway

UHasselt and JRC independently modeled Jatropha-HEFA, in line with the other oilseed-HEFA pathways, and the results were presented at FTG/06. The co-products of the oil extraction process from jatropha are meal, husk, and shell. However, jatropha meal is toxic and therefore cannot be used as fodder unless it is detoxified. During the FTG/06 meeting, experts suggested the development of different pathway values as a function of the meal use and the use of husk and shell as additional co-products. The UHasselt team performed an extensive literature review on jatropha and identified the most likely pathways for oil extraction by-products (see Figure 4). The team then calculated a set of GHG emission values for different scenarios and presented the work to FTG/08. Three different pathways were analyzed, in which it was assumed that jatropha meal could be used as fertilizer, fodder (after detoxification), or combusted for electricity production. All scenarios assumed that the shells and the husks from the process were combusted for electricity generation.

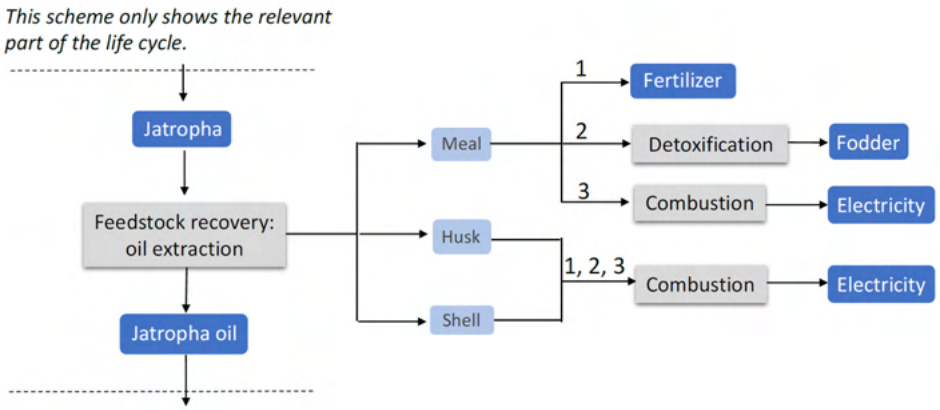

Figure 4. Analyzed pathways for jatropha co-products.

The U.S. and India were considered as world regions for the analysis, and regional electricity mixes were used for each country. UHasselt calculated the CLCA values using the Greenhouse Gases, Regulated Emissions, and Energy Uses in Technologies (GREET) model, and the Argonne National Laboratory verified the calculations. CLCA values for these scenarios ranged between 42.1 and 50.1 gCO_2e/MJ (see Table 1). These values are within the 8.9 gCO2e/MJ envelope that can constitute a fuel production pathway within CORSIA.

Table 1. CLCA values for different scenarios of the jatropha HEFA pathway (in gCO_2e/MJ).

Scenario	Region	Feedstock cultivation	Feedstock transportation	Oil extraction	Oil transportation	Jet fuel production	Jet fuel transportation	Total emissions	Midpoint value
1	US	24.9	0.71	3.66	0.38	12.1	0.37	42.1	
	India	25.9	0.72	3.67	0.38	12.5	0.38	43.6	
2	US	27.3	0.78	4.26	0.38	12.1	0.37	45.2	**46.0**
	India	28.4	0.79	4.29	0.38	12.5	0.38	46.8	
3	US	29.8	0.85	4.87	0.38	12.1	0.37	48.3	
	India	31.0	0.86	4.88	0.38	12.5	0.38	50.1	

CLCA Validation and verification
The UHasselt team served as the verifier for lifecycle analysis on the integrated and standalone waste gas ethanol-to-jet pathway.

Milestones

The work described above has been documented in numerous Working Papers and Information Papers submitted to the FTG. UHasselt and MIT experts participated in and contributed to numerous FTG meetings, including FTG/06 (November 2020), FTG/08 (March 2021), FTG/09 (May 2021), and FTG/10 (July 2021), where these topics were discussed.

Major Accomplishments

The MIT and UHasselt team accomplished the following under this task:

1. The team contributed to analyses and methods that established a default CLCA value for co-processed fuels and provided guidance for calculating actual CLCA values for co-processed fuels.
2. The team provided detailed analyses on the CLCA value for the Jatropha HEFA pathway, which informed discussions within FTG and lead to the approval of default jatropha CLCA default values.
3. The team acted as verifier to the integrated and standalone waste gas to ethanol pathway that led to the approval of default CLCA values for these pathways.

Publications

CAEP/12-FTG/06-WP/02. Summary of the progress of the CLCA Subgroup since FTG/03. November 2020.

CAEP/12-FTG/06-WP/03. Default values for jatropha to HEFA pathways. November 2020.
CAEP/12-FTG/06-IP/04. Summary of progress since FTG/05 on calculating LCA values for fuels produced through co-processing of biogenic feedstock with petroleum feedstock. November 2020.
CAEP/12-FTG/06-FL/02. Proposed Jatropha Assessment Cases. November 2020.
CAEP/12-FTG/08-WP/04. Summary of the progress of the CLCA Subgroup since FTG/07. March 2021.
CAEP/12-FTG/09-WP/04. Life-cycle analysis of co-processed sustainable aviation fuels. May 2021.
CAEP/12-FTG/10-WP/03. Summary of the progress of the CLCA Subgroup since FTG/09. July 2021.

Outreach Efforts

Progress on these tasks was communicated during weekly briefing calls with the FAA and other U.S. delegation members to FTG, as well as during numerous FTG teleconferences between meetings. In addition, UHasselt and MIT experts participated in and contributed to numerous FTG meetings, including FTG/06 (November 2020), FTG/07 (February 2021), FTG/08 (March 2021), FTG/09 (May 2021), and FTG/10 (July 2021).

Awards

None

Student Involvement

TJ Park, Master's degree student at MIT, contributed to the analysis on co-processing.

Plans for Next Period

The team will continue to perform attributional CLCA to establish default values for use under CORSIA. More specifically, the team expects to support efforts to determine CLCA values for co-processed fuels and novel fuel pathways (e.g., catalytic thermolysis), as well as establish additional default CLCA values for pathways such as jatropha HEFA.

References

ASTM International. (2020). Standard specification for aviation turbine fuels (Report No. D1655-20). ASTM International, West Conshohocken, PA. https://doi.org/10.1520/D1655-20

Bezergianni, S., & Dimitriadis, A. (2013). Temperature effect on co-hydroprocessing of heavy gas oil-waste cooking oil mixtures for hybrid diesel production. Fuel *103*, 579–84.

CARB. (2020). California LCFS Tier 2 fuel pathway application: GREET Pathway for the Production of Renewable Diesel from Animal Tallow. (GREET modelling technical support document). CARB, Sacramento, CA, https://ww2.arb.ca.gov/sites/default/files/classic/fuels/lcfs/fuelpathways/comments/tier2/b0079_report.pdf

CARB. (2019). California LCFS Tier 2 fuel pathway application: Renewable diesel produced from co-processed animal fat at the BP Products North America Inc Cherry Point Refinery using natural gas, steam, and electricity as process energy (GREET modelling technical support document). CARB, Sacramento, CA. Retrieved from ww3.arb.ca.gov/sites/default/files/classic/ fuels/lcfs/fuelpathways/comments/tier2/b0018_report.pdf

Garrain, D., Herrara, I., Lechon, Y., & Lago, C. (2014). Well-to-tank environmental analysis of a renewable diesel fuel from vegetable oil through co-processing in a hydrotreatment unit. Biomass and Bioenergy, *63*, 239-249.

ICAO., (2019). CORSIA Eligible Fuels – Life Cycle Assessment Methodology (CORSIA supporting document). ICAO, Montreal, Canada. Retrieved from https://www.icao.int/environmentalprotection/CORSIA/Documents/CORSIA%20Supporting%20Document_CORSIA%20Eligible%20Fuels_LCA%20Methodology.pdf

Task 3 – Contribute to the Development of the Fuel Production Assessment for CORSIA-eligible Fuels

Hasselt University
Massachusetts Institute of Technology

Objective

The UHasselt team aimed to contribute to the development of the fuel production assessment for CORSIA-eligible fuels out to the year 2035. The results of this will then be extrapolated to 2050 and fed into the CAEP Modelling and Databases

Group (MDG) process. During the reporting period, this work was accelerated and re-scoped to inform efforts under ICAO's Long-Term Aspiration Goals (LTAG) Task. The research was completed jointly with researchers from Washington State University and Purdue University.

In addition, the MIT team analyzed potential availability scenarios for fuels leveraging either waste CO_2 sources or atmospheric CO_2 sources, using pathway modeling completed under ASCENT Project 52 as well as data from future hydrogen production scenarios, grid scenarios, and sectoral CO_2 emission projections. The research was completed jointly with researchers from the Argonne National Laboratory.

Research Approach

Fuel production assessment for CORSIA eligible fuels

A short-term projection database on proposed SAF production was generated. This database includes data and references from publicly available production announcements from companies planning to make SAF over the next five years. It only tallies potential SAF production, not LCAF. Using this database, and a set of criteria and assumptions, we modeled a short-term SAF production ramp-up under five production scenarios (low, moderate, high, high+, and max). These scenarios differed with respect to the type of companies included, the maturity of the production plans, and the assumptions concerning product slate and the success rate of announced production plans (see Tables 2 and 3). The resulting ramp-ups from each scenario were then taken as a starting point to forecast SAF production out to 2035 assuming a diffusional approach that will be extended out to 2050.

Table 2. Definition of the short-term SAF production scenarios.

Scenario	Code[a]	Maturity[a]	Facility Jet Fuel Ratio	Overall Success Rate for A Maturity	Overall Success Rate for B Maturity	Overall Success Rate for C Maturity
Low	1	A, B	Actual or low %	25%	10%	0%
Moderate	1-2	A, B, C	Actual or low %	50%	25%	10%
High	1-3	A, B, C	Actual or high% for codes 1-2, Actual or low% for code 3	75%	50%	25%
High+	1-3	A, B, C	High%	75%	50%	25%
Max	1-3	A, B, C	High%	100%	100%	100%

[a] See Table 3.

Figure 5 shows the SAF production estimates derived from the short-term projection database and the developed scenarios, as well as the fit considering the diffusional approach. Figure 6 presents the forecast for SAF production out to 2050. We projected that SAF replaces about 0.5% and 47% of the conventional jet fuel production by 2035 under the most pessimistic and optimistic scenarios, respectively. By 2050, these values could rise to about 7% and 87%, respectively.

Table 3. Codes and maturity level definitions given to the announcements in the short-term database.

Parameter	Criterion
Code	
1	SAF production/facility planned.
2	SAF targeted/mentioned. The company has no specific plans regarding SAF production but mentions something like "we will make green diesel and jet fuel."
3	Process relevant to SAF. The company does not indicate their willingness to produce jet fuel, but the process could theoretically do so.
Maturity level	
A (Very high)	The company is already producing and selling renewable fuel produced using an ASTM qualified pathway.
B (High)	1. The company has one or more of the following: • A plant under construction • A demo or pilot plant built by the company or a partner. These plants depend on their technology maturity (e.g., for HEFA, a newcomer can build a plant) • Credibility of the partnership (e.g., financial backing) 2. Fuel is already certified for use by aviation
C (Moderate)	1. The company has not yet started to produce but has financial partners, off-take agreement, and/or some government support for technology scale-up to commercial demo. 2. The fuel readiness level is greater than or equal to 6 (equivalent to being under evaluation for approval). 3. The company has made some kind communication and/or public information regarding on-going activities over the last 12–18 months.

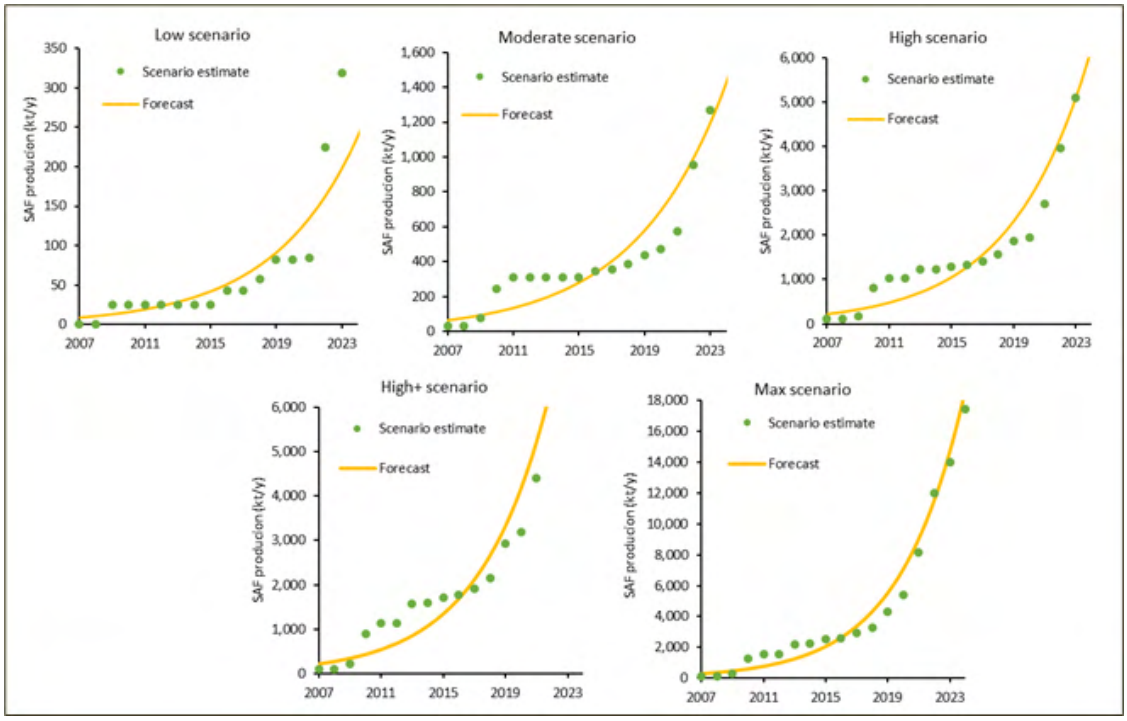

Figure 5. Ramp-up and curve fitting of the SAF production scenario results out to 2025.

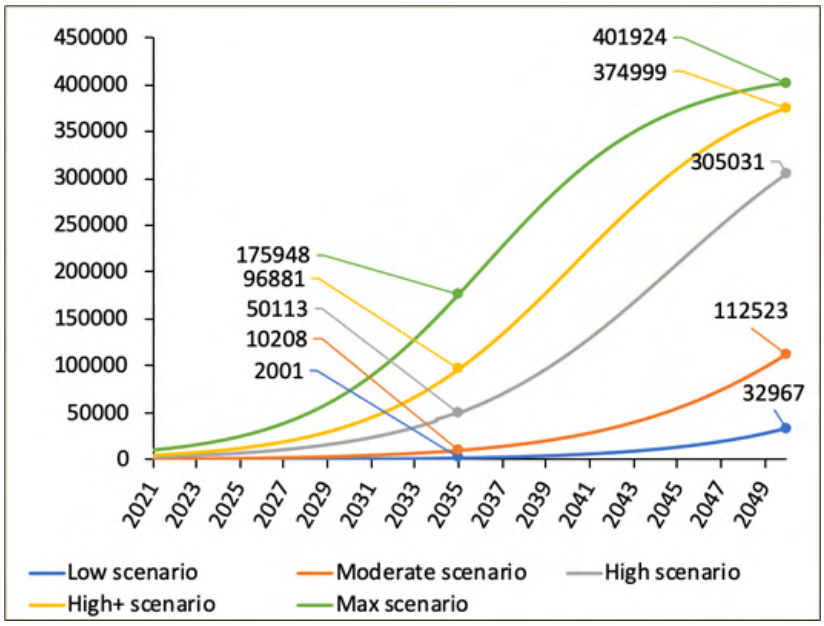

Figure 6. Forecasted SAF production out to 2050 under the analyzed scenarios. Data in kt.

Feedstock portfolios for short-term SAF production were estimated for 2021 considering the information included in the short-term projection database. The feedstock portfolio to 2035 was inferred considering the set of feedstock group-specific SAF production for the year 2050, which was developed during CAEP/10 (see CAEP/10-IP13) assuming a linear evolution of the feedstock breakdown (from 2021 to 2050). These feedstock groups differ in their sustainability assumptions (the "S"-dimension of the analysis with five scenarios), their price and policy emphasis on bioenergy in general (the "A" dimension with 3 scenarios), and their emphasis on SAF production (the "F" dimension with 5 scenarios). Lower A and F values indicate a higher emphasis on bioenergy and SAF, respectively. Thus, the max, high+, high, moderate, and low SAF production scenarios considered a high (A1 and F1 dimensions), moderate (average A1/A2 and F2 dimensions), middle (A2 and F2 dimensions), low (average A2/A3 and F3 dimensions), and very low (A3 and F3 dimensions) emphasis on bioenergy and SAF production, respectively. All SAF production scenarios considered a middle availability of primary sustainable feedstocks (average S2/S3 dimension). Figure 7 shows the evolution of the feedstock portfolio to produce SAF under the analyzed scenarios.

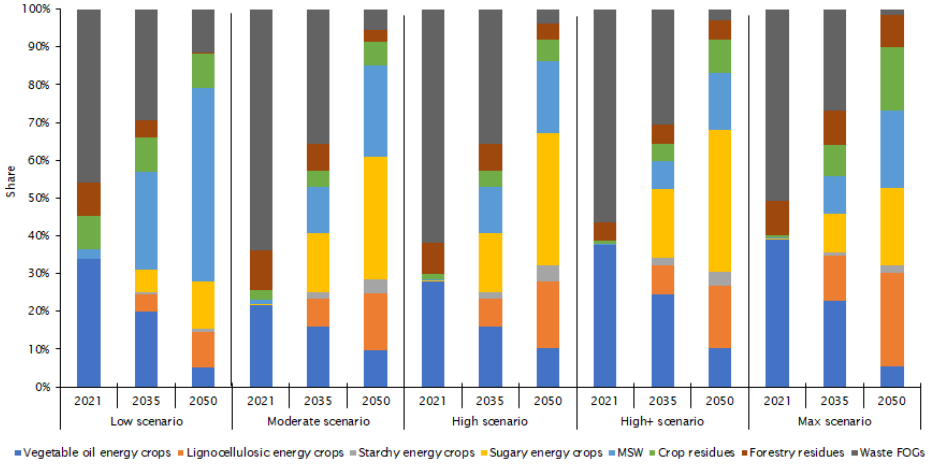

Figure 7. Feedstock portfolio for SAF production in 2021, 2035, and 2050.

Availability scenarios for fuels using waste CO_2 and atmospheric CO_2

We considered three scenarios for fuel availability, defined based on the attainability and readiness of advanced fuel production technologies and certification processes:

- IS1 (low end of the range of potential GHG reductions): high attainability and readiness of fuel production technologies and certification processes. However, waste CO_2 volumes are limited to the most economic sources. Few incentives exist for SAF production.
- IS2 (the middle-of-the-range of potential GHG reductions): medium attainability and readiness for fuel production technologies and certification processes. Use of waste gases for SAF production with expanded waste resource volumes is acknowledged. Increased incentives exist for SAF and LCAF production.
- IS3 (high end of the range of potential GHG reductions): Low attainability and readiness of advanced fuel production technologies and certification processes. Use of both waste and atmospheric gases is assumed. High incentives for GHG emissions reduction.

In each of the integrated scenarios, we assumed that CO_2 came from different subsets of waste CO_2 streams:

- IS1 considers only CO_2 capture from ethanol and ammonia sources with relatively low cost ($20-30 USD per tonne CO_2 for ammonia and ethanol vs. ~$110 USD per tonne CO_2 for iron, steel and cement sources). Fuel conversion is modeled based on the alcohol-to-jet process, with a fuel yield of 0.204 t fuel/t CO_2 at a fraction of jet fuel in the output slate of 70%. In addition, the availability of renewable electricity is considered a potentially limiting factor for producing waste CO_2-based fuels, with power generation limits derived from the International Energy Agency's Stated Policy Scenario.
- IS2 considers CO_2 capture from ethanol and ammonia sources, as well as from the production of iron, steel and cement, given the wide availability of waste CO_2 capture technologies. Fuel conversion is modeled based on the Fischer-Tropsch process, with a fuel yield of 0.272 t fuel/t CO_2 at a fraction of jet fuel in the output slate of 41%. In addition, the availability of renewable electricity is considered a potentially limiting factor for producing waste-CO_2-based fuels, with power generation limits derived from the International Energy Agency's Sustainable Development Scenario.
- IS3 considers the same waste CO_2 sources as IS2, but we model reduced CO_2 availability due to the use of carbon capture and storage following Paltsev et al., 2021. Fuel conversion is assumed based on the Fischer-Tropsch process with a fuel yield of 0.272 t fuel/t CO_2 at a fraction of jet fuel in the output slate of 41%in the same way as IS2. Direct air capture is considered as another source of CO_2 under IS3, with its scale-up being limited according to additional capacity build-up beyond the International Energy Agency's Net Zero Emissions Scenario 2050. In addition, the availability of renewable electricity is considered a potentially limiting factor for production of waste- and atmospheric-CO_2-based fuels, with power generation limits derived from the International Energy Agency's Net-Zero 2050 Scenario.

The potential volumes of fuel from waste gases and atmospheric CO_2 are shown in Figure 8. The integrated scenarios allow the use of different sources of CO_2 and therefore produce different volumes of fuel over time. In IS1 (considering waste CO_2 from ethanol and ammonia only), up to 0.05 Gt/y of jet fuel can be produced from 2040 on. In IS2, the additional use of CO_2 from iron, steel, and cement plants allows a scale-up to 0.3-0.35 Gt/y in the year 2070. In IS3, a mix of fuel production leveraging waste and atmospheric CO_2 reaches 0.35 Gt/y, with an increasing share of direct air capture-based fuels over time as the availability of direct air capture scales up and waste CO_2 streams decrease due to the increased use of carbon capture and storage technologies.

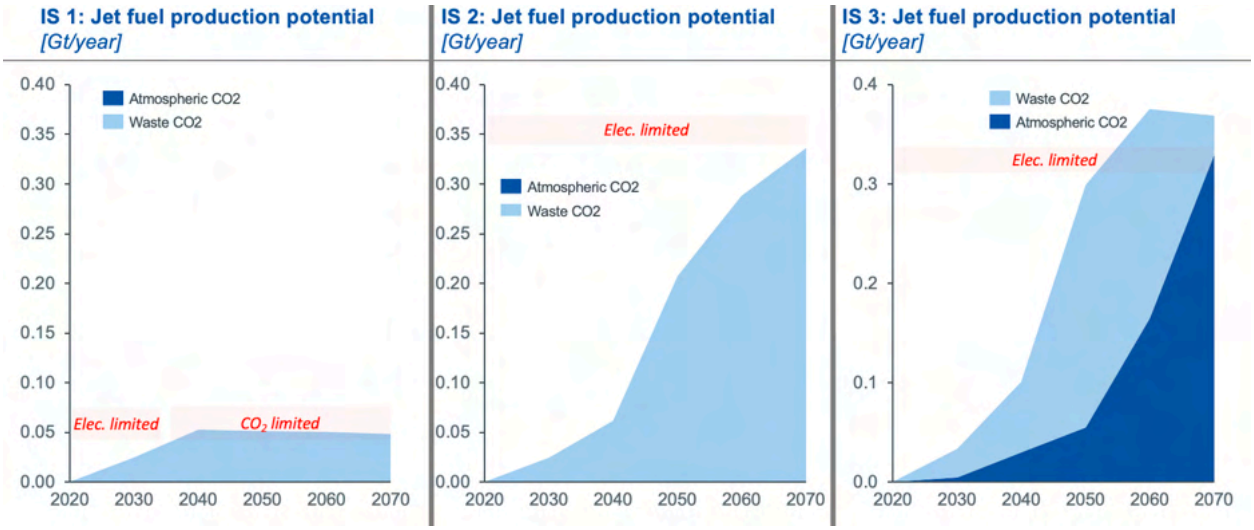

Figure 8. Production potential of PtL fuels in three integrated scenarios using either waste CO_2 (IS1, IS2) or both waste and atmospheric CO_2 (IS3).

Milestone

The work described above has been documented in several Working Papers submitted to the FTG. In addition, both the SAF production scenarios and the fuel production scenarios for fuels produced from waste CO_2 and atmospheric CO_2 provide the scientific basis for the fuel availability assessments under LTAG.

Major Accomplishments

- The team developed comprehensive scenarios of future availability of SAF, presented them to FTG, and provided the data as input to LTAG.
- The team developed comprehensive scenarios of future availability of drop-in fuels produced using Waste CO_2 or Atmospheric CO_2 sources. The data is an input to the LTAG analyses.

Publications

CAEP/12-FTG/06-WP/07: Summary of progress of the Technology Production Policy Task Group. November 2020.
CAEP/12-FTG/07-WP/04: Method for SAF production projections out to 2035. February 2020.
CAEP/12-FTG/07-FL/06: Proposal for the addition of a "SAF-emphasis scenario". February 2021.
CAEP/12-FTG/08-WP/02: Summary of SAF production scenarios and associated GHG emissions reductions. March 2021.
CAEP/12-FTG/08-IP/02: SAF production scenarios and associated GHG emissions reductions. March 2021.
CAEP/12-FTG/08-FL/04: Additional caveats for the reporting of the SAF production scenarios and associated GHG emissions reductions as presented in CAEP/12-FTG/08-WP/02 and IP/02. March 2021.

Outreach Efforts

Progress on these tasks was communicated during weekly briefing calls with the FAA and other U.S. delegation members to FTG, as well as during numerous FTG teleconferences between meetings. In addition, UHasselt and MIT experts participated in and contributed to numerous FTG meetings, including FTG/06 (November 2020), FTG/07 (February 2021), FTG/08 (March 2021), FTG/09 (May 2021), and FTG/10 (July 2021).

Furthermore, results on fuels from waste CO_2 and atmosphericCO_2 were briefed to the LTAG Fuels subgroup in a detailed presentation on May 12, 2021. The team also engaged in detailed discussions with LTAG experts and participated in bi-weekly meetings of the LTAG Fuels subgroup.

The results from the fuel production assessment for CORSIA-eligible fuels were also presented during the ASCENT meeting in Spring 2021.

Awards
None

Student Involvement
None

Plans for Next Period
The team will continue to update scenarios and projections as needed.

Task 4 – Develop Methods for Probabilistic Life-cycle Analyses and Probabilistic Techno-economic Analyses of SAF
Massachusetts Institute of Technology

Objective
Previous studies have shown significant variability and uncertainty in the life cycle emissions of renewable drop-in fuels (e.g., Sills et al., 2012, Fortier 2014). This variability has been addressed by calculating local sensitivities and generating a deterministic range of estimates including maximum, minimum, and most likely values (e.g., Staples et al. 2014, Stratton et al., 2011, Seber et al. 2014, Galligan 2018, Rosen 2017). Uncertainty has been quantified for selected pathways (Suresh et al., 2018); however, a probabilistic quantification of uncertainty across SAF pathways has not yet been performed.

Similarly, MIT previously conducted stochastic techno-economic analysis (TEA) studies for a wide set of feedstock-to-fuel pathways to convert biomass or industrial and household wastes into alternative aviation fuel in the U.S. The resulting literature (e.g., Bann et al., 2017; Yao et al., 2017; Suresh et al., 2018; Pearlson et al., 2013, Seber et al., 2014; Bond et al., 2014; Staples et al., 2014) shows that alternative aviation fuels will remain more expensive to produce than conventional jet fuel in the short- to medium-term, but also highlights the range of potential cost outcomes.

Previous TEA and LCA studies have evaluated nationwide uncertainty but did not intend to capture or disentangle nationwide uncertainty from regional variability in key inputs. Regional variability manifests itself in factors such as yield, utility prices, emissions factors, and capital area cost factors. Under this task, we aim to develop a high-resolution stochastic TEA and LCA model to disentangle the impacts of regional variability and nationwide uncertainty in key input parameters on costs and lifecycle impacts. The results of a combined probabilistic LCA would help researchers, policymakers, technology developers, and investors systematically evaluate the risks and likely emissions outcomes of SAF production and use. In addition, disentangling variability from uncertainty would guide decisionmakers in choosing the most efficient implementation strategies.

These analyses are presented in the context of a fuel production assessment for the U.S. by the year 2035 and provide further insights into the potential for the U.S. to meet certain SAF production goals through domestic SAF production, while accounting for the uncertainties and variabilities associated with future production.

Research Approach
The analysis followed a three-step approach as shown in Figure 9.

First, we calculated feedstock availability in 2035 (for the 15 feedstocks considered) at the county level. Mass and energy balances, for the six feedstock-to-fuel pathways we considered, were modeled based on existing literature. The costs and lifecycle emissions associated with feedstock production, transportation, fuel production, and fuel transportation were quantified using regional data and while accounting for uncertainty. Airport jet fuel demand was calculated at the county level from flight schedule data. For any uncertain inputs or assumptions, Monte Carlo analysis was performed.

Second, based on the costs and emissions model for each feedstock and pathway at each viable location, we ran a supply chain optimization model to determine the minimal-cost SAF supply chain for each run case, subject to the airport jet fuel demand requirements. The model was run across four different land use scenarios for 2035, which make different assumptions about the amount of land that will become available for energy crop cultivation. Additionally, the optimization

model was run for two different carbon emissions costs ($0/tonne CO_2e and $100/tonne CO_2e), to evaluate the impact of carbon pricing on supply chain costs and emissions.

Third, we calculated key outputs, including cost-minimal SAF availability, costs, and GHG emission savings. These metrics allow us to compare the proposed SAF system and traditional petroleum-derived jet fuel.

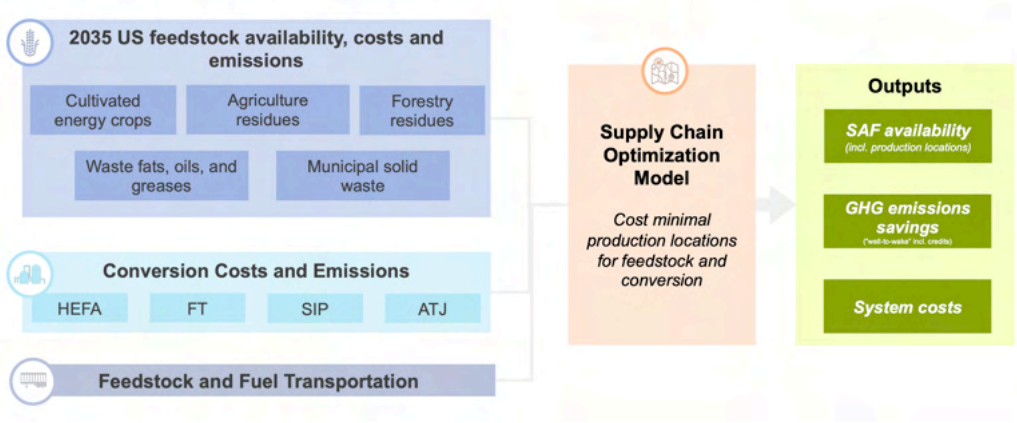

Figure 9. Method of the year-2035 fuel production assessment with stochastic LCA and TEA.

Across all land use scenarios considered, the maximum fraction of jet fuel demand that can be reached is 77.6%. Figure 10 shows the cost-optimal locations for feedstock farms and biorefineries to meet 50% of jet fuel demand in 2035.

Introducing a carbon price had significant impacts on the supply-chain layout. Specifically, a carbon price increased the share of feedstock and conversion pathways with slightly higher costs but lowered lifecycle GHG emissions. In fact, the average per-unit SAF emissions across the supply chain was calculated at 54.1 gCO_2e/MJ without a carbon price. this value declined to 36.6 gCO_2e/MJ with the introduction of a US$100/t$CO_2$e carbon price. The average per-unit SAF costs were $0.75/L and $0.78/L without and with a carbon cost, respectively. Detailed insights into the supply-chain changes are shown in Figure 11.

Supply chain map of a cost-optimized supply chain meeting 50% jet fuel demand

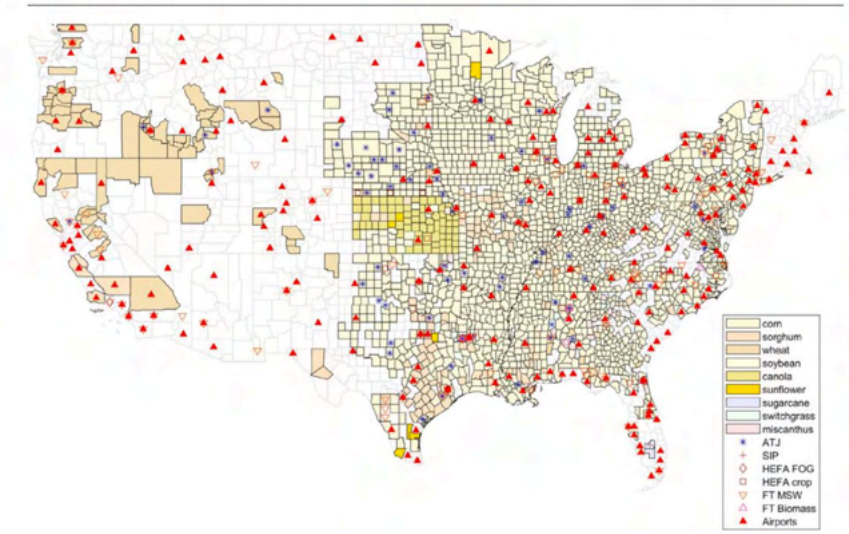

	SAF cost ($/L)	GHG emissions (gCO_2e/MJ)	SAF produced [bn gal]	# plants
AtJ	0.71 [0.63-0.81]	64 [56.5-74.4]	7.33 [4.3-9.9]	72 [44-93]
HEFA crop	0.68 [0.59-0.79]	71.7 [60.9-83.5]	0.60 [0-1.6]	7 [0-22]
HEFA FOG	0.60 [0.49-0.75]	22.7 [21.0-25.0]	0.40 [0.3-0.4]	6 [4-6]
SIP	0.84 [0.52-1.14]	49.5 [34.7-67.9]	0.4 [0.3-0.4]	1 [0-19]
FT Biomass	0.88 [0.79-1.01]	7.6 [4.4-10.3]	2.44 [0.2-5.1]	72 [4-144]
FT MSW	0.36 [0.29-0.46]	25.6 [19.5-31.6]	1.95 [1.8-2.0]	106 [100-111]

Figure 10. Results from the supply chain optimization under a 50% mandate and optimistic yield.

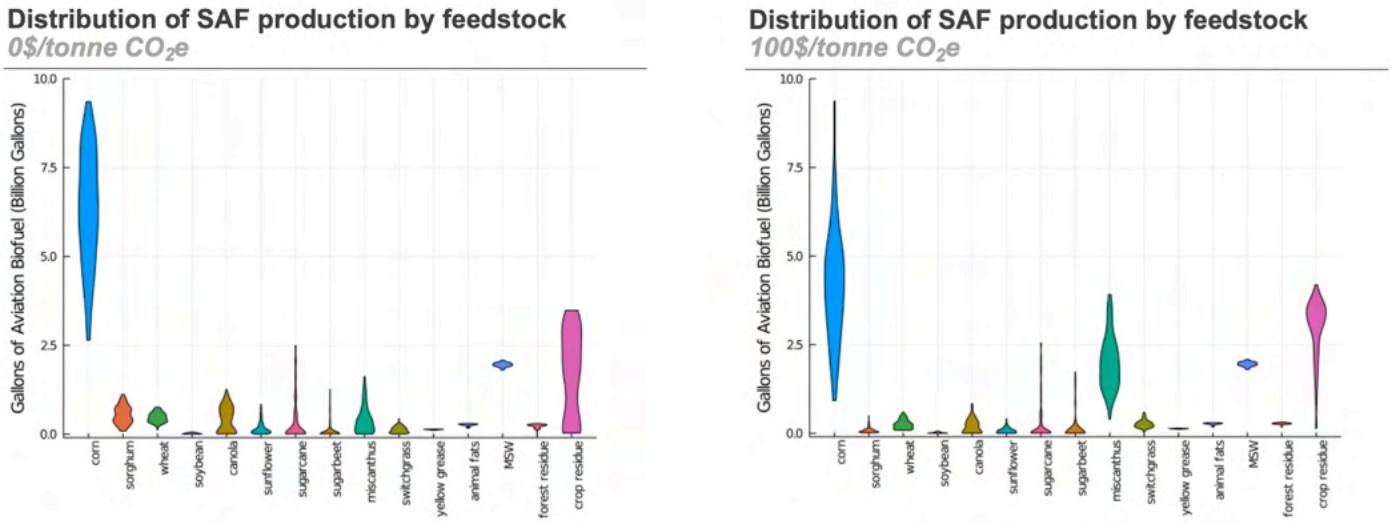

Figure 11. Carbon price sensitivity of the year-2035 feedstock mix under a 50% mandate and optimistic yield.

Milestone
A baseline analysis has been completed and is being prepared for publication in the scientific literature.

Major Accomplishments
A baseline analysis has been completed and is being prepared for publication in the scientific literature.

Publications
Kelso, W. (2021). Cost optimization of U.S. sustainable aviation fuel supply chain under different policy constraints [S.M. Thesis, Massachusetts Institute of Technology]. *To be released soon via MIT DSpace*: https://dspace.mit.edu/

Wang, Z., Staples, M. D., Tyner, W., Zhao, X., Malina, R., Olcay, H., Allroggen, F., & Barrett, S. R. H. (2021). Quantitative policy analysis for sustainable aviation fuel production technologies. Frontiers in Energy Research, *9*. https://doi.org/10.3389/fenrg.2021.751722

Outreach Efforts
MIT presented the work under this task to the ASCENT 1 Team meeting in August 2021.

Awards
None

Student Involvement
The MIT graduate student involved in this task was Walter Kelso, who graduated in the Summer of 2021.

Plans for Next Period
MIT will continue to apply and refine the model. Specifically, the team will add Power-to-Liquid and Power-and-Biomass-to-Liquid pathways and will add assessments of water use. With these additions, the team will conduct further policy analyses.

References
Bann, S. J., Malina, R., Staples, M. D., Suresh, P., Pearlson, M., Tyner, W. E., Hileman, J. I., & Barrett, S. (2017). The costs of production of alternative jet fuel: A harmonized stochastic assessment. Bioresource Technology, *227*, 179-187. https://doi.org/10.1016/j.biortech.2016.12.032

Bond, J. Q., Upadhye, A. A., Olcay, H., Tompsett, G. A., Jae, J., Xing, R., Alonso, D. M., Wang, D., Zhang, T., Kumar, R., Foster, A., Sen, S. M., Maravelias, C. T., Malina, R., Barrett, S. R. H., Lobo, R., Wyman, C. E., Dumesic, J. A., & Huber, G. W. (2014). Production of renewable jet fuel range alkanes and commodity chemicals from integrated catalytic processing of biomass. Energy & Environmental Science, *7*(4), 1500-1523. https://doi.org/10.1039/c3ee43846e

Fortier, M. P., Roberts, G. W., Stagg-Williams, S. M., & Sturm, B. S. (2014). Life cycle assessment of bio-jet fuel from hydrothermal liquefaction of microalgae. Applied Energy, *122*, 73-82. https://doi.org/10.1016/j.apenergy.2014.01.077

Galligan, T. (2018). *Carbon dioxide emissions reduction potential of aviation biofuels in the US* [Master's thesis, Massachusetts Institute of Technology]. Unpublished.

Pearlson, M., Wollersheim, C., & Hileman, J. (2013). A techno-economic review of hydroprocessed renewable esters and fatty acids for jet fuel production. Biofuels, Bioproducts and Biorefining, *7*(1), 89-96. https://doil.org/10.1002/bbb.1378

Rosen, C. (2017). Scenario based lifecycle analysis of greenhouse gas emissions from petroleum-derived transportation fuels in 2050 [Master's thesis, Massachusetts Institute of Technology].

Seber, G., Malina, R., Pearlson, M. N., Olcay, H., Hileman, J. I., & Barrett, S. R. (2014). Environmental and economic assessment of producing hydroprocessed jet and diesel fuel from waste oils and tallow. Biomass and Bioenergy, *67*, 108-118. https://doi.org/10.1016/j.biombioe.2014.04.024

Sills, D. L., Paramita, V., Franke, M. J., Johnson, M. C., Akabas, T. M., Greene, C. H., & Tester, J. W. (2012). Quantitative uncertainty analysis of life cycle assessment for algal biofuel production. Environmental Science & Technology, *47*(2), 687-694. https://doi.org/10.1021/es3029236

Staples, M. D., Malina, R., Olcay, H., Pearlson, M. N., Hileman, J. I., Boies, A., & Barrett, S. R. (2014). Lifecycle greenhouse gas footprint and minimum selling price of renewable diesel and jet fuel from fermentation and advanced fermentation production technologies. Energy & Environmental Science, *7*(5), 1545-1554. https://doi.org/10.1039/c3ee43655a

Stratton, R. W., Wong, H. M., & Hileman, J. I. (2011). Quantifying variability in life cycle greenhouse gas inventories of alternative middle distillate transportation fuels. Environmental Science & Technology, *45*(10), 4637-4644. https://doi.org/10.1021/es102597f

Suresh, P., Malina, R., Staples, M. D., Lizin, S., Olcay, H., Blazy, D., Pearlson, M. N., & Barrett, S. R. H. (2018). Life cycle greenhouse gas emissions and costs of production of diesel and jet fuel from municipal solid waste. Environmental Science & Technology, *52*(21), 12055-12065. https://doi.org/10.1021/acs.est.7b04277

Yao, G., Staples, M. D., Malina, R., & Tyner, W. E. (2017). Stochastic techno-economic analysis of alcohol-to-jet fuel production. Biotechnology for Biofuels, *10*(1). h10.1186/s13068-017-0702-7

Task 5 – Support Coordination of All A01 Universities' Work on SAF Supply-chain Analyses

Massachusetts Institute of Technology

Objective

The objective of this task is to provide support for coordination of all ASCENT Project 1 (A01) Universities' work on SAF supply-chain analysis. The sharing of methods and results decreases the replication of A01 Universities' work on similar topics.

Research Approach

The MIT A01 team performed several functions to accomplish this task. Specifically, the team:

- Participated in the bi-weekly A01 coordination teleconferences, which were used as a venue to discuss progress on various grant tasks and learn about the activities of other ASCENT universities. The team also presented current research on co-processing to the A01 universities.
- Contributed to efforts for developing a special journal issue on SAF based on the research conducted under A01.

Milestone

The MIT ASCENT A01 team presented current research to other ASCENT universities.

Major Accomplishments
The major accomplishments associated with this task include participation in bi-weekly A01 coordination teleconferences; presentation of current research to other ASCENT universities; and contribution to the development of a journal special issue.

Publications
N/A

Outreach Efforts
See above.

Awards
None

Student Involvement
N/A

Plans for Next Period
Continued engagement in bi-weekly teleconferences and other events to disseminate MIT's A01 work.

Project 002 Ambient Conditions Corrections for Nonvolatile Particulate Matter Emissions Measurements

Missouri University of Science and Technology, Aerodyne Research Inc., and Honeywell

Project Lead Investigator

Philip D. Whitefield
Chancellor's Professor of Chemistry
Missouri University of Science and Technology
400 W 11th Street, Rolla, MO 65409
573-341-4420
pwhite@mst.edu

University Participants

Missouri University of Science and Technology (MS&T)

- PI: Philip D. Whitefield, Chancellor's Professor of Chemistry
- FAA Award Number: 13-C-AJFE-MST, Amendments 002, 003, 005, 008, 010, and 012
- Period of Performance: September 18, 2014, to October 31,2022
- Task: Collect nonvolatile particulate matter (nvPM) data in a combustor rig to assess ambient effects on nvPM emissions

Project Funding Level

PROJECT	FUNDING	MATCHING	SOURCE
13-C-AJFE-MST-002	$1,288,836.34	$1,288,836.34	EMPA LETTER
	$284,613.66	$284,613.66	TRANSPORT CANADA
13-C-AJFE-MST-003	$500,000.00	$500,000.00	EMPA LETTER
13-C-AJFE-MST 005	$500,000.00	$500,000.00	EMPA LETTER
13-C-AJFE-MST-008	$579,234.00	$579,234.00	EMPA LETTER
13-C-AJFE-MST-010	$725,500.00	$725,500.00	EMPA LETTER
13-C-AJFE-MST-012	$1,217,221.00	$1,217,221.00	EMPA LETTER

Investigation Team

- Professor Philip Whitefield, Missouri University of Science and Technology
- Steven Achterberg, research technician, Missouri University of Science and Technology
- Max Trueblood, research technician, Missouri University of Science and Technology
- Dr. Richard Miake-Lye, subcontractor, Aerodyne Research, Inc.
- Rudy Dudebout, subcontractor, Honeywell Aerospace
- Paul Yankowich, subcontractor, Honeywell Aerospace

Project Overview

During this reporting period, the MS&T/Aerodyne team collaborated with Honeywell to collect nvPM data for a combustor rig to assess ambient effects on nvPM emissions.

Task 1 – Collect nvPM Data in a Combustor Rig to Assess Ambient Effects on nvPM Emissions

Missouri University of Science and Technology

Objectives

nvPM emissions from aircraft engines are affected by changing inlet conditions. A combustor rig test provides the most flexibility for quantifying the impact of changing conditions on nvPM emissions and developing methods for use in inventory modeling. The MS&T/Aerodyne team has worked with Honeywell to conduct combustor rig tests, collect nvPM mass and number emissions data, and to perform data analysis to determine nvPM ambient corrections.

Research Approach

- Define and assemble a standardized nvPM measurement system that will include the same Mobile Measurement System (MMS) that was used to sample nvPM from 25 Honeywell HTF7350 production engines in 2017
- Design and fabricate the nvPM emission rakes and combustor rig adaptive hardware required to enable nvPM and gaseous emissions data to be acquired from Honeywell's existing HTF7000 Combustor Test Rig
- Perform four combustor rig tests with Jet A and three alternative fuels
- Vary combustor test conditions (derived from engine cycle performance analysis, covering a range of engine ambient inlet conditions on the ground and at altitude) and measure nvPM emissions
- Analyze data to inform performance-based nvPM emissions modeling for all altitudes

Milestones

A rig test matrix has been devised and executed for exclusively burning jet A. Preliminary data analysis has been performed during this reporting period. An outstanding dataset has been acquired albeit under the constraints of the ongoing pandemic protocol restrictions. It was not possible to deploy the entire North American Reference System (NARS) due to travel restrictions associated with the pandemic protocol; however, critical nvPM size measurement capabilities (Cambustion DMS500) were deployed, and their operation was monitored remotely, thus yielding a synchronized size dataset. Analysis of the size data is underway.

Major Accomplishments

- Honeywell and the MS&T/Aerodyne team have assembled two standardized nvPM emissions measurement systems.
- Honeywell has completed the design and fabrication of rakes and adaptive rig hardware required to enable nvPM emissions measurements in the HTF7000 Combustor Test Rig.
- Honeywell has completed the initial set-up of the sampling system and performed the shake-down test.
- Honeywell found some hardware interferences in the shake-down tests, and the necessary corrections have been made. During the pandemic delay, the calibrations required for the Honeywell and NARS nvPM measurement systems expired. Thus, these instruments have undergone recalibration.
- Specifically, data for six different temperature points ranging from idle to 100% thrust with associated variations in corrected flow, fuel air ratio, and pressures were studied with Jet A as the candidate fuel. Facility pressure limitations resulted in a pressure limit of approximately one half of the 100% landing and take-off full-engine pressure. The reported mass-based emissions index (EIm) and noise- based emissions index (Ein) data were corrected for thermophoretic loss. A typical data example is given in Figure 1.

Publications

An informational paper was provided to the Emissions Characterization Task Group of Emissions Technical Working Group 3 (WG3-7) in the 12th cycle of the Committee on Aviation Environmental Protection (CAEP/12) on September 20–24, 2021.

Outreach Efforts

Results were presented at the 7th meeting of the Emissions technical Working group 3 (WG3-7) in the 12th cycle of the Committee on aviation environmental protection (CAEP/12) on September 20-24

Awards

None

Student Involvement

No graduate students were employed in this task; however, three undergraduate research assistants (Christian Hurst, Nicholas Altese, and Susan Donaldson) were employed in pretest activities, including individual component testing and calibration and data reduction and interpretation. This work was halted during Covid restrictions.

Plans for Next Period

- Re-install and perform a shake-down test of the nvPM combustor rig measurement system with rig in the test cell
- Conduct a rig test with Jet A and three sustainable aviation fuel (SAF) blends (Phase II)

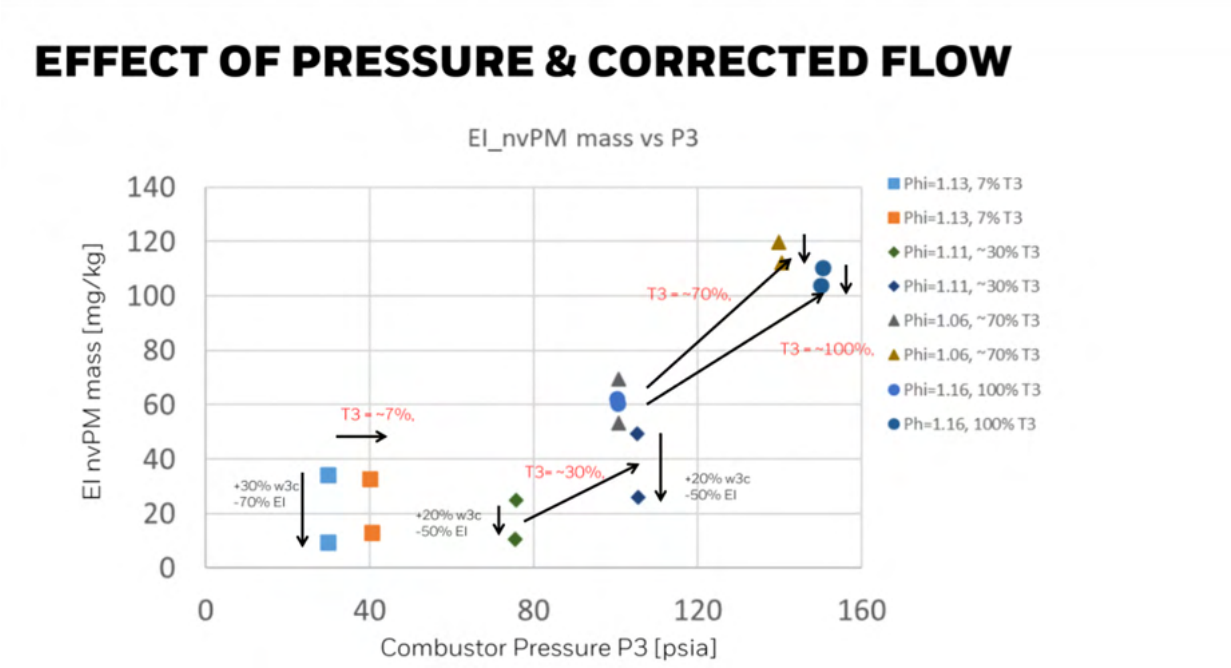

Figure 1. Example of typical data from a preliminary analysis of the test matrix results.

Project 003 Cardiovascular Disease and Aircraft Noise Exposure

Boston University

Project Lead Investigator

Junenette L. Peters
Assistant Professor
Department of Environmental Health
Boston University School of Public Health
715 Albany St., T4W, Boston, MA 02118
617-358-2552
petersj@bu.edu

University Participants

Boston University (BU)

- PIs: Prof. Jonathan Levy (university PI), Prof. Junenette Peters (project PI)
- FAA Award Number: 13-C-AJFE-BU-016
- Period of Performance: October 1, 2020 to September 30, 2021

Massachusetts Institute of Technology (MIT)

- Sub-PI and Co-I: Prof. R. John Hansman, Dr. Florian Allroggen

Tasks (Performance Period)

Related to 2018 FAA Reauthorization, Section 189, Tasks 1-3

1. Write up and publish final results of analysis of hypertension and aircraft noise exposure.
2. Generate results for supporting analyses.
   a. Trends of aircraft noise exposure (preliminary)
   b. Sociodemographic patterning of aircraft noise exposure (final)
3. Generate preliminary results of analysis of sleep quantity and quality and aircraft noise exposure.
4. Generate preliminary results for cardiovascular disease (CVD) and aircraft noise exposure.

Related to 2018 FAA Reauthorization, Section 189, Task 4

5. Develop a model for measuring change in business activities attributable to aircraft noise exposure, prototyping a model city.

Project Funding Level

Total funding (three-year funding): $1,729,286
Matching: $1,729,286
Source of matching funds: Nonfederal donors to the Nurses' Health Study (NHS), Health Professional Follow-up Study (HPFS), and Women's Health Initiative (WHI) cohorts.

Investigation Team

Junenette Peters, PI, Boston University
Dr. Peters is responsible for directing all aspects of the proposed study, including study coordination, design and analysis plans, and co-investigator meetings.

Jonathan Levy, Boston University
Dr. Levy will participate in noise exposure assessment and provide expertise in the area of predictive modeling and air pollution.

Francine Laden, Jaime Hart, and Susan Redline, Harvard Medical School/Brigham and Women's Hospital
Dr. Laden is our NHS and HPFS sponsor for this ancillary study. Dr. Hart will assign aircraft noise exposures to the geocoded address history coordinates of each cohort member. Dr. Laden and Dr. Hart will also assist in documenting data from the NHS and HPFS based on their previous experience in air pollution and chronic disease outcome research in these cohorts and in appropriate analyses of hypertension and cardiovascular outcomes. Dr. Redline will lead efforts related to noise and sleep disturbance in the NHS and WHI.

John Hansman and Florian Allroggen, Massachusetts Institute of Technology
Dr. Hansman will participate in the economic impact assessment and will provide expertise on analytical approaches for quantifying noise. Dr. Allroggen will perform an economic impact assessment based on his expertise in analyzing the societal costs and benefits of aviation.

Project Overview

Exposure to aircraft noise is "the most readily perceived environmental impact of aviation" in communities surrounding airports (Wolfe et al., 2014). Exposure to aircraft noise has been associated with physiological responses and psychological reactions (Bluhm & Eriksson, 2011; Hatfield et al., 2001), including sleep disturbances, sleep-disordered breathing, nervousness, and annoyance (Hatfield et al., 2001; Rosenlund et al., 2001). Recent literature, primarily from European studies, provides evidence of a relationship between aircraft noise and self-reported hypertension (Rosenlund et al., 2001), increased blood pressure (Evrard et al., 2017; Haralabidis et al., 2008; Haralabidis et al., 2011; Jarup et al., 2008; Matsui et al., 2004), antihypertensive medication use (Bluhm & Eriksson, 2011; Floud et al., 2011; Franssen et al., 2004; Greiser et al., 2007), and incidence of hypertension (Dimakopoulou et al., 2017; Eriksson et al., 2010). However, the extent to which aircraft noise exposure increases the risk of adverse health outcomes is not well understood. Impacts related to annoyance have been empirically studied using the stated preference approach (Bristow et al., 2015) and the revealed preference approach, which often relies on analyses of house prices (Almer et al., 2017; Kopsch, 2016; Wadud, 2013). Although the impacts of aircraft noise on individuals are well understood, little evidence has been presented on the impact of aircraft noise exposure on businesses in communities located beneath flight paths. Section 189 of the 2018 FAA Authorization has called for a study on the potential health and economic impacts attributable to aircraft overflight noise.

The goal of this ongoing project is to examine the potential health impacts attributable to noise exposure resulting from aircraft flights; this project will leverage ongoing work within ASCENT to respond to Section 189. This study aims to assess the potential association between aircraft noise exposure and outcomes such as sleep disturbance and elevated blood pressure. The study will leverage existing collaborations with well-recognized and respected studies that have followed over 250,000 participants through the course of their lives to understand factors that affect health. These studies include the NHS and HPFS. Furthermore, this work is aligned with an ongoing National Institutes of Health (NIH)-funded effort to examine these associations in the WHI. The research team will leverage aircraft noise data for 90 U.S. airports from 1995 to 2015, as generated using the Aviation Environmental Design Tool (AEDT); these data will then be linked to demographic, lifestyle, and health data for the participants of long-term health studies. These studies provide considerable geographic coverage of the United States, including all the geographic areas specified in Section 189.

This work will also respond to the aspect of Section 189 calling for the study of economic harm or benefits for businesses located in communities underneath regular flight paths. The study will involve a first-of-its-kind empirical assessment of the economic impacts on businesses located beneath flight paths at selected U.S. airports. Such impacts are expected to be driven by (a) potential positive economic impacts related to the airport and its connectivity, and (b) environmental impacts such as noise, which may reduce the revenue and productivity of businesses beneath flight paths. The team will evaluate whether such impacts can be empirically identified while considering economic outcome metrics such as the gross domestic product (GDP), employment, and revenue.

The overall aims for the three-year project are as follows:

- Perform Tasks 1–3 [*Sec. 189. (b)(1–3)*]: Potential health impacts attributable to aircraft overflight noise.
    - Investigate the relationship between aircraft noise exposure and the incidence of hypertension in the NHS and HPFS, accounting for other individual- and area-level risk factors.
    - Investigate the relationship between aircraft noise exposure and the incidence of cardiovascular disease (CVD) in the NHS and HPFS cohorts and determine whether sufficient data exist to prove a causal relationship.

    - Determine whether a relationship exists between annual average aircraft noise exposure and general sleep length and quality in the NHS and the Growing Up Today Study (GUTS) and report whether sufficient data exist to prove a causal relationship.
    - Evaluate the potential relationship between residing under a flight path and measures of disturbed sleep in the WHI WHISPER sub-study.
- Perform Task 4 [*Sec. 189. (b)(5)*]: Potential economic impacts attributable to aircraft overflight noise.
    - Model noise exposure before and after the introduction of area navigation (RNAV) procedures on the basis of FAA flight trajectory data.
    - Combine noise data with yearly county-level data from the Bureau of Economic Analysis (BEA) (e.g., GDP, employment) and with city-level statistics for the years 2007, 2012, and 2017 from the Economic Census (e.g., revenue, employment).
    - Compare economic outcomes using state-of-the-art econometric approaches while controlling for regional and national economic trends.
    - Evaluate whether the spatial resolution of the available data can significantly impact the study results.

Task 1 - Generate Final Results for Analyses of Aircraft Noise and Hypertension

Boston University

Objective

To generate final results of analyses of aircraft noise (day-night average sound level [DNL]) and hypertension.

Research Approach

We intersected modeled noise exposure surfaces for 1995, 2000, 2005, 2010, and 2015 with geocoded addresses of the participants over the follow-up period. We selected a large set of a priori variables to be examined as confounders and/or effect modifiers and used time-varying Cox proportional hazards models to estimate hypertension or CVD risks associated with time-varying aircraft noise exposure, while adjusting for both fixed and time-varying covariates. We also performed a sensitivity analysis to address potential biases.

Milestones

Generate and submit final results from analyses of aircraft noise (DNL) and hypertension for publication (October 2021).
Present to the Airport Council International (ACI) (March 2021).
Present at the International Commission on Biological Effects of Noise (ICBEN) Congress (June 2021).

Major Accomplishments

- Generated final results of analysis of aircraft noise (DNL) and risk of hypertension.
- Drafted manuscript reporting results of analysis of aircraft noise and hypertension.
- Gained all Harvard/BWH Channing manuscript approvals including undergoing scientific, program, and technical reviews. We also so submitted manuscript for FAA review.
- Submitted the manuscript to a peer-reviewed journal.
- In response to journal reviewer comments, reevaluated the inclusion of variables that could be mediators or colliders (variables that could introduce bias because of their relationships with other variables). We ended up with three models – crude, parsimonious (multivariable excluding potential mediators and colliders), and fully adjusted. The crude model controlled for age and calendar year; the parsimonious model additionally controlled for race, physical activity, smoking status, alcohol use, DASH (dietary approaches to stop hypertension), spouse's education attainment, neighborhood-level socioeconomic status (nSES), and region of residence; and the fully adjusted model additionally controlled for menopausal status, family history of hypertension, and body mass index (BMI).
- We generated results for NHS (original) and NHS II and performed a meta-analysis combining the results from the two cohorts (Figure 1).
- Presented research at the ACI Meeting.
- Presented research at the ICBEN Congress.

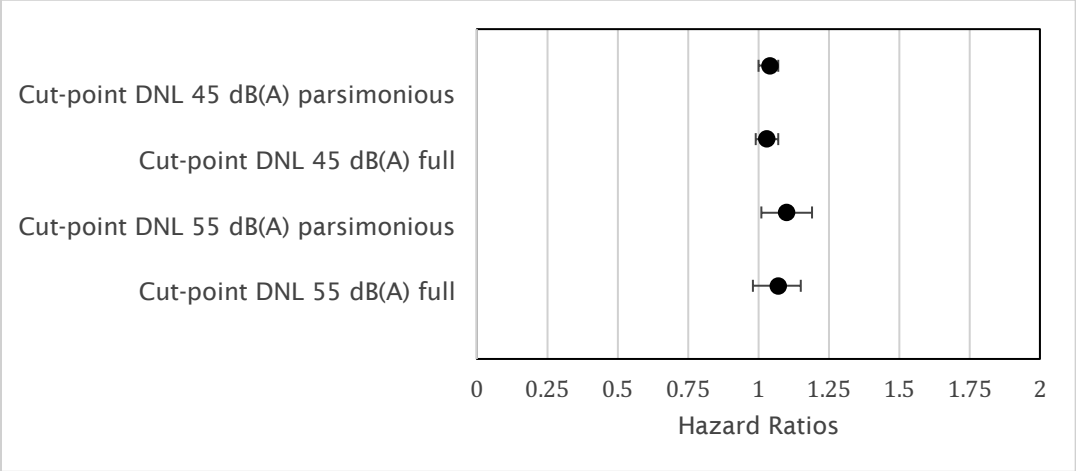

[1]Parsimonious model: Adjusted for age, calendar year, race, physical activity, smoking status, alcohol use, DASH (dietary approaches to stop hypertension), spouse's education attainment, neighborhood-level socioeconomic status (nSES), and region of residence.
[2]Fully-adjusted model: Adjusted for age, calendar year, race, physical activity, smoking status, alcohol use, DASH, spouse's education attainment, nSES, region of residence, menopausal status, family history of hypertension, and body mass index (BMI).

Figure 1. Hazard ratios (95% confidence intervals) for hypertension associated with aircraft noise in the Nurses' Health Study (NHS) and NHS II (meta-analysis), comparing results for day-night average sound level (DNL) ≥45 dB with those for DNL <45 dB and for DNL ≥55 dB with those for DNL <55 dB in the parsimonious[1] and fully adjusted[2] models.

Interpretation using the DNL 55 dB cut-point as an example: In the combined parsimonious model, using a DNL 55 dB cut-point, participants in NHS and NHS II exposed to levels ≥ DNL 55 dB had a 10% increased risk of hypertension compared to participants exposed to levels < DNL 55 dB, with a 95% confidence interval (CI) of 1% to 19%. In the combined fully adjusted model, participants exposed to ≥ DNL 55 dB had a 6% increased risk (95% CI: −2%, 15%) compared with the unexposed. The hazard ratios were relatively stable across the sensitivity analyses including controlling for air pollution. There was an indication that smoking modified the relationship between noise and hypertension.

Task 2 - Generate Preliminary Results from Supporting Analyses: (a) Trends in Aircraft Noise Exposure and (b) Sociodemographic Patterning of Aircraft Noise Exposure

Boston University

Objective

To understand changes in exposure that will facilitate our interpretation of time-varying exposure measures in noise-health analyses and to understand sociodemographic patterning of noise exposure that may confound or modify potential associations of noise and health.

Research Approach

For (a) (Noise Trend), we overlaid noise contours for 2000, 2005, 2010, and 2015 and census block data from the U.S. Census Bureau and American Community Surveys for 2000, 2010, and 2015 in a geographic information system to estimate population changes within noise levels. We will utilize linear fixed-effects models to estimate changes in the sizes of exposure areas based on U.S. census regions/divisions with DNL values ≥65 dB or ≥55 dB. For (b) (Sociodemographic Patterning), we described the characteristics of populations exposed to aviation noise by race/ethnicity and income/education using the U.S. Census Bureau and American Community Survey for 2010 and performed univariate and multivariable hierarchical and multinomial analyses.

Milestones

- Perform supporting analyses characterizing aircraft noise trends and sociodemographic patterns of exposure to aviation noise.
- Submit manuscript reporting results of sociodemographic patterns of exposure to aviation noise.

Major Accomplishments

- Overlaid noise contours for 2000, 2005, 2010, and 2015 and census block data from the U.S. Census Bureau and American Community Surveys for 2000, 2010, and 2015.
- Evaluated the sociodemographic pattern of exposure to aircraft noise over time (2000–2015).
- Evaluated geographic and airport characteristics as predictors of patterns of exposed area over time.
- We determined social patterning of aircraft noise exposure by race/ethnicity and income/education for 2010 using univariate and multivariable analysis (mixed effects, hybrid, and Bayesian approaches) at three DNL cut-points: 45 dB, 55 dB, and 65 dB. Preliminary results are presented in Table 1 (multivariable mixed effects) for airports with at least 100 census block groups at the DNL 65 dB cut-point with and without controlling for distance to the airport.
- In response to journal reviewer/editor comments, we also ran a multivariable model by category of noise exposure DNL 45 to <55 dB, 55 to <65 dB, and ≥65 dB compared with DNL <45 dB (multinomial analysis).

Table 1. Within-airport odds ratio for block group exposure to day-night average sound level (DNL) ≥65 dB (for 15 airports with ≥100 block groups within the study area) for a 10% increase in percent of block group with characteristic using multivariable hybrid mixed-effect logistic model with random intercept by airport.

(N airports = 15; N block groups = 4,031; N block groups exposed = 58)	Main Model[1]	Main model + adjustment for distance to airport
Variables	Odds Ratio (95% CI)	Odds Ratio (95% CI)
% Race/Ethnicity		
Non-Hispanic Black	0.96 (0.89, 1.04)	0.99 (0.90, 1.07)
Non-Hispanic Asian	0.44 (0.30, 0.66)	0.51 (0.34, 0.77)
Hispanic	1.09 (0.96, 1.23)	1.08 (0.96, 1.23)
Non-Hispanic Other	0.82 (0.54, 1.25)	0.88 (0.57, 1.35)
Non-Hispanic White	Reference	Reference
% Education		
< High school diploma or GED	1.08 (0.89, 1.30)	1.10 (0.91, 1.33)
High school diploma or GED	1.11 (0.93, 1.32)	1.15 (0.96, 1.38)
> High school diploma or GED	Reference	Reference
% Household Income		
<$25k	0.99 (0.84, 1.15)	1.01 (0.86, 1.18)
$25k to <$50k	1.10 (0.92, 1.31)	1.13 (0.94, 1.34)
$50k to <$75k	1.17 (0.95, 1.43)	1.20 (0.97, 1.49)
≥$75k	Reference	Reference

[1]Main model adjusted for variables on race/ethnicity, education, household income, and airport.

Task 3 - Assess Suitability of Data on Sleep Quality and Develop a Noise-Sleep Analysis Plan

Boston University

Objective

To identify sleep measures that may be used to evaluate potential associations between noise and sleep outcomes and to perform preliminary analysis of aircraft noise (DNL) and nighttime equivalent sound levels and identified sleep outcomes.

Research Approach

We reviewed the available measures of sleep quality and sleep quantity for the NHS to determine their timing and frequency and their relationship to the timing of the noise exposure data. We also determined which measures were relevant to the average exposure measures. Suitable measures were found, so we developed an analysis plan and presented it to the NHS

and HPFS committees. We selected a large set of a priori variables to be examined as confounders and/or effect modifiers and are using generalized estimating equations to estimate odds from repeated measures of sleep insufficiency over multiple survey years and using conditional logistic regression models of sleep quality to estimate odds for the one survey year.

Milestone

Preliminary results of analysis of DNL and nighttime aircraft noise and sleep quantity and sleep quality in NHS (August 2021)

Major Accomplishments

- Determined timing of sleep measures relevant to exposure for NHS (original).
- Produced descriptive statistics of sleep measures and numbers exposed by measure in NHS.
- Determined relevant confounders and effect modifiers.
- Performed preliminary analysis on noise and sleep quantity (insufficiency) and sleep quality.
- Requested access to data on other environmental factors that could confound or modify the relationship between noise and sleep - light at night and greenness. Incorporated these data and tested variables.
- Wrote and submitted abstract on noise and sleep quantity to International Society of Environmental Epidemiology (ISEE).
- Presented results of analysis at ISEE Conference (example of preliminary results in Figure 2).

Figure 2 shows the odds of sleep insufficiency (defined as ≤6 hr/night) by category of noise exposure (DNL) for models controlling for age and sequentially further adjusted as indicated with (1) other demographics: U.S. region of residence, race, living alone, spouse's education; (2) behaviors: smoking status, alcohol consumption; (3) comorbidities: diabetes, hypertension; and (4) ambient environmental: particulate matter of size 2.5 μm or smaller ($PM_{2.5}$), greenness (normalized difference vegetation index, NDVI), light at night (LAN).

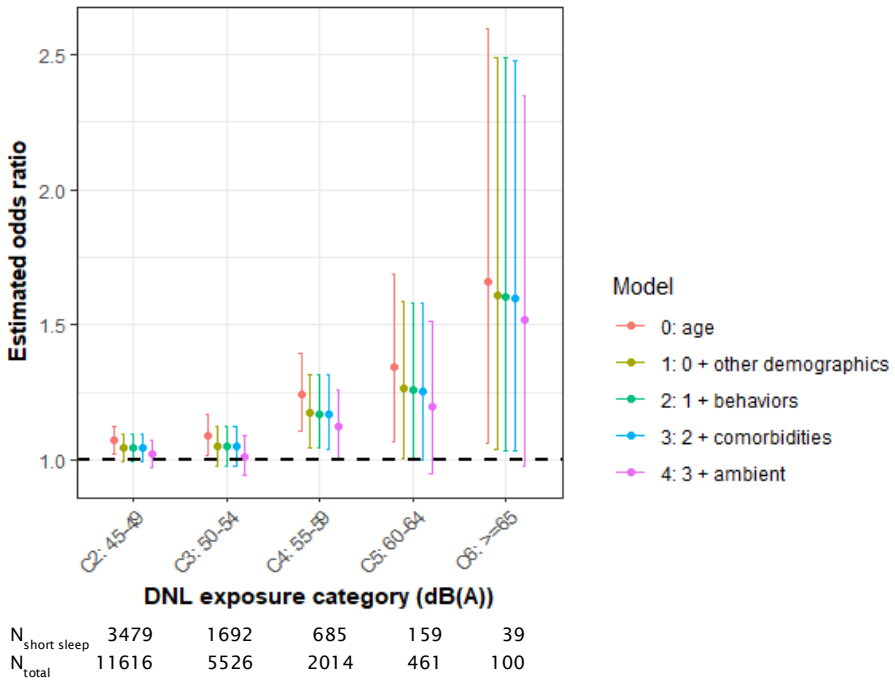

Figure 2. Potential dose-response relationship between DNL (5 exposure categories compared to the reference category <45 dB(A)) and sleep insufficiency.

Task 4 - Develop an Analysis Plan for Cardiovascular Disease and Aircraft Noise and Generate Descriptive Statistics

Boston University

Objective

To generate an analysis plan for studying the potential relationship between CVD and aircraft noise and perform preliminary analyses.

Research Approach

We developed an analysis plan for studying CVD and aircraft noise and gained approval from the NHS and HPFS oversight committees. We designed the statistical analysis and selected a large set of a priori variables to be examined as confounders and/or effect modifiers. We compiled appropriate data sets and ran descriptive statistics. We are using time-varying Cox proportional hazards models to estimate CVD risk associated with time-varying aircraft noise exposure.

Milestone

Preliminary results of analysis of aircraft noise and CVD (August 2021).

Major Accomplishments

- Updated the person-time of people free of CVD at baseline (1995) and number of cases (Table 2).
- Incorporated updated NHS and NHS II data relevant to this analysis.
- Ran preliminary analysis of noise and CVD risk for NHS (Figure 3).

Table 2. Number of CVD cases, including number of exposed cases at different exposure cut-points. DNL = day-night average sound level; NHS = Nurses' Health Study.

	NHS
Total CVD cases	**8,730**
Exposed cases	
≥DNL 45 dB	*599*
≥ DNL 55 dB	*87*
≥ DNL 65 dB	2

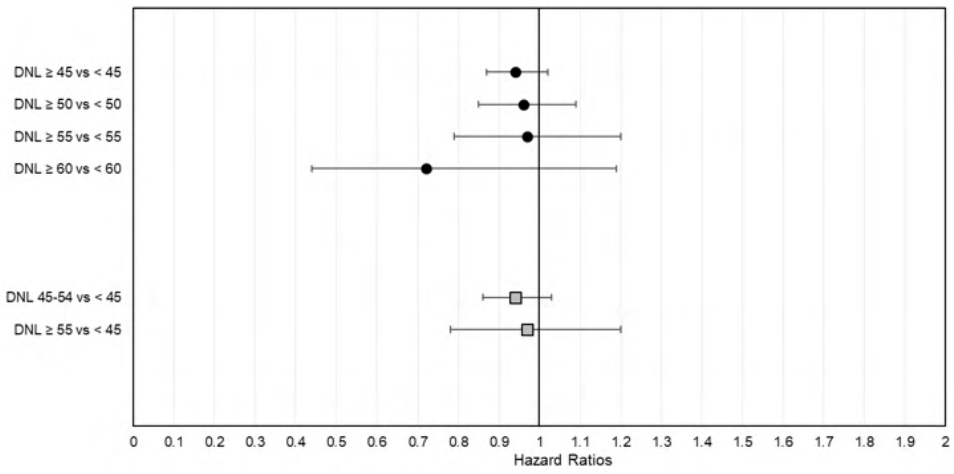

Figure 3. Hazard ratios (95% confidence intervals (CIs)) for CVD associated with aircraft noise in the NHS, comparing results for ≥DNL 45 dB with those for <DNL 45 dB and ≥ DNL 55 dB with those for < DNL 55 dB in crude models and in categorical variables comparing DNL 45-54 dB and > DNL 55 dB to those for < DNL 45 dB (all adjusting for age and calendar years).

Interpretation using DNL 55 dB as an example: In the crude models comparing exposure to DNL ≥55 dB, participants in NHS exposed to DNL ≥55 dB had a 3% decreased risk of CVD compared to participants exposed to DNL <45 dB, with a 95% confidence interval of −22% to 20%.

Task 5 - Develop a Model for Measuring Change in Business Activities Attributable to Aircraft Noise Exposure, Prototyping a Model City

Massachusetts Institute of Technology

Objective

To develop a model for measuring changes in business activities attributable to aircraft noise exposure and begin data analysis to assess potential impacts on business dynamics, controlling for confounding, prototyping one or two cities.

Research Approach

During the current reporting period, the economic impact of noise exposure changes was studied for Boston Logan Airport and Chicago O'Hare Airport. The methods centered on the difference-in-difference approach, which was applied to identify differences between changes in business trends before and after exogenous noise exposure changes such as the introduction of performance-based navigation (PBN) procedures at Boston Logan Airport or the opening of new runway infrastructure at Chicago O'Hare Airport.

The analyses included the following:

- Mapping changes in both noise trends and business activities, which gives insights into the geographical distribution of noise changes and changes in business activities.
- Correlation analysis, which was used to identify whether changes in aviation noise are strongly correlated with local trends in business activities.
- Treatment group analyses, which test whether regions with noise increases or decreases (treatment groups) show business trends that differ significantly from regions where no changes in noise exposure are observed. Treatment groups were defined using different noise change thresholds. In addition to using simple noise-increase and noise-decrease treatment groups, we also studied a set of geographically contiguous treatment groups, which would capture prevalent neighborhood trends).

Milestone

Empirical studies of the impacts of noise exposure changes on local business dynamics were completed for Boston Logan Airport and Chicago O'Hare Airport (September 2021).

Major Accomplishments

- Completed a review of the validity and internal consistency of high-resolution business data that is used to determine changes in economic outcomes; business data were cleaned and reorganized.
- Identified necessary noise data required for comparing between and within cities and determined the timeline for obtaining that data.
- In our preliminary case studies for Boston Logan Airport (BOS), no significant relationship between noise exposure and business dynamics has yet been found (see Figures 5 and 6).
- Ran a full set of analyses for Boston Logan Airport and Chicago O'Hare Airport (ORD). By way of example, we include here results for selected analyses of noise trends and changes in business activity in Figures 4 to 7.

Figure 4 shows changes in both noise exposure and local business dynamics (measured through the number of businesses) for Chicago O'Hare Airport. The mapping does not reveal a strong visible relationship between noise changes and changes in business dynamics. Figure 5 plots local changes in noise exposure and business activity, again revealing no clearly visible trends. Outliers were studied in detail to ensure that they are not case studies for situations in which strong impacts of noise on business activities must be suspected.

Figure 6 shows the results of empirical testing procedures, which were conducted to identify significant differences in business dynamics between treatment and nontreatment areas (see Research Approach for definitions). The results do not

point toward any statistically significant differences, irrespective of the applied noise thresholds. The analysis was repeated for geographically contiguous treatment groups, which again did not yield significant results (see Figure 7).

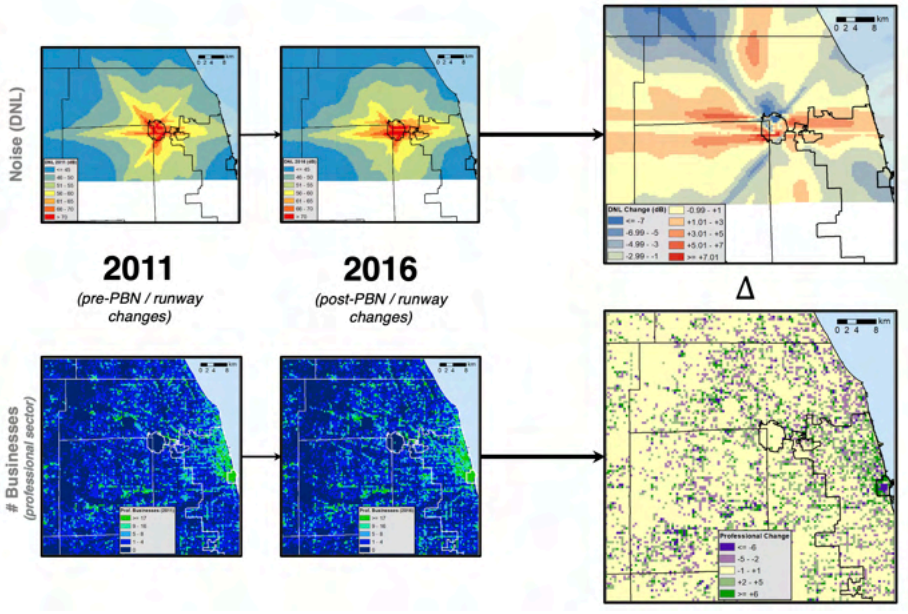

Figure 4. Geospatial analysis of changes in noise exposure and business activities for Chicago O'Hare Airport. PBN = performance-based navigation.

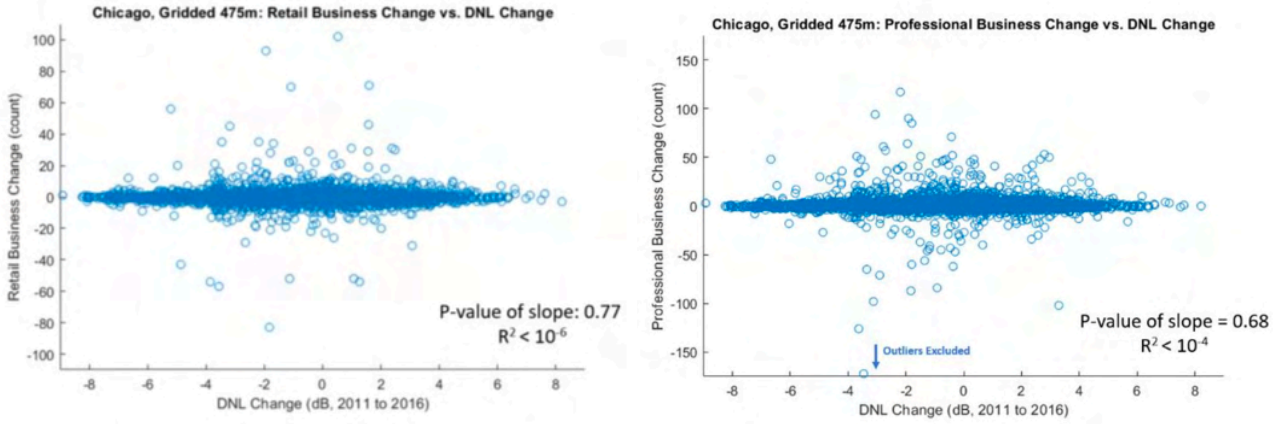

Figure 5. Correlation analysis of noise exposure changes and local business dynamics in the retail sector (left panel) and the professional business sector (right panel) for Chicago O'Hare Airport. DNL = day-night average sound level.

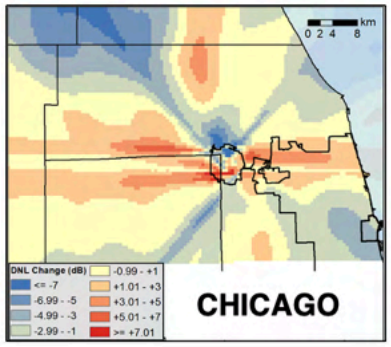

Nontreatment : Noise Change ≥ -1 and ≤ +1	Noise increase ≥ 1 dB	Noise increase ≥ 2 dB	Noise increase ≥ 4 dB	Noise decrease ≤ -1 dB	Noise decrease ≤ -2 dB	Noise decrease ≤ -4 dB
Mean: -0.15	Mean: -0.25 DoM: +0.10	Mean: -0.24 DoM: +0.09	Mean: +0.09 DoM: -0.24	Mean: -0.22 DoM: +0.07	Mean: -0.25 DoM: +0.10	Mean: -0.12 DoM: -0.03

Mean = Average change in business # by grid cell 2011-2016 * α < 0.1 ** α < 0.05
DoM = Difference in mean between control group vs. treatment group

Figure 6. Significance testing of business trends in treatment groups vs. control groups for the retail sector around Chicago O'Hare Airport.

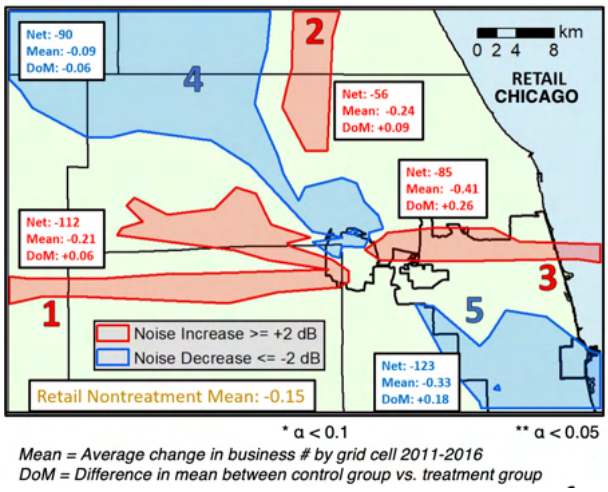

Figure 7. Significance testing of business trends in geographically contiguous treatment versus control groups for the retail sector around Chicago O'Hare Airport.

Publications

Bullock, C. (2021). Aviation effects on local business: Mapping community impact and policy strategies for noise remediation. [S.M. thesis, Massachusetts Institute of Technology].

Kim, C. S., Grady, S. T., Hart, J. E., Laden, F., VoPham, T., Nguyen, D. D., Manson, J. E., James, P., Forman, J. P., Rexrode, K. M., Levy, J. I., & Peters, J. L. (2021). Long-term aircraft noise exposure and risk of hypertension in the Nurses' Health Studies. Environmental research, 112195. Advance online publication. https://doi.org/10.1016/j.envres.2021.112195

Outreach Efforts

Presented on current progress orally during the ASCENT Spring Meeting (April 27–29, 2021) and during the ASCENT Fall Meeting (October 26–28, 2021).

Presented on "Associations between aircraft noise exposure and insufficient sleep in the US-based prospective Nurses' Health Study I cohort" at the International Society of Environmental Epidemiology (ISEE) conference, August 23-26, 2021.

Presented on "Long-term aircraft noise exposure and incident hypertension in national US cohort studies" at the International Commission on Biological Effects of Noise (ICBEN) Congress on June 15, 2021.

Presented on "Aircraft Noise and Health Research" to the Airport Council International (ACI) on March 23, 2021.

Awards

None.

Student Involvement

The dissertation of Chloe Kim (doctoral graduate, BU) included the development and implementation of statistical analyses on the noise and hypertension risk. Chloe Kim graduated in the fall of 2019 and is currently working for the Environmental Science, Policy, and Research Institute.

The dissertation of Daniel Nguyen (doctoral candidate, BU) includes a characterization of the temporal trends in aviation noise surrounding U.S. airports.

The research rotation of Stephanie Grady (doctoral student, BU) includes the development and running of statistical analyses on noise and cardiovascular event risk, which will continue as part of her dissertation. Stephanie also worked with Chloe Kim on noise and hypertension risk.

Carson Bullock (master's student, MIT) conducted economic impact analysis and graduated in the summer of 2021.

Plans for Next Period

(October 1, 2020 to September 30, 2022)

Related to 2018 FAA Reauthorization, Section 189, Tasks 1–3

- Assign noise exposure estimates to participants for nighttime equivalent sound level metrics to NHS II.
- Continue analyses to estimate the risk of CVD events associated with aircraft noise exposure.
- Complete analyses to evaluate the relationship between noise and sleep.
- Verify, document, and publish results.

Related to 2018 FAA Reauthorization, Section 189, Task 4

- Verify and document results.
- Consider analyses of additional airports.

References

Allroggen, F., & Malina, R. (2014). Do the regional growth effects of air transport differ among airports? Journal of Air Transport Management. *37*,1-4.

Brueckner, J. K. (2003). Airline traffic and urban economic development. Urban Studies. *40*(8),1455-1469.

Campante, F., & Yanagizawa-Drott, D. (2018). Long-range growth: Economic development in the global network of air links. Quarterly Journal of Economics. *133*(3),1395-1458.

Lakshmanan, T. R. (2011). The broader economic consequences of transport infrastructure investments. Journal of Transport Geography. *19*(1),1-12.

Project Overview References

Almer, C., Boes, S., & Nuesch, S. (2017). Adjustments in the housing market after an environmental shock: Evidence from a large-scale change in aircraft noise exposure. Oxford Economic Papers. *69*(4),918-938.

Bluhm, G., & Eriksson, C. (2011). Cardiovascular effects of environmental noise: Research in Sweden. Noise and Health. *13*(52), 212-216.

Bristow, A. L., Wardman, M., & Chintakayala, V. P. K. (2015). International meta-analysis of stated preference studies of transportation noise nuisance. Transportation. *42*(1), 71-100.

Dimakopoulou, K., Koutentakis, K., Papageorgiou, I., Kasdagli, M. I., Haralabidis, A. S., Sourtzi, P., Samoli, E., Houthuijs, D., Swart, W., Hansell, A. L., & Katsouyanni, K. (2017). Is aircraft noise exposure associated with cardiovascular disease and hypertension? Results from a cohort study in Athens, Greece. Occupational and Environmental Medicine. *74*(11), 830-837.

Eriksson, C., Bluhm, G., Hilding, A., Ostenson, C. G., & Pershagen, G. (2010). Aircraft noise and incidence of hypertension--gender specific effects. Environmental Research. *110*(8), 764-772.

Evrard, A. S., Lefevre, M., Champelovier, P., Lambert, J., & Laumon, B. (2017). Does aircraft noise exposure increase the risk of hypertension in the population living near airports in France? Occupational and Environmental Medicine. *74*(2), 123-129.

Floud, S., Vigna-Taglianti, F., Hansell, A., Blangiardo, M., Houthuijs, D., Breugelmans, O., Cadum, E., Babisch, W., Selander, J., Pershagen, G., Antoniotti, M. C., Pisani, S., Dimakopoulou, K., Haralabidis, A. S., Velonakis, V., Jarup, L., & HYENA Study Team. (2011). Medication use in relation to noise from aircraft and road traffic in six European countries: Results of the HYENA study. Occupational and Environmental Medicine. *68*(7), 518-524.

Franssen, E. A., van Wiechen, C. M., Nagelkerke, N. J., & Lebret, E. (2004). Aircraft noise around a large international airport and its impact on general health and medication use. Occupational and Environmental Medicine. *61*(5), 405-413.

Greiser, E., Janhsen, K., & Greiser, C. (2007). Air traffic noise increases prescriptions of cardiovascular drugs in the vicinity of a major airport. Epidemiology. *18*(5), S33-S33.

Haralabidis, A. S., Dimakopoulou, K., Vigna-Taglianti, F., Giampaolo, M., Borgini, A., Dudley, M. L., Pershagen, G., Bluhm, G., Houthuijs, D., Babisch, W., Velonakis, M., Katsouyanni, K., Jarup, L., & HYENA Consortium. (2008). Acute effects of night-time noise exposure on blood pressure in populations living near airports. European Heart Journal. *29*(5), 658-664.

Haralabidis, A. S., Dimakopoulou, K., Velonaki, V, Barbaglia, G., Mussin, M., Giampaolo, M., Selander, J., Pershagen, G., Dudley, M. L., Babisch, W., Swart, W., Katsouyanni, K., Jarup, L., & HYENA Consortium. (2011). Can exposure to noise affect the 24 h blood pressure profile? Results from the HYENA study. Journal of Epidemiology and Community Health. *65*(6), 535-541.

Hatfield, J., Job, R., Carter, N. L., Peploe, P., Taylor, R., & Morrell, S. (2001). The influence of psychological factors on self-reported physiological effects of noise. Noise and Health. *3*(10), 1-13.

Jarup, L., Babisch, W., Houthuijs, D., Pershagen, G., Katsouyanni, K., Cadum, E., Dudley, M. L., Savigny, P., Seiffert, I., Swart, W., Breugelmans, O., Bluhm, G., Selander, J., Haralabidis, A., Dimakopoulou, K., Sourtzi, P., Velonakis, M., Vigna-Taglianti, F., & HYENA Study Team. (2008). Hypertension and exposure to noise near airports: The HYENA study. Environmental Health Perspectives. *116*(3), 329-333.

Kopsch, F. (2016). The cost of aircraft noise - does it differ from road noise? A meta-analysis. Journal of Air Transport Management. *57*, 138-142.

Matsui, T., Uehara, T., Miyakita, T., Hiramatsu, K., Yasutaka, O., & Yamamoto, T. (2004). The Okinawa study: Effects of chronic aircraft noise on blood pressure and some other physiological indices. Journal of Sound and Vibration. *277,* 469-470.

Rosenlund, M., Berglind, N., Pershagen, G., Jarup, L., & Bluhm, G. (2001). Increased prevalence of hypertension in a population exposed to aircraft noise. Occupational and Environmental Medicine. *58*(12), 769-773.

Wolfe, P. J., Yim, S. H. L., Lee, G., Ashok, A., Barrett, S. R. H., & Waitz, I. A. (2014). Near-airport distribution of the environmental costs of aviation. Transport Policy. *34*, 102-108.

Project 009 Geospatially Driven Noise Estimation Module

Georgia Institute of Technology

Project Lead Investigators

Dimitri N. Mavris
Director, Aerospace Systems Design Laboratory
School of Aerospace Engineering
Georgia Institute of Technology
(404) 894-1557
dimitri.mavris@ae.gatech.edu

Holger Pfaender
Research Engineer II
Aerospace Systems Design Laboratory
School of Aerospace Engineering
Georgia Institute of Technology
(404) 385-2779
holger.pfaender@ae.gatech.edu

University Participants

Georgia Institute of Technology

- PI(s): Dr. Dimitri Mavris, Director, Aerospace Systems Design Laboratory; Dr. Holger Pfaender, Research Engineer II
- FAA Award Number: 13-C-AJFE-GIT-059
- Period of Performance: October 1, 2020 to September 30, 2021
- Tasks:
    1. Literature review and GIS software evaluation
    2. Investigation of emerging computational technologies
    3. Collaboration with the unmanned aircraft systems (UAS) Computation Module Development Team
    4. Noise computation engine integration

Project Funding Level

This project is funded at the following levels. Georgia Institute of Technology: $249,999. The Georgia Institute of Technology has agreed to a total of $83,333 in matching funds. This total includes salaries for the project director, research engineers, and graduate research assistants, and funds for computing, financial, and administrative support, including meeting arrangements. The institute has also agreed to provide tuition remission for students whose tuition is paid via state funding.

Investigation Team

Georgia Institute of Technology

- PI: Dimitri Mavris
- Co-Investigator: Holger Pfaender
- Graduate Students: Aroua Gharbi, Joaquin Matticoli, and Martin Delage

Project Overview

The goal of this task is to develop a novel geospatially driven noise estimation module to support the computation of noise resulting from the operation of UAS and other upcoming vehicle concepts. The development of the module will leverage emerging computational technologies to achieve fast and efficient modeling of a potentially large number of vehicles and operations. The module will be designed to be integrated as a component module or plug-in to other applications relying on a Geographic Information System (GIS) interface. The noise estimation approach will be based on the concept of precomputed

noise grid tiles addition. The module's design phase will identify which emerging open-source geospatial and data processing technologies would be best suited to serve as the module's computational infrastructure and assess whether these technologies could provide innovative, maintainable, and affordable solutions.

Task 1 – Literature Review and GIS Software Evaluation

Georgia Institute of Technology

Objectives

This task aims to identify the most appropriate open-source GIS software according to preset evaluation criteria.

Research Approach

This review focused on open-source options. For adequate evaluation of the options, six preset criteria were determined:

1. Data import: ability to read the shapefile format of input geometrical data and rasterized (gridded) data
2. Data storage: ability to store geospatial data in either shape/vector formats, or rasterized data
3. Geometric calculations: conversion to and from a Cartesian coordinate system and other Earth model coordinates, and ability to compute polygon areas and lengths, as well as unions and intersections.
4. Geospatial calculations: ability to perform calculations on given vector or raster data and draw contour plots
5. Display: ability to print raw or processed geospatial data as various map displays
6. Map data: ability to display results with relation to landmasses, political boundaries (such as states and counties), and roads and buildings

In addition to software evaluation, GIS applications were investigated to examine the option of creating a stand-alone, customized library or component.

GIS Libraries

QGIS

QGIS is a user-friendly open-source GIS written in C++. It runs on Linux, Unix, Macintosh OSX, Windows, and Android, and it supports numerous vector, raster, and database formats and functionalities. Beyond the built-in functionalities, QGIS allows users to install and create their own plugins. New applications can also be created In QGIS with the C++ and Python languages.

Figure 1. Screenshot of QGIS.

Evaluation Criteria

1. Data import: imports files in shapefile and raster format
2. Data storage: stores geospatial data in vector and raster formats
3. Geometric calculations: supports Cartesian (*x*, *y*), polar (length, angle), and projected (*x*, north; *y*, east) coordinate systems; calculates lengths or areas of geometry features; and provides overlay, union and difference between areas.

4. Geospatial calculations: creates vector contour maps from an elevation raster; performs raster-to-vector conversion
5. Display: web mapping with QGIS2Web
6. Map data: displays geospatial data, such as countries, states, and counties, as well as roads

Open JUMP
OpenJUMP is a Java-based open-source GIS. It works on the Windows, Linux, and Macintosh platforms with Java 1.7 or later. OpenJUMP's features include reading and writing vector formats, displaying geospatial data, and executing geometric calculations. Additional plugins for more capabilities are also available.

Evaluation Criteria
1. Data import: imports files in shapefile and raster format
2. Data storage: stores geospatial data in vector and raster formats
3. Geometric calculations: supports coordinate reference system (CRS), and Cartesian (*x*, *y*, *z*), geographic (longitude, latitude, height), and projected (*x*, north; *y*, east) coordinate systems; provides a CRS transformation library called PROJ; calculates lengths or areas of geometry features; provides overlay, union, and subtraction capabilities
4. Geospatial calculations: enables conversion between desired file formats (raster-to-vector conversion); does not feature a contour plot
5. Display: does not provide a web application
6. Map data: displays geospatial data, such as countries, states, and counties, as well as roads

System for Automated Geoscientific Analyses (SAGA)
SAGA is an open-source cross-platform GIS software written in C++. It can be run on Windows, Linux, FreeBSD, and Macintosh OS X. SAGA provides multiple libraries for GIS calculations, such as digital terrain analysis, image segmentation, fire-spreading analysis and simulations. In addition, SAGA allows for scripting of custom models through the command line interface and the Python interface.

Evaluation Criteria
1. Data import: imports files in shapefile and raster format
2. Data storage: stores geospatial data in vector and raster formats
3. Geometric calculations: supports geographic coordinate system (latitude, longitude) and universal transverse Mercator coordinate systems
4. Geospatial calculations: performs raster-to-vector conversion and can create contour lines
5. Display: displays data with histograms and scatter plots; provides a web-mapping service
6. Map data: enables visualization of spatial data in cartographic maps; can also import maps from Web Map Service and OpenStreetMap

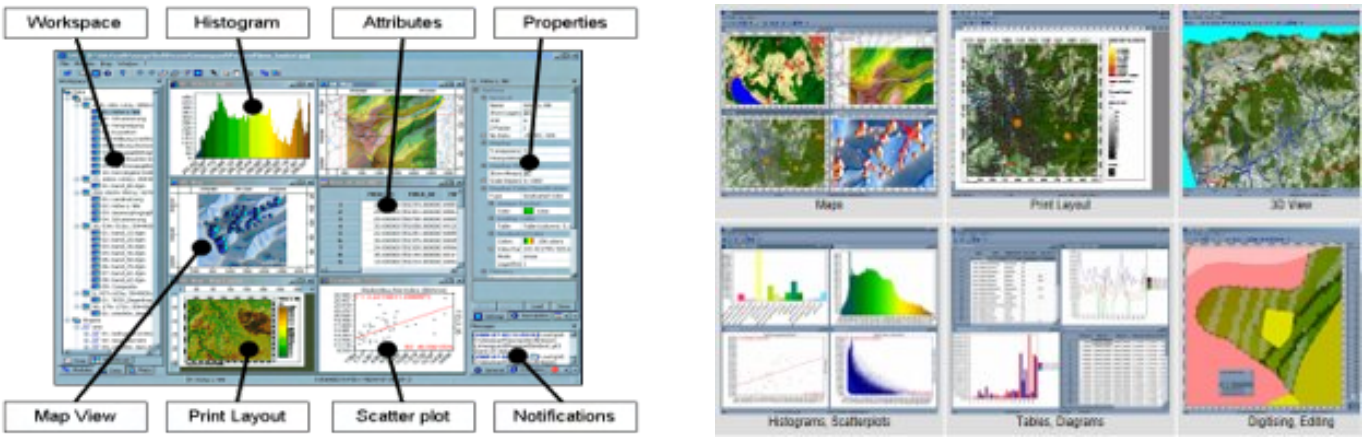

Figure 2. Screenshot of SAGA.

Deck.gl
Deck.gl is a WebGL visualization framework for large data sets. It allows users to map data (JSON objects, csv) into stacks of layers. These layers can be imported directly from a catalog or built by the user.

Evaluation Criteria
1. Data import: reads only csv files
2. Data storage: does not store geospatial data in vector or shapefile format
3. Geometric calculations: supports geographic coordinate system (latitude, longitude), using Web Mercator
4. Geospatial calculations: does not convert raster data to vector data; creates contour lines for a given threshold and cell size
5. Display: offers an architecture for packaging advanced WebGL based visualizations; enables users to quickly and easily obtain impressive visual results
6. Map data: easily displays geospatial data with relation to roads and buildings

Geographic Resources Analysis Support System (GRASS) GIS
GRASS GIS is an open-source Java-based software for vector and raster geospatial-data management, geoprocessing, spatial modeling, and visualization. Because is compatible with QGIS, QGIS can run some features of GRASS GIS as a plugin. Developed add-ons are available, and users can also develop their own add-ons.

Evaluation Criteria
1. Data import: imports vector and raster files
2. Data storage: stores geospatial data in vector and raster formats
3. Geometric calculations: supports CRS, Cartesian (*x*, *y*, *z*), and geographic (longitude, latitude, height) coordinate systems; provides a CRS transformation library called PROJ; calculates lengths or areas of geometry features; provides overlay, union, and subtraction capabilities
4. Geospatial calculations: enables conversion between desired file formats (raster-to-vector conversion); creates contour lines
5. Display: provides a web-mapping service
6. Map data: displays geospatial data, such as countries and states, by using Inkspace

GeoPandas
GeoPandas is an open-source project developed in Python to provide a useful library for working with geospatial data. It is able to run on distributions of Linux and Windows. It primarily uses the Python packages pandas (as a basis for its data storage), shapely (to manipulate the shapes stored in the advanced database), Fiona (for file access), and Descartes and matplotlib (for plotting the visualizations of the data). It is most adept at displaying discrete sections of data in a geospatial visualization. It is limited in its ability to display graphics outside the Python environment, and it does not support conversion to the desired raster/vector formats.

Evaluation Criteria
1. Data import: reads almost any vector-based spatial data format
2. Data storage: stores geospatial data in vector and raster formats
3. Geometric calculations: supports CRS; cannot calculate lengths or areas of geometry features; has functions for overlay, such as intersections between two or more areas, union (merges the areas of one layer to one single area), difference (A–B areas), and polygons
4. Geospatial calculations: no conversion to any desired file formats (no raster-to-vector formats); does not provide a contour-plot function
5. Map data: uses various map projections with CartoPy or other Python libraries
6. Display: does not provide a web application; good representation in 3D colorspace with matplotlib

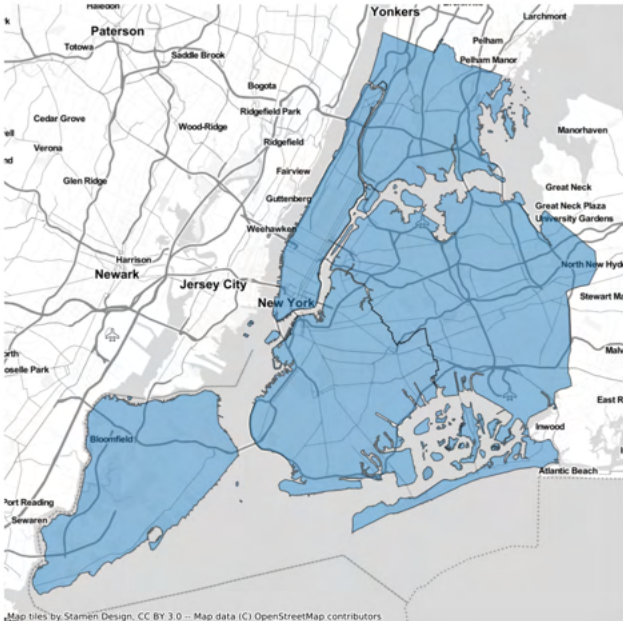

Figure 3. GeoPandas can overlay processed geospatial data over existing maps.

WorldWind

WorldWind is an open-source API for virtual 3D globe visualization developed by NASA in partnership with the European Space Agency. It is written in both Java (for desktop and Android devices) and JavaScript (for web applications). After being suspended from development in 2019, it was re-funded in August of 2020. It can import a variety of input files with geospatial data, store the data in both raster and vector formats, perform sufficient geometric and geospatial calculations for what is desired here, and produce good visualizations with comprehensive map data.

Evaluation Criteria

1. Data import: imports files in formats including shapefile, KML, VPF, GML, GeoJSON, GeoRSS, GPX, and NMEA
2. Data storage: stores geospatial data in vector and raster formats
3. Geometric calculations: supports geographic coordinate system (latitude, longitude), universal transverse Mercator, and draws and measures distances and areas across the terrain
4. Geospatial calculations: displays contour lines on surface terrain at a specified elevation
5. Map data: visually represents scalar values, such as noise, over a grid of geographic positions; visualizes the results on web and Android platforms
6. Display: displays geospatial data divided into countries, states, and cities

Overall Evaluation

The overall evaluation of all investigated libraries is provided in the table below. QGIS appears to surpass all other libraries with respect to the metrics previously set.

	Intuitive GUI	Compatibility	Statistical Analyses	Data Import	Data Storage	Geometric Calculations	Geospatial Calculations	Map Data	Display	Total
QGIS	3	5	3	5	5	5	5	5	4	40
Open JUMP										
SAGA	3	3	4	5	5	4	5	5	4	38
Deck.gl	4	3	1	1	1	3	3	5	5	26
Kepler.gl										
GRASS										
gvSIG										
MapWindow										
GeoPandas		*3*		5	5	4	1	2	2	19
WorldWind		*5*		5	5	4	4	5	5	28

GIS Applications

GIS applications can be broadly classified into two categories: desktop- and web-based applications.
WebGIS applications use web technologies to display and communicate geospatial information to an end user. Five common elements exist in every WebGIS application:

1. Web application
   - The web application is the interface used by the client. It has tools to visualize, analyze, and interact with geographic information. It can be run on a web browser or a GPS-enabled device.
2. Digital basemaps
   - Digital basemaps provide geographical context for the application, e.g., transportation, topography, or imagery.
3. Operational layers
   - The operational layers display the results of an operation, e.g., observations, sensor feeds, query results, or analytic results.
4. Tasks and tools in the WebGIS application
   - Tools to perform operations beyond mapping are included.
5. Geodatabase(s)
   - The containers of geo data can be geodatabases, shapefiles, tabular databases, CAD files, etc.

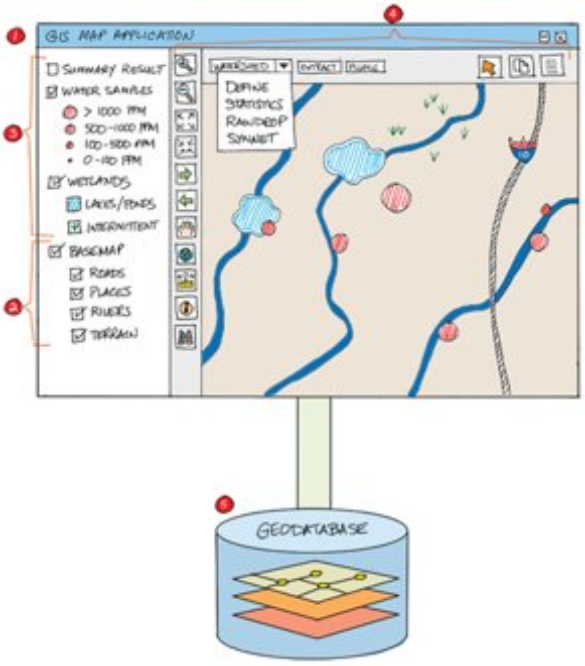

Figure 4. Sketch of a WebGIS application.

WebGIS applications have multiple advantages as well as limitations, some of which are show in the table below:

Advantages of WebGIS	Drawbacks of WebGIS
• **WebGIS provides a potential to host data online rather than traditional desktop applications.** • **WebGIS has better cross-platform capability with various web browsers.** • **Customers with different levels of GIS expertise can easily use WebGIS.** • **WebGIS is extendable to cloud services, thus allowing for manipulation and use of big GIS data.**	• WebGIS is relatively difficult to build: developers must have good knowledge of multiple scripting languages to build the app (e.g., Python, JavaScript, or HTML). • Data security might be dependent on a third party. • The application might need to be hosted outside the organization.

• **WebGIS has a low cost to entry, because most of the libraries and tools are open source with good community support.** • **WebGIS enables real-time analysis.**	

The team has also started a dialogue with the Aviation Environmental Design Tool (AEDT) development team regarding which GIS functionalities will be required to enable integration of the UAS noise engine into AEDT in the future.

Task 2 – Investigation of Emerging Computational Technologies

Georgia Institute of Technology

Objectives

This task aims to investigate various emerging computational technologies by using a sample test problem.

Research Approach

The ASCENT9 team identified three main areas of investigation for this task:

- GIS visualization techniques
- Parallel computation
- Data pre/post-processing

The team has also investigated graphics processing unit (GPU) technologies and cloud-computing platforms as a secondary area of interest. Figure 5 highlights these areas.

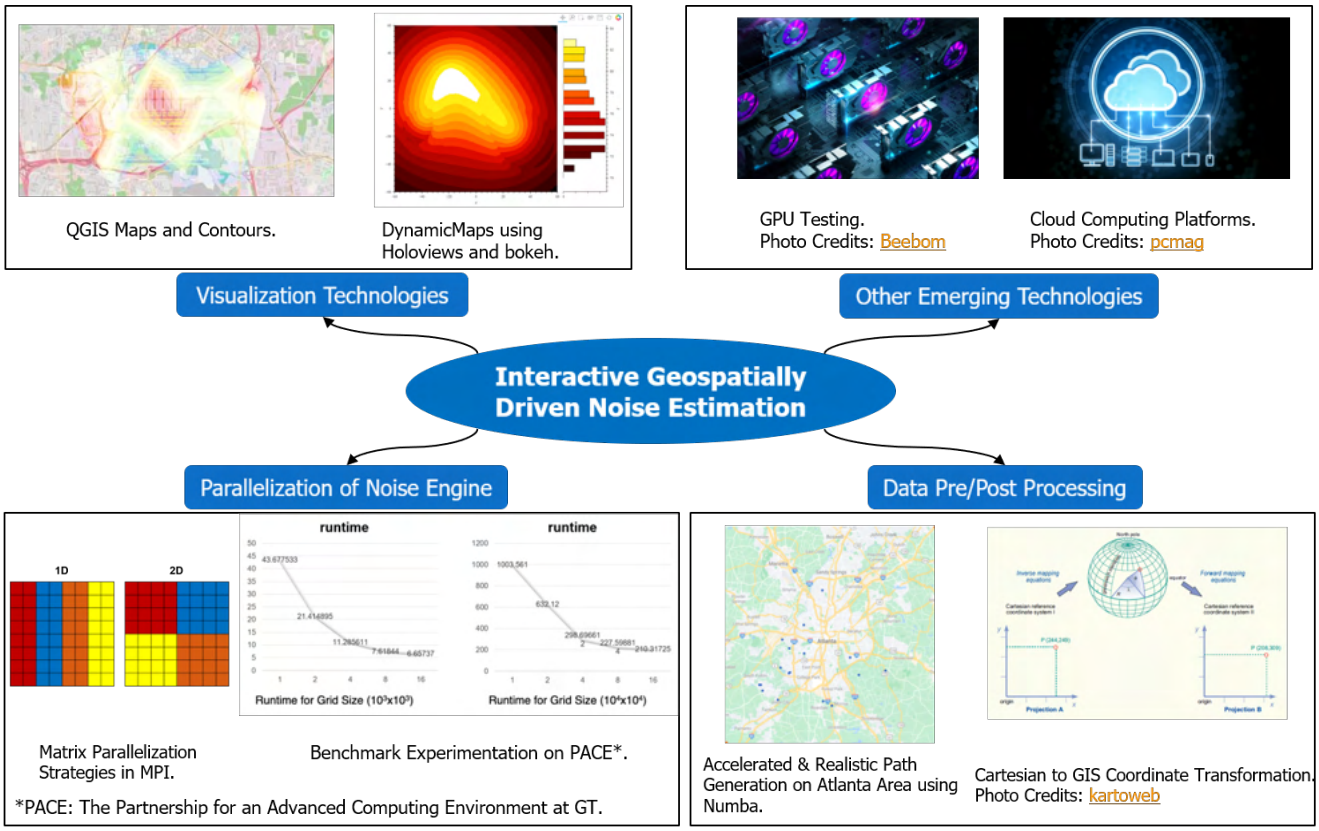

Figure 5. Emerging technologies investigated.

GIS Visualization Technologies

The team's efforts focused on technologies that provide interactive visualization of large data on maps. The choices were narrowed to QGIS and interfaces based on Python or JavaScript. Working with large datasets in QGIS requires a SQL plugin as a conduit for data communication. Furthermore, the GUI aspect limits the interactive capabilities. Therefore, we focused on JavaScript and Python libraries and interfaces—in this context, D3 library for JavaScript and bokeh for Python. Bokeh emerged as the preferable choice, because it builds on JavaScript visualizations without a need to explicitly use JavaScript. Furthermore, with this library, both the front-end and back-end of a web application can be coded with Python.

Parallel Computing Technologies

Parallel computing technologies are critical for calculations involving large grids. These grids can be expressed as matrices, whose regular structures are advantageous for the partitioning of the computation tasks.

The team initiated the analysis by exploring the standards for parallel programming through the Message Passing Interface (MPI) implemented in various libraries, such as OpenMPI, MPICH, and MVAPICH. Because the noise computation engine is built from common mathematical and computational operations, OpenMPI was selected for its portability and ability to support most existing platforms.

Parallel algorithms for matrix computation are well documented in the literature. Typically, the data are partitioned along either one axis of the matrix or both axes, as shown in Figure 6. These algorithms are usually designed with consideration of the communication overhead and the computation cost on individual processors.

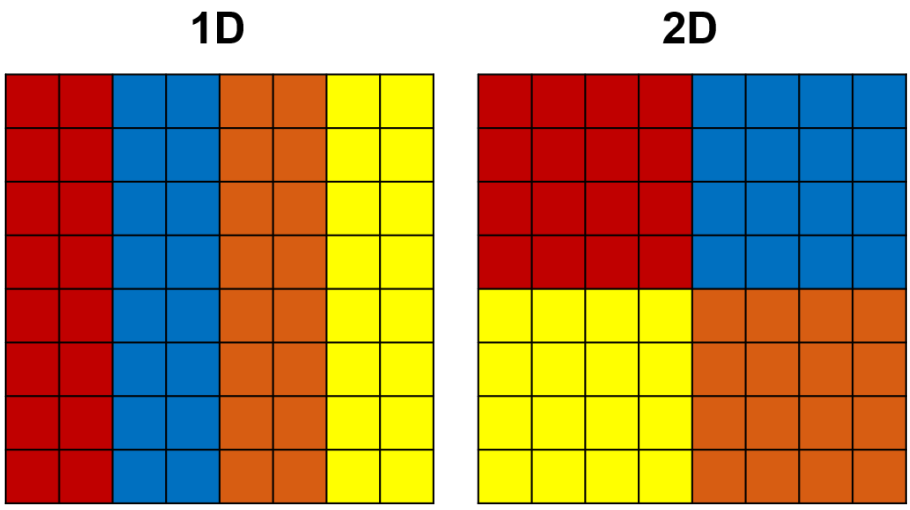

Figure 6. Common partition strategies for matrix computations.

The noise engine can considered as a large dense matrix problem in which the calculations for its elements depend not on its neighbors but on the path of the noise source, which can be modeled as a vector. Hence, the partition strategies shown in Figure 6 are theoretically the same: the main challenge is the management of the data communicated. In addition to the communication of the path data to each partition, the engine must collect the results and send them to the visualization tool.

Therefore, we needed to examine the input/output (IO) operations in parallel. The three main approaches to parallel IO operations are briefly defined as follows:

- Non-parallel: a central unit is uniquely responsible for the IO operations
- Independent parallel: each process writes to a separate file
- Cooperative parallel: all processors collaboratively written to one file

The main advantages and drawbacks of each approach are summarized in the table below. Although the cooperative parallel approach has the potential to deliver the best performance, the limitation of the allowable file types is undesirable and might

also result in poorer performance than the sequential algorithm. Therefore, a parallel IO approach was not chosen; the choice instead was based on other characteristics of the overall noise module.

Parallel IO Approach	Advantages	Drawbacks
Non-Parallel	Easy to code	Poor performance (worse than sequential)
Independent Parallel	• Easy to parallelize • No inter-process communication	Generation of many small files to manage
Cooperative Parallel	• Potentially excellent performance • Only one file needed	• Complex coding • Dependence on implementation of concurrent updates in rare file types

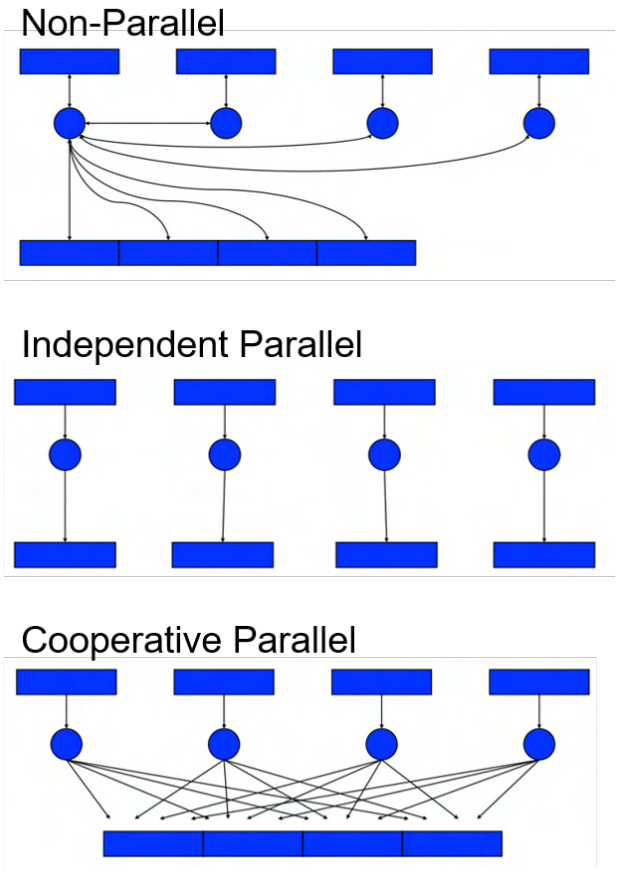

Figure 7. IO operations in MPI. Source: William Gropp, "Introduction to MPI I/O."

The analysis of parallel IO approaches led to a need to also examine the file formats used in parallel. Three major categories of file formats can be listed:

- ASCII
- Binary
- Standard scientific libraries (HDF5, NetCDF, etc.)

Their major benefits and drawbacks are listed in the table below.

File Format	Advantages	Drawbacks
ASCII	• Human readable • Portable	• Large storage requirement • Costly read/write operations
Binary	• Efficient storage • Less costly read/write operations	Formatting required to read
Standard Scientific Libraries	• Data portability across platforms • Data stored in binary • Data description included	Risk of corruption

This analysis was conducted with the gridded data format in mind. Instances of these files that are encoded in binary format are relatively straightforward to create and manage in parallel, because MPI writes to binary format by default. Instances with ASCII characters are more difficult to use, because a binary-ASCII conversion is needed to format them.

To demonstrate the runtime difference between ASCII files and binary files, we ran a test case with a fixed problem size and a variable number of processors (p). The test used the independent parallel approach to eliminate the need for a central unit that collects the results. Figure 8 illustrates the runtimes of the text-file problems and the binary problems on a number of processors ranging from 2 to 16. The "runtime no IO" scenario was included as a baseline to demonstrate the cost of communication due to the IO operations. As expected, for a fixed problem, the runtime decreased as the number of processors increased; however, the difference with respect to the file formats was quite apparent.

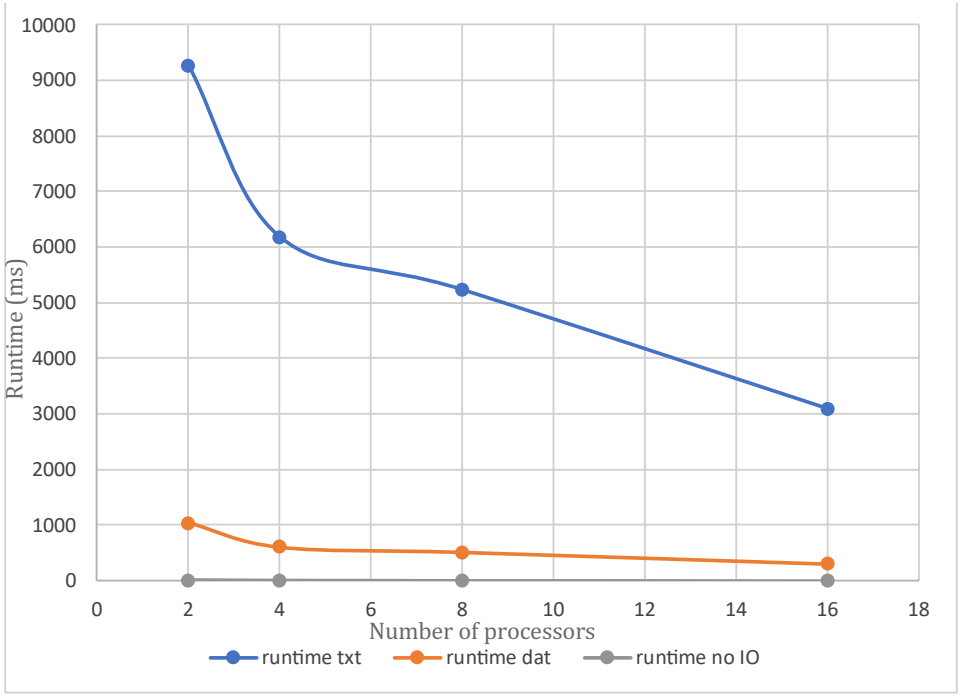

Figure 8. Runtime vs. number of processors for different IO formats.

Furthermore, for any format used, storage space is needed to contain the data. Figure 9 shows an exponential growth in size as the grid becomes finer. This test case indicates that the hardware's available memory plays an important role in the calculation of large grids.

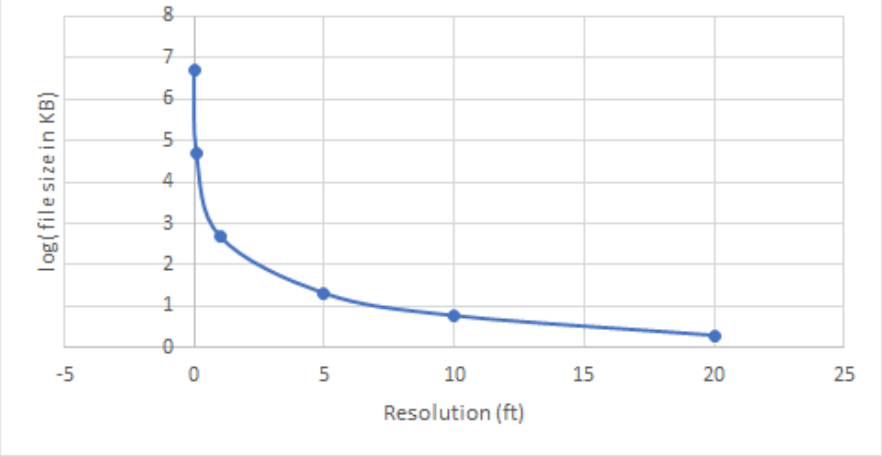

Figure 9. log (file size in kB) vs resolution (ft).

The choice of programming language is another important aspect in this investigation. Programming languages such as C and C++ combined with MPI libraries are the primary choice of many HPC practitioners, who often have some access to low-level machine language, thus resulting in good performance for parallel computations. The main challenge in using these languages is the integration with interactive GIS visualization tools. Higher-level languages, such as Matlab and Python, provide these libraries with much less scripting and easier integration, at the expense of speed in running parallel code. Matlab in particular requires the setup of a Virtual Network Computing session before any calculations are launched. Python, despite being slower than C/C++, emerged as an adequate choice for the noise module, because it is well equipped to facilitate large interactive GIS visualizations without substantially sacrificing speed for this particular application, while still being able to act as a wrapper for fast C/C++ implementations of the computational code.

Data Processing Technologies

The team investigated processing libraries for GIS data. Because the investigation of visualization techniques favored the use of Python to code the application, libraries such as GeoPandas and GeoTIFF were explored to assess their compatibility with the goals of this project.

GeoPandas is a library that brings the powerful functionalities of pandas to geospatial operations. GeoTIFF is a format allowing geospatial data to be embedded in images. GeoPandas is more suited to work with vector data, whereas GeoTIFF supports both raster and vector formats. Each of these libraries has its own merits and applications, and could be used in the noise calculation engine. The final choice would depend on the data pipeline from the computation to the visualization and the data conversions required in this process.

Other Emerging Technologies

Task 2 also included the investigation of GPUs and the potential to use them in the noise engine. GPUs are designed for fast creation and rendering of graphics. They are widely used in visualization tasks and therefore were included in this study. Although the calculation process for a GPU implementation is similar to that of a central processing unit (CPU) implementation, some considerations must be accounted for. For this project, the open-source machine-learning library Torch was selected to test the GPU implementation of a noise engine. The choice was based on the ability of this library to handle *N*-dimensional tensors as well as providing generic linear algebra functionalities. This library is also capable of running on CPUs or the NVIDIA CUDA platform.

GPU use depends on the operating system of the machine. Windows has a video-driver timeout limit of 2 s, after which the video driver of the video card being used for display output is forced to restart. A similar limit of 5 s exists in Linux. This limit can be disabled for workstation cards that are not being used for video display. Therefore, the calculations generally must be broken up into small parts that ensure CPU control before the driver timeout is reached. The calculations must be split according to the speed of the available hardware. The other limitation is the speed of moving data from main memory to GPU memory. GPU-based calculations require the data to reside in GPU memory. The transfer to and from the GPU is limited by the PCI bus speed, which, although fast, is orders of magnitude slower than direct memory access. Generally, the

speed is only marginally faster than modern SSD data access, depending on the number of PCI bus lanes being used. Because of the size of memory required, the entire noise calculation must be split into many smaller tasks, as well as smaller storage arrays that are constantly moved between the main memory and GPU memory. Therefore, the potential acceleration that can be gained by GPU-based calculations is limited. The potential speed still remains high but is still under investigation.

A toy problem was run on different architectures using various hardware. With increasing resolution, local CPU calculations were fastest, because of the fast access to memory and the absence of communication between the processes (Figure 10). A distributed calculation requires more time, because of the communication cost. GPUs can accelerate the calculations. An ideal solution would eliminate any need to communicate data but is not realistic in this case.

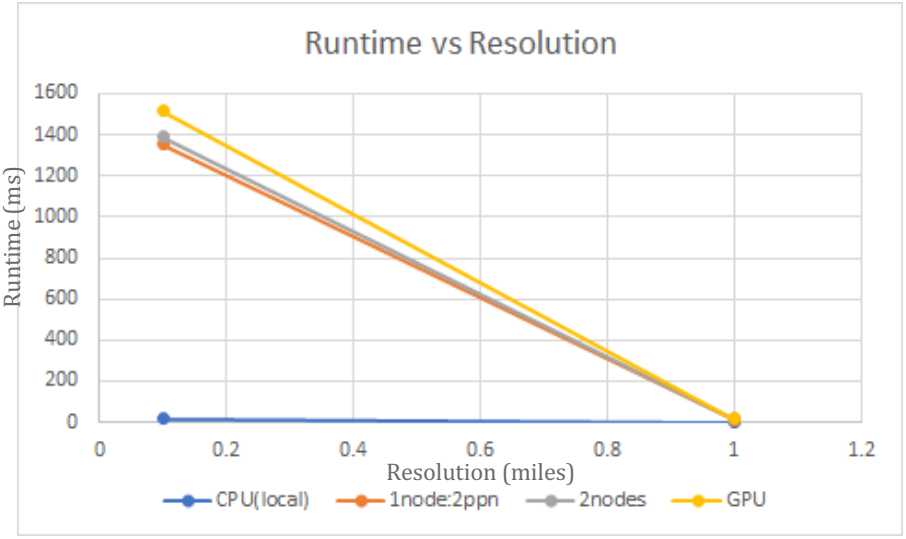

Figure 10. Runtimes for different hardware.

Task 3 – Collaboration with the UAS Computation Module Development Team

Georgia Institute of Technology

Objectives

This task focuses on a collaboration with the UAS Computation Module Development team at Mississippi State University (MSU) to explore how both teams can effectively exchange data and ideas.

Research Approach

The ASCENT9 Team met with the team working on the eCommerce project at MSU on a biweekly basis. This team, led by Dr. Adrian Sescu, provided demand data and a data generator to create random UAS paths. The teams discussed the simulation of noise footprints from a notional UAS delivery network in the Memphis area. The ASCENT9 team shared an early version of the noise engine calculation with the MSU team.

The eCommerce project focused on emerging UAS networks and their implications on National Airspace System integration. The project's case study is an analysis of the Amazon UAS delivery network with ground support. The MSU team collected data on warehouses in the greater Memphis area and the residential addresses served by these warehouses. Trucks were placed in the area to reduce the UAS flight time and assist with last-mile delivery. These warehouses are shown in Figure 11. Multiple scenarios were considered in this study:

- 8 drones per warehouse and 4 drones per truck (1,132 drones)
- 12 drones per warehouse and 6 drones per truck (1,698 drones)
- 16 drones per warehouse and 8 drones per truck (2,264 drones)

- 24 drones per warehouse and 12 drones per truck (3,396 drones)
- 32 drones per warehouse and 16 drones per truck (4,528 drones)
- 55 drones per warehouse and 50 drones per truck (12,305 drones)

The ASCENT9 team shared an early version of the noise engine developed under Task 4 with the MSU team and successfully verified the ability to run the noise engine on their systems.

The ASCENT9 team used the first scenario to test the noise engine with variable grid precision. These trajectories are shown in Figure 12. They span an area of approximately 40 miles, with each trajectory's length varying between 3,000 and 8,000 ft.

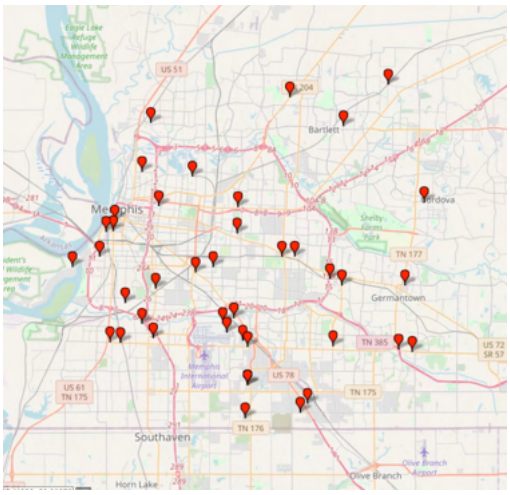

Figure 11. Warehouses in the Memphis, Tennessee area.

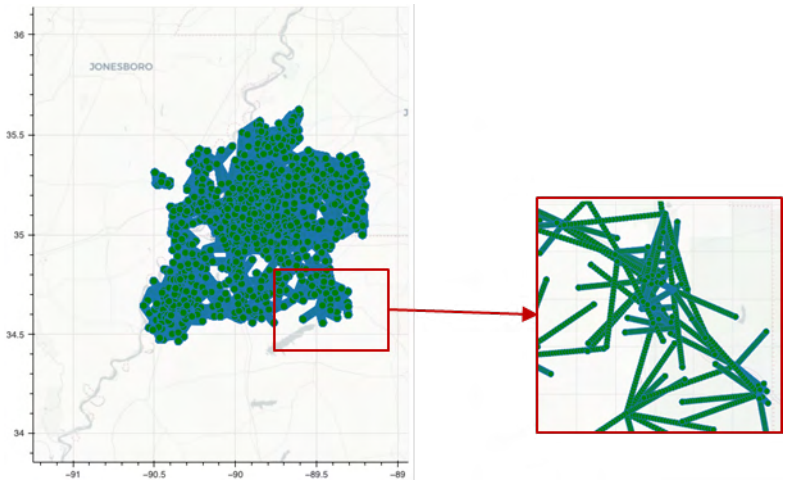

Figure 12. Random trajectories provided by MSU.

In addition to collaborating with MSU, the ASCENT9 team collaborated with the Volpe Research Center to acquire national transportation noise data consisting of the combined gridded road, aviation, and railroad noise for the entire United States, provided in A-weighted 24-h exposure levels. The data were used as background noise, which was added to the calculated noise by the engine module. A cropped overview of this data on the greater Memphis area is shown in Figure 13.

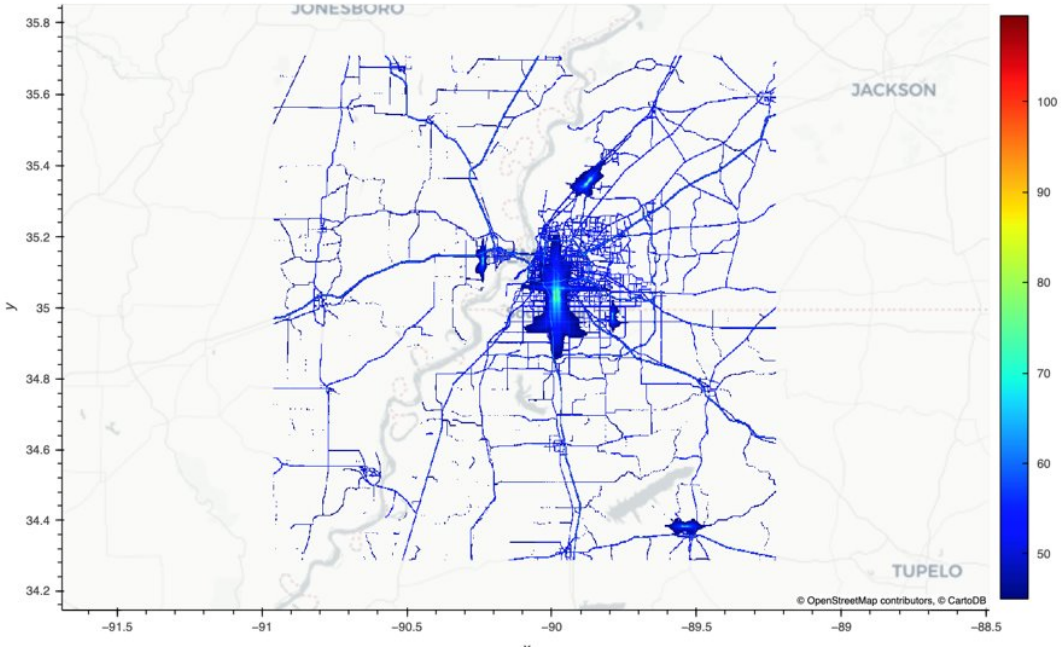

Figure 13. National transportation noise data plotted in the greater Memphis area.

Beyond these external collaborations, this research was also supported in part through research cyberinfrastructure resources and services provided by the Partnership for an Advanced Computing Environment (PACE) at the Georgia Institute of Technology. This computing environment consists of a large compute cluster, which was used to develop and test the noise engine under Task 4. This cluster was also used to conduct experiments and tune various parameters and aspects of how the noise engine is executed in parallel. For example, choices include the number of compute nodes, the amount of memory per node, and the number of parallel processes per node.

Task 4 – Noise Computation Engine Integration

Georgia Institute of Technology

Objectives

This task aims to create a noise calculation module by using the UAS trajectories provided by the Mississippi State University research team.

Research Approach

The investigation conducted in Task 2 led to the identification of adequate tools to build the high-performance, interactive, GIS-based noise module for UAS. A Python web application was planned to be built with the ability to be run either locally or in a distributed setting provided by the HPC infrastructure at the Georgia Institute of Technology Partnership for an Advanced Computing Environment (PACE). Because Python was already selected as the programming language for this module, libraries enabling parallel matrix computation and large interactive visualization were explored. The selection process resulted in four libraries, as briefly described in Figure 14.

bokeh	• Python library for interactive visualizations on web browsers • Developers use bokeh to create dashboards with graphs and interaction for the users
DASK	• Python library for parallel computing • Enables the use of computer clusters to handle heavy computation
Datashader	• Accurate rendering of large datasets • Allows users to easily represent and analyze large datasets
xarray	• Efficient handling of multi-dimensional arrays (including raster and GeoTiff files) • Implements operations on labeled arrays (e.g., array of longitude and latitude coordinates) for clearer and faster manipulation of datasets

Figure 14. Enabling capabilities for the UAS noise engine prototype.

Before describing the architecture of the web application, the structure of the Python object for the grid must be discussed. Noise metrics are built on the distances between the grid and the path of the noise source. That is, for each point in the path, the distance to every point in the grid must be calculated. This calculation can use a 3D matrix in which the third dimension matches the number of the points in the path. A notional sketch of this structure is shown in Figure 15. This choice actually benefits from the highly optimized methods of numpy, a Python library for multidimensional arrays.

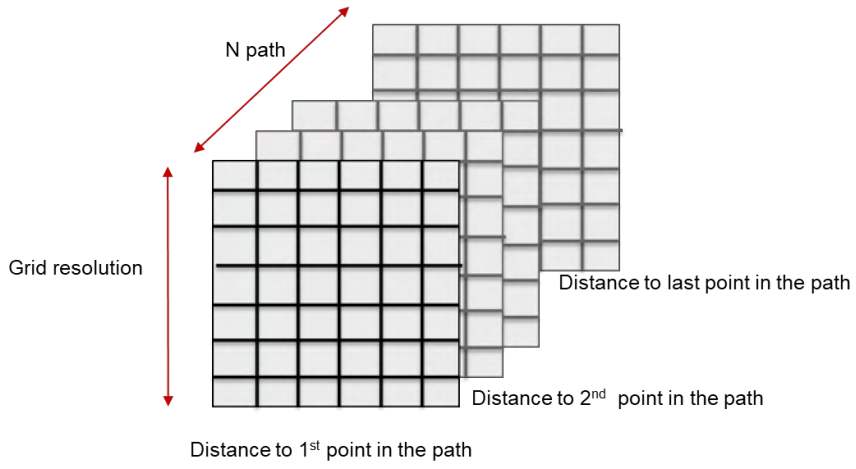

Figure 15. Notional structure of the noise module object.

The UAS prototype was required to demonstrate the calculation and visualization of two types of noise metrics: peak metrics and exposure metrics. The individual steps to calculate each are shown in Figure 16.

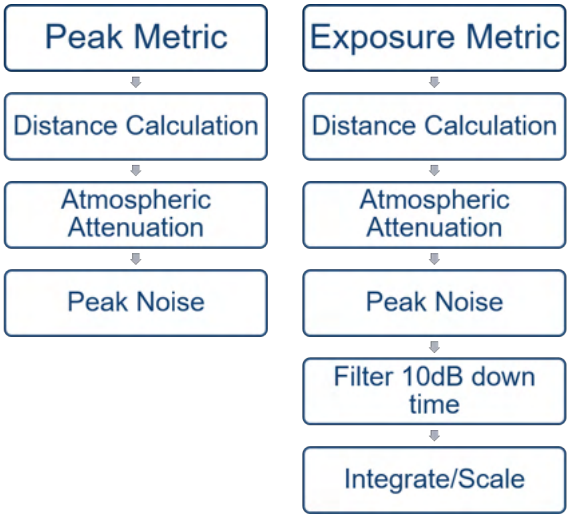

Figure 16. Steps in the calculation of peak noise metrics and exposure noise metrics.

The parallel execution of the noise engine is performed with dask library through the following implementation phases:

1. Definition of the computational steps as operations on generic datasets
2. Preparation of the datasets
3. Definition of the computational resources
4. Launch of the dynamic scheduler and mapping/application of the operations on the datasets
5. Collection of the results

The computational resources are defined according to the available hardware for parallel computation, characterized by the number of cores or workers, and the available memory per core. In addition to allowing parallel computations on single machines, dask supports clusters schedulers, such as PBS and Slurm, and is supported by Amazon Web Services.

The dynamic scheduler is one of the most powerful features of dask, because it performs partitioning of the data and calculations without extensive user involvement. This scheduler creates an optimized directed acyclic task graph to transfer data and apply computations using the given resources. An example of such task graphs is shown in Figure 17. This graph corresponds to a peak metric event calculation using 10 workers.

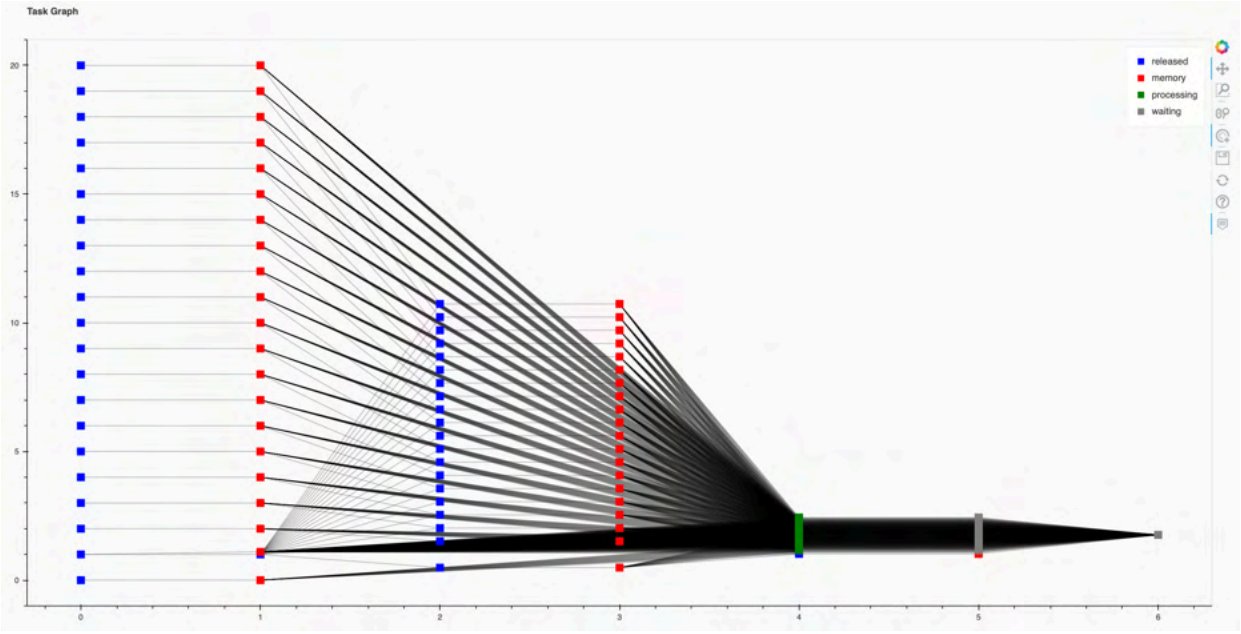

Figure 17. Task graph generated by the dask dynamic scheduler.

The generic implementation steps in dask are illustrated in Figure 18, in which the client refers to the web browser used to visualize the noise contours.

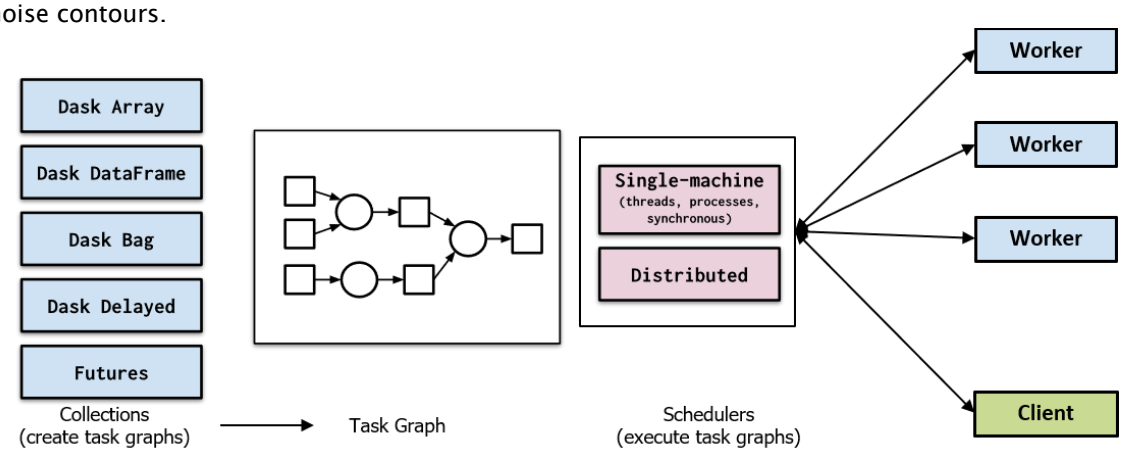

Figure 18. Implementation steps in dask.

To finally visualize these contours in the browser, the dask data objects must undergo several packaging operations with xarray and datashader. Because the number of points that a browser can support is limited, datashader was used to allow sampling of the data points and meaningful visualization of the data. Datashader objects are integrated in bokeh, but they do not support dask arrays. Xarray was used to wrap the dask objects for use within datashader. The data pipeline is illustrated in Figure 19.

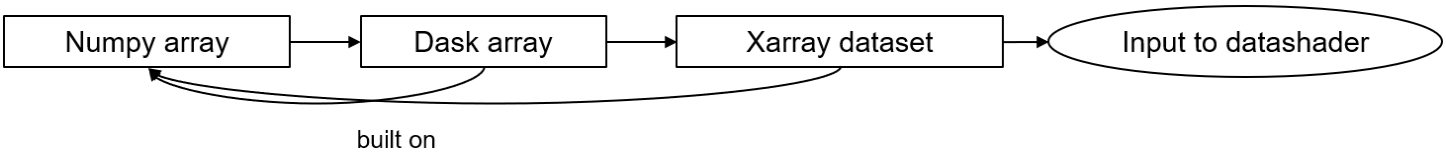

Figure 19. The data pipeline from dask to bokeh.

The overall architecture of the UAS noise calculation prototype is shown in Figure 20. The noise contours are calculated and stored on the distributed cluster at PACE. For visualization, bokeh requests a portion of the data that are aggregated and projected by using datashader. This process requires continuous communication between dask scheduler, and the workers writing the data to files has been bypassed. Alternatively, a central file could be created to collect the results, but the high communication cost would need to be accounted for. The data are accessible from the bokeh server through secure SSH tunneling to the PACE interface. This aspect is a major advantage of web applications over desktop applications, because it enables broader cross-platform access to clients.

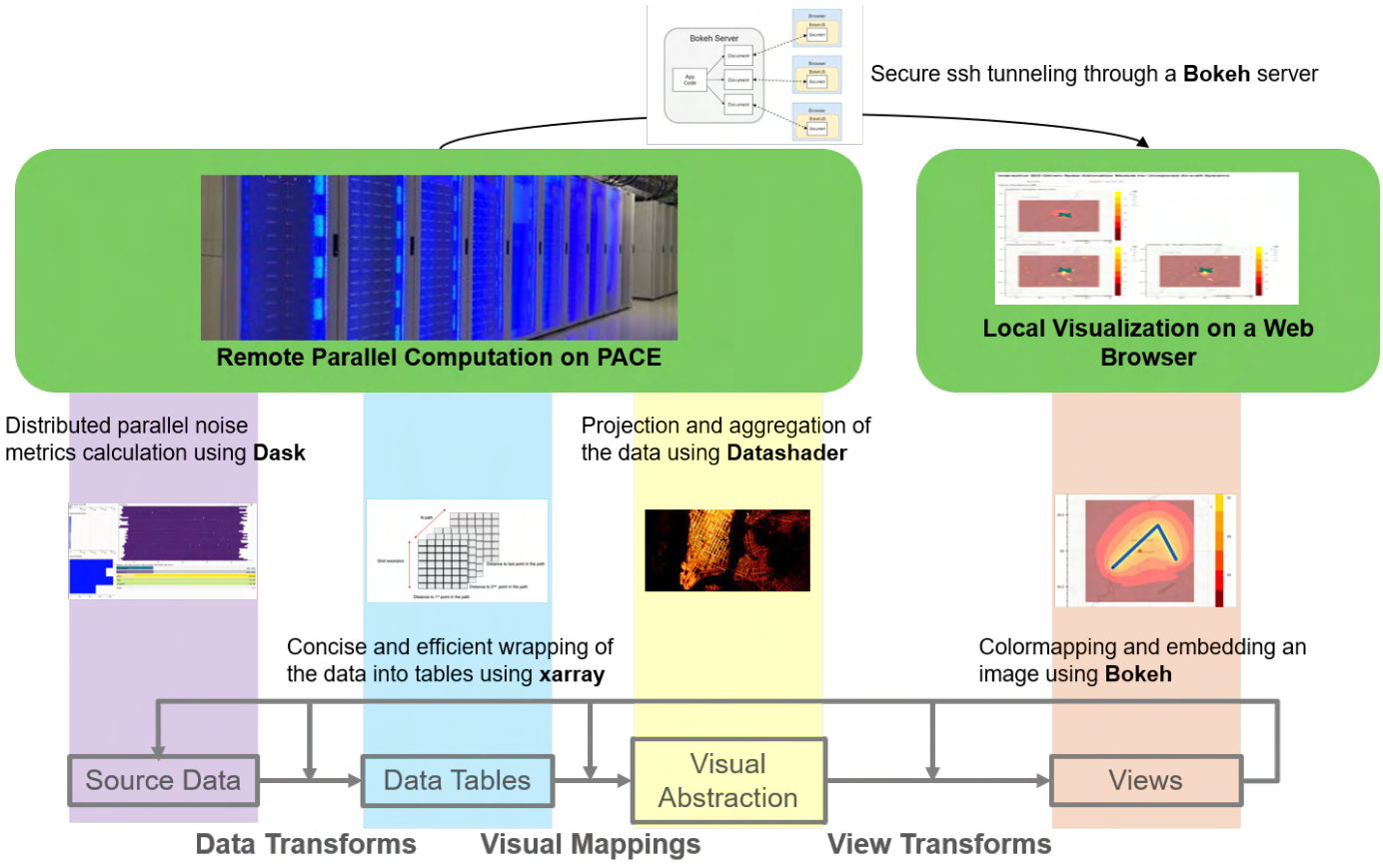

Figure 20. Overview of the noise module.

Benchmark Demonstration

The benchmark study aimed to simulate the noise footprint from a notional UAS delivery network in the greater Memphis area. In this study, 40 warehouses serving approximately 30,000 residential addresses were considered. Trucks that serve

as UAS staging platforms were positioned near some neighborhoods to reduce UAS range requirements and delivery times. For this study, eight UAS per warehouse were considered, with four UAS per truck and a total of 1,132 total flights. The paths for these flights are shown in Figure 21.

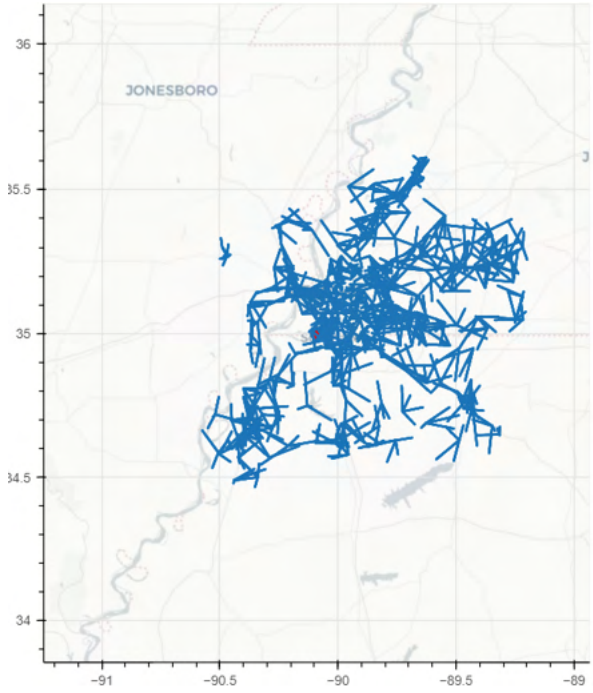

Figure 21. Flight paths in the benchmark study.

The national transportation noise map was used as a background to supplement the engine's computations. The noise contours of this background noise are shown in Figure 22. The cumulative LAE noise contours generated uniquely from the UAS activities are shown in Figure 23. The effect of UAS activity on the existing noise in the greater Memphis area is shown in Figure 24.

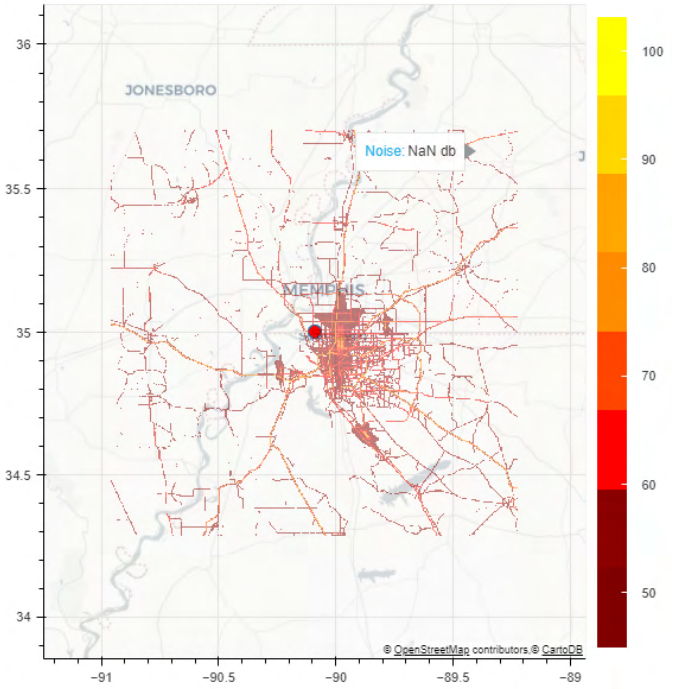

Figure 22. National transportation noise map in the greater Memphis area.

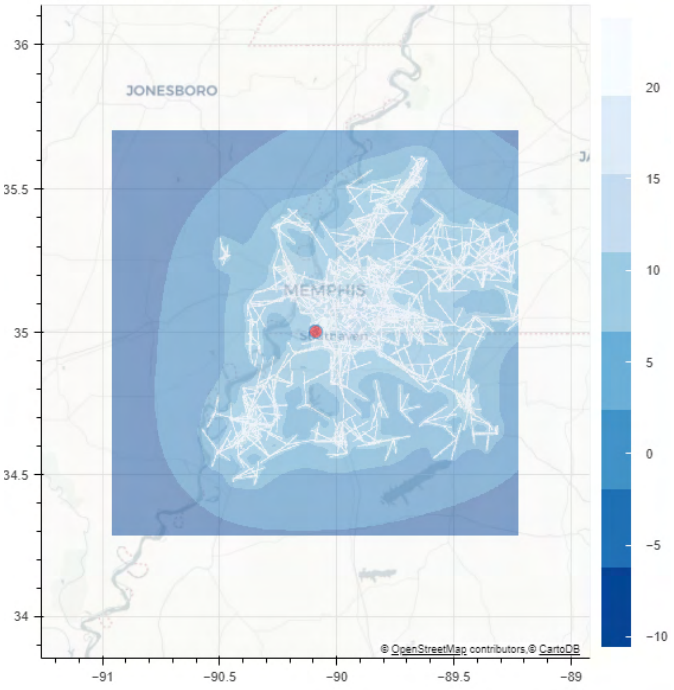

Figure 23. Computed UAS noise $L_{Aeq,24h}$

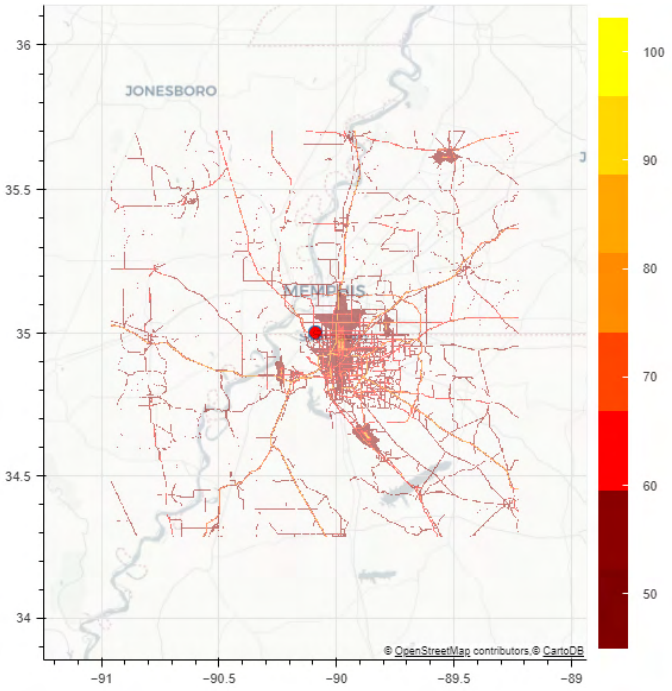

Figure 24. Combined noise $L_{Aeq,24h}$

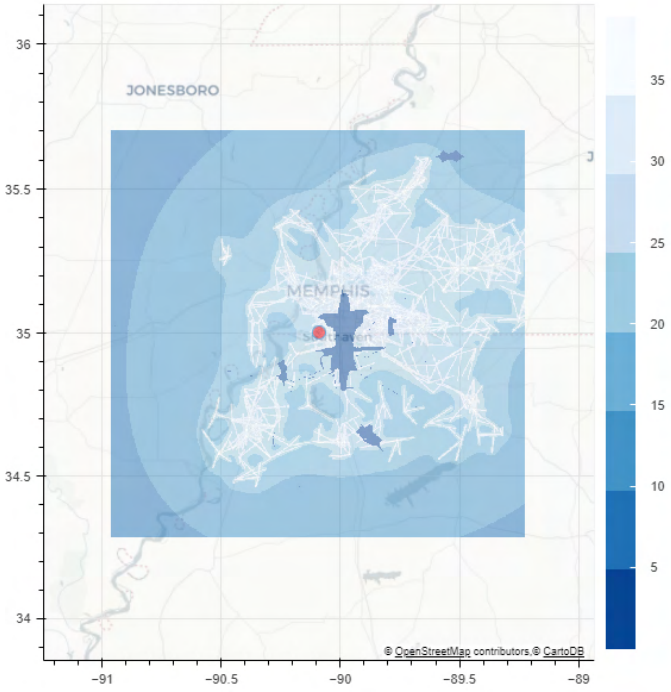

Figure 25. Change in $L_{Aeq,24h}$

A side-by-side zoomed-in comparison between the total combined noise and change in $L_{Aeq,24h}$ is illustrated in Figure 26. This figure indicates that areas that already have high noise exposure levels are not strongly affected in this particular sample problem. Nonetheless, more analysis must be conducted before a final deduction is made.

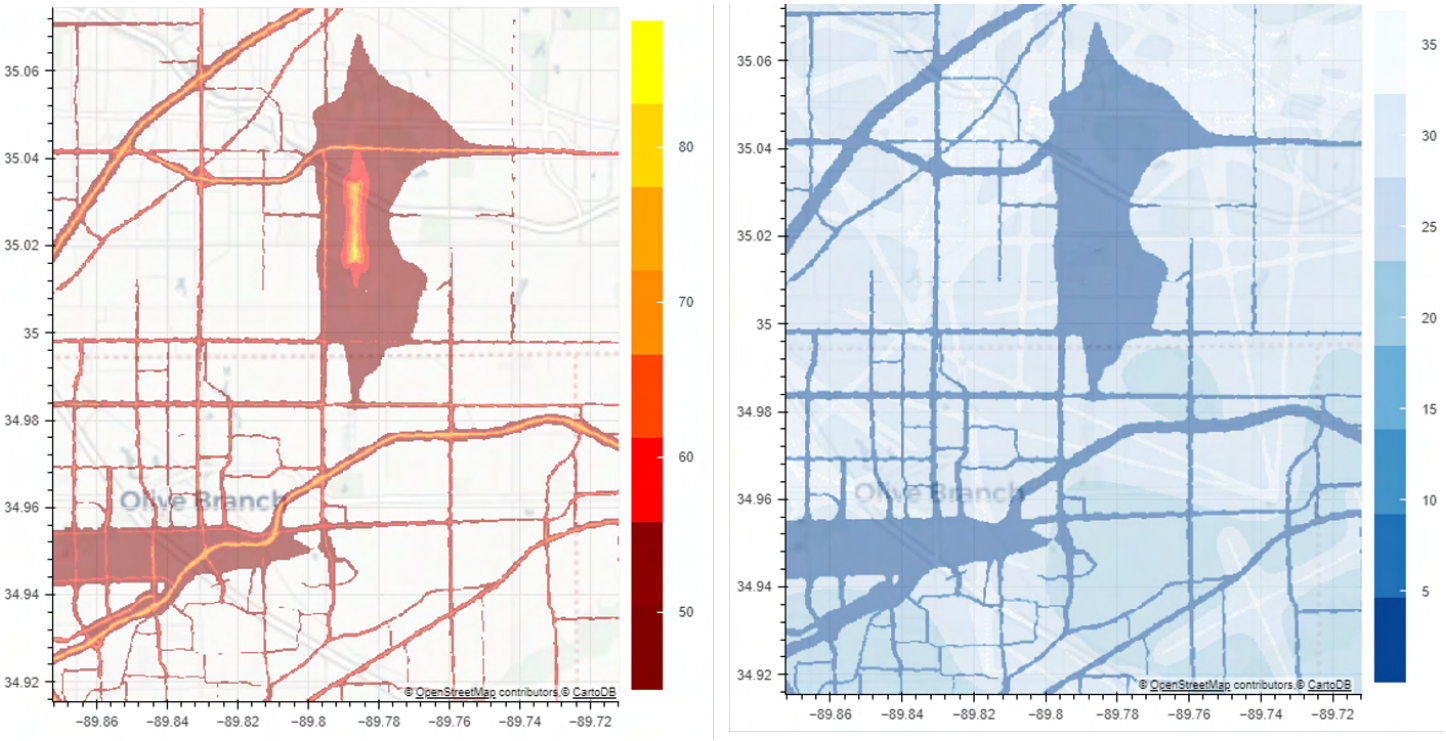

Figure 26. Combined noise $L_{Aeq,24h}$ (left) and change in $L_{Aeq,24h}$ (right).

With the noise engine prototype created after these tasks, the next steps will involve conducting more benchmarking studies to test the limits and sensitivity of the module. These tests will include demonstrating the scaling with increasing levels of UAS operations and how the computational time scales with variations in computational approaches. Furthermore, the team will work on eventually transitioning the noise engine to FAA or the Department of Transportation Volpe Center.

Milestone

The team delivered a recommendation for an updated GIS system to FAA and members of the AEDT development team.

Major Accomplishments

The team presented an initial prototype of the UAS noise engine with an interactive display while running on a parallel computing cluster to FAA.

Publications

None

Outreach Efforts

Initial outreach and coordination were conducted with the ASSURE Center of Excellence team at Mississippi State University.

Awards

None

Student Involvement

The Georgia Institute of Technology student team consists of three graduate research assistants. At the beginning of the project, all graduate research assistants engaged in the GIS background research. The team has now been divided to address different aspects: the implementation of the noise engine; the novel computational technology testing; and the creation of benchmark studies that will serve as a test bed for testing the computational scaling of different approaches.

Plans for Next Period

The plan for the next reporting period is to finish the current work plan and perform more testing with the emerging computational technologies on a defined sample problem. After further discussion with FAA, the team will seek to support FAA in potential applications of the UAS noise engine, through studies on varying flight operations for different operation concepts. The UAS noise engine will also be improved with more realistic atmospheric attenuation calculations as well as better UAS source noise data.

References

1. Aftomis, M. J., Berger, M. J., & Alonso, J. J. (2006). Applications of a cartesian mesh boundary-layer approach for complex configurations. Presented at the 44th AIAA Aerospace Sciences Meeting, Reno, NV.
2. Gropp, W. (n.d.). Introduction to MPI I/O. CS 598 Lecture Notes. University of Illinois Urbana-Champaign, Urbana, IL.
3. The Office of Spatial Analysis and Visualization at the Bureau of Transportation Statistics, U.S. Department of Transportation. Retrieved December 6, 2021 from https://maps.dot.gov/BTS/NationalTransportationNoiseMap/
4. Bokeh Development Team. (2018). Bokeh: Python library for interactive visualization. Retrieved December 6, 2021 from http://www.bokeh.pydata.org.
5. Dask Development Team. (2016). Dask: Library for dynamic task scheduling. Retrieved December 6, 2021 from https://dask.org
6. Cottam, J. A., Lumsdaine, A., & Wang, P. (2014). Abstract rendering: Out-of-core rendering for information visualization., Presented at the IS&T/SPIE Electronic Imaging Conference, San Francisco, CA. https://doi.org/10.1117/12.2041200

Project 010 Aircraft Technology Modeling and Assessment

Georgia Institute of Technology and Purdue University

Project Lead Investigators

Dimitri Mavris (PI)
Regents Professor
School of Aerospace Engineering
Georgia Institute of Technology
Mail Stop 0150
Atlanta, GA 30332-0150
404-894-1557
dimitri.mavris@ae.gatech.edu

William Crossley (PI)
Professor
School of Aeronautics and Astronautics
Purdue University
701 W. Stadium Ave
West Lafayette, IN 47907-2045
765-496-2872
crossley@purdue.edu

Jimmy Tai (Co-PI)
Senior Research Engineer
School of Aerospace Engineering
Georgia Institute of Technology
Mail Stop 0150
Atlanta, GA 30332-0150
404-894-0197
jimmy.tai@ae.gatech.edu

Daniel DeLaurentis (Co-PI)
Professor
School of Aeronautics and Astronautics
Purdue University
701 W. Stadium Ave
West Lafayette, IN 47907-2045
765-494-0694
ddelaure@purdue.edu

University Participants

Georgia Institute of Technology

- PI(s): Dr. Dimitri Mavris (PI), Dr. Jimmy Tai (Co-PI)
- FAA Award Numbers: 13-C-AJFE-GIT-006, 13-C-AJFE-GIT-012, 13-C-AJFE-GIT-022, 13-C-AJFE-GIT-031, 13-C-AJFE-GIT-37, 13-C-AJFE-GIT-041, 13-C-AJFE-GIT-50, 13-C-AJFE-GIT-52, 13-C-AJFE-GIT-56, 13-C-AJFE-GIT-76, 13-C-AJFE-GIT-94
- Period of Performance: September 1, 2020 to August 31, 2021

- Task(s):
    1. Demand assessment
    2. Fleet analysis
    3. Aviation Environmental Design Tool (AEDT) supersonic modeling
    4. Support Committee on Aviation Environmental Protection (CAEP) supersonic exploratory study
    5. SST modeling in AEDT
    6. Coordination

Purdue University

- PI(s): Dr. William A. Crossley (PI), Dr. Daniel DeLaurentis (Co-PI)
- FAA Award Numbers: 13-C-AJFE-PU-004, 13-C-AJFE-PU-008, 13-C-AJFE-PU-013, 13-C-AJFE-PU-018, 13-C-AJFE-PU-026, 13-C-AJFE-PU-032, 13-C-AJFE-PU-035, 13-C-AJFE-PU-044
- Period of Performance: September 1, 2020 to August 31, 2021
- Task(s):
    1. Demand assessment
    2. Fleet analysis
    4. Support CAEP supersonic exploratory study
    5. SST modeling in AEDT

Project Funding Level

The project is funded by FAA at the following levels: Georgia Institute of Technology: $1,200,000; Purdue University; $222,116. Cost-sharing details are below:

The Georgia Institute of Technology has agreed to a total of $1,200,000 in matching funds. This total includes in-kind cost-sharing from GE and Boom; salaries for the project director, research engineers, and graduate research assistants (GRAs); and funding for computing, financial, and administrative support, including meeting arrangements. The institute has also agreed to provide tuition remission for the students, paid by state funds.

Purdue University provides matching support through salary support for the faculty PIs, and through salary support and tuition and fee waivers for one of the GRAs working on this project. OAG Aviation Worldwide Limited also provided in-kind cost-sharing to the Purdue team.

Investigation Team

Georgia Institute of Technology

- PI: Dimitri Mavris
- Co-Investigator: Jimmy Tai (Task 4)
- Vehicle Modeling Technical Leads: Greg Busch, Russell Denney, Jai Ahuja, Christian Perron, and Chung Lee
- Fleet Modeling Technical Leads: Holger Pfaender, Dushhyanth Rajaram, Michelle Kirby, Mayank Bendarkar, and Mohammed Hassan (Tasks 1, 2, and 5)
- Graduate Students: Nikhil Iyengar, Barbara Sampaio, Edan Baltman, Kaleb Cornick, Brennan Stewart, Ezgi Balkas, David Shalat, Mengzhen Chen, Joao De Azevedo, Colby Weit, Jiajie (Terry) Wen, and Ted Vlady

Purdue University

- PI: William Crossley (Tasks 1,2, 4, and 5)
- Co-Investigator: Daniel DeLaurentis (Tasks 1, 2, 4, and 5)
- Graduate Students: Samarth Jain, Suzanne Swaine, Tien-Yueh Fung, and Boning Yang

Project Overview

Georgia Institute of Technology (Georgia Tech) and Purdue University have partnered to investigate the future demand for supersonic air travel and the environmental impact of supersonic transports (SSTs). In the context of this research, environmental impacts include direct carbon dioxide (CO_2) emissions and fuel consumption. The research is conducted as a collaborative effort to leverage the capabilities and knowledge available from the multiple entities that make up the ASCENT university partners and advisory committee. The primary objective of this research project is to support the Federal Aviation Administration (FAA) in modeling and assessing the potential future evolution of the next-generation supersonic aircraft

fleet. The research in this project consists of five integrated focus areas: (a) establishing fleet assumptions and performing demand assessment; (b) performing preliminary SST environmental impact prediction; (c) testing the ability of the current Aviation Environmental Design Tool (AEDT) to analyze existing supersonic models; (d) performing vehicle and fleet assessments of potential future supersonic aircraft; and (e) modeling SSTs by using the modeling and simulation environment Framework for Advanced Supersonic Transport (FASST).

To better understand the potential demand for supersonic air travel, the team developed a parametric airline operating-cost model to explore the sensitivities of key vehicle, operational, and cost parameters on the required yield that an airline would need to target for ticket prices on potential new supersonic aircraft. The current model, however, assumes fixed parameters for key vehicle metrics, which can be changed but do not include sensitivities to key vehicle design choices such as vehicle size, design cruise Mach number, and maximum range. This task will examine the implications of the physical and technical dependencies on airline operational cost. Through the vehicle performance sensitivities, such as passenger capacity and design cruise Mach number, the combined "sweet spot," i.e., the most profitable vehicle for an airline to operate, can be determined. To accomplish this goal, the existing vehicle models created in the prior year will be utilized and supplemented with the additional vehicles proposed in Task 4. These vehicles together will serve as the foundation to create credible sensitivities regarding parameters such as vehicle size and design cruise Mach number. These sensitivities will then be embedded in the airline operating-cost estimation model and used to explore the combined vehicle and airline operational space to identify the most economically feasible type of supersonic vehicle.

In an independent complementary approach to consider the demand and routes for supersonic aircraft, the Purdue team developed a ticket pricing model for possible future supersonic aircraft that relies on the "as-offered" fares before the novel coronavirus (COVID-19) pandemic for business-class and first-class tickets on routes expected to have passenger demand for supersonic aircraft. Via an approach considering the number of passengers potentially demanding fares at business class or above on a city-pair route, the distance of that city-pair route, an adjustment to increase the over-water distance of the route where the aircraft can fly supersonically to allow for the shortest trip time, and the range capability of a low-fidelity modeled medium SST (55-passenger [pax] capacity) to fly that route with the shortest trip time, the Purdue team identified 258 potential routes that could potentially allow for supersonic aircraft service in a network of routes with at least one end (i.e., the origin or destination) in the United States. Of these 258 potential routes, 241 are direct, and 17 would require fuel stops but would still save travel time with respect to a subsonic non-stop flight on the same route. By providing these potential routes as input to the Fleet-Level Environmental Evaluation Tool (FLEET) simulation, the allocation problem in FLEET then determines which routes would be profitable for the airline to offer supersonic transportation and how many supersonic aircraft would operate on these routes, providing a prediction of which routes might have supersonic aircraft use and the number of supersonic flights operated on those routes at dates in the future. The analysis also explored the possible reaction of an airline to losing business-class passengers on subsonic aircraft, by including the allocation of a high-passenger-density aircraft on routes with supersonic service and considering various ticket pricing schema and associated changes in passenger demand. With the onset of the COVID-19 pandemic, the Purdue team updated the demand modeling to reflect the decrease in air travel and provided several scenarios for post-pandemic recovery. Near the end of this reporting period, the Purdue team began an effort to expand the fleet analysis tool, FLEET, from the United States-touching route network to a worldwide network.

One major accomplishment of the project during the performance period is the preliminary results for the design Mach trade study, which encompasses nine SST models developed in FASST. These nine vehicles make up three vehicle classes: business jet, medium, and large vehicle classes. The business jets were modeled to carry eight passengers for 4,240 nmi at Mach 1.4, 1.6, and 1.8. The medium-class SSTs were modeled to carry 55 passengers for 4,500 nmi at Mach 1.8, 2.0, and 2.2. Finally, the large-class SSTs were modeled to carry 100 passengers for 5,000 nmi at Mach 1.6, 1.8, and 2.0. All noise analyses incorporated Variable Noise Reduction System (VNRS), and all associated propulsion systems were of a clean-sheet design.

Georgia Tech and Purdue used their respective fleet analysis tools—Global and Regional Environmental Analysis Tool (GREAT) and the aforementioned FLEET—to produce estimates of the fleet-level impact of a potential fleet of supersonic aircraft operating in the future. The SSTs required for these fleet-level analyses were provided by the vehicle modeling tasks with FASST, a derivative framework from Environmental Design Space (EDS). The outcomes of this study provide a glimpse into the future potential state of supersonic air travel by using physics-based models of supersonic vehicle performance. Future work should build on current estimates to conduct more detailed analyses of vehicle and fleet performance.

Table of Acronyms and Symbols [Someone]

%Nc Fan	percent *corrected fan speed*
α	T/T_{SL}, installed full-throttle thrust lapse
A4A	Airlines for America
A_C	inlet capture area
ADP	aerodynamic design point
AEDT	Aviation Environmental Design Tool
ANP	aircraft noise performance
A_O	reference inlet area
AoA	angle of attack
ASDL	Aerospace System Design Lab
APU	auxiliary power unit
β	multiplier used to capture impacts of both fuel burn and utilization on airline costs
BADA	Base of aircraft data
BFFM	Boeing fuel flow method
BPR	bypass ratio
BTS	Bureau of Transportation Statistics
CAEP	Committee On Aviation Environmental Protection
$C_{all\text{-}other}$	all other costs
CART3D	NASA INVISCID computational fluid dynamics program
CAS	calibrated airspeed
C_{D_O}	profile drag
C_{D_R}	additional drag caused by flaps, ground friction, etc.
C_{fixed}	fixed proportions of airline operating cost
C_{fuel}	fuel cost of airline operating cost
CG	center of gravity
C_L	lift coefficient
CLEEN	continuous lower energy, emissions, and noise
CMPGEN	NASA program for compressor map generation
CO_2	carbon dioxide
d	distance between center of inoperative engine and aircraft longitudinal axis
δ_{amb}	ratio of total pressure
Δt	total segment flight time
ΔT	change in temperature from standard atmospheric temperature
ΔX	distance between CG of vehicle and aerodynamic center of tail
Δz_e	total change in segment energy height
D	drag
DNL	day-night level
DoE	design of experiment
EDS	Environmental Design Space
EEDB	Engine Emissions Databank
eff_{REF}	reference fuel efficiency metric
EI	emissions index
$EINO_X$	NOx emissions index
EIS	entry into service
EPNdB	effective perceived noise in decibels
EPR	engine pressure ratio
EXTR	extraction ratio
ϕ	cooling effectiveness
FAA	Federal Aviation Administration
FAR	Fuel to air ratio
FASST	Framework for Advanced Supersonic Transport
FB_A	fuel penalty to accelerate
$FB_{D\&L}$	fuel penalty to descend from cruising altitude and land

FB_{REF}	reference subsonic fuel burn
FB_{SST}	supersonic fuel burn
$FB_{T\&C}$	fuel penalty to takeoff and climb to cruising altitude
FF	fuel flow
FLEET	Fleet-level Environmental Evaluation Tool
FLOPS	Flight Optimization System
FPR	fan pressure ratio
γ	acquisition multiplier used to scale the proportion of ownership costs
$\gamma_{airline}$	average yield per unit distance for a commercial subsonic airline
GC	great circle
GRA	graduate research assistant
GREAT	Global and Regional Environmental Analysis Tool
HPC	high-pressure compressor
HPCPR	high-pressure-compressor pressure ratio
HPT	high-pressure turbine
ICAO	International Civil Aviation Organization
IDEA	Interactive Dynamic Environmental Analysis
IGV	inlet guide vanes
ISA	international standard atmosphere
K_1	coefficients of parabolic lift-drag polar
K_2	coefficients of parabolic lift-drag polar
KEI	key environmental indicators
JFK	John F. Kennedy International Airport
LAX	Los Angeles International Airport
L/D	lift-to-drag ratio
LE	leading edge
LPC	low-pressure compressor
LPCPR	low-pressure-compressor pressure ratio
LPP MRA	lean pre-mixed pre-vaporized multi radial axial
LPT	low-pressure turbine
LSA	large single aisle
LTA	large twin aisle
LTO	landing and takeoff
M or MN	Mach number
$Mach_{sub}$	subsonic cruise Mach number
$Mach_{super}$	supersonic cruise Mach number
MDP	multi-design point
MFTF	mixed flow turbofan
MTOM	maximum takeoff mass
MTOW	maximum takeoff weight
n	load factor or number of flight segments
n_a	number of accelerations
NASA	National Aeronautics and Space Administration
n_f	number of fuel stops
NOx	nitrogen oxide
NPD	noise power distance
NPR	nozzle pressure ratio
NPSS	Numerical Propulsion System Simulation
nvPM	non-volatile particulate matter
OEI	one engine inoperative
OGV	outlet guide vanes
OpenVSP	open vehicle sketch pad
OPR	overall pressure ratio
PACI	passenger airline cost index
PAX_{REF}	reference subsonic number of passengers
PAX_{SST}	number of passengers of the supersonic aircraft
PCBOOM	NASA PC software for predicting sonic boom on the ground
PDEW	passengers daily each way
PI	principal investigator

PIPSI	Performance Of Installed Propulsion System Interactive
PLdB	sound pressure level in db
P_{t2}	total pressure entering the fan
P_{t21}	total pressure exiting the fan
P_{t3}	total pressure exiting the HPC
P_{t16}	total pressure entering mixer from core side
P_{t56}	total pressure entering the mixer from bypass side
P_S	weight-specific excess power
q	dynamic pressure
ρ	air density
R	rolling resistance force
$R_{C,max}$	maximum cruise range for supersonic vehicles
RJ	regional jet
RQL	rich burn, quick quench, lean burn
S	wing area
SAR	specific air range
SAR_{sub}	specific air range for subsonic aircraft
SAR_{super}	specific air range for supersonic aircraft
S_C	cruise range
SA	single aisle (includes both SSA and LSA classes)
SEL	single event level
SFTF	separate-flow turbofan
SLS	Sea level static
SP	switching percentage
SSA	small single aisle
SST	supersonic transport
STA	small twin aisle
S_{tail}	tail area
θ_{amb}	ratio of total temperature
T	thrust
T_{t3}	compressor exit temperature
T_{t4}	burner exit temperature
T_{t41}	turbine rotor entrance temperature
T_{t41max}	maximum turbine rotor temperature
T_{gas}	gas temperature
T_{metal}	metal temperature
T_{cool}	cooling air temperature
T_{t41SLS}	turbine rotor inlet temperature at sea-level static
t_{cool}	cooled temperature
$t_{C,sub}$	cruise time for subsonic vehicle
$t_{C,sup}$	cruise time for supersonic vehicle
t_{DandL}	time to descent from cruising altitude and land
TE	trailing edge
t_{gas}	gas temperature
TO	takeoff
t_{metal}	metal temperature
TOC	top of climb
t_{REF}	flight times for reference subsonic aircraft
$t_{re\text{-}fuel}$	time delay (90 min) for fuel stops
TSFC	thrust-specific fuel consumption
T_{SL}	thrust at sea level
t_{SST}	flight time for supersonic aircraft
t_{TandC}	time to takeoff and climb to cruising altitude
$t_{total,sub}$	total subsonic flight time
$t_{total,sup}$	total supersonic flight time
U_{REF}	utilization for subsonic aircraft used as reference
U_{SST}	utilization for supersonic aircraft
V	velocity

V_{jet}	nozzle jet velocity
V_C	cruise speed
$V_{C,sub}$	subsonic cruise speed
$V_{C,sup}$	supersonic cruise speed
V_{SR1}	reference stall speed
VT	vertical tail
VTTS	value of travel time savings
WATE	Weight Approximation for Turbine Engines
W_E	empty weight
W_F	fuel weight
W_f	weight of aircraft at the end of a mission segment
W_i	weight of aircraft at the beginning of a mission segment
W_P	payload weight
W_{TO}	takeoff weight
x	percentage of flight over water

Project Introduction

Georgia Tech and Purdue partnered to investigate the effects of supersonic aircraft on the future environmental impacts of aviation. Impacts assessed at the fleet level include direct CO_2 emissions and fuel consumption. The research is conducted as a collaborative effort to leverage capabilities and knowledge available from the multiple entities that make up the ASCENT university partners and advisory committee.

The primary objective of this research project is to support the FAA in modeling and assessing the potential future evolution of the next-generation supersonic aircraft fleet. Research under Task 1 of this project focuses on the development of fleet demand drivers for supersonic transport. This task explores and estimates the potential demand for supersonic travel. Task 2 assesses fleet impact by using the scenarios and vehicle performance metrics developed in Task 1. In Task 3, Georgia Tech will continue to support the development of supersonic aircraft analysis capabilities in AEDT, identify modeling issues, and work with the AEDT development team to identify required modifications. Of note, Task 3 has been combined with Task 5. Task 4 will develop a detailed supersonic aircraft model for the 100-passenger class for three design Mach numbers and will support CAEP supersonic exploratory study. Task 5 involves developing the capability to generate Base of aircraft data (BADA) 4 coefficients to provide additional BADA4 vehicles for AEDT.

Table 1 summarizes the four updated objectives for ASCENT Project 10 with high-level division of responsibilities delineated between Georgia Tech and Purdue.

Table 1. University contributions for year 4.

Objectives		Georgia Tech	Purdue
1	Demand Assessment	Improve airline cost model; improve SST routing tool; improve SST demand estimation Develop assumptions for supersonic scenarios relative to 12 previously developed subsonic focused fleet scenarios	Not applicable
2	Fleet Analysis	Perform fleet analysis with the gradual introduction of SST vehicles into the fleet, including additional SST vehicle types	Develop assumptions for supersonic scenarios relative to 12 previously developed subsonic focused fleet scenarios; perform fleet-level assessments, including additional SST vehicle types; develop FLEET-like tool for supersonic business jet operations; use simple SST sizing to support FLEET development and studies
3	Support CAEP Efforts	FASST vehicle modeling: develop an additional SST class for 100 passengers; perform trade studies to inform CAEP exploratory study	Provide representative supersonic demand scenarios; develop and assess airport noise model to account for supersonic aircraft
4	SST Modeling in AEDT	Develop, implement, and test propulsion and aero coefficient generation algorithms for incorporation within AEDT; identify gaps and challenges in coefficient generation for SSTs; develop an independent method for modeling SST performance by using regression; provide a plan for implementation in AEDT	Not applicable
5	Coordination	Coordinate with entities involved in CAEP supersonic exploratory study Coordinate with clean-sheet supersonic engine design project	Coordinate with entities involved in CAEP MDG/FESG, particularly the SST demand task group; maintain ability to incorporate SST vehicle models that use the engine design from ASCENT project 47 and/or NASA-developed SST models

Georgia Tech is leading the development of a supersonic routing tool to provide basic information about potential time savings and additional costs. This information is then used to develop a demand forecast for commercial supersonic travel.

This work is performed under Objective 1, and the outcome is used to support Objective 2. Under Objective 2, Georgia Tech also produces results for multiple scenarios to assess the fleet-level impacts of supersonic vehicles.
Purdue has applied their FLEET tool under Objective 2, using a subset of the fleet assumptions defined in Objective 1 and preliminary vehicle impact estimates from Objective 4. This activity has demonstrated the capabilities of FLEET for assessing fleet-level environmental impacts as a result of new aircraft technologies and distinct operational scenarios.

Under Objective 4, Georgia Tech is responsible for developing additional aircraft concepts in FASST to support a trade study that will inform the CAEP supersonic exploratory study. For Objective 4, Georgia Tech explores the requirements for modeling supersonic vehicles in AEDT and develops an approach to generate both aerodynamics and propulsion regression coefficients for incorporation into AEDT.

Under Objective 5, Georgia Tech is supporting coordination and meetings with the member entities of the CAEP Modeling and Database Group/Forecasting and Economic Support Group (MDG/FESG), as well as NASA and ASCENT Project 47. This task involves a series of frequent (weekly) meetings as well as ad hoc groups and in-person meetings, or virtual meetings if in-person meetings are not possible.

Milestones

Georgia Tech had four milestones for this year of performance:

1. Fleet assumptions and demand analysis
2. Fleet analysis and demand results
3. FASST SST descriptions and characteristics in Microsoft PowerPoint format

For Purdue, the proposal covering this year of performance included several milestones:

1. Expand the FLEET route network to include global routes
2. Provide updated supersonic demand scenario information in support of CAEP efforts
3. Implement a simultaneous allocation model for FLEET to consider airport capacity and potential airport noise considerations
4. Develop a separate FLEET-like tool to assess supersonic business jet (SSBJ) operations and their subsequent impacts on fleet allocation
5. Assessment of airlines possibly introducing high-passenger-density subsonic aircraft on routes that also have supersonic aircraft service, to provide an estimate of how airlines might respond to high-fare passengers switching to supersonic aircraft (milestone added after additional discussions with our FAA colleagues)

The Purdue team is using its in-house low-fidelity “placeholder” representation of the A10 notional medium SST aircraft to identify the potential supersonic routes based on multiple filters. The team identified 258 potential “supersonic-eligible” routes, comprising 241 nonstop routes and 17 routes with fuel stops. The potential supersonic routes and their associated passenger demand are used in FLEET to determine which of those routes are profitable for the airline and should be served. Early in the project period, the Purdue team used FLEET to indicate which routes had supersonic aircraft service, how many flights per day operated on those routes, and the number of passengers carried on those routes.

The Purdue team has also incorporated the detailed A10 notional medium SST aircraft flown on the detailed supersonic routing path (both provided by Georgia Tech) in FLEET and performed fleet-level assessments for the single “current trends best guess” (CTBG) scenario. The FLEET allocation results indicate routes where supersonic aircraft might be used and might be profitable for the airline, the number of operations performed, along with changes in the utilization of the subsonic aircraft in the fleet. As the Georgia Tech team completes additional supersonic aircraft models with different passenger capacities, ranges, and cruise Mach numbers, the Purdue team will incorporate these aircraft into FLEET.

Because the introduction of SST on certain routes may affect the demand for subsonic travel, the Purdue team developed alternate subsonic aircraft with a higher passenger density (high-passenger-density aircraft) and used them in the FLEET allocation model to provide airlines with an option to use these aircraft to maintain or increase profit on routes using supersonic aircraft. The results show that airlines could maintain or increase existing profit levels by converting existing subsonic aircraft to higher passenger density.

Major Accomplishments

The following major tasks were completed under ASCENT Project 10 during the period of performance:

Fleet-Level Assumptions and Demand Assessment (Task 1)

The Georgia Tech team has developed a parametric airline operating-cost model to allow exploration of the sensitivities of key vehicle, operational, and cost parameters on the required yield that an airline would need to target ticket prices for a potential new supersonic aircraft. This model was integrated with the subsonic forecast to estimate a potential switching percentage on a per-route basis for the estimated cost for an airline to provide commercial SST service. Fuel, a major cost component, was estimated on a per OD pair optimized routing and validated by an aircraft performance model. This procedure resulted in a future-year estimate of the potential demand for SSTs given certain assumptions regarding vehicle performance and cost.

The Purdue team updated FLEET's passenger demand and route network by using historical Bureau of Transportation Statistics (BTS) data for the years 2005–2018, and model-based predictions for the years 2019 and beyond. The team used the previously developed "back of the envelope" representation of the A10 notional medium SST aircraft to identify supersonic-eligible routes including both nonstop routes and routes with one fuel stop. The team also incorporated the detailed A10 notional medium SST aircraft from Georgia Tech into FLEET along with the detailed supersonic routing path (also from Georgia Tech).

Fleet Analysis (Task 2)

One major accomplishment during the period of performance for this task is the capability analyze routes by using the vehicle performance model from Task 4. This allows the detailed evaluation of each route by vehicle capability as well as fuel burn and emissions, which are then fed back to the demand task to refine the demand estimates.

Purdue conducted fleet-level assessments for the updated route network in FLEET by using the detailed A10 notional medium SST aircraft (flown on a detailed supersonic routing path). The outputs included the number of operations and number of passengers served by supersonic aircraft on profitable supersonic-eligible routes, and similar details regarding subsonic aircraft on both supersonic and subsonic routes. In addition, to explore the potential adaptation of an airline that "loses" business-class passengers on its subsonic aircraft, the team developed a high-passenger-density subsonic aircraft model that was used in FLEET to assess the operations of an airline that tries to remain profitable by increasing the number of economy-fare passengers. With these higher-passenger-density aircraft in operation on routes that also have supersonic aircraft service, FLEET can predict the associated impacts on CO_2 emissions.

Because of the continued impact of the COVID-19 pandemic on air travel, the Purdue team updated the historical passenger travel demand to include the reduction in travel in 2019 and 2020, and modified the estimations of future passenger demand to include several recovery scenarios and future demand growth. These adjustments make the FLEET results more relevant and provide a more realistic picture of the potential utilization of supersonic aircraft and associated environmental impacts.

AEDT Supersonic Modeling (Task 3)

The original intent of Task 3 was to develop methods for AEDT to model supersonic transports. At the time of writing of the proposal, AEDT used BADA3 for vehicle modeling; therefore, the proposal focused on BADA3 approaches. Since then, at the time of writing of this report, AEDT is transitioning to BADA4 for new vehicle representation in AEDT, thus rendering the proposed tasks obsolete. On the basis of conversations with FAA technical monitors at Spring of 2019 ASCENT Advisory Board meeting, Georgia Tech has been directed to focus on BADA4 coefficient generation for supersonic transport, which is described in Task 5.

Support of CAEP Supersonic Exploratory Study (Task 4)

Although EDS was originally developed for subsonic vehicles, its structure is still relevant and useful to adapt for the design of supersonic vehicles. One major accomplishment during the previous period of performance was the continual refinement of FASST, specifically the noise assessment for supersonic vehicles, including a variable noise reduction system. Several major modeling accomplishments have been completed during the period of performance by using FASST. The first accomplishment (or more accurately, the first nine accomplishments) is the development of nine closed vehicles ranging from business jets to large SSTs. The second accomplishment is the automation of FASST to generate data for cycle and trajectory optimization. The final accomplishment is the generation of final results of the design Mach trade study for three classes of SSTs.

SST Modeling in AEDT (Task 5)
The Georgia Teach team developed an approach for conducting regression analysis akin to the existing AEDT formulation, and implemented a similar approach for both subsonic and supersonic aircraft. With the current functional form, the accuracy of the regression models has been deemed insufficient. As a result, the team has proposed possible alternative functional forms that are more representative of the underlying physics. The implementation of the proposed approach is under active development and discussion with the FAA.

The Georgia Tech team has developed, and is actively validating and improving, an independent, in-house, physics-informed regression approach that specifically focuses on modeling the propulsive performance and aerodynamic characteristics of supersonic aircraft. The approach has been validated on several GT_SST concepts. The Georgia Tech team has also built a mission simulator to compare the performance of the regressors against truth data across a variety of missions. The mission simulator also provides a framework for implementation of the regression approach within AEDT and has proven to be an effective implementation-related discussion enabler.

Coordination (Task 6)
The Georgia Tech team attended—either in person or virtually after travel became restricted—11 CAEP-related meetings of Working Group 1 (Noise), Working Group 3 (Emissions), and the Modeling and Database Group/Forecasting and Economic Support Group (MDG/FESG) meetings. These meetings included as many as six teleconferences per week, depending on schedules and needs. The Georgia Tech team authored and presented eight papers in these meetings and contributed additional presentations and technical data in support of the CAEP supersonic exploratory study and related progress reports.

The Georgia Tech modeling team provided a medium SST vehicle definition and mission requirement to ASCENT Project 47 Massachusetts Institute of Technology (MIT) researchers for their work on derivative versus clean-sheet propulsion design. In addition, Georgia Tech collaborated with MIT to investigate the impact of a variable noise reduction system on climb-out nitrogen oxide (NO_x) under 3,000 ft for terminal area operations. Finally, Georgia Tech provided detailed results for a Mach 2.2 medium SST in the form of mission-level segment-based results to ASCENT Project 22 and 58. These segment-based results will then be converted to global gridded emissions suitable for global atmospheric analyses,

Task 1 - Demand Assessment

Georgia Institute of Technology

Objective(s)

The primary objective for demand assessment is to first develop a good understanding of the benefits provided by commercial supersonic travel (in terms of time savings) and the increase in ticket cost (proportional to fuel consumption) associated with the faster cruise speed. The model then predicts, for each route, given the corresponding time advantage and ticket cost, the percentage of premium-class passengers expected to switch from existing subsonic service to supersonic offerings.

Demand assessment was conducted on seven SST vehicle models developed at the Aerospace Systems Design Laboratory (ASDL). The SSBJ models were not considered here, because they cater to the business aviation market, and many of the modeling assumptions used for the commercial aviation market no longer hold. The seating capacity and supersonic design cruise Mach number for the seven SST vehicle models are listed in Table 2.

Table 2. ASDL-developed SST vehicle models.

Vehicle Seating Capacity	Supersonic Cruise Mach Number		
55 - Pax	1.8	2.0	2.2
75 - Pax	2.2		
100 - Pax	1.6	1.8	2.0

The flight routing tool optimizes the flight trajectory for each vehicle according to its supersonic and subsonic cruise Mach numbers, as well as the fuel burn characteristics (supersonic specific air range, subsonic specific air range, and transonic acceleration fuel burn). After fuel burn feasibility is verified by flying the optimized flight profile through mission analysis,

viability criteria are then applied to further down-select the final set of routes. This final network differs for each vehicle, because although the demand from premium-class passengers remains constant, different vehicles require different amounts of fuel and provide different time savings.

Research Approach

The demand analysis methodology for commercial SSTs developed by the Georgia Tech team have already been thoroughly described in last year's report. In this year, we have made a slight update to the demand assessment (which changes the estimated switching percentages), because of the use of more accurate trip times obtained from the high-fidelity aircraft mission analysis tool Flight Optimization System (FLOPS). This model capability is described under Task 2.
When performing flight path planning, a more time-optimal setting is first used to calculate all trajectories. If that mission profile cannot be completed by the aircraft because of insufficient fuel capacity, the failed routes are rerun with a more fuel-optimal setting. For a given SST model, all routes that can be flown within the fuel limit are considered feasible. However, whether that route is included in the final network (for that specific SST model) depends on the viability filters.

The criteria for route viability checking are provided below (and are the same as last year's). For a route to be deemed viable, it must meet the following criteria:

1. Time savings relative to the reference subsonic aircraft are more than 20%
2. Time savings relative to the reference subsonic aircraft are more than two hours
3. Number of accelerations are less than four, if no fuel stop is needed
4. Number of accelerations are less than six, if fuel stops are needed
5. Number of flights per day in 2050 are at least one
6. Change in fare per hour saved is less than $1,000

The reasoning for each of these filters is as follows:

- The relative time savings limit is present to enforce a minimum time savings as a percentage of the conventional subsonic trip time, thus allowing for the removal of routes for which the relative time savings might not justify the additional expense for passengers. This filter is similar to but different from the second filter, which is based on a minimum absolute time savings and focuses on removing routes for which the time savings might be less than two hours because passengers may not be able to make use of the small amount of time saved, and therefore their willingness to pay might be low.
- The third and fourth filters are present to eliminate routes that would require too many supersonic accelerations, which, even without detailed performance analysis, would exceed any vehicle performance capability.
- The fifth filter is present to focus on routes that would allow for regular daily service in the highest-demand year in the forecast period. Although more sporadic service (e.g., only several days per week) would also be an option for airlines to offer regular scheduled service, the focus was on the best routes with sufficient demand to enable this service.
- The sixth and final filter is present to limit the maximum fare per hour differential with respect to subsonic service. This filter eliminates routes that meet the other filter criteria but, for various reasons, would require very expensive tickets in order for the service to be offered. The reasons may include excessive circuity (wherein the aircraft, to avoid sonic boom, is forced to fly a long additional distance while still having good relative time savings) or burning large amounts of fuel by maneuvering the aircraft. This final filter removes these routes because passengers willing to pay a very high premium for limited time savings could potentially be served better by business jet service, either subsonic or supersonic.

Results

By analyzing the route data for commercial aviation and forecasting its growth (details were discussed in the previous report), the team identified a set of 1,114 feasible global routes with potential demand from premium-class passengers to support commercial supersonic service in the year 2050. However, routes failing to meet the viability criteria will not be considered in the final network. Several key assumptions are listed below:

1. The forecast year is 2050.
2. The passenger load factor is 70%.
3. Available seat kilometers (ASKs) and revenue passenger kilometers (RPKs) are calculated using great-circle distance and not rerouted distance.

4. The refuel stops last 90 minutes.

Figure 1 shows the relationship between the percentages of feasible routes that are also viable for the seven SST designs, which can be understood as a measure of market-capture capability for different vehicles. It can be seen that the slower Mach numbers (Mach 1.6) have a noticeable impact on the viability of routes, because slower vehicles generally cannot provide as much time savings. Additionally, the larger passenger capacity also adversely affects large SSTs' market capture, because there is a feasibility requirement for the minimum flight frequency, and more passengers are needed to fill a large SST's seats. The 75-Pax Mach 2.2 design performed reasonably well, with very similar market capture compared to that of the Mach 1.8 and the Mach 2.0 variants of the 55-pax SST, although its seating capacity is higher. However, the Mach 2.2 variant of the 55-pax SST still offered the highest market capture. In summary, the general trend is that a higher Mach number and lower seating capacity will lead to greater market capture.

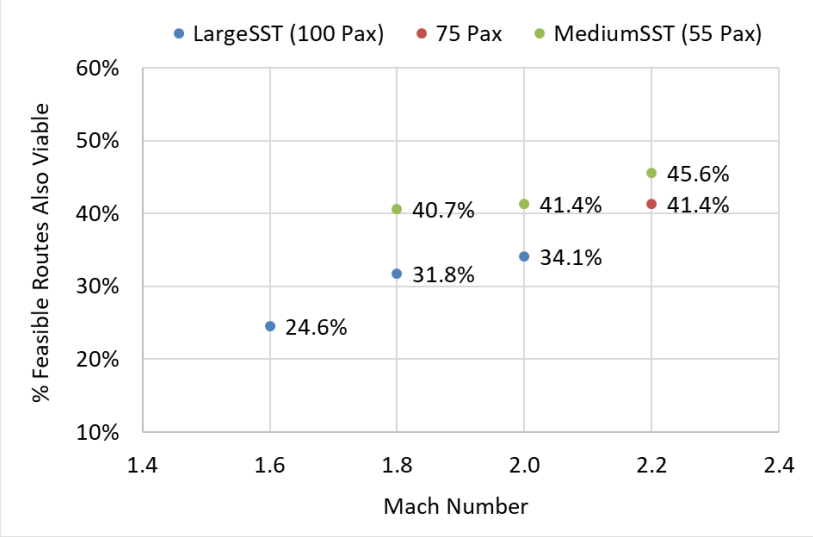

Figure 1. Percentage of feasible routes that are also viable for the seven SST designs.

Figure 2 shows what percentage of viable routes that must be completed with a refuel stop. Because the large SSTs are designed with 5000 nmi of supersonic range, those vehicles are less likely to require refueling. Here, the 75-Pax again shows good performance, considering that it is carrying 20 more passengers but performs on a similar level to that of the Mach 1.8 variant of the medium SST. Moreover, the Mach 2.0 large SST does not require more refuel stops than the Mach 1.8 large SST, because of multiple competing effects, such as the time penalty of refueling against the speed advantage of a higher supersonic cruise Mach number. The overall trend is that SSTs with a higher design Mach number are more likely to require refueling, and the large SST with a supersonic design range of 5000 nmi reduced the need for refueling (approximately 30%–40% reduction) when compared to the medium SST with 4,500 nmi of range.

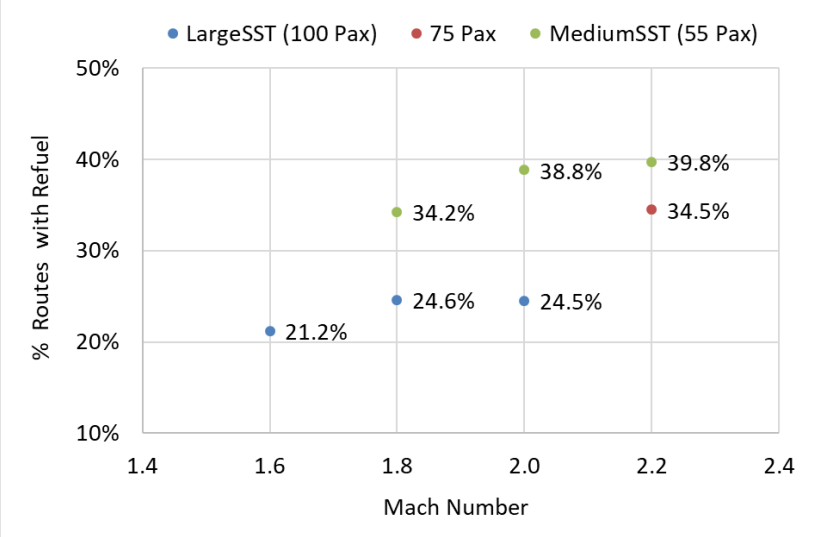

Figure 2. Percentage of viable routes requiring a refuel stop for the seven SST designs.

Table 3 summarizes several key air transportation metrics to aid in understanding the forecasted scale and volume of commercial SST operations for different vehicle designs.

Table 3. Key transportation metrics for the seven SST designs.

SST Type	Mach Number	Sum of Annual Flights (Thousands)	Sum of Annual Passengers (Millions)	Sum of Annual Flight Distance (Billion km)	Sum of Annual Flight Hours (Millions)	Sum of Annual ASK (Billions)	Sum of Annual RPK (Billions)
Large SST (100 Pax)	1.6	211	14.8	1.447	1.226	144.7	101.3
	1.8	281	19.7	1.955	1.600	195.5	136.9
	2.0	308	21.6	2.124	1.666	212.4	148.7
75 -Pax	2.2	469	24.6	3.269	2.536	245.2	171.6
Medium SST (55 Pax)	1.8	616	23.7	4.455	3.748	245.0	171.5
	2.0	631	24.3	4.509	3.662	248.0	173.6
	2.2	690	26.6	4.879	3.837	268.4	187.9

Continuing the same trend observed in market capture, Table 3 shows that smaller, faster designs generally lead to an increased scale of operations (in terms of available seat kilometers). Notably, the 75-Pax (Mach 2.2) design is ranked second in terms of total passengers flown and provides similar total ASKs to the Mach 1.8 medium SST, although the total number of flights and the total flight distance are significantly lower.

Task 2 - GT Fleet Analysis

Georgia Institute of Technology

Objective(s)

The fleet analysis conducted by Georgia Tech mainly focused on the fuel burn, CO_2, and NO_x emissions for the seven aforementioned ASDL-developed SST vehicle models.

Research Approach

The routing algorithm developed by ASDL and described in last year's annual report was updated to accommodate the different performance characteristics of SST vehicle models. Additionally, the flight routing algorithm's output is now merged with aircraft mission analysis output from FLOPS, thus enabling output of the geographic location and the altitude at which the emissions occur. A sample trajectory output is visualized in Figure 3.

In Figure 3, two main types of points are shown on the SST trajectory. The original track points, marked by purple crosses, are the waypoints generated by the flight routing algorithm. The orange dots indicate locations where the discretized FLOPS mission analysis output is available. The mission analysis output is tightly spaced during the acceleration and climb, thus capturing the dynamic behavior of the aircraft during these phases of flight in detail.

The emission species considered and the associated emission indices are listed below:

- NO_x (kg): taken from FLOPS output (details regarding NO_x modeling discussed the Emissions Modeling section of this report)
- CO_2 (kg) based on fuel burn, constant emissions index (EI) of 3.159 kg/kg-fuel (AEDT 3c Tech Manual)
- H_2O (kg) based on fuel burn, constant EI of 1.237 kg/kg-fuel (AEDT 3c Tech Manual)
- Non-volatile particulate matter (nvPM) (g) based on fuel burn, constant EI of 0.05 g/kg-fuel
- Organic particulate matter (PM) (g) based on fuel burn, constant EI of 0.05 g/kg-fuel
- SO_2 (g) and SO_4 (g) based on fuel burn, fuel sulfur concentration (FSC) = 600 mg/kg-fuel
    - E = 2% conversion to SO_4 and estimate the sulfate PM emissions
    - SO_2: FSC/1,000 × [(100% − E)/100%] × fuel × 64/32
    - SO_4: FSC/1,000 × (E/100%) × fuel × 96/32

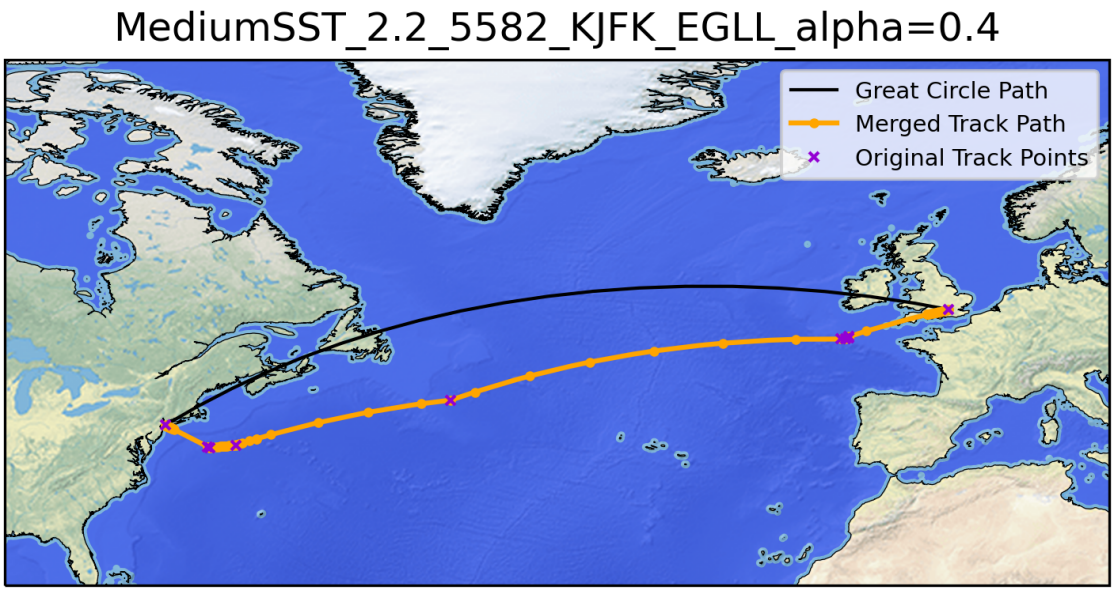

Figure 3. Flight routing tool waypoints and mission analysis data points for KJFK–EGLL.

Results

A jet fuel density of 0.8 kg/L was used. The previously mentioned assumptions regarding passenger load factor and distance measure (great-circle distance [GCD] instead of rerouted distance) still apply.

Table 4. Key emissions metrics for the seven SST designs.

SST Type	Mach Number	Total Annual Fuel Burn (Megatonnes)	Total Annual CO_2 (Megatonnes)	Total Annual NO_x (Kilotonnes)	Fuel Intensity (kg/ASK)	Fuel Efficiency (RPK/L)
Large SST (100 Pax)	1.6	11.52	36.35	150.28	0.080	7.03
	1.8	17.78	56.10	247.60	0.091	6.16
	2.0	22.18	70.01	334.96	0.104	5.36
75-Pax	2.2	33.16	104.65	633.78	0.135	4.14
Medium SST (55 Pax)	1.8	26.80	84.58	391.08	0.109	5.12
	2.0	34.37	108.46	563.81	0.139	4.04
	2.2	43.39	136.95	768.57	0.162	3.46

Of note, the amounts of total fuel consumption, carbon dioxide and nitrogen oxides result from different market capture and scale of operations. To directly compare the fuel efficiency of different vehicles, examining the fuel intensity and fuel efficiency is more reasonable. The general trend is that larger vehicles are more fuel efficient on a per-ASK or per-RPK basis. Additionally, increasing the supersonic design cruise number obviously leads to higher fuel consumption.

Another point that must be emphasized is that the fuel intensity and fuel efficiency values reported here are network-averaged values. If a vehicle were to fly only simple supersonic missions, then the fuel efficiency would be significantly higher. Operating on routes requiring a substantial portion of subsonic overland flight or additional transonic accelerations would have a big impact on the overall network-averaged fuel efficiency.

The detailed results for the Mach 2.2 medium SST were saved as mission-level segment-based results, which were shared with Ascent Project 22 and 58. These segment-based results will be converted to global gridded emissions, which are suitable for global atmospheric analyses,

Task 2 - Purdue Fleet Analysis

Purdue University

Objectives

The Purdue team conducted four sub-tasks as a part of this task. For this year, the Purdue team used a U.S.-touching route network to study the impact of supersonic aircraft operations on subsonic aircraft operations, predict the changes in future supersonic travel demand due to the COVID-19 pandemic, and develop a simultaneous aircraft allocation approach for supersonic and subsonic aircraft. Additionally, the team extended the U.S.-touching route network in FLEET to a worldwide route network; the task is still underway and will be completed next year.

Supersonic Demand and Route Characterization

The ticket fares associated with supersonic aircraft travel will be higher than those of current economy-class tickets, which indicates that there will only be a small segment of passengers who would be willing to pay for the supersonic aircraft service. In addition, the supersonic aircraft characteristics (particularly the restriction from overland supersonic operations and the range of the aircraft) will limit the routes on which the aircraft could operate. Hence, the number of passengers on a given route who would be willing to pay for and use supersonic aircraft must be determined, and the potential routes with supersonic aircraft operations must be identified.

Supersonic Passenger Demand

The Purdue team assumed that the potential supersonic passengers are the current passengers paying fares at business class or above. In FLEET, the travel demand is split such that supersonic demand (business class or above) is a fixed percentage (5%) of the total travel demand on each route, and the remaining demand is from passengers only willing to pay subsonic fares.

Potential Supersonic Routes (U.S.-Touching Route Network)

In this report, the team considered potential airport pairs that are nonstop (direct) or include a fuel stop (indirect) as potential supersonic routes. The potential supersonic routes were identified from FLEET's existing U.S.-touching route network of 1,974 routes in year 2018 (the route network in the year 2018 is the most recent route network in FLEET, and the network stays constant for all years beyond 2018), by using a set of route filters based on the performance characteristics of a placeholder supersonic aircraft (different from the high-resolution supersonic aircraft provided by Georgia Tech). The potential supersonic routes were filtered according to the placeholder supersonic aircraft's maximum design range (thus differentiating between routes that require a fuel stop and those that do not), the aircraft's maximum range capability for different percentages of supersonic and subsonic flight segments, and the block time savings incurred by flying supersonic aircraft rather than subsonic aircraft. To calculate the minimum time flight path for a supersonic route, the Purdue team used a very simple supersonic route path adjustment strategy that outputs the block time, percentage of flight path over water, updated departure heading for the route, and minimum time route distance.

Nonstop Routes (U.S.-Touching Route Network)

The route filters for nonstop routes led to the identification of 241 nonstop potential supersonic routes in the FLEET network. Of these 241 routes, with our simplistic route path adjustment, 191 routes have greater than or equal to 75% of flight overwater, 35 routes have flight segments between 50% and 75% over water, and the remaining 32 routes have flight segments less than 50% over water.

Routes with Fuel Stops (U.S.-Touching Route Network)

Some intercontinental routes exceed the un-refueled range of the supersonic aircraft with sufficiently high passenger demand to suggest the potential for profitable supersonic operations. These routes show total time savings even with the increase in distance flown, and the time required to land, refuel, and take off again, with the assumption that the fuel stops are just technical stops (i.e., there is no boarding of new passengers from the fuel-stop airport into the flight or debarkation of any existing passengers from the flight). Only airports currently in the FLEET network were considered for potential fuel stops. There are two trans-Pacific potential fuel-stop airports (Honolulu, Hawaii (HNL) and Anchorage, Alaska (ANC); and five trans-Atlantic potential fuel-stop airports (Shannon, Ireland (SNN); Keflavik, Iceland (KEF); Oslo, Norway (OSL); Dublin, Ireland (DUB); and San Juan, Puerto Rico (SJU). The fuel stop adds 60 minutes to the block time of the supersonic aircraft flying on the with-fuel-stop route (this is based on the team's judgement, including the time for final descent, landing, taxi, refueling, taxi, takeoff, and climb out).

U.S.-Touching Supersonic-Eligible Route Network in FLEET

The supersonic-eligible route network in FLEET consists of a total of 258 potential supersonic routes, 241 of which are nonstop and 17 of which include a fuel stop. Figure 4 depicts the potential supersonic route network for FLEET on a world map. The route paths for the 258 potential routes plotted in this figure are based on airport minimum time connections and are only illustrative.

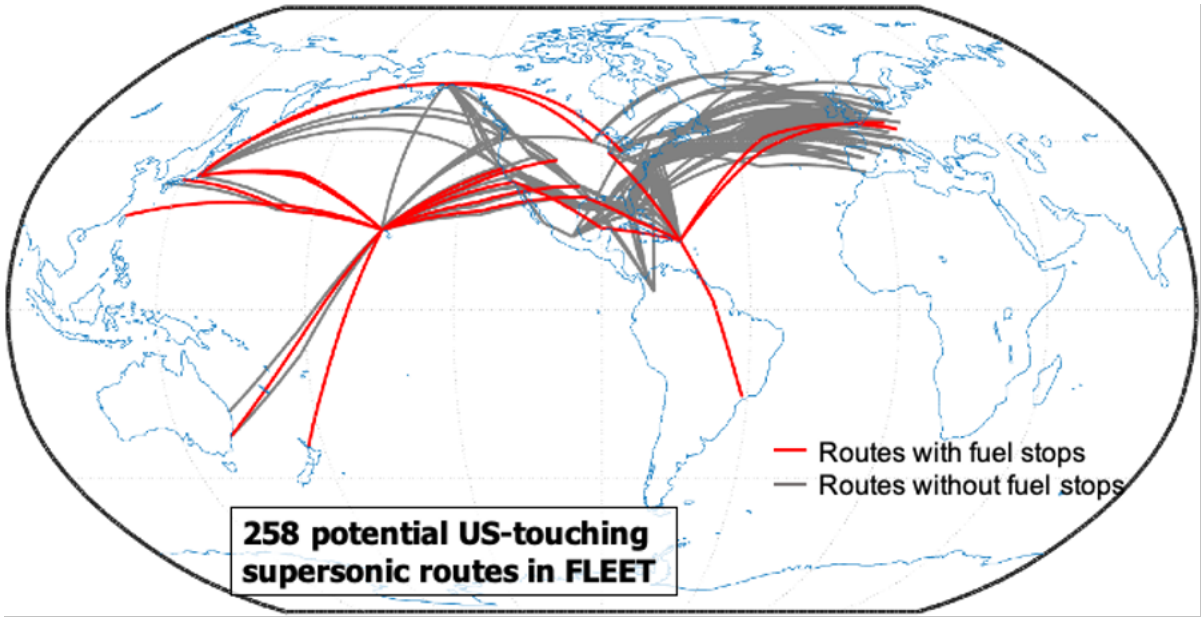

Figure 4. U.S.-touching supersonic-eligible route network in FLEET (airport minimum time connections, not the exact route path flown, are shown).

Impact of Supersonic Aircraft Operations on Subsonic Operations

The Purdue team predicted how commercial supersonic aircraft operations as part of an airline's fleet might alter subsonic operations across the network in an effort to maintain profitability. The current work was based on the assumption that the potential supersonic passengers are the current subsonic passengers who pay "business class or above" fares. Considering current ticket pricing on many over-ocean routes where future supersonic aircraft would operate, the ticket prices for business class or above tend to subsidize the economy-class ticket prices. When the airline loses a portion of its subsonic high-revenue passengers to supersonic service, the airline might want to alter the economy ticket prices to compensate for the loss of business-class seats and associated fares. As these passengers shift from subsonic business class or above to supersonic service, airlines may need to change how they operate their subsonic fleet of aircraft to maintain or increase profit. One possible way to do so is to reconfigure the current subsonic aircraft by removing premium seats and replacing them with a higher number of "economy" seats to limit the impact of the loss of revenue, from business class or above fares, on profits. With changes to the subsonic aircraft seating configuration, the team considered four possibilities for how airlines might adjust ticket pricing to continue to make similar (or even greater) profit. This work simulated those four different ticket pricing possibilities and estimated their potential future effects on airline profits and emissions when high-passenger-density aircraft are introduced alongside supersonic aircraft.

<u>High-Passenger-Density Subsonic Aircraft Modeling Approach</u>

This work considered high-passenger-density versions for the "new-in-class" and "future-in-class" generations of class 3 (SA – single aisle), class 4 (STA – small twin aisle), class 5 (LTA – large twin aisle), and class 6 (VLA – very large aircraft) subsonic aircraft in FLEET. As mentioned above, the concept for modeling a higher-passenger-density subsonic aircraft is that some of the larger premium (business class or first class) seats are removed and replaced with a larger number of smaller economy-class seats. A study of recent multi-class cabin configurations—which vary by aircraft among airlines, and even among sub-models of aircraft within a given airline—has determined the ratio of "small" seats added to "large" seats removed. For modeling in FLEET, the team adjusted the operating load factor of the subsonic aircraft operating on routes where supersonic service is also available, to mimic operating an aircraft with more seats in a higher-passenger-density cabin. The major assumption was that the aircraft operating empty weight remains constant even when a higher number of seats is present in the aircraft; therefore, the weight of the seats in business class or above removed from the aircraft equals the weight of the economy-class seats added to the aircraft. This assumption allowed the team to reuse existing subsonic aircraft FLOPS models. The team acknowledges that a higher-fidelity approach to model the high-density version of the existing subsonic aircraft would be to modify the existing aircraft models in FLOPS by using a different operating empty weight (with the

difference in the operating empty weight resulting from the replacement of some large seats with a larger number of small seats); however, the team believes that the simplistic modeling approach described here is sufficient to demonstrate the fleet-level impacts of introducing high-density subsonic aircraft on routes with supersonic aircraft operations.

High-Passenger-Density Subsonic Aircraft Seat Configuration

This work was based on the assumption that 50% of the passengers in business class or above are the potential supersonic passengers. This assumption is based on observations that approximately 10% of the seats in multi-class cabin aircraft are premium seats, and approximately half the passengers who sit in premium seats pay the premium fare (whereas the remainder use some form of upgrade or reward). The team configured the high-passenger-density subsonic aircraft by replacing half the seats in business class or above (large) with twice the number of economy-class (small) seats. Figure 5 compares the seat areas of various seat configurations for long-haul flights across different airlines, where the seat area is estimated as the product of the seat pitch and seat width. On average, the first-class, business-class, and premium-economy seat areas are 3.2 times, 2.3 times, and 1.3 times larger than the basic economy-class seat areas, respectively, according to data obtained from SeatGuru (by Tripadvisor) in March 2019.

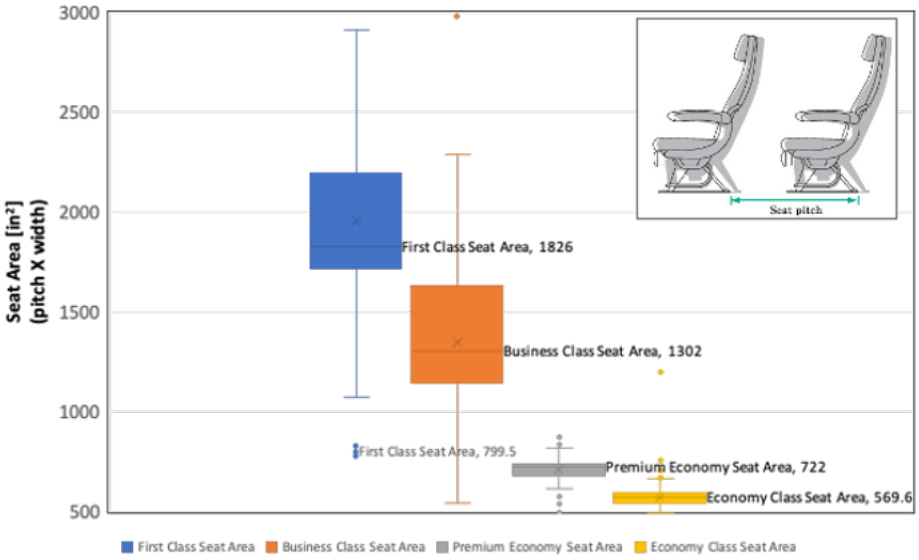

Figure 5. Seat area comparison for aircraft seat configurations for long-haul flights across different airlines.

On the basis of these findings, the team assumed that one large seat is approximately equal to two small seats. For example, a class 3 aircraft in FLEET has 12 large seats and 165 small seats, with a total of 177 seats in its standard configuration. Using the aforementioned approach, the high-passenger-density version of a class 3 aircraft would have (12 – 12/2) = 6 large seats and (165 + 2 × 12/2) = 177 small seats, with a total of 183 seats. Table 5 shows the seat configuration for all four classes of high-passenger-density aircraft. Prior to the study described here, all the subsonic aircraft (referred to as standard configuration in this paper) in FLEET operated at a load factor of 80% for the allocation problem and did not require differentiation between classes of seats. The values for the high passenger density at an 80% load factor provide an estimate of how the seats would be filled in each cabin class.

Table 5. Seat configuration for all four classes of high-passenger-density aircraft (*seat capacity: economy class [small seats] + business class or above [large seats]).

	Single-Aisle, SA (Class 3)		Small Twin-Aisle, STA (Class 4)		Large Twin-Aisle, LTA (Class 5)		Very Large, VLA (Class 6)	
Configuration	Standard	High-pax-density	Standard	High-pax-density	Standard	High-pax-density	Standard	High-pax-density
Max Seat Capacity [pax]	177 (165 + 12)*	**183 (177 + 6)***	261 (237 + 24)*	**273 (261 + 12)***	305 (227 + 78)*	**344 (305 + 39)***	417 (309 + 108)*	**471 (417 + 54)***
Pax capacity w/ 80% load factor	142	**147 (142 + 5)***	209	**219 (209 + 10)***	245	**275 (244 + 31)***	335	**377 (334 + 43)***

Maximum Passenger Capacity of Subsonic Aircraft

For models of the new-in-class and future-in-class aircraft, the smaller class 3 (single aisle) and class 4 (small twin aisle) high-passenger-density aircraft cannot fly most of the popular trans-Atlantic and trans-Pacific routes at an 80% load factor, whereas their counterparts with standard configuration can. The reason for this difference is the highly efficient nature of these notional future subsonic aircraft models. Figure 6 shows modified payload-range diagrams for class 3 and class 4 aircraft in standard configuration, that uses load factor rather than payload on the vertical axis. The new-in-class, class 3 aircraft has an intersection of the maximum takeoff weight limit and the fuel volume limit at a load factor of approximately 90%, whereas that of the future-in-class aircraft is at approximately 50%. For class 4 aircraft, this intersection for both the new- and future-in-class is at approximately 90%. The new-in-class, class 3 aircraft could only complete routes approximately 3,400 nmi or less at an 80% load factor in standard configuration, and the future-in-class aircraft could complete routes of approximately 4,400 nmi or less. Similarly, the class 4 aircraft at an 80% load factor could complete routes of only approximately 6,400 nmi or less for both the new-in-class and future-in-class versions in standard configuration. The aircraft with high-passenger-density configuration would be at a lower load factor for the same payload weight, which would make the maximum range for these aircraft even narrower at an 80% load factor. These findings suggest the need to consider the maximum number of passengers that could be carried by any of the class 3–6 aircraft on the trans-oceanic routes, because those trans-oceanic routes are where the supersonic aircraft might also operate.

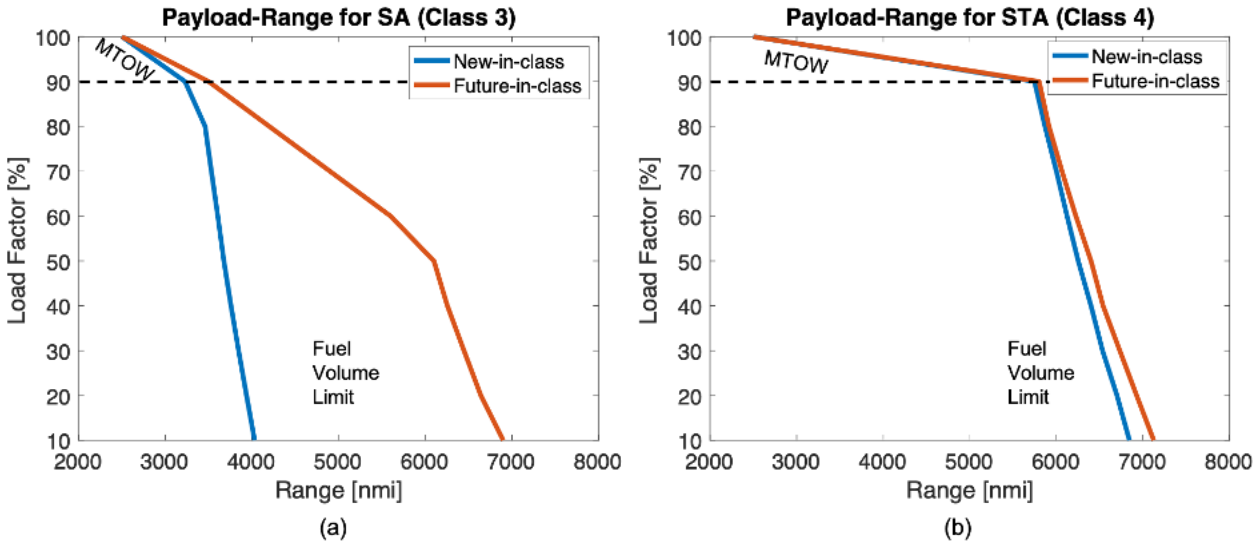

Figure 6. Payload-range charts for (a) class 3 subsonic aircraft, and (b) class 4 subsonic aircraft in FLEET.

The team reran the subsonic aircraft FLOPS models to determine the maximum passenger capacity for a given range. Figure 7 shows how the maximum load factor for the standard configuration varies with route length. As expected, the maximum load factor decreases as the route length increases. Because the high-passenger-density subsonic aircraft are introduced only on routes that see supersonic aircraft operations, the authors only considered the route lengths of the 258 supersonic-

eligible routes in this effort. Consequently, all the high-passenger-density subsonic aircraft (new-in-class and future-in-class aircraft for classes 3, 4, 5, and 6 to have a unique maximum passenger capacity for each of the 258 supersonic-eligible routes.

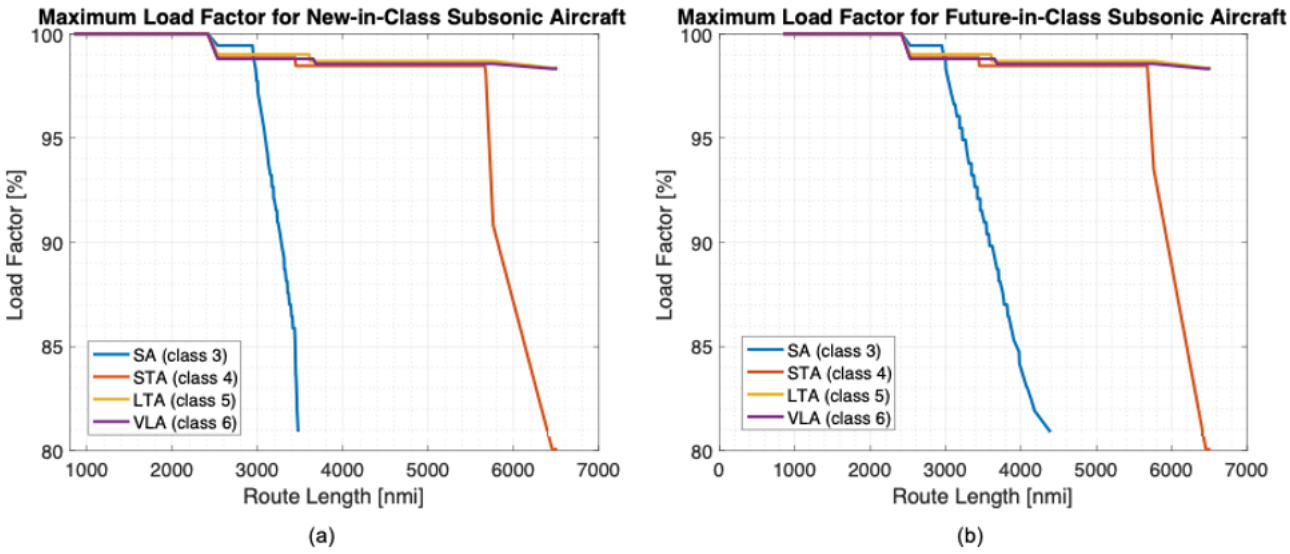

Figure 7. Maximum load factor for the standard configurations, as a function of route length for (a) new-in-class subsonic aircraft and (b) future-in-class subsonic aircraft, in FLEET.

Implementation of High-Passenger-Density Subsonic Aircraft in FLEET

To determine the number of subsonic seats available in FLEET for a specific subsonic aircraft class on a route with supersonic service, the team chose the lower value of the passenger capacity corresponding to an 80% load factor of the high-passenger-density configuration or the maximum number of passengers that the standard configuration aircraft could carry on the route. For example, if the number of seats available using the high-passenger-density configuration class 3 aircraft with an 80% load factor is 147 passengers on a hypothetical route A–B, and the maximum capacity for a class 3 standard configuration aircraft is 135 passengers on that route, then the high-passenger-density aircraft could only carry 135 passengers. Therefore, the payload weight limitation may restrict the high-passenger-density configuration aircraft to carry the same number of passengers as in the standard configuration, and the airline would see no revenue benefit to using this class of aircraft on this route.

To introduce these high-passenger-density subsonic aircraft into FLEET, the team generated the FLEET relevant aircraft performance and cost coefficients for all the high-passenger-density subsonic aircraft (similar to the standard versions of these aircraft) by using the updated load factor for each of the 258 routes. The updated load factor is calculated as the percentage ratio of the available seats for the high-passenger-density aircraft to the maximum number of seats available in the standard configuration.

For a route where the 80% load factor on the high-passenger-density configuration is not restricted by the payload-range diagram, the updated load factor will be greater than 80%. For instance, a high-passenger-density class 5 aircraft at an 80% load factor will carry 275 passengers; the FLEET updated load factor will be (275/305) × 100 = 90%. For the above example of the high-passenger-density class 3 aircraft with a payload-range limitation, the FLEET updated load factor on that route will be (135/177) × 100 = 76%.

Table 6 shows sample aircraft performance and cost coefficients for a new-in-class, class 3 aircraft on the John F. Kennedy International Airport (JFK)–London Heathrow International Airport (LHR) route; this route of approximately 3,000 nmi is not payload-range limited for this aircraft in either the standard or high-passenger-density configuration. As expected, the high-passenger-density configuration of subsonic aircraft burns more fuel (because of the higher payload weight) and has higher crew and indirect operating costs (because of the relationship to the number of passengers carried).

Table 6. Sample aircraft performance and cost coefficients for new-in-class, class 3 aircraft on the JFK–LHR route.

Coefficients for new-in-class 3 aircraft on JFK – LHR route	Standard	High-Pax-Density	Increment
Block time [hrs.]	7.2	7.2	**0.0 %**
Fuel burn [lbs.]	31,663	32,825	**+3.7 %**
Crew cost [$]	5,848	5,872	**+0.4 %**
Indirect operating cost [$]	19,966	20,338	**+1.9 %**
Servicing cost [$]	1,318	1,318	**0.0 %**
Maintenance cost [$]	2,030	2,030	**0.0 %**

The team currently uses a sequential allocation approach for allocating the supersonic and subsonic passengers in FLEET. In the sequential allocation approach, the allocation of the airline's supersonic aircraft occurs before the allocation of the airline's subsonic aircraft. Because the supersonic aircraft are allocated first, introducing high-density subsonic aircraft only on routes with supersonic aircraft allocation is straightforward. Hence, the team was able to implement the high-passenger-density subsonic aircraft in FLEET without modifying the allocation problem itself.

High-Passenger-Density Subsonic Aircraft Ticket Pricing

With the "densification" of the subsonic aircraft, 50% of the passengers in business class or above would switch from subsonic to supersonic aircraft, which could cause the airlines to adjust ticket pricing for the high-passenger-density aircraft operations to continue to make similar (or even higher) profits. The team considered four ticket pricing possibilities for the high-passenger-density aircraft; each possibility affects the profitability of a given aircraft type on a given trip, and the aircraft allocation changes to maximize profit.

Currently, FLEET uses an average ticket price for all its simulations. To capture the ticket price possibilities when the seating configuration changes, business and economy ticket prices must be considered separately. To break down the average ticket price in FLEET into business-class and economy-class prices, the team assumed that a business-class ticket price costs twice as much as the economy-class ticket price. Using the seat configuration information for the existing subsonic aircraft in FLEET and the ratio of business-class to economy-class ticket prices, the team determined the business and economy ticket prices for each aircraft type on every route in FLEET (using Equations 1 and 2). Equations 3 and 4 depict the relationship between average ticket price, ticket price margin, and trip margin in the existing subsonic ticket pricing model in FLEET.

Equation 1 $$\mathbf{avg_{ticketprice}} = \frac{\mathbf{ticketprice_{business} * seats_{business} + ticketprice_{economy} * seats_{economy}}}{\mathbf{seats_{total}}}$$

Equation 2 $$\mathbf{ticketprice_{business}} = \mathbf{2} \times \mathbf{ticketprice_{economy}}$$

Equation 3 $$\mathbf{avg_{ticketprice}} = \frac{\mathbf{cost_{trip}}}{\mathbf{seats_{total}}} + \mathbf{ticketprice_{margin}}$$

Equation 4 $$\mathbf{trip_{margin}} = \mathbf{avg_{ticketprice}} \times \mathbf{seats_{total}} - \mathbf{cost_{trip}}$$

There are four possible high-passenger-density ticket price modeling approaches in FLEET:

Case 1: Constant Average Ticket Price

In this case, the average ticket price for the high-passenger-density aircraft is set to be the same as the average ticket price for the standard subsonic aircraft. The higher number of seats with the high-passenger-density version causes both the business and economy ticket prices to increase, thus leading to a higher ticket price margin and trip margin (Table 7). The airline is expected to earn a higher profit when this approach is implemented in FLEET.

Case 2: Constant Ticket Price (Business and Economy)
In this case, the business and economy ticket prices for the high-passenger-density aircraft are set to be equal to the business and economy ticket prices for the standard subsonic aircraft. Because of the increased number of seats in the high-passenger-density version, the ticket price margin and trip margin increase slightly (but remain lower than those in case 1), while the average ticket price decreases (Table 7). The airline is expected to earn a slightly higher profit when this approach is implemented in FLEET (but lower than that in case 1).

Case 3: Constant Trip Margin
In this case, the trip margin for the high-passenger-density aircraft is set to be the same as the trip margin for the standard subsonic aircraft. With the constant trip margin spread out over more seats for the high-passenger-density version, the business and economy ticket prices are slightly lower, along with the average ticket price. However, the ticket price margin remains higher than that the standard subsonic aircraft case (Table 7). The airline is expected to earn a slightly lower profit when this approach is implemented in FLEET, because the passengers end up paying less for the business-class and economy-class tickets.

Case 4: Constant Ticket Price Margin
In this case, the ticket price margin for the high-passenger-density aircraft is set to be the same as the ticket price margin for the standard subsonic aircraft. The economy-class tickets have a much lower margin than business-class tickets. With a smaller number of business-class seats available in the high-passenger-density version, the trip margin, prices of business and economy tickets, and average ticket price decrease (Table 7). This case indicates that the airline is unable to compensate for the loss of business-class seats, and the airline's profit is expected to be lowest.

Table 7 summarizes the four possible airline actions with respect to ticket pricing for high-passenger-density subsonic aircraft and their required FLEET inputs. Table 8 considers the JFK–LHR route as an example to provide ticket price values for a new-in-class, class 3 subsonic aircraft; the numbers in this example help demonstrate the actual changes in trip and ticket price margins as different ticket pricing strategies are adopted.

Table 7. Possible airline actions with respect to ticket pricing for high-passenger-density subsonic aircraft and their required FLEET inputs.

Possible airline actions	Inputs				
	Average Ticket Price	Economy Ticket Price	Business Ticket Price	Trip Margin	Ticket Price Margin
No high-pax-density	–	–	–	–	–
Case 1: Constant average ticket price	–	↑	↑	↑	↑
Case 2: Constant ticket price	↓	–	–	↑ (slightly)	↑ (slightly)
Case 3: Constant trip margin	↓	↓ (slightly)	↓ (slightly)	–	↑ (slightly)
Case 4: Constant ticket price margin	↓	↓	↓	↓	–

Impact of COVID-19 on Passenger Demand and Fleet-Level Assessments
The novel coronavirus (COVID-19) pandemic has caused severe disruptions in the aviation industry by inducing one of the sharpest declines in air travel demand in aviation history. The full-year global passenger traffic results from both the International Air Transport Association (IATA) and the International Civil Aviation Organization (ICAO) indicate that 2020 was the worst year in history for air travel demand (IATA Press Release, 2021; ICAO, 2021). According to IATA, the global passenger demand in 2020 fell by 65.9% with respect to the pre-COVID-19 levels of 2019 (IATA Press Release, 2021; IATA Economic Reports, 2020). ICAO has provided similar estimates for the decrease in travel demand in 2020 (ICAO, 2021), with an overall reduction of 50% of seats offered by airlines, which translates to approximately 2,699 million fewer passengers

worldwide compared to the pre-COVID-19 levels (2019). In 2021, IATA estimates indicate that the demand may recover to between 38% to 52% of pre-COVID-19 levels (2019), and complete recovery to 2019 levels may be possible by 2023 or 2024 (IATA Press Release No: 33, 2021; Pearce, 2021), depending on the continuation of travel restrictions imposed worldwide because of the spread of more contagious COVID-19 variants.

Table 8. Ticket pricing example for new-in-class, class 3 aircraft on the JFK–LHR route (*based on the assumption that a business-class ticket costs twice as much as an economy ticket).

JFK-LHR route / Class 3 aircraft	Possible airline actions	Average Ticket Price [$]	Economy Ticket Price [$]*	Business Ticket Price [$]*	Trip Margin [$]	Economy Ticket Margin [$]*	Business Ticket Margin [$]*
Standard (132 + 10)	Existing	342.8	320.2	640.4	1759.3	-10.2	310.1
High-pax-density (142 + 5)	Case 1: Constant average ticket price	342.8	331.5	663.0	3587.6	13.1	344.6
	Case 2: Constant ticket price	331.1	320.2	640.4	1873.8	1.9	322.1
	Case 3: Constant trip margin	330.3	319.5	638.9	1759.3	1.1	320.6
	Case 4: Constant ticket price margin	319.1	308.2	628.4	107.3	-10.2	310.1

Future Demand Scenarios

For this report, the Purdue team considered two different scenarios for airline operations recovery after the current decrease in operations due to COVID-19-related travel restrictions imposed worldwide. The team also considered three GDP growth scenarios from the year of passenger demand recovery to pre-COVID-19 levels (2019) to the year 2030; the GDP growth rate directly impacts the inherent passenger demand in FLEET. Thus, a total of six scenarios for future demand projections are examined. The total passenger demand in 2020 for all six scenarios is set to 34% of the passenger demand levels in 2019, signifying a 66% decrease in total passenger demand (IATA Press Release No: 33, 2021).

The first three scenarios consider that the passenger demand returns to pre-COVID-19 levels (2019) by the year 2023. The total passenger demand is set to recover to 52% of pre-COVID-19 levels by 2021, 88% of pre-COVID-19 levels by 2022, and 100% of pre-COVID-19 levels by 2023 (IATA Press Release No: 33, 2021). These three scenarios are distinguished by the inherent passenger demand growth rate, which is based on the GDP growth rate assumed in the FLEET simulation. The first scenario, 2023 recovery, assumes that the passenger demand continues to grow based on the GDP growth rate in FLEET beyond 2023. This scenario does not consider the long-term economic impacts of the COVID-19 pandemic and assumes that the GDP will continue to grow in a manner unaffected by the pandemic after 2023. The second scenario, 2023 recovery + GDP slowdown to 75% until 2030, considers that the passenger demand grows corresponding to 75% of the GDP growth assumptions in FLEET from the years 2023–2030. This scenario considers the long-term economic impacts of the COVID-19 pandemic and assumes that the GDP will grow at a slower rate until the year 2030. The third scenario, 2023 recovery + GDP inflation to 125% until 2030, assumes that the passenger demand grows at 125% of the inherent demand and GDP growth assumptions in FLEET from the years 2023–2030. This scenario assumes that the GDP will rebound and become stronger in the longer term and grow at a faster rate until the year 2030.

The remaining three scenarios consider that the passenger demand returns to pre-COVID-19 levels (2019) by the year 2024 (1 year later than in the previous three scenarios). The total passenger demand is set to recover to 38% of pre-COVID-19 levels by 2021, considering the possibility that the severe travel restrictions in response to new COVID-19 variants might persist (IATA Press Release, 2021). The passenger demand is then assumed to recover to 50% of pre-COVID-19 levels by 2022, 75% of pre-COVID-19 levels by 2023, and pre-COVID-19 levels by 2024. Similarly to the previous three scenarios, the fourth scenario, 2024 recovery, assumes that the GDP will continue to grow in a manner unaffected by the pandemic after 2024; the fifth scenario, 2024 recovery + GDP slowdown to 75% until 2030, assumes that the passenger demand will grow corresponding to 75% of the GDP growth assumptions in FLEET until the year 2030; and the sixth scenario, 2024 recovery +

GDP inflation to 125% until 2030, assumes that the passenger demand will grow at 125% of the GDP growth assumptions in FLEET until the year 2030.

Table 9 summarizes the future demand scenarios considered; passenger demand for different years is listed as a percentage of pre-COVID-19 levels (2019), and the GDP growth rate is listed as a percentage of the "nominal" GDP growth rate in FLEET (Mavris et al., 2017).

Table 9. Future demand scenarios.

Scenario #	Description	Passenger Demand (% of pre-COVID-19 levels)					GDP Growth Rate (as % of 'Nominal')
		2020	2021	2022	2023	2024	
1	2023 recovery	34%	52%	88%	100%	--	No change
2	2023 recovery + GDP slowdown to 75% until 2030	34%	52%	88%	100%	--	75% (- 25%)
3	2023 recovery + GDP inflation to 125% until 2030	34%	52%	88%	100%	--	125% (+25%)
4	2024 recovery	34%	38%	50%	75%	100%	No change
5	2024 recovery + GDP slowdown to 75% until 2030	34%	38%	50%	75%	100%	75% (- 25%)
6	2024 recovery + GDP inflation to 125% until 2030	34%	38%	50%	75%	100%	125% (+25%)

Extending the Airline Network to a Global Network

As part of the efforts in previous years, FLEET adopts a semi-dynamic route network that changes according to Bureau of Transportation Statistics (BTS) (Airline Origin and Destination Survey – DB1B) data from 2005 to 2018, followed by a static route network from the year 2019 onward. The final route network consists of 1,974 different routes defined by a subset of the list of 257 airports from the Worldwide Logistics Management Institute Network (WWLMINET). The motivation for using 2005 as the baseline year for FLEET came from numerous stated CO_2 emissions goals that also use 2005 as their baseline year. With the BTS-reported data providing the basis for most of the initial airline fleet and yearly route demand up to 2018, FLEET is limited to modeling U.S.-touching routes (those with at least one airport of the origin-destination pair in the United States) and only flights operated by U.S. flag carrier airlines.

To extend FLEET's capability to provide supersonic and subsonic aircraft allocation data on global international routes (in addition to those already present in the FLEET network), the Purdue team is updating FLEET's U.S.-touching route network to a worldwide route network. This task is currently underway and will be fully completed as part of the next year's work.

To model the behavior of an aggregate global airline, the Purdue team purchased global fleet demand data from the Official Aviation Guide (OAG) Traffic Analyzer. The data were extracted from the OAG Traffic Analyzer for the years 2011–2020; OAG did not have relevant global fleet demand data available for any year earlier than 2011. On the basis of global data availability, the team decided to change the initial year of the FLEET simulation from 2005 to 2011, and update the initial network, passenger demand, and fleet composition accordingly.

Passenger Demand

The team accessed the raw passenger demand data from OAG for the years 2011–2020. The raw data contained information irrelevant to FLEET and therefore required filtering before being used to generate the route network in FLEET. The application of the filters numbered from 0 to 5 in Table 10 trims the raw data from OAG to relevant data that can be used as an input for further processing in FLEET. After these filters are applied to the raw data in the order listed in Table 10, the final demand data contain information on the number of passengers per year on directional routes by all global carriers combined. For example, to capture regularly scheduled airline traffic, the team considered only routes with a passenger demand of at least 7,800 passengers per year (i.e., 150 passengers per flight, one flight per week, and 52 weeks per year) among the 257

WWLMINET airports (257 most popular airports around the world according to Institute Network Queuing Model (WWLMINET). The resulting filtered OAG data have 364,672 segments (routes) over the 10-year time window from 2011 to 2020.

Table 10. List of filters for extracting and processing OAG data.

ID	Step	Purpose	Data
0	Initial worldwide routes and passenger demand data for 2011using OAG Traffic Analyzer		Yearly records of numbers of passengers who traveled on directional routes by all carriers
1	All origin and destination airports are in the WWLMINET network of 257 airports	Keep entries for routes with origin and destination within only the WWLMINET 257 airport network	Same as above
2	Filter out routes with the same origin and destination	Remove entries with same origin and destination for directional routes only	Same as above
3	Filter out all routes that have less than 7,800 passenger counts	Keep only entries for routes with regular operations (at least 150 passengers per flight for at least one flight per week or 52 flights per year, performed on directional routes)	Yearly record numbers of passengers who traveled on directional routes with regular operations via all carriers
4	Turn each subset into a 257 × 257 matrix	Prepare for input to FLEET	Same as above, in matrix form
5	Process in FLEET	Filter for minimum passengers per day, minimum runway length, etc. Convert yearly demand to daily demand	Daily demand on bidirectional routes by one large “aggregate” airline representing all carriers

To conduct a sanity test of the filtered OAG data, the team compared the U.S.-touching demand from the BTS data with the OAG demand on the existing U.S.-touching route network in FLEET from 2011 to 2020. Figure 8 shows a coefficient of determination for the OAG and BTS data of 0.9918, indicating that the passenger demand for at least the U.S.-touching route network is highly similar between BTS and OAG data. This finding allowed the team to verify that the filtered OAG data make sense.

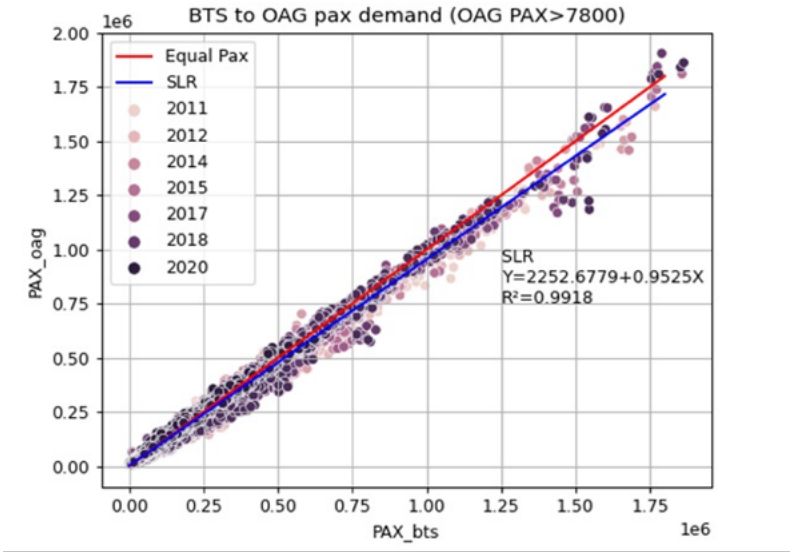

Figure 8. Comparison of U.S.-touching network demand in OAG and BTS data by using a simple linear regression (SLR) model.

Figure 9 compares the passenger demand for the existing U.S.-touching route network (according to the BTS database) with the passenger demand for the worldwide network (according to the OAG database) for the years 2011–2020. The passenger demand for the worldwide route network is significantly higher than that for the U.S.-touching network, and the demand growth rate for the worldwide route network is also higher than that of the U.S.-touching route network.

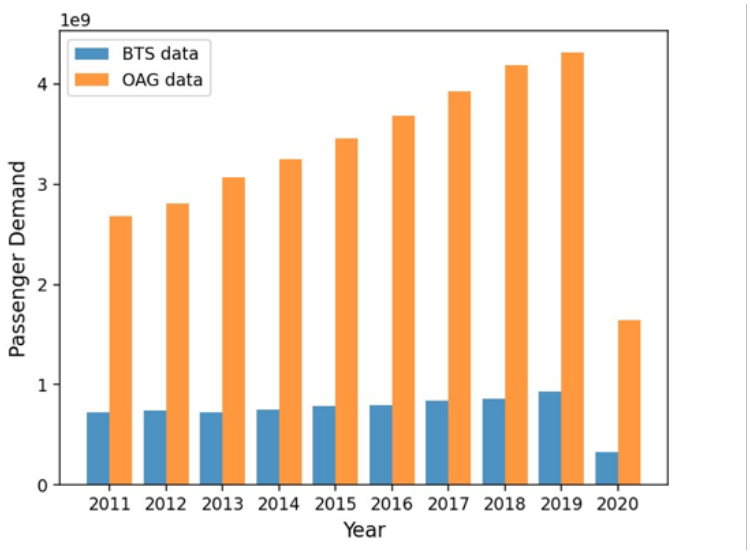

Figure 9. Comparison of passenger demand for the existing U.S.-touching route network and the updated worldwide route network.

Worldwide Route Network

The updated worldwide route network builds upon passenger demand data from OAG for the years 2011–2019; the team did not use the data for the year 2020 because of the pandemic-related decrease in demand. FLEET uses a semi-dynamic route network that follows how worldwide airlines updated their route networks from 2005 to 2019, as reported in the OAG

data, followed by a static route network from 2019 and beyond (i.e., FLEET does not predict the addition or deletion of routes in the future). In 2019 (and all subsequent years), there were 5,317 routes in the FLEET network that connect a subset of WWLMINET 257 airports. Comparison with the previous U.S.-touching route network in FLEET indicates a 170% increase in the number of routes, from 1,974 routes (U.S.-touching only) to 5,317 routes (worldwide). Figure 10 compares the worldwide route network with the U.S.-touching network, visually highlighting the increased routes in the new network.

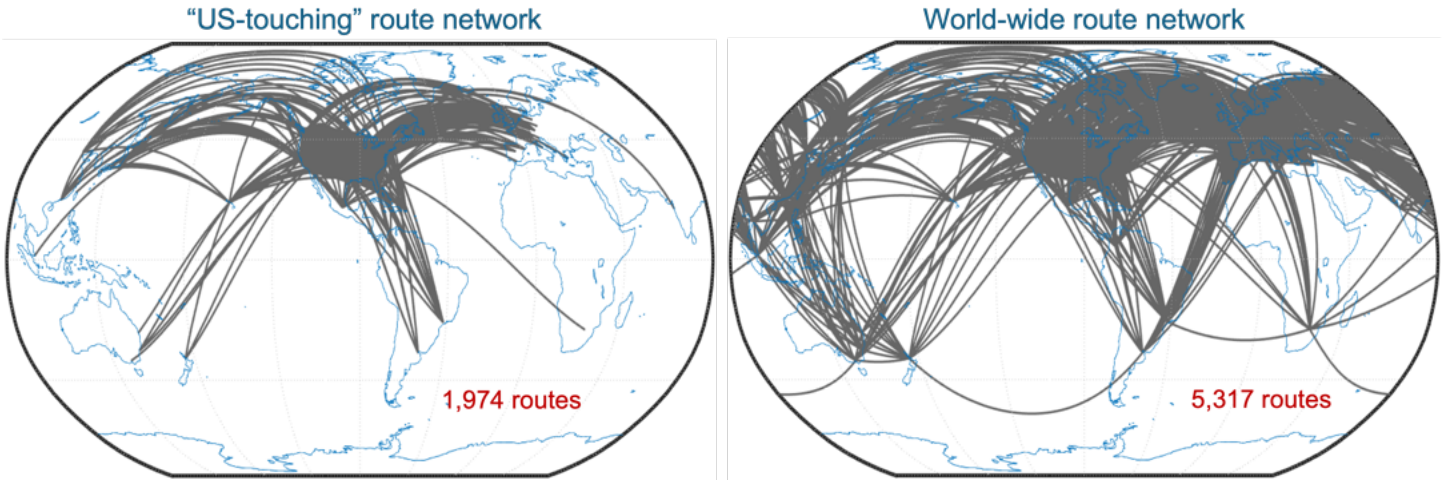

Figure 10. Comparison of the worldwide route network with the existing U.S.-touching route network in FLEET.

Aircraft Classification

The team used the 2011 BTS data of the U.S.-fleet composition to determine the classification method and the representative models of aircraft operating in the new FLEET network. The new worldwide network of FLEET is represented by 14 aircraft models, divided into six classes based on seat capacity, and then grouped into representative-in-class, best-in-class, new-in-class, and future-in-class. The representative-in-class and best-in-class models have the most aircraft within an average age group; representative-in-class models usually have an average age of approximately 15–20 years, and best-in-class models have an average age of approximately 5–10 years. The new-in-class category includes the models that entered service around the years 2015–2020, and the future-in-class category includes the models that will enter service in a future year (around 2030, depending on the seat class) and will have substantial technology improvements over the new-in-class models. The initial fleet (in 2011, the starting year of the worldwide network FLEET simulation) consists of representative-in-class and best-in-class models only. New-in-class and future-in-class models enter the fleet as the simulation proceeds to later years. The resulting representative models of each class are shown in Table 11. Class 1 and 2 are not available for the new-in-class and future-in-class technology classes, because the team determined that the demand for class 1 and 2 aircraft will be low, and these aircraft are not expected to be a significant part of the future global fleet.

Table 11. Aircraft classifications used in FLEET with the worldwide network; FLEET now uses 2011 as the baseline year.

Class	Seats	Representative-in-class	Best-in-class	New-in-class	Future-in-Class
Class 1	20-50	Saab 340B	Canadair RJ200	-	-
Class 2	51-99	ATR 72	Canadair RJ700	-	-
Class 3	100-149	McDonnel Douglas MD-80	Boeing 737-700	Airbus A220	Aircraft X3
Class 4	150-199	Boeing 757-200	Airbus A320-200	Airbus A320 neo	Aircraft X4
Class 5	200-279	Boeing 767-200	Airbus A330-200	Boeing 787	Aircraft X5
Class 6	280+	Boeing 747-400	Boeing 777-200ER	Airbus A350 XWB	Aircraft X6

Global Fleet Composition

The Purdue team used Boeing's 2012–2031 Current Market Outlook (CMO) Report (Boeing Market Outlook, 2012) and Oliver Wyman's 2017 Global Fleet & MRO Market Forecast Summary (Wyman, 2017) as primary sources to determine the size of the 2011 global fleet. Both Boeing and OW provide only "high-level" global fleet size numbers. The current work relies on the U.S. fleet's BTS data for further details, such as dividing the global fleets into different classes. The initial fleet in FLEET's worldwide network is set up by decomposing the fleet into six seat classes and taking an average of the Boeing and Oliver Wyman 2011 global fleet, followed by rounding to the nearest 10, as shown in Table 12. The composition of representative-in-class/best-in-class and age distributions was also determined with the 2011 BTS U.S.-fleet data.

Table 12. Global fleet composition in FLEET (for worldwide route network) for 2011.

	Africa	Middle East	APAC	Latin America	North America	CIS	Europe	World
Class 1	250	40	410	240	1510	210	530	3190
Class 2	150	20	250	150	920	130	320	1940
Class 3	240	230	1760	570	2150	410	1650	7010
Class 4	160	150	1140	360	1380	270	1050	4510
Class 5	70	290	670	40	510	70	400	2050
Class 6	40	170	360	10	250	40	190	1060
Total	910	900	4590	1370	6720	1130	4140	19760

Aircraft Production

At present, the aircraft production and delivery curves as well as the entry-into-service dates of the new-in-class aircraft and future-in-class aircraft for FLEET with the worldwide route network remain unchanged with respect to the previous U.S.-touching version of FLEET. However, only 40% of the total aircraft produced were previously available for purchase by the U.S. flag carrier airline in FLEET. With the update to the worldwide network, all the produced aircraft are eligible to be purchased by the global airlines in FLEET.

As mentioned before, the FLEET update to a worldwide network is still underway and will be completed in the next phase of the project. Current progress has allowed us to visualize the updated worldwide route network and updates to the passenger demand in FLEET. Figure 11 shows the normalized passenger demand in FLEET for the years 2011–2040, considering the worldwide network.

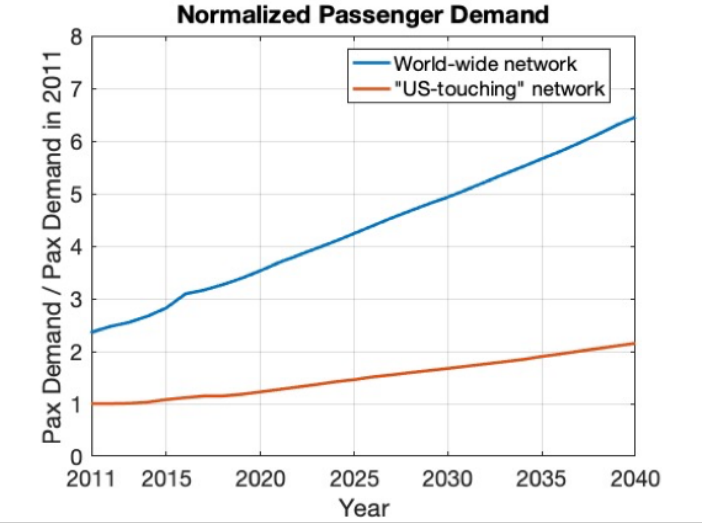

Figure 11. Normalized passenger demand in FLEET for the years 2011–2040.

Simultaneous Aircraft Allocation Approach

Currently, the Purdue team uses a sequential aircraft allocation approach for allocating the supersonic and subsonic passengers, i.e., FLEET accommodates the premium passengers first. The sequential allocation problem satisfies as much of the available supersonic demand on a set of supersonic eligible routes using the supersonic aircraft in the airline fleet. Any remaining, unsatisfied supersonic demand is then added to the subsonic travel demand, and a second allocation problem satisfies this demand by using the subsonic aircraft in the airline fleet. However, the sequential allocation approach does not allow FLEET to incorporate noise and/or airport capacity constraints and is inherently based on the assumption that airlines will always satisfy supersonic passenger demand.

To mitigate these limitations of the sequential allocation approach, the Purdue team developed another approach for allocating supersonic and subsonic aircraft at the same time in FLEET: simultaneous aircraft allocation. The simultaneous aircraft allocation treats the supersonic aircraft as options for allocation on supersonic-eligible routes alongside subsonic aircraft in the same problem. All FLEET simulations conducted to date use sequential aircraft allocation.

In the simultaneous allocation problem, the FLEET airline has the ability to use both supersonic and subsonic aircraft in any combination that yields the most profit. The problem restricts supersonic aircraft to the routes identified as supersonic eligible, similarly to how the problem limits subsonic aircraft to routes based on aircraft range capability. As with the current sequential version of the allocation problem, the simultaneous allocation approach also treats the passengers desiring SST as if they are business class or above, whereas subsonic passengers are treated as a homogenous class of passengers most closely reflecting economy-class passengers. Currently, the model still uses 5% of the total passenger demand in FLEET as the demand that exists for supersonic travel; the simultaneous allocation problem reflects both the supersonic and subsonic demand as separate types of demand, while constraints ensure that the allocation meets all demand.

The simultaneous supersonic and subsonic allocation approach has several useful advantages over the sequential aircraft allocation approach. This approach provides insights into passengers' travel preferences via supersonic and subsonic aircraft while allowing for the enforcement of noise and/or airport capacity constraints in FLEET; therefore, it is pertinent to conducting the noise-related FLEET work.

The Purdue team has completed the development of the sequential allocation approach and plans to use this allocation approach for all upcoming FLEET runs. The team has conducted several test runs by using some of the previous-year supersonic aircraft models operating on the U.S.-touching FLEET. The team will conduct runs for the updated FLEET with a worldwide route network by using simultaneous allocation in the upcoming year.

Results

Impact of Supersonic Aircraft Operations on Subsonic Operations

The FLEET simulation is run from years 2005 to 2050, with a first-generation supersonic aircraft introduced in 2025 and a second-generation supersonic aircraft introduced in 2038; the second-generation supersonic aircraft has the same block time on routes but consumes less fuel for the mission, assuming incremental improvements in empty weight, aerodynamics, and propulsive efficiency. In FLEET simulations, the aircraft are available for the airline to use 1 year after the entry into service (EIS) date (i.e., the aircraft was first available during the EIS year, but the representative day when that aircraft was part of regular service is the year following the EIS). Hence, the first-generation supersonic aircraft becomes available for allocation by the airline for a representative day in 2026. Similarly, the second-generation supersonic aircraft becomes available for allocation in 2039.

The high-passenger-density subsonic aircraft (for new-in-class and future-in-class, (classes 3, 4, 5, and 6) are made available only on routes with supersonic aircraft allocation; FLEET allocates the standard subsonic aircraft on all other routes. For simplicity in implementation, the team assumed that the airline can quickly "convert" a standard configuration subsonic aircraft to a high-passenger-density configuration, thus allowing for use of the existing subsonic aircraft acquisition and retirement models.

The simulation results presented here use the sequential aircraft allocation approach for allocating the supersonic and subsonic passengers, i.e., FLEET accommodates premium passengers first. The FLEET run presented here is based on the U.S.-touching route network and has no constraints on the number of airport operations. In addition, this work considered only the Current Trends Best Guess (CTBG) scenario from previous work (Mavris et al., 2017), which comprises nominal aircraft technology development, nominal economic growth, and nominal energy price evolution. The previously obtained

subsonic-only CTBG results were used for comparing and analyzing the supersonic with high-passenger-density FLEET CTBG allocation and fleet fuel burn results.

With the current modeling, the possible airline response to the introduction of high-passenger-density subsonic aircraft on routes with supersonic service impacts fleet-wide subsonic aircraft utilization and total fuel burn. The different ticket price approaches lead to differences in subsonic aircraft allocation, fleet-level fuel burn, and overall airline profit. The supersonic aircraft allocation and emissions remain the same for all the ticket price approaches, because supersonic aircraft are allocated first. Considering the fleet-wide fuel burn, case 1 (constant average ticket price) leads to the maximum overall fuel burn, case 2 (constant ticket price) leads to the maximum fuel burn in 2050, and case 4 (constant ticket price margin) leads to the lowest overall fuel burn among the four ticket price cases discussed. The fleet-wide fuel burn from all four cases with high-passenger-density aircraft (along with supersonic aircraft) and the case with supersonic aircraft but no high-passenger-density aircraft are higher than the fuel burn from the subsonic-only case. Figure 12 shows the fleet-wide normalized fuel burn for all cases considered. Figure 13 shows the aircraft flown miles, the passenger flown, and fuel burn from the whole subsonic fleet. The class-wise contributions (from classes 3, 4, 5, and 6 subsonic aircraft) to aircraft flown miles, the passenger flown, and fuel burn are depicted in Figures 14–16.

Case 1: Constant Average Ticket Price

Analysis of case 1 indicates a slight change in the passenger demand combined with a significant change in the subsonic aircraft allocation, as compared with the case with no high-passenger-density aircraft. The constant average ticket price approach causes the profit per trip for the high-passenger-density configuration to be higher than the standard configuration. The airline maximizes its profit by flying as many passengers as possible per trip, favoring larger aircraft to earn more profit. The airline ultimately flies more trips with class 5 and class 6 aircraft instead of the smaller class 3 aircraft, thus increasing the overall fuel burn. Figures 14c and 14d show that the aircraft flown miles (and subsequently the passenger flown) for class 5 and class 6 aircraft are much higher than those in other cases, depicting that the airline tends to fly more larger aircraft to earn a higher profit, thereby leading to higher emissions (visible in Figures 13c, and Figures 16c & d, depicted by red dotted lines).

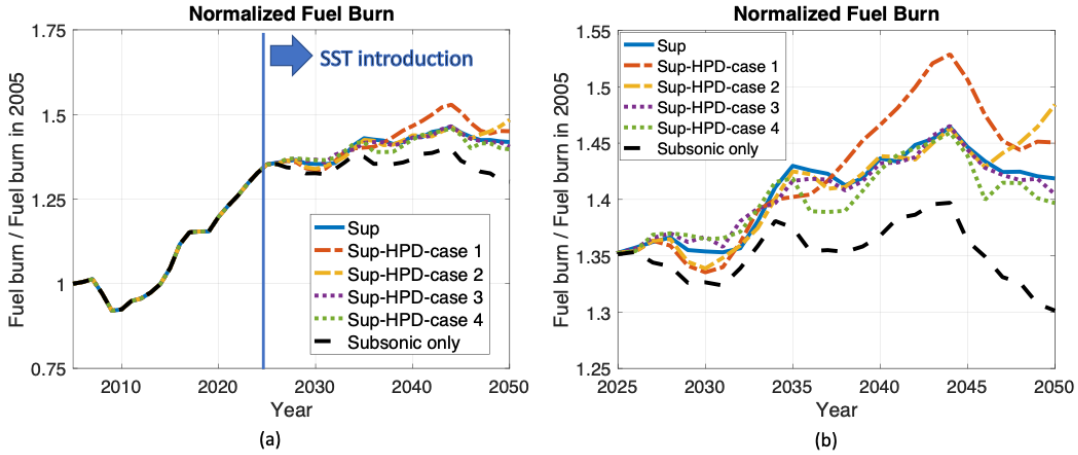

Figure 12. (a) Normalized fuel burn from FLEET simulation. (b) Zoomed-in view of normalized fuel burn starting from the year 2025.

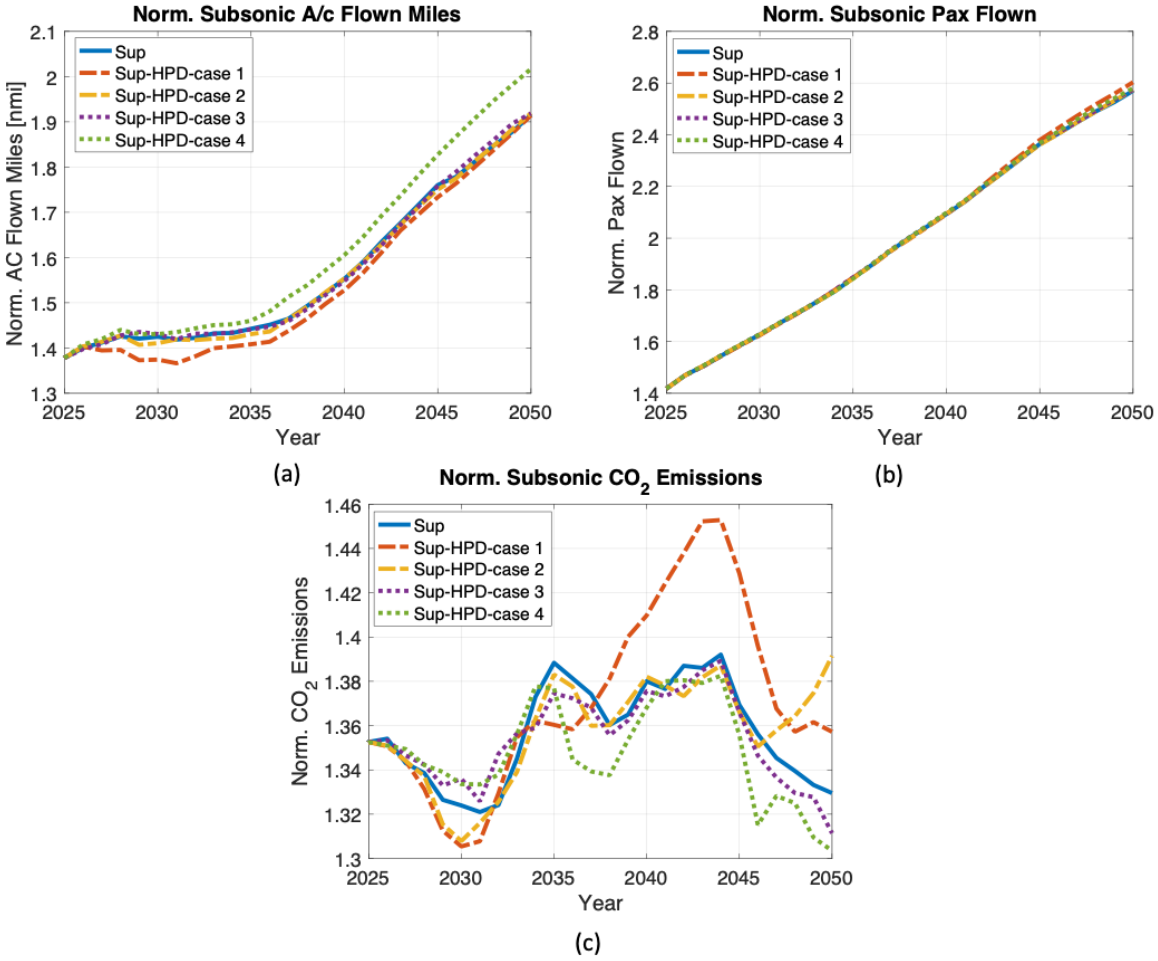

Figure 13. (a) Aircraft flown miles for subsonic fleet. (b) Passengers flown for subsonic fleet. (c) Fuel burn from a subsonic fleet. All data are normalized to respective 2005 values.

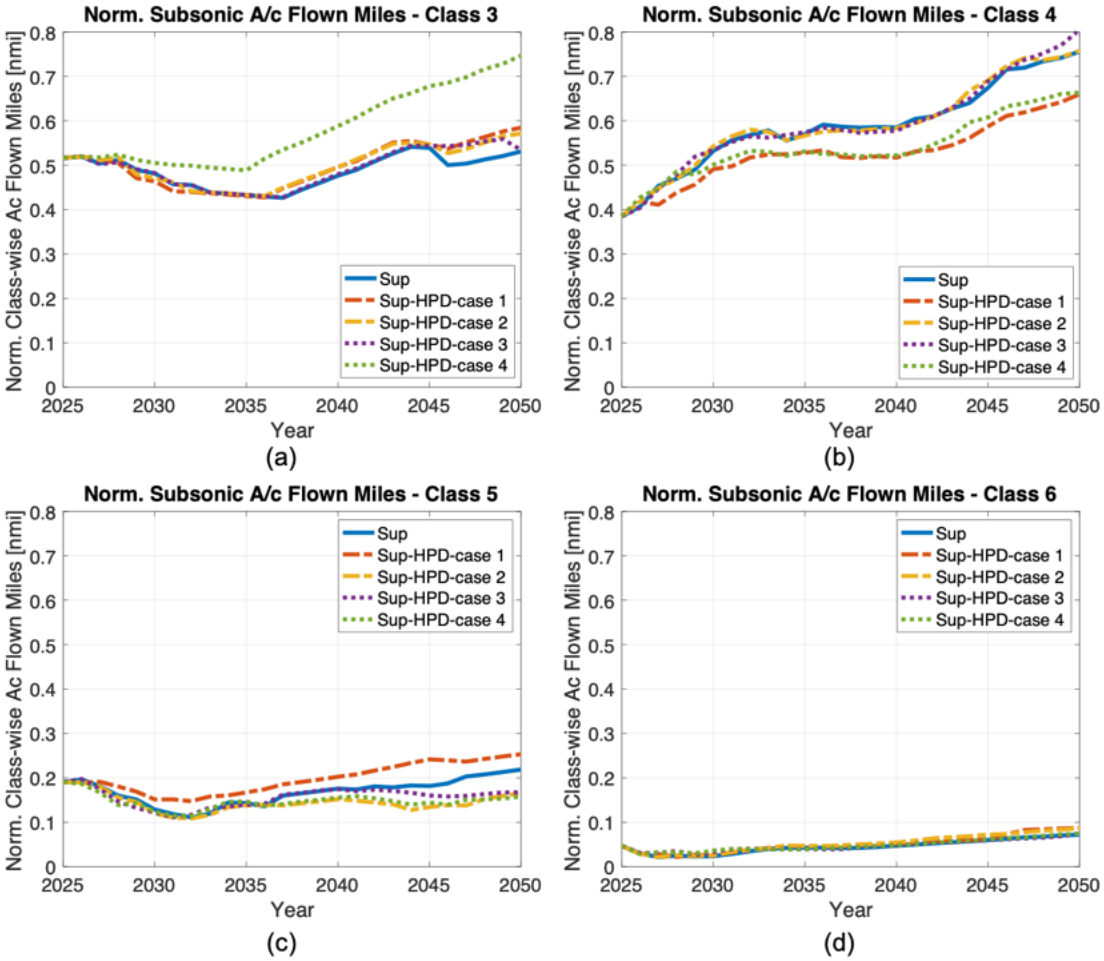

Figure 14. Normalized class-wise aircraft flown miles for subsonic fleet: (a) class 3, (b) class 4, (c) class 5, and (d) class 6. All data are normalized to 2005 total subsonic aircraft flown miles.

Case 2: Constant Ticket Price

For case 2, there is almost no change in passenger demand; the subsonic aircraft allocation changes slightly with respect to the case with no high-passenger-density aircraft. The constant business-class and economy-class ticket prices approach causes the total trip profit to increase (ticket prices remain constant, but the increase in the number of seats results in an increased trip profit). The airline maximizes its profit by flying more trips, favoring smaller aircraft to minimize the loss of business-class revenue. The airline ultimately flies more trips using class 3 aircraft and fewer trips using class 5 aircraft; after 2046, utilization of newer technology aircraft (classes 3 and 4) further increases because of higher trip margins for these aircraft. This shift in allocation after 2046 shows that the profit margin difference between differently sized aircraft plays a role in prioritizing more trips vs. carrying more economy passengers. In this case, the airline makes more profit by prioritizing more trips using smaller aircraft. The overall fuel burn is similar to that in the case with no high-passenger-density aircraft until the year 2046 (yellow dotted line in Figure 13c). Figures 16a and 16b show increased fuel burn from class 3 and class 4 aircraft after the year 2046 (depicted by yellow dotted lines).

Case 3: Constant Trip Margin

For case 3, there is a slight change in passenger demand and subsonic aircraft allocation compared to the case with no high-passenger-density aircraft. The constant trip margin approach causes the profit per trip for the high-passenger-density configuration to be same as that of the standard configuration. As in case 2, the airline maximizes its profit by flying more trips using smaller aircraft, flying more trips using class 3 aircraft and fewer trips using class 5 aircraft. Figure 14a–c (purple dotted lines) shows an increase in the aircraft flown miles for class 3 and class 4 aircraft, and a decrease in aircraft flown

miles for class 5 aircraft. The overall fuel burn is similar to that in the case with no high-passenger-density aircraft (purple dotted line in Figure 13c).

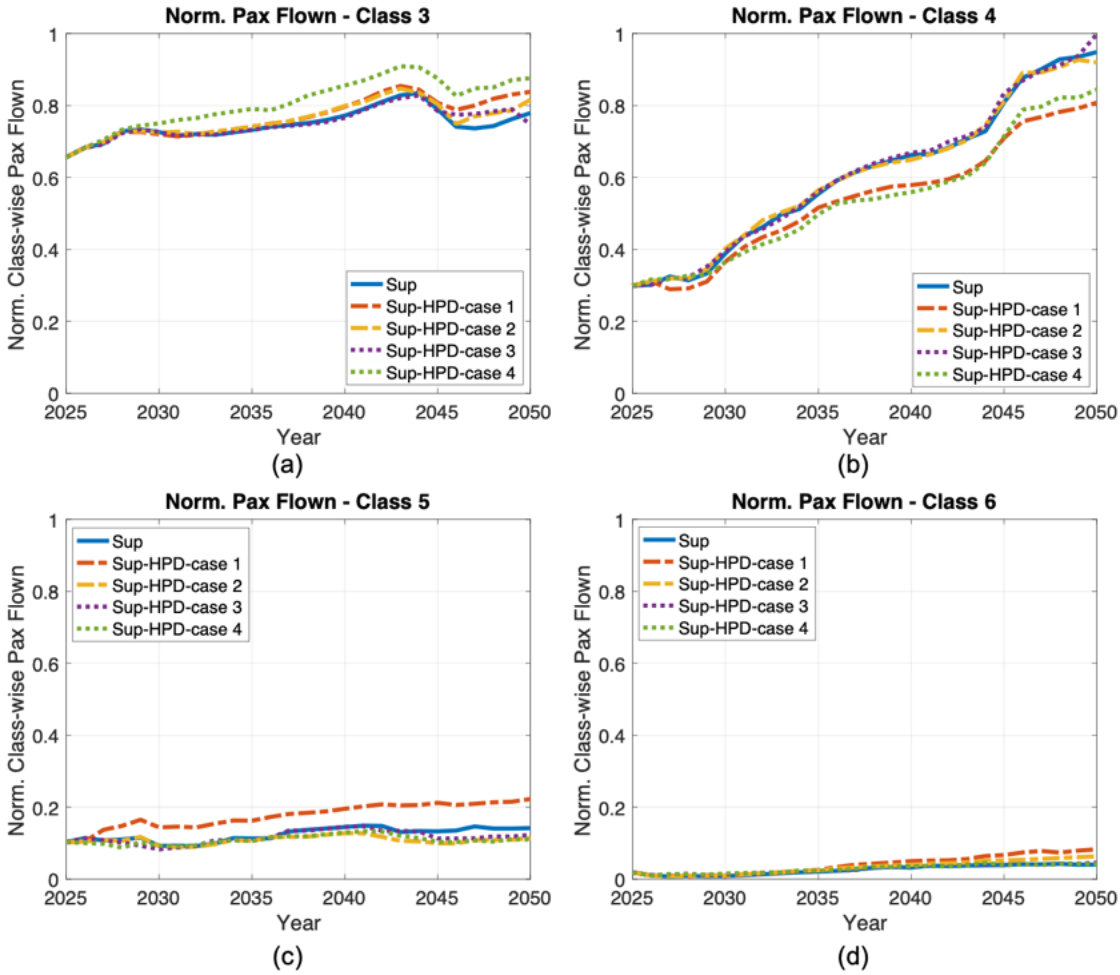

Figure 15. Normalized class-wise passengers flown for subsonic fleet: (a) class 3, (b) class 4, (c) class 5, and (d) class 6. Data are normalized to 2005 total subsonic passengers flown.

Case 4: Constant Ticket Price Margin

For case 4 (constant ticket price margin), there is a slight change in demand, but the subsonic aircraft allocation changes significantly compared to the case with no high-passenger-density aircraft. Because the airline does not alter profit margins from economy ticket prices to compensate for the loss of business-class seats, this approach causes the total trip profit to decrease as business seats are reduced by 50%. The airline maximizes its profit by flying more trips using the smaller aircraft, which allow more trips to be flown. Interestingly, the airline ultimately flies many more trips with class 3 aircraft, and fewer trips with class 4 and class 5 aircraft. Figure 13a and b show that the subsonic aircraft flown miles are highest for case 4, although the number of passengers flown remains relatively unchanged. The increase in trips on smaller aircraft (green dotted line in Figure 14a), with a decrease in the use of larger aircraft, results in a net reduction in the fleet-wide fuel burn (visible in Figures 16 and 13c, depicted by green dotted lines).

The plots in Figures 14–16 show that changes in the utilization of class 3, 4, 5, and 6 subsonic aircraft drive the changes in fuel burn for the four different ticket price approaches. Hence, the changes in fuel burn are a function of changes in passenger demand and subsonic aircraft allocation due to ticket price variations.

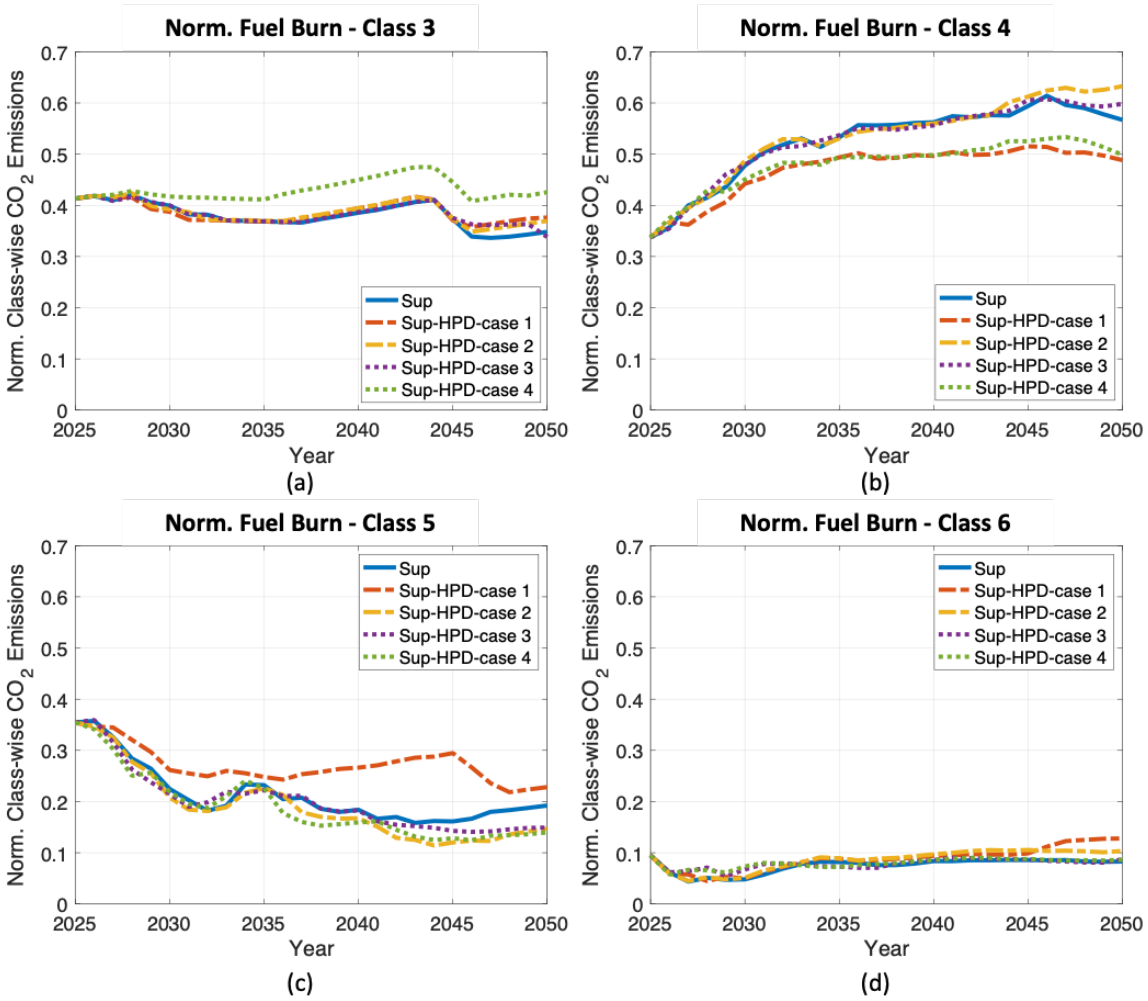

Figure 16. Normalized class-wise fuel burn for a subsonic fleet: (a) class 3, (b) class 4, (b) class 5, and (d) class 6. Data are normalized to 2005 total subsonic fuel burn.

Most Likely and Least Likely Cases

Given the current modeling assumptions, the team estimated the likelihood of occurrence of the four high-passenger-density cases in the future based on airline profit and impact on passengers, i.e., changes in ticket price. The likelihood estimation process led to the identification of a most likely case and a least likely case.

The team identified case 2, maintaining a constant ticket price, as the most likely case. In this case, the airline makes high profit, and there is no cost that is transferred to the passengers as the subsonic ticket prices stay constant. The least likely case would be maintaining a constant ticket price margin, i.e., case 4. The airline makes the lowest profit in this case, because it does not change the ticket price margins to compensate for the loss of business-class passengers—a profit-seeking airline will not follow this approach. Table 13 provides an overview of the outcomes with respect to the case with no high-passenger-density aircraft; the table also includes the team's judgement regarding the likelihood of occurrence of the four cases considered.

Impact of COVID-19 on Passenger Demand and Fleet-Level Assessments

The FLEET simulation was run from years 2005 to 2050 with a first-generation supersonic aircraft introduced in 2025 and a second-generation supersonic aircraft introduced in 2038. The simulation results presented here utilize the sequential aircraft allocation approach for allocating the supersonic and subsonic passengers, i.e., FLEET accommodates the premium

passengers first. The FLEET run presented here is based on the U.S.-touching route network and has no constraints on the number of airport operations. In addition, this work considered only the CTBG scenario from previous work (Mavris et al., 2017), utilizing the previously obtained subsonic-only CTBG results for comparing and analyzing the supersonic FLEET CTBG results, and considering the 2020 decrease in passenger demand and the possible demand recovery paths due to the COVID-19 pandemic.

Table 13. Overview of outcomes with respect to predictions when no high-passenger-density aircraft are available in FLEET (considering sequential aircraft allocation on a U.S.-touching route network).

Possible Airline Actions	Preference (Likelihood of Occurrence)	Impact on Passengers (Ticket Pricing)			Impact on Fleet-Level Fuel Burn	Impact on Airline (Profit)
		Average Ticket Price	Economy Ticket Price	Business Ticket Price		
Case 1: Constant average ticket price	2	–	↑	↑	↑	↑
Case 2: Constant ticket price	1 (most likely)	↓	–	–	↑ (slightly after 2046)	↑ (slightly)
Case 3: Constant trip margin	3	↓	↓ (slightly)	↓ (slightly)	~ (similar)	↓ (slightly)
Case 4: Constant ticket price margin	4 (least likely)	↓	↓	↓	↓ (slightly)	↓

Figure 17 shows the normalized passenger demand for the projected demand scenarios along with the baseline scenario. There is a maximum 16.8% reduction in the 2050 total passenger demand (for scenario 5) and a minimum 11.2% reduction in the 2050 total passenger demand (for scenario 3) when compared to the baseline scenario. Figure 17 also shows the normalized fuel burn for the projected demand scenarios along with the baseline scenario (depicted by a black solid line) in FLEET; the fuel burn for all six scenarios is always lower than the pre-COVID baseline scenario. There is a maximum reduction of 17.3% (for scenario 4) and a minimum reduction of 11.7% (for scenario 3) in the 2050 fleet-level fuel burn when compared to the baseline scenario. The differences between COVID-19 scenarios and the pre-COVID baseline are a combination of two factors: 1) the lower passenger demand leads to a smaller number of flights, and 2) lower passenger demand initiates early retirement of less profitable aircraft and the introduction of more profitable (more fuel-efficient) aircraft during passenger demand recovery.

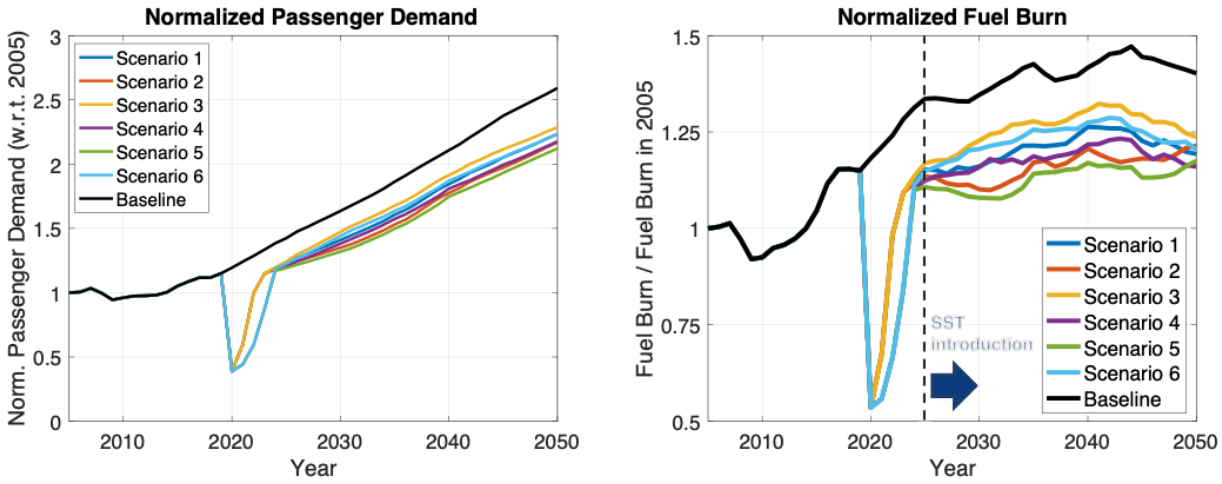

Figure 17. Normalized passenger demand and fleet-level fuel burn for different passenger demand recovery scenarios (based on a U.S.-touching route network).

Considering the year 2038, the FLEET simulation results using the projected demand scenarios show a maximum 42% reduction in supersonic passenger demand (for COVID-19 recovery scenario 6) compared with the pre-COVID baseline scenario. Analysis of COVID-19 recovery scenario 6 indicates that the 42% reduction in supersonic passenger demand leads to a 39% reduction in the number of supersonic routes allocated, from 57 routes to 37 routes, and a 43% reduction in supersonic roundtrips flown per nominal day, from 79 round trips to 45 round trips. Figure 18 shows the normalized supersonic passenger demand, number of supersonic routes allocated, and supersonic round trips flown for all six COVID-19 demand recovery scenarios and the pre-COVID baseline scenario.

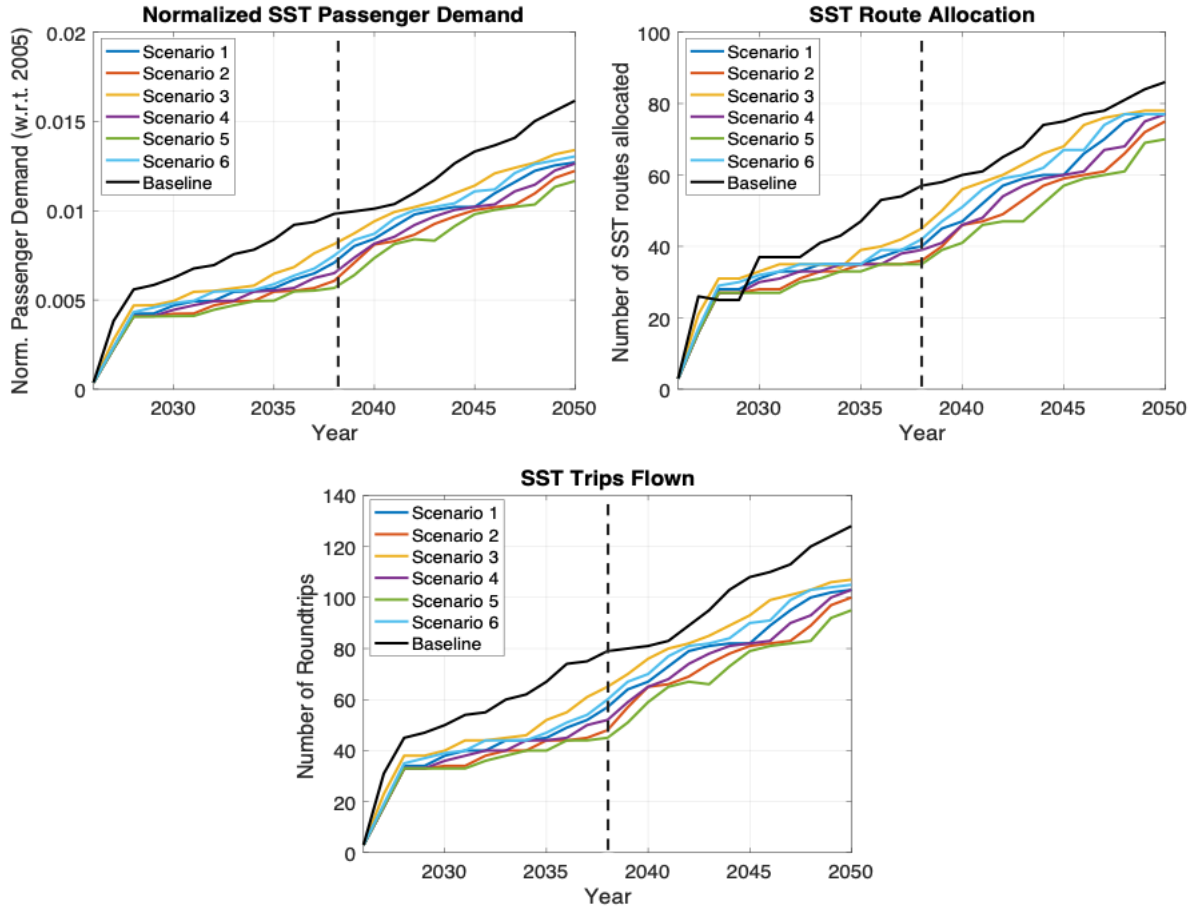

Figure 18. Normalized passenger demand, number of supersonic routes allocated, and number of supersonic trips flown for different passenger demand recovery scenarios in the year 2038.

Task 3 - AEDT Supersonic Modeling

Georgia Institute of Technology

The original intent of Task 3 was to develop methods for AEDT to model SST. At the time of writing of the proposal, AEDT utilized BADA3 for vehicle modeling; therefore, the proposal focused on BADA3 approaches. Since then, and at the time of writing of this report, AEDT is transitioning to BADA4 for new vehicle representation in AEDT, thus rendering the proposed tasks obsolete. Based on conversations with FAA technical monitors at the Spring 2019 ASCENT Advisory Board meeting, Georgia Tech was directed to focus on BADA4 coefficient generation for SST, which is described in Task 5.

Task 4 - Support CAEP Supersonic Exploratory Study

Georgia Institute of Technology

Objectives

In support of the CAEP supersonic exploratory study, or E-Study, Georgia Tech engaged in two major activities. One activity was attending CAEP meetings and authoring or contributing to numerous working papers and information papers at the working-group meetings. Specifically, Georgia Tech supported Working Group 1 (Noise), Working Group 3 (Emissions), and the CAEP Forecast and Economic Analysis Support Group. Specific results and products from this activity are discussed in

the Results section of this task. The second major activity was supersonic vehicle modeling. The Research Approach section for this task describes the methodology used to model major disciplines, such as aerodynamics, propulsion, noise, and mission analysis. Finally, the Results section discuss the results of the Design Mach Trade Study using the nine vehicles modeled.

Research Approach

As with previous work, the Georgia Tech researchers leveraged the Framework for Advanced Supersonic Transports (FASST) M&S environment to model the supersonic vehicles for this task. This framework is based on the Environmental Design Space (EDS) [,]. The goals of EDS and FASST are the same: to provide a modeling and simulation environment that enables tradeoffs and interdependencies among aircraft system-level metrics. The difference is that EDS was designed for subsonic aircraft; therefore, modifications were implemented to enable the modeling and simulation of supersonic aircraft. In the case of FASST, the system-level metrics of highest interest are the vehicle weight, design mission fuel burn, and landing and takeoff (LTO) or certification noise. The flow diagram for the FASST environment (Figure 19) shows the inputs, outputs, and interconnections between each discipline's analysis module in the modeling and simulation environment.

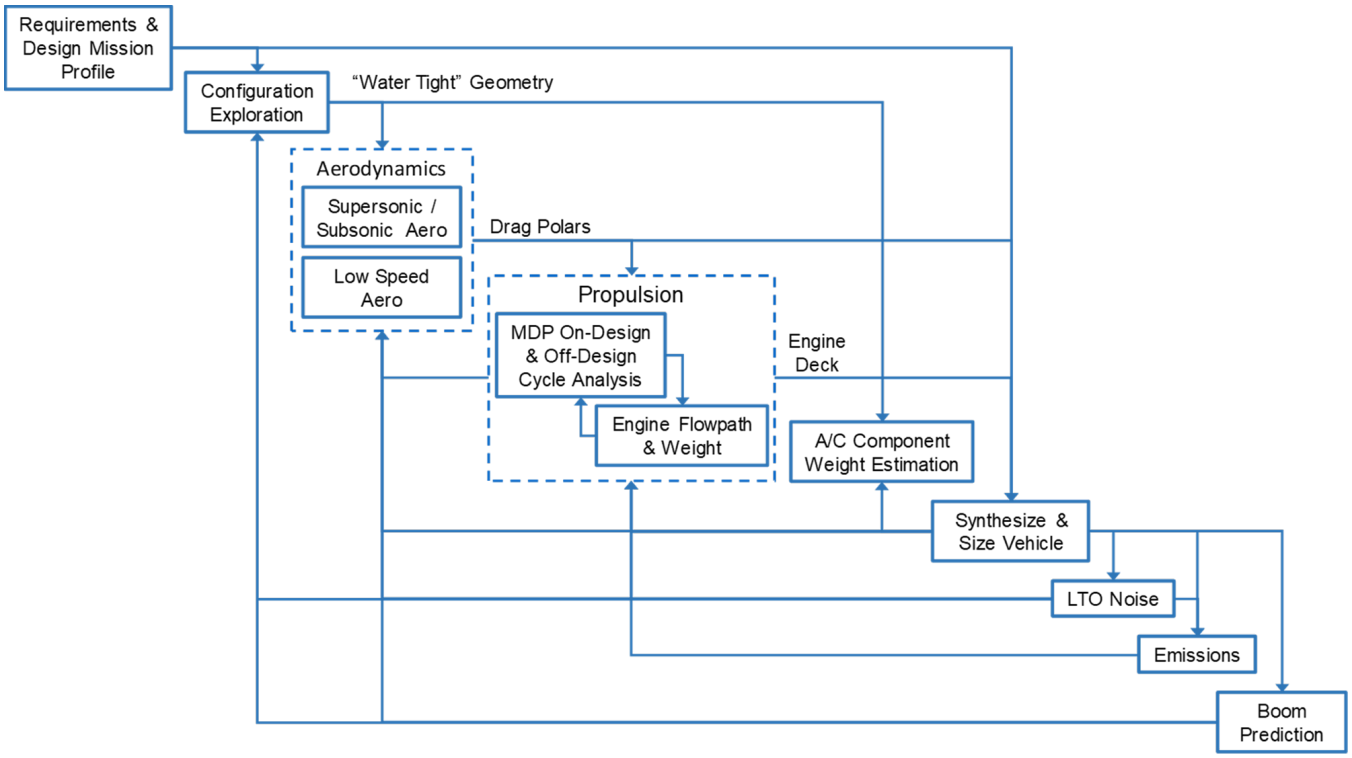

Figure 19. FASST flow diagram.

The requirements and design mission are specified by the research team and are outlined in the following sections. Some of the high-level requirements are the number of passengers, the design Mach number, and the design mission range.

The configuration exploration and aerodynamics drag polar generation are performed in a local setting, outside of FASST. This process involves parametrically generating a 3D model of the airplane in Engineering Sketch Pad (ESP). From this model, a CFD mesh is generated that can then be run through CART3D to analyze the vehicle's supersonic aerodynamic performance. For this task, a design of experiments (DoE) was conducted to properly shape the planform, keeping the fuselage, engine, and tail geometry fixed. From the data collected from executing FASST for this DoE, a set of surrogates are generated, and the cruise lift-to-drag ratio (L/D) is used to select the best vehicle. After a design is selected, the complete high-speed drag polar is developed with CART3D and a takeoff and landing drag polar is generated in NASA's Vehicle Sketch Pad, AERO2S, and WINGDES. Both sets of drag polars are fed into the mission analysis and vehicle sizing module. More details on the aerodynamic module are included in the Aerodynamics Modeling section.

The engine cycle modeling is performed in Numerical Propulsion System Simulation (NPSS), and flowpath and weight estimation is conducted with Weight Approximation for Turbine Engines (WATE). This process provides an engine deck and engine weight to the mission analysis and vehicle sizing module. The propulsion analysis is detailed further in the Propulsion Modeling section. For the vehicle mission analysis and sizing, NASA's FLOPS is used. FLOPS uses the inputs of engine deck, drag polar and other vehicle configuration parameters to estimate the weight, and it then iterates on the vehicle gross weight to complete the mission prescribed by the designer. FLOPS scales the engine and wing as required to achieve the required thrust and wing area based on a specified wing loading and thrust-to-weight ratio. If the engine is scaled in FLOPS, it is subsequently rescaled in the engine analysis to obtain an updated engine performance and weight. This iteration continues until the engine no longer requires scaling. After sizing, the vehicle is analyzed through a series of design missions. Specifically, the takeoff and climb-out trajectory is of interest because of its importance to LTO emissions and noise. The modeling assumptions for emissions and noise are also included below.

Propulsion Modeling

Cycle Architecture Selection

A mixed-flow turbofan (MFTF) engine cycle was selected for this work. Most modern subsonic aircraft use a high-bypass-ratio separate-flow turbofan (SFTF). This type of engine allows for high overall efficiency by moving a greater amount of air for high propulsive efficiency while being able to maintain a high overall pressure ratio (OPR) for high thermal efficiency. As a result of the higher mass flow rate, high bypass SFTF have lower jet velocities for the same thrust, an aspect also beneficial for from a noise perspective. However, moving more air comes at the cost of larger engine diameters and greater thrust lapse due to altitude as density decreases. Supersonic aircraft face high drag in transonic acceleration and cruise at higher altitudes than subsonic aircraft; therefore, the greater thrust lapse of engines with a high bypass ratio (BPR) is not ideal. Additionally, supersonic engines have longer inlets and nozzles than subsonic engines, to efficiently decelerate and accelerate the flow. Therefore, higher airflow and fan diameter result in very large and heavy inlets and nozzles. An MFTF is a simple modification of the SFTF accomplished by mixing the bypass and core flow before the stream exits through a single exhaust nozzle. The mixing of the two streams offers some efficiency gains and higher specific thrust, which in turn reduces the thrust lapse problem [3]. MFTFs have been shown to offer a good compromise of thrust-specific fuel consumption (TSFC), jet velocities (i.e., specific thrust), weight, complexity, and fuel burn relative to other cycles, such as the turbojet, turbine-bypass engine, and variable-cycle engines [5].

Cycle Modeling

A schematic is included in Figure 20, depicting the components in the engine model and their connectivity. The inlet, fan, high-pressure compressor (HPC), both turbines, and the nozzle are modeled with parametric performance maps. Each vehicle uses a different inlet map from the Performance of Installed Propulsion System Interactive (PIPSI)/INSTAL maps [8]. The inlet chosen (Table 14) for each vehicle class was based on the range of Mach numbers and the inlet type. The nozzle map used in all configurations is the plug nozzle map from the PIPSI/INSTAL library [**Error! Bookmark not defined.**]. The fan and HPC maps are generated with the NASA tool CMPGEN within the FASST environment to avoid the need for map scaling. The turbine maps are notional maps that are scaled, because the FASST environment does not currently include a routine to parametrically generate turbine maps. The design point performance of all turbomachinery was estimated using a simple mean-line approximation. In addition to performance, the mean line calculation also estimates the gross dimensions, number of stages, and RPM, which are required inputs for the engine flowpath and weight analysis.

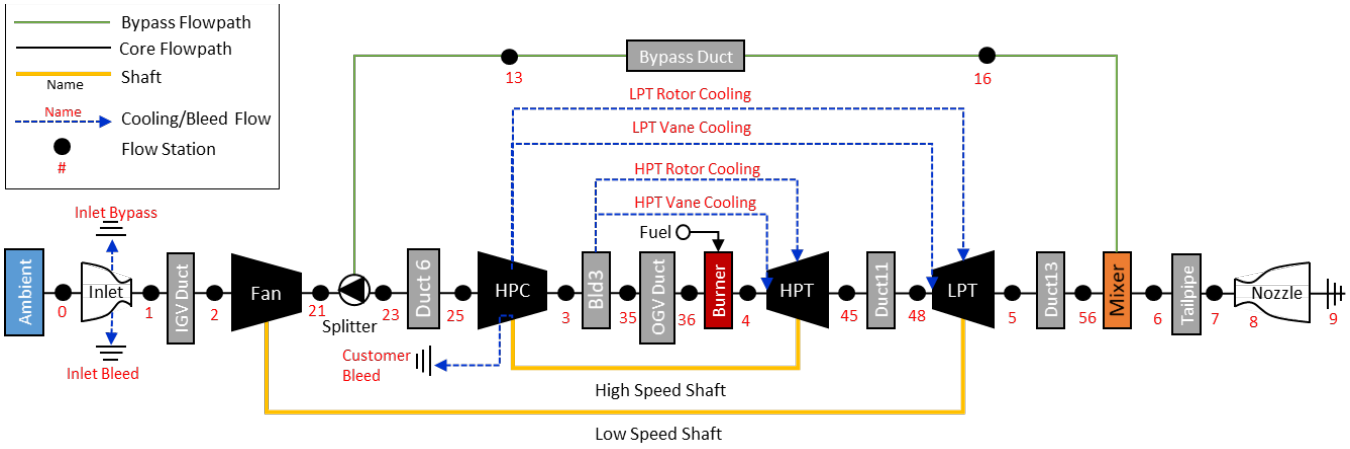

Figure 20. Engine schematic of a clean-sheet design for a medium SST.

Turbine cooling flows are determined from the NASA-developed CoolIt model [10], which computes the required cooling flow as a function of metal temperature and the cooling effectiveness parameter $\phi = (T_{gas} - T_{metal})/(T_{gas} - T_{cool})$. An advanced impingement and film cooling technology is assumed to cool the turbine blades [11]. The rotor blades were assumed to be made of an advanced single-crystal nickel superalloy, and the vanes were assumed to be made of a ceramic matrix composite material. The mixer, combustors, and ducts were all modeled with constant nominal loss metrics. Estimates for horsepower extraction, and customer bleed were based on the passenger class of the aircraft.

Table 14. Inlet selection for each vehicle class.

Vehicle	Inlet Name	Description
GT_SSBJ	NVSTOL	Axisymmetric, 3-ramp, expanding centerbody, external compression
GT_MediumSST	R2DSST	2D, 4-ramp, variable geometry, mixed compression
GT_LargeSST	ATS2	2D, 4-ramp, variable geometry, external compression

Cycle Design Methodology

A clean-sheet engine design was conducted rather than a fixed-core refan design. In a clean-sheet engine design, the entire engine is a brand-new design with all of its components sized as required. In contrast, a fixed-core refan design involves selecting a fixed core from an existing engine and designing a new low-pressure spool (fan and low-pressure turbine), inlet, and exhaust system. A simultaneous, multi-design-point (MDP) approach was used in this work to size the engine. Classical single-point analysis sizes the engine at single flight condition and subsequently iterates to ensure that requirements are met under other flight conditions. The MDP method enables simultaneously meeting design requirements and sizing components under multiple flight conditions [12]. The flight conditions considered in this work are listed in Table 15. The aerodynamic design point (ADP) is the sizing point of the engine and a reference point for defining the turbomachinery component performance. The ADP selected in this study was the transonic acceleration point at which having enough thrust is critical to overcome the high drag. The top of climb (TOC) point is typically a critical point at which adequate thrust for a minimum specific excess power is needed. Additionally, this point is part of the supersonic cruise segment, and thus efficiency is a critical concern. The takeoff point is critical to ensure sufficient thrust at rotation and for one engine inoperative. The cooling flow sizing point sizes the turbine cooling flows for the condition of maximum gas temperature and maximum cooling flow temperature.

The NPSS solver is then used to determine a set of independent parameters (fuel flow, airflow, BPR, etc.) that would meet specified target values of certain dependent parameters. An MFTF engine cycle is defined by the following five parameters: fan pressure ratio (FPR) = P_{t21}/P_{t2}, OPR = P_{t3}/P_{t2}, throttle ratio (TTR) = T_{t41max}/T_{t41SLS}, maximum turbine rotor inlet temperature (T_{t41max}), and extraction ratio □(EXTR) = P_{t16}/P_{t56} [13]. The selection of the throttle ratio is the same as the selection of the design turbine inlet temperature and in turn the Mach number at which the engine reaches T_{t41max}. In this study, an assumed technology limit for T_{t41max} is set at 3300 $°R$. Bypass ratio is another key metric but will be a fallout of

selecting the above five cycle variables. For this study, the extraction ratio is set to 1.1 to increase the bypass ratio without significant mixing losses. The ADP airflow is set to meet a TOC thrust requirement subject to constraints on thrust requirements at other points. The thrust requirements are scaled as the vehicle is run through mission analysis. The inlet capture area is sized to ensure that the inlet and engine are perfectly matched at the TOC.

Table 15. Cycle design points for a medium SST engine.

Design Point	Mach	Altitude (ft)	ΔISA ($°F$)	Purpose
Aerodynamic Design Point (ADP)	1.2	39,000	0	Size turbomachinery and engine
Top of Climb (ToC)	Design Mach	55,000	0	Match thrust requirements for top of climb/cruise
Takeoff	0.3	0	18	Match thrust requirements for takeoff
Cooling-Flow Sizing	Design Mach	45,000	0	Size cooling flows

Off-Design Power Management

This section describes how the engine operates in off-design mode through the entire flight envelope. Full power at any flight condition is defined as running the fuel control to target 100% corrected fan speed, constrained by maximum temperature limits on the compressor discharge ($T_{t3max} = 1790\,°R$) and turbine rotor entrance ($T_{t41} = 3300\,°R$). In addition, the nozzle throat is variable and set to hold the design stall margin. At part power, the fuel flow and fan speed are reduced to hit the thrust target, and the nozzle throat is varied to maintain a high fan efficiency. For noise analysis only, a different power management logic is used wherein part power is achieved by initially moving along the 100% speed line of the fan map, thereby decreasing the pressure ratio and increasing the stall margin. This is less efficient but results in a greater reduction of jet velocity for the same reduction in thrust by holding the airflow. This is constrained by a maximum stall margin, to avoid adverse choking effects, at which point the fan speed is reduced to further reduce thrust.

Flowpath and Weight Model

The flowpath and weight of the engine are estimated using a model developed with WATE++ and inherited from a previous supersonic study in which Georgia Tech was involved [**Error! Bookmark not defined.**]. The model is modified for a 2D supersonic inlet and an axisymmetric plug nozzle, and changes were made to some turbomachinery parameters based on a preliminary analysis method developed for this study. The inlet weight is modeled by using the regressions from PIPSI [**Error! Bookmark not defined.**]. The nozzle model is modified for an axisymmetric plug nozzle by extending the internal plug outside the nozzle with a 15° half-angle and setting the external convergent flap to match the plug half-angle. A custom module for calculating the weights of variable geometry actuators was also developed. A preliminary analysis code based on constant-meanline assumptions was developed to estimate the number of stages of turbomachinery required, and parameters such as the hub-tip ratio, area, radii, and blade speeds. This preliminary turbomachinery code is run in conjunction with cycle analysis to set the component efficiency and the geometric parameters, and the results are then passed to the WATE++ input to ensure consistency in the geometry used to compute both final component efficiency and component weight.

Emissions Modeling

One important issue in the development of any aircraft is environmental acceptability [14] particularly for SSTs, which consume more fuel than their subsonic counterparts. To predict the NO_x emissions, a NASA High Speed Civil Transport rich burn, quick quench, lean burn (RQL) combustor technology correlation is assumed [15] and is shown below. This equation is used to predict the NO_x emissions index ($EINO_x$), which determines the number of grams of NO_x produced per kg of fuel used at each of the NO_x certification points. The $EINO_x$ in turn is used to estimate the total NO_x emitted through the entire mission and for assessing CAEP certification limits in terms of grams of NO_x per kN of thrust.

$$\mathrm{EINO_x} = 23.8\,(\frac{P_3}{432.7})^{0.4}\exp\,[\frac{(T_3 - 1{,}027.6)}{349.9} + 0.014]$$

The nvPM emissions for several supersonic engine candidates were also estimated in this study through a procedure based on the Döpelheuer–Lecht equation, as described in CAEP11-WG3-PMTG09-IP06, with a suitable reference engine selected for each case. The Döpelheuer–Lecht equation is:

$$\mathrm{EI} = \mathrm{EI}_{\mathrm{ref}} * \left(\frac{\mathrm{FAR4}}{\mathrm{FAR4}_{\mathrm{ref}}}\right)^{2.5} * \left(\frac{\mathrm{P3}}{\mathrm{P3}_{\mathrm{ref}}}\right)^{1.35} * \frac{\exp(-20000/T_{fl})}{\exp(-20000/T_{fl,ref})}$$

where FAR is the fuel-to-air ratio, and the flame temperature is given by:

$$T_{fl} = 2281 * \{\mathrm{P3}^{0.009375} + [0.000178 * \mathrm{P3}^{0.055} * (\mathrm{T3} - 298)]\}$$

Note that the units of P3 are bars, and the units of T3 are degrees Kelvin.

Issue 28 of the ICAO Emissions Databank (issued December 23, 2020) reported, for the first time, measured mass and number EI nvPM data for the subsonic LTO cycle. In the present study, these new data were used for the reference engines, along with updated estimates of the supersonic engine cycles.

Three supersonic engine candidates were considered in this study: the NASA STCA engine, the Boom study engine, and the Gulfstream study engine. For both the NASA STCA and Boom engines, the reference engine was selected to be the CFM56-7B. Two different estimates of the Gulfstream engine cycle were considered, but in both cases, the reference engine was the BR700-725A1-12 engine. Both of the CFM56 and BR700 reference engines have reported mass and number EI nvPM values in issue 28 of the ICAO Emissions Databank. Only the mass EI nvPM was considered in this study.

For use of the Döpelheuer–Lecht equation, reference engine values for P3 and FAR4 are required as a function of T3. The reference engine data were generated using the ASDL EDS estimates of the CFM56 and BR700 engines. In each case, a sea-level static standard day power hook was run, and the resulting P3 and FAR4 values were curve fit (polynomial) vs. T3. The accuracy of the P3 and FAR4 estimates was evaluated indirectly by comparison of the thrust-SFC curves predicted by the EDS models to the fuel flow data available in the ICAO Emissions Databank.

The supersonic engine cycle data consist of P3, T3, and FAR4 for both the subsonic LTO cycle (four power settings) and the supersonic LTO cycle (five power settings). For each value of T3 given, reference engine values of P3 and FAR4 were read from the EDS data curve fits. The reference EI nvPM was interpolated (linear) from the ICAO data as a function of T3. Then the Döpelheuer–Lecht equation was used to estimate the mass EI nvPM for the supersonic engine. The normalized results are tabulated in the Propulsion Results section.

Aerodynamic Modeling

Analysis Workflow

A general analysis process was developed, as illustrated in Figure 21, to obtain the aerodynamic performance of multiple aircraft designs. This process was then automated with Python and implemented by using Georgia Tech's high-performance computing (HPC) facilities. Because the analysis workflow was automated and easily parallelizable, many designs could be analyzed at once. Thousands of aerodynamic analyses could be completed in a matter of hours, thus allowing for rapid evaluation of designs and generation of drag polars.

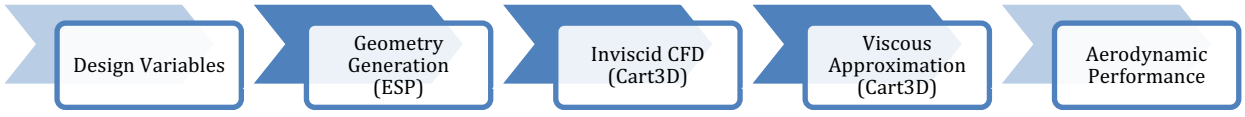

Figure 21. Analysis workflow for aerodynamic performance predictions.

Starting from a set of design variables, the first step was to generate a CAD representation of the aircraft geometry. This process was done using Engineering Sketch Pad (ESP), a lightweight, open-source CAD tool developed by MIT. ESP allows users to easily script generation of complex geometries and to expose design parameters. Therefore, changing global parameters, such as the sweep angle or taper ratio, would automatically and seamlessly scale and reposition the different sections of the wing. After a new geometry was defined, it was then saved to a generic CAD file (the EGADS format in the current workflow) and tessellated for later use in CFD analysis.

With the tessellated geometry, the aerodynamic performance of the aircraft was then obtained by using CFD. These simulations were performed with CART3D, an INVISCID CFD code with immersed boundaries that was developed by NASA. The reason for using CART3D in the current process was its rapid execution with reasonable accuracy. In fact, a single design could be evaluated in approximately 15 min on the Georgia Tech Phoenix cluster, thus allowing us to quickly assess many designs within a relatively short time frame. The code also provides a viscous drag estimation tool that uses the computed surface pressure distribution together with boundary layer equations. Although the viscous drag estimated in this manner is reasonable, it should not be perceived as having the same accuracy as RANS results. However, for initial design analysis, the costs of a RANS based analysis were deemed too high, and consequently the viscous drag module was used instead.

Design Selection Process

The objective of the design selection process was to select the best design for each SST vehicle class, i.e., the vehicle configuration that maximized L/D at its design Mach number; therefore, a purely supersonic aerodynamic design effort. Although this exercise could have been conducted by directly linking CART3D to an optimization algorithm, such an approach would have had substantial drawbacks. First, because of the lack of an adjoint solution for the viscous component of drag, any gradient-based optimization would have required finite differencing, which is wasteful. Gradient-free approaches, in contrast, would not have been efficient either, owing to the number of design variables considered. Additionally, optimization is a sequential process in which designs are evaluated one after the other. This approach fails to take advantage of the parallelization afforded by the high-performance computing clusters available to Georgia Tech. As such, a surrogate-based design optimization (SBO) strategy was selected. SBO approaches are robust, thus eliminating the risk of premature termination from CART3D crashing. Surrogates also typically tend to smooth out the impacts of noisy data and outliers on the responses, making it easier for the optimization algorithm to converge. The design space can be visualized easily with the surrogates, especially with the help of profiler plots in the statistical software JMP, thereby providing valuable diagnostic information and qualitative checks on expected trends. Finally, with surrogates of key responses, the optimization problem can be modified quite easily, such as by adding constraints or changing the objective function, without a need to rerun CFD from the beginning.

The first step in the SBO approach is the formulation of a sampling plan. In this case, the goal was to create a globally accurate surrogate model for L/D, and thus a DoE with 1,000 samples was created for each of the SST vehicle classes. These designs were obtained using a Latin Hyper Cube sampling plan to ensure that the samples were spread across the design space. For a given SST vehicle class, each of the 1,000 designs was evaluated in CART3D at the design Mach number, and then at the off-design Mach numbers where appropriate. For C_D, the INVISCID and viscous components were computed separately. The solutions from the CART3D viscous module were noisy, with respect to variations in some design parameters, as shown in Figure 22 for an aspect-ratio variation, for example. Of note, the INVISCID L/D trends are smooth, indicating no issues with the primary CART3D solver. However, the noise introduced by the viscous component of drag affects the viscous L/D trends with AR to a point where the viscous and INVISCID L/D optima with respect to the aspect ratio are different. Given that no justifiable physical explanation could be provided for the C_D^{visc} trends, we took steps to address this issue.

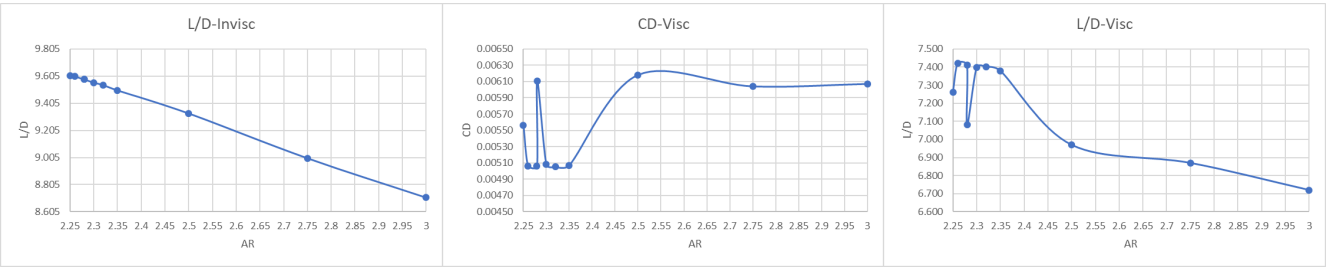

Figure 22. INVISCID and viscous trends with aspect ratio for a generic SST.

To minimize the adverse impacts of such noise in the selection of the optimum designs, we averaged out the viscous component of C_D over the 1,000 samples in each DOE to obtain one representative value of C_D^{visc} for each Mach and altitude combination at which the optimization exercise was conducted. This average value was then added to each individual value of C_D^{inv} to obtain an estimate for the viscous L/D for each of the 1,000 designs in the DOE. Surrogate models were then fit to this response.

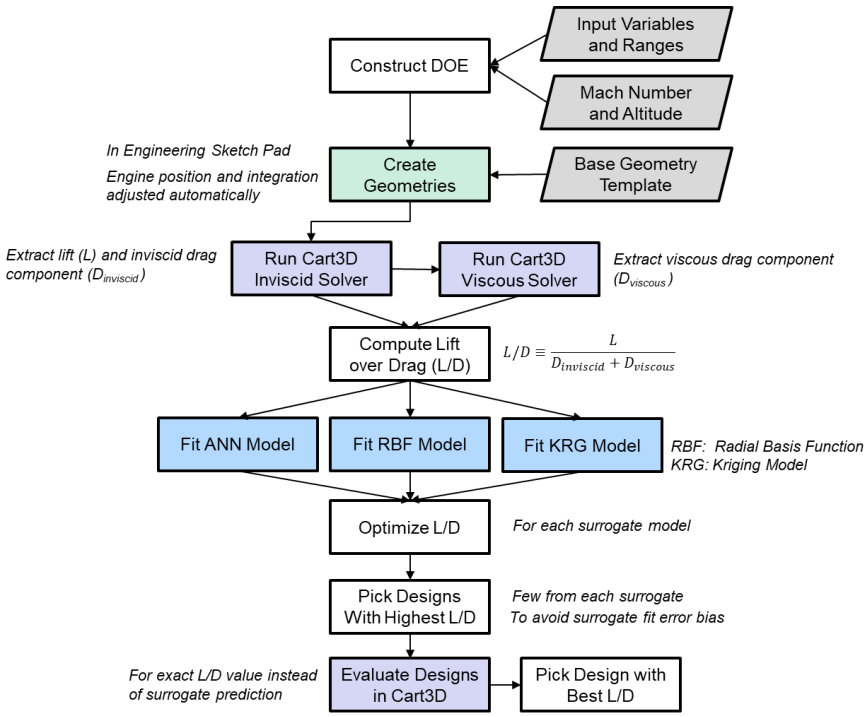

Figure 23. Aerodynamic optimization process.

The main outcomes of this exercise were a triplet of vehicle designs for a given SST passenger class, each optimized at a different Mach number. These vehicles were then evaluated at different Mach–altitude points to generate a series of drag polars encompassing the entire mission. For the polars, the values of C_D^{visc} directly predicted by CART3D were used, because a geometry-averaged, or a flight-condition-averaged C_D^{visc} value does not make sense in this context. Ideally, each vehicle in the triplet should have the highest L/D at the Mach number at which it was optimized, with the other two optimized vehicles showing a lower L/D at the same conditions. This condition is necessary for the vehicle to be "optimal" at a given Mach number. However, given the noisy nature of the C_D^{visc} trends discussed above, this expected behavior was not observed in some instances. As such, the vehicle designs were manually perturbed in this scenario to ensure that the resulting L/D was indeed the highest at the chosen Mach number.

Geometry Parametrization

A major modeling challenge has been defining a parametric representation of the nacelle in the ESP model. To simplify this task, because both the airframe and engine cycle were undergoing constant updates, unpowered flow through nacelles was used to represent the engines. Inlet ramps, exhaust nozzles, and any internal components were neglected at this stage to further reduce the complexity of parameterizing this model. Although greatly simplified, modeling the nacelle installation parametrically remained a difficult task. The primary issue was parametrically shaping the nacelle to the curvature of the wing to remove any gaps between the nacelle and the forward and aft sections of the wing. If the parametric definition of the nacelle resulted in any gaps, high- or low-pressure pockets would build up in the gaps that would adversely affect the aerodynamic efficiency of the aircraft. Because the parametric model needed to be able to handle thousands of DoE cases,

designing custom integration and cowling for any gaps with the wing, as would probably be the case in detailed design, was not an option. Figure 24 shows how a gap between the leading edge of the nacelle and the wing results in a high-pressure zone (of note, between the early and final nacelle model, the nacelle inlet had also undergone significant modeling changes, but forces on the interior the nacelle were neglected from aero analysis and bookkept in propulsion). The presence or lack of these gaps effectively created noise when trying to determine the aerodynamic efficiency of a design, because some designs generated by the DoE would have gaps, whereas others would not. A method that consistently integrated the nacelle into the wing without any gaps was needed to effectively explore the aeroshaping of these concepts. The solution that wimplemented involved taking a rectangular slice of the bottom surface and using it as the top and bottom surface of the nacelle; the rest of the nacelle geometry was built by lofting between these two faces and making the appropriate cuts for the flow through. Consequently, the intersection of the bottom of the wing and the top surface featured two identical faces, thus eliminating the possibility of any gaps.

Figure 24. Comparison between the initial nacelle-wing integration (left) and Improved nacelle-wing integration (right).

Table 16. Range of DoE variables used in geometry selection.

Variable	LB	UB
REFAREA	Fixed based on an initial estimate for each vehicle	
TAPER_RATIO_I	0.25	0.5
TAPER_RATIO_O	0.25	0.5
TWIST_R	0	1.5
TWIST_M	−3	3
TWIST_T	−6	6
SWEEP_TE_I	−5	5
SWEEP_TE_O	−5	5
AR	2.2	3.0
REL_Y_M	0.4	0.6
DIHEDRAL_I	−5	5
DIHEDRAL_O	−5	5
ANGLE OF ATTACK	1	4

The SSBJ required some special considerations for its geometry compared to the other vehicle classes. Instead of using a clean sheet-of-paper design for the aeroshaping for the SSBJ, the GT_SSBJ utilized the fuselage, nacelles, and vertical tail design from the NASA STCA, with only the wing planform being parametrized. NASA's VSP model of the STCA was used to export an IGS file that could be imported into traditional CAD software. This initial segmentation of the bodies did leave the

inner core of the nacelle free floating, which would have caused issues in the triangulation of the model for CART3DTherefore, we added a small cylindrical tube to the internal section of the engine, which connected the inner core and nacelle. The fuselage, nacelles, vertical tail, and nacelle pylons were then isolated as individual components and exported as STEP files that could individually be imported into ESP. The ESP model then unions these fixed components and a parametrically defined wing. Because the SSBJ model was a derivative of the STCA, utilizing the STCA planform as a baseline rather than enforcing the design constraints present on the other vehicle classes in this study was determined to be more appropriate. From the baseline variable ranges, the minimum trailing edge sweep needed to be substantially decreased, and the outboard taper ratio minimum needed to be slightly decreased, to ensure that the STCA baseline planform was captured in the design space.

Table 17. Cabin layout for the 55- Pax and 100- Pax aircraft.

	Cabin Layout
100 PAX	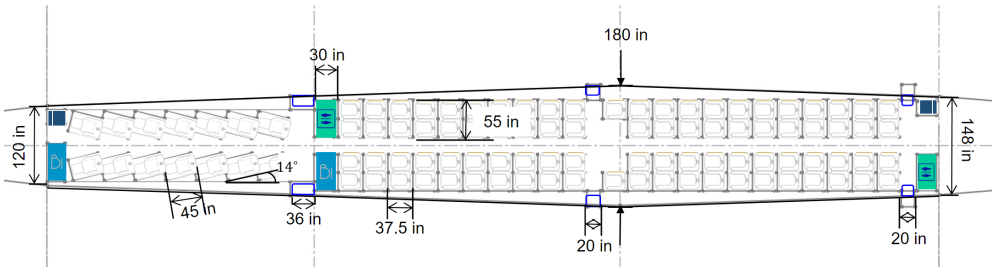 Cabin Length: 111.6 ft (1340.0 in) Cabin Diameter: 10-15 ft (120-180 in)
55 PAX	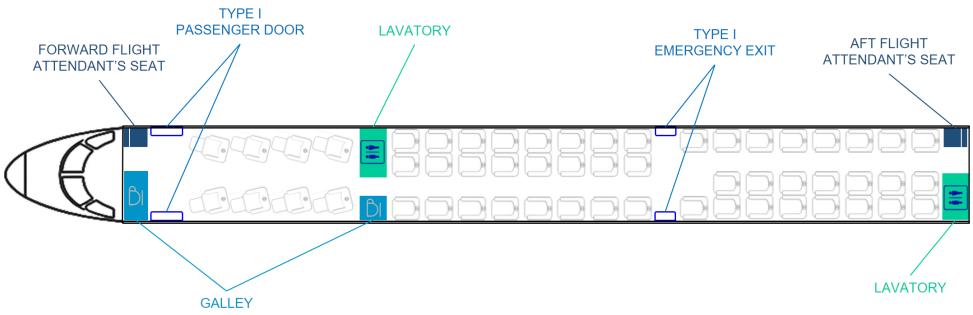 Cabin Length: 80 ft (1340.0 in) Cabin Diameter: 10 ft (120-180 in)

Mission Analysis

The mission analysis was performed by using NASA's FLOPS. For FLOPS to size and synthesize the SST, a geometry definition from the ESP is required, i.e., the L/D optimized configuration from aerodynamics, the engine deck generated from NPSS, and both the high-speed and low-speed aerodynamic drag polars. The aircraft component weights were predicted by using internal FLOPS empirical weight equations based on the vehicle gross weight and geometric information provided. A certain amount of composites were assumed in the wing, fuselage, and empennage. Two major vehicle scaling parameters, wing loading (W/S) and the thrust-to-weight ratio (T/W), were varied with each mission analysis execution to satisfy balanced field length and approach speed constraints while minimizing takeoff gross weight.

Noise Modeling

The noise assessment for each aircraft configuration was performed with NASA's Aircraft Noise Prediction Program (ANOPP). In performing these assessments, several assumptions were made in selecting and using different ANOPP modules. Table 18 lists the components of the ANOPP input file structure along with a rationale applicable to each particular module or section.

Table 18. Modules used in aeroacoustics analysis.

Component	ANOPP Module	Acronym	Rationale
Trajectory	Source Flyover Module	SFO	Considered separate trajectories (prescribed by FLOPS) for the sideline and the cutback/approach noise assessments – the difference being that the sideline trajectory did not include a cutback section after the second segment acceleration – and both cases used a VNRS takeoff trajectory
Airframe	Fink's Airframe Noise Module	FNKAFM	Standard module to predict the broadband noise from the dominant components of the airframe and based on a method developed by Fink for the FAA
Jet	Single Stream Circular Jet Noise Module	SGLJET	The single stream jet mixing noise is calculated with a methodology based on SAE ARP 876, because it is known to be the best representation of the current nozzle type.
Fan	Heidmann Fan Noise Module	HDNFAN	The fan inlet and discharge noises were assessed separately for their tone and broadband contributions using a methodology based on correlations to model and full-scale test data.
Treatment	Fan Noise Treatment Module	TREAT	Given that the chosen fan module assumes that the inlet and discharge ducts are without acoustic treatment, the attenuation spectra are applied to separate predictions of the inlet and aft radiated source noise produced by the source noise module, and a total attenuated fan noise prediction is produced.
Combustor	Combustion Noise Module	GECOR	The combustor noise was predicted with a methodology developed by General Electric and later adopted by the SAE A-21 Committee.
Shielding	Wing Module	WING	Used to compute the geometric effects of wing shielding or reflection on the propagation of engine noise (depending on the engine placement/configuration).

The VNRS previously mentioned consisted, for the purpose of the present study, of automatic (i.e., no pilot control) changes to the engine and airframe configurations during a takeoff run to help reduce noise. The following were included:

- Programmed high-lift devices (PHLD): flap deflections are controlled by the flight management system to optimize the aerodynamic efficiency for the required lift at each point in the takeoff trajectory.
- Programmed thrust lapse rate (PLR): automatic thrust reduction is controlled by FADEC and implemented immediately after the aircraft clears the obstacle during takeoff.
- Second segment acceleration (2SA): an acceleration during the second segment of the takeoff procedure (i.e., between the obstacle and the cutback point). The acceleration takes place at a fixed flight path angle and thrust until the final climb-out speed is reached. The aircraft then holds airspeed and thrust, varying the flight path angle, until the cutback altitude is reached.

The takeoff trajectory thus follows the following general procedure:

1. Takeoff at full power
2. After obstacle: reduce power to specified PLR level, pitch to specified flight path angle and climb and accelerate to final climb-out speed
3. At final climb-out speed: adjust flight path angle to hold final climb-out speed at constant thrust
4. At cutback altitude: reduce thrust to cutback level and hold constant thrust and speed; continue climbing

Table 19 shows how the takeoff trajectory (VNRS) used for all aircraft in this study differs from other common takeoff trajectories. Figure 25 shows how the trajectory and throttle settings vary for each of these options.

Table 19. Differences between trajectory types.

	Cutback	Programed Lapse Rate	Programed High-Lift Device
No Cutback Trajectory	No	No	No
Standard Trajectory	Yes	No	No
Advanced Trajectory	Yes	Yes	No
VNRS Trajectory	Yes	Yes	Yes

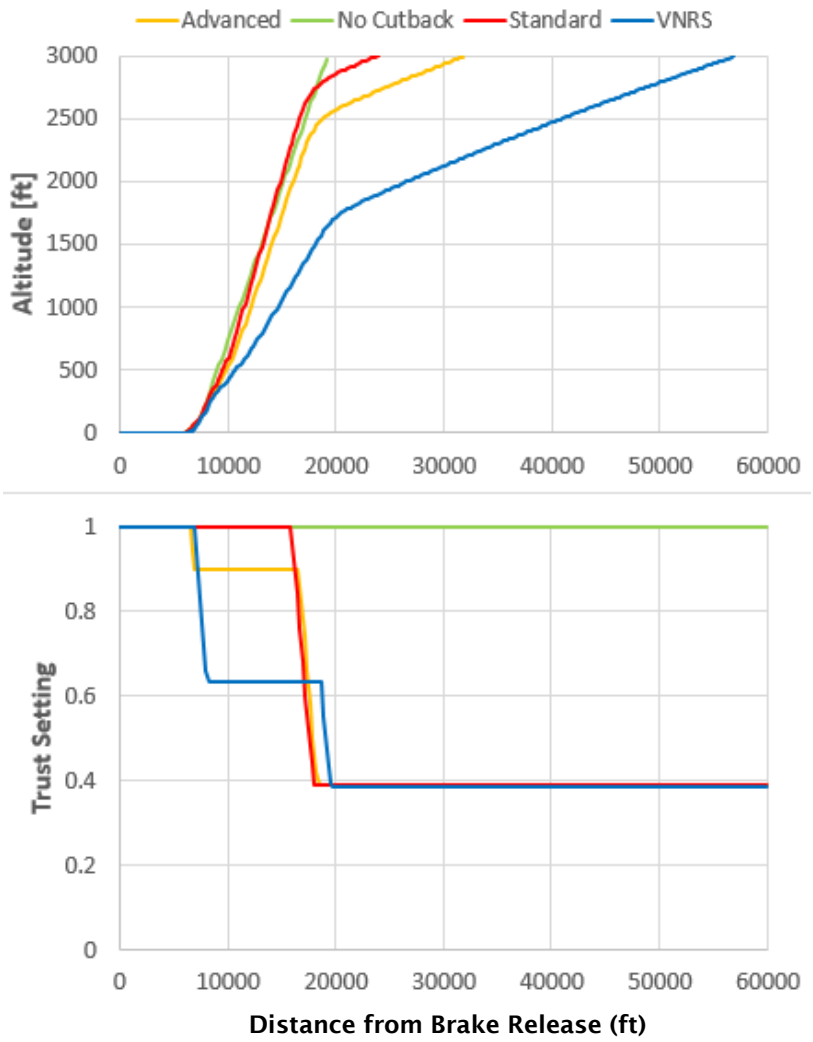

Figure 25. Altitude (top) and thrust setting (bottom) vs. distance from brake release for GT_MediumSST.

Design Mach Number Trade Study

Introduction

No explicit LTO noise standards currently exist for commercial supersonic aircraft. Related regulations are currently being discussed in ICAO WG1, with a focus on two primary questions. First, should LTO noise certification trajectory requirements remain the same as subsonic requirements? Second, what should the stringency level be for commercial supersonic aircraft? At the request of the FAA Office of Aviation Environment and Energy (AEE), technology trade studies were added to the work scope to examine the interdependencies between design fuel burn, LTO NO_x, and LTO noise as a function of design Mach number for several classes of vehicles, as listed in Table 20. To aid in answering the previous two questions, this work posed several additional questions:

- What is the rate of change in fuel burn per effective perceived noise in dB (EPNdB) reduction in LTO noise and noise margin?
- How does that rate of change vary with Mach number and vehicle class?
- Can a commercial supersonic vehicle with moderate noise technology meet current subsonic Chapter 14 rules?

Table 20. Design Mach number trade study for different vehicles.

Passenger Class	Baseline Design Mach Number	Design Mach Number Range for Trades	Design Range (nm)	Number of Engines and Location
8	1.4	1.4, 1.6, 1.8	4,240	2 fuselage & 1 empennage
55	2.2	1.8, 2.0, 2.2	4,500	4 under-wing
100	1.8	1.6, 1.8, 2.0	5,000	4 under-wing

Approach

To establish the interdependencies a set of vehicle and operational design variables were explored for each vehicle. The variables used in this study are shown in Table 21. Ranges for each of these variables were established, and a DoE was created to explore the design space. The design process for each discipline was as detailed in the previous sections. After all the simulations were run for each vehicle and Mach number over their respective design spaces, the data were filtered to ensure that all requirements and constraints were met, and the set of nondominated solutions composing the Pareto frontier were obtained with JMP. An illustration of the Pareto front for fuel burn and noise is shown in Figure 26. Results of this study are presented below in the Results section.

Table 21. Design variables for establishing interdependencies.

Airframe Geometry	Engine Cycle	Vehicle Sizing	Takeoff Trajectory
• Trailing edge sweep (inboard and outboard) • Twist (root, mid, and tip) • Taper ratio (inboard and outboard) • Dihedral (inboard and outboard) • Wing break location	• Fan pressure ratio • HPC pressure ratio • Turbine inlet temperature (i.e., throttle ratio)	• Thrust loading (thrust-to-weight ratio) • Wing loading (weight-to-wing area ratio)	• % Programmed lapse rate • Initial climb angle • Constant speed transition altitude • Cutback altitude

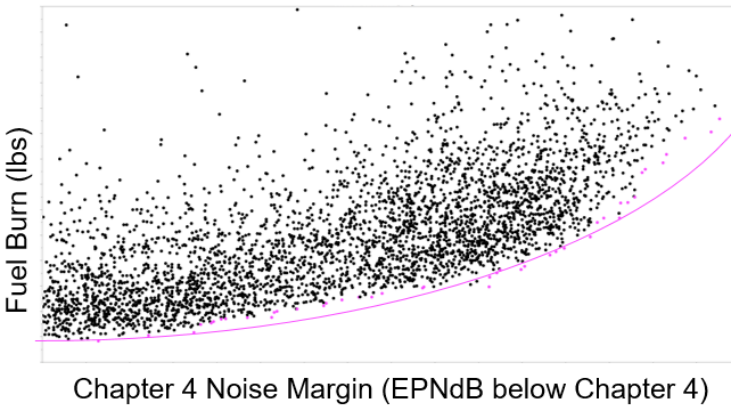

Figure 26. Example scatter plot of fuel burn vs. noise margin for all designs simulated with the Pareto frontier (pink).

Results

Design Mach Number Trade Study

The results in this section demonstrate that the LTO noise of an SST is a strong function of passenger class (i.e., maximum takeoff mass [MTOM]), Mach number, and engine placement. More specifically, several key findings were as follows.

1. Fuel burn and fuel burn vs. noise margin slope increases with:
   - Mach number (Figures 27 and 28),

  - Noise margin (Figures 27 and 28), and
  - Vehicle class (Figures 27 and 28).
2. A tradeoff (V-shape) exists in the effects of a quieter engine cycle (lower jet velocity) and fuel burn (heavier/louder vehicle; Figure 29).
3. LTO noise increases:
  - Mach number (Figure 29) and
  - Vehicle class (Figure 29).
4. Minimum noise does not necessarily meet the current subsonic Chapter 14 noise rules (Figures 29 and 30).
5. Relatively smaller SSTs are less sensitive to supersonic/subsonic cruise split (Figures 35–37).
6. LTO NO_x increases as fuel burn decreases, owing to increasing FPR and OPR (Figure 31).
7. LTO NO_x also exhibits a tradeoff (V-shape; Figure 32):
  - OPR and FPR increase from the minimum, the vehicle becomes smaller, and the noise decreases, but NO_x increases (Pareto optimal points).
  - At a certain point, the OPR and FPR increase past the minimum noise optimum, and both NO_x and noise increase.
8. LTO NO_x vs. Mach as the OPR increases for the selected designs (Figures 33 and 34).

The data points shown in Figures 27–29 are the series of non-dominated designs composing the Pareto front of design mission block fuel and certification noise margin. Figures 27 and 28 were plotted separately for ease of visibility due to the differences in the scale of block fuel between the large SST, medium SST, and SSBJ. The figures show that larger vehicle classes consume more fuel for designs with the same noise margin. In addition, within a vehicle class, a higher Mach number increases fuel requirements, as can be seen by the vertical position of each curve. Similarly, moving to the right along the noise margin axis shows that a design with a greater noise margin results in increased block fuel. The same conclusions hold for the slope of block fuel with respect to noise margin. That is, the increase in block fuel per dB of increase in noise margin increases with vehicle class, Mach number, and noise margin. Figure 29 swaps the axes of Figures 27 and 28, and replaces fuel burn with MTOM, and noise margin with absolute cumulative LTO noise level, to provide a typical plot of noise limits. The same results seen in Figures 27 and 28 can also be seen in Figure 29, but several additional conclusions can be drawn. The first is the tradeoff or V-shape of the curves. To the left of the minimum are the designs for which the noise is dominated by the jet velocity, and to the right are designs dominated by vehicle size effects on noise. That is, at a certain point, design changes that further reduce jet velocity are outweighed by the adverse effects on vehicle and engine size, partly because of the higher fuel burn requirements. Another conclusion is that, for the choice of architecture and technologies, the minimum noise design may not meet Chapter 14 requirements. A design to the right of the Chapter 14 limit line could be chosen but this design would not only have worse fuel burn but also would be louder in terms of absolute noise. This can be seen more clearly in Figure 30, where the final selected designs for the MediumSST and LargeSST do not meet Chapter 14 requirements. Figure 29 shows the raw data, whereas the designs in Figure 30 were based on subsequent optimization. This was done by first constructing a surrogate model and attempting to minimize fuel burn within 1dB of the raw data minimum noise design. A subsequent DoE on just the LTO operational variables was conducted to assess whether any further reductions in noise might be possible for the same fuel burn and to ensure that the trajectory met all requirements. This essentially shifted the design to the left, such that it was no longer compliant with Chapter 14 but had a better fuel burn for approximately the same noise. The SSBJ designs differ significantly partly because the differences in requirements were in a lower range and involved much fewer passengers, but also because of the choice of three over-wing engines. As such, the region of the design space sampled did not yield the right side of the tradeoff seen in Figure 29 for the MediumSST and LargeSST. The SSBJ was also a three-engine over-wing design so it is likely that fewer engine and engine placement, in addition to the vehicle class, played a role in its sensitivity relative to the larger vehicles.

The data in Figures 31 and 32 show the Pareto front on LTO NO_x (subsonic rules) vs. block fuel and LTO noise, respectively. Both plots show that as fuel and noise decrease, the LTO NO_x increase. This effect is caused by an increase in the OPR, which drives the increase in NO_x. However, this result is somewhat misleading, because lower fuel burn is generally observed to be the result of higher OPR and higher FPR, but noise generally has an inverse relationship with fuel burn. This aspect is explained in Figure 29, although the data sets between the plots are different. To the left of the minimum in Figure 29, the fuel burn (i.e., MTOM) decreases as a result of the increased FPR and OPR, and this drives an increase in LTO NO_x as well as LTO noise, because of the lower BPR and higher jet velocities. To the right of the minimum in Figure 29, the fuel burn continues to increase as a result of lower FPR and OPR. This results in higher LTO noise due to the size of the vehicle dominating the effect of a lower jet velocity engine. However, because LTO NO_x is normalized by thrust, it is only a function of OPR, and thus it continues to decrease as fuel burn increases, as seen in Figure 31. If it were not normalized by thrust, the amount of NO_x would also show a tradeoff (V-shape) similar to that in Figure 29. As the OPR further decreases, the growth

in vehicle size and fuel burn will dominate, and the non-normalized amount of LTO NO_x will begin to increase as the OPR decreases and fuel burn increases. In Figure 32, only the design space to the left of the minimum in Figure 29 is shown. Moving from right to left in Figure 29, the noise reduces as a result of increasing FPR and OPR, which reduce the vehicle size and thereby reduce the noise, which in turn increases the LTO NO_x. However, to the left of the minimum, as FPR and OPR continue to increase, both LTO noise and LTO NO_x increase and are therefore not included on the Pareto front. In essence, LTO NO_x vs. LTO noise (Figure 32) has a similar V-shape to that in Figure 29, in which the area to the right of the minimum is not Pareto optimal, except that the points where both NO_x and noise increase are not shown. The only reason why they are shown in Figure 29 is that those points were obtained on the Pareto front of block fuel vs. noise margin. Figures 33 and 34 plot the LTO NO_x for each selected vehicle design, as described above, as a function of OPR. Because the chosen designs were selected primarily with consideration for noise and fuel burn, these plots show the expected trend in which that as Mach number decreases the optimal OPR increases resulting in an increase in LTO NO_x.

Figures 35–37 plot the results of fuel fraction for a fixed-range off-design mission with varying amounts of subsonic cruise. As the Mach number increases, the fuel burn increases more steeply for a greater amount of subsonic cruise. An observation from this analysis was that as the Mach number decreases, a Mach number exists at which the design is always more efficient in subsonic flight despite being optimized for supersonic flight. That is not to say it is better than a vehicle optimized for subsonic flight; instead, it may just be more optimal in subsonic flight than supersonic flight. Additionally, larger vehicle classes tend to have a steeper slope for the same Mach number, as shown in Figure 36. Finally, the rightmost point, the 100% subsonic cruise, deviates below the trend line of the preceding points, because it does not ever go supersonic and saves fuel by avoiding the transonic acceleration segment. These results are only initial observations and warrant further investigation to provide a comprehensive understanding of the behavior or supersonic vehicles when operated subsonic at some percentage.

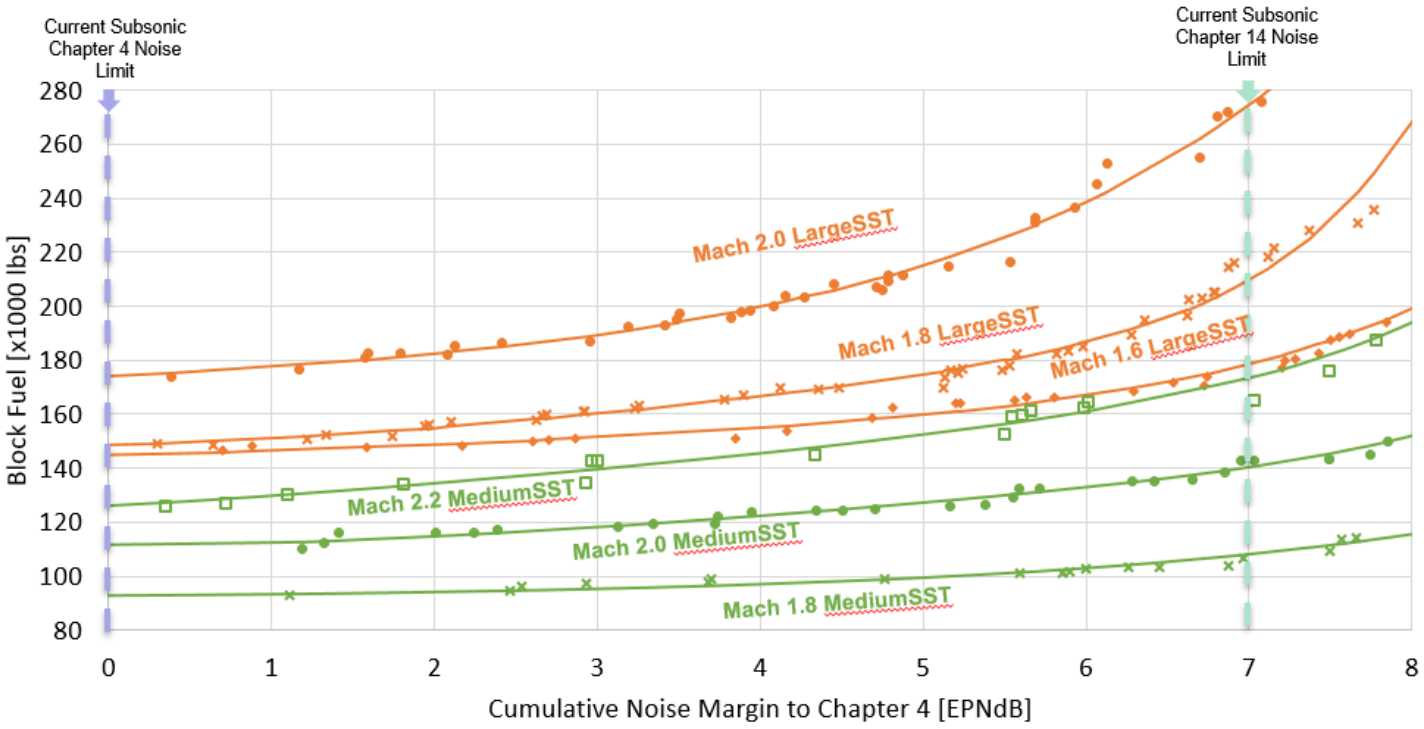

Figure 27. Design mission block fuel vs. cumulative LTO noise margin for large SST and medium SST.

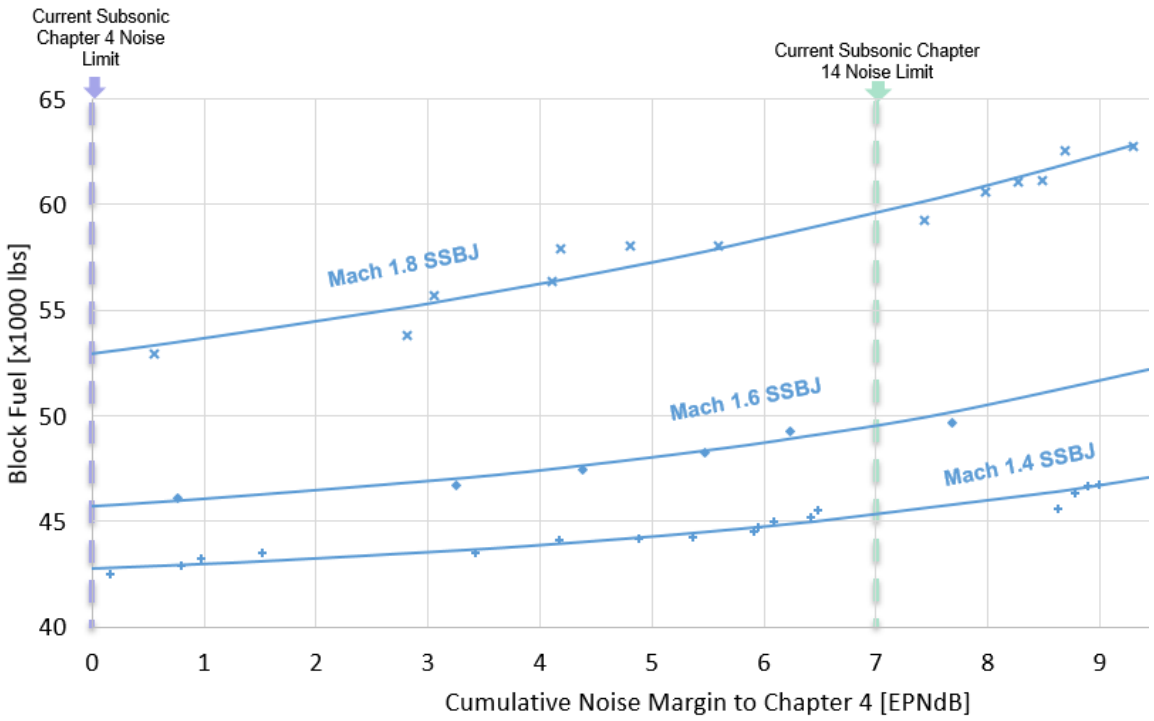

Figure 28. Design mission block fuel vs. cumulative LTO noise margin for SSBJ.

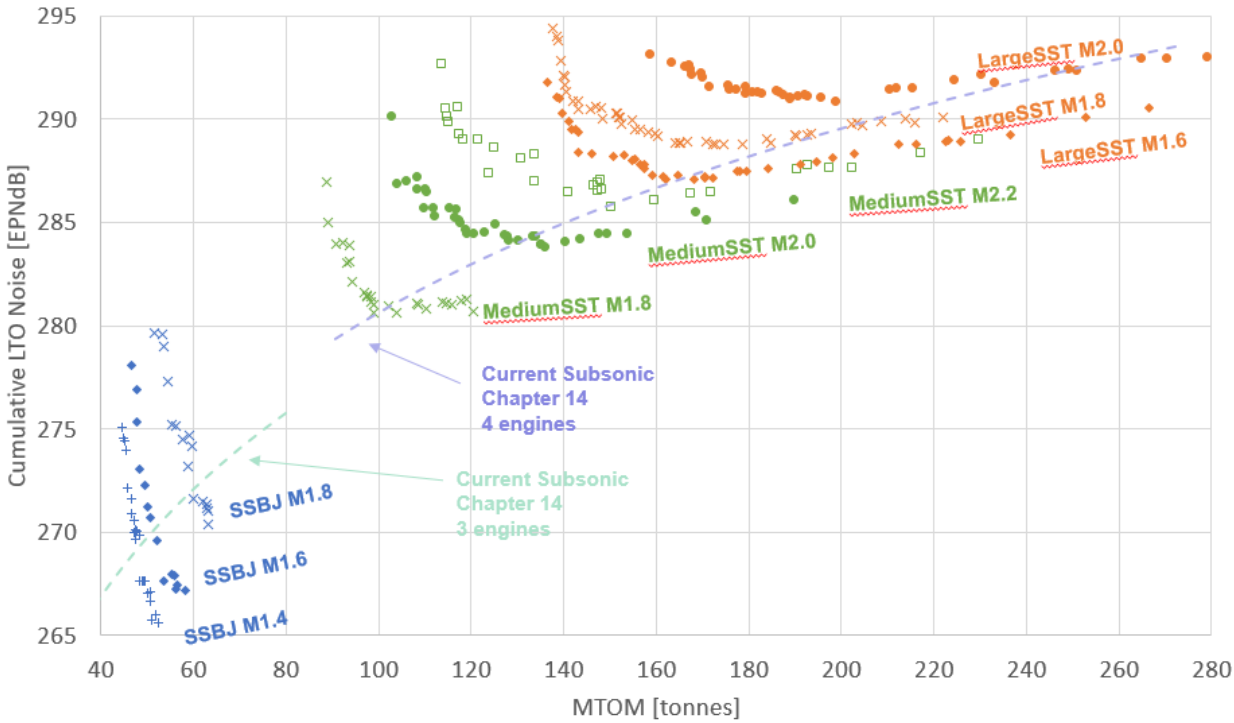

Figure 29. Cumulative LTO noise vs. maximum takeoff mass.

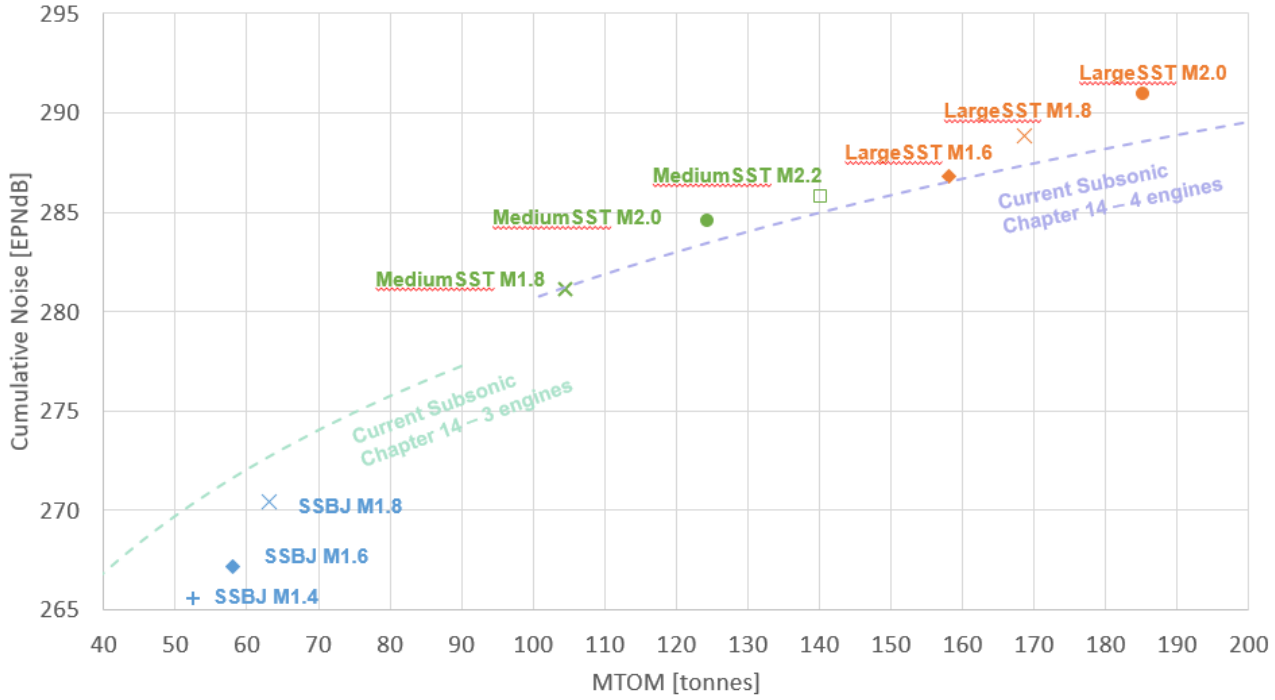

Figure 30. Final designs selected.

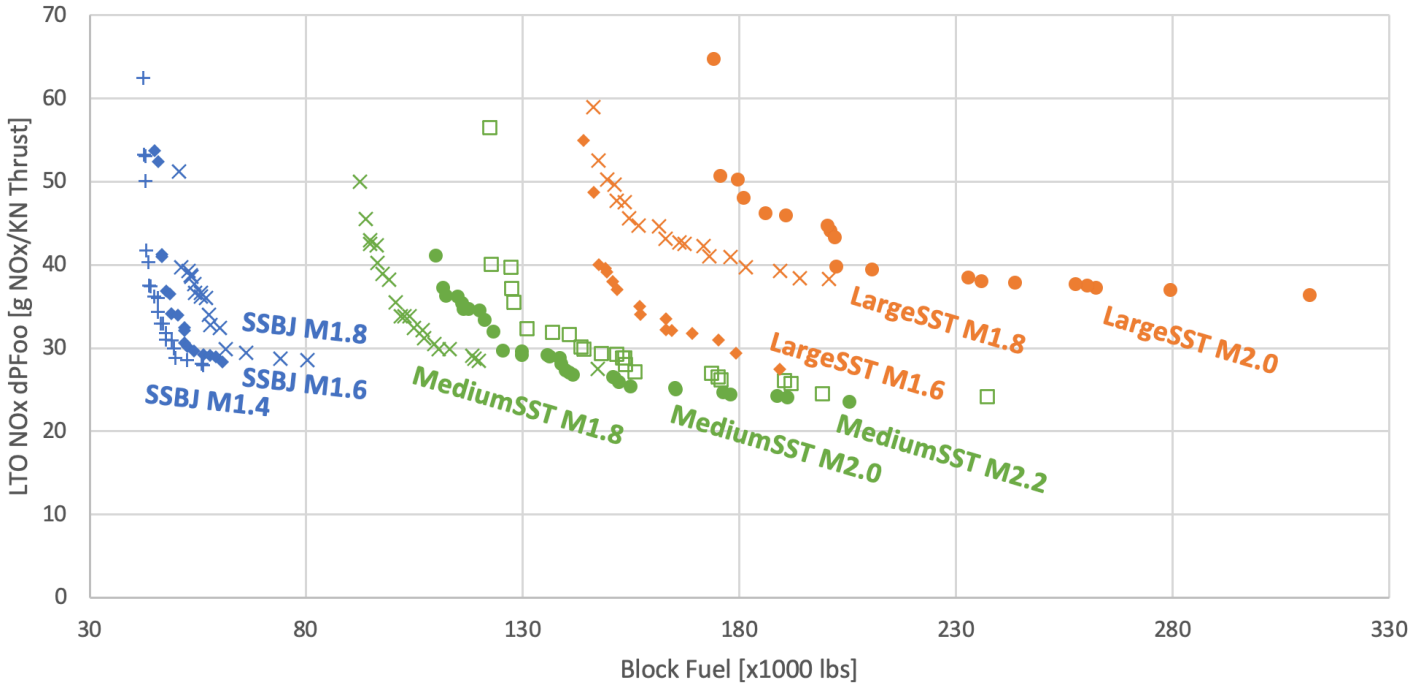

Figure 31. LTO NO_x dPFoo vs. design mission block fuel.

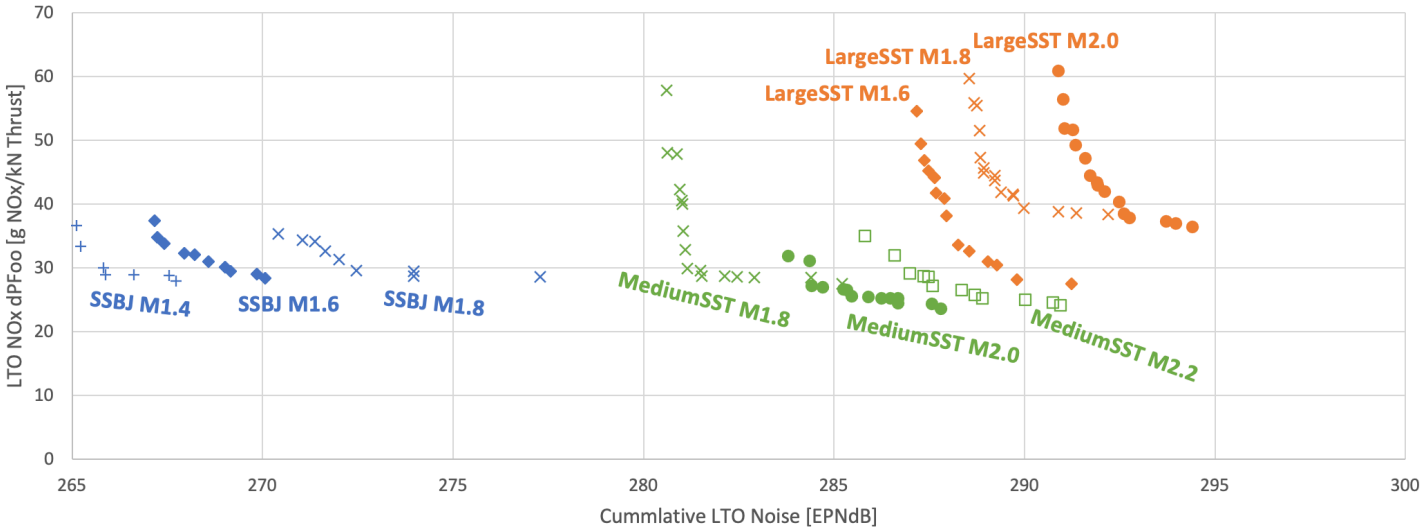

Figure 32. LTO NO_x dpFoo vs. cumulative LTO noise.

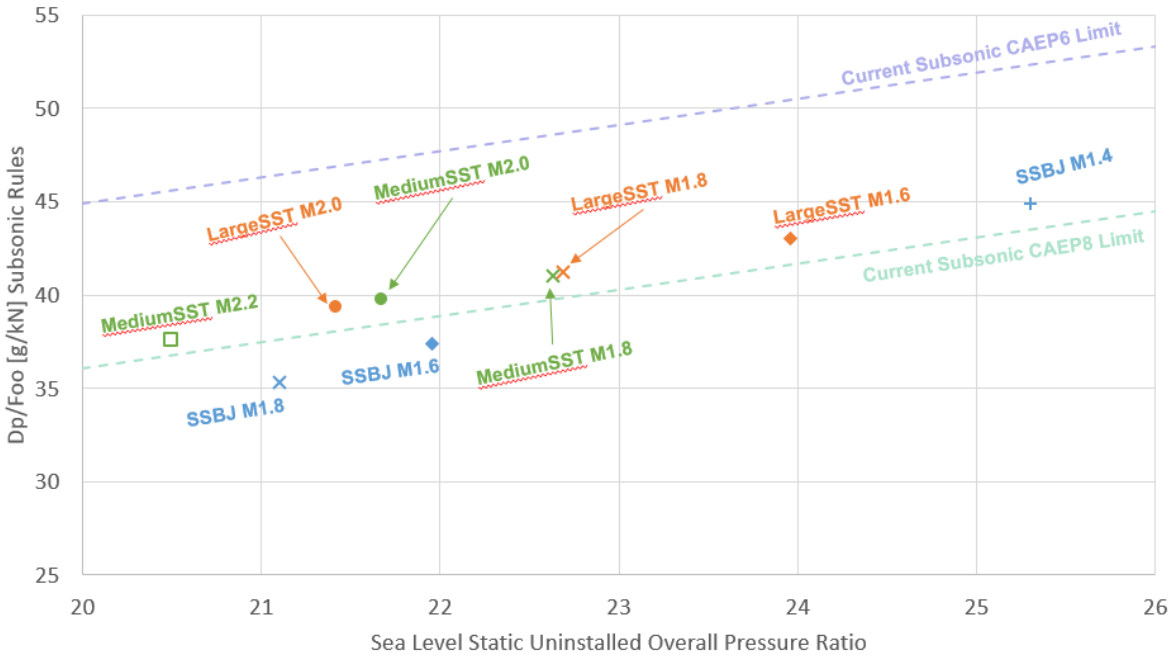

Figure 33. LTO NO_x subsonic rules vs. OPR for selected vehicle designs.

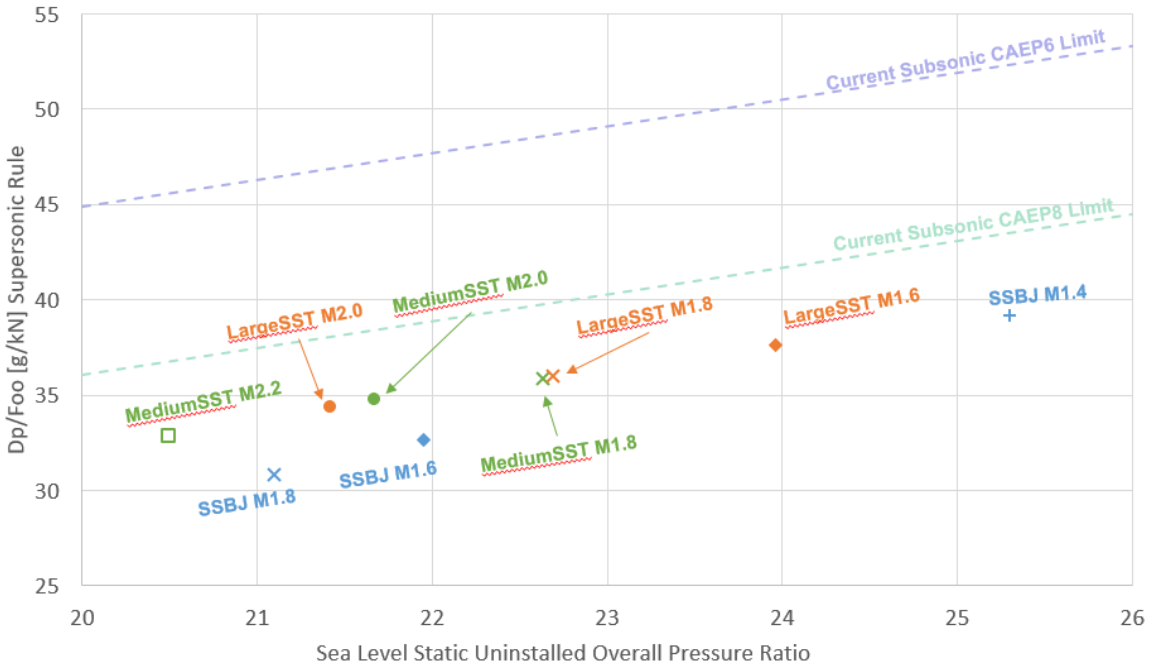

Figure 34. LTO NO_x supersonic rules vs. OPR for selected vehicle designs.

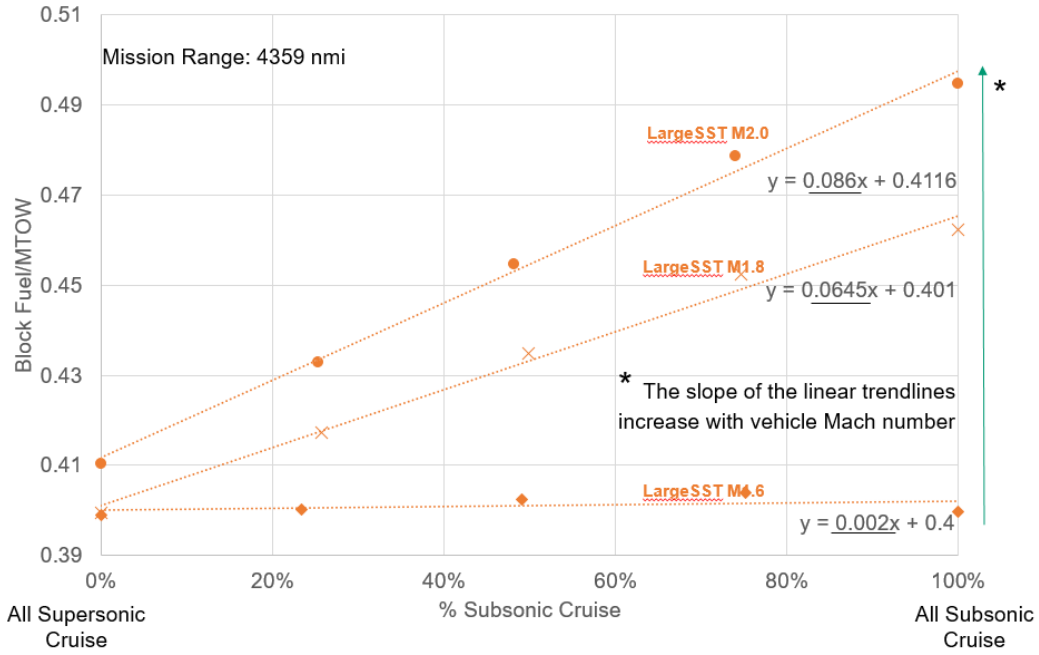

Figure 35. Large SST fuel fraction vs. percentage of cruise subsonic.

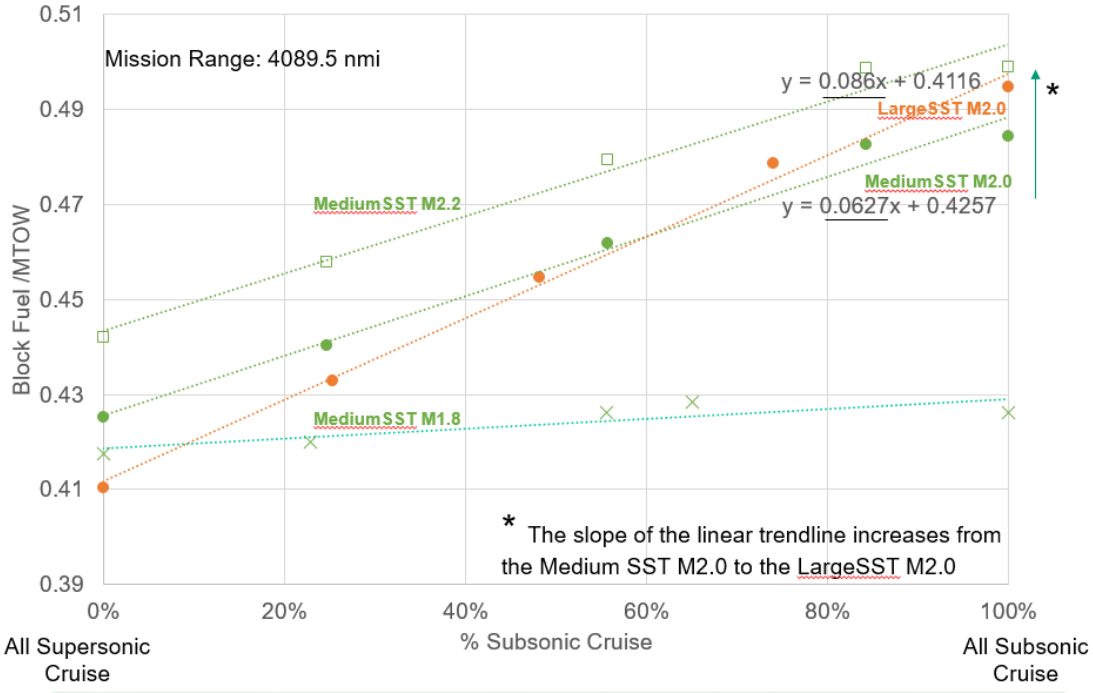

Figure 36. Medium SST fuel fraction vs. percentage of cruise subsonic.

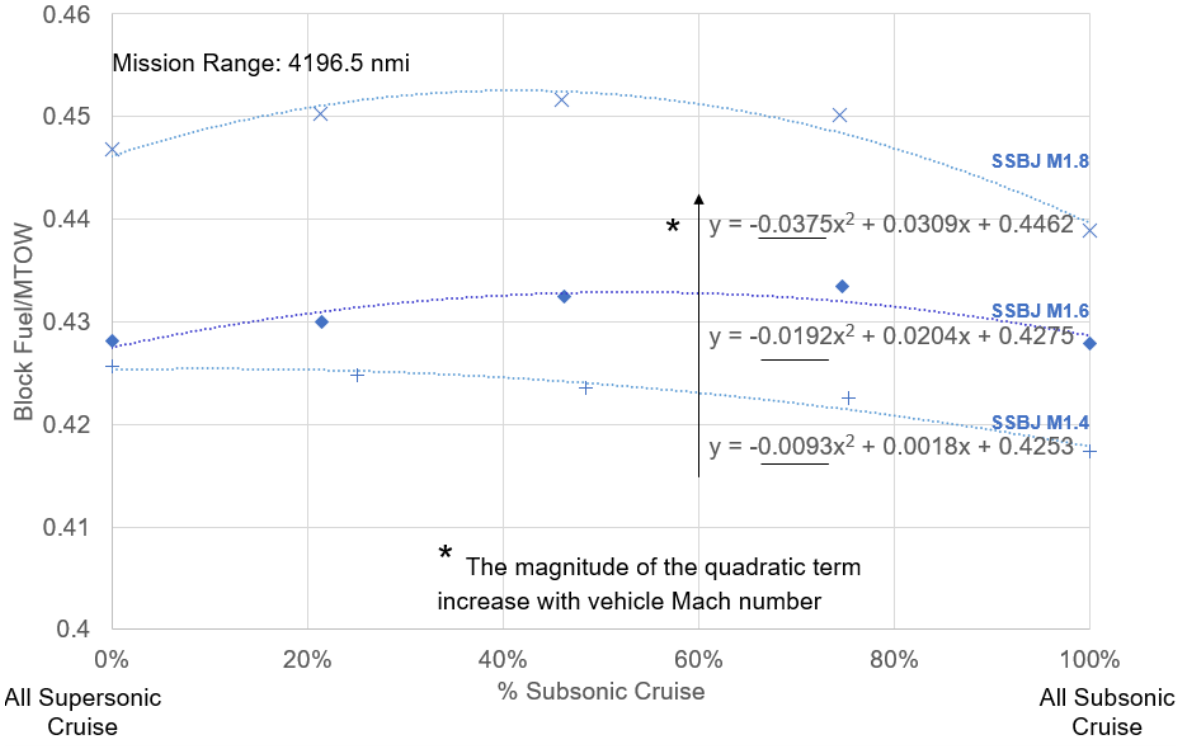

Figure 37. SSBJ fuel fraction vs. percentage of cruise subsonic.

Propulsion Results

Since the last report, the propulsion design has changed because of the inclusion of noise analysis and optimizing primarily for LTO noise. In the previous report, Georgia Tech optimized for fuel burn, constrained by a jet velocity constraint. The results below show the engine performance, dimensions, and weight for the selected vehicle designs, as described in the results of the Design Mach Number Trade Study section. As a result of optimizing primarily for noise, the FPR is much lower than that in the last report to increase the BPR and decrease the jet velocity. Similarly, the throttle ratio is much lower (design turbine inlet temperature higher) to further improve the BPR and low-speed performance. However, specific thrust is sacrificed, thus resulting in a greater loss of thrust with altitude. Consequently, the engine must be oversized at takeoff to have sufficient thrust during the transonic acceleration. Supersonic performance is also sacrificed, because the higher design turbine inlet temperature results in the engine being more severely constrained by the maximum turbine inlet temperature during cruise. The result is an engine that is much heavier and less efficient than is optimal for fuel burn when optimizing primarily for takeoff noise. In addition, as with the whole vehicle, the engine size increases with the Mach number. Furthermore, the OPR tends to decrease with the Mach number, and the FPR tends to increase with the Mach number. The following pages contain a table for each vehicle with metrics grouped by flight condition and then design Mach number. Tables 23–25 show the selected engine designs for the SSBJ, medium SST (55 pax), and large SST (100 pax), respectively. Some metrics do not change with flight conditions for a given design Mach number and may be repeated across flight conditions. The metrics shown in the subsequent tables are defined in Table 22.

Table 22. Propulsion metric description.

Metric	Description
FPR	Fan pressure ratio
BPR	Bypass ratio
OPR	Overall pressure ratio
T3 [R]	High-pressure compressor/combustor entrance total temperature
T4 [R]	Combustor exit total temperature
T41 [R]	High pressure turbine 1st rotor inlet temperature
%Nc Fan	Percentage corrected fan speed
TSFC $\left[\frac{\text{lbm}}{\text{lbf}\cdot\text{h}}\right]$	Thrust-specific fuel consumption
EPR	Engine pressure ratio
NPR	Nozzle pressure ratio
Vjet [ft/s]	Nozzle exit fully expanded jet velocity
LTO NO_x [g/kN] subsonic	Certification LTO NO_x in grams per kN of thrust according to subsonic rules
LTO NO_x [g/kN] supersonic	Certification LTO NO_x in grams per kN of thrust according to supersonic rules
Thrust [lbf]	Installed net thrust
Wc Fan [lbm/s]	Corrected airflow entering the fan
Nozzle Throat Area [in^2]	Flow area of the nozzle throat
Inlet Capture Area [in^2]	Forward projected area of the inlet
Fan Diameter [in]	Diameter of the fan
Engine Length [in]	Length of the installed engine pod
Engine Weight [lbf]	Installed engine weight

Table 23. Eight-PAX engine cycle, performance, dimensions, and weight.

	ADP Mach 1.2/39 kft/ISA			TOC Design Mach/50 kft/ISA			TKO M 0.3/SL/ISA + 18F		
Design Mach	**1.4**	**1.6**	**1.8**	**1.4**	**1.6**	**1.8**	**1.4**	**1.6**	**1.8**
FPR	2.03	2.02	2.03	2.03	1.98	1.70	2.03	2.02	2.03
BPR	3.67	3.44	3.65	3.65	3.49	4.30	3.68	3.45	3.66
OPR	25.16	21.85	20.98	25.07	21.14	15.33	25.17	21.84	20.99
T3 [R]	1371	1314	1298	1480	1512	1482	1474	1414	1397
T4 [R]	2989	2947	3081	3271	3379	3381	3130	3090	3233
T41 [R]	2930	2877	3004	3206	3300	3300	3071	3019	3156
%Nc Fan	100	100	100	100	99	91	100	100	100
TSFC $\left[\frac{\text{lbm}}{\text{lbf}\cdot\text{h}}\right]$	0.86	0.89	0.86	0.92	0.97	1.06	0.60	0.61	0.61
EPR	1.82	1.82	1.85	1.82	1.78	1.53	1.82	1.81	1.86
NPR	4.20	4.19	4.28	5.50	7.15	8.23	1.86	1.85	1.90
Vjet [ft/s]	1880	1885	1913	2112	2312	2358	1352	1354	1390
LTO NO_x [g/kN] subsonic	44.87	37.37	35.30	44.87	37.37	35.30	44.87	37.37	35.30
LTO NO_x [g/kN] supersonic	39.17	32.67	30.83	39.17	32.67	30.83	39.17	32.67	30.83
Thrust [lbf]	4621	4905	5658	3583	4989	4857	15504	16985	18760
Wc Fan [lbm/s]	494	540	576	490	532	517	500	547	583
Nozzle Throat Area [in^2]	1084	1192	1257	1081	1199	1289	1087	1196	1264
Inlet Capture Area [in^2]	1966	2240	2297	1966	2240	2297	1966	2240	2297
Fan Diameter [in]	50.7	53.0	54.7	50.7	53.0	54.7	50.7	53.0	54.7
Engine Length [in]	293	313	328	293	313	328	293	313	328
Engine Weight [lbf]	5304	6228	6721	5304	6228	6721	5304	6228	6721

Table 24. Medium SST engine cycle, performance, dimensions, and weight.

	ADP Mach 1.2/39 kft/ISA			TOC Design Mach/55 kft/ISA			TKO M 0.3/SL/ISA + 18F		
Design Mach	**1.8**	**2.0**	**2.2**	**1.8**	**2.0**	**2.2**	**1.8**	**2.0**	**2.2**
FPR	2.02	2.1	2.20	1.73	1.66	1.58	2.02	2.1	2.20
BPR	3.38	2.93	2.59	3.91	3.63	3.44	3.38	2.93	2.58
OPR	22.66	21.70	20.53	17.29	14.41	11.47	22.59	21.64	20.47
T3 [R]	1331	1317	1294	1544	1584	1604	1433	1418	1395
T4 [R]	2994	2957	2954	3382	3384	3385	3173	3138	3137
T41 [R]	2918	2879	2874	3300	3300	3300	3094	3057	3054
%Nc Fan	100	100	100	92	88	83	100	100	100
TSFC $\left[\frac{\text{lbm}}{\text{lbf·h}}\right]$	0.84	0.87	0.90	1.04	1.13	1.25	0.62	0.63	0.64
EPR	1.84	1.93	2.03	1.56	1.50	1.42	1.84	1.93	2.03
NPR	4.35	4.58	4.84	8.36	10.80	13.93	1.89	1.98	2.09
Vjet [ft/s]	1926	1988	2060	2397	2580	2757	1394	1465	1547
LTO NO_x [g/kN] subsonic	41.00	39.76	37.60	41.00	39.76	37.60	41.00	39.76	37.60
LTO NO_x [g/kN] supersonic	35.85	34.79	32.90	35.85	34.79	32.90	35.85	34.79	32.90
Thrust [lbf]	7208	8565	9504	5079	6615	9504	22862	27419	30828
Wc Fan [lbm/s]	695	780	817	629	670	817	703	789	826
Nozzle Throat Area [in^2]	1533	1678	1705	1565	1722	1737	1541	1694	1724
Inlet Capture Area [in^2]	2993	3598	4001	2993	3598	4001	2993	3598	4001
Fan Diameter [in]	60.1	63.7	65.2	60.1	63.7	65.2	60.1	63.7	65.2
Engine Length [in]	538	578	601	538	578	601	538	578	601
Engine Weight [lbf]	9671	11706	13106	9671	11706	13106	9671	11706	13106

Table 25. Large SST engine cycle, performance, dimensions, and weight.

	ADP Mach 1.2/39 kft/ISA			TOC Design Mach/50 kft/ISA			TKO M 0.3/SL/ISA + 18 F		
Design Mach	**1.6**	**1.8**	**2.0**	**1.6**	**1.8**	**2.0**	**1.6**	**1.8**	**2.0**
FPR	2.07	2.08	2.20	1.86	1.75	1.68	2.07	2.08	2.2
BPR	3.74	3.38	2.87	4.14	3.97	3.63	3.73	3.37	2.87
OPR	23.98	22.71	21.45	19.93	16.76	13.57	23.91	22.65	21.39
T3 [R]	1354	1332	1312	1487	1524	1552	1458	1434	1413
T4 [R]	3127	3062	3037	3379	3380	3381	3310	3245	3221
T41 [R]	3052	2987	2959	3300	3300	3300	3233	3167	3141
%Nc Fan	100	100	100	95	92	87	100	100	100
TSFC $\left[\frac{\text{lbm}}{\text{lbf}\cdot\text{h}}\right]$	0.82	0.85	0.88	0.96	1.06	1.17	0.61	0.63	0.64
EPR	1.88	1.90	2.02	1.67	1.57	1.52	1.88	1.90	2.02
NPR	4.39	4.45	4.75	6.63	8.30	10.92	1.92	1.94	2.06
Vjet [ft/s]	1931	1960	2043	2229	2397	2594	1406	1434	1530
LTO NO_x [g/kN] subsonic	43.05	41.19	39.36	43.05	41.19	39.36	43.05	41.19	39.36
LTO NO_x [g/kN] supersonic	37.61	36.00	34.41	37.61	36.00	34.41	37.61	36.00	34.41
Thrust [lbf]	9649	10684	11766	7200	8922	10592	30275	33814	37532
Inlet Capture Area [in^2]	3350	3871	4250	3350	3871	4250	3350	3871	4250
Fan Diameter [in]	69.0	72.0	72.7	69.0	72.0	72.7	69.0	72.0	72.7
Wc Fan [lbm/s]	917	998	1017	859	897	859	928	1010	1029
Nozzle Throat Area [in^2]	1983	2162	2124	2024	2221	2188	1997	2179	2147
Engine Length	546	579	595	546	579	5955	546	579	595
Engine Weight	12470	13979	15293	12470	13979	15293	12470	13979	15293

NASA STCA Engine Emissions Results

The supersonic engine data for the NASA STCA engine was provided by Mr. Jeff Berton at NASA Glenn Research Center. The normalized results are presented in the following tables.

Table 26. NASA STCA nvPM, subsonic LTO cycle.

	TO (100%)	C_L (85%)	AP (30%)	ID (7%)
Normalized EI Mass	1.0000	0.5942	0.0223	0.0197

Table 27. NASA STCA nvPM, Supersonic LTO cycle.

	TO (100%)	C_L (65%)	DE (15%)	AP (34%)	ID (5.8%)
Normalized EI Mass	1.0000	0.2318	0.0205	0.0285	0.0197

Boom Engine Emissions Results

The supersonic engine data for the Boom engine were generated from the Boom engine NPSS model run by Georgia Tech. The normalized results are presented in the following tables.

Table 28. Boom nvPM, subsonic LTO cycle.

	TO (100%)	C_L (85%)	AP (30%)	ID (7%)
Normalized EI Mass	1.0000	0.4503	0.1205	0.1472

Table 29. Boom nvPM, supersonic LTO cycle.

	TO (100%)	C_L (65%)	DE (15%)	AP (34%)	ID (5.8%)
Normalized EI Mass	1.0000	0.1769	0.1487	0.1185	0.1528

Gulfstream Engine Emissions Results

Two different estimates for the Gulfstream engine were available, generated from NPSS models developed by ASDL. The second model had lower thrust but higher T3 and P3 than the first model. The normalized results are presented in the following tables.

Table 30. Gulfstream nvPM, subsonic LTO cycle No. 1.

	TO (100%)	C_L (85%)	AP (30%)	ID (7%)
Normalized EI Mass	1.0000	0.7310	0.3457	0.1447

Table 31. Gulfstream nvPM, supersonic LTO cycle No. 1.

	TO (100%)	C_L (65%)	DE (15%)	AP (34%)	ID (5.8%)
Normalized EI Mass	1.0000	0.2085	0.3089	0.1936	0.1306

Table 32. Gulfstream nvPM, subsonic LTO cycle No. 2.

	TO (100%)	C_L (85%)	AP (30%)	ID (7%)
Normalized EI Mass	1.0000	0.8401	0.2236	0.1422

Table 33. Gulfstream nvPM, supersonic LTO cycle No. 2.

	TO (100%)	C_L (65%)	DE (15%)	AP (34%)	ID (5.8%)
Normalized EI Mass	1.0000	0.5026	0.2012	0.1905	0.1328

Airframe Aerodynamic Results

This section presents planform views of the optimized vehicles, with pressure coefficient contours overlaid, as well as drag polars and L/D trends at 55,000 ft for the 100- pax (Figures 38–40) and 55-pax (Figures 41–43) aircraft, and SSBJ (Figures 44–46). Table 34 captures all designs and also shows the optimized vehicles at off-design Mach numbers. A decrease in peak L/D with Mach number is observed, which is consistent with the physics. In addition, the peak L/D decreases with passenger class, probably because of a reduction in the wing planform area as the vehicle size reduces. The exception to this rule is the SSBJ; however, the highly swept wings for this concept are likely to provide a high-speed L/D benefit that counteracts the smaller planform area. The design space selected appears to have been overly constrained, particularly by the trailing edge sweep bounds. As such, most planforms ultimately appear similar across vehicles. The SSBJ in contrast, with a different baseline and variable bounds, shows a noticeable change in wing sweep as the Mach number is increased, thus justifying the conclusion of a narrow design space for the other vehicles.

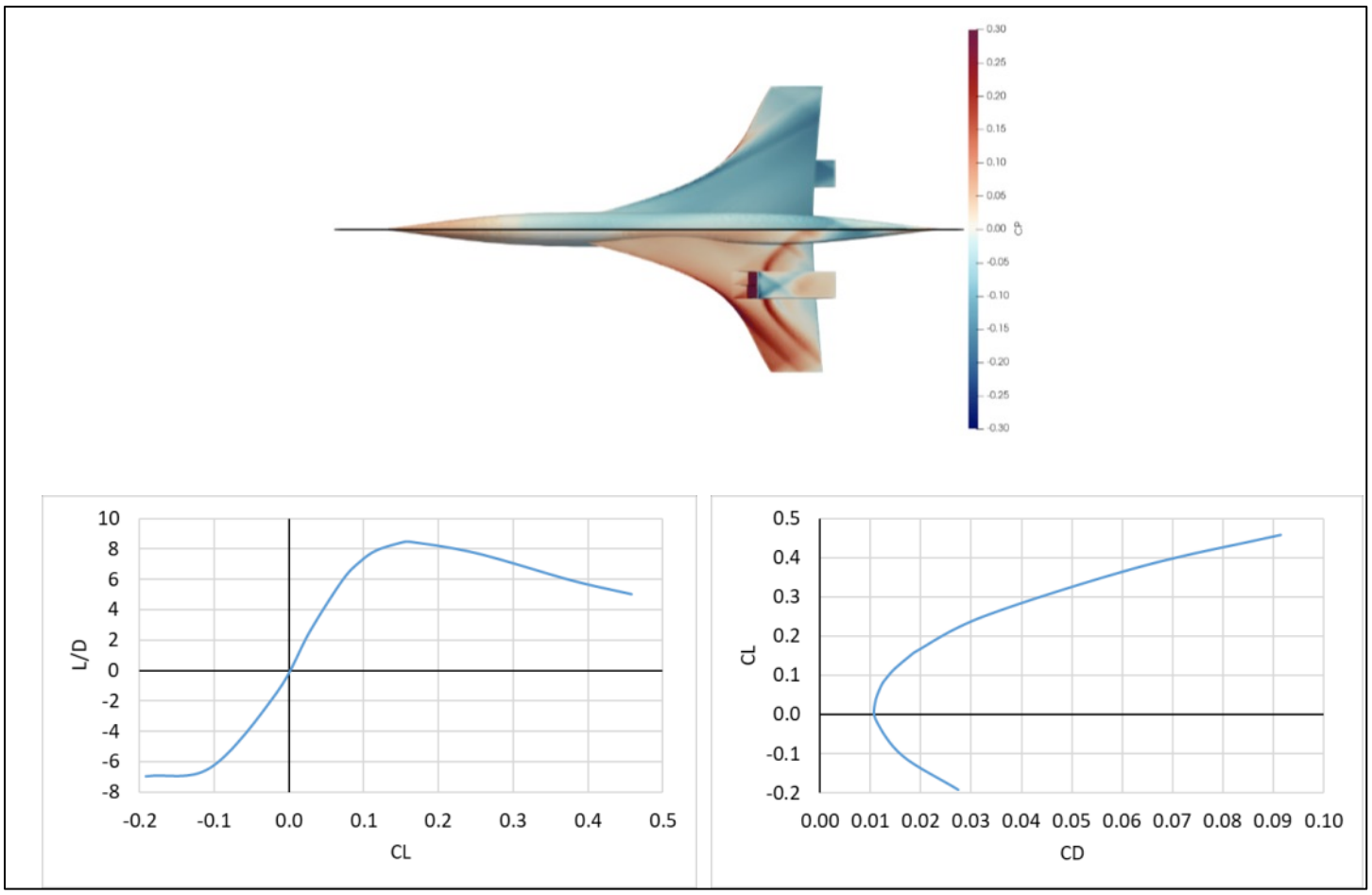

Figure 38. Large SST Mach 1.6 design at Mach 1.6/55,000 ft (peak L/D = 8.46 at C_L = 0.162).

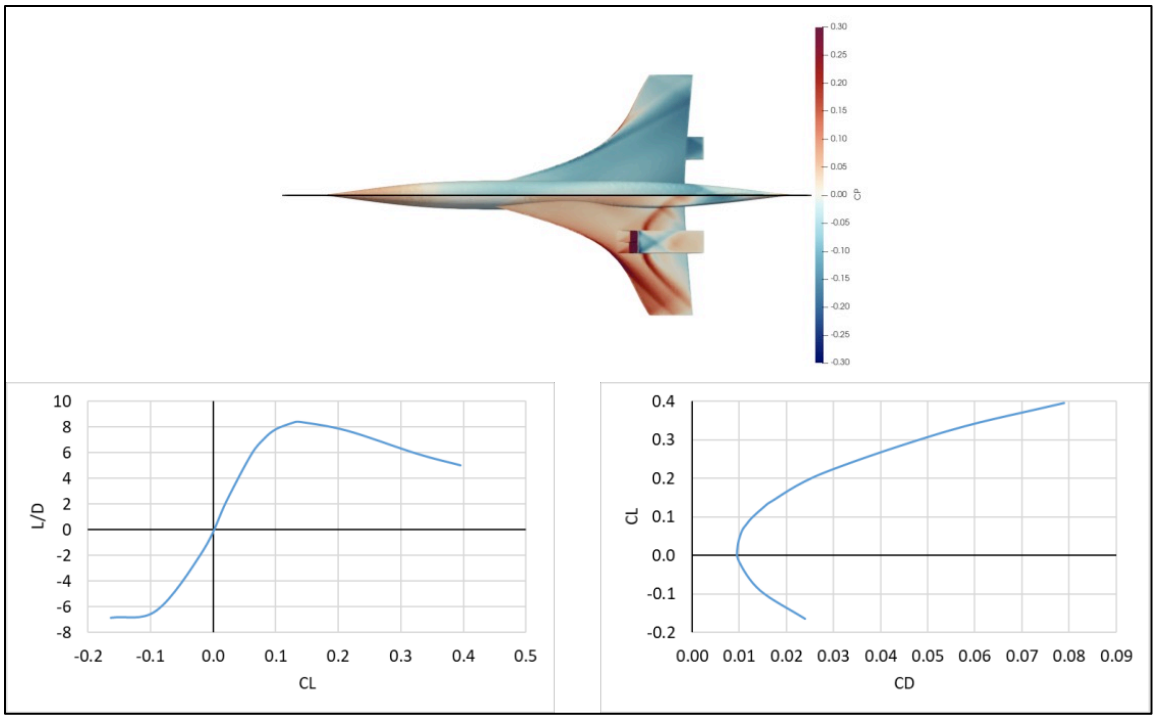

Figure 39. Large SST Mach 1.8 design at Mach 1.8/55,000 ft (peak L/D = 8.39 at C_L = 0.138).

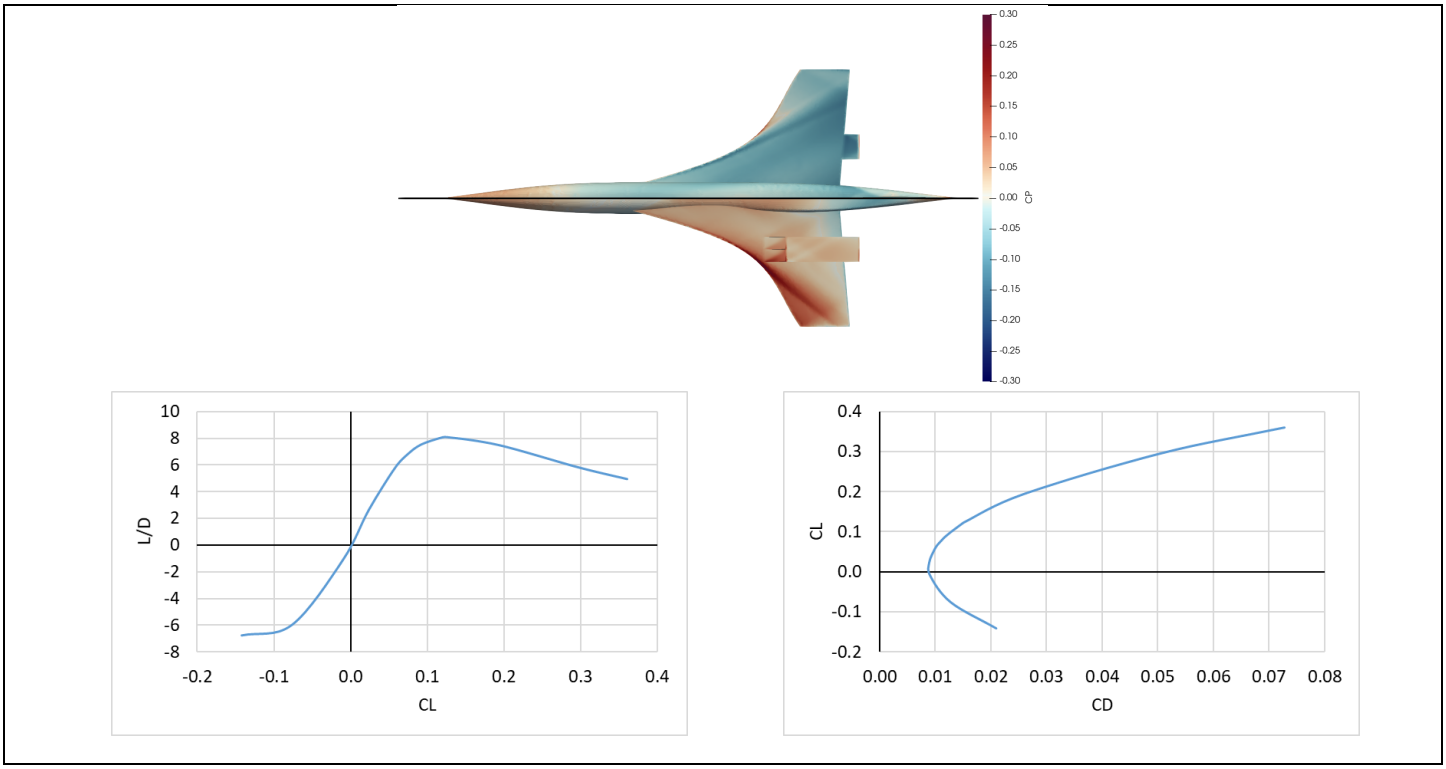

Figure 40. Large SST Mach 2.0 design at Mach 2.0/55,000 ft (peak L/D = 8.09 at C_L = 0.126).

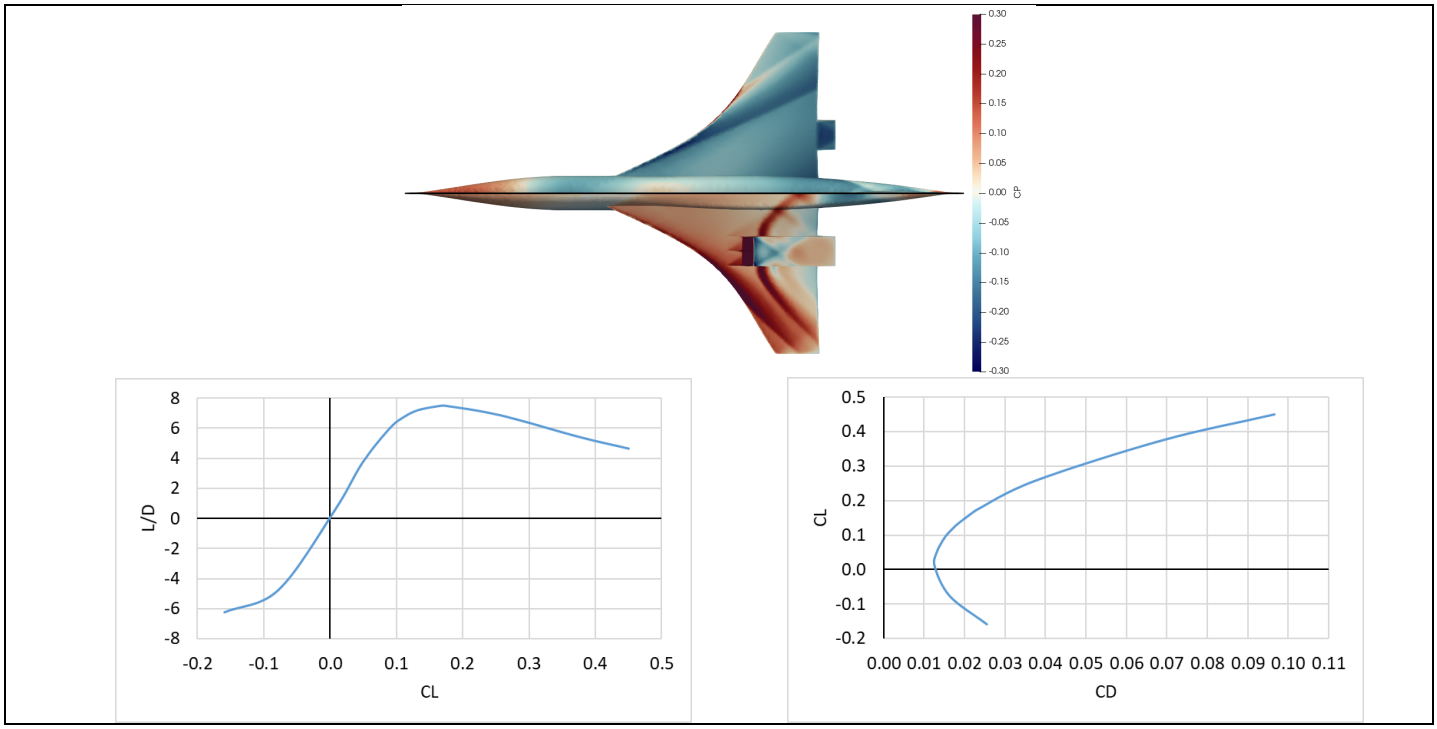

Figure 41. Medium=SST Mach 1.8 design at Mach 1.8/55,000 ft (peak L/D = 7.51 at C_L = 0.174).

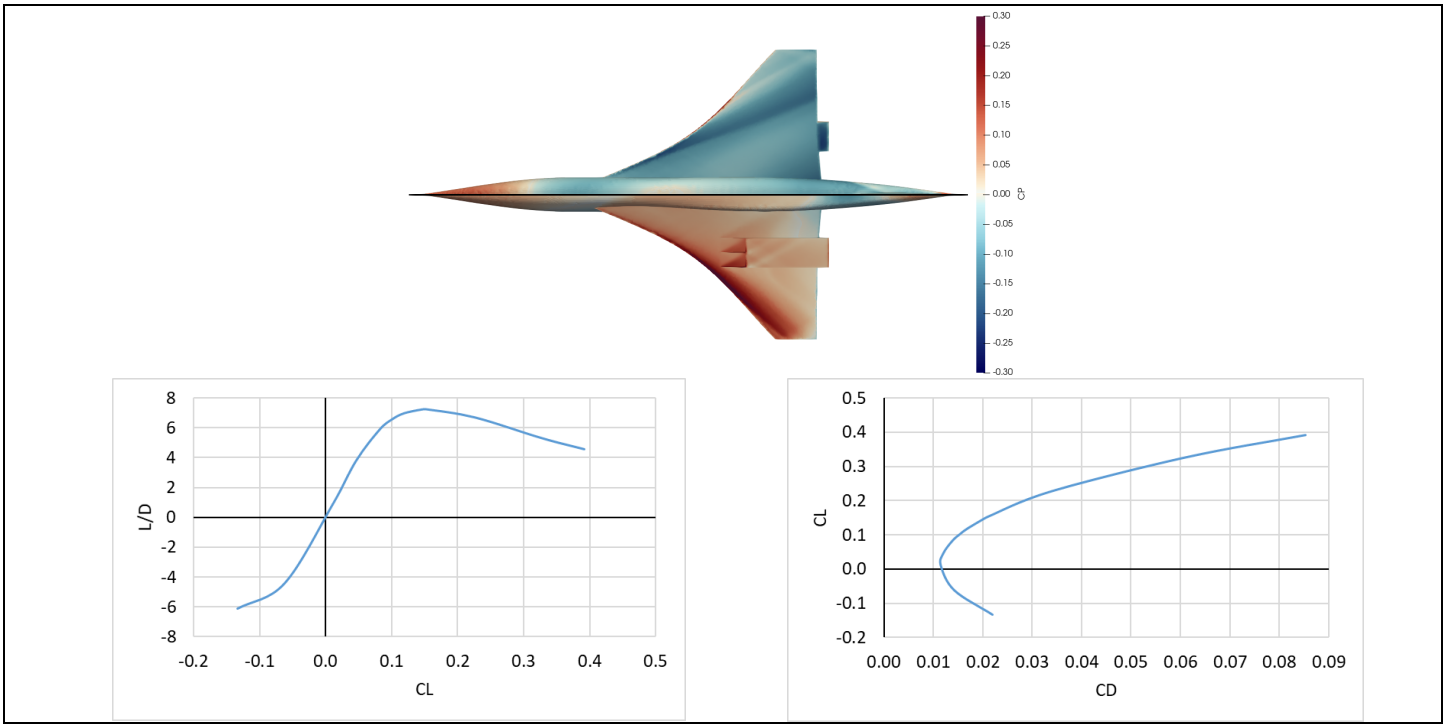

Figure 42. Medium SST Mach 2.0 design at Mach 2.0/55,000 ft (peak L/D = 7.26 at C_L = 0.153).

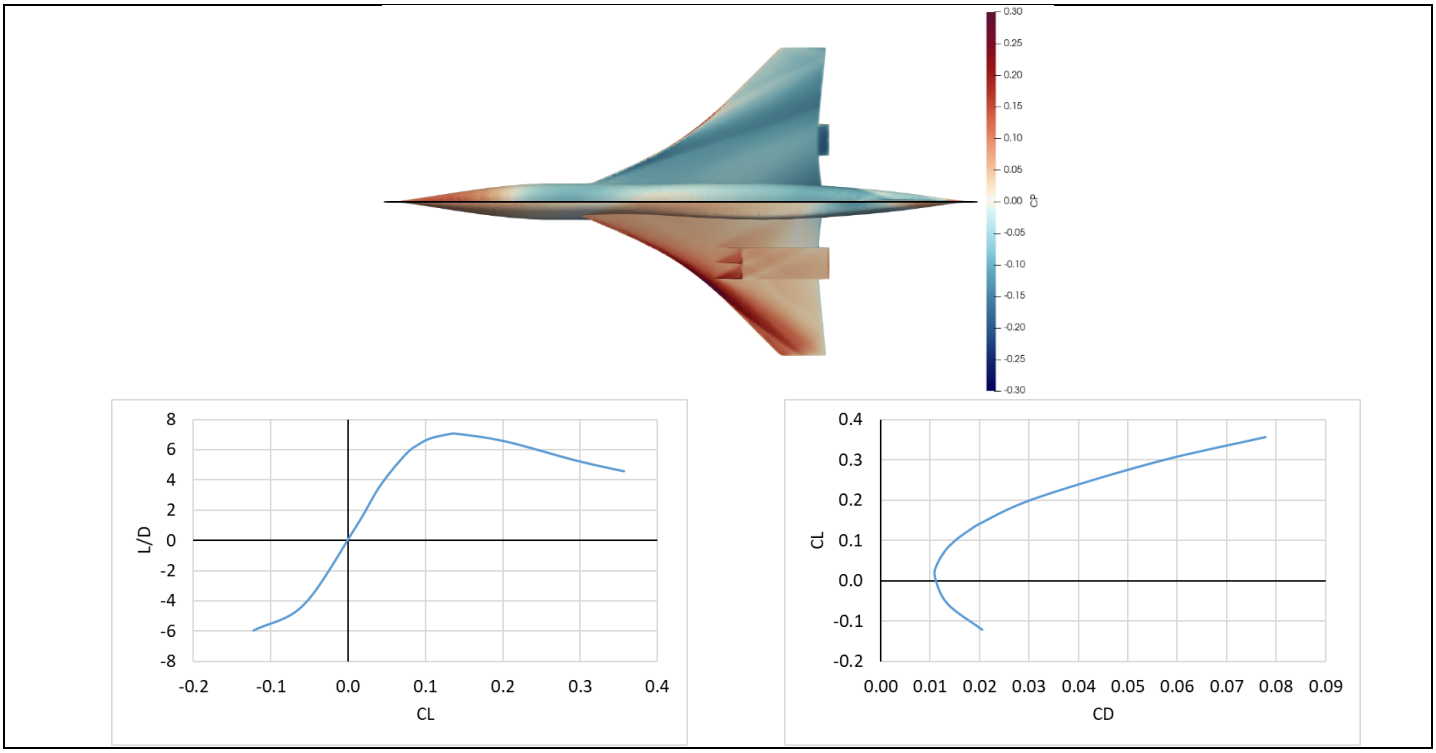

Figure 43. Medium SST Mach 2.2 design at Mach 2.2/55,000 ft (peak L/D = 7.07 at C_L = 0.139).

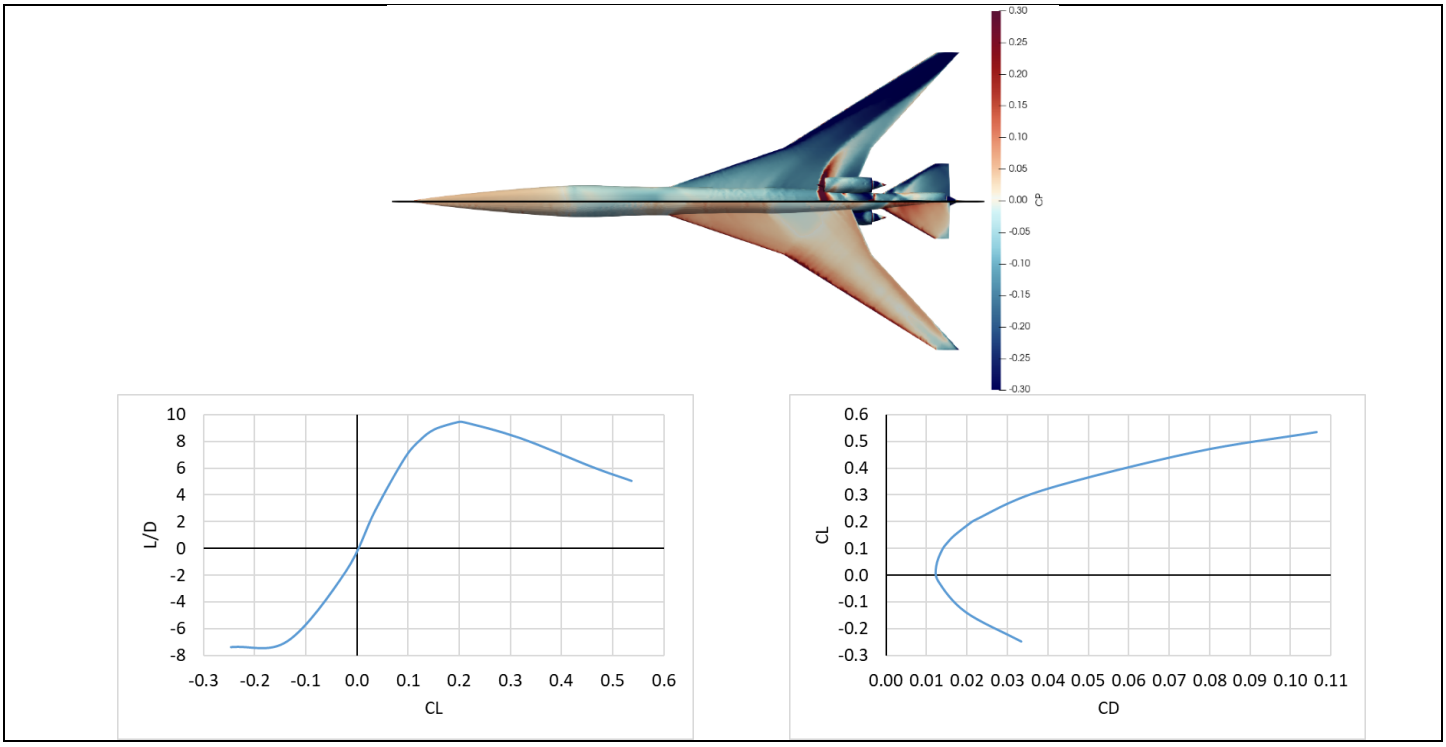

Figure 44. SSBJ Mach 1.4 design at Mach 1.4/55,000 ft (peak L/D = 9.41 at C_L = 0.209).

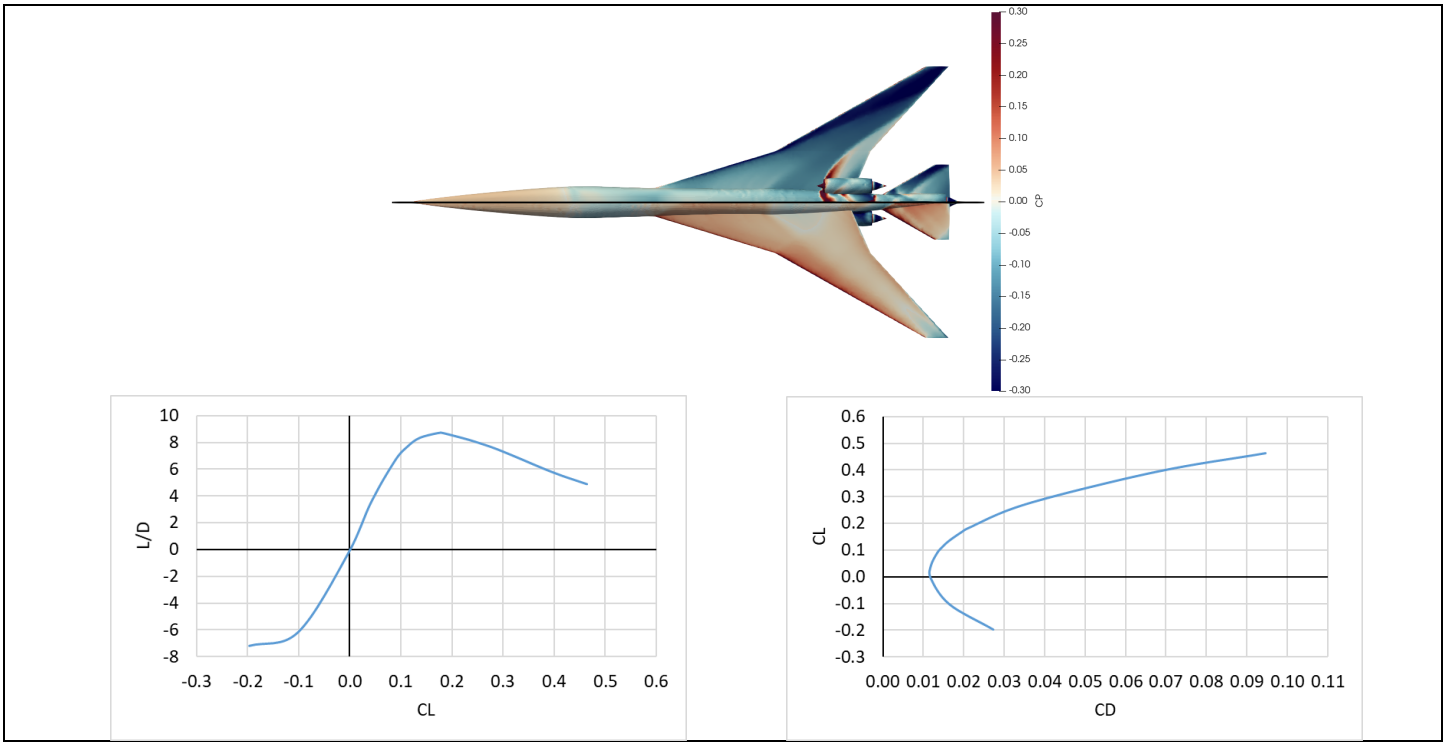

Figure 45. SSBJ Mach 1.6 design at Mach 1.6/55,000 ft (peak L/D = 8.72 at C_L = 0.172).

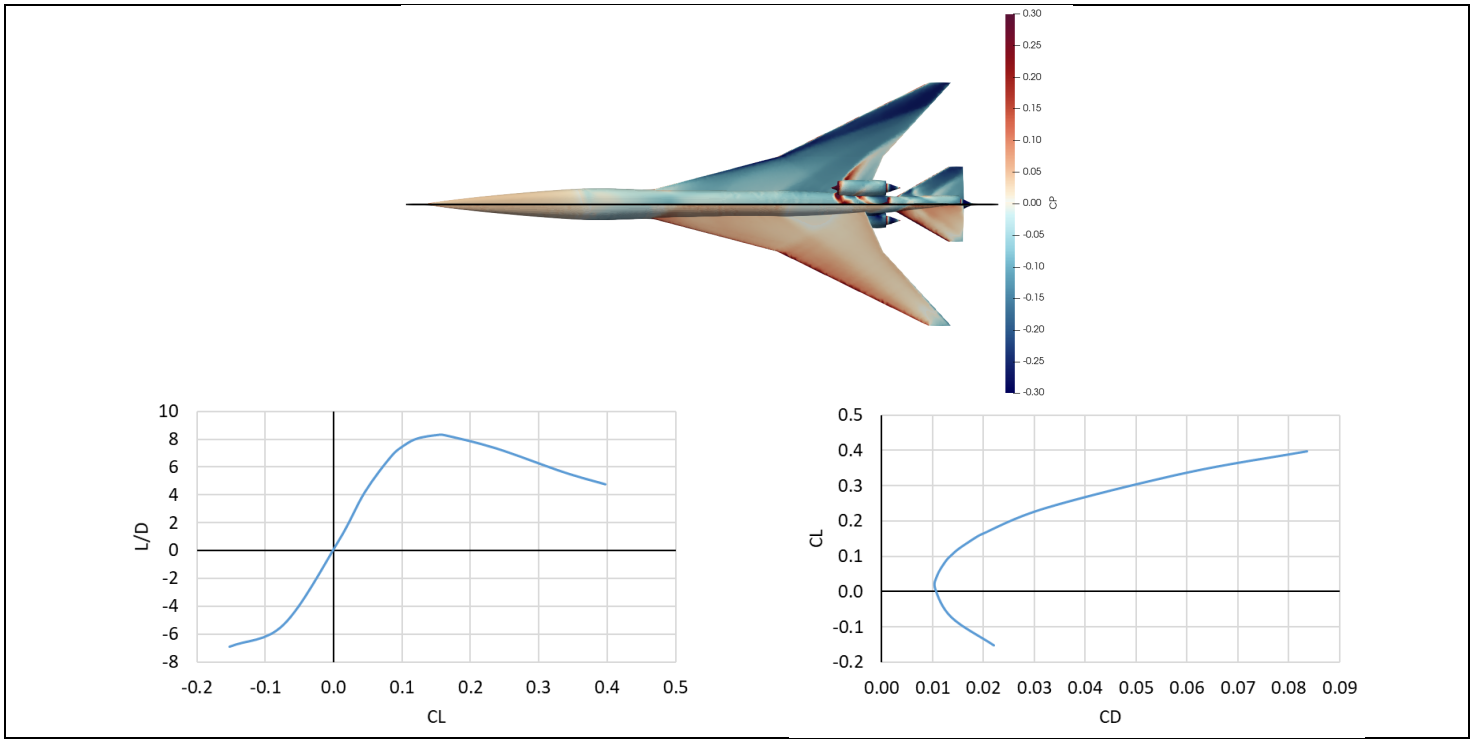

Figure 46. SSBJ Mach 1.8 design at Mach 1.8/55,000 ft (peak L/D = 8.29 at C_L = 0.153).

Table 34. Table of optimum designs with maximum L/D (as computed by **CART3D**) and surface pressure coefficients shown for an altitude of 55,000 ft.

	$M_\infty = 1.4$	$M_\infty = 1.6$	$M_\infty = 1.8$	$M_\infty = 2.0$	$M_\infty = 2.2$
Large SST		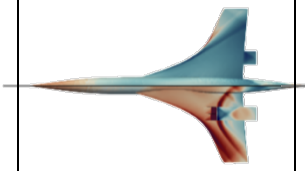 *Max L/D = 8.46*	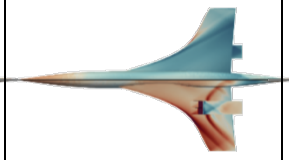 *Max L/D = 8.39*	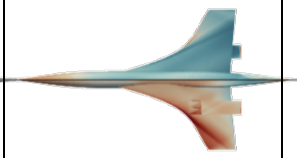 *Max L/D = 8.09*	
Medium SST			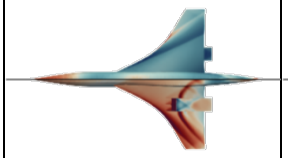 *Max L/D = 7.51*	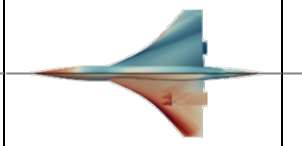 *Max L/D = 7.26*	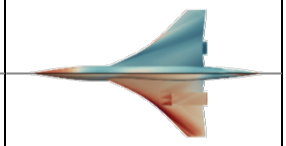 *Max L/D = 7.07*
SSBJ	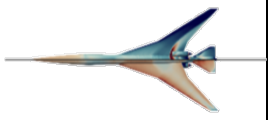 *Max L/D = 9.41*	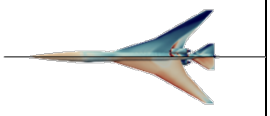 *Max L/D = 8.72*	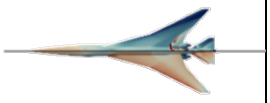 *Max L/D = 8.29*		

Mission Analysis/Vehicle Sizing Results

The vehicle sizing results for all nine vehicles are summarized in Table 35, and the associated aircraft component weight breakdowns are also summarized in Table 36. In addition, Figures 47–49 summarize the resulting mission profiles for each SST class.

Table 35. Summary of SST sizing results.

	SSBJ (8 pax)			Medium SST (55 pax)			Large SST (100 pax)		
	Mach 1.4	**Mach 1.6**	**Mach 1.8**	**Mach 1.8**	**Mach 2.0**	**Mach 2.2**	**Mach 1.6**	**Mach 1.8**	**Mach 2.0**
Design Range (nmi)	4,240	4,240	4,240	4,500	4,500	4,500	5,000	5,000	5,000
Payload (Passengers)	8	8	8	55	55	55	100	100	100
Maximum takeoff weight (lbs)	116,371	128,825	140,070	231,554	275,256	310,752	350,735	374,313	411,435
OEW (lbs)	57,922	63,449	66,760	96,453	113,926	124,369	141,928	151,371	162,172
Fuel Weight (lbs)	56,767	63,697	71,630	123,550	149,780	174,884	187,807	201,942	228,263
Block Fuel (lbs)	49,591	55,904	63,358	109,567	132,728	155,453	167,771	179,658	203,466
Block Time (hr)	5.85	5.23	4.68	5.00	4.60	4.31	6.08	5.49	5.07
T/W	0.469	0.464	0.468	0.420	0.420	0.415	0.365	0.380	0.380
W/S	77	74	76	101	102	106	102	102	105
TOFL (ft)	6,409	6,440	6,695	7,527	7,710	7,996	8,684	8,359	8,523
LDFL (ft)	5,346	5,044	4,781	7,747	7,601	7,619	7,730	7,645	7,618
Vapp (kts)	151.2	147.7	147.2	164.9	164.3	164.5	164.9	164.6	164.7
Wing Area (ft^2)	1,609	1,733	1,838	2,293	2,699	2,932	3,439	3,670	3,918
Sized Thrust (lbf)	18,199	19,924	21,874	24,313	28,902	32,241	32,005	35,560	39,085
Aspect Ratio	3.26	2.72	2.18	2.75	2.25	2.25	2.70	2.35	2.25

Table 36. Summary of SST weight breakdown.

	SSBJ			Medium SST			Large SST		
	M1.4	M1.6	M1.8	M1.8	M2.0	M2.2	M1.6	M1.8	M2.0
WING	12,614	13,991	14,852	17,667	19,828	22,736	31,689	33,491	37,163
HORIZONTAL TAIL	681	856	950	-	-	-	-	-	-
VERTICAL TAIL	630	718	722	253	346	396	338	375	419
VERTICAL FIN	-	-	-	-	-	-	-	-	-
CANARD	-	-	-	-	-	-	-	-	-
FUSELAGE	8,832	8,832	8,832	18,972	18,972	18,972	27,393	27,393	27,393
LANDING GEAR	4,746	5,147	5,393	2,521	8,461	9,250	11,224	11,881	12,624
NACELLE (AIR INDUCTION)	-	-	-	-	-	-	-	-	-
STRUCTURE TOTAL	*27,504*	*29,544*	*30,749*	*39,414*	*47,607*	*51,254*	*70,643*	*73,140*	*77,599*
ENGINES	15,914	18,682	20,163	38,675	46,830	52,443	49,893	55,942	61,200
THRUST REVERSERS	-	-	-	-	-	-	-	-	-
MISCELLANEOUS SYSTEMS	21	22	23	163	178	188	187	197	207
FUEL SYSTEM-TANKS AND PLUMBING	1,854	2,075	2,312	1,917	2,221	2,510	2,348	2,549	2,836
PROPULSION TOTAL	*17,789*	*20,779*	*22,498*	*40,755*	*49,230*	*55,141*	*52,428*	*58,688*	*64,243*
SURFACE CONTROLS	1,062	1,239	1,341	2,433	2,692	3,091	1,583	1,675	1,858
AUXILIARY POWER	459	459	459	706	706	706	903	903	903
INSTRUMENTS	528	564	599	863	910	954	990	1,050	1,107
HYDRAULICS	868	947	1,004	1,652	1,790	1,894	2,278	2,412	2,546
ELECTRICAL	2,094	2,094	2,094	2,713	2,713	2,713	3,157	3,157	3,157
AVIONICS	1,130	1,130	1,130	1,329	1,329	1,329	1,556	1,556	1,556
FURNISHINGS AND EQUIPMENT	3,397	3,397	3,397	-	-	-	-	-	-
AIR CONDITIONING	1,195	1,352	1,509	2,827	3,131	3,434	3,343	3,746	4,149
ANTI-ICING	150	158	163	125	132	140	162	167	170
SYSTEMS AND EQUIPMENT TOTAL	*10,885*	*11,343*	*11,698*	*12,650*	*13,404*	*14,262*	*13,973*	*14,666*	*15,446*
WEIGHT EMPTY	*56,179*	*61,666*	*64,945*	*92,829*	*110,241*	*120,657*	*137,044*	*146,494*	*157,288*
CREW AND BAGGAGE-FLIGHT,	450	450	450	450	450	450	450	450	450
-CABIN,	155	155	155	310	310	310	310	310	310
UNUSABLE FUEL	647	678	700	806	863	901	943	973	1,010
ENGINE OIL	252	268	284	233	260	279	278	298	317
PASSENGER SERVICE	240	232	226	1,486	1,452	1,421	2,203	2,146	2,096
CARGO CONTAINERS	-	-	-	350	350	350	700	700	700
OPERATING WEIGHT	*57,922*	*63,449*	*66,760*	*96,453*	*113,926*	*124,369*	*141,928*	*151,371*	*162,171*
PASSENGERS	1,440	1,440	1,440	9,900	9,900	9,900	18,000	18,000	18,000
PASSENGER BAGGAGE	240	240	240	1,650	1,650	1,650	3,000	3,000	3,000
CARGO	-	-	-	-	-	-	-	-	-
ZERO FUEL WEIGHT	*59,502*	*65,129*	*68,440*	*108,003*	*125,476*	*135,919*	*162,928*	*172,371*	*183,171*
MISSION FUEL	56,769	63,697	71,630	123,550	149,780	174,834	187,807	201,942	228,248
RAMP (GROSS) WEIGHT	*116,371*	*128,825*	*140,070*	*231,554*	*275,256*	*310,752*	*350,735*	*374,313*	*411,419*

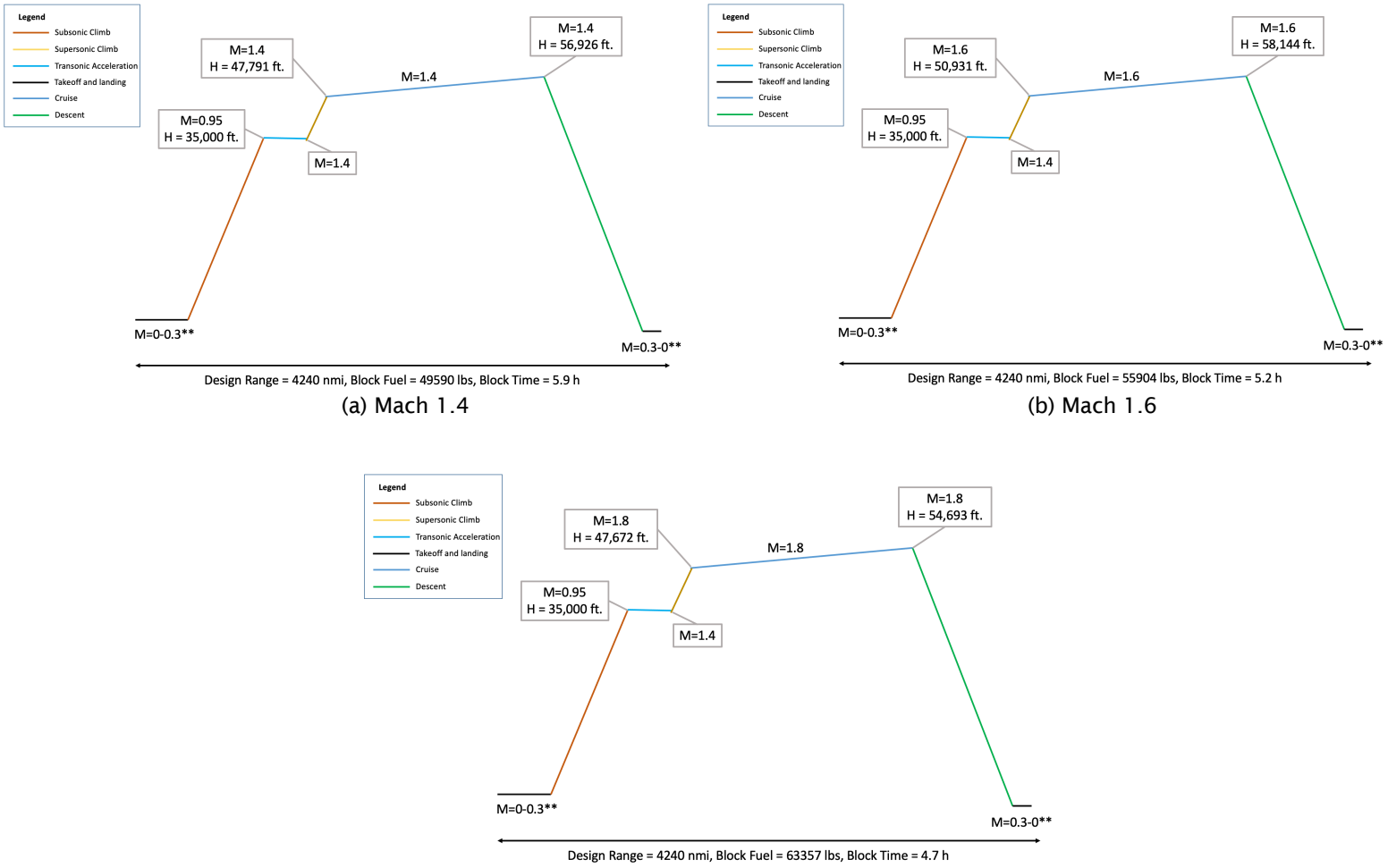

Figure 47. Summary of SSBJ mission profiles.

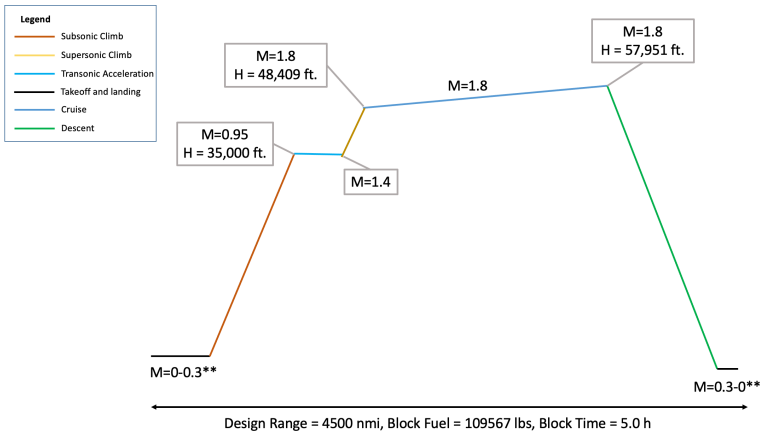

(a) Mach 1.8

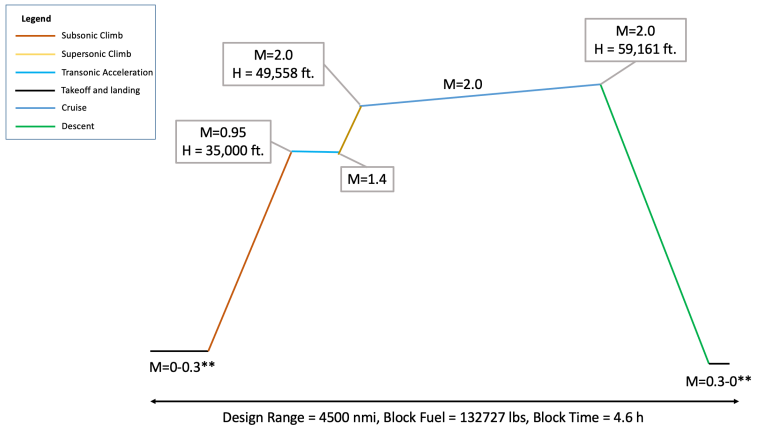

(b) Mach 2.0

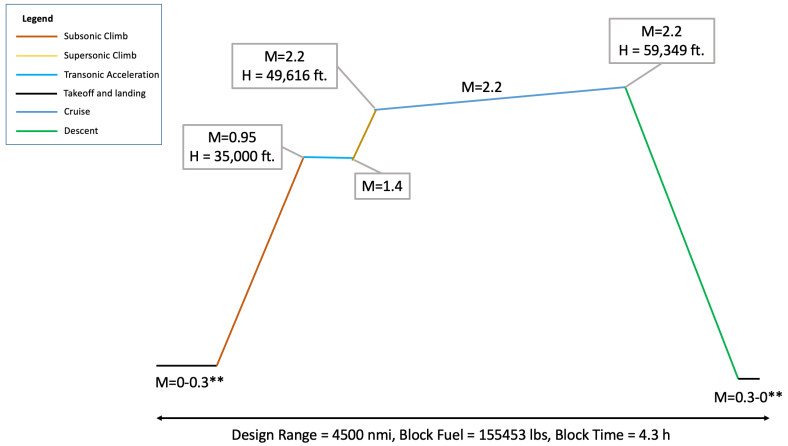

(c) Mach 2.2

Figure 48. Summary of medium SST mission profiles.

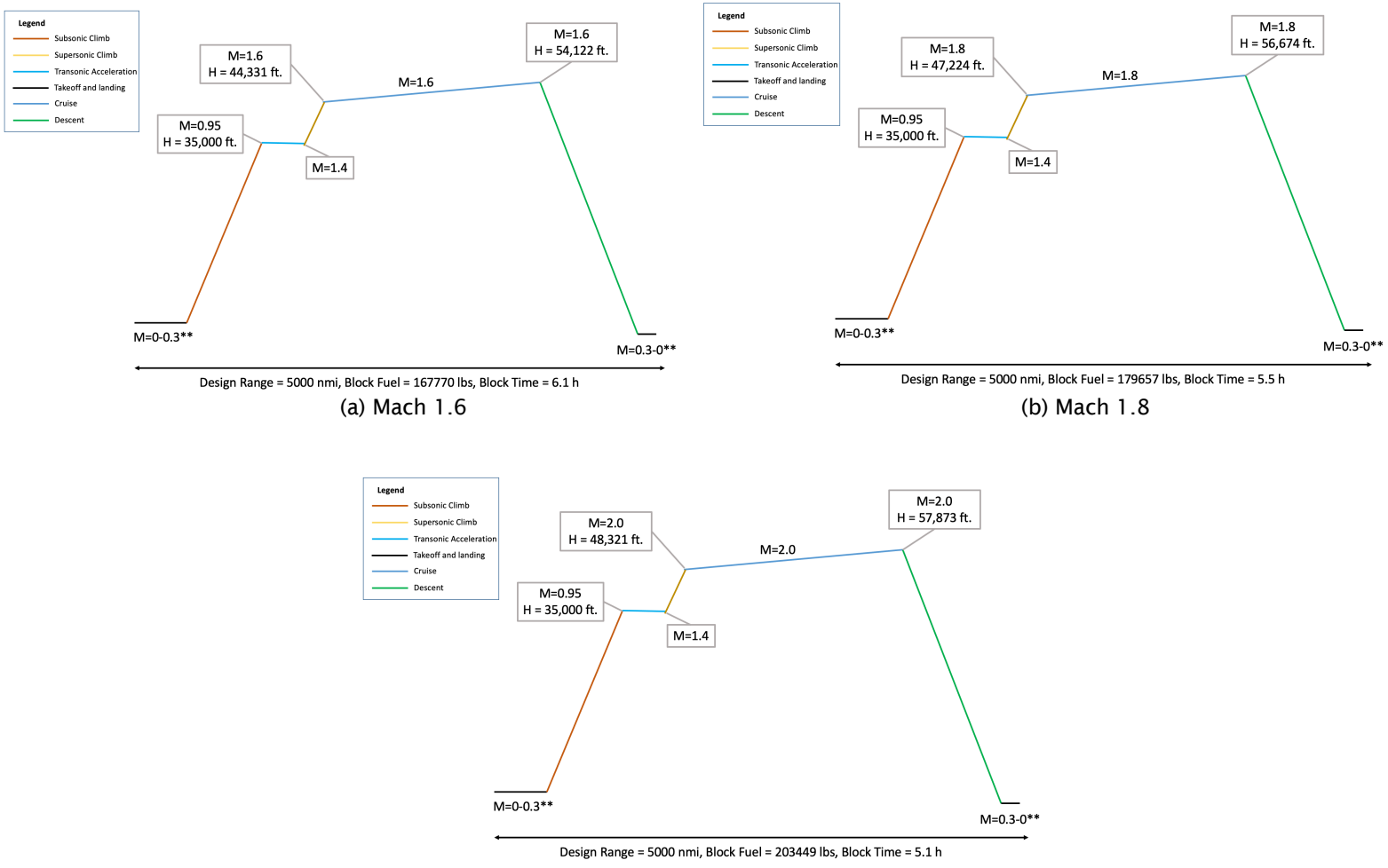

Figure 49. Summary of large SST mission profiles.

Noise Analysis Results

For the takeoff noise analysis, the accumulated data resulting from the DoEs were filtered to include the relevant parameters, i.e., the trajectory variables and the noise values (and corresponding noise margins) associated with each configuration. Although the following analysis focuses on the five main variables described in the Methodology section, many other variables were also included to help assessing the validity of the design point. A collection of viable design points can be seen in Figure 50 where each point represents a simulated configuration and is colored by the total cumulative noise margin for visualization purposes.

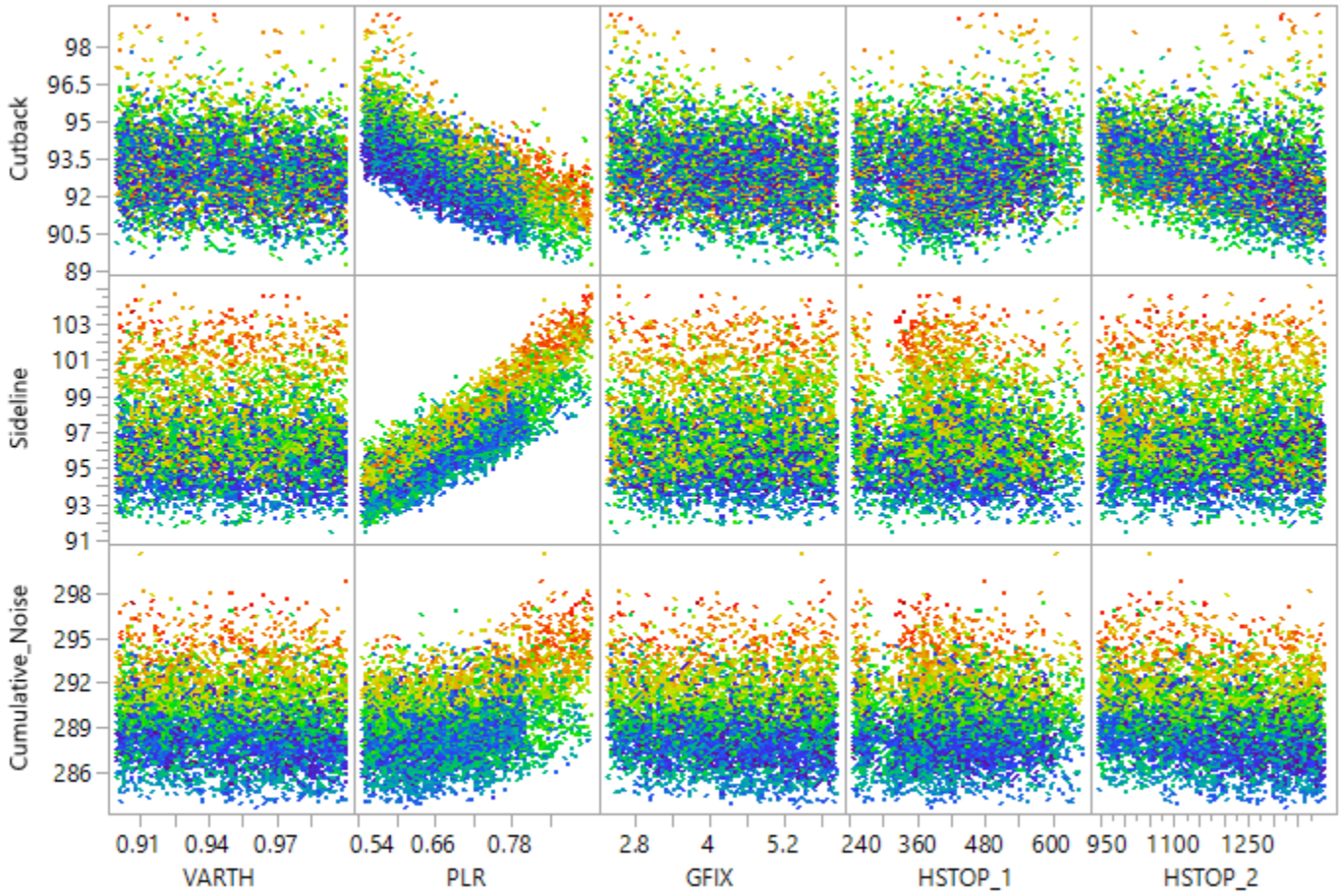

Figure 50. Takeoff noise DoE visualization.

The next step in the analysis is to fit a predictive model (e.g., a neural net) over the data. This process enables use of a prediction profiler, similar to that shown in Figure 51, to a setting for the trajectory variables with the optimal noise configuration. In the present study, the optimal condition was set to a weighted minimum noise, taking the cutback and sideline components into consideration but relying heavily on the total cumulative noise.

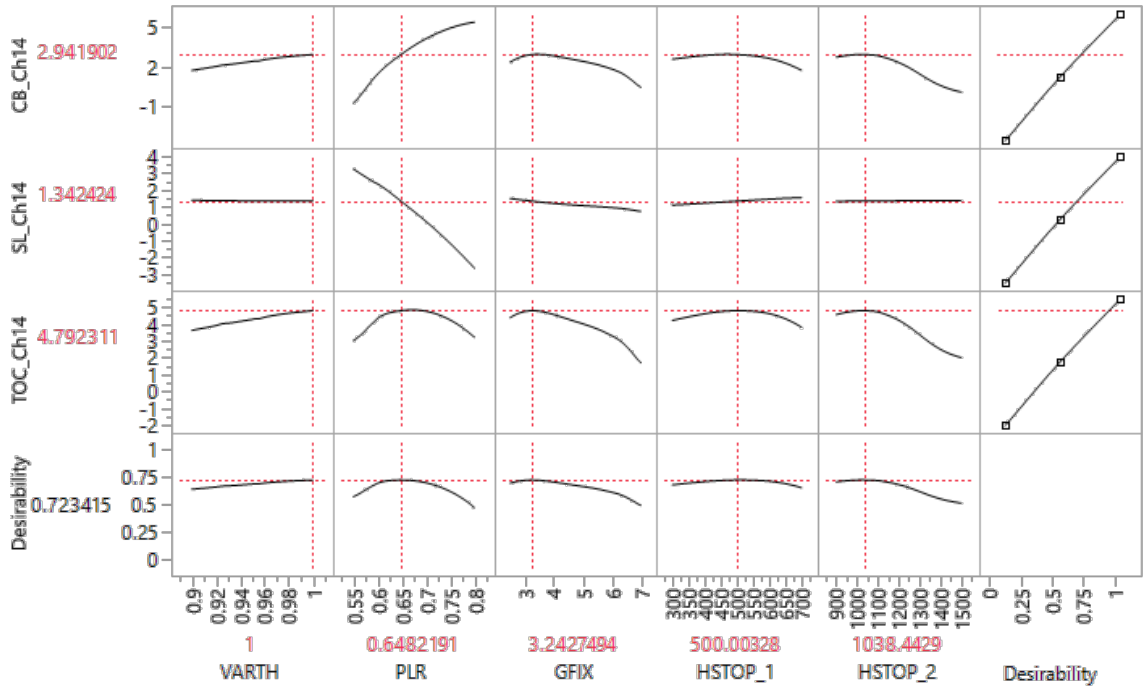

Figure 51. Takeoff noise prediction profiler.

Repeating this process for each aircraft's design Mach number configuration yielded the values shown in Table 37.

Table 37. Takeoff trajectory variable values.

Aircraft	Design Mach	VARTH	PLR	GFIX	HSTOP_1	HSTOP_2
100 PAX	1.6	1.0	0.720	5.51	532.39	1479.58
	1.8	1.0	0.703	5.40	646.48	1371.83
	2.0	1.0	0.717	5.58	416.90	1416.20
55 PAX	1.8	1.0	0.561	6.39	429.58	1536.62
	2.0	1.0	0.613	5.37	405.63	1517.61
	2.2	1.0	0.633	6.21	598.59	1572.54
SSBJ	1.4	1.0	0.739	3.45	512.68	1314.79
	1.6	1.0	0.739	3.45	512.68	1314.79
	1.8	1.0	0.763	2.50	480.00	1150.00

The final variable values from the Noise DoE cases were selected to minimize total noise EPNdB and maximize noise margin. The values selected are shown in Figure 13 under the Mach study section. Figures 52–54 show the contributions of the airframe and each major engine component to the total noise. For each aircraft, for approach airframe noise significantly contributes due to the landing gear, but is negligible for cutback and sideline. Additionally, for cutback and sideline for each aircraft, the jet, exhaust, and core noise are the most dominate noise sources.

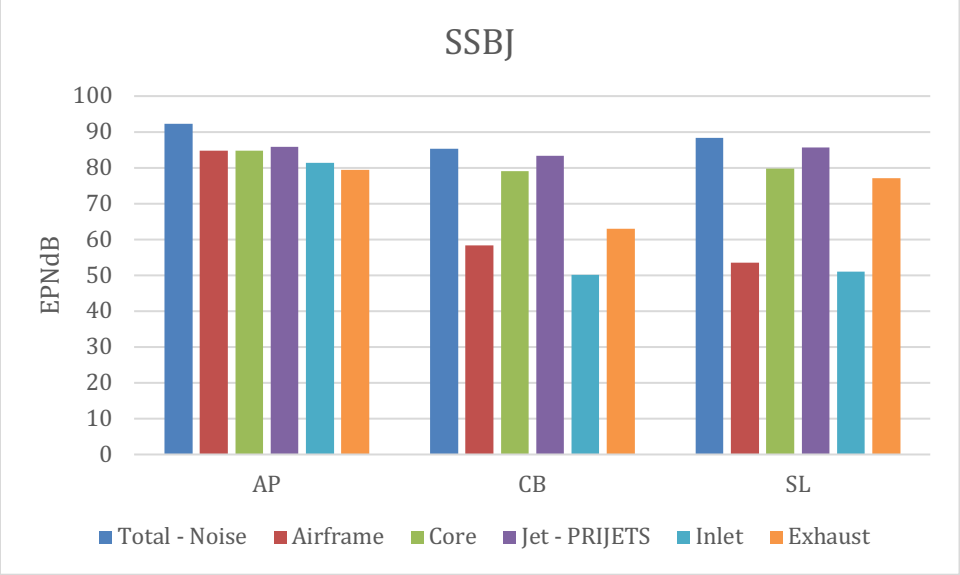

Figure 52. Component noise breakdown for the SSBJ, Mach 1.4.

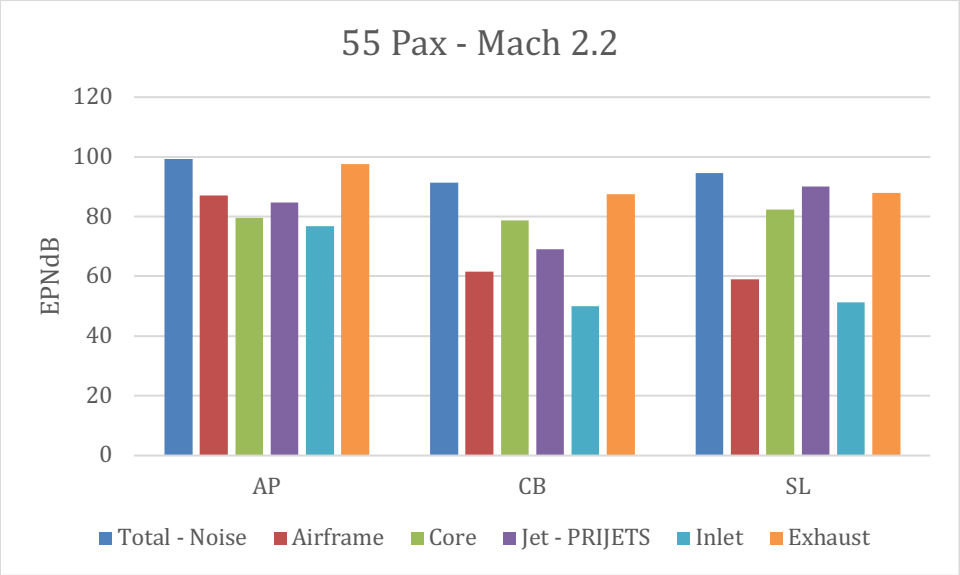

Figure 53. Component noise breakdown for the 55-Pax, Mach 2.2.

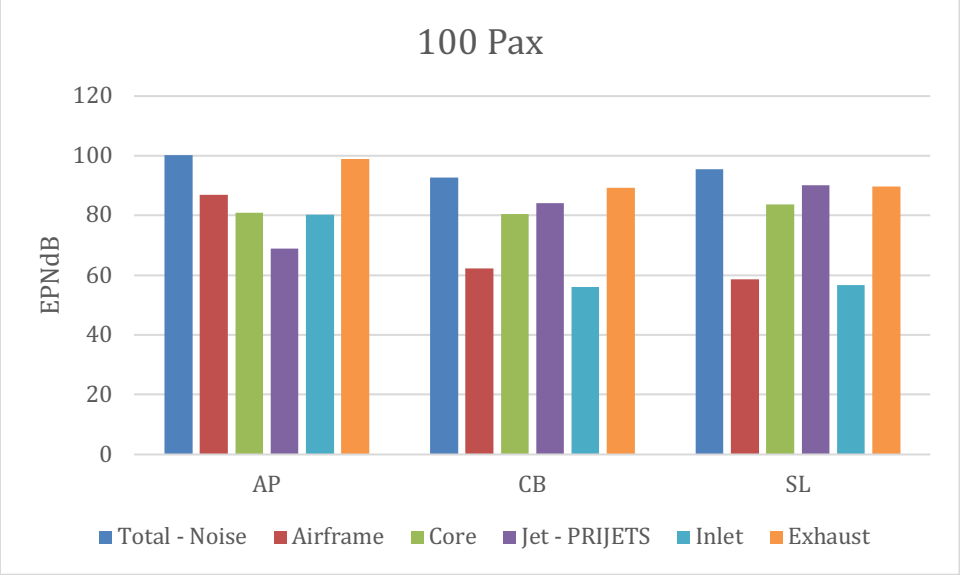

Figure 54. Component noise breakdown for the 100- Pax, Mach 1.8.

Task 5 - SST Modeling in AEDT

Georgia Institute of Technology

Objectives

The primary objective of this task is to develop a method to construct regression models that accurately predict the propulsive performance and aerodynamic characteristics of SST aircraft. In addition, the GT team will validate and provide an implementation plan for the developed approach within AEDT.

Research Approach

Propulsion Regressions

To generate coefficients for net thrust and fuel consumption for each SST concept, the engine deck data are regressed by using a 5th order least-squares linear regression through JMP. In this case, net thrust and fuel flow are both regressed against static pressure ratio, total temperature ratio, Mach number, and power code (δ_s, θ_t, M, and PC, respectively). This process results in two regression equations with 31 coefficients (the unknowns) plus the intercept. For the sake of simplicity and efficient implementation within AEDT, both net thrust and fuel flow have the same regression equation form. An example of the regression equation is shown below.

$$R = a_0 + a_1 * \mathrm{M} + a_2 * \mathrm{M}^2 + a_3 * \mathrm{M}^3 + a_4 * \mathrm{M}^4 + a_5 * \mathrm{M}^5 + a_6 * \mathrm{PC} + a_7 * \mathrm{PC}^2 + a_8 * \mathrm{PC}^3 + a_9 * \mathrm{PC}^4 + a_{10} * PC^5 + a_{11} * \delta_s + a_{12} * \delta_s^2 + a_{13} * \delta_s^3 + a_{14} * \delta_s^4 + a_{15} * \delta_s^5 + a_{16} * \theta_t + a_{17} * \theta_t^2 + a_{18} * \theta_t^3 + a_{19} * \theta_t^4 + a_{20} * \theta_t^5 + a_{21} * \mathrm{M} * \mathrm{PC} + a_{22} * \mathrm{M} * \delta_s + a_{23} * \mathrm{M} * \theta_t + a_{24} * \mathrm{PC} * \delta_s + a_{25} * \mathrm{PC} * \theta_t + a_{26} * \delta_s * \theta_t + a_{27} * \mathrm{M} * \mathrm{PC} * \delta_s + a_{28} * \mathrm{M} * \mathrm{PC} * \theta_t + a_{29} * \mathrm{M} * \delta_s * \theta_t + a_{30} * \mathrm{PC} * \delta_s * \theta_t + a_{31} * \mathrm{M} * \mathrm{PC} * \delta_s * \theta_t$$

Because a good fit cannot be obtained for the whole engine deck data with one regression equation, boxes of different Mach number, altitude, and power code (PC) interval combinations are designated such that the union of the set of boxes encapsulates the design mission and other notional missions for the specific SST concept in question. These boxes were carefully chosen, and the team defined them to minimize the regression errors. The data from the engine deck are then filtered according to these boxes, and the regression exercise explained above is then used for each box, thus resulting in two regression equations, one for net thrust and one for fuel flow, for each designated box. Figure 55 shows the box selection for the 55- Pax Mach 1.8 SST concept, with the box selection for the ascent phase of the design mission in green

and the descent phase in blue. In this case, seven boxes would result in 14 equations. In addition, the box selection is unique for each SST concept, because each concept has a different design mission. A concept with a higher cruise speed and altitude might require more boxes to be defined to obtain good regression results than a concept with lower cruise speed and altitude.

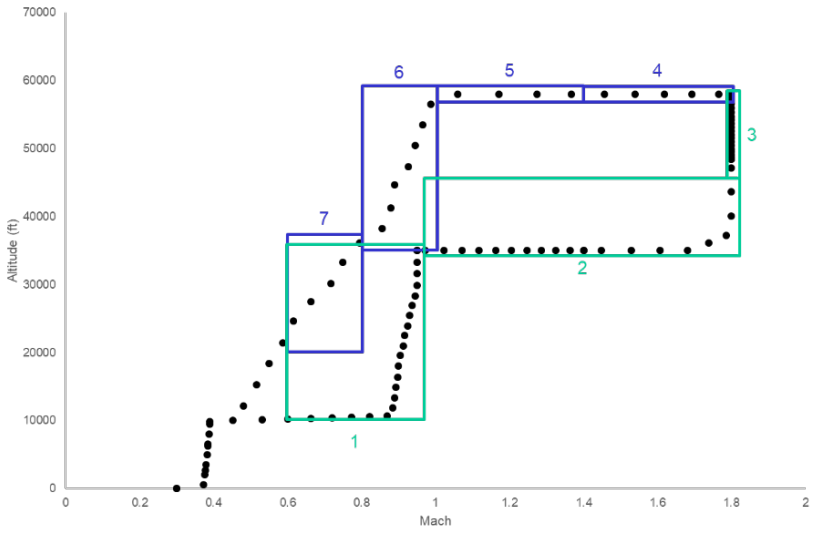

Figure 55. Propulsion box selection for the 55- Pax Mach 1.8 SST concept.

For evaluating the goodness of the fits for each box, the values for predicted value for net thrust and fuel flow that can be obtained with the regression equations and the values for net thrust and fuel flow from the concept engine deck are used to calculate the percentage error. Probability density function distributions are then constructed using JMP to visualize the error for each box individually. A standard deviation of less than 1, a mean equal to 0, and a percentage error values lower than 4% at the 97.5% and 2.5% quantiles are all indicative of a good regression. An example of these percentage error distributions is shown in Figure 56.

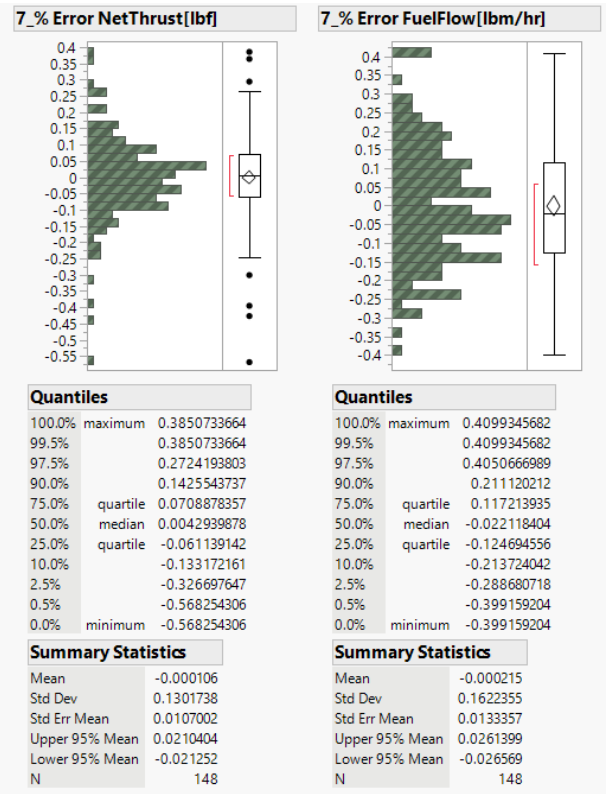

Figure 56. Percentage error distribution example.

After obtaining a promising set of regressions for a particular concept, the next step is to validate them against the concept's design mission and off-design mission data generated using FLOPS. This process is explained in more detail in the validation section below.

Aerodynamic Regressions

To generate coefficients for the regression of the coefficient of drag for each SST concept, the design team provided raw FLOPS data containing cardinal values of Mach number, C_L, altitude, and their corresponding C_D. The adopted strategy first regresses the drag coefficient on those cardinal values by using a stepwise fit before conducting a quadratic interpolation. This strategy was established after a comparison was performed between other strategies including the use of a stepwise fit on continuous variables (errors ranged between −25% and 50%), introduction of a large number of the cardinal values of C_L in the regression by using a stepwise fit coupled with a quadratic interpolation (error ranged between −6.1% and 8.6%). Using the latter strategy with fewer C_L cardinal values and introducing the Mach number as a cardinal value, empowering quadratic interpolation rather than stepwise regression, resulted in significantly better predictions (errors ranged between -1.4% and 1.8%). Hence, the team decided to exploit this strategy for all future aerodynamic regressions, using the latter strategy with fewer C_L cardinal values.

JMP was used to perform the stepwise regression of the drag coefficient on Mach number, altitude, and C_L number. Because the behavior of the drag coefficient is quite different between subsonic, transonic, and supersonic phases, we defined three boxes, one for each speed regime. The set of cardinal values was always chosen to encompass the design mission to avoid extrapolation. Figure 57 shows an example of a supersonic regime equation obtained with the stepwise fit analysis. Figure 58 allows for a graphical understanding of how the cardinal values were exploited to perform the regression.

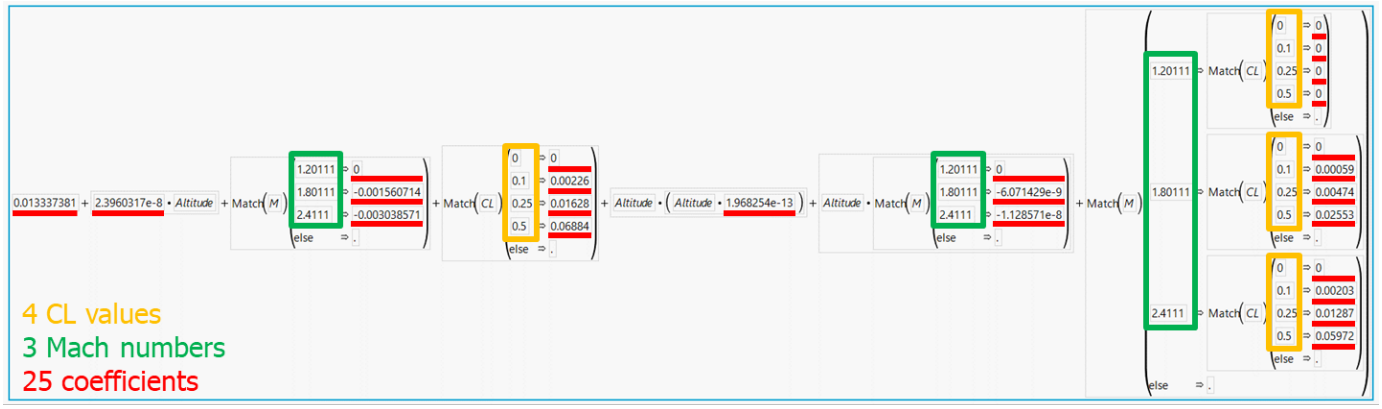

Figure 57. Form of the equation yielded by the stepwise fit on the cardinal values of Mach number (green) and C_L (yellow) and a continuous altitude.

	Altitude	Mach	CL	CD	Pred Formula CD - Subsonic	Pred Formula CD - Transonic	Pred Formula CD - Supersonic
1	0	0.3	0	0.00877	•	•	•
2	0	0.4	0	0.00813	•	•	•
3	0	0.5	0	0.00765	•	•	•
4	0	0.6	0	0.00748	0.007486633	•	•
5	0	0.7	0	0.00739	0.0073944108	•	•
6	0	0.8	0	0.00743	•	•	•
7	0	0.88	0	0.00771	0.0077230774	0.0077705694	•
8	0	1.05	0	0.01669	•	0.0167487013	•
9	0	1.2	0	0.01422	•	0.014294965	0.014
10	0	1.4	0	0.01271	•	•	•
11	0	1.6	0	0.01191	•	•	0.0117775
12	0	1.8	0	0.01085	•	•	•
13	0	2	0	0.01023	•	•	0.0101275
14	0	2.2	0	0.00982	•	•	•
15	0	0.3	0.05	0.00916	•	•	•
16	0	0.4	0.05	0.00853	•	•	•
17	0	0.5	0.05	0.00806	•	•	•
18	0	0.6	0.05	0.00792	•	•	•
19	0	0.7	0.05	0.00786	•	•	•

Figure 58. Example of the regression performed on cardinal values of Mach number, C_L, and altitude in JMP for the different regimes.

The design mission against which the regressions were validated did not have specific cardinal values; the Mach number, altitude, and C_L number were continuous. To enable good predictive capability for any input combination between the original cardinal values of the inputs, we developed a custom-made script to perform quadratic interpolation. The quadratic interpolation form is shown in Figure 59.

$$C_D = a_1 + a_2 h + a_3 h^2 + b_1 + b_2 h + c_1 + d_1$$

$$b_1 = \begin{cases} b_{1,1}, & if M = M_1 \\ b_{1,2}, & if M = M_2 \\ b_{1,3}, & if M = M_3 \end{cases} \quad b_2 = \begin{cases} b_{2,1}, & if M = M_1 \\ b_{2,2}, & if M = M_2 \\ b_{2,3}, & if M = M_3 \end{cases}$$

$$c_1 = \begin{cases} c_{1,1}, & if C_L = C_{L,1} \\ c_{1,2}, & if C_L = C_{L,2} \\ c_{1,3}, & if C_L = C_{L,3} \\ c_{1,4}, & if C_L = C_{L,4} \end{cases} \quad d_1 = \begin{cases} d_{1,1,1}, & if M = M_1 \text{ and } C_L = C_{L,1} \\ d_{1,2,1}, & if M = M_2 \text{ and } C_L = C_{L,1} \\ \vdots & \\ d_{1,3,4}, & if M = M_3 \text{ and } C_L = C_{L,4} \end{cases}$$

Figure 59. Form of the quadratic interpolation.

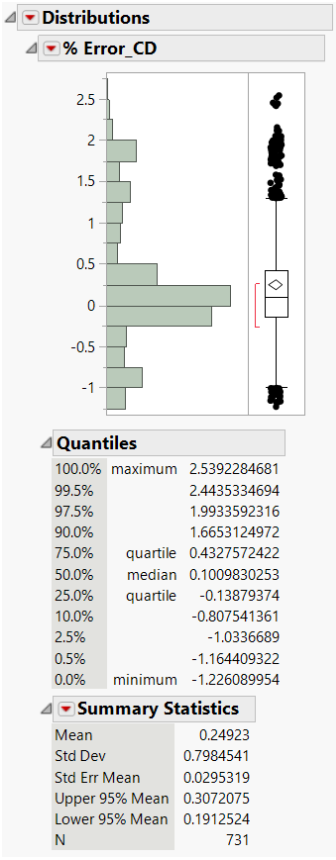

Figure 60. Total C_D error distribution example.

Figure 60 shows an example of total C_D error distribution after the quadratic interpolation. After the fit is satisfactory, the Mach-Alt combinations in the design mission are considered as the validation points.

Validation

The validation exercise consisted of using the propulsion and aerodynamic regressions to obtain values for thrust, fuel flow, and drag coefficient for the SST concept's design mission and off-design mission data generated through FLOPS, and comparing the predicted values to the actual values from those data by calculating the percentage error and constructing error distributions to visualize the results. To perform this exercise in a quick and efficient manner, a Python script was

created that takes the propulsion and aerodynamic regression equations, as well as the data from the FLOPS mission as inputs and calculates the percentage error between the predicted regression outputs and the actual FLOPS outputs for the net thrust, fuel flow, and drag coefficient. A flow chart indicating how the validation process works and how the Python script was developed is shown in Figure 61.

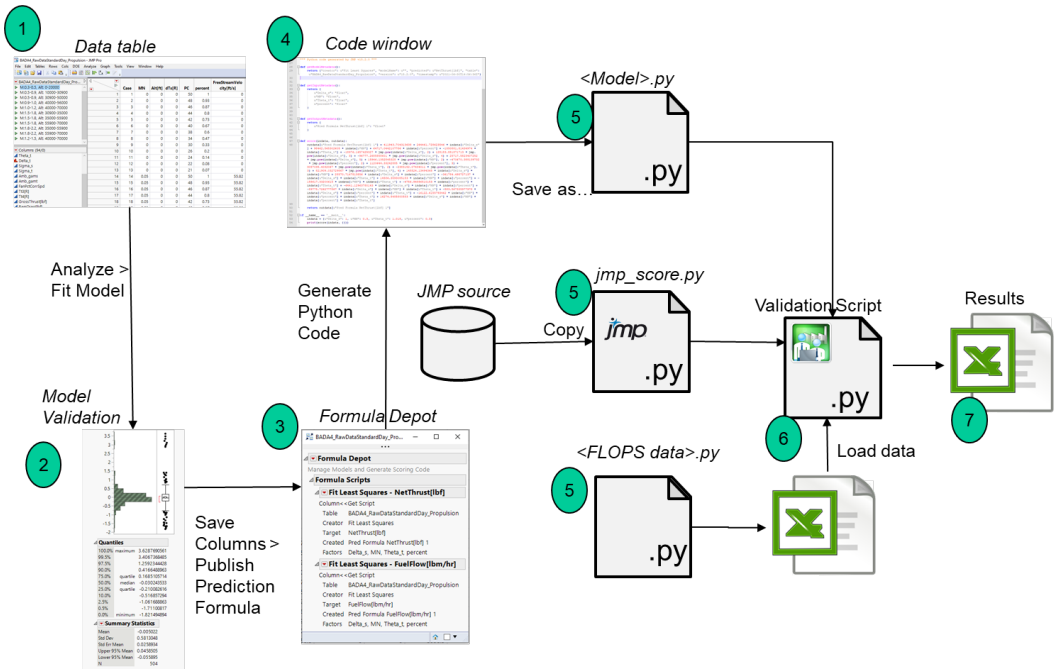

Figure 61. Validation process flow chart.

In addition to serving as a validation tool, the developed mission simulator also serves as a testbed to mimic the eventual implementation of the developed approach within AEDT. It has proven valuable in enabling discussions related to the eventual implementation within AEDT.

Because the FLOPS mission data do not contain values for static pressure ratio and total temperature ratio, atmospheric models must be incorporated into the code to calculate these values as functions of the altitude and Mach number. Various models were used for the troposphere (altitude < 36,089 ft) and stratosphere (altitude > 36,089 ft) portions of the mission data to account for the differences in how the static pressure ratio and total temperature ratio behave between the two regimes. The box selection used for the propulsion and aerodynamic regressions is also incorporated into the script, and the script automatically uses the corresponding regression equation for the segments of the mission data that fall into the designated boxes.

Results

The design mission validation results are presented below for the various SST concepts performed to date. For each, the box selection for the propulsion and aerodynamic regressions is shown, followed by the error distribution results from the validation exercise for each box. For the descent phases, residuals were calculated instead of percentage errors for net thrust, because FLOPS defaults the net thrust to 0 during descent, and therefore the percentage error cannot be calculated.

55- Pax Mach 1.8 SST

The propulsion and aerodynamic box selection of the 55- Pax Mach 1.8 aircraft are depicted in Figure 62. Boxes 1-3 correspond to the ascent phase of the flight, and boxes 4-7 correspond to the descent phase of the flight. Ideally, different boxes would be used as soon as an important change in the behavior occurs, so that the boxes would correspond to a single climb or a single cruise and for a single regime (subsonic, transonic, and supersonic); however, that practice would lead to an enormous number of boxes and some predictive ability would be lost when performing the off-design missions.

Tables 38–41 display the results of the validation mission regarding the propulsion (net thrust and fuel flow) and the aerodynamic (drag coefficient) analysis.

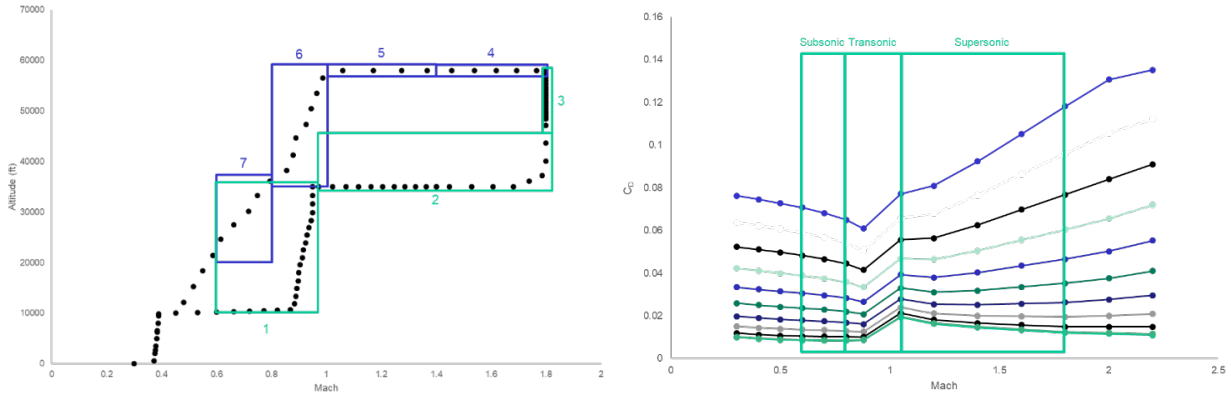

Figure 62. Box selection for the 55- Pax Mach 1.8 SST concept.

Table 38. Ascent net thrust design mission validation results for the 55- Pax Mach 1.8 SST concept.

Box	Minimum % Error	Maximum % Error	Mean	Std. Dev.
1	−0.2720	7.238	1.668	2.337
2	−6.012	1.444	−0.4509	2.181
3	−14.87	−5.453	−10.14	2.091

Table 39. Descent net thrust design mission validation results for the 55- Pax Mach 1.8 SST concept.

Box	Minimum Residual (lbf)	Maximum Residual (lbf)	Mean	Std. Dev.
4	1005	1043	-	-
5	645.6	958.0	-	-
6	649.7	1415	-	-
7	1521	2104	-	-

Table 40. Fuel flow design mission validation results for the 55- Pax Mach 1.8 SST concept.

Box	Minimum % Error	Maximum % Error	Mean	Std. Dev.
1	−0.8251	8.247	1.855	2.700
2	−4.196	1.617	−0.1447	1.585
3	−7.586	−3.662	−6.138	0.8677
4	1.295	5.914	3.788	2.031
5	−44.49	22.72	−2.264	29.88
6	−13.97	13.82	4.280	11.29
7	14.76	21.56	19.05	3.015

Table 41. Drag coefficient design mission validation results for the 55- Pax Mach 1.8 SST concept.

Box	Minimum % Error	Maximum % Error	Mean	Std. Dev.
Subsonic	−0.2149	0.09529	−0.06381	0.09991
Transonic	−3.083	0.3130	−0.1688	0.8298
Supersonic	−3.817	3.610	0.01050	1.509

55- Pax Mach 2.0 SST

As with the previous concept, box selection is depicted in Figure 63, and the propulsion and aerodynamic results are shown in Tables 42–45. A different strategy was implemented in this box selection. Four boxes were chosen for the ascent phase, and three boxes were chosen for the descent phase.

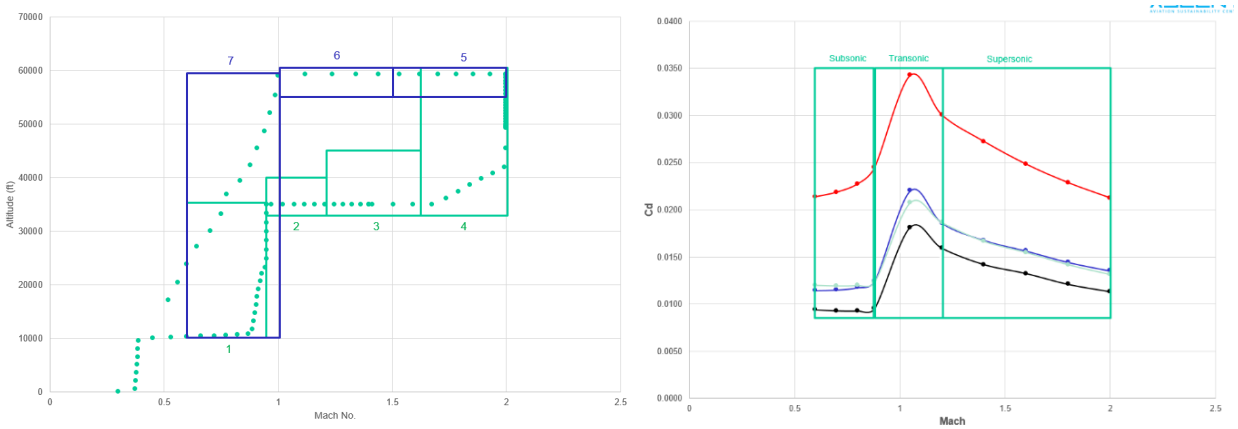

Figure 63. Box selection for the 55- Pax Mach 2.0 SST concept.

Table 42. Ascent net thrust design mission validation results for the 55 Pax Mach 2.0 SST concept.

Box	Minimum % Error	Maximum % Error	Mean	Std. Dev.
1	−0.6312	7.4679	2.1939	2.302
2	−0.6447	0.8229	0.0775	0.1855
3	−1.3195	0.5997	−0.2022	0.5306
4	−14.396	−0.0836	−8.26	4.8826

Table 43. Descent net thrust design mission validation results for the 55- Pax Mach 2.0 SST concept.

Box	Minimum Residual (lbf)	Maximum Residual (lbf)	Mean	Std. Dev.
5	1264.985	1357.4	-	-
6	378.317	1122.76	-	-
7	829.867	2626.8	-	-

Table 44. Fuel flow design mission validation results for the 55- Pax Mach 2.0 SST concept.

Box	Minimum % Error	Maximum % Error	Mean	Std. Dev.
1	−0.6	8.228	2.3948	2.6487
2	−0.5468	0.0735	−0.1963	0.2386
3	−0.2555	0.1888	−0.08954	0.1499
4	−6.7475	−0.07597	−4.2064	2.6087
5	1.146	7.995	4.6834	2.8265
6	−100	0.4387	−37.28	43
7	−11.53	22.80	11.05	11.015

Table 45. Drag coefficient design mission validation results for the 55- Pax Mach 2.0 SST concept.

Box	Minimum % Error	Maximum % Error	Mean	Std. Dev.
Subsonic	−0.5295	0.26315	−0.22175	0.2723
Transonic	−0.053	17.08	9.828	5.1841
Supersonic	−0.8344	2.46127	0.178	0.9405

The propulsion validation exercise for the different SST concepts revealed a clear distinction between the regression equation predictions for net thrust and fuel flow using the data from the engine deck and FLOPS calculations for these values in the design missions. This behavior was observed even though the goodness-of-fit exercise showed no significant error. To investigate this further, data from the engine deck was regressed and validated against themselves to ensure that the Python script was not the source of the error. This exercise yielded near-zero errors for net thrust and fuel flow. The cause of the small discrepancies was in the atmospheric models used by the script to obtain the static pressure ratio and total temperature ratio, which do not exactly match the values of these parameters in the engine deck.

The next step in investigating this issue was to take a point from the FLOPS design mission (Mach, altitude, and PC) and find two very similar points from the engine deck and check what the regressions equation predictions both cases. The results of this exercise are shown in Table 46. The results showed no significant error for the engine deck data points while showing a significant error for the FLOPS data point, although the data were similar. This result suggests that the method used by FLOPS to obtain values of net thrust and fuel flow for a given set of inputs does not match the data from the engine deck. For instance, the engine deck has no values of net thrust for any point close to zero, whereas FLOPS yields values of zero net thrust for any point in the mission categorized as part of the descent phase by default. Any differences in the behavior of the data, as in this example, are bound to cause some errors when the sets of data are validated against each other. This issue is currently being investigated further.

Table 46. FLOPS and engine deck propulsion data comparison.

Parameter	FLOPS Mission	Engine Deck 1			Engine Deck 2		
		Value	Predicted	% Error	Value	Predicted	% Error
MN	1.2734	1.25	1.25	-	1.3	1.3	-
Altitude (ft)	57981	58000	58000	-	58000	58000	-
PC	21	21	21	-	21	21	-
Net Thrust (lbf)	0	200.7	200.69	0.004983	216.2	216.3	-0.04163
Fuel Flow (lbm/hr)	2197	975.7	983.14	-0.7625	587.9	582.4	0.9304

The results for the aerodynamic regressions are promising overall and show no significant errors for most of the concepts. However, for a specific concept (55 Pax Mach 2.0 SST), the team is observing unexpected errors in the transonic phase, not in the entirety of the box/speed regime, but exclusively in between the cardinal number of Mach 0.88 and 1.05. The team is currently investigating the root cause of this issue.

Table 47. Aero data comparison 1.

Parameters	Validation Mission	Data Used for the First Interpolation			Data Used for the First Interpolation		
		Value	Predicted	% Error	Value	Predicted	% Error
MN	0.9453	0.88	0.88	-	1.05	1.05	-
Altitude (ft)	22,226	20,000	20,000	-	20,000	20,000	-
C_L	0.18679	0.19	0.19	-	0.1769	0.1769	-
C_D	0.01855	0.0166	0.01661	0.06	0.0252	0.025193	0.088

Table 48. Aero data comparison 2.

Parameters	Validation Mission	Data Used for the First Interpolation			Data Used for the First Interpolation		
		Value	Predicted	% Error	Value	Predicted	% Error
MN	0.9453	0.88	0.88	-	1.05	1.05	-
Altitude (ft)	22,226	25,000	25,000	-	25,000	25,000	-
C_L	0.18679	0.19	0.19	-	0.1769	0.1769	-
C_D	0.01855	0.0167	0.01671	0.04	0.0253	0.025321	0.066

Tables 47 and 48 above display the closest points found in the data table that were used to perform the initial regression. Their respective errors are all below 1% when the error for the validation mission point is at 17%.

Task 6 - GT Coordination

Georgia Institute of Technology and Purdue University

Objective

The main aim of this coordination task for Georgia Tech is to document interactions with other ASCENT projects as well as other stakeholders such as CAEP Working Groups, original equipment manufacturers (OEMs), and NASA. The research approach highlights only two interactions during the period of performance. The interactions with CAEP Working Groups are documented in the Results section of Task 4.

Research Approach (Georgia Tech)

The Georgia Tech modeling team has provided ASCENT Project 47 MIT researchers with results for the medium SST. During the period of performance, the Georgia Tech modeling team compiled the following information for the GT medium v11.4 closed vehicle and the v11.5 closed vehicle:

- General aircraft properties
  - Number of engines
  - Wing area
  - Wing inclination angle with the horizontal
  - Thrust inclination angle with the horizontal
  - Maximum takeoff weight (MTOW)
- Overall mission analysis
  - Design mission design
  - Total fuel wing capacity
  - Drag polar for clean configuration
  - Detailed mission segment performance
- Airframe constraint on engine size
- Takeoff and landing trajectories
  - Low speed (M < 0.35) aerodynamic properties of the full aircraft
- Noise footprint analysis
  - Airframe flap area
  - Horizontal tail area
  - Vertical tail area
  - Wing area
  - Flap span
  - Horizontal tail span
  - Vertical tail span
  - Wing span
  - Tire diameter of main landing gear
  - Tire diameter of nose landing gear

- Main landing gear strut length
- Nose landing gear strut length
- Number of wheels in main landing gear
- Number of wheels in nose landing gear
- Number of main landing gear
- Number of nose landing gear
- Number of slots for trailing edge flaps
- Flap setting (degrees deflected)
- Coordinates of the wing planform relative to the engine (i.e., top view of the aircraft)

Results (Georgia Tech)

VNRS Takeoff Trajectory

To examine the effects of takeoff trajectories on emission under 3,000 ft. The first step was to generate the relevant takeoff trajectories adhering to regulations. This was performed for both Georgia Tech's 55- passenger, Mach 2.2 SST (GT_MediumSST), and 8 passenger, Mach 1.4 representative supersonic business jet (GT_SSBJ). Four trajectories were established for comparison: 1) No cutback, 2) standard cutback, 3) advanced procedure and 4) a variable noise reduction systems (VNRS). The no cutback trajectory was a maximum thrust takeoff included as the antithesis to the "VNRS Min Noise" trajectory. After the obstacle, the aircraft holds a flight path angle (γ_{obs}) and accelerates to 250 kts (V_{trans}). It then transitions to holding 250 kts, increasing the flight path angle for the rest of the climb. The standard trajectory augmented the no cutback trajectory with a standard pilot-initiated cutback at some altitude (h_{cb}), which was optimized to minimize the combined takeoff certification noise levels at the lateral and flyover observers. The thrust setting for the cutback was determined in accordance with Title 14 CFR Part 36: Noise Standards: Aircraft Type and Airworthiness Certification. The advanced trajectory augmented the standard procedure with a programmed lapse rate (PLR) which is a FADEC initiated thrust reduction after gear retraction and is completed by 150 ft AG. PLR can be overridden by the pilot in emergencies, thus allowing for trading lower engine noise for a shallower/longer initial climb. A PLR with 90% thrust setting was used to match the assumptions of NASA. The advanced trajectory optimized the initial flight path angle, transition speed, and cutback height for the minimum combined takeoff certification noise levels at the lateral and flyover observers. The VNRS Min Noise trajectory used both PLR and PHLD controlled by the flight management system (FMS). For this trajectory, the amount of PLR, the initial flight path angle, the transition speed, and the cutback height were optimized for minimum cumulative noise. All trajectories were constrained (climb gradients, maximum airspeeds, etc.) to ensure compliance with all airworthiness requirements laid out in Title 14 CFR Part 25: Airworthiness Standards: Transport Category Airplanes. The engine deck used to assess the trajectories was for an $\mathrm{ISA} + 18\,°F$, a noise analysis standard condition. The trajectory parameters for GT_MediumSST-GT and GT_SSBJ are shown in Tables 49 and 50, respectively. A comparison of the flight path and thrust settings is shown in Figure 64 for the GT_MediumSST-GT and Figure 65 for the GT_SSBJ. The GT_MediumSST-GT VNRS trajectory had an increased climb time of 1.4 min relative to the standard trajectory. The GT_SSBJ VNRS trajectory had an increased climb time of 0.33 min relative to the standard trajectory.

Table 49. GT_MediumSST trajectory comparison.

Name	TS_{TO}	PLR					Cutback		PHLD	Time from 35 to 3,000 ft [s]	Average Thrust [%]
		h_{PLR} [ft]	TS_{PLR} [%]	γ_{obs}	V_{trans} [kts]	h_{trans} [ft]	h_{cb} [ft]	TS_{cb} [%]			
No Cutback	100%	–	–	12.75°	250	1999	–	–	No	31	100
Standard		–	–	9.6°	235.5	457	2290	39.2	No	44	76.2
Advanced		35	90	8.4°	235	500	2127	38.9	No	64	61.3
VNRS Min Noise		35	63	6.21°	232	583	1573	38.8	Yes	128	45.2

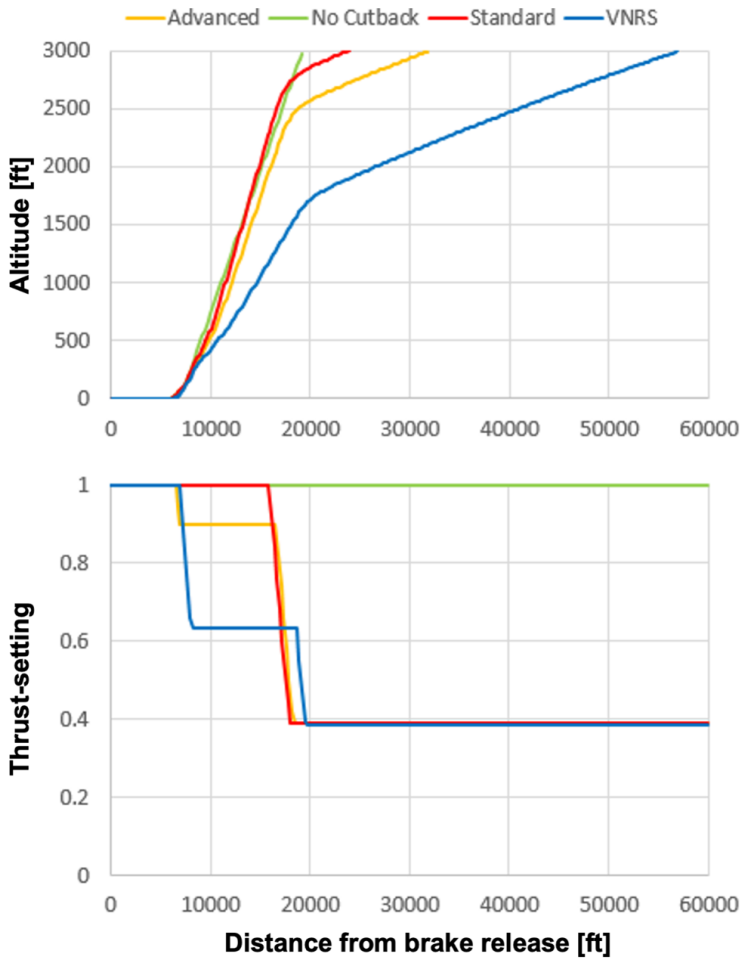

Figure 64. Altitude (top) and thrust setting (bottom) vs. distance from brake release for GT_MediumSST-GT trajectories.

Table 50. GT_SSBJ trajectory comparison.

Name	TS_{TO}	PLR					Cutback		PHLD	Time from 35 to 3,000 ft [s]	Average Thrust [%]
		h_{PLR} [ft]	TS_{PLR} [%]	γ_{obs}	V_{trans} [kts]	h_{trans} [ft]	h_{cb} [ft]	TS_{cb} [%]			
No Cutback	100%	-	-	3.5°	250	433	-	-	No	43.1	100
Standard		-	-	3.1°	250	374	1573	52.6	No	84.9	69.8
Advanced		35	90	2.9°	232	313	1522	53.9	No	82.5	67.8
VNRS Min Noise		35	78.4	3.3°	232	563	1143	53.8	Yes	105	62.2

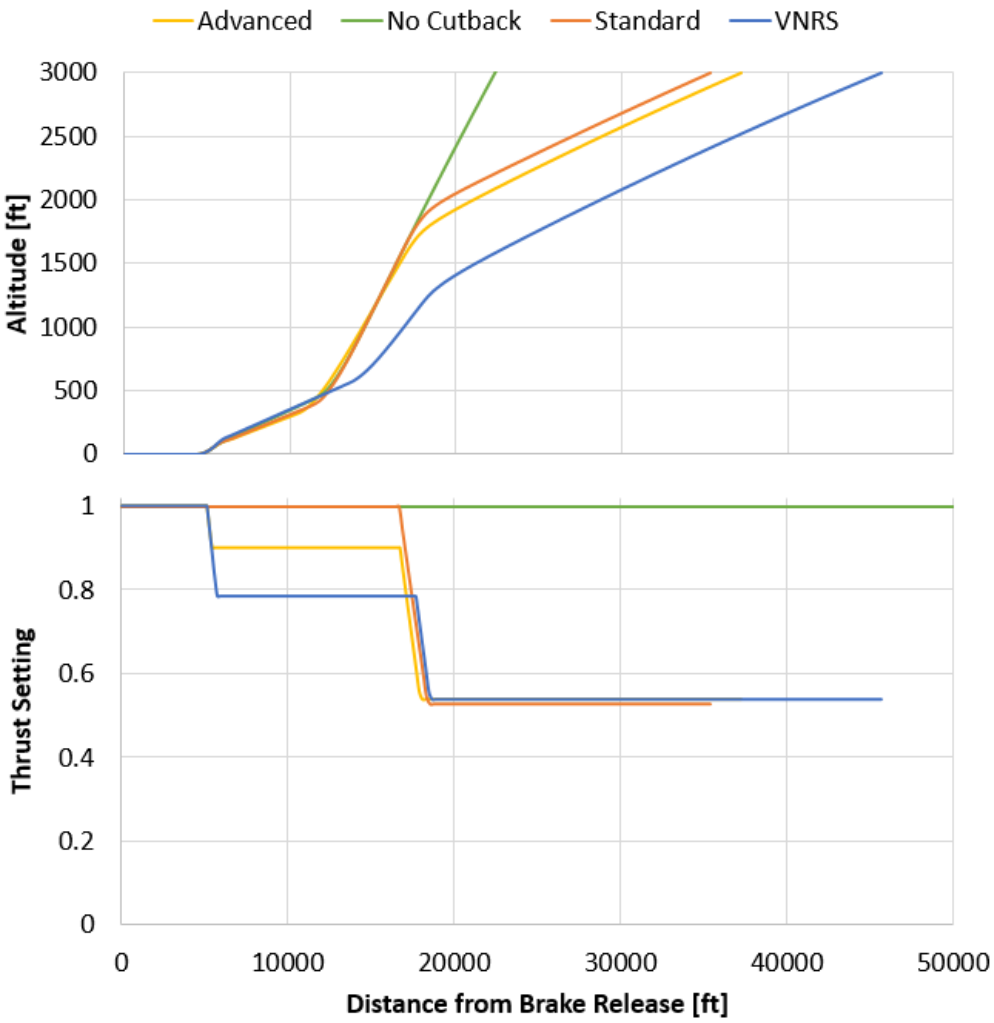

Figure 65. Altitude (top) and thrust setting (bottom) vs. distance from brake release for GT_SSBJ trajectories.

Emission Calculations

After the trajectories were determined, the cumulative NO_x as a function of time between 35 ft and 3,000 ft (i.e., climb out) was determined by integration over the discretized flight profile. The values for fuel flow and EI came from the engine deck. The GT_MediumSST-GT and GT_SSBJ assumed an RQL combustor technology based on the GE correlation, Equation 1, for EI_{NOx} from Niedzwiecki [**Error! Bookmark not defined.**]. The resultant cumulative NO_x for each trajectory of the GT_MediumSST-GT and GT_SSBJ is shown in Table 51.

$$\mathrm{EI_{NOx}} = 23.8 \left(\frac{P_3}{432.7\ \mathrm{psia}}\right)^{0.4} \exp\left(\frac{T_3 - 1027.6°\mathrm{F}}{349.9°\mathrm{F}} + \frac{6.29 - H_0}{53.2}\right) \quad \text{Equation 1}$$

where

P_3 is combustor entrance total pressure

T_3 is combustor entrance total temperature

H_0 is percentage humidity

Table 51. Cumulative NO_x[g] from 35 to 3,000 ft.

Trajectory	GT_MediumSST_GT			GT_SSBJ		
	NO_x [g]	Time from 35 to 3,000 ft [s]	Average Thrust [%]	NO_x [g]	Time from 35 to 3,000 ft [s]	Average Thrust [%]
No Cutback	1279	31	100	558	43.1	100
Standard	1182	44	76.2	626	84.9	69.8
Advanced	1122	64	61.3	572	82.5	67.8
VNRS Min Noise	1159	128	45.2	583	105	62.2
Subsonic Certification Rule	2568	132	85	1612	132	85
Supersonic Certification Rule	1202	120	65	752	120	65

Variability in Pt3, Tt3, FAR and EINO$_x$

As Pt_3, Tt_3, and fuel flow all affect EI and absolute NO_x production, these values are plotted as a function of the percentage maximum available thrust, Mach, and altitude for the VNRS trajectory. Additionally, an upper bound (Mach = 0.5, altitude = 0 ft) and a lower bound (Mach = 0, altitude = 2,500 ft) are included for reference to illustrate the ranges explored in CAEP12_WG3-5_ESTG_WP04 presented by [16]. All values are relative to the ICAO emissions 85% F00 climb point. The GT_MediumSST-GT is plotted in Figure 66, and the GT_SSBJ is plotted in Figure 67.

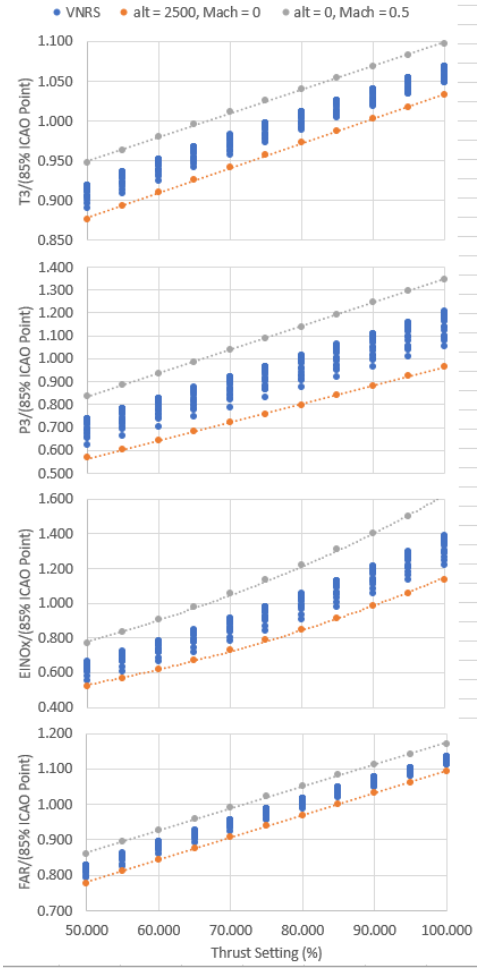

Figure 66. Variability in T_3, P_3, $\mathbf{EINO_x}$, and $\mathbf{FAR}$ with thrust setting for GT_MediumSST-GT.

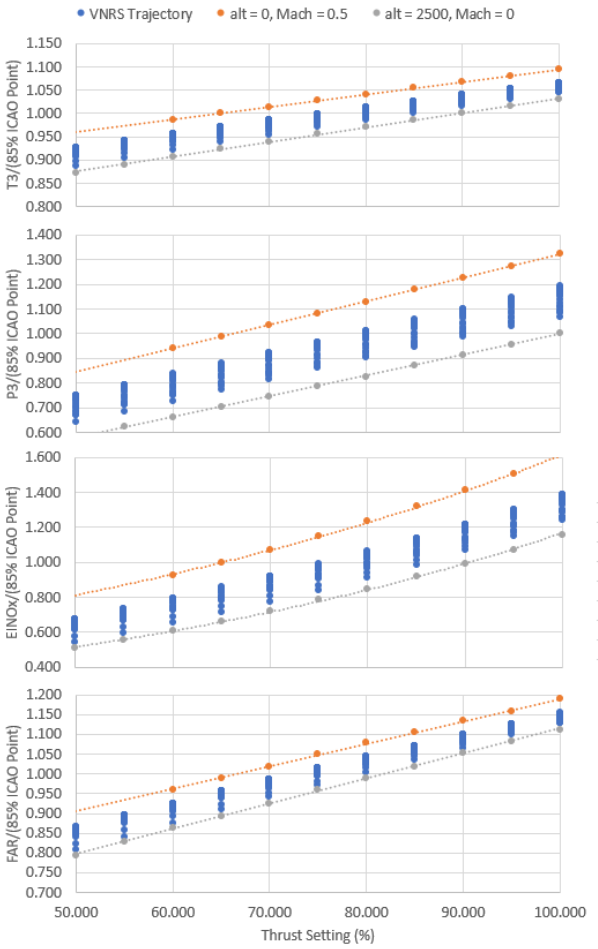

Figure 67. Variability in T_3, P_3, $\mathbf{EINO_x}$, **and FAR** with thrust setting for GT_Medium_SST-GT.

Task 6 - Purdue Coordination

Objectives

This objective comprised coordinating with entities involved in CAEP MDG/FESG, particularly the SST demand task group. In addition, this objective included maintaining the ability to incorporate SST vehicle models designed by our Georgia Tech colleagues and/or SST models developed by others.

Research Approach

For the period of performance covered in this report, the Purdue team was not asked to participate directly in many coordination activities. We did provide updates when requested by our FAA technical monitors, who were active in the CAEP efforts. We have also maintained an approach in FLEET that will allow, with low effort, representation of the performance of aircraft other than the notional lA10 medium SST. To date, the Purdue team has considered only the notional A10 medium SST, but we are prepared to incorporate other aircraft models.

Publications

Jain, S., Mane, M., Crossley, W. A., & DeLaurentis, D. A. Investigating How Commercial Supersonic Aircraft Operations Might Impact Subsonic Operations and Total CO_2 Emissions, AIAA 2021-3014. AIAA Aviation 2021 Forum. August 2021

Mane M., Jain, S., Crossley, W. A. Estimating Market Size for Supersonic Passenger Transport Aircraft, AIAA 2021-2442. AIAA Aviation 2021 Forum. August 2021.

Submitted conference proceedings

Fung, T., Yang, B., Jain, S., Chao, H., Mane, M., Crossley, W. A., & DeLaurentis, D. Fleet-Level Impacts of Different Commercial Supersonic Aircraft Configurations Considering A World-Wide Route Network. Abstract submitted to AIAA Aviation Forum for presentation in June 2022

Yang, B., Fung, T., Jain, S., Chao, H., Mane, M., Crossley, W. A., & DeLaurentis, D. A. Estimating Future Fleet-Level CO2 Emissions Considering a World-Wide Network. Abstract submitted to AIAA Aviation Forum for presentation in June 2022

Outreach Efforts

Multiple interactions with government, industry, and academia have occurred during the course of the project.

ASCENT 10: Aircraft Technology Modeling and Assessment, oral presentation to ASCENT Fall Advisory Committee Meeting, GT, Virtual, September 2020.
ASCENT 10: Aircraft Technology Modeling and Assessment, poster presentation to ASCENT Spring Advisory Committee Meeting, GT, Virtual, April 2021.

Awards

None

Student Involvement

The Georgia Tech student team consists of 11 graduate research assistants (GRA). During the period of performance, the GRA team was organized by vehicle class, i.e., SSBJ, medium SST, and large SST. However, the student members of the team each also supported the disciplinary analysis that best matched their research interests. The disciplinary areas included geometry, aerodynamics, propulsion, weights, noise, mission analysis, and fleet assessment. GRA leads were identified for each topic. Ms. Barbara Sampaio and Mr. Brennan Stewart are the student leads for aerodynamics; Mr. Edan Baltman is the student lead for propulsion; Mr. Brennan Stewart is the student lead for geometry; Mr. Joao De Azevedo is the student lead for noise; Mr. Colby Weit is the student lead for mission analysis; and Mr. Jiajie (Terry) Wen is the student lead for demand and fleet assessment.

The Purdue team included four graduate students over the 1-year period, all of whom have been conducting tasks in support of the effort. Samarth Jain, a continuing PhD student at Purdue, worked on the effort for the entire period. Hsun Chao, a PhD student, moved primarily to another research project but still supports the ASCENT 10 effort in an advisory capability. Suzanne Swaine, a PhD student, participated in the Purdue team through most of this reporting period. In addition, the Purdue team added Boning “Willis” Yang and Tien-Yueh “Edward” Fung, both MS students in Aeronautics and Astronautics, to the team during this reporting period.

Plans for Next Period

Georgia Tech

The plans for the next period include two focus areas: AEDT supersonic modeling implementation and supersonic fuel burn and LTO noise interdependencies. The AEDT supersonic modeling includes working with supersonic airframers and engine OEMs to generate aerodynamics and propulsion regression coefficients to be tested in AEDT. The Georgia Tech modeling team will continue to improve on the SST designs to capture both fuel burn and LTO noise and examine the interdependencies between these two metrics. The modeling team will also be working with both supersonic airframers and engine OEMs to verify assumptions and review results. Other SST classes, i.e., 25 and 75 passenger aircraft, will also be investigated.

Purdue

The Purdue team successfully demonstrated FLEET’s capabilities for modeling and analyzing the introduction of commercial supersonic aircraft to an existing all-subsonic airline fleet model. This demonstration has shown that FLEET is capable of predicting the changes in subsonic aircraft operations on routes where supersonic aircraft also operate (to compensate for the shifting of subsonic business class and above passengers to supersonic aircraft – based on supersonic demand), along with predicting the number of round trips and the number of passengers carried on such routes. The Purdue team also predicted the changes in future supersonic demand and its impacts on supersonic and subsonic operations, depending on various COVID-19-related projected demand scenarios. Additionally, the team successfully developed a “simultaneous”

allocation approach wherein the supersonic and subsonic aircraft are allocated together on the basis of supersonic and subsonic passenger demand. The Purdue team is in the process of updating its route network from a U.S.-touching-only network to a worldwide network.

Future work will include completing FLEET's airline network update to a global network (moving away completely from the U.S. flag carrier airlines only route network currently implemented in FLEET). The team will also assess the fleet-level advantage of having different types and sizes of supersonic aircraft, defined by certain operational specifications (e.g., Mach cutoff over land) and passenger capacity (e.g., 100-seat supersonic aircraft), available to the FLEET global airline. Future work will also include developing a FLEET-like tool for SSBJ operations.

References

Airline Origin and Destination Survey – DB1B [online database], U.S. Dept. of Transportation, Bureau of Transportation Statistics.

Boeing Market Outlook, "Boeing Current Market Outlook 2012-2031", 2012, Retrieved October, 2021. URL http://libraryonline.erau.edu/online-full-text/books-online/Boeing_Current_Market_Outlook_2012.pdf.[19]

IATA Economic Reports, "Air Passenger Market Analysis", December 2020, Retrieved June, 2021. URL https://www.iata.org/en/iata-repository/publications/economic-reports/air-passenger-monthly-analysis---december-2020/.

IATA Press Release, "2020 Worst Year in History for Air Travel Demand", February 2021, Retrieved June, 2021. URL.

IATA Press Release No: 33, "Optimism When Borders Reopen", May 2021, Retrieved June, 2021. URL https://www.iata.org/en/pressroom/pr/2021-05-26-01/.

ICAO, "Effects of Novel Coronavirus (COVID-19) on Civil Aviation: Economic Impact Analysis,", June 2021, Retrieved June, 2021. URL https://www.icao.int/sustainability/Documents/COVID-19/ICAO_Coronavirus_Econ_Impact.pdf.

Mavris, D., DeLaurentis, D., Crossley, W., and Alonso, J. J. (2017), "Project 10 Aircraft Technology Modeling and Assessment: Phase I Report", 2017.

OAG Traffic Analyzer [online database], Official Aviation Guide, Retrieved Dec. 2020. URL https://www.oag.com/traffic-analyzer.

Pearce, B., "COVID-19: An almost full recovery of air travel in prospect," IATA Economic Reports, May 2021, Retrieved June, 2021. URL https://www.iata.org/en/iata-repository/publications/economic-reports/an-almost-full-recovery-of-air-travel-in-prospect/.

"SeatGuru by Tripadvisor", Retrieved Mar. 2019. URL https://seatguru.com/.17.

Wyman, O., "Oliver Wyman Global Fleet & MRO Market Forecast Summary 2017-2027", 2017, Retrieved October, 2021. URLhttps://www.oliverwyman.com/our-expertise/insights/2017/feb/2017-2027-fleet-mro-forecast.html.

Aftomis, Michael J., Berger, Marsha J. and Alonso, Juan J. (2006) "Applications of a Cartesian Mesh Boundary-Layer Approach for Complex Configurations". 44th AIAA Aerospace Sciences Meeting, Reno NV,

Blake, M., Smith, J., Wright, K., Mediavilla, R., Kirby, M., Pfaender, H., Clark, J.P., Volovoi, V., Dorbian, C., Ashok, A. (2010). "Advanced Vehicle concepts and implications for NextGen." NASA CR-2010-216397

Dubois, D. & Paynter, G.C. (2006), "Fuel flow method 2 for estimating aircraft emissions," SAE Transactions Vol. 115, pp. 1-14, Section 1: Journal of Aerospace

The Concorde Flying Manual Volume II. (1976). British Airways Overseas Division with later amendments.

Annual Energy Outlook 2011. (2011). U.S. Energy Information Administration

Bachman, J. (2016). "Supersonic is coming back. Will the airlines buy it?" Bloomberg

Barnhart, P. J. *IPAC - Inlet Performance Analysis Code*. 1997.

Bogaisky, J. (2018). "GE reveals engine that could make Aerion's ambitious supersonic business jet take flight." Forbes

Crichton, D., de la Rosa Blanco, E., Law, T., & Hileman, J. (2007). "Design and operation for ultra-low noise take-off," AIAA 45th Aerospace Sciences Meeting and Exhibit, January 8-11, 2007.

de la Rosa Blanco, E., Hall, C., & Crichton, D. (2007). "Challenges in the silent aircraft engine design," AIAA 45th Aerospace Sciences Meeting and Exhibit, January 8-11, 2007.

Hartmann, A. (1967). "Theory and test of flow mixing for turbofan engines," AIAA 3rd Propulsion Joint Specialist Conference, Vol. 5, No. 6, pp. 522–527. DOI:10.2514/3.43978

Kowalski, E.J. & Atkins Jr., R.A. (1979). "A computer code for estimating installed performance of aircraft gas turbine engines." Advanced Airplane Branch Boeing Military Airplane Company, Vol. I - Final Report

Kuchar, A.P. (1989). "Variable convergent-divergent exhaust nozzle. General Electric Company Aircraft Engine Group", AIAA Education Series, 1989, Chapter 5 of Aircraft Propulsion Systems Technology and Design.

Li, W., Shields, E., & Le, D. (2008). "Interactive inverse design optimization of fuselage shape for low-boom supersonic concepts." Journal of Aircraft, Vol. 45, No. 4, July – August 2008.

Mattingly, J. (2002). Aircraft engine design, AIAA Education Series.
Ozgen, S. (2017). AE 451 aeronautical engineering design I. Middle East Technical University
Pearson, H. (1962). "Mixing of exhaust bypass flow in bypass engine," Journal of The Royal Aeronautical Society, Vol. 66, No. 620, pp. 528–530.
Pratt & Whitney, and General Electric Aircraft Engines. Critical Propulsion Components Volume 1: Summary, Introduction, and Propulsion Systems Studies. 2005.
Raymer, D. (2004). Aircraft design: A conceptual approach. AIAA 1992
Rech, J. & Leyman, C.S. (1981). A case study by Aerospatiale and British aerospace on the Concorde. AIAA Professional Study Series
Scholz, E. (2017). Aircraft design – an open educational resource. Hamburg Open Online University
Schutte, J.S. (2009). "Simultaneous multi-design point approach to gas turbine on-design cycle analysis for aircraft engines," Ph.D. Thesis, Georgia Institute of Technology, May 2009.
Thornock, R.L. & Brown, E.F. (1972). "An experimental study of compressible flow through convergent-conical nozzles, including a comparison with theoretical results," Journal of Basic Engineering, pp.926-930.
Welge, H.R., Bonet, J., Magee, T., Chen, D., Hollowell, S. Kutzmann, A., Mortlock, A., Stengle, J., Nelson, C., Adamson, E., Baughcum, S., Britt, R., Miller, G., Tai, J. (2010). "N+2 supersonic concept development and systems integration," NASA-CR-2010-216842.
Whitcomb, R.T. (1966). "Some consideration regarding the application of the supersonic area rule to the design of airplane fuselages,' NACA Research Memorandum, National Advisory Committee for Aeronautics, Washington, July 1966.
Young, J.B. & Wilcock, R.C. (2002). "Modeling the air-cooled gas turbine part 2-coolant flows and losses," Journal of Turbomachinery, 124(2): pp. 214-221.
Air France, 2003. Manuel d'utilisation Concorde.
Airlines for America, 2017. A4A Passenger Airline Cost Index (PACI).
Boeing, 2019. Commercial market outlook 2019–2038.
Bresenham, J.E., 1965. Algorithm for computer control of a digital plotter. IBM Systems Journal 4, 25–30.
BTS, 1995. American Travel Survey (ATS) 1995. https://www.transtats.bts.gov/.
Daniel, K., Nash, A., Koeing, S., Felner, A., 2010. Theta*: Any-angle path planning on grids. Journal of Artificial Intelligence Research 39, 533–579.
FAA, 2015. 2015 inventory as modeled in Aviation Environmental Design Tool (AEDT).
FAA, 2018. FAA aerospace forecast – fiscal years 2018-2038.
FAA, 2020. Aviation Environmental Design Tool (AEDT) version 3c – user manual.
Graver, B., Rutherford, D., 2018. Transatlantic airline fuel efficiency ranking, 2017.
Hassan, M., Pfaender, H., Mavris, D., 2020. Design tools for conceptual analysis of future commercial supersonic aircraft, in: AIAA Aviation 2020 Forum. doi:10.2514/6.2020-2620.
Henne, P.A., 2005. Case for small supersonic civil aircraft. Journal of Aircraft 42, 765–774.
IATA, 2019. IATA economics chart of the week: Air travel frequency flattens in developed markets, rises in emerging markets.
Liebhardt, B., 2019. Sonic boom carpet computation as a basis for supersonic flight routing, in: AIAA Aviation 2019 Forum, p. 3387.
Liebhardt, B., Gollnick, V., Lütjens, K., 2011. Estimation of the market potential for supersonic airliners via analysis of the global premium ticket market, in: 11th AIAA Aviation Technology, Integration, and Operations (ATIO) Conference, p. 6806.
Liebhardt, B., Linke, F., Dahlmann, K., 2014. Supersonic deviations: Assessment of sonic-boom-restricted flight routing. Journal of Aircraft 51, 1987–1996. doi:10.2514/1.C032591.
Liebhardt, B., Lütjens, K., Tracy, R., Haas, A., 2017. Exploring the prospect of small supersonic airliners – A case study based on the Aerion AS2 jet, i17th AIAA Aviation Technology, Integration, and Operations (ATIO) Conference, p. 3588.Mavris, D., DeLaurentis, D., Crossley, W., & Alonso, J. J. (2017). Project 10 aircraft technology modeling and assessment: Phase I report.
Sun, Y., Smith, H., 2017. Review and prospect of supersonic business jet design. Progress in aerospace sciences 90, 12–38.
WID, 2019. World Inequality Database (WID). https://wid.world/data/.
Zheng, X.S., Rutherford, D., 2019. U.S.–Latin America airline fuel efficiency ranking, 2017–2018.

Task 4 References

[1] Salas Nunez, L., Tai, J. C., & Mavris, D. N. (2021). The Environmental Design Space: Modeling and Performance Updates. January, 1–15. https://doi.org/10.2514/6.2021-1422

[2] Kirby, M. R., & Mavris, D. N. (2008). The Environmental Design Space. 26th International Congress of the Aeronautical Sciences ICAS, 1–9.

[3] HARTMANN, A. (1967). Theory and test of flow mixing for turbofan engines. AIAA 3rd Propulsion Joint Specialist Conference, 5(6), 522–527. https://doi.org/10.2514/3.43978

[4] Pearson, H. (1962). Mixing of Exhaust Bypass Flow in Bypass Engine. Journal of the Royal Aeronautical Society, 66(620), 528–530.

[5] Berton, J. J., Haller, W. J., Senick, P. F., Jones, S. M., & Seidel, J. A. (2005). A comparative propulsion system analysis for the high-speed civil. Nasa/Tm—2005-213414, December.

[6] SEIDEL, J., HALLER, W., & BERTON, J. (1991). Comparison of turbine bypass and mixed flow turbofan engines for a high-speed civil transport. AIAA Aircraft Design Systems and Operations Meeting. https://doi.org/10.2514/6.1991-3132

[7] Welge, H. R., Bonet, J., Magee, T., Chen, D., Hollowell, S., Kutzmann, A., Mortlock, A., Stengle, J., Nelson, C., Adamson, E., Baughcum, S., Britt, R. T., Miller, G., & Tai, J. (2010). N+2 Supersonic Concept Development and Systems Integration. http://www.sti.nasa.gov

[8] Kowalski, E.J. & Atkins Jr., R.A. (1979). “A computer code for estimating installed performance of aircraft gas turbine engines.” Advanced Airplane Branch Boeing Military Airplane Company, Vol. I - Final Report

[8] https://software.nasa.gov/software/LEW-19686-1

[10] Gauntner, J. W. (1980). Algorithm for Calculating Turbine Cooling Flow and Resulting Decrease in Turbine Efficiency. https://ntrs.nasa.gov/search.jsp?R=19800011581

[11] Grondahl, C. M., & Tsuchiya, T. (2001). Performance benefit assesment of ceramic components in an MS9001FA gas turbine. Journal of Engineering for Gas Turbines and Power, 123(3), 513–519. https://doi.org/10.1115/1.1335476

[12] Schutte, J. S. (2009). SIMULTANEOUS MULTI-DESIGN POINT APPROACH TO GAS TURBINE ON-DESIGN CYCLE ANALYSIS FOR AIRCRAFT ENGINES.

[13] Denney, R. K., Tai, J. C., Kestner, B. K., & Mavris, D. N. (2005). Variable Cycle Optimization for Supersonic Commercial Applications. In Source: SAE Transactions (Vol. 114).

[14] Pratt & Whitney, & General Electric Aircraft Engines. (2005). Critical Propulsion Components Volume 2: Combustor. https://ntrs.nasa.gov/citations/20050185254

[15] Niedzwiecki, R. W. (1992). Low Emissions Combustor Technology for High-Speed Civil Transport Engines.

[16] ICCAIA CAEP12_WG3-5_ESTG_WP04

Project 018 Community Measurements of Aviation Emission Contributions to Ambient Air Quality

Boston University School of Public Health

Project Lead Investigator

Kevin J. Lane
Assistant Professor
Department of Environmental Health
Boston University School of Public Health
715 Albany St. T4W
Boston, MA 02118
617-414-8457
klane@bu.edu

University Participants

Boston University School of Public Health (BUSPH)

- PI(s): Kevin J. Lane, Assistant Professor; Jonathan I. Levy, Professor and Associate Chair
- FAA Award Number: 13-C-AJFE-BU, Amendment 7
- Period of Performance: September 30, 2020 to August 30, 2021
- Task(s):
    - **Task 1**: Continue long-term monitoring of air pollution at both new and existing stationary sites to assess temporal variations in aviation source contributions in greater Boston area communities
    - **Task 2**: Incorporate particle size distributions at each of our monitoring sites to inform our understanding of in-flight contributions to community ultrafine particles (UFPs) relative to background sources
    - **Task 3**: Conduct mobile monitoring in selected communities near Logan Airport to determine spatial and short-term temporal variations in aviation emission contributions to concentrations at ground level
    - **Task 4**: From FAA essential flight activity, compile covariates needed for regression modeling under Project 18 and dispersion modeling under Project 19 for a data-sharing platform that allows comparisons between atmospheric dispersion models implemented by collaborators on ASCENT Project 19 and monitored pollutant concentrations and related regression models from Project 18
    - **Task 5**: In Year 1, construct regression models using 2017–2018 data and the flight activity data and covariates developed under Task 4 to determine the contributions of aviation sources to UFP and black carbon (BC) concentrations measured during our 2017–2018 monitoring campaign; in Year 2, analyze the combined mobile monitoring and stationary data collected under Tasks 1–3 for the 2020 sampling campaign for community-level contributions from aviation sources

Project Funding Level

FAA provided $599,999 in funding. Matching funds were provided by a non-federal donor to the Women's Health Initiative cohort studies as cost-sharing support to Boston University through Project 3.

Investigation Team

- ASCENT BUSPH Director and Project 18 Co-Investigator: Jonathan I. Levy, ScD (Professor of Environmental Health, Chair of the Department of Environmental Health, BUSPH). Dr. Levy is the Boston University PI for ASCENT. He initiated ASCENT Project 18 and serves as the director of BUSPH ASCENT research.
- ASCENT Project 18 PI: Kevin J. Lane, PhD (Assistant Professor of Environmental Health, Department of Environmental Health, BUSPH). Dr. Lane joined the Project 18 team in July 2017. Dr. Lane has expertise in the assessment of UFP exposure, geographic information systems, statistical modeling of large datasets, and cardiovascular health outcomes associated with air pollution exposure. He has contributed to study design and data analysis strategies

and, as of October 1, 2017, has taken over the primary responsibility for project execution. Dr. Lane also contributes to the manuscripts and reports produced.
- Tufts University Associate Professor Dr. John Durant, PhD. Dr. Durant oversees the Tufts Air Pollution Monitoring Laboratory (TAPL) team, leads the development of field study design, and contributes to scientific manuscript preparation.
- Tufts University Research Professor Dr. Neelakshi Hudda, PhD. Dr. Hudda joined the Project 18 team in September 2020 and is managing the TAPL team and the mobility data analysis, field study design and implementation, and scientific manuscript preparation.
- BUSPH Assistant Professor Dr. Prasad Patil. Dr Patil is a machine learning and regression modeling expert who is assisting Dr. Lane with modeling of the 2017–2019 UFP data.
- Graduate Student: Sean Mueller is a doctoral student at BUSPH.
- Postdoctoral Research Associate: Dr. Tiffany Duhl at Tufts University is managing mobile monitoring and analyzing the mobile particle number concentration (PNC) and fast-scanning mobility particle sizer (FMPS) size distribution data.
- Undergraduate Students: Ida Weiss and Taylor Adams at Tufts University are working on the mobile monitoring platform and helping to clean the air pollution data and create map plots.

Project Overview

The primary goal of this project was to conduct a new air pollution monitoring campaign beneath flight paths to and from Boston Logan International Airport, using a protocol specifically designed to determine the magnitude and spatial distribution of UFPs in the vicinity of arrival flight paths. Data were collected to assess whether aircraft emissions, particularly arrival emissions, significantly contribute to UFP concentrations at appreciable distances from the airport. Tasks 1–3 are an extension of the previous air pollution monitoring performed under ASCENT Project 18. Tasks 2 and 3 leverage the infrastructure developed for our field campaign and enable measurements that address a broader set of research questions than those evaluated in the previous monitoring year, with additional data collection for UFP size distributions and a new air pollutant (NO/NO_2). These tasks provide a strong foundation for Tasks 4 and 5, which increases the potential for future collaborative efforts with Project 19, in which we interpret and apply the collected measurements to inform ongoing dispersion modeling efforts at the University of North Carolina (UNC) and regression modeling at BUSPH.

We have continued our monitoring campaign to collect and analyze community air pollution measurements to determine the contributions of in-flight arrival and departure aircraft to ground-based concentrations. Previous studies have not had the monitoring infrastructure and real-time flight activity data necessary to determine how much of the measured pollution arises from aviation sources. We have used state-of-the-art air pollution monitoring technology that can measure different air pollutants every 1–5 s. Stationary sites have been established at varying distances from flight paths for Boston Logan International Airport, with measurements collected across multiple seasons. We have also employed a mobile monitoring system (electric vehicle [EV]) outfitted with the same monitoring equipment to drive throughout these communities to better characterize geographic variations in air pollution. Statistical analyses will compare the stationary and mobile measurements with flight activity data from the U.S. FAA and meteorology to determine aircraft contributions to ground measurements. We will compare these source attribution estimates with comparable outputs from atmospheric dispersion models.

A summary of the current project methods and data collection is included below to describe the continued application of Project 18 data, including bivariate statistical analysis and multiple regression model development conducted under Task 5.

Task 1 - Continue Long-term Monitoring of Air Pollution at Both New and Existing Stationary Sites to Assess Temporal Variations in Aviation Source Contributions in Greater Boston Area Communities

Boston University School of Public Health

Objective(s)

We have focused on designing and implementing an air pollution monitoring study that will enable us to identify contributions from arriving aircraft to ambient air pollution in a near-airport setting. The objective of this task was to determine whether aircraft emissions, particularly in-flight arrival and departure emissions, significantly contribute to ground-level UFP concentrations at appreciable distances from the airport.

Research Approach

An air pollution monitoring campaign was conducted at five sites located at varying distances from the airport and arrival/departure flight paths for Boston Logan Airport (Figure 1). Sites were selected through a systematic process, considering varying distances from the airport and laterally from each flight path and excluding locations close to major roadways or other significant sources of combustion. These sites were specifically chosen to isolate the contributions of in-flight aircraft, which is important for the flight activity source attribution task. PNC (a proxy for UFP) monitoring instruments were established at each monitoring site in a preselected scheme to allow for multiple levels of comparison (e.g., sites beneath vs. not beneath flight paths given prevailing winds, sites at varying distances from the airport, sites at varying lateral distances beneath flight paths). The PNC was measured using a TSI condensation particle counter (CPC) (model 3783).

Field monitoring: We have collected air pollution data at Chelsea since April 2020, allowing us to capture nearly the entire COVID-19 time period with a full mobile and stationary monitoring launch that began September 2020. UFP data have been collected from four long-term monitoring sites in Chelsea, Revere, South Boston, and Winthrop, allowing for a comparison of PNC results within our monitored communities. Each monitoring site is located more than 200 m from major roadways and intersections and is near the arrival and takeoff locations on runways (4R, 22, and 9). The map in Figure 1 indicates the locations of the stationary monitoring sites in relation to the airport.

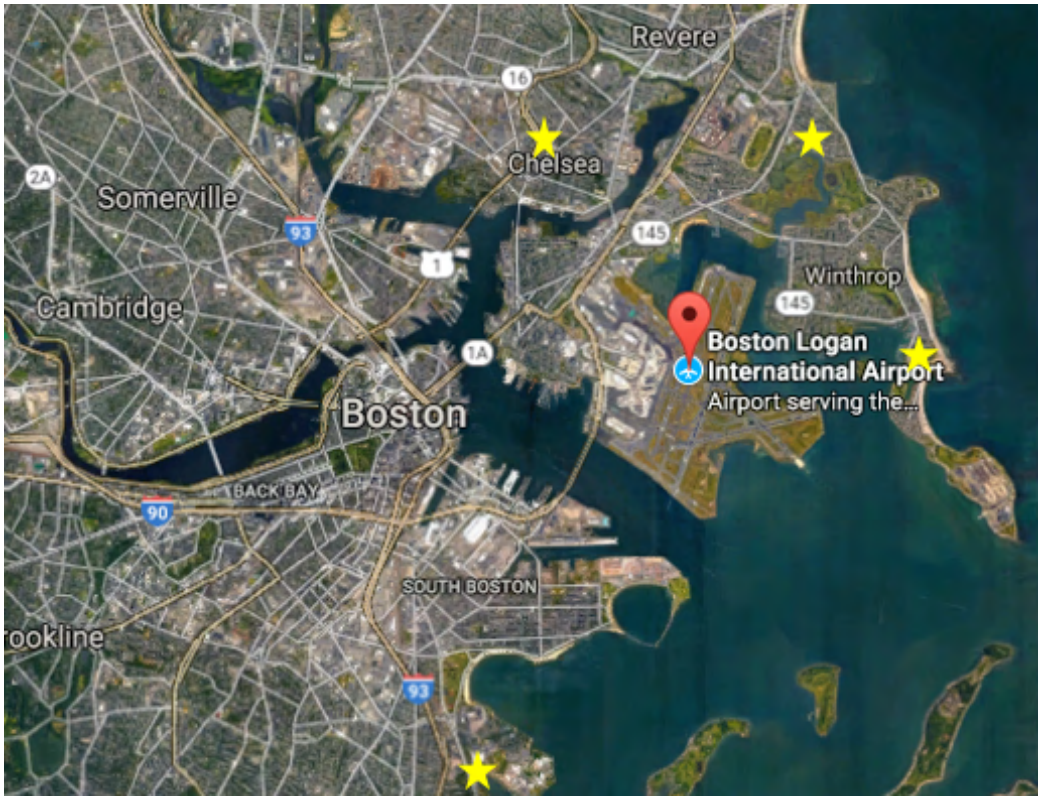

Figure 1. Stationary sites for the 2020–2021 monitoring campaign.

Each stationary site is outfitted with a climate-controlled enclosure that allows for year-round sampling. Monitoring sites have a combination of UFP (TSI CPC or TSI FMPS), $NO/NO_2/NO_x$ (2BTechnology), and BC (Magee Scientific AE22) monitors. An example of the box setup with climate control is shown in Figure 2.

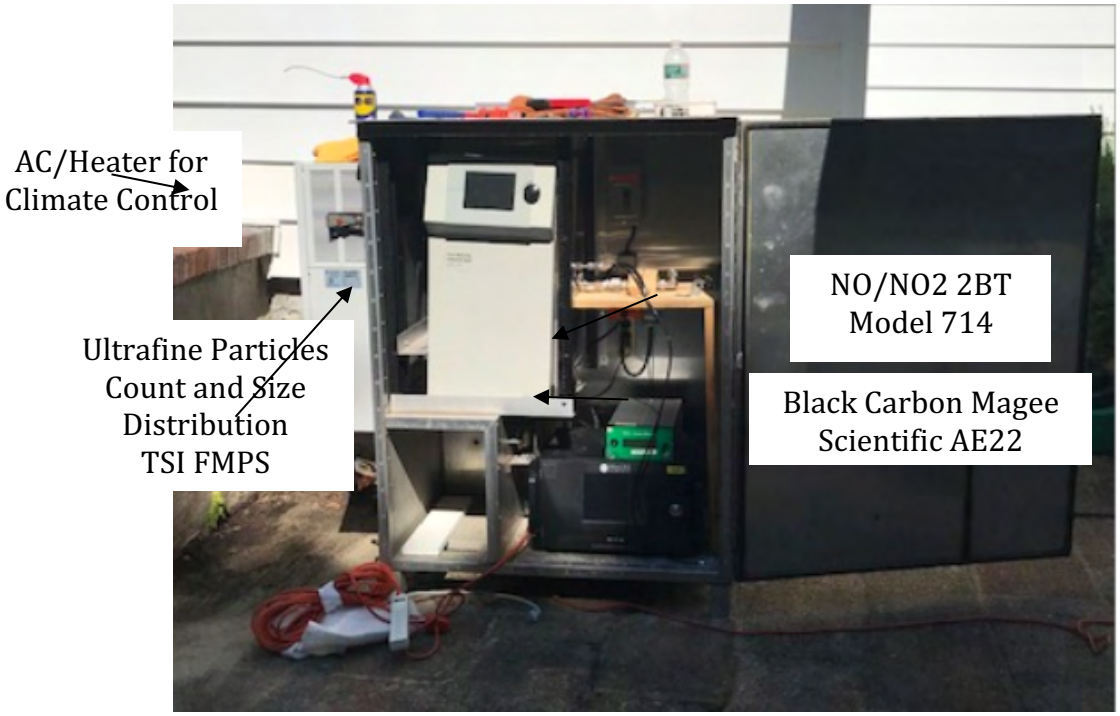

Figure 2. BUSPH long-term air pollution monitoring box.

The other sites configured with the following monitoring equipment.

- **Chelsea**
  - UFP – CPC
  - BC – micro-aethalometer
- **Revere**
  - UFP –CPC
  - NO/NO_2 – 2BT model 714
  - BC – micro-aethalometer
- **Winthrop**
  - UFP – FMPS
  - NO/NO_2 – 2BT model 714
  - BC – Magee AE33
- **South Boston**
  - UFP – FMPS

Milestone(s)

On August 15, 2021, we completed a full year of ambient data across our monitoring platform. As additional milestones for continued monitoring, we:

- Obtained permission to continue monitoring at each stationary site,
- Completed annual manufacturer cleaning and calibration of CPCs and FMPS, and
- Continued sixth-month side-by-side calibration.

Major Accomplishments

We have completed a full year of ambient stationary monitoring and have implemented quality assessment (QA) and quality control (QC) procedures on the data, allowing the team to analyze for aviation source attribution during the COVID-19 pandemic. Field tests were periodically performed to compare CPCs for low and high air pollution exposure sampling scenarios. Comparisons between instruments were made using recently factory-calibrated instruments and exhibited good

agreement, with r ≥ 0.97 – 0.99 and a within-device comparison of 0.96. These tests will continue to be conducted every six months or when a monitor requires factory recalibration. The CPC monitors have been recalibrated and will continue to be examined for retesting and factory calibration. Stationary monitors have been collecting data that are compiled and merged with meteorological data. Figure 3 provides a time-series plot for three of our monitoring locations as an example of the UFP data being collected. The PNC histogram depicts the 95th percentile for 1-hr average PNC results by month for data collected during the 2020–2021 monitoring campaign and analyzed in section 5 to determine the impact of the COVID-19 pandemic on transportation and UFP concentrations. Although formal statistical analyses are still underway, we can observe a meaningful variation in the PNC that shifts for each season, corresponding to the dominant wind direction during each month. Regression analysis with flight activity needs to be conducted to examine the contributions from aviation.

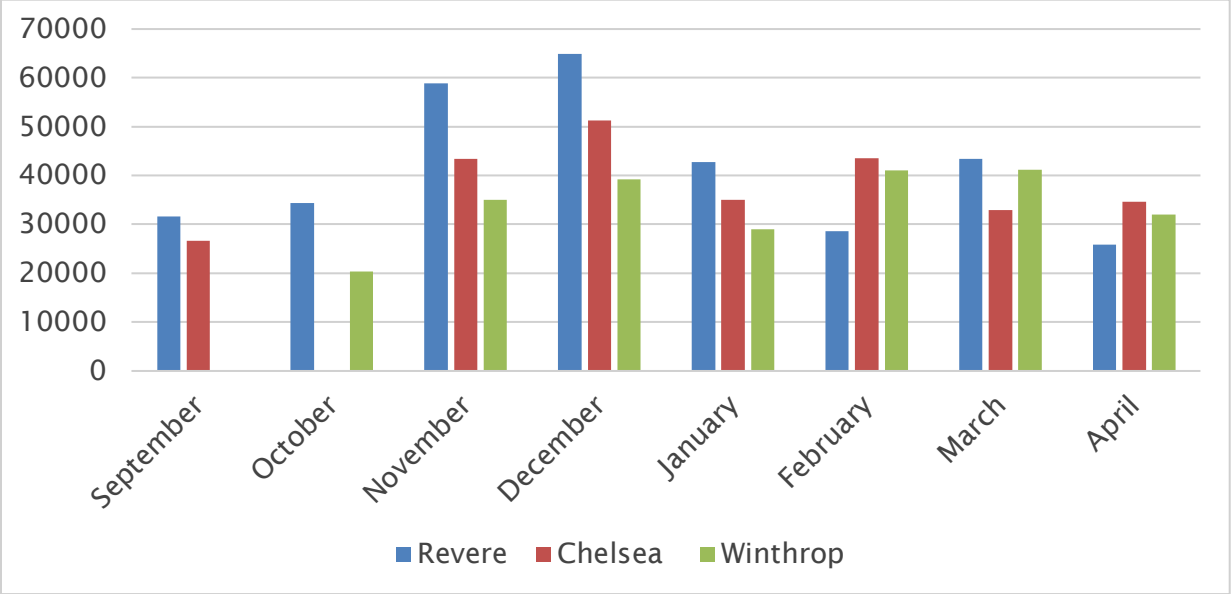

Figure 3. Multiple-site comparison of 95th percentile UPCs, measured as hourly 95th percentile of the PNC in Chelsea, Revere, and Winthrop by month for 2020–2021.

Figure 4 provides NO, NO_2, and NO_x distributions for the study period at the Winthrop site during the ramp-up phase at Logan Airport from November 2020 to May 2021. Figure A presents 95th percentile data for NO, NO_2, and NO_x at different times of the day, indicating significantly higher concentrations at night for NO_2 and NO_x but not for NO.

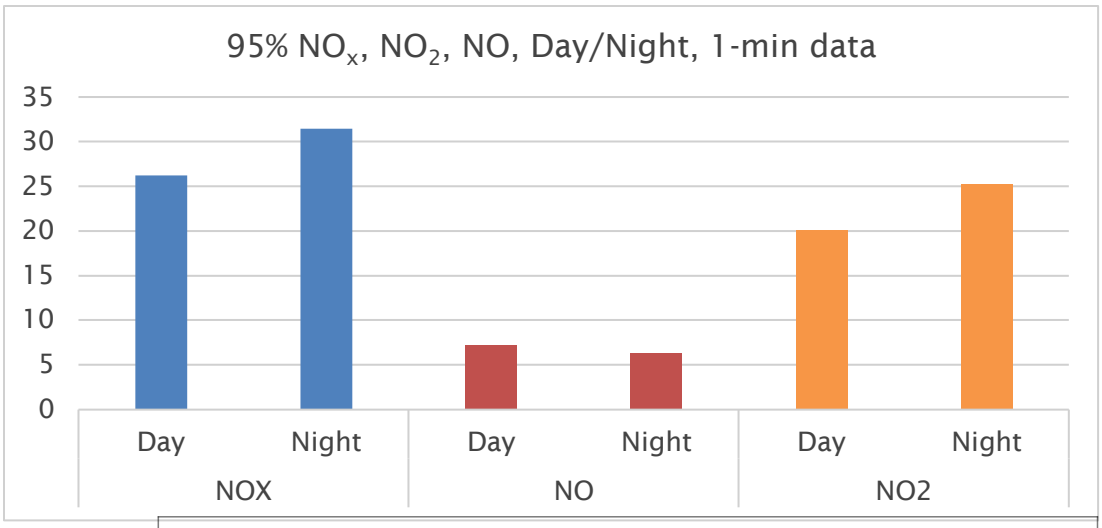

	n=140179	sunrise-sunset		n=54261	sunset-sunrise	
	Day			Night		
	NOX	NO	NO2	NOX	NO	NO2
0.10%	0	0	0	0	0	0
1%	1	0	0	1	0	0
5%	2	0	0	2	0	1
50%	6	2	4	8	2	6
95%	26	7	20	31	6	25
99%	47	21	29	54	22	35
99.90%	86	50	40	82	46	41

Figure 4. Hourly averages of NO, NO_2, and NO_x in parts per billion (ppb) by day and night, shown as a histogram and time of day distribution, for Winthrop, MA.

Publications
None

Outreach Efforts
None

Awards
None

Student Involvement
Sean Mueller, a doctoral student involved in this study, has been analyzing descriptive statistics of the stationary monitoring data. Ida Weiss and Tyler Tatro, undergraduate students at Tufts University, have been assisting with the collection of stationary site monitoring data.

Plans for Next Period
As proposed tasks for the next study period (October 1, 2021 to September 30, 2022), we will continue monitoring at our stationary sites and will add NO_2 and SO_2 to our monitoring efforts. Validation and refinement of aviation-specific air pollution

dispersion models require (1) the collection of monitoring data, (2) the use of federal reference methods and/or federal equivalency methods, and (3) the application of statistical approaches for source attribution. We will expand on this work to add a new monitoring site that is in close proximity to the airport, in consultation and collaboration with Massport.

Task 2 – Incorporate Particle Size Distribution at Each of Our Monitoring Sites to Inform our Understanding of In-flight Contributions to Community UFPs Relative to Background Sources

Boston University School of Public Health

Objective(s)

In this task, we aimed to incorporate particle size distribution into our UFP monitoring campaign using two TSI FMPSs. FMPSs are routinely used to make accurate nanoparticle size measurements to assess the shape of the particle size distribution, providing a broad size range of 1–1,000 nm at a fine temporal scale (< 10-s scans) that can bin categorize a wide concentration range up to 10^7 particles/cm^3. The method is independent of the refractive index of the particle or fluid and has a high degree of absolute sizing accuracy and measurement repeatability.

The inclusion of two FMPSs in our study design allows the particle size distribution to be examined. Given that the literature has shown differences in particle size distributions for aircraft versus motor vehicles, as well as for aircraft plumes at different points in time, this approach could advance our understanding of in-flight contributions to community UFPs relative to background sources.

Research Approach

We will deploy two different particle size distribution monitors in stationary monitoring platforms, two FMPSs. During the summer, we began our comparison of FMPS and SMPS laboratory testing. The FMPS and SMPS particle numbers obtained for different particle size channels were compared under 10 test runs, with a correlation coefficient average of r = 0.97 and differences in time coincident points that were below the instrument error for both monitors (< 800 particles/cm^3). The SMPS can measure many more size channels than the FMPS, but has a higher limit of detection on the particle size at 10 nm; in contrast, the FMPS can accurately measure sizes as low as 6 nm. Therefore, we conducted statistical analyses only on the channels that were able to detect coincident size distribution values.

Milestone(s)

The core milestones for Task 2 include incorporating particle size distributions into our monitoring campaign, testing for comparability between UFP monitoring instruments, and deploying these instruments in the field.

Major Accomplishments

We successfully integrated monitoring of particle size distribution into our Year 2020–2021 monitoring campaign.

Below is an example of PNC data from an FMPS, which uses an electrical mobility measurement technique to classify particles into the following 32 size channels (sizes reported in nm):

6.04	6.98	8.06	9.31	10.8	12.4	14.3	16.5	19.1	22.1	25.5	29.4	34	39.2
45.3	52.3	60.4	69.8	80.6	93.1	107.5	124.1	143.3	165.5	191.1	220.7	254.8	294.3
339.8	392.4	453.2	523.3										

The FMPS uses multiple low-noise electrometers and can measure particles simultaneously for multiple channels at 1-Hz resolution, enabling measurements of rapidly changing particle size distributions in the study area. Figure 5 illustrates the different types of size distributions observed at the Winthrop monitoring location, indicating that rapid (within a 2-min period) changes in the distributions are commonly observed in the study area. We show data for one day (December 26, 2020), and during the afternoon hours, the presence of a size distribution with a mode of ~10 nm is evident. The winds were westerly, indicating potential for arrivals over the site during this sampling period. We are using these plots to inform our regression modeling approach for the size distribution data.

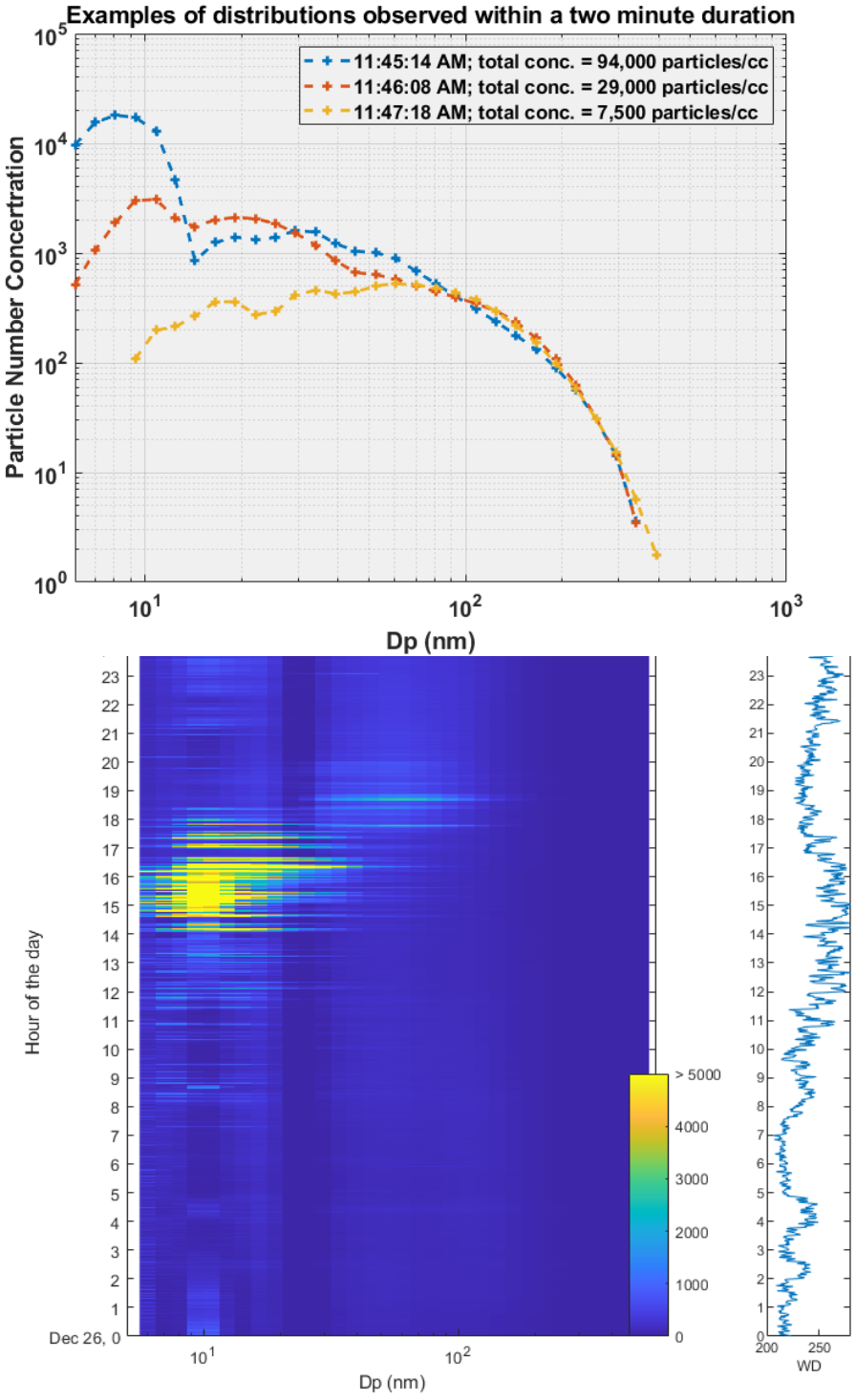

Figure 5. Particle size distribution at the Winthrop monitoring site. (a) Particle size distribution averaged over a 2-min duration as the natural log of PNC by particle size bin in nanometers. (b) Plot of 1-minute average PNC by size distribution with wind direction for a 24-hr time period.

Publications
None

Outreach Efforts
None

Awards
None

Student Involvement
Doctoral student Sean Mueller will analyze the particle distribution data as part of a source apportionment analysis.

Plans for Next Period
We will continue monitoring particle size distribution as part of the ongoing community monitoring campaign and will use these plots to inform our regression modeling approach for the size distribution data.

Task 3 – Conduct Mobile Monitoring in Selected Communities Near Logan Airport to Determine Spatial and Short-term Temporal Variations in Aviation Emission Contributions to Concentrations at Ground Level
Boston University School of Public Health

Objective(s)
New to our scope of work in 2019–2021, we added high-resolution mobile monitoring to improve the spatial characterization of UFPs and other air pollutants in near-airport communities. Under the current project, we are collaborating with Drs. John Durant and Neelakshi Hudda at Tufts University to deploy a mobile monitoring platform concurrent with our stationary monitoring under Tasks 1 and 2, which will allow us to efficiently monitor more spatially diverse communities near Logan Airport in less time, with a limited number of monitoring devices. Dr. Durant has the mobile monitoring infrastructure and expertise to allow us to collect these data in a reliable and robust manner, as described in detail below. Real-time measurements of air pollutants will be acquired with the Tufts Air Pollution Monitoring Laboratory TAPL, a mobile platform equipped with fast-response instruments for monitoring gas- and particle-phase pollutants.

Research Approach
The TAPL is a 2017 Chevrolet Bolt EV equipped with instruments powered by six 12-V marine deep cycle batteries, which are connected in parallel to a 2-kW inverter/charger (Xantrex 2000). The TAPL is driven slowly (~10 m/s) to allow measurements of local-scale (~20 m) changes in pollutant concentrations. Individual measurements are matched to location by 1-s-interval global positioning system (GPS) readings. The TAPL monitoring setup can be outfitted to include a combination of air pollution monitoring equipment, including a CPC (model 3775, TSI; 4–2,000 nm), a particle size classifier (SMPS; model 3080 electrostatic classifier and model 3085 Nano DMA, TSI; 6–200 nm)), a photoelectrical aerosol sensor to detect particle-bound polycyclic aromatic hydrocarbons (model PAS2000, EcoChem Analytics, Inc.), an aethalometer to measure BC (model AE-16, Magee Scientific), and a laser photometer (Dusttrak DRX Aerosol Monitor, 8533, TSI) to measure particulate matter (PM2.5). Nitric oxide (NO) and nitrogen oxides (NO_x; sum of NO_2 and NO concentrations) are measured using a chemiluminescence analyzer (model 42i, Thermo Scientific). The measurement cycle of the instruments ranges from 1 s for the CPC to 135 s for a full scan (32 bins) with the SMPS. Real-time measurements of air pollutants were acquired with the TAPL, an electric-powered vehicle equipped with fast-response instruments for monitoring gas- and particle-phase pollutants. The TAPL is shown in Figure 6, with a description of the monitoring devices given in Table 1.

Figure 6. Exterior and interior images of the TAPL.

TAPL Instruments

The monitoring instruments used in the TAPL are listed in Table 1. Measurements were acquired every 1 s to 1 min, depending on the instrument. All instruments were factory-calibrated by the equipment manufacturers prior to the start of the campaign. QA measures were performed before each monitoring run, including a flow rate and zero-concentration check and instrument clock resets to the National Institute of Standards and Technology. Periodic side-by-side tests of the instrument area were also performed as part of the QA process to determine instrument-specific measurement differences prior to data analysis.

Table 1. Air pollution monitoring equipment in the TAPL used for this study.

Instrument	Parameter measured	Instrument flow rate (L min-1)	Response time	Detection limit, sensitivity
TSI portable CPC (ethanol-based) model 3007	UFP count, 10 nm–1 um	0.8	< 9 s for 95% response	10 nm, < 0.01 particles/cm^3
TSI EPC (water-based) model 3783	UFP count, 7 nm–3 um	3	< 3 s for 95% response	7 nm, < 0.01 particles/cm^3
2BTechnology model 408	NO	1	8 s	Greater of 3 ppb or 3% of reading
Magee Scientific aethalometer AE-33	BC	5	< 60 s	Proportional to time base and sample flow rate settings: approximately 0.03 µg/m^3 @ 1 min, 5 L/min
Garmin GPSMAP 76CSx	GPS location	N/A	1	3 m

Data Acquisition and QA/QC Checks

Data from the instruments are recorded in real time on a laptop in the TAPL. After each monitoring day, the data files are screened and collated in a master database. Air pollution measurements are matched to location by 1-s-interval GPS readings. The database then goes through a QA and quality check process, where the data are screened for errors flagged by instruments and quality criteria developed by the research team. Both the raw data and QA-processed database are stored on a secure server.

Monitoring Routes

We have developed two monitoring routes that encompass the communities impacted by the most commonly used runways at Logan: (1) a route to the north (north route) that includes all or parts of the communities of Winthrop, Revere, Chelsea, East Boston, and Lynn located 1–4 miles from the airport and (2) a route to the south (south route) that includes all or parts of the communities of South Boston, Dorchester, and Quincy located 1–6 miles from the airport. The routes are shown in Figure 7. The following criteria were applied in determining the routes:

(1) Coverage of communities in proximity to the airport,
(2) Coverage under main flight paths,
(3) Spacing of transects underneath flight paths such that spatial gradients of air pollutants can be assessed over a large area,
(4) Ability to perform measurements on multiple transects in an area within a relatively short period of time (1-2 hr) to capture both spatial and temporal changes in aviation impacts within the study area, and
(5) Ability to cover the entire route within the period associated with peak and off-peak flight activity periods (3-4 hr).

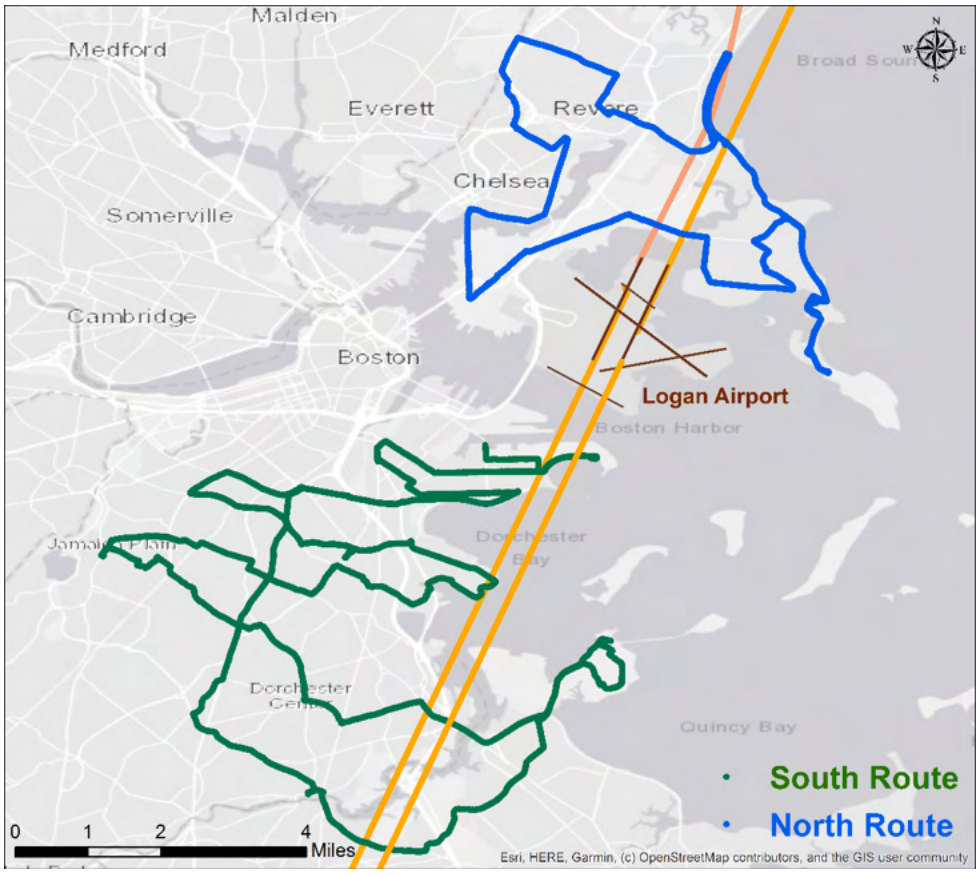

Figure 7. Map showing the north and south monitoring routes, the airport, and typical flight trajectories for arrivals on multiple runways at Logan Airport.

Monitoring Schedule

We are collecting measurements on these two routes under a variety of meteorological and airport-activity conditions. We have adopted a purposeful, flexible monitoring approach rather than a rigid, repetitive schedule. The advantage of this approach is that it allows us to capture a much wider range of meteorological and airport-activity conditions and to thereby more fully characterize the main factors that influence aviation-related pollutant concentrations in the two study areas. The following criteria are being used to guide the monitoring schedule:

1. Maximal coverage of the periods of the day associated with peak and off-peak flight activity,
2. Coverage of the periods of the day associated with predictable diurnal variations in air pollution due to changes in meteorological factors (e.g., temperature, mixing height, on-shore and off-shore winds),
3. Coverage of the seasonal wind patterns (we are aiming to reasonably mimic the natural distribution [2/3 westerly flow vs. 1/3 easterly flow] that is prevalent in the research area and are scheduling the monitoring runs to cover different wind speed/direction combinations),
4. Coverage of various temperature regimes (e.g., seasonal and diurnal), and
5. Coverage of various active runway configurations.

Mobile Monitoring Protocol

Mobile monitoring has continued with two to three routes per week. The decision to monitor the north or south route is based on weather, current flight activity patterns, and arrivals and takeoffs for day of the sampling. Route selection is being designed to maximize variations in meteorology and landing and takeoff (LTO) activity over a community to inform regression modeling. The standard operating procedure for preparation of a mobile monitoring route (see Figure 8) begins with (a) checking weather conditions as the wind direction and speed are used by Massport to identify LTO runways, (b) checking a real-time flight tracker to identify flight paths and which communities are being flown over, (3) preparing monitoring equipment and driving to the starting point of the route, and (4) driving the route and then downloading QA/QC data.

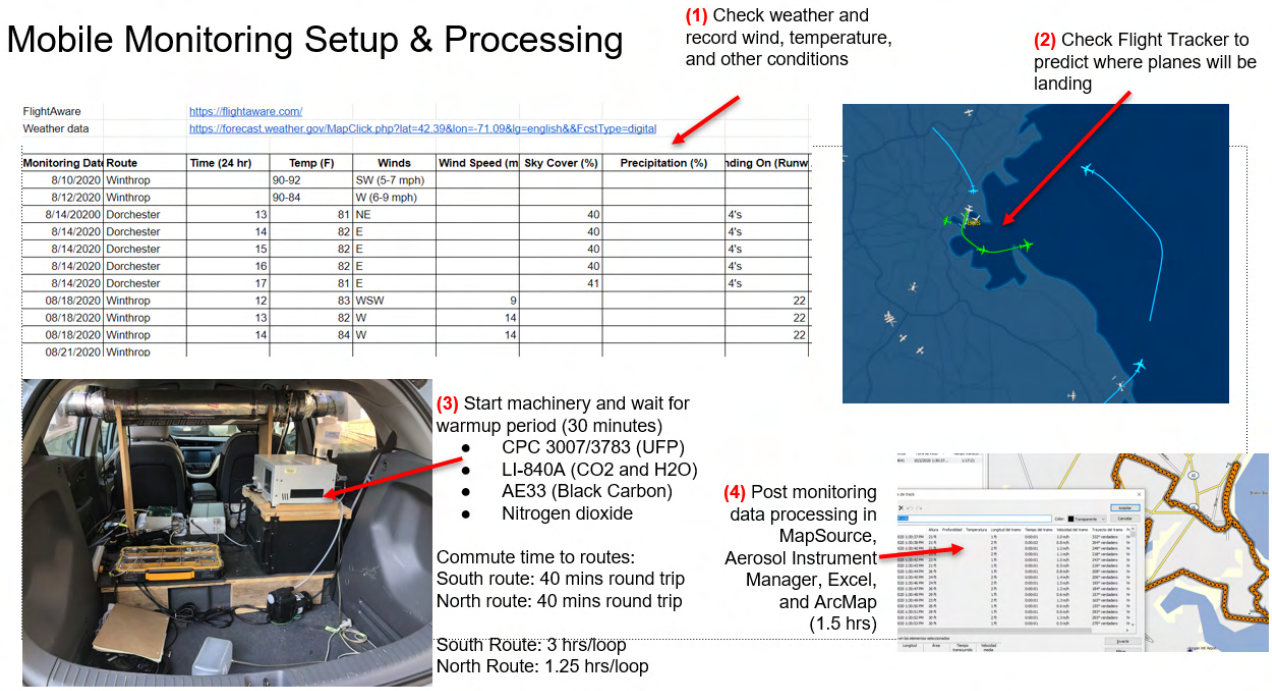

Figure 8. Standard operating procedure for mobile monitoring route preparation.

Data are cleaned on a weekly basis and integrated with the stationary monitoring data platform at BUSPH.

Milestone(s)

We have designed monitoring routes and protocols to integrate mobile monitoring for community measurements of aviation-related UFPs. Data are being compiled and examined for wind rose plotting and for inclusion in regression modeling for UFPs.

Major Accomplishments

Over 400 hours of mobile air pollution data have been collected using the Tufts EV, covering a wide variation of meteorology and ramp-up of aviation activities during the COVID-19 time period. Table 2 provides a breakdown of the number of days sampled during different months of the year after the full launch of the simultaneous mobile and stationary monitoring platform.

Table 2. Number of mobile monitoring sampling runs by month and year.

Mobile Monitoring Runs: South Route				
Year	Dec-Feb	Mar-May	Jun-Aug	Sept-Nov
2020			3	12
2021	15	22	16	8
Total	**15**	**22**	**19**	**20**
Mobile Monitoring Runs: North Route				
Year	Dec-Feb	Mar-May	Jun-Aug	Sept-Nov
2020			3	16
2021	16	24	16	9
Total	**16**	**24**	**19**	**25**

Mobile monitoring sampling compared with stationary site meteorology: We aim to capture the meteorology in a representative manner in both our mobile and stationary monitoring campaigns. We conducted mobile monitoring using the Tufts EV approximately one in every three days. The wind rose plots in Figure 9 show the wind speed and wind direction distribution for (a) average daily wind speed and direction at Logan Airport, (b) mobile monitoring average wind speed and direction by day, and (c) mobile monitoring average wind speed and direction by hour. Moving forward, monitoring will be conducted purposefully to address any gaps in meteorology representativeness (for example, southwest winds).

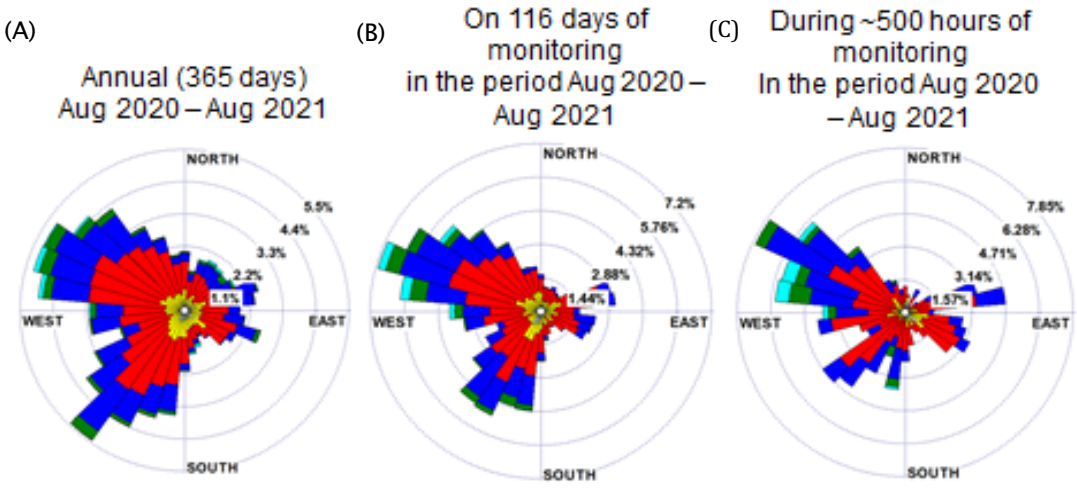

Figure 9. Comparison of long-term stationary and mobile monitoring data meteorology by days and hours.

Mobile monitoring maps: Figure 10 presents PNC data from our mobile monitoring routes with consistent prevailing winds throughout the sampling period that would allow for a descriptive understanding of the meteorological impacts on PNC distribution. In Figure 10, maps A and B were obtained from the northern route and include cases in which the mobile and stationary platform for Chelsea and Revere would be downwind and upwind, respectively. Maps C and D show results from the southern monitoring route and include downwind and upwind cases, respectively. When the community is downwind, we

can see a more concentrated elevation spread near the communities with our monitoring sites, indicating potential arrival flight activity. However, further analysis pairing the mobile monitoring data in aggregate with the flight trajectory data is currently ongoing.

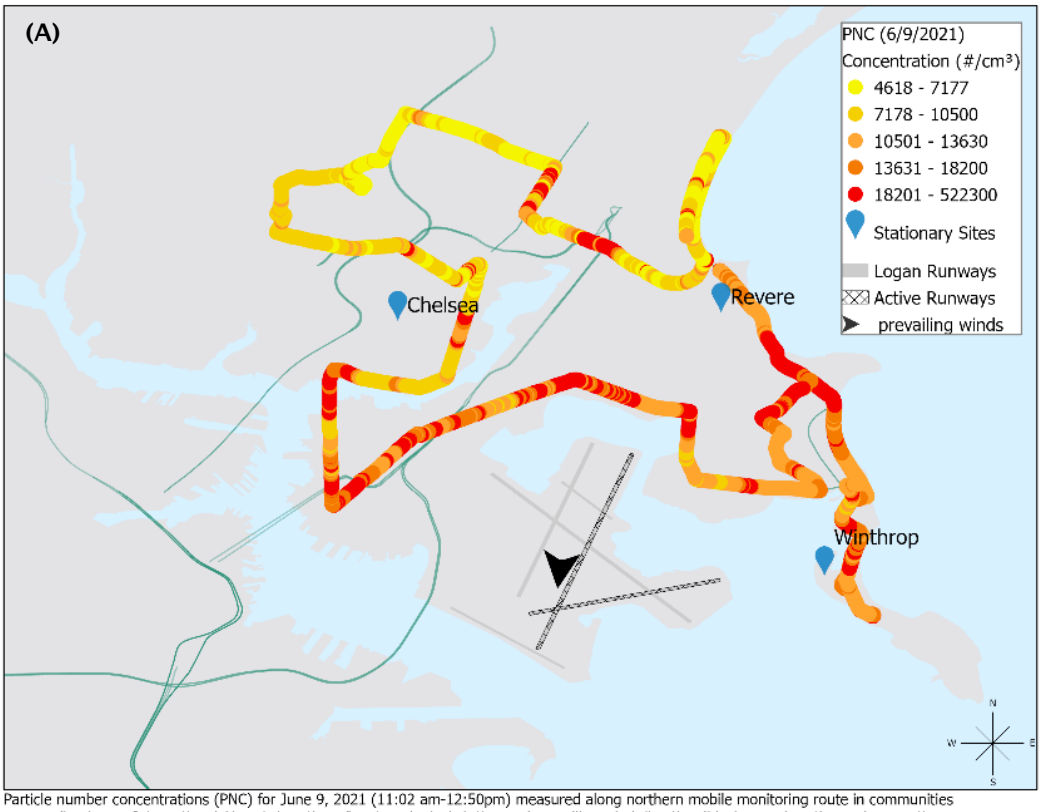

Particle number concentrations (PNC) for June 9, 2021 (11:02 am-12:50pm) measured along northern mobile monitoring route in communities surrounding Logan International Airport. Location of meteorological station and prevailing wind direction (black arrow), active and non-active runways (dark and light grey bars, respectively) for sampling period, location of stationary air monitoring sites (blue pins), and primary and secondary roadways (dark green lines) are also shown. During the measurement period the prevailing winds were out of the N at 9.3 mph.

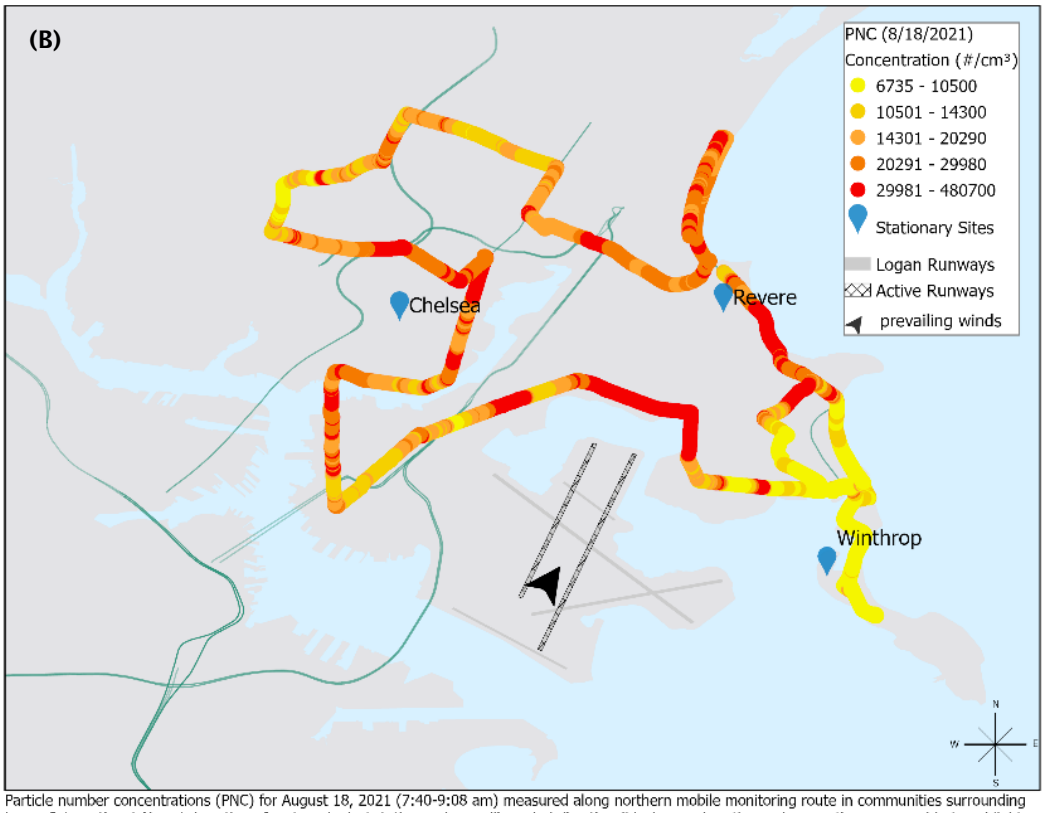

Particle number concentrations (PNC) for August 18, 2021 (7:40-9:08 am) measured along northern mobile monitoring route in communities surrounding Logan International Airport. Location of meteorological station and prevailing wind direction (black arrow), active and non-active runways (dark and light grey bars, respectively) for sampling period, location of stationary air monitoring sites (blue pins), and major roadways (dark green lines) are also shown. During the measurement period the prevailing winds were out of the SW at 8.5 mph.

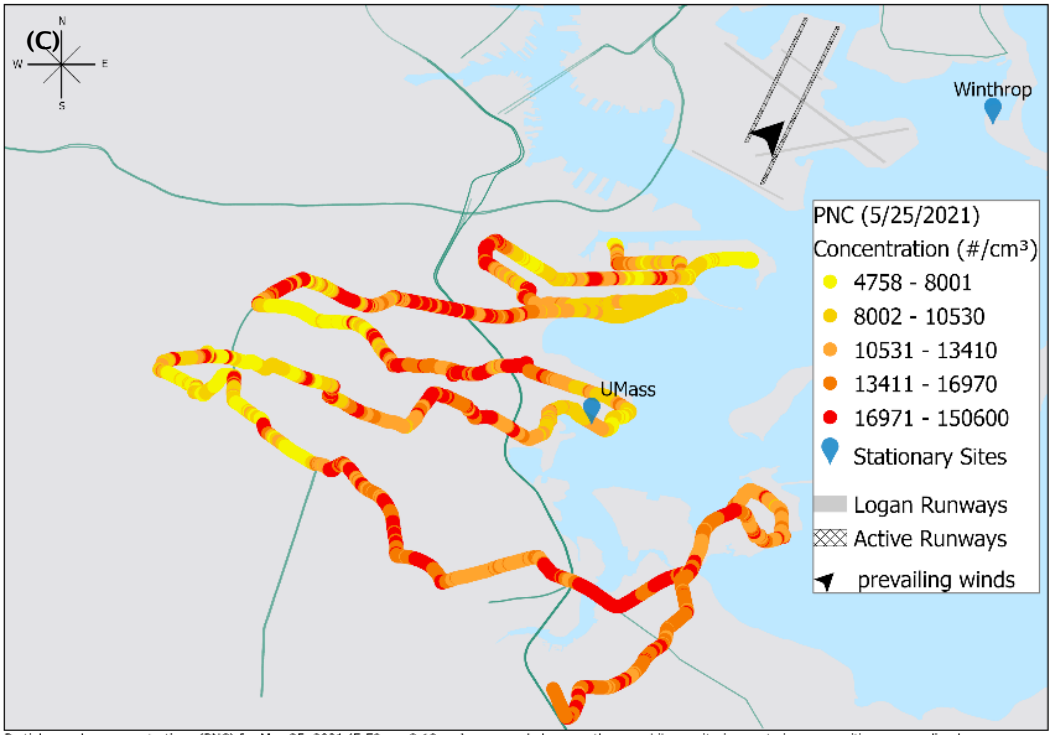

Particle number concentrations (PNC) for May 25, 2021 (5:50 am-8:19 am) measured along southern mobile monitoring route in communities surrounding Logan International Airport. Location of meteorological station and prevailing wind direction (black arrow), active and non-active runways (dark and light grey bars, respectively) for sampling period, location of stationary air monitoring sites (blue pins), and major roadways (dark green lines) are also shown. During the measurement period the prevailing winds were out of the SW at 13.7 mph.

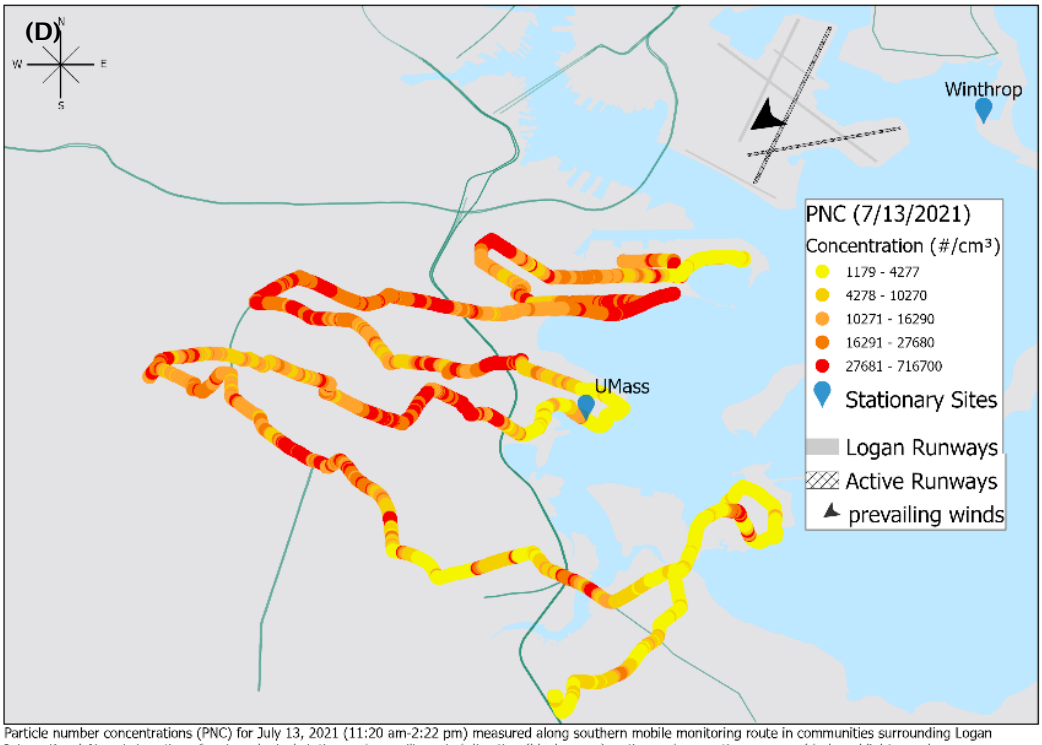

Particle number concentrations (PNC) for July 13, 2021 (11:20 am-2:22 pm) measured along southern mobile monitoring route in communities surrounding Logan International Airport. Location of meteorological station and prevailing wind direction (black arrow), active and non-active runways (dark and light grey bars, respectively) for sampling period, location of stationary air monitoring sites (blue pins), and major roadways (dark green lines) are also shown. During the measurement period the prevailing winds were out of the NE at 10.25 mph.

Figure 10. Mobile monitoring PNC maps for a time period under different prevailing winds.

Publications
None

Outreach Efforts
None

Awards
None

Student Involvement
Two undergraduate students at Tufts University (Ida Weiss and Taylor Adams) and doctoral candidate (now postdoctoral associate) Tiffany Duhl have been trained on the air pollution monitoring equipment and are driving the TAPL as part of their degrees in environmental engineering.

Plans for Next Period
As a proposed task for the the next study period (October 1, 2021 to September 30, 2022), we will continue mobile monitoring, with an expansion to include monitoring of NO_2 and SO_2.

Task 4 - From FAA Essential Flight Activity, Compile Covariates Needed for Regression Modeling Under Project 18 and Dispersion Modeling Under Project 19 for a Data-Sharing Platform that Will Enable Comparisons Between Atmospheric Dispersion Models Implemented by Collaborators on ASCENT Project 19 and Monitored Pollutant Concentrations and Related Regression Models from Project 18

Boston University School of Public Health

Objective(s)

We are currently analyzing data from the 2017 stationary site monitoring campaign to provide insight regarding the ability of statistical analyses of real-time UFP concentration measurements to capture arrival aircraft source contributions to UFPs, providing a roadmap for future investigations. Thus far, our analyses indicate that we can explain significant variability in UFPs across multiple monitoring sites, with statistically significant terms for aviation flight activity as well as meteorology and other site attributes. We are also examining the contribution of aviation activity to UFP concentrations in communities. This task includes the concurrent collection of UFP concentrations at multiple sites, with sites selected specifically for the purpose of aircraft source attribution, the application of insight about detailed flight activity tracks, and the use of statistical methods to separate the aviation signal from other sources of UFPs.

Research Approach

The monitoring data and regression model outputs can directly inform UFP dispersion model development under ASCENT Project 19 directed by Dr. Sarav Arunachalam at the University of North Carolina. Under this task, we plan to work directly with Project 19 and improve both dispersion and regression modeling approaches to quantify arrival and takeoff aircraft contributions to UFP concentrations in communities near Logan Airport. In collaboration with Project 19, we will develop a data-sharing platform to provide UFP monitor data and to coordinate the collection of flight activity data to be used in both projects. The use of accurate and highly resolved flight activity data from the FAA (e.g., aircraft type, number of engines, engine type, latitude, longitude, elevation, tail number) is essential for both Projects 18 and 19 in the development of a UFP regression model and emission inventory for dispersion modeling, respectively. We will use Boston Tracon data and other related data as the foundation of the shared data inputs needed for both projects.

Using a shared data platform will allow us to (a) compare UFP and NO_2 monitoring data collected under Project 18 to SCICHEM and CMAQ dispersion model outputs developed under Project 19, (b) identify key predictors in both dispersion and regression modeling of UFPs, (c) use the same flight activity data and covariates to develop a regression model (Project 18) and dispersion model (Project 19) of UFPs, and (d) compare our results with dispersion model outputs. Future modeling efforts will incorporate mobile monitoring data to enhance the spatial resolution of UFP prediction. Comparisons of both project models will guide future efforts toward the development of a robust hybrid regression and dispersion model to predict fine-scale concentrations of aviation-attributable UFPs and other air pollutants.

Milestone

Monitoring site information and preliminary data are being shared with ASCENT Project 19.

Major Accomplishments

Monitoring site information and preliminary data are being shared with ASCENT Project 19.

Publications

None

Outreach Efforts

None

Awards

None

Student Involvement
None

Plans for Next Period
We will continue to share data and outputs with ASCENT Project 19. We are also collaborating to establish new sites for NO_2 and SO_2 monitoring under the next phase of this project.

Task 5 – In Year 1, Construct Regression Models Using 2017–2018 Data and the Flight Activity Data and Covariates Developed Under Task 4 to Determine the Contributions of Aviation Sources to UFP and BC Concentrations Measured During our 2017–2018 Monitoring Campaign; in Year 2, Analyze the Combined Mobile Monitoring and Stationary Data Collected Under Tasks 1–3 for the 2020 Sampling Campaign for Community-level Contributions from Aviation Sources

Boston University School of Public Health

Objective(s)
From 2017 to 2019, we conducted a monitoring campaign to inform an aviation source attribution analysis as an expansion of the regression model development in Task 1. In our 2020 report, we presented a preliminary analysis for regression modeling of source attribution for aviation-related UFP contributions. In this year's report, we leverage our new set of UFP measurements for a community near a major airport across multiple years to evaluate time trends and contributions from transportation sources by:

1. Analyzing PNC patterns before and during the COVID-19 pandemic to ascertain changes in transportation sector contributions and
2. Utilizing high-temporal resolution data, including wind speed and wind direction, to discern impacts from aviation activity, an intermittent but impactful UFP source.

Research Approach
Utilizing air pollution, flight activity, and meteorological data collected across multiple monitoring campaign years under ASCENT Project 18, we developed insights as part of our ongoing analyses of stationary site monitoring data collected during our initial 2017 monitoring campaign through 2021 by using the downturn in primary UFP sources (i.e., roads and aviation) to inform source attribution. We began by analyzing concentrations as a function of wind conditions and flight activity to help inform the structure and form of subsequent regression models. The contributions of aircraft to ambient UFP concentrations were preliminarily examined by comparing measurements obtained prior to the COVID-19 state of emergency declaration in Massachusetts (before April 2020), during the COVID-19 state of emergency (April–June 2020), and after the state of emergency (July 2020–June 2021). During the Massachusetts state of emergency, both vehicle and aviation travel was considerably reduced, presenting an opportunity to compare low transportation-related air pollution with previous normal operating conditions as well as to track a ramp-up for both aviation and vehicle activity. We can observe the contributions of aviation activity to community-level exposure by considering concentration patterns as a function of meteorological conditions and other key predictors across sites and pollutants using a natural experiment study design that captures incremental increases in aviation and vehicles at different time periods throughout the COVID-19 pandemic.

Milestone(s)
- Submitted a manuscript with descriptive data for publication in *Environmental Science and Technology*
- Completed regression modeling analysis of aviation-related contributions to community-level UFPs and presented our findings at conferences
- Drafted two additional manuscripts for submission on generalized regression modeling of aviation-related UFPs and machine learning regression modeling of UFPs

Major Accomplishments

Stationary monitor analysis of the COVID-19 lockdown period by wind direction: Here, we present a preliminary analysis of the monthly distribution of PNC compared with changes in source activity levels before and during the COVID-19 lockdown. Figure 11 identifies the Chelsea monitoring site in relation to the airport. The Chelsea site is located approximately 3 miles north of Logan International Airport.

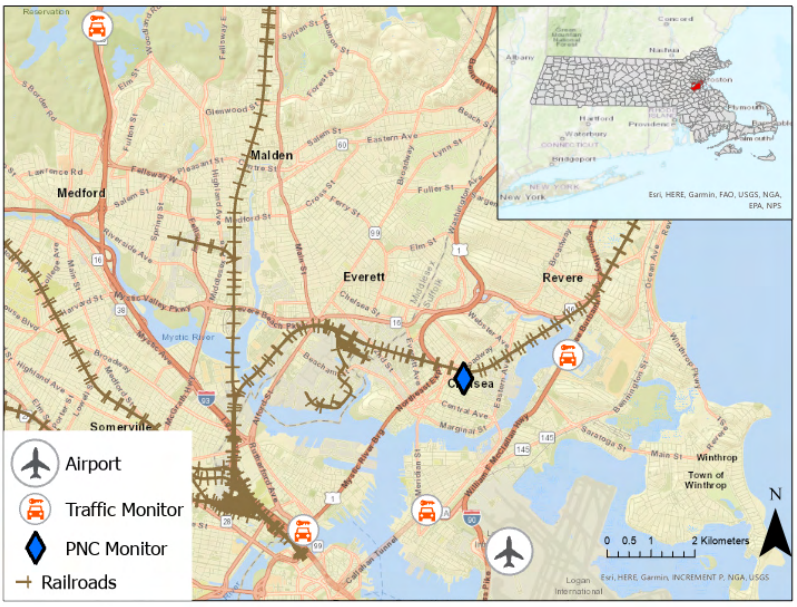

Figure 11. Map of the Chelsea monitoring site.

We have leveraged a set of UFP measurements in a community near a major airport across multiple years to evaluate time trends and contributions from transportation sources to analyze PNC patterns before and during the COVID-19 pandemic to ascertain changes in transportation sector contributions. We utilized high-temporal-resolution data, including wind speed and wind direction data, to discern impacts from aviation activity, an intermittent but impactful UFP source. Figure 12 presents a comparison of data analyzed during the last month, showing reductions in both vehicle and flight activity during the pandemic period.

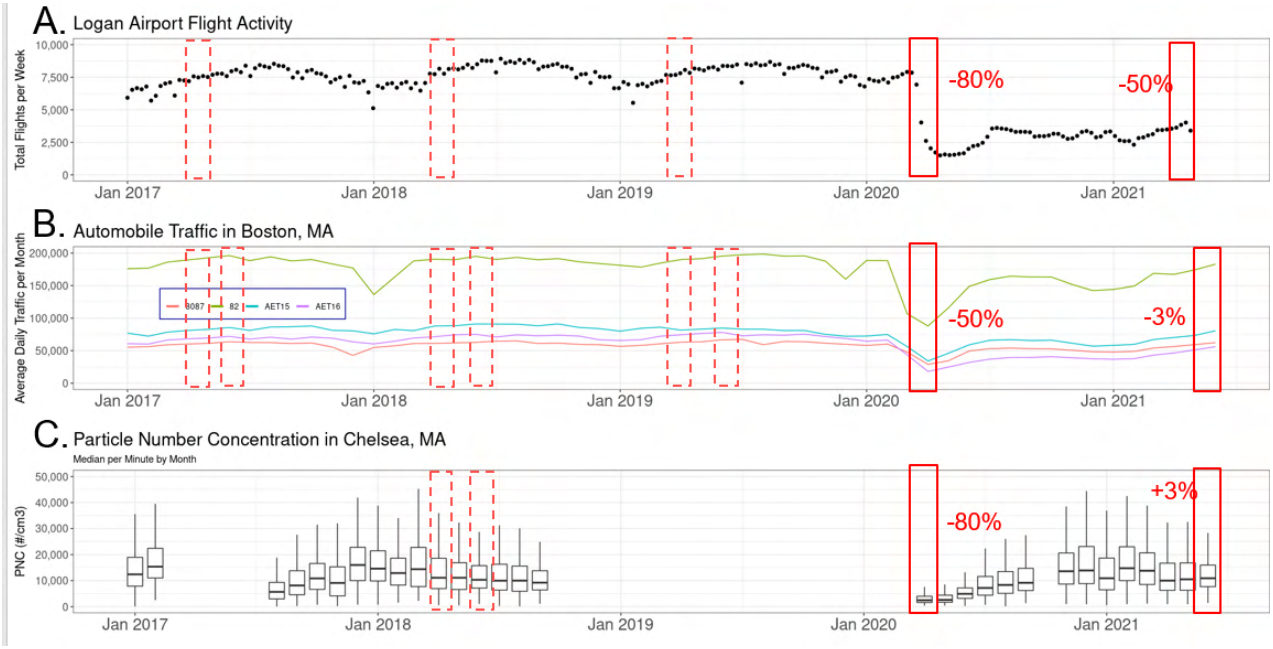

Figure 12. For the Chelsea site, 95th percentile UFP concentrations measured as the hourly 95th percentile of PNC by month for the 2017–2018 and 2020–2021 campaigns.

The 1-s-resolution PNC dataset was aggregated across several aggregation categories: the 25th percentile, average, median, 75th percentile, and 95th percentile per minute, resulting in a total sample size of 977,224 min of PNC data. The 1-min aggregated PNC data were merged with flight activity (1-hr resolution), meteorological (1-min resolution), and automobile traffic (monthly average traffic volumes) data. Figure 13 presents monthly polar plots of PNC that depict the 1-min average PNC by wind direction and wind speed for data collected during the 2017–2018 and 2020–2021 monitoring campaigns. Although formal statistical analyses are still underway, we can observe lower PNC values for April–August in 2020 compared with 2017 or 2018. Regression analysis with flight activity needs to be conducted to examine the contributions from aviation activity versus other sources during the pandemic.

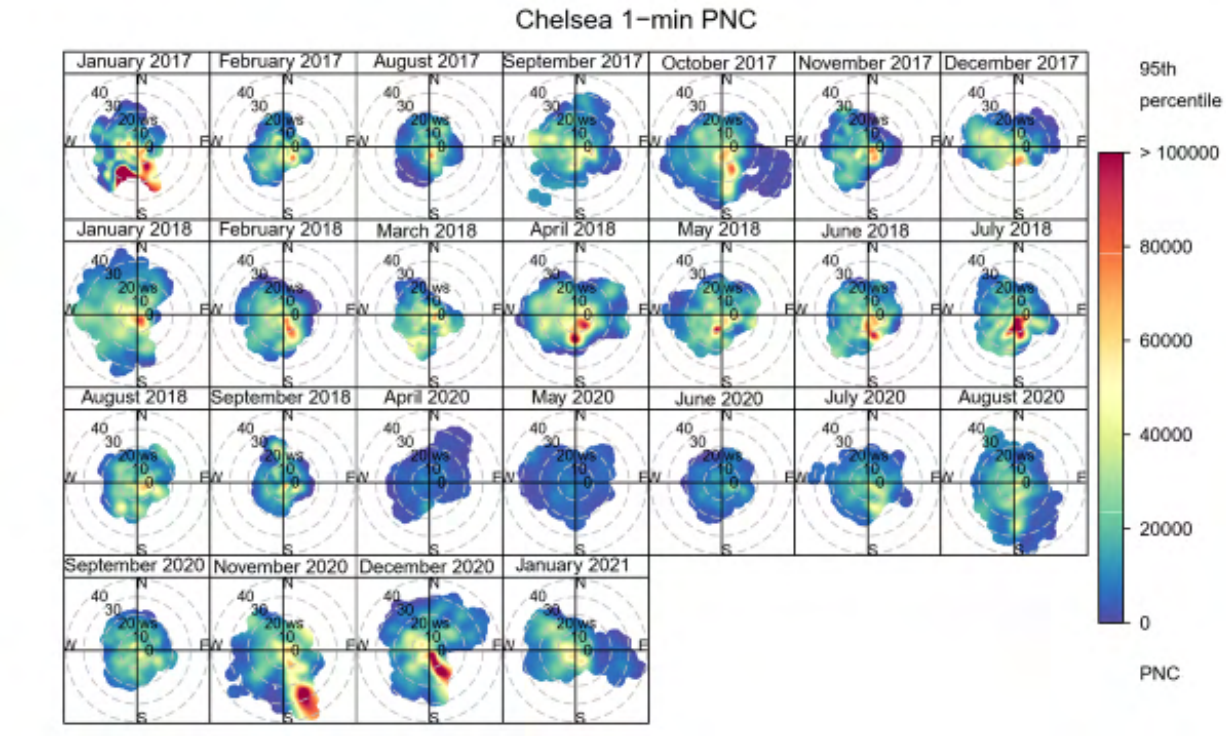

Figure 13. Chelsea UFP concentrations measured as the PNC by month for the 2017–2018 and 2020–2021 campaigns.

We are also tracking data on flight activity and traffic data during the different periods of monitoring to work toward regression modeling. Additional variables of interest associated with anthropogenic emissions were created, chiefly indicating whether the wind direction positioned the PNC monitor site downwind of the Logan Airport, referred to as an impact sector wind, previously defined as 128°–172° (Figure 14).

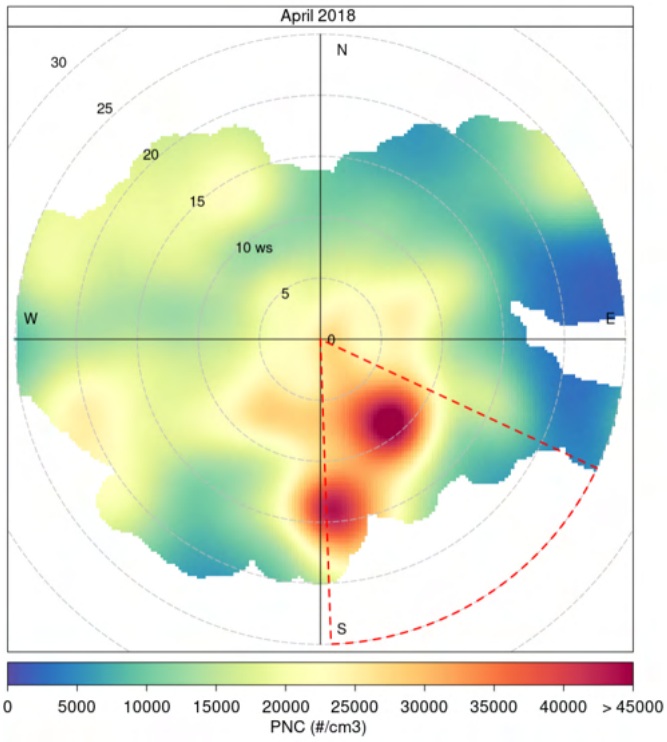

Figure 14. Polar plot of PNC, with the impact sector for the Chelsea site identified as a red dashed line.

To quantify the change in air pollution and transportation sector activity during the pandemic, we compared during-pandemic data to pre-pandemic data on a month-by-month basis to control for seasonal variations between the two time periods. We also detected more rapid changes in activity levels in response to the phased re-opening, which frequently changed on a weekly and monthly basis. Table 3 presents a comparison of the analyzed data, which presents drops in both the vehicle and flight activity during the pandemic period. Ratios of the impact sector versus non-impact sector PNC were consistent between median and 95th percentile 1-min aggregated PNC data for the pre-COVID-19 (2017–2018), lockdown (2020), and post-lockdown (2021) periods. The 95th percentile 1-min PNC values for the impact sector were 1.6 times higher than those of the non-impact sector for the pre-COVID-19 months of April, May, and June. The pre-COVID-19 April results showed the highest ratio of impact sector PNC (22,100 particles/cm^3) to non-impact sector PNC (12,600 particles/cm^3). During the initial lockdown months of April–June 2020, the impact sector PNC was 1.3 times greater than the non-impact sector PNC. For the post-lockdown period, one year after the initial lockdown period, the impact sector PNC was 1.5 times greater than the non-impact sector PNC. The ratio of impact sector to non-impact sector PNC was nearly the same for April–June 2020 and April–June 2021. During the post-lockdown period, the absolute magnitude of the non-impact sector PNC was nearly equal to the pre-COVID-19 non-impact sector PNC; however, impact sector PNC levels were lower during the post-lockdown period than during the pre-COVID-19 monitoring period.

Table 3. Comparison of PNC during the pre-COVID-19, COVID-19 lockdown, and post-lockdown periods by impact sector winds.

			Pre-COVID (2017-2018)	Lockdown (2020)	Post Lock down (2021)
95th and IQR (# / cm3)	April	Impact Sector	22100 [28200]	3800 [3100]	16800 [19000]
		Non-Impact Sector	12600 [14300]	2700 {2400]	12400 [15700]
	May	Impact Sector	18300 [23300]	3500 [2600]	15300 [16000]
		Non-Impact Sector	12700 [11800]	2800 [3000]	12400 [12300]
	June	Impact Sector	18800 [25500]	6800 [5300]	16600 [25700]
		Non-Impact Sector	11900 [11100]	5300 [4400]	12300 [10000]
			Pre-COVID (2017-2018)	Lockdown (2020)	Post Lock down (2021)
Median and IQR (# / cm3)	April	Impact Sector	19800 [23900]	3700 [3200]	14600 [16600]
		Non-Impact Sector	11100 [12200]	2500 [2200]	10300 [12900]
	May	Impact Sector	16900 [20200]	3300 [2600]	13100 [12900]
		Non-Impact Sector	11200 [10500]	2600 [2800]	10400 [10800]
	June	Impact Sector	16000 [21200]	6100 [4500]	14900 [21900]
		Non-Impact Sector	10400 [9400]	4800 [4000]	11000 [8500]
			Pre-COVID (2017-2018)	Lockdown (2020)	Post Lock down (2021)
Sample size (minutes)	April	Impact Sector	2981	445	1775
		Non-Impact Sector	39106	15897	28432
	May	Impact Sector	1452	666	1484
		Non-Impact Sector	26747	22463	35868
	June	Impact Sector	2379	2154	2466
		Non-Impact Sector	28890	26823	35403

Publications
None

Outreach Efforts
- Preliminary results were presented at the Seattle–Tacoma Airport Community Advisory Committee, September 2021.
- Results were presented at the FAA Aviation Emissions Characterization meeting, May 2021.

Awards
None

Student Involvement
Sean Mueller, a doctoral student at BUSPH, has been involved in field monitoring, data cleaning, and calculations of the COVID-19 UFP analysis.

Plans for Next Period

We are developing descriptive data plots of wind roses under various flight conditions to inform regression modeling. We will continue to develop new models that include NO_2 analysis. We are including mobile monitoring data in the 2020–2021 campaign to inform UFP source attribution over a wider spatial spread. This effort necessitates an analogous but slightly different statistical analysis approach, given concurrent spatial and temporal variations in concentrations. With each of these regression models, we will be able to estimate the amount of measured air pollution attributable to flight activity. In other words, by zeroing out the flight activity terms and determining the predicted concentrations, we will ascertain the portion of measured concentrations attributable to aircraft arrivals and departures. These predictions will be shared with Project 19, which is focused on the development of comparable estimates of aviation-attributable concentrations near Logan Airport, and we will conduct analyses to compare predictions from dispersion models and regression models.

Project 019 Development of Aviation Air Quality Tools for Airshed-Specific Impact Assessment: Air Quality Modeling

University of North Carolina at Chapel Hill

Project Lead Investigator

Saravanan Arunachalam, PhD
Research Professor
Institute for the Environment
University of North Carolina at Chapel Hill
100 Europa Drive, Suite 490
Chapel Hill, NC 27517
919-966-2126
sarav@email.unc.edu

University Participants

University of North Carolina at Chapel Hill

- PI: Saravanan Arunachalam, Research Professor and Deputy Director
- FAA Award Number: 13-C-AJFE-UNC, Amendments 1–15
- Period of Performance: October 1, 2020 to September 30, 2021
- Task: Develop a framework for a new dispersion model for aircraft sources

Project Funding Level

FAA provided $569,000 in funding. Matching cost-sharing was provided by EU-AVIATOR and the Environmental Defense Fund.

Investigation Team

Prof. Saravanan Arunachalam (UNC) (PI) [Task 1]
Dr. Chowdhury Moniruzzaman (UNC) (Co-Investigator) [Task 1]
Dr. Gavendra Pandey (UNC) (Co-Investigator) [Task 1]
Mr. Brian Naess (UNC) (Co-Investigator) [Task 1]
Mr. Praful Dodda (UNC) (Graduate Research Assistant) [Task 1]
Prof. Akula Venkatram (University of California, Riverside) (Consultant) [Task 1]

Project Overview

Aviation is predicted to grow steadily in upcoming years;[1] thus, a variety of aviation environmental policies will be required to meet emission reduction goals in aviation-related air quality and health impacts. Tools are needed to rapidly assess the implications of alternative policies for an evolving population and atmosphere. In the context of the International Civil Aviation Organization (ICAO), Committee on Aviation Environmental Protection (CAEP), additional approaches are required to determine the implications of global aviation emissions.

The overall objective of this project is to develop a new aircraft-specific dispersion model and continue the development and implementation of tools, both domestically and internationally, to allow for an assessment of year-to-year changes in significant health outcomes. These tools must be acceptable to the FAA (in the context of Destination 2025) and/or other decision-makers. More importantly, this new model must have the capability to address the 1-hour form of the NO_2 National Ambient Air Quality Standard (NAAQS) in the United States (U.S.) and to support National Environmental Policy Act (NEPA)

[1] Boeing Commercial Airplane Market Analysis, 2010.

and/or NAAQS analyses that may be needed by airports. The developed methods must also rapidly provide output to support a variety of "what-if" analyses and other investigations. While the tools for use within and outside the United States need not be identical, a number of goals are desirable for both cases:

- Enable the assessment of premature mortality and morbidity risks due to aviation-attributable particulate matter (PM) with a diameter up to 2.5 μm ($PM_{2.5}$), ozone, and other pollutants known to exert significant health impacts;
- Capture airport-specific health impacts at regional and local scales;
- Account for the impact of landing/takeoff (LTO) versus non-LTO emissions, including a separation of effects;
- Allow for an assessment of a wide range of aircraft emission scenarios, including differential growth rates and emission indices;
- Account for changes in nonaviation emissions;
- Allow for assessments of sensitivity to meteorology;
- Provide domestic and global results;
- Include quantified uncertainties and differences with respect to Environmental Protection Agency (EPA) practices, which are to be minimized when scientifically appropriate; and
- Ensure computational efficiency such that tools can be used in time-sensitive rapid turnaround contexts and for uncertainty quantification.

During this period of performance, the (UNC) Institute for the Environment (UNC-IE) team performed work on a single task with four subtasks, as described below.

1. Develop a new dispersion model for aircraft sources with four subtasks:
    1. Source Characterization
    2. Physical Processes
    3. Chemical Processes
    4. Model Evaluation

Task 1 – Develop a Framework for a New Dispersion Model for Aircraft Sources

University of North Carolina at Chapel Hill

Objective(s)

The FAA's Aviation Environmental Design Tool (AEDT) is currently coupled with the U.S. EPA's AERMOD dispersion model for modeling aircraft sources and is the required regulatory model in the U.S. for modeling airport-level aircraft operations during LTO cycles.

Recent studies have shown several limitations in the use of AERMOD for modeling aircraft sources. In 2011, the Airport Modeling Advisory Committee (AMAC) developed a series of recommendations to improve jet exhaust modeling. Since then, Airport Cooperative Research Program (ACRP) project 02-08 has developed guidance for airport operators on conducting measurements and modeling for air quality at airports, published in ACRP Report 70 (Kim et al., 2012). This study conducted a measurement and modeling study at Washington Dulles International Airport (IAD). More recently, ACRP project 02-58 developed a final ACRP Report 171 (Arunachalam et al., 2017a) for providing dispersion modeling guidance for airport operators regarding local air quality and health. This study applied four dispersion models—AERMOD, CALPUFF, SCICHEM, and the U.K.'s ADMS-Airport—for the Los Angeles International Airport (LAX) and compared model predictions with high-resolution measurements taken during the Los Angeles Air Quality Source Apportionment Study (AQSAS). Each of these reports identified several limitations with AERMOD and developed a series of recommendations for improving dispersion modeling of aircraft emissions for airport-level air quality.

UNC recently developed the C-AIRPORT dispersion model for application to LAX (Arunachalam et al., 2017c). Initially, C-AIRPORT was designed to be part of the C-TOOLS series of community-scale, web-based modeling systems. The objective of C-TOOLS was to create a web-based interface to model multiple source types for short-term or long-term pollutant concentration averages and to perform various what-if scenarios that assess changes in air quality at local scales due to changes in inputs. C-AIRPORT uses a line-source-based approach to model aircraft sources, based upon the C-LINE modeling system (Barzyk et al., 2015), and a preliminary evaluation of the algorithms in comparison with LAX AQSAS was conducted.

Under the previous year's funding, UNC-IE developed a comprehensive plan for a modeling framework that addresses known limitations from the above Tasks and proposed a viable, more suitable approach for modeling pollutants from aircraft sources. The primary objective of this plan is to demonstrate that a robust, improved pollutant dispersion model for aircraft can be developed for U.S. regulatory compliance purposes. The proposed new model will disperse pollutants from aircraft sources in a more technically and scientifically advanced manner (compared with current AERMOD capabilities), with the ultimate goal of use as a potential U.S. regulatory compliance tool, based on ongoing discussions between the FAA and EPA. This plan will include an itemized list of known limitations along with a corresponding proposed developmental approach providing recommendations on how to address these limitations.

As part of this Task, we proposed implementing the plan with specific focus on four broad areas over a period of two years.

Our approach aims to ensure that the new model will be "robust" and based on the state of science on source and plume characterization and associated algorithms.

1) **Source Characterization**
   In this area, we explore alternate options beyond the current area-source-based approach in the AERMOD model. Some approaches we explored include:
   - Volume treatment in AERMOD,
   - Puff-based treatment, as in SCICHEM,
   - Line-based treatment, as in C-AIRPORT, and
   - Line-puff or jet sources, as in ADMS-Airport.
2) **Physical Process Assessment**
   In this area, we assess all relevant processes for aircraft dispersion, including the treatment of plume rises, wing tip vortices, and low-wind-speed conditions. Some specific approaches include:
   - A coupled plume rise-wake model for assessing the effects of wake vortices on plume rise, dispersion, and ground-level concentrations and
   - An integral approach called the fluid-mechanical entrainment model (FEM), which has been evaluated against light detection and ranging (LIDAR) observations from Heathrow Airport (see Arunachalam et al., 2017a).
3) **Chemical Process Assessment**
   We will go beyond the initial implementation from last year, with a specific focus on the following aspects:
   - Recognition that the 1-hr form of the NO_2 NAAQS is a critical issue for air quality around U.S. airports, with several modeling studies showing overestimates of these compared with observations; it is important that the new model performs adequately to capture this short-term form of the NO_2 NAAQS;
   - A new detailed chemical mechanism for NO_2 including the generic reaction set (GRS) mechanism (Venkatram et al., 1994; Valencia et al., 2017) or others; and
   - A condensed version of the aerosol treatment, as included in CMAQ and SCICHEM and described by Chowdhury et al. (2015).
4) **Model Evaluation**
   Ongoing model evaluation has involved evaluating model predictions using only measurements from the LAX AQSAS for 2012. We will now work to develop and test the model for other case studies, including the following:
   - One of three airports (Copenhagen, Madrid, and Zurich) with measurements being undertaken as part of the EU-AVIATOR project (see https://aviatorproject.eu/) and
   - The Long Island Sound Tropospheric Study (LISTOS) project-based high-resolution measurements of NO_2 (and other pollutants) around the John F. Kennedy (JFK) International Airport in New York City (see https://ui.adsabs.harvard.edu/abs/2018AGUFM.A34B..01M/abstract).

   Model evaluation will focus on the model's ability to capture the behavior of the plume related to aircraft sources during LTO cycles at an airport in comparison with available observations and identifying strengths and weaknesses compared with other existing models.

Research Approach

In this report, we describe progress made on the four subtasks. Results from Subtask 1d are embedded in the descriptions for Tasks 1a–1c.

1. Source Characterization

1.1 Emissions Processing of AEDT Emissions (AEDT2ADM)

A Python-based emission processor, named "AEDT2ADM", has been developed to produce emission files of both new ADM and AERMOD dispersion models using AEDT flight segment data. We have updated the emission processor and evaluated the flight segment data for both winter and summer 2012 AEDT files.

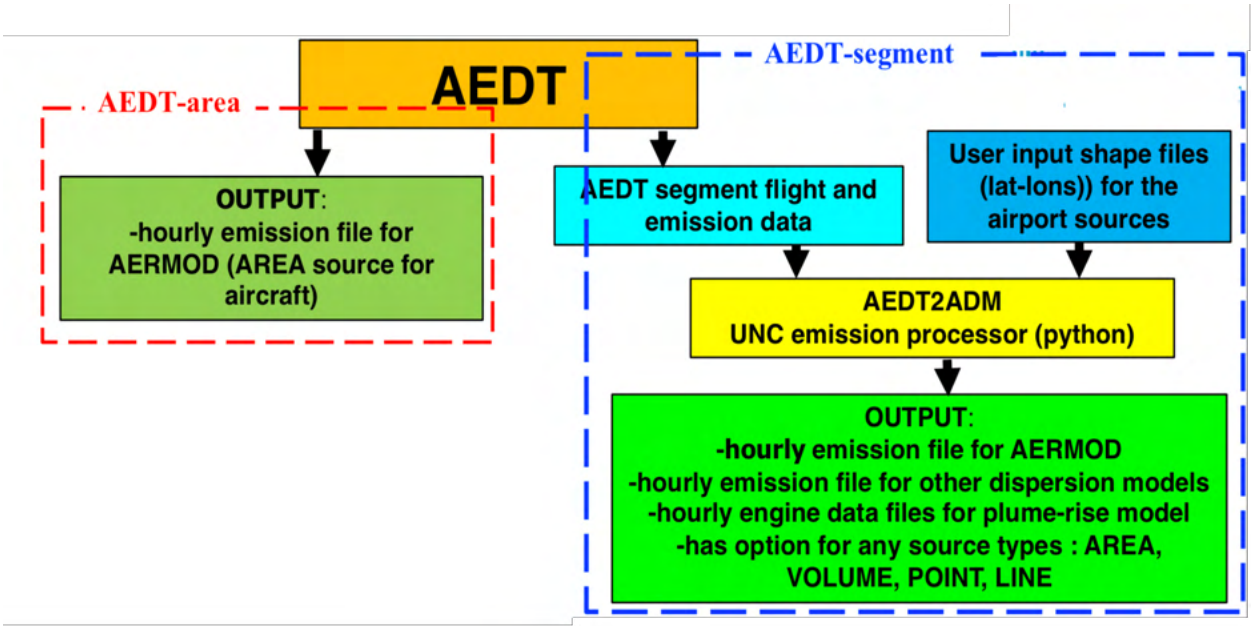

Figure 1.1. Schematic of the input/output data flow for the AEDT2ADM emission processor.

1.1.1 Update of the AEDT2ADM emission processor

The AEDT2ADM emission processor has been updated to include multiple new features since the last version reported in the UNC's ASCENT 2020 annual report. The new updates are described in section 1.1.1.1 to 1.1.1.5.

1.1.1.1 Added capability to produce emission files for all species for all dates in a single run

The 2020 version of the code was designed for only two species (NO_x and SO_x) and for only a single day. The code needed to run 29 times for 29 days to produce February 2012 data. The AEDT2ADM emission processor has been updated and can now produce emission files for all species present in the AEDT segment files for each day for an entire time period in a single run.

1.1.1.2 Added capability to produce ADM-formatted emission files

The AEDT2ADM emission processor has been updated to produce emission files in the desired format for ADM models.

1.1.1.3 Increase of spatial resolution of the surface source design

AEDT2ADM has been updated so that the user can provide source files (latitude and longitude of each area source) based on the user's source design. In this way, AEDT2ADM now has the capability to increase or decrease the spatial resolution of sources. The 138 surface sources in the latest version are shown in Figure 1.2, where sources are grouped in 5 categories shown in 5 colors.

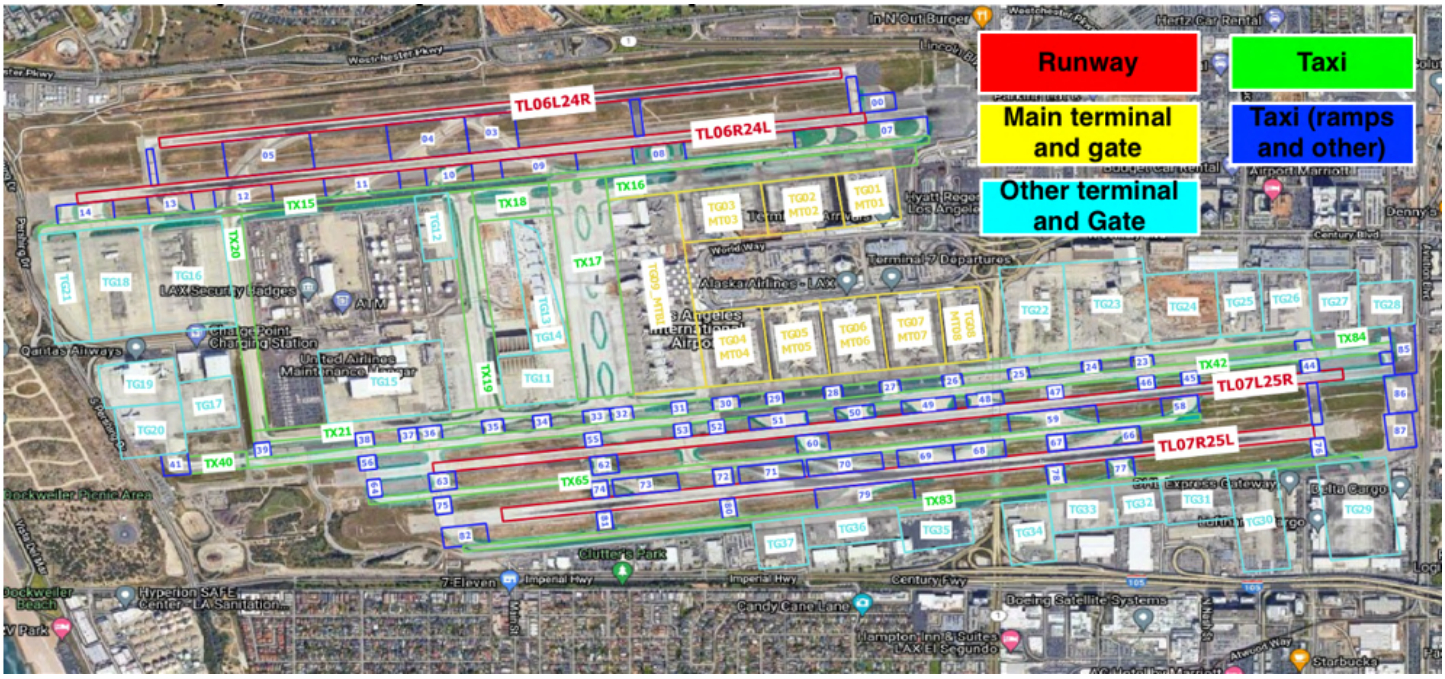

Figure 1.2. The 138 surface sources for LAX for the AEDT2ADM emission processor.

A sensitivity study was performed in which three sensitivity runs for the following three cases were performed by three AERMOD run cases:

- AEDT-area: 1440 area sources
- AEDT2ADM: 138 surface sources
- AEDT2ADM: 31 surface sources

A sensitivity study was performed to determine the model performance for these three source-number cases. The sensitivity results on the effect of a reduced number of surface sources on surface pollutant concentration in AERMOD dispersion modeling (Figure 1.3) showed that although the number of sources decreased from 1440 to 138 and to as few as 31, the diurnal profile showed little change from the results for the case of AEDT with 1440 surface sources.

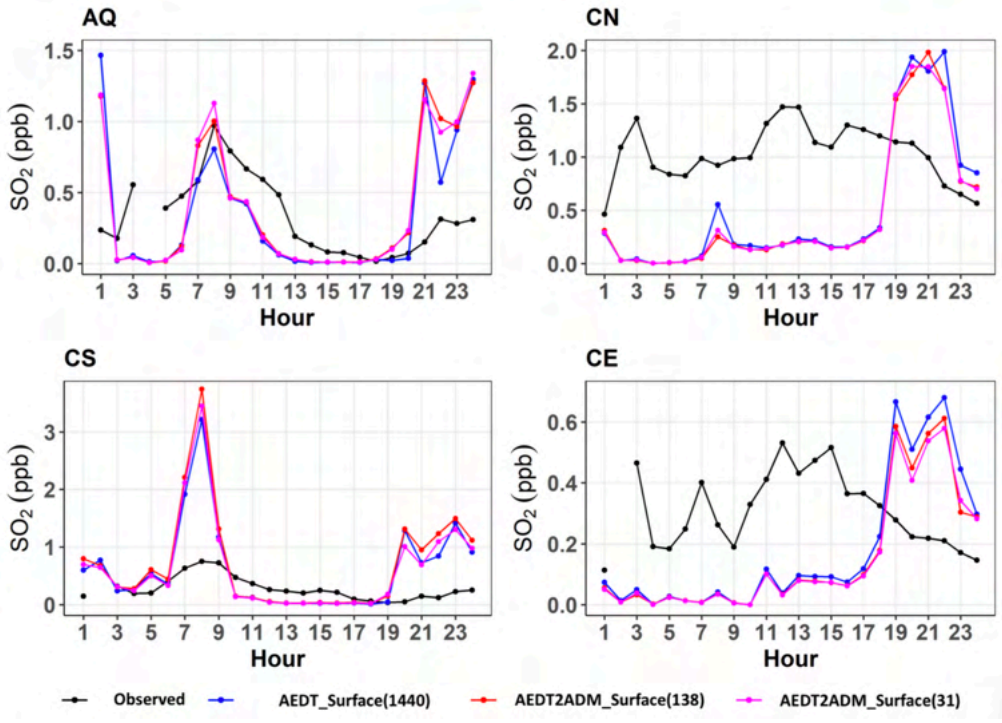

Figure 1.3. Diurnal profiles of SO_2 concentrations for one-month average data for each hour for three source-number cases: (1) AEDT 1440 surface sources (blue line), (2) AEDT2ADM 138 surface sources (red line), and (3) AEDT2ADM 31 surface sources for LAX in February 2012.

AERMOD modeling results for one month (February 2012) showed that a 90% surface source reduction (from 1440 to 138) decreased the computation time by 90% and increased the mean absolute error (MAE) by 3.5% and 12.3% at the AQ (Air Quality) and CS (Community South) sites and decreased the MAE by 2.8% and 4.8% at the CN (Community North) and CE (Community East) sites, respectively. A 98% reduction in surface sources (from 1440 to 31) decreased the computation time by 95% and increased the MAE by 3.9% and 1.2% at AQ and CS and decreased the MAE by 3.2% and 5.2% at CN and CE, respectively.

1.1.1.4 Added capability to produce emission files for AERMOD

The AEDT2ADM emission processor has been updated to produce emission files for AERMOD for user-provided surface source shape (latitude–longitude) files.

1.1.1.5 Added capability to produce aircraft-engine data files for the plume rise model for ADM

We updated the Python emission processor code AEDT2ADM and produced five ADM-formatted hourly average aircraft engine variables for the plume rise model. The five engine variables are:

- Fuel burn rate (segment number average fuel burn rate over one hour for a source),
- Thrust (fuel-burn-weighted average thrust for all segments over one hour for a source),
- Aircraft speed (segment number average aircraft speed over one hour for a source),
- Bypass ratio (average bypass ratios for all segments over one hour for a source) from AEDT data files, and
- Air–fuel ratio (average air–fuel ratios for all segments over one hour for a source) estimated for four LTO scenarios from a reference paper (Wayson et al., 2009).

The fuel burn rate, thrust, and aircraft speed for one source's data are shown in Table A1 in Appendix A for the plume rise model, whose values seem reasonable. The thrust (fuel-burn-rate-weighted average thrust for all segments over one hour for

a source) was compared with the segment number average thrust of a Boeing 737-300 aircraft engine from the AEDT-segment data file, as shown in Figure A1 in Appendix A, which shows hourly average thrust values within the normal range.

The newly developed plume rise model was applied to AEDT-segment data for different flights. We compared the average buoyancy for different segments for five different aircrafts with reported values for ADMS-Airport (https://www.cerc.co.uk/environmental- software/ADMS-Airport-model.html), as shown in Figure 1.4. The buoyancy was similar to results obtained by ADMS-Airport for B737 and B777, with an underprediction for B747 and an overprediction for A320 and A330, as shown in Figure 1.4. The buoyancy equation in the latest plume rise model successfully produced the buoyancy trend for aircraft engine size, where the largest engine (B777) has the highest buoyancy, which is consistent with the ADMS-Airport model results shown in Figure 1.4.

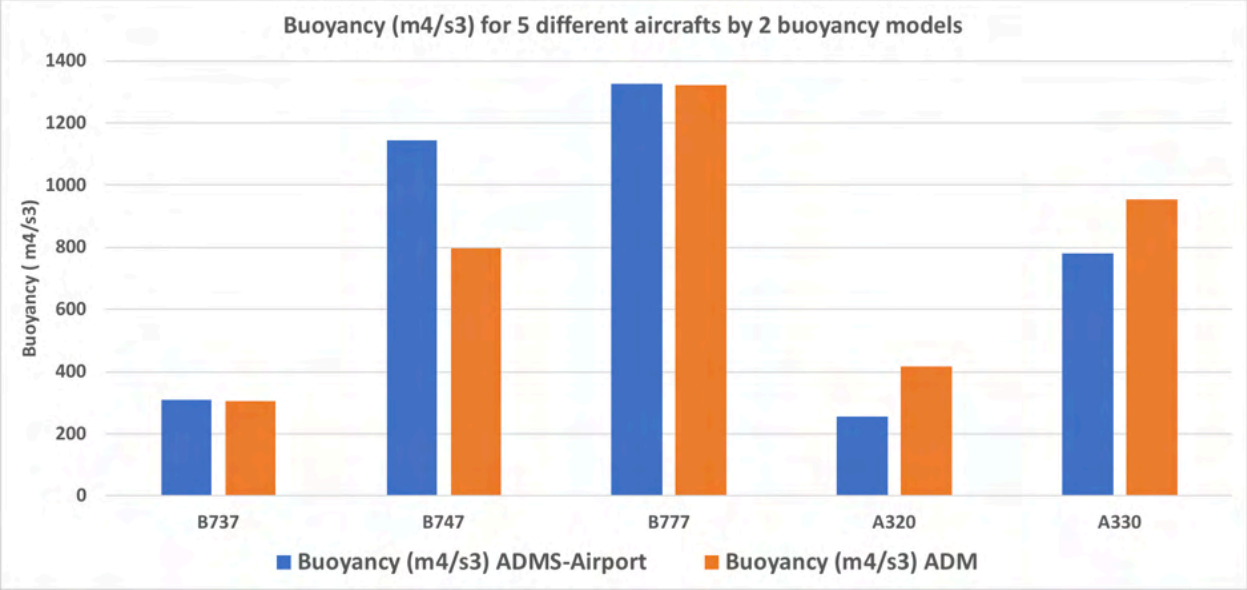

Figure 1.4. Comparison of buoyancy for the ADM with ADMS-Airport models (https://www.cerc.co.uk/environmental-software/ADMS-Airport-model.html) for five different aircraft.

1.1.2 Evaluation of winter and summer 2012 AEDT-segment data files

The values of variables in the summer and winter 2012 AEDT-segment files have been evaluated through a comparison with reference or typical values. Some findings are summarized in subsections 1.1.2.1–1.1.2.3.

1.1.2.1 Removal of zero-duration segments

The winter 2012 AEDT-segment data file has some rows with a zero value for "Duration." Analysis of the zero-duration segments provided the following findings:

- There are 1,815 zero-duration segments among 1,996,543 segments for 29 days in the February 2012 file, corresponding to 0.09%, as shown in Table A2 in Appendix A.
- In our initial postprocessing, we removed these 1,815 zero-duration ("00:00:00.00") segments from the main file and produced an emission inventory, which may have caused a 0.09% reduction in NO_x and SO_x emissions.
- Removing the 0.09% of segments may not cause any problems in the emission inventory.

1.1.2.2 Negative thrust

The winter and summer AEDT-segment data files have some rows with negative thrusts. A comprehensive analysis was performed on the negative thrust values and was described in a report to the FAA. Our findings were as follows:

- Approximately 1.7% of the segments in a 1.5-month winter file and 5.7% of segments in a 2-month summer file had negative thrusts for all altitudes, and approximately 1.4% and 2.3% of segments within LTO (3,000 ft) height had negative thrusts for one specific day in the winter and summer files, respectively, as shown in Table 1.1.
- The winter file had negative thrust values both at the surface and in air, but the summer file had negative thrust values only in air, as shown in Table A3 (can be seen in the minimum altitude for negative thrust segments in the winter and summer files).
- Analysis of the winter 2012 data file showed both civilian aircrafts and military aircrafts with negative thrusts.

Table 1.1. Number of segments with negative thrust values in winter and summer 2012 AEDT data files for LAX.

Files	Height	Total no of segments	No of negative thrust segments	% Negative thrust segments
Winter 2012 files				
1.5 months winter file	all height	3,603,655	62,155	1.72
1 day: Feb 1, 2012	all height	84,047	1,555	1.85
1 day: Feb 1, 2012	LTO height (<3000 ft)	62,485	898	1.44
Summer 2012 files				
2 months summer file	all height	5,983,658	315,176	5.27
1 day: July 1, 2012	all height	93,715	4,983	5.32
1 day: July 1, 2012	LTO height (<3000 ft)	64,573	1,531	2.37

1.1.2.3 Comparison of winter and summer 2012 AEDT-segment files

A comprehensive analysis has been performed to evaluate the winter and summer 2012 AEDT-segment files for LAX.

a. Comparison of non-emission parameters

We reviewed the FAA-AEDT summer file and compared it with the winter file, whose summary is given in Table A4 in Appendix A. The comparison shows that the AEDT-segment summer file has 126 variables whereas the winter file has 38. The summer file has 6 million rows for 2 months of data whereas the winter file has 3.7 million rows for 1.5 months of data. The summer file has two useful variables: (1) the number of engines per aircraft and the bypass ratio, which will be used to calculate air mass flow rate; and (2) the propulsion efficiency, which will be used in the plume rise model. The AEDT-area (AERMOD) summer file has three species (NO_x, SO_x, and CO), and the winter file has two species (NO_x and SOx). The AEDT-area (AERMOD) summer file has 21,660 sources whereas the winter file has 5,919 sources.

b. Comparison of emissions

The total emissions of all species have been compared between the winter and summer files. A summary of the comparison for SO_x and NO_x only is given in Tables A5 and A6 in Appendix A, respectively. The results of the comparison of other species can be shared with the FAA upon request. Some findings for SO_x and NO_x are as follows:

- **SO_x and NO_x emissions in winter and summer files**
  - The SO_x emission rate is approximately 27% lower for surface + air, 18% lower for surface only, and 35% lower for air only in the summer file than in the winter file, as shown in Table A5 in Appendix A.
  - The NO_x emission rate is approximately 40% lower (for surface + air, surface only, and air only) in the summer file than in the winter file, as shown in Table A6 in Appendix A.

- **Comparison of emission rates in winter and summer files with reference values**
  - The NO_x and SO_x emission rates for the winter file are consistent with the LAWA2013 report (Arunachalam et al., 2013) and Next-Gen JPDO report (CSSI, 2009), as shown in Tables A5 and A6 in Appendix A, respectively.
  - Instances in which both the NO_x and SO_x emission rates in the summer file are inconsistent with the LAWA2012 summer values are shown in Tables A5 and A6 in Appendix A, respectively.
- **Comparison of emissions below and above 3,000 ft**
  - SO_x emissions were 68% below 3,000 ft and 32% above 3,000 ft for both the winter and summer files, as shown in Table A5 in Appendix A.
  - NO_x emissions were 58% below 3,000 ft and 42% above 3,000 ft for both the winter and summer files, as shown in Table A6 in Appendix A.

1.2 Area-S vs. Area-A vs. Volume Characterization

In aircraft dispersion modeling, characterization of the aircraft sources presents a challenging problem. To address this issue, we performed a sensitivity analysis based on source treatments such as AREA and VOLUME in the AERMOD dispersion model. For this task, we used SO_2 aircraft emissions from AEDT-area (directly generated by AEDT) and AEDT-segment (generated from AEDT2ADM). Here, we modeled only the aircraft sources. AERMOD results from AREA and VOLUME sources were compared with each other and with observed concentrations reported in the LAWA study for February 2012. The simulated results are presented in the form of diurnal plots and quantile–quantile (Q-Q) plots with a fractional bias (FB) based on the robust highest concentration and factor of two (FAC2) for the observations. The following results were obtained using 1) AEDT-Area emissions, and 2) AEDT-Segment emissions.

1.2.1 AEDT-area emissions

- The diurnal concentration behaviors are similar for both source treatments (AREA and VOLUME) at all sites due to the large number of VOLUME sources (Figure 1.5 (a)).
- For VOLUME source treatment, the model's ability to predict low SO_2 concentrations improved slightly, approaching a one-to-one line at all sites except CN (Figure 1.5 (b)).
- FAC2 improved from 14%, 21%, and 22% to 20%, 55%, and 38% at the AQ, CS, and CE sites, respectively, under VOLUME source treatment (Figure 1.5 (b)).
- The FBs for both source treatments are comparable for all four core sites (Figure 1.5 (b)).

1.2.2 AEDT-segment emissions

- Significant changes were observed in diurnal concentration behavior at all sites, especially the CS site, under the AEDT-segment-based VOLUME source treatment. These differences are likely due to the lower number of volume sources (Figure 1.5).

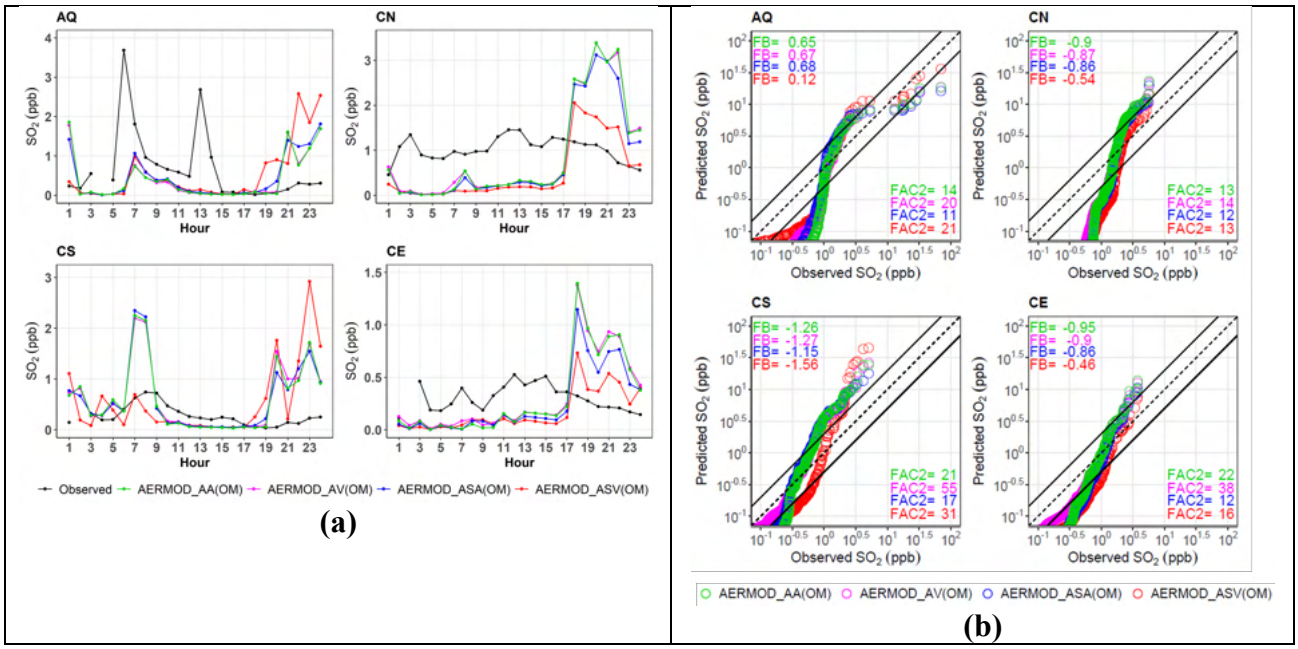

Figure 1.5 (a) Diurnal variability between observed and modeled SO_2 concentrations. **(b)** Q-Q plots for observed and predicted SO_2 concentrations for February 2012 at all four core sites (AQ, CN, CS, and CE). AA-AEDT: area-area source treatment; AV-AEDT: area-volume source treatment; ASA-AEDT: segment-area source treatment; ASV-AEDT: segment-volume source treatment; OM: original meteorology.

In addition, we conducted a sensitivity analysis based on the number of runway sources in AEDT-segment emissions. Here, we have depicted only the diurnal behavior of SO_2 predictions at the CS site (Figure 1.6). We found that as we increase the number of volume sources from 15 to 128, the results from VOLUME source treatment capture the characteristic patterns of diurnal concentrations obtained via AREA source treatment (Figure 1.6). Hence, the use of a larger number of volume sources enhances accuracy, and the results are comparable to those obtained from area sources.

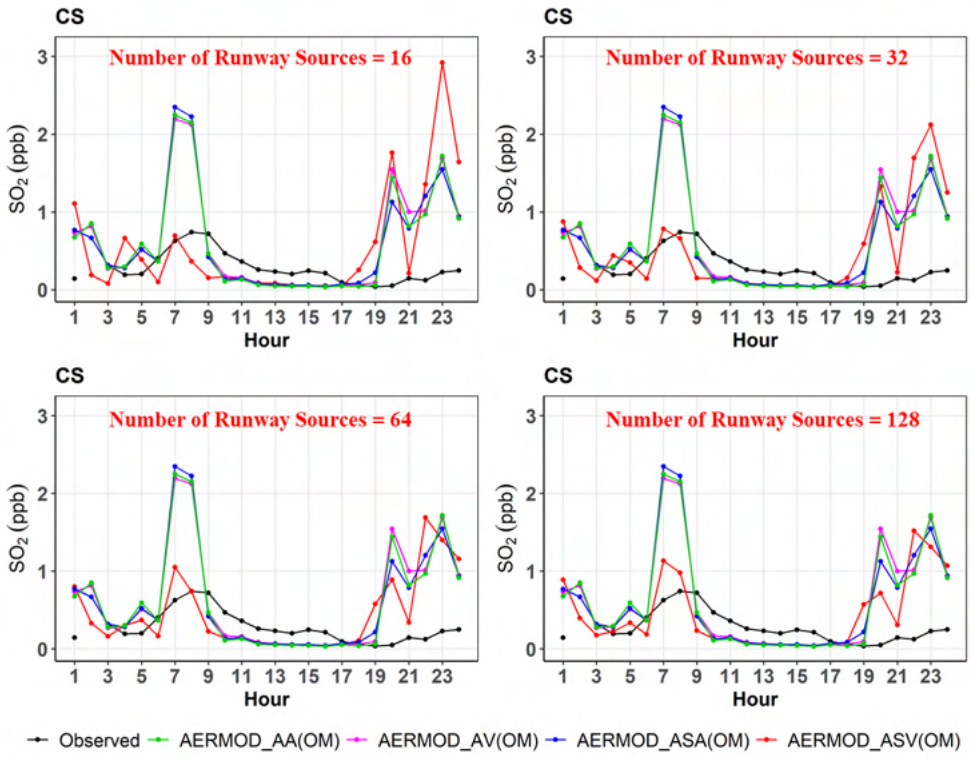

Figure 1.6. Diurnal variability between observed and modeled SO_2 concentrations for February 2012 at all four core sites (AQ, CN, CS, and CE). The notations are the same as those in Figure 1.5.

2. Physical Process Assessment

2.1 Plume Rise Treatment

In view of the incompleteness of the dispersion models used in aircraft dispersion modeling, we have developed a plume rise algorithm that builds upon our current understanding of the plume rise of emissions from stationary point sources.

The buoyancy parameter, F_b, that governs the plume rise from a point source is associated with energy output from an aircraft engine. The buoyancy parameter, F_b, of the exhaust plume is given by the following expression (Briggs, 1965):

$$F_b = \frac{g}{T_a} v_e r_0^2 \left(T_e - T_a\right), \quad (1)$$

where v_e and T_e are the velocity and temperature of the exhaust plume, T_a is the ambient temperature, and g is the acceleration due to gravity. The plume rise, h_{pb}, associated with a buoyant release from a point source in a neutral atmosphere is given by (Briggs, 1965):

$$h_{pb} = \left(\left(\frac{r_0}{\beta} \right)^3 + \frac{3}{2\beta^2} \frac{F_b}{U_{eff}^3} x^2 \right)^{1/3} - \left(\frac{r_0}{\beta} \right), \quad (2)$$

where $\beta = 0.6$ is an entrainment constant, x is the effective distance between the source and receptor, U_{eff} is the effective velocity within the plume, and r_0 is the initial radius of the plume. The final plume rise is calculated with the aid of two main plume rise parameters, such as buoyancy and momentum-induced plumes.

2.1.1 Computation of the buoyancy parameter from engine characteristics

Equation (1) for the buoyancy parameter can be written in terms of Q_e, the thermal power added to the air passing through the engine:

$$F_b = \frac{g}{T_a}\frac{Q_e}{\pi\rho_e C_p}, \quad (3)$$

where ρ_e is the exhaust density and C_p is the specific heat of the exhaust gas, which is mostly air.

After applying an energy balance for Q_e and performing further calculations for the thermal efficiency (η_t), we obtain the final buoyancy parameter term as:

$$F_b = \frac{g}{T_a}\frac{\dot{m}_f H_f \left(1-\eta_t\right)}{\pi\rho_e C_p}, \quad (4)$$

where the exit density, ρ_e, is computed from the energy conservation equation and the equation of state:

$$T_e = T_a + \frac{Q_e}{\dot{m}C_p}$$

$$\rho_e = \frac{p_a}{R_a T_e}. \quad (5)$$

Here, T_e is the average temperature of the exhaust gases, p_a is the ambient pressure, and R_a is the gas constant of air. We see that the inputs required to compute F_b are the thrust T, aircraft velocity v_a, fuel burn rate $\dot{m}_f$, air–fuel ratio AF, and engine bypass ratio, $bypr$.

2.1.2 Computation of jet momentum term

We assume that the horizontal momentum is conserved as the radius of the horizontal plume grows with distance from a stationary point within the area source. For a top-hat profile of velocity within the plume, the momentum balance can be written as:

$$\rho_p U_p \left(U_p - U_a\right)\pi r^2 = T, \quad (6)$$

where U_p is the velocity inside the plume relative to a stationary observer, U_a is the ambient velocity at the level of the plume, and ρ_p is the plume density. The initial momentum flow inside the plume is the thrust, T, exerted by the engine on the air. A version of this equation is derived in the appendix of Arunachalam et al. (2017).

As in Barrett et al. (2013), we assume that the radius of the jet exhaust grows linearly with distance from a point within the area source:

$$r = \alpha x + r_0, \quad (7)$$

where α is an entrainment constant and r_0 is the radius of the engine exhaust. The radius of the momentum plume is taken to grow until the difference between the plume and ambient velocities is comparable to the standard deviation of the ambient horizontal velocity fluctuation, $\sigma_u = 2.0u_*$, where u_* is the surface friction velocity. Then, the maximum plume radius is given by the following relationship:

$$T = \pi\rho_a r_m^2 \left(U_a + \sigma_u\right)\sigma_u, \quad (8)$$

where U_a is evaluated at $z = r_m$ and ρ_a is the ambient density. Then, r_m is given by:

$$r_m = \left(\frac{T}{\pi\rho_a (U_a + \sigma_u)\sigma_u}\right)^{1/2}. \quad (9)$$

The plume rise associated with momentum, h_{pm}, is taken to be the radius of the plume:

$$h_{pm} = r_0 + \alpha x \quad x \le x_m$$
$$= r_m \qquad x > x_m \,, \tag{10}$$

where x_m is the distance at which the radius reaches its maximum value:

$$x_m = \frac{(r_m - r_0)}{\alpha} \,. \tag{11}$$

The effect of buoyancy is considered by assuming that the buoyancy acts independently on the expanding jet plume.

We estimate the plume rise associated with buoyancy by applying a formulation applicable to point releases in a neutral atmosphere (Briggs, 1965):

$$h_{pb} = \left(\left(\frac{R}{\beta} \right)^3 + \frac{3}{2\beta^2} \frac{F_b}{U_{eff}^3} x^2 \right)^{1/3} - \left(\frac{R}{\beta} \right) \,, \tag{12}$$

where $\beta = 0.6$ is an entrainment constant, x is the effective distance between the area source and receptor, and U_{eff} is the effective velocity, which is taken to be the maximum of the velocity in the jet and the ambient velocity at plume height.

The buoyant plume rise interacts with that associated with horizontal momentum through the initial radius, R, in Equation (12). It is taken to be the average value of the radius of the momentum plume between 0 and x to account for the impact of momentum on the initial radius of the buoyant plume:

$$R = \frac{1}{x} \int_0^x r(x) dx \,, \tag{13}$$

which yields

$$R = r_0 + \alpha x / 2 \qquad x \le x_m$$
$$R = \frac{x_m}{x} \left(r_0 + \frac{\alpha x_m}{2} \right) + r_m \left(1 - \frac{x_m}{x} \right) \qquad x > x_m \,. \tag{14}$$

The buoyancy parameter, F_b, is computed from the equations described above. Equation (12) must be solved iteratively because the wind speed at the plume height is not known a priori.

The total plume rise is then:

$$h_p = h_{pb} + h_{pm} \,, \tag{15}$$

where the second term on the right-hand side is the plume rise associated with the momentum jet, given by Equation (10).

From Figure 2.1, we can clearly see how the plume rise varies with downwind distance for takeoff and landing for an individual area source. The maximum plume rise reaches 70 m for takeoff, whereas it reaches approximately 45 m for landing.

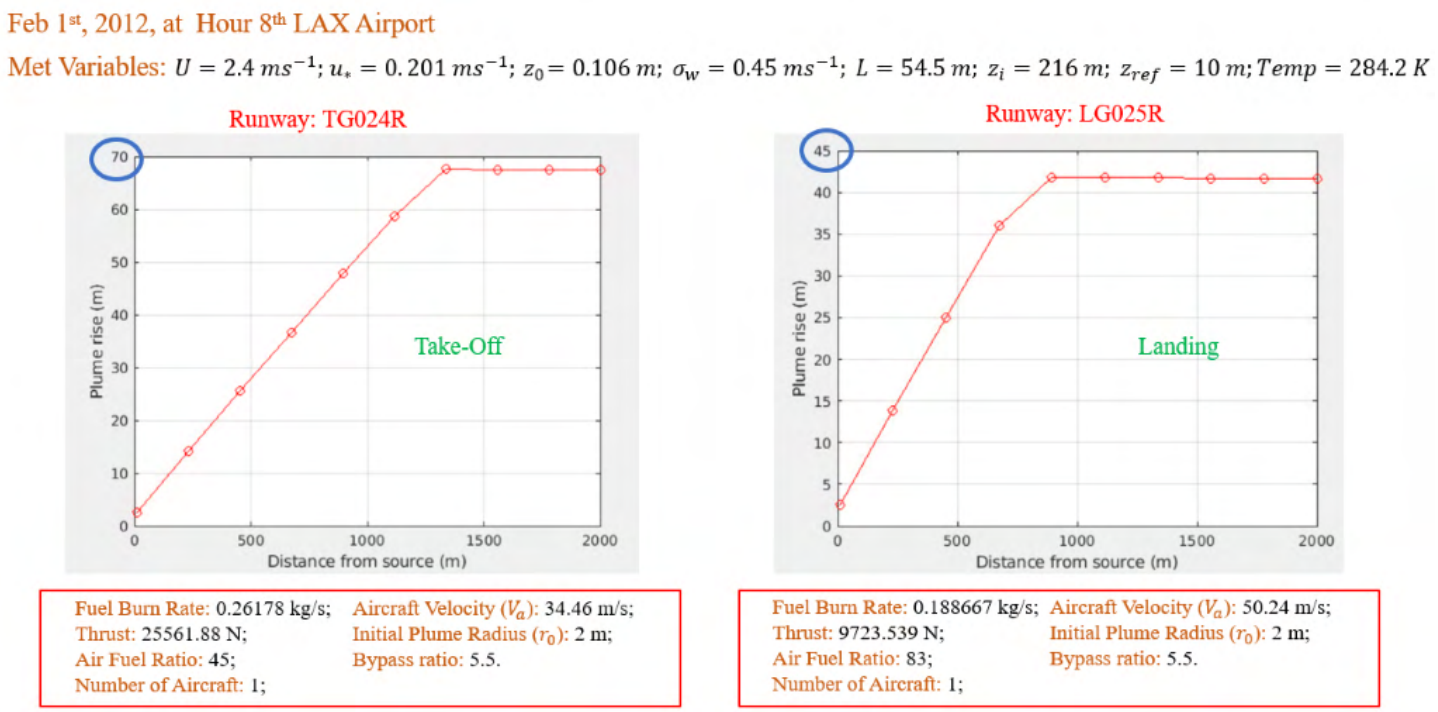

Figure 2.1. Plume rise for a single source at one hour for take-off and landing at LAX.

2.2 Alternate Treatment of Meteorological Inputs

Air quality assessments in and around an airport become more difficult when the airport is located near a shoreline or coastal region, where meteorological conditions are far from spatially uniform. In these conditions, the airport region never become highly unstable or highly stable due to the cold breeze from the ocean. The input preprocessor (AERMET) of AERMOD does not account for important features of the boundary layer present on the shoreline. We have modified the meteorological outputs from AERMET to account for the formation of an internal boundary layer when stable air from the ocean flows onto the warmer land surface of the airport. The sensitivity analysis led to the following changes:

- To account for the shoreline effect at LAX, stable and convective conditions in the AERMET file were replaced by neutral conditions: the Monin–Obukhov length was set to 1000 m, and the friction velocity was computed using the neutral formulation:

$$u_* = k\frac{U_r}{ln\left(\frac{z_r}{z_0}\right)}, \qquad (16)$$

  where k is the von-Karman constant, U_r is the wind speed at z_r (reference height), and z_0 is the roughness length.
- The roughness lengths (z_0) changed when the winds blew from the northeast quadrant to reflect flow passing over the Los Angeles urban core with tall buildings.

Here, the set of AERMET output parameters based on the above modifications is termed the modified meteorology (MM), whereas the AERMET-generated meteorological output is called the original meteorology (OM). For this analysis, we used SO_2 concentration measurements from the LAX AQSAS obtained for four core locations (AQ, CN, CS, and CE) for a 42-day period during February and March 2012, accounting for all airport and non-airport source emissions from the EDMS inventory (Arunachalam et al., 2017; ACRP Report 179).

In addition to applying the above meteorological inputs, we performed a sensitivity analysis based on sub-hourly treatment of the meteorological inputs.

2.3 Sub-hourly Treatment of Meteorological Inputs (SHARP)

Aircraft sources emit pollutants in short bursts, especially during LTO operations. It is difficult to quantify these short bursts of emissions and model the governing processes. Additional complexity arises when the wind speed is low and variable. In these conditions, winds can blow to/from several directions within a duration of one hour, resulting in multiple concentration "lobes" and large plume spread. Classical steady-state models such as AERMOD do not account for the meandering effect and short bursts of aircraft emissions resulting in hourly variations of inputs and outputs in typical applications. To account for these features characterizing the dispersion of aircraft emissions, a sensitivity analysis based on a sub-hourly approach is described here. To create meteorological inputs for these sub-hourly time scales, we used AERMINUTEplus (developed by AECOM), an enhanced version of the AERMET preprocessor AERMINUTE that outputs sub-hourly wind averages based on 1-minute ASOS data. The output from AERMINUTEplus is used in AERMET, AERMOD is run multiple times for each portion of an hour, and then output concentration files are simply averaged for that hour using a previously developed approach called the Sub-Hourly AERMOD Run Procedure (SHARP) (Figure 2.2).

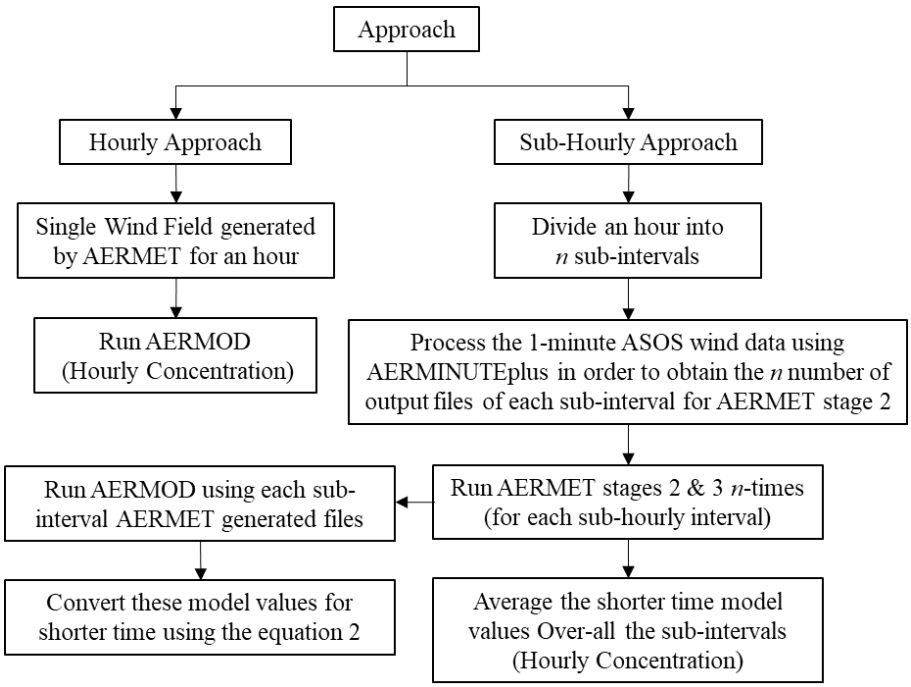

Figure 2.2. Hourly and sub-hourly calculations.

The diurnal concentration peaks decrease with the sub-hourly approach, particularly for the CS site (Figure 2.3(a)). In addition, the sub-hourly approach with MM showed a greater improvement in the results and largely captured most of the high peaks at all sites (Figure 2.3(a)). Hourly AERMOD simulations produced concentrations that were significantly greater than those at AQ and CS and significantly lower than those at CN and CE in the Q-Q distribution (Figure 2.3 (b)). The FB based on the top 26 robust highest concentrations increased from -1.50 and -1.37 to -0.91 and -0.79 at sites AQ and CN with the sub-hourly approach, whereas with MM, these values are improved as -0.05 and 0.15 respectively at sites AQ and CN. However, these approaches showed little change at sites CS and CE (Figure 2.3(b)). The use of the SHARP approach with MM magnifies the mid- to lower-range concentrations, and the lower concentrations nearly match the observations. The fraction of model estimates within a factor of two of the observations increased from 32% to 47% at the CN site and by up to 46% at the CS site (Figure 2.3(b)). Overall, our sub-hourly modeling results using SHARP and MM are relatively closer to the observations and demonstrate that this alternate approach should be seriously explored in circumstances when low-wind meander conditions predominate for modeling aircraft sources.

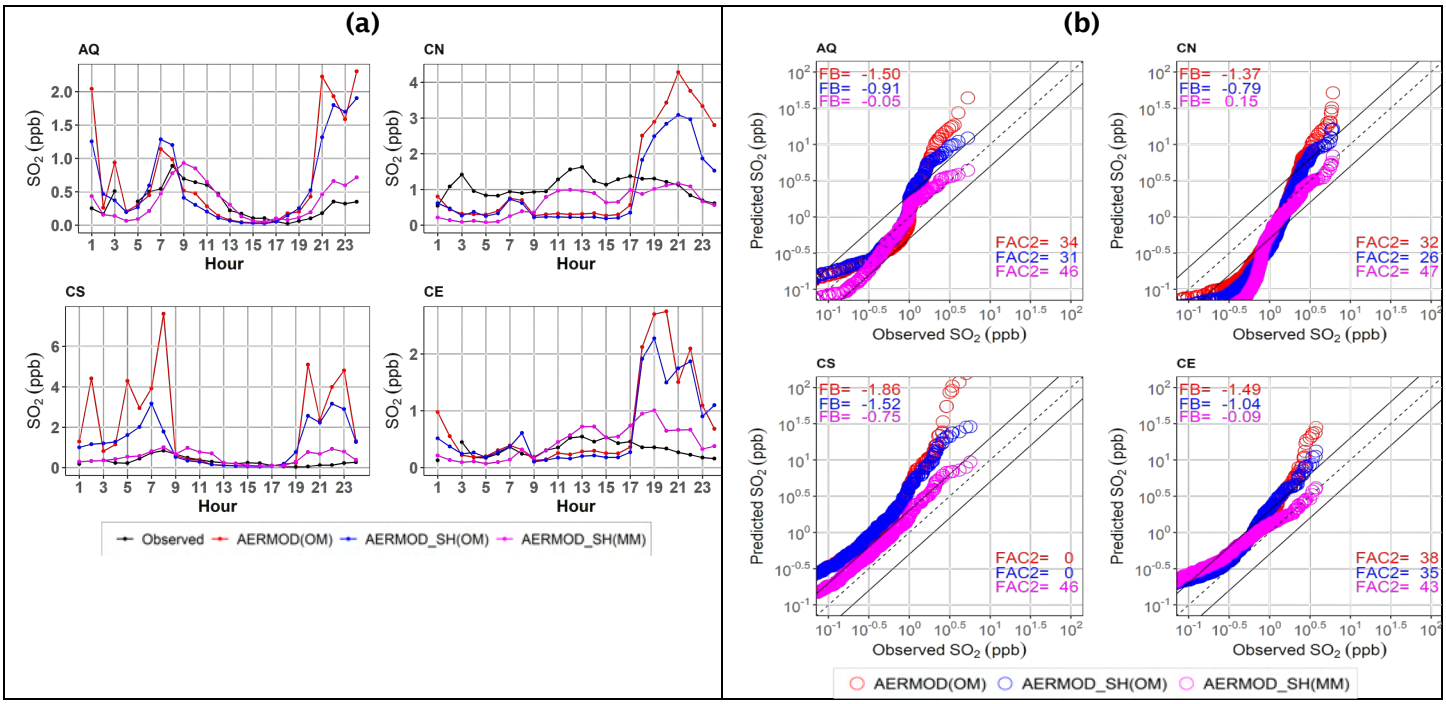

Figure 2.3. (a) Diurnal variability between observed and modeled SO_2 concentrations. **(b)** Q-Q plots for observed to predicted SO_2 concentrations for winter 2012 (42 days) at all four core sites (AQ, CN, CS, and CE). SH: sub-hourly area source treatment; OM: original meteorology; MM: modified meteorology.

3. Chemical Process Assessment

3.1 Gas-phase Treatment

Different reaction mechanisms have been reviewed for the chemistry module for the ADM. One reaction mechanism named Generic Reaction Set (GRS) mechanism (Azzi et al., 1992), as shown in Table B1 in Appendix B, was chosen for the initial tests. The second reaction mechanism (Venkatram et al., 1997), shown in Figure B1 in Appendix B, has a higher number reactions with an empirical aerosol formation reaction, which is modified from the GRS mechanism (Azzi et al., 1992) and is denoted hereafter as the MGRS mechanism. Box model simulations were performed for these two reaction mechanisms for initial tests.

3.1.1 Box model simulation of the GRS mechanism by rate constant for three different reference sources

Box model simulations were performed for the GRS mechanism using the rate constants shown in Figure B2 in Appendix B, which were obtained from three papers: (1) GRS mechanism, Azzi et al., (1992), (2) Valencia et al. (2018), and (3) Pournazeri et al. (2014), as shown in Table B1 in Appendix B. Few reactions are different among the three papers shown in Table B1 in Appendix B. The rate constants from Valencia et al. (2018) give the best results in comparison with the observations shown in Figure B2 in Appendix B. Both NO and O_3 results from box models for the three reaction rate cases follow the trend and magnitude of the observation (right figure) shown in Figure B2 in Appendix B. The reaction rate for the GRS mechanism (Valencia et al., 2018) can be used for the chemistry module of the ADM.

3.1.2 Determination of the reactive organic carbon/volatile organic compound (ROC/VOC) ratio

The lumped hydrocarbon VOC species may not be as reactive as individual real reactive organic carbon (ROC) species (Venkatram et al., 1994). Hence, ROC estimations from VOC were proposed by Venkatram et al. (1994). The ROC/VOC ratio has been estimated based on Venkatram et al. (1994). The ROC emission rate was estimated through the following steps:

- The mole fraction, molecular formula, and molecular weight of VOCs were estimated based on the speciation of VOCs from Wilkerson et al. (2010) and the VOC definition from the FAA-EPA Report (EPA, 2009), as shown in Table 3.1.

- The following were calculated based on the nine lumped VOC species and their reactivity from Venkatram et al. (1994):
    - The mass ratio of ROC/VOC in emissions must be 14.11 (ROC emission in the GRS model must be 14.11 times the VOC emission).
    - The molar ratio of ROC/VOC in emissions must be 17.30.
    - The VOC average molecular formula is $C_{3.2}H_6O_{0.43}$.
    - The VOC average molecular weight is 51.38.

Table 3.1 Estimating the ROC emission rate (ROC/VOC mass ratio) based on the reactivity of eight lumped VOC species (Venkatram et al., 1994) and speciated VOCs from Wilkerson et al. (2010) and the average elemental composition of VOCs.

VOC	Reactivity (RA)	ADOM VOC Species	Mass Fraction (MSF)	Mole fraction (MLF)	ROC/VOC Ratio MSF*RA	ROC/VOC Ratio MLF*RA	Average Molecular Formula	Average Molecular Weight
Propane, benzene	0.170	C3H8	0.023	0.012	0.004	0.002	C5.77H6.15	
Higher alkane (C>4)	0.430	ALKA	0.177	0.063	0.076	0.027	C10.17H22.33	
Ethylene	10.370	ETHE	0.239	0.420	2.482	4.354	C2.13H3.89	
Higher alkene, biogenics (C>2)	24.970	ALKE	0.135	0.082	3.363	2.039	C6.12H11.85	
Mono-alkyl-benzenes	8.760	TOLU	0.009	0.005	0.078	0.042	C7.30H8.61	
Di- and tri-alkyl-benzenes	24.850	AROM	0.038	0.016	0.948	0.396	C9.40H11.06	
Formaldehyde	42.170	HCHO	0.123	0.213	5.190	8.964	C1H2O1	
Higher aldehyde	6.700	ALD2	0.190	0.136	1.271	0.912	C4.025H7.851	
Ketones	10.490	MEK	0.067	0.054	0.700	0.563	C2.77H3.54O1.50	
Sum Total (VOC)			**1.000**	**1.000**	**14.112**	**17.299**	**C3.20H6.00O0.43**	**51.38**

3.1.3 Output of ROC emission files for February 2012 using the AEDT VOC emission files

ROC emission files were produced for February 2012 by using the VOC emission rate from the AEDT2ADM emission processor and the estimated ROC/VOC ratio, which will be used in the GRS chemistry mechanism in the chemistry module of the ADM.

3.2 Aerosol-phase Treatment

Currently, we are planning to use the empirical aerosol formation reaction from the MGRS reaction mechanism (Venkatram et al., 1994) shown in Figure B1b, reaction 2, 3, 9, 10, 11, and 12. The rate constants of these new reactions in the MGRS

mechanism will be determined by box model simulations compared with box model measurements in which aerosol is produced and measured.

Milestone(s)

We submitted drafts of the following documents to the FAA:

- A design document for the ADM,
- Version 1 of the ADM, and
- A white paper on plume rise treatment.

Major Accomplishments

- Updated a design document detailing the features that will be included in the new ADM
- Developed a white paper on plume rise treatment with a focus on AERMOD
- Developed an initial version of plume rise treatment
- Drafted a paper on improved meteorology and evaluation at LAX AQSAS
- Completed initial work on creating sub-hourly meteorological inputs for AERMOD and evaluated the results against LAX AQSAS data

Publications

- Arter, C. A., Buonocore, J. J., Moniruzzaman, C., Yang, D., Jiaoyan, J., & Arunachalam, S. (2022). Air quality and health-related impacts of traditional and alternate jet fuels from airport aircraft operations in the U.S. Environment International, *158*, 106958. https://doi.org/10.1016/j.envint.2021.106958
- Arter, C. A., & Arunachalam, S. (2021). Assessing the importance of nonlinearity for aircraft emissions' impact on O_3 and $PM_{2.5}$. Science Of the Total Environment, *777*, 1462021. https://doi.org/10.1016/j.scitotenv.2021.146121
- Moniruzzaman, C. G., Bowden, J., & Arunachalam, S. (2020). Aircraft landing and takeoff emission impacts on surface O_3 and $PM_{2.5}$ through aerosol direct feedback effects estimated by the coupled WRF-CMAQ model. Atmosoheric Environment, *243*, 117859. https://doi.org/10.1016/j.atmosenv.2020.117859
- Pandey, G., Moniruzzaman, C., Venkatram, A., & Arunachalam, S. (2021, October 18-22). Effect of atmospheric stability on modeling air quality in and around a major airport [Presentation]. International Technical Meeting on Air Pollution Modeling and Its Applications (ITM), Barcelona, Spain.

Outreach Efforts

- Presentation at semi-annual ASCENT stakeholder meetings in the spring and fall of 2021, held virtually
- Presentation and collaborative discussion during monthly meetings with the FAA and EPA
- Presentation at monthly and annual AEC Roadmap meetings hosted by the FAA

Awards

None

Student Involvement

Mr. Praful Dodda contributed to Task 1.

Plans for Next Period

Finalize the ADM with all physical and chemical processes and perform a complete evaluation

References

Arunachalam, S., Blanchard, C., Henry, R., & Tombach, I. (2013). *LAX Air Quality and Source Apportionment Study Volume 1: Executive Summary.* Los Angeles World Airports. Retrieved from https://www.lawa.org/lawa-environment/lax/lax-air-quality-and-source-apportionment-study/final-report-and-materials

Arunachalam, S., Valencia, A., Woody, M., Snyder, M., Huang, J., Weil, J., Soucacos, P., & Webb, S. (2017). Dispersion modeling guidance for airports addressing local air quality concerns, Appendix G (Report No. 179). Transportation Research Board Airport Cooperative Research Program (ACRP), Washington, DC. http://nap.edu/24881

Azzi, M., Johnson, G. M., & Cope, M. (1992, July 5-10). An Introduction to the generic reaction set photochemical smog mechanism In: CSIRO Division of Coal and Energy Technology, North Ryde (Ed.) 11th International Conference of the Clean Air Society of Australia and New Zealand. Brisbane, Australia, 451–462.

Barrett, S. R. H., Britter, R. E., Waitz, I. A. (2013). Impact of aircraft plume dynamics on airport local air quality. Atmospheric

Environment, *74*, 247–258. https://doi.org/10.1016/j.atmosenv.2013.03.061
Briggs, G. A. (1965). A plume rise model compared with observations. Journal of the Air Pollution Control Association, *15*, 433–438. https://doi.org/10.1080/00022470.1965.10468404
CSSI, 2009, JPDO-NextGen-TDM23: Investigation of Aviation for Future Aviation Activity Scenario, Washington, DC.
Federal Aviation Administration, & U.S. Environmental Protection Agency. (2009), Recommended best practice for quantifying speciated organic gas emissions from aircraft equipped with turbofan, turbojet, and turboprop engines – Version 1.0. Federal Aviation Administration Office of Environment and Energy and U.S. Environmental Protection Agency Office of Transportation and Air
Quality. https://www.faa.gov/regulations_policies/policy_guidance/envir_policy/media/FAA-EPA_RBP_Speciated%20OG_Aircraft_052709.pdf
Pournazeri, S., Tan, S., Schulte, N., Jing, Q., Venkatram, A. (2014). A computationally efficient model for estimating background concentrations of NO_x, NO_2, and O_3. Environmental Modelling & Software, *52*, 19–37. https://doi.org/10.1016/j.envsoft.2013.10.018
Valencia, A., Arunachalam, S., Heist, D., Carruthers, D., & Venkatram, A. (2018). Development and evaluation of the R-LINE model algorithms to account for chemical transformation in the near-road environment. Transportation Research Part D: Transport & Environment, 59, 464 – 477. https://doi.org/10.1016/J.TRD.2018.01.028
Venkatram, A., Karamchandani, P., Pai, P., & Goldstein, R. (1994). The development and application of a simplified ozone modeling system (SOMS). Atmospheric Environment, *28*, 3665–3678. https://doi.org/10.1016/1352-2310(94)00190-V
Venkatram, A., Karamchandani, P., Pai, P., Sloane, C., Saxena, P., & Goldstein, R. (1997). The development of a model to examine source-receptor relationships for visibility on the colorado plateau. Journal of the Air & Waste Management Association, *47*, 286–301. https://doi.org/10.1080/10473289.1997.10464453
Wayson, R. L., Fleming, G. G. & Iovinelli, R. (2009). Methodology to estimate particulate matter emissions from certified commercial aircraft engines. Journal of the Air & Waste Management Association *59*(1), 91-100. https://doi.org10.3155/1047-3289.59.1.91

Appendix A: Emission Processing

Table A1. Hourly average aircraft engine data (fuel burn rate, thrust, aircraft speed, bypass ratio [BPR], and air-fuel ratio [AFR]) for runway 24L takeoff produced by the emission processor code AEDT2ADM (all data for runway sources have been produced and saved in the ADM format; only one source is shown here).

Time	24L-Take-Off_Fuel_Burn (kg/s)	24L-Take-Off_Thrust (kN)	24L-Take-Off_Aircraft_Speed (m/s)	24L-Take-Off_BPR	24L-Take-Off_AFR
2/1/12 0:00	1.28	124.10	37.29	5.5	45
2/1/12 1:00	1.21	102.53	35.72	5.5	45
2/1/12 2:00	1.58	88.79	33.87	5.5	45
2/1/12 3:00	1.29	94.63	32.23	5.5	45
2/1/12 4:00	1.36	98.85	33.90	5.5	45
2/1/12 5:00	1.53	146.79	35.70	5.5	45
2/1/12 6:00	0.94	110.23	34.79	5.5	45
2/1/12 7:00	1.72	266.78	38.48	5.5	45
2/1/12 8:00	1.06	127.00	34.47	5.5	45
2/1/12 9:00	0.73	99.18	33.05	5.5	45
2/1/12 10:00	1.59	239.19	37.50	5.5	45
2/1/12 11:00	1.53	152.05	36.01	5.5	45
2/1/12 12:00	1.50	148.65	34.20	5.5	45
2/1/12 13:00	1.50	150.24	33.19	5.5	45
2/1/12 14:00	1.00	96.23	30.32	5.5	45
2/1/12 15:00	0.58	67.49	30.11	5.5	45
2/1/12 16:00	1.44	153.81	31.77	5.5	45
2/1/12 17:00	1.21	157.33	33.16	5.5	45
2/1/12 18:00	1.46	212.36	34.58	5.5	45
2/1/12 19:00	1.31	147.13	32.59	5.5	45
2/1/12 20:00	1.32	136.42	32.99	5.5	45
2/1/12 21:00	1.97	178.12	37.93	5.5	45
2/1/12 22:00	1.89	233.65	36.33	5.5	45
2/1/12 23:00	1.54	97.43	36.42	5.5	45

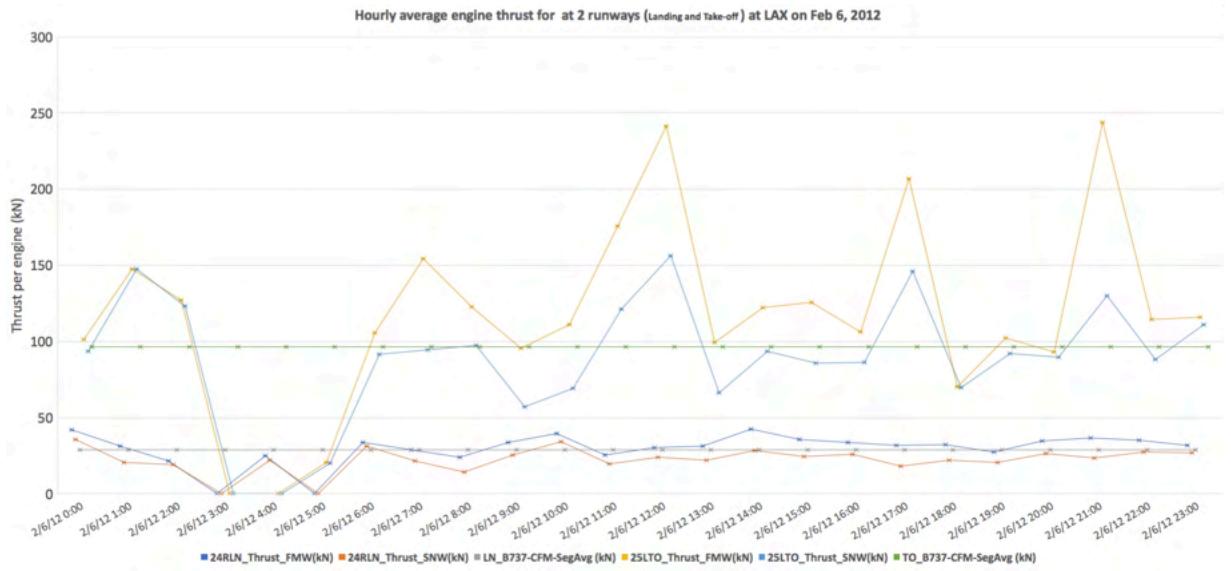

Figure A1. Comparison of hourly average thrust averaged by two methods: 1) fuel-burn-weighted (FBW) average thrust and 2) segment number average thrust (SNW) for 24R landing (24RLN) and 24L takeoff (24LTO) with the corresponding segment average thrust of the CFM engine of a Boeing 737-300 aircraft for landing (LN_B737-CFM-SegAvg(kn)) and takeoff (TO_B737-CFM- Seg Avg(kn)).

Table A2. Number of segments in the one-month AEDT file with and without zero-duration rows for February 2012 at LAX.

Type	Maximum altitude in data (ft)	No. of segments with zero-duration rows	No. of segments without zero-duration rows	Change in no. of segments when zero-duration rows are removed	% change in no. of segments when zero-duration rows are removed
All heights	13,865	269,2749	2,690,620	2,129	0.08
Used for ADM for 3000 ft	3,000	1,996,543	1,994,728	1,815	0.09

Table A3. Summary statistics of negative thrust segments and the altitude for negative thrust segments for one day in both winter (Feb. 1, 2012) and summer (July 1, 2012) AEDT data files.

	Winter 2012 file		Summer 2012 file	
Statistical parameters	Summary statistics of negative thrust (lb) segments	Summary statistics of altitude AFE (ft) of the negative thrust segments	Summary statistics of negative thrust (lb) segments	Summary statistics of altitude AFE (ft) of the negative thrust segments
Count	898	898	4983	4983
Mean	-201.68	2861.79	-315.22	4105.72
Standard deviation	238.23	534.89	209.35	1072.77
Minimum	-2740.30	-14.90	-1325.4	2582.00
25 Percentile	-322.37	2991.20	-444.32	2999.98
50 Percentile	-128.60	2991.20	-287.88	3873.98
75 Percentile	-74.60	3000.00	-140.74	5063.88
Maximum	-16.80	3000.00	-0.89	5999.98

Table A4. Comparison of AEDT-segment data for summer and winter 2012 files for LAX.

	Winter 2012 file	Summer 2012 file
AEDT-segment file		
Time duration	1.5 months (Feb. and Mar.)	2 months (July and Aug.)
File size		
Variables (columns)	38	126
No. of rows	3.7 million rows (3,661,723)	6 million (5,983,659)
Some new useful variables		Number of engines per aircraft, bypass ratio of the engine (will be used to calculate the air mass flow rate, propulsion efficiency, and exhaust speed to be used in the plume rise model)
Some new useful variables		Runway and gate number for both departure and arrival (will help to more easily extract direction-based emissions for each runway easier than the winter file)
AEDT-area (AERMOD file)		
Species files available	NO_x and SO_x	NO_x, SO_x, CO
# of sources	5,919	21,660

Table A5. Comparison of SO_x emissions between winter and summer AEDT-segment files for 2012 for LAX.

H	I	J	K	L	M
Data Period	**All height**	**Below 3000 ft (914.4 m)**	**Above 3000 ft (914.4 m)**	**Surface (height <= 0 ft)**	**Air (height 0-3000 ft)**
	SOx	**SOx**	**SOx**	**SOx**	**SOx**
	Total emission (surf+air) (g)	**Total emission (surf+air) (g)**	**Total emission (surf+air) (g)**	**Total emission (surface) (g)**	**Total emission (air) (g)**
Feb-12	26,525,852.59	17,423,672.72	9,102,179.87	8,107,894.32	9,315,778.40
Jul-12	20,239,295.90	13,685,934.80	6,553,361.09	7,129,882.36	6,556,052.48
Aug-12	19,766,199.69	13,332,544.60	6,433,655.09	6,883,357.60	6,449,187.00
July-Aug-12	40,005,495.62	27,018,479.44	12,987,016.17	14,013,239.96	13,005,239.48
	% OfTotalAllHeight	**% OfTotalAllHeight**	**% OfTotalAllHeight**	**% OfTotal-3000ft-Height**	**% OfTotal-3000ft-Height**
Feb-12	100	65.686	34.314	46.534	53.466
Jul-12	100	67.621	32.379	52.096	47.904
Aug-12	100	67.451	32.549	51.628	48.372
July-Aug-12	100	67.537	32.463	51.865	48.135
	Emission rate (ton/day)	**Emission rate (ton/day)**	**Emission rate (ton/day)**	**Emission rate (ton/day)**	**Emission rate (ton/day)**
Feb-12	**0.915**	**0.601**	**0.314**	**0.28**	**0.321**
Jul-12	**0.653**	**0.441**	**0.211**	**0.23**	**0.211**
Aug-12	**0.638**	**0.43**	**0.208**	**0.222**	**0.208**
July-Aug-12	**0.645**	**0.436**	**0.209**	**0.226**	**0.21**
Ref1: LAWA2013 Winter		**0.720**			
Ref1: LAWA2013 Summer		**0.716**			
Ref2: CSSI 2009	**1.004**				
	% Change of emission rate from Feb-2012	**% Change of emission rate from Feb-2012**	**% Change of emission rate from Feb-2012**	**% Change of emission rate from Feb-2012**	**% Change of emission rate from Feb-2012**
Jul-12	**-28.63387978**	**-26.62229617**	**-32.80254777**	-17.85714286	-34.26791277
Aug-12	**-30.27322404**	**-28.45257903**	**-33.75796178**	-20.71428571	-35.20249221
July-Aug-12	**-29.50819672**	**-27.45424293**	**-33.43949045**	-19.28571429	-34.57943925
LAWA 2013, Arunachalam, S. et al., 2013. LAX Air Quality and Source Apportionment Study Volume 1. Executive Summary. Los Angeles World Airports, Environ. Serv. Div. 2					
CSSI 2009 , JPDO – NextGen – TDM23: Investigation of Aviation Emissions for Future Aviation Activity Scenario. Washington DC					

Table A6. Comparison of NO_x emissions between winter and summer AEDT-segment files for 2012 for LAX.

H	I	J	K	L	M
Data Period	**All height**	**Below 3000 ft (914.4 m)**	**Above 3000 ft (914.4 m)**	**Surface (height <= 0 ft)**	**Air (height 0-3000 ft)**
	NOx	**NOx**	**NOx**	**NOx**	**NOx**
	Total emission (surf+air) (g)	**Total emission (surf+air) (g)**	**Total emission (surf+air) (g)**	**Total emission (surface) (g)**	**Total emission (air) (g)**
Feb-12	403,315,277.26	234,493,560.84	168,821,716.42	88,480,752.27	146,012,808.57
Jul-12	261,576,175.00	151,265,262.00	110,310,913.00	58,907,836.40	92,357,425.60
Aug-12	249,171,734.84	143,614,031.93	105,557,702.92	55,585,079.38	88,028,952.55
July-Aug-12	510,747,909.57	294,879,293.94	215,868,615.63	114,492,915.78	180,386,378.16
	% OfTotalAllHeight	**% OfTotalAllHeight**	**% OfTotalAllHeight**	**% OfTotal-3000ft-Height**	**% OfTotal-3000ft-Height**
Feb-12	100	58.142	41.858	37.733	62.267
Jul-12	100	57.828	42.172	38.943	61.057
Aug-12	100	57.637	42.363	38.704	61.296
July-Aug-12	100	57.735	42.265	38.827	61.173
	Emission rate (ton/day)	**Emission rate (ton/day)**	**Emission rate (ton/day)**	**Emission rate (ton/day)**	**Emission rate (ton/day)**
Feb-12	**13.907**	**8.086**	**5.821**	**3.051**	**5.035**
Jul-12	**8.438**	**4.88**	**3.558**	**1.9**	**2.979**
Aug-12	**8.038**	**4.633**	**3.405**	**1.793**	**2.84**
July-Aug-12	**8.238**	**4.756**	**3.482**	**1.847**	**2.909**
Ref: LAWA2013 Winter		**8.634**			
Ref: LAWA2013 Summer		**8.033**			
Ref2: CSSI 2009	**12.988**				
	% Change of emission rate from Feb-2012	**% Change of emission rate from Feb-2012**	**% Change of emission rate from Feb-2012**	**% Change of emission rate from Feb-2012**	**% Change of emission rate from Feb-2012**
Jul-12	**-39.32551952**	**-39.64877566**	**-38.8764817**	-37.72533596	-40.83416087
Aug-12	**-42.20176889**	**-42.70343804**	**-41.50489607**	-41.23238283	-43.59483615
July-Aug-12	**-40.76364421**	**-41.18229038**	**-40.1820993**	-39.46247132	-42.224429

LAWA 2013, Arunachalam, S. et al., 2013. LAX Air Quality and Source Apportionment Study Volume 1. Executive Summary. Los Angeles World Airports, Environ. Serv. Div. 2

CSSI 2009 , JPDO – NextGen – TDM23: Investigation of Aviation Emissions for Future Aviation Activity Scenario. Washington DC

Appendix B: Chemistry Modeling in Dispersion Models

a) 7 reaction mechanism (Azzi et al., 1992)

1	ROC + hv >[O2]> RP + ROC
2	RP + NO >[O2]> NO2
3	NO2 + hv >[O2]> NO + O3
4	NO + O3 > NO2
5	RP+RP > RP
6	RP+NO2 > SGN
7	RP+NO2 > SNGN

b) 12 reaction mechanism (Venkatram et al., 1997)

1	ROC1 + hv > RP +ROC1
2	AROM+hv > RP + AROM
3	TERP+hv > RP + TERP
4	RP + NO > NO2
5	NO2+hv > NO + O3
6	NO + O3 > NO2
7	RP + RP > RP + alfa*H2O2
8	RP + NO2 > RNO3
9	OH + SO2 > SO4
10	OH + NO2 > HNO3
11	OH + AROM > y1OC
12	OH + TERP > y2OC

Figure B1. Two reaction mechanisms for the chemistry module in the ADM dispersion model.

Table B1. Comparison of rate constants of Generic Reaction Set (GRS) mechanism (Azzi et al., 1992) with rate constants from two additional papers: (1) Valencia et al. (2018) and (2) Pournazeri et al. (2014).

No.	Reaction	Rate constant (ppm, min) Valencia et al. (2018)	Rate constant (ppm, min) Pournazeri et al. (2014)
1	ROC + hv > RP + ROC	k1=10000*exp(-4710/T) * k3 (min-1)	k1= 0:0067 k3 exp(-1000Gamma(1/T-1/316)) (min-1) where Gamma=4.7
2	RP + NO > NO_2	k2=5482 * exp(242/T) (ppm-1 min-1)	k2=3.58e6/T (ppm-1 min-1)
3	NO2 + hv > NO + O_3	k3=function of solar zenith angle (min-1)	k3= exp(-0.575/sin(theta)) where theta is the sun elevation angle (min-1)
4	NO + O_3 > NO_2	k4=2643 * exp(-1370/T) (ppm-1 min-1)	k4=9.24 *e5 (1/T)exp(-1450/T) (ppm-1 min-1)
5	RP + RP > RP	k5=10000 (ppm-1 min-1)	K5=10200
6	RP + NO_2 > SGN	k6=125 (ppm-1 min-1)	K6=120
7	RP + NO_2 > SNGN	k7=k6 (ppm-1 min-1)	K7=120

ROC: Reactive organic compounds
RP: Radical pool
SGN: Stable gaseous nitrogen products
SNGN: Stable nongaseous nitrogen products

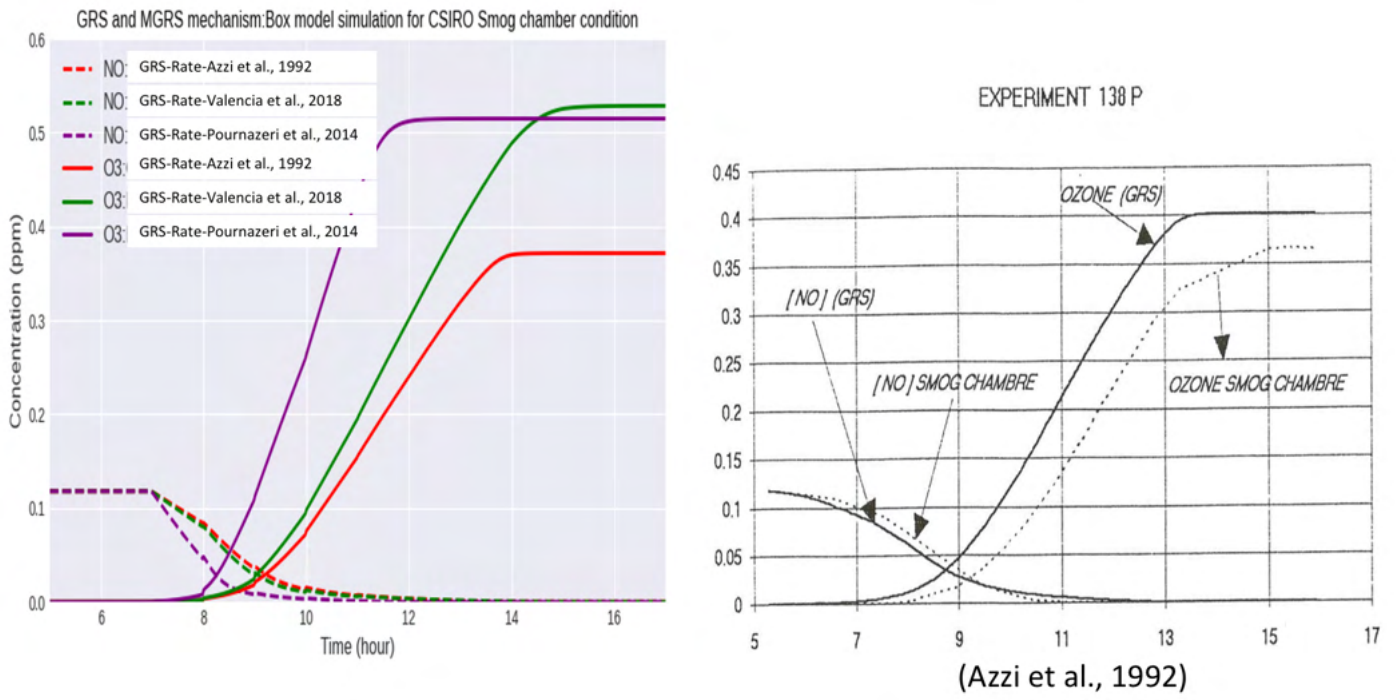

Figure B2. Left: A comparison of rate constants for the GRS mechanism (Azzi et al., 1992) with those from two additional papers (Valencia et al., 2018; Pournazeri et al., 2014). Right: A comparison with observations from Azzi et al. (1992) for the same conditions employed in the left figure.

Project 022 Evaluation of FAA Climate Tools: Aviation Portfolio Management Tool (APMT)

University of Illinois at Urbana-Champaign

Project Lead Investigator

Dr. Donald Wuebbles
Department of Atmospheric Sciences
University of Illinois
105 S. Gregory Street
Urbana, IL 61801
Tel: 217-244-1568
Fax: 217-244-4393
Email: wuebbles@illinois.edu

University Participants

University of Illinois at Urbana-Champaign

- PI: Dr. Donald Wuebbles
- Period of Performance: October 1, 2020 to September 30, 2021 (project started January 31, 2020)
- Tasks:
    1. Examine effects of fleets of supersonic aircraft on ozone and climate using the state-of-the-art Whole Atmosphere Community Climate Model (WACCM), a global climate-chemistry model.
    2. Analyze emissions provided to us for fleets of proposed supersonic aircraft designs.

Project Funding Level

Support from the FAA over this time period was about $70,000, with an additional $70,000 in matching support, including about $70,000 from the University of Illinois at Urbana-Champaign.

Investigation Team

Dr. Donald Wuebbles: project oversight
Jun Zhang (graduate student; recently graduated): conduct studies and perform analyses using the Community Earth System Model (CESM) WACCM, a 3-dimensional (3D) atmospheric climate-chemistry model.

Task 1 - Revisiting High-Speed Civil Transports and Their Potential Effects on Ozone and Climate

University of Illinois at Urbana-Champaign

Objective

This project has the primary objective of understanding how atmospheric processes over the last few decades have affected analyses of the potential environmental effects on ozone and climate from assumed future fleets of supersonic transport (SST) aircraft. The aim was to conduct a series of sensitivity global chemistry-climate modeling studies that revisit case studies run for High-Speed Civil Transport (HSCT) emission scenarios for a mature fleet of aircraft. The emission scenarios analyzed in this study were developed from the NASA HSCT program from the late 1990s through the early 2000s and/or from the 1999 Intergovernmental Panel on Climate Change (IPCC) special assessment on aviation. Future studies will consider new emissions for proposed fleets of SSTs.

Research Approach

The study will use the WACCM of the CESM, developed by the National Center for Atmospheric Research (NCAR). This model has 66 layers from the ground to the middle of the mesosphere and provides a comprehensive treatment of tropospheric and stratospheric chemical processes.

Results and Discussions

The calculated total column ozone percentage change from the HSCT emission scenarios are shown in Table 1 for different nitrogen oxides (NOx) emission indexes and fleet sizes in a 2015 background atmosphere. The results from the earlier 1999 NASA Atmospheric Effects of Aviation Project (AEAP) and IPCC aviation assessments (Kawa et al., 1999; Penner et al., 1999) using 2-dimensional (2D) and 3-dimensional (3D) models from that time period are shown here for comparison. The calculated percentage change in total column ozone from this study with WACCM is shown in the last row. All total column ozone changes are shown here for each emission scenario relative to the subsonic-only background atmosphere.

The results are more similar to the earlier results from the 2D models than the early-stage 3D models. For the baseline scenario Case A, this study determines a change in percentage ozone of −0.21% and −0.13% for the Northern Hemisphere (NH) and Southern Hemisphere (SH), respectively. This change falls into the range of +0.2 to −0.4% in the NH and +0.05 to −0.8% in the SH calculated from previous models shown in Table 1. For Cases B and C, with increasing NOx Emissions Index (EINOx) to either 10 g or 15 g of NO_2/kg of fuel, the WACCM-derived ozone loss in the NH tends to be larger than that from most of the earlier models. Case D, for only NOx emissions with EINOx = 15g of NO_2/kg of fuel, was not considered in the earlier assessments.

For the water vapor (H_2O)-only emissions scenario (Case E), the WACCM results are lower than all of the earlier models in the NH. Doubling the fleet to the 1000 HSCTs assumed to be in operation (Case F), the total column ozone percentage change calculated from WACCM is −0.45% and −0.27% in the NH and SH, respectively, which is in the range of values calculated from previous models.

Figure 1 shows the sensitivity of ozone depletion in the NH as a function of NOx emission indices (EINOx) for a fleet of 500 supersonic aircraft calculated from WACCM and the comparison with earlier models. In general, WACCM derives a higher sensitivity in the NH between the levels of NOx emissions and the resulting ozone changes. As the EINOx goes from no NOx emission (the H_2O-only perturbation case) to 5 g/kg fuel, WACCM has a higher sensitivity in ozone depletion than all of the earlier models. Increasing the EINOx from 5 to 15 g/kg of fuel also shows WACCM having a stronger sensitivity compared to most of the earlier models, with one exception, the THINAIR 2D model.

Table 1. Percentage changes (%) in total column ozone for the WACCM results relative to the earlier NASA Atmospheric Effects of Aviation Project (AEAP) and Intergovernmental Panel on Climate Change (IPCC) aviation assessment results taken from Kawa et al. (1999) and Penner et al. (1999). The first and second values are for the Northern Hemisphere and Southern Hemisphere average percent change in total column ozone, respectively.

Model	Case A EINOx = 5 with H_2O	Case B EINOx = 10 with H_2O	Case C EINOx = 15 with H_2O	Case D EINOx = 15 without H_2O	Case E EINOx = 0 H_2O only	Case F EINOx = 5 with H_2O Fleet 1000
AER 2D	−0.3, −0.1	−0.3, −0.1	−0.3, −0.05	—	−0.6, −0.3	−0.7, −0.3
GSFC 2D	−0.4, −0.8	−0.6, −0.7	−0.8, −0.7	—	−0.4, −0.8	−0.9, −1.4,
LLNL 2D	−0.2, −0.2	−0.3, −0.1	−0.4, −0.01	—	−0.3, −0.3	−0.5, −0.3
CSIRO 2D	−0.2, −0.1	−0.3, −0.2	−0.5, −0.3	—	−0.2, −0.07	−0.5, −0.2
UNIVAQ 2D	−0.002, +0.02	+0.2, +0.1	+0.4, +0.2	—	−0.4, −0.2	−0.06, +0.005
SUNY 2D	−0.2, −0.1	−0.2, −0.06	—	—	−0.2, −0.1	−0.3, −0.2
THINAIR 2D	−0.2, −0.2	−0.5, −0.3	−0.9, −0.5	—	—	−0.4, −0.3
GMI 3D	+0.2, +0.05	—	—	—	—	—
LaRC 3D	−0.05, −0.1	+0.07, −0.03	—	—	—	—
SLIMCAT 3D	−0.4, −0.6	−0.5, −0.7	—	—	−0.6, −0.7	—
This study	**−0.21, −0.13**	**−0.38, −0.11**	**−0.66, −0.14**	**−0.62, −0.003**	**−0.13, −0.16**	**−0.45, −0.27**

EINOx = NOx Emissions Index; values in g/kg of fuel.

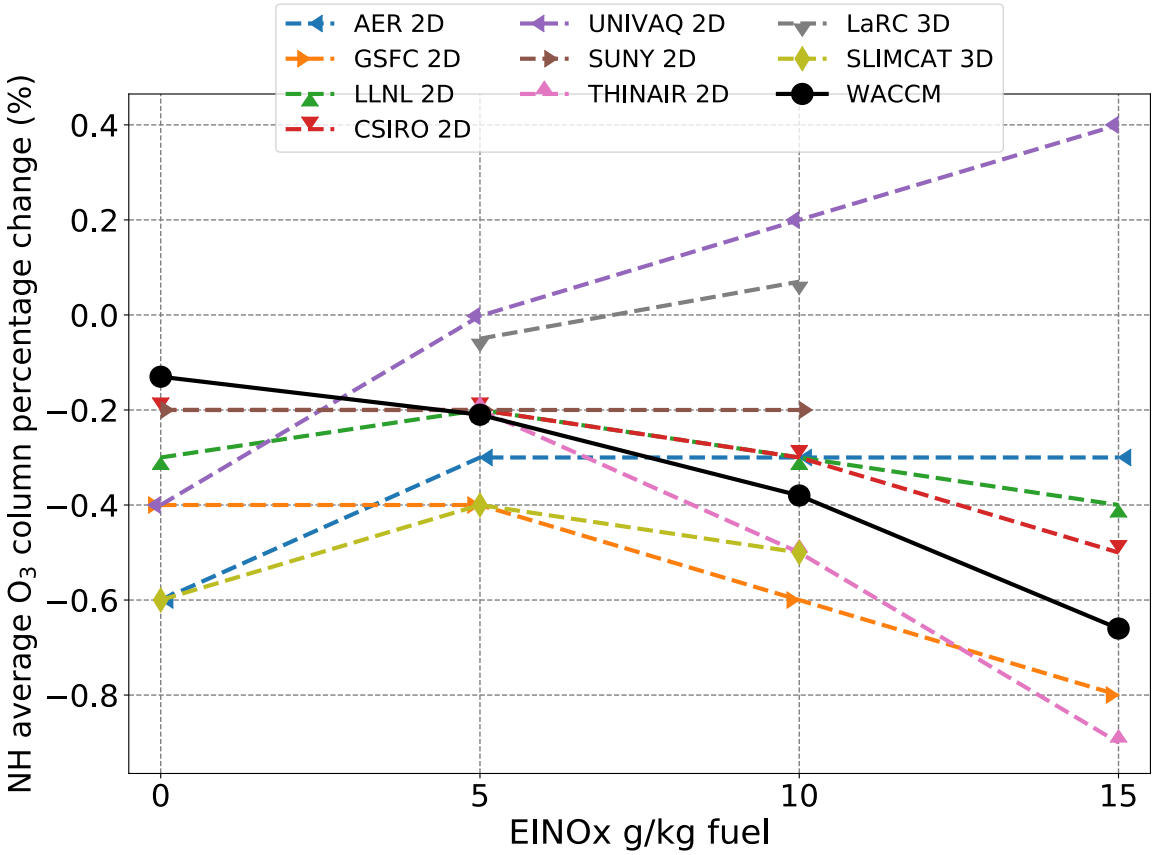

Figure 1. Northern Hemisphere (NH) total ozone column change (%) as a function of NOx Emissions Index (EINOx) for a fleet size of 500 supersonic aircraft. Results from earlier 2- and 3-dimensional models are shown in dashed lines, and the WACCM results are shown by the solid black line.

Milestones

- Journal paper now published by the *Journal of Geophysical Research* after revisions were made during this past year. This paper provides a historical context for further studies of supersonic aircraft effects on ozone and climate.
- NOx and H_2O emissions from fleets of HSCTs can potentially affect stratospheric ozone and climate.
- New analyses on ozone change from HSCTs are similar to results from the 1999 NASA and IPCC aviation assessments, although with a greater sensitivity to NOx emissions.
- Ozone effects from an HSCT fleet depend on the amount of NOx and H_2O emissions and resulting chemical interactions through ozone-destroying catalytic cycles.
- These studies provide important context for the studies of actual projected fleets that we will be examining next in our studies.

Task 2 - Conducting Sensitivity Studies on Cruise Altitude

University of Illinois at Urbana-Champaign

Objectives

This study was intended to show how the stratosphere responds to different cruise altitudes. The potential effects from hypothetical fleets of stratospheric-flying aircraft will be evaluated by conducting a series of sensitivity studies in a projected realistic 2050 background atmosphere.

Research Approach

We used a state-of-the-art 3D chemistry-transport model to evaluate the sensitivity of the atmosphere, especially the stratosphere, to different cruise altitudes from a possible supersonic aircraft fleet. A parametric approach is applied in which the fleet fuel use, NOx emission index, and geographical distribution of the emissions are all kept constant while the emission altitude varies systematically at a 2-km cruise range. The cruise emissions are assumed to be uniformly distributed vertically over a 2-km band ranging from 13 to 23 km, with a total of eight emission scenarios.

Results and Discussion

This study evaluated the sensitivity of the potential environmental effects at different cruise altitudes of SSTs on atmospheric ozone and radiative forcing. A series of sensitivity studies of possible future cruise altitudes were conducted to evaluate the relative atmospheric response from NOx and H_2O emissions for a fleet of supersonic aircraft assumed to be fully operational by 2050. For these calculations, a fixed fleet fuel use and geographical distribution were assumed.

For the range of cruise altitudes from 13 to 23 km evaluated in this study, the resulting ozone impacts depend on the altitude and can be either positive or negative when examining the annual and global averaging total ozone column change (Figure 2). For emissions in the upper troposphere and lower stratosphere, such as for cruise altitudes between 13 and 17 km, total column ozone indicates a slight increase. At these altitudes, the ozone chemistry is affected by the coupling of hydrogen, nitrogen, chlorine and bromine oxides (HOx/NOx/ClOx/BrOx) chemistry, and the resulting ozone impact is less significant and much less dependent on the altitude of the aircraft emissions. At higher cruise altitudes, from 17 to 23 km, where the ozone chemistry is dominated by NOx and the stratospheric lifetimes are longer, stratospheric ozone is reduced, primarily as a result of the NOx-Ox catalytic cycles, and the magnitude of the ozone destruction increases with higher cruise altitudes. The resulting changes in total column ozone at these altitudes is highly dependent on the cruise altitude. A cruise altitude from 16 to 18 km shows a minimal total column ozone change resulting from the offsetting effects of ozone production and reduction at different heights. The inflection point is at around 17 km, where the effect of supersonic emission on ozone transitions from ozone production to ozone depletion. The maximum total column ozone loss occurs in NH high latitudes in the fall to winter season. With higher cruise altitudes, greater ozone depletion is found in the SH as more emitted NOx and H_2O are lifted upward and transported southward across the equator.

This study looked at a range of cruise altitudes that encompass the range of the concepts currently being discussed by the industry for supersonic business jets and smaller supersonic airliners. The sensitivity study is based on an assumed Mach-2.4, 300-passenger conceptual supersonic airliner and a projected network based on its 5000-nautical-mile range that was developed in the 1990s. As a consequence, the fleet fuel use in these studies is likely larger than any of the much smaller business jets being considered. Likewise, their range, projected markets, utilization, and fleet sizes could be much different, which would result in changes to the geographical patterns of the emissions. If developers succeed in developing designs with low sonic boom, then the geographical distributions could also be quite different because of flights occurring over land. When viewed as impact scaled by fleet fuel use, this study provides insights on the potential impacts on ozone relative to cruise altitudes (Figure 2). As such, our results suggest that developing low-NOx combustors could be important if large fleets of supersonic aircraft flying at the highest altitudes ever become viable. In future studies, the environmental effects of other design and operation parameters need to be evaluated thoroughly to facilitate technological development in order to make widespread supersonic travel more environmentally feasible.

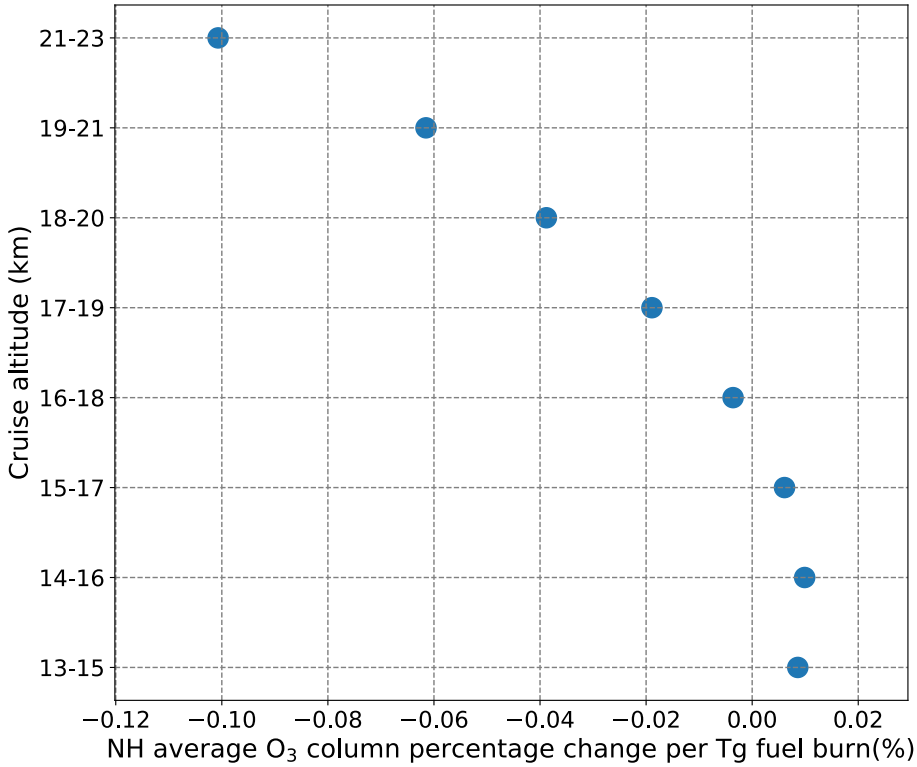

Figure 2. Northern Hemisphere total column ozone change (%) per Tg of fuel burn as a function of cruise altitudes.

Milestones

- Journal paper published (in August) by the *Journal of Geophysical Research* after revision. This study provides further context for future studies of the environmental effects from future fleets of supersonic aircraft.
- Established that the stratospheric ozone response of supersonic aircraft emissions depends on cruise altitudes and the sensitivity of ozone to emissions was found to increase with altitudes.
- The calculated ozone impact was found to be small for cruise altitudes below 17 km; ozone depletion increases sharply as cruise altitudes increase above 17 km.
- Low-NOx combustors may be important to consider for fleets of potential future supersonic aircraft with cruise altitudes above 17 km.
- These studies provide important context for the studies of actual projected fleets that we will be examining next in our studies.

Major Accomplishments

- The model performs well and the results establish a new paradigm for studying the impacts from fleets of supersonic aircraft, while also being consistent with earlier studies.
- Completed the sensitivity studies.
- Journal paper accepted and published.

Task 3 - Analyses for Supersonic Transport Fleet Proposed by Georgia Tech University

University of Illinois at Urbana-Champaign

Objectives

This study examines the effect of a proposed fleet of supersonic commercial aircraft on stratospheric ozone and on climate.

Research Approach

We used the state-of-the-art 3D WACCM chemistry-transport model to evaluate emissions from a fleet of supersonic aircraft proposed by Georgia Tech University. Distribution of aircraft emissions was obtained from Georgia Tech, analyzed, and then put into the model for the steady-state run, assuming a background atmosphere for the 2050 time period (based on climate projections).

Milestone

Model runs have been completed and analyses of results are now underway.

Publications

Zhang, J., D. Wuebbles, D. Kinnison, and S.L. Baughcum. 2021. Potential impacts of supersonic aircraft emissions on ozone and resulting forcing on climate. An update on historical analysis. *J. Geophys. Res.*, https://doi.org/10.1029/2020JD034130.

Zhang, J., D. Wuebbles, D. Kinnison, and S.L. Baughcum. 2021. Stratospheric ozone and climate forcing sensitivity to cruise altitudes for fleets of potential supersonic transport aircraft. *J. Geophys. Res.*, 126, e2021JD034971, https://doi.org/10.1029/2021JD034971.

Zhang, J. 2021. On Potential Effects from the Aviation and Refrigeration Sectors on Ozone and Climate. Ph.D. Thesis, University of Illinois at Urbana-Champaign, Urbana.

Outreach Efforts

Presentation at ASCENT Meeting, April 2021
Biweekly meeting with project manager.
ICAO Impacts and Science Group (ISG) meetings (monthly) for Dr. Wuebbles.

Student Involvement

Graduate student Jun Zhang was responsible for the analyses and modeling studies within the project and leading the initial preparation of the project reports.

Plans for Next Period

- Begin studies based on the emission inventories developed by ASCENT Project 10 to consider specific designs of SSTs from MIT and compare those results to model analyses done by MIT for the same scenario plus their similar analyses of the Georgia Tech SST fleet.
- Use the results from this study to inform the development of Aviation Portfolio Management Tool – Impacts Climate (APMT-IC) for supersonic impacts (ASCENT Project 58).

References:

Kawa, S. R., Anderson, J. G., Baughcum, S. L., Brock, C. A., Brune, W. H., Cohen, R. C., ... & Waugh, D. (1999). Assessment of the effects of high-speed aircraft in the stratosphere: 1998. National Aeronautics and Space Administration report. NASA/TMM1999-209237.

Penner, J. E., Lister, D. H., Griggs, D. J., Dokken, D. J., & McFarland, M. (Eds). (1999). Aviation and the global atmosphere (pp. 1–373). Cambridge, UK: Cambridge University Press.

Project 023 Analytical Approach for Quantifying Noise from Advanced Operational Procedures

Massachusetts Institute of Technology

Project Lead Investigator

R. John Hansman
T. Wilson Professor of Aeronautics & Astronautics
Department of Aeronautics & Astronautics
Massachusetts Institute of Technology
Room 33-303
77 Massachusetts Ave, Cambridge, MA 02139
617-253-2271
rjhans@mit.edu

University Participants

Massachusetts Institute of Technology

- PI: R. John Hansman
- FAA Award Number: 13-C-AJFE-MIT, Amendment Nos. 008, 015, 022, 031, 046, and 051
- Period of Performance: October 1, 2020 to September 30, 2021
- Tasks:
    1. Evaluate the noise impacts of flight track concentration or dispersion associated with performance-based navigation (PBN) arrival and departure procedures.
    2. Identify the key constraints and opportunities for procedure design and implementation of noise-minimizing advanced operational procedures.
    3. Develop concepts for arrival and departure procedures that consider noise impacts in addition to operational feasibility constraints.
    4. Analyze location-specific approach and departure design procedures in partnership with affected industry stakeholders.

Project Funding Level

FAA provided $860,000 in funding, and matching funds totaling $860,000 were provided by the Massachusetts Institute of Technology (MIT) (approximately $80,000) and the Massachusetts Port Authority (Massport) (approximately $780,000).

Investigation Team

- Professor R. John Hansman (PI)
- Sandro Salgueiro (graduate student)
- Clement Li (graduate student)
- Ara Mahseredjian (graduate student)
- Kevin Zimmer (graduate student)

Project Overview

This project is evaluating the noise reduction potential from advanced operational procedures in the terminal (arrival and departure) phases of flight. The noise impact from these procedures is not well understood or modeled in current environmental analysis tools, presenting an opportunity for further research to facilitate air traffic management (ATM) system modernization. The project leverages a noise analysis framework developed at MIT under ASCENT Project 23 to evaluate a variety of sample procedures. In conjunction, the project is contributing to the memorandum of understanding between the FAA and Massport to identify, analyze, and recommend procedure modifications at Boston Logan International Airport (hereafter, Boston Logan).

Task 1 - Evaluate the Noise Impacts of Flight Track Concentration or Dispersion Associated with Performance-Based Navigation (PBN) Arrival and Departure Procedures

Massachusetts Institute of Technology

Objectives

This task evaluates the impact of flight track concentration arising from PBN procedure implementation and the potential noise mitigation impact of track dispersion. The effects of track concentration due to PBN procedure implementation have not been fully explored. Although the potential benefits of PBN for flight efficiency and predictability are well understood, the resulting environmental impact has caused increased community awareness and concern over the procedure design process. Current methods and noise metrics do not provide adequate information to inform policy decisions relating to noise concentration or dispersion due to PBN implementation.

In this task, models were used to evaluate noise concentration scenarios using a variety of metrics and procedure design techniques. Noise data from Massport were used to support the simulation effort. The impact of track dispersion was compared with potential community noise reduction through noise-optimal required navigation performance procedure designs that avoid noise-sensitive areas and use background noise masking where possible.

Research Approach

- Evaluate the impact of noise dispersion directly through modeling of a dispersed set of flight tracks in the Aviation Environmental Design Tool (AEDT).
- Analyze population exposure impact using multiple metrics, including day-night average sound level (DNL) and N_{above}.
- Validate which metrics best capture the impacts of noise concentration and dispersion.

Major Accomplishments

- Created new visualization methods to allow communities to more easily understand the impact of flight procedure changes at different scales.
- Evaluated noise complaints at Boston Logan and began development of method to correlate them with specific overflights, allowing a data-driven review of annoyance criteria.
- Published the final Block 2 Report for the Boston Logan project, containing a series of low-noise procedure recommendations based on the analysis of flight tracks and complaints from both before and after the implementation of area navigation (RNAV).

Task 2 - Identify the Key Constraints and Opportunities for Procedure Design and Implementation of Noise-Minimizing Advanced Operational Procedures

Massachusetts Institute of Technology

Objectives

Arrival and departure procedure design is subject to physical, regulatory, and workload constraints. Procedures must be flyable by transport-category aircraft using normal, stabilized maneuvers and avionics. The procedures must comply with Terminal Instrument Procedures (TERPS) guidelines for obstacle clearance, climb gradients, and other limitations. The procedures must be chartable and work within the limitations of current flight management systems. Advanced operational procedures must also be compatible with airport and air traffic control operations, avoiding workload saturation for air traffic controllers and pilots.

This task involved evaluating the key constraints affecting advanced operational procedures and opportunities to improve noise performance, identifying those that may affect design and implementation. This process involved collaboration with pilots, air traffic controllers (ATC), procedure designers, and community members. The task also considered current research and evidence on physical, psychological, and social impacts of aircraft noise, as well as emerging issues such as community perceptions of equity and the effect of overflight frequency on noise perception.

Research Approach

- Meet with key stakeholders in the implementation pathway to understand procedure development processes, timeline, and constraints.
- Research documentation on regulations and operational standards influencing new flight procedure development.
- Consult with stakeholders during candidate advanced operational procedure development to identify potential implementation obstacles.

Major Accomplishments

- Finalized the design of proposed Boston Block 2 procedures and held meetings with operational stakeholders (ATC, pilots, FAA safety staff) to conduct preliminary assessments of feasibility. All proposed procedures for runways 22L/R, 27, and 33L have passed these preliminary checks.
- Identified categories of constraints (1) flight standards design criteria, (2) ATC rules and procedures, (3) aircraft limitations and standard operator practices—and recorded lessons learned in satisfying constraints in these three key areas.
- Shared key lessons learned regarding flight procedure constraints at the Fall 2021 ASCENT meeting.

Task 3 - Develop Concepts for Arrival and Departure Procedures that Consider Noise Impacts in Addition to Operational Feasibility Constraints

Massachusetts Institute of Technology

Objectives

This task applied the findings from task 2 to identify a set of generic flyable advanced operational procedures to minimize noise perception as measured by traditional metrics (e.g., 65 dB DNL) and alternative metrics that address noise concentration concerns introduced by PBN procedures and emerging equity issues. Given an understanding of technology capabilities and operational constraints, in this task we developed potential operational concepts and identified potential implementation pathways for both specific locations and generalizable operational concepts. Some of the approaches considered were:

- Lateral track management approaches (e.g., dispersion, parallel offsets, equivalent lateral spacing operations, multiple transition points, vectoring, high background noise tracks, and critical point avoidance tracks)
- Vertical/speed thrust approaches (e.g., thrust tailoring, steep approaches, and delayed deceleration approaches).

In addition, procedures were identified and categorized for the noise reduction effort at Boston Logan. These included Block 1 procedures, which were characterized by clear predicted noise benefits, limited operational/technical barriers, and a lack of equity issues, and Block 2 procedures, which exhibited greater complexity due to potential operational and technical barriers, as well as equity issues (defined as noise redistribution between communities).

Research Approach

- Use feedback from task 2 to identify procedures with noise reduction potential.
- Model procedures using AEDT and the Aircraft Noise Prediction Program (ANOPP) for generic runways to evaluate noise impacts for candidate procedures on a single-event or integrated basis.
- Determine noise impacts based on multiple metrics that are location-agnostic (i.e., contour area) as well as location-specific (i.e., population exposure at specific runways).

Major Accomplishments

- Investigated a *thrust cutback* concept for departure procedures, in which aircraft momentarily reduce engine thrust by flying a procedural level segment on departure, therefore also reducing engine noise.
- Published an academic paper at the 2021 AIAA SciTech conference on the thrust cutback concept, titled "Operational Noise Abatement through Control of Climb Profile on Departure."

Task 4 - Analyze Location-Specific Approach and Departure Design Procedures in Partnership with Affected Industry Stakeholders

Massachusetts Institute of Technology

Objectives

Advanced operational procedures may be particularly applicable for specific airports based on local geography, population density, operational characteristics, fleet mix, and local support for procedure modernization (among other factors). Specific procedures were evaluated for Boston Logan through a project with Massport. This task involved collaborating with airport stakeholders, air carriers, and local air traffic controllers on potential opportunities for developing lower-noise procedures for Boston Logan.

Research Approach

- Identify opportunities for procedural noise abatement through the evaluation of current flight trajectories, local noise complaint data, and community input.
- Develop new alternative procedures and modify existing procedures that both show potential for noise reduction and meet procedure implementation constraints.
- Work closely and communicate with affected stakeholders throughout the procedure evaluation, design, and analysis process to ensure that key constraints and objectives are appropriate for the selected location on a procedure-by-procedure basis.

Major Accomplishments

- Held regular meetings with airport and operational stakeholders to assess preliminary feasibility of procedures developed specifically for Boston Logan.
- Published the final Block 2 Report for the Boston Logan project, containing a series of low-noise procedure recommendations based on the analysis of flight tracks and community input.
- Continued regular meetings and collaboration with Massport and its Community Advisory Committee, ensuring that communities have the data needed to decide on what procedures to support.

Publications

- "Block 1 Procedure Recommendations for Logan Airport Community Noise Reduction," 2017. Link: http://hdl.handle.net/1721.1/114038
- Thomas, J; Hansman, J. "Framework for Analyzing Aircraft Community Noise Impacts of Advanced Operational Flight Procedures," *Journal of Aircraft*, Volume 6, Issue 4, 2019. https://doi.org/10.2514/1.C035100

- Thomas, J., Yu, A., Li, C., Toscano, P., and Hansman, R.J. "Advanced Operational Procedure Design Concepts for Noise Abatement" *In Thirteenth USA/Europe Air Traffic Management Research and Development Seminar*, Vienna, 2019.
- Yu, A., and Hansman, R.J. "Approach for Representing the Aircraft Noise Impacts of Concentrated Flight Tracks" *AIAA Aviation Forum 2019*, Dallas Texas, 2019.
- Salgueiro, S., Thomas, J., Li, C., and Hansman, R.J. "Operational Noise Abatement through Control of Climb Profile on Departure" *AIAA SciTech Forum 2021*.

Outreach Efforts

- September 27, 2017: Poster to ASCENT Advisory Board
- December 5, 2017: Call with Boeing to discuss procedure noise impact validity
- March 16, 2018: Discussion with Minneapolis-St. Paul (MSP) Airport about metrics
- April 4, 2018: Poster to ASCENT Advisory Board
- May 7, 2018: Presentation to FAA 7100.41 PBN Working Group
- June 24, 2018: Discussion with air traffic controllers about dispersion concepts
- July 23, 2018: Briefing to FAA Joint University Program research update meeting
- October 9, 2018: Poster to ASCENT Advisory Board
- November 8, 2018: Presentation to Airline Industry Consortium
- March 3, 2019: Presentation to the Aviation Noise and Emissions Symposium
- October 15, 2019: Presentation to the ASCENT Advisory Board
- November 12, 2019: Presentation to Airline Industry Consortium
- May 21, 2020: Meeting with operational stakeholders from FAA 7100.41 process to discuss Block 2 concepts
- September 23, 2021: Public hearing to present Block 2 procedure recommendations for Boston Logan
- Numerous community meetings
- Numerous briefings to politicians representing eastern Massachusetts (local, state, and federal)
- Briefing to FAA Management Advisory Council
- In-person outreach and collaboration with Massport, operator of Boston Logan and ASCENT Advisory Board member

Awards

2018 Dept of Transportation/FAA COE Outstanding Student of the Year Award to Jacqueline Thomas.
2021 Massachusetts Port Authority Logan Stars Award to the MIT International Center for Air Transportation research group.

Student Involvement

Graduate students have been involved in all aspects of this research in terms of analysis, documentation, and presentation.

Plans for Next Period

The next phase of this project will focus on the documentation of lessons learned from the Boston Logan project, during which several low-noise flight procedures were developed with considerable input from operational and community stakeholders. Based on findings from this step, areas of opportunity for future work will be considered in coordination with the Project Managers.

Project 025 Shock Tube and Flow Reactor Studies of the Kinetics of Jet Fuels - Rapid IR Fuel Screening

Stanford University

Project Lead Investigator

Ronald K. Hanson
Woodard Professor
Mechanical Engineering Department
Stanford University
452 Escondido Mall
650-723-6850
rkhanson@stanford.edu

University Participants

Stanford University

- PIs: Professor Ronald K. Hanson
- FAA Award Number: 13-C-AJFE-SU, Amendments 27, 28
- Period of Performance: October 1, 2020 to September 30, 2021
- Task:
    1. Area #1: Chemical kinetics combustion experiments

Project Funding Level

2020–2021: $300,000 from FAA with 1:1 matching funds of $300,000 from Stanford University

Investigation Team

- Professor Ronald K. Hanson, PI, research direction
- Alison Ferris, research scientist, research management
- Vivek Boddapati, graduate student, research assistant

Project Overview

The seventh year of this program has focused on developing and refining strategies for the accurate prediction of jet fuel properties (chemical and physical) and composition. To achieve this goal, the research focused on two areas: (a) new spectroscopic measurements of infrared (IR) spectra of jet fuels and pure hydrocarbons and (b) correlation of chemical, physical, and combustion fuel properties with IR spectral features. The results of the IR spectral analysis work will be used to establish the strong sensitivity of the physical and chemical properties of jet fuels to their molecular structure, with the ultimate goal of developing a rapid pre-screening approach, requiring minimal fuel volume, to simplify the certification process for alternative jet fuels. These IR-spectra-based correlation models will also potentially aid in the development of future kinetic models for jet fuel combustion.

Task 1 - Chemical Kinetics Combustion Experiments

Stanford University

Objective(s)

This work aims to develop fuel prescreening tools based on the IR absorption cross-section measurements of jet fuels and their constituent molecules. Specific fuel analysis objectives include developing effective strategies for correlating (a) chemical, physical, and combustion properties of jet fuels and (b) functional group and molecular species composition with their IR spectra.

This multi-year research program has culminated in the completion of American Institute of Aeronautics and Astronautics (AIAA) book chapters describing the research progress during the past 7 years, notably the advancements in the understanding of jet fuel chemical kinetics and fuel prescreening techniques.

Research Approach

An important goal of the current research is to characterize jet fuel composition and properties on the basis of the fuel's mid-IR absorption spectrum, measured with a Fourier transform IR (FTIR) spectrometer. Over the past 2 years, a database of spectroscopic measurements and property data for a variety of jet fuels and jet fuel components has been acquired. Using this database, we have developed correlations between the spectroscopic properties of neat jet fuel and the fuel composition as well as with important physical/combustion properties, such as the initial boiling point (IBP), density, derived cetane number (DCN), and ignition delay times (IDT). Here, an overview of the two research areas (FTIR spectroscopic measurements and IR fuel analysis) is presented along with experimental and modeling results obtained over the past year.

FTIR Spectroscopic Measurements: Methods and Results

An FTIR instrument (Nicolet 6700) and heated cell are used to measure the mid-IR spectra of gas-phase fuel samples. Analysis of gas-phase samples allows for the detection of sharp spectral features, even individual absorption transitions, which can in turn be tied directly to structural characteristics of fuel molecules. This work focuses on the analysis of mid-IR absorption spectra, because of the strong sensitivity of the mid-IR region to hydrocarbon bonding. Initial work in the previous year of the program focused solely on the 3-μm spectral region, which contains the C–H stretch absorption features corresponding to the -CH_2 and -CH_3 functional groups in hydrocarbon molecules. These features are characteristic of *n*-paraffins and isoparaffins, but do not offer any distinctive information about cycloparaffins and aromatic compounds, which are often important constituents of jet fuels. To capture additional features corresponding to these molecular classes, we extended the wavelength range of acquired IR spectra to cover the entire 2- to 15-μm region.

The 2- to 15-μm FTIR spectra of approximately 35 pure hydrocarbons were sourced from the Pacific Northwest National Laboratory (PNNL) spectroscopic database. The spectra of 24 pure hydrocarbon blends were calculated by using the mole-fraction-weighted sums of the spectra of individual components. The measurement of the extended-wavelength spectra of additional pure hydrocarbons and jet fuels required modification of our in-house FTIR spectrometer facility. To this end, the sapphire optical windows on the heated cell were replaced with new ZnSe windows that transmit IR light across 2–15 μm. The system was then subjected to leak testing to ensure that the optical cell was well sealed. A new IR light source was installed in the FTIR spectrophotometer to improve the signal at long wavelengths (12–15 μm). Because a portion of the optical path length of the FTIR setup passed through open atmosphere, interfering absorbance from atmospheric water and carbon dioxide was observed in the spectral measurements. To mitigate the effects of this interfering absorbance on our measurements, we constructed a purge system to enclose the entire optical path, as shown in Figure 1. A line was provided to purge the setup with nitrogen gas, which, unlike water and carbon dioxide, does not absorb IR light.

Figure 1. The modified FTIR spectrometer facility, with a purge system constructed to enable purging of the entire optical path length with nitrogen gas during measurements.

Preliminary 2- to 15-μm spectra of toluene, *n*-octane, and iso-octane were measured with the modified system and were found to be in agreement with spectra taken from the PNNL database. Subsequently, the spectra of several jet-fuel-relevant pure hydrocarbons (*n*-dodecane, isocetane, methylcyclohexane, *n*-propylcyclohexane, *trans*-decalin, and 1-methylnaphthalene) were measured at a temperature of 150 °C and added to our database of FTIR spectra. Multiple fuel concentrations were used during the measurement of each fuel to capture the weaker absorption features with a high signal-to-noise ratio. An example measurement of methylcyclohexane (MCH) is shown in Figure 2, with the important spectral features labeled. The dataset was further expanded by measuring the spectra of 17 A and C category jet fuels A1–A8 and C1–C9. These, spectra along with the pure hydrocarbon spectra from PNNL and the calculated blends' spectra were compiled into the training dataset, thus bringing the total to 81 fuels, representing a considerable improvement with respect to the dataset size of 63 fuels in the previous year.

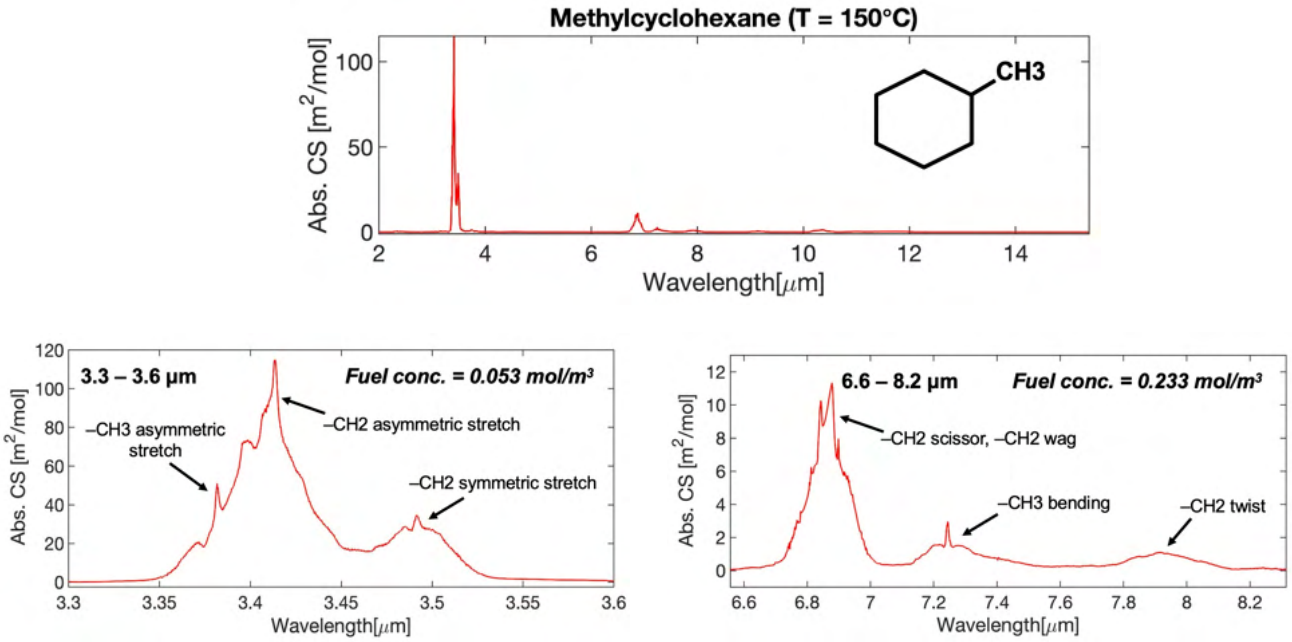

Figure 2. Measured 2- to 15-μm spectrum of methylcyclohexane (top); strong -CH_2 and -CH_3 stretch features in the 3.3- to 3.6-μm region, captured by using a using low fuel concentration (bottom left); relatively weaker -CH_2 and -CH_3 bending features in the 6.6- to 8.2-μm region captured by using a high fuel concentration (bottom right).

IR Fuel Analysis: Methods and Results

In the past 2 years of this program, four strategies (strategies 1–4) were developed for estimating physical and chemical properties, functional group fractions, and molecular species constituents of fuels directly from mid-IR spectra in the 3-μm region. In the current year of this program, two of these developed strategies (strategies 1 and 4) were further refined to improve their predictive performance. The methods and results for each strategy are discussed below.

The first iteration of strategy 1 implemented cross-validated linear models with Lasso regularization to correlate the FTIR spectra from 3300 to 3500 nm with a fuel's physical and chemical properties. Although these preliminary models showed good prediction accuracy for *n*-paraffins and isoparaffins, they had higher property prediction error for aromatic compounds. To improve the performance of these models, we modified the training dataset to include the full 2- to 15-μm FTIR spectra of fuels. Furthermore, the models were modified to use Elastic Net regularization instead of Lasso regulation, enabling the selection of optimal model parameters for each property during training. For implementation, a grid search was first performed to choose the combination of model parameters resulting in the minimum cross-validation error (CVE), which were then used to train the final model for each property. Figure 3 demonstrates this improvement in strategy 1 performance on the training data for the property IBP.

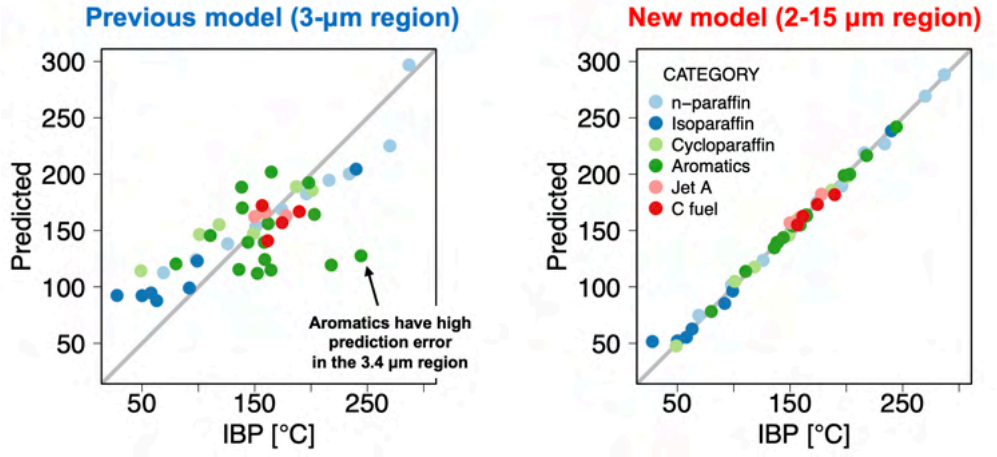

Figure 3. Actual versus predicted values of IBP by using strategy 1 models: previous model based on 3-μm FTIR spectra (left); new model based on 2- to 15-μm FTIR spectra (right).

These two plots indicate that the new model (based on 2- to 15-μm spectra) fits the data much better than the previous model (based only on the 3-μm spectral region). The previous model shows poor prediction for aromatic compounds in particular, which do not have distinctive absorption features in the 3-μm region. The performance improvement is further evidenced by the decrease in CVE (indicative of future predictive performance) and an increased R^2 value (measure of goodness of fit). These results are summarized in Table 1. Similar performance improvements were observed for all properties considered.

Table 1. Strategy 1 performance metrics for IBP: CVE, mean absolute error (MAE) on the training data, and R^2 value.

Method	CVE (%)	MAE (%)	R^2 value
Previous model (3-μm region)	18.93	17.72	0.59
New model (2-15 μm region)	5.61	1.95	0.99

Figure 4 shows the 38 wavelengths selected by the new strategy 1 model, along with their relative contributions to the variation in IBP. This plot clearly shows that the model selects multiple wavelengths outside the 3-μm region, which contribute considerably to IBP prediction, thus explaining the gain in prediction accuracy due to the extended spectral range.

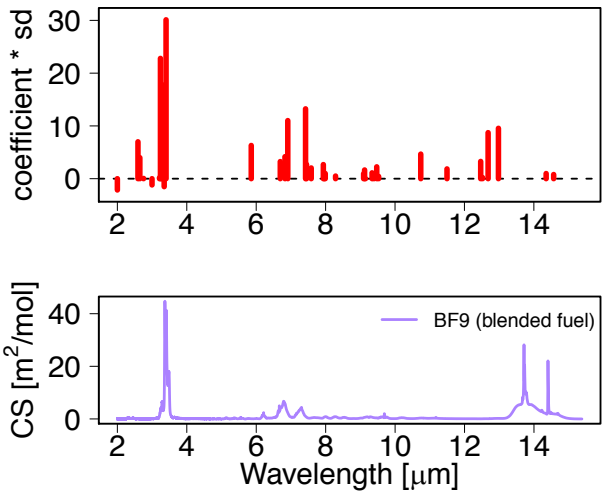

Figure 4. Wavelengths selected by the new strategy 1 model (based on 2- to 15-μm spectra) and their contributions to the variation in IBP (top); representative IR spectrum of BF9, a three-component hydrocarbon blend (bottom).

Strategy 4 was developed to infer the molecular species content of a fuel from its IR spectrum. This strategy uses a constrained least-squares optimization approach to accurately identify the components of a blended fuel and predict their respective mole fractions. This strategy, which was previously restricted to the 3-μm spectral region, was modified to estimate the molecular species composition of fuels based on the extended 2- to 15-μm FTIR spectra. To test this approach, we calculated the spectrum of a six-component mixture of pure hydrocarbons (35% *n*-decane, 7% 3-methylhexane, 22% isooctane, 9% mesitylene, 16% *o*-xylene, and 11% *m*-xylene) with a mole-fraction-weighted sum of the individual components' spectra. Strategy 4 was then used to estimate the composition of this simulated mixture from a set of 35 pure hydrocarbon spectra, all from the PNNL database. Particular emphasis was placed on quantifying the uncertainty in the predicted mole fractions by using a Monte Carlo method and simultaneously varying the spectra of the 35 database components within the FTIR experimental uncertainty range (±1.25%). This method is demonstrated in Figure 5.

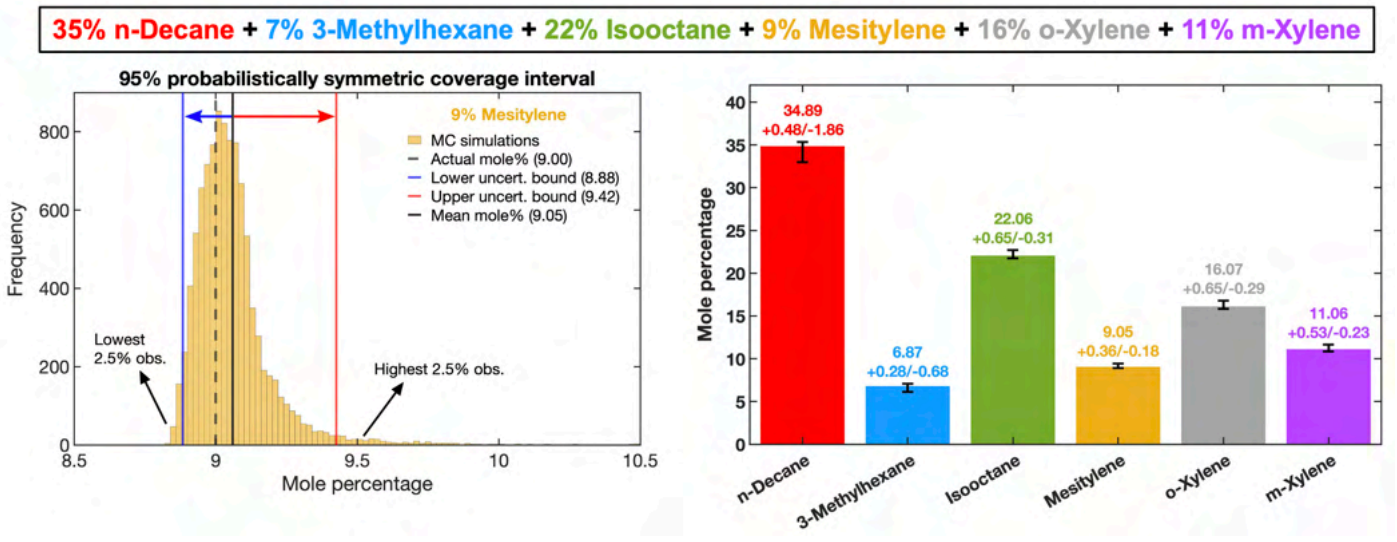

Figure 5. Strategy 4 uncertainty quantification for a simulated six-component mixture. Estimation of 95% confidence interval with Monte Carlo simulations for each component, shown here for mesitylene (left); estimated uncertainties in the mole percentages of the six components predicted with strategy 4 (right).

As seen above, strategy 4 can be used to estimate the molecular composition of blended fuels within tight uncertainty bounds. This information can then be used to accurately determine the basic properties of the composite fuel, such as the C and H number, and the average molecular weight (MW), by using additive models. Figure 6 below draws a comparison between the uncertainties in the predicted MW of the simulated six-component mixture for strategy 1 (both the previous model and the new model) and strategy 4. As seen in this plot, the new strategy 1 model, as expected, is more accurate than the previous model in predicting the mixture MW. However, strategy 4 clearly outperforms strategy 1 in terms of the prediction uncertainty for MW. Hence, strategy 4 provides a more accurate way of predicting certain linearly additive properties of complex fuel mixtures.

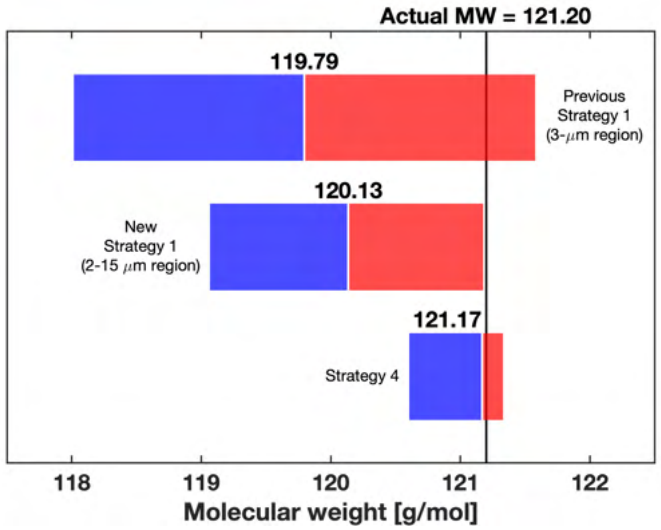

Figure 6. Comparison of uncertainty in the prediction of MW of the simulated six-component mixture by using the previous strategy 1 model (3-μm region), the new strategy 1 model (2- to 15-μm region), and strategy 4.

Overall, the IR analysis results obtained with the two refined strategies (strategies 1 and 4) developed over the past year show improved predictive performance relative to that of the initial spectral analysis strategies developed in the previous 2 years of this work. Together, these strategies provide the capability to accurately predict the physical and chemical properties, and the molecular composition of jet fuels directly based on their IR spectra.

Milestone(s)

Major milestones included regular reporting of experimental results and analysis at the National Jet Fuels Combustion Program (NJFCP) teleconferences (October, 2020 and February, 2021), as well as the Fall and Spring ASCENT meetings (September 2020 and April 2021).

Major Accomplishments

During the seventh year of this program, major advances were made in several areas:

- The FTIR spectrometer facility was modified to enable spectroscopic measurements in the extended wavelength region spanning 2- to 15-μm.
- New 2- to 15-μm FTIR spectra of jet-fuel-relevant pure hydrocarbons, and A and C category real fuels were measured.
- An expanded training dataset of FTIR spectra and property data was compiled by using a combination of in-house measurements and the PNNL spectral database.
- The previously developed strategy 1 model was modified with the extended spectral range and hyperparameter tuning methods to select the optimal model parameters for each property.
- The strategy 4 model was refined by implementing a Monte Carlo method to quantify uncertainties in the predicted mole fractions of a simulated six-component mixture and was further used to accurately estimate the mixture's MW with high confidence.

- Our contribution to the jet fuel prescreening section of the AIAA volume titled *Fuel Effects on Operability of Aircraft Gas Turbine Combustors* was completed.

Publications

Peer-reviewed journal publications

Wang, Y., Wei, W., Hanson, R. K. (2021). A new strategy of characterizing hydrocarbon fuels using FTIR spectra and generalized linear model with grouped-Lasso regularization. Fuel, *287*, 119419. https://doi.org/10.1016/j.fuel.2020.119419

Published book chapters

Park, J. W., Xu, C., Gao, Y., Lu, T. F., Shao, J. K., Pinkowski, N. H., Wang, S., Wang, Y., Cao, Y., Hanson, R. K., Davidson, D. F., & Colket, M. B. (2021). Chemical kinetics. In: J. Heyne, & M. Colket (Eds.), *Fuel effects on operability of aircraft gas turbine combustors* (pp. 255-293). American Institute of Aeronautics and Astronautics, Inc.

Heyne, J., Yang, Z., Boehm, R., Rauch, B., Le Clercq, P., Hanson, R., Ferris, A., Dooley, S., Ure, A., Blakey, S., Lewis, C., Colket, M. (2021). Prescreening of sustainable aviation jet fuels. In: J. Heyne, & M. Colket (Eds.), *Fuel effects on operability of aircraft gas turbine combustors* (pp. 487-523). American Institute of Aeronautics and Astronautics, Inc.

Outreach Efforts

Our IR fuel analysis work was presented at the Joint NJFCP Meetings on October 20, 2020 and February 2, 2021; the Virtual Fall ASCENT Advisory Board Meeting, September 29–30, 2020; and the Virtual Spring ASCENT Advisory Board Meeting, April 27–29, 2021. We have also begun collaborating with Professor Joshua Heyne's group at the University of Dayton in examining the effects of isomeric structure on jet fuel combustion properties.

Awards

None

Student Involvement

Graduate students are actively involved in the acquisition and analysis of all experimental data. Vivek Boddapati (current graduate student) performed the IR spectral analysis/fuel prescreening. Yu Wang successfully defended his PhD thesis, which was partly based on work performed under this contract. Alison Ferris (current research scientist) has additionally contributed to the project through research management, compilation of experimental results, and report writing.

Plans for Next Period

In the next period, we plan to perform the following:

- Acquire additional FTIR measurements and property data of neat hydrocarbons and real fuels to further expand the current dataset
- Train strategy 3 models (principal component analysis + support vector regression) by using the expanded 2- to 15-μm spectra and assess the improvement in predictive performance compared with just the 3-μm region, particularly for highly non-linear properties (e.g., kinematic viscosity)
- Apply these wide-spectrum IR analysis methods to the prescreening and characterization of real, sustainable aviation fuel (SAF) candidates.
    - Acquire candidate SAF samples and property data from ASCENT/NJFCP partners
- Investigate further refinement of IR analysis strategies to enhance their predictive accuracy and applicability to a wider range of jet fuels, particularly those from bio-derived feedstocks
- Explore the potential of IR spectral analysis methods for predicting important combustion parameters and subsequently guiding the development of kinetic models for jet fuel combustion

Project 029(A) National Jet Fuel Combustion Program – Area #5: Atomization Test and Models Final Report

Purdue University

Project Lead Investigator

Robert P. Lucht
Ralph and Bettye Bailey Distinguished Professor of Combustion
School of Mechanical Engineering
Purdue University
West Lafayette, IN 47907-2088
Cell: 765-714-6020
Lucht@purdue.edu

University Participants

Purdue University

- PIs: Robert P. Lucht, Jay P. Gore, Paul E. Sojka, and Scott E. Meyer
- FAA Award Number: 13-C-AJFE-PU, Amendments: 05, 11,16, 21, 28, 30
- Period of Performance: December 1, 2014 to December 19, 2020
- Tasks:
    1. Obtain phase Doppler anemometry (PDA), Mie scattering, and fuel laser-induced fluorescence data in the variable ambient pressure spray (VAPS) test rig operated with the referee rig nozzle for numerous fuels under near-lean blowout (near-LBO) conditions and under cold fuel/cold air flow conditions approximating ground light-off (GLO) and high-altitude relight conditions (HAR).
    2. Perform computational fluid dynamics (CFD) simulations of the referee rig under near-LBO and LBO conditions for different fuels.

Project Funding Level

The funding level from FAA was $1,020,000 to Purdue University. Purdue University provided cost-sharing funds.

Investigation Team

- PI Dr. Robert Lucht, Bailey Distinguished Professor of Mechanical Engineering, is responsible for overseeing the project at Purdue University. He is also responsible for mentoring one of the graduate students, coordinating activities with Stanford, working with all parties for appropriate results, and reporting results as required.
- Co-PI Dr. Jay P. Gore, Reilly Professor of Mechanical Engineering, works closely with the PI and oversees the work performed by one of the graduate students. He is also responsible for interacting with the CFD groups to suggest comparisons with experiments and with results of an adaptive grid solver.
- Co-PI Dr. Paul Sojka, Professor of Mechanical Engineering, is mentoring one of the graduate students and is responsible for supervising the spray measurements.
- Co-PI Scott Meyer, Managing Director of Maurice J. Zucrow Laboratories, is responsible for coordinating facility upgrades and for performing facility design reviews.
- Dr. Sameer V. Naik, Senior Research Scientist, is responsible for direct supervision of two graduate students involved in the experimental portion of the project.
- Graduate students Andrew Bokhart and Daniel Shin are responsible for performing the phase Doppler anemometry (PDA) measurements and for modifying the Rules & Tool Spray (RTS) test rig for operation at near-LBO conditions.
- Graduate student (until December 2019) and current research assistant professor, Hasti Veeraraghava Raju has conducted simulations with an adaptive grid solver and has performed comparisons with experimental results and results from the other CFD groups.

- Graduate student Neil Rodrigues contributes to the project by providing advice for the PDA measurements and technical editing.

Project Overview

The objectives of this project, as stated in the invitation for ASCENT COE Notice of Intent (COE-2014-29), are to "measure the spray characteristics of the nozzles used in the Referee Combustor used in Area 6 tests and to develop models for characterizing the atomization and vaporization of the reference fuels." We are conducting experiments within the joint experimental and modeling effort. The experimental tasks are being performed at Purdue University, and the modeling tasks are being performed by Professor Matthias Ihme's group at Stanford University, Prof. Suresh Menon's group at Georgia Tech, and Vaidya Sankaran's group at United Technologies Research Center (UTRC). Nader Rizk (Rolls Royce, retired) is developing spray correlations based on the measurements.

Purdue University has highly capable test facilities for measuring spray characteristics over wide ranges of pressure, air temperature, and fuel temperature. The experimental diagnostics applied in this project include PDA and high-frame-rate shadowgraphy. The atomization and spray dynamics for multiple reference and candidate alternative fuels have been characterized for the referee rig nozzle operating under near-LBO conditions. In the future, measurements will be performed for these fuels under operating conditions characteristic of HAR. A new fuel, IH^2 (Shell CPK-0), has been added to the test matrix and is being investigated under LBO and cold-start conditions.

Experimental Contributions

Objectives

The primary objectives of the work at Purdue University are to visualize and measure the nonreacting spray characteristics, including drop size distributions and axial velocity components of the sprays generated by a nozzle being used in the referee combustor rig in the Area 6 tests for standard and alternative aviation fuel candidates under a wide range of engine operating conditions. The upgraded Variable Ambient Pressure Spray (VAPS) test rig at Purdue allows us to investigate the spray characteristics for a variety of standard and alternative aviation fuels near LBO, engine cold-start, and high-ambient-pressure conditions. PDA has emerged as a technique of choice for obtaining fundamental drop size distribution and axial and radial velocity data for comparison with numerical simulations. The VAPS facility has been upgraded to allow us to test over the entire range of fuel and air temperatures and air pressures of interest.

The resulting data will be used for the development of spray correlations by consultant Nader Rizk and for the purpose of submodel development for detailed computer simulations being performed by Matthias Ihme, Suresh Menon, and Vaidya Sankaran. The experimental tasks are being performed at Purdue University, and the resulting data will be shared with FAA team members developing modeling, simulations, and engineering correlation-based tools.

The experimental data will support continued development and evaluation of engineering spray correlations, including the dependence of Sauter mean diameter (SMD), spray cone angle, and particle number density per unit volume on the fuel properties at fuel and air temperatures of interest. The experimental data will provide detailed statistical measurements for comparisons with high-fidelity numerical simulations of mixing and combustion processes. The prediction of the spatial distribution of the liquid fuel and the resulting vapor and breakdown components from the liquid fuels critically affect the ignition, flame-stabilization, and pollutant formation processes.

Major Accomplishments

Investigation at LBO Conditions

The representative diameters are used to characterize the spray: D_{10}, D_{32}, and *MMD*. D_{10} is the arithmetic mean diameter (first order mean) that represents the average drop diameter. The arithmetic mean diameter can be expressed as:

$$D_{10} = \frac{\sum N_i D_i}{\sum N_i}$$

where N_i is the number of droplets and D_i indicates the drop diameter. The subscription, i, indicates the drop size class.

D_{32} is a fifth order mean diameter that represents the ratio of drop volume to drop surface area. This is also called Sauter Mean Diameter (SMD). D_{32} is a representative diameter that typically used for drop size comparisons in mass transfer and reaction applications. The Sauter Mean Diameter (D_{32}) can be expressed as:

$$D_{32} = \frac{\sum N_i D_i^3}{\sum N_i D_i^2}$$

Lastly, *MMD* indicates the mass median diameter, which represents the diameter at which 50% of the total liquid volume is contained within smaller diameters. The expression for *MMD* is:

$$0.5 = \int_0^{MMD} f_3(D)dD$$

where, f_3 (D) indicates the volume probability density functions and *dD* is the drop size bin.

The mean axial drop velocity, U_z, measured by the PDA system was also used to represent the drop size velocity at different spray locations. The PDA system measures 20,000 sample droplets at each radial location within the spray, and U_z is the mean of 20,000 axial drop velocity values.

Effect of pressure drop

The pressure drop across the swirler ($\Delta P/P$) was observed to have a significant effect on the D_{10}, D_{32}, *MMD*, and the axial velocity U_z for both standard (Jet A) and alternative aviation fuels (C-1, C-5, C-7, and C-8). Figure 1 shows that D_{10}, D_{32}, and *MMD* decreased with increasing $\Delta P/P$ for all radial locations. The magnitude of the drop velocity was observed to increase for greater $\Delta P/P$, as shown in Figure 1d. Higher $\Delta P/P$ results in a higher atomizing gas velocity, which leads to greater inertial and aerodynamic forces to overcome the viscous and surface tension forces of the bulk liquid and, in turn, results in smaller drop diameters. The drop velocities near the center of the spray were negative, which confirms that a majority of the droplets near the center were traveling back toward the injector within the hollow cone. No significant variation was observed at r = 15 mm, where the transition of the spray from the hollow cone to the fuel cone exists. Similar trends in drop size and velocity as functions of $\Delta P/P$ were observed at the measurement planes (z) of 12.7 and 38.1 mm and for C-1, C-5, C-7, and C-8 fuels.

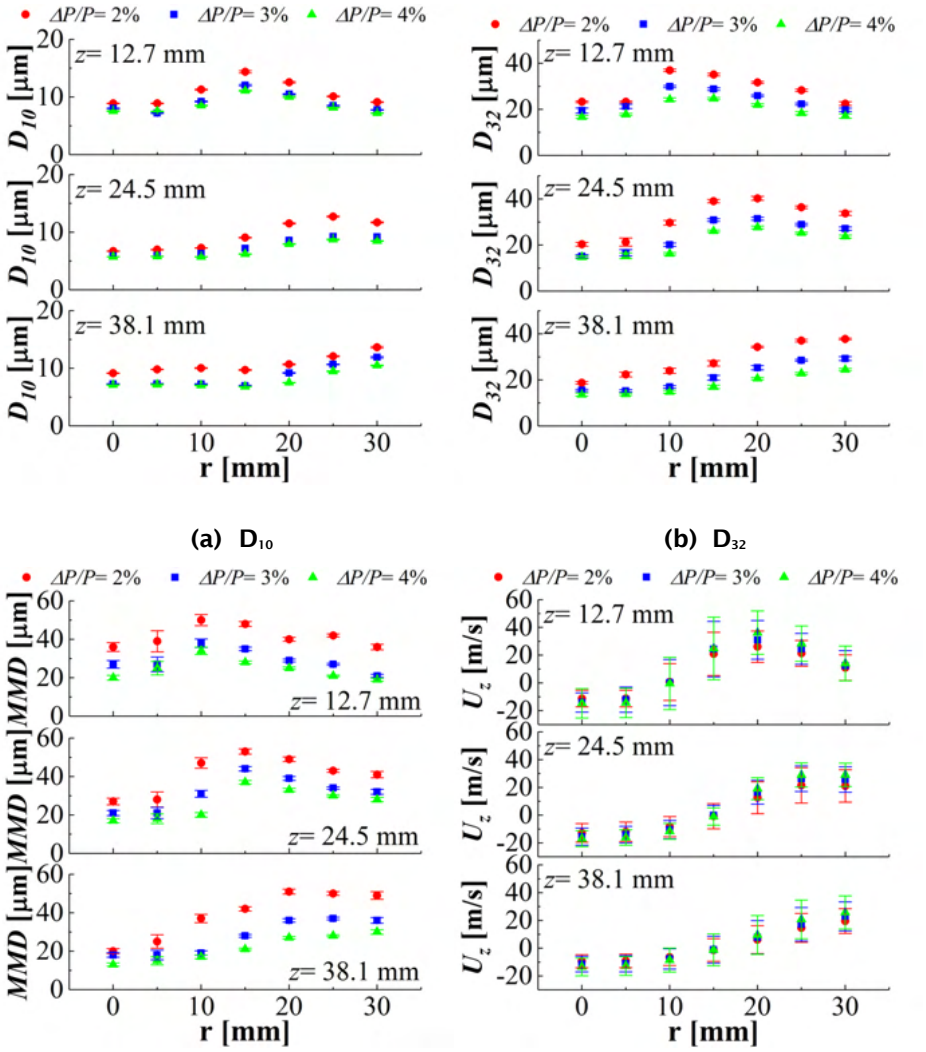

Figure 1. Drop diameter (D_{10}, D_{32}, *MMD*) and drop velocity (U_z) distributions for A-2 at pressure drop ($\Delta P/P$) = 2, 3, and 4% for measurement plane (z) = 12.7, 25.4, and 38.1 mm. D_{10} = arithmetic mean diameter; D_{32} = Sauter Mean Diameter; MMD = mass median diameter; r = radial location.

Effect of fuel injection pressure

The fuel injection pressure differential across the pilot nozzle, ΔP_{Pilot}, was varied to values of 1.72, 3.45, and 5.17 bar to investigate the effect of fuel mass flow rate on drop size and drop velocity. ΔP_{Pilot} dictates the total fuel mass flow rate through the pilot nozzle. The mass flow rates as measured by a Coriolis flow meter for each fuel injection pressure were 2.52, 3.56, and 4.59 g/s, respectively. Figure 2 shows D_{32} and U_z for the A-2 fuel. The effect of the fuel injection pressure on the mean drop size and velocity was found to be minimal. We considered that the variations in fuel injection pressure (1.72–5.17 bar) were not significant enough to affect mean drop size due to the dominating effect of the atomizing gas from the airblast component of the atomizer.

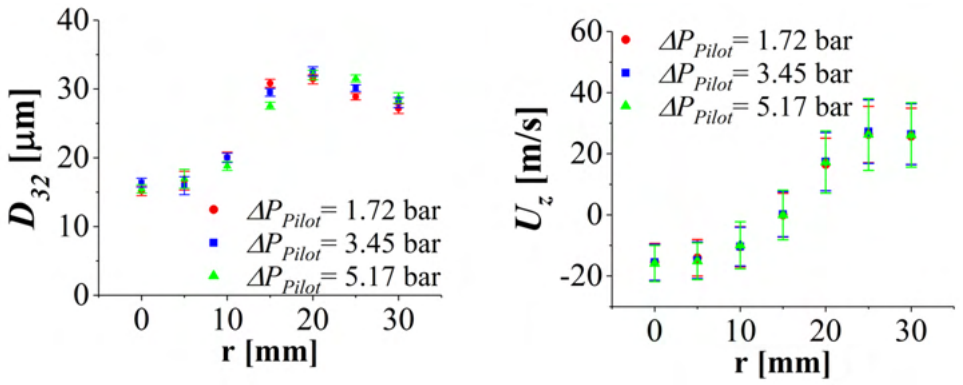

(a) D_{32} **(b) Uz**

Figure 2. Drop diameter (D_{32}) and drop axial velocity (U_z) with variation in fuel injection pressure (ΔP_{Pilot}). r = radial location.

Effect of fuel type

The effect of fuel type (A-2, C-1, C-5, C-7, and C-8) was investigated under LBO conditions for $\Delta P/P$ = 2, 3, and 4%. Figure 3 shows D_{32} and U_z for each fuel at the 25.4-mm measurement plane. The D_{32} measurement showed that C-7 formed the largest droplets and C-1 formed the smallest. We observed that the effect of viscosity on drop size was minimal, with approximately 60% variation in viscosity value among fuels at LBO conditions. The drop size trend, however, seemed to follow the surface tension near the spray edge (r >15 mm). The U_z measurements showed no significant variations among the fuels tested.

Figure 4 shows the relationships between line-of-sight D_{32} (D_{32o}) and viscosity and surface tension for all six fuels. D_{32o} is an averaged D_{32} value of the overall radial profile that is weighted by the volume flux at each radial location. As shown in Figure 4, no definitive relationship between the viscosity and drop size was observed. Drop size, however, tended to increase slightly with increasing surface tension. This was thought to be due to the high atomizing gas impingement angle onto the ligament that is formed at the prefilmer tip. It is hypothesized that if the atomizing gas impingement angle was lower than or parallel to the ligament axis, the effect of viscosity may not be negligible due to its resistance force to flow. However, if the gas impingement angle is close to normal, the surface tension is only responsible for the ligament breakup related to atomization energy. The model also successfully demonstrated drop size trends observed with viscosity and surface tension in Figure 4.

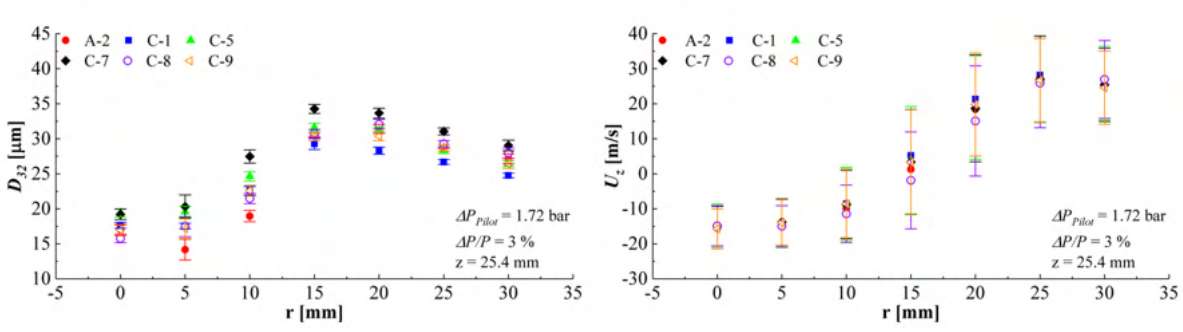

(a) D_{32} **(b) Uz**

Figure 3. Comparison of drop diameters (D_{32}) and drop velocities (U_z) for six fuels (A-2, C-1, C-5, C-7, C-8, and C-9) at lean blowout conditions. ΔP_{Pilot} = variation in fuel injection pressure; $\Delta P/P$ = pressure drop; z = measurement plane; r = radial location.

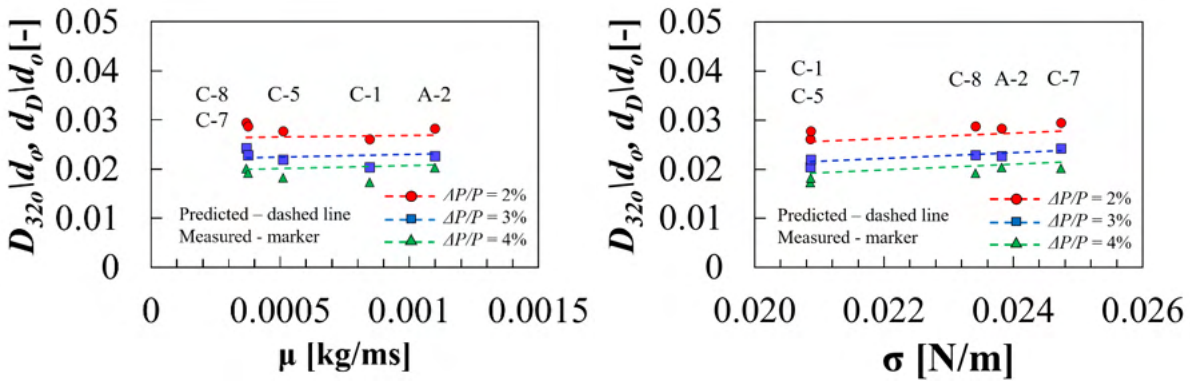

(a) D_{32o}/do and dD/do vs. viscosity **(b) D_{32o}/do and dD/do vs. surface tension**

Figure 4. Relationships between measured D_{32} and viscosity and surface tension for jet fuels A-2, C-1, C-5, C-7, and C-8. Dashed lines indicate the model predictions. D_{32o} = line of sight D_{32}; d_o = orifice diameter; d_D = predicted D_{32}; $\Delta P/P$ = pressure drop; μ = viscosity; σ = surface tension.

Investigation at Engine Cold Start Conditions

Effect of pressure drop

The pressure drop across the swirler ($\Delta P/P$) was found to have a significant effect on parameters D_{32} and U_z for the A-2, A-3, and C-3 fuels. Figure 5 shows the spatial distributions of D_{32} and U_z for pressure drops of 2, 3, and 4%, at a constant fuel injection pressure differential ($\Delta P/P$) of 1.72 bar and at a measurement plane (z) of 25.4 mm for A-2 and C-3 fuels. The air-to-liquid ratios of the atomizer for pressure drops of 2, 3, and 4% were calculated to be 12, 15, and 17, respectively. Drop size D_{32} was observed to decrease significantly as the pressure drop increased. The mean drop axial velocity, in contrast, increased in magnitude with increasing pressure drop. An increase in pressure drop results in a higher atomizing gas velocity, which corresponds to greater inertial and aerodynamic forces for the gas flow. This amplified the hydrodynamic instabilities of the bulk fuel and resulted in smaller droplets. Similar drop size and drop velocity trends were observed for A-3 fuel.

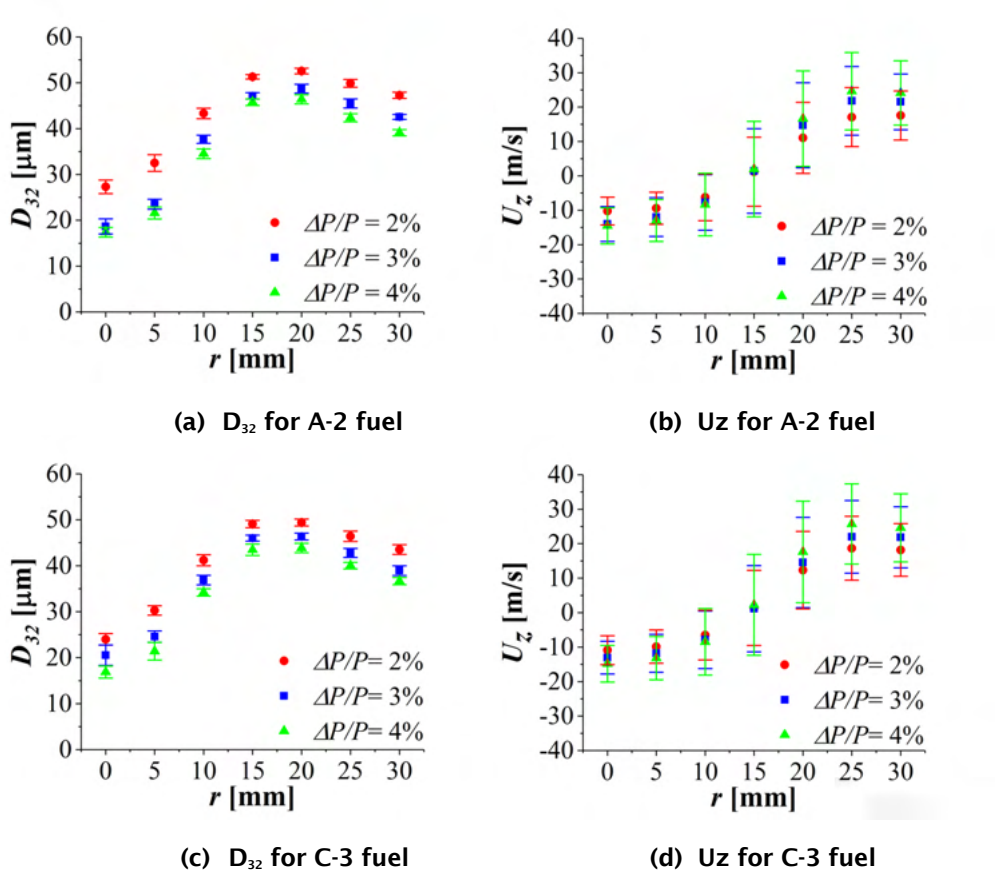

(a) D_{32} for A-2 fuel (b) Uz for A-2 fuel

(c) D_{32} for C-3 fuel (d) Uz for C-3 fuel

Figure 5. Comparisons of drop diameters (D_{32}) and drop velocities (U_z) for A-2 and C-3 fuels at $\Delta P/P$ = 2, 3, and 4%, ΔP_{Pilot} = 1.72 bar, T_{fuel} = 239 K, and T_{airbox} = 239 K for measurement plane (z) = 25.4 mm. ΔP_{Pilot} = variation in fuel injection pressure; $\Delta P/P$ = pressure drop; r = radial location; T_{fuel} = fuel temperature; T_{airbox} = airbox temperature.

Effect of fuel type

Three fuels (A-2, A-3, and C-3) were compared to investigate the effects of fuel properties on drop diameters and axial velocities. Figure 6 shows the comparisons of D_{32} and U_z for the three fuels at $\Delta P/P$ = 3% at the 25.4-mm measurement plane. The C-3 fuel had the highest viscosity value among the fuels and was expected to form larger droplets. However, it formed droplets with the smallest D_{32}. The largest D_{32} was observed for the A-3 fuel within the recirculation zone, whereas the A-2 and C-3 fuels formed droplets with similar D_{32} in the same region. The A-2 fuel was observed to form droplets with the largest D_{32} near the edge of the spray, and C-3 fuel formed droplets with the smallest D_{32}.

Figure 7 shows the relationship between the line-of-sight D_{32} (D_{32o}) and viscosity and surface tension for all three fuels under cold-start conditions. Based on these observations, we determined that the effect of surface tension dominated the effect of viscosity on drop sizes. The model (dashed lines) successfully demonstrated these drop size trends with viscosity and surface tension for three different pressure drop values.

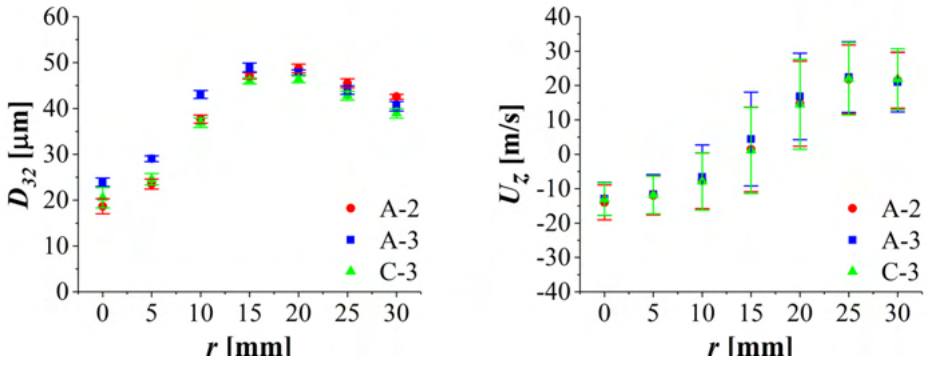

(a) D_{32} for A-2, A-3, and C-3 fuels **(b) Uz for A-2, A-3, and C-3 fuels**

Figure 6. Comparisons of drop diameters (D_{32}) and drop velocities (U_z) for A-2, A-3 and C-3 fuels at $\Delta P/P$ = 3%, ΔP_{Pilot} = 1.72 bar, T_{fuel} = 239 K, and T_{airbox} = 239 K for measurement plane (z) = 25.4 mm. $\Delta P/P$ = pressure drop; r = radial location; ΔP_{Pilot} = variation in fuel injection pressure; T_{fuel} = fuel temperature; T_{airbox} = airbox temperature.

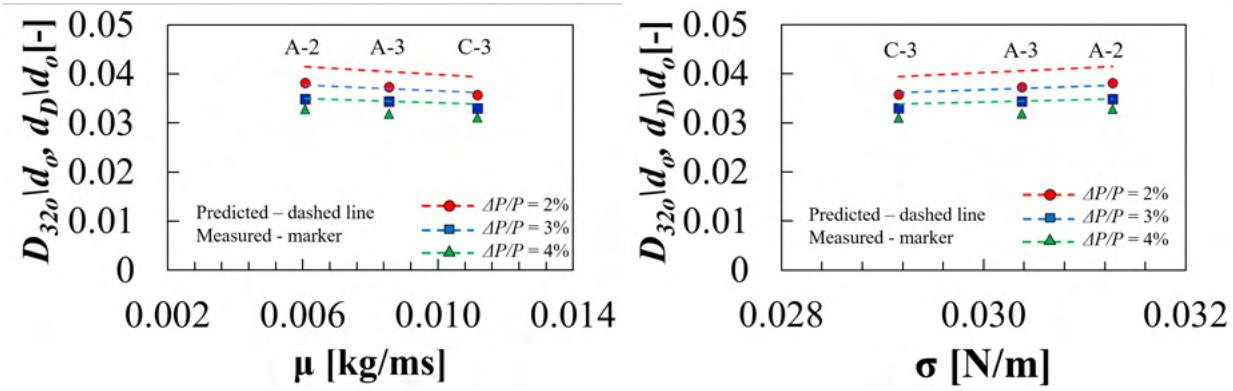

(a) D_{32o}/do and dD/do vs. viscosity **(b) D_{32o}/do and dD/do vs. surface tension**

Figure 7. Relations between measured D_{32} and viscosity and surface tension. Dashed lines indicate the model predictions. D_{32o} = light of sight D_{32} ; d_o = orifice diameter; d_D = predicted D_{32}; $\Delta P/P$ = pressure drop; μ = viscosity; σ = surface tension

Investigation at High Ambient Pressure Conditions

Effect of ambient pressure

Ambient pressure (P_{vessel}) was found to significantly affect mean drop size. As shown in Figure 8, a significant decrease in D_{32} was observed as P_{vessel} increased from 1 bar to 9.5 bar. However, the effect of P_{vessel} on drop diameters diminished with a further increase in P_{vessel}. Furthermore, the spray tended to have a monodisperse drop size at higher P_{vessel}. The greater inertial and drag forces on a droplet and ligament with increasing density of the ambient gas resulted in smaller droplets. The drop axial velocity was observed to be similar for all ambient pressures, as shown in Figures 8(b) and 8(d). However, droplets near the spray edge were observed to slow down with increasing pressure because they were more affected by the drag force. The hollow-cone region boundary was observed to be preserved at higher ambient pressure.

The effect of pressure drop ($\Delta P/P$) on D_{32} and U_z was observed to be significant at P_{vessel} = 5 bar, as shown in Figure 9 for A-2 fuel. The pressure drop was varied to values of 2, 3, and 6% at ΔP_{pilot} = 1.72 bar, T_{fuel} = 332 K, T_{airbox} = 394 K, and z = 25.4 mm. The D_{32} decreased with increasing $\Delta P/P$ and tended to be monodisperse across the radial locations at higher $\Delta P/P$. Drop axial

velocity was observed to increase with increasing $\Delta P/P$, as shown in Figure 9(b). Greater inertial force of the gas flow with increasing $\Delta P/P$ led to the formation of smaller droplets.

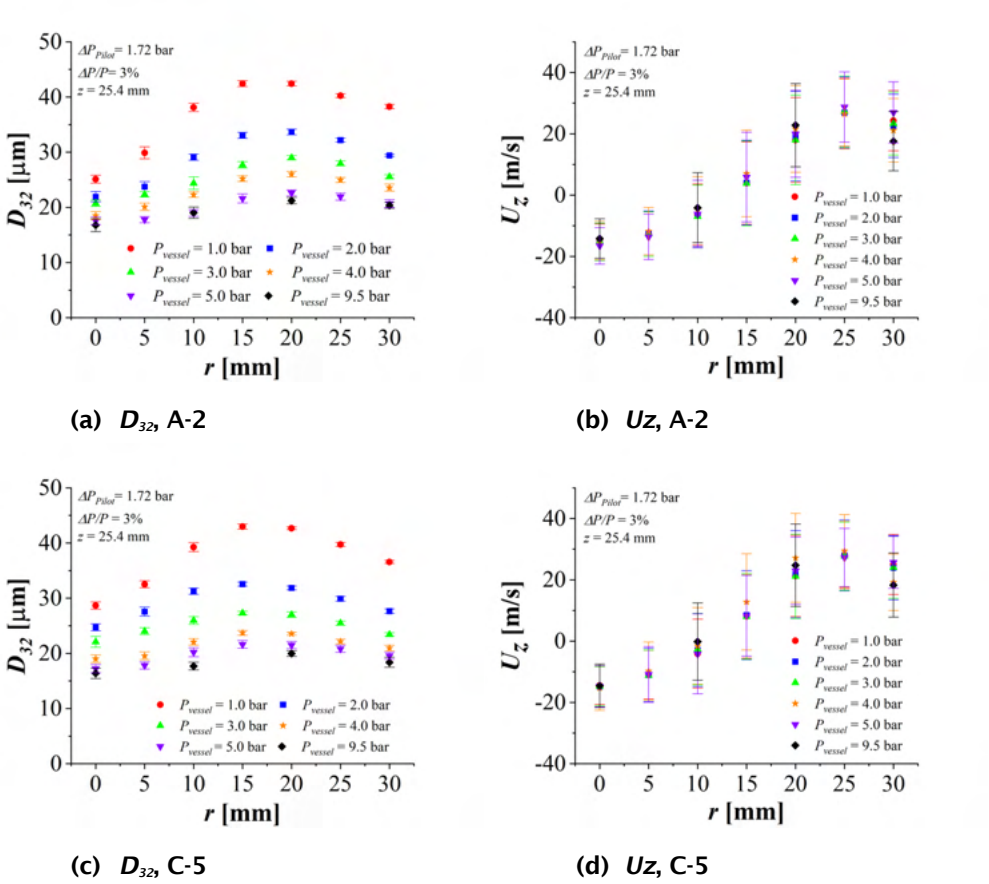

(a) D_{32}, A-2 **(b)** Uz, A-2

(c) D_{32}, C-5 **(d)** Uz, C-5

Figure 8. Comparisons of drop diameters (D_{32}) and drop velocities (U_z) for A-2 and C-5 fuels at P_{vessel} = 1,2,3,4,5, and 9.5 bar, $\Delta P/P$ = 3%, ΔP_{pilot} = 1.72 bar, T_{fuel} = 332 K, and T_{airbox} = 394 K for measurement plane (z) = 25.4 mm. P_{Vessel} = ambient pressure; ΔP_{Pilot} = variation in fuel injection pressure; $\Delta P/P$ = pressure drop; r = radial location ; T_{fuel} = fuel temperature; T_{airbox} = airbox temperature.

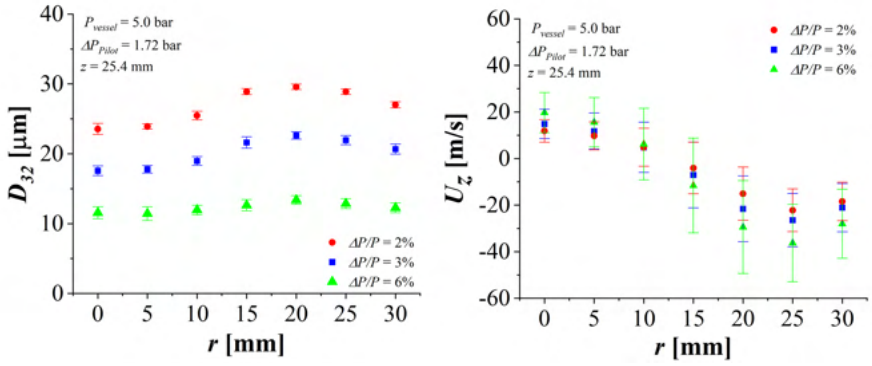

(a) D_{32} **(b) U_z**

Figure 9. Comparisons of drop diameters (D_{32}) and drop velocities (U_z) for A-2 fuel at $\Delta P/P$ = 2, 3, and 6 %, P_{vessel} = 5 bar, ΔP_{pilot} = 1.72 bar, T_{fuel} = 332 K, and T_{airbox} = 394 K for measurement plane (z) = 25.4 mm. P_{Vessel} = ambient pressure; ΔP_{Pilot} = variation in fuel injection pressure; $\Delta P/P$ = pressure drop; r = radial location; T_{fuel} = fuel temperature; T_{airbox} = airbox temperature.

Figure 10(a) shows the effect of ambient pressure on the drop size by comparing average drop size (D_{32o}/d_o) and predicted drop size (d_D/d_o) at different ambient pressures for A-2 and C-5 fuels. The effect of ambient pressure on drop size was observed to diminish as ambient pressure increased for both fuels. The model successfully demonstrated the drop size trend with increasing ambient pressure within ±20% error compared to measured drop sizes. Figure 10(b) shows the effect of pressure drop on drop size at elevated ambient pressure of 5 bar for A-2 fuel using dimensionless measured line-of-sight D_{32} (D_{32o}/d_o). The model was also able to demonstrate the drop size trend with increasing pressure drop.

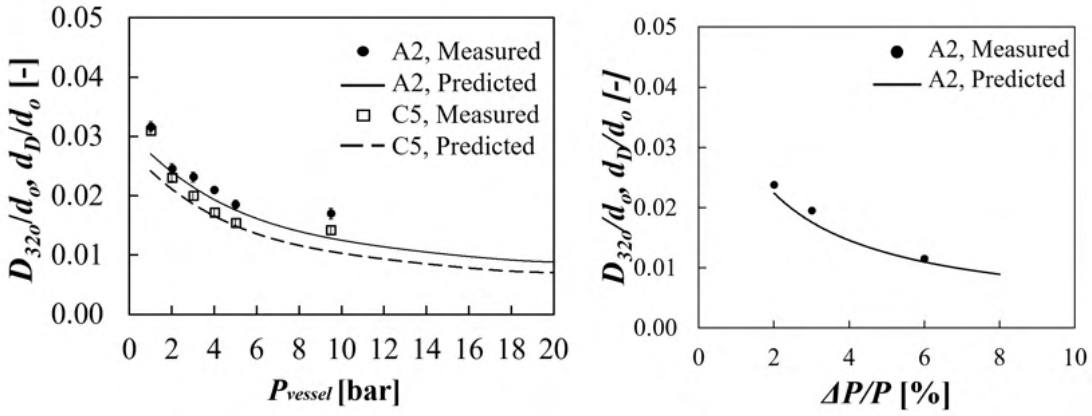

(a) D_{32o}/do and dD/do vs. P_{vessel} **(b) D_{32o}/do and dD/do vs. $\Delta P/P$**

Figure 10. Comparison of nondimensionalized measured average drop sizes (D_{32o}/d_o) and predicted drop size (d_D/d_o) at different ambient pressures and different pressure drops for A-2 and C-5 fuels at $\Delta P/P$ = 3%, ΔP_{pilot} = 1.72 bar, T_{fuel} = 332 K, and T_{airbox} = 394 K for measurement plane (z) = 25.4 mm. P_{Vessel} = ambient pressure; ΔP_{Pilot} = variation in fuel injection pressure; $\Delta P/P$ = pressure drop; T_{fuel} = fuel temperature; T_{airbox} = airbox temperature.

Liquid and vapor discrimination

Liquid and vapor discrimination analysis were performed using planar laser-induced fluorescence (PLIF) and Mie images. Figure 11 shows pairs of simultaneously captured PLIF (left) and Mie (middle) images and the normalized difference image

from PLIF and Mie images (right) at P_{vessel} = 1, 2, and 9.5 bar. Although the comparison between the Mie and PLIF images presented in this section is nonquantitative, it can be a useful approach to identify and distinguish liquid and vapor regions in the spray.

From Figures 11(b), 11(e), and 11(h), it can be seen that the number of droplets near the spray center increased at higher ambient pressure. This is thought to be due to an increased number of smaller droplets at higher ambient pressure being recirculated into the hollow cone region, increasing the number of scattering events and signals. Smaller droplets at P_{vessel} = 9.5 bar were observed to have a greater tendency to follow the gas flow compared with those observed at lower P_{vessel}, as shown in Figures 11(c), 11(f), and 11(i).

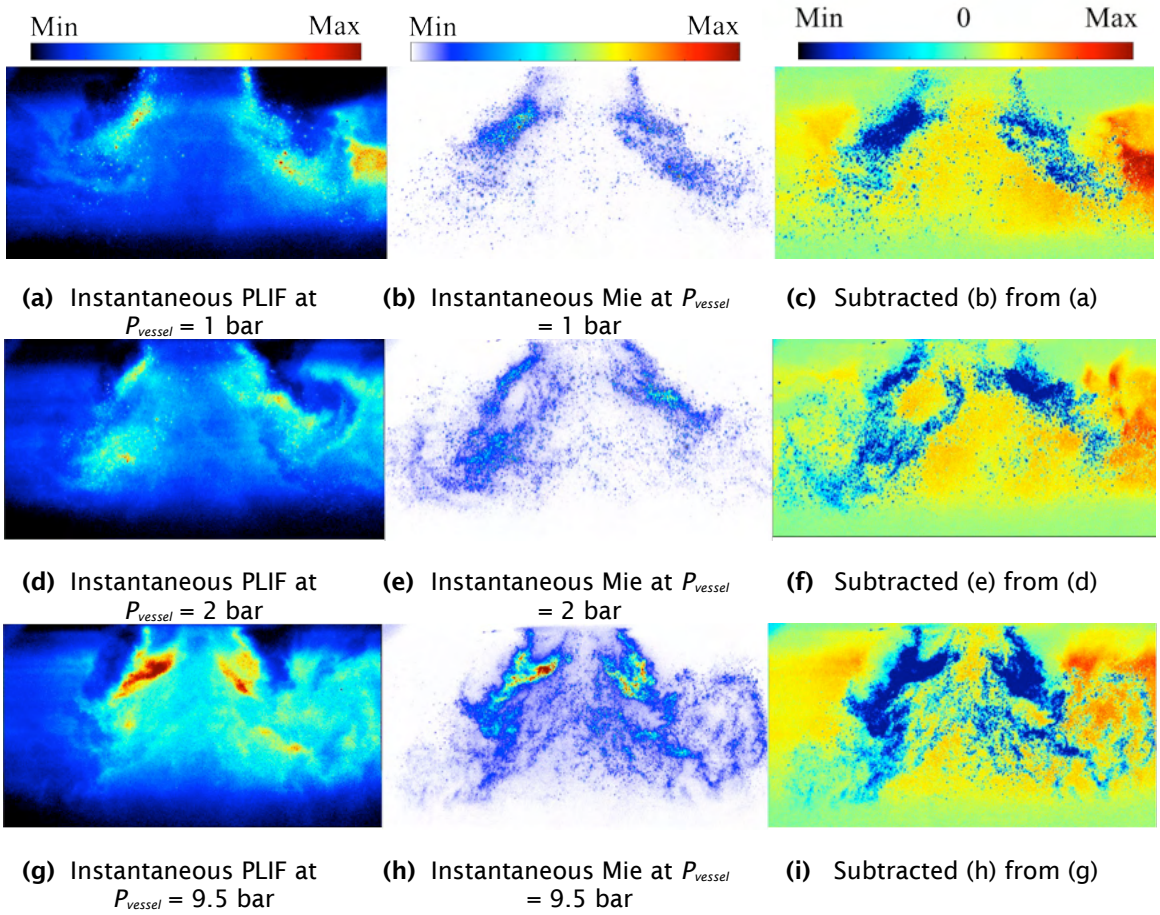

(a) Instantaneous PLIF at P_{vessel} = 1 bar **(b)** Instantaneous Mie at P_{vessel} = 1 bar **(c)** Subtracted (b) from (a)

(d) Instantaneous PLIF at P_{vessel} = 2 bar **(e)** Instantaneous Mie at P_{vessel} = 2 bar **(f)** Subtracted (e) from (d)

(g) Instantaneous PLIF at P_{vessel} = 9.5 bar **(h)** Instantaneous Mie at P_{vessel} = 9.5 bar **(i)** Subtracted (h) from (g)

Figure 11. Liquid–vapor discrimination A-2 fuel at P_{vessel} = 1, 2, and 9.5 bar, $\Delta P/P$ = 3%, ΔP_{pilot} = 1.72 bar, T_{fuel} = 332 K, and T_{airbox} = 394 K. PLIF = planar laser-induced fluorescence; P_{Vessel} = ambient pressure; ΔP_{Pilot} = variation in fuel injection pressure; $\Delta P/P$ = pressure drop; T_{fuel} = fuel temperature; T_{airbox} = airbox temperature.

Publications

Bokhart, A. J., Shin, D., Rodrigues, N. S., Lucht, R. P., Gore, J. P., & Sojka, P. E. (2018) Spray characteristics of a hybrid airblast pressure-swirl atomizer at near lean blowout conditions using phase doppler anemometry [Presentation]. AIAA SciTech 2018 Forum, Atlanta, GA.

Bokhart, A. J., Shin, d., Gejji, r., Buschhagen, T., Naik, S. V., Lucht, R. P., Gore, J. P., Sojka, P. E., & Meyer, S. E. (2017). Spray measurement at elevated pressures and temperatures using phase doppler anemometry [Presentation]. AIAA SciTech 2017 Forum, Grapevine, TX.

Shin, D., Bokhart, A. J., Rodrigues, N. S., Gore, J. P., Sojka, P. E., & Lucht, R. P. (2019). Non-reacting spray characteristics for alternative aviation fuels at near lean blowout conditions. Journal of Propulsion and Power, *36*(3), 323–334.
Shin, D., Bokhart, A. J., Rodrigues, N. S., Lucht, R. P., Gore, J. P., & Sojka, P. E. (2019). Experimental study of spray characteristics at cold start and elevated ambient pressure using hybrid airblast pressure-swirl atomizer [Presentation]. AIAA SciTech 2019 Forum, San Diego, CA.
Shin, D., Rodrigues, N. S., Bokhart, A. J., Gore, J. P., Sojka, P. E., & Lucht, R. P. (2020). *Spray characteristics of standard and alternative aviation fuels at cold start conditions* [Manuscript submitted for publication].
Shin, D., Hasti, V. R., Rizk, N., Bokhart, A. J., Rodrigues, N. S., Corber, P. A., Sojka, P. E., Lucht, R. P., & Gore, J. P. (2021). *Chapter VIII. Spray characteristics of conventional and alternative fuels,* Fuel Effects on Operability of Aircraft Gas Turbine Combustors, Edited by Meredith Colket and Joshua Heyne, ISBN: 978-1-62410-603-3, Progress in Astronautics and Aeronautics, American Institute of Aeronautics and Astronautics, 2021. https://doi.org/10.2514/4.106040
Shin, D., Aman, S., & Lucht, R. P. (2021). *Spray characteristics of standard and alternative aviation fuels at high ambient pressure conditions* [Manuscript in preparation].

Summary: Modeling and Simulation of Fuel Effects on Lean Blowout (LBO)

Objectives

The main objective of the computational research at Purdue was to establish modeling and simulation methodology to predict the fuel composition effects on LBO in the referee combustor at engine-relevant conditions. The CFD methodology to predict LBO in a liquid-fueled gas turbine combustor is not well established in the literature. As part of this National Jet Fuel Combustion Program (NJFCP) FAA project, we have focused on developing CFD methodology, including all the hardware features as-it-is on the real engine combustor. The successful demonstration of these computational tools will help identify the best CFD models and best practices to predict the fuel sensitivity to LBO limits in a swirl-stabilized gas turbine combustor. Another objective was to demonstrate the methodology for conventional Jet A fuel (denoted A-2) and an alternative aviation fuel (C-1). The experimental data from the Maurice J. Zucrow Laboratory (Purdue) were used to determine the spray boundary conditions. The reacting spray measurements, OH* chemiluminescence from the referee experiments at University of Illinois Urbana-Champaign (UIUC), Illinois, and the LBO equivalence ratios from the rig tests at University of Dayton Research Institute/Air Force Research Laboratory (UDRI/AFRL), Ohio, were utilized to evaluate the CFD models. Then, we used the results from successful high-fidelity large-eddy simulations (LES) to understand flame structure under stable flame conditions and during blowout and to identify markers for early detection of combustion instabilities and LBO. This research effort also aimed to identify new measurements for model validation.

Accomplishments

Computational method

The Reynolds Averaged Navier-Stokes (RANS) and LES were performed for the referee combustor using the finite volume-based compressible CFD solver CONVERGE. The gas-phase equations are described using an Eulerian approach, and the liquid spray was modeled with discrete injections of droplets using a Lagrangian approach. The subgrid stress tensor terms in the momentum equations were modeled using a non-viscosity-based one-equation model to obtain closure. Two different combustion models—namely, the detailed chemistry solver utilizing the laminar finite-rate chemistry (FRC) model and flamelet approach using the FGM model—were evaluated for LBO predictions. The HyChem kinetic models and compact kinetic models based on fuel surrogates were used to represent chemical reactions. The FGM model accounts for the effects of turbulence on reaction rates via a joint probability density function of the mixture fraction, the mixture fraction variance, and a reaction progress variable. A fully automated on-the-fly meshing strategy, combined with the cut-cell Cartesian method and adaptive mesh refinement (AMR), was employed, and the mesh parameters were selected based on a grid sensitivity study. More than 90% of the turbulent kinetic energy is resolved in the combustor region with appropriate mesh size and distribution. Additional details on the boundary conditions and the spray can be found in Hasti et al. (2018; 2018).

The spray is represented by an ensemble of six ring injectors, each with prescribed cumulative distribution functions for droplet diameter, average velocity, cone angle, mass flow rate, and parcel number. The spray boundary conditions (droplet diameter, average velocity, and cone angle) at 2 mm from the nozzle exit were obtained from the PDA measurements (from detailed measurements described in our experimental contribution section) at 25.4 mm from the deflector plate. An ensemble of six ring injectors, each with its own droplet size and velocity distribution, represents the nozzle. Taylor analogy secondary breakup and dynamic drag models were used to estimate the secondary breakup and resulting spray droplet

dynamics. A droplet dispersion model was used to include the effects of the sub-grid-scale flow field on the discrete parcels. The droplet evaporation rates were calculated using the Frossling correlation based on the laminar mass diffusivity of the fuel vapor, mass transfer number, and Sherwood number. The prescribed fuel properties were set as those determined for the A-2 and C-1 fuels.

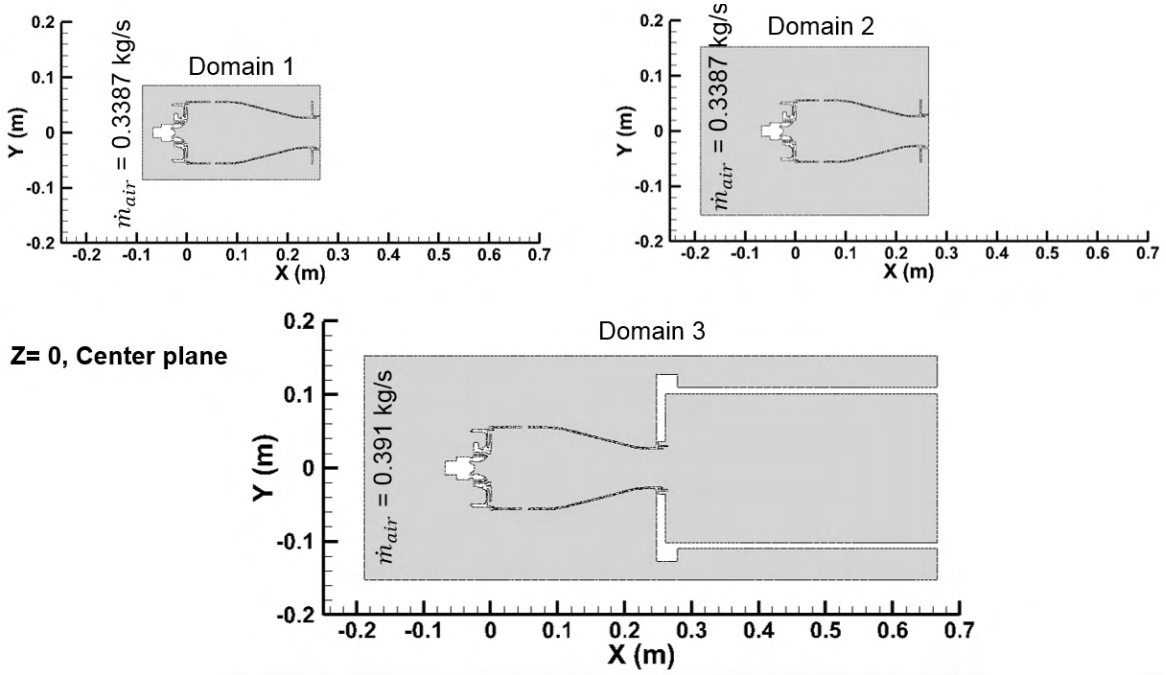

Figure 12. Comparison of computational domains at the Z=0, Center plan for the three computational domains. $\dot{m}_{air}$ is the mass flow rate of air.

Nonreacting flow simulations were carried out for the referee combustor with three different computational domains as shown in Figure 12. The flow splits comparison between these three domains is shown in Table 1. This sensitivity study was carried out to understand the sensitivity of the plenum size on the combustor flow splits and flow field in the primary zone. For domain 1, the dilution jets in the first row enter the combustor at a higher velocity because of the smaller width of the annulus and therefore show an $8°$ greater angle. The results showed that domain size does not have a significant effect on flow patterns or velocity magnitudes in the critical primary flame stabilization zone. This zone is dominated by swirling flow. Domain 1 was used for the reacting LES, and the computational domain external to the combustor was reduced in order to focus on better resolving the complex swirling flowfield with fine mesh in the combustor region and gridding through the cooling holes in the combustor. Reductions in the length of the plenum upstream of the swirler section and the annular region beyond the combustor walls, and elimination of the large circular outlet section beyond the combustor exit were not expected to significantly affect the highly swirling flowfield in the primary zone. Results of the cold-flow simulations showed that the flow features of the primary zone in the vicinity of the injector were indeed insensitive to the reduced plenum size for domain 1. The 3-dimensional view of the domain 1 with a swirler and 2-dimensional cross-section at Z=0 are shown in Figure 13. The flow through all passages, including tiny effusion holes on the liners, was resolved in this CFD model. The computational grid for flow simulations with all passages open is shown in Figure 14. The grid is locally refined in the regions with the steepest gradients and is relatively coarse in sections with weaker gradients, based on AMR.

Table 1. Comparison of flow splits.

	Exp (g/s)	Domain 1 Non-Reacting (g/s)	Domain 1 Reacting A2-0.096 (g/s)	Domain 2 Non-Reacting (g/s)	Domain 3 Non-Reacting (g/s)
Dilution Row 1	39.5	45.22	46.3	47.03	47.45
Dilution Row 2	45.4	50.01	52.4	50.57	51.27
Total swirler	60.7	75.37	72.9	73.12	74.17
Radial swirler	14.3	15.56	14.7	15.68	15.34
Axial int. swirler	18.9	25.18	23.8	23.92	24.93
Axial ext. swirler	24.6	32.37	31.9	31.3	31.64
Swirler cooling	2.9	2.25	2.3	2.22	2.24
Effusive plate	245.4	167.66	166.7	164.82	210
Total (sum)	391	338.26	338.3	335.54	382.89

LBO simulation approach

LES were performed for a global equivalence ratio (Φ) of 0.096, which was experimentally found to produce stable combustion. From this condition, the fuel flow rate was reduced in a gradual stepwise manner; larger time steps were initially applied, and the flow rate steps were progressively reduced as impending blowout behavior was observed. The simulations were run with a fixed global equivalence ratio for at least two flow-through durations of approximately 30 ms. The fixed equivalence ratio was maintained beyond 30 ms if a quasi-steady heat release rate was not reached within either of those limits. The heat release rate was used as a criterion for identifying LBO. The global equivalence ratio steps resulting from this process are plotted in Figure 15 as a function of time for fuels A-2 (left) and C-1 (right). The experimental data shown by red filled circles indicate that the C-1 fuel blows out at a higher equivalence ratio than the A-2 fuel. The evolutions of the heat release rate for varying equivalence ratios and for two fuels with the FGM combustion model are shown in Figure 16. The flame is initially stable; subsequently, a steady decrease followed by a sharp reduction in the heat release rate is observed for both fuels. The heat release rates reach a steady state before the next step. In this figure, the dotted black line shows the mean heat release rate, and the dotted pink line shows the ideal heat release rate.

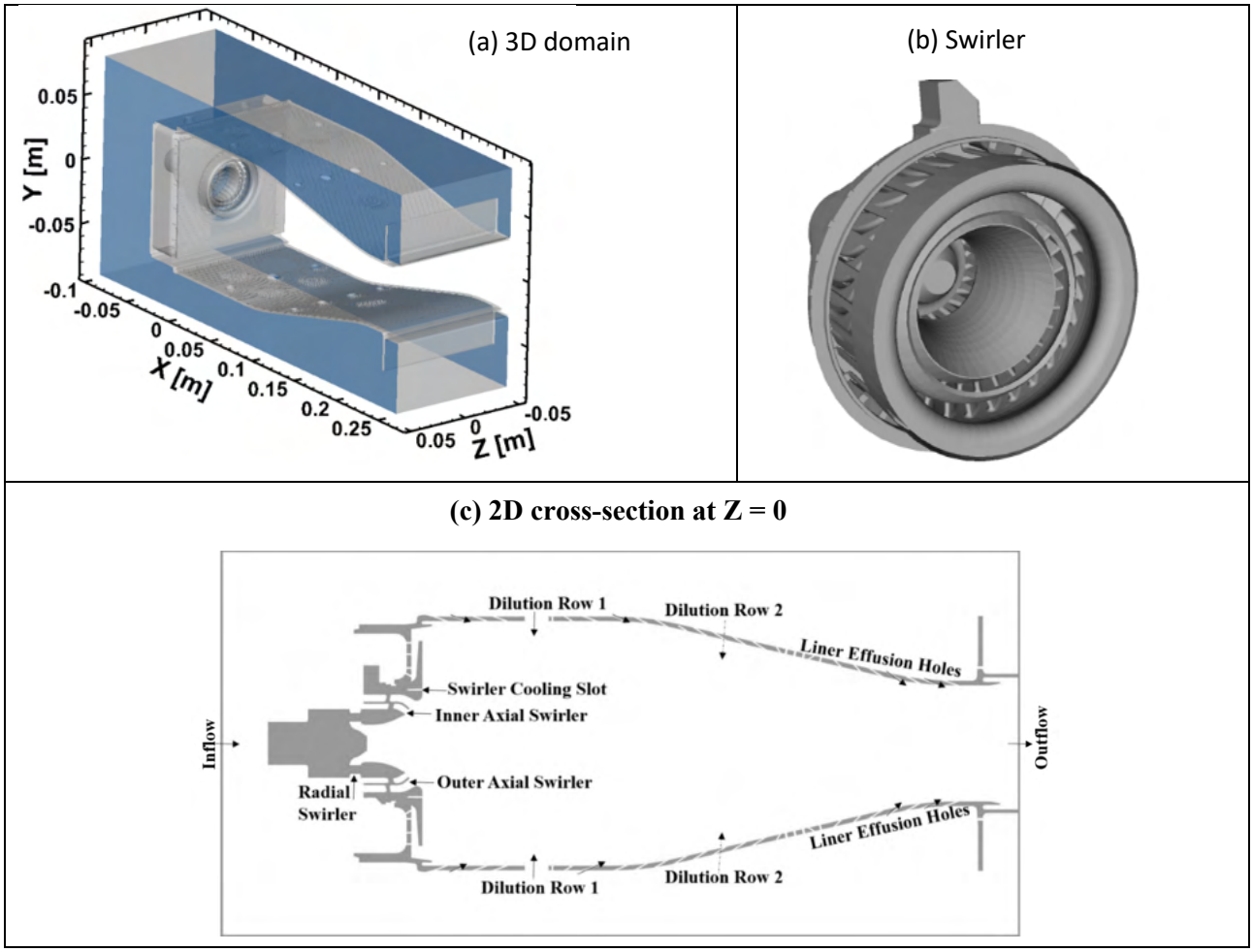

Figure 13. (a) Three-dimensional (3D) computational domain, (b) magnified view of the 3D swirler, and (c) magnified view of the 2-dimensional cross-section at Z=0 (mid-plane).

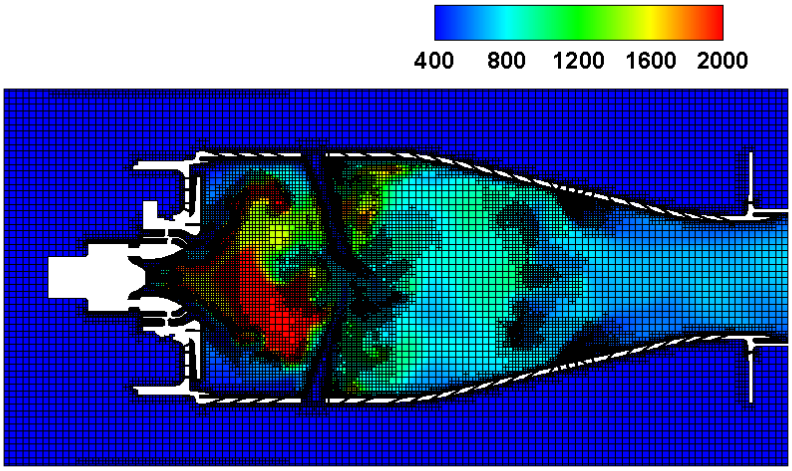

Figure 14. Computational grid with adaptive mesh refinement (AMR) on the mid-plane (Z=0) of the referee combustor for a reacting case with the flamelet-generated manifold (FGM) combustion model, with colored temperature [K] contours.

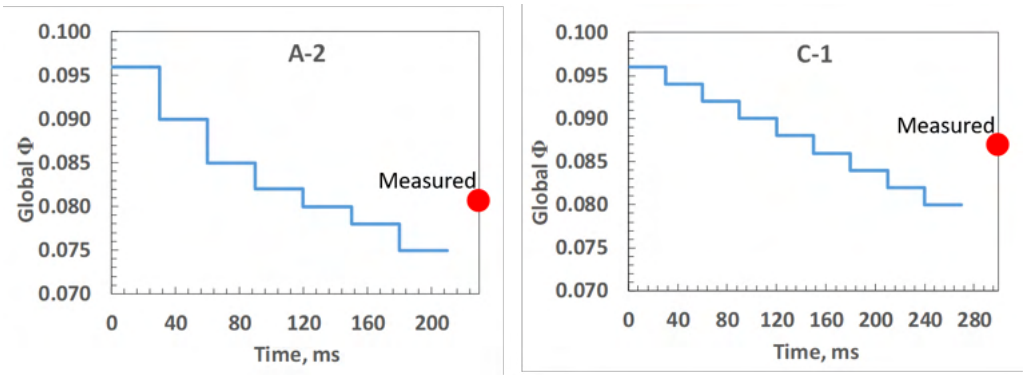

Figure 15. Staged fuel ramp-down approach for lean blowout (LBO) prediction using A-2 and C-1 fuels. The red dot represents the measured LBO global equivalence ratio (Φ).

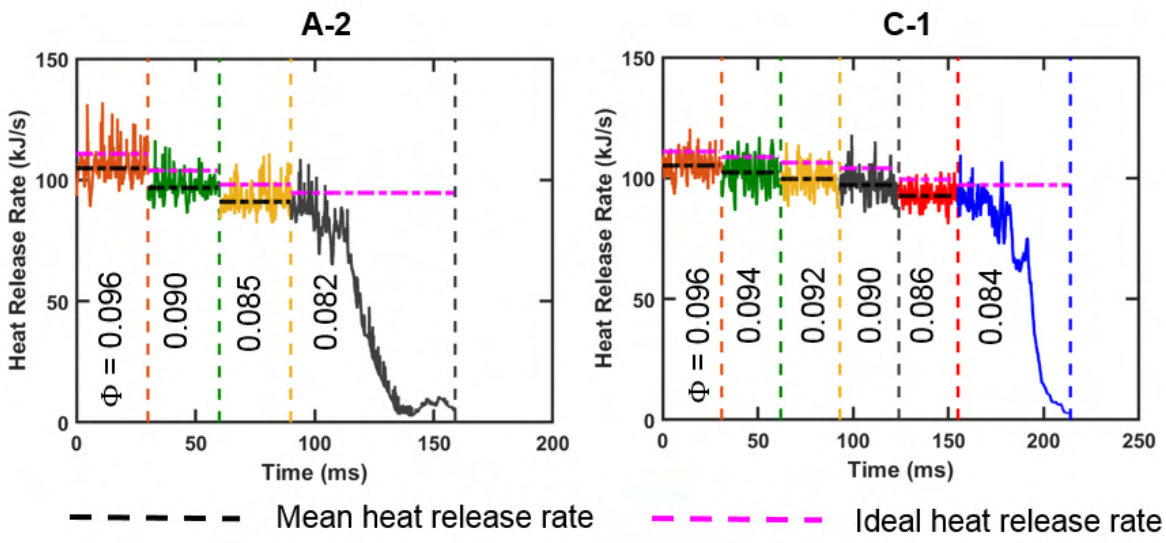

Figure 16. Heat release rate calculation with the flamelet-generated manifold (FGM) combustion model for A-2 and C-1 fuels. Φ = global equivalence ratio.

Reacting spray comparison under near-LBO conditions

Spray statistics were collected via LES calculations at a stable operating point over two flow-through durations. The averaging process over two flow-through durations was started after the flame and heat release rate reached a quasi-steady state. Figure 17 shows the experimental data and predicted droplet statistics as a function of radial distance for the FRC and FGM combustion models at four axial stations. The fuel spray exhibited a pattern with smaller-diameter droplets near the hollow cone surface 10 mm downstream of the nozzle exit. This distribution widened in the radial direction toward the downstream locations, with larger droplets toward the center and smaller droplets in the outer regions. The two combustion models satisfactorily captured this trend for both fuels, and better agreement with the experiments was observed for the downstream locations. The axial and radial velocities increased away from the center and decreased with increasing spray cone angle. These trends were accurately captured for the near-nozzle regions as well as the downstream regions for both fuels. Overall, the Lagrangian spray setup accurately captures spray breakup and evaporation.

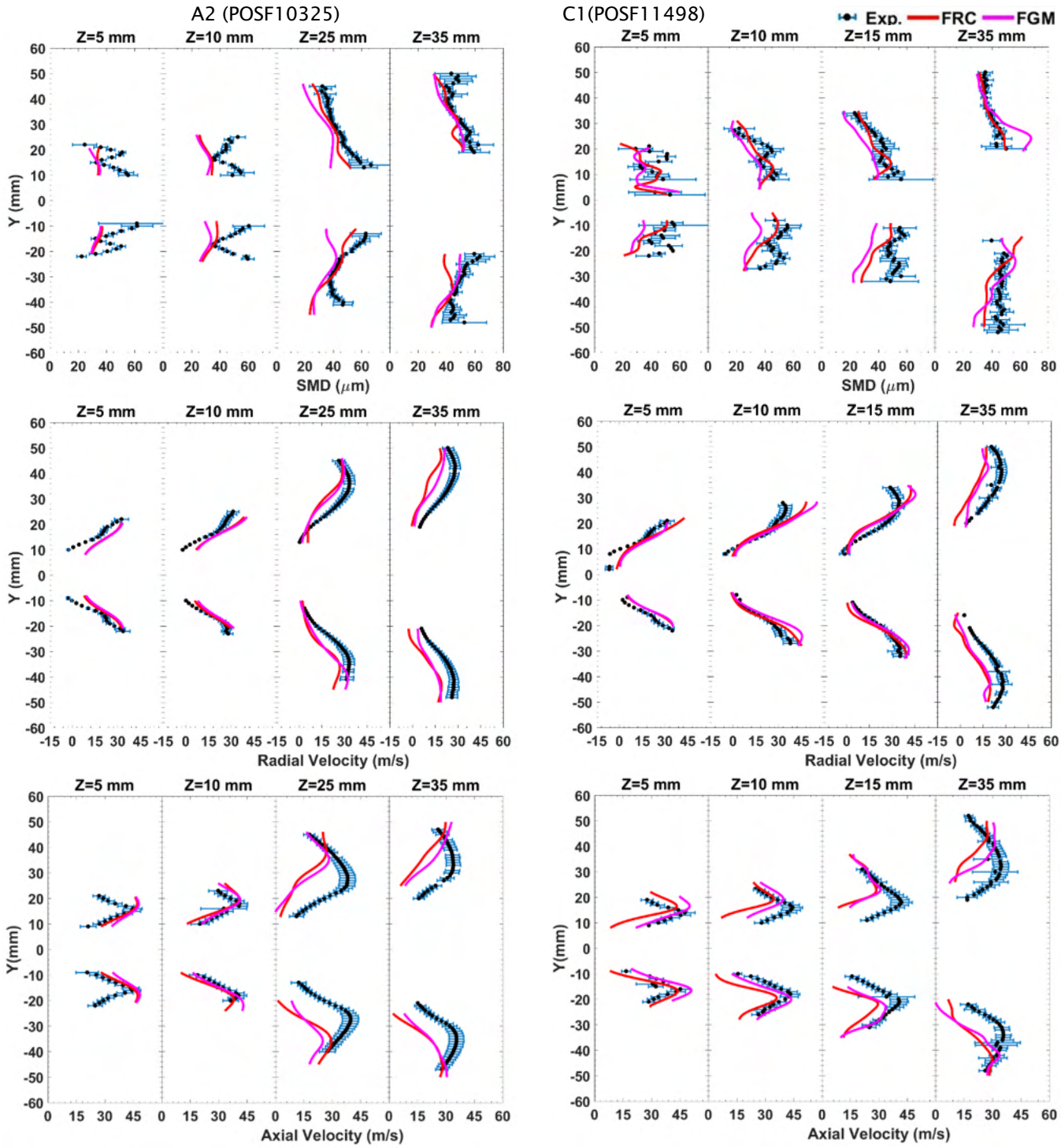

Figure 17. Comparison of spray statistics and phase Doppler anemometry (PDA) data for a stable flame at global equivalence ratio Φ = 0.096. FRC = finite-rate chemistry model; FGM = flamelet-generated manifold model; SMD = Sauter mean diameter.

Flame shape comparison

OH* chemiluminescence data from the UIUC experiments were used to compare the line-of-sight average OH mass fraction from LES for four kinetic mechanisms and two combustion models. The results for the detailed, skeletal, reduced, and compact mechanisms are displayed in Figure 18, alongside the experimentally observed OH* chemiluminescence. The results from the detailed, skeletal, and reduced mechanisms were qualitatively similar, and the experimental data (OH* chemiluminescence) and detailed mechanism calculations (OH) showed similar spreads in the radial and axial directions. However, it must be noted that these comparisons are qualitative. The experimental images are based on false color and do not indicate a quantitative measurement of the OH field. The horizontal position of 0 mm corresponds to the deflector plate. OH formation marks the high-temperature heat release region, which extends 50 mm downstream of the deflector plate and corresponds to the downstream location of the first row of dilution holes. This area is the stable region of the swirl-stabilized flame and exhibits a truncated cone shape, with regions of high OH/heat release corresponding to the cone angle of the hollow spray cone. This trend indicates strong burning and heat release near the spray cone surface downstream of the swirl cup. The A-2 fuel exhibited a higher degree of asymmetry in OH* for this configuration and measurement. These regions of intense heat release were qualitatively captured by all four chemistry mechanisms. The flame shape computed for the FGM combustion model showed a stronger and larger reaction zone compared with the FRC model.

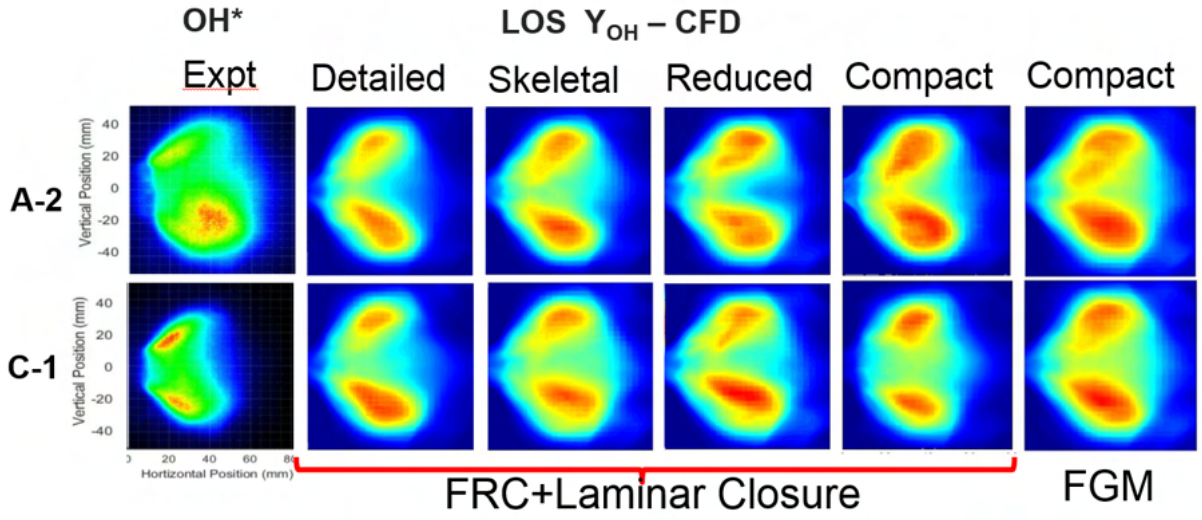

Figure 18. Line-of-sight (LOS) average OH mass fraction (Y_{OH}) obtained from large-eddy simulations (LES) compared with experimental (Expt.) OH* obtained from chemiluminescence. FRC = finite-rate chemistry model; FGM = flamelet-generated manifold model. CFD = computational fluid dynamics.

LBO equivalence ratio comparison

The LBO trends for both fuels were compared with experimental results in Figure 19. The C-1 fuel was shown to blow out at a higher equivalence ratio compared with A-2 in the experiments. This LBO dependence on the fuel's physical and chemical properties is very complex. The simulations with the FRC and FGM combustion models captured accurate LBO trends and relative behaviors for each fuel. However, the FGM model predicted that LBO would occur at a lower equivalence ratio compared with the FRC model because of the stronger flame root and larger reaction zone, as shown in Figure 20.

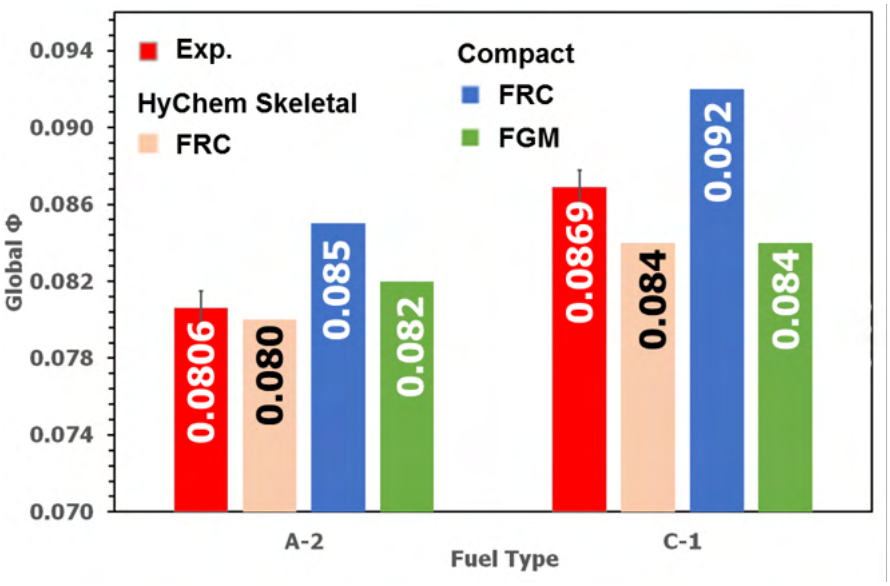

Figure 19. Comparison of lean blowout (LBO) global equivalence ratio (Φ) with experimental data for two different mechanisms—HyChem Skeletal and Compact—and two combustion models—finite-rate chemistry (FRC) and flamelet-generated manifold (FGM).

Evaluation of combustion models

The computed velocity, temperature, and mean OH mass fraction contours are compared for the FRC and FGM combustion models in Figure 20. The results for the FRC model show a pointed flame root and a smaller reaction zone, whereas the FGM model results show a stronger flame root and a much larger reaction zone. However, experimental validation data would be highly beneficial to verify the computational model results and to obtain further enhancements.

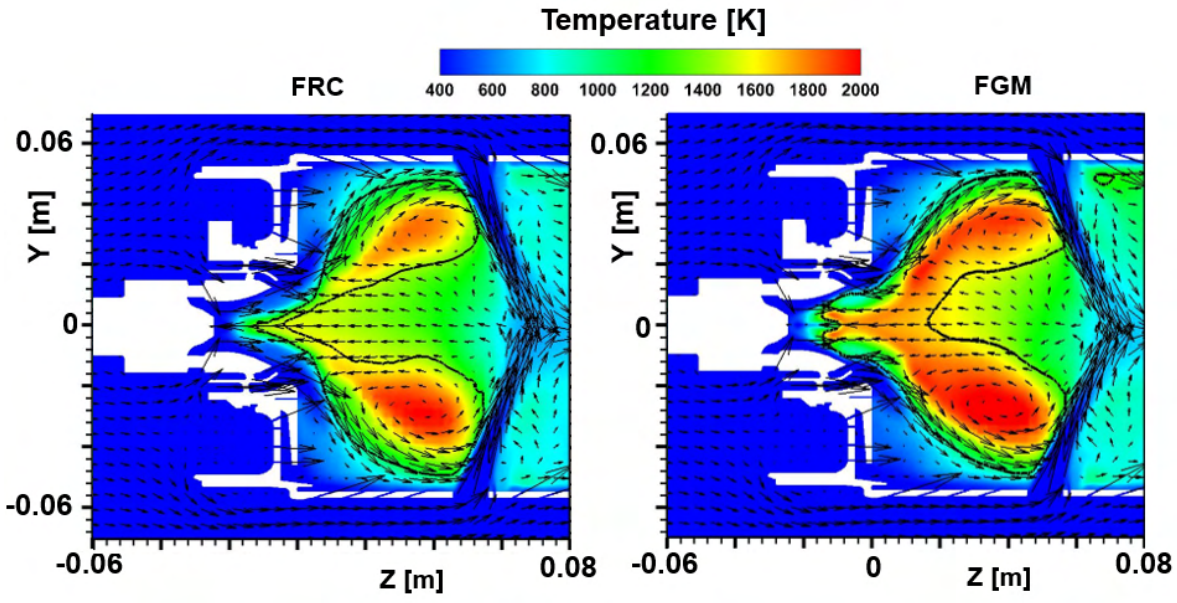

Figure 20. Comparison of temperature (filled contours), velocity (vectors), and an isocontour for a mean OH mass fraction of 5e-04 (black line) for C-1 fuel. FRC = finite-rate chemistry model; FGM = flamelet-generated manifold model.

Flame structure analysis under stable conditions and during LBO

The LES results from the HyChem skeletal mechanism were chosen for understanding the flame extinction process during LBO for the A-2 and C-1 fuels. Qualitative analysis of the flame during LBO is shown in Figure 21. Instantaneous temperature contour plots at the combustor mid-plane are shown on the left for both fuels, and corresponding formaldehyde mass fractions are shown on the right. The primary recirculation zone corresponds to the region of intense heat release rate. These regions correspond to the high OH formation regions described in the previous section. For A-2 fuel, after the final step-down, at an equivalence ratio of 0.080, a lifted flame was observed to stabilize inside the swirler cup region within the 0 to 5 ms window. Formaldehyde was observed to form very close to the nozzle tip and to follow the spray regions. Formaldehyde is oxidized to form the high-temperature regions. As time progressed, the flame stabilization point started to move in the axial direction and a remarkable shift in the CH_2O regions was observed, away from the nozzle tip. Finally, by 15 ms, the heat release in the primary recirculation region decreased considerably, with a considerable shift of CH_2O formation in the downstream regions. Finally, the flame was observed to blow out by 25 ms. A similar trend was observed for the C-1 fuel, but at a much higher global equivalence ratio of 0.084. The C-1 fuel had significantly greater CH_2O formation, even at 0 ms. To summarize these plots overall, the flame was observed to shift downstream as LBO was approached, along with downstream movement of intermediate species. The reduction of heat release rates and overall temperatures led to partial oxidation of these intermediate species, which is shown as a corresponding downstream shift in the contour plots.

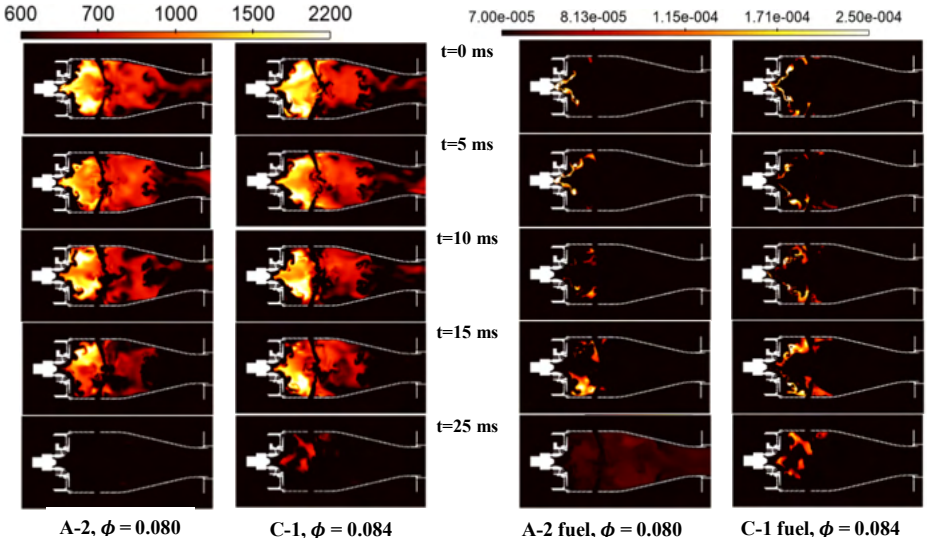

Figure 21. Instantaneous temperature [K] contour plots (left) at the combustor mid-plane and formaldehyde mass fractions (right) for A-2 and C-1 fuel during lean blowout. Φ = global equivalence ratio.

To understand flame stabilization and key factors governing LBO limits, we analyzed species formation in the mixture fraction space in the primary zone of the combustor. These are reported in Figure 22. The aim was to identify key markers or events that are universal, with respect to different fuels. Temperatures from the primary zone (upstream of the primary dilution holes) were isolated from the 3D CFD domain and further filtered based on their axial velocities. Computational cells that had axial velocities in the negative direction were selected for analysis. Because this was a nonuniform grid, these points were weighted with their respective cell volumes. These sets of points represent the recirculating fluid that flows from the high-temperature regions toward the base of the flame. Each point in the T-Z space is colored by CH_2O mass fraction. The red dotted line corresponds to the stoichiometric mixture fraction. These data points were also reported for the stable configuration at 0.096. We first considered the stable operating point for A-2. CH_2O was observed to form in the rich regions in the temperature range of 1000 to 1600 K. These regions were subsequently oxidized in the high-temperature regions. After a series of step-downs in equivalence ratio to 0.080, CH_2O formation shifted toward the richer regions, highlighted by the dotted lines. This shift indicated partial oxidation of the HC fuel due to a global reduction in heat release and corresponding temperatures. The C-1 fuel, in contrast, indicated relatively higher CH_2O concentrations in the rich regions, even for the stable operating point. This is an early indication of both partial oxidation and the likelihood of the flame

blowing out at relatively higher equivalence ratios. As expected, as the equivalence ratios were reduced, formaldehyde formation shifted to the richer regions, indicating partial oxidation and subsequent flame blowout by 15 ms. The higher concentration of intermediates in the rich regions can be attributed to the lowered temperature and a corresponding decrease in oxidation rates of intermediate species. The reduction in heat release rate (HRR) and overall temperatures further leads to a reduction in the overall evaporation efficiency, which finally leads to a blowout. The oxidation of the intermediate species to high-temperature radicals and saturated combustion products is the step that has a huge impact on LBO limits.

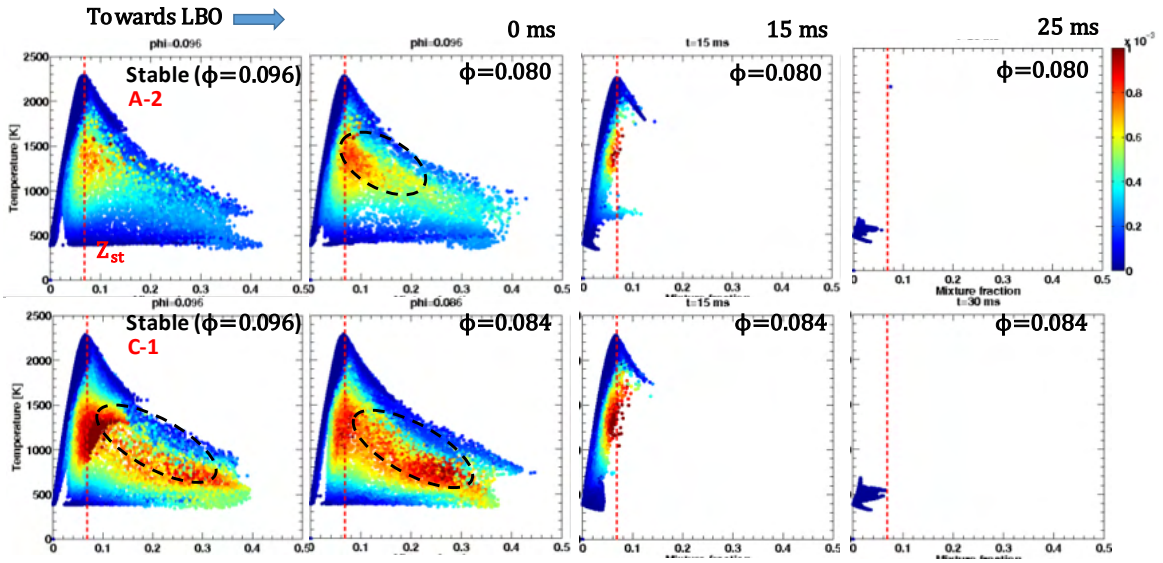

Figure 22. Temperature versus mixture fraction scatterplots for A-2 fuel (top) and C-1 fuel (bottom) sampled from the primary zone. Colored with CH_2O mass fraction. LBO = lean blowout; Φ = global equivalence ratio; Z_{st} = stoichiometric mixture fraction.

The intermediate radical OH is formed in the high-temperature stoichiometric regions and does not shift with lower global equivalence ratios, as shown in Figure 23. This study showed that the trend of increasing concentrations of intermediate species in rich regions is an important marker during the LBO process.

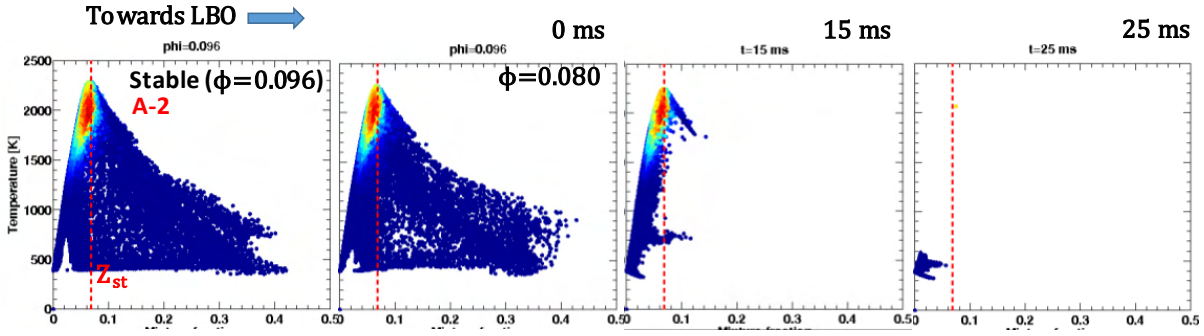

Figure 23. Temperature versus mixture fraction scatterplots for A-2 fuel sampled from the primary zone. Colored with OH mass fraction. LBO = lean blowout; Φ = global equivalence ratio; Z_{st} = stoichiometric mixture fraction.

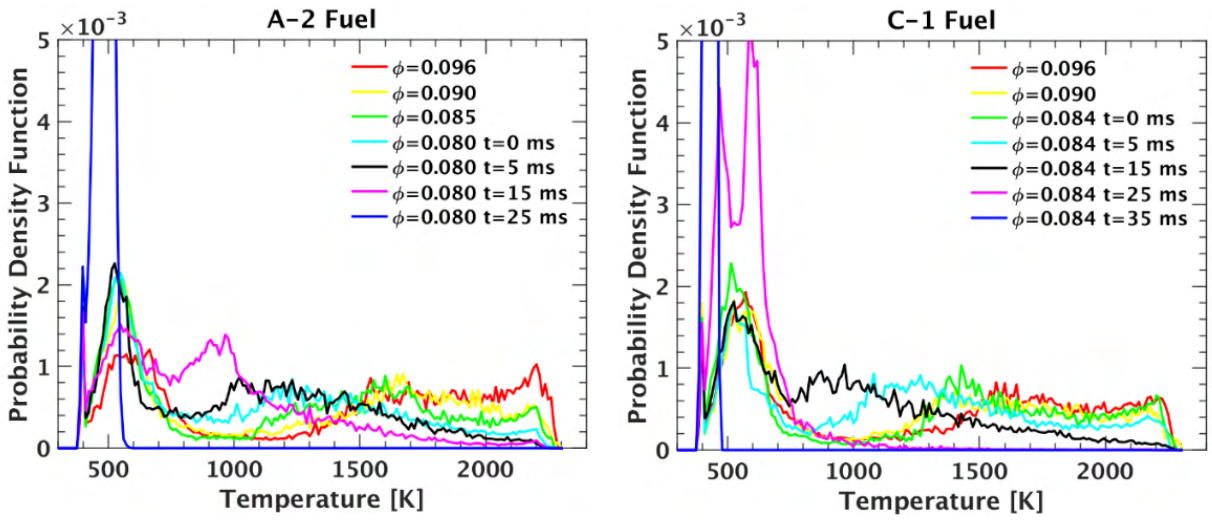

Figure 24. Probability density function of the temperatures of the recirculating gases in the primary zone for A-2 fuel (left) and C-1 fuel (right). Φ = global equivalence ratio.

Statistical analysis was carried out by generating a probability density function (PDF) of the temperature distribution in the recirculation zone, as demonstrated for fuels A-2 and C-1 in Figure 24. The temperature distribution of the recirculation zone shows a nonuniform, multi-modal distribution with a peak in the 500 K zone, and a major part of the distribution spread in the range of 1500 K to 2300 K. This indicates that high temperatures are a major part of the recirculation zone and play a significant role in stabilizing the flame. The reduced fuel flow rates corresponding to the stable operation condition exhibit a similar distribution; however, the distributions show more bias toward the low temperatures. At the blowout equivalence ratio, the distribution was observed to have shifted significantly. The second peak of the bimodal distribution corresponding to the high-temperature region was now at a significantly lower temperature compared with the previous equivalence ratios. As the flame finally approached LBO, we observed that this distribution shifted toward the low temperature region and merged into a delta PDF type of distribution. Thus, it can be seen that, as the flame blows out, the recirculation zone cools due to the decrease in overall heat release rates. This lowers evaporation rates and further triggers a reduction in heat release, leading to a cyclical process. This weakening of the recirculation zone is a key marker of flame stability. A significant shift in the PDF distribution of temperatures of the recirculating fluid can be marker for the start of LBO.

Conclusions

A comprehensive CFD LES methodology using autonomous meshing and AMR was developed for simulating the as-it-is realistic engine combustor and successfully demonstrated for the referee combustor. Flow through all combustor passages, including the tiny effusion holes, was resolved in this approach for accurate estimation of the combustor flow field. Flow rate calculations were performed for component-wise and total flow splits for all passages in the referee combustor. RANS and LES models with different mesh resolutions captured the flow splits correctly. The computational results agreed reasonably well with experimental data of nonreacting flow splits from a complex combustor.

LES successfully captured the fuel sensitivity for A-2 and C-1 fuels on the LBO limits with HyChem skeletal and compact kinetic mechanisms. Predicted LBO trends agreed well with experimental data. Several sensitivity studies were performed to identify best practices: (1) computational domain sensitivity: we analyzed the influence of plenum size on the combustor flow fields; (2) mesh sensitivity; (3) combustion model sensitivity: we evaluated a detailed chemistry solver with laminar FRC and FGM models; (4) chemical kinetic mechanisms sensitivity: HyChem and compact kinetic mechanism model. The model setup consists of a detailed spray injection along with well-defined flow boundary conditions. The modeling approach was initially validated against a stable operating point, where the global equivalence ratio was 0.096. The Lagrangian spray setup was able to capture the trends in spray SMD and velocities for both fuels. Qualitative comparisons of flame shapes were made by comparing line-of-sight averaged OH mass fraction from the computations with OH* from the chemiluminescence.

All kinetic mechanisms predicted similar flame shapes. The overall flame shape and the peak location of the OH were found to be in reasonable agreement with experimental data, providing confidence in the further calculation for LBO computations for both fuels.

The blowout process was studied in detail by analyzing the heat release rate, temperatures, and intermediate species distributions in the primary zone of the referee combustor. The main aim was to identify key markers across different conditions and fuels that could be used to identify stability limits. Two main observations were identified that mark the onset of an unstable flame. We observed in simulations that formation of intermediate species such as formaldehyde moves toward the richer regions of the flame as the LBO limit is approached. These high concentrations indicate incomplete oxidation near the LBO limits. Compared with A-2, C-1 fuel showed significantly higher CH_2O formation in richer regions for the same equivalence ratio and exhibited a higher LBO limit. The temperature in the recirculation zone was also an important indicator of flame stability. The temperature distributions showed a remarkable shift as an unstable configuration is approached. The observation was consistent for both fuels with different LBO limits. Overall, our results support the feasibility of using CFD models to evaluate different fuels and their figures of merit, like LBO, for a realistic gas turbine combustor in a predictive fashion. Further work is needed to understand why CFD models with certain kinetic mechanisms did not produce the correct LBO trends. Future work will involve predicting LBO trends for other alternative fuels, as well as simulating cold-start ignition and high-altitude relight and developing an improved feature sensitivity analyses of LBO's dependence on individual physical and chemical kinetic characteristics. These efforts will help to develop a robust LES CFD methodology for accurate prediction of fuel sensitivity on combustion, operability limits, and emissions. These high-fidelity computational tools can be very helpful in the industry for combustor design evaluations and fuel certification process.

Publications

1. Veeraraghava Raju Hasti, Robert P. Lucht, and Jay P. Gore, "Large eddy simulation of hydrogen piloted CH_4 / air premixed combustion with CO_2 dilution", Journal of the Energy Institute, Volume 93,Issue3,June2020,Pages1099-1109 https://doi.org/10.1016/j.joei.2019.10.004
2. Veeraraghava Raju Hasti, Abhishek Navarkar, and Jay P. Gore , "A data-driven discovery using machine learning for identification of the critical flame location and early detection of the lean blowout in a gas turbine combustor", Energy and AI (Submitted – Under Review)
3. Veeraraghava Raju Hasti, Prithwish Kundu, Sibendu Som, and Jay P. Gore, "Numerical simulations and analysis of the complex turbulent flow field in a realistic gas turbine Combustor", Proceedings of the Institution of Mechanical Engineers, Part A: Journal of Power and Energy (Submitted – Under Review)
4. M.S. Anand, Jeffery A. Lovett, Jeff Moder, Thomas Wey, Matthias Ihme, Lucas Esclapez, Peter C. Ma, Suresh Menon, Achyut Panchal, Veeraraghava Raju Hasti, Jay Gore, Pritwish Kundu, Sibendu Som, Venkat Raman, Yihao Tang, Fang Xu, Vaidya Sankaran, "Chapter IX. CFD Modeling of Lean Blowout and Ignition Fuel Sensitivity", AIAA Book Series (Submitted - Under Review)
5. Veeraraghava Raju Hasti, Prithwish Kundu, Gaurav Kumar, Scott A. Drennan, Sibendu Som, and Jay P. Gore. "A Numerical Study of Flame Characteristics during Lean Blow-Out in a Gas Turbine Combustor", 2018 Joint Propulsion Conference, AIAA Propulsion and Energy Forum, (AIAA 2018-4955)
6. Veeraraghava Raju Hasti, Prithwish Kundu, Gaurav Kumar, Scott A. Drennan, Sibendu Som, Sang Hee Won, Frederick L. Dryer, and Jay P. Gore. "Lean blow-out (LBO) computations in a gas turbine combustor", 2018 Joint Propulsion Conference, AIAA Propulsion and Energy Forum, (AIAA 2018-4958).
7. Veeraraghava Raju Hasti, Prithwish Kundu, Gaurav Kumar, Scott A. Drennan, Sibendu Som, and Jay P. Gore. "Numerical Simulation of Flow Distribution in a Realistic Gas Turbine Combustor", 2018 Joint Propulsion Conference, AIAA Propulsion and Energy Forum, (AIAA 2018-4956).
8. Veeraraghava Raju Hasti, Gaurav Kumar, Shuaishuai Liu, Robert P. Lucht, and Jay P. Gore. "Large Eddy Simulation of Pilot Stabilized Turbulent Premixed CH4+Air Jet Flames", 2018 AIAA Aerospace Sciences Meeting, AIAA SciTech Forum, Kissimmee, Florida, USA (AIAA 2018-0675)
9. Veeraraghava Raju Hasti, Shuaishuai Liu, Gaurav Kumar, and Jay P. Gore. "Comparison of Premixed Flamelet Generated Manifold Model and Thickened Flame Model for Bluff Body Stabilized Turbulent Premixed Flame", 2018 AIAA Aerospace Sciences Meeting, AIAA SciTech Forum, Kissimmee, Florida, USA (AIAA 2018-0150)

Project 31 Alternative Jet Fuel Test and Evaluation

University of Dayton Research Institute

Project Lead Investigator

Steven Zabarnick, PhD
Division Head, Fuels and Combustion
University of Dayton Research Institute
300 College Park
Dayton, OH 45469-0043
937-255-3549
Steven.Zabarnick@udri.udayton.edu

University Participants

University of Dayton Research Institute

- PIs: Steven Zabarnick, Division Head
- FAA Award Number: 13-C-AJFE-UD
- Overall Period of Performance: April 8, 2015 to September 30, 2021
- Tasks:
  - Period of Performance: April 8, 2015 to March 14, 2016 – Amendment No. 006
    1. Evaluate the performance of candidate alternative fuels via the ASTM D4054 approval process
  - Period of Performance: August 13, 2015 to August 31, 2016 – Amendment No. 007
    2. Evaluate the performance of candidate alternative fuels via the ASTM D4054 approval process
  - Period of Performance: August 5, 2016 to August 31, 2017 – Amendment No. 012
    3. Manage the evaluation and testing of candidate alternative fuels
  - Period of Performance: July 31, 2017 to August 31, 2019 – Amendment No. 016
    4. Manage the evaluation and testing of candidate alternative fuels
  - Period of Performance: August 30, 2018 to August 31, 2019 – Amendment No. 021
    5. Manage the evaluation and testing of candidate alternative fuels
  - Period of Performance: Extended period of performance end from September 10, 2019 to September 9, 2020 – Amendment No. 023
  - Period of Performance: February 5, 2020 to February 4, 2021 – Amendment No. 25
    6. Manage the evaluation and testing of candidate alternative fuels
  - Period of Performance: Extended period of performance end from September 9, 2019 to September 9, 2021 – Amendment No. 028.
  - Period of Performance: February 4, 2021 to February 5, 2022 – Amendment No. 32
    7. Manage the evaluation and testing of candidate alternative fuels
  - Period of Performance: August 10, 2021 to February 10, 2022 – Amendment No. 33
    - No cost extension. Amendment 33 is not task specific.

Project Funding Level

Amendment No. 006	$309,885
Amendment No. 007	$99,739
Amendment No. 012	$693,928
Amendment No. 016	$999,512
Amendment No. 021	$199,966
Amendment No. 025	$1,926,434
Amendment No. 032	$1,049,700

Amendment 33	No cost extension
Total	**$5,279,164**

In-kind cost sharing has been obtained from the following organizations:

Organization	Amount	Year
LanzaTech	$55,801	2015
LanzaTech	$381,451	2016
University of Dayton Research Institute (UDRI)	$43,672	2016
Neste	$327,000	2017
Boeing	$2,365,338	2017
Shell	$280,000	2019
IHI	$1,150,328	2019
Shell	$325,000	2020
Global Bioenergies	$6,875,900	2021
Global Bioenergies	$290,000	2021
Total	**$12,094,490**	

Investigation Team

- Steven Zabarnick, PI, New candidate fuel qualification and certification
- Richard Striebich, Researcher, Fuel chemical analysis and composition
- Linda Shafer, Researcher, Fuel chemical analysis and composition
- John Graham, Researcher, Fuel seal swell and material compatibility
- Zachary West, Researcher, Fuel property evaluation
- Rhonda Cook, Technician, Fuel property testing
- Sam Tanner, Technician, Fuel sampling and shipping
- Carlie Anderson, Researcher, Fuel chemical analysis
- Marlin Vangsness, Researcher, Fuel chemical analysis

Project Overview

Alternative jet fuels offer the potential benefits of reduced global environmental impacts, greater national energy security, and stabilized fuel costs for the aviation industry. The FAA is committed to the advancement of “drop-in” alternative fuels. The successful adoption of alternative fuels requires approval for use by the aviation community, followed by large-scale production of fuel that is cost competitive and meets the safety standards of conventional jet fuel. Alternative jet fuels must undergo rigorous testing to become qualified for use and to be incorporated into ASTM International specifications.

Cost-effective, coordinated performance testing capability (in accordance with ASTM D4054) is needed to support the evaluation of promising alternative jet fuels. The objective of this project is to provide the necessary capability to support fuel testing and evaluation of novel alternative jet fuels.

The proposed program should provide the following capabilities:

- Identify alternative jet fuels, including blends with conventional jet fuel, with the potential to be economically viable and to support FAA’s NextGen environmental goals for testing
- Perform engine, component, rig, or laboratory tests or any combination thereof to evaluate the performance of alternative jet fuels in accordance with ASTM International standard practice D4054
- Identify and conduct unique testing, beyond that defined in ASTM International standard practice D4054, to support the evaluation of alternative jet fuels for inclusion in ASTM International jet fuel specifications
- Obtain baseline and alternative jet fuel data to assess any effects of an alternative jet fuel on aircraft performance, maintenance requirements, and reliability

- Coordinate efforts with activities sponsored by the Department of Defense and/or other governmental parties that may be supporting relevant work
- Report relevant performance data for the alternative fuels tested, including quantified effects of the alternative fuel on aircraft and/or engine performance and on air-quality emissions relative to conventional jet fuel; share reported data with the FAA National Jet Fuel Combustion Program (NJFCP), the broader community (e.g., ASTM International), and the ASCENT COE Program 33 "Alternative Fuels Test Database Library."

Tasks 1 and 2 - Evaluate the Performance of Candidate Alternative Fuels via the ASTM D4054 Approval Process and Manage the Evaluation and Testing of Candidate Alternative Fuels

University of Dayton Research Institute

Objective

Cost-effective, coordinated performance testing capability (in accordance with ASTM D4054) is needed to support the evaluation of promising alternative jet fuels. The objective of this project is to provide the capability necessary to support either (a) the evaluation of to-be-determined alternative fuel(s) selected in coordination with the FAA or b) a fuel test and evaluation project with a specific alternative fuel(s) in mind.

Research Approach

The intent of this program is to provide the capability needed to perform specification and fit-for-purpose evaluations of candidate alternative fuels, with the aim of providing a path through the ASTM D4054 approval process. The UDRI team is capable of performing a large number of these evaluations and is prepared to work with other organizations, such as Southwest Research Institute (SwRI) and engine original equipment manufacturers (OEMs), with unique test capabilities, as needed. These assessments include additional engine, auxiliary power unit (APU), component, and rig evaluations. The UDRI testing capabilities include efforts at the laboratories of the Fuels Branch of the Air Force Research Laboratory (AFRL) and at our campus laboratory facilities.

The following lists provide examples of the evaluations that can be provided by UDRI:

Tier 1

1. Thermal stability (quartz crystal microbalance)
2. Freeze point (ASTM D5972)
3. Distillation (ASTM D86)
4. Hydrocarbon range (ASTM D6379 and D2425)
5. Heat of combustion (ASTM D4809)
6. Density, API gravity (ASTM D4052)
7. Flash point (ASTM D93)
8. Aromatics (ASTM D1319)

Tier 2

1. Color, Saybolt (ASTM D156 or D6045)
2. Total acid number (ASTM D3242)
3. Aromatics (ASTM D1319 and D6379)
4. Sulfur (ASTM D2622)
5. Sulfur mercaptan (ASTM D3227)
6. Distillation temperature (ASTM D86)
7. Flash point (ASTM D56, D93, or D3828)
8. Density (ASTM D1298 or D4052)
9. Freezing point (ASTM D2386, D5972, D7153, or D7154)
10. Viscosity at −20 °C (ASTM D445)
11. Net heat of combustion (ASTM D4809)
12. Hydrogen content (ASTM D3343 or D3701)
13. Smoke point (ASTM D1322)

14. Naphthalenes (ASTM D1840)
15. Calculated cetane index (ASTM D976 or D4737)
16. Copper strip corrosion (ASTM D130)
17. Existent gum (ASTM D381)
18. Particulate matter (ASTM D2276 or D5452)
19. Filtration time (MIL-DTL-83133F Appendix B)
20. Water reaction interface rating (ASTM D1094)
21. Electrical conductivity (ASTM D624)
22. Thermal oxidation stability (ASTM D3241)

Extended physical and chemical characterization

1. Lubricity evaluation: ball-on-cylinder lubricity evaluator (BOCLE) test (ASTM D5001)
2. Evaluation of low-temperature properties: scanning Brookfield viscosity
3. Detection, quantification, and/or identification of polar species, as necessary
4. Detection, quantification, and/or identification of dissolved metals, as necessary
5. Initial material compatibility evaluation: optical dilatometry and partition coefficient measurements to determine the fuel-effected swell and fuel solvency in three O-ring materials (nitrile, fluorosilicone, and fluorocarbon) and as many as two additional fuel system materials
6. Experimental thermal stability evaluation: quartz crystal microbalance to measure thermal deposition tendencies and oxidation profiles at elevated temperatures
7. Evaluation of viscosity versus temperature: ASTM D445 to determine the fuel viscosity at 40 °C and −40 °C to assess the viscosity variation with temperature

In addition to the above physical and chemical fuel evaluation capabilities, UDRI has extensive experience in evaluating microbial growth in petroleum-derived and alternative fuels. These evaluations include standard laboratory culturing and colony counting methods, as well as advanced techniques, such as quantitative polymerase chain reaction (QPCR) and metagenomic sequencing. These methods enable quantitative measurements of microbial growth rates in candidate alternative fuels for comparison with petroleum fuels.

UDRI also has extensive experience in the evaluation of elastomer degradation upon exposure to candidate alternative fuels. Various methods are used to evaluate seal swell and O-ring fixture leakage, including optical dilatometry, sealing pressure measurements, fuel partitioning into the elastomer, and the use of a pressurized temperature-controlled O-ring test device.

Moreover, UDRI can perform fuel–material compatibility testing by using the D4054 procedures for fuel soak testing, postexposure nonmetallic and metallic material testing, and surface and microstructural evaluation. The 68 “short-list” materials and the 255 materials on the complete list can be tested.

Milestone(s)

The schedule for this project is dependent on the receipt of alternative fuel candidates for testing. As candidate fuels are received, a testing schedule will be established via coordination with the FAA and collaborators. Our existing relationships with these organizations will help expedite this process.

Major Accomplishments

Shell IH^2 testing

Discussions with Shell on their IH^2 fuel and process (hydropyrolysis and hydrotreating of woody biomass, municipal solid waste (MSW), and agriculture residue) began in 2017 and proceeded through 2018. In January 2019, samples of their CPK-0 (zero aromatics) fuel were received by the Clearinghouse for testing. Testing proceeded at UDRI and SwRI through the spring of 2019, and a draft research report was produced in the summer. In October 2019, initial warm lean blowout (LBO) testing of the CPK-0 fuel blends was performed in the referee combustor. We await the production of larger quantities of IH^2 fuel for additional cold LBO and ignition studies in the referee rig. In addition, a Phase 1 research report was presented to the OEM committee in June 2020, with the anticipation of OEM APU and engine combustor sector testing in 2022. Feedback from the OEM committee resulted in additional testing being performed. The unusually high cycloparaffin content (>95%) of this fuel will dictate the need for additional Tier 3 testing. Due to the fuel’s excellent performance in the referee rig, the extent of additional testing may be limited. OEM feedback from the Phase 1 research report was provided to Shell and plans are being made to perform combustion testing via CLEEN 3 and this ASCENT project.

IHI Bb-Oil SPK testing
Discussions with IHI of Japan on their Bb-oil fuel and process (algae cultivation with hydrocarbon and oil extraction) began in 2018, and initial fuel samples were received in January 2019. Testing proceeded during the winter and spring of 2019, and the resulting Fast Track research report was submitted for OEM review in June 2019. This fuel consists of approximately 40% cycloparaffins and thus has a higher density than specified in the Fast Track guidelines. The OEM review was completed in August 2019, and we completed additional testing on another production sample to address the OEM's questions during the year. The ASTM ballot was approved in March 2020 for the creation of D7566-20 Annex 7, with the fuel now referred to as HC-HEFA SPK (hydroprocessed hydrocarbons, esters, and fatty acids).

Fischer–Tropsch coprocessing
Fulcrum Bioenergy is interested in adding Fischer–Tropsch (FT) coprocessing to the D1655 fuel specification to permit small quantities (<10%) of FT waxes to be used as feed to petroleum refinery hydrocracking reactors. This change would allow for the use of FT waxes produced from the gasification of MSWs in petroleum refinery operations, thus enabling jet fuel to be produced without operation modifications. To support this effort, this project received jet fuel produced from vacuum gas oil (VGO), and fuel produced from a co-feed of VGO and FT wax product. We assessed the D1655 Table 1 properties, jet fuel total oxidation test (JFTOT) thermal stability, trace metals, GCxGC hydrocarbon type, GCxGC polars, lubricity additive responses, and conductivity additive responses. A research report was produced, and FT coprocessing was balloted in an ASTM October 2019 ballot. The FT coprocessing ballot was approved in March 2020 with subsequent publication of D1655-20 which includes this process in paragraphs A1.2.2.2 of Annex A1.2, "Acceptable Fuels from Non-Conventional Sources."

Publications

Written reports

(n.d.). (2019). Modification of ASTM D1655: Co-processing of Fischer-Tropsch feedstocks with petroleum hydrocarbons for jet production using hydrotreating and hydrocracking (Modification of Report No. ASTM D1655). ASTM International.

(n.d). (2019). Evaluation of synthesized paraffinic kerosene from algal oil extracted from *botryococcus braunii* (IHI Bb-SPK) (Report No. D4054).

(n.d). (2020). Standard specification for aviation turbine fuels (Report No. ASTM D1655-20). ASTM International. https://astm.org/d1655-20.html

Outreach Efforts

Presentations on Project 31 activities were given at the April 2021 and October 2021 ASCENT virtual meetings. Meetings were held with the OEM team, FAA, fuel producers, and others at numerous virtual (generally two per month) FAA/OEM meetings.

Awards

None

Student Involvement

None

Plans for Next Period

We are awaiting the receipt of larger quantities of the Shell IH^2 fuel for further evaluation, which will include cold LBO testing, ignition testing, APU cold start and ignition evaluation, and engine OEM sector evaluation. We will continue discussions with new fuel producers and expect new candidates to enter the process in the coming months, such as fuels from Global Bioenergies, OMV, Revo, CSIR-IIP.

Tasks 3 and 4 - Manage the Evaluation and Testing of Candidate Alternative Fuels

University of Dayton Research Institute

Objective

The objective of this work is to manage the evaluation and testing of candidate alternative jet fuels in accordance with ASTM International standard practice D4054 (Figure 1).

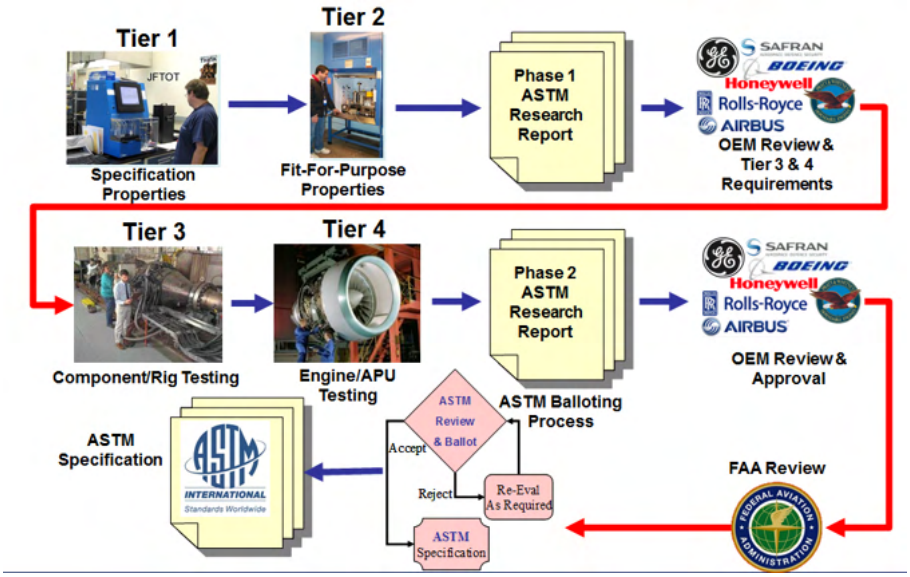

Figure 1. ASTM D4054 qualification process.

Research Approach

UDRI will subcontract with other research organizations, test laboratories, and/or OEMs to conduct the following tasks in support of the evaluation and ASTM specification development for alternative jet fuels. The purpose of this project is to manage and coordinate the D4054 evaluation process illustrated in Figure 2 to facilitate the transition of alternative fuels to commercial use.

Subtask 1: General support

- Develop and make available a D4054 process guide describing logistical procedures for the handling of test fuels, documentation requirements, test report issuance and delivery, and contact information, to provide clear instructions for candidate fuel producers for entering the ASTM D4054 process.

Subtask 2: Phase 1 support

- Coordinate the handling of Phase 1 candidate test fuel samples for Tier 1 and 2 testing.
- Review process descriptions provided by the fuel producer to determine the acceptability for incorporation into the Phase 1 research report
- Review test data from Tier 1 and 2 testing to determine acceptability for incorporation into the Phase 1 research report
- Issue and deliver a Phase 1 research report to OEMs
- In conjunction with the fuel producer, review and respond to comments regarding the Phase 1 research report, as submitted by the OEMs
- Conduct additional Tier 1 or 2 testing in response to OEM comments, as required
- Review and consolidate OEM requirements for D4054 Tier 3 and 4 testing, as submitted by the OEMs
- Deliver consolidated D4054 Tier 3 and 4 testing requirements to the fuel producer.

Subtask 3: Phase 2 support

- Coordinate the funding and scheduling of D4054 Tier 3 and 4 testing with OEMs and other test facilities.
- Coordinate the handling of Phase 2 candidate test fuel samples for Tier 3 and 4 testing.
- Review test data from Tier 3 and 4 testing to determine acceptability for incorporation into the Phase 2 research report.
- Issue and deliver the Phase 2 research report to OEMs
- In conjunction with the fuel producer, review and respond to comments submitted by OEMs regarding the Phase 2 research report
- Conduct additional Tier 3 or 4 testing in response to OEM comments as required
- Issue and deliver Phase 2 research report addenda reporting the additional Tier 3 or 4 test results, as required

Subtask 4: OEM review meetings

- Schedule periodic OEM meetings to review the testing status and the research report evaluations
- Identify suitable meeting venues and support equipment
- Develop agendas and coordinate with attendees for participation in these meetings
- Record meeting minutes, including agreements, commitments, and other action items
- Issue and distribute meeting minutes to all attendees

Subtask 5: Single-laboratory GCxGC method documentation

- Document UDRI GCxGC methods for hydrocarbon type analysis
- Develop reference materials for the creation of GCxGC hydrocarbon type templates
- Measure single-laboratory precision of the GCxGC methods

Subtask 6: Multi-laboratory GCxGC method documentation

- Validate the precision of GCxGC methods across multiple laboratories
- Identify alternative GCxGC methods, including column selection and order, and modulation techniques
- Perform a correlation study to determine the agreement among laboratories, methods, and hardware choices

Milestone(s)

The schedule for this project is dependent on the receipt of alternative fuel candidates for testing. As candidate fuels are received, a testing schedule will be established via coordination with the FAA and collaborators. Our existing relationships with these organizations will help expedite this process. Figure 3 shows a Gantt chart schedule for the testing and approval of candidate fuels that are either currently under evaluation or will soon enter the evaluation process.

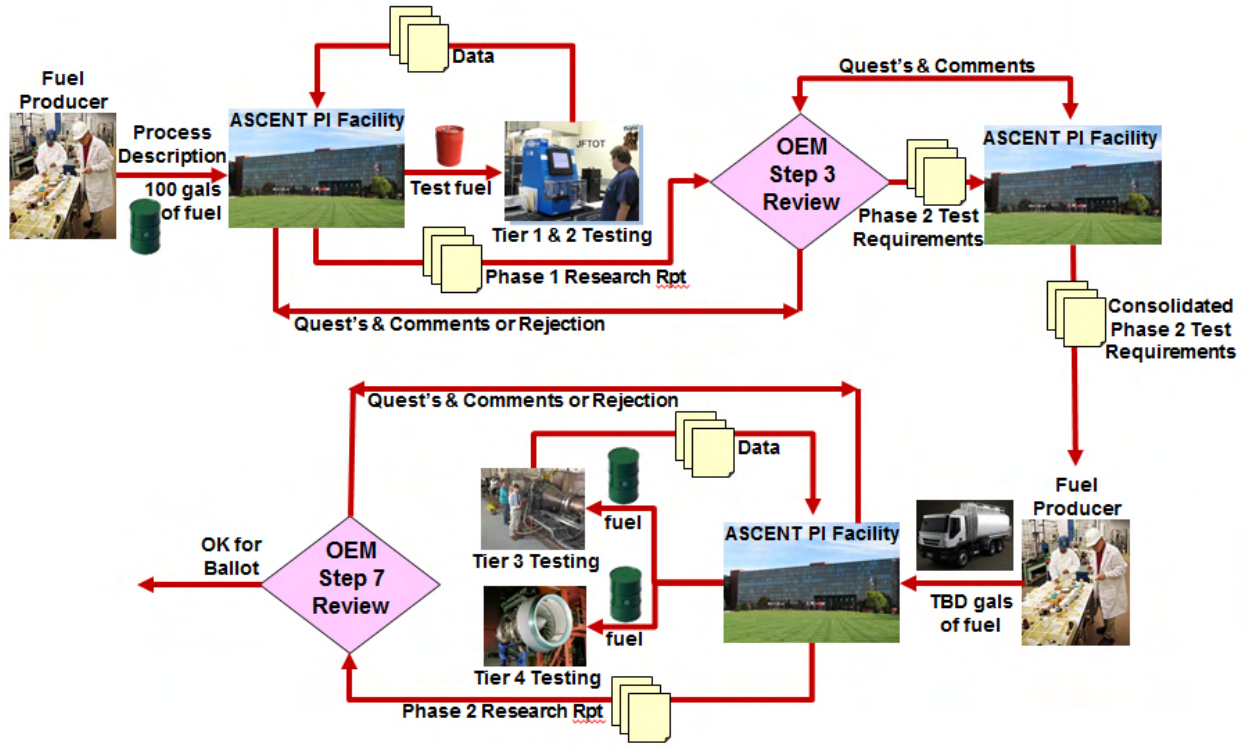

Figure 2. D4054 evaluation process.

D4054 Clearinghouse
Forecasted Fuel Evaluation Schedule

ID	Task Name	Start	Finish
1	**Shell IH2**	**Thu 2/1/18**	**Tue 5/31/22**
2	Step 5 - Phase 2 Testing & Report	Mon 3/1/21	Tue 5/31/22
3	Step 6 - Entry Screening		
4	Step 7 - OEM Engineering Review		
5	Ballot		
6	**Global BioEnergies**	**Sun 5/31/20**	**Fri 4/29/22**
7	Testing and Report	Sun 5/31/20	Mon 1/31/22
8	Entry Screening	Mon 1/31/22	Tue 3/1/22
9	OEM Engineering Review	Tue 3/1/22	Fri 4/29/22
10	**Swedish Biofuels**	**Tue 12/8/20**	**Tue 11/30/21**
11	Testing & Report	Tue 12/8/20	Sat 7/31/21
12	Entry Screening	Sun 8/1/21	Tue 8/31/21
13	OEM Engineering Review	Wed 9/1/21	Tue 11/30/21
14	**CSIR-IIP**	**Tue 12/8/20**	**Sun 7/31/22**
15	Testing & Report	Tue 12/8/20	Wed 3/30/22
16	Entry Screening	Fri 4/1/22	Sat 4/30/22
17	OEM Engineering Review	Sun 5/1/22	Sun 7/31/22
18	**Virent SAK**	**Thu 7/1/21**	**Tue 5/31/22**
19	Step 5 - Phase 2 Testing & Report	Thu 7/1/21	Fri 12/31/21
20	Step 6 - Entry Screening	Fri 12/31/21	Wed 3/2/22
21	Step 7 - OEM Engineering Review	Wed 3/2/22	Tue 5/31/22
22	**ARA CHJ 100%**	**Tue 6/1/21**	**Wed 6/1/22**
23	Step 5 - Phase 2 Testing & Report	Tue 6/1/21	Sun 1/30/22
24	Step 6 - Entry Screening	Mon 1/31/22	Tue 3/1/22
25	Step 7 - OEM Engineering Review	Wed 3/2/22	Wed 6/1/22

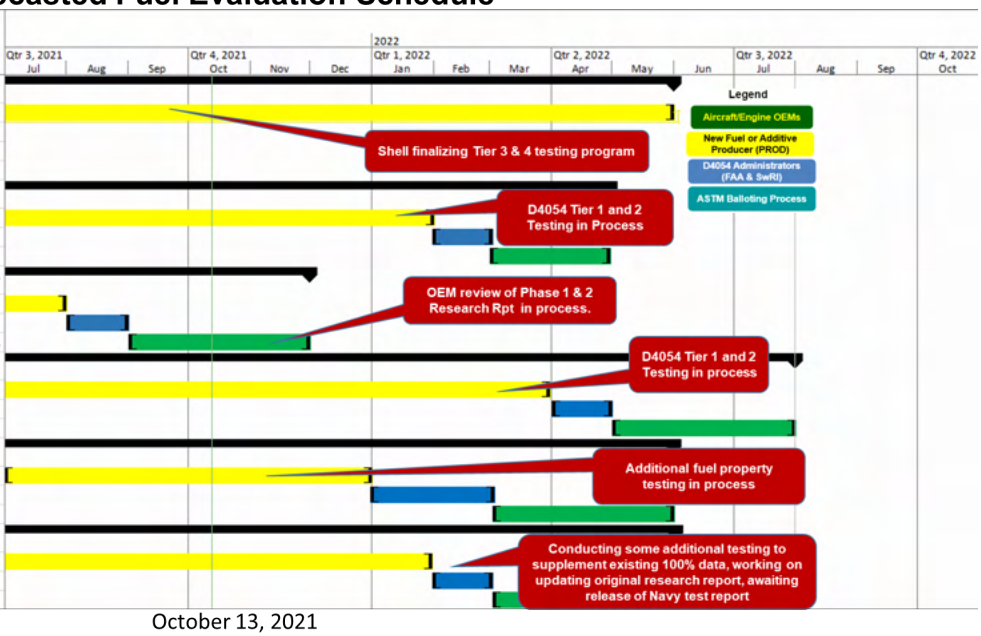

October 13, 2021

Figure 3. Schedule for fuel evaluations.

Major Accomplishments

Fast Track annex development

A D7566 Generic Annex concept was originally presented to the OEM committee, in which a set of highly stringent property requirements would be used to create a D7566 annex without the feedstock or process being defined. This annex would enable the rapid approval of a wide variety of fuels that closely resemble already approved fuels with regard to composition and physical properties. However, the OEM committee was concerned about the lack of OEM review for each fuel approved through this process. Thus, the Generic Annex pathway was abandoned in the spring/summer of 2018. In response to OEM concerns, a Fast Track Annex to D4054 was proposed in the winter of 2018–2019, which included a list of stringent properties and chemical composition requirements. This Fast Track Annex would require identification of the feedstock and processing, along with a required OEM review of the research report results. The goal would be an allowed 10% blend limit with a much more rapid approval pathway. Fast Track approval would result in the creation of a D7566 annex for each approved fuel. Ultimately, the Fast Track Annex was balloted in the spring of 2019 and approved in April 2019. To date, one candidate fuel has been approved via the Fast Track process, the IHI HC-HEFA D7566 Annex 7 fuel.

GCxGC method documentation

Two GCxGC method reports were completed and made available to the fuel community (UDRI Method FC-M-101, Flow Modulation GCxGC for Hydrocarbon Type Analysis of Conventional and Alternative Aviation Fuels; UDRI Method FC-M-102, Identification and Quantitation of Polar Species in Conventional and Alternative Aviation Fuels Using SPE-GCxGC). The first report documents the UDRI/AFRL hydrocarbon type analysis method based on flow modulation GCxGC and “normal phase” column order (nonpolar followed by polar columns). The second report documents the UDRI/AFRL polar analysis, which uses a solid-phase extraction pre-separation technique to separate and concentrate trace polar species. After pre-separation, the fuel polars are analyzed by GCxGC separation. These reports are being made available to any parties that express interest. These documents are now included in the ASTM D4054 Fast Track Annex A4 (ASTM D4054 Annex A4, Fast Track OEM Qualification and Approval Process for New Aviation Turbine Fuels). These methods provide the fuel community with new tools to enable accurate fuel composition analysis and improved techniques for evaluating and qualifying new candidate alternative fuels.

GCxGC precision: intra- and interlaboratory comparisons

To investigate the precision of GCxGC hydrocarbon type analyses, we assessed a single fuel over several years with a single instrument (intralaboratory comparison). We also compared two different GCxGC systems: flow modulation with a nonpolar initial column and a polar secondary column versus thermal modulation with a polar initial column and a nonpolar secondary column. We also compared measurements between two laboratories (UDRI/AFRL versus NASA Glenn) for multiple fuels with the same instrument type and column configuration. In addition, we have recently compared measurements between multiple laboratories using a number of different GCxGC systems and methods.

A report describing these results has been drafted and submitted to the FAA for comments (UDR-TR-2021-159). This report details the following:

- 2.0 Phase 1 results: single-laboratory GCxGC method documentation
  - 2.1 Methods and documents describing UDRI methods
  - 2.2 Development of reference materials
  - 2.3 Single-laboratory precision
- 3.0 Phase 2 results: multi-laboratory GCxGC method documentation
  - 3.1 Precision validation of normal phase GCxGC, flow modulation with an outside laboratory (reproducibility)
  - 3.2 Identification of alternative methods
  - 3.3 Correlation study

OEM committee coordination

The ongoing effort of ASTM OEM committee coordination continued during this period. This effort involves coordinating the engine and airframer OEM meetings, which have ordinarily occurred in concert with the biannual ASTM Committee D02 sessions and at the annual U.K. Ministry of Defense Aviation Fuels Committee meeting in London. During travel restrictions due to the COVID-19 pandemic, these meetings have been occurring virtually and more frequently, once or twice per month. SwRI continues to receive funding to aid in coordinating the OEM meetings and in communicating with the OEMs for discussions and research report reviews of new candidate alternative jet fuels. In addition, a Gantt schedule is updated monthly; this schedule shows a queue of candidate fuels and the completed and expected schedules as these fuels move through the ASTM D4054 process of testing, review, balloting, and approval. A recent version of this schedule is shown in

Figure 3. In support of the ongoing OEM committee coordination, subcontracts are being extended to our ASCENT grant end date of September 2022 with Boeing, GE Aviation, Honeywell, Rolls Royce, Pratt & Whitney, and SwRI.

Publications

Written reports

(n.d.). (2018). UDRI Method FC-M-101: Flow modulation GCxGC for hydrocarbon type analysis of conventional and alternative aviation fuels (Report No. UDR-TR-2018-40).

(n.d.). (2018). UDRI Method FC-M-102: Identification and quantification of polar species in conventional and alternative aviation fuel using SPE-GCxGC (Report No. UDR-TR-2018-41).

(n.d.). (2020). Evaluation of integrated hydropyrolysis and hydroconversion (IH^{2}®) cycloparaffinic kerosene (CPK-0) (Report No. D4054).

(n.d.). (2019). Evaluation of synthesized paraffinic kerosene from algal oil extracted from *Botryococcus braunii* (IHI Bb-SPK) (Fast Track Research Report).

(n.d.). (2021). Alternative jet fuel evaluation and specification development support: GCxGC methods draft report (Report No. UDR-TR-2021-159).

Outreach Efforts

Presentations on Project 31 activities were given at the April 2021 and October 2021 ASCENT virtual meetings. Meetings were held with the OEM team, FAA, fuel producers, and other attendees at numerous virtual FAA/OEM meetings (generally two per month). We have had occasional teleconferences with Shell on their IH^{2} fuel candidate. We have also met with multiple candidate fuel producers, including Global Bioenergies, OMV, CSIR-IIP, and Revo.

Awards

None

Student Involvement

None

Plans for Next Period

We plan to continue coordination of the OEM committee reviews. We will continue to hold virtual OEM committee meetings until the COVID-19 restrictions allow business travel.

Project 033 Alternative Fuels Test Database Library

University of Illinois at Urbana–Champaign

Project Lead Investigator

Tonghun Lee
Professor
Mechanical Science & Engineering
University of Illinois at Urbana–Champaign
1206 W. Green St.
Urbana, IL 61801
517-290-8005
tonghun@illinois.edu

University Participants

University of Illinois at Urbana–Champaign

- PI: Tonghun Lee, Professor
- FAA Award Number: 13-C-AJFE-UI, Amendment 33
- Period of Performance: October 1, 2020, to September 30, 2021
- Tasks:
    1. Generation II online database: JETSCREEN, ALIGHT and NewJET and domestic airport connection
    2. Machine-learning-based online analysis

Project Funding Level

FAA funding Level: $200,000
Cost sharing: Software license support from Reaction Design (ANSYS)

Investigation Team

- Tonghun Lee (Professor, University of Illinois at Urbana–Champaign): overall research supervision
- Ji Hun Oh (graduate student, University of Illinois at Urbana–Champaign): database development and machine-learning-based analysis
- Alex Solecki (graduate student, University of Illinois at Urbana–Champaign): database development

Project Overview

This study seeks to develop a comprehensive and foundational database of current and emerging alternative jet fuels by integrating relevant pre-existing jet fuel data into a common archive that can support scientific research, enhance operational safety, and provide guidelines for the design and certification of new jet fuels. In light of the September 2021 White House statement on advancing the future of sustainable aviation fuels (SAFs) in America, the database now has even greater potential to serve the national agenda. In previous years of this project, efforts were focused on the integration and analysis of pre-existing jet fuel data from various government agencies and individual research groups. In 2020, we converted all the compiled data to a new nonstructured query language (NoSQL) format by using a JavaScript object notation (JSON) schema, thus allowing the data to be analyzed in a flexible manner with various programming languages. To this end, we have launched the second generation of our online database, the Alternative Jet Fuels Test Database (AJFTD), which utilizes the new nonrelational database structure. This version is equipped with interactive analysis functions for users and flexible methods for plotting and downloading data. In the previous year, we extended this effort to incorporate advanced machine-learning algorithms in the analysis process. Additionally, we have integrated our database with the database assembled by the European Jet fuel screening and optimization (JETSCREEN) program. In the future, data acquisition from domestic and international airports will help further develop the database and support its use as a destination for all sustainable-aviation-related property and test data.

Figure 1. Generation II national Alternative Jet Fuels Test Database web interface (altjetfuels.illinois.edu).

We hope that the database will ultimately serve not only as a comprehensive centralized knowledge base utilized by the jet fuel research community but also as a resource that can enhance global operation efficiency and safety. Future efforts will include linking real-time fuel usage and certification data from domestic and international airports. Connecting our database with ongoing European projects, such as ALIGHT and NewJET, will help create avenues for future database development in this area. With the expected prolific diversification of new alternative jet fuels in the near future, the ability to track critical fuel properties and test data from both research and operation perspectives will be highly valuable for the future of commercial aviation. Furthermore, increasing the breadth of data categories available in the database - from fuel data to global usage trends—will increase its relevance to a broader audience. We hope that the ongoing website development and improvement of the user interface will also allow the general public to engage with high-level information thus increasing the awareness of SAFs and further supporting the nationwide visibility of sustainable aviation.

Task 1- Generation II Online Database Updates: JETSCREEN, ALIGHT, NewJET, and Domestic Airport Connection

University of Illinois at Urbana-Champaign

Objective(s)

The main objective of this task is to upgrade and debug the generation II online national AJFTD functions and link the database to the European JETSCREEN, ALIGHT, and NewJET programs. The generation II database has been designed with a new architecture allowing for flexible analysis and scaling based on a NoSQL data format. This format can accommodate various data types that can be easily accessed by any common programming language, and basic analysis functions have been directly built into the web interface. After the launch of the generation II web interface, extensive efforts in the past year have been focused on upgrading the functionality and addressing bugs according to user feedback. We have also converted much of the data to comma-separated value (CSV) format to enable future machine-learning-based analysis, as further discussed in Task 2. The specific goals in Task 1 are:

- Test and improve the functionality of the generation II online web interface and database structure
- Pilot connection with the European ALIGHT and NewJET programs
- Establish methods for acquiring real-time airport fuels data (previously delayed because of the COVID-19 pandemic; efforts restarted as of September 2020)

Research Approach

Generation II Database Debugging and Upgrade

A beta version of the generation II database was launched online in the summer of 2019. The web interface of the generation II database is shown in Figure 1. All functionality of the previous database has been maintained, and the security login features have been migrated from the previous version. The generation II web interface, much like that of generation I, is an HTML-oriented program built on a layer of metadata, which supports search functions for users. The tree structure applied to organize the data folders in the first database has been retained in this version, thus allowing users to access the data in a similar manner. The main difference is the addition of an inner core that houses the JSON files and is where the test data reside. Currently, the database has grown to contain more than 25,000 separate fuel records.

The catalog of data currently available in the database is assembled primarily from four separate sources. The fuels with POSF (Air Force Research Laboratory [AFRL] fuel database code) number designations were added from the internal database maintained by the AFRL at the Wright Patterson Air Force Base. The second dataset was obtained from the Petroleum Quality Information System (PQIS) reports of the Naval Air Systems Command (NAVAIR) and corresponds to a compilation of fuel data geared primarily toward government use. The third set was provided by Metron Aviation, which compiled fuel properties from samples collected at airports through a previous ASCENT project. The dataset resulting from this study has proven valuable by providing a landscape of fuels currently used in commercial aviation and will guide our future efforts focused on capturing this type of data in real time. The final dataset was obtained from the National Jet Fuel Combustion Program (NJFCP) within ASCENT.

After the launch of the generation II database, significant changes have been made to fix bugs and upgrade various aspects of the database. Several key changes to the database are summarized below.

- During the integration of the database with JETSCREEN, we modified the labeling structure to ensure that files were coded as JETSCREEN data and were separately searchable. Similar to how the Metron data are labeled according to the airport from which the data were retrieved, JETSCREEN has been added as a separate search label. This search filter can be integrated with additional search filters to allow users to view tests for a specific fuel type from the JETSCREEN group if desired.

- The Export and Compare features also required updates. Although we had worked with JETSCREEN extensively to create a standard JSON format, the files generated from the AJFTD and JETSCREEN had minor differences, which caused the current code on the database to fail occasionally. Slight differences among the JETSCREEN files themselves were also causing errors in attempts to compare the data with FAA files as well as with other JETSCREEN files. The Export and Compare features were updated to work around these issues and to support the comparison of all test files in the database.

- The display of data in the database was also changed to allow for more privacy and security. Authors of the files (which included student names) were removed from the JETSCREEN display. The sharing function, which was added to share selected FAA data with JETSCREEN via Amazon Web Services (AWS), was set to display for only administrator accounts. These shared FAA files sync with the AWS S3 bucket every hour. The JETSCREEN bucket on AWS is checked each day for new files, which are then downloaded to the website.

- Efforts were made to convert the JSON format in the database to CSV format for select files to enable machine-learning-based analysis, which will be addressed further in Task 2. The actual files being stored will use the NoSQL JSON format, which is more conducive to maintaining a flexible database. However, certain parts of the data to be analyzed with machine learning will need to be converted to CSV format, for which multiple Python-based machine-learning scripts are available. In the future, a process to automate this conversion in real time may be necessary.

- Online viewing of 2D gas chromatography (GCxGC) data is being made available to users (beta testing in progress). The scripts that process data uploads have been revised to properly process the section containing GCxGC data and now present this information on the web portal. This development is important because it is the first of many upcoming improvements to the user interface that will allow users to engage with data on the website itself in a comprehensive and high-level fashion before downloading and processing raw files. The data are available in both tabulated format and bar chart format by carbon number. Figure 2 shows an example of the tabulated GCxGC data for a sample fuel. The table organizes compositional data by chemical family and further by subgroups within that family, and the final values are the species within the subgroup, ordered by carbon number. The Expand feature allows for more focused viewing of

compositional data by chemical family and subgroup. Users can choose to view composition data by weight or volume percent with a toggle switch at the top of the table. Figure 3 depicts a graphical representation of the fuel composition by carbon number and chemical family, which further elucidates the distribution of the fuel species by carbon number and also gives users a general idea of the most abundant species in the fuel sample. The scroll-over feature allows users to preview numerical data for a given bar section. Users may also zoom by using a mouse scroll wheel. For ease of viewing of less abundant species, the chemical families represented in the bar chart can be toggled on and off. The *y* axis automatically adjusts accordingly for optimal viewing. As with the table, the bar chart can also be viewed by weight percent or volume percent.

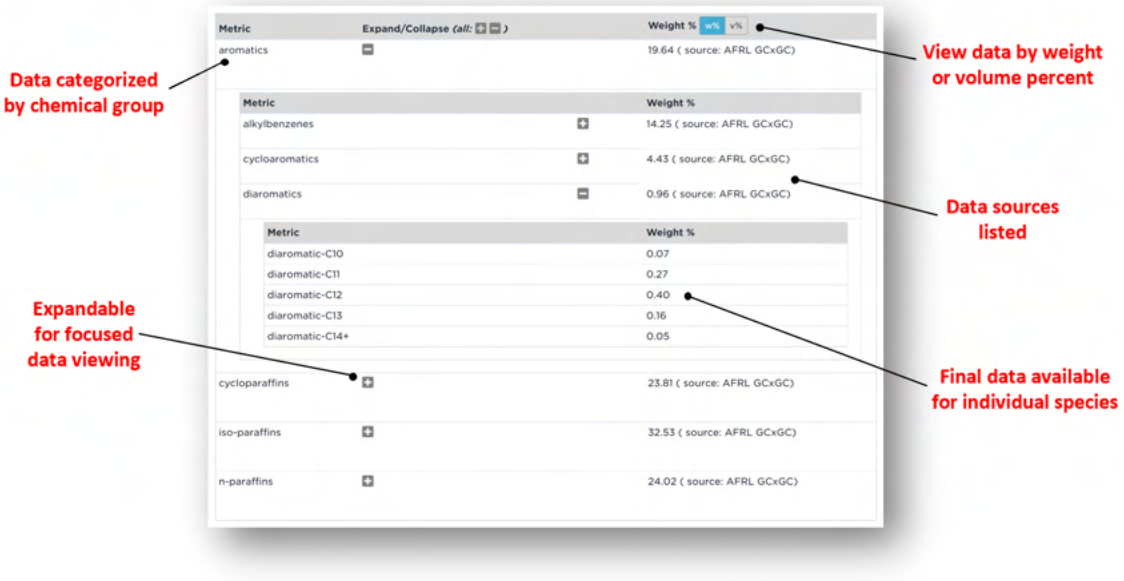

Figure 2. Updates to data viewing on the AJFTD website: view of GCxGC data in tabulated format.

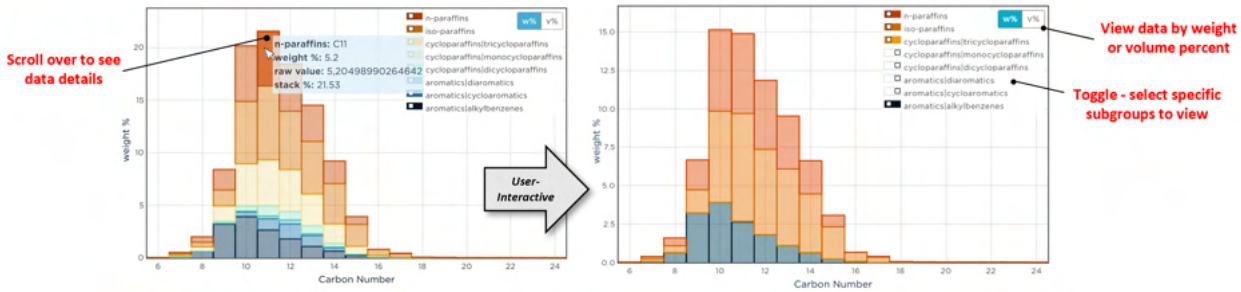

Figure 3. Updates to data viewing on AJFTD website: view of GCxGC data in carbon number bar chart format.

Integration of the Database with JETSCREEN, ALIGHT, and NewJET

In 2020, we completed the integration of our database with the European JETSCREEN program. The JETSCREEN program was initiated to provide fuel producers, air framers, and aero-engine and fuel system original equipment manufacturers (OEMs) with knowledge-based screening tools for fuels and have a similar database that could be linked with ours. We first started discussing a potential merger with the JETSCREEN database in 2018, after which we started methodically synchronizing the data structure so that a merger could be possible. After extensive beta testing, the two databases were first linked in the spring of 2020. Data sharing between AJFTD and JETSCREEN ended in 2020, when the JETSCREEN project was completed and archived.

After the completion of JETSCREEN, AJFTD will continue acquiring new data through connections with new European programs ALIGHT and NewJET. ALIGHT is a program aiming to assess and improve the supply chain, integration, and use of SAFs and smart energy solutions through examining and optimizing operations at Copenhagen Airport. NewJET is a research program headed by the University of Birmingham aiming to improve pathways for production of new SAFs. We anticipate using a similar data-sharing structure to that used by JETSCREEN to connect these programs with AJFTD (process outlined in Figure 4).

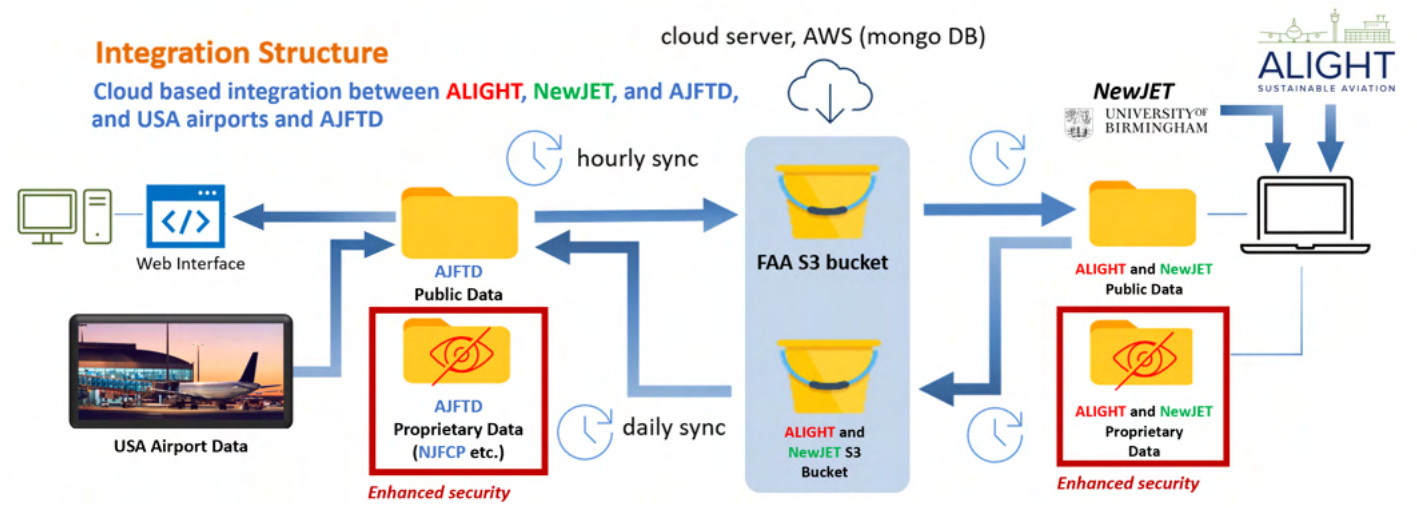

Figure 4. Plans for future data sharing with the European sustainable aviation programs ALIGHT and NewJET.

The JETSCREEN integration process has helped streamline a data-sharing method that ensures frequently updated and well-secured data flow between two projects; thus, this method of data sharing is expected to be used in future integration with the aforementioned ALIGHT and NewJET programs. Previously, the JETSCREEN and FAA databases were joined by a common cloud storage. AWS was selected as the server to store the shared data, mainly because of its affiliation with the University of Illinois. S3 buckets (Amazon database structure) were created for both FAA and JETSCREEN to share their JSON files. Each could pull files from the other's folder, but read and write access was granted to only the owners of the bucket. The FAA data are shared with its S3 bucket via altjetfuels.illinois.edu. All public FAA data on the website will have an option to be shared with JETSCREEN, which can be toggled by administrators. The website syncs hourly with the bucket to upload newly shared data. No proprietary data are shared with the FAA S3 bucket. Any files uploaded to the FAA bucket can be viewed and downloaded by JETSCREEN. For downloading new JETSFCREEN data to the website, a script is run daily to check JETSCREEN's S3 bucket for newly shared data. Any new files are then downloaded to our local database and can be accessed by users.

We note that the actual interface of the database is decided by each entity. We have adopted an open web interface; ALIGHT has an operational website; and NewJET is currently in the process of developing their web interface. Additionally, we note that near the end of the JETSCREEN data integration period, new security measures were implemented for protecting proprietary data at both JETSCREEN's and AJFTD's ends. As database integration with new programs continues, the process of handling proprietary data from different sources may need to be streamlined to account for variations in preferences between different program managers.

The completion of the JETSCREEN database integration process was a major first step in linking many other fuel databases across the globe. From this joint effort between FAA and JETSCREEN, we established a foundation for data sharing that can be used again with other programs, such as ALIGHT and NewJET. The ultimate goal of international database integration is to help monitor and evaluate fuels used in international airspace and provide an accurate picture of how fuel composition and usage trends are changing with time. As new fuels are integrated into the global supply chain, having a means to keep track of their properties will become critical. Such an interconnected database will ensure our ability to provide the most representative information needed for research on, and certification of, new SAFs. The impacts of database integration are outlined below in Figure 5.

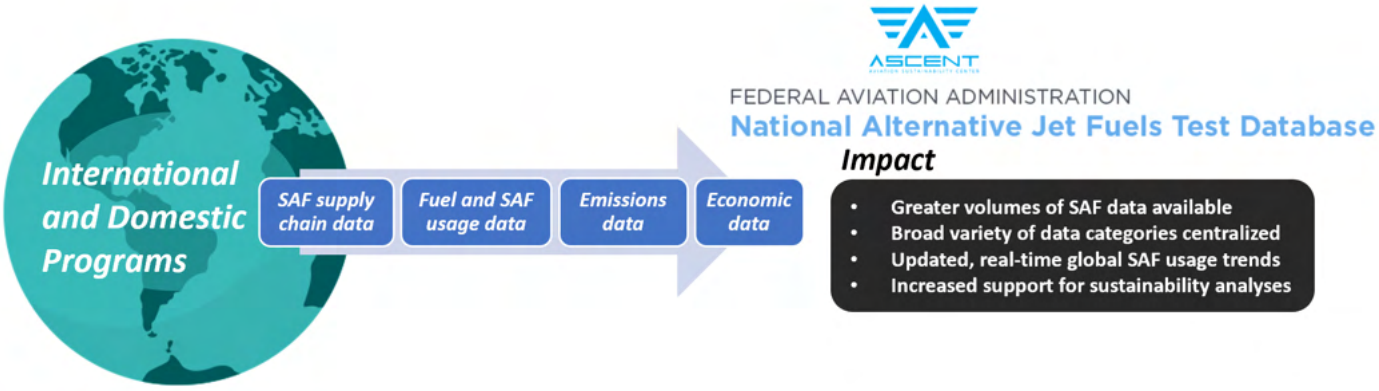

Figure 5. Plan to expand AJFTD's available data categories through data sharing with domestic airports and the current international SAF projects ALIGHT and NewJET.

This year, in addition to opening pathways for international database integration, we have resumed our efforts to intercept fuel samples and usage data from a selection of US airports (activities previously delayed because of the COVID-19 pandemic). National motivation to achieve a more sustainable and emission-free aviation sector grew in the Fall of 2021 with the launch of the White House Sustainable Aviation Fuel Grand Challenge. This initiative outlines various public and private grants, as well as policy changes, supporting the research, development, and implementation of SAFs. As this topic gains national visibility, the platform for further development of the AJFTD will also grow.

The goal of connecting AJFTD with domestic airports is to be able to assess the potential for zero-carbon operation via integration of SAFs. This aim can be accomplished by collecting actual fuel supply data from domestic airports and applying advanced analysis techniques to determine both the current status and future prospects for optimal integration of SAF. Real-time fuel property data can be used to analyze the current fuel supply infrastructure, thus enabling the determination of optimal SAF integration strategies for the future. This effort is expected to lay a foundation for achieving the sustainability targets set by both the United States (SAF Grand Challenge) and the global community (Renewable Energy Directive [RED II] of the European Union and the Paris agreement) by providing the data and analytic tools for sustainable pathways toward zero-emission airport operation through SAF integration.

Milestone(s)

3 months
- Debugging and optimization of the data structure in the generation II database
- Completion of JETSCREEN database integration security features

6 months
- Communication initiated with Airlines for America (A4A) contacts for the airport data integration plan
- Completion of most of the debugging of the generation II database and further improvements to online analysis tools

9 months
- File upload script supporting the identification of fuel compositional data along with property data
- Discussions with domestic airport contacts to establish the next steps for real-time airport data interception.

12 months
- Modification of View, Compare, and other functions to include the presentation of fuel compositional data
- Planning and communication with ALIGHT and NewJET contacts

Major Accomplishments

Initiation of Domestic Airport, ALIGHT, and NewJET Connections

Correspondence with the relevant program contacts for the aforementioned programs has been initiated and plans to proceed with international program integration are in place. These three connections will serve as new sources for acquiring greater amounts of fuel data as well as the expansion of the data categories available in the database to include categories such as usage and emissions data. Continued international collaboration will increase the long-term potential for support and data sharing with other international programs as they are formed. Connections with domestic airports will also support the long-term reliability of in-country data acquisition if consistent avenues for data sharing are built and maintained, thus providing the database with the most up-to-date and relevant information available.

Modifications to the Generation II Online Database and Inclusion of Fuel Compositional Data on the Website

Continuing improvements to the online database will include the availability of fuel compositional data viewing, representing a significant step in streamlining the use of the database as an analytic tool as well as a source of raw data files. Such modifications will not only improve the user experience, by enabling more meaningful inspection and interaction with fuel data, but also support further development of the machine-learning interactive capabilities we hope to include in future versions of the database.

Publications

Blakey, S., Rauch, B., Oldani, A., & Lee, T. (2019). Advanced fuel property data platform: Overview and potential applications [Presentation]. 16th International Conference on Stability, Handling, and Use of Liquid Fuels Dresden, Germany.

Outreach Efforts

The database has been made accessible through https://altjetfuels.illinois.edu/

Awards

None

Student Involvement

This project was primarily conducted by two graduate students, Ji Hun Oh and Alex Solecki.

Plans for Next Period

In the future, detailed planning regarding the integration of the database with ALGIHT and NewJET will be undertaken. A more formal outline of the intents and goals of collaboration with these programs will guide the anticipated progress for the coming years. Interception of domestic airport data will be an increasingly important process to streamline as the national focus on SAFs increases in accordance with the 2021 Grand Challenge. Detailed planning in close coordination with our contacts at selected target airports will be the next step.

In addition, efforts to improve the functional and aesthetic features of the database are ongoing, as summarized below.

- Data presentation: Similar to the updates to data viewing and interaction on the online portal, we plan to implement a series of additional visual aids to support more meaningful user interaction with the data before downloading and analysis of raw files. One way to achieve this goal is by optimizing the Compare feature. We are currently working on presenting GCxGC data comparisons, with which users can quickly judge significant compositional differences between selected fuels. We are also redesigning the comparison graphs that are generated automatically during the use of the fuel comparison feature to make it more logical and account for situations in which the fuels being compared have different information types.

- Navigation: A site navigation guide, accessible on the main page, will outline the information available on the database website and indicate where it is located, to help new users locate relevant information more quickly. Because the prospective plans for the database include the addition of new data categories, which may reflect airport and emissions data, this feature is expected to become more important to supporting effective and efficient use of the database resources. To make finding specific fuels easier and more intuitive, we will also improve the fuel search function, by revising the tags for each fuel to include a broader range of search terms that could be used to locate a fuel of interest.

- User feedback: To implement more relevant improvements in the web portal's main interface and functionality, efforts are underway to gather more data on how the database is being used. We will be including a user feedback window on every page, through which users can submit feedback or questions directly to the website managers, thus improving the response time and the frequency of contact between our team and users. Surveys may be introduced to frequent users to allow us to better understand how the database is being used, and further improve the website's organization and functionality.

Task 2 - Machine-Learning-Based Analysis

University of Illinois at Urbana-Champaign

Objective(s)

The main objective of this task was to develop advanced methods based on machine-learning algorithms for analysis of the data in the alternative jet fuel database. The effort is inspired by the notion that the intricate relationships between the properties of fuels and their chemical signatures are critical but potentially too complex to be addressed with routine, classical, regression-based analysis. The effort has become increasingly important with the advent of new analytic techniques, such as GCxGC, that yield large amounts of data that are difficult to process with simple analytic algorithms. Machine learning can enable the most advanced analysis to be applied to our current data and is expected to become even more powerful as the size and diversity of data increase in the future. Previous studies have verified the efficacy of artificial neural networks in modeling the complex and obscure correlations between jet fuels' chemical compositions or structures and their physicochemical properties. The next step in this task is to exploit neural networks and deep-learning methods to address realistic challenges in SAF databases. The specific major goals are as follows:

- Identify real-world challenges in the analyses of jet fuel, specifically SAF, datasets
- Devise deep-learning-based strategies for addressing these challenges
- Perform composition–property modeling by using GCxGC and advanced machine-learning techniques

Research Approach

Data-driven Streamlining Based on Novelty Fuel Composition

A major challenge in SAF evaluation and qualification is the diversity and sparsity of SAF chemical compositions. If a SAF candidate exhibits compositions not explicitly characterized by D1665 conventional aviation fuels, its properties cannot be accurately correlated via existing data-driven approaches, such as quantitative structure–property relationships. This conclusion was corroborated by our preliminary studies attempting to map the comprehensive features of GCxGC to key properties in a diverse dataset: fuels with compositions not represented during the training (referred to as "novelty fuels" herein) showed high predictive errors. Therefore, there is a need to establish a means for preemptive detection and handling of such novelty fuels within the analyses pipeline. Unfortunately, most studies and literature have focused on conventional fuels, and only a few have addressed this topic.

Motivated by this challenge, we began to develop a deep-learning-based strategy to detect and quantify the degree of GCxGC novelty with respect to an existing pool of known (i.e., labeled) fuels. Using the labeled pool, our novelty-detection scheme utilizes an autoencoding neural network trained to encode more than 80 hydrocarbon groups to a few latent representations with the highest variance (or "energy") and optimal clustering characteristics, then decodes the output back to the original input. This network is implemented in Python by using PyTorch and is trained via stochastic gradient descent to update network parameters. After training, the novelty of unknown target fuels can be computed via decoded reconstruction error and outlying distances to the latent embeddings. Our preliminary results have indicated that our hybrid approach is more robust than traditional anomaly detection techniques such as *K*-nearest neighbors because it (a) accounts for all GCxGC information, (b) uses artificial neural networks that permit intricate nonlinear mappings, and (c) extracts the final score from more than one criterion.

The calculated novelty score dictates the next course of action for the target fuels. Low-scoring "normal" fuels can be evaluated with high fidelity with data-driven models built from the pool of labeled fuels. We have successfully demonstrated that key properties, such as distillation, flashpoint, viscosity, and net heat of combustion, can be accurately predicted. In contrast, the remaining novelty fuels require other means, e.g., labeling by conducting fuel tests and compiling the results. We further propose a labeling strategy based on prioritizing the fuels with the highest novelty scores. This corresponds to active learning, a subfield of machine learning in which the goal is to query the unlabeled data that are richer in information

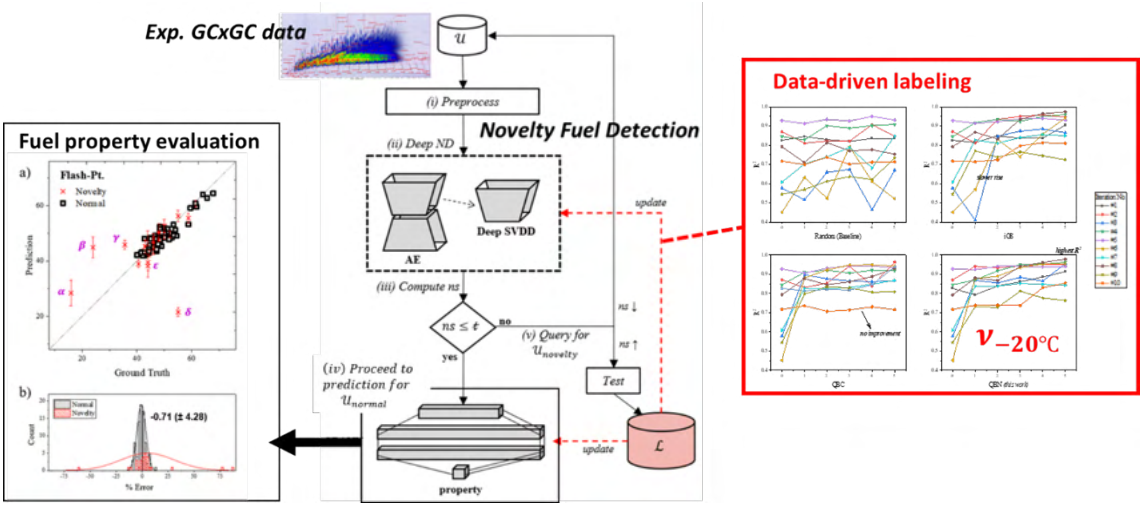

Figure 6. Framework for streamlining based on novelty fuel composition.

This framework is schematically shown in Figure 6. From top to bottom, the target fuel's GCxGC is screened on the pre-trained novelty fuel detection agent before being approved for downstream predictive analyses (left) or deferred/rejected to manual labeling (right). This framework was validated on a diverse and sparse dataset of 100 total fuels comprised of petroleum-based aviation fuels or SAF derived from various sources, methods, and blending ratios. The results indicated that our framework is highly effective.

Missing Data Imputation Algorithms

Another major challenge of real SAF databases is missing or noisy data. Such occurrences compromise the implementation of machine-learning algorithms. In these scenarios, the most frequently used approach is consolidating the dataset by discarding fuels containing missing elements (listwise deletion) or substituting missing data with averages or means computed from the available data. However, these approaches lead to either (a) reduced dataset sizes, which are known to affect the performance of machine-learning models, or (b) induce biases, because missing and non-missing data possess systemic differences; for example, achievable temperature measurements of certain properties (e.g., flashpoint or freezing point) are restricted by the apparatus, and thus the missingness mechanisms are not strictly random (Figure 7, top left diagram).

To combat these issues, we have devised a machine-learning strategy to impute missing data more accurately and reliably. We use a two-fold algorithm in which missing data are fist approximated via multiple imputations via chained equations (MICE), and this is followed by a refinement stage using a denoising autoencoder, as shown in the top right schematic in Figure 7. We have implemented this process on a hydroprocessed esters and fatty acids (HEFA) property dataset with data instances randomly omitted according to a defined missingness mechanism. The results have indicated that missing data can be accurately imputed for all properties under moderate missingness scenarios. For certain properties, imputations are feasible (although with limited accuracy), even for extreme circumstances where up to 60%–70% of the data are missing, and only 5% of the fuel instances are completely labeled. In future studies, we will investigate the impact of using these imputations for machine-learning applications, to demonstrate the advantages over using a reduced dataset.

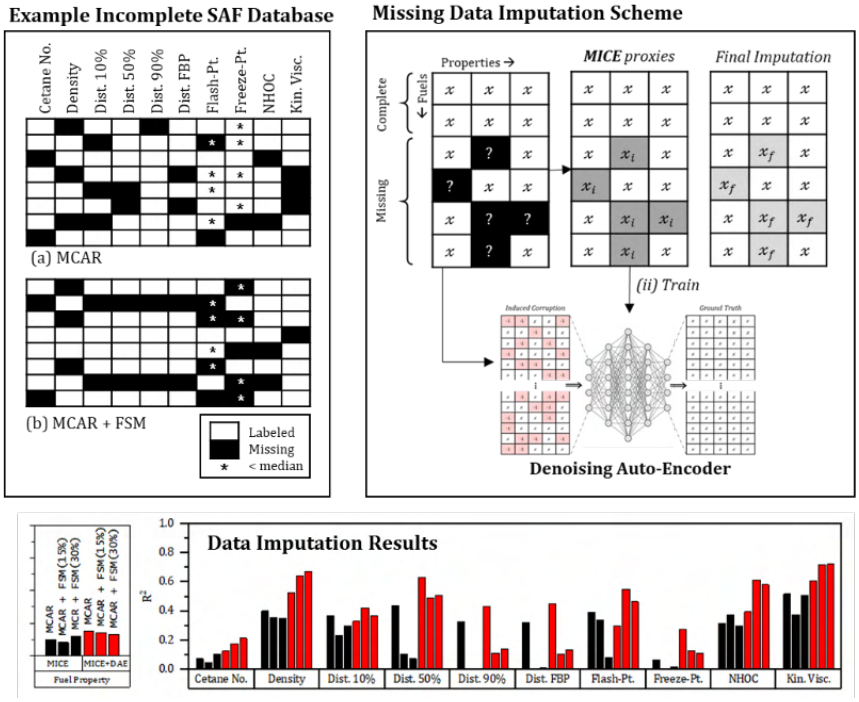

Figure 7. Missing fuel property data imputations.

Milestone(s)

3 months

- Formalization of a machine-learning implementation plan

6 months

- Setting up scripts and algorithms for implementation of machine learning
- Organization of target data from the database for implementation of machine learning

9 months

- Implementation and optimization of machine-learning algorithms

12 months

- Finalization of all machine-learning tasks for publication

Major Accomplishments

We have continued to implement advanced machine-learning algorithms in the analysis of data in our database. Specifically, we have devised deep-learning-based strategies to address relevant challenges in existing SAF databases, such as how to accommodate fuels exhibiting low predictive confidence due to novelty fuel chemical compositions and missing data. Although this work is in nascent stages, our preliminary results showed promise in tackling these challenges, especially when compared to traditional machine-learning methods. Current efforts are devoted to finalizing and refining the methods, and we plan to publish our findings, integrate our algorithms into the website database as an online analysis tool, and test the feasibility of using these methods to aid in the rapid assessment of SAF in real-world scenarios.

Publications

The following two publications are in progress, with anticipated publication in AIAA SciTech:

Oh, J., Oldani, A., Lee, T., & Shafer, L. (2021).*Deep learning algorithms for assessing sustainable jet fuels from two-dimensional gas chromatography* [Manuscript in preparation].

Oh, J., Oldani, A., Shafer, L., & Lee, T. *Data-driven streamlining of sustainable aviation fuels via deep novelty GCxGC detection and query* [Manuscript in preparation].

Outreach Efforts
The database has been made accessible through https://altjetfuels.illinois.edu/

Awards
None

Student Involvement
This project was conducted primarily by two graduate students, Ji Hun Oh and Alex Solecki.

Plans for Next Period
We will expand our machine-learning capabilities and provide tangible performance metrics for various datasets in the database. Furthermore, we acknowledge the importance of obtaining high-fidelity assessments of chemically novel SAFs, and thus we plan to extend or rebuild our current novelty fuel detection framework. In particular, we plan to investigate more advanced deep learning techniques, such as propagation or synthesis of data via generative AI or physical structure-property relationship models, to improve model robustness to outlying cases.

Project 034 National Jet Fuels Combustion Program – Area #7: Overall Program Integration and Analysis

University of Dayton

Project Lead Investigator

Joshua Heyne
Associate Professor
Mechanical Engineering
University of Dayton
300 College Park
Dayton, OH 45458
937 229-5319
Jheyne1@udayton.edu

University Participants

University of Dayton

- P.I.: Joshua Heyne
- FAA Award Number: 13-C-AJFE-UD (Amendment Nos. 9, 10, 13, 17, 18, and 24)
- Period of Performance: Sept. 18, 2015 to Sep. 30, 2021
- Task:
    1. Overall integration and coordination of the National Jet Fuels Combustion Program (NJFCP)
    2. Investigation of alternative jet fuel dependencies between combustors of different sizes and mixing approaches

Project Funding Level

Amendment No. 9: $134,999.00 (September 18, 2015, to February 28, 2017)
Amendment No. 10: $249,330.00 (July 7, 2016, to December 31, 2017)
Amendment No. 13: $386,035.00 (August 30, 2016, to December 31, 2017)
Amendment No. 17: $192,997.00 (August 3, 2017, to September 30, 2018)
Amendment No. 18: $374,978.00 (December 7, 2017, to December 31, 2018)
Amendment No. 24: $582,983.00 (February 5, 2020, to February 4, 2022)
Cost share is from the University of Dayton, DLR Germany, Raytheon Technologies Research Center (RTRC), and the National Research Council (NRC) Canada.

Investigation Team

- Joshua Heyne (University of Dayton) is the project's lead investigator and is responsible for coordinating all NJFCP teams (both ASCENT and non-ASCENT efforts).
- Randall Boehm (University of Dayton) is a research engineer combining the results from various combustor observations.
- Jen Colborn (University of Dayton) is a graduate student research assistant helping with fuel testing on the Referee Rig.
- Zhibin Yang (University of Dayton) is a graduate student research assistant working on Tier Alpha and Tier Beta.

Project Overview

The NJFCP is composed of over two dozen member institutions that contribute information and data, including expert advice from gas turbine original equipment manufacturers (OEMs), federal agencies, and other ASCENT universities as well as corroborating experiments at the German Aerospace Center (DLR Germany), National Research Council Canada, and other

international partners. This project involves coordinating and integrating research among these diverse program stakeholders and academic PIs; cross-analyzing results from other NJFCP areas; collecting data from a well-stirred reactor for modeling and fuel comparison purposes; conducting large eddy simulations of sprays for the Area 3 high-shear rig; and procuring additional swirler geometries for the NJFCP areas and allied partners while developing an interface for NJFCP modeling capabilities and OEM requirements. Work under this program consists of, but is not limited to:

- conducting meetings with member institutions to facilitate the consistency of testing and modeling,
- coordinating timely completion of program milestones,
- documenting results and procedures,
- creating documents critical for program processes (e.g., fuel down selection criteria),
- soliciting and incorporating program feedback from OEMs,
- reporting and presenting on behalf of the NJFCP at meetings and technical conferences,
- integrating state-of-the-art combustion and spray models into user-defined-functions (UDFs), and
- advising the program steering committee.

Task 1 - Integration and Coordination of NJFCP Teams

University of Dayton

Objective(s)

The objective of this task is to integrate and coordinate all ASCENT and non-ASCENT team efforts by facilitating meetings, summarizing results, presenting results external to the NJFCP, communicating regularly with the steering committee, and performing other related activities.

Research Approach

The NJFCP is integrated and coordinated via two main techniques: (1) the structural combining of various teams into six topic areas; and (2) routine meetings and discussions both internal and external to individual topic areas. The topic areas are distinguished by the dominant physics associated with them (topics I and IV), the culmination of all relevant combustion physics (topics II, III, V), and the wrapping of all work into a single OEM graphical user interface package (topic VI). These six topic areas are as follows:

Topic I. Chemical kinetics: A chemical kinetic model, with the validation data to anchor modeling predictions, is foundational to any combustion model.
Topic II. Lean blowout (LBO): This topic covers data, screening, and validation, under relevant conditions, to statistically and theoretically anticipate the effects of fuel properties on this figure of merit (FOM).
Topic III. Ignition: Similar to Topic II, the focus of this topic is obtaining experimental screening and validation data for statistical and theoretical predictions.
Topic IV. Sprays: Historically, the dominant effect of fuel FOM behavior has been the spray character of the fuel relative to others. Experiments in this topic area focus on measuring the effects of fuel properties on spray behavior. Like Topic I, spray behavior is not a FOM (like Topics II and III), but it is critical to bounding the effects of physical properties on combustion behavior relative to other processes (i.e., chemical kinetics).
Topic V. Computational fluid dynamics (CFD) modeling. Complementary to the empirical Topics II, III, and IV, CFD modeling focuses on the theoretical prediction of measured data and facilitates the development of theoretical modeling approaches.
Topic VI. User-defined function development: Once the theoretical modeling approaches established in Topic V are validated, user-defined functions are developed for OEM evaluation of fuel performance in proprietary rigs.

The topic area teams meet and coordinate regularly. At minimum, NJFCP-wide meetings are held monthly, and topic area meetings typically occur every 2 to 3 weeks.

Milestone(s)

- NJFCP American Institute of Aeronautics and Astronautics (AIAA) Book was published.
- Developed Tier Alpha prescreening tool for novel sustainable aviation fuel (SAF) prescreening.

Major Accomplishments

- Edited, coordinated, and published a NJFCP AIAA book.

- Developed and published a Civil Aviation Alternative Fuels Initiative (CAAFI) R&D prescreening document to aid novel companies and producers in the refinement and development of fuels that can most easily eclipse the Tier 3 and 4 testing.
- Reported the alternative jet fuel dependencies between combustors of different sizes and mixing approaches.

Publications

Peer-reviewed journal publications

Boehm, R. C., Colborn, J. G., & Heyne, J. S. (2021). Comparing alternative jet fuel dependencies between combustors of different size and mixing approaches. Frontiers in Energy Research, *9*. https://doi.org/10.3389/FENRG.2021.701901

Book publication

Colket, M., & Heyne, J. (2021). *Fuel effects on operability of aircraft gas turbine combustors*. American Institute of Aeronautics and Astronautics. https://doi.org/10.2514/4.106040

Book chapters

Colket, M., Heyne, J., Andac, G., Rumizen, M. (2021). Chapter I. Introduction. In T. C. Lieuwen (Ed.), *Fuel effects on operability of aircraft gas turbine combustors* (pp. 1-20). American Institute of Aeronautics and Astronautics.

Rock, N., Stouffer, S., Hendershott, T., Heyne, J., Blunck, D., Lukai, Z., Khandelwal, B., Emerson, B., Mastorakos, E., Colket, M. (2021). Chapter V. Lean blowout studies., In T. C. Lieuwen (Ed.), *Fuel effects on operability of aircraft gas turbine combustors* (pp. 143–196). American Institute of Aeronautics and Astronautics.

Heyne, J., Rauch, B., Hanson, R., Dooley, S., Blakey, S., Yang, Z., Ferris, A., Ure, A., Le Clercq, P., Boehm, R., Lewis, C., & Colket, M. Chapter XII. Prescreening of Sustainable Aviation Jet Fuels. In T. C. Lieuwen (Ed.), *Fuel effects on operability of aircraft gas turbine combustors* (pp. 487–523). American Institute of Aeronautics and Astronautics.

Heyne, J., Colket, M., Edwards, T., Moder, J., Rumizen, M., & Oldani, A. (2021). Chapter XIII. Summary. In T. C. Lieuwen (Ed.), *Fuel effects on operability of aircraft gas turbine combustors* (pp. 525–534). American Institute of Aeronautics and Astronautics.

Outreach Efforts

Invited talks

- Heyne, J. (2020, November). High value drop-in aviation fuels: From molecule selection to mission benefits [Panel presentation]. Fuel Quality Matters, DOE BETO/PNNL HTL Workshop, Virtual meeting.
- Heyne, J. (2020, November). Prescreening of HTL SAFs: Rapid low-volume, low-cost testing. Sustainable Aviation Fuel Certification, DOE BETO/PNNL HTL Workshop, Virtual meeting.
- Heyne J. (2021, May). Summative results of the national jet fuels combustion program [Panel presentation]. Properties and Emissions, CRC Aviation Fuels Meeting, Virtual meeting.
- Heyne, J. (2021, June). Prescreening of sustainable aviation fuels [Panel presentation]. CAAFI Virtual Mini-Symposium.
- Heyne, J. (2021, June 2). Sustainable aviation fuel prescreening, benefits, and a proposed streamlined evaluation process [Panel presentation]. National Academies, Transportation Research Board (AV030), Sustainable Aviation Fuels subcommittee midyear meeting.
- Heyne, J. (2021, August 17). Sustainable aviation fuel: Properties, compositions, and qualification requirements [Sponsored seminar]. Sandia National Laboratory.
- Heyne, J., (2021, August 17). Sustainable aviation fuel property needs and some solid waste candidates [Panel presentation]. Seminar on Hydrothermal Liquefaction: biocrudes and advances towards drop-in fuel potential, Aalborg University, Denmark.
- Heyne, J. (2021, November). Sustainable aviation fuel: Properties, compositions, and qualification requirements [Sponsored travel]. Center for Multiphase Flow Research and Education, Iowa State University.

Conference presentations

None.

Awards

Joshua Heyne

- 2021 Net Good Summit on sustainable travel, honored guest
- 2021 US Frontiers of Engineering Symposium, National Academies of Engineering, selected participant

- 2021 Vision Award for Excellence in Scholarship, School of Eng., University of Dayton

Student Involvement

Jen Colborn, graduate research assistant, leads this effort.
Zhibin (Harrison) Yang, Ph.D. student (October 2020 to September 2021), is working on developing the Tier Alpha prescreening tool.

Plans for Next Period

Continue to coordinate across various federal agencies and research institutions for SAF testing.

Task 2 – Investigation of Alternative Jet Fuel Dependencies Between Combustors of Different Size and Mixing Approaches

University of Dayton

Objective

The objective of this task is to investigate alternative jet fuel dependencies between combustors of different sizes and mixing approaches.

Research Approach

1. Introduction

As global fuel demand increases, various environmental, economic, and security interests have led to the investigation of SAFs for broader use. Due to differences in composition between SAFs and petroleum-derived fuels, SAFs must undergo a certification and qualification process before being deployed. The process for SAF qualification, known as ASTM D4054, focuses on developing “drop-in” hydrocarbon fuels, meaning that no changes need to be made to engine, aircraft, or airport infrastructure for a fuel to be compatible. Unless a candidate fuel qualifies for fast-track approval, this evaluation is an extensive process that takes years to complete, millions of dollars, and thousands of gallons of fuel (Oldani [1]). As shown in Figure 1, the approval process for non-fast-track jet fuel qualification involves four levels of testing as well as two stages of research reports with comprehensive stakeholder review. Fuel is first tested for general specifications and fit-for-purpose properties before the Phase 1 report is released to the stakeholders, who then complete a technical review of the data before the fuel can proceed to Tier 3 and Tier 4 testing. Both rig and engine testing are then conducted in Tiers 3 and 4. The amount of fuel required for testing increases about 10-fold with every tier in the qualification process.

A renewable jet fuel called RediJet, which was produced through catalytic hydrothermolysis, was recently submitted to ASTM subcommittee J for aviation fuels for approval. According to Coppola [2] , approximately 72,000 gallons of RediJet was required to complete the test plan. Component and rig tests were performed by three different engine manufacturers across nine different test conditions. Engine testing was completed by two engine manufacturers and included a flight test with a twin-engine Falcon 20. Three fuel mixtures were used for each test condition: neat Jet A as a baseline, neat RediJet, and a 50:50 blend. Overall, 144,000 gallons of jet fuel were used for full qualification of the new “drop-in” SAF. Reducing the volume of fuel required for the qualification process would be advantageous for both fuel manufacturers and the sponsors who have a vested interest in SAF.

The aim of the NJFCP was to shorten and redirect the process for jet fuel qualification (Colket et al. [3]). By developing predictive models for fuel behavior and adding some tailored, low-volume testing prior to the phase I research report, additional feedback would be provided to the ASTM evaluation committee and fuel manufacturers to guide early fuel development. The scope of tier 3 and tier 4 testing could then be directed toward a narrower range of potential concerns, thereby reducing the total amount of fuel required. Alternatively, the candidate fuel could be reformulated into a product that has a higher probability of achieving qualification. Importantly, there is a need to understand how fuel effects in small-scale rigs compare with engine observations. Validating small-scale rigs against full-scale engines is also essential for developing predictive models and testing methodology.

At the program level, we identified a range of operating conditions where lean blowout (LBO) or ignition is most likely to be impacted by differences in fuel composition and properties (Colket & Heyne [4]). The most sensitive LBO conditions involve

(i) a throttle-chop from cruise to flight idle and (ii) a start transient where the increase in fuel flow rate may not sufficiently keep up with the increase in airflow rate if the control schedule is improperly set for the fuel being used. Fuel impacts on ignition are most important at cold conditions such as a cold-soaked auxiliary power unit (APU) at altitude or a cold-soaked main engine on the ground. Figure 2 shows operating conditions for the typical temperatures (T_{cmb}) and pressures (P_{cmb}) in the combustion chamber. In this figure, "altitude relight" and "cold start" both refer to ignition cases. These conditions were selected because they are some of the most extreme conditions that can exist within an engine and are consistent with the tests required by ASTM D4054 (Coppola [2]; Colket et al. [3]). Similar fuel dependencies have been noted for cold ground start and altitude relight (Hendershot et al. [5]; Stouffer et al. [6]).

Nine experimental rigs within the NJFCP, featuring a wide range of geometries and time scales, were used to observe fuel effects (Colket & Heyne, 2021). As shown in Figure 3, eight of the nine rigs showed a correlation between the derived cetane number (DCN) and the relative equivalence ratio at LBO (Φ_i). The parameter Φ_i is defined as the LBO performance of fuel (i) relative to the LBO performance of the reference fuel (A2) and is expressed as a percentage (see Equation 1).

$$\Phi_{\mathrm{i}} = \frac{\phi_i - \phi_{A2}}{\phi_{A2}} \quad (1)$$

The only rig that did not show a correlation between DCN and Φ_i was the Honeywell 131-9 APU combustor rig (APU-CR), one of the two industry combustors used in the program. This result appears to be incongruent with the goal of the NJFCP; namely, to reduce tier 3 or tier 4 testing. However, closer examination of results from both the Referee Rig (RR) and a GE9X full annular combustor rig (GE9X-FAR) showed that fuel dependencies vary with operating conditions.

Colborn et al. [7] showed that the relative LBO in the RR at an air temperature and pressure of 65 °C and 107 kPa, respectively, is dominated by the Ohnesorge number (Oh) at 2% DP/P. In contrast, the DCN dominates at 6% DP/P, with a smooth transition from one extreme to the other. At 3.5% DP/P and 107 kPa, the fuel with the lowest DCN and most favorable atomization properties (hereafter labeled as C1) showed no sensitivity to air temperature between 65 °C and 83 °C. Boehm et al. [8] found this same fuel (C1) had measurably worse LBO performance in a GE9X combustor than the other three fuels tested at three of their four test conditions. At a lower air temperature, C1 showed the same LBO performance as the reference petroleum-derived fuel when the two fuels were heated to 60 °C, which was the reference fuel temperature for this set of tests. These results are summarized in Figure 4. Overall, the data suggest that the physical and chemical properties of the fuel are both important near the low-temperature boundary of the GE9X engine operating range at conditions important to the aircraft engine LBO margin, whereas only chemical properties are important at higher air temperatures and loadings.

In this report, we show that the results introduced above are consistent with LBO theory (Plee & Mellor [9]; Mellor [10]) and that the RR, in concert with a well-thought-out test plan, can show the same fuel dependencies as the APU-CR and the GE9X-FAR. The timescales of evaporation and chemical reactions are impacted significantly by fuel and air temperature, suggesting that the range of operating conditions being tested is critical to a thorough investigation of fuel dependencies. We assert that commercial combustor geometry does not need to be matched with specific operating conditions if the test combustor is tested over a sufficiently wide range of operating conditions to sweep through the range of timescale ratios that are relevant to commercial combustor operability.

2. Background

2.1 Previous work

Several investigations of how fuel affects LBO have already been completed. For example, Rock et al. [11] measured the LBO threshold in an un-cooled flame tube using 18 different fuels and three different inlet air temperatures. They noted a correlation to DCN, T10, T90, or surface tension, dependent depending on the inlet air temperature. Using the same set of 18 fuels, Casselberry et al. [12] demonstrated a correlation between pyrolysis products at 625 °C and the LBO threshold in the RR when the RR was operated at chop-like (warm) conditions. Won et al. [13] investigated the role of preferential vaporization and suggested that the DCN of the front end of the distillation may be a better indicator of LBO than the DCN of the fully vaporized fuel. They also observed that LBO is more strongly correlated with fuel physical properties than with fuel chemistry at low temperature operation. Grohmann et al. [14] similarly observed that both physical and chemical properties of a fuel influence combustor LBO. In a study of the effects of atomization, Muthuselvan et al. [15] related atomization quality with timescales relevant to LBO.

Many experiments and analyses of the ignition characteristics of hydrocarbon fuels have focused on either pre-vaporized and premixed fuel or other fuels and conditions that depart significantly from the most extreme start-up requirements for

gas turbines used in aviation. Excellent reviews on these topics have been published by Aggarwal [16] and, more recently, by Colket and Heyne [4]. Mayhew [17] observed correlation between ignition probabilities at cold altitude relight conditions in a derivative of the RR and each of four fuel properties: viscosity, surface tension, 20% recovered temperature (T_{20}), and flash point. Opacich et al. [18] observed similar correlations within datasets derived from both the RR and the APU-CR, although they represented volatile properties using vapor pressure and heat capacity instead of T_{20} and flash point. Part of this work directly follows up on the work introduced by Opacich et al. [18].

2.2 LBO Theory

A common theme in several of the works cited above is that LBO performance can be evaluated by considering three timescales that impact LBO limits, as shown in Equation 2: chemical, mixing and evaporative timescales (Plee & Mellor, 1979; Mellor, 1980). This theory is further illustrated in Figure 5.

$$\frac{1}{\phi_{LBO}} \sim \left(\frac{1}{\tau_{chem}} + \frac{1}{\tau_{mix}} + \frac{1}{\tau_{evap}} \right)^{-1} \quad (2)$$

Fuel physical properties, along with aerodynamic shear forces, flow field, fuel nozzle design, and fuel pressure all affect fuel spray atomization, including droplet size distribution and spray distribution. While combustor design and operating conditions are important to atomization, fuel properties are also an important factor for some commercial combustors at relevant, in-service operating conditions.

Fuel vapor pressure (and/or thermal conductivity), spray characteristics, and combustor aerodynamics all influence the evaporation timescale. From the perspective of fuel dependencies on LBO, it is important to note that the evaporation timescale of some commercial combustors will be impacted significantly by vapor pressure, which varies not only with droplet surface temperature but also with the time-varying composition of the liquid fuel throughout the evaporation process. In systems that are evaporation-limited, fuels with a higher vapor pressure at a given temperature are expected to ignite more readily than fuels with a lower vapor pressure.

The mixing of fuel vapor with air depends on the flow field, turbulence intensity, and the spatial relationship between the fuel spray, the eddies within the flow field, and the flame. Because turbulence is overwhelmingly more important than laminar diffusion in most commercial combustors, there is ample technical justification for neglecting this term when considering fuel effects. Moreover, the characteristic mixing time of a given commercial combustor at any well-defined operating condition is likely to be kept proprietary by the engine companies.

The specifics of fuel-air mixing also influence the gaseous mixture residence time and reactant concentration. These two variables, along with species reactivity, determine the fuel chemistry of combustion and blowout. The chemical timescale is relevant to the physics and may be comprised of different pieces, such as autoignition and extinction.

2.3 Cold Ignition

At extremely low fuel temperatures, the fuel vapor pressure is low. When the inlet air temperature is equally low, fuel droplets are not heated until they reach a heat source, which could be either a plasma discharge or the kernel of a previously ignited fuel/air mixture. The size and spatial distribution of liquid fuel droplets within the combustor flow field at extremely cold conditions is expected to be critical for most, if not all, combustors in aviation service. Very little evaporation occurs outside of the domain of the plasma discharge (spark), and it must therefore supply enough energy to both evaporate the fuel and overcome the critical kernel radius (Kim et al., 2013). Each kernel must release enough heat to both sustain the flame and sufficiently evaporate enough surrounding liquid fuel droplets to replenish the fuel consumed by combustion within the kernel. Only under these conditions can the flame kernel grow, propagate upstream to an anchor point, and transition to a self-sustaining flame. This process can be influenced significantly by fuel volatility, thermal properties, and the physical properties that influence atomization.

2.4 Atomization

Atomization is affected by the viscosity, density, and surface tension of the fuel [(Guildenbecher et al., 2019; Lefebvre & McDonnell, 2017). Increased surface tension inhibits fuel breakup, increased viscosity dampens the instabilities that allow for breakup, and increased density drives lower flow rates in engines that are controlled to deliver a scheduled enthalpy flux or equivalence ratio. This in turn reduces the gage pressure, which supplies the energy that drives atomization.

3. Experiments, Data and Methods

3.1 Referee Rig Experiments

Experiments performed in the RR were completed at the Air Force Research Laboratory (AFRL) located at Wright-Patterson Air Force Base and have previously been published (Henderschott et al., 2018; Colborn et al., 2020). The RR is a non-proprietarty, single-cup, swirl-stabilized combustor designed by GE (this article's corresponding author) with input from four other leading engine manufacturers. The rig simulates representative aerodynamic characteristics of both legacy and emerging swirl-stabilized combustors (Colket & Heyne, 2021). It is a classic rich-quench-lean combustor with effusion-cooled liners, a flat dome protected by an impingement-cooled heat shield, primary dilution holes located at ½ the dome height downstream from the dome, and seconday dilution holes located just aft of the primary reaction zone. The rig features a modular construction to facilitate swapping of fuel injectors and swirlers, which allows researchers to evaluate different swirler effective areas, swirl numbers, spray angles and flow numbers. However, most of the data collected from the RR to date has come from just one design configuration. The AFRL modified the rig's original four-cup design to a single-cup design, and the University of Dayton Research Institute (UDRI) custom-buillt a thryatron-based exciter to achieve better control over spark energy and frequency relative to jet engine exciters. Readers interested in fabricating a copy of this combustor should contact the authors for information on where to find a copy of the drawings.

In this study, we analyzed four operating conditions of the RR (Table 1). Fuel and air temperature were matched in each condition, and LBO was determined after each successful ignition. For all test conditions, the normalization described by Equation 1 was reset so that its value, corresponding to the fuel sample designated as A2, was always zero. This normalization reduces the dependencies on operating conditions and highlights fuel dependencies.

3.2 APU-CR Experiments

The APU-CR experiments were performed in the combustor component test facility at Honeywell Aerospace. For all experiments, the APU-CR was operated at simulated engine conditions (Culbertson & Williams [22]). APUs are small gas turbine engines used to provide power to spool-up the main engine during starter-assisted air starts. APUs are particularly sensitive to the physical properties that influence atomization and vaporization (Pfeiffer et al. [23]) because of their small volume and correspondingly low combustor residence time ($t_{cmb}= r_{air}V_{cmb}/W_{air}$). The 131-9 combustor is swirl-stabilized and relies on a rich-quench-lean combustion process, like many of the much larger, main engine combustors. A standard 131-9 ignition system was used with the igniter located at approximately the eight o'clock position of the combustor (Culbertson & Williams [22]). Readers who wish to reproduce any of the data presented in the noted publications should contact Honeywell Aerospace.

The warm ignition (T_{fuel} = 15 °C) light-off boundary was determined at a baseline air temperature (-35 °C) and pressure (1.05 atm) along with single-point derivatives to higher temperature or lower pressure, as listed in Table 1. The cold ignition (T_{fuel} = -37 °C) light-off boundary was determined at each of the conditions used for warm ignition, plus two additional points at a colder air temperature and low pressure (also listed in Table 1). The LBO data set included six operating conditions. As with the RR data, the equivalence ratios for all test conditions were normalized using Equation 1.

3.3 GE9X-FAR Experiments

The GE9X-FAR experiments were performed in the GE's combustor component test facility. The combustor was operated at simulated engine conditions; although these conditions are proprietary information, sanitized data are publicly available through reference (Boehm et al., 2020), and readers who wish to reproduce this data may contact GE. Unlike the RR and the APU-CR, the GE9X is a large combustor that achieves lean combustion for low NOx emissions using a twin annular premixing swirler. Limited details about this combustor design have been published by Dhanuka et al. [24]. The understandable restrictions around sharing proprietary test data, procedures, and combustor designs from fuel evaluation tests such as these remain one of the prime motivators behind the development of the RR.

The GE data was not available in a format appropriate for the statistical analyses used in this study. The LBO data shown in Figure 4 was normalized at the baseline operating condition using an equation like Equation 1, but it was not reset at each operating condition because dependence on operating condition was part of the story GE communicated. The un-disclosed constant denoted by 'Δ' in the axis label of Figure 4 represents the difference between the actual and displayed equivalence ratio at the reference condition, which disguises proprietary engine LBO performance. However, the original source indicates that the tested points track along a reference velocity, which scales with the log of air flow multiplied by the square of air temperature and occurs in the same order presented in Figure 4 with roughly equal spacing.

3.4 Fuel Property Data

The RR and APU-CR experiments were directly or indirectly part of the NJFCP, and the fuels used in this study were distributed to affiliated labs by a control center led by Tim Edwards at the AFRL. Dr. Edwards was also responsible for acquiring and publishing fuel property data (Edwards, [25]), which is available through the National Alternative Jet Fuels Test Database ([26]. The fuel samples designated as A1, A2, A3, C1, C2, and C5 were tested in both the RR and APU-CR, whereas the fuel samples designated as C3, C4, and C7 were only tested in the RR. The GE9X experiments were part of a different program but included one fuel (C1) provided by the AFRL. Various properties of the fuels used by GE are provided in Table 2.

The fuel densities used in the analyses of the LBO datasets were as measured at 15 °C. For analyses of the ignition datasets, all fuel properties were transformed into their respective values at the tested fuel temperature following the approach described by Opacich et al. (Opacich et al . [18). Fuel properties that were measured over a range of temperatures that bounded the tested fuel temperature (e.g., density) were interpolated to the test temperature. Temperature-dependent fuel properties that were not measured over a sufficient temperature range to warrant interpolation (e.g., vapor pressure) were determined as outlined here. First, we derived a surrogate fuel composition by matching measured fuel property data and GCxGC-determined hydrocarbon class concentration data, using published blending rules (Flora et al. [27]) to relate molecular properties and compositions to mixture properties. Next the molecular properties over a range of temperatures were calculated based on using the models provided in the molecular properties database published by the National Institute of Standards and Technology (Kroenlein et al. [28]), and the blending rules were applied at each modeled temperature. The resulting temperature-dependent mixture properties were then curve-fitted, and those models were used to estimate the fuel properties at each tested fuel temperature.

3.5 Analysis

The previously described random forest statistical analysis (Colborn et al. [7]; Pfeiffer et al. [23]) was used for this investigation. In summary, the method uses random sampling and replacement to decrease overfitting and allows for one dependent variable (e.g. LBO or ignition performance) to be evaluated against multiple independent variables (e.g. fuel properties) (Hastie et al. [29]). Standard Monte Carlo methods were used to simulate uncertainties in each independent variable based on measurement reproducibility, as quoted in the relevant ASTM standard with an assumed Gaussian distribution. These distributions represent the uncertainty domain within the random forest method. We used the same regression approach as Peiffer et al. [18] and Opacich et al. [23]. The simulation included numerous trials to capture the full distribution of possible values within the reproducibility domain of each measured value. The relative importance values of each independent variable were recorded during each trial. Using this approach, we estimated confidence bands around each relative importance value.

One set of random forest analyses was used to assess the relative importance of atomization, evaporation rate, autoignition and extinction in each of two LBO datasets. Because none of these fundamental processes were clearly known or regress-able for all the fuels used in both test articles, it was necessary to choose a set of four independent, orthogonal properties that are known to strongly correlate with each of these four fundamental processes. Primary and secondary droplet breakup at incipient LBO conditions were represented by fuel density at 15 °C. T_{20} was selected to represent the evaporation rate. Extinction was represented by the radical index (RI), and autoignition was represented by the DCN. The idea here was to compare these two analyses and assess how well one dataset (i.e., LBO in the RR at cold conditions) represents the other (i.e., LBO in the APU-CR at normal operating conditions).

A second set of random forest analyses was used to assess the relative importance of five independent variables in each of three cold ignition datasets. We represented atomization dependencies using the Ohnesorge Number, which combines dynamic viscosity (μ), density, surface tension (σ), and the nozzle diameter, D, into a single dimensionless parameter (Equation 3):

$$Oh = \frac{\mu(T)}{[\rho(T)\sigma(T)D]^{0.5}} \quad (3)$$

Fuel dependency on the evaporation rate was represented by vapor pressure, and fuel dependency on droplet heating was represented by specific heat. The definition of the dependent variable, representing ignition performance, was somewhat different between the RR dataset and the APU-CR datasets. In the APU-CR datasets, the ignition variable was defined by the minimum equivalence ratio required to achieve ignition within a Honeywell-standard duration of time, during which the ignitor is firing periodically as it would in a commercial APU. In the RR dataset, the ignition variable was defined by the equivalence ratio corresponding to a 10% ignition probability per spark along a binomial regression fitted curve to the

equivalence ratio and light/no-light data corresponding to each spark. Details of this binomial regression have been published by Hendershot et al. (2018).

4. Results

4.1 LBO Results

Although several laboratory rigs showed a strong correlation between LBO and the DCN (Figure 3), the APU-CR did not. Instead, it showed a strong correlation to physical and volatility properties such as viscosity (ν), and 20% recovered temperature (T_{20}) as shown in Figure 6. At cold conditions, in contrast to the results at warm conditions, the RR also showed a correlation to physical and volatility properties, but not the DCN. Due to the relatively low fuel temperatures at cold start, temperature-dependent physical properties such as density, viscosity, and surface tension trend higher, which is detrimental to fuel atomization. In addition, vapor pressure trends lower, which is detrimental to evaporation. It is therefore not surprising that the effects of such properties would be more observable at these conditions. In essence, the cold temperature in the cold LBO experiments with the RR serves to prolong the time scale of the physical processes necessary for combustion (namely, evaporation) and drive this time scale closer to the combustor residence time.

Main effects plots of Φ versus fuel properties, shown in Figure 6, suggest that both the RR and the APU-CR show a correlation between Φ and fuel physical properties when the time scale of evaporation is on the same order as the combustor residence time. To further analyze this fuel property dependency, we repeated a random forest statistical analysis 100 times. The results of the random forest analyses are summarized in Figure 7.

Overall, three important results were observed from the random forest analysis. First, each rig showed nearly the same relative importance of T_{20} (representing evaporation rate) and density (representing atomization) on LBO, which suggests that the RR, when operated at cold conditions, adequately represents the relevant physics that largely determine LBO performance in the APU-CR operated at representative engine conditions. Second, the fuel properties that influence evaporation rate are clearly more important than those that correlate strongly with chemical reactivity. This result suggests that the LBO performance of the RR and APU-CR, as operated in these tests, is affected by evaporation more than chemical reactivity. Data collected in this way should therefore be used to evaluate the impact of variation in fuel physical properties, not fuel chemistry, on LBO. Third, the relative importance of the DCN and RI at these conditions was not equal between the RR and the APU-CR, which suggests that the RR is not a good surrogate for the APU-CR in this context. However, that is not a requirement because the LBO performance in the APU-CR is not determined by the DCN or RI. In contrast, the LBO performance of the GE9X-FAR was more strongly determined by the fuel chemical properties. A useful surrogate laboratory combustor for the GE9X-FAR should therefore produce similar relative importance values for influential fuel chemical properties.

With respect to the data from the GE9X-FAR, Table 2 documents the notable differences between the petroleum-derived reference fuel and the SAF blend component (designated as C1). Sample C1 is 6.3% lighter, has 1.7% higher specific energy, and has a much lower DCN than the reference fuel. The lower density and higher specific energy of C1 are expected to push LBO toward a lower (and more favorable) Φ_{C1}. The lower density leads to a higher volumetric flow rate, which leads to higher fuel pressure and, consequently, finer atomization, whereas the higher LHV leads to a higher flame temperature for a given equivalence ratio. Conversely, the lower DCN of C1 is expected to lead to a higher (i.e., less favorable) Φ_{C1} based on the empirical trends shown in Figure 3. The data shows higher Φ_{C1} at three of the four test conditions, which is consistent with the much lower DCN of C1 relative to the reference fuel. However, at the lowest air temperatures that were tested, Φ_{C1} and Φ_{Ref} were essentially the same, presumably because the favorable density and specific energy of C1 compensate for its unfavorable DCN.

GE also provided LBO data for Jet A fuel at two different temperatures. Although these two tests did not employ fuel from a quarantined tank dedicated for such tests, the commercial jet fuel was acquired from the same supplier, and we therefore assumed that the properties of the two fuels are comparable. The colder fuel had higher density, viscosity, and surface tension and lower initial vapor pressure, but the chemical properties of the fuel vapor were the same. These differences in physical properties were reflected in the data: at the lowest air temperatures, $\Phi_{Ref,32C}$ was higher than $\Phi_{Ref,60C}$. At the three conditions where C1 showed measurably worse LBO performance than the reference fuel, the colder reference fuel performed as well as the warmer reference fuel. Together, these trends suggest that the LBO phenomenon in the GE9X-FAR is governed by fuel chemistry at three of the four test conditions, but evaporation becomes important when the air temperature is reduced. The two SAF fuels that were partially derived from hydrogenated esters and fatty acids (HEFA) showed similar results to each other at all conditions and outperformed the reference fuel at the lowest-temperature test condition, as expected based on their lower viscosity and density relative to the reference fuel.

4.2 Ignition Results

Main effects plots of Φ versus fuel properties, shown in Figure 8, suggest that both the RR and APU-CR showed a correlation between Φ and both fuel physical properties (viscosity) and volatile properties (T_{20}). To further analyze this property dependency, we performed a random forest statistical analysis with 2,000 iterations. Figure 9 provides a summary of the random forest results. As noted in section 3.1, $Oh(T_{fuel})$, $C_p(T_{fuel})$ and $P_{vap}(T_{fuel})$ were used to represent atomization, droplet heating, and droplet evaporation rate, respectively, for the random forest analyses.

The three fuel properties we selected were of similar importance in the RR at cold conditions and in the APU-CR at both cold and warm conditions. Each property accounted for about 27% of the observed variation in ignition performance. The random forest analysis suggested that 4-5% of the observed variation in ignition performance within each of the three datasets could be attributed to variation in combustor air temperature and pressure, and the remaining ten percent of the variation could not be accounted for.

Ideally, the ignition performance data would be normalized, and the datasets would be selected in such a way as to remove all dependencies on combustor operating conditions. However, data are collected prior to the analysis, and pre-test predictions are not yet capable of informing the researchers with enough information to make this possible. Moreover, the highly non-linear dependencies of ignition performance on operating conditions are difficult to completely obscure using any straightforward normalization. Although the unexplained variation in our results (~10% for each dataset) is not as low as some may like it to be, it is nevertheless excellent for a one-dimensional ignition model that does not resort to overfitting. Machine learning analyses, such as the random forest regressions used here, could be integrated with a physical two- or three-dimensional model, but further development of such an approach is still needed.

Overall, the main result of our ignition analysis is that the fuel property dependencies within each of the three datasets are nearly the same, which suggests that a small, standardized set of test articles can be used to characterize fuel dependencies on ignition within the industry-wide fleet of combustors. This result has important practical implications for the evaluation of potential SAFs. From a more fundamental perspective, our observation that two fuel properties were required to account for the evaporation timescale suggests a need for more detailed data relating to fundamental heat and mass transfer processes within the intersecting region of cold fuel droplets and plasmas or pre-existing flame kernels. Such data could lead to an even better understanding of the fundamental processes that govern fuel property dependencies on kernel initiation and growth.

5. Conclusion

In this study, we suggested that combustor operating conditions can be used to vary the relative importance of the evaporation, chemical, and mixing timescales that are characteristics of combustion phenomena. By adjusting the operating conditions of the LBO experiments the ratio of the evaporation time to residence time can be matched. For example, we demonstrated that the RR, when operated at cold fuel and air conditions, exhibits the same fuel property dependencies on LBO (i.e., density and the 20% recovered temperature) as the APU-CR at normal operating conditions in spite of large difference in residence time between these two combustors. Furthermore, when operated at representative flight idle conditions, the RR exhibits the same LBO dependencies on fuel properties (i.e., DCN) as the GE9X-FAR at similar operating conditions. We additionally observed that when the GE9X-FAR is operated at lower temperatures, the LBO phenomenon is governed by a combination of chemical and physical fuel properties rather than by the DCN. This result is consistent with previous work in the RR [7] exploring the transition in operating condition space between evaporation- and chemistry-governed LBO.

Analysis of data from cold ignition in the RR and both standard-day and cold ignition in the APU-CR, shows that the Ohnesorge number (which represents atomization), specific heat (which represents heat absorption from a nearby plasma or flame kernel into a fuel droplet), and vapor pressure (which represents evaporation from the surface of a droplet that has been transported into the path of the plasma or flame kernel) were all equally important to the ignition phenomenon. This was true, independent of the large differences in combustor cup volume between the RR and APU-CR and in the operating conditions being tested.

Collectively, our data indicate that results from the RR are strongly correlated to those from real engines in tests designed to gage the fuel dependencies of combustor operability. The RR therefore shows potential as a standard, laboratory-scale test article for representing swirl-stabilized combustors in the ASTM fuel evaluation process for SAFs.

References

1. Oldani, A. (2020). FAA ASCENT & clearinghouse programs [Presentation]. PNNL HTL Workshop, Pacific Northwest National Laboratory
2. Coppola, E. N. (2018). CHJ pathway readijet renewable jet fuel produced by catalytic hydrothermolysis (CH) [Presentation]. ASTM Committee D02 on Petroleum Products and Lubricants, Subcommittee D02.J0.06 on Emerging Turbine Fuels.
3. Colket, M., Heyne, J. Rumizen, M., Gupta, M., Edwards, T., Roquemore, W. M., Andac, G., Boehm, R., Lovett, J., Williams, R., Condevaux, J., Turner, D., Rizk, N., Tishkoff, J., Li, C., Moder, J., Friend, D., & Sankaran, V. (2017). Overview of the national jet fuels combustion program. AIAA Journal, *55*(4), 1087-1104.
4. Colket, M., & Heyne, J. (2021). *Fuel effects on operability of aircraft gas turbine combustors*. Manuscript submitted for publication.
5. Hendershott, T. H., Stouffer, S., Monfort, J. R., Diemer, J., Busby, K., Corporan, E., et al. (2018). Ignition of Conventional and Alternative Fuels at Low Temperatures in a Single-Cup Swirl-Stabilized Combustor [Presentation]. AIAA Aerospace Sciences Meeting. Kissimmee, FL.
6. Stouffer S D, Hendershott T H, Colborn J, Monfort J R, Corporan E, Wrzesinski P, et al. Fuel Effects on Altitude Relight Performance of a Swirl Cup Combustor. In: AIAA Scitech 2020 Forum. Orlando, Florida; 2020.
7. Colborn, J. G., Heyne, J. S., Stouffer, S. D., Hendershott, T. H., & Corporan, E. (2020). Chemical and physical effects on lean blowout in a swirl-stabilized single-cup combustor. Proceedings of the Combustion Institute, *38*(4), 6309–6316.
8. Boehm, R., Thomsen, D. D., & Andac, M. G. (2020). GE-Aviation program update [Public plenary presentation], FAA CLEEN II Consortium.
9. Plee, S. L., & Mellor, A. M. (1979). Characteristic time correlation for lean blowoff of bluff-body-stabilized flames. Combustion and Flame, *35*, 61–80.
10. Mellor, A. M. (1980). Semi-empirical correlations for gas turbine emissions, ignition, and flame stabilization. Progress in Energy and Combustion Science, *6*(4), 347–58.
11. Rock, N., Chterev, I., Emerson, B., Won, S. H., Seitzman, J., & Lieuwen, T. (2019). Liquid fuel property effects on lean blowout in an aircraft relevant combustor. Journal of Engineering for Gas Turbines and Power, *141*(7).
12. Casselberry, R. Q., Corporan, E., & DeWitt, M. J. (2019). Correlation of combustor lean blowout performance to supercritical pyrolysis products. Fuel, *252*, 504–511.
13. Won, S. H., Rock, N., Lim, S. J., Nates, S., Carpenter, D., Emerson, B., et al. (2019). Preferential vaporization impacts on lean blow-out of liquid fueled combustors. Combustion and Flame, *205*, 295–304.
14. Grohmann, J., Rauch, B., Kathrotia, T., Meier, W., & Aigner, M. (2018). Influence of single-component fuels on gas-turbine model combustor lean blowout. Journal of Propulsion and Power, 97–107. 10.2514/1.B36456
15. Muthuselvan, G., Suryanarayana, R. M., Iyengar, V. S., Pulumathi, M., Thirumalachari, S., & Srinivasan, K. (2020). Effect of atomization quality on lean blow-out limits and acoustic oscillations in a swirl stabilized burner. Combustion Science and Technology, *192*(6), 1028–1052. https://doi.org/10.1080/00102202.2019.1607846
16. Aggarwal, S. K. (1998). A review of spray ignition phenomena: Present status and future research. Progress in Energy and Combustion Science, *24*(6), 565–600.
17. Mayhew, E. K. Impact of alternative jet fuels on gas turbine combustion systems [Ph.D. thesis, University of Illinois at Urbana-Champaign]. IDEALS. https://www.ideals.illinois.edu/handle/2142/101653
18. Opacich, K. C., Peiffer, E., & Heyne, J. S. (2019, January 1-10). Analyzing the relative impact of spray and volatile fuel properties on gas turbine combustor ignition in multiple rig geometries [Presentation]. AIAA Scitech 2019 Forum, San Diego, CA.
19. Kim, H. H., Won, S. H., Santner, J., Chen, Z., & Ju, Y. (2013). Measurements of the critical initiation radius and unsteady propagation of n-decane/air premixed flames. Proceedings of the Combustion Institute, *34*(1), 929–936. https://doi.org/10.1016/j.proci.2012.07.035
20. Guildenbecher, D. R., López-Rivera, C., & Sojka, P. E. (2009). Secondary atomization. Experiments in Fluids, *46*(3), 371–402. https://doi.org/10.1007/s00348-008-0593-2
21. Lefebvre, A. H, & McDonell, V. G. (2017). Atomization and sprays (2nd ed.) [Internet]. CRC Press Taylor & Francis Group.
22. Culbertson, B., & Williams, R. (2017). Alternative aviation fuels for use in military APUs and engines: Versatile affordable advanced turbine engine (VAATE), Phase II and III (Report No. 0007 : AFRL-RQ-WP-TR-2017-0047). Honeywell International, Inc.
23. Peiffer, E. E., Heyne, J. S., & Colket, M. (2019). Sustainable aviation fuels approval streamlining: Auxiliary power unit lean blowout testing. AIAA Journal, *57*(11), 4854–4862. https://doi.org/10.2514/1.j058348

24. Dhanuka, S. K., Temme, J. E., & Driscoll, J. F. (2011). Unsteady aspects of lean premixed prevaporized gas turbine combustors: Flame-flame interactions. Journal of Propulsion and Power, *27*(3), 631–641. https://doi.org/10.2514/1.B34001
25. Edwards, J. T. (2017). Reference jet fuels for combustion testing [Presentation]. 55th AIAA Aerospace Sciences Meeting. Grapevine, TX.
26. Home | AJF:TD | U of I [Internet]. [cited 2021 Jun 5].
27. Flora, G., Kosir, S., Behnke, L., Stachler, R., Heyne J, Zabarnick S, & Gupta, M. Properties calculator and optimization for drop-in alternative jet fuel blends [Presentation]. AIAA Scitech 2019 Forum. https://doi.org/10.2514/6.2019-2368
28. Kroenlein, K., Muzny, C., Kazakov, A., Diky, V., Chirico, R., & Magee, J. (2019). *NIST standard reference 203: TRC web thermo tables (WTT)* [Internet]. National Institutes of Standards and Technology.
29. Hastie, T., Tibshirani, R., & Friedman, J. (2008). *The elements of statistical learning, data mining, inference, and prediction* (2nd ed.). Stanford University.

Figures and Tables

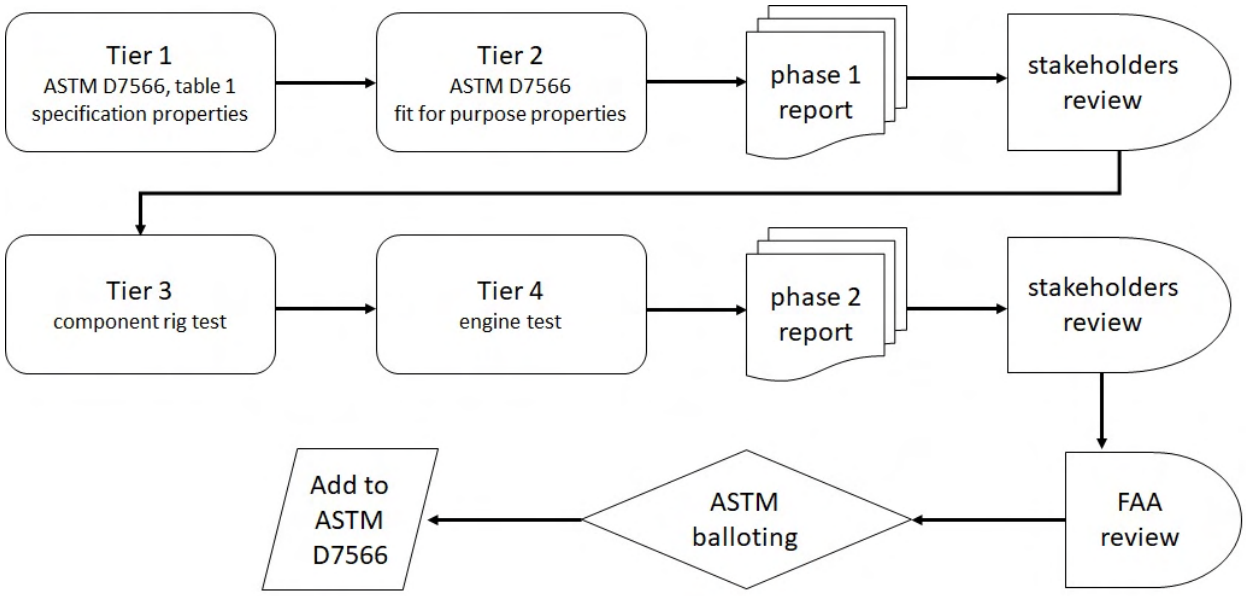

Figure 1. ASTM D4054 fuel evaluation process.

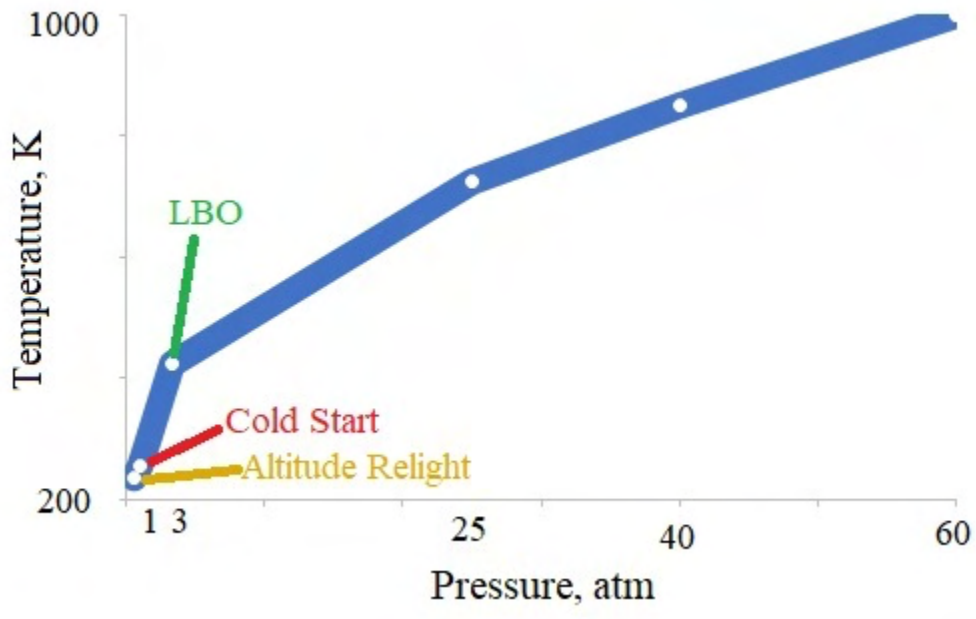

Figure 2. Visual representation of operating conditions relevant to combustion figures of merit.

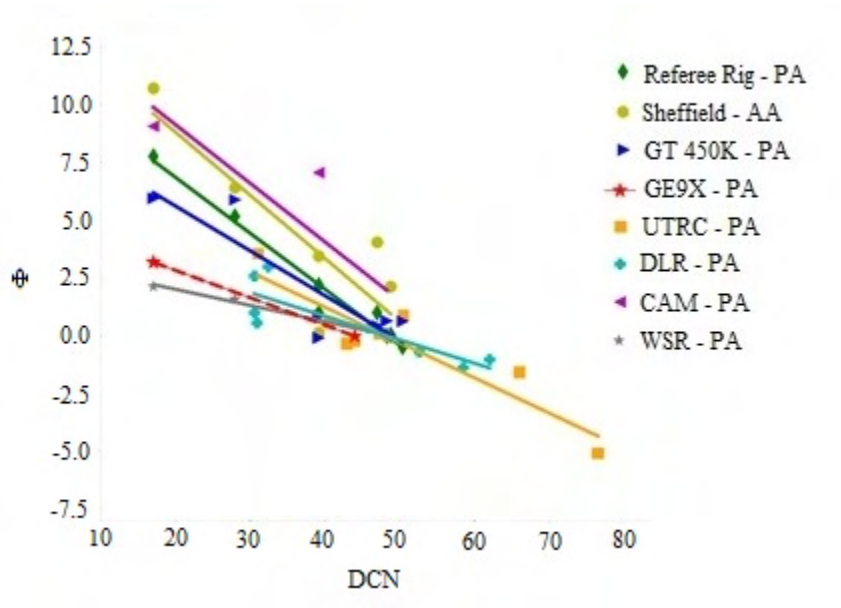

Figure 3. Lean blowout limit as a function of derived cetane number (DCN) for eight different rigs used within the National Jet Fuels Combustion Program.

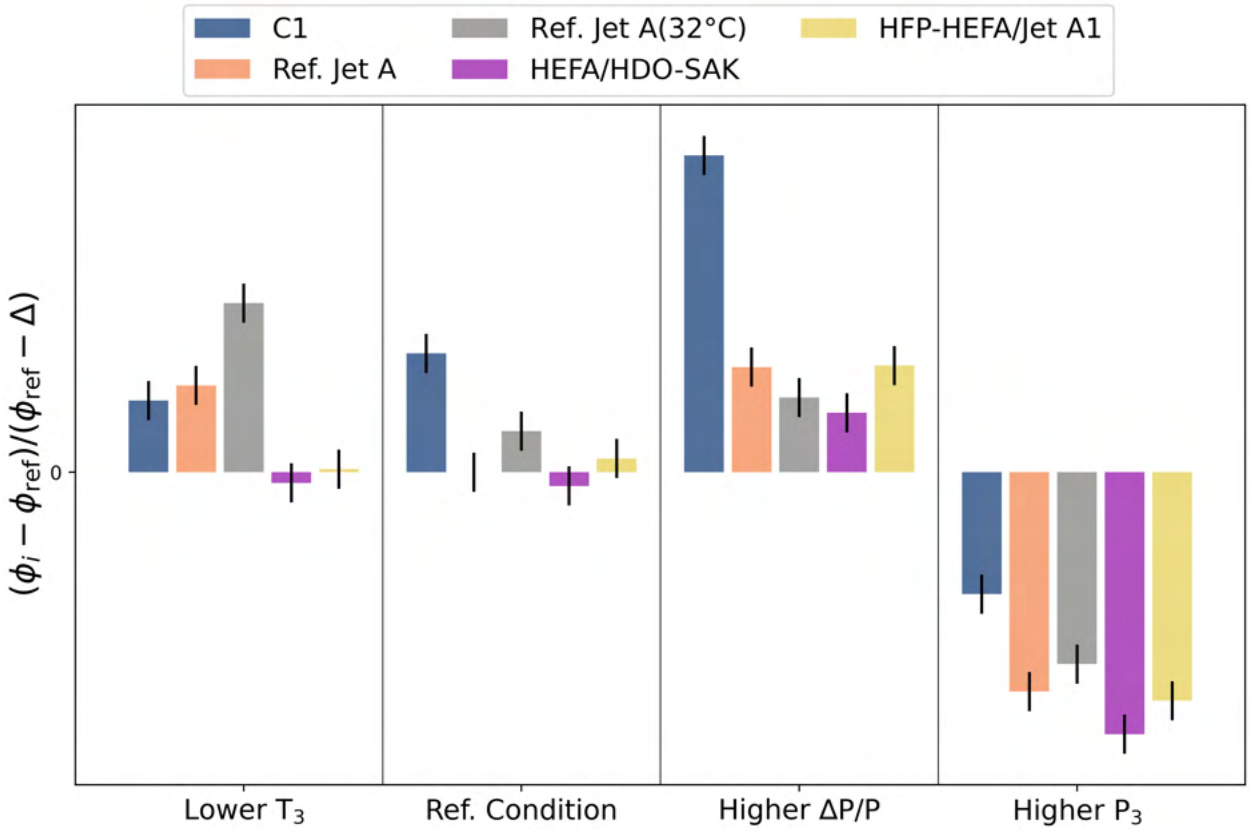

Figure 4. Relative lean blowout at four operating conditions in the GE9X full annular combustor rig. This figure was redrawn using data that was digitally extracted from the GE report to the FAA, which was part of the CLEEN II Consortium Program Update Public Plenary.

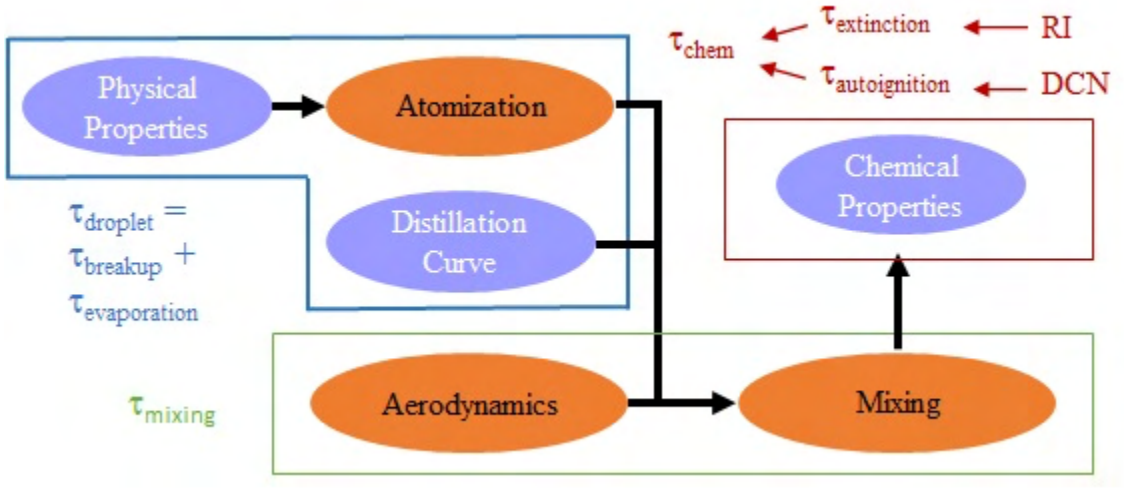

Figure 5. Available lean blowout pathways. Orange ovals represent combustor-specific characteristics and purple ovals show any fuel-dependent properties that can impact lean blowout limits.

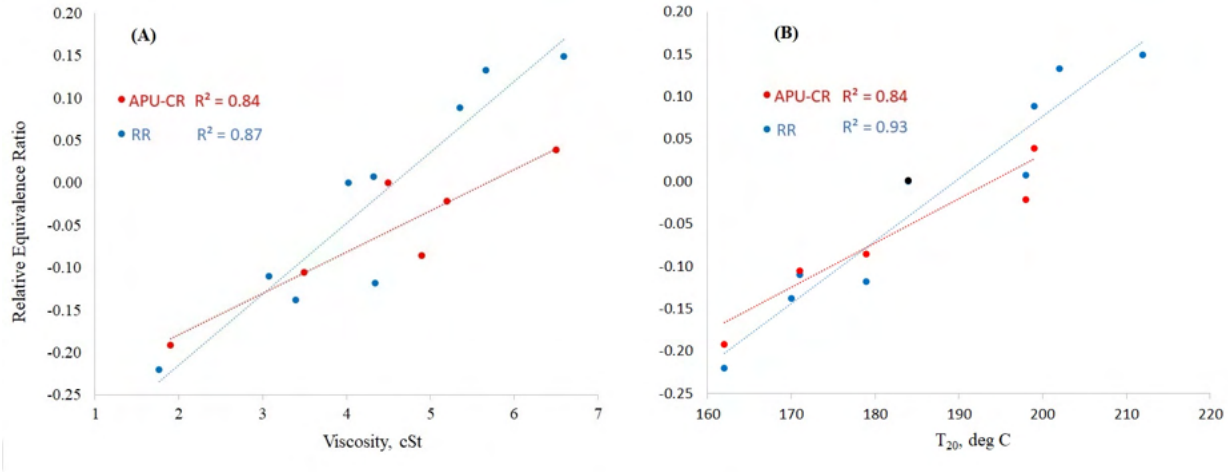

Figure 6. APU combustor rig (APU-CR) and Referee Rig (RR) LBO performance correlation with (a) viscosity (ν) and (b) 20% recovered temperature (T_{20}). Data is from Colborn et al. [?].

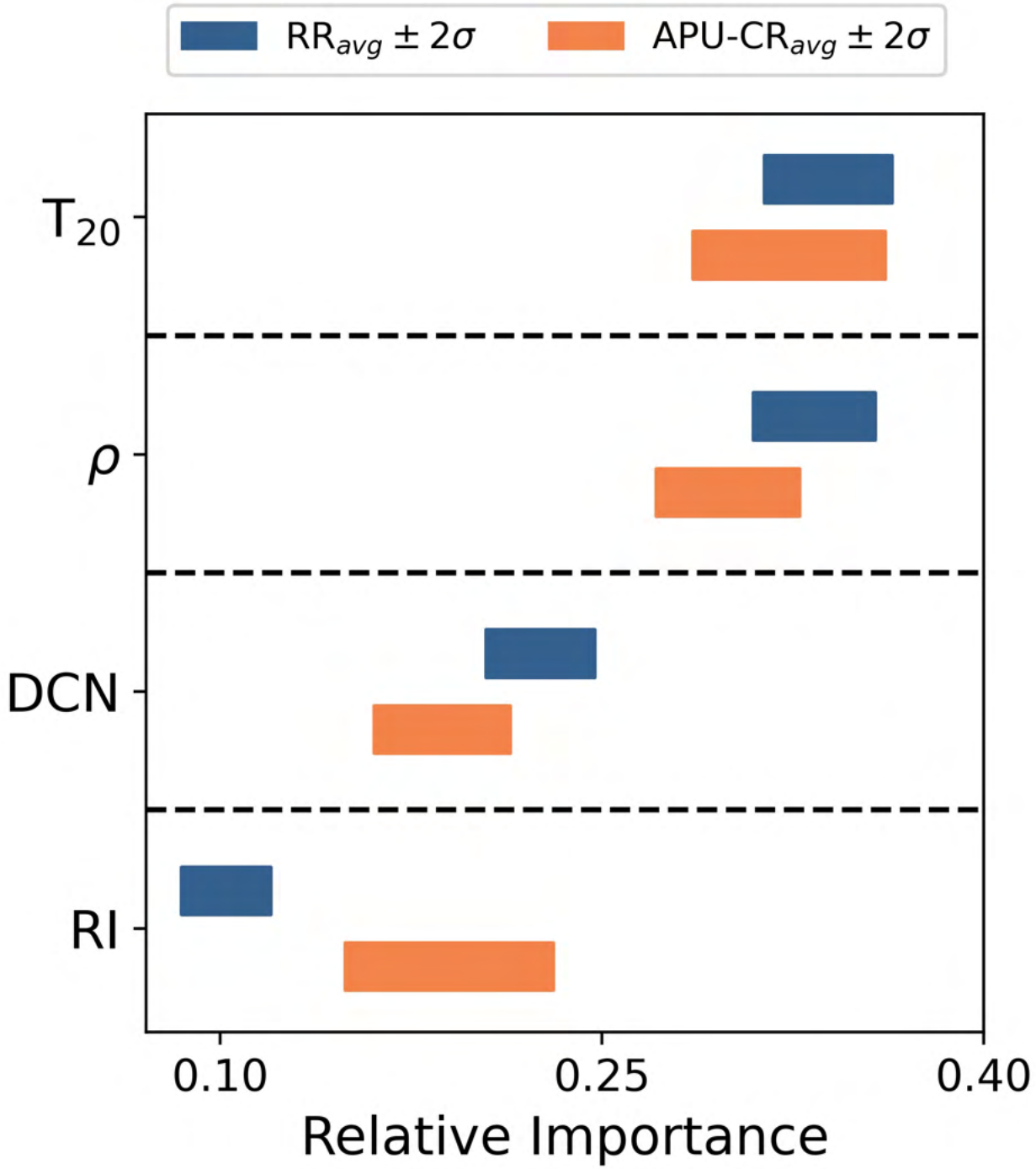

Figure 7. LBO determinants importance values for the RR at cold conditions and the APU-CR at normal operating conditions. On average, 98.6% of the LBO performance variance in the RR is explained by the chosen independent variables, while 91.8% of the LBO performance variance in the APU-CR is explained. Abbreviations: T20, 20% recovered temperature; ρ, density; DCN, derived cetane number; RI, radical index.

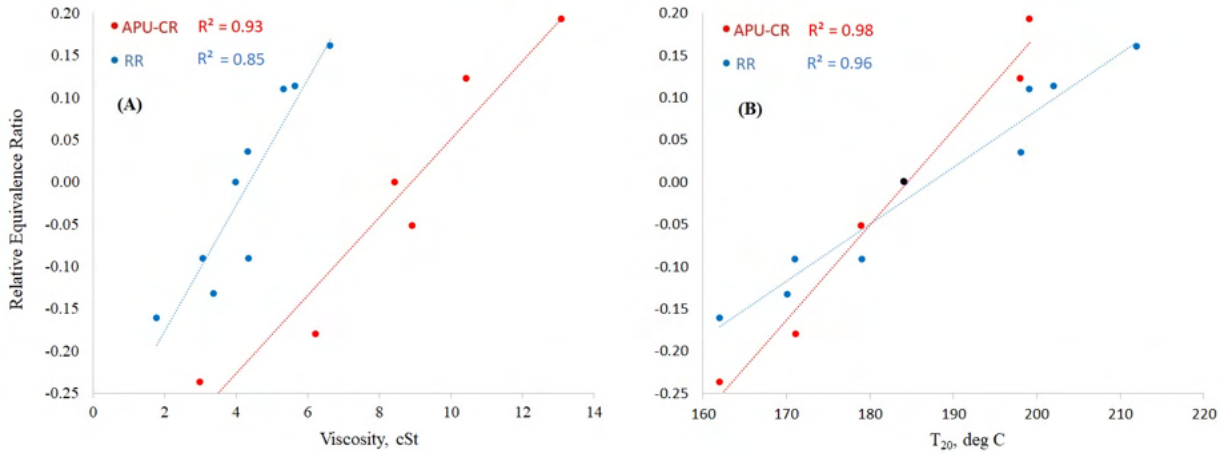

Figure 8. RR and APU-CR ignition equivalence ratio as a function of (a) Viscosity and (b) 20% recovered temperature (T_{20}). Data is from Hendershot et al. [5].

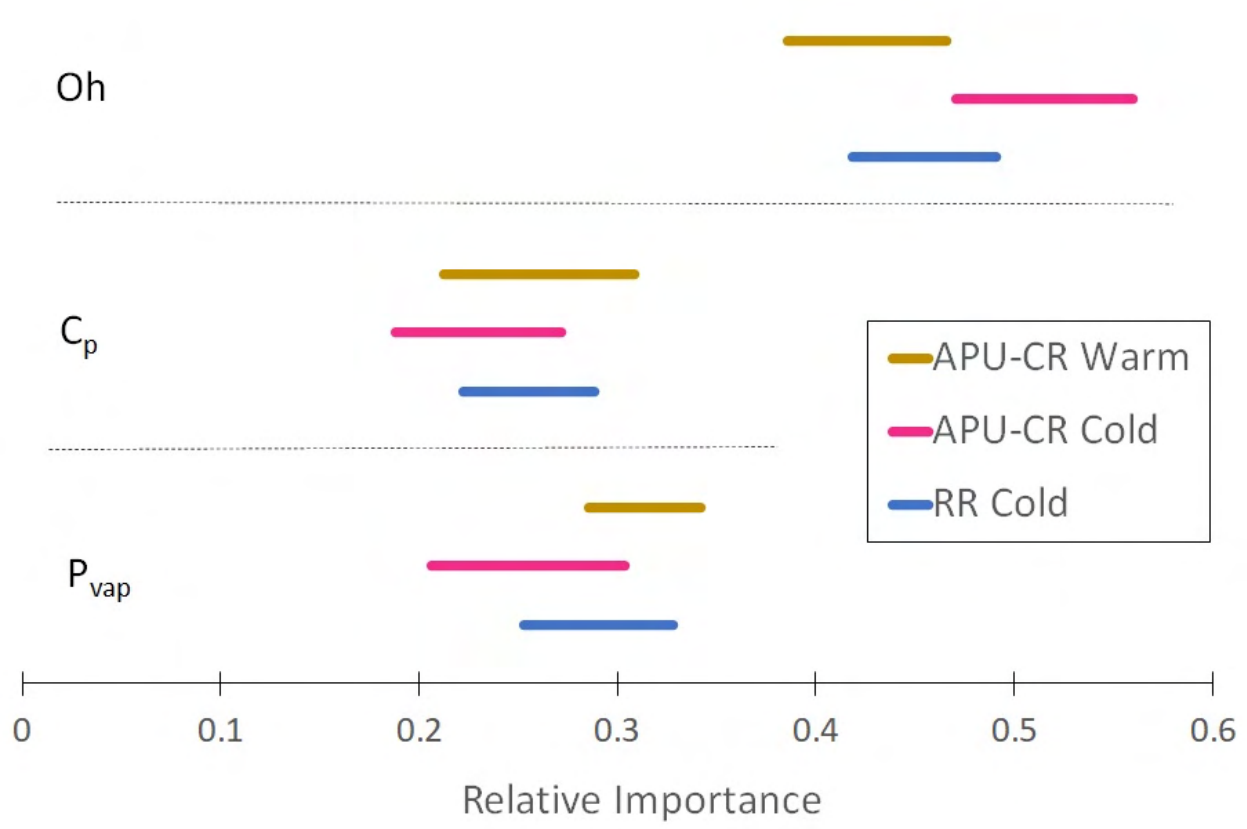

Figure 9. Ignition equivalence ratio determinants importance values for the RR at cold conditions and the APU-CR at both cold and warm conditions. On average, 89% of the ignition performance variance in the RR is explained by the chosen independent variables, 91% of the ignition performance variance in the APU-CR at cold conditions is explained, and 87% of the ignition performance variance in the APU-CR at warm conditions is explained.

Table 1. Operating conditions for the APU combustor rig (APU-CR) and Referee Rig (RR).

Rig	Operating Condition	Fuel Temperature [°C]	Air Temperature [°C]	Pressure [atm]	$\Delta P/P_{cmb}$ [%]
RR	Cold Lean Blowout [7]	-34, -15	-34, -15	1.02	2%
	Cold Start [5]	-34, -15	-34, -15	1.02	2%, 3.5%
APU-CR	Lean Blowout [22]	15	51 to 314	1.0, to 5.7	
	Cold Ignition [22]	-37	-44, -35, 15	1.05, 0.2, 0.3	
	Warm Ignition [22]	15	-38, 15	1.05, 0.2	

Table 2. Properties of fuels used in GE9X-FAR testing

Property	Jet A	C1	HFP-HEFA / Jet A1	HEFA / HDO-SAK
Density@15.6C (g/ml)	0.809	0.758	0.786	0.789
LHV (MJ/kg)	43.3	44.0	43.4	43.2
Hydrogen (wt%)	13.91	15.25	14.23	13.90
Viscosity@37.8C (cSt)	1.49	1.53	1.16	1.21
Viscosity@-20C (cSt)	5.02	4.99	3.15	
Viscosity@15.6C (cSt)		2.41 (curve fit)		1.66
DCN	~48	17.1		

Milestone(s)

- Determined alternative jet fuel dependencies between combustors of different sizes and mixing approaches.

Major Accomplishments

- Reported the alternative jet fuel dependencies between combustors of different sizes and mixing approaches.
- Published the NJFCP book.

Publications

Peer-reviewed journal publications

Boehm, R.C., Colborn, J. G., & Heyne, J. S. (2021). Comparing alternative jet fuel dependencies between combustors of different size and mixing approaches. Frontiers in Energy Research,*440*. https://doi.org/10.3389/FENRG.2021.701901.

Book publication

Colket, M., & Heyne, J. (2021). *Fuel effects on operability of aircraft gas turbine combustors*. American Institute of Aeronautics and Astronautics. https://doi.org/10.2514/4.106040

Book chapters

Colket, M., Heyne, J., Andac, G., Rumizen, M. (2021). Chapter I. Introduction. In T. C. Lieuwen (Ed.), *Fuel effects on operability of aircraft gas turbine combustors* (pp. 1-20). American Institute of Aeronautics and Astronautics.

Rock, N., Stouffer, S., Hendershott, T., Heyne, J., Blunck, D., Lukai, Z., Khandelwal, B., Emerson, B., Mastorakos, E., Colket, M. (2021). Chapter V. Lean blowout studies., In T. C. Lieuwen (Ed.), *Fuel effects on operability of aircraft gas turbine combustors* (pp. 143–196). American Institute of Aeronautics and Astronautics.

Heyne, J., Rauch, B., Hanson, R., Dooley, S., Blakey, S., Yang, Z., Ferris, A., Ure, A., Le Clercq, P., Boehm, R., Lewis, C., &Colket, M. Chapter XII. Prescreening of Sustainable Aviation Jet Fuels. In T. C. Lieuwen (Ed.), *Fuel effects on operability of aircraft gas turbine combustors* (pp. 487–523). American Institute of Aeronautics and Astronautics.

Heyne, J., Colket, M., Edwards, T., Moder, J., Rumizen, M., & Oldani, A. (2021). Chapter XIII. Summary. In T. C. Lieuwen (Ed.), *Fuel effects on operability of aircraft gas turbine combustors* (pp. 525–534). American Institute of Aeronautics and Astronautics.

Outreach Efforts

Invited talks

Heyne, J. (2020, November). High value drop-in aviation fuels: From molecule selection to mission benefits [Panel presentation]. Fuel Quality Matters, DOE BETO/PNNL HTL Workshop, Virtual meeting.

Heyne, J. (2020, November). Prescreening of HTL SAFs: Rapid low-volume, low-cost testing. Sustainable Aviation Fuel Certification, DOE BETO/PNNL HTL Workshop, Virtual meeting.

Heyne J. (2021, May). Summative results of the national jet fuels combustion program [Panel presentation]. Properties and Emissions, CRC Aviation Fuels Meeting, Virtual meeting.

Heyne, J. (2021, June). Prescreening of sustainable aviation fuels [Panel presentation]. CAAFI Virtual Mini-Symposium.

Heyne, J. (2021, June 2). Sustainable aviation fuel prescreening, benefits, and a proposed streamlined evaluation process [Panel presentation]. National Academies, Transportation Research Board (AV030), Sustainable Aviation Fuels subcommittee midyear meeting.

Heyne, J. (2021, August 17). Sustainable aviation fuel: Properties, compositions, and qualification requirements [Sponsored seminar]. Sandia National Laboratory.

Heyne, J., (2021, August 17). Sustainable aviation fuel property needs and some solid waste candidates [Panel presentation]. Seminar on Hydrothermal Liquefaction: biocrudes and advances towards drop-in fuel potential, Aalborg University, Denmark.

Heyne, J. (2021, November). Sustainable aviation fuel: Properties, compositions, and qualification requirements [Sponsored seminar]. Center for Multiphase Flow Research and Education, Iowa State University.

Conference presentations

None.

Awards

Joshua Heyne:

- 2021 Net Good Summit on sustainable travel, honored guest
- 2021 US Frontiers of Engineering Symposium, National Academies of Engineering, selected participant
- 2021 Vision Award for Excellence in Scholarship, School of Eng., University of Dayton

Student Involvement

Jen Colborn, graduate research assistant, leads this effort.

Plans for Next Period

Continue to coordinate across various federal agencies and research institutions regarding SAF testing.

Project 037 CLEEN II System-level Assessment

Georgia Institute of Technology

Project Lead Investigator

Dimitri Mavris
Regents Professor
School of Aerospace Engineering
Georgia Institute of Technology
Mail Stop 0150
Atlanta, GA 30332-0150
404-894-1557
dimitri.mavris@ae.gatech.edu

University Participants

Georgia Institute of Technology

PI(s): Dr. Dimitri Mavris (PI), Dr. Jimmy Tai (Co-PI)
FAA Award Number: 13-C-AJFE-GIT-055
Period of Performance: October 1, 2020 to September 30, 2021

Project Funding Level

FAA provided $240,000 in funding to Georgia Institute of Technology.

The Georgia Institute of Technology has agreed to a total of $240,000 in matching funds. This total includes salaries for the project director and research engineers, as well as funding for computing, financial, and administrative support, including meeting arrangements. The institute has also agreed to provide tuition remission for students, paid from state funds.

Investigation Team

PI: Dimitri Mavris
Co-Investigator: Jimmy Tai
Fleet Modeling Technical Lead: Holger Pfaender
Supporting Engineers: Joshua Brooks, and Brennan Stewart
Students: Joao De Azevedo, Madelyn Focaracci, and Sebastian Seubert

Project Overview

The objective of this research project is to support the FAA by independently modeling and assessing the technologies that are being developed under the CLEEN II and CLEEN III programs. This will involve direct coordination and data sharing with the CLEEN funded companies in order to accurately model the environmental benefits of these technologies at the vehicle and fleet levels.

Georgia Institute of Technology (GT) was previously selected to perform all system-level assessments for the CLEEN program under PARTNER Project 36 and ASCENT Project 10. As a result, GT is in a unique position from both technical and programmatic standpoints to continue the system-level assessments for CLEEN II. From a technical perspective, GT has significantly enhanced the Environmental Design Space (EDS) over the past 5 years to incorporate advanced, adaptive, and operational technologies targeting fuel burn, noise, and emissions. EDS has been successfully applied to all CLEEN I contractor technologies including the following: GE open rotor, twin annular premixing swirler (TAPS) II combustor, Flight Management System (FMS)-Engine, and FMS-Airframe; Pratt & Whitney geared fan; Boeing adaptive trailing edge and ceramic matrix composite (CMC) nozzle; Honeywell hot section cooling and materials; and Rolls-Royce turbine cooling technologies. GT has also gained extensive experience in communicating system-level modeling requirements to industry engineers and translating the impacts to fleet-level fuel burn, noise, and emissions assessments. This broad technical knowledge base

covering detailed aircraft and engine design as well as high-level benefits assessments places GT in a unique position to assess CLEEN II technologies.

Because the ultimate goal of this work is to conduct fleet-level assessments for aircraft representative of future "in-service" systems, GT will need to create system-level EDS models using a combination of both CLEEN II and other public domain N+1 and N+2 technologies. The outcomes of the technology and fleet assumptions setting workshops conducted under ASCENT Project 10 will be heavily leveraged for this effort. Non-CLEEN II technologies for consideration, along with potential future fleet scenarios, will help to bound the impact of CLEEN II on future fleet fuel burn, emissions, and noise.

Because the FAA will also be performing a portion of the EDS technology modeling work, EDS training was provided to the FAA in 2016 under ASCENT Project 10. The training provided the requisite skill set for using EDS. In the prior year of this project, Georgia Tech continued modeling activities with Collins, Honeywell, Boeing, and Pratt & Whitney. This modeling process included validation of underlying EDS models; information and data exchange necessary to model the individual technologies; and related EDS modeling activities. In addition, GT has assisted the FAA with in-house EDS modeling. This process has increased the number of FAA personnel performing EDS system-level assessment modeling.

Next year's work will focus on moving toward the end of the project by completing vehicle- and fleet-level assessments for CLEEN II. This will include final technology modeling details for each CLEEN II industry contractor generation of vehicle-level assessments of fuel burn, emissions, and noise compared to current best-in-class values, along with fleet-level estimates of fuel burn, emissions, and noise, including community noise impact estimates at multiple relevant airports. Individual technology impacts to the vehicle airframe and engine will not be reported, to preserve contractor confidentiality. Quantifying this impact will provide an understanding of the number of increased operations per day that CLEEN II technologies enable without worsening the surrounding community's noise exposure. Although airports in the United States are not generally noise constrained, some European airports have limited capacity to meet noise constraints. Understanding the impact of technologies on the future U.S. fleet will be critical to quantifying the interaction between economic growth (i.e., increased flight operations at a given airport) and community noise impacts.

GT has completed most of the technology modeling to date. Remaining items include updating technology models by using the most recent data from contractors and conducting a final fleet assessment. The table in the next section shows the current status of the technology modeling. Where work remains, a brief description is provided after the table.

Milestone(s)

The major milestones and planned due dates are listed in the table below:

Task No.	Milestone	Planned Due Date
Task 1	Attend CLEEN II Contractor Kickoff Meetings	8/31/2022
Task 2	Identify Required EDS Modeling Enhancements	8/31/2022
Task 2	Develop CLEEN II 5-year System Modeling Roadmaps for Each Contractor	8/31/2022
Task 3	Document EDS Modeling Approaches	8/31/2022

Major Accomplishments

- The modeling for GE More Electric Systems and Technologies for Aircraft in the Next Generation (MESTANG) is complete.
- The modeling for the GE Flight Management System is complete.
- The modeling for the Collins slim nacelle is complete.
- The audit of CLEEN I and II technology impacts is complete.
- Updated fuel burn assessment is complete.
- The data exchange and assumptions were defined for the Honeywell compact combustor.
- Efforts to model Collins zoned liner technology are ongoing.
- Efforts to model GE low pressure ratio advanced acoustic technology are ongoing.
- Efforts to model the Boeing compact nacelle acoustic liner are ongoing.

- Efforts to model the Honeywell blade outer air seal are ongoing and awaiting contractor review.
- Efforts to model the Pratt & Whitney compressor and turbine aero-efficiency technologies are ongoing and awaiting contractor review.

Task 1 – Establish Working Relationship with CLEEN III Contractors

Georgia Institute of Technology

Working relationships with CLEEN III contractors has been largely established through Georgia Tech's participation at contractor kickoff meetings held in the second half of 2021. Non-disclosure agreements where necessary are either standing or are in the initialization process.

Task 2 - Modeling of Aircraft Technologies and Advanced Configurations

Georgia Institute of Technology

Objective(s)

In order to estimate the impact of CLEEN relevant technologies at the vehicle system-level, each of these technologies must be modeled regarding their impacts to aircraft fuel burn, noise, and emissions using EDS.

Research Approach

Georgia Institute of Technology (GT) was previously selected to perform all system-level assessments for the CLEEN program under ASCENT Project 10. Because the ultimate goal of this work is to conduct fleet-level assessments for aircraft representative of future "in-service" systems, GT will need to create system-level EDS models using a combination of both CLEEN II and other public domain N+1 and N+2 technologies. Vehicle system-level modeling for all relevant CLEEN II technologies will be performed using EDS.

Table 1 presents an update on the vehicle system-level modeling effort regarding each of the CLEEN II relevant technologies.

Table 1. Update on CLEEN II technology modeling.

Contractor	Technology/Model Impact Area	Initial Modeling Discussions Held with Contractor?	Modeling Underway	Percentage Complete
Aurora (Technologies Listed are Sub-parts of Double Bubble Fuselage)	D8 configuration	✓	✓	100%
Boeing	Structurally efficient wing	✓	✓	100%
	Compact nacelle	✓	✓	100%
	Compact nacelle (noise liner)	✓	✓	50%
Delta/MDS/America's Phenix	Leading edge protective fan blade coating	✓	✓	100%
GE	TAPS III low NOx combustor	✓	✓	90%
	More Electric Systems and Technologies for Aircraft in the Next Generation (MESTANG)	✓	✓	100%
	Flight Management System (FMS)	✓	✓	100%

Contractor	Technology/Model Impact Area	Initial Modeling Discussions Held with Contractor?	Modeling Underway	Percentage Complete
	Low pressure ratio advanced acoustic	✓		15%
Honeywell	Compact combustor	✓	✓	75%
	Advanced acoustic fan rotor/liner			0%
	Advanced high-pressure compressor		✓	5%
	Turbine blade outer air seal	✓	✓	85%
Pratt & Whitney	Compressor and turbine aero-efficiency technologies	✓	✓	85%
Collins/Rohr/UTAS	Slim nacelle	✓	✓	100%
	Noise liner technologies	✓	✓	85%
Rolls-Royce	Advanced rich-quench-lean low NOx combustor	✓		25%

Remaining Modeling Work

- GE low pressure ratio advanced acoustic
  - We are awaiting information from GE.
  - Modeling has not yet started. The modeling approach has been formulated.
- Boeing compact nacelle noise liner
  - We have held several working meetings with Boeing. The modeling approach has been agreed upon. The required modeling data have been provided by Boeing.
  - Baseline aircraft modeling results have been reviewed by Boeing.
  - Technology modeling study is underway, and results will be presented to Boeing for verification.
- Honeywell compact combustor
  - We have received preliminary combustor correlation estimates from Honeywell.
  - When Honeywell completes high-pressure testing at NASA, correlations will be updated, and the model will be finalized. Only minor modeling changes will be required.
- Honeywell turbine blade outer air seal
  - We have received modeling impacts from Honeywell. Preliminary sensitivity studies have been completed, and the results have been communicated to Honeywell. Work with Honeywell to verify trends is ongoing.
- Honeywell advanced high-pressure compressor
  - The GT modeling approach formulation has begun. We will initiate modeling conversations with Honeywell before proceeding to results generation.
- Honeywell advanced acoustic fan rotor/liner
  - Modeling has not yet started.
- Pratt & Whitney compressor and turbine aero-efficiency technologies
  - We have held several working meetings with Pratt & Whitney. The modeling approach has been agreed upon. The required modeling data have been provided by Pratt & Whitney. Preliminary sensitivity studies have been completed, and the results have been communicated to Pratt & Whitney. Work with Pratt & Whitney to verify trends is ongoing.
- Collins noise liner technologies
  - GT has developed a new modeling approach based on feedback from Collins and is currently in the process of implementing this approach. Preliminary results have been generated.
- Rolls-Royce advanced rich-quench-lean (RQL) low nitrogen oxides (NOx) combustor
  - When Rolls-Royce completes testing, we will use the same modeling approach as that with Honeywell, but with an empirical NOx model specific to Rolls-Royce.

Task 3 - Finalize CLEEN II Analysis

Georgia Institute of Technology

Objective(s)

To evaluate the impact of CLEEN relevant technologies as propagated forward into the United States civil fleet of domestic and international departing aircraft. Specifically interested in the impact of CLEEN technologies to fleet-level noise, fuel burn, and NOx emissions.

Research Approach

Vehicle system-level modeling for all relevant CLEEN II technologies will be performed using EDS. Fleet benefit assessments for aircraft fleet fuel burn, oxides of nitrogen (NOx), and noise through the year 2050 will be performed using the information delivered by the vehicle system-level modeling effort alongside fleet replacement matrices, technology integration scenarios, and projected aviation demand schedules.

Updated Fuel Burn Assessment

GT and FAA have updated the preliminary fleet-level fuel burn assessment from 2020. This update includes the results of an audit of the previously presented study, with the objective of ensuring the traceability of all relevant technology impacts and the repeatability of the fleet benefit assessment. Technologies included in the fuel burn assessment update include:

- All relevant CLEEN I technologies
- Aurora double bubble (fuselage weight reduction)
- Boeing structurally efficient wing (SEW)
- Boeing compact nacelle
- Delta/MDS/America's Phenix leading edge protective coating
- GE MESTANG
- GE FMS
- Honeywell turbine blade outer air seal
- Pratt & Whitney compressor and turbine aero-efficiency technologies
- Collins slim nacelle

The fuel burn assessment update does not represent the entire set of CLEEN II technologies. It is important also to note that this analysis only includes domestic US flights and US departures, which may represent lower growth rates than a more global analysis. The applied fleet analysis definition and underlying assumptions have remained consistent throughout the CLEEN program.

A technology impact matrix (TIM) has been introduced to rigorously, transparently, and reproducibly manage the impacts of all technologies included in GT's CLEEN program assessment. The TIM was implemented across all five vehicle classes considered in this assessment.

In addition, a comprehensive review was conducted of technology impacts and all the associated design of experiments (DoEs) considered, to date. Based on this review, updates were made within vehicle analysis DoE.

Figure 1 is provided to display the percentage fuel savings relative to the evolutionary scenario. Results are estimated for the fleet of U.S. domestic and internationally departing aircraft.

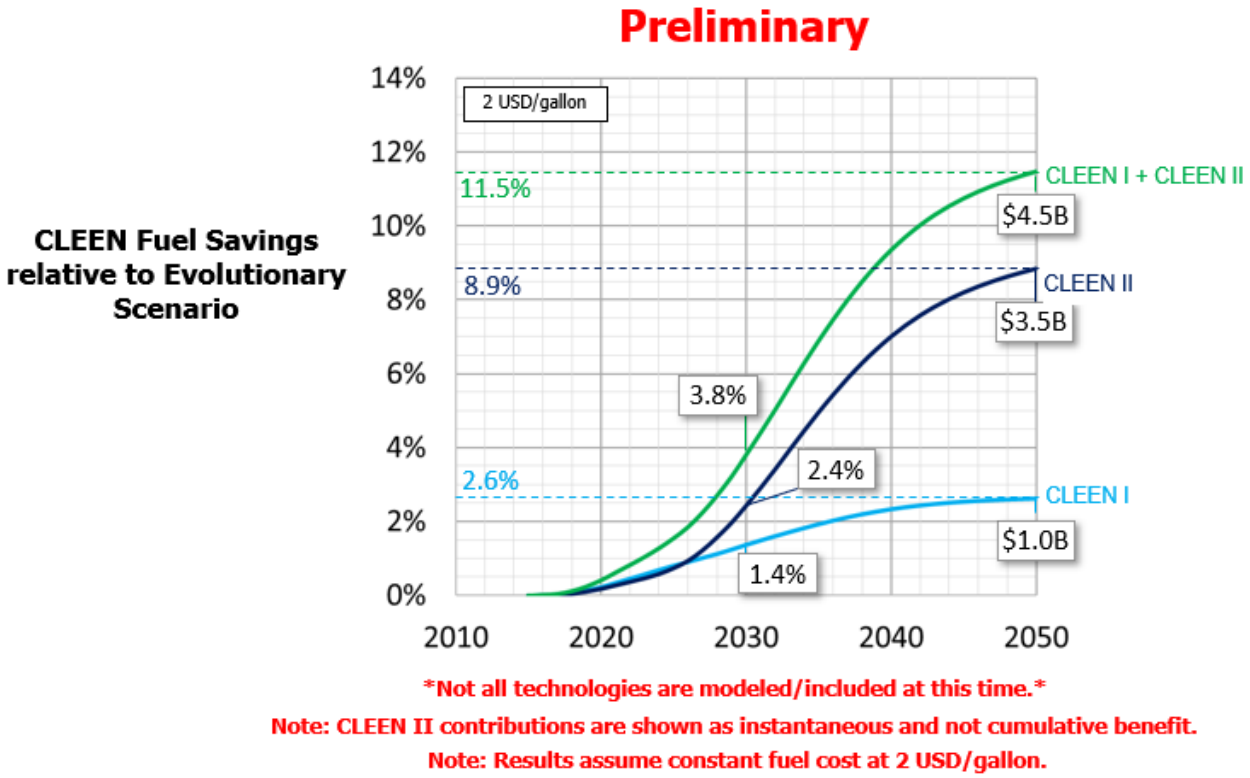

Figure 1. Preliminary fuel burn assessment: savings relative to evolutionary scenario (updated).

According to the analysis performed above, the technologies matured in the first 5-year phase of CLEEN will reduce U.S. fleet-wide fuel burn by 1.4% by the year 2030 and 2.6% by the year 2050 relative to the evolutionary scenario, thus providing a cumulative savings of 9.3 billion gallons of jet fuel. The CO_2 savings are the equivalent of taking 781,000 cars off the road in the years 2020–2050.

This preliminary analysis projects the technologies matured in the CLEEN Phase II program to reduce fuel consumption 2.4% by 2030 and 8.9% by 2050 relative to the evolutionary scenario, thus bringing the contribution of CLEEN Phase I and II to 11.5% fuel burn reduction in the fleet by 2050.

Cumulatively, CLEEN Phase I and II are estimated to save 34.7 billion gallons of fuel by 2050, with a savings worth approximately 69.5 billion dollars for airlines, and resulting in a reduction in CO_2 emissions of approximately 404 million metric tons. These CO_2 reductions are equivalent to removing 2.9 million cars from the road in the years 2020–2050.

Assessment of other areas of benefit of CLEEN Phase II are ongoing. Quantification of the program's fleet-level noise benefits is expected to be complete in 2022.

Publications
None

Outreach Efforts
CLEEN Consortium

Awards
None

Student Involvement

Three graduate students are currently receiving funding from this effort.

Plans for Next Period

Future work will focus on completing technology modeling and updating fleet analysis assessments with the remaining technologies. The next period will also include the transition of efforts toward the incoming CLEEN III initiative (e.g., Non-disclosure agreements).

This work will also support attendance at CLEEN consortium meetings and contractor preliminary and detailed design reviews to identify any updates required to the technology models developed in prior years.

References

None

Project 038 Rotorcraft Noise Abatement Procedure Development

The Pennsylvania State University, Continuum Dynamics, Inc.

Project Lead Investigator

Kenneth S. Brentner
Professor of Aerospace Engineering
Department of Aerospace Engineering
The Pennsylvania State University
233 Hammond Building
University Park, PA
(814) 865-6433
ksbrentner@psu.edu

University Participants

The Pennsylvania State University (Penn State)

- PI: Kenneth S. Brentner, Professor of Aerospace Engineering
- FAA Award Number: 13-C_AJFE-PSU-038, Amendment No. 63
- Period of Performance: August 11, 2020 to August 10, 2021
- Task(s) (during this period):
  18. Compare the effectiveness of noise abatement procedures by helicopter class using 2017 and 2019 flight test data
  19. Analyze 2019 FAA/NASA acoustic flight test data
  20. Develop a method for coupling the noise prediction system with FAA noise prediction and analysis tools
  21. Continue efforts to develop noise abatement flight procedures for various helicopter classes
  22. Develop documentation and training materials for the noise prediction system

Project Funding Level

FAA Funding $150,000; Continuum Dynamics, Inc. (points of contact: Dan Wachspress and Mrunali Botre) will provide $150,000 of cost sharing in the form of a 1-year license for the Comprehensive Hierarchical Aeromechanics Rotorcraft Model (CHARM) rotorcraft comprehensive analysis software to Penn State and a second 1-year license to the FAA or its designee. Penn State will provide $21,787 as an academic year salary for the PI.

Investigation Team

- Kenneth S. Brentner, PI, The Pennsylvania State University; acoustic prediction lead on all tasks
- Joseph F. Horn, Co-PI, The Pennsylvania State University; flight simulation lead supporting all tasks
- Daniel A. Wachspress, Co-PI, Continuum Dynamics, Inc.; responsible for rotor loads, wake integration, and CHARM coupling
- Damaris Zachos and Lauren Weist, Graduate Research Assistants, The Pennsylvania State University; primarily responsible for establishing new aircraft models, developing simulations for new helicopter types, performing acoustic predictions, and developing flight abatement procedures; Damaris Zachos was involved in all tasks; Lauren Weist started working on this project near the end of the year.

Project Overview

Rotorcraft noise consists of several components, including rotor noise, engine noise, and gearbox and transmission noise. Rotor noise is typically the dominant component of rotorcraft noise to which the community is exposed upon takeoff and landing and along the flight path of the helicopter. Rotor noise arises from multiple noise sources, including thickness noise

and loading noise (the combination of these two is known as rotational noise), blade–vortex interaction (BVI) noise, high-speed impulsive (HSI) noise, and broadband noise. Each noise source has its own unique directivity pattern around the helicopter. Furthermore, aerodynamic interactions among rotors, interactions between the airframe wake and a rotor, and unsteady time-dependent loading generated during maneuvers typically result in significant increases in loading noise. The combination of all potential rotor noise sources makes the prediction of rotorcraft noise highly complex, even though not all noise sources are present at any given time in the flight (e.g., BVI noise usually occurs during the descent, and HSI noise only occurs during high-speed forward flight).

In ASCENT Project 6, "Rotorcraft Noise Abatement Operating Conditions Modeling," the project team coupled a MATLAB-based flight simulation code with CHARM and PSU-WOPWOP to perform rotorcraft noise prediction. This noise prediction system was used to develop noise abatement procedures through computational and analytical modeling. Although this noise prediction system cannot predict engine noise or HSI noise, it was thoroughly validated via a comparison between predicted noise levels for a Bell 430 aircraft and flight test data (Snider et al., AHS Forum, 2013) for several observer positions and operating conditions.

In previous work for ASCENT Project 38, representative helicopters were recommended for noise abatement procedure development. These helicopters were selected to enable a determination of whether noise abatement procedures could be developed for various categories of helicopters (two-blade light, four-blade light, two-blade medium, etc.) or whether aircraft-specific design considerations would be required. Aircraft models were established for the following aircraft: Bell 430, Sikorsky S-76C+ and S-76D, Bell 407 and 206L, Airbus EC130 and AS350, and Robinson R66 and R44. Predictions were made before the 2017 FAA/NASA noise abatement flight test to provide guidance for the flight test. After the flight test, a comparison of L_A (A-weighted sound pressure level) time histories and sound exposure level (SEL) contour plots revealed a problem in the broadband noise prediction, which was subsequently corrected. Initial validation comparisons demonstrated that the simulations were within a few dBA of the flight test data; however, some discrepancies in the simulations (simplifications) remained, requiring a detailed examination. Work was also performed on the noise prediction system, including modifying PSU-WOPWOP to output plots of the maximum dBA, as plotted in the flight test. Further work was conducted to enhance the postprocessing of noise data to enable a direct comparison with flight test. Detailed analysis of the noise components and noise sources was performed for several of the helicopters in the 2017 FAA/NASA flight test.

The objective of this continuing project is to reduce the need for flight testing of each rotorcraft of interest for continued development of low-noise operating procedures. Current guidelines provided to pilots and operators in the Fly Neighborly guide are based on recommendations from manufacturers, but this guidance is not required and often not provided. Other methods for developing noise abatement procedures at the FAA and NASA are empirical, based on previous flight measurements of specific aircraft. The tasks described below will enable analyses of new flight procedures and noise analysis strategies through computations alone. This year's efforts included detailed analyses and investigation of the 2017 and 2019 FAA/NASA noise abatement flight tests, along with documentation and training materials for the FAA to use the tools more effectively.

Task 18 - Compare the Effectiveness of Noise Abatement Procedures by Helicopter Class Using 2017 and 2019 Flight Test Data

The Pennsylvania State University

Objective(s)

In this task (Task 8.1 in the 2020–2021 proposal), helicopter models in the 2019 FAA/NASA flight test will continue to be analyzed. Several of the noise abatement procedures performed during the flight test will be simulated with the noise prediction system. Using both noise predictions and measured data, noise abatement procedures will be examined. The effectiveness of the procedures for the heavier helicopters in the 2019 test will be compared with that for the lighter helicopters in the 2017 test. The noise predictions will allow a deeper understanding of the noise sources and their relative importance to help explain differences in noise abatement procedures for helicopters of different weight classes and technology levels.

Research Approach

The noise prediction system developed in ASCENT Projects 6 and 38 was used and updated as necessary. The PSU-WOPWOP code was used for noise prediction and was coupled with the PSUHeloSim flight simulator and CHARM to form a rotorcraft

noise prediction system. The flight test data were examined, and the measured and predicted results were compared to help explain any significant details in the noise measurements. This evaluation can also identify the primary and secondary noise sources involved in each flight procedure and can clarify how noise abatement was achieved (which can lead to generalized procedures for other helicopter categories, weights, etc.). After the prediction system is validated with 2019 flight test aircraft, a comparison between similar aircraft from the 2017 and 2019 flight tests will be developed. Identical maneuver cases will be developed for comparable aircraft, and various noise metrics will be evaluated for signs of significant differences in noise sources between heavier and lighter designs. The results of this study will provide guidance on the importance of aircraft weight in the development of noise abatement procedures and determine if separate procedures are necessary for aircraft in different weight classes.

In previous work performed as part of Project 38, M. Botre [Botre, Ph.D. dissertation, 2020] found that the Pegg broadband loading model overpredicts broadband noise for some helicopters and underpredicts broadband noise in other cases. The source of this over- and underprediction is not understood; however, the Pegg model is a simple empirical model, and changes in weight or other helicopter design features may be related to this discrepancy. In this work, we propose to determine whether it would be useful to include a simple shift in the Pegg broadband noise models, i.e., a scaling of the Pegg broadband noise prediction. To determine the scaling for each case, the measured flight test maximum dBA level is used at a single observer position to determine the necessary scale factor for each aircraft. Then, that Pegg scale factor is applied to plot the predicted ground contour results. Each aircraft has its own distinct scale factor. It would be beneficial to assess whether these unique scale factors follow any trends that could be used to improve Pegg broadband noise predictions.

Milestone(s)

The milestones for this task include (a) using validated helicopter noise prediction models for aircraft from the 2019 and 2017 flight tests to simulate identical flight maneuvers for multiple aircraft and (b) evaluating noise prediction results for each noise source (thickness, loading, and broadband) to determine similarities between noises produced by aircraft in different weight classes. In this task, we will examine various predicted noise sources and will investigate which sources are important in simulated predictions (for several different observer locations). Dissimilarities between comparable aircraft with differences in weight will be used to determine the use of noise abatement procedures to reduce noise.

Major Accomplishments

The required modeling parameters for the Bell 205 and Sikorsky S-76 helicopters were used to generate HeloSim flight path models that mimicked test trajectories from 2019 flight tests. These models have been validated against flight test data as part of Task 19 (8.2 in the 2020–2021 proposal). The S-76 model uses elements from S-76 models A–D because the needed parameters were not publicly available for S-76D. This “S-76” model was used to provide an initial view of the comparison between measured and predicted noise. The Bell 205 model was also validated using flight test data, and key parts of the noise predictions were assessed to determine areas for improvement in the prediction models. This work is also discussed in Task 19.

Models for aircraft flown during 2017 flight tests (Bell 206 and Bell 407) were updated during this past year to revalidate the models with system improvements made by Damaris Zachos. The system improvements (including Pegg broadband scaling) are described in more detail in Task 19. These efforts demonstrate the noise prediction system’s ability to predict maneuvering aircraft noise. Comparisons for these new models against 2017 flight test data are shown in Figures 1 and 2.

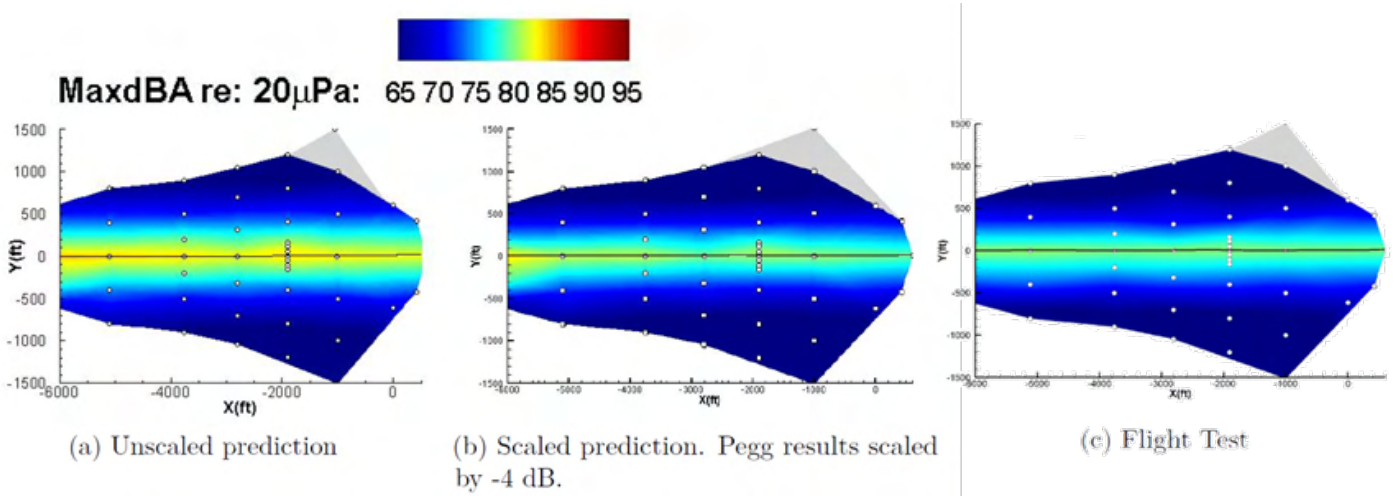

Figure 1. Comparison of maximum dBA results for the Bell 407 flying nominally at 80 knots in a level flight (run 283107) measured with the Amedee flight test grid.

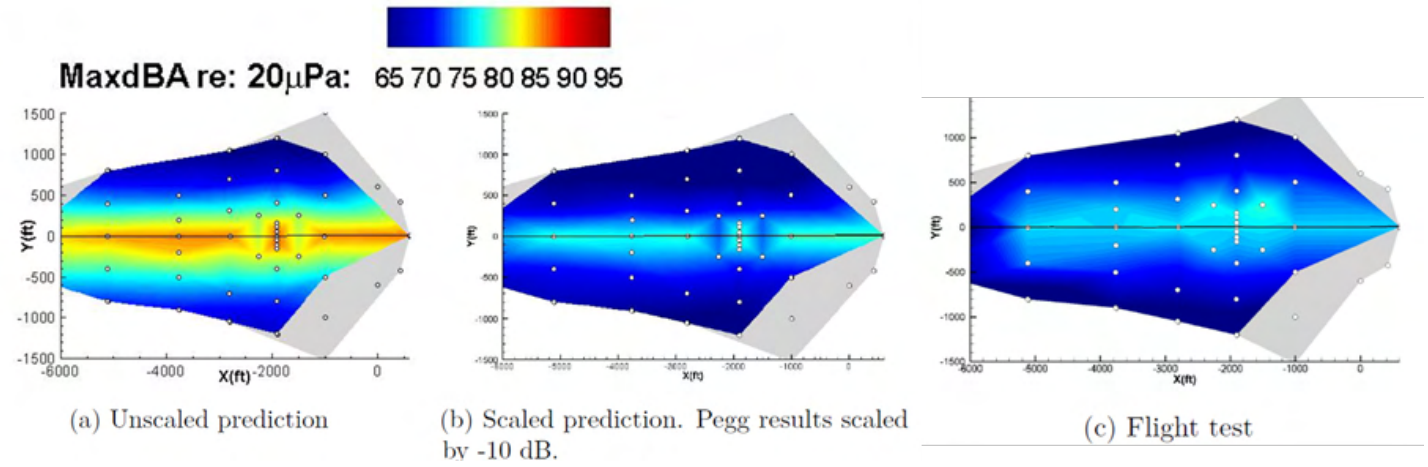

Figure 2. Comparison of maximum dBA results for the Bell 206 flying nominally at 94 knots in a level flight (run 278187) measured with the Amedee flight test grid.

With validated models for various aircraft of different weight classes, the helicopters were grouped into categories with similar design characteristics. The Bell 205 helicopter was compared against the Bell 206 because both of these aircraft have a main rotor and tail rotor with two blades each. The S-76 was compared against the lighter Bell 407 model because both aircraft utilize four-bladed main rotors (although the number of blades on the tail rotor of each aircraft is different). Comparing in this manner makes the comparisons between the differences in noise for each of these aircraft more isolated to the vehicle weight. The comparisons between the Bell 205 and Bell 206 aircraft are shown in Figure 3. The S-76 is compared with the Bell 407 in Figure 4.

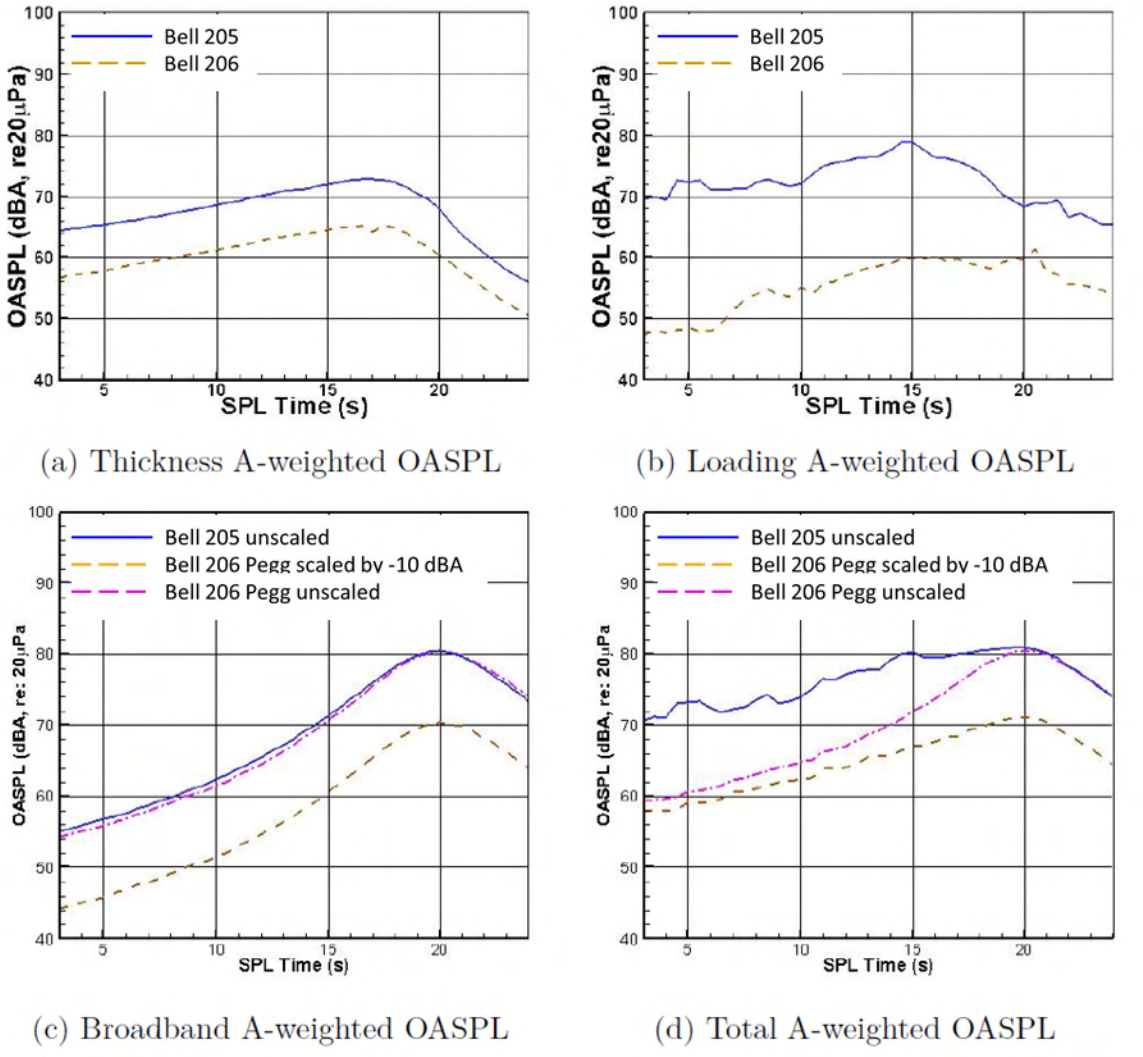

Figure 3. A-weighted Overall sound pressure level (OAPSL) comparison results for the Bell 205 versus Bell 206 simulated at 80 knots in a level flight.

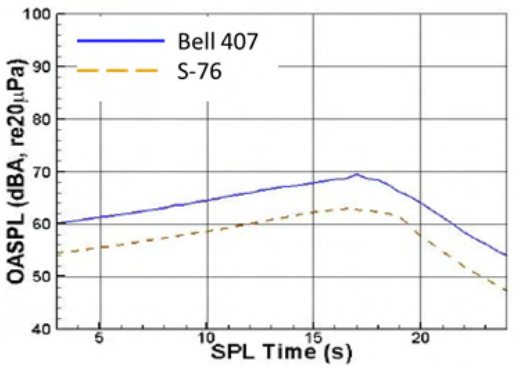

(a) Thickness OASPL

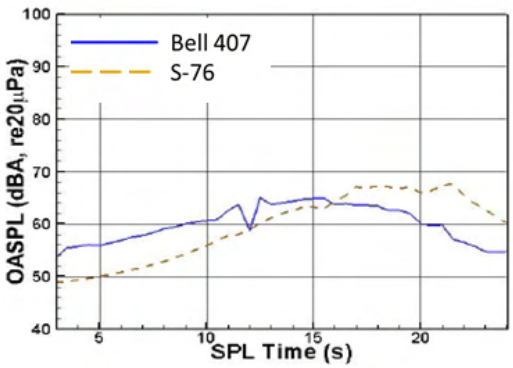

(b) Loading OASPL

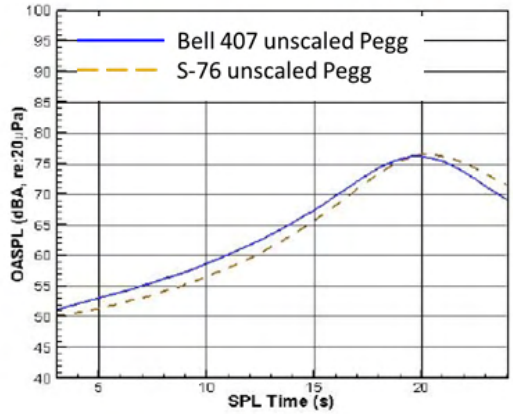

(c) Pegg Broadband OASPL

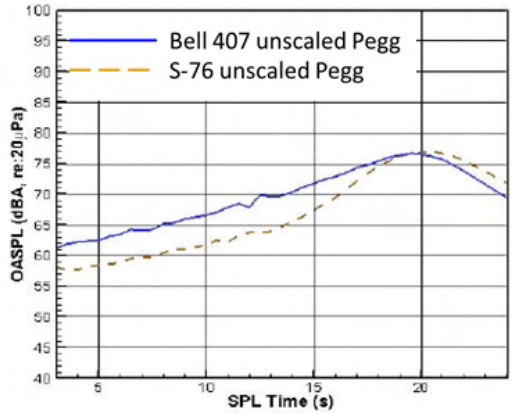

(d) Total OASPL

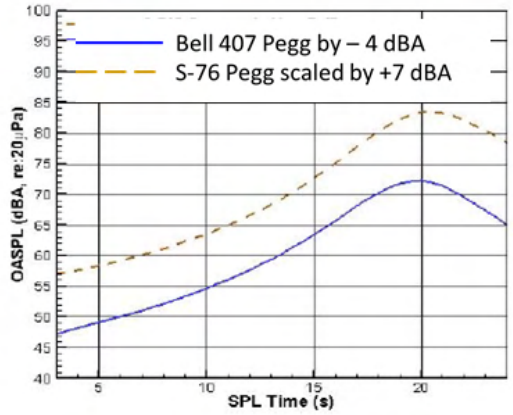

(e) Pegg Broadband OASPL. Pegg scaled by 7 dB for S-76 and -4 dB for Bell 407

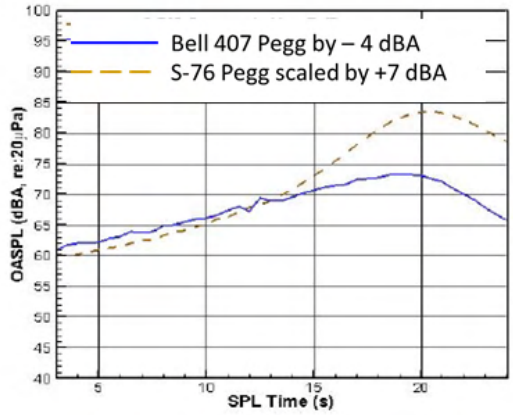

(f) Total OASPL. Pegg scaled by 7 dB for S-76 and -4 dB for Bell 407

Figure 4. A-weighted OASPL comparison of the Bell 407 versus S-76 simulated at 80 knots in a level flight.

A detailed analysis of the difference in predicted noise for each noise source can be found in Damaris Zachos' master's thesis.

Publications
Zachos, D. R. (2022). Noise prediction for helicopter noise abatement and EVTOL design [M.S. thesis, The Pennsylvania State University]. Manuscript in preparation.

Outreach Efforts
None

Awards
None

Student Involvement
Damaris R. Zachos, a graduate assistant currently working toward her master's degree at Penn State, generated predictions for the Bell 407, Bell 206, Bell 205, and S-76. She also developed the simulated flight trajectories necessary to compare exactly identical flight maneuvers between aircraft.

Plans for Next Period
During the next period, simulated trajectories for the four aircraft studied during 2021 will be developed for maneuvering flight, including descent and turn trajectories. The broadband scaling method developed during this year will be evaluated to determine whether there is a better approach for predicting broadband noise for conventional helicopter designs. This effort might lead to a re-evaluation of the comparisons presented in this section.

Task 19 - Data Analysis of 2019 FAA/NASA Acoustic Flight Test Data
The Pennsylvania State University

Objective
The goal of this task (Task 8.2 in the 2020–2021 proposal) is to provide continued assistance in evaluating the 2019 FAA/NASA flight test data and assessing the effectiveness of various noise abatement procedures. This task will involve evaluating flight test data and examining and comparing measured and predicted results to help explain any significant unexpected differences in noise measurements. This evaluation can also identify which sources are the primary and secondary noise sources involved in a flight procedure and provide understanding about how the noise abatement was achieved (which can lead to generalized procedures for other helicopter categories, weights, etc.).

Research Approach
In this task, we will perform detailed noise predictions of noise abatement procedures executed in the 2017 and 2019 FAA/NASA flight tests (with an emphasis on the 2019 flight test) and will explain how noise abatement was achieved or why procedures did not work as expected. Specifically, the thickness, loading, and broadband noise from both the main and tail rotors will be predicted to determine which noise sources were increased or reduced. Variations in the flight procedure may also be predicted to help understand if the procedures applied in the flight test were optimal. This evaluation is expected to lead to better noise abatement procedures and perhaps even procedures tailored to particular helicopter models.

Milestone(s)
The milestones for this task include (a) replication of identical cases in PSU-WOPWOP, (b) comparison of noise predictions with flight test data to identify possible deficiencies in the noise prediction models, and (c) development of an improved model for Pegg broadband noise prediction.

Major Accomplishments
Flight test predictions for two of the aircraft flown during the 2019 flight test (Bell 205 and S-76D) have been generated. Predictions for various maneuvers (level flight, descents, and turns) were modeled, and prediction results were compared against flight test data. The discrepancy between noise levels noted during modeling of 2017 flight test aircraft was addressed via a scaling method for Pegg broadband noise prediction. By changing the peak level of the OASPL broadband

noise prediction, the maximum dBA value for various observers was adjusted to match flight test data (see Figure 5). In Figure 5, the difference in time when the peak occurs (flight test data vs. prediction) is thought to be a time shift when reading the data or plotting the prediction. The source of this discrepancy will be addressed in continuing work.

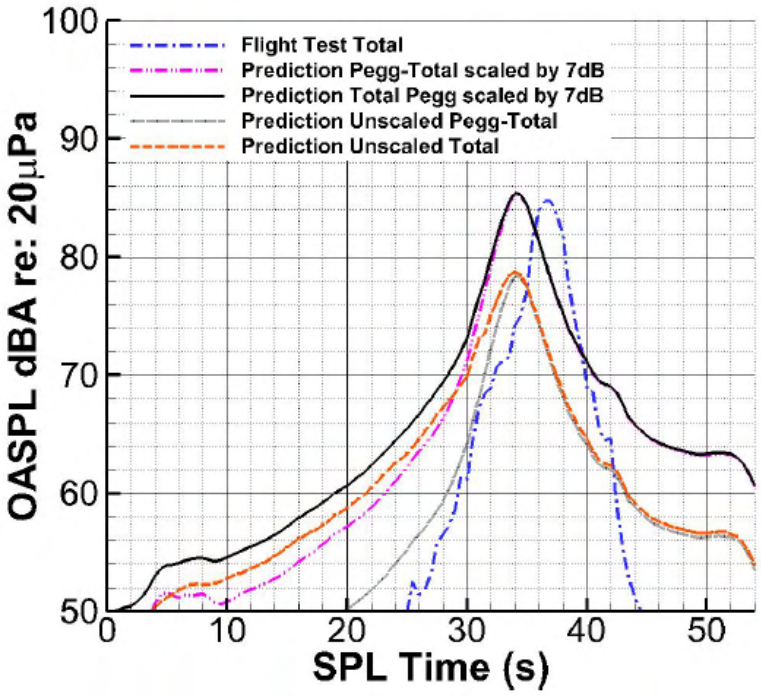

Figure 5. A-weighted OASPL noise breakdown. Flight Test Total refers to the measured flight test data for S-76D in a nominal 88-knot level flight (run 178301) at the Coyle Field, microphone location 26. The predictions are for the S-76 prediction model. Both scaled and unscaled broadband and total noise predictions are shown.

A single scaling value was found for the S-76 model. The Bell 205 model was not scaled because there were issues with the loading noise prediction that must be addressed first. Pegg scaling improved the correlation between the flight test maximum dBA ground noise contours and predicted ground noise contours during steady level flight (see Figure 6). Although this figure is not a good image to use for evaluating the noise generated by this aircraft, it does show how the use of Pegg scaling can improve the correlation between the peak flight test level and the maximum dBA predicted by the noise prediction system.

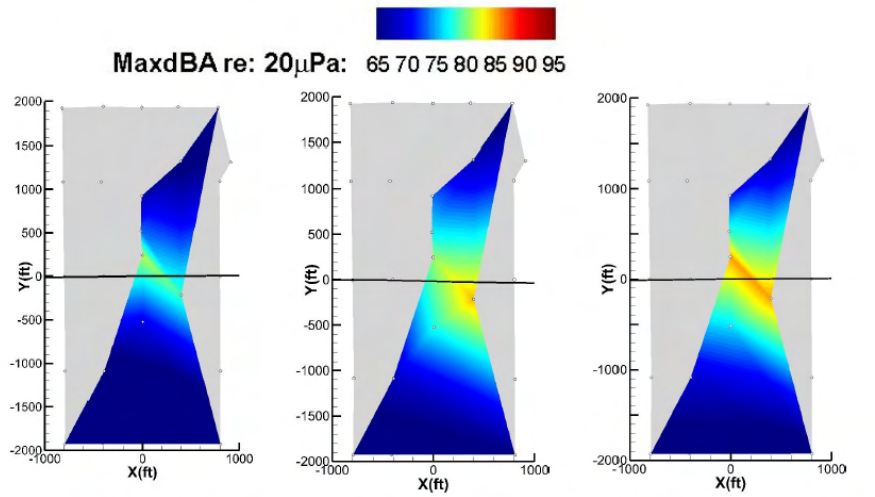

(a) Unscaled prediction (b) Flight test (c) Scaled prediction. Pegg results scaled by 7 dB.

Figure 6. Comparison of maximum dBA for a nominal 88-knot level flight (run 78301) measured on a flight test grid for measured S-76D versus modeled S-76 results. Note that the contours are skewed because there were too many inoperable microphones for this run.

Maneuvers, including descents and turns, were also modeled during 2021. These predictions provided initial insights into changes in noise for the Bell 205 and S-76D that are induced when the pitch of the aircraft changes during descent. Figure 7 shows the change in amplitude and directivity of the total S-76D noise generated during one of these descents. Because these results are predictions, the noise can be divided into components to determine whether the change in noise is caused by thickness, loading, or broadband noise. Descent cases for the Bell 205 were also modeled during this working period.

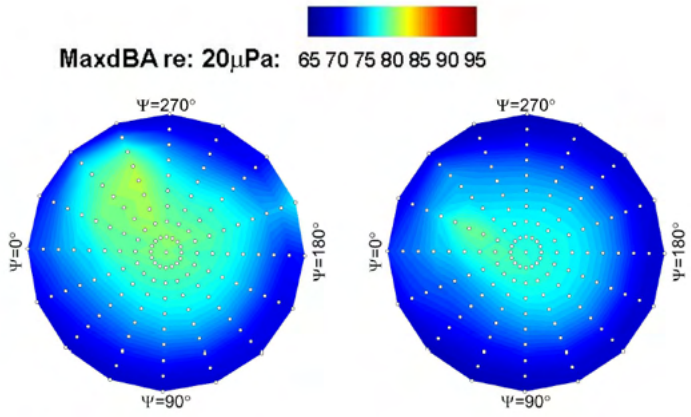

(a) 3 degree descent total noise prediction (b) 4.5 degree descent total noise prediction

Figure 7. Comparison of the total maximum dBA of descent cases for the S-76D over a hemisphere. The hemisphere has been distorted by using constant elevation spacing to better show the contours at the top edge of the hemisphere near an elevation angle of 0˚.

Left and right turn cases with multiple bank angles were also modeled with the noise prediction system. Both the Bell 205 and S-76 models yielded results regarding the changes in noise caused by these maneuvers. A normalization method was

developed and implemented to remove the effects of distance from noise predictions to show peak noise levels in a ground noise contour as a turn was performed. Figure 8 shows the noise predictions for a Bell 205 performing various bank angle turns with this normalization method. Note that the transitions of entering or leaving the turn produced the highest noise levels in the predictions.

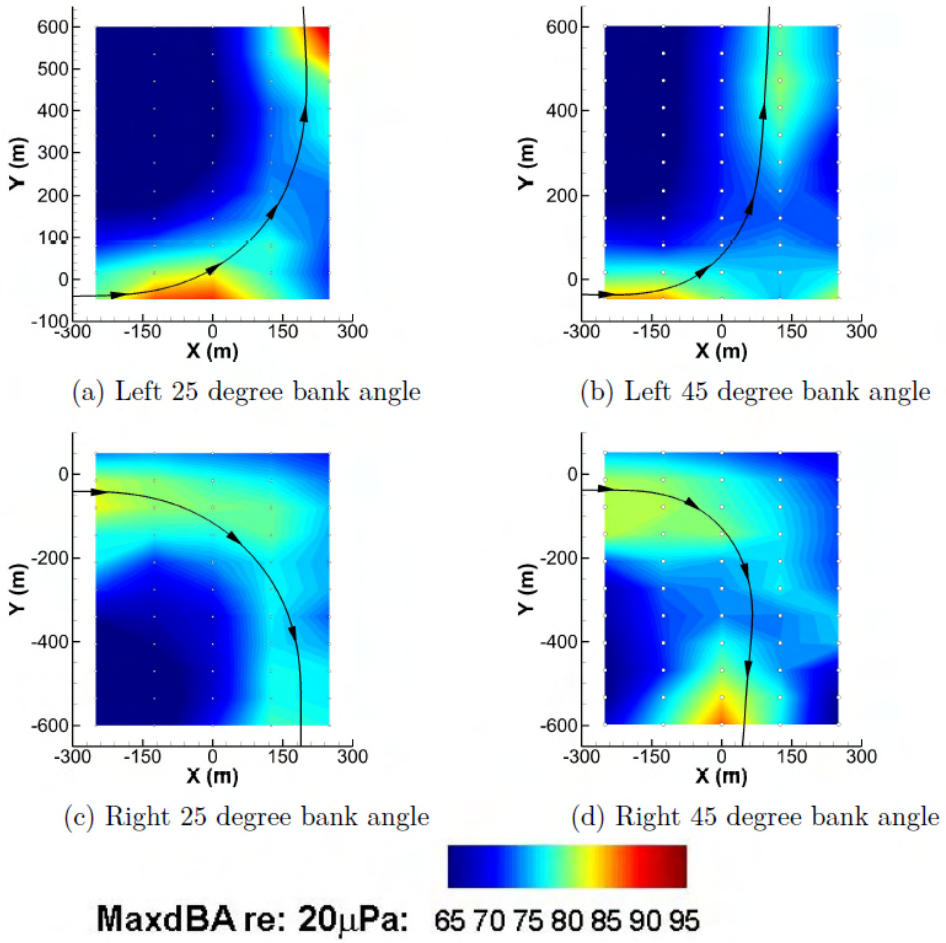

Figure 8. Comparison of maximum dBA ground noise contours for various turns and bank angles in the Bell 205.

Publications

Zachos, D. R. (2022). Noise prediction for helicopter noise abatement and EVTOL design [M.S. thesis, The Pennsylvania State University]. Manuscript in preparation.

Outreach Efforts

None

Awards

None

Student Involvement
Damaris R. Zachos, a graduate assistant at Penn State, postprocessed the flight test data for this task, added the capability to scale Pegg broadband noise predictions, implemented distance normalization to turning noise predictions, and generated and evaluated much of the processed flight test data to determine key noise aspects during various maneuvers.

Plans for Next Period
More maneuvering flight trajectories need to be modeled to better understand what happens to the noise of a helicopter as maneuvers are performed. Descents at different flight speeds and flight path angles must be modeled to determine an optimal descent rate for low-noise procedures. Additional runs are also needed for turns to evaluate the changes in noise induced at various flight speeds and flight path angles. The variability included in the 2019 flight test data must also be quantified to determine which noise abatement procedures can reliably be implemented by pilots.

Task 20 - Develop a Method for Coupling the Noise Prediction System with FAA Noise Prediction and Analysis Tools
The Pennsylvania State University

Objective
In this task (Task 8.3 in the 2020–2021 proposal), the goal is to increase the usability of the noise prediction system for the FAA and Volpe by creating tools to allow PSU-WOPWOP outputs in the Volpe Advanced Acoustic Model (AAM) format. The tool will be written in the Fortran language. This tool will then be included within PSU-WOPWOP in close collaboration with FAA/Volpe to ensure that the workflow and outputs are in the desired form for use with AAM.

Research Approach
The noise prediction system developed and validated in Projects 6 and 38 provides significantly more detailed noise and component analyses than is needed for routine noise assessment and abatement procedure analysis. However, the system has the unique capability to predict the noise from existing helicopter models for which noise measurements are not available in part or at all. Furthermore, notional aircraft or innovative changes to a helicopter can be analyzed because the noise prediction is a first-principles physical model. This capability could be more fully utilized if there were a more streamlined process to provide information in the correct format for FAA/Volpe tools, particularly AAM. It is anticipated that we will work closely with the Volpe Center to ensure that the correct format files are produced by the noise prediction system and that the process is efficient.

Milestone(s)
The milestones for this task are (a) creation of a tool external to PSU-WOPWOP in Fortran, (b) direct merging of the tool into PSU-WOPWOP, and (c) creation of documentation and training for the tool for use by FAA/Volpe.

Major Accomplishments
Initial coordination with Volpe was established, and Volpe provided AAM documentation to PSU to help develop the NetCFD file format used by AAM. PSU also obtained a site license for AAM so that testing can occur at PSU before the tool is sent to Volpe for testing. Finally, as part of another project, a tool was developed to convert PSU-WOPWOP output into AAM format, but this tool has not been well documented and is not ready for inclusion in PSU-WOPWOP.

Publications
None

Outreach Efforts
None

Awards
None

Student Involvement
Lauren Weist, a graduate assistant currently working toward her master's degree at Penn State, took over as the lead graduate researcher in 2021 and will develop a method for coupling the noise prediction system and the FAA/Volpe AAM tool.

Plans for Next Period
An existing tool written in the D coding language, developed as part of another project, will be updated. This step will guide the development of a Fortran language tool external to PSU-WOPWOP. Because the new code will be written in Fortran, once it is operational, it will be encapsulated in a Fortran module and incorporated in PSU-WOPWOP for ease of use within the noise prediction system. FAA/Volpe feedback will be sought to ensure that the most-needed features for Volpe are easy to use.

Task 21 - Continue Efforts to Develop Noise Abatement Flight Procedures for Various Helicopter Classes
The Pennsylvania State University

Objective
This task (Task 8.4 in the 2020–2021 proposal) will continue the development of noise abatement procedures. Based on the understanding developed by analyzing and predicting flight test noise procedures, potential new noise abatement strategies can be evaluated and demonstrated through simulations. The process will be documented and will provide a basis for future low-noise operational guidelines.

Research Approach
Following the validation of noise predictions with 2019 FAA/NASA flight test data (Task 18), the prediction system has been validated for multiple maneuvers. Using both predicted and experimental data, a flight path optimizer tool will be created to develop flight paths with the lowest noise. Optimal flight paths will be tested in the noise prediction system to verify that the noise is minimized. Predictions from these generated flight paths will yield new insight about noise abatement procedures for different size-class aircraft. Evaluations of noise results from these optimized flight paths will be compared against flight path recommendations from the Fly Neighborly guide to update the guidance as needed.

Milestone(s)
The milestones for this task are (a) creation of a noise-optimized flight trajectory generator, (b) evaluation of noise metrics for fully simulated flight test cases, and (c) recommendation of noise abatement flight maneuvers for aircraft.

Major Accomplishments
The flight path generation code created in August 2020 set the groundwork for a noise-optimized trajectory generator, which will be used to determine optimal noise abatement maneuvers. Preliminary work, which will incorporate the ability to turn in this command generation code, was continued in 2021. This code was used in 2021 to generate a simulated 80-knot level flight trajectory for several aircraft from 2017 and 2019 flight tests (see Figure 9). Preliminary tests have been performed using this tool to evaluate predicted noise from a simulated descent flight path, which is the next step for the maneuvering noise prediction tool.

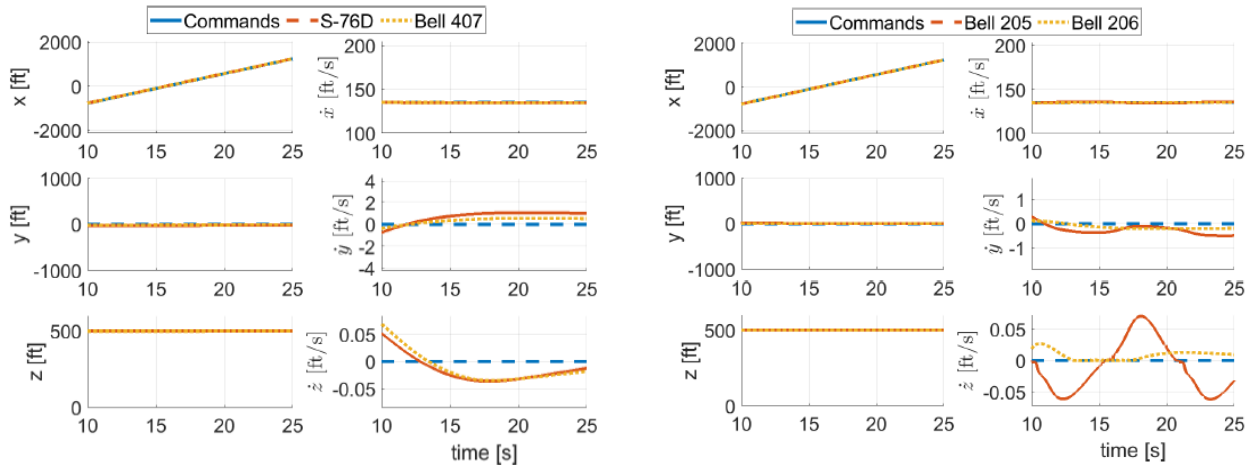

Figure 9. Results for an 80-knot simulated trajectory for S-76, Bell 407, Bell 205, and Bell 206.

Publications
None

Outreach Efforts
None

Awards
None

Student Involvement
Damaris R. Zachos, a graduate assistant at Penn State, used the tool to simulate level flight procedures and started the evaluation of noise prediction for aircraft using the descent flight path planning code.

Plans for Next Period
Further development of the waypoint trajectory generator will be needed to perform more complicated maneuvers and to add the capability to optimize the flight path based on noise results. An in-depth analysis of the changes in noise sources during each point in a maneuver is also required to determine which sound sources may be causing high noise levels. This information should be included in an optimizer tool for determining low-noise flight maneuvers. Evaluations of the effects of pilot commands on generated noise may also be assessed.

Task 22 - Develop Documentation and Training Materials for the Noise Prediction System

The Pennsylvania State University

Objective

In this task (Task 8.5 in the 2020–2021 proposal), we will develop documentation and collect other available information for applying the noise prediction system. Sample test cases will be developed for use in a training course. This material could be taught in a small class setting (perhaps at Volpe) or used as self-study materials by FAA, Volpe, or other designated persons.

Research Approach

As we work to use the noise prediction system to evaluate simulated helicopter noise, we will create documentation about the program's use, significant debugging issues, and necessary knowledge for use. Training documentation in both written and presentation form will be created to better enable a new user to start using the necessary programs.

Milestone(s)

The milestones for this task are (a) documentation of the steps necessary to use the noise prediction system, (b) identification and documentation of common mistakes made when using the noise prediction system, and (c) a description of acoustic knowledge that will help users understand the results provided by the system.

Major Accomplishments

A guide for helping new students at Penn State on the use of the PSU noise prediction system was written, which documents the steps necessary to install and use PSUHeloSim, CHARM, and PSU-WOPWOP at Penn State. The information contained within was tested when the new graduate assistant for Project 38, Lauren Weist, was introduced to the project. Any omissions in information during the installation and first use of the program were identified and added to the guide.

New debugging and common mistakes were documented while generating many of the noise prediction models necessary to progress on Tasks 18, 19, and 21. These issues were documented, and resolutions were recorded. A first attempt at the basic principles summary for effectively operating these tools was included in Damaris Zachos' master's thesis. As more prediction models are generated, the documentation will be updated and refined.

Publications

Zachos, D. R. (2022). Noise prediction for helicopter noise abatement and EVTOL design [M.S. thesis, The Pennsylvania State University]. Manuscript in preparation.

Outreach Efforts

None

Awards

None

Student Involvement

Damaris R. Zachos, a graduate assistant at Penn State, created a "Getting Started" guide for Penn State users and conducted the training for Lauren Weist based on this guide. Zachos also wrote a summary of the necessary helicopter aero-acoustics knowledge necessary for correct use of these modeling tools.

Plans for Next Period

As more users request access to the noise prediction system, Penn State will provide training and consultation when necessary. New errors and issues will be documented and resolved as more companies and users begin to use the tools.

Project 039 Naphthalene Removal Assessment

Massachusetts Institute of Technology

Project Lead Investigator

Steven R. H. Barrett
Professor of Aeronautics and Astronautics
Department of Aeronautics and Astronautics
Massachusetts Institute of Technology
77 Massachusetts Avenue, Bldg. 33-316
Cambridge, MA 02139
(617)-452-2550
sbarrett@mit.edu

University Participants

Massachusetts Institute of Technology

- PI(s): Professor Steven R. H. Barrett, Dr. Raymond Speth (Co-PI)
- FAA Award Number: 13-C-AJFE-MIT
- Period of Performance: July 8, 2016 to February 28, 2021
- Task(s):
    1. Preliminary screening of the naphthalene removal refining processes
    2. Calculation of process requirements and fuel composition effects for selected refining processes
    3. Estimate capital and operating costs of naphthalene removal
    4. Develop a kinetic model of polycyclic aromatic hydrocarbon (PAH) formation with fuel-composition effects
    5. Compare kinetic model results to laser flash-photolysis photoionization mass spectrometry (LFP/PIMS) experimental data
    6. Evaluate the relationship between PAH formation and aircraft particulate matter (PM) emissions
    7. Calculate air quality and climate impacts of naphthalene removal
    8. Conduct integrated cost–benefit analysis of impacts of naphthalene removal in the United States

Investigation Team

- Professor Steven Barrett (Massachusetts Institute of Technology [MIT]) served as PI for the A39 project as head of the Laboratory for Aviation and the Environment. Professor Barrett both coordinates internal research efforts and maintains communication among investigators in the various MIT research teams described below.
- Dr. Raymond Speth (MIT) served as co-PI for the A39 project. Dr. Speth directly advised students performing research in the Laboratory for Aviation and the Environment, with a focus on assessment of naphthalene removal refinery options; climate and air quality modeling; and fuel alteration life-cycle analysis. Dr. Speth also coordinated communication with FAA counterparts.
- Professor William Green (MIT) served as a co-investigator for the A39 project, as head of the Green Research Group. Professor Green advised students on work in the Green Research Group focusing on computer-aided chemical kinetic modeling of PAH formation.
- Mr. Randall Field (MIT) is the Executive Director of the MIT Energy Initiative and was a co-investigator of the A39 project. Drawing upon his experiences as a business consulting director at Aspen Technology Inc., Mr. Field provided mentorship to student researchers in the selection and assessment of naphthalene removal refining options and process engineering in general.
- Mr. Drew Weibel (MIT) was a graduate student researcher in the Laboratory for Aviation and the Environment. Mr. Weibel was responsible for conducting selection and assessment of naphthalene removal refining options; calculation of refinery process requirements and fuel composition effects from selected processes; estimation of capital and operating costs of naphthalene removal processes; air quality and climate modeling; and integrated cost–benefit analysis.
- Mr. Lukas Brink (MIT) was a graduate student researcher in the Laboratory for Aviation and the Environment. Mr. Brink was responsible for the development of a combustor model quantifying the effect of naphthalene removal on soot emissions, and the use of this model to assess air quality and climate impacts of naphthalene removal.

- Dr. Mica Smith (MIT) was a postdoctoral associate in the Green Research Group. Ms. Smith was responsible for the experimental measurements being used for the validation of the chemical kinetic mechanisms.
- Dr. Agnes Jocher (MIT) was a postdoctoral associate in the Green Research Group. Ms. Jocher was responsible for evaluating microphysical models that link the presence of PAH molecules to the formation of soot particles and for providing modeling expertise in combining these models with the kinetic models being developed.

Project Overview

The composition of aviation fuels affects the formation of pollutants that contribute to climate change and to reduced air quality that leads to adverse health impacts, including an increased risk of premature mortality. The objective of this project was to assess the societal costs and benefits of removing naphthalenes from jet fuel produced in the United States. Removal of naphthalene by extractive distillation has been found to be less expensive than hydrotreatment. Hydrotreatment has the additional effect of removing sulfur from the fuel, while fuel processed by extractive distillation has larger reductions in nvPM emissions. The largest environmental benefits come from reductions in air quality damages due to sulfur emissions, although the removal of sulfur also results in a net warming effect on the climate. The climate benefits due to reductions in nvPM emissions are mainly associated with reductions in contrail radiative forcing (RF). However, this benefit is more than offset by the increased CO_2 emissions required for the naphthalene removal processes. These results suggest that naphthalene removal on a nationwide basis is unlikely to be cost beneficial with either extractive distillation or hydrotreatment. However, naphthalene removal could be beneficial under certain circumstances, for example, if applied to fuels used at individual airports with particular air quality concerns, or if used at times and locations where the formation of warming contrails is most likely.

References

Brem, B. T., Durdina, L., Siegerist, F., Beyerle, P., Bruderer, K., Rindlisbacher, T., Rocci-Denis, S., Andac, M. G., Zelina, J., Penanhoat, O., & Wang, J. (2015). Effects of fuel aromatic content on nonvolatile particulate emissions of an in-production aircraft gas turbine. Environmental Science and Technology *49*, 13149–13157.

Moore, R. H., Shook, M., Beyersdorf, A., Corr, C., Herndon, S., Knighton, W. B., Miake-Lye, R., Thornhill, K. L., Winstead, E. L., Yu, Z., Ziemba, L. D. & Anderson, B. E. (2015). Influence of jet fuel composition on aircraft engine emissions: A synthesis of aerosol emissions data from the NASA APEX, AAFEX, and ACCESS missions. Energy Fuels *29*, 2591–2600.

Task 1 - Preliminary Screening of the Naphthalene Removal Refining Processes

Massachusetts Institute of Technology

Objective

Naphthalene is present at varying levels in the straight-run crude oil distillation cuts used to produce jet fuel and is currently not targeted for removal in the treatments used to meet industry standard fuel specifications. Consequently, reducing the naphthalenic content in jet fuel requires the introduction of an additional refinery treatment process. The objective of this task is to identify suitable refinery processes that could be used to remove or convert naphthalenes. Once identified, data for key refining process parameters will be collected to inform future cost estimation of applying the selected processes for jet fuel naphthalene removal.

Research Approach

Introduction

Refining processes, and chemical processes in general, are focused on subjecting chemical species to various environments to allow for conversion, combination, separation, etc. thus yielding useful products with increased value. When considering removal of a chemical component from a mixture, e.g., naphthalenic species from a kerosene feed, a process designer must consider the unique properties shared by the chemical component that allow for its conversion, combination, separation, etc. without affecting the underlying mixture.

Although naphthalenes are not currently targeted for removal to meet industry standards, several mature refining technologies, once tuned, could perform this reduction or removal with high efficiency. We selected suitable, readily accessible refining technologies for the removal of naphthalenes from the U.S. jet pool. Our focus is on technologies currently used in industry, to determine possible policies that could be implemented in the near term.

Methods

To select various refining processes for the large-scale removal of naphthalenes from the U.S jet fuel pool, we completed a literature review of current technologies, then performed a qualitative evaluation of those technologies in terms of their applicability to naphthalene removal, the scope of economic and process data available, and the level of naphthalene removal achievable. Particular attention was paid to preserving non-naphthalenic aromatic compounds, because reducing the amounts of these components would limit the ability to blend paraffinic alternative jet fuels while still meeting the minimum requirements for aromatics.

To evaluate each candidate process, we leveraged the existing literature to estimate the utility requirements (e.g., process fuel, electricity, or hydrogen) for each process, the effect on the composition of the resulting jet fuel, and the capital costs of new refinery equipment required. We included the effects of any potentially necessary pre-processing. We then compared processes side-by-side to demonstrate the trade-offs associated with naphthalene removal at the refinery.

In analyzing a range of different refining pathways, we will also be able to assess the tradeoffs associated with different levels of naphthalene removal. Those efforts, together with ongoing work regarding the relationship between jet fuel composition and PAH formation, will allow us to assess the level at which naphthalenes should be removed to optimize costs and benefits.

Results

This task concluded with the selection of extractive distillation and selective hydrotreating as candidate refinery processes for the large-scale removal of naphthalenes from the U.S. jet fuel pool.

Naphthalenes are unsaturated, double-ring aromatic species, that may contain alkylated or impurity groups. They are most readily removed via conversion to mono-aromatic or saturated species—via hydrogen addition or carbon removal—or separated on the basis of polarity. A desired refinery process would remove naphthalenic species with high efficiency without affecting the remaining aromatic content, would result in minimal changes to other fuel properties, and would produce limited emissions and economic impact; the removal of other impurities (e.g., sulfur or nitrogen) would also be preferable. A list of potential refining processes is shown in Figure 1 (Gary et al., 2007).

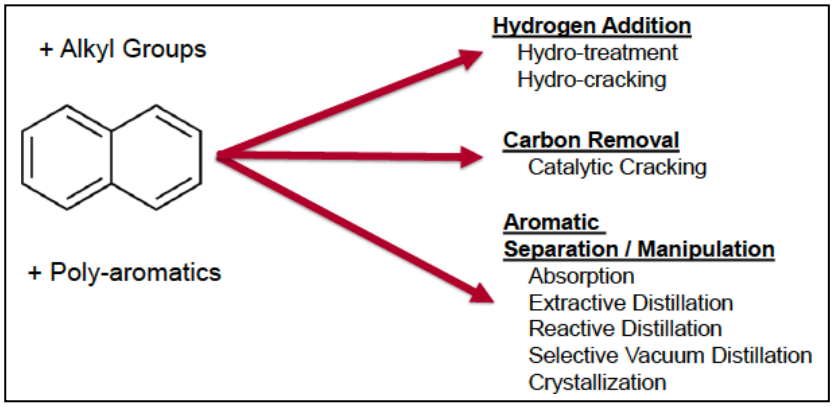

Figure 1. Categories of potential processes for naphthalene removal.

As noted, three families of processes are pertinent to the removal of naphthalenes: conversion by hydrogen addition (saturation), conversion by carbon removal (cracking), and aromatic separation. Hydrogen addition and aromatic separation are often used as finishing processes and can be performed under mild conditions. Carbon removal, in contrast, is often associated with molecular cracking, has the potential to radically convert the feed, is associated with the production of olefins, and often cannot break apart stable aromatic rings. As a result, only hydro-conversion and aromatic separation processes were considered.

Hydro-conversion processes are a family of refining units that react a petroleum feed with gaseous hydrogen at elevated temperatures and pressures to saturate—and in severe processes, crack—hydrocarbon molecules. Hydrotreating is a mild hydro-conversion finishing process used to remove impurities and saturate olefin and aromatic species. Selective hydro-treating for the conversion of naphthalenes is a viable process candidate because the second ring of naphthalenic species tends to be fully saturated before the saturation of mono-aromatic species. Because of the relative selectivity of fuel

components, we also expect desulfurization and di-nitrogenation to occur. As a result, with a robust catalyst selection and finely tuned process parameters, we expect that a selective hydrotreating process could reduce or remove naphthalenes by converting them to mono-aromatics, while resulting in little change to the overall aromatic content and other fuel characteristics, and having reasonable hydrogen requirements (Fahim et al., 2009).

Separation processes enable mixtures to be divided into their components according to defining species characteristics, such as weight, size, polarity, etc. Extractive distillation enables the separation of petroleum components based on polarity, by introducing a heavy, high-boiling point polar solvent to the feed. Highly polar components, including all aromatic and impurity-containing species, will bind to the solvent and be separated from other species according to weight. The solvent is then separated by simple distillation. Finally, mono-aromatic and naphthalene species can be roughly separated in a second distillation step, and the prior cut is returned to the feed. Extractive distillation, although less common for feed mixture separations, was identified as a second candidate for naphthalene removal from the U.S. jet fuel pool (Meyers, 2004).

After selection of extractive distillation and selective hydrotreating as candidate refining processes for the removal/reduction of naphthalene from the U.S. jet fuel pool, we collected further details on each process to define their offsite needs and fuel composition impacts. Table 1 shows the relevant process requirements and fuel effects.

Table 1. Process requirements and fuel impacts for hydrotreatment and extractive distillation.

Process Name	Hydrotreatment	Extractive Distillation
Description	Hydrogenation of naphthalenes to mono-aromatic and cyclo-paraffinic components	Separation of all aromatics via a polar solvent; separation of mono-aromatics from naphthalenes via distillation and subsequent blending back into the jet fuel product
Process Type	Conversion (H_2 addition)	Aromatic separation
Existing Uses	Desulfurization, impurity removal, aromatic hydrogenation	Separation of polar feed components, benzene, toluene, xylene (BTX) separation
Removal of Naphthalenes	Assumed 95% efficient	Assumed 95% efficient
Effect on Mono-Aromatics	Limited (<10%) hydrogenation	Fully separated; fraction returned to product can be controlled
Impurity Removal	S and N removal to < 50 ppm	Little removal of S and N impurities
Supporting Processes Required	Hydrogen production, sulfur gas removal, sulfur post-treatment, steam generation and cooling facilities	Naphthalene/mono-aromatic post distillation, steam generation and cooling facilities
Process Innovation Required	Minimal required; very similar to existing units	Efficient solvent with impurity (S and N) resiliency

Milestone

This task concluded with the selection of extractive distillation and selective hydrotreating as candidate refinery processes for the large-scale removal of naphthalenes from the U.S. jet fuel pool. The results were described in a presentation provided to the FAA on February 28, 2017.

Major Accomplishments

During this period, two refining processes—selective hydrotreating and extractive distillation—were chosen as suitable candidates for large-scale naphthalene removal from the U.S. jet fuel pool. A summary of this work is contained in the Deliverable 1 presentation provided to the FAA on February 28, 2017.

Publications

Weibel, D. (2018). Techno-economic assessment of jet fuel naphthalene removal to reduce non-volatile particulate matter emissions [S.M. thesis, Massachusetts Institute of Technology]. DSpace@MIT. https://hdl.handle.net/1721.1/124174

Outreach Efforts

ASCENT advisory board presentations/posters (April 2017, September 2017, and April 2018)

Student Involvement

Drew Weibel, a Master's student in the Laboratory for Aviation and the Environment, worked directly with Professor Steven Barrett and Dr. Raymond Speth to conduct the research objectives of Task 1.

References

Gary, J. H., Handwerk, G. E., & Kaiser, M. J. (2007). *Petroleum refining: Technology and economics* (5th ed.). CRC Press.

Fahim, M. A., Al-Sahhaf, T., & Elkilani, A. (2009). *Fundamentals of petroleum refining*. Elsevier Science.

Meyers, R. (2004). *Handbook of petroleum refining processes* (3rd ed.). McGraw-Hill.

Task 2 - Calculation of Process Requirements and Fuel Composition Effects for Selected Refining Processes

Massachusetts Institute of Technology

Objective

In Task 1, selective hydrotreating and extractive distillation were selected as candidate refinery processes for large-scale reduction or removal of naphthalene from the U.S. jet fuel pool. In addition, data were collected regarding the offsite (or supporting process) requirements and fuel composition effects of each process.

The objective of this task was to continue quantitative analysis of both processes to develop simplified estimation models of process requirements and fuel composition effects. The result of this task will be cost estimation for individual selective hydrotreating and extractive distillation refinery units, modeled as brown-field additions to existing refinery operations.

Research Approach

Methods

Based on the process parameters defined as part of Task 1, utility requirements and capital cost data were collected for distillate hydro treating, extractive distillation, and their supporting processes. The supporting processes of selective hydrotreating are steam methane reforming for hydrogen production, amine separation for hydrogen sulfide separation from off-gasses, and the Claus process for sulfur recovery. Because these supporting processes are often connected to several units at a refinery, costs were determined based on both the size of the modelled refinery and the capacity of the modelled hydro-treatment unit. The sole supporting process for extractive distillation is post-distillation.

To calculate the net present value (NPV) of an added refinery finishing process for the reduction or removal of naphthalene from jet fuel, the methods described by Gary et al. (2007) were adopted. Fixed capital investment was estimated from the desired process capacities and the collected cost data. Operating cost was calculated as a function of the fixed costs, and as a function of the utility requirements and estimated utility costs (depicted in Figure 2). Catalyst/solvent and process water utility costs were assumed to be constant (Gary et al. 2007, Peters et al., 2003). Historical and predicted natural gas and electricity prices, by U.S. census region, were taken from the U.S. Energy Information Administration. We used an autoregressive moving average model, calibrated to the predicted trend and historical price variations, to estimate natural gas and electricity prices stochastically. The NPV was then calculated with a discounted cash flow rate of return (DCFRoR) model over the lifetime of the process unit. A discount factor of 2.74%, according to the 20-year constant maturity rate, was used for the estimated cost to society.

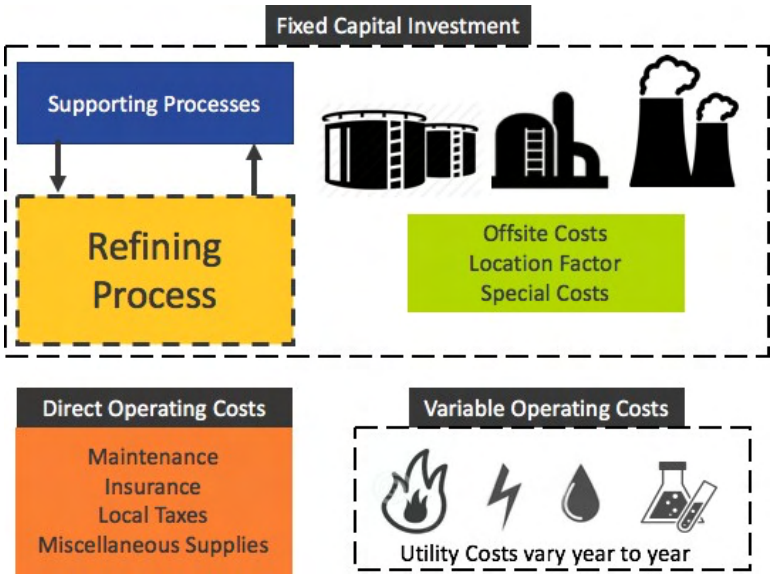

Figure 2. Schematic of factors affecting costs of refinery processes.

Results
The model successfully estimated the cost of the reduction or removal of naphthalene from U.S. jet fuel via operation of an additional finishing process (either selective hydrotreating or extractive distillation) at U.S. refineries. Preliminary cost data were presented in the Deliverable 3 presentation provided to the FAA on August 31, 2017.

Milestone
This work was completed in August 2017 and is summarized in the Deliverable 1-3 presentation provided to FAA on August 31, 2017.

Major Accomplishments
During this period, a simplified model was created for the purpose of cost estimation of individual selective hydrotreating and extractive distillation process units. This model included effects on fuel composition, utility requirements, and estimated costs over the lifetime of the unit. Results collected from the discounted cash flow model are presented as the NPV of the unit over its lifetime. A summary of this work is contained in Deliverable 1-3, provided to the FAA on August 31, 2017.

Publications
Weibel, D. (2018). Techno-economic assessment of jet fuel naphthalene removal to reduce non-volatile particulate matter emissions [S.M. thesis, Massachusetts Institute of Technology]. DSpace@MIT. https://hdl.handle.net/1721.1/124174

Outreach Efforts
- ASCENT advisory board presentations/posters (September 2017, April 2018, and October 2018)
- Presentation at the Coordinating Research Council Aviation Meeting (May 2018) titled “Naphthalene Removal Assessment: Cleaning up Jet Fuel for Reduced Environmental Impacts”
- Presentations at the Aviation Emissions Characterization (AEC) Roadmap Annual Meetings (May 2018 and May 2020)

Student Involvement
Drew Weibel, a Master’s student in the Laboratory for Aviation and the Environment, worked directly with Professor Steven Barrett and Dr. Ray Speth to conduct the research objectives of this task.

References

Gary, J. H., Handwerk, G. E., & Kaiser, M. J. (2007). *Petroleum refining: Technology and economics* (5th ed.). CRC Press.
Peters, M. S., Timmerhaus, K. D., & West, R. E. (2003). *Plant design and economics for chemical engineers*. (5th ed.). McGraw-Hill.

Task 3 - Estimate Capital and Operating Costs of Naphthalene Removal

Massachusetts Institute of Technology

Objective

The objective of this task was to evaluate refinery technologies that could be used to remove naphthalene, and to determine their feasibility, costs, and effects on fuel composition. This process included calculating the costs of constructing new refinery unit processes and determining additional utility and other operating costs associated with using the process units responsible for naphthalene removal.

Research Approach

Naphthalene is present at varying levels in the straight-run crude oil distillation cuts used to produce jet fuel. For cuts exceeding the 3% volume limit on naphthalenes (ASTM D1655 2016), this excess can be resolved solely through blending, because the average naphthalene content of commercial Jet A fuel is ~1.4% (DLA Energy 2013). Reducing or eliminating the naphthalene content of jet fuel would therefore require the introduction of additional refinery processing. After reviewing several candidate refining processes in the prior year of this project, we decided to further explore two processes in detail: selective hydrotreatment and extractive distillation. These processes are used in industry for the reduction or separation of aromatics, and they show promise in their ability to reduce and remove naphthalene from jet fuel. Selective hydrotreatment reacts hydrogen with the feedstock and leads to the removal of impurities and saturation of aromatic compounds. Extractive distillation allows for the full separation of aromatics from the feedstock via polar solvents. The aromatics stream can then be processed to separate mono-aromatics and naphthalenes, and the former stream is then returned to the jet fuel blending pool. These processes were chosen because of their low added complexity and energy, and their minimal effect on the resultant fuel properties. However, changes in fuel density, specific energy, fuel sulfur content, hydrogen content, and aromatic content will occur and were considered.

We have developed fundamental process models to estimate the effects of fuel constituents and completed a literature search to collect data on process energy requirements, capital costs, and operating costs for both hydrotreatment and extractive distillation. To evaluate each candidate process, we leveraged the existing literature to estimate the utility (e.g., process fuel, electricity, or hydrogen) requirements for each process, the effect on the composition of the resulting jet fuel, and the capital costs of new refinery equipment required, including the effects and costs of pre-processing and auxiliary process units that might be required. We then compared processes side by side to demonstrate the trade-offs associated with naphthalene removal at refinery.

We considered the hypothetical adoption of a policy whereby jet fuel naphthalene content in the U.S. is reduced by 95% via either hydrotreatment or extractive distillation, at each of the 116 operational U.S. refineries with capacities > 1,000 barrels per day (BPD). We calculated costs using a stochastic discounted cash flow model of each refinery. Refinery capital costs were calculated using standard cost curve estimation methods, which relate process unit costs to capacity. Cost curves were used for both the primary naphthalene-removing process units (e.g., extractive distillation column or hydrotreater) as well as auxiliary process units (e.g., steam-methane reformer, Claus sulfur recovery unit, pressure-swing hydrogen recovery units, and steam generators). Direct operating costs included maintenance, local taxes, insurance, and supplies, calculated as a percentage of capital costs. Variable operating costs, such as process water and chemicals, were calculated according to the process unit utility requirements. The stochastic refinery model was used to determine the NPV of each naphthalene removal process over its operating lifetime. The NPV could also be used to calculate the cost premium (i.e., cents per gallon) associated with the production of naphthalene-free fuel. Cost estimates were considered from two perspectives: that of the fuel market and that of society. The market perspective involved computation of cost premiums including all cash flows incurred by fuel producers, by estimating the expected increase in the market price for naphthalene-free jet fuel. The societal cost estimate was computed from a resource-based perspective, placing it on the same basis as the monetization of potential benefits from improved air quality and potential climate impacts. From that perspective, redistribution of resources, e.g., taxes or loan payments, was disregarded, and the discount rate was assumed to be equivalent to society's long-term cost of capital.

Milestone

The work completed for this task was documented in Deliverable 2-1, provided to the FAA on November 30, 2017.

Major Accomplishments

The resource-based (societal) cost premium and market cost premium estimate distributions for a policy in which all U.S.-produced jet fuel has its naphthalene content reduced by 95% (to 0.06 vol%) are shown in Figure 3, with cost data presented in 2016 USD. The mean societal cost premium was found to be 2.4 cents/liter (95% confidence interval (CI): 2.0–2.7) for hydrotreating and 1.7 cents/liter (95% CI: 1.5–1.0) for extractive distillation.

The mean market cost premium of hydrotreating was found to be 3.1 cents/liter (95% CI: 2.4–3.7), and that for extractive distillation was found to be 2.1 cents/liter (95% CI: 1.7–2.5). Given that the average U.S. Gulf Coast cost of jet fuel in 2016 was $0.33/liter, this represents a 9% and 6% increase in the cost of jet fuel for naphthalene removal via hydrotreatment and extractive distillation, respectively.

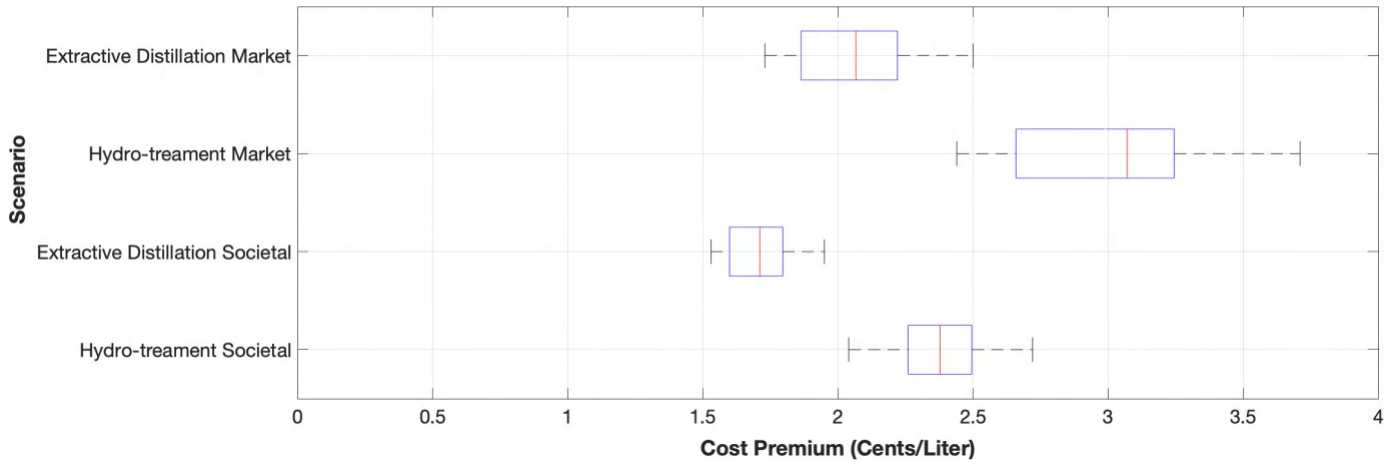

Figure 3. Box plot showing the societal and market cost premiums of hydrotreatment and extractive distillation. All values are in cents/liter. Red markers represent the distribution means, blue boxes represent the first and third quartiles, and whiskers represent the 95% CI.

Publications

Weibel, Drew (2018). Techno-economic assessment of jet fuel naphthalene removal to reduce non-volatile particulate matter emissions [S.M. thesis, Massachusetts Institute of Technology]. DSpace@MIT. https://hdl.handle.net/1721.1/124174

Outreach Efforts

- ASCENT advisory board presentations (September 2017, April 2018, and October 2018)
- Presentation at the CRC Aviation Meeting (May 2018) titled “Naphthalene Removal Assessment: Cleaning up Jet Fuel for Reduced Environmental Impacts”
- Presentation at the AEC Roadmap Annual Meeting (May 2018 and May 2020)
- Presentation at the CAEP/12-WG3/2 meeting (October 2019) titled “Economic and Environmental Assessment of Jet Fuel Naphthalene Removal”

Student Involvement

This task was conducted primarily by Drew Weibel, a Master’s student in the Laboratory for Aviation and the Environment, working directly with Professor Steven Barrett and Dr. Raymond Speth.

References

ASTM. (2016) *D1655: Standard Specification for Aviation Turbine Fuels*. ASTM International. https://doi.org/10.1520/D1655-16C

DLA Energy. (2013). Petroleum quality information system 2013 annual report (Report No. ADA619019). Defense Logistics Agency, Fort Belvoir, VA.

Task 4 · Develop a Kinetic Model of PAH Formation with Fuel Composition Effects

Massachusetts Institute of Technology

Objective

The formation of black carbon (soot) from hydrocarbon fuels can be considered to occur in two stages. First, fuel components and combustion intermediates react to form polycyclic aromatic hydrocarbons (PAHs). Subsequently, large PAHs act as soot nuclei, which grow as they absorb both PAH and other species, coagulate through collisions with other soot particles, carbonize, and partially oxidize (Richter and Howard, 2000). The details of fuel composition mainly affect the first step of this process, the formation of PAHs. In this project, we used the Reaction Mechanism Generator (RMG) to develop a detailed chemical kinetic mechanism for jet fuel combustion including the formation of PAH (Gao et al., 2016).

The objective of this task was to update the RMG algorithm to accommodate aromatic species, and to include aromatic reactions up to three-ring species, for use as identifiers for soot precursors in later models. The updates to RMG also underwent preliminary validation according to experimental results from shock-tube pyrolysis and co-pyrolysis studies.

Research Approach

Introduction

RMG (http://rmg.mit.edu) is an automatic chemical reaction mechanism generator that constructs kinetic models composed of elementary chemical reaction steps using a general understanding of how molecules react. This tool provides a powerful method to computationally identify reaction mechanisms and ensure full coverage of pertinent species and reactions according to the current literature. RMG has been used to analyze various fuels including JP-10 and di-isopropyl ketone combustion and pyrolysis (Gao et al., 2015; Allen et al., 2014).

We will add updates to the RMG algorithm to accurately accommodate aromatic species, and to include aromatic reactions up to three-ring species, which will be used as identifiers for soot precursors in later models.

Method

Previously, RMG was unable to robustly represent aromatic structures. The algorithm depended primarily on representations using Kekulé structures, thus resulting in their incorrect treatment as aliphatic species. To correctly represent aromatic species, RMG was updated to generate Clar structure representations of PAHs. As result, aromatic species are more clearly differentiated from aliphatic species, and the number of representations has been reduced in many cases. An example of the decreased number of representations for a phenanthrene radical is shown in Figure 4.

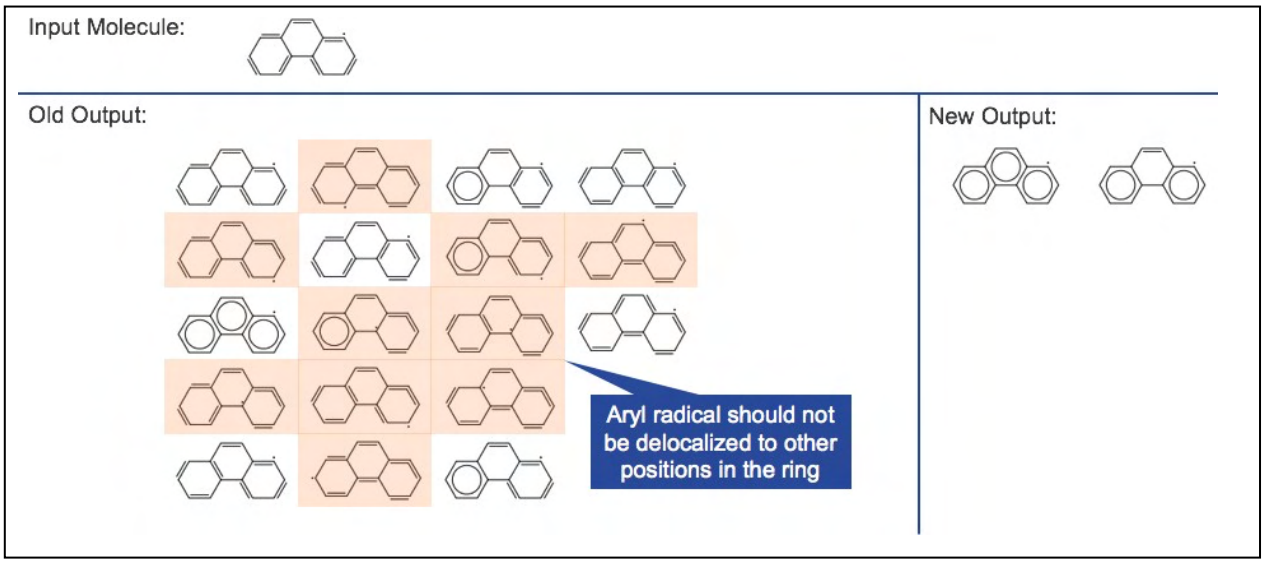

Figure 4. Kekulé and Clar structures for a phenanthrene radical.

Other changes were made to further improve the reaction rate predictions. An algorithmically challenging task of allowing aromatic bond types was completed after implementing a custom kekulization algorithm. This allows rate rules for aromatic species to be specified separately from those for aliphatic species. Moreover, ring perception was implemented for rate rules to allow for the separation of rates for linear versus cyclic species.

To validate the updates described previously, we tested the RMG model against experimental shock-tube pyrolysis data (Lifshitz et al., 2009). Additional co-pyrolysis models were also generated, although without experimental comparisons.

Results

The improvements described above successfully enabled RMG to handle aromatic species. Prior to the updates, program crashes were inevitable when modeling any aromatic system. To support the algorithm changes, new literature data for aromatic thermochemistry and kinetics were added to the database.

For preliminary validation, a model was generated for pyrolysis of 1-iodonaphthalene and acetylene for comparison to shock-tube data. The model predictions for the major products, acenaphthalene and naphthalene, matched the experimental data well, as shown in Figure 5. The RMG model predicted a higher yield of 1-ethynyl naphthalene than the literature model, although none was observed in the experiment. The RMG model also predicted smaller side products, such as vinylacetylene and 1,3-butadiene, which were not reported in the experiment, although the authors do note that small molecule products from acetylene reactions were assumed to be negligible.

Co-pyrolysis models for equimolar naphthalene or tetralin with acetylene were also generated to obtain an initial view regarding whether RMG could capture the differences in reactivity. For naphthalene and acetylene, RMG predicted the major products to be acenaphthalene and hydrogen, a finding that was initially surprising, because other PAHs such as anthracene or phenanthrene were also expected. However, these observations were corroborated by Parker et al. (2015), who have also observed that acenaphthalene is the main product, in contrast to the generally accepted hydrogen abstraction-C_2H_2 addition (HACA) mechanism for PAH growth. The model for tetralin and acetylene displayed markedly different behavior, as expected. Major products were hydrogen, naphthalene, methane, and ethene. No three-ring aromatics were formed, possibly because of the overall higher hydrogen/carbon ratio.

Overall, these modeling results are very promising and show that RMG is now much better at modeling aromatics.

Milestone(s)

This work was completed in June 2017 and is contained in the Deliverable 2 presentation provided on Jun 30, 2017.

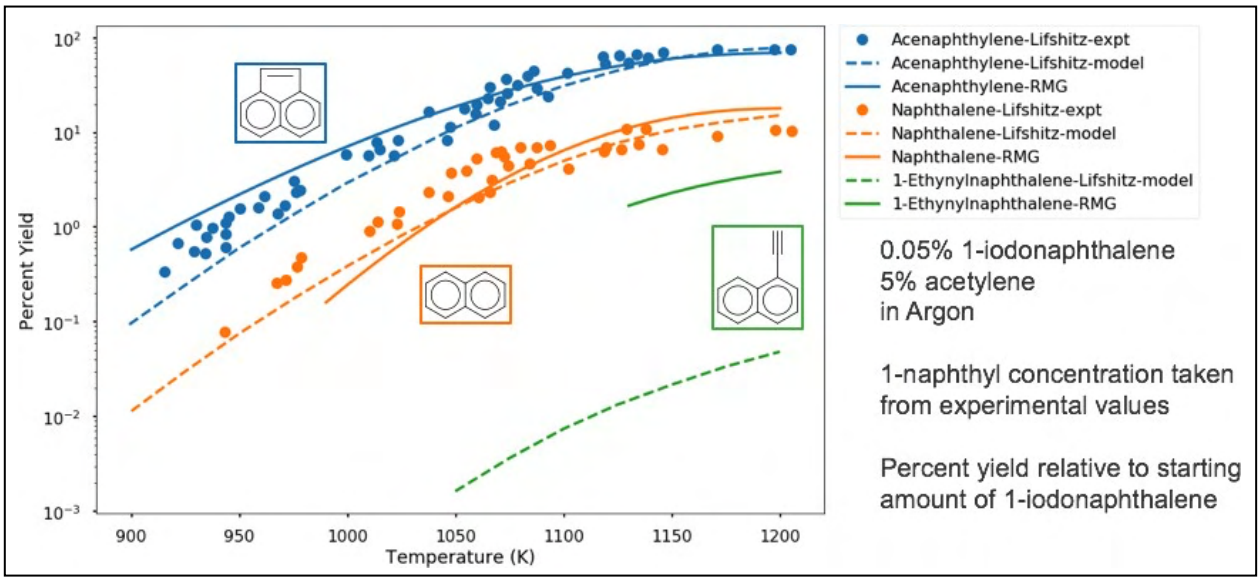

Figure 5. Comparison of yields for selected PAH species in shock tube experiments and kinetic models.

Major Accomplishments

During this period, the RMG algorithm was successfully updated to accommodate aromatic species, and kinetics data were added for aromatic species. These updates also underwent preliminary validation through comparison to experimental shock-tube pyrolysis data. A summary of this work is contained in the Deliverable 2 presentation provided to the FAA on June 30, 2017.

Publications

Liu, M., & Green, W. H. (2019). Capturing aromaticity in automatic mechanism generation software. Proceedings of the Combustion Institute, *37*(1), 575–581. https://doi.org/10.1016/j.proci.2018.06.006

Liu, M. (2020). Predictive modeling of polycyclic aromatic hydrocarbon formation during pyrolysis [Ph.D. thesis, Massachusetts Institute of Technology]. DSpace@MIT. https://hdl.handle.net/1721.1/129925

Outreach Efforts

- Presentation at the International Conference on Chemical Kinetics (May 2017) titled "Going Bigger: Capturing PAH Chemistry in RMG"
- Presentation at the Aviation Emissions Characterization (AEC) Roadmap Annual Meeting (June 2017)
- Presentation at the 37th International Symposium on Combustion (August 2018) titled "Capturing Aromaticity in Automatic Mechanism Generation Software"

Student Involvement

Mengjie (Max) Liu, a PhD student in the Green Research Group at MIT's Department of Chemical Engineering, completed the majority of the updates to the RMG, and validation and refinement of the RMG models.

References

Allen, J. W., Scheer, A. M., Gao, C. W., Merchant, S. S., Vasu, S. S., Welz, O., Savee, J. D., Osborn, D. L., Lee, C., Vranckx, S., Wang, Z., Qi, F., Fernandes, R. X., Green, W. H., Hadi, M. Z., & Taatjes, C. A. (2014). A coordinated investigation of the combustion chemistry of diisopropyl ketone, a prototype for biofuels produced by endophytic fungi. Combustion and Flame, *161*(3), 711–724. https://doi.org/10.1016/j.combustflame.2013.10.019

Gao C. W., Allen J. W., Green W. H., & West R. H. (2016). Reaction mechanism generator: Automatic construction of chemical kinetic mechanisms. Computer Physics Communications, *203*, 212–225. https://doi.org/10.1016/j.cpc.2016.02.013

Gao, C. W., Vandeputte, A. G., Yee, N. W., Green, W. H., Bonomi, R. E., Magoon, G. R., Wong, H.-W., Oluwole, O. O., Lewis, D. K., Vandewiele, N. M., & Van Geem, K. M. (2015). JP-10 combustion studied with shock tube experiments and modeled with automatic reaction mechanism generation. Combustion and Flame, *162*(8), 3115–3129. https://doi.org/10.1016/j.combustflame.2015.02.010

Lifshitz, A., Tamburu, C., & Dubnikova, F. J. (2009). Reactions of 1-naphthyl radicals with acetylene. Single-pulse shock tube experiments and quantum chemical calculations. Differences and similarities in the reaction with ethylene. Journal of Physical Chemistry A, *113*(39), 10446–10451. https://doi.org/10.1021/jp905448g

Parker, D. S. N., Kaiser, R. I., Bandyopadhyay, B., Kostko, O., Troy, T. P., & Ahmed, M. (2015). Unexpected chemistry from the reaction of naphthyl and acetylene at combustion-like temperatures. Angewandte Chemie, *54*(18), 5421–5424. https://doi.org/10.1002/ange.201411987

Richter, H., & Howard, J. B. (2000). Formation of polycyclic aromatic hydrocarbons and their growth to soot—a review of chemical reaction pathways. Progress in Energy and Combustion Science, *26*(4–6), 565–608. https://doi.org10.1016/S0360- 1285(00)00009-5

Task 5 - Compare Kinetic Model Results to LFP/PIMS Experimental Data

Massachusetts Institute of Technology

Objective

The growth of aromatic rings as part of PAH formation is controlled by radical reactions, particularly the HACA mechanism. The objective of this task was to produce experimental data that can be used to improve estimates of rate coefficients used in chemical kinetic models of PAH formation.

Research Approach

Laser flash-photolysis photoionization mass spectrometry (LFP/PIMS) is an experimental technique in which a photolysis laser pulse initiates controllable, quantifiable radicals in a temperature- and pressure-controlled reactor. The evolution of the chemical composition in the reactor is then monitored by ionization with VUV light and detection with a mass spectrometer. Experimental conditions were simulated with reactor modeling software, using rate coefficients estimated from the literature. Because these rate coefficients are often pressure dependent, quantum chemistry calculations were used to extrapolate from the low-pressure experimental values to the high pressures relevant to engine operations. Simulations using RMG-generated mechanisms were compared with rates in the literature and experimental results to improve important pathway parameters for aromatic growth.

For this task, two pathways were evaluated. The first was the addition of a vinyl radical (C_2H_3) to acetylene (C_2H_2), which is key step in a formation pathway for benzene (C_6H_6). Studying this system allowed us to confirm that we can observe ring formation in our experiment and measure the kinetics and branching ratios which describe C_4H_5/C_4H_4 formation and the yield of benzene, as shown in Figure 6.

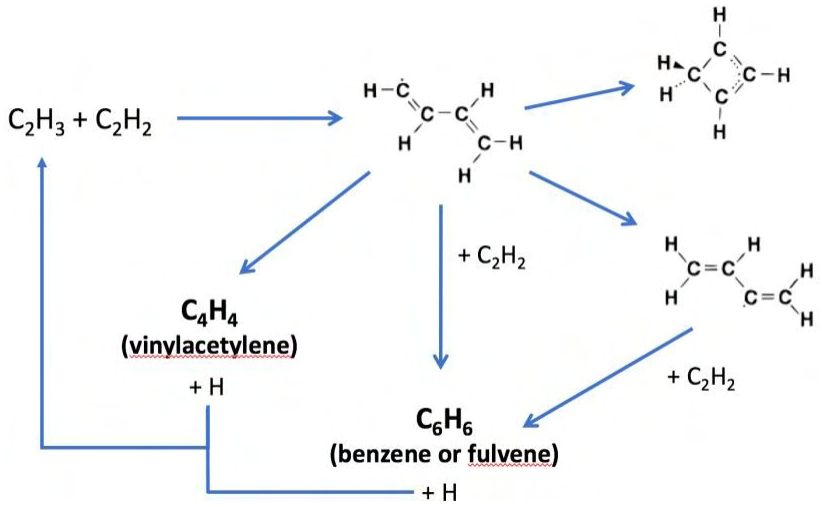

Figure 6. Formation pathways of benzene from vinyl radical and acetylene.

The second pathway explored was acetylene addition to naphthyl radicals. Although aromatic growth from naphthalene is thought to be dominated by the HACA mechanism, under experimental conditions, three-ring PAHs have generally

not been observed, thus prompting the question of what other pathways might exist that convert naphthalenes to PAHs. This question was explored with LFP/PIMS.

Milestone

The work completed for this task was documented in Deliverable 2-3, provided to the FAA on April 30, 2018.

Major Accomplishments

Results for the vinyl radical–acetylene pathway, comparing experimental time profiles with simulations, are shown in Figure 7. Kinetics calculated from LFP/PIMS were found to generally agree with the results of the RMG-generated model over a range of temperatures. Preliminary experiments for 1-naphthyl addition to C_2H_2 revealed branching between stable $C_{12}H_8$ products (e.g., acenaphthalene) and $C_{12}H_9$ adducts, as shown in Figure 8. Work to incorporate this finding into RMG is ongoing.

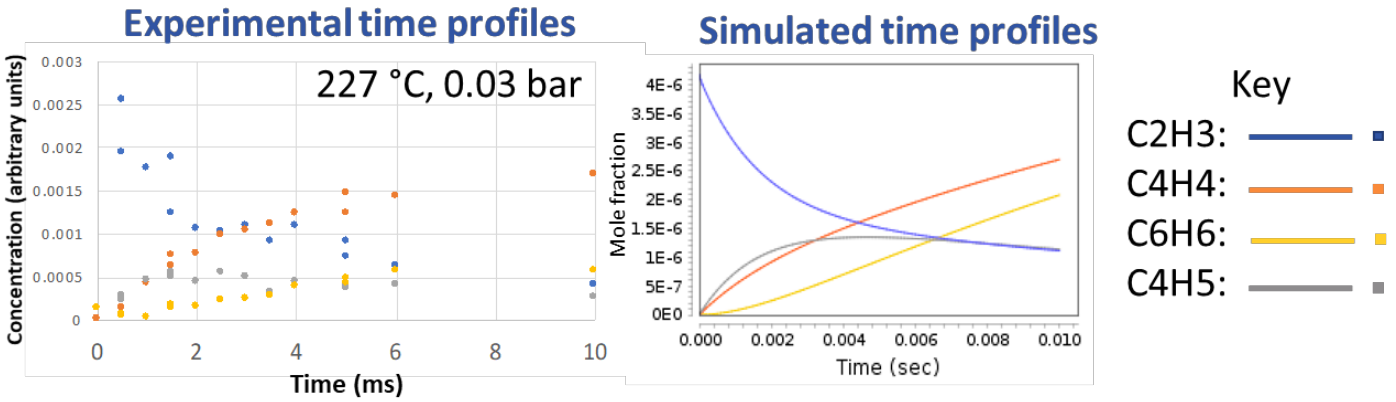

Figure 7. Comparison of experimental and simulated concentration profiles for the reaction of vinyl radical and acetylene.

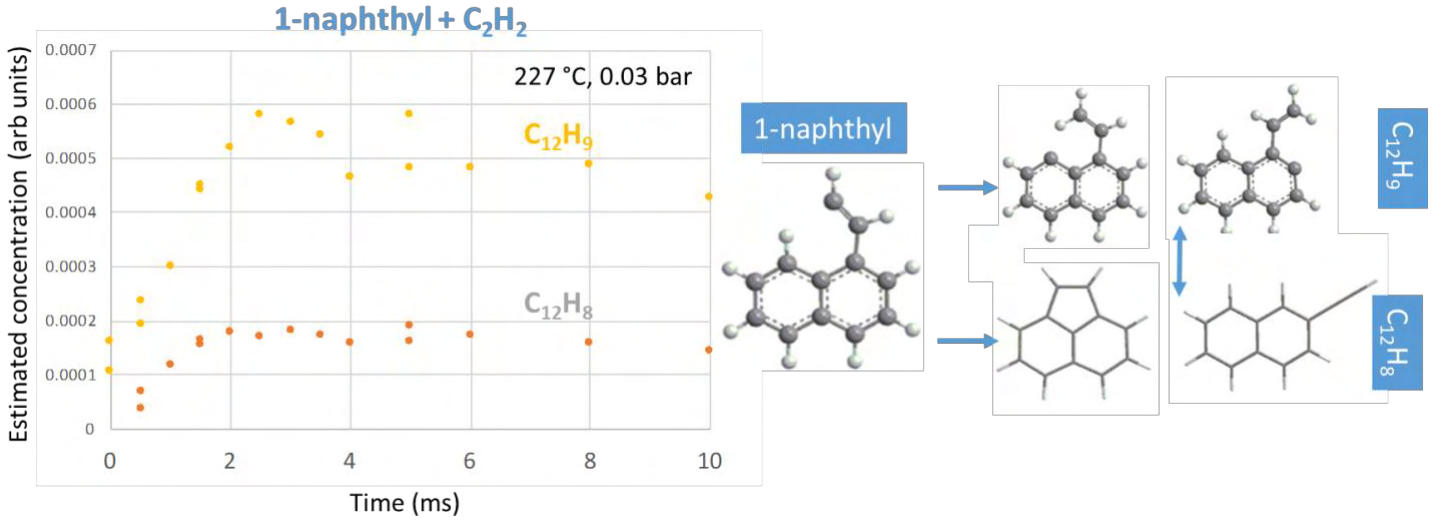

Figure 8. Experimentally-observed branching ratios between stable $C_{12}H_8$ species and $C_{12}H_9$ adducts formed by the reaction of 1-naphthyl radicals with acetylene.

Student Involvement

This work was conducted primarily by Dr. Mica Smith, a postdoctoral associate working under the supervision of Professor William Green.

Task 6 - Evaluate Changes in Emissions Resulting from Removal of Naphthalene

Massachusetts Institute of Technology

Objective

Changes to jet fuel composition, such as those achieved by the removal of naphthalene using available refining technologies, affect the chemical kinetics of the combustion process in gas turbine engines, which in turn affects the resulting emissions. The formation of black carbon (soot) from hydrocarbon fuels can be considered to occur in two stages. First, fuel components and combustion intermediates react and form PAHs. Large PAHs then act as soot nuclei, which grow as they absorb both PAH and other species, coagulate through collisions with other soot particles, carbonize, and partially oxidize (Richter & Howard, 2000). The details of the fuel composition mainly affect the first step of this process: the formation of PAHs. To enable evaluation of the sensitivity of soot emissions to fuel composition, in this task, we developed a combustor model that includes the detailed chemical kinetic pathways for the formation of (PAH) species from different fuel components and the conversion of these PAH species to soot particles or nvPM emissions. The model also provides the ability to predict changes in CO and nitrogen oxide (NO_x) emissions resulting from changes to fuel composition.

Research Approach

The aircraft engine emissions model developed herein has three main components: a soot model, an engine model, and a combustor model. The combustor model consists of a reactor network coupled with a gas-phase kinetic mechanism, which was modeled using Cantera (Goodwin et al., 2018). A soot model was added to the reactor network, and the interactions between the gas phase and the solid soot phase were modeled in detail. The altitude- and thrust-specific input conditions for the combustor were generated with the engine model, Pycaso (Python Cantera Soot). The model was used to predict emissions for a CFM56-7B/3 engine, because it is one of the most prevalent engines in the commercial fleet, and measurement data for soot emissions from this engine have been published.

Soot model

Because of the uncertainty in soot modeling in gas turbine combustors, we used a two-equation model, which captures all major soot formation and depletion processes while minimizing complexity. In a two-equation model, the soot number density (N) and mass density (M) were modeled with two equations representing the change in soot N and M in response to four soot formation and depletion steps. The standard two-equation model is based on the assumption that oxidation affects solely M and does not directly destroy soot particles. However, experiments have indicated that oxidation can destroy particles and can thus reduce N (Garo et al., 1988; Lindstedt, 1994). Therefore, an additional term was included in the number density equation to capture the effect of particle destruction through oxidation. Every change in soot mass equivalent to the average soot particle mass was assumed to also destroy a variable fraction of a particle. The resulting equations for N and M are as follows:

$$\frac{dN}{dt} = C_{\text{nuc}}\left(\frac{dN}{dt}\right)_{\text{nuc}} + C_{\text{coag}}\left(\frac{dN}{dt}\right)_{\text{coag}} + C_{\text{ox},N}\frac{N}{M}C_{\text{ox}}\left(\frac{dM}{dt}\right)_{\text{ox}}, \tag{1}$$

and

$$\frac{dM}{dt} = C_{\text{nuc}}\left(\frac{dM}{dt}\right)_{\text{nuc}} + C_{\text{sg}}\left(\frac{dM}{dt}\right)_{\text{sg}} + C_{\text{ox}}\left(\frac{dM}{dt}\right)_{\text{ox}}. \tag{2}$$

During nucleation, the inception of soot particles occurs through collisions of precursor species (Blanquart & Pitsch, 2009). These precursor species are considered to primarily consist of heavy PAH molecules (Dobbins et al., 1998; Schuetz & Frenklach, 2002). When two PAH molecules collide and stick together, they form a PAH dimer, which again increases in size through collisions with other PAH species and dimers. This growth through collisions allows for transitioning from the gas phase to the solid phase and results in the first solid incipient soot particle (Martini, 2008). PAH-PAH collision rates were considered for nucleation in the model, while PAH-soot collisions are modeled as surface growth. The nucleation rate resulting from collisions of PAH species i and j was based on the collision frequency $\beta i,j$ and is given by the following:

$$\left(\frac{dN}{dt}\right)_{\text{nuc},ij} = \frac{\gamma_i + \gamma_j}{2}\varepsilon\sqrt{\frac{8\pi k_B T}{\mu_{i,j}}}N_A^2\left(r_i + r_j\right)^2[\text{PAH}_i][\text{PAH}_j], \tag{3}$$

where ε = 2.2 is the Van der Waals enhancement factor, k_B is the Boltzmann constant, N_A is Avogadro's constant, r_i and r_j are the radii of PAH species i and j, $\mu_{i,j}$ is the reduced mass of PAH species i and j and $[\mathrm{PAH}_i]$ is the concentration of PAH species i (An et al., 2016; Atkins et al., 2018; Blanquart & Pitsch, 2009). The sticking coefficient $\gamma < 1$ was computed using the assumption that it scales with PAH mass to the fourth power (Blanquart & Pitsch, 2009). The PAH species were chosen such that no direct pathways from species in the fuel surrogates to soot mass through nucleation exist, as these pathways might result in an overestimation of sensitivities to fuel composition. The total nucleation rate was calculated by taking the sum over all the PAH species in the gas-phase mechanism.

Nucleation is followed by surface growth and coagulation. During surface growth, the soot particles grow in size and mass, because of the adsorption of gas phase molecules, mainly acetylene (Omidvarborna et al., 2015). Growth rates have been found to be much higher than nucleation rates, and most of the soot mass is thought to form during this step in the process (Martini, 2008). Here, two types of surface growth mechanisms were implemented. The first was based on an assumption of surface growth solely by acetylene, whereas the second also included surface growth through condensation of PAH species on the soot surface. To include surface growth through the adsorption of PAH species, the surface growth source term was expanded with an additional term based on the collision frequency of soot particles with PAH species i, given by:

$$\left(\frac{dM}{dt}\right)_{\mathrm{sg,PAH}} = \sum_{i=1}^{L} n_{\mathrm{C},i} W_{\mathrm{C}} \frac{\gamma_i + \gamma_{soot}}{2} \varepsilon \sqrt{\frac{8\pi k_B T}{\mu_{\mathrm{soot},i}}} \left(r_i + \frac{d_p}{2}\right)^2 [\mathrm{PAH}_i] N. \tag{4}$$

Because this term is similar to the nucleation term, it was scaled with C_{nuc} instead of C_{sg}.

During coagulation, soot particles grow further through particle-particle collisions (Blanquart & Pitsch, 2009; Omidvarborna et al., 2015). The total number of soot particles decreases during coagulation, whereas the total mass across all particles remains constant. The implemented coagulation mechanism was based on the collision of two spherical particles with a collision rate, as defined by Puri et al. (1993). The resulting source term for the number density equation is given by:

$$\left(\frac{dN}{dt}\right)_{\mathrm{coag}} = -K_{\mathrm{coag}} \sqrt{\frac{24 R_u T}{\rho_{\mathrm{soot}} N_A}} \sqrt{d_p} N^2, \tag{5}$$

where ρ_{soot} was a ssumed to be equal to 2000 kg/m^3 and K_{coag} is a constant ranging between 1 and 9 in literature (Brookes & Moss, 1999; Wen et al., 2003).

In contrast to the previous three steps, soot is destroyed during oxidation. Oxidation significantly reduces the amount of soot and measurements have suggested that most of the soot formed at the start of the combustion process is oxidized before reaching the combustor exit (Toone, 1968). Carbon and hydrogen atoms are removed from the soot agglomerates by reactions with primarily diatomic oxygen (O_2), hydroxyl radicals (OH) and atomic oxygen (O) (Louloudi, 2003; Neoh et al., 1981). Their respective contributions to the oxidation source term (Guo et al., 2016; Martini, 2008; Schiener & Lindstedt, 2018) are given by:

$$\left(\frac{dM}{dt}\right)_{\mathrm{ox},O_2} = -745.88 \eta_{O_2} W_{\mathrm{C}} \sqrt{T} \exp\left(-\frac{19{,}680}{T}\right) [O_2] A_s, \tag{6}$$

and

$$\left(\frac{dM}{dt}\right)_{\mathrm{ox,OH}} = -\eta_{\mathrm{OH}} W_{\mathrm{C}} \sqrt{T} [\mathrm{OH}] A_{s,} \tag{7}$$

and

$$\left(\frac{dM}{dt}\right)_{\mathrm{ox,O}} = -1.82 \eta_{\mathrm{O}} W_{\mathrm{C}} \sqrt{T} [\mathrm{O}] A_s, \tag{8}$$

where the collision efficiencies for O_2 and O ($\eta_{O_2}$and η_{O}) are assumed to be unity (Mueller et al., 2009; Wen et al., 2003). For oxidation through OH, collision efficiency values ranging from 0.01 to 0.65 have been proposed (Fenimore & Jones,

1967; Ghiassi et al., 2017; Guo et al., 2016; Haudiquert et al., 1997; Neoh et al., 1981; Puri et al., 1994; Richter et al., 2005; Schiener & Lindstedt, 2018). We used a value of 0.13, determined by Neoh et al. (1981), as the baseline value in this model.

Engine model

The combustor inlet temperature (T_3) and pressure (P_3), as well as the mass flows of fuel ($\dot{m}_{\mathrm{fuel}}$) and air ($\dot{m}_{\mathrm{air}}$) entering the combustor were computed using a detailed engine model of the CFM56-7B engine. The engine model is developed using the Numerical Propulsion System Software (NPSS) and matches the fuel flows, thrust levels and pressure ratios from the International Civil Aviation Organization (ICAO) engine emissions databank (EDB) within 5%. The temperature of the gas-phase mixture entering the combustor was corrected for vaporization of the fuel by adjusting the specific enthalpy of the gas-fuel mixture as follows:

$$h_{\mathrm{mix}} = \frac{1}{\dot{m}_{\mathrm{air}}}\left[\dot{m}_{\mathrm{air}} h_{\mathrm{air},P_3T_3} + \dot{m}_{\mathrm{fuel}} h_{\mathrm{fuel},P_3T_3} - \dot{m}_{\mathrm{fuel}}(L + \Delta h)\right], \tag{9}$$

where L represents the enthalpy of vaporization at standard conditions (T =298.15 K and P = 101,325 Pa), h is the specific enthalpy and Δh is the change in specific enthalpy going from standard conditions to T_3 and P_3. $\dot{m}_{\mathrm{fuel}}$ and $\dot{m}_{\mathrm{air}}$ are the mass flow rates of fuel and air, respectively.

Combustor model

The combustor model developed for this project represents a rich-burn quick-mix Lean-Burn (RQL) combustor. Figure 9 shows a schematic overview of the model. The model is divided into two parts: the primary zone and the secondary zone. In the primary zone, air and fuel are mixed at a certain equivalence ratio. Quenching then occurs at the start of the secondary zone through to the addition of secondary air in the slow and fast mixing zones. In the second part of the secondary zone, dilution air is added to represent the lean burn zone. Because NO_x, CO and soot reactions have been found to be quenched at the end of the secondary zone, the turbine was not modeled. The gas phase chemistry inside the combustor model was modeled using a kinetic mechanism that determines the structure of the flame and specifies the species profile (Appel et al., 2000). A high temperature kinetic mechanism for transportation fuels was coupled with a NO_x mechanism, thus resulting in a chemical mechanism consisting of 218 species and 7047 reactions (Ranzi et al., 2012, 2014, 2015).

The combustor model can be used to represent different (RQL) combustors. To represent a specific combustor design, combustor model parameters were calibrated by using emissions data from the EDB for an engine containing that specific combustor. Because the combustor model can be considered a "black box" function, and obtaining a (numerical) gradient is computationally expensive, gradient-free optimization was used to calibrate the model parameters. More specifically, the DIvided RECTangles (DIRECT) method was applied (Finkel, 2003; Hicken et al., 2012; Jones, 2009).

Milestone

The combined combustor, soot, and engine model described above were implemented, then used to explore the impacts of different jet fuel compositions on NO_x, CO, and soot emissions.

Major Accomplishments

Model validation

Eight different soot model configurations (C1 – C8) were developed. Each configuration consists of a different set of reaction rate coefficients and/or soot mechanisms. These eight configurations were selected to capture a range of soot mechanisms in literature and to quantify the impact and behavior of each step of the soot formation process. The performance of the configurations against measurements for both emissions index (EI) mass and number is summarized in Figure 10. Starting with EI soot mass, two clusters of configurations are visible. Configurations 1-5 capture the trends in the validation data for thrust levels >= 30%. On the other hand, configurations 6-8 capture the trend in the data for thrust settings larger than approximately 75% but underpredict soot mass emissions thrust settings lower than 75%. For soot number EI, the models all capture the trend in the validation data of decreasing number EI with increasing thrust between approximately 60% and 100% thrust. Configurations 4,5, and 6 also capture the 30% thrust point, whereas configurations 1,2,7, and 8 underpredict soot number at this thrust setting, while configuration 3 overpredicts it.

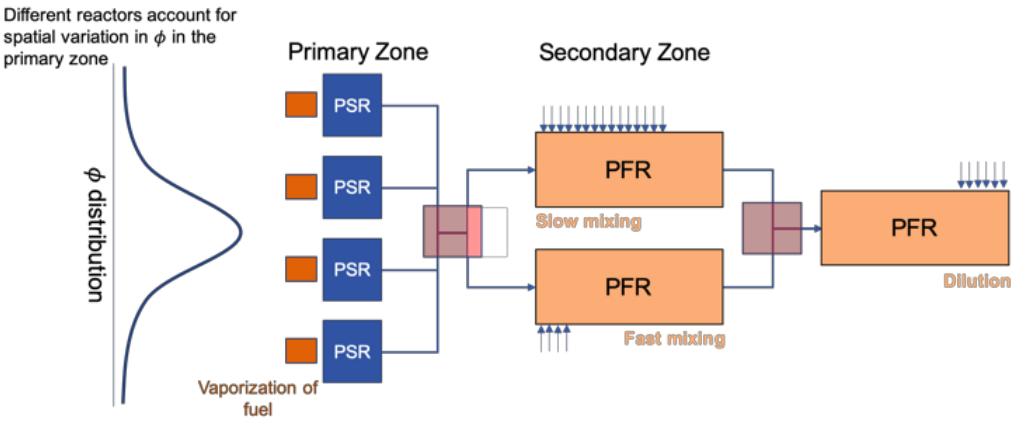

Figure 9. Schematic overview of the combustor model. Multiple well-stirred reactors (WSR) are used in the primary zone. The secondary zone uses a combination of plug flow reactors (PFR) to simulate different mixing times. The arrows represent secondary and dilution air entering the combustor.

We found primary zone soot mass formation peaks at $\varphi \approx 2.3$, where the EI soot was approximately seven times higher than that at $\varphi \approx 3.0$ and $\varphi \approx 2.0$. In contrast, the soot number increased with the equivalence ratio, and peak EI soot number values were observed in the richest reactors. This difference can be explained by the PAH concentration being the limiting factor for nucleation (soot number), whereas temperature and C_2H_2 concentration are the limiting factors for soot mass (surface growth).

To validate the model's ability to predict changes in soot emissions in response to changing fuel compositions, we simulated a subset of the experiments conducted by Brem et al. (2015), in which soot emissions were measured for two fuel blends with differing naphthalene and aromatic content. The soot predictions of each of the model configurations for two versions of each of the five surrogates were evaluated. The content of total aromatics (% v/v), naphthalene (% v/v), and hydrogen of these two fuels matched the values used in experiments by Brem et al. (2015). The resulting changes in EI soot mass and

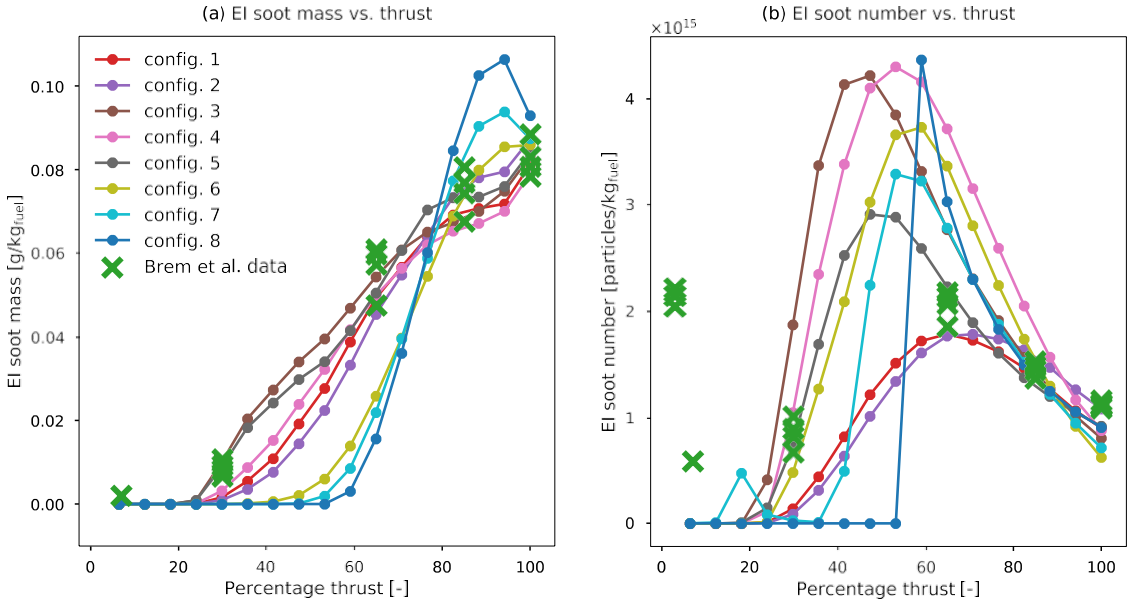

Figure 10. Comparison of EI soot (a) mass and (b) number with validation data (surrogate 4).

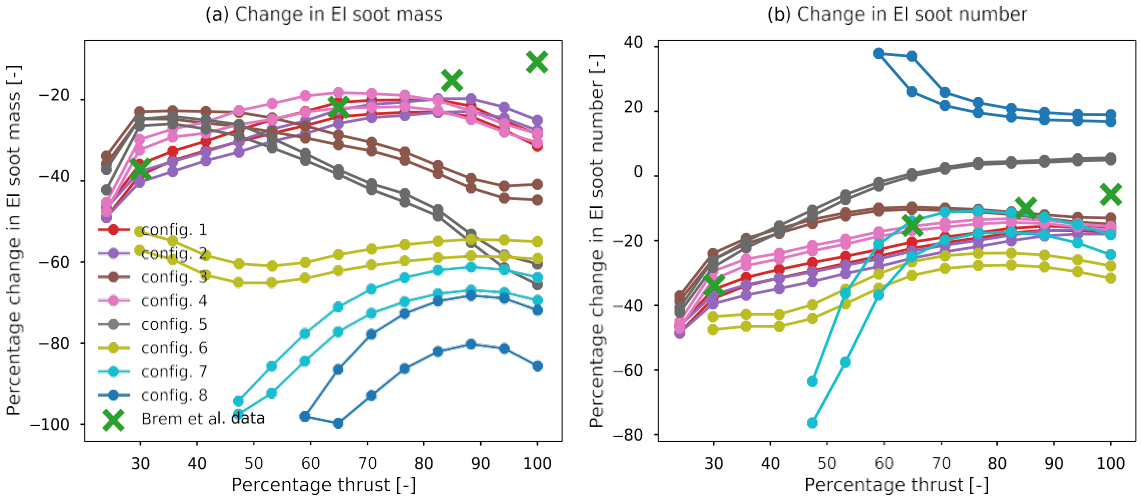

Figure 11. Comparison of model predictions with experimental data by Brem et al. (2015). Percentage change in EI soot (a) mass and (b) number for all eight configurations.

number are shown in Figure 11. The three configurations using the HACA mechanisms showed large discrepancies for both soot mass and number. The five other configurations could be grouped based on their values for C_{coag} and $C_{ox,N}$. The three configurations (1, 2, and 4) with relatively low coagulation factors (< 30) and relatively large $C_{ox,N}$ values (> 0.65) matched the soot mass data from Brem et al. (2015) within 5 percentage points (p.p.) at 30% and 65% thrust, 8 p.p. at 85% thrust and 18 p.p. at 100% thrust, and within 15 p.p. of the soot number data for all thrust conditions. When increasing the coagulation factor and decreasing $C_{ox,N}$ (configurations 3 and 5), these differences grew to a maximum of 51 p.p. at 100% thrust for configuration 5. A possible explanation for the relatively large discrepancies at high thrust for the configuration using high coagulation factors is that these configurations rely on a large N in the PZ to increase the average particle size (and thus the M/A_s ratio). When reducing the naphthalene content of the fuel, less nucleation occurs, and the soot number density decreases. Consequently, coagulation is decreased and M/A_s is increased thus leading to more oxidation in the secondary zone. In contrast, configurations relying on $C_{ox,N}$ to reduce N are relatively less affected by a decreasing N. Because of their superior performance with respect to the validation data, configurations 1, 2, and 4 were selected to assess the sensitivity of soot to naphthalene removal and biofuels in the subsequent analysis of fuel composition effects.

Effects of fuel composition

Figure 12 shows the computed ranges of soot mass and number emissions reductions associated with naphthalene removal through extractive distillation and hydrotreating. These ranges represent both variations in the three soot model configurations as well as the five baseline fuel compositions. The mean reductions in EI mass were approximately 20 p.p. higher for extractive distillation than for hydrotreating. For EI soot number, the differences between the means of the two methods ranged from 12 p.p. at 100% thrust to 28 p.p. at 30% thrust. These differences are explained by tetralin, the product of hydrotreating naphthalene, being an aromatic species and having a relatively short pathway to becoming a PAH species during combustion. Reductions in mass are predicted to be larger than those in number (for >35% thrust), in agreement with the literature (Brem et al., 2015; Speth et al., 2015).

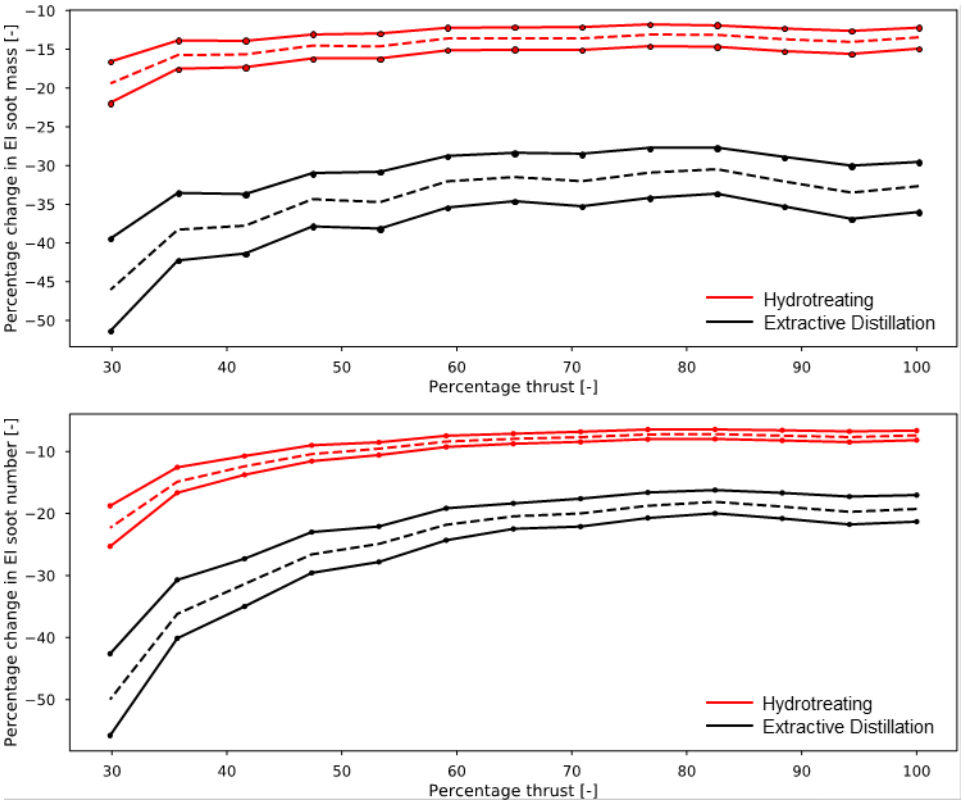

Figure 12. Ranges of predicted effects of naphthalene removal from jet fuel by hydrotreating (red) and extractive distillation (black) on EI soot (a) mass and (b) number emissions indices. The dashed lines represent the means of the prediction ranges, which capture variations in three different soot configurations and five different surrogates.

Furthermore, particularly for number emissions, reductions increase with decreasing thrust. This effect has also been observed in experiments in the literature (Brem et al., 2015; Corporan et al., 2007; Naegeli & Moses, 2015; Speth et al., 2015). We found that the increasing change in soot emissions with decreasing thrust can be explained by two main factors. The first factor is that sensitivity to fuel composition increases with decreasing PZ equivalence ratio. The changes in EI soot mass and number due to naphthalene removal were found to be approximately 1.5 and 2–3 times higher at φ=2.2 compared to φ=3.0, respectively. The lower the thrust setting, the lower the primary zone equivalence ratio(s), and thus the higher the sensitivity to fuel composition. The second factor is that for a given φ, the reductions in both soot mass and number increase with decreasing thrust. This is explained by the temperature difference between the thrust conditions. Higher temperatures at higher thrust settings make the reactor more resilient to changes in naphthalene concentrations.

Figure 13 shows the predicted effects of using 20%, 50%, and 100% biofuel blends on soot emissions. As expected, the mean reductions increase with increasing biofuel fraction and decreasing thrust. The predicted reductions for soot mass range from 17%, 37%, and 55% at 100% thrust to 25%, 56%, and 92% at 30% thrust. For soot number, the mean reductions at 100% thrust are 11%, 26%, and 51%, as compared with reductions of 24%, 56%, and 92% at 30% thrust.

The effects of using 20%, 50%, and 100% biofuel blends on NO_x and CO emissions are shown in Figure 14. The model predicts the mean reductions in NO_x emissions of 2%, 5%, and 10% and those in CO emissions of 1%, 2%, and 5% for the three blends, respectively. The sharp drop in CO at the lowest thrust setting is a consequence of the finite number of reactors in the model; the corresponding CO values were therefore not considered. This sharp drop in CO occurs because the leanest reactor blows out for the standard surrogate but does not do so for the 50% and 100% biofuel blends, thus leading to an increase in SZ mixing temperature and consequently CO depletion.

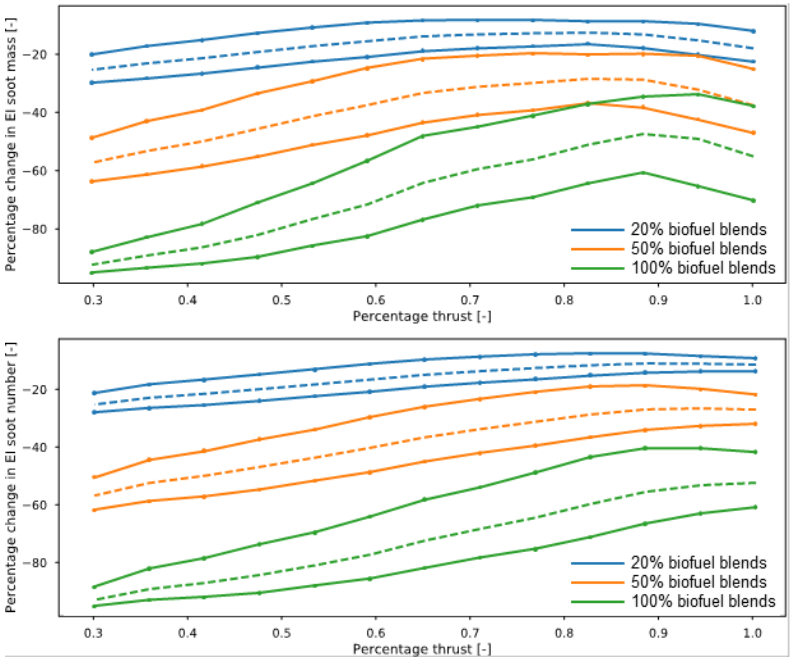

Figure 13. Effects of using 20% (blue), 50% (orange), and 50% (green) biofuel blends on EI soot (a) mass and (b) number. The dashed lines represent the means of the prediction ranges, which capture variations in three soot mechanisms and five surrogates.

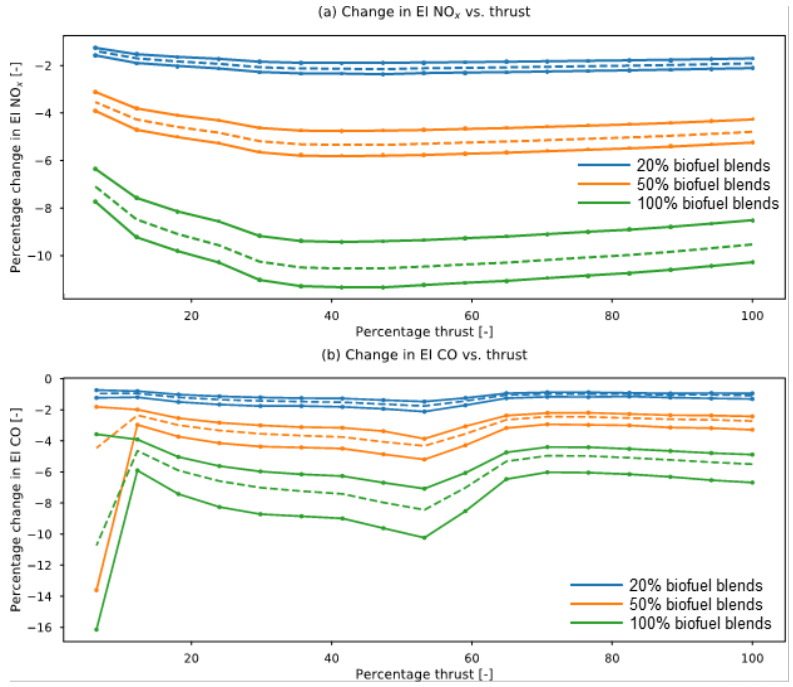

Figure 14. Effects of using 20% (blue), 50% (orange), and 100% (green) biofuel blends on (a) NO_x and (b) CO emissions. The dashed lines represent the means of the prediction ranges, which capture variations in five surrogates.

Publications

Brink, L. (2020). Modeling the impact of fuel composition on aircraft engine NO_x, CO and soot emissions [S.M. thesis, Massachusetts Institute of Technology]. DSpace@MIT. https://hdl.handle.net/1721.1/129181

Outreach Efforts

- ASCENT advisory board presentations (October 2018, October 2019, and March 2020)
- Presentations at the Aviation Emissions Characterization (AEC) Roadmap Annual Meeting (June 2017 and May 2020)

Student Involvement

This task was conducted primarily by Lukas Brink, working directly with Professor Steven Barrett and Dr. Raymond Speth. Mr. Brink graduated with a Master of Science degree in 2020.

References

An, Y., Li, X., Teng, S., Wang, K., Pei, Y., Qin, J., & Zhao, H. (2016). Development of a soot particle model with PAHs as precursors through simulations and experiments. Fuel, *179*, 246–257. https://doi.org/10.1016/j.fuel.2016.03.100

Appel, J., Bockhorn, H., & Frenklach, M. (2000). Kinetic modeling of soot formation with detailed chemistry and physics: Laminar premixed flames of C_2 hydrocarbons. Combustion and Flame, *121*(1–2), 122–136.

Atkins, P. W., De Paula, J., & Keeler, J. (2018). *Atkins' physical chemistry*. Oxford University Press.

Blanquart, G., & Pitsch, H. (2009). A joint volume-surface-hydrogen multi-variate model for soot formation. Combustion Generated Gine Carbonaceous Particles, 437–463.

Brem, B. T., Durdina, L., Siegerist, F., Beyerle, P., Bruderer, K., Rindlisbacher, T., Rocci-Denis, S., Andac, M. G., Zelina, J., Penanhoat, O., & Wang, J. (2015). Effects of fuel aromatic content on nonvolatile particulate emissions of an in-production aircraft gas turbine. Environmental Science and Technology, *49*, 13149–13157.

Brookes, S. J., & Moss, J. B. (1999). Predictions of soot and thermal radiation properties in confined turbulent jet diffusion flames. Combustion and Flame, *116*(4), 486–503. https://doi.org/10.1016/S0010-2180(98)00056-X

Corporan, E., DeWitt, M. J., Belovich, V., Pawlik, R., Lynch, A. C., Gord, J. R., & Meyer, T. R. (2007). Emissions characteristics of a turbine engine and research combustor burning a Fischer–Tropsch jet fuel. Energy and Fuels, *21*(5), 2615–2626. https://doi.org/10.1021/ef070015j

Dobbins, R. A., Fletcher, R. A., & Chang, H.-C. (1998). The evolution of soot precursor particles in a diffusion flame. Combustion and Flame, *115*(3), 285–298. https://doi.org/10.1016/S0010-2180(98)00010-8

Fenimore, C. P., & Jones, G. W. (1967). Oxidation of soot by hydroxyl radicals. The Journal of Physical Chemistry, *71*(3), 593–597. https://doi.org/10.1021/j100862a021

Finkel, D. (2003). *DIRECT optimization algorithm user guide*. North Carolina State University Center for Research in Scientific Computation.

Garo, A., Lahaye, J., & Prado, G. (1988). Mechanisms of formation and destruction of soot particles in a laminar methane-air diffusion flame. Symposium (International) on Combustion, *21*(1), 1023–1031. https://doi.org/10.1016/S0082- 0784(88)80333-3

Ghiassi, H., Lignell, D., & Lighty, J. S. (2017). Soot oxidation by OH: Theory development, model, and experimental validation. Energy and Fuels, *31*(3), 2236–2245. https://doi.org/10.1021/acs.energyfuels.6b02193

Goodwin, D. G., Speth, R. L., Moffat, H. K., & Weber, B. W. (2018). Cantera: An object-oriented software toolkit for chemical kinetics, thermodynamics, and transport processes (2.4.0) [Computer software]. https://www.cantera.org.

Guo, H., Anderson, P. M., & Sunderland, P. B. (2016). Optimized rate expressions for soot oxidation by OH and O2. Fuel, *172*, 248–252. https://doi.org/10.1016/j.fuel.2016.01.030

Haudiquert, M., Cessou, A., Stepowski, D., & Coppalle, A. (1997). OH and soot concentration measurements in a high-temperature laminar diffusion flame. Combustion and Flame, *111*(4), 338–349. https://doi.org/10.1016/S0010- 2180(97)00003-5

Hicken, J., Alonso, J., & Farhat, C. (2012). Chapter 6: Gradient-free optimization. In *Introduction to multidisciplinary design optimization* (pp. 133-161). Stanford University.

Jones, D. R. (2009). Direct global optimization algorithm. Encyclopedia of Optimization, *1*(1), 431–440.

Lindstedt, P. R. (1994). Simplified soot nucleation and surface growth steps for non-premixed flames. In H. Bockhorn (Ed.), *Soot formation in combustion: Mechanisms and models* (pp. 417–441). Springer. https://doi.org/10.1007/978-3-642-85167-4_24

Louloudi, S. (2003). *Transported probability density function: Modelling of turbulent jet flames*. Imperial College London (University of London).

Martini, B. (2008). *Development and assessment of a soot emissions model for aircraft gas turbine engines* [S. M. thesis, Massachusetts Institute of Technology]. DSpace@MIT. https://dspace.mit.edu/handle/1721.1/45256

Mueller, M. E., Blanquart, G., & Pitsch, H. (2009). Hybrid method of moments for modeling soot formation and growth. Combustion and Flame, *156*(6), 1143–1155. https://doi.org/10.1016/j.combustflame.2009.01.025

Naegeli, D. W., & Moses, C. A. (2015, April 17). Effect of fuel molecular structure on soot formation in gas turbine engines [Presentation]. ASME 1980 International Gas Turbine Conference and Products Show. https://doi.org/10.1115/80-GT-62
Neoh, K. G., Howard, J. B., & Sarofim, A. F. (1981). Soot oxidation in flames. In D. C. Siegla & G. W. Smith (Eds.), *Particulate carbon: Formation during combustion* (pp. 261–282). Springer US. https://doi.org/10.1007/978-1-4757-6137-5_9
Omidvarborna, H., Kumar, A., & Kim, D.-S. (2015). Recent studies on soot modeling for diesel combustion. Renewable and Sustainable Energy Reviews, *48*, 635–647. https://doi.org/10.1016/j.rser.2015.04.019
Puri, R., Richardson, T. F., Santoro, R. J., & Dobbins, R. A. (1993). Aerosol dynamic processes of soot aggregates in a laminar ethene diffusion flame. Combustion and Flame, *92*(3), 320–333.
Puri, R., Santoro, R. J., & Smyth, K. C. (1994). Oxidation of soot and carbon monoxide in hydrocarbon diffusion flames. Combustion and Flame, *97*, 125–144.
Ranzi, E., Cavallotti, C., Cuoci, A., Frassoldati, A., Pelucchi, M., & Faravelli, T. (2015). New reaction classes in the kinetic modeling of low temperature oxidation of n-alkanes. Combustion and Flame, *162*(5), 1679–1691. https://doi.org/10.1016/j.combustflame.2014.11.030
Ranzi, E., Frassoldati, A., Grana, R., Cuoci, A., Faravelli, T., Kelley, A. P., & Law, C. K. (2012). Hierarchical and comparative kinetic modeling of laminar flame speeds of hydrocarbon and oxygenated fuels. Progress in Energy and Combustion Science, *38*(4), 468–501. https://doi.org/10.1016/j.pecs.2012.03.004
Ranzi, E., Frassoldati, A., Stagni, A., Pelucchi, M., Cuoci, A., & Faravelli, T. (2014). Reduced kinetic schemes of complex reaction systems: Fossil and biomass-derived transportation fuels. International Journal of Chemical Kinetics, *46*(9), 512–542. https://doi.org/10.1002/kin.20867
Richter, H., Granata, S., Green, W. H., & Howard, J. B. (2005). Detailed modeling of PAH and soot formation in a laminar premixed benzene/oxygen/argon low-pressure flame. Proceedings of the Combustion Institute, *30*(1), 1397–1405. https://doi.org/10.1016/j.proci.2004.08.088
Schiener, M. A., & Lindstedt, R. P. (2018). Joint-scalar transported PDF modelling of soot in a turbulent non-premixed natural gas flame. Combustion Theory and Modelling, *22*(6), 1134–1175. https://doi.org/10.1080/13647830.2018.1472391
Schuetz, C. A., & Frenklach, M. (2002). Nucleation of soot: Molecular dynamics simulations of pyrene dimerization. Proceedings of the Combustion Institute, *29*(2), 2307–2314. https://doi.org/10.1016/S1540-7489(02)80281-4
Speth, R. L., Rojo, C., Malina, R., & Barrett, S. R. H. (2015). Black carbon emissions reductions from combustion of alternative jet fuels. Atmospheric Environment, *105*, 37–42. https://doi.org/10.1016/j.atmosenv.2015.01.040
Toone, B. (1968). A review of aero engine smoke emission. In I. E. Smith (Ed.), *Combustion in advanced gas turbine systems* (pp. 271–296). Pergamon. https://doi.org/10.1016/B978-0-08-013275-4.50019-2
Wen, Z., Yun, S., Thomson, M. J., & Lightstone, M. F. (2003). Modeling soot formation in turbulent kerosene/air jet diffusion flames. Combustion and Flame, *135*(3), 323–340. https://doi.org/10.1016/S0010-2180(03)00179-2

Task 7 - Calculate Air Quality and Climate Impacts of Naphthalene Removal

Massachusetts Institute of Technology

Objective

The objective of this task was to calculate the air quality and climate impacts of a policy in which naphthalene is removed from jet fuel used in the United States.

Research Approach

The air quality effects of changes in aircraft PM emissions were evaluated by using the GEOS-Chem adjoint model, which we previously used for assessing the health impacts of emissions (Dedoussi & Barrett, 2014). The use of an adjoint model, a computationally efficient approach to calculating the sensitivity of an aggregate objective function (e.g., population exposure to $PM_{2.5}$), enables evaluation of a range of scenarios in a single run, thus allowing for incorporation of upstream uncertainty in the emissions indices for different species. The PM exposure calculated by using GEOS-Chem included both the effects of changes in black carbon emissions and changes due to sulfur reductions that accompany the removal of naphthalenes (in the case in which hydrotreating is used to remove naphthalenes). The spatial patterns of emissions of nvPM, and sulfur compounds were taken from the 2015 inventory from the Aviation Environmental Design Tool(AEDT).

Climate impacts of naphthalene removal include contributions at both the fuel production and fuel consumption stages.

The additional refinery processing required to reduce or remove naphthalene requires process fuel, steam, electricity, and, in the case of hydrotreating, hydrogen production. The greenhouse gas (GHG) emissions associated with each of these processes increase life-cycle jet fuel GHG emissions. Using the results calculated as part of the refinery modeling work conducted in the previous project year, we found that the GHG emissions associated with naphthalene removal were 135 g CO_2e per kg fuel for hydrotreating and 144 g CO_2e per kg fuel for extractive distillation.

The consumption of reduced-naphthalene fuel decreases RF from aviation black carbon, and reductions in sulfur content decrease the cooling effect of sulfates (Mahashabde et al., 2011). Contrail impacts are estimated according to studies on the impact of reducing the number of ice nuclei available for contrail formation. Caiazzo et al. (2017) have found that decreasing ice nuclei by 67% (an amount representative of a fully paraffinic biofuel) reduces contrail RF by <13%. Burkhardt et al. (2018) have found that reducing ice nuclei by 50% reduces contrail RF by ~20%. Here, the reductions in contrail RF found in these studies were scaled by the estimated reduction in nvPM emissions from naphthalene removal.

The combined climate impacts of these effects were evaluated by using the APMT-Impacts Climate model, a policy-oriented rapid assessment tool that provides probabilistic estimates of climate impacts.

Milestone

The work completed for this task was documented in Deliverable 2-4, provided to the FAA on May 31, 2018.

Major Accomplishments

On the basis of a literature review of nvPM emissions measurements from engines using fuels with varying levels of naphthalene (Brem et al., 2015; DeWitt et al., 2008), we estimated the potential range of reduction in nvPM emissions associated with 95% naphthalene removal to be 15–40%, or 5.0–12.5 mg nvPM per kg fuel. Monetized climate impacts for the different climate forcing pathways are summarized in Table 2, presented on a cents-per-gallon basis, with both median values and a range indicating the 90% CI. Monetized air quality impacts of naphthalene removal are similarly summarized in Table 3.

Table 2. Monetized climate benefits of naphthalene removal.

Impact Pathway	Impact (¢/gallon)
Black carbon RF (15% nvPM reduction)	0.09 (90% CI: 0.01 to 0.23)
Black carbon RF (40% nvPM reduction)	0.23 (90% CI: 0.04 to 0.61)
Contrail RF (15% nvPM reduction)	1.06 (90% CI: 0.30 to 2.59)
Contrail RF (40% nvPM reduction)	2.77 (90% CI: 0.77 to 6.89)
Hydrotreating CO_2 emissions	−1.82 (90% CI: −0.30 to −4.70)
Extractive distillation CO_2 emissions	−1.89 (90% CI: −0.31 to −5.01)
Sulfate aerosol (hydrotreating only)	−4.17 (90% CI: −0.61 to −11.23)

Table 3. Monetized air quality benefits of naphthalene removal.

Impact Pathway	Impact (¢/gallon)
nvPM emissions (15% nvPM reduction)	0.04 (90% CI: 0.02 to 0.06)
nvPM emissions (40% nvPM reduction)	0.11 (90% CI: 0.06 to 0.16)
Sulfur emissions (hydrotreating only)	1.92 (90% CI: 1.04 to 2.76)

Outreach Efforts

- ASCENT advisory board presentations (October 2018 and October 2019)
- Presentation at the CAEP/12-WG3/2 meeting (October 2019) titled “Economic and Environmental Assessment of Jet Fuel Naphthalene Removal”

Student Involvement

This task was conducted primarily by Drew Weibel, a Master's student in the Laboratory for Aviation and the Environment, working directly with Professor Steven Barrett and Dr. Raymond Speth.

References

Brem, B. T., Durdina, L., Siegerist, F., Beyerle, P., Bruderer, K., Rindlisbacher, T., Rocci-Denis, S., Andac, M. G., Zelina, J., Penanhoat, O., & Wang, J. (2015). Effects of fuel aromatic content on nonvolatile particulate emissions of an in-production aircraft gas turbine. Environmental Science and Technology, *49*, 13149–13157.

Burkhardt, U., Bock, L., & Bier, A. (2018). Mitigating the contrail cirrus climate impact by reducing aircraft soot number emissions. Climate and Atmospheric Science, *1*, 37.

Caiazzo, F., Agarwal, A., Speth, R. L., & Barrett, S. R. H. (2017). Impact of biofuels on contrail warming. Environmental Research Letters, *12*, 114013.

Dedoussi, I. C., & Barrett, S. R. H. (2014). Air pollution and early deaths in the United States. Part II: Attribution of PM2.5 exposure to emissions species, time, location and sector. Atmospheric Environment, *99*, 610–617.

DeWitt, M. J., Corporan, E., Graham, J. & Minus, D. (2008). Effects of aromatic type and concentration in Fischer–Tropsch fuel on emissions production and material compatibility. Energy and Fuels, *22*, 2411–2418.

Mahashabde, A., Wolfe, P., Ashok, A., Dorbian, C., He, Q., Fan, A., Lukachko, S., Mozdzanowska, A., Wollersheim, C., Barrett, S. R. H., Locke, M., & Waitz, I. A. (2011). Assessing the environmental impacts of aircraft noise and emissions. Progress in Aerospace Sciences, *47*, 15–52.

Punger, E. M., & West, J. J. (2013). The effect of grid resolution on estimates of the burden of ozone and fine particulate matter on premature mortality in the USA. Air Quality, Atmosphere & Health, *6*, 563–573.

Task 8 · Conduct Integrated Cost-Benefit Analysis of Impacts of Naphthalene Removal in the United States

Massachusetts Institute of Technology

Objective

The objective of this task was to produce an integrated cost–benefit analysis of naphthalene removal in the United States, accounting for the additional refining cost as well as the air quality and climate impacts.

Research Approach

The overall cost–benefit assessment of naphthalene removal includes fuel production costs, air quality benefits, and climate impacts from fuel production and fuel consumption. Fuel production costs were evaluated in tasks that were completed in previous project years. Air quality benefits and non-contrail climate impacts were calculated per unit reduction in nvPM mass and number emissions, based on the results of Grobler et al. (2019). These impacts were then scaled by using the emissions reductions determined in the results of Task 1. Contrail impacts were estimated on the basis of contrail modeling studies investigating the effects of reductions in the soot number emissions index (Caiazzo et al., 2017; Bier & Burkhardt, 2019). Finally, all effects were placed on a common monetized basis to compare different naphthalene removal scenarios. We considered uncertainties in the assessment of each component and used these uncertainties to compute the likelihood of a net benefit for different scenarios.

Milestone

The work completed for this task was documented in Deliverable 2-5, provided to the FAA on July 31, 2018.

Major Accomplishments

The processing costs, air quality benefits, and climate impacts of naphthalene removal were converted to a common basis of cents per liter, as presented in Table 4. The results indicate that the benefits of widespread naphthalene removal are outweighed by the costs of processing the fuel and the CO_2 emissions associated with that processing.

Table 4. Costs (positive) and benefits (negative) of naphthalene removal.

Component		Hydrotreatment (¢/liter)		Extractive Distillation (¢/liter)	
		Median	95% CI	Median	95% CI
Processing	Refinery	2.4	2.0 to 2.7	1.7	1.5 to 2.0
Air Quality	nvPM	−0.004	0 to −0.01	−0.009	0 to −0.03
	Fuel sulfur	−0.51	−0.28 to −0.73	0	
Climate	nvPM	−0.02	0 to −0.04	−0.04	−0.01 to −0.09
	Fuel sulfur	1.06	0.15 to 2.85	0	
	Contrails	−0.16	−0.04 to −0.44	−0.38	−0.09 to −1.0
	Refinery CO_2	0.46	0.08 to 1.19	0.48	0.08 to 1.27
Total		**3.2**	**2.2 to 4.7**	**1.8**	**1.0 to 2.5**

For hydrotreatment, the climate impacts of the refinery CO_2 emissions exceed the expected air quality and climate benefits associated with the reduction in soot emissions. Furthermore, the NPV of the climate warming associated with sulfur removal is greater than the NPV of the reduced air-quality-related damages. For extractive distillation, the median air quality and climate benefits are approximately equal to the societal cost of the refinery CO_2 emissions. In addition to these environmental costs, the costs associated with processing jet fuel in the refinery must also be considered. These results suggest that, in the absence of a strong contrail effect, naphthalene removal on a nationwide basis is unlikely to be cost beneficial using either extractive distillation or hydrotreatment. However, it may be possible that naphthalene removal could be beneficial under certain circumstances, e.g., if applied to fuels used at individual airports with particular air quality concerns, or if used at times in locations where the formation of net warming contrails is most likely.

Outreach Efforts

- ASCENT advisory board presentations (April 2017, April 2018, October 2018, and October 2019)
- Presentation at the CAEP/12-WG3/2 meeting (October 2019) titled "Economic and Environmental Assessment of Jet Fuel Naphthalene Removal"
- Presentation at the Aviation Emissions Characterization (AEC) Roadmap annual meeting (May 2020)

Student Involvement

This task was conducted primarily by Drew Weibel, a Master's student in the Laboratory for Aviation and the Environment, working directly with Professor Steven Barrett and Dr. Raymond Speth.

References

Bier, A., & Burkhardt, U. (2019). Variability in contrail ice nucleation and its dependence on soot number emissions. Journal of Geophysical Research: Atmospheres, *124*(6), 3384–3400. https://doi.org/10.1029/2018JD029155

Caiazzo, F., Agarwal, A., Speth, R. L., & Barrett, S. R. H. (2017). Impact of biofuels on contrail warming. Environmental Research Letters, *12*(11), 114013. https://doi.org/10.1088/1748-9326/aa893b

Grobler, C., Wolfe, P. J., Dasadhikari, K., Dedoussi, I. C., Allroggen, F., Speth, R. L., Eastham, S. D., Agarwal, A., Staples, M. D., Sabnis, J., & Barrett, S. R. H. (2019). Marginal climate and air quality costs of aviation emissions. Environmental Research Letters, *14*(11), 114031. https://doi.org/10.1088/1748-9326/ab4942

Project 040 Quantifying Uncertainties in Predicting Aircraft Noise in Real-World Scenarios

The Pennsylvania State University
Purdue University

Project Lead Investigator

Victor W. Sparrow
United Technologies Corporation Professor of Acoustics
Graduate Program in Acoustics
The Pennsylvania State University
201 Applied Science Bldg.,
University Park, PA 16802
+1 (814) 865-6364
vws1@psu.edu

University Participants

The Pennsylvania State University (Penn State)

- PI: Victor W. Sparrow, United Technologies Corporation Professor of Acoustics
- Co-PI: Philip J. Morris, Boeing/A.D. Welliver Professor of Aerospace Engineering
- FAA Award Number: 13-C-AJFE-PSU, Amendment 49
- Period of Performance: May 31, 2019 to April 30, 2021
- Tasks:
  1. Assess uncertainty in aircraft noise events, examining the background noise levels and noise levels from enroute aircraft (BANOERAC) and similar datasets.
  2. Assess uncertainty in realistic noise source models in the Aircraft Noise Prediction Program (ANOPP).

Purdue University

- PI: Kai Ming Li, professor of mechanical engineering
- FAA Award Number: 13-C-AJFE-PU, Amendment 31
- Period of Performance: May 31, 2019 to December 31, 2020
- Task: No tasks in 2021

Project Funding Level

FAA funding to Penn State in 2019–2020 is $170,000. FAA funding to Purdue in 2019–2020 is $85,000.

Airbus has committed in-kind cost share for both Penn State and Purdue regarding the SILENCE-R data set, and this in-kind cost share is currently in process, awaiting a nondisclosure agreement. The point of contact for the cost sharing is Stefan Moal (Stefan.moal@airbus.com), who took over for the recently retired Pierre Lempereur.

Investigation Team

The Pennsylvania State University

Victor W. Sparrow, PI
Philip J. Morris, co-PI
Harshal P. Patankar, graduate research assistant

Purdue University

Kai Ming Li, PI
Yiming Wang, graduate research assistant
Jianxiong Feng, graduate research assistant

Special Acknowledgments

European Union Aviation Safety Agency
Illimar Bilas, section manager
Anotec Engineering, S.L.
Nico van Oosten

The BANOERAC data were provided to Penn State and Purdue by the European Union Aviation Safety Agency (EASA) via a special licensing agreement, with the assistance of Anotec Engineering, S.L. This in-kind data contribution is greatly appreciated.

Project Overview

The ASCENT R&D portfolio is designed to assist the FAA in meeting the overarching environmental performance goal for the Next-Generation Air Transportation System (NextGen) to attain environmental protection that allows sustained aviation growth. This project is part of the aviation modeling and analysis work in the ASCENT R&D portfolio that has the goal of improving the accuracy of the FAA's environmental modeling tools. Specifically, this project provides data and methods to improve the aircraft weight and takeoff thrust modeling capabilities within the FAA Aviation Environmental Design Tool (AEDT). Atmospheric conditions and ground properties have significant impacts on accurate predictions of aircraft noise. It is well known that the accuracy of these inputs is critical for accurate predictions. The research performed by Penn State and Purdue through FAA ASCENT research grants has informed the FAA regarding the limitations of existing noise tools and helped advance the state of the art in aircraft noise modeling. Appropriate models were enhanced and developed to account for the effects of meteorological conditions, atmospheric absorption, and the Doppler effect caused by source motion on the propagation of aircraft noise. The purpose of this project is to understand and quantify uncertainty in the prediction of noise propagation of aircraft.

ASCENT Project 40 is developing numerical methods that could later be used in FAA tools for predicting aircraft noise. The current research addresses an improved approach to extend the uncertainty quantification methods of Wilson et al. (2014) and other algorithms. Realistic aircraft trajectories and meteorology in the atmosphere are being used to predict aircraft flyover noise levels. The results will be compared with field data already acquired in Discover-AQ Acoustics, the Vancouver Airport Authority, BANOERAC, and SILENCE(R) databases. In addition, uncertainties on geometric locations of source and receivers, effective surface impedance and ground topography, and source motion have been incorporated in this year's work.

ASCENT Project 40 is expected to lead to the development of methodologies that could be used to improve the FAA tools for predicting aircraft noise in the presence of real-world weather. By having faster predictions and predictions verified with field data, the project will help to improve confidence when making decisions regarding aircraft noise. Examples of these decisions include choosing sites for new runways and implementing new landing approach and takeoff patterns overpopulated areas. The project team has identified key drivers for quantifying uncertainties in predicting aircraft noise. An integrated approach will be used to assess and understand uncertainties in (a) the aircraft state and resulting noise levels and directivity (source), (b) atmospheric and meteorological conditions (propagation), and (c) ground impedance and terrain model (receiver). This integrated approach will include all predominant uncertainties between the source and receiver. One of the main motivations of the current project is to guide these recent advancements for reaching a sufficient Research Readiness Level (RRL) that leads to a possible implementation in AEDT in the future.

This research will enhance the accuracy of AEDT through improved aircraft noise propagation modeling. This improvement is needed to support the evaluation and development of aircraft flight routes and procedures that could reduce community noise. These improvements will also facilitate the implementation of NextGen through improved characterization of the efficiency benefits it would deliver. If this research is not performed, then the accuracy of the noise prediction tool may not be representative of real-world operations affecting studies used by airport authorities.

In 2020–2021, the Project 40 team continued the collaborative initiative with National Aviation University of Ukraine and close cooperation with the Georgia Tech team working on ASCENT Project 43. The team continued to work with Airbus regarding a nondisclosure agreement to use the SILENCE-R dataset.

Task 1 - Assess the Propagation Uncertainty in Aircraft Noise Events, Examining the BANOERAC and Similar Data Sets

The Pennsylvania State University

Research Approach

Overview of the BANOERAC data

Background noise level and noise levels from en route aircraft (BANOERAC) was a project initiated by EASA in 2009 (contracted to Anotec Consulting, S.L.; Aspuru & van Oosten, 2009). The project had two main goals, the first of which was to prepare maps for Europe showing background noise levels. The calculation method relied on population density to determine background noise levels (based on work done earlier by SINTEF). Measurements of background noise and enroute aircraft noise were conducted in Spain (see Figure 1). The first part of the BANOERAC study focused on correcting the SINTEF model for areas of extremely low population density by taking background noise measurements. (This correction will not be the focus of the analysis presented here.) The second goal of the study involved measurements of enroute aircraft noise. These measurements were conducted from February 2009 to July 2009 (to cover winter and summer seasons). The data collection was spread across 20 days over the six-month period.

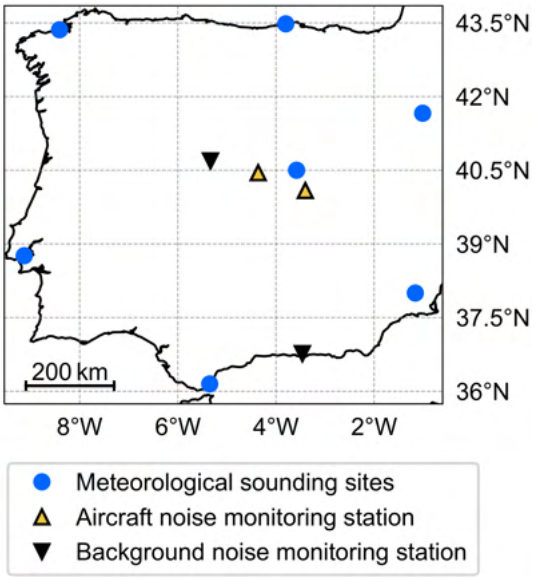

Figure 1. Map of Spain showing locations of measurement sites.

The measured data included time histories of aircraft tracking data and noise measurement data (one-third octave band levels) obtained from two microphones, one placed 1.2 m above the ground, and the second inverted and placed on a flat plate on the ground. The locations of the noise monitors can be seen in Figure 1 (yellow triangles). Meteorological data from a ground meteorological station (time synchronized with the noise monitors) and seven faraway sounding stations (seven Spanish airports shown by blue circles in Figure 1) are also provided.

Choosing noise events for analysis

In total, there are 1056 aircraft events in the BANOERAC dataset. Events that were reported to be contaminated (by noise from helicopters, general aviation, motorized vehicles, wind, birds, and other natural sources) were removed, and only events that had audible commercial aircraft noise were selected. This reduced the number of events to 537. Up to this point, only the information in the BANOERAC report (Aspuru & van Oosten, 2009) was utilized for the data filtering process. All data from the 537 events were visualized to inspect the quality of the data. Based on the preliminary visualization, the number

of usable aircraft noise events was further reduced to 68. The visualization procedure and the resulting summary of the fleet-mix of the potentially usable data are shown in the ASCENT Project 040 annual report (2019).

Knowing the aircraft source level and directivity is one of the key challenges in analyzing aircraft noise events. Because the project team had a good understanding of modeling a 'Boeing 737-800' aircraft in NASA Aircraft Noise Prediction Program 2 (ANOPP2; see Task 2 in this report and in last year's report: ASCENT Project 040 annual report, 2020), we decided to focus on aircraft events involving the same aircraft. Out of the 68 potentially usable events, only 14 involved a Boeing 737-800 aircraft. After carefully skimming through the events involving a Boeing 737-800, we selected events that seemed to have the least amount of non-aircraft noise for further investigation. Out of those events, three (a descent event, a cruise event, and a climb event) involving Boeing 737-800 aircraft are analyzed and discussed in this report. To gain a brief understanding of aircraft altitudes, slant distances, and the maximum overall sound pressure levels (OASPL) involved in these events, a brief summary is provided in Table 1. Note that the cruise event selected here (Event ID 40305) is different from the one (Event ID 120301) in last year's annual report (ASCENT Project 040 annual report, 2020). The cruise event shown in the 2020 report did not have sufficiently clean measurement data for the noise monitors; hence, it was discarded and replaced with a cleaner event.

Table 1. Brief Summary of the Noise Events Selected for Analysis

	Event ID 30609	Event ID 40305	Event ID 30214
Event type	Descent	Cruise	Climb
Aircraft altitude (min. to max.)	4.6 km to 5.9 km	11.3 km	6.4 km to 8 km
Maximum OASPL (50 Hz to 5000 Hz) for the ground microphone	58 dB	48 dB	60 dB
Slant distance (min. to max.)	4.6 km to 18 km	11 km to 37 km	7.2 km to 28.6 km

OASPL = overall sound pressure level.

Data associated with the selected events

The data available for each of the three selected events are shown in Figures 2 to 5 (the descent event), Figures 12 to 15 (the cruise event), and Figures 21 to 24 (the climb event), respectively. Because the figures corresponding to each event are laid out identically, only Figures 2 to 5 are explained in detail in the following subsection.

Detailed explanation of the data visualization for the descent event

The event shown in Figures 2 to 5 involves a descending Boeing 737-800 aircraft. Figure 2 shows the aircraft track (with timestamps) along with the location of the noise monitor (the yellow triangle). Figure 3 shows the time history of the aircraft altitude (solid black line on the left-hand Y-axis) as well as the slant distance (dashed blue line on the right-hand Y-axis). Figure 4 shows the time history of the aircraft ground speed (solid black line on the left-hand Y-axis) and the time history of the aircraft heading (dashed blue line on the right-hand Y-axis). As can be seen from Figure 4, aircraft ground speed drops from 650 km/h to about 600 km/h during the event (a slow descent). The heading angle time history shown in Figure 4 can be corroborated with the aircraft track shown in Figure 2. The time history of one-third octave band sound pressure levels (SPLs) is shown in Figure 5 using a colormap (dark blue to yellow) along with the OASPL in red (right-hand Y-axis). The upper part of Figure 5 shows the data from the microphone on the ground and the lower part shows the data from the microphone placed at 1.2 m above the ground. The aircraft is approaching the noise monitor until about 65 seconds, as can be seen from Figure 2 (aircraft track), which is reflected in the time history of the slant distance (dashed blue line reaching its minimum value) in Figure 3. After that point in time, the aircraft continues to move away from the noise monitor. The direct effect of this kind of trajectory is evident in the noise monitor data, where the OASPL is seen to be increasing for the first part of the event and then starts dropping off as the aircraft flies away from the noise monitor.

The sound energy observed at the start of an event (time = 0 s) corresponds to the energy emitted a finite amount of time in the past (since sound must travel from aircraft to receiver over a finite distance). To account for this, the data shown in Figures 2 to 5 (the descent event), Figures 12 to 15 (the cruise event), and Figures 21 to 24 (the climb event) include an additional amount of time before the start of the event (before the zero-second mark). In the previous annual report (ASCENT Project 040 annual report, 2020), data before the start of the event were not shown because the project team had not accessed the data and had instead extrapolated the aircraft trajectory to obtain aircraft track before the start of the event.

Descent event (event ID 30609):

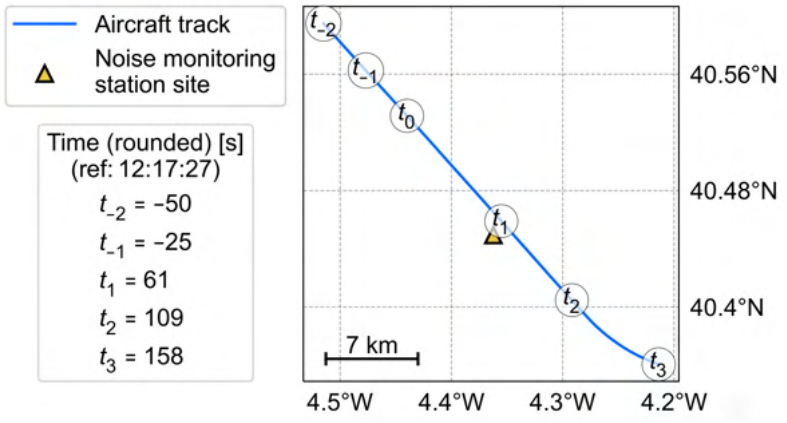

Figure 2. Time history of the aircraft trajectory (descent event).

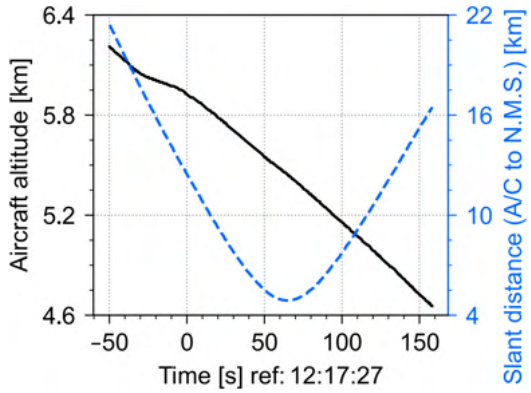

Figure 3. Time history of the aircraft altitude and the slant distance between the aircraft (A/C) and the noise monitor station (N. M. S.) (descent event).

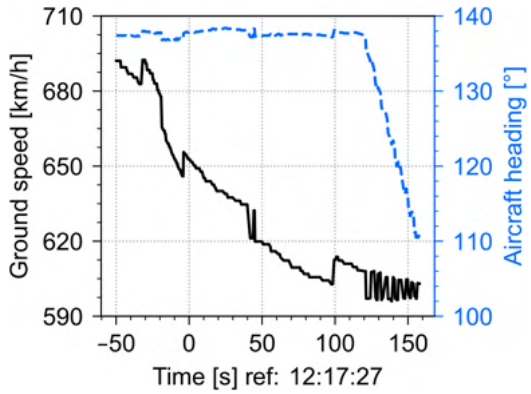

Figure 4. Time history of the aircraft ground speed and heading angle (descent event)

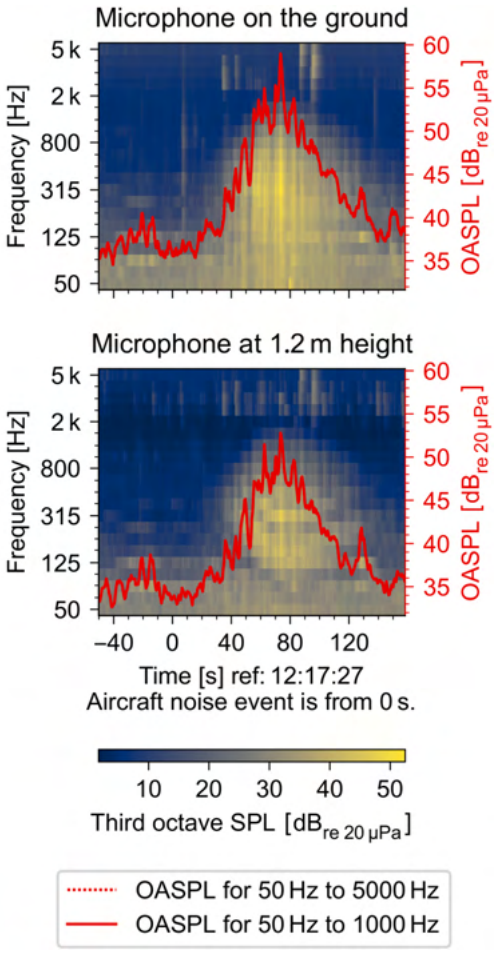

Figure 5. Time history of one-third octave band SPLs and OASPL for microphones on the ground and at 1.2 m height (descent event).

Modeling the acoustic propagation
The Penn State team developed an in-house acoustic ray-tracing code that takes into account wind (vector), sound speed profile, and ground reflections. The in-house code assumes a vertically stratified atmosphere (i.e., temperature and wind profiles are specified as functions of the vertical coordinate). The code was validated using a benchmark problem.

Atmospheric absorption was modeled using ISO 9613-1 and used SAE-ARP-5534 to correctly calculate the losses when dealing with the one-third octave band data. To take into account the inhomogeneity in the humidity and temperature profile (since both affect absorption), atmospheric absorption was successively calculated every 10 m along the slant range from the source to the receiver (assuming a vertically stratified atmosphere).

The effect of a moving source on the frequency content of the noise (Doppler effect) is included in the in-house calculations. For amplitude, the effect of convection on the received SPL is included as a function of the Mach number and the emission angle (Ruijgrok, 1994; Burley, C., & Rawls, J., 2011); please see last year's annual report for details (ASCENT Project 040 annual report, 2020).

Limitations of the available meteorological data
The BANOERAC data provide two types of meteorological data. The first are from a ground meteorological system. The data from this system (placed on a 1.8-m-high mast at the noise measurement site) consist of temperature, relative humidity, wind speed, wind direction, and atmospheric pressure. Although the data are synchronized in time with the noise measurement data, the data only provide information at one physical location (i.e., not along a vertical profile).

The second type of data are from meteorological sounding stations (seven Spanish airports shown by blue circles in Figure 1). Data from the seven stations do provide vertical profiles of the meteorological variable but are only available every 12 hours (and not in sync with the noise events). In addition, the sounding stations are far away from the noise measurement sites. For the noise events under consideration, the closest meteorological sounding station (Madrid airport) is about 66 km away from the noise monitor; hence, sounding station data might not be the best choice for use in acoustic propagation calculations.

Obtaining the meteorological conditions necessary to analyze the events
As explained in the last year's annual report (ASCENT Project 040 annual report, 2020), the Penn State team had considered alternative sources (such as ERA5 [Copernicus Climate Change Service, 2017], CFSv2 [Saha et al., 2011], and HRRR [Horel and Blaylock, 2015]) for obtaining meteorological conditions relevant to the noise events under consideration. Because of the geographical location of the BANOERAC test sites (in Spain), the meteorological data source with the best possible resolution (both spatial and temporal) seems to be the ERA5 reanalysis product. It is hosted by the European Centre for Medium-Range Weather Forecasts (ECMWF). The horizontal grid of the ERA5 product has a 0.25° resolution in both latitude and longitude (which corresponds to about 15–20 km for Spain). The temporal resolution of the product is 1 hour, and the vertical grid consists of 37 pressure levels from 1000 hPa to 1 hPa.

As shown in last year's annual report (ASCENT Project 040 annual report, 2020), the meteorological profiles do not vary drastically within the span of 15 to 20 km; hence, data from the grid point closest to the aircraft track were used for the propagation calculations. Note that this grid point is about 8 km away from the noise monitor. It is important to note that because the ERA5 reanalysis product has a temporal resolution of 1 hour, and the data obtained are from the closest hour to the actual event time. Refer to last year's annual report for the process followed to validate and gain confidence in the data from ERA5.

Aircraft source levels and directivity
Preliminary noise propagation predictions (shown in the ASCENT Project 040 annual report, 2019) demonstrated the importance of using a realistic noise source directivity when estimating ground-based measurements. To provide such a noise source description, ANOPP2 is being used. The details of obtaining the noise source description are explained in Task 2 from the 2020 annual report (ASCENT Project 040 annual report, 2020). The noise directivity data obtained from ANOPP2 are used along with the in-house ray-tracing code to predict aircraft noise levels near the ground.

Focus of this year's work
The work presented in the last year's report focused only on the OASPL predictions for the microphone on the ground. Last year, the emphasis was on investigating the impact of correctly modeling the propagation path (inhomogeneity in meteorological conditions). This year, we focused on comparing the results for the ground microphone and the microphone

at 1.2 m. Instead of looking only at the OASPL, we also present a detailed analysis of one-third octave band level comparisons. To assess the quality of the measured data as well as the predictions, the project team has taken a closer look at the background noise data before and after the aircraft noise events.

Differences between the ground microphone and the microphone at 1.2 m

The noise monitor station site (shown in Figure 6) for the events under consideration was in Cebreros (Ávila), Spain. As mentioned in the BANOERAC report (2009), the ground near the noise monitor had "relatively soft soil" and the surroundings were flat. The exact ground condition varied from "no vegetation" to "low wheat plants" (in spring) during the measurement period (February–July 2009). Unfortunately, the exact conditions of the ground near the noise monitor are not known for the aircraft noise events under consideration.

Figure 6. Representative image from the BANOERAC report (2009) showing the ground conditions and the microphone at 1.2 m.

Because the ground conditions during the test are not precisely known, typical soft ground was modeled using Attenborough's four-parameter model. The parameters used to define the ground are (1) static flow resistivity σ = 200 kPa·s/m^2, (2) porosity Ω = 0.27, (3) grain shape factor g = 0.5, and (4) pore shape factor s_f = 0.75. Using these values, ground impedance was incorporated in the in-house ray-tracing code, and the reflected ray from the ground was correctly accounted for when making predictions for the microphone at 1.2 m height.

Figure 7 shows the comparison of OASPL for the ground microphone and for the microphone at 1.2 m above the ground for the descent event. The black line and red line indicate measured data from the ground microphone data and the microphone at 1.2 m height, respectively. The ray-tracing predictions for the same two microphones are shown by the blue line (with asterisks) and the orange line (with upward-pointing triangles), respectively. Qualitatively, the ray-tracing results follow similar trends for both microphones. Until about 70 seconds, the ray-tracing results overpredict the OASPL by a maximum of 5 dB but after the 70-second mark, the overprediction goes as high as 15-20 dB.

Figure 8 shows the difference between OASPL measured by the microphone on the ground and the microphone at 1.2 m. The red line indicates measured data and the black line shows predicted data. As expected, the OASPL for the microphone on the ground was higher than that for the microphone at 1.2 m (for both measured and predicted data). The difference between the predicted levels for the two microphones was lower when the aircraft was far away from the noise monitor (i.e., toward the start and the end of the event). In addition to the qualitative agreement between prediction and measurement throughout the event, the quantitative agreement between 20 and 60 seconds is reassuring.

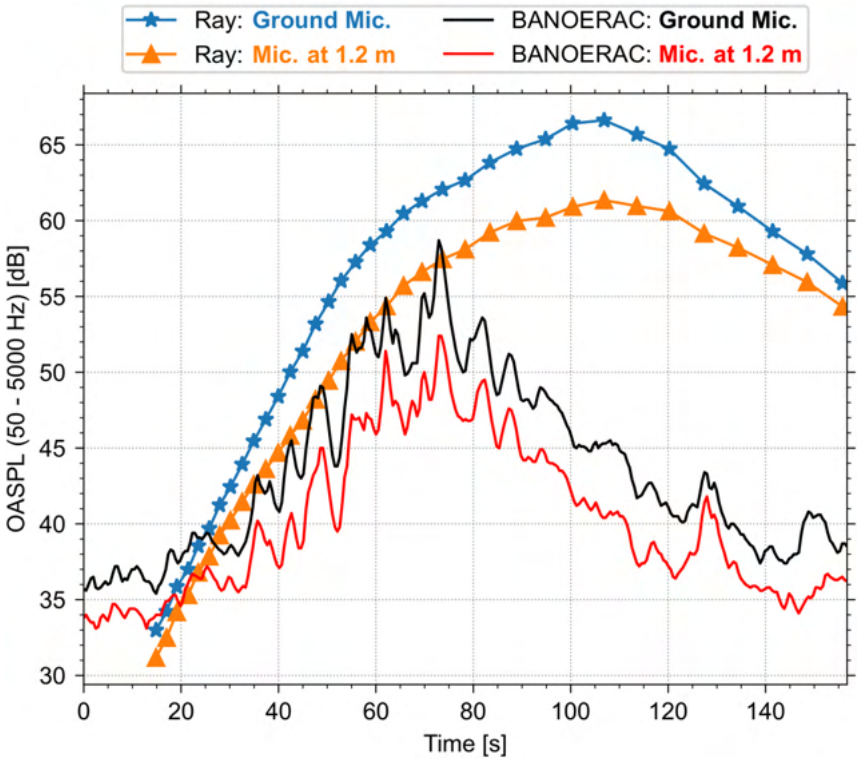

Figure 7. Comparing the ray-tracing overall sound pressure level (OASPL) results with measurements for the ground microphone (Mic.) and that at 1.2 m height (descent event, event ID 30609).

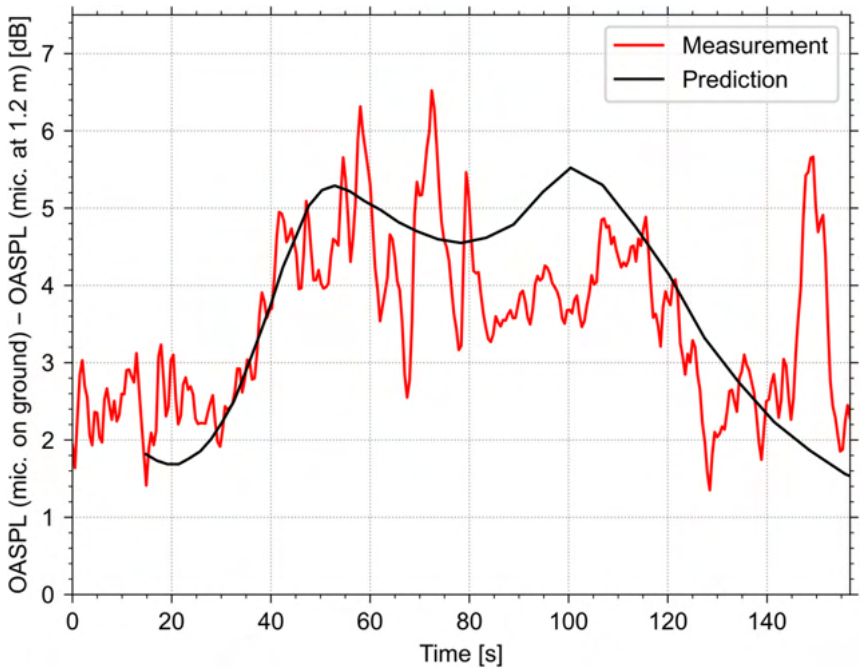

Figure 8. Comparing measurements and prediction (ray-tracing): difference between overall sound pressure level (OASPL) for the ground microphone (mic.) and that at 1.2 m height (descent event, event ID 30609).

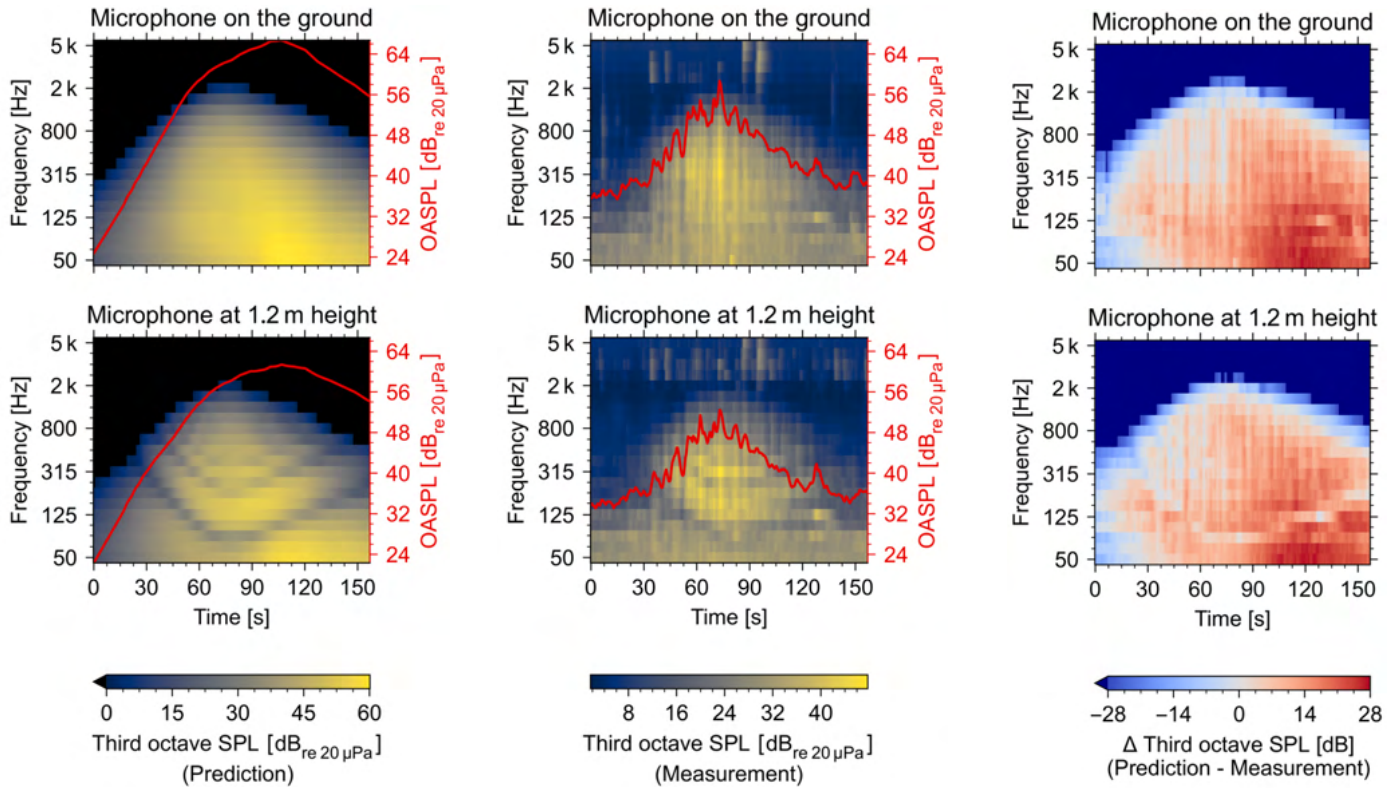

(a) Prediction using ray-tracing **(b)** Measured data (BANOERAC) **(c)** Prediction − measurement

Figure 9. Comparing the ray-tracing one-third octave band prediction results with the measurement for the ground microphone and the microphone at 1.2 m height (descent event, event ID 30609). SPL = sound pressure level.

To investigate the differences between measurements and predictions, the project team looked at the one-third octave band data, as shown in Figure 9. The predicted one-third octave band data are shown in Figure 9(a), the measured data in Figure 9(b), and the difference between them in Figure 9(c). It is reassuring to see the destructive interference pattern for the microphone at 1.2 m at similar locations in both predictions and measurements. The destructive interference pattern is not as prominent in the measured data (Figure 9(b)) as in the predicted data (Figure 9(a)). One possible reason for this is contamination of the measured data by background noise. The assumptions made about the nature of the ground (a soft, flat surface with no vegetation) might not be consistent with reality and could have led to a less prominent destructive pattern in the measured data. If narrow band data (e.g., one-twelfth octave) were available, we could have investigated the details of the destructive pattern and its relation to the nature of the ground surface. From the predicted data in Figure 9(a), we concluded that there is no perceivable aircraft noise above 2 kHz (even in the middle of the event when the slant distance is close to 5 km). At the start of the event, there is almost no contribution from the frequency bands above 125 Hz because of the large propagation distance involved (around 20 km). This is attributed to atmospheric attenuation. From Figure 9(c), it can be seen that the overprediction in the later part of the event is due to a strong contribution from bands between 125 Hz and 315 Hz (notice the darker shades of red toward the end of the event in Figure 9(c)).

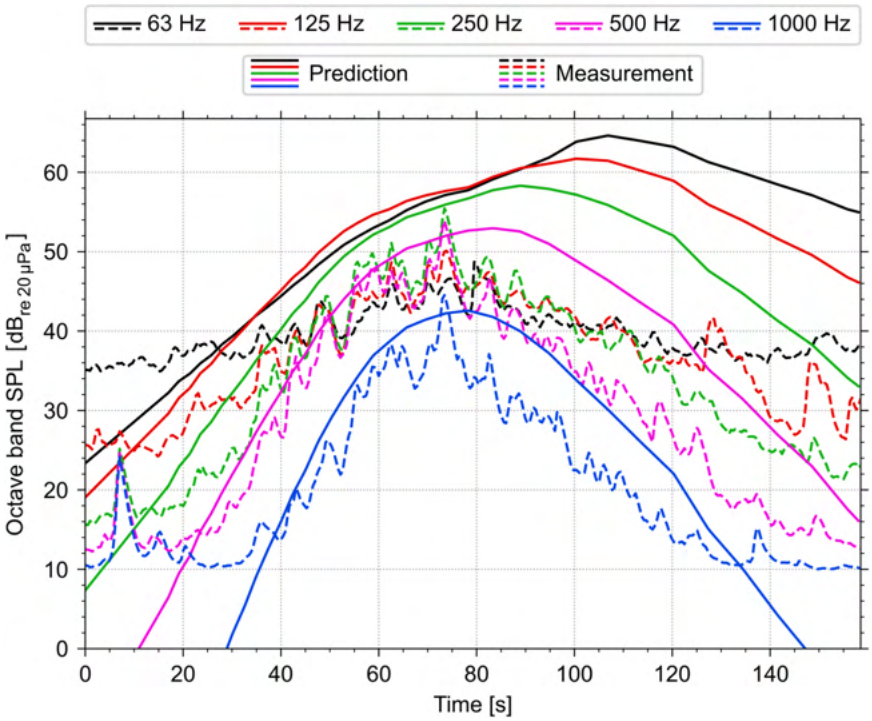

Figure 10. Octave band data for the ground microphone for the duration of the event (descent event, event ID 30609). SPL = sound pressure level.

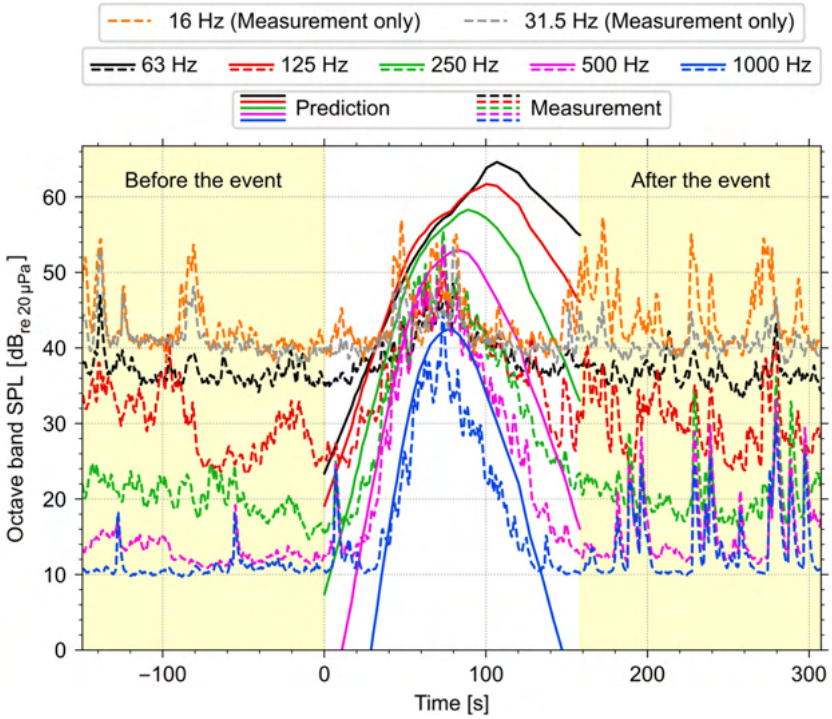

Figure 11. Octave band data for the ground microphone before, during, and after the event (descent event, event ID 30609). SPL = sound pressure level.

Investigating the reliability of the measured data by looking at the background noise levels
As can be seen from the measured data (and the summary presented in Table 1), the OASPL values are relatively low and almost approaching background noise toward the start and end of the noise events (when the aircraft is further away from the noise monitors). To assess the quality of the measurements, both the measured and predicted data for the microphone on the ground were analyzed for octave bands below 1 kHz, as shown in Figures 10 and 11. The ground microphone data were chosen for this purpose because they are not affected by interference from ground reflections. Figure 10 shows the octave band data from 63 Hz to 1 kHz for the duration of the event. Figure 11 includes two additional lower octave bands (16 Hz and 31.5 Hz; measured data only). The data shown in Figure 11 also include the measured data before the start of the aircraft noise event and after the end of the aircraft noise event.

From Figures 10 and 11, it is evident that the octave band data for 250 Hz (green line), 500 Hz (magenta line), and 1 kHz (blue line) can be reliably attributed to aircraft noise, since the peak level is more than 20 dB above the background noise level for those bands. Despite the contamination from background noise, the 125 Hz (red line) octave band data appears to be borderline acceptable. It follows the qualitative trend expected for an aircraft approaching and then going away from the noise monitor. The data in the 63 Hz octave band (black line) are clearly dominated by background noise. The measured data from the lower octave bands (16 Hz and 31.5 Hz) are consistently at a high level before, during, and after the event. The data do not show any trend (consistent with aircraft trajectory) and are unusable for validation work.

The analysis shown in the rest of the report (for the cruise and climb events) follows a structure similar to that shown for the descent event.

Cruise event (Event ID 40305):

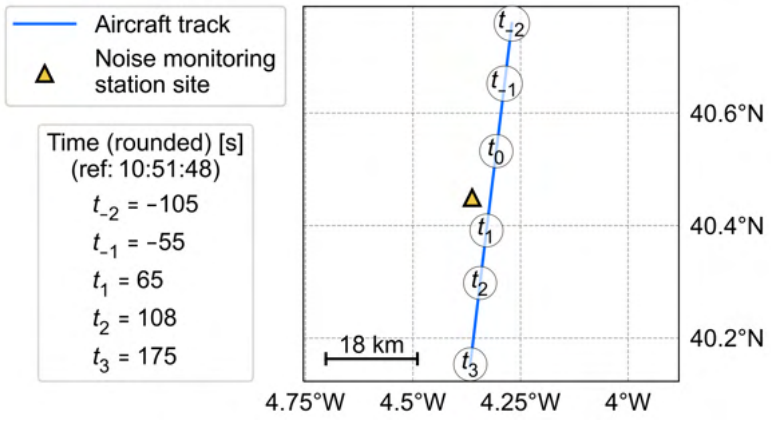

Figure 12. Time history of the aircraft trajectory (cruise event).

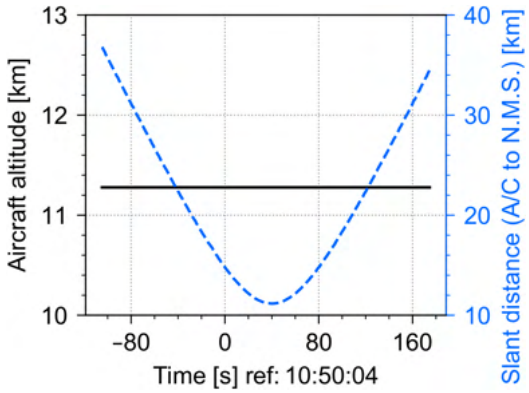

Figure 13. Time history of the aircraft altitude and the slant distance between the aircraft (A/C) and the noise monitor (N.M.S.) (cruise event).

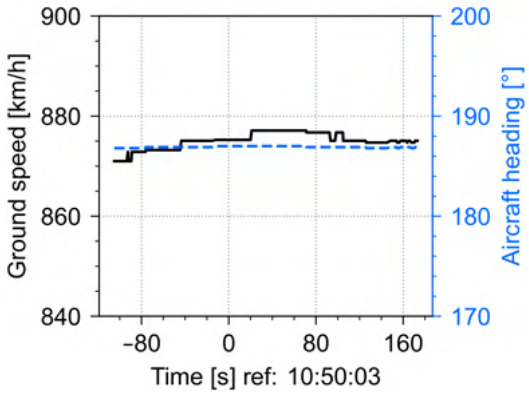

Figure 14. Time history of the aircraft ground speed and heading angle (cruise event).

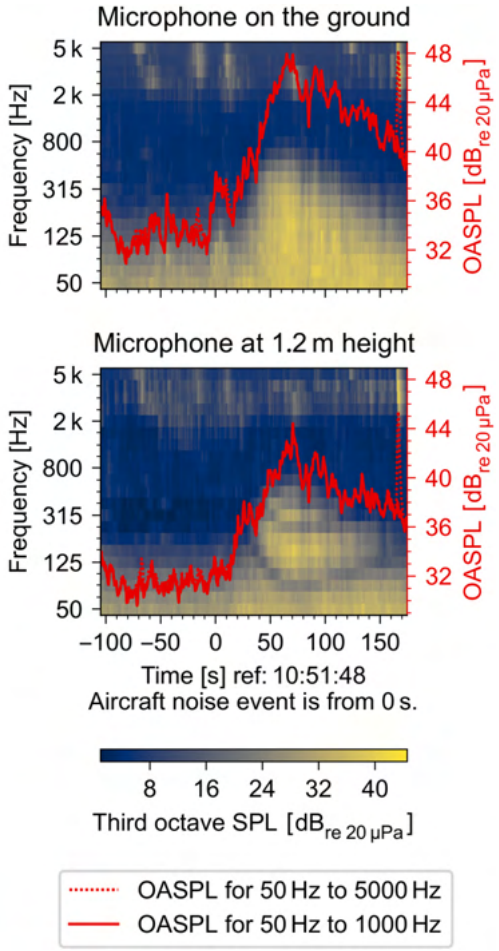

Figure 15. Time history of one-third octave band SPLs and OASPL for the microphones on the ground and at 1.2 m (cruise event).

Figures 12 to 15 show the detailed visualization of the cruise event selected for analysis. The description of these figures closely follows the details provided for the descent event.

For the cruise event, the ray-tracing results obtained for the microphone on the ground and the microphone at 1.2 m are shown in Figure 16. Qualitatively, the predictions follow the trend seen in the measured data after 40 seconds, where predictions are off by 5 dB, at most, for both microphones. The predicted levels at the start of the event (prior to 40 seconds) are much lower than the measurements. During this part of the event, the slant distance is on the order of 30 km, which explains the low predicted levels due to atmospheric attenuation. The measured data are likely dominated by background noise during this part of the event. Figure 17 shows the difference between the OASPL measured by the microphone on the ground and the microphone at 1.2 m. The red line in Figure 17 shows measured data and the black line shows predicted data. Throughout the event, the maximum difference between the OASPL measured by the ground microphone and the microphone at 1.2 m was about 6 dB for both the measured and predicted levels (consistent with our expectation).

Similar to the analysis conducted for the descent event, Figure 18 shows the one-third octave band data for predictions, measurements, and the difference between the two. As reported for the descent event, the in-house ray-tracing is able to correctly predict the interference pattern in the data for the microphone at 1.2 m. In the case of the cruise event under consideration, the lowest slant distance (corresponding to the middle portion of the event) is about 12 km. For this reason, almost no aircraft noise will be detected above 800 Hz throughout the event (as evident by the predictions shown in Figure 18(a)).

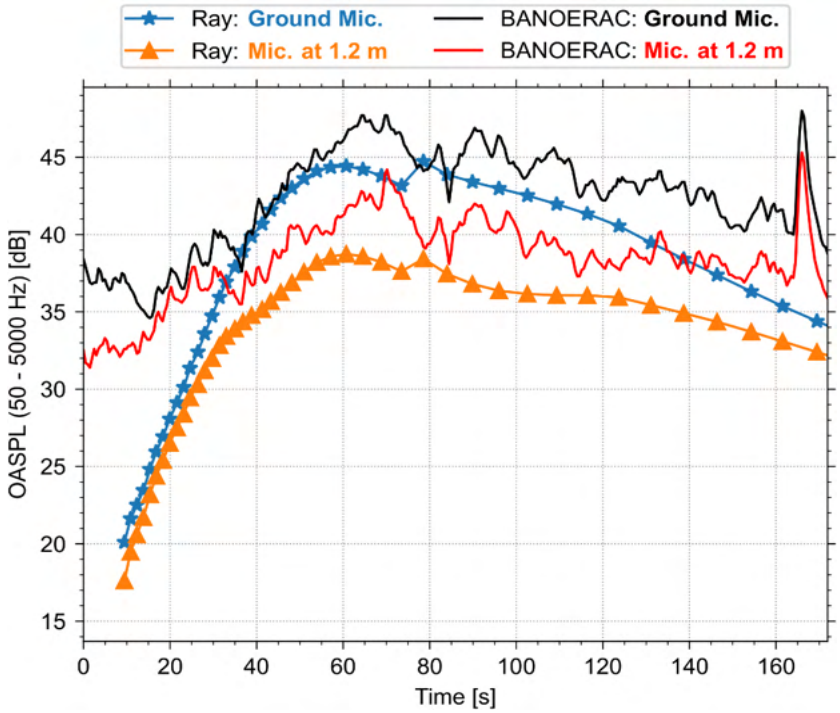

Figure 16. Comparing the ray-tracing overall sound pressure level (OASPL) results with measurements for the ground microphone (Mic.) and the microphone at 1.2 m (cruise event, event ID 40305).

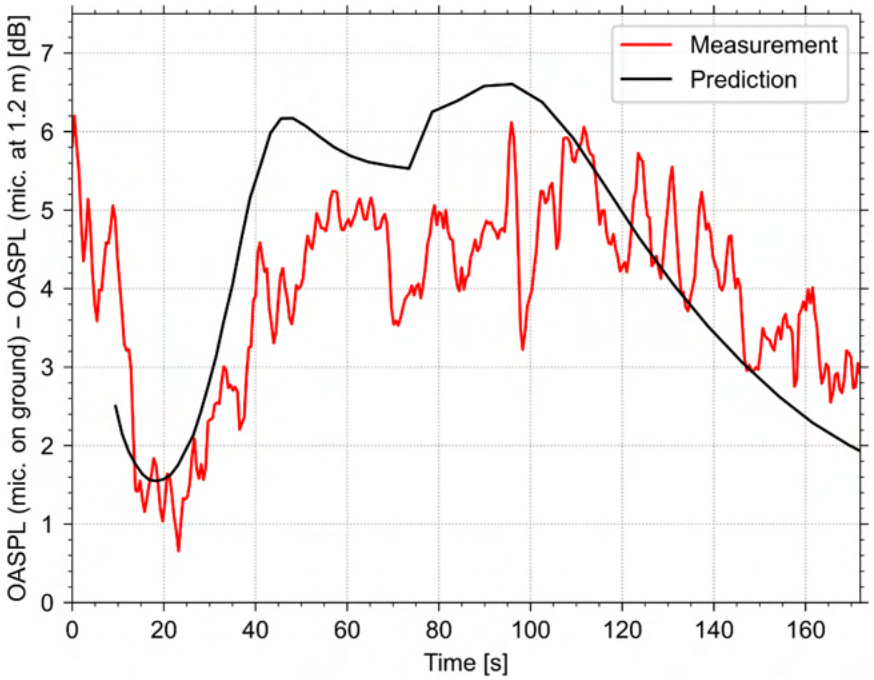

Figure 17. Comparing measurements and prediction (ray-tracing): difference between overall sound pressure level (OASPL) for the ground microphone (mic.) and that at 1.2 m (cruise event, event ID 40305).

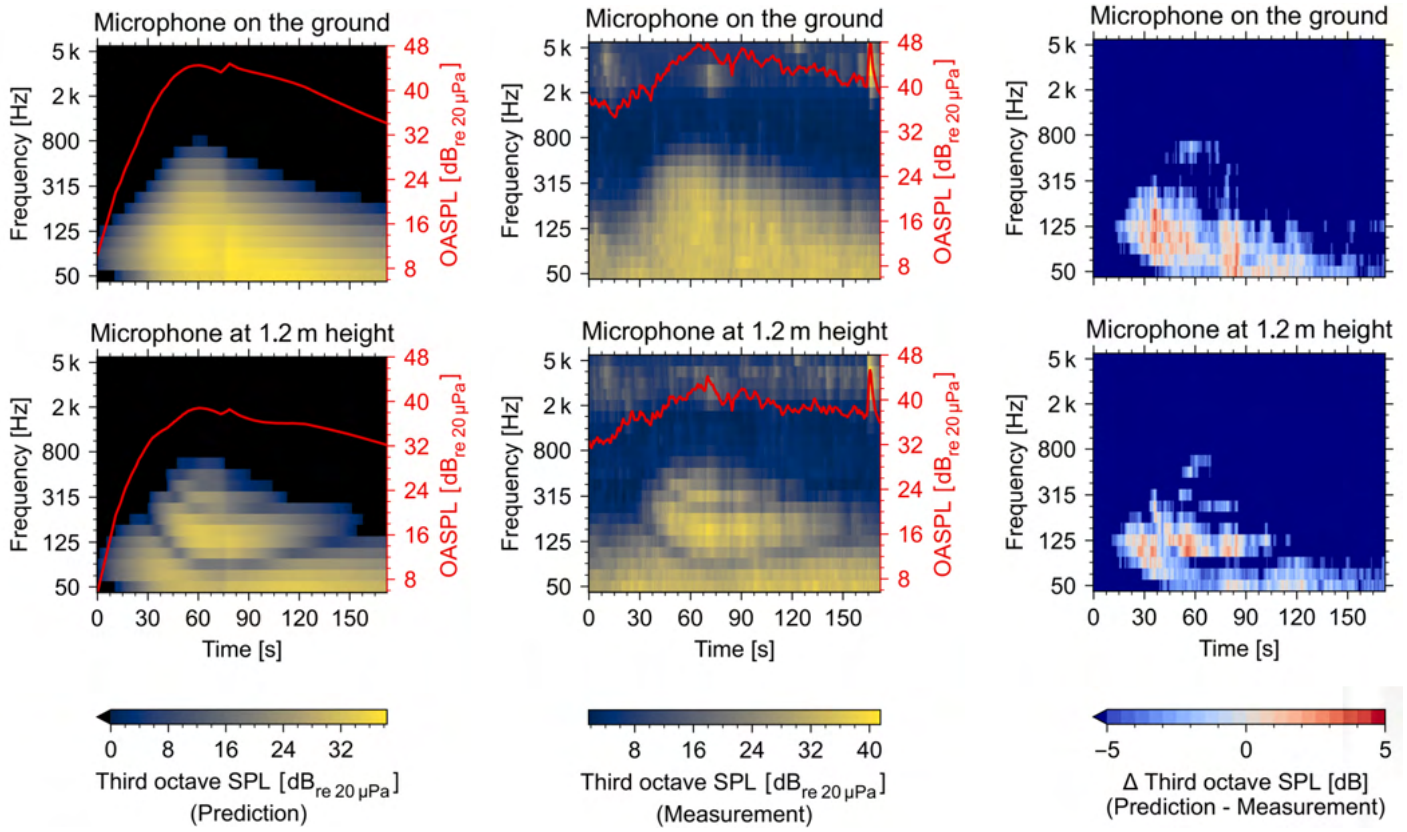

(a) Prediction using ray-tracing **(b)** Measured data (BANOERAC) **(c)** Prediction − measurement

Figure 18. Comparing the ray-tracing one-third octave band prediction results with measurements for the ground microphone and that at 1.2 m (cruise event, event ID 40305). SPL = sound pressure level.

The contamination of the measured data below 125 Hz and above 2 kHz (seen in Figure 18(b)) explains the large discrepancy between the OASPL predictions and measurements in the initial part of the event. This is confirmed by looking at Figures 19 and 20, which show the octave band data for the event and for 180 seconds before and after the event. From Figures 19 and 20, it can be seen that the 63 Hz and 1 kHz octave band data are dominated by background noise. In the context of the background noise before and after the event, only the data from the 250 Hz and 500 Hz octave bands seem reliable (the peak level in these bands is more than 20 dB above the background level). The agreement between the measured data and the prediction for the 125 Hz octave band is barely acceptable. As with the descent event, the data in the lower octave bands (16 and 31.5 Hz) are unusable for validation work.

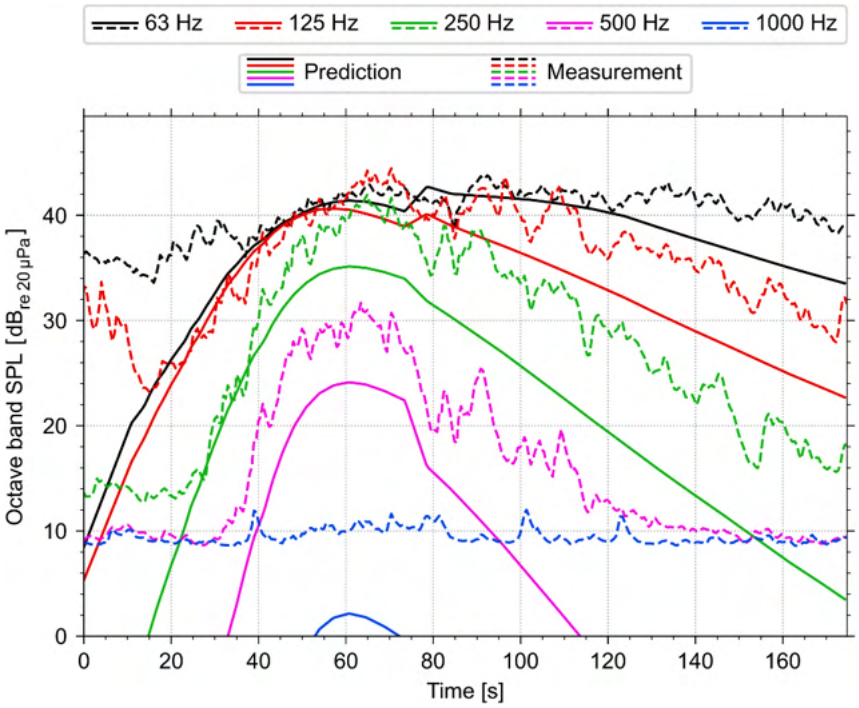

Figure 19. Octave band data for the ground microphone for the duration of the event (cruise event, event ID 40305). SPL = sound pressure level.

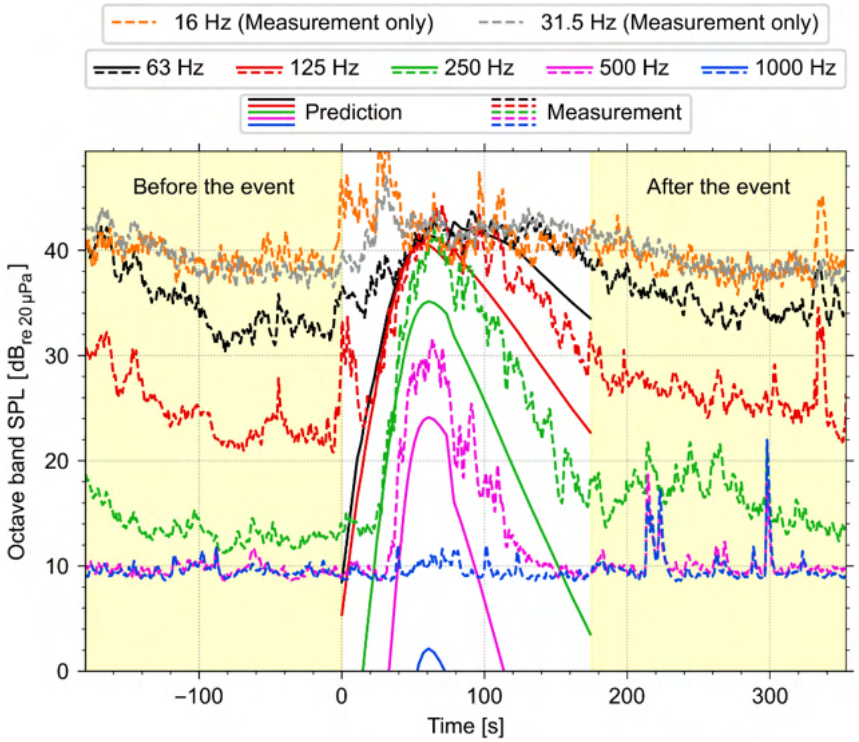

Figure 20. Octave band data for the ground microphone before, during, and after the event (cruise event, event ID 40305). SPL = sound pressure level.

Climb event (event ID 30214):

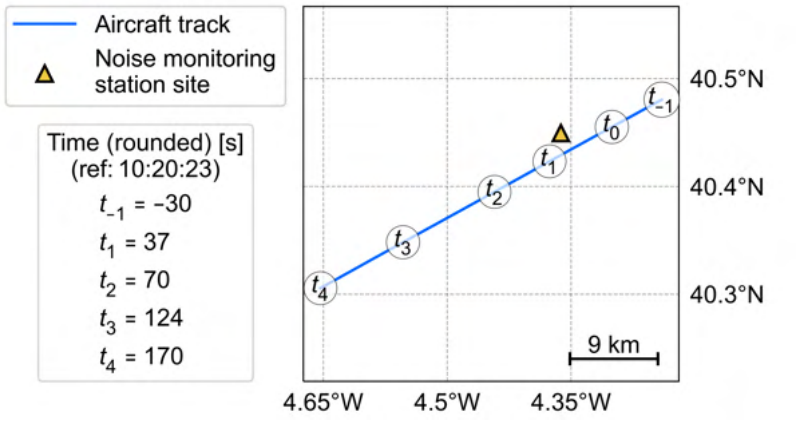

Figure 21. Time history of the aircraft trajectory (climb event).

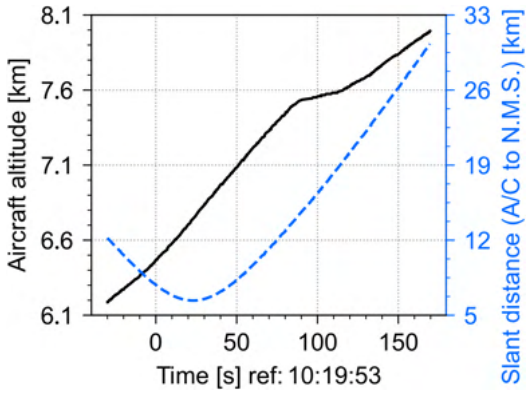

Figure 22. Time history of the aircraft altitude and the slant distance between the aircraft (A/C) and the noise monitor (N.M.S.) (climb event).

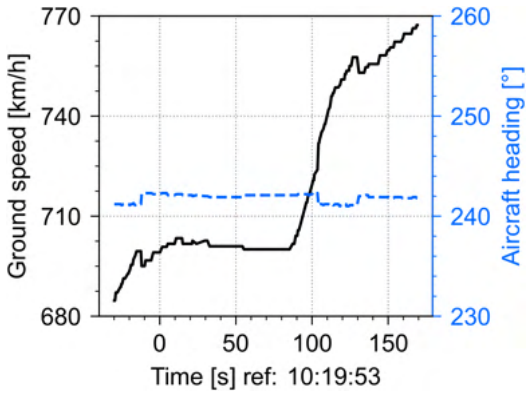

Figure 23. Time history of the aircraft ground speed and heading angle (climb event).

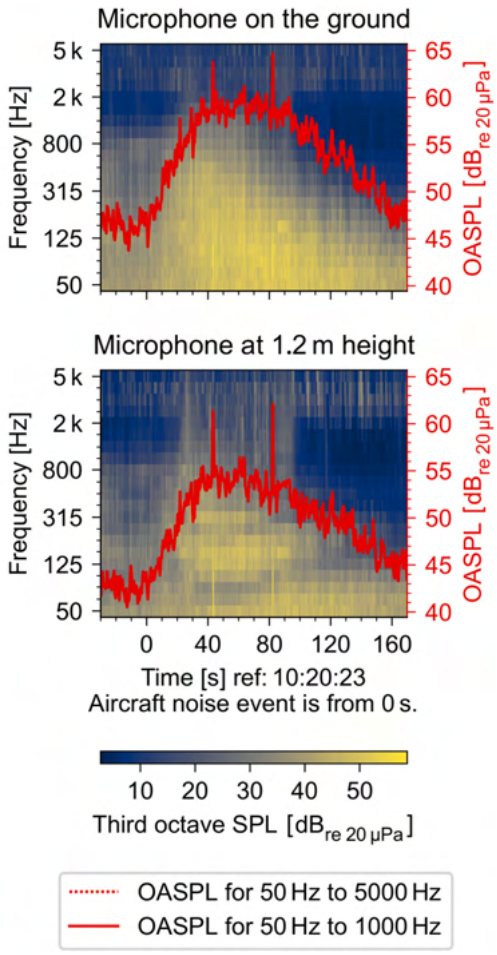

Figure 24. Time history of one-third octave band sound pressure levels (SPLs) and overall sound pressure level (OASPL) for the microphone on the ground and the microphone at 1.2 m (climb event).

Figures 21 to 24 show the detailed visualization of the climb event selected for analysis. The description of these figures closely follows the details provided for the descent event.

For the climb event, the ray-tracing results obtained for the microphone on the ground and that at 1.2 m are shown in Figure 25. Qualitatively, the predictions follow the trend seen in the measured data throughout the event. The predictions for both microphones match the measurements for the first 30 seconds. After the first 30 seconds, the OASPL is underpredicted by 6 dB. Figure 26 shows the difference between the OASPL measured by the microphone on the ground and that at 1.2 m. The difference between the levels for the two microphones drops off toward the end of the event (for both measurement and predictions). In Figure 26, good quantitative agreement can be seen between the measured and predicted values for the difference between OASPLs measured by the two microphones.

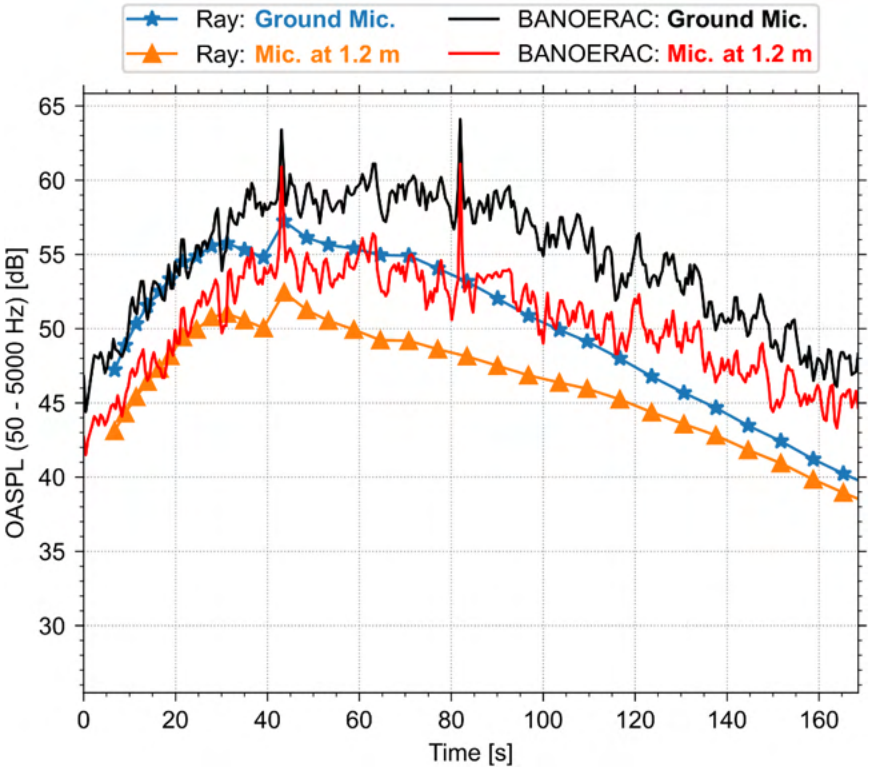

Figure 25. Comparing the ray-tracing overall sound pressure levels (OASPL) results with measurements for the ground microphone (Mic.) and that at 1.2 m (climb event, event ID 30214).

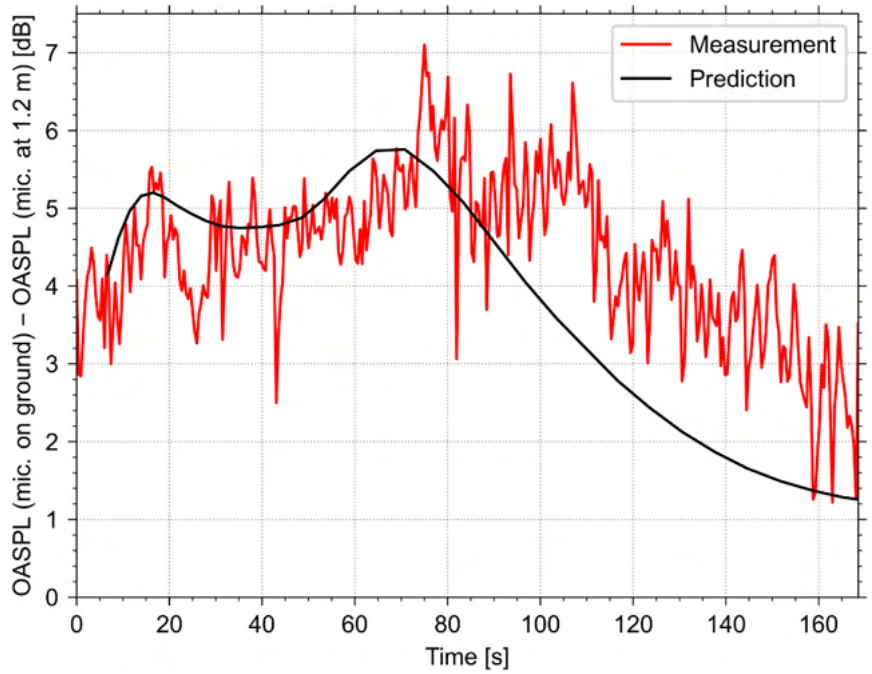

Figure 26. Comparing measurements and prediction (ray-tracing): difference between overall sound pressure levels (OASPL) for the ground microphone (mic.) and that at 1.2 m (climb event, event ID 30214).

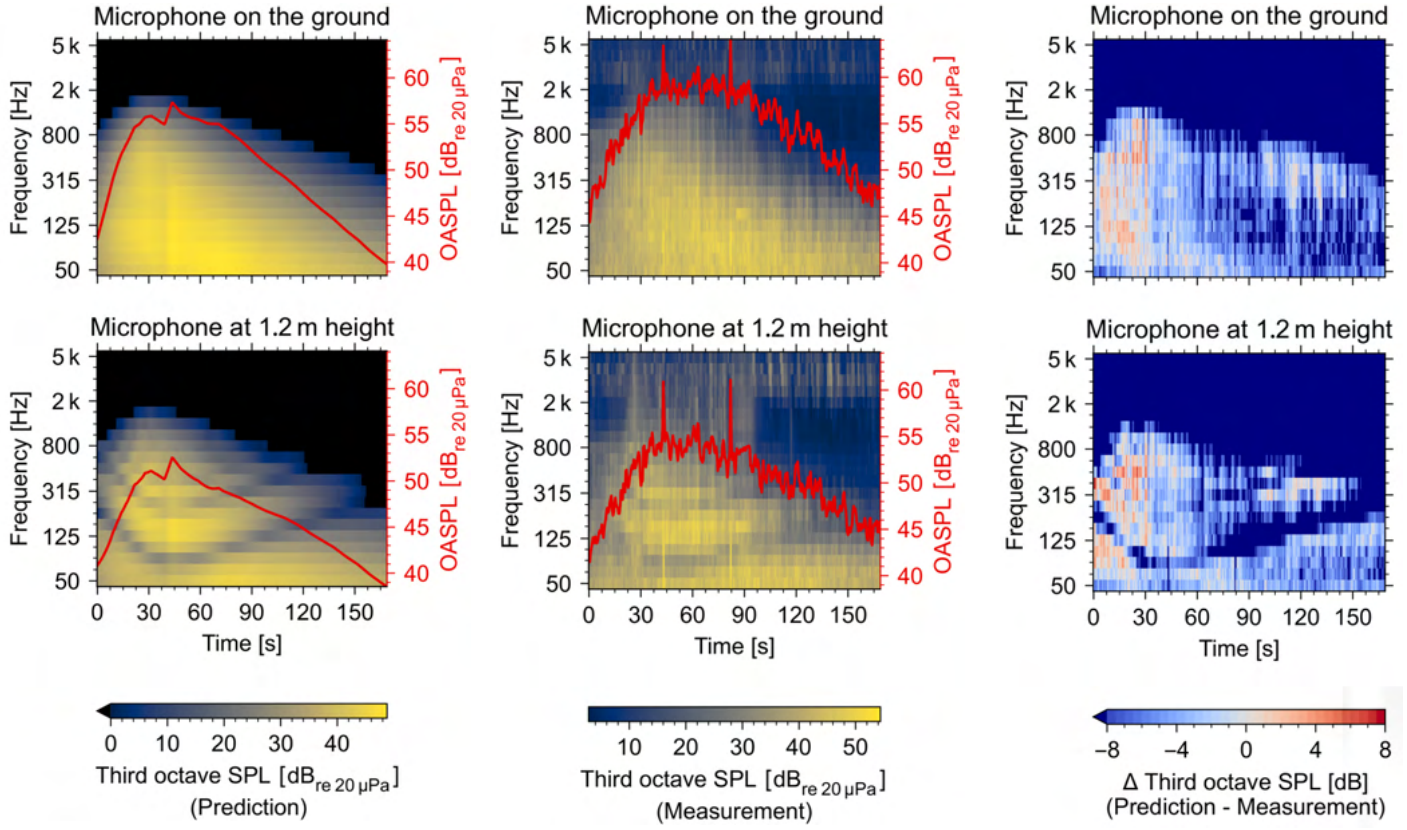

(a) Prediction using ray-tracing **(b)** Measured data (BANOERAC) **(c)** Prediction − measurement

Figure 27. Comparing the ray-tracing third octave band prediction results with the measurement for the ground microphone and that at 1.2 m (climb event, event ID 30214). SPL = sound pressure level.

Repeating a similar exercise as for the descent and cruise events, Figure 27 shows the one-third octave band time histories for (a) predictions, (b) measurements, and (c) the difference between the two. As with the previously discussed events, the in-house calculations correctly predicted the interference pattern seen in the data for the microphone at 1.2 m. There seems to be good qualitative agreement between the predictions in Figure 27(a) and the measurements in Figure 27(b), even though the measured data seem to be contaminated (especially above 1 kHz). In Figure 27(c), for the microphone on the ground, the darker blue regions around the 125 Hz band explain the underprediction in OASPL in the later part of the event.

To assess the quality of the measured data in the context of background noise, the octave band data for the event are shown in Figure 28, and the additional time history (before and after the event) is shown in Figure 29. Based on Figures 28 and 29, we can infer that the quality of the data measured at the lower end of the spectrum seems to be acceptable for this event (the data follow the trend in predictions in the higher octave bands). In Figure 28, the pattern in octave band data just before the aircraft noise event is certainly not random. The pattern in the data before the start of the event might point to a moving source like a car passing by or another aircraft flying over. The possibility of a car passing was ruled out because such an event would have appeared in the measurement log provided with the BANOERAC data. Also, it is important to note that the event is reported to be uncontaminated (i.e., after time 0 s). Fortunately, the project team had access to additional aircraft tracking data (before the start of the event). Based on the time history of the trajectory of an A-320 aircraft, it was established to be the source of the noise that appeared before the start of the climb event under consideration. The A-320 aircraft was about 18 km away (and moving away) at the start of our noise event of interest, thereby reducing the likelihood of contamination for the climb event. Nevertheless, this exercise underscores the importance of looking at the background noise data before and after the noise event of interest.

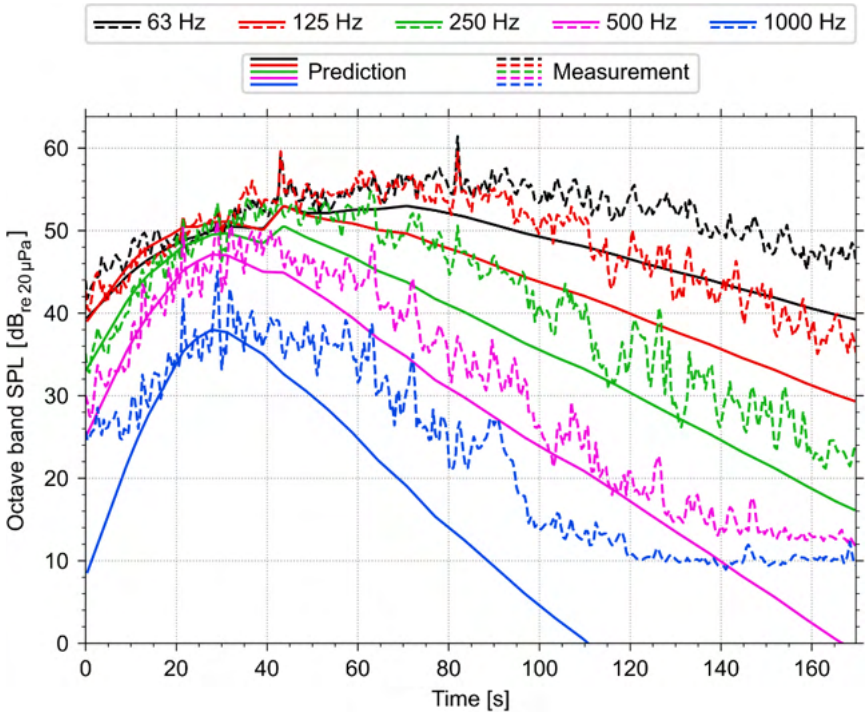

Figure 28. Octave band data for the ground microphone for the duration of the event (climb event, event ID 30214). SPL = sound pressure level.

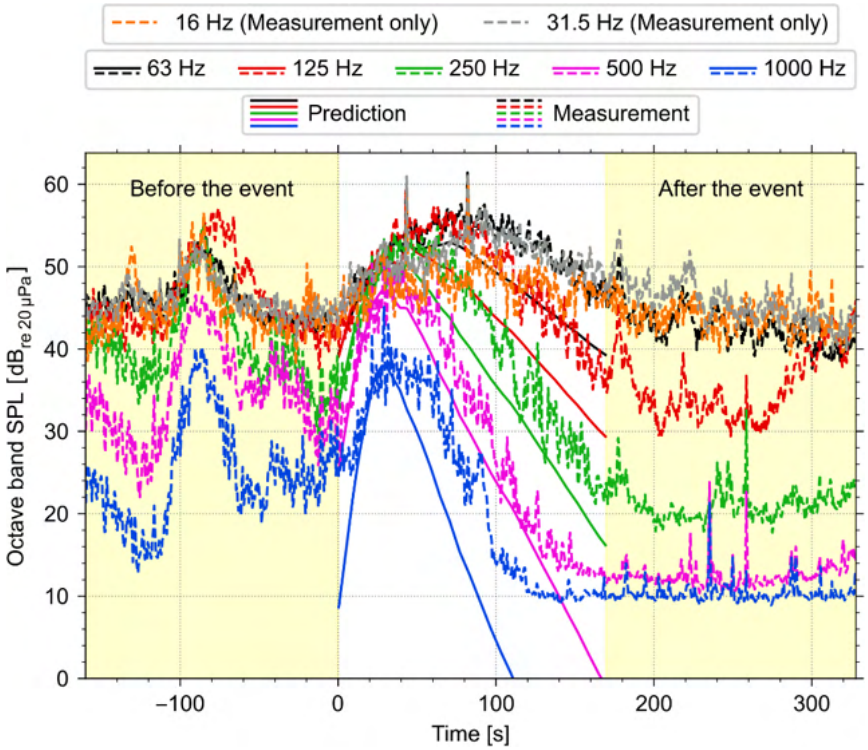

Figure 29. Octave band data for the ground microphone before, during, and after the event (climb event, event ID 30214). SPL = sound pressure level.

Conclusions based on analyzing three aircraft events using real-world measurements
The results shown in the last year's report (ASCENT Project 040 annual report, 2020) emphasized the importance of correctly including the moving source effects (for both frequency and amplitude). We achieved good qualitative agreement between measurements and predictions for the noise monitor on the ground by incorporating the inhomogeneity in meteorological variables. Inhomogeneity in the humidity profile was shown to have a more significant impact on predictions than that in the temperature profile. The effect of wind on the broadband OASPL predictions was shown to be negligible. To achieve quantitative agreement between predictions and measurements, we demonstrated the important role played by aircraft source levels and directivity (see Task 2 from the 2020 ASCENT annual report). The work presented in this report highlights the importance of looking at the one-third octave band time histories of the measured data to gain confidence in the measurements.

Milestones
A descent event, a cruise event, and a climb event, involving Boeing 737-800 aircraft, from the BANOERAC data were analyzed. To achieve this, appropriate meteorological data were extracted using the ERA5 meteorological product. Acoustic propagation was modeled using an in-house ray-tracing code and an atmospheric absorption routine that can handle inhomogeneities in temperature, humidity, and wind profiles. Given the limited or lack of information about the state of the aircraft, we attempted to correctly model the noise source and directivity (see Task 2 from ASCENT annual report 2020). The effects of high-speed source motion (convective amplification, Doppler effect) have been included in the in-house code used for making predictions. Although sufficient information about ground conditions near the noise monitors is not available, we attempted to predict levels recorded by the microphone at 1.2 m above the ground. The in-house predictions and the measured data from the noise monitors were analyzed by looking at the details of the octave and one-third octave band levels.

Major Accomplishments
Using real-world aircraft trajectories and realistic (inhomogeneous) meteorological conditions, aircraft flyover noise levels were predicted and compared with field data. Despite the very low overall levels, qualitative agreement was achieved between predicted and measured aircraft noise on the ground.

Publications
None.

Outreach Efforts
None.

Awards
None.

Student Involvement
Graduate research assistant Harshal P. Patankar has been the primary person working on this task.

Plans for Next Period
Not applicable.

References
Aspuru, I., & van Oosten, N. (2009). BANOERAC project final report (Report No. PA074-5-0). Anotec Consulting S.L. https://www.easa.europa.eu/sites/default/files/dfu/Banoerac%20final%20report.pdf

Burley, C., & Rawls, J. (2011). Aircraft Noise Prediction Program (ANOPP) Theoretical Manual. Currently maintained at NASA Langley by the ANOPP team in electronic format and provided upon request.

Horel, J., & Blaylock, B. (2015). Archive of the high-resolution rapid refresh model. University of Utah, Salt Lake City, UT. Retrieved February, 2020, from https://hive.utah.edu/concern/datasets/47429912h

Ruijgrok, G.J. (1994). *Elements of aviation acoustics*. Delft University Press.

Saha, S., Moorthi, S., Wu, X., Wang, J., Nadiga, S., Tripp, P., Behringer, D., Hou, Y., Chuang, H., Iredell, M., Ek, M., Meng, J., Yang, R., Mendez, M. P., van den Dool, H., Zhang, Q., Wang, W., Chen, M., & Becker, E. (2011). *NCEP Climate Forecast System Version 2 (CFSv2) 6-hourly Products*. Research Data Archive at the National Center for Atmospheric Research,

Computational and Information Systems Laboratory. Retrieved January, 2019, from https://doi.org/10.5065/D61C1TXF
Wilson D. K., Pettit C. L., Ostashev V. E., and Vecherin S. N. (2014). Description and quantification of uncertainty in outdoor sound propagation calculations. The Journal of the Acoustical Society of America 136(3), 1013–1028
(2017). *Copernicus Climate Change Service (C3S) (2017): ERA5: Fifth generation of ECMWF atmospheric reanalyses of the global climate*. Copernicus Climate Change Service Climate Data Store. Retrieved February, 2020, from https://cds.climate.copernicus.eu/cdsapp#!/home
(2019). ASCENT Project 040 2019 Annual Report (V. Sparrow, Ed.). FAA, Washington, DC. https://s3.wp.wsu.edu/uploads/sites/2479/2020/05/ASCENT-Project-040-2019-Annual-Report.pdf
(2020). ASCENT Project 040 2020 Annual Report (V. Sparrow, Ed.). FAA, Washington, DC. https://s3.wp.wsu.edu/uploads/sites/2479/2021/03/ASCENT-Project-040-2020-Annual-Report.pdf

Task 2 - Assess Uncertainty in Realistic Noise Source Models in ANOPP

Pennsylvania State University

Objectives

The first objective of this task was to provide source spheres for cases from the BANOERAC dataset for noise prediction with ANOPP. All events chosen were for Boeing 737-800 aircraft. The event flightpaths corresponded to a climb event, a cruise event, and a descent event. ANOPP input decks were generated for each event, and noise was predicted for the BANOERAC ground monitor location.

Second, source spheres of 1-m radius around the aircraft were developed. The acoustic predictions from ANOPP included OASPL and one-third octave band SPLs for each event. These were necessary for the use of ray-tracing techniques through a realistic atmosphere.

Sound source spheres

The approach to the generation of the source input decks was described in the previous annual report (ASCENT Project 040 annual report, 2020). Sound source spheres with a radius of 1 m were generated at the location where the aircraft was closest to the ground observer station. The available flightpath information allowed for the generation of aircraft body Euler angles, ground speeds, and Mach number, needed as inputs in ANOPP. Separate source spheres were generated for jet and fan noise, core noise, and airframe noise. Fifty-eight source locations on the source spheres were used, and the OASPL and one-third octave band SPLs at these locations were provided in tabular form for propagation calculations. Two key improvements were made to the previous methodology. A technique was developed to overcome the difficulty in using ANOPP2 to generate sound source spheres at a distance of 1-m radius from the aircraft noise source point. The difficulty was in allowing for the motion of the aircraft during the extraction of the sound source sphere. The problem was overcome by generating the rear half of the source sphere at one time step and the forward half at the next time output. This ensured that the sphere radius was kept constant at 1 m. The effect of this correction can be seen in Figure 30.

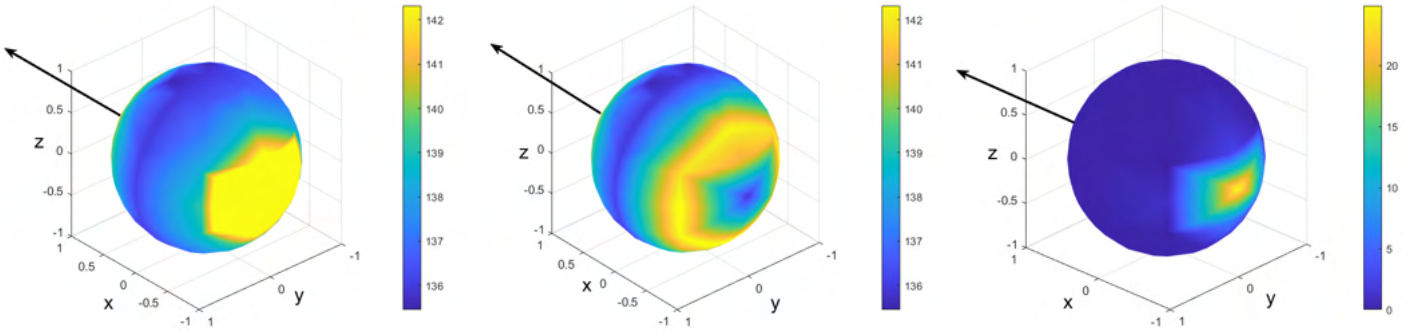

a) uncorrected b) corrected c) error

Figure 30. Sound source sphere calculations showing effect of correction for aircraft motion during ANOPP2 outputs.

A second check on the sound source sphere outputs was made to determine the effect of spatial resolution on the sphere of the predicted OASPL and one-third octave band levels on the acoustic predictions at the ground observer. Figure 31 shows the high-resolution sphere. This should be contrasted with the lower resolution sphere shown in Figure 30b. Despite the obvious differences, the predicted observer levels were virtually identical. Since the time taken to generate a high-resolution sphere is computationally much longer, all predictions have continued to be made using the lower resolution.

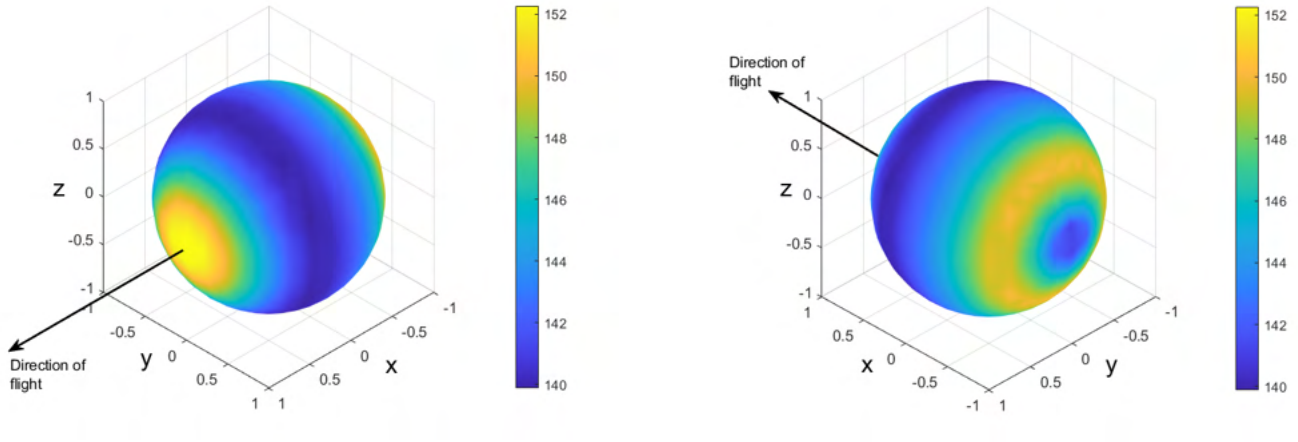

a) from front b) from rear

Figure 31. High-resolution sound source sphere calculations for cruise event.

Milestones
Not applicable.

Major Accomplishments
Sound source spheres were generated for a new cruise event. The source resolution on the 1-m source sphere was shown not to affect the predicted noise levels at the observer. A method was developed to correct source spheres to allow for synchronization of the source sphere location to account for the finite time step output from ANOPP2.

Publications
None.

Outreach Efforts
None.

Awards
None.

Student Involvement
Stephen Willoughby has contributed strongly to this task, initially as an undergraduate student and later as a graduate research assistant during the fall of 2020.

Project 041 Identification of Noise Acceptance Onset for Noise Certification Standards of Supersonic Airplanes

The Pennsylvania State University

Project Lead Investigator

Victor W. Sparrow
Director and United Technologies Corporation Professor of Acoustics
Graduate Program in Acoustics
The Pennsylvania State University
201 Applied Science Building
University Park, PA 16802
(814) 865-6364
vws1@psu.edu

University Participants

The Pennsylvania State University (Penn State)

- PI: Victor W. Sparrow, United Technologies Corporation Professor and Director, Graduate Program in Acoustics
- FAA Award Number: 13-C-AJFE-PSU Amendment Nos. 45 and 60
- Period of Performance: March 29, 2019 to February 28, 2021
- Tasks:
  1. Obtaining confidence in signatures, assessing metrics sensitivity, and adjusting for reference day conditions
  2. Assessing secondary sonic boom propagation

Queensborough Community College, City University of New York

- Co-Investigator: Kimberly A. Riegel, subrecipient to Penn State

Volpe National Transportation Systems Center

- Co-Investigators: Juliet Page and Robert Downs, subrecipient to Penn State

Project Funding Level

This project supports the identification of noise acceptance onset for noise certification standards of supersonic airplanes through research on multiple tasks conducted at Penn State. The FAA funding to Penn State in 2019–2021 was $390,000. Matching funds are expected to meet cost share on both tasks. Boom Supersonic has pledged $300,000, and Gulfstream has pledged $100,000.

Investigation Team

For 2019–2021, the investigation team included:

- Victor W. Sparrow, PI, Penn State (Tasks 1 and 2)
- Joshua Kapcsos, graduate research assistant, Penn State (Task 1)
- Kimberly A. Riegel, coinvestigator, Queensborough Community College, City University of New York, subrecipient to Penn State (Task 2)
- Juliet Page and Robert Downs, coinvestigators, Volpe National Transportation Systems Center, subrecipient to Penn State (Task 2)
- Michael Rybalko, Joe Salamone, et al., Boom Supersonic (industrial partner)
- Brian Cook and Charles Etter, Gulfstream (industrial partner)

Project Overview

FAA participation continues in International Civil Aviation Organization, Committee on Aviation Environmental Protection (ICAO CAEP) efforts to formulate a new civil supersonic aircraft sonic boom (noise) certification standard. This research investigates elements related to the potential approval of supersonic flight over land for low-boom aircraft. The efforts include investigating certification standards, assessing community noise impact, and developing methods to assess the public acceptability of low-boom signatures. The proposed research will support NASA in the collaborative planning and execution of human response studies gathering data to correlate human annoyance with low-level sonic boom noise. As the research progresses, this work may involve the support of testing, data acquisition and analyses, field demonstrations, laboratory experiments, or theoretical studies; for example, Maglieri et al. (2014).

Task 1 - Obtaining Confidence in Signatures, Assessing Metrics Sensitivity, and Adjusting for Reference Day Conditions

The Pennsylvania State University

This task has transitioned into the new ASCENT Project 57. Please see the 2020 and 2021 reports for ASCENT Project 57, “Support for Supersonic Aircraft En-route Noise Efforts in ICAO CAEP,” which describes developments on this task.

Task 2 - Assessing Secondary Sonic Boom Propagation

The Pennsylvania State University
Queensborough Community College, City University of New York
Volpe National Transportation Systems Center

Research Approach

Background

As both conventional “N-wave” (normal) boom and low-boom supersonic aircraft approach implementation, assessing all aspects of the sonic boom noise that reaches the ground is important. Such assessment includes the need to better understand secondary sonic booms, when and why they occur, and the resulting signatures.

Most of the research done in the United States was completed in 1980 to understand the regular occurrence of secondary sonic booms observed along the New England coastline as a result of Concorde flights approaching New York. Two main types of secondary sonic booms exist: type I is the ground boom resulting from shock waves emanating from the top of the aircraft that refract downward under certain atmospheric conditions, and type II is the boom that bounces off the ground or water surface, is bent in the atmosphere, then travels back down to the ground a second time. To better predict the conditions resulting in these secondary sonic booms, the variations in atmospheric conditions, type of aircraft, and trajectories should be examined.

In the recent work for Project 41 in 2019, the original work of Rickley and Pierce (1980) was recreated by using the PCBoom (Plotkin et al., 2007) modeling software. The sound ray arrival locations, resulting from the PCBoom simulations showed very good agreement with the original Rickley and Pierce arrival locations.

Given this confidence that PCBoom appropriately predicts the ray trajectories for secondary sonic booms, the work for this year focused on predicting the arrival locations for a variety of atmospheric conditions and locations in the United States. The Climate Forecast System (CFS) v2 (Saha et al., 2014) was used to obtain weather conditions for different times and locations.

Boom Supersonic Cylinder Data

The research team continued to study the results for aircraft other than the Concorde with the CFD data supplied by Boom Supersonic for their XB-1 demonstrator aircraft. These data were adapted to create cylinder input data for PCBoom. Previously, the ray arrival locations were successfully run with the cylinder option in PCBoom for the atmospheric conditions provided by Rickley and Pierce for the 1980 atmospheric data. The simulations were extended to examine the behavior of the XB-1 data for the year 2018. Figure 1 shows a comparison of the two aircraft in the summer and winter months. The

arrival locations are highly similar for both aircraft. The arrivals impact the coastline for both aircraft during the summer months but have no secondary sonic boom impact during the winter months.

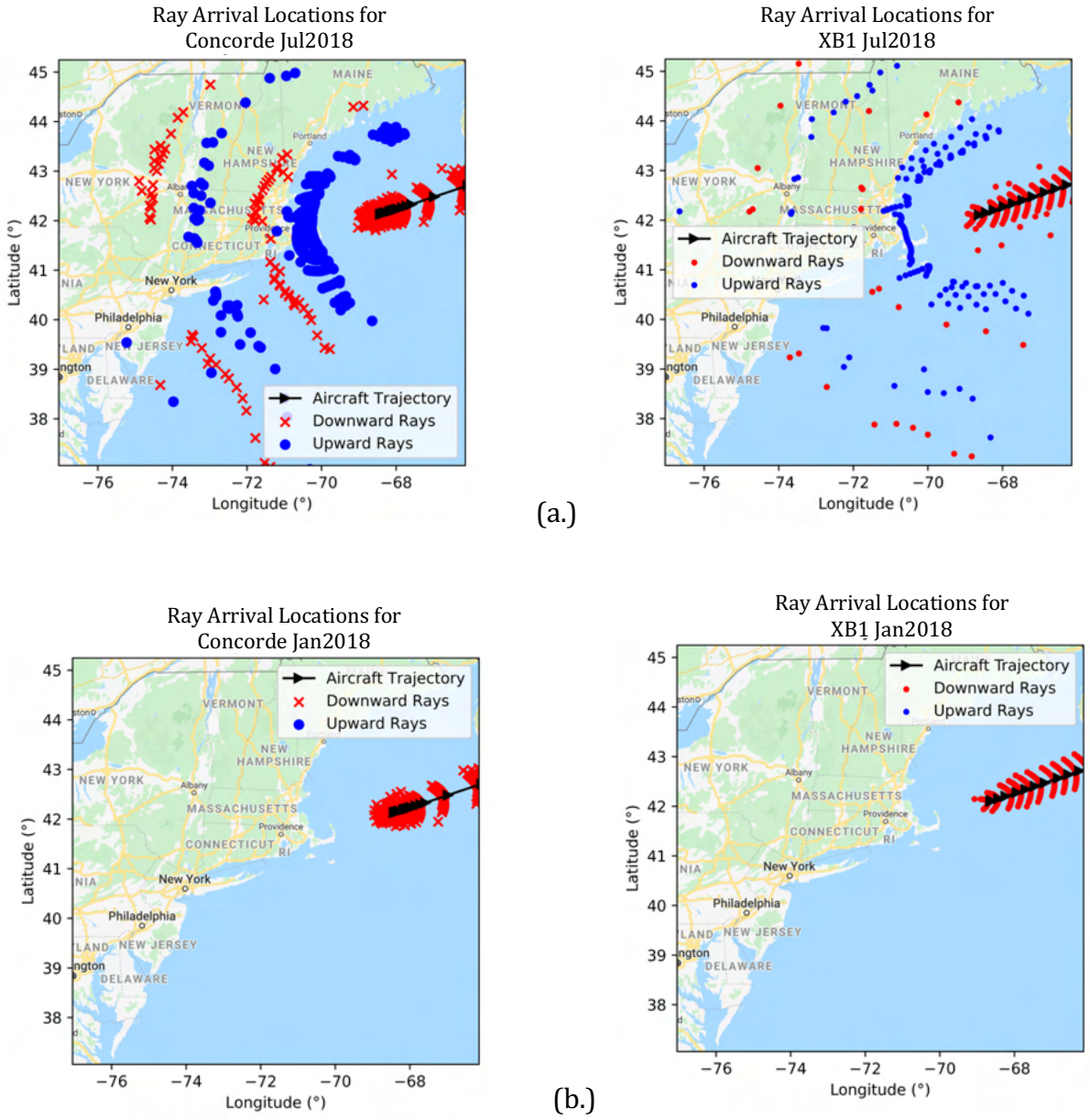

Figure 1. Predicted ray arrival locations for the XB-1 demonstrator aircraft approaching New York City, flying the original trajectory flown by the Concorde, according to 2018 weather data. Figure 1a shows the comparison for the summer months between the Concorde arrivals and XB1 arrivals for similar weather and trajectory. Figure 1b shows the comparison for the winter months.

Comprehensive Literature Review

As mentioned in the 2020 Annual Report for Project 41, a comprehensive literature review of known references on the subject of secondary sonic boom was prepared. This paper was presented at the e-Forum Acusticum in late 2020 and is now available online as an open-access resource (https://hal.archives-ouvertes.fr/FA2020/hal-03229476).

Obtaining Historical Concorde Secondary Boom Data

ASCENT Project 41 renewed interest in the secondary boom measurements described by Rickley and Pierce (1980). Volpe engaged in a task to examine media and files from National Transportation System Center archives and evaluate the possibility of extracting high-resolution digital data from the original measurement tapes. The archived materials were found to include tapes of both infrasonic measurements (the primary data type from the Rickley and Pierce report) and measurements from a secondary "acoustic measuring system," which was intended to record events as perceived by a listener but had limited frequency response below approximately 20 Hz. As will be described, this effort was able to extract measurement data from the acoustic measurement tapes but not the infrasonic measurement tapes. The primary system was a four-track frequency-modulated (FM) instrumentation tape recorder, HP model 3960A, which recorded three channels of infrasonic data that were band-filtered (0.5–30 Hz) and the signal from an IRIG-B time code generator. The secondary recording system was a Nagra model IV-SJ instrumentation tape recorder (half-track) that measured outdoor acoustic data in the frequency band 15–20 kHz. Both systems used 0.25-inch magnetic tape on 7-inch open reels as recording media.

Because recording logs were not found with the measurement tapes, the initial effort began with decoding the alphanumeric tape-labeling scheme. The investigation led to the discovery of key details not included in the Rickley and Pierce report, such as tape speed. Voice annotations made on both systems were used for positive identification and also provided useful measurement details. We determined that the 21 tapes attributable to the secondary boom measurement program are a subset of the reported measurements: acoustic measurements from 5 days in August of 1979 and infrasonic measurements from 8 days in August and September of 1979 (some measurement dates used multiple tapes).

As of February of 2021, Volpe had access to only a Nagra IV-SJ tape recorder; therefore, the infrasonic data tapes could not be played back. However, a half-track recorder was able to play back voice annotation from the tapes recorded on the four-track HP 3960A tape recorder, because the voice annotation channel was not frequency modulated. Evaluation of the infrasonic data tapes would probably require the same device model used in the original recording. Communication with E. Rickley confirmed that the Transportation Systems Center owned an HP 3960A, which was shared with another laboratory, but attempts to locate the device in the Volpe inventory were unsuccessful. However, we were able to play back audio from the acoustic measurement tapes by using the Nagra IV-SJ while digitally recording the output at 24-bit resolution with a sampling rate of 48 kHz. An IRIG-B timing signal recorded on the cue track of the acoustic measurement tapes allowed the digitized data to be compared with plotted measurements in the original report.

Digitized secondary boom measurements are plotted in Figures 2 and 3 and compared with Figure 13 from Rickley and Pierce (1980). Although the measurement system used to produce Figure 13 in Rickley and Pierce (1980) was not directly specified, Figure 2 is likely to represent a comparison between infrasonic and acoustic data.

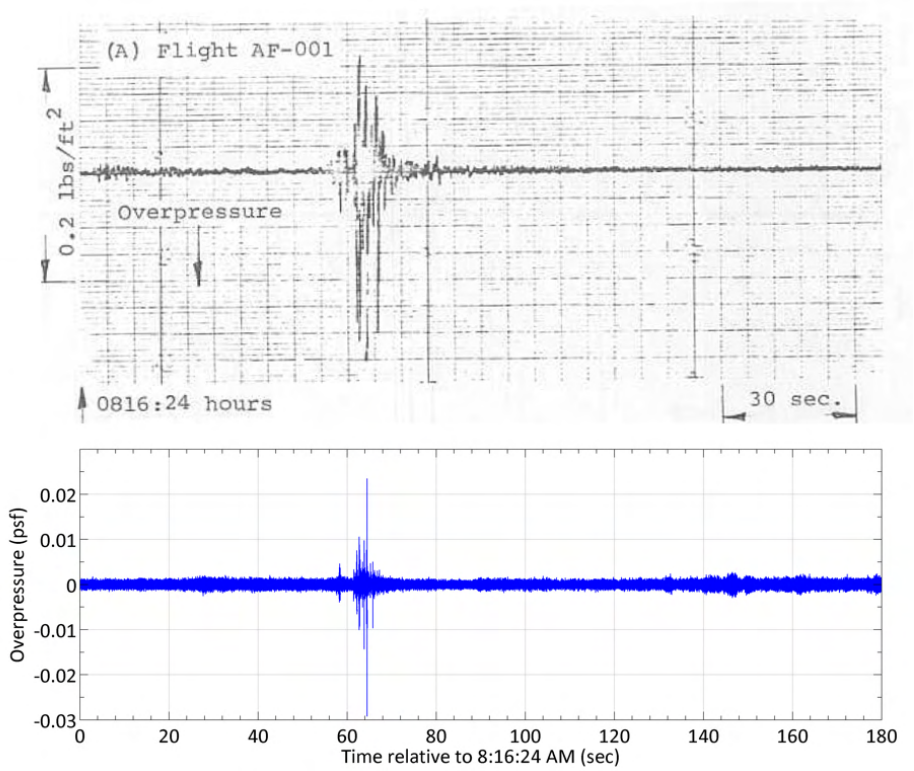

Figure 2. Pressure time series from flight AF-001 on August 15th, 1979, at the Malden, Massachusetts site. The top plot is reproduced from Rickley and Pierce (1980); the bottom plot shows data extracted from the original acoustic measurement system data tape.

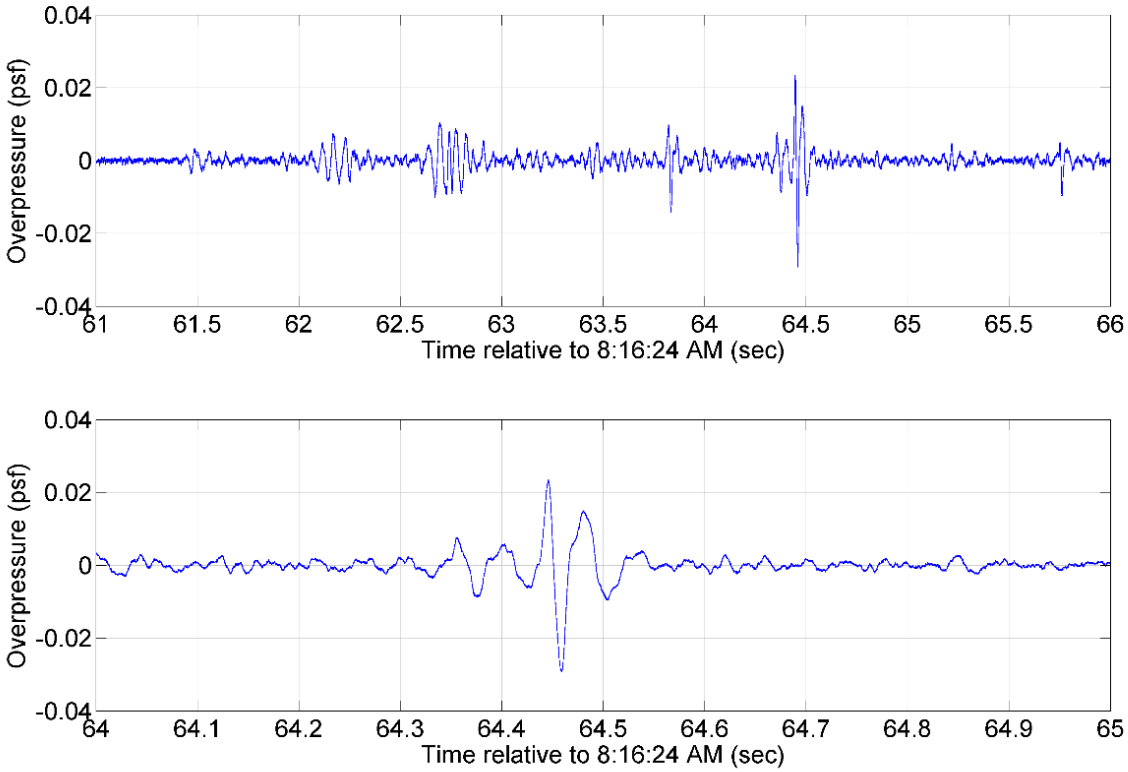

Figure 3. Magnified portions of the signal from Figure 2, flight AF-001 on August 15, 1979, at the Malden, Massachusetts site.

The overpressure levels in the extracted acoustic data are significantly lower than those reported by Rickley and Pierce (1980). The report data are likely to refer to the infrasonic measurements, and the acoustic system measurement had limited response below 20 Hz. The overpressure discrepancy appears to be due to the limited low-frequency response of the original acoustic measurement system. Of note, however, waveforms can be observed in the acoustic measurement system data that correlate well with the reported arrival times. The ability to read the secondary boom signatures from the acoustic measurement tapes suggests that the infrasonic measurement tapes may also be in usable condition, because both sets of tapes were stored in the same physical box. This effort has also demonstrated that sufficient information concerning the measurements is available to extract and analyze the data of interest if a suitable functioning four-track recorder becomes available.

Milestone

The team successfully compared the XB-1 demonstrator secondary boom predictions to those for the Concorde.

Major Accomplishments

The team successfully demonstrated that secondary sonic booms are expected near the coastline of the United States due to an aircraft other than the Concorde. Furthermore, a comprehensive literature review on secondary sonic booms was published. Initial attempts to read Concorde secondary boom acoustic data were successful, and additional work is required to obtain infrasonic data.

Publications

Sparrow, V., & Riegel, K. (2020, December). 2020 literature review of secondary sonic boom [Paper presentation]. Proceedings of the 2020 e-Forum Acusticum, European Acoustics Association, Virtual meeting. https://hal.archives-ouvertes.fr/FA2020/hal-03229476

Outreach Efforts
None

Awards
None

Student Involvement
None for Task 2

Plans for Next Period
Project 41 is now completed. All efforts have now shifted to the follow-on project, ASCENT 57.

References
Maglieri, D.et al. (2014), "Signature Deturbing," Sonic Boom: Six Decades of Research, NASA Technical Report. NASA/SP-2014-622. pp 51-52

Plotkin, K., Page, J., & Haering, E. (2007). Extension of PCBoom to over-the-top booms, ellipsoidal earth, and full 3-D ray tracing [Presentation]. 13th AIAA/CEAS Aeroacoustics Conference, Rome, Italy.

Rickley, E., & Pierce, A. (1980). Detection and assessment of secondary sonic booms in New England. The Journal of the Acoustical Society of America, *69*(S1), S100–S100. https://doi.org/10.1121/1.386524

Saha, S., Moorthi, S., Wu, X., Wang, J., Nadiga, S., Tripp, P., Behringer, D., Hou, Y.-T., Chuang, H., Iredell, M., Ek, M., Meng, J., Yang, R., Mendez, M. P., van den Dool, H., Zhang, Q., Wang, W., Chen, M., & Becker, E. (2014). The NCEP Climate Forecast System Version 2. Journal of Climate, *27*, 2185-2208. https://doi.org/10.1175/JCLI-D-12-00823.1

Project 043 Noise-Power-Distance Reevaluation

Georgia Institute of Technology

Project Lead Investigator

Dimitri Mavris
Regents Professor
School of Aerospace Engineering
Georgia Institute of Technology
Mail Stop 0150
Atlanta, GA 30332-0150
404-894-1557
dimitri.mavris@ae.gatech.edu

University Participants

Georgia Institute of Technology

- PIs: Dr. Dimitri Mavris (PI), Mr. Christopher Perullo (Co-PI), and Dr. Michelle Kirby (Co-PI)
- FAA Award Number: 13-C-AJFE-GIT-048
- Period of Performance: June 28, 2016 to May 31, 2022
- Tasks:
    1. Development and testing of the NPD+C correction function (CF)

Project Funding Level

This project is funded at the following levels: Georgia Institute of Technology, $200,000. In addition, $200,000 in matching funds has been provided through in-kind contributions from a major airline. This total includes salaries for the project director, research engineers, and graduate research assistants, as well as funding for computing, and financial and administrative support, including meeting arrangements. The institute has also agreed to provide tuition remission for students whose tuition is paid via state funds.

Investigation Team

- Dimitri Mavris, PI, Georgia Institute of Technology
- Michelle Kirby, Co-Investigator, Georgia Institute of Technology
- Yongchang Li, Research Faculty, Georgia Institute of Technology
- Dushhyanth Rajaram, Research Faculty, Georgia Institute of Technology
- Mohammed Hassan, Research Faculty, Georgia Institute of Technology
- Ameya Behere, graduate student, Georgia Institute of Technology
- Max Geissbuhler, graduate student, Georgia Institute of Technology

Project Overview

The standard technique for evaluating fleet noise is to estimate the flight procedure source noise by using noise-power-distance (NPD) curves. Noise calculations within the Aviation Environmental Design Tool (AEDT) rely on NPD curves provided by aircraft manufacturers. This dataset reflects representative aircraft categories at set power levels and aircraft configurations. Noise levels are obtained as a function of slant distance via spherical spreading through a standard atmosphere, and other correction factors are applied to obtain the desired sound field metrics at the location of the receiver. The current NPD model does not consider the aircraft configuration (e.g., flap settings) or alternative flight procedures being implemented. These factors are important, because the noise characteristics of an aircraft depend on the thrust, aircraft speed, and airframe configuration, among other contributing factors such as ambient conditions. The outcome of this research is an approach based on the suggested NPD + configuration (NPD+C) format, which will enable more accurate noise predictions because of its inclusion of aircraft configuration and speed changes.

This project is currently in its fourth year. During the third year, this work focused on two main topics. First, prior work was extended to examine the impact of NPD spectral (frequency) content on noise contours. This first focus was divided into two aspects: (a) the manner in which the spectral data are used within AEDT while all other parameters are held constant and (b) the manner in which the noise contours change when spectral data generated from the Environmental Design Space (EDS) are utilized in a manner similar to that of the NPD+C approach. Second, the NPD+C approach was validated with available aircraft operation and airport noise monitoring data. A brief description of the prior work is provided for reference.

Task 1 - Development and Testing of the NPD+C Correction Function

Georgia Institute of Technology

Objectives

The objective of this task was to create a correction function (CF) to correct the baseline NPD for an aircraft class to match a given flight configuration, incorporating flight velocity (FV), flap deflection angle (FDA), and gear setting (gear).

Research Approach

Overview

Before a CF was created, several categories of commercial transportation aircraft were identified according to their payload capacity. Ultimately, four categories were identified: 50, 150, 210, and 300 passenger (pax) categories. Fitting the NPD CF involved four steps. The first was the aircraft class definition, in which the bypass ratios (BPR), overall pressure ratios (OPR), and rated thrusts (i.e., sea-level static [SLS] thrust) were collected for a given aircraft class. Next, these values were used to create a series of engine variants for the aircraft class and were evaluated with the EDS software to generate engine state tables for use in the Aircraft Noise Prediction Program (ANOPP). The final step of this process was to fit a model to these data, so that the difference between a given configuration and a baseline condition could be predicted. The model itself would be a function of both engine parameters and aircraft configuration, i.e., *fcn* (BPR, OPR, S*LS Thrust, FDA, FV, Gear*). This process is shown in the left column of Figure 1. A general form of the CF equation can be found in which *a, b, c, d,* and *e* are constants, and the remaining terms are cross-products, raised to powers (up to the fifth power) and multiplied by constants. The authors of this report did not actively write the equations for the CFs; instead, the JMP statistical program suite was used to calculate the best linear fit to the ANOPP data. The actual equations were approximately 100 lines long when typed out.

Equation 1. Correction Function General Form.

$$\boldsymbol{CF(BPR, OPR, SLS\ Thrust, FDA, FV, Gear) = a * BPR + b * OPR + c * (FDA * FV)^2 + d * (SLS\ Thrust - e)^4 + \cdots}$$

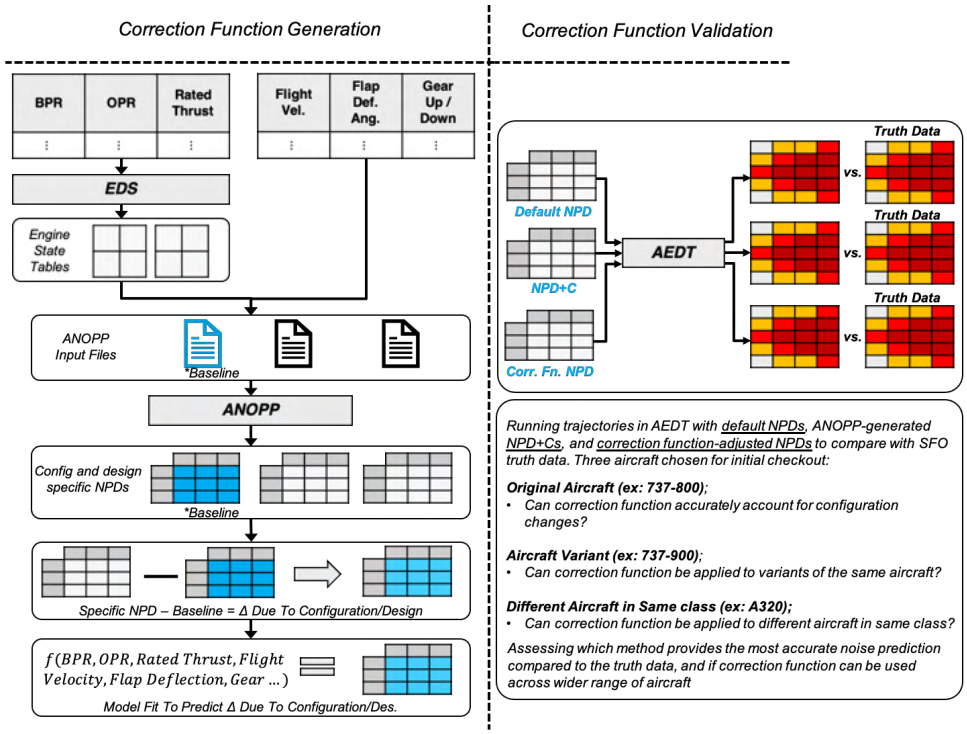

Figure 1. CF generation and validation processes.

Class Definition

The first phase of the CF modeling process involved defining the scope of the model, specifically selecting the aircraft and corresponding engines from AEDT on which the model would be based. A baseline engine was also selected to match the baseline aircraft represented in the ANOPP model. After this list was compiled, the engine BPR, OPR, and SLS thrust values were collected from AEDT by exporting each aircraft's definition as an .XML file and compiling the engine parameters via a Python script. With this information, a customized design of experiments (DoE) could be created. This DoE captured both corner and interior points within the design space, for a total of 25 cases. A 26th case would also be added to account for the baseline engine settings. The AEDT IDs of the aircraft applicable to each CF are shown in Table 1.

Table 1. AEDT IDs for each CF

50–100 pax	100–210 pax	210–300 pax	300–400 pax
EMB145	737700	767300	777200
EMB170	737800	A330-301	777300
EMB175	A319-131	A330-343	7773ER
EMB190	A320-211		7878R
EMB195	A320-232		A350-941
CRJ9-ER	A320-271N		
CRJ9-LR	A320-272N		
	A321-232		

Environmental Design Space (EDS) Simulations

The next phase of the CF modeling process involved creating the engine variants to model in EDS. EDS is a computational program, created by the Aerospace Systems Design Laboratory (ASDL), which performs aircraft sizing (utilizing NASA's FLOPS program) and includes a routine for generating ANOPP input files. The engine variants were modeled by modifying the baseline EDS engine input of the same class by adjusting the values of the SLS thrust, takeoff thrust, top-of-climb thrust, fan pressure ratio, low-pressure compressor pressure ratio, and high-pressure compressor pressure ratio. After the values were modified to match the engine settings from the DoE, the simulation was initiated, and the resulting outputs were compiled. These results were then post-processed to extract the specific engine and thrust information needed for use in ANOPP.

ANOPP Simulations

Next, the post-processed EDS data were used to modify aircraft input files for use in ANOPP to generate NPD curves. The engine state tables were processed for use in ANOPP such that ANOPP would generate NPDs at 4%, 8%, 20%, and 35% of the SLS thrust for each engine variant. A customized DoE was then created for aircraft configurations, capturing 64 different combinations of flap and ground speed for both gear-up and gear-down settings, for a total of 128 configurations. In combination with the 26 engine variants generated in EDS, a total of 128 × 26 = 3,328 ANOPP cases were simulated, producing engine-specific NPDs. To reduce the computation time, we distributed the simulations across eight computers. After the ANOPP simulations were complete, the outputs were compiled and transferred to the statistical software package JMP. The same ANOPP DoE was used for each CF. The independent parameters and corresponding DoEs are detailed in Tables 2 and 3, respectively.

Table 2. Variable definitions

Variable	Acronym	Units
Flight Velocity	FV	Knots
Flap Deflection Angle	FDA	Degrees
Landing Gear Position	Gear	N/A

Table 3. ANOPP DoEs

Case No.	FV	FDA	Gear
1	220	5	Up
2	180	10	Up
3	220	15	Up
4	200	5	Up
5	180	5	Up
6	200	15	Up
7	180	0	Up
8	200	0	Up
9	220	10	Up
10	180	15	Up
11	160	15	Up
12	160	10	Up
13	160	5	Up
14	220	0	Up
15	200	10	Up
16	160	0	Up
17	164	0	Up
18	168	0	Up
19	172	0	Up
20	176	0	Up

Case No.	FDA	FV	Gear
1	30	180	Down
2	10	140	Down
3	10	180	Down
4	20	180	Down
5	20	160	Down
T			
6	20	120	Down
7	40	180	Down
8	20	140	Down
9	30	160	Down
10	40	160	Down
11	10	160	Down
12	10	120	Down
13	30	120	Down
14	40	120	Down
15	30	140	Down
16	40	140	Down
17	10	124	Down
18	10	128	Down

21	184	0	Up
22	188	0	Up
23	192	0	Up
24	196	0	Up
25	204	0	Up
26	208	0	Up
27	212	0	Up
28	216	0	Up
29	164	5	Up
30	168	5	Up
31	172	5	Up
32	176	5	Up
33	184	5	Up
34	188	5	Up
35	192	5	Up
36	196	5	Up
37	204	5	Up
38	208	5	Up
39	212	5	Up
40	216	5	Up
41	164	10	Up
42	168	10	Up
43	172	10	Up
44	176	10	Up
45	184	10	Up
46	188	10	Up
47	192	10	Up
48	196	10	Up
49	204	10	Up
50	208	10	Up
51	212	10	Up
52	216	10	Up
53	164	15	Up
54	168	15	Up
55	172	15	Up
56	176	15	Up
57	184	15	Up
58	188	15	Up
59	192	15	Up
60	196	15	Up
61	204	15	Up
62	208	15	Up
63	212	15	Up
64	216	15	Up

19	10	132	Down
20	10	136	Down
21	10	144	Down
22	10	148	Down
23	10	152	Down
24	10	156	Down
25	10	164	Down
26	10	168	Down
27	10	172	Down
28	10	176	Down
29	20	124	Down
30	20	128	Down
31	20	132	Down
32	20	136	Down
33	20	144	Down
34	20	148	Down
35	20	152	Down
36	20	156	Down
37	20	164	Down
38	20	168	Down
39	20	172	Down
40	20	176	Down
41	30	124	Down
42	30	128	Down
43	30	132	Down
44	30	136	Down
45	30	144	Down
46	30	148	Down
47	30	152	Down
48	30	156	Down
49	30	164	Down
50	30	168	Down
51	30	172	Down
52	30	176	Down
53	40	124	Down
54	40	128	Down
55	40	132	Down
56	40	136	Down
57	40	144	Down
58	40	148	Down
59	40	152	Down
60	40	156	Down
61	40	164	Down
62	40	168	Down
63	40	172	Down
64	40	176	Down

Model Fit

The final phase of the CF modeling process involved creating models within JMP. For a given aircraft class, two models were fit: one with gear down and one with gear up. The model was fit to the difference between configuration-specific NPDs and the baseline NPD (both coming from the set of ANOPP cases) at the thrust settings corresponding to the approach. With this prediction formula, a default NPD could be adjusted to represent different flap, gear, and speed configurations. For analysis of the quality of the fit, the ANOPP data were partitioned into two sets: a training set containing 75% of the data and a testing

set containing 25% of the data. The training set was used exclusively to create the model fit, whereas the testing set was used exclusively to compare the error between the ANOPP results and the model results.

50pax Model Fit

The first correction function to be created was the 50pax CF, which would be suitable for aircraft such as the Bombardier CRJ series or the Embraer E-Jet series. More broadly, the 50pax CF can be applied to any regional jet whose engine parameters fall within the ranges listed in Table 4.

Table 4. 50pax correction function engine parameter ranges

BPR	OPR	SLS Thrust (lb_f)
4.3–6.3	17–28	7,500–18,500

A graphical depiction of the 26 engines used to generate the correction function is shown in Figure 4.

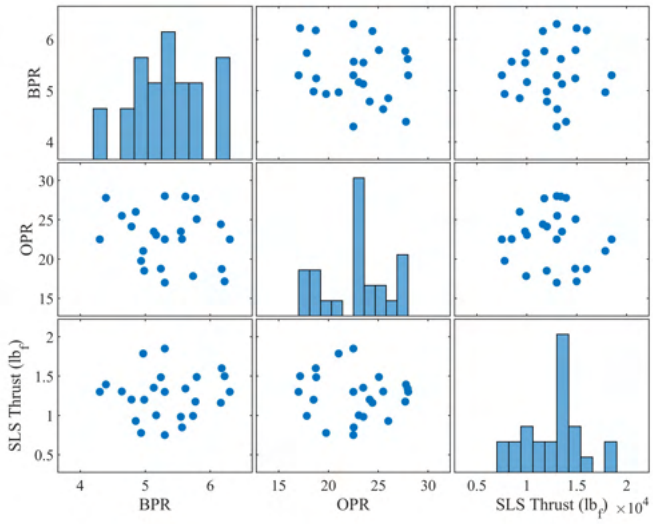

Figure 2. 50pax correction function engine parameters.

Next, the engines identified via the DoE were simulated with EDS, and the results were post-processed for use in ANOPP simulations. ANOPP was used to generate the baseline NPD for this aircraft (at a setting of 160 kts, 30° flaps, and gear down) and configuration-specific NPDs, with simulations completed at higher speeds and lower flap deflection angles for the gear-up cases and lower speeds and higher flap deflection angles for the gear-down cases. The configurations used for the gear-up and gear-down simulations are shown in Figure 3.

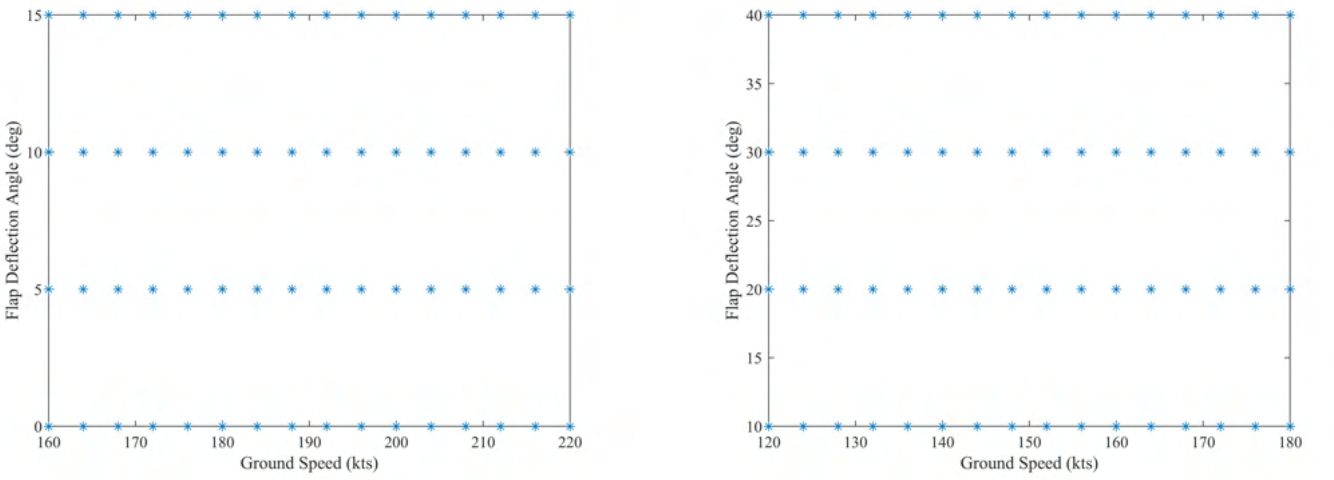

(a). Gear-Up **(b).** Gear-Down

Figure 3. ANOPP design of experiments for gear-up and gear-down configurations.

The resulting NPDs from the ANOPP cases were post-processed and imported into JMP. With this tool, two models were fit for approach thrust settings: one with gear up and another with gear down. The models were fit on the difference between the configuration-specific NPDs and the baseline NPD as a function of BPR, OPR, SLS thrust, flap deflection angle, gear setting, aircraft speed, thrust fraction, and distance. After the two models were created, they were tested by comparison of the predicted configuration-specific NPDs from the correction function with the original configuration-specific NPDs from ANOPP. The sound exposure level (SEL) error distributions for this comparison are shown in Figure 4.

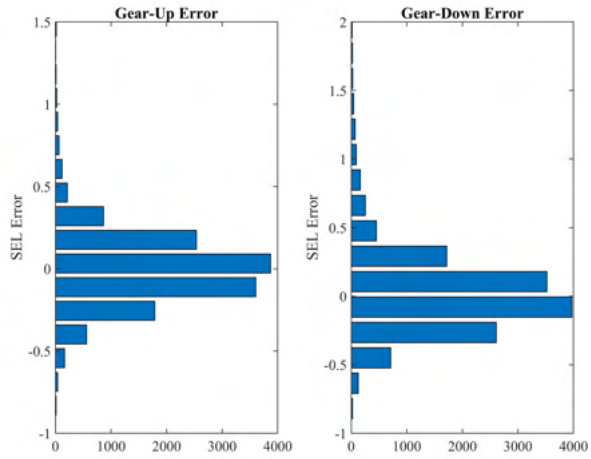

Figure 4. 50pax correction function error distribution.

As shown in Figure 4, the error is clearly centered around 0 dB for both gear-up and gear-down settings. The mean errors were 3.1×10^{-4} dB and 0.033 dB for the gear-up and gear-down models, respectively. The standard deviations of the errors were 0.24 dB and 0.36 dB for the gear-up and gear-down models, respectively.

To compare the outputs of the 50pax correction factor with a baseline NPD, we plotted a sample comparison (Figure 5), by using a notional CRJ-900ER aircraft. In this comparison, two configurations were compared. The first was for the CRJ at a

ground speed of 170 kts, a flap deflection of 15°, and the gear-up setting. The second was for a ground speed of 150 kts, a flap deflection of 30°, and the gear-down setting.

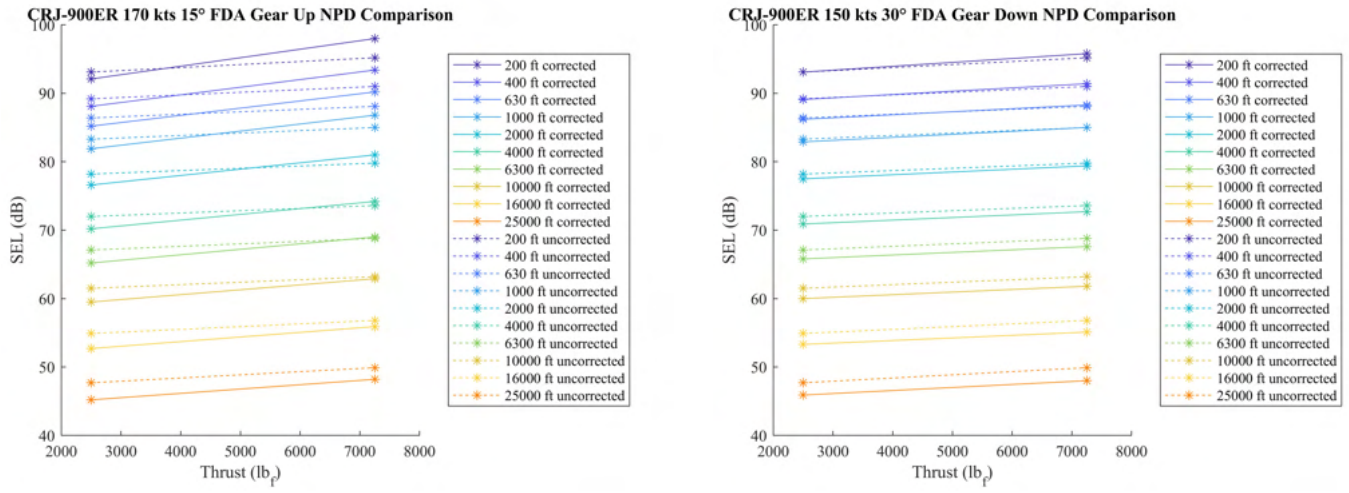

(a). Gear-Up **(b).** Gear-Down

Figure 5. 50-pax sample application.

100- to 210-pax Model Fit

When determining the simulation cases to use in creating the CF, we found that both the engine parameters and approach NPD for the 100-pax model (represented in ANOPP as a 737-700) were close to those of the 150-pax model (represented in ANOPP as a 737-800). Therefore, we decided to fit a model for both classes simultaneously. Engine variants for the Boeing 737-700/800/900 and the Airbus A318/319/320 were obtained from the equipment database in AEDT, and the minimum and maximum values were found. The ranges of engine parameters applicable to the 100- to 210-pax CF are shown in Table 5.

Table 5. 100- to 210-pax correction function engine parameters

BPR	OPR	SLS Thrust (lb_f)
4.43–13.78	19–42	22,000–30,000

The exact parameters of the 26 engines used to create the correction function are shown in Figure 6.

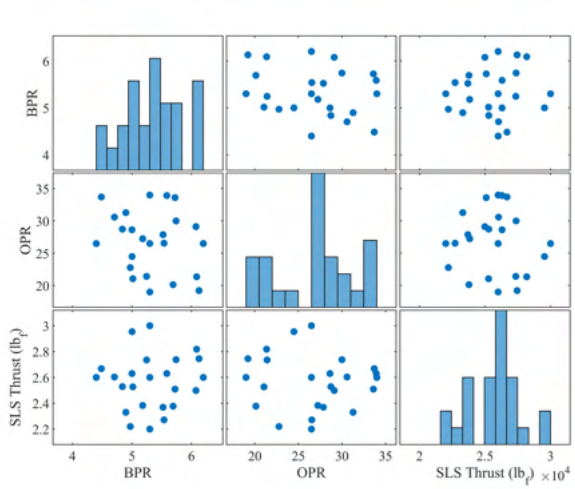

Figure 6. 100- to 210-pax correction function domain.

Figure 6 shows the sweep of engine parameters that were covered by the 100- to 210-pax correction function Of note, the diagonal of Figure 6 depicts the histogram of each variable, showing the ranges covered by this CF. Next, the ANOPP simulations were conducted by using the same DoEs as shown in Figure 3. The resulting data were imported into JMP to fit the model and analyze its error; the error distributions for the 100- to 210-pax CF are plotted in Figure 7.

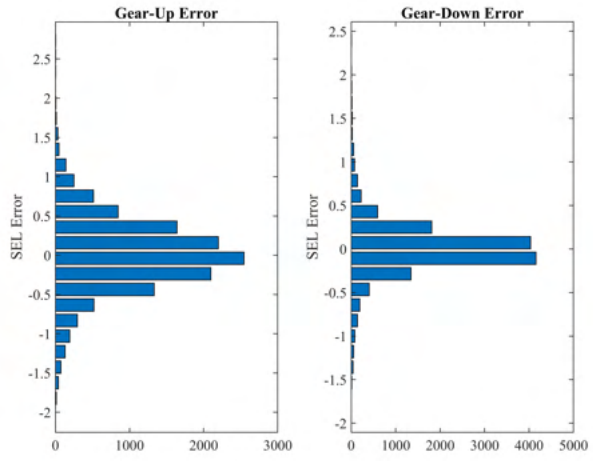

Figure 7. SEL error distributions for the 150-pax correction function.

Again, the error distributions were centered around 0 dB, and the majority of the error was within ±1.5 dB. The mean errors were 5.5×10^{-3} dB and 3.7×10^{-3} dB for the gear-up and gear-down models, respectively. The standard deviations of the errors were 0.48 dB and 0.33 dB for the gear-up and gear-down models, respectively.

To visually demonstrate the 100- to 210-pax CF, we calculated and plotted two sample applications which are shown in in Figure 8. The first application is for a notional Boeing 737-800 at a flight configuration of 20˚ of flap deflection, ground speed of 160 knots, and gear-up setting. The second application was for the same notional 737 at a flight configuration of 150 knots, 30˚ of flap deflection, and gear-down setting.

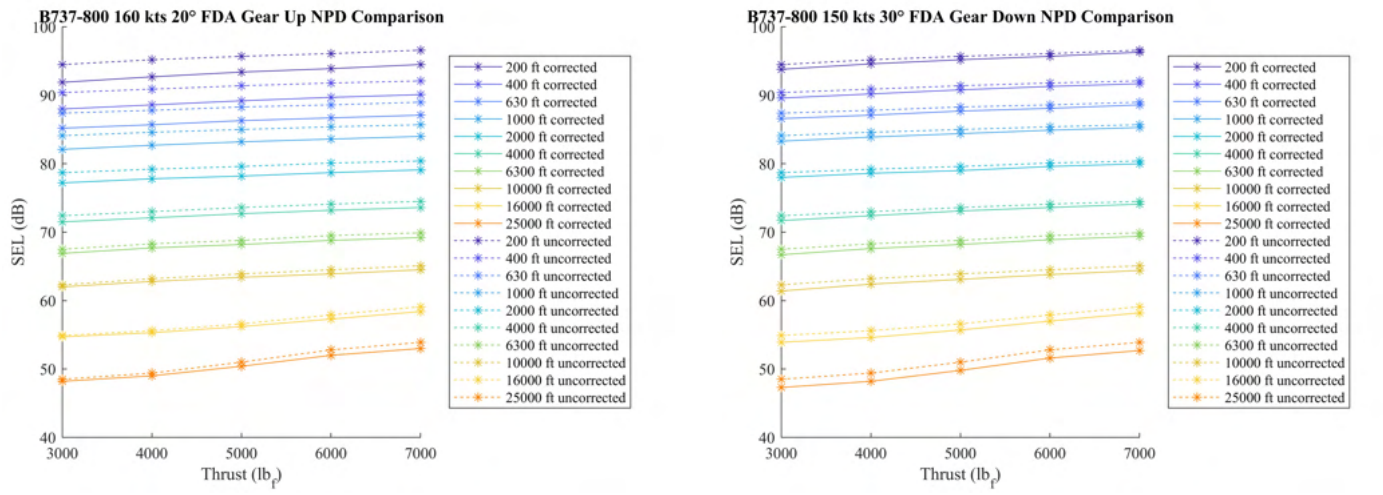

(a). Gear-Up **(b)**. Gear-Down

Figure 8. 100- to 210-pax CF sample application.

The plots indicate that, in both cases, the correction function predicts less noise than the baseline NPD for the notional aircraft as defined in AEDT. This is, primarily because of the reference condition defined for the correction function ofCF160 kts ground speed, 30˚ flap deflection, and gear-down setting. To demonstrate the effect of the correction function on noise contours, we performed a sample study using AEDT. This study used a notional Boeing 737-800, and was performed with both uncorrected and corrected NPDs in AEDT. The resulting contours are shown in Figure 9. In this plot, the contours generated with the corrected NPDs are shown with dashed lines, and the contours generated with the uncorrected NPDs are shown with solid lines. Shading indicates the difference in the corrected and uncorrected contours: a negative value (blue regions) indicates that the correction function predicts less noise than the default AEDT calculations. Of note, these results are preliminary, and several efforts are underway to improve the accuracy of NPD+C corrections. In particular, the region on the top left of the plot shows a small red region indicating that the NPD+C corrected case predicts higher noise. However, this region is also affected by the reverse thrust during the landing ground roll segment of the arrival operation. Efforts are underway to assess the accuracy of the noise prediction during the landing ground roll segment.

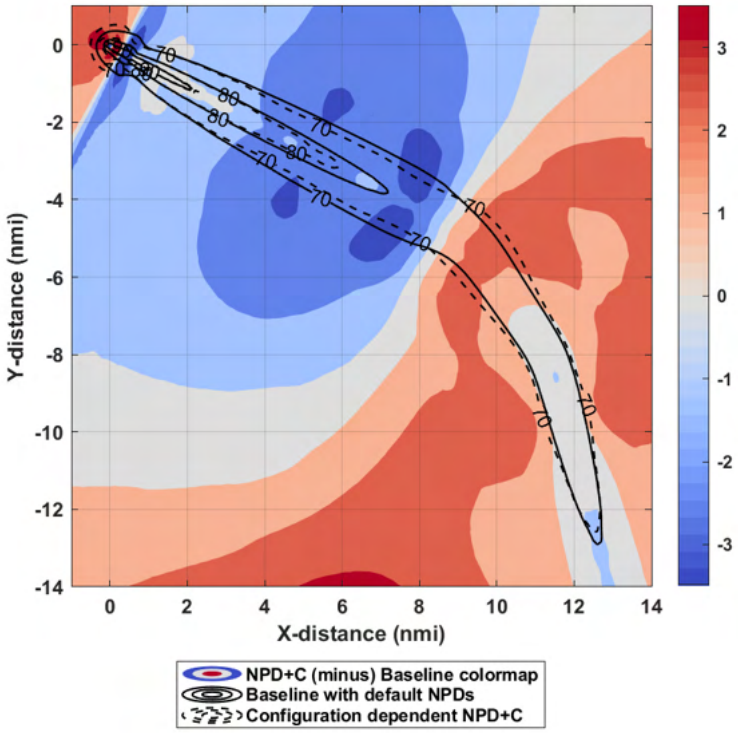

Figure 9. 150-pax CF sample application contours.

210-pax Model Fit

Next, a correction function was created for the 210-pax category, encompassing aircraft such as the Boeing 767 and the Airbus A330. The exact ranges of engine parameters applicable to this correction function are shown in Table 6.

Table 6. 210pax correction function engine parameter ranges

BPR	OPR	SLS Thrust (lb_f)
4.2–9.0	22.8–45.4	48,000–71,100

The parameters of the 26 engines used to create the 210-pax correction factor are shown in Figure 10.

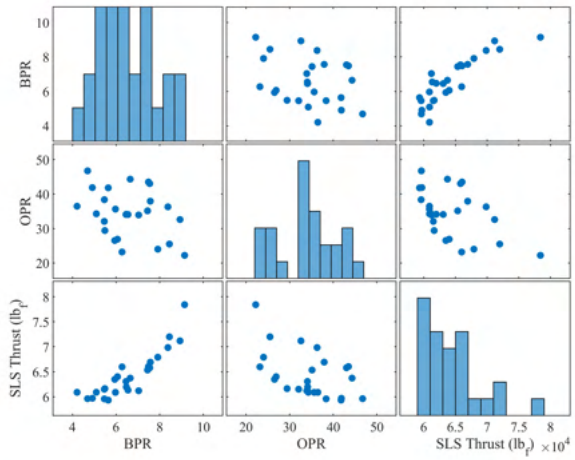

Figure 10. 210-pax engine parameters.

Next, the ANOPP simulations were conducted, again with the same configurations shown in Figure 3. After the simulations were complete, the data were imported into JMP, and the correction function model fit. The error distributions for this correction function are shown in Figure 11.

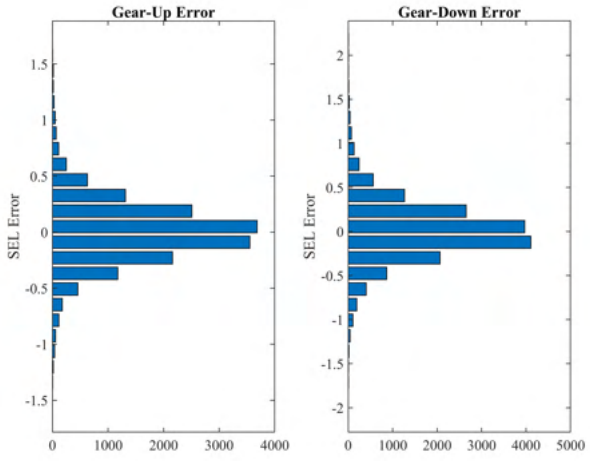

Figure 11. 210pax correction function error distribution.

For the 210-pax CF, the mean errors were 1.3×10^{-4} dB and 3.6×10^{-3} dB for the gear-up and gear-down models, respectively. The standard deviations of the errors were 0.29 dB and 0.35 dB for the gear-up and gear-down models, respectively.

300-pax Model Fit

The final correction function created was for the 300-pax category, suitable for application to aircraft such as the Boeing 777 and the Airbus A350. The engine parameter ranges for this model are shown in Table 7. The parameters for the 26 engines used to create the 300-pax CF are shown in Figure 12.

Table 7. 300pax correction function engine parameter ranges.

BPR	OPR	SLS Thrust (lb_f)
4.4 - 9.23	25.4 - 48.7	70000 - 115000

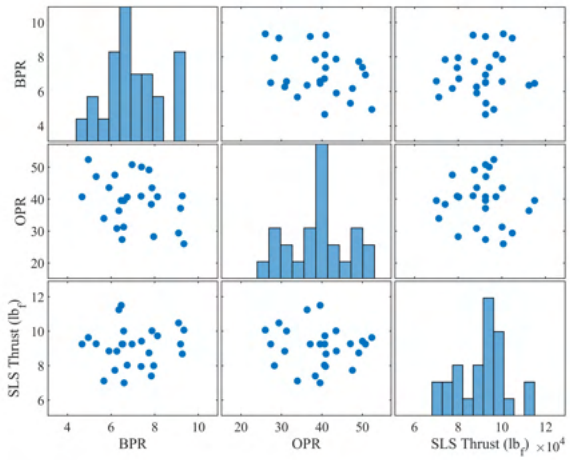

Figure 12. 300-pax correction function engine parameters.

Next, the ANOPP simulations were initiated, and the resulting data were imported into JMP. The resulting models' error distributions are shown in Figure 13.

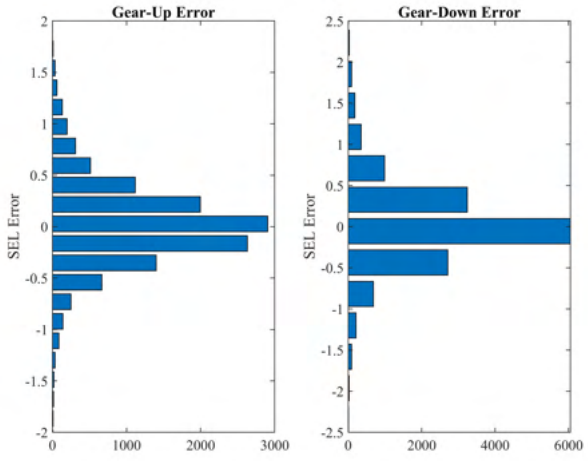

Figure 13. 300-pax correction function error distribution.

For the 300-pax correction factor, the resulting mean errors were 0.013 and 0.019 for the gear-up and gear-down models, respectively. The standard deviations of the errors were 0.42 and 0.54 for the gear-up and gear-down models, respectively. One point of interest with the 300-pax correction factor is that its error distribution was wider than that of the previous aircraft classes, probably because of two factors. The first is the relatively larger size of the engines in the 300-pax correction factor vs. the other correction factors, with the 300-pax correction factor capturing the highest SLS thrust values of any of the correction factor s. The second factor is the large space captured by the 300-pax correction factor. To capture as many commercial aircraft in the 300-pax category as possible, the DoE was created to be as large as possible, including the largest spread of SLS thrusts of any CF. Because of these factors, it is reasonable that the error is constrained to ±2 dB.

Milestone

Develop correction functions across vehicle classes

Major Accomplishments

Correction factors were developed across vehicle classes and compared with real-world noise monitoring data. In addition, original equipment manufacturers were engaged to review the approach used. Finally, draft scoping and requirement implementation plans were created and provided to the AEDT development team.

Plans for Next Period

- Continue engagement of the manufacturers to obtain "fit for purpose" application of the correction function within AEDT
- Compare noise contours against "truth data" in the form of real-world noise observations for aircraft of the same class
- Finalize implementation plan to AEDT
- Complete an airport-level study to determine the impact on the DNL contours

Publications

None

Outreach Efforts

A21
Manufacturers

Awards

None

References

AEDT. (2016). Aircraft Environmental Design Tool (2.c) [Computer software]. FAA, Washington, DC.

ANOPP. (1998). Aircraft noise prediction program (1.0) [Computer software]. NASA, Langley, VA. Aratani, L. (2018, August 9). D.C. residents suffer major setback in fight over plane noise from National Airport. *The Washington Post*. https://www.washingtonpost.com/news/dr-gridlock/wp/2018/08/09/d-c-residents-suffer-major-setback-in-fight-over-plane-noise-from-national-airport/

Federal Aviation Administration (FAA). (Retrieved December 2019) Aircraft noise issues. United States Department of Transportation

Page, J. A., Hobbs, C. M., Plotkin, K. J., Stusnick, E., & Shepherd, K. P. (2000). Validation of aircraft noise prediction models at low levels of exposure (Report No. CR-2000-210112). National Aeronautics and Space Administration, Arlington, VA.

Plotkin, K. J., Page, J. A., Gurovich, Y., & Hobbs, C. M. (2013). Detailed weather and terrain analysis for aircraft noise modeling (Report No. 13-01). John A. Volpe National Transportation Systems Center, Cambridge, MA.

Raymer, D. P. (2006). Aircraft design: A conceptual approach (4th ed.). AIAA, Reston, VA.

(n.d.). (2008). Integrated Noise Model (INM) version 7.0 technical manual (Report No. FAA-AEE-08-01). John A. Volpe National Transportation Systems Center, Cambridge, MA.

(n.d). (2016). Aviation Environmental Design Tool (AEDT) (2c) technical manual (Report No. DOT-VNTSC-FAA-16-11). FAA, Washington, DC.

(n.d). (2017). Aviation Environmental Design Tool (AEDT) (2d) technical manual (Report No. DOT-VNTSC-FAA-17-16). John A. Volpe National Transportation Systems Center, Cambridge, MA.

Project 044 Aircraft Noise Abatement Procedure Modeling and Validation

Massachusetts Institute of Technology

Project Lead Investigator

R. John Hansman
T. Wilson Professor of Aeronautics & Astronautics
Department of Aeronautics & Astronautics
Massachusetts Institute of Technology
Room 33-303
77 Massachusetts Ave
Cambridge, MA 02139
617-253-2271
rjhans@mit.edu

University Participants

Massachusetts Institute of Technology (MIT)

- PI: R. John Hansman
- FAA Award Number: 13-C-AJFE-MIT, Amendment Nos. 050, 057, and 073
- Period of Performance: September 1, 2018 to August 31, 2021
- Tasks:
    1. Evaluate general approaches to aircraft noise validation
    2. Develop validation approach options
    3. Develop flight test plans
    4. Initial experimental runs on targets of opportunity
    5. Evaluate experimental results and implications for advanced operational flight procedure noise modeling and low-noise procedures

University of California - Irvine (sub-award from MIT)

- PI: Jacqueline Huynh
- Award Number: MIT Subaward Purchase Order No. S5171 – PO 523807
- Period of Performance: September 1, 2020 to August 31, 2021
- Tasks:
    1. Evaluate general approaches to aircraft noise validation
    2. Develop validation approach options
    3. Develop flight test plans
    4. Initial experimental runs on targets of opportunity
    5. Evaluate experimental results and implications for advanced operational flight procedure noise modeling and low-noise procedures

Project Funding Level

FAA provided $720,000 in funding. A total of $720,000 in matching funds were provided: approximately $125,000 from MIT and $595,000 from the Massachusetts Port Authority.

Investigation Team

- Professor R. John Hansman (PI), MIT
- Professor Jacqueline Huynh (PI), UCI

- Clement Li (graduate student), MIT
- Sandro Salgueiro (graduate student), MIT
- Madeleine Jansson (graduate student), MIT
- Ara Mahseredjian (graduate student), MIT

Project Overview

This project utilizes empirical noise data to develop validation methods from noise and flight surveillance datasets and improve existing noise models. Field measurements of aircraft noise on approach and departure have historically shown significant variation (on the order of 10 dB), which have traditionally been attributed to factors such as varied power settings, aircraft configuration differences, and propagation effects. Recent analyses in this and other ASCENT projects have attempted to account for these factors but have been constrained by limited detailed flight data. This project explores approaches to combine emerging sources of flight data from flight data recorders and other sources such as ADS-B with current and emerging networks of ground noise monitors, to validate or improve aircraft noise models and to validate proposed noise abatement procedures. The rise of data mining techniques has substantially enabled new insights and modeling capabilities based on the use of large datasets without requiring full a priori knowledge of all the relevant physics. The development of advanced data mining approaches applied to noise modeling is expected to provide insight into aircraft noise prediction for refining or validating noise models and developing strategies for noise mitigation, through either new aircraft technologies or operational changes. Furthermore, improved noise modeling capabilities would enable more informed decision-making for stakeholders considering the options and consequences of operational or technological changes, thus facilitating the minimization of noise impacts on communities. As noise is becoming an increasingly important factor in operational decisions regarding airports in the National Airspace System, an accurate understanding of noise impacts is necessary to minimize unnecessary disruptions to, or inefficiencies in, National Airspace System operations.

Task 1 - Evaluate General Approaches to Aircraft Noise Validation

Massachusetts Institute of Technology

Objective(s)

This goal of this task is to evaluate the different options for validation of the Aircraft Noise Prediction Program (ANOPP) source component models and to confirm noise reductions from proposed low-noise procedures. Approaches to experimental design were considered, including dedicated engineering flight trials that involve parametric sweeps of velocity and aircraft configuration at various power conditions. This process would involve collaborating with airline operators, who would need to be willing to fly trials of procedures, and air traffic control (ATC), which would need to approve the procedures. A ground measurement system would need to be in place under the departure tracks.

Potential monitoring approaches will also be considered, including distributed microphone arrays or single microphone installations, as well as potential phased-array microphone configurations. In addition, alternative flight data sources will be obtained, either through airline sources or through available surveillance data. Sources of noise data from existing and emerging noise monitoring systems will be identified. Boston Logan International Airport (BOS) has agreed to provide data, and additional airports will be approached to participate in the effort. Emerging open source and community noise monitoring systems such as those being developed under ASCENT Project 53 will also be investigated. Opportunities for collaboration will be explored, with a focus on providing correlated flight data and noise datasets.

This task will use a systems approach and will explore options with potential collaborators on experimental opportunities to validate research concepts.

Research Approach

- Evaluate the different options for validation of the ANOPP source component models and confirm any noise reductions from proposed procedures
- Identify potential existing data sources for noise validation
- Model aircraft flight profiles by using existing surveillance (e.g., ADS-B or ASDE-X) data to generate noise estimates (Readily available surveillance data are easier and less expensive to acquire than Flight Data Recorder (FDR) data and dedicated flight tests.)
- Evaluate flight profiles to understand why some procedures are quieter than others

Major Accomplishments

- Flight radar and noise monitoring data were collected at BOS. ADS-B and noise monitoring data were collected at Seattle–Tacoma International Airport (SEA).
- A framework was developed to generate flight profiles by using raw ADS-B and atmospheric data. Noise monitor recordings were correlated with ADS-B data.
- Flight profiles were generated for various approaches to landing at BOS and SEA. Flight profiles were used to model aircraft noise at various monitor locations, and noise estimates were compared with monitor recordings.
- Quieter flyover cases were analyzed, and trends in aircraft altitude, airspeed, and lateral position were identified.
- Sources of weather data as a function of altitude were identified to make atmospheric absorption corrections for noise modeling validation.

Task 2 - Develop Validation Approach Options

Massachusetts Institute of Technology

Objective(s)

On the basis of the results of Task 1 and initial discussions with potential collaborators (measurement experts, model developers, manufacturers, operators, and test locations), one or more validation options will be identified. Targets of opportunity will be explored in which noise measurements may supplement other planned flight trials. For each option, the potential advantages and disadvantages will be identified, and preliminary flight test plans will be developed in coordination with the identified collaborators and in consultation with subject-matter experts such as NASA. Potential advantages include the willingness of operators or collaborators to participate and provide test resources, including aircraft and measurement systems. Other factors include measurement system resolution and the discrimination of noise sources. Timing and location may also be considered. On the basis of this analysis, recommendations for the next steps will be made.

Research Approach

- Identify methods to correct variations in modeled noise due to flap setting, aircraft weight, and ambient atmospheric conditions; apply these methods to approaches at BOS and SEA
- Acquire ADS-B data from the OpenSky Network and atmospheric data from NOAA High-Resolution Rapid Refresh; use these data to estimate weight from true airspeed and atmospheric attenuation from relative humidity
- Model noise at various flap configurations to identify the noise impact of high-lift devices

Major Accomplishments

- Demonstrated the impacts of aircraft configuration and relative humidity on modeled and measured noise over noise monitors of interest at the BOS and SEA
- Presented noise modeling methodology and results at the 2021 InterNoise and American Institute of Aeronautics and Astronautics (AIAA) Aviation conferences, respectively
- Demonstrated the noise benefit of delayed-deceleration approaches using empirical data; analyzed flyovers of various monitors at BOS and SEA, and demonstrated a correlation between the fastest flyovers, flying at indicated airspeeds consistent with clean or almost-clean flap configurations, and the quietest noise monitor recordings

Task 3 - Develop Flight Test Plans

Massachusetts Institute of Technology

Objective(s)

For the recommended validation options identified in Task 2, detailed flight test plans will be developed. Flight test plans for dedicated engineering flights would involve detailed planning of the speed, configuration, and thrust of each trial. Test plans for flight trials in collaboration with airline operators would focus on documenting the flown profiles to analyze the associated data measurements. Opportunity exists in both of these types of trials to validate not only the expected effects of aircraft speed versus noise in the analysis models, but also the expected noise impacts of procedures including delayed deceleration approaches, steeper approaches, and continuous approaches.

Research Approach
- Develop flight test plans where appropriate for the validation of low-noise procedures
- Collaborate with airline operators and industry to determine appropriate data collection for trial flight tests

Major Accomplishments
- Modeled noise from flight tests that were conducted during the ecoDemonstrator flight demonstration in the previous period was compared with identified noise monitoring data collected at SEA.
- Determined that validation for low-noise flight procedures such as the delayed deceleration approach can be performed by using available surveillance and noise monitoring data, if reasonable assumptions regarding the weight, flap and slat configuration, and atmospheric attenuation are made. Partnerships with operators for FDR data were sought, but MIT was unable to obtain FDR data because of operator restrictions on the sharing of flight data.

Task 4 - Initial Experimental Runs on Targets of Opportunity
Massachusetts Institute of Technology

Objective
If targets of opportunity are identified in Task 2 that would occur within the period of performance of this proposed research, initial experimental runs will be conducted after consultation with the FAA Office of Environment and Energy and other relevant parties.

Research Approach
- Document procedural recommendations to enable flight trials
- Meet with airline technical pilots and representatives from aircraft manufacturers to discuss operational constraints and test opportunities
- Develop test plans and protocols for potential flight trials
- Develop test plans and protocols for potential noise measurement campaigns
    - Specific flight test locations
    - Operational field measurements

Major Accomplishments
- Flight data collected from an aircraft performing a conventional deceleration approach during the ecoDemonstrator tests that were flown in the previous cycle were used to model the noise impacts of the procedure, and those impacts were compared with noise data collected by the Port of Seattle.
- Additional conventional and delayed deceleration approach procedures were observed in surveillance data at BOS and SEA and were identified for noise analysis.
- Instead of using dedicated flight test plans, flights from this surveillance data were grouped by altitude and analyzed with varied speed, configuration, and thrust. The noise monitor readings from these flights were then compared. This approach removed flyover altitude as a variable and enabled a direct comparison between the noise levels and the speed, configuration, and thrust levels of the flights.
- Flights for which the speeds were more likely to have been in the clean configuration when they flew over the monitors were shown to correlate with lower recorded noise levels than flights that were more likely to have been in a dirty configuration when they flew over the monitors.

Task 5 - Evaluate Experimental Results and Implications for Advanced Operational Flight Procedure Noise Modeling and Low-Noise Procedures
Massachusetts Institute of Technology

Objective(s)
Contingent on data availability from Task 4 or other data identified as part of the experimental approach and discussions with collaborators, this task, in coordination with NASA, will involve the following:

- Evaluating the Advanced Operational Flight Procedure Noise Modeling relative to experimental results
- Identifying discrepancies requiring correction
- Determining whether the results and data are sufficient to improve discrepancies or whether continued validation and testing are required

The implications for Advanced Operational Flight Procedure Noise Modeling from the data will be evaluated.

Validation of procedures, such as delayed deceleration approaches, will also create opportunities for the development of further low-noise procedures.

Research Approach

- Treat noise monitoring data from SEA and BOS as experimental data, which could serve as a benchmark for comparison against ANOPP component-based noise models
- Model departure noise for various departures from SEA, and identify the characteristics of the quietest departures; determine whether learning can be applied to future departure noise abatement procedure designs

Major Accomplishments

- Noise models demonstrated similar trends to monitor recordings for approach procedures when proper assumptions regarding flap configuration were made. Both speed and configuration were shown to impact the noise model results.
- Aircraft weight and thrust levels were shown to impact the noise modeling results for approach procedures.

Publications

Jensen, L., Thomas, J., Brooks, C., Brenner, M., & Hansman, R. J. (2017). Analytical approach for quantifying noise from advanced operational procedures [Presentation]. European Air Traffic Management Research and Development Seminar. Seattle, Washington.

Jensen, L. & Hansman, R. J. (2018). Data-driven flight procedure simulation and noise analysis in a large-scale air transporation system (Report No. ICAT-2018-02). Massachusetts Institute of Technology, Cambridge, MA.

Jensen, L., O'Neill, G., Thomas, J., Yu, A., & Hansman, R. J. (2018). Block 1 procedure recommendations for Logan Airport community noise reduction (Report No. ICAT-2017-08). Massachusetts Institute of Technology, Cambridge, MA.

Mahseredjian, A., Thomas, J., & Hansman, R. J. (2021). Advanced procedure noise model validation using airport noise monitor networks [Presentation]. Inter-Noise 2021, Washington, DC. https://doi.org/10.3397/IN-2021-2842.

Reynolds, T., Sandberg, M., Thomas, J., & Hansman, R. J. (2016). Delayed deceleration approach noise assessment [Presentation]. 16th AIAA Aviation Technology, Integration, and Operations Conference, Washington, DC.

Salgueiro, S., Thomas, J., Li., C. & Hansman, R. J. (2021). Operational noise abatement through control of climb profile on departure [Presentation]. AIAA Scitech 2021 Forum, Washington, DC. https://doi.org/10.2514/6.2021-0007.

Thomas, J., & Hansman, R. J. (2017). Modeling performance and noise of advanced operational procedures for current and future aircraft [S. M. thesis, Massachusetts Institute of Technology]. DSPace@MIT. https://dspace.mit.edu/handle/1721.1/108937

Thomas, J., Jensen, l., Brooks, C., Brenner, M., & Hansman, R. J. (2017). Investigation of aircraft approach and departure velocity profiles on community noise [Presentation]. AIAA Aviation 2017 Forum, Grapevine, TX.

Thomas, J., & Hansman, R. J. (2019). Framework for analyzing aircraft community noise impacts of advanced operational flight procedures. Journal of Aircraft, *6*(4), 1407-1417. https://doi.org/10.2514/1.C035100

Thomas, J., Yu, A., Li., C., Maddens Toscano, P., & Hansman, R. J. (2019). Advanced operational procedure design concepts for noise abatement [Presentation]. 13th USA/Europe Air Traffic Management Research and Development Seminar, Vienna, Austria.

Thomas, J., Yu, A., Li, C., Toscano, P., & Hansman, R. J. (2019). Advanced operational procedure design concepts for noise abatement [Presentation]. 13th USA/Europe Air Traffic Management Research and Development Seminar, Vienna, Austria.

Thomas, J., & Hansman, R. J. (2020). Systems Analysis of Community Noise Impacts of Advanced Flight Procedures for Conventional and Hybrid Electric Aircraft [Ph.D. thesis, Massachusetts Institute of Technology]. DSpace@MIT. https://dspace.mit.edu/handle/1721.1/125995

Thomas, J., & Hansman, R. J. (2020). Evaluation of the impact of transport jet aircraft approach and departure speed on community noise (Report No. ICAT-2020-03). Massachusetts Institute of Technology, Cambridge, MA.

Thomas, J., & Hansman, R. J. (2020). Modeling and assessment of delayed deceleration approaches for community noise reduction [Presentation]. AIAA Aviation Forum, Dallas, TX.
Thomas, J., & Hansman, R. J. (2021). Modeling of delayed deceleration approaches for community noise reduction. Journal of Air Transportation, *29*(3), 127-136. https://doi.org/10.2514/1.D0237
Thomas, J., Mahseredjian, A., & Hansman, R. J. (2021). Delayed deceleration approach procedure noise modeling validation using noise measurements and radar data [Paper presentaiton]. AIAA Aviation 2021 Forum, Virtual Meeting. https://doi.org/10.2514/6.2021-2135.
Yu, A., & Hansman, R. J. (2019). Aircraft noise modeling of dispersed flight tracks and metrics for assessing impacts [S. M. thesis, Massachusetts Institute of Technology]. DSpace@MIT. https://hdl.handle.net/1721.1/122382
Yu, A., & Hansman, R. J. (2019). Approach for representing the aircraft noise impacts of concentrated flight tracks [Presentation]. AIAA Aviation Forum 2019, Dallas, TX. https://doi.org/10.2514/6.2019-3186

Outreach Efforts

- October 28, 2021: presentation to the ASCENT Advisory Board
- September 9,2021: presentation to the Port of Seattle
- April 29, 2021: presentation to the ASCENT Advisory Board
- September 30, 2020: presentation to the ASCENT Advisory Board
- September 9, 2020: presentation to the Port of Seattle
- October 15, 2019: presentation to the ASCENT Advisory Board
- November 8, 2019: presentation to NASA
- November 12, 2019: presentation to the Airline Industry Consortium
- Weekly meetings with industry
- Biweekly teleconferences and meetings with FAA Technical Monitors
- In-person outreach and collaboration with Massport, operator of BOS and ASCENT Advisory Board member

Awards

2021, 2020 AIAA Air Transportation Systems Best Student Paper Award “Modeling, Assessment, and Flight Demonstration of Delayed Deceleration Approaches for Community Noise Reduction” (AIAA-2020-2874) by Jacqueline L. Thomas and R. John Hansman
2018 Department of Transportation/FAA COE Outstanding Student of the Year Award to Jacqueline Thomas.

Student Involvement

Graduate students have been involved in all aspects of this research in terms of analysis, documentation, and presentation.

Plans for Next Period

The next phase of this project will evaluate the departure and arrival noise of various aircraft at SEA, starting with the Boeing 737-800 and Airbus A320 and eventually expanding to larger widebody aircraft. A main goal of the upcoming work is to understand the causes of variation in departure noise. Instead of examining and modeling the noise of individual flights of interest, a large number of flights will be analyzed over all monitors in the system. This approach will provide a large dataset for which many quiet and loud cases can be identified over various monitor locations. Flight profiles and noise models will be generated for these cases of interest. Trends in variables affecting aircraft noise, including aircraft weight, thrust, distance to monitor, airspeed, and ambient atmospheric conditions will be identified. Understanding how these variables impact aircraft noise will inform the design of future advanced flight procedures intended to reduce aircraft noise.

Project 046 Surface Analysis to Support AEDT Aircraft Performance Model (APM) Development

Massachusetts Institute of Technology and Massachusetts Institute of Technology Lincoln Laboratory

Project Lead Investigator

Hamsa Balakrishnan
William E. Leonhard (1940) Professor
Aeronautics and Astronautics
Massachusetts Institute of Technology
77 Massachusetts Ave., 33-328
Cambridge, MA 02139
617-253-6101
hamsa@mit.edu

University Participants

Massachusetts Institute of Technology (MIT) and MIT Lincoln Laboratory

- PI: Hamsa Balakrishnan
- FAA Award Number: 13-C-AJFE-MIT, Amendment Nos. 021, 035, 044, 047, 063, 068, and 077
- Period of Performance: July 7, 2016, to August 31, 2022
- Task(s):
    1. Undertake more detailed studies to extend Aviation Environmental Design Tool (AEDT) capabilities to model surface noise and emissions impacts
    2. Identify representative application scenarios and estimate the impact of improved surface movement modeling capability
    3. Develop implementation plan to transition appropriate surface modeling enhancements into the operational AEDT product
    4. Support initial implementation of appropriate surface modeling enhancements in the operational AEDT product.

Project Funding Level

$625,000 in FAA funding and $625,000 in matching funds from MIT.

Investigation Team

- Prof. Hamsa Balakrishnan, co-PI (MIT)
- Dr. Tom Reynolds, co-PI (MIT Lincoln Laboratory)
- Sandeep Badrinath, PhD student (graduated in April 2021)
- Emily Joback, MIT Lincoln Laboratory staff

Project Overview

The objective of this research project is to identify and evaluate methods for improving airport taxi performance modeling in the AEDT) [1] to better reflect actual operations. This objective is being met through the analysis of relevant data sources, including surface surveillance (Airport Surface Detection Equipment, ASDE-X), Aviation System Performance Metrics (ASPM) taxi time, flight data recorder (FDR), and air quality monitor datasets. Prior phases of the ASCENT 46 project have identified first-order enhancements to the AEDT Aircraft Performance Model (APM) for surface operations. Specific improvement areas include enhanced baseline taxi fuel flow models; improved taxi times at different airports; and estimation of pre-taxi engine

and auxiliary power unit (APU) fuel burn. These enhancements were described in prior reports. This phase of the work has extended and refined fuel burn modeling in these areas, and we have undertaken initial studies to explore whether improved surface emissions models can leverage these enhanced fuel models. In particular, the research team has undertaken a detailed assessment of surface operations and associated air quality impacts at Los Angeles International Airport (LAX) due to extensive data availability at that location. In doing so, we demonstrated development of a machine learning model of the spatial distribution of airport surface emissions, given pollutant measurements, air traffic demand, and prevailing weather conditions. In addition, we developed a clustering-based method to evaluate the generalizability of our surface operations modeling framework.

Background: Two categories of analyses are important when considering the environmental impacts of airport surface operations:

- **Inventory analysis:** The objective of such an analysis is to determine aggregate total fuel burn or emissions over a period of time for current or potential future scenarios. These analyses often support higher-level analysis objectives; for example, to assess system-wide fuel and emissions impacts of different procedures or technologies.
- **Spatial distribution analysis:** This type of analysis requires more fine-grained models that reflect *where* on the airport surface fuel and emissions are released and is relevant for assessing spatial and temporal impacts of fuel burn and emissions, which are essential for local air quality analysis. Applications of such analyses include the assessments of impacts on communities close to an airport.

AEDT was developed as a single tool to replace a suite of existing models for predicting aviation environmental impacts. The previous legacy models included the following:

- Integrated Noise Model (INM) [2], used for obtaining noise estimates
- Model for Assessing Global Exposure to the Noise of Transport Aircraft (MAGENTA) [3], used for determining the global impact of aircraft noise
- Noise Integrated Routing System (NIRS) [4], used for comparing the noise impact between different routes and procedures
- Emissions and Dispersion Modeling System (EDMS) [5], used to estimate emissions on the airport surface
- System for Assessing Aviation's Global Emissions (SAGE) [6], which predicted global totals of fuel burn and emissions across all commercial flights, or alternatively the impact from a single aircraft.

A tool similar to AEDT is EUROCONTROL's Advanced Emission Model (AEM), which is used to estimate aircraft fuel burn and emissions [23]. AEM is a part of the Fuel Burn and Emission Inventory System (FEIS) used by EUROCONTROL for annual inventory analysis, which helps drive policy decisions for the European Environmental Agency [23]. Another commercial tool that has been used to estimate flight-specific fuel burn and emissions is Piano-X [24]. In addition to these industry tools, researchers have proposed various enhancements and standalone models to improve the estimation accuracy (a recent review can be found in [25]).

Prior Work: We present a brief discussion about our proposed enhancements for inventory analysis; our earlier paper [7] and prior reports contain more detailed discussions. As mentioned earlier, inventory analysis involves determining the aggregate fuel burn and emissions over a period of time. The current taxi phase model in AEDT calculates fuel burn as the product of a baseline taxi fuel burn rate and a nominal taxi time, as illustrated in the top portion of Figure 1.

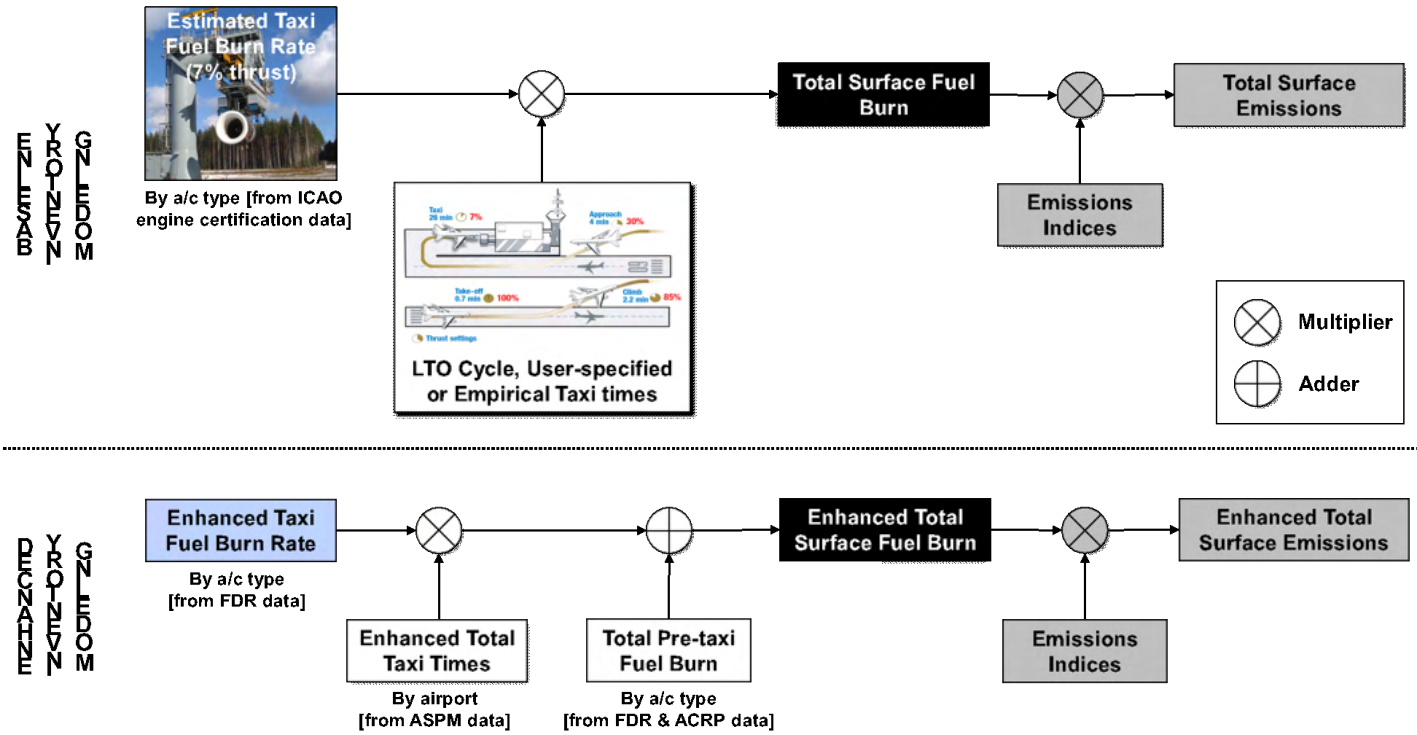

Figure 1. Fuel & Emissions Inventory Analysis Model Baseline & Enhancements.

Emissions are calculated by multiplying the resulting total fuel burn by an emissions index [8] for the emissions species of interest. The estimated baseline taxi fuel burn rate for a given aircraft type is based on a constant engine-specific 7% thrust level (and resulting fuel flow rate) during taxi, determined from engine manufacturer certification data. This can differ significantly from the actual fuel burn characteristics during operational conditions for a given aircraft because of factors such as the age of the engine (as the engine gets older, the amount of fuel it burns changes), as well as pilot technique (e.g., choosing a slightly higher or lower taxi thrust setting or "riding the brakes" instead of throttling down the engines when coming to a stop on the airport surface). The nominal taxi times are often based on the standard certification Landing and Take-Off (LTO) cycle which assumes 26 minutes of taxi time on the airport surface, typically broken into 19 minutes for taxi-out and 7 minutes for taxi-in. Different airports may have very different taxi times depending on topology, configuration, congestion levels, and so on, which can lead to a large range of taxi times. In addition, the current AEDT approach uses simplified assumptions regarding emissions (but no explicit modeling of fuel burn) contributions from the pushback and engine start events, including engine and auxiliary power unit (APU) contributions [9]. These events can be significant contributors to the overall surface fuel burn and emissions and therefore need to be modeled accurately.

New data availability and modeling techniques provide opportunities to make model enhancements to the taxi fuel burn rate, taxi time, and pre-taxi (gate and engine start) elements shown in the bottom portion of Figure 1. In our previous work [7], we had proposed enhancements in each of these elements, which are summarized below.

Enhanced Taxi Fuel Burn Rate

The recent (limited) availability of FDR data provides direct observability of engine fuel flow rates during realistic operational conditions to address many of the shortcomings identified above with previous baseline fuel flow models. Using FDR data, we have developed ordinary least squares regression-based models for the mean baseline fuel flow rate as a function of the mean values of the ambient temperature (θ_∞) and pressure (δ_∞) ratios (these input features are used for consistency with the Boeing Fuel Flow Method [9]). Table 1 shows the proposed model equations for different aircraft types in our dataset, where $\dot{m}_f$ represents the ICAO Databank fuel burn index during taxi-out. The table also shows a comparison of the error statistics of the taxi-out fuel burn obtained using our proposed model and the current AEDT model, evaluated over an independent

test set. The error statistics indicate that the proposed models are more accurate than the current AEDT model, and the reduction in mean absolute error is up to about 93% for some aircraft types.

Table 1. Proposed Model for Baseline Fuel Flow Rate and Error Statistics.

A/C type	Engine type	Proposed model	Mean error (%)		Mean absolute error (%)	
			Proposed model	AEDT	Proposed model	AEDT
A320-214	2 × CFMI CFM56-5B4/2	$0.81\ \dot{m}_f\delta_\infty^{-0.12}\theta_\infty^{-0.48}$	1.0	36.3	13.3	39.4
A321-111	2 × CFMI CFM56-5B1/2	$0.80\ \dot{m}_f\delta_\infty\theta_\infty^{0.21}$	3.8	47.1	14.9	50.1
A330-343	2 × RR Trent 772B-60	$0.78\ \dot{m}_f\delta_\infty\theta_\infty^{0.35}$	-3.0	36.4	5.8	39.1
A340-313	4 × CFMI CFM-56 5C4/P	$1.02\ \dot{m}_f\delta_\infty\theta_\infty^{0.60}$	-0.7	7.8	9.1	12.5
B777-300ER	2 × GE GE90-115BL	$0.75\ \dot{m}_f\delta_\infty^{-6.7}\theta_\infty^{0.72}$	-2.2	42.3	3.1	43.1
C Series-100	2 × PW PW1542G	$0.97\ \dot{m}_f\delta_\infty\theta_\infty^{0.19}$	0.1	17.7	5.5	19.3

$\dot{m}_f$= ICAO Databank fuel burn index during taxi-out; δ_∞ = ambient pressure ratio; θ_∞ = ambient temperature ratio; AEDT = Aviation Environmental Design Tool.

Enhanced Total Taxi Times

Airport-specific taxi-out times are available in current versions of AEDT but these can be outdated. For this part of the study, recent taxi-out data were collected from the FAA's ASPM database [10]. This dataset contains flight-specific taxi-out times, available to the nearest minute. ASPM data from flights across 25 major US airports were aggregated for dates between October 2016 and September 2017 to provide a recent model of the distribution of taxi-out times at a given airport. The boxplot in Figure 2 gives a side-by-side comparison of all airport taxi-out distributions across the 25 airports studied (which were clustered into six sets of airports with similar taxi characteristics: see [7] for more details). The 19-minute taxi-out simplification is provided as a reference, along with the error between this assumption and median of each of the distributions. The 19-minute default taxi-out time assumption is intended to represent average airport taxi time. This chart shows that the errors in this estimate vary from 0% to 72.7% for these particular airports, which is one reason why users typically do not use the 19-minute default taxi time. By using recent historical data at an airport, the error resulting from predicting the taxi-out time for a given flight can be decreased drastically. This analysis could be updated regularly to reflect evolving taxi time behaviors, and/or extended to taxi-in operations and to other US or international airports as needed.

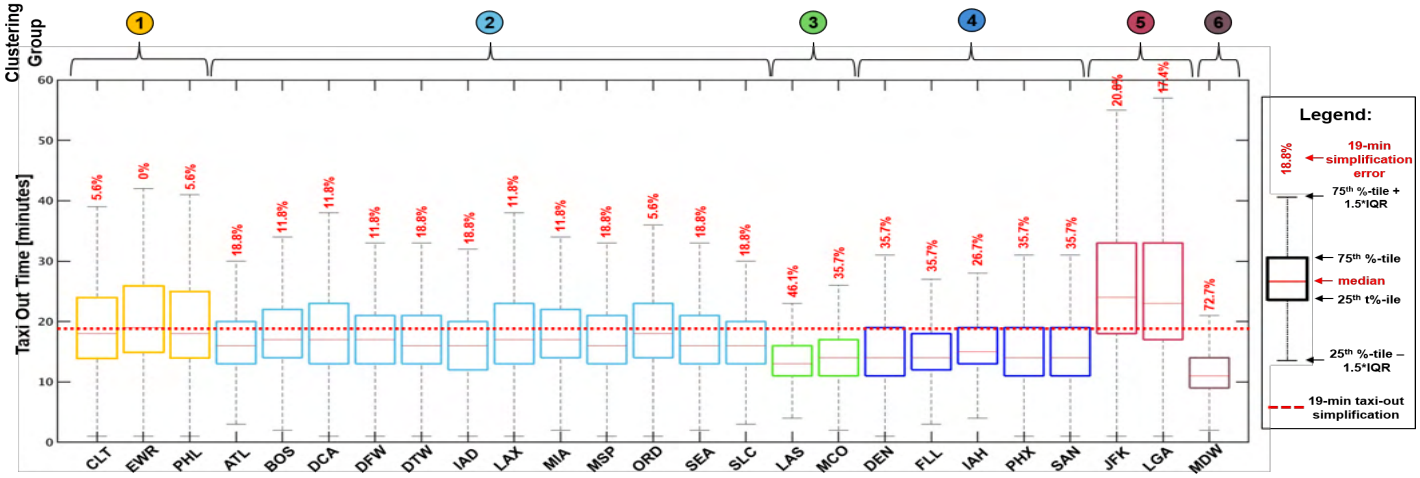

Figure 2. Enhanced Taxi-out Times Based on Recent ASPM Data [7].

Enhanced Pre-Taxi Fuel Burn

To establish a more accurate model of fuel burn, enhanced estimates of the fuel consumed by both the engine and APU during the "pre-taxi" phases at the gate, pushback, and engine startup have been developed. The engine startup fuel burn was obtained using the FDR data, and the APU fuel burn was determined from [11] and through discussions with an experienced commercial pilot. The fuel burn totals for the gate/pushback/engine start processes were aggregated over all flights of a given aircraft type available in the FDR data as a statistical approach to building fuel burn histograms from historical data. The resulting pre-taxi fuel burn distributions for the types studied are shown in Figure 3 (solid curves). The relationship between fuel burn and aircraft weight was then investigated as a means to predict the pre-taxi fuel burn of aircraft types not within the FDR dataset. The total fuel burned during gate/pushback/engine start was seen to be linearly related to the weight of the aircraft type, and this correlation was used to then predict the approximate fuel burn for aircraft types not available in the FDR data set. The results of this process for a number of wide-body aircraft are presented as the dashed lines in Figure 3.

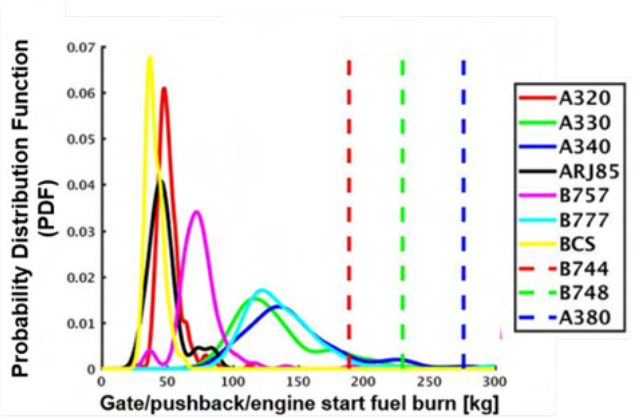

Figure 3. Pre-taxi fuel burn estimates by aircraft type [7].

Task Progress and Plans

This report summarizes the latest accomplishments in each of the ASCENT46 task areas.

Task 1 - Undertake More Detailed Studies to Extend AEDT Capabilities to Model Surface Fuel Burn and Emissions Spatial Distributions

Massachusetts Institute of Technology

The ideal approach to determining spatial distributions of fuel burn and emissions from airport surface operations is shown on the top portion of Figure 4. Fuel burn as a function of time and location would be available from FDR data (as used in the previous analysis) given that time, fuel flow for each engine, and latitude and longitude locations are then readily available. Multiplying by emissions indices for the species of interest would enable emissions as a function of time and location on the airport surface to be easily determined. Air quality impacts of surface emissions are often accomplished by deploying air quality monitors at strategic locations around the airport and its perimeter.

In practice, FDR data are not routinely available, and approximations are needed for the different elements outlined above. These are illustrated in the bottom half of Figure 4. The enhanced taxi fuel burn rates from the analysis detailed in the previous section can also be used here.

The taxi time by airport location is more critical for this type of analysis because of its sensitivity to the accuracy of the amount of time spent (and emissions created) at different airport locations. The updated taxi time analysis from the previous section does not apply for this type of analysis because it only represents *total* taxi time. To determine the amount of time spent by the aircraft at different locations on the airport surface, we can utilize trajectory data from airport surface radar

data (e.g., Airport Surface Detection Equipment, ASDE-X). However, airport surface radar data are insufficient if we are interested in evaluating fuel burn and emissions under infrastructure changes and different airport operating conditions (traffic levels, runway usage patterns etc.) not seen in historical operations. Performing such what-if analysis under different operating conditions is the primary use case for airport environmental assessment tools such as AEDT. Therefore, we need to develop traffic models of the airport surface that are capable of estimating the time spent by the aircraft at different airport locations given the airport operating conditions as the input. Queuing models have been shown to be able to reflect surface traffic congestion at airports.

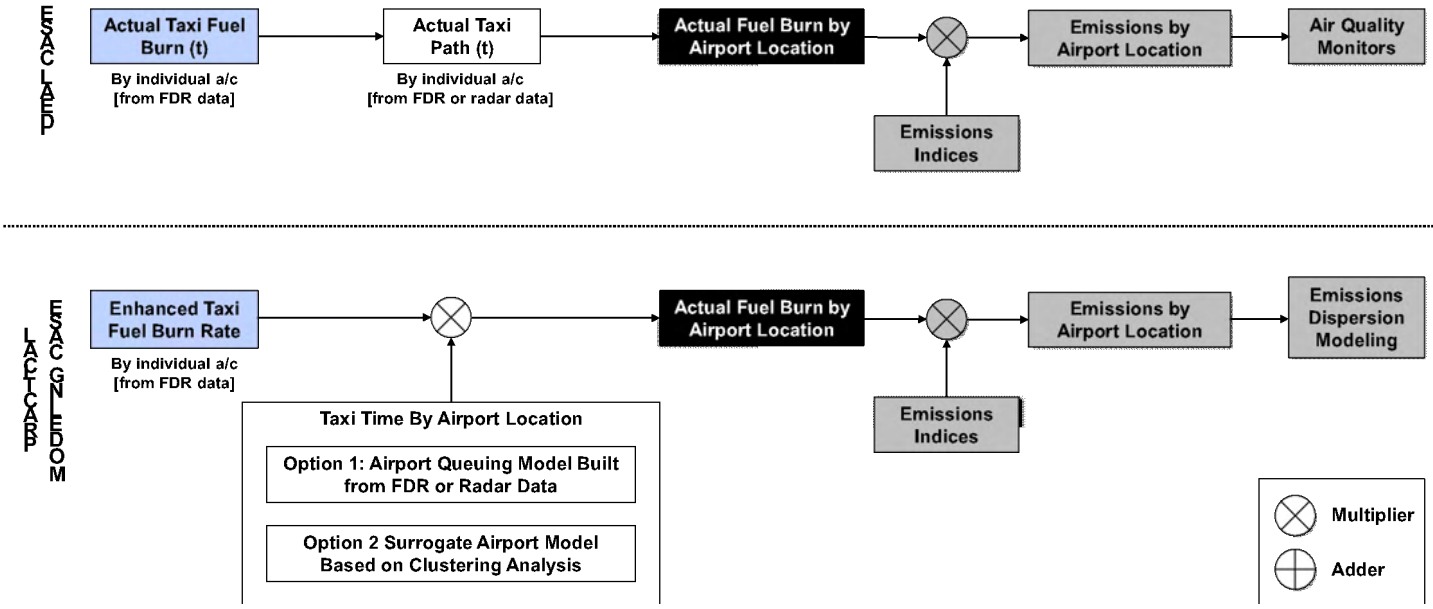

Figure 4. Fuel and emissions spatial distribution analysis ideal and practical models. FDR = flight data recorder.

Airport Queuing Model

When developing a queuing model for an airport, the queuing locations on the surface must first be known. To this end, we use airport traffic density from surface radar data (e.g., ASDE-X) to create heat maps, where hot spots within the image correspond to locations of airport surface congestion. To illustrate this, ASDE-X flight track data from LAX were analyzed. These data contained details on aircraft trajectories such as latitude, longitude, and time recorded at 1-second intervals. To identify airport dynamics during congested periods, we considered data only from the time periods when the taxi-out time was greater than the 99th percentile of the taxi-out time calculated from ASPM data. For all time windows containing a mean taxi-out time greater than the 99th percentile, the ASDE-X data were aggregated and interpolated to a 500-by-500 cell grid laid on top of the airport, where the value of a grid point represented the number of flight track points at that spot. A flight in a queue at a particular grid point increased that grid point's count every second. The count at each grid point was then normalized by the number of flights that passed over that location. Therefore, when plotting the point density of the grid as a heat map image, bright spots represent locations where aircraft were queued over a given period. The heat map for sample data at LAX from February to April 2012 (see later for why this period was selected) is shown in Figure 5. Queuing spots are seen as bright yellow in the image, where markups have been added to the image to highlight what different queuing spots represent from an operational perspective. For example, queues are seen for flights departing on runways 24L and 25R, as well as for flights arriving on the remaining two outer runways, which then must cross the inner runways to reach the terminal. Such details inform what queue spots need to be considered when developing a queuing model for LAX. A similar approach could be applied at any other airport of interest to determine what queuing model elements are appropriate.

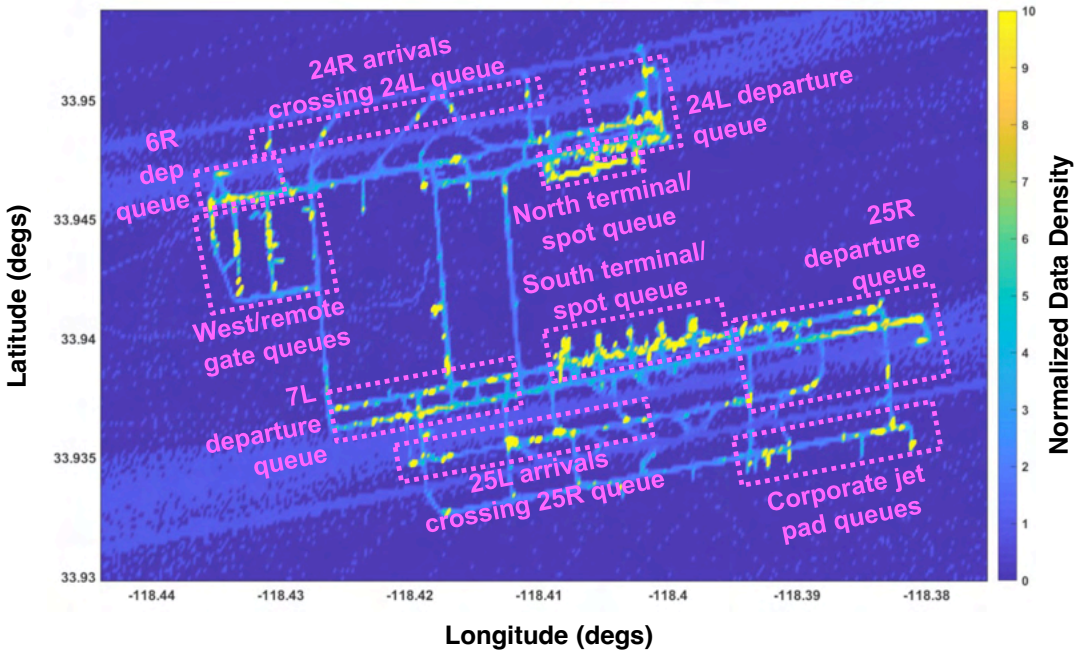

Figure 5. Data density heat map for LAX Airport (analysis period February 1, 2012 – April 30, 2012).

The objective of the queuing model is to determine macroscopic quantities of interest such as queue length and taxi-out time as a function of demand (pushback-time) and other parameters such as meteorological conditions. We next focused on developing the queuing model for West-flow runway configuration (24L, 25R|24R, 25L) at LAX, which represents the most frequently used configuration, with around 90% of the operations during the period considered in our analysis (February 1 – March 15, 2012).

In Figure 5, we see that departing flights are queued up predominantly near the departure runways. Therefore, the taxi-out process was represented using a single queue, one for each departure runway, as shown in Figure 6. After pushback, the taxi-out flights enter the departure runway queue after spending an unimpeded gate-to-runway time. Note that we use airline-specific unimpeded taxi-out time (terminal-to-runway) as a surrogate for the unimpeded gate-to-runway travel time due to the lack of gate information in the ASPM data. However, this assumption serves as a good approximation, as will be shown later in the model validation. Additionally, the unimpeded times are determined as the 10th percentile of the taxi-out time distribution for each airline-runway pair.

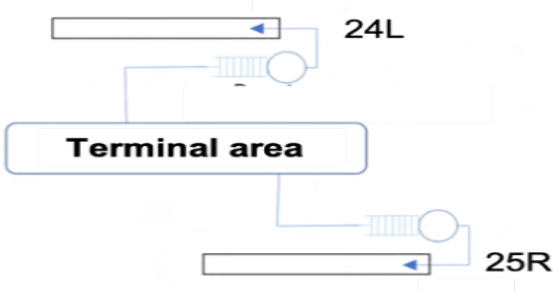

Figure 6. LAX taxi-out queuing network representation (West-flow configuration).

The dynamics for the evolution of the queuing process were obtained using a fluid-flow model, which is a continuum approximation to the discrete queuing process. Such a fluid-flow model for the queuing process has been used previously

to accurately predict queue lengths and taxi times for major airports [12]. The dynamics governing the evolution of the departure runway queue are as follows:

$$\dot{x}_i = -\mu_i(t)\frac{C_i(t)x_i(t)}{C_i(t)x_i(t)+1} + u_i(t-\tau_i),\ \ i = 1,2$$

where x_i represents the queue length of the ith departure runway, τ_i is the average unimpeded travel time from the gate to the ith departure runway, u_i represents the pushback rate to the ith departure runway, C_i is a positive parameter that depends on the coefficient of variation of the service time distribution of the server [12]], and μ_i is the mean service rate of the departure runway server. The parameters of the service time distribution of the runway server are determined from operational data [13]. The pushback rate is computed as the number of aircraft pushing back from the gate in a given time interval (5 min in this analysis). The time delay in the dynamics accounts for the travel time from the gate to the departure runway. The queue length can be predicted by integrating the dynamics forward in time with appropriate server parameters and pushback rate. The wait times of aircraft entering the queue are determined using the predictions of queue length and time-varying mean service rates [12]. The taxi-out time is then determined as the sum of the unimpeded gate-to-runway time plus the waiting time in the queue.

Figure 7 shows a comparison between the predicted and observed departure queue length at LAX for runway 24L, on a typical good weather day (March 7, 2012) in the test data set. The data correspond to a time-based definition of queue length, in which an aircraft is said to be in the runway queue if it has spent unimpeded gate-to-runway time after pushback but is yet to take-off. The time-based definition of queue length is validated by comparing against the physical queues seen at the airport using trajectory data. The deviation was found to be small, with a mean absolute error of 0.6.

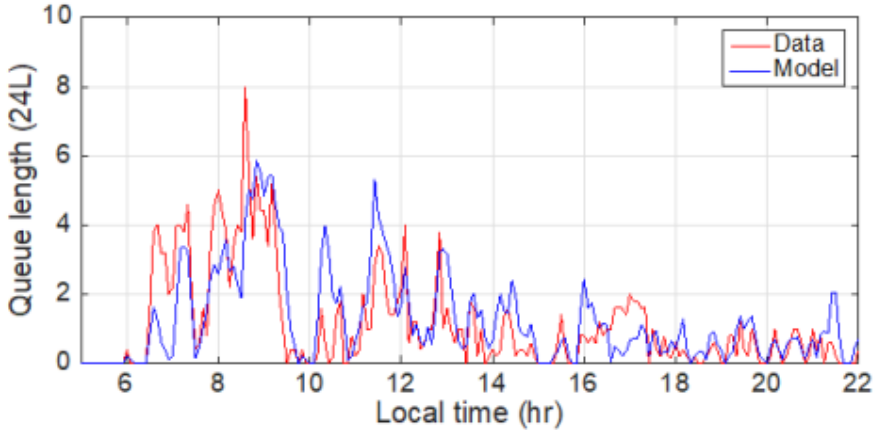

Figure 7. Queue length comparison between model predictions and data for LAX (March 7, 2012).

The taxi-out times for this particular day, averaged over 15-min windows, are shown in Figure 8. These figures show a good match between the model predictions and observed values. Aggregate error statistics of the taxi-out time prediction for individual flights were computed for an independent test set of 6,536 departures over a 9-day period. Here, the errors were computed as the predicted taxi-out time minus the actual value. The mean error was found to be 0.9 min and mean absolute errors was found to be 3.9 min, which are small relative to the mean taxi-out time of 14.2 min. These results indicate that we can predict the congestion level and locations on the airport surface to a good degree of accuracy. Although the focus of the discussion above was departure movements, a similar approach can be adopted for arriving aircraft as well.

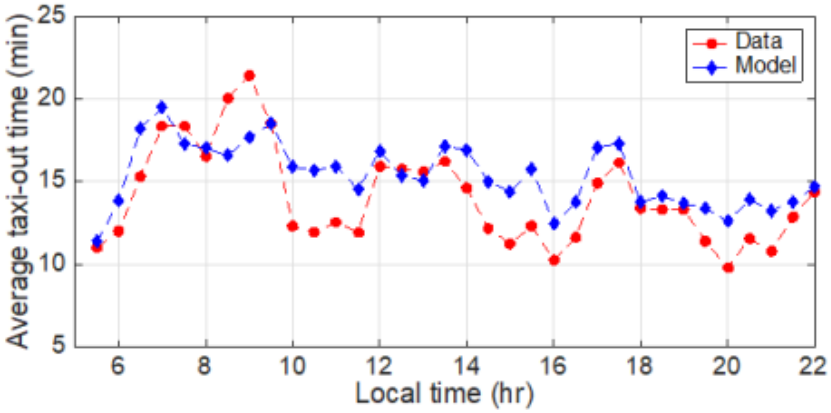

Figure 8. Taxi-out time comparison between model predictions and data for LAX (March 7, 2012).

Validation: Modeling Emissions Dispersions at LAX

The airport traffic models (such as the queuing model presented earlier) provide the total taxi time as well as the wait time in congested regions on the airport surface. Using such models or flight trajectories (if available), we can obtain a spatial distribution of fuel burn on the airport surface by multiplying the residence time of flights at a particular location with the engine-specific fuel flow rate (as detailed earlier). Further, the spatial distribution of fuel burn can be used to compute the spatial sources of emissions by multiplying the fuel burn by the corresponding engine-specific emissions index for each pollutant [8].

Figure 9. Location of LAX emissions monitoring sites AQ, CN, CE, and CS.

To demonstrate that a model could be developed to estimate pollutant concentrations around an airport, we developed regression-based emissions dispersion models for LAX. Note that this exercise was carried out to check whether we could correlate airport surface traffic with pollutant concentrations recorded at the monitoring sites around the airport; we do not follow the typical methodology for dispersion computation as done in industry toolboxes (as shown earlier in Figure 4). Figure 9 shows the locations of the four emissions monitoring sites (called AQ, CN, CE, and CS) around LAX that were considered in the analysis. The monitoring sites are located 500 to 5000 ft from the airport boundary. The emissions data consist of pollutant concentrations of CO, NOx, SO_2, PM2.5 and ultrafine particles (UFP, i.e., PM with diameter <100 nm) sampled every minute for the period February 1 to March 16, 2012.

Figure 10 shows the median pollutant concentrations of CO and NOx at the four emissions monitoring sites around the airport evaluated over the period considered in our analysis.

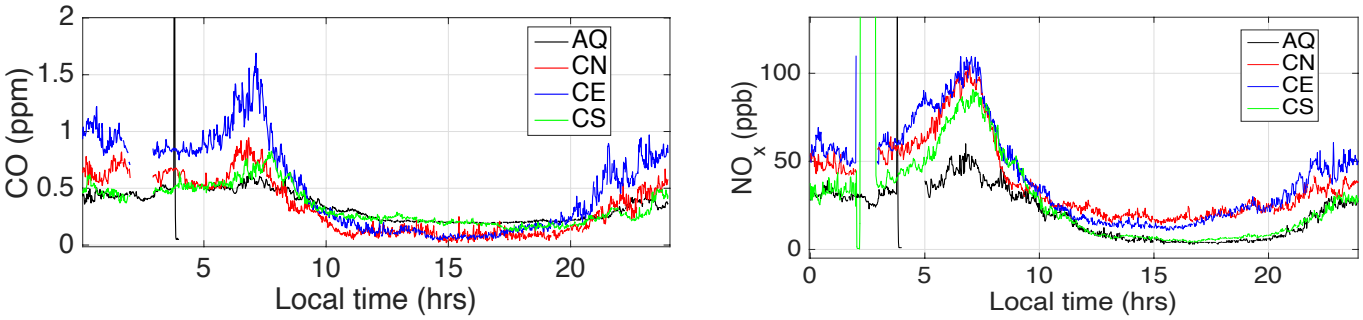

Figure 10. Pollutant Concentrations of CO and NOx at the four emissions monitoring sites.

We can see that the pollutant concentrations of CO and NOx are higher during the night than during the day, which does not follow the trend in air traffic movements. The unexpected discrepancy between nighttime and daytime pollutant concentrations is because of various factors, including changes in mixing height and smog formation in the Los Angeles region [18]. Therefore, the variations in the pollutant concentrations in Los Angeles region are largely influenced by external factors, such as photochemical reactions, but not by airport traffic. This makes these pollutants ineffective signals for analyzing the environmental impact of airport operations. It is important to note that the impact of smog formation or other background sources is not specific to LAX but could impact other airports as well [19]. Therefore, we need to consider other pollutants that correlate well with airport traffic to better understand the impact of airport operations.

Figure 11 shows the median of the counts (normalized by the sum of the counts over the entire period) of aircraft movements (arrivals and departures) on the airport surface and UFP particle number concentrations (corresponding to particle diameter of 10 nm) at the CE emissions monitoring site for the period February 1 to March 16, 2012. We can observe a strong correlation between traffic counts and UFP concentrations, indicating that UFP concentrations are a good signature for studying the effect of airport traffic. The particle size diameter from aircraft emissions are much lower than that from vehicular emissions or other sources, and are thus an excellent candidate for analyzing the impact of airport operations [20]. Additionally, the particulate matter diameter depends on the aircraft thrust setting, which helps us isolate taxi emissions from other phases of flight [21]. In our analysis, we considered 10-nm UFP concentrations because it corresponds to a diameter lower than the particulate matter from vehicular sources (which tend to be greater than 30 nm) [20]. Unlike PM2.5 or other pollutants, there is currently no regulation on UFP, but recent studies indicate that UFP can have serious health consequences, given their smaller size [22].

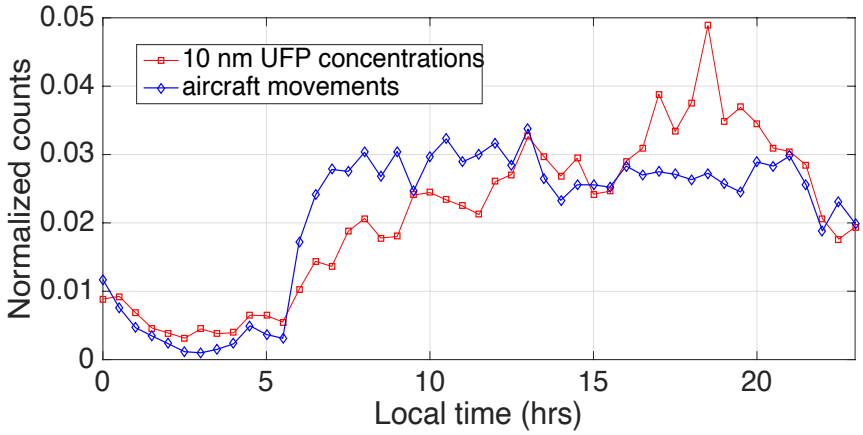

Figure 11. Normalized counts of aircraft movements and 10-nm ultrafine particle (UFP) concentrations.

We developed a model for 10-nm UFP concentrations as a function of airport traffic and meteorological data to illustrate an emissions dispersion model. In particular, we developed a *temporal model* and a *spatial model* to showcase different methodologies and their performance.

Temporal Model

In the temporal model, we estimated the 10-nm UFP concentrations at one of the monitoring sites using historical data from the same monitoring site and a set of inputs that depend on the airport traffic and meteorological conditions. For illustration, we present a model that was trained using data from the CE site located to the east of departure runway 25R (see Figure 9). We consider a regression model of the following form:

$$Y = f(C_{k,m}, W_{EW}, W_{NS}, T_{amb}, S_{rad})$$

Here, Y denotes the normalized 10-nm UFP concentration sampled at 15-min intervals. $C_{k,m}$ represents the traffic counts weighted by the baseline aircraft fuel flow rate for arrivals ($k = a$) or departures ($k = d$) in the queue ($m = q$) or actively taxiing aircraft ($m = t$), that have been assigned one of the southern runways (25R, 25L). W_{EW} and W_{NS} represent the wind speed along east-west and north-south directions, respectively. T_{amb} and S_{rad} denote the ambient temperature and solar irradiance, respectively. The regression function, $f()$, is determined using Gaussian process regression (GPR), with 70% of the data (1657 samples) used for training the model and the remainder used to test the model. The input features were selected based on careful feature engineering, and we omit the details here for conciseness. For example, we found that the magnitude and direction of wind play a significant role in emissions dispersion, as might be expected. Additionally, we found that departure and arrival traffic using runway 25R had a significant influence on the pollutant concentrations at the CE site, and including other traffic did not improve the model performance. Figure 12 shows the model predictions (and 95% confidence intervals) and the actual data from an independent test set. We can see a good match between the predicted and actual data. The mean error and mean absolute error evaluated using the test set were found to be 0.009 and 0.038, respectively. Here, the errors are computed as the difference between the estimated normalized UFP concentrations from the model and the data.

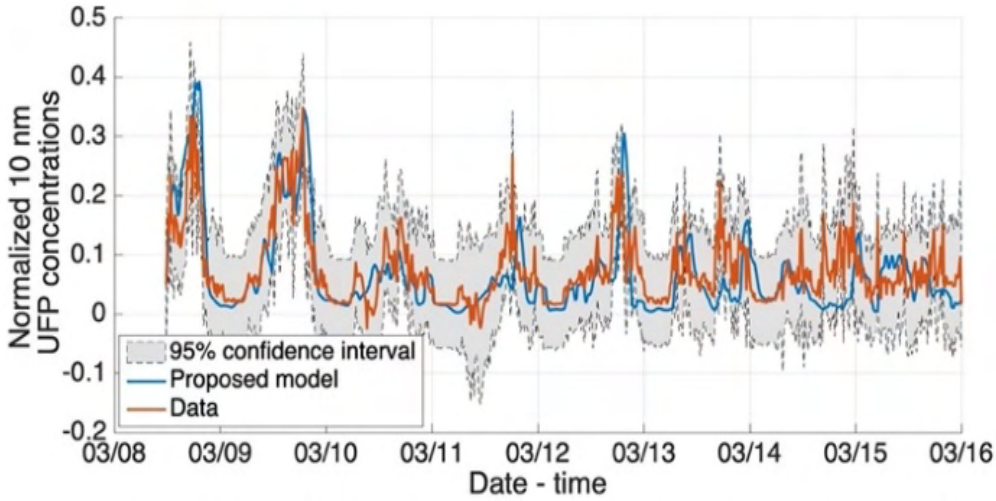

Figure 12. Predictions of the Normalized UFP Concentrations using temporal model.

Spatial Model

The spatial model allows us to estimate the UFP concentration at any location around the airport. The model is trained using data from multiple monitoring sites, and we considered the spatial component (location) of emission sources by accounting for the distance between the various sources and the location where the pollutant concentration needs to be estimated. Here, the sources represent the queuing traffic and actively taxiing traffic for each runway. The input features include traffic at different sources weighted by the baseline fuel flow rate, distance between source and monitor, bearing between wind vector and position vector of monitors, temperature, and solar irradiance. Additionally, we included time-delay terms of the input features (the previous two 15-min intervals) to account for advection of pollutants from the source to the monitor. For illustration, we present a model that was trained using data from two monitoring locations (CE and CS sites) and tested the

performance of the model using data from a different location (CN site) that is located to the east of runway 24L. The model was determined using GPR. Figure 13 shows the model predictions along with 95% confidence intervals and the actual data from an independent test set. We observed a good match between the model predictions and actual data. The mean error and mean absolute error evaluated using the test set were found to be 0.013 and 0.039, respectively. However, the temporal model performed better than the spatial model because it was trained on data from the same monitor. Nonetheless, the advantage of the spatial model is that it can estimate UFP concentrations at any location around the airport. Overall, these results indicate that queuing models that estimate the airport traffic can be used to predict UFP concentrations around the airport. Therefore, this framework shows that we can estimate the environmental impact of taxi operations without interference from other background sources of emissions.

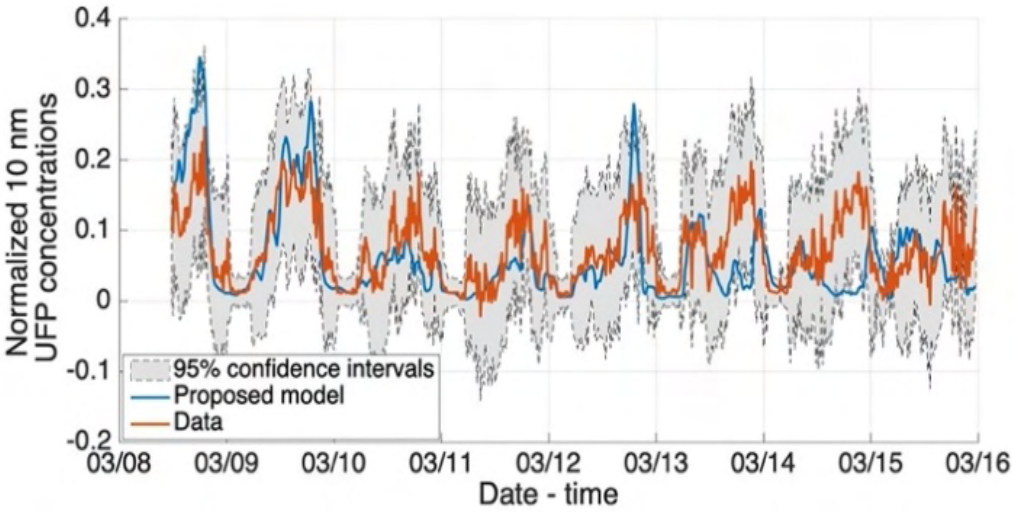

Figure 13. Predictions of the Normalized UFP Concentrations Using Spatial Model.

Task 2 - Identify Representative Application Scenarios and Estimate the Generalization of the Modeling Approach

Massachusetts Institute of Technology

Surface operations assessments are needed at many major airports around the world but tailoring the fuel burn and emissions model to each airport individually would not be feasible. Rather than developing a queuing model and validating the framework for every major airport, we used clustering to determine groupings of airports with similar features. We then noted that validated queuing models exist in the literature for representative airports in each group, suggesting that the approach generalizes well to a large number of airports.

For this approach, we used a *k*-means clustering algorithm [14]. The features used for the clustering algorithm were chosen with the intent to capture major differences between airports:

- **Mean, standard deviation, and skew of taxi-out delay:** The taxi-out time delay was calculated as the difference between the unimpeded taxi-out time (the 10th percentile of the taxi-out time for that year for that airport), and the actual taxi-out time for each flight. The mean value of the taxi-out time delay is useful in determining whether an airport typically has a lot of delayed flights, but the standard deviation and skew of this distribution yield additional insight. For example, an airport may not experience high delay on average, and thus have a "normal" mean taxi-out time delay, but the delay distribution could be skewed, indicating that periods still exist when departing flights experience high delay.
- **Mean taxi-out time:** Whereas the previous three features consider the level of congestion on the airport surface, mean taxi-out time serves as a metric for measuring the size of the airport (i.e., higher taxi time equates to larger airport size).

- **Number of runway configurations:** The number of runway configurations can vary greatly between airports. For example, at LAX, the majority of annual air traffic operations are performed in the same configuration. In contrast, Boston Logan International Airport (BOS) has multiple configurations that are commonly utilized, with seasonal traffic patterns from weather effects. This feature measures how many configurations account for the top 75% of annual operations, each of which could have very different queue dynamics and locations.
- **Percentage of operations in visual meteorological conditions (VMC):** This accounts for weather impacts.

For all of these features, the data were obtained from ASPM. This database contains flight-level information (such as taxi-out time) and airport information (such as the weather operating conditions), which is updated hourly. The full 2018 dataset was pulled for the ASPM Core 30 airports [15] and used to calculate the six features identified above. Each feature was normalized across all 30 airports by subtracting out the mean value and dividing by the standard deviation. This step prevents improper weighting between features that have differing magnitudes (e.g., the mean taxi-out time delay will always be a much larger number than the percentage of operations in VMC, but is not a necessarily more important feature). To determine *k*, the sum of the squared error was plotted against chosen *k* values, and the knee in this curve was seen to be at seven clusters. Repeated use of *k*-means can sometimes yield varying results on the same set of data due to randomized initial centroids used at the start of the algorithm. To account for this, the *k*-means algorithm was repeatedly applied to our dataset for 1 million iterations to ensure the final clustering result was consistent. To further verify the fit of the final clustering result, we used the silhouette coefficient [16], where a larger value for the silhouette coefficient corresponds to clusters that better fit the data. The silhouette coefficient plot for our final clustering results is shown in Figure 14, and shows that the final clustering is a good fit given the all-positive scores.

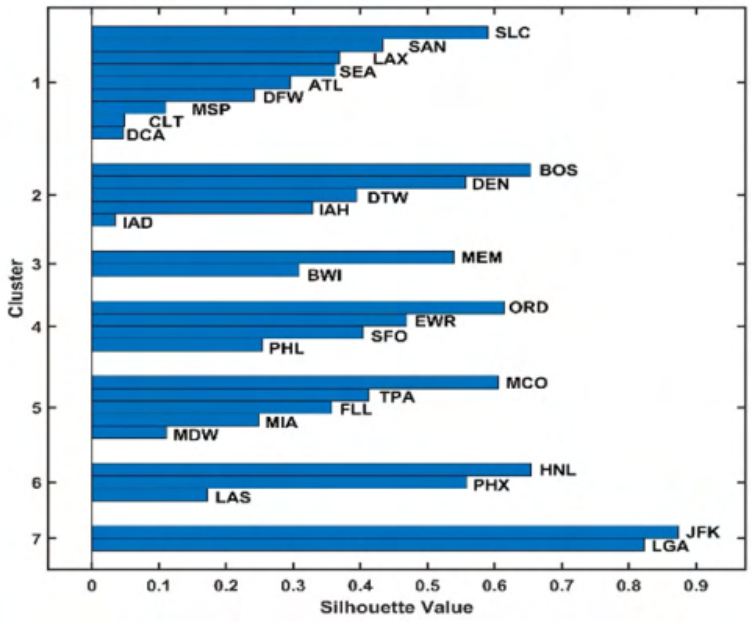

Figure 14. Core 30 airport clusters.

Additional insight into why certain airports were paired together can be gleaned from looking at the mean feature values across the airports in each cluster: see Figure 15. Features with values close to zero are within the normal range when compared against all 30 airports, whereas a largely negative or positive feature indicates that the feature is significant for the airports in that cluster, and one of the drivers for why those airports were paired. For example, airports in cluster 2 contain features that are relatively normal, but the number of commonly used configurations is high, and the percentage of operations in VMC is slightly low. The airports in this cluster, such as BOS and DEN (Denver International Airport), are airports that often switch configuration due to weather effects. For such airports, the model would need to consider the current airport configuration and potentially the season of the year when making taxi time, fuel burn, and emissions predictions. In contrast, cluster 6 contains airports with lower-than-average taxi-out time and delays, and the highest percentage of operations in VMC. The three airports in this cluster are HNL (Daniel K. Inouye International Airport, Hawaii), PHX (Phoenix),

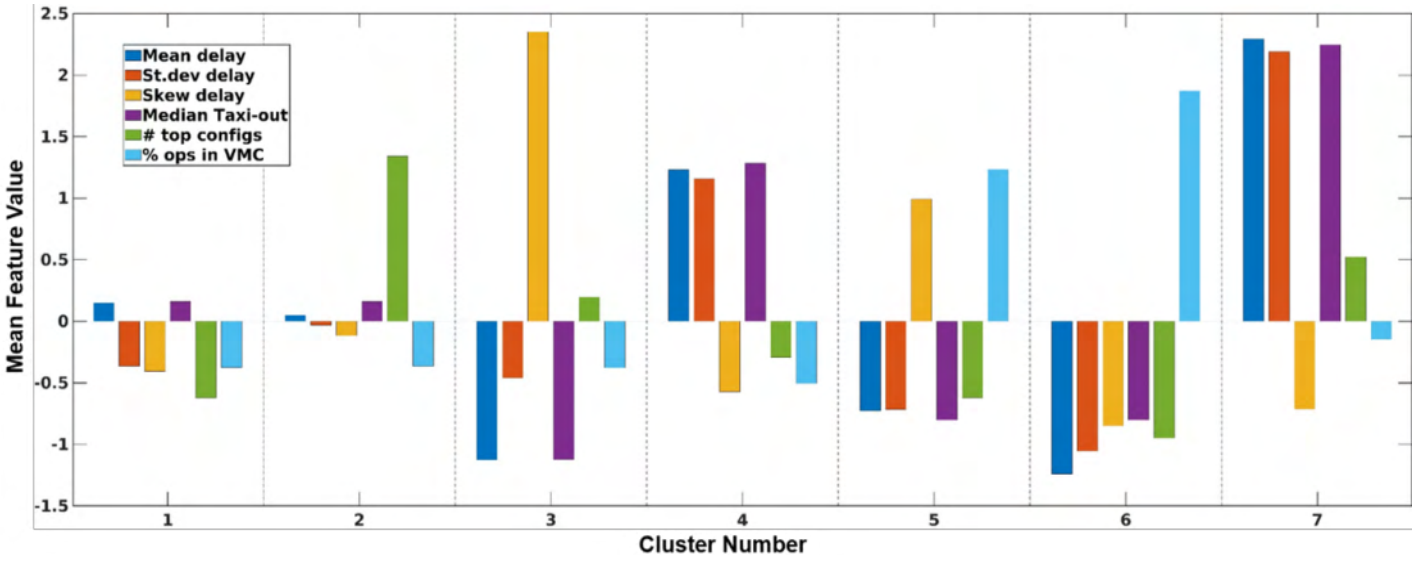

Figure 15. Core 30 airport cluster feature values.

Task 3 - Develop Implementation Plan to Transition Appropriate Surface Modeling Enhancements into the Operational AEDT Product

Massachusetts Institute of Technology

The research team conducts regular analysis, status, and results reviews with FAA sponsors and AEDT developers. This will continue, with the intent to identify an implementation plan and schedule to transition specific surface modeling enhancements into appropriate versions of the operational AEDT product given their developmental maturity and programmatic priorities. We will also further engage with AEDT developers as prior phases of the work identified the need for functionality tailored to different user classes, including:

1. **Basic users** wanting the ability to select "canned" options representative of typical operating conditions; for example, based on ASPM-derived empirical distributions. We can also analyze the impact of infrastructure development (e.g., runway construction) that can change airport capacity and traffic flows on the surface, and have a subsequent effect on fuel burn, noise, and emissions.
2. **Intermediate users** wanting the ability to modify behaviors based on appropriate modeled parameters; for example, available in the existing AEDT delay and sequence model.
3. **Advanced users** wanting complete control over all aspects of aircraft and airport dynamics; for example, based on ASDE-X data.

Task 4 - Support Initial Implementation of Appropriate Surface Modeling Enhancements in the Operational AEDT Product

Massachusetts Institute of Technology

The research team will continue to support the initial implementation of the enhanced surface queuing model into the operational AEDT product (i.e., the replacement of the DSQM module within AEDT). This task includes recommendations on default model parameters for the departure runway service rates and their coefficient of variations, as well as a recommended methodology for calculating the mean service times for new runways or types of operations, when needed. An AEDT surface modeling enhancement scoping document has recently been completed in close collaboration with AEDT developers. The initial focus has been on implementing the departure queuing model developed in this work, and AEDT software requirements based on this scoping document are currently under development. The research team is poised to assist with validation cases once this enhanced queuing capability has been implemented. The team is also helping to socialize other enhancements recommended in this work to key stakeholders; for example, briefing the enhanced taxi fuel flow rate recommendations the SAE A21 Committee.

Milestones

The work to date has focused on Tasks 1-3 above; more recently (and going forward) we have been focusing on Task 4.

Publications

S. Badrinath, E. Joback, J. Abel, T.G. Reynolds, and H. Balakrishnan. "Spatial Modeling of Airport Surface Fuel Burn for Environmental Impact Analysis," *US-Europe ATM R&D Seminar*, September 2021.

Outreach Efforts

None

Awards

Best Paper in the Environment and Energy Efficiency Track at the US-Europe ATM R&D Seminar, September 2021.

Student Involvement

MIT students have been involved in this research. Sandeep Badrinath was a PhD candidate in Aeronautics and Astronautics at MIT who graduated in April 2021. We also had an undergraduate student, James Abel, involved in this project.

Plans for Next Period

In the next period, the research team will continue to support the initial implementation of the enhanced surface queuing model into the operational AEDT product (i.e., the replacement of the DSQM module within AEDT), including default model parameters for the departure runway service rates and their coefficient of variations, as well as a recommended methodology for calculating the mean service times for new runways or types of operations, when needed. The team will also explore extending the activities reported here to help improve surface thrust and noise modeling capabilities, as well as potentially exploring applications to general aviation operations and airports.

References

[1] FAA, "Aviation Environmental Design Tool (AEDT)". Retrieved from https://aedt.faa.gov/ on February 24, 2021.
[2] FAA, "Integrated Noise Model (INM)". Retrieved from https://www.faa.gov/about/office_org/headquarters_offices/apl/research/models/inm_model/ on February 24, 2021.
[3] FAA, "Model for Assessing Global Exposure to the Noise of Transport Aircraft (MAGENTA). Retrieved from https://www.faa.gov/about/office_org/headquarters_offices/apl/research/models/ on February 24, 2021.
[4] FAA, "Noise Integrated Routing System (NIRS) & NIRS Screening Tool (NST)". Retrieved from https://www.faa.gov/about/office_org/ headquarters_offices/apl/research/models/nirs_nst/ on February 24, 2021.
[5] FAA, "Emissions and Dispersion Modeling System (EDMS). Retrieved from https://www.faa.gov/about/office_org/headquarters_offices/apl/ research/models/edms_model/ on February 24, 2021.

[6] FAA, "System for Assessing Aviation's Global Emissions (SAGE) incorporated into the Aviation Environmental Design Tool (AEDT)". Retrieved from https://www.faa.gov/about/office_org/headquarters_ offices/apl/research/models/sage/ on February 24, 2021.

[7] E. Clemons, T. G. Reynolds, Y. Chati, and H. Balakrishnan, "Enhancing Aircraft Fuel Burn Modeling on the Airport Surface," *AIAA AVIATION Forum*, June 2018.

[8] ICAO, Aircraft Engine Emissions Databank, Retrieved from https://www.easa.europa.eu/domains/environment/icao-aircraft-engine-emissions-databank on March 30, 2021.

[9] M. Ahearn et al., "Aviation Environmental Design Tool (AEDT) Technical Manual", Version 2b, Service Pack 3, U.S. Department of Transportation John A. Volpe National Transportation Systems Center, Report No. DOT-VNTSC-FAA-16-11, 2016.

[10] FAA, "Aviation System Performance Metrics (ASPM)" database, https://aspm.faa.gov/, 2021.

[11] ACRP 02-25, "Handbook for Evaluating Emissions and Costs of APUs and Alternative Systems", Transportation Research Board, 2012.

[12] S. Badrinath, H. Balakrishnan, E. Joback., & T. G. Reynolds, "Impact of Off-block Time Uncertainty on the Control of Airport Surface Operations" *Transportation Science*, *54*(4), 920-943, 2020.

[13] I. Simaiakis, & H. Balakrishnan "Probabilistic Modeling of Runway Interdeparture Times," *Journal of Guidance, Control, and Dynamics*, *37*(6), 2044-2048, 2014.

[14] J. A. Hartigan & M.A. Wong, "A K-means Clustering Algorithm," *Journal of Royal Statistical Society: Series C*, Vol. 28 pp. 100-108, 1979.

[15] FAA, Core 30. Retrieved from https://aspm.faa.gov/aspmhelp/ index/Core_30.html. on April 8, 2021.

[16] Peter J. Rousseeuw, "Silhouettes: A Graphical Aid to the Interpretation and Validation of Cluster Analysis," *Journal of Computational and Applied Mathematics*, Volume 20, Pages 53-65, 1987.

[17] I. Simaiakis, "Analysis, Modeling and Control of the Airport Departure Process," Ph.D. thesis, Massachusetts Institute of Technology, 2013.

[18] G. C. Tiao, G. E. P. Box, & W. J. Hamming, "Analysis of Los Angeles Photochemical Smog Data: A Statistical Overview," *Journal of the Air Pollution Control Association*, 25(3), 260-268, 1975.

[19] A. Baklanov, L. T. Molina & M. Gauss., "Megacities, Air Quality and Climate," *Atmospheric Environment*, *126*, 235-249, 2016.

[20] E. A. Riley, T. Gould, K. Hartin, S. A. Fruin, C. D. Simpson., M. G. Yost, & T. Larson, "Ultrafine Particle Size as a Tracer for Aircraft Turbine Emissions," *Atmospheric Environment*, *139*, 20-29, 2016.

[21] J. S. Kinsey, Y. Dong, D. C. Williams & R. Logan, "Physical Characterization of the Fine Particle Emissions from Commercial Aircraft Engines during the Aircraft Particle Emissions eXperiment (APEX) 1–3," *Atmospheric Environment*, *44*(17), 2147-2156, 2010.

[22] G. R. Cass, L. A. Hughes, P. Bhave, M. J. Kleeman, J. O. Allen & L. G. Salmon, "The Chemical Composition of Atmospheric Ultrafine Particles," *Philosophical Transactions of the Royal Society of London: Series A,* 358 (1775), 2581-2592, 2000.

[23] M. Whiteley, "European Aviation Fuel Burn & Emissions Inventory System (FEIS)," Retrieved from https://www.eurocontrol.int/database/ aviation-fuel-use-and-emission-inventory-system on April 8, 2021.

[24] Piano-X. Retrieved from https://lissys.uk/PianoX.html on April 9, 2021.

[25] J. Yanto, & R. P. Liem, "Aircraft Fuel Burn Performance Study: A Data-Enhanced Modeling Approach," *Transportation Research Part D: Transport and Environment*, *65*, 574-595, 2018.

Project 47 Clean-Sheet Supersonic Aircraft Engine Design and Performance

Massachusetts Institute of Technology

Project Lead Investigator

Prof. Steven R. H. Barrett
Professor of Aeronautics and Astronautics
Department of Aeronautics and Astronautics
Massachusetts Institute of Technology
77 Massachusetts Avenue
Cambridge, MA 02139
617-452-2550
sbarrett@mit.edu

University Participants

Massachusetts Institute of Technology

- PI: Prof. Steven R. H. Barrett
- FAA Award Number: 13-C-AJFE-MIT, Amendment Nos. 052, 059, 074, 076, and 090
- Period of Performance: March 29, 2019, to September 30, 2022 (with the exception of funding and cost-share information, this report covers the period from October 1, 2020, to September 30, 2021)
- Tasks:
    1. Identify mission profiles and operating requirements for propulsion systems
    2. Develop an engine cycle model for a supersonic aircraft propulsion system
    3. Assess environmental footprint of an engine for a supersonic transport aircraft
    4. Assess the effect of variable noise reduction systems (VNRS) on landing and take-off (LTO) emissions of supersonic aircraft

Project Funding Level

$1,250,000 in FAA funding and $1,250,000 matching funds. Sources of match are approximately $288,000 from MIT, plus third-party in-kind contributions of $177,000 from Byogy Renewables Inc., and $634,000 from NuFuels LLC, and $151,000 from Savion Aerospace Corp.

Investigation Team

- Prof. Steven Barrett (MIT) serves as PI for the ASCENT 47 (A047) project as head of the Laboratory for Aviation and the Environment. Prof. Barrett coordinates internal research efforts and maintains communication between investigators in the various MIT research teams.
- Dr. Raymond Speth (MIT) serves as co-PI for the A47 project. Dr. Speth directly advises student research in the Laboratory for Aviation and the Environment focused on assessment of fuel and propulsion system technologies targeting reduction of aviation's environmental impacts. Dr. Speth also coordinates communication with FAA counterparts.
- Dr. Choon Tan (MIT) serves as co-PI for the A47 project. Dr. Tan directly advises student research in the Gas Turbine Laboratory focused on unsteady and three-dimensional flow in turbomachinery and propulsive devices, aerodynamic instabilities in aircraft gas turbine engines, and propulsion systems.
- Dr. Jayant Sabnis (MIT) serves as co-investigator for the A47 project. Dr. Sabnis co-advises student research in the Laboratory for Aviation and the Environment. His research interests include turbomachinery, propulsion systems, gas turbine engines, and propulsion system–airframe integration.

- Mr. Prashanth Prakash is a PhD student in the Laboratory for Aviation and the Environment. Mr. Prakash is responsible for developing engine models in the Numerical Propulsion System Simulation (NPSS) tool, for developing the combustor reactor network model, and for analyzing the sensitivity of engine emissions to design parameters.
- Mr. Laurens Voet is a PhD student in the Gas Turbine Laboratory. Mr. Voet is responsible for determining propulsion system requirements for supersonic aircraft designs, for relating the noise footprint to the relevant engine parameters, for estimating the effective perceived noise level (EPNL) for given aircraft trajectories, and for proposing clean-sheet engine design solutions to reduce its noise footprint.

Project Overview

A number of new civil supersonic aircraft designs are currently being pursued by industry in different Mach regimes and for different size classes (e.g., supersonic business jets at low-supersonic Mach numbers and airliners at high-supersonic Mach numbers). Compared with those for subsonic aircraft, engines for supersonic aircraft present unique challenges in terms of their fuel consumption, noise, and emissions impacts because of their unique operating conditions. The propulsion systems currently proposed by the industry are developed around the core (high-pressure compressor, combustor, and high-pressure turbine) of existing subsonic engines, with modifications to the low-pressure spool (fan and low-pressure turbine).

ASCENT Project 47 aims to evaluate the design space of "clean-sheet" engines designed specifically for use on civil supersonic aircraft, and to determine the resulting environmental performance of such engines. Unlike previous commercial supersonic engines, which were adapted from military aircraft, or planned propulsions systems derived from current commercial engines, a clean-sheet engine takes advantage of recent advances in propulsion system technology to significantly improve performance and reduce emissions and noise footprints. This project will quantify these benefits for a range of engine designs relevant to currently proposed civil supersonic aircraft.

Specific goals of this research are to:

- Develop a framework for quantifying the noise and emissions footprints of propulsion systems used on civil supersonic aircraft
- Assess the difference in environmental footprint between a derived engine and a clean-sheet engine for a civil supersonic aircraft
- Assess variable noise reduction systems (VNRS) used during noise certification of Supersonic Level 1 (SSL1) type aircraft and their effect on landing and take-off (LTO) emissions
- Develop a roadmap for technology development, focusing on reducing the environmental footprint associated with engines for civil supersonic aircraft

A summary of accomplishments to date includes the following:

- A survey of supersonic transport concepts and existing designs was carried out, and the Stanford University Aerospace Vehicle Environment (SUAVE) was selected to analyze mission profiles and derive propulsion system requirements.
- Multiple engine models were developed in the NPSS tool. The baseline engine chosen for the derivative engine analysis was the CFM56-5B engine.
- The engine cycle model was used to evaluate the sensitivities of performance measures to design variables, technology assumptions, and propulsion system requirements.
- A reactor network framework was developed to estimate NO_x emissions. The model was calibrated to the International Civil Aviation Organization (ICAO) data for the CFM56-5B3 engine.
- A framework was developed to estimate the noise footprint (sound pressure level [SPL], tone-corrected perceived noise level [PNLT] and EPNL) of the engine given the relevant engine parameters using a semi-empirical model. The framework provides sensitivities of acoustic objective functions to engine operating variables, enabling multi-disciplinary design optimization and optimal control of low-noise aerospace vehicles.
- The difference of pollutant emissions of engines for supersonic transport (SST) aircraft flying trajectories with and without VNRS has been estimated.

Task 1 - Identify Mission Profiles and Operating Requirements for Propulsion Systems

Massachusetts Institute of Technology

Objectives

The first objective of this task is to identify representative mission profiles of commercial SST aircraft (i.e., characterize stages of the mission by defining parameters such as climb rates and accelerations). A second objective is to use these mission profiles and representative aircraft parameters (e.g., wing area, drag and lift polars) of civil supersonic aircraft operating in different Mach regimes to derive propulsion system requirements for supersonic aircraft.

Research Approach

Mission profiles and operating requirements are identified for two vehicles spanning a wide range in the possible supersonic fleet.

NASA Supersonic Technology Concept Aeroplane (STCA): 8-passenger, Mach 1.4 business jet

The NASA STCA is a 55-tonne, 8-passenger business tri-jet cruising at a Mach number of 1.4 between 41 and 51 kft altitude. The mission profile of the NASA STCA is used to obtain propulsion system requirements (Berton, 2019). The four critical sizing points of the NASA STCA, as illustrated in Table 1, are used in a multiple-design-point (MDP) model in the engine design process.

Table 1. Propulsion system requirements (per engine) for the NASA STCA. The top-of-climb conditions are chosen as the aerodynamic design point for any component that is purpose-designed for the application.

	Sea-level static (SLS)	Take-off (TO)	Top-of-climb (TOC)	End-of-cruise (EOC)
Altitude [kft]	0	0	41	51
Mach [-]	0	0.25	1.4	1.4
Thrust [lbf]	16,617	14,140	5,500	3,300

M2.2 Medium SST: 55-passenger, Mach 2.2 airliner

The mission requirements of a 55-passenger, 4-engine, Mach 2.2 SST, designed by Georgia Tech, were obtained through collaboration with the ASCENT 10 Project.

Publications

None.

Outreach Efforts

None.

Awards

None.

Student Involvement

This work was primarily carried out by graduate research assistants Prashanth Prakash and Laurens Voet.

Plans for Next Period

This task is complete.

References

Berton, J. & Geiselhart, K. (2019). NASA 55-tonne Supersonic Transport Concept Aeroplane (STCA) release package. NASA GRC/NASA LaRC.

Task 2 - Impact of Design Space Constraints on Noise and Emissions from Derivative Engines for Supersonic Civil Transport Aircraft

Massachusetts Institute of Technology

Objectives

The objectives of this task are to:

- Use an engine cycle deck to analyze derivative and clean-sheet propulsion systems for commercial supersonic aircraft.
- Assess the sensitivities of engine performance metrics to constraints and propulsion system requirements to analyze the impact of design requirements and technology constraints on the engine performance.
- Evaluate the design space constraints imposed by a constraint donor engine core on the environmental footprint.

Research Approach

The NPSS software (Claus, 1991) is chosen to develop the engine cycle decks for clean-sheet and derivative engines because it is an industry standard tool that facilitates future collaboration with other users of the tool.

Donor engine model

To develop the derivative engine, a baseline engine was first chosen and modeled. The CFM56-5B engine was chosen for this task because it was the initial donor engine for the proposed GE Affinity engine. The engine architecture of the donor engine is illustrated in the bottom half of Figure 1. The baseline engine was modeled using published data from Jane's Aero Engines and data published in the Emissions Databank (EDB) by the European Union Aviation Safety Agency (EASA). The thrust versus fuel flow characteristic of the engine model is compared with data from the EDB of six CFM56 variants. The root mean square (RMS) error between the engine model results and the EDB data is 1.3%.

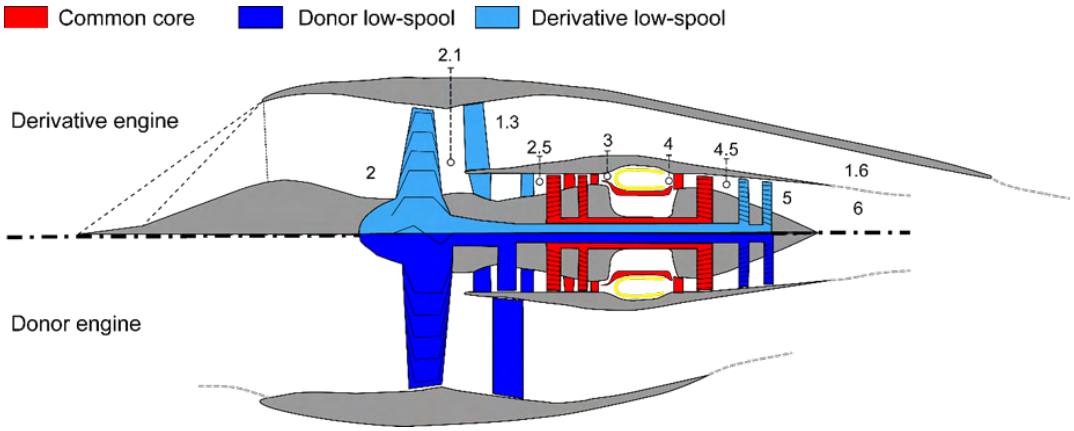

Figure 1. Engine architecture schematic. Lower half shows the subsonic donor engine. The high spool (red) core is used in the derivative engine along with modifications to the inlet, fan, and nozzle, as shown in the top half.

Derivative engine model

The thrust requirements of the derivative engine are given in Table 1. As shown in the engine architecture diagram in Figure 1, the derivative engine for supersonic application uses the high-pressure core of the donor subsonic engine. The low-pressure spool consists of a two-stage fan and a low pressure turbine (LPT). An external compression supersonic inlet with two oblique shocks is mounted upstream of the fan, with a pressure recovery modeled using standard oblique shock equations. A fully mixed, variable-area nozzle is added downstream of the LPT. The engine is designed such that the nozzle is at the cusp of choke at take-off conditions, to avoid shock-cell noise. Polytropic efficiencies of the turbomachinery components are set to values representative of the CFM56-5B3 technology level. The map scalars of the turbomachinery components in the engine cycle model, the flow areas, and the cooling bleed flow fractions of the CFM56 donor engine core are applied as fixed constants to the derivative engine model.

Clean-sheet engine model
The clean-sheet engine is also designed to meet the propulsion system requirements outlined in Table 1. The engine architecture for the clean-sheet design is the same as that of the derivative design. However, all components for the clean-sheet engine, along with the high-pressure core, are purpose-designed. To have a fair comparison between the derivative and clean-sheet engines, the polytropic efficiencies of the turbomachinery are set to the CFM56 values to model the same technology level, and turbine cooling flow requirements are met using semi-empirical methods.

Engine performance sensitivities
An optimizer coupled with the NPSS models is used to optimize the cycle subject to any constraints (temperature limits and fan diameter limits) for various thrust requirements.

Environmental footprint calculations
A first-principles approach is used to evaluate design space constraints imposed by the donor core on the environmental footprint of the derivative engine. The engine cycle deck described above is used to calculate the engine performance in terms of specific fuel consumption (SFC), emissions index, and noise of both the derivative and clean-sheet engines. Engine gaseous NO_x emissions are quantified using the P_3-T_3 method (DuBois and Paynter, 2006). The emission index of NO_x is assumed to be proportional to $P_{t3}^{0.4}$ and a polynomial fit in T_{t3}, constructed based on engine emission data from the ICAO emission data bank, leading to the correlation

$$\frac{\mathrm{EI(NO_x)}}{P_{t3}^{0.4}} = 6.26 \cdot 10^{-8} T_{t3}^3 - 0.00117 T_{t3}^2 + 0.0074 T_{t3} - 15.04 \quad (1)$$

The aircraft certification cumulative noise levels are computed based on standard methods as summarized in Task 3 (Table 2).

Milestones

Multiple engine models were developed in NPSS. The CFM56-5B engine for the supersonic derivative core was chosen to be the donor engine. The derivative engine model was used to evaluate the impact of design space constraints on the performance of the engine relative to the clean-sheet model. The performance of the clean-sheet and derivative engines was compared for different thrust requirements.

Major Accomplishments

Derivative engine design space constraints
Because the core of the derivative engine is sized by the donor engine (CFM56) cycle, the pressure ratio of the high-pressure compressor (HPC) of the derivative engine is not an independent design variable (in contrast to a clean-sheet engine where the HPC pressure ratio is a design variable that can be optimized). The design space of the derivative engine is illustrated in Figure 2. The core of the derivative engine also has cooling flows for the high-pressure turbine sized by the donor engine cycle. Therefore, there are regions of the design space where insufficient cooling flow can result in turbine blade metal temperatures exceeding the set limits. Therefore, the constraints from the donor core limit the feasible design space that can be used for the derivative engine.

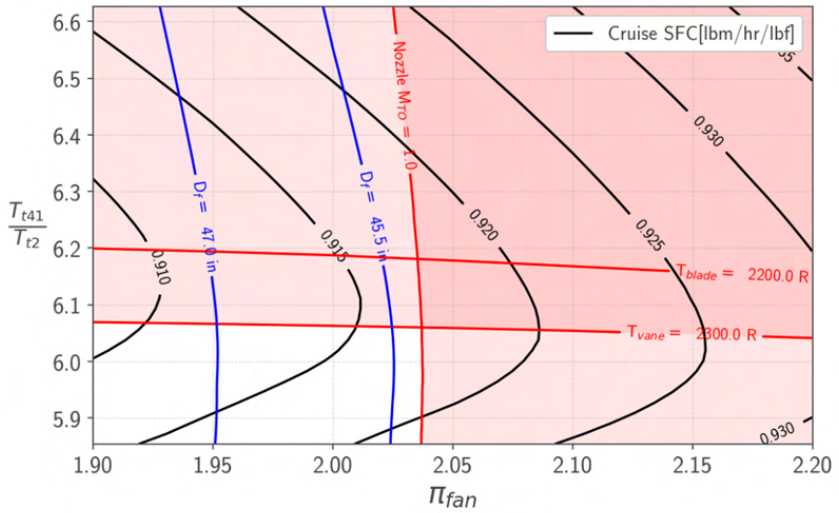

Figure 2. Design space of the derivative engine: turbine inlet temperature over compressor inlet temperature ratio, T_{t41}/T_{t2}, vs. fan pressure ratio, π_{fan}, at the engine aerodynamic design point. The performance contours show the cruise specific fuel consumption (SFC). The resulting fan diameter, D_f, for different designs in the design space is indicated.

Engine performance sensitivities

The required thrust of the aircraft affects the performance of the clean-sheet and derivative engines. At each thrust level, the clean-sheet and derivative engines are optimized to provide minimum SFC. Figure 3 shows the impact that the thrust required has on fuel consumption and emissions of NO_x. The fan size for both engines is constrained to be 45.5 inches (consistent with the STCA airframe requirement).

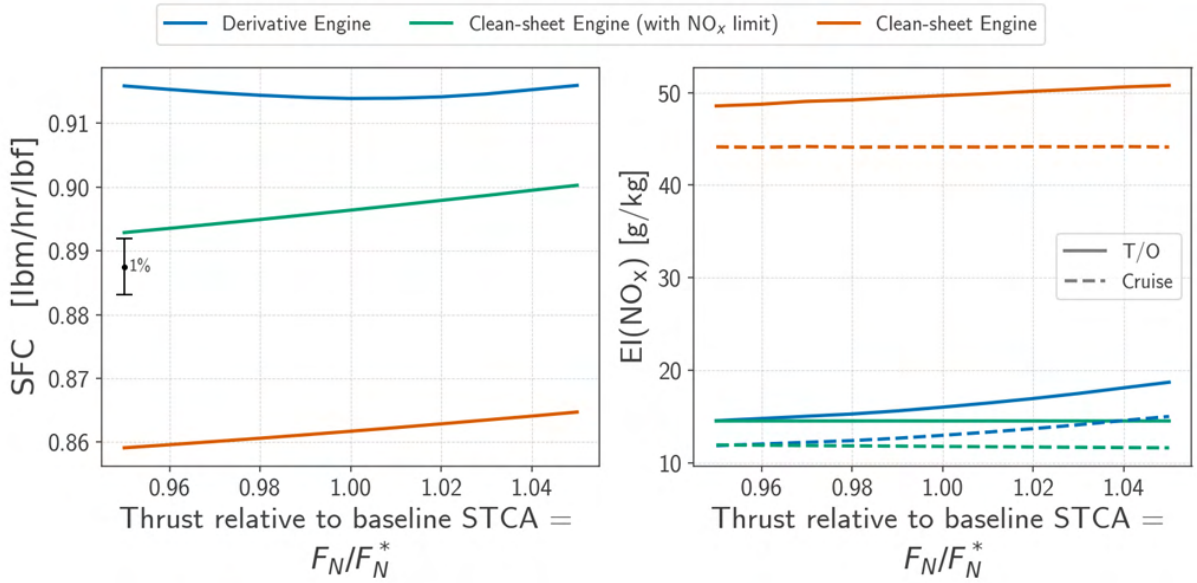

Figure 3. Sensitivities of engine performance parameters (specific fuel consumption at cruise, SFC, and NO_x emission index, EIN, at both design and sea-level static take-off conditions) for a range of thrust requirements. The thrust required is shown as a fraction of the STCA design thrust.

As seen in Figure 2, the clean-sheet engine designed for minimum SFC results in a 5.5% to 6.5% reduction in SFC relative to the derivative engine. However, assuming the same combustor technology is applied in the clean-sheet engine as in the

derivative, the emissions of NO_x from the clean-sheet engine that is optimized for minimum SFC is ~3 times greater than that of the derivative engine. An alternate clean-sheet engine sizing strategy is to impose a NO_x emissions constraint. This results in a 2% to 3% reduction in SFC relative to the derivative engine. This highlights the need to switch to advanced combustor designs that minimize NO_x emissions if the potential SFC benefits of a clean-sheet engine design are to be realized.

Publications

- Voet, L., Prashanth, P., Speth, R., Sabnis, J., Tan, C., & Barrett, S. (2021). The impact of design space constraints on the noise and emissions from derivative engines for civil supersonic aircraft. In *AIAA Scitech 2021 Forum* (p. 1272).
- Prashanth, P., Voet, L., Speth, R., Sabnis, J., Tan, C., & Barrett, S. The impact of design space constraints on the noise and emissions from derivative engines for civil supersonic aircraft. Manuscript in preparation.

Outreach Efforts

Mr. Prashanth Prakash and Mr. Laurens Voet gave a presentation titled "Clean-sheet supersonic engine design and performance" at the virtual ASCENT meeting on April 27, 2021.

Mr. Prashanth Prakash gave a presentation titled "Civil Supersonic Transport Emissions" at the Aviation Emissions Characterization Roadmap 2021 Annual Meeting on May 26, 2021.

Awards

None.

Student Involvement

This task was conducted primarily by Prashanth Prakash, a graduate research assistant working under the supervision of Dr. Jayant Sabnis, Dr. Raymond Speth, and Dr. Choon Tan.

Plans for Next Period

The effect of various notional donor cores (scaled from existing cores) are to be evaluated to quantify the sensitivity of the derivative engine performance to donor core characteristics (expected completion: May 2022).

A clean-sheet approach that uses advanced metallurgy/cooling technology and combustor design is to be developed that will allow us to quantify the sensitivity of clean-sheet engine performance to technology parameters (expected completion: July 2022).

References

Claus, R. W., Evans, A.L., Lylte, J.K., & Nichols, L.D. (1991). Numerical propulsion system simulation. Computing Systems in Engineering *2*(4), 357-364.

DuBois, D., & Paynter, G. C. (2006). Fuel Flow Method 2 for estimating aircraft emissions (SAE Technical Report No. 2006-01-1987). SAE International.

Task 3 - Assess Environmental Footprint of an Engine for a Supersonic Transport Aircraft

Massachusetts Institute of Technology

Objective

The objective of this task is to develop models to assess the environmental footprint of a supersonic transport aircraft. Models for both the noise footprint and the emissions footprint will be developed.

Research Approach

The flow chart in Figure 4 illustrates the approach to model the environmental footprint of engines for supersonic transport.

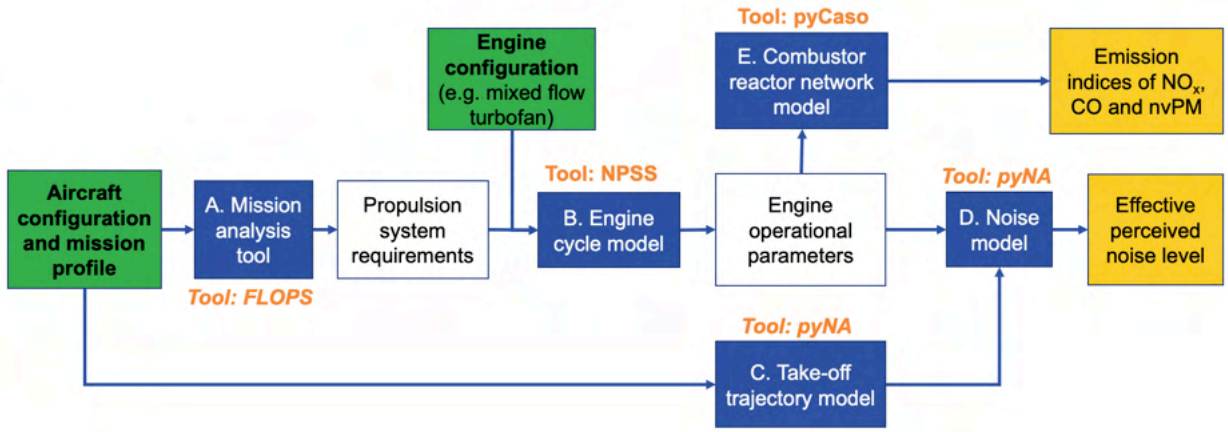

Figure 4. Overview of the framework to model environmental footprint of engines for supersonic transport (SST). The mission analysis is performed using the NASA Flight Optimization System (FLOPS) software, the engine cycle model is made in the Numerical Propulsion System Simulation (NPSS) tool, and the combustor reactor network model (pyCaso) and the aircraft noise and take-off trajectory model (pyNA) are used to calculate emission indices and effective perceived noise levels of the engines.

Emissions modeling

A chemical reactor network combustor model (pyCaso) was developed to assess the emissions of the engines for supersonic transport. The combustor model represents CFM56-TechInsertion rich-quench-lean (RQL) combustor technology. The combustor model is illustrated in Figure 5. A series of perfectly stirred reactors in parallel, representing the primary zone of the combustor, are coupled to a secondary zone plug flow reactor. Similar to the engine model, the emission characteristics of the combustor model are validated against publicly available data from the EDB.

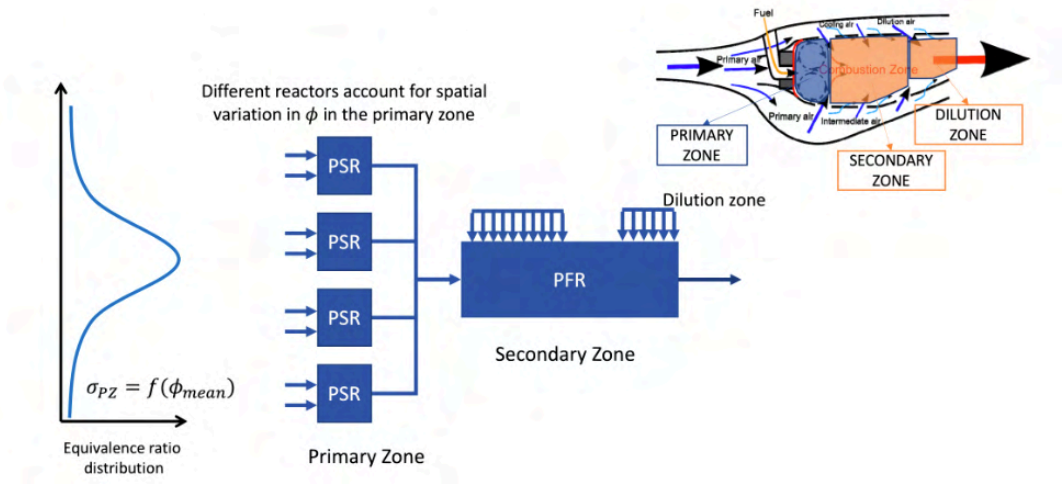

Figure 5. Chemical reactor network combustor model: a series of perfectly stirred reactors (PSR) in parallel, representing the primary zone, combined in parallel with a secondary zone plug flow reactor (PFR). The series of PSR represents a gaussian distribution, with standard deviation, $\boldsymbol{\sigma_{PZ}}$ being a function of the mean equivalence ratio, $\boldsymbol{\phi_{mean}}$.

Noise footprint modeling

A Python Noise Assessment (pyNA) model was developed to estimate the engine certification noise levels and assess their sensitivities with respect to engine operating variables. The model is developed in Python within the OpenMDAO framework (Gray et al., 2019); the individual noise modules were implemented in Julia to be able to use its automatic differentiation

(AD) libraries for the Jacobian computation. The different noise modules in pyNA, as shown in Figure 6, are developed based on the methods from literature listed in Table 2, based on the NASA Technical Memorandum TM-83199 (Zorumski, 1981).

Table 2. Methods for the noise source, propagation, and levels modules.

Module	Method from literature
Noise source modules • Jet mixing noise • Jet shock-cell noise • Combustor noise • Fan broadband and tones (inlet and discharge) • Airframe noise	 Single-stream, shock-free jet mixing noise (SAE ARP876, 2012) Circular jet shock-cell noise (SAE ARP876, 2012) Emmerling method FAA-RD-74-125 (Emmerling et al., 1976) Heidmann method NASA TM X-71763 (Heidmann, 1975) • with GEAE revision NASA CR-195480 for BB (Kontos et al., 1996) • with AlliedSignal revision for RS tones (Hough et al., 1996) • with fan treatment NASA CR-202309 (Kontos et al., 1996) Fink method FAA-RD-77-29 (Fink, 1977) • with HSR calibration *NASA CR-2004-213014 (*Golub et al., 2004)
Noise propagation modules • Spherical spreading/characteristic impedance • Atmospheric absorption • Ground reflection and attenuation • Lateral attenuation • Wing shielding module	R^2 law and characteristic impedance ratio Exponential decay using atmospheric absorption coefficient (Montegani, 1979) Chien-Soroka method (Chien et al., 1975) SAE AIR 5662 method (SAE-AIR5662, 2006), Berton method (Berton, 2021) Maekawa method (copied shielding factors from STCA) (Maekawa, 1968)
Certification noise levels modules • Perceived noise level, tone-corrected (PNLT) • Effective perceived noise level (EPNL)	ICAO Annex 16 Volume I: Aircraft noise App. 2-13 (ICAO, 2008) ICAO Annex 16 Volume I: Aircraft noise App. 2-13 (ICAO, 2008)

The extended design structure matrix (Lambe et al., 2012) of the aircraft noise estimation model is shown in Figure 6.

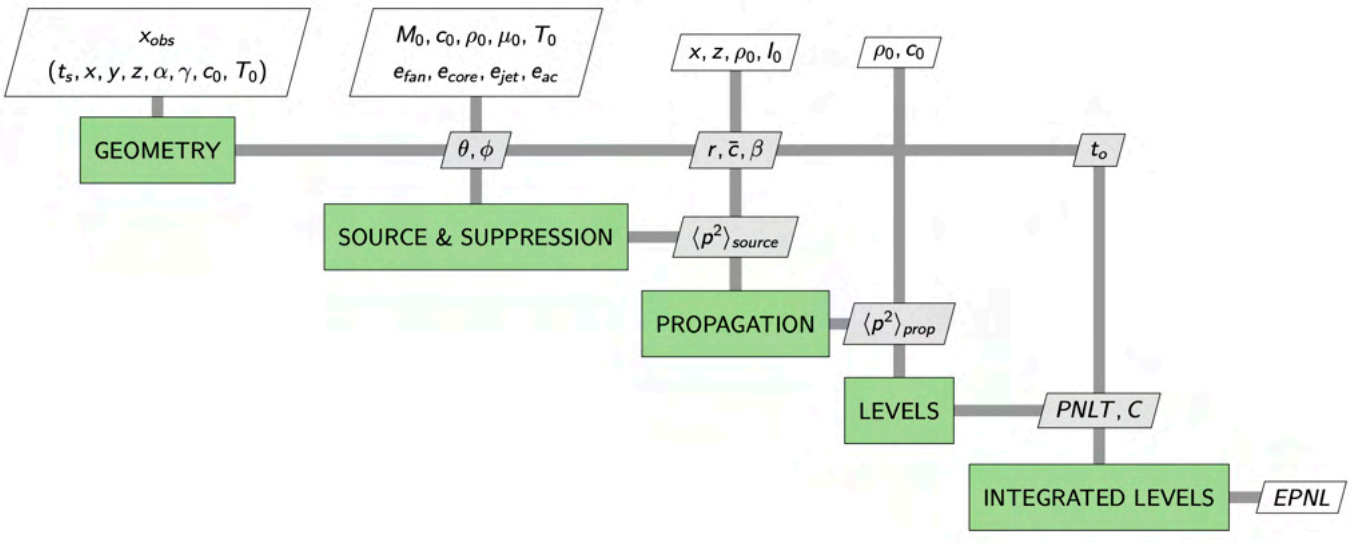

Figure 6. Flow chart of the python Noise Assessment (pyNA) model showing the different modules required to estimate the effective perceived noise level (EPNL) from engine cycle and fan parameters.

The *Geometry* component computes geometrical variables related to the aircraft trajectory relative to the observer position, x_{obs}, i.e., source-observer distance, r; polar and azimuthal directivity angle, (θ, ϕ); elevation angle, β; and observer time, t_O. In the *Source and Suppression* modules, the mean-square acoustic pressure of the different noise sources is computed, and noise suppression is applied to the fan and airframe mean-square acoustic pressure, for the fan liner treatment and the SST airframe calibration, respectively. In the *Propagation* component, the source mean-square acoustic pressure is propagated to the observer through the atmosphere, using the propagation effects listed in Table 1. Finally, the noise levels at the observer, including overall SPL, PNLT, and EPNL, are computed in the *Levels* and *Integrated Levels* components.

The Jacobian of the individual noise modules in Figure 2 are computed using an automatic differentiation (AD) method. AD provides more accurate derivative computations compared to finite-difference (FD) methods, as well as faster computations compared to FD and complex-step (CS) differentiation methods. The Julia ForwardDiff package (Revels et al., 2016) is used to implement the partial derivatives of the aircraft noise estimation model.

Milestones

A chemical reactor network–based combustor model was developed, and NO_x and CO emissions were calibrated to the EDB data using combustor inlet values obtained from the NPSS model of the CFM56-5B engine.

An open-source aircraft noise estimation model estimating the static noise database from relevant engine parameters, the static-to-flight noise projection, and the certification noise levels was developed. Sensitivities of the certification noise levels to engine operating parameters are provided by the model to enable multi-disciplinary design optimization and optimal control.

Major Accomplishments

Emissions model

A framework was developed to estimate the NO_x and CO emissions indices of the donor engine, given the relevant engine parameters using a reactor network model. A comparison of the model developed and the EDB data is shown in Figure 7. The derivative and clean-sheet engine analyzed in the work described here assumes that the combustor technology used is similar to that of the donor engine; therefore, the calibrated parameters are assumed to hold for the clean-sheet engine as well. A soot model to estimate the nonvolatile particulate matter (nvPM) concentrations is currently being integrated into the combustor model.

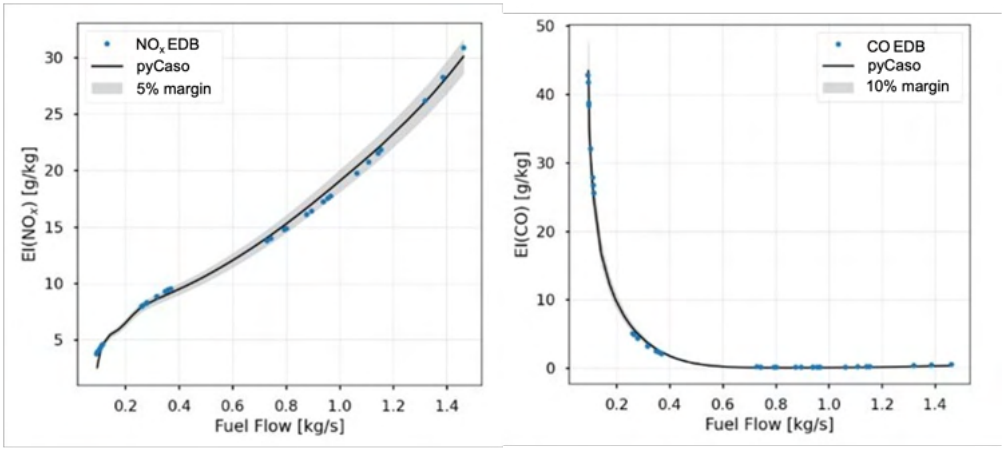

Figure 7. Comparison of NO_x emission indices (EI) (left), and CO EI (right) of the combustor model and International Civil Aviation Organization (ICAO) data from the Emissions Databank (EDB).

Aircraft noise model (pyNA)

A framework was set up to estimate the noise levels (SPL, PNLT, and EPNL) of the engine given the relevant engine parameters using a semi-empirical model.

Aircraft noise estimation model: verification

The utility of the aircraft noise model is evaluated based on the noise assessment of the STCA, designed by NASA to evaluate environmental and economic impacts of SST (Berton et al., 2020). The noise modules are evaluated on the Standard take-off trajectory, denoted by Berton et al. as a trajectory that abides by the noise regulation procedures in ICAO Annex 16 for subsonic transport-category airplanes (Berton et al., 2018; ICAO, 2017). The STCA is a 55-tonne, 8-passenger, Mach 1.4 business tri-jet, cruising at altitudes between 12.5 and 15.5 km (Berton et al., 2020). The STCA noise assessment was performed by Berton et al. (2018) using the NASA Aircraft Noise Prediction Program (ANOPP) (Zorumski, 1982).

The spectral and polar directivity SPL distribution of the fan inlet and discharge, core, jet mixing, and airframe source modules are determined at the zenith point of the flyover observer for a series of one-third octave frequencies, as shown in the polar plots in Figure 8. The engine noise sources are independent of the azimuthal directivity angle, ϕ; the airframe noise source module is plotted for an azimuthal directivity angle, ϕ = 0 deg. The SPL distribution is computed along a circular arc with a 0.3048 m (1 ft) radius from the noise source. The SPL distributions are compared to the NASA STCA ANOPP noise assessment in the polar plots of Figure 8. Excellent agreement is found—a RMS error <0.1 dB across polar directivity angles and frequencies—between the current noise model (pyNA) and the STCA data for the core, jet mixing, and airframe source SPL. Good agreement is found, with an RMS error <1.3 dB, for the fan inlet and discharge broadband component, although discrepancies can be found in the fan tonal components of the fan inlet and discharge noise.

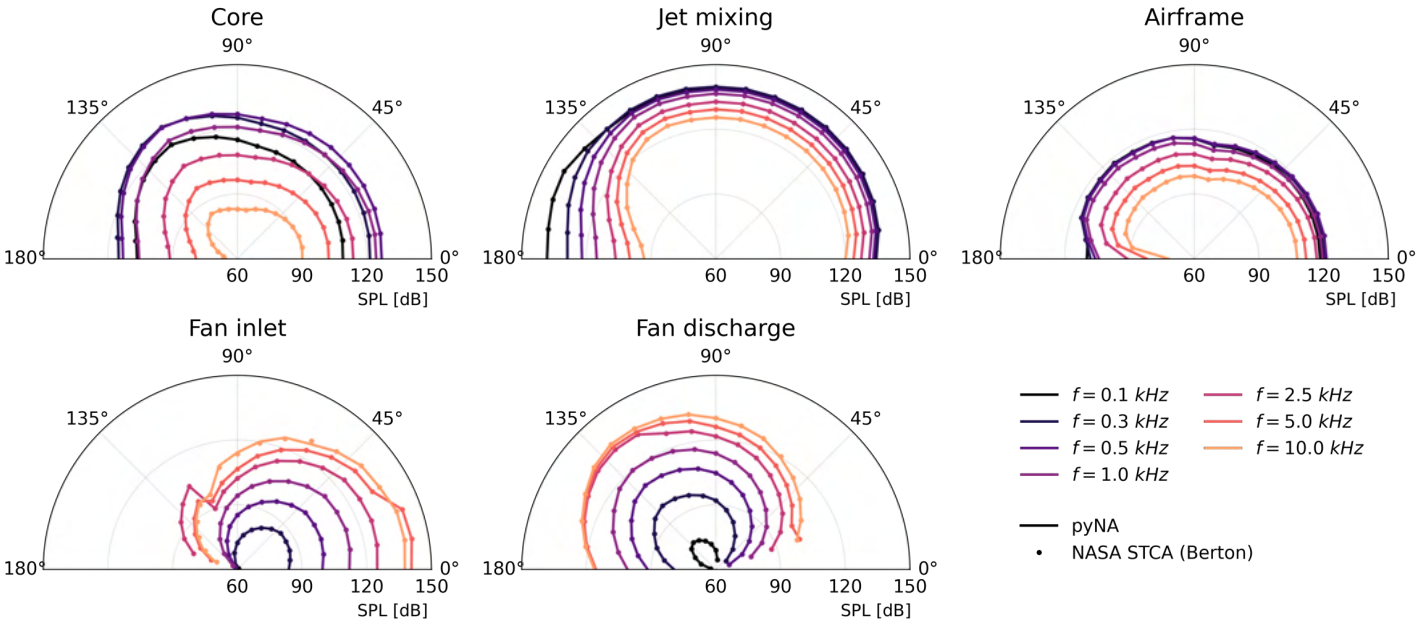

Figure 8. Comparison of the spectral and directional sound pressure level (SPL) distribution at the zenith point of the flyover microphone determined using the current noise model (pyNA) and NASA STCA ANOPP (Berton et al., 2018).

The total PNLT at the lateral and flyover microphones computed by the current noise model (pyNA) is compared with the NASA STCA ANOPP noise assessment in Figure 9. The PNLT curves computed by pyNA have an RMS error of 0.35 PNdB in the domain of dependence of EPNL, compared to those computed by ANOPP.

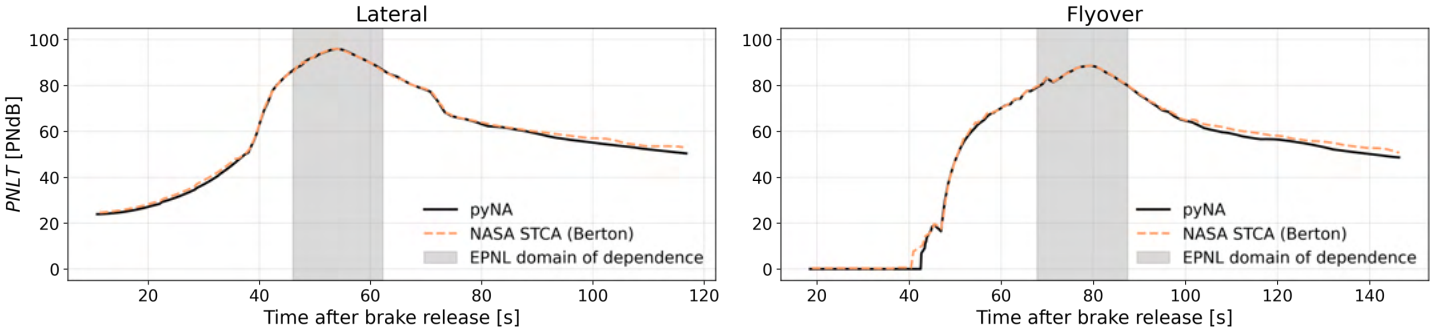

Figure 9. Comparison of the tone-corrected perceived noise level (PNLT) at the lateral (left) and flyover (right) microphone determined using the current noise model (pyNA) and NASA STCA ANOPP (Berton et al., 2018).

The EPNL for individual noise sources as well as the total EPNL are compared with the NASA STCA ANOPP noise assessment in Table 3. A maximum difference across all noise sources of −1.4 EPNdB (effective perceived noise in decibels) is found for fan inlet noise source module. This difference is considered acceptable because the fan inlet noise is not the dominating noise source for the lateral or flyover microphone. For the total EPNL, a maximum difference of −0.1 EPNdB is found for the flyover microphone, set mostly by the good agreement for the jet mixing noise source module.

Table 3. Comparison of the individual noise source and total effective perceived noise level (EPNL) determined using the current noise model (pyNA) and NASA ANOPP (Berton et al., 2018). The lateral microphone position is assumed to be at the x-location where the aircraft reaches 304.8 m (1000 ft) altitude (i.e., $x_{lateral}$ = 3756 m).

Noise source	Lateral microphone [EPNdB]			Flyover microphone [EPNdB]		
	pyNA	STCA	Δ	pyNA	STCA	Δ
Fan inlet	50.4	49.5	+0.9	35.6	37.0	−1.4
Fan discharge	77.0	76.9	+0.1	71.8	71.8	0.0
Combustor	76.9	77.0	−0.1	73.3	73.6	−0.3
Jet mixing	94.6	94.6	0.0	87.8	87.9	−0.1
Airframe	62.0	—*	—*	64.7	64.8	−0.1
Total	**95.0**	**95.0**	**+0.0**	**88.5**	**88.6**	**−0.1**

*The NASA STCA results for airframe noise source were not available at the lateral microphone.

Sensitivities of noise levels to engine operating variables

The aircraft noise estimation model provides sensitivities of acoustic objective functions with respect to engine operating variables to enable multi-disciplinary design optimization and optimal control. Figure 10 shows the sensitivities of EPNL at the lateral and flyover microphones with respect to key engine operating variables driving the aircraft noise signature. From Figure 10 it can be seen that noise levels are dominantly sensitive to the jet velocity, as is expected from high-specific-thrust engines for supersonic transport.

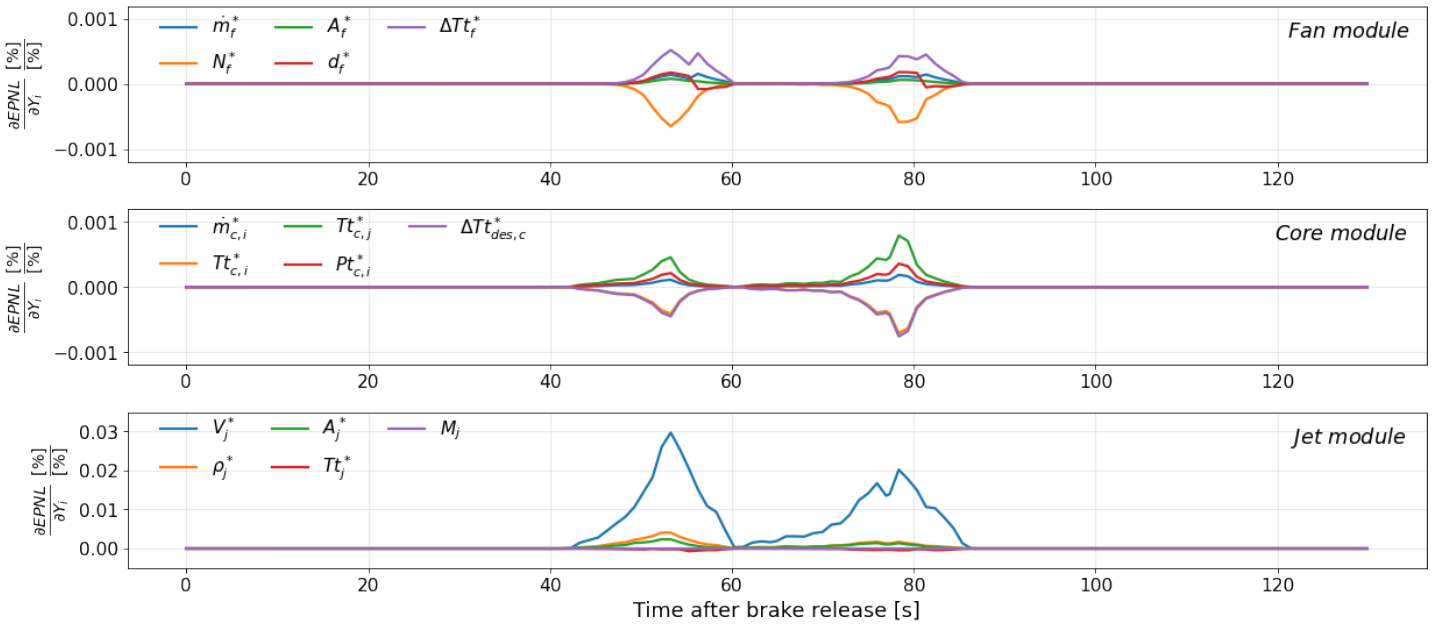

Figure 10. Sensitivities of effective perceived noise level (EPNL) along NASA STCA Standard take-off trajectory with respect to engine operating variables (fan: top; core: middle; jet: bottom) for the lateral and flyover microphones.

Sensitivities of noise levels to engine design variables

The sensitivities of the environmental performance metrics of a clean-sheet engine with respect to a set of engine design variables is assessed for the NASA STCA business jet. The sensitivities of the environmental performance metrics to engine design variables, $\frac{\partial Y_{env}}{\partial X_{des}}$, are normalized; that is, $\frac{\partial Y_{env}}{\partial X_{des}}|_{norm} = \frac{\partial Y_{env}}{\partial X_{des}} \cdot \frac{X_{des}}{Y_{env}}$. The normalized sensitivities are given in units of [%]/[%], also known as [pts]. These sensitivities give insight into the design trades of new engine designs configurations during the preliminary design process. The impact of the derivative engine design space constraints imposed by a donor core on the engine environmental performance is briefly considered.

The sensitivities of the environmental performance metrics to engine design variables of the clean-sheet engine without fan size constraint are shown in Table 4. The effect of the change in design variables on the fan size is shown in Table 5.

Table 4. Sensitivity of environmental performance metrics with respect to engine design parameters ([%]/[%]). The environmental performance metrics are found to be most sensitive to the fan pressure ratio, π_{fan}.

Environmental performance metric	π_{fan}	π_{HPC}	$T_{t,4}/T_{t,2}$	ER_{mix}
Take-off effective perceived noise level, $EPNL_{TO}$	+0.198	−0.019	−0.020	+0.080
Top-of-climb thrust-specific fuel consumption, $TSFC_{TOC}$	+0.165	−0.114	−0.063	+0.117
Cruise thrust-specific fuel consumption, $TSFC_{cruise}$	−0.040	−0.097	−0.059	+0.013
Take-off NO_x emission index, $EI(NO_x)_{TO}$	+1.978	+1.257	−0.066	+0.259
Cruise NO_x emission index, $EI(NO_x)_{cruise}$	+1.638	+1.786	−0.026	−0.106

Table 5. Sensitivity of fan diameter with respect to engine design parameters ([%]/[%]).

	π_{fan}	π_{HPC}	$T_{t,4}/T_{t,2}$	ER_{mix}
Fan diameter, d_{fan}	−0.750	+0.063	+0.057	−0.295

From Table 4, it can be seen that the take-off EPNL is most sensitive to the design fan pressure ratio, π_{fan}. The increase in design fan pressure ratio causes an increase in mixed jet velocity and thus, for a given thrust requirement, reduces the fan size, as shown in Table 5. A similar effect happens for the mixer extraction ratio, ER_{mix}. The increase in jet velocity caused

by the increase in fan pressure ratio is the dominant driver of the increased take-off noise levels. Furthermore, from all design variables, the fan diameter is found to have the highest sensitivity to the design fan pressure ratio. This behavior is well known for subsonic transport engines.

The sensitivity of the take-off noise levels to the engine core design variables (i.e., π_{HPC} and $T_{t,4}/T_{t,2}$) is significantly smaller (by a factor of 10) than that of the design fan pressure ratio. This also shows that, even if the core design variables were constrained by the donor core of a derivative engine design, the impact of such constraints would be relatively small because the take-off noise levels are mainly sensitive to design fan pressure ratio. The low-spool of the derivative engine is purpose-designed to meet the propulsion system requirements. This is unlike the cruise thrust-specific fuel consumption and the take-off NO_x emission index, where the sensitivities to the HPC pressure ratio are of the same order of magnitude as those of the design fan pressure ratio.

At the engine design point; that is, the top-of-climb operating point, the sensitivity of thrust-specific fuel consumption (TSFC) with respect to fan pressure ratio is positive, governed by the decrease in propulsive efficiency at higher fan pressure ratios. The sensitivity with respect to HPC pressure ratio and $T_{t,4}/T_{t,2}$ is negative, driven by an increase in thermal efficiency. At the cruise operating point, the sensitivity of TSFC with respect to fan pressure becomes negative due to off-design effects.

At the take-off and cruise operating point, the dominant sensitivities of the NO_x emissions are those with respect to the fan and HPC pressure ratio. Both sensitivities are positive since increases in the fan and HPC pressure ratios cause an increase in the overall pressure ratio (OPR), resulting in higher $T_{t,3}$ and $P_{t,3}$, and thus higher NO_x emissions.

Finally, increasing the HPC pressure ratio for a fixed $T_{t,4}/T_{t,2}$ and ER_{mix} results in a lower total temperature at the HPT exit. Consequently, the mixed jet velocity is lower and, therefore, to meet the engine thrust requirement, the engine mass flow and necessary fan size increases. This results in a positive sensitivity $\partial d_{fan}/\partial \pi_{HPC}$. An increase in $T_{t,4}/T_{t,2}$ at a fixed ER_{mix} similarly results in lower mixed jet velocity, thus increasing the necessary fan size. The sensitivity $\partial d_{fan}/\partial (T_{t,4}/T_{t,2})$ is thus also expected to be positive.

The sensitivities of the environmental performance metrics to engine design variables of the clean-sheet engine with fan size constraint are shown in Table 6.

Table 6. Sensitivity of environmental performance metrics with respect to engine design parameters ([%]/[%]). A constrained fan size results in limited sensitivity of the take-off noise levels with respect to engine design variables.

Environmental performance metric	π_{fan}	π_{HPC}	$T_{t,4}/T_{t,2}$
Take-off effective perceived noise level, $EPNL_{TO}$	−0.007	−0.002	−0.005
Top-of-climb thrust-specific fuel consumption, $TSFC_{TOC}$	−0.134	−0.088	−0.041
Cruise thrust-specific fuel consumption, $TSFC_{cruise}$	−0.074	−0.094	−0.057
Take-off NO_x emission index, $EI(NO_x)_{TO}$	+1.319	+1.313	−0.016
Cruise NO_x emission index, $EI(NO_x)_{cruise}$	+1.907	+1.763	−0.046

Compared to the results in Table 4, the additional fan size constraint causes the sensitivity of the take-off EPNL with fan pressure ratio, πfan, to become equally insignificant as the sensitivities to the engine core design variables. Because the fan size and fan face Mach number are fixed, the mass flow through the engine is also fixed. Therefore, the necessary jet velocity to meet the required thrust demand is fixed, resulting in approximately constant take-off noise levels. This effect is specific to high-specific-thrust engines for SST, which have a noise signature dominated by jet noise.

As can be seen from Table 6, the cruise thrust-specific fuel consumption and the take-off NO_x emission index can still be traded by varying the three design variables (π_{fan}, π_{HPC}, and T_{t4}/T_{t2}). The sensitivities of TSFC with respect to all design variables in Table 6 are negative; an increase in both fan and HPC pressure ratios as well as T_{t4}/T_{t2} results in an increase in engine thermal efficiency. The effect of the fan pressure ratio on the propulsive efficiency is now limited because of the constrained fan size. The signs of the sensitivities of engine NO_x emissions with respect to the set of design variables do not change when adding a fan size constraint.

Publications

Voet, L., Speth, R., Sabnis, J., Tan, C., & Barrett, S. R. H. (2021). Sensitivities of aircraft acoustic metrics to engine design variables for multi-disciplinary optimization. Manuscript submitted for publication in AIAA Journal.

Outreach Efforts

None.

Awards

Mr. Laurens Voet received the “AIAA 2021 Luis de Florez Graduate Award”.

Student Involvement

This task was conducted primarily by Prashanth Prakash and Laurens Voet, graduate research assistants working under the supervision of Dr. Jayant Sabnis, Dr. Raymond Speth, and Dr. Choon Tan.

Plans for Next Period

This task is complete.

References

Berton, J., & Geiselhart, K. (2019). *NASA 55-tonne Supersonic Transport Concept Aeroplane (STCA) release package* [Computer software]. NASA GRC/NASA LaRC.

Berton, J., Jones, S. M., Seidel, J. A., & Huff, D. L. (2018). Noise predictions for a supersonic business jet using advanced take-off procedures. Aeronautical Journal, *122*(1250) 556– 571.

Berton, J. (2021). Simultaneous use of ground reflection and lateral attenuation noise models. AIAA Aviation Forum and Exposition, pages 7–11.

W. E. Zorumski (1982). Aircraft Noise Prediction Program Theoretical Manual Part 1-2, Technical report, NASA.

Society of Automotive Engineers (1994). ARP-876: Gas Turbine Jet Exhaust Noise Prediction, SAE.

J. Emmerling, S. Kazin, R. Matta, Core engine noise program (1976). Volume III. Prediction methods – Supplement I: Extension of prediction methods, technical report, General Electric Co Cincinnati OH Air- craft Engine Business Group.

J. S. Gray, J. T. Hwang, J. R. Martins, K. T. Moore, and B. A. Naylor (2019). OpenMDAO: An open-source framework for multidisciplinary analysis and optimization. Structural and Multidisciplinary Optimization, 59(4): 1075–1104.

ICAO (2017). Annex 16 to the Convention on International Civil Aviation Environmental Protection Volume 1: Aircraft Noise (Edition 8). Technical report, ICAO.

M. F. Heidmann (1995). Interim prediction method for fan and compressor source noise. NASA-TM-x71763.

K. B. Kontos, B. Janardan, P. Gliebe (1996). Improved NASA-ANOPP noise prediction computer code for advanced subsonic propulsion systems. Volume 1: ANOPP evaluation and fan noise model improvement. NASA CR-195480.

K. B. Kontos, R. E. Kraft, P. R. Gliebe (1996). Improved NASA-ANOPP noise prediction computer code for advanced subsonic propulsion systems. Volume 2: Fan suppression model development.NASA-CR- 202309..

J. W. Hough, D. S. Weir (1996). Aircraft noise prediction program (ANOPP) fan noise prediction for small engines. NASA-CR-198300.

Lambe A.B. and Joaquim R.R.A. Martins (2012). Extensions to the design structure matrix for the description of multidisciplinary design, analysis, and optimization processes. Structural and Multidisciplinary Optimization, 46(2): 273–284.

M. R. Fink (1977). Airframe noise prediction method, technical report, United Technologies Research Center East Hartford, CT.

Francis J Montegani (1979). Computation of atmospheric attenuation of sound for fractional- octave bands. NASA Technical Paper, 100(1): 1.

J. Revels, M. Lubin, and T. Papamarkou (2016). Forward-Mode Automatic Differentiation in Julia. arXiv preprint, 1607.07892.

Golub, Robert, John W. Rawls Jr, and Jessie C. Yeager (2004). High Speed Research Noise Prediction Code (HSRNOISE) User's and Theoretical Manual.

C. Chien, W. Soroka (1975). Sound propagation along an impedance plane, Journal of Sound and Vibration 43 (1): 9–20.

Z. Maekawa (1968). Noise reduction by screens, Applied Acoustics 1 (3): 157–173.

ICAO (2017). Annex 16 environmental protection. Volume I: Aircraft engine emissions (eight edition).

SAE Aerospace (2006). Prediction of Lateral Attenuation of Airplane Noise. Technical report, SAE International.

Task 4 - Assess the Effect of Variable Noise Reduction Systems on LTO Emissions for Engines for Supersonic Transport Aircraft

Massachusetts Institute of Technology

Objective

The engine configurations currently being pursued for the second-generation supersonic transport (SST) are low- or medium-bypass turbofans, instead of the afterburning turbojets used on Concorde. Such engines, sized for supersonic cruise, are likely to have higher thrust capability at the take-off condition and therefore, may be able to use a programmed thrust cutback (PTCB), allowing the aircraft to perform a take-off at less than 100% of the thermodynamically available thrust. Unlike thrust lapse, PTCB is not a thermodynamic, aerodynamic, or atmospheric phenomenon; rather, it is a computer-programmed reduction in thrust during the take-off procedure of the aircraft for the purpose of reducing certification noise.

A PTCB designed to reduce certification noise affects the amount of gaseous emissions from the engines during take-off procedures (in this work, only NO_x emissions are considered). The objective of this task is to analyze whether a single thrust setting for the climb-out phase of the engine emissions LTO cycle is representative, or whether the PTCB should be accounted for in the engine emissions LTO cycle.

The objective of this task involves interdependencies between aircraft operations related to PTCB and engine emission certification standards. The noise certification flight profile is chosen as a reference flight profile to analyze these interdependencies. The in-flight emissions during the climb phase (between 35 and 3000 ft) of the noise reference trajectories resulting from different PTCB trajectories are compared to the emissions of the climb mode of the engine emission LTO certification standard. The comparison is done for both the existing subsonic and the supersonic engine emission LTO certification standard to assess which is more representative.

Research Approach

The approach to address the above-mentioned research objective is shown in Figure 11. We start from a supersonic aircraft model and an engine model for that aircraft. These are input in a take-off trajectory model that is coupled to a noise model. Minimizing the noise footprint using a VNRS gives us a PTCB, characterized by a thrust-setting schedule as a function of time, $\mathrm{TS}(t)$. This thrust-setting schedule is put into a combustor model to estimate take-off emissions (i.e., Method 1 in Figure 11). These emissions are then compared to those in a baseline trajectory, using a simple power setting schedule, without VNRS being applied (i.e., Method 2 in Figure 11). We are interested in comparing the take-off emissions of both these methods.

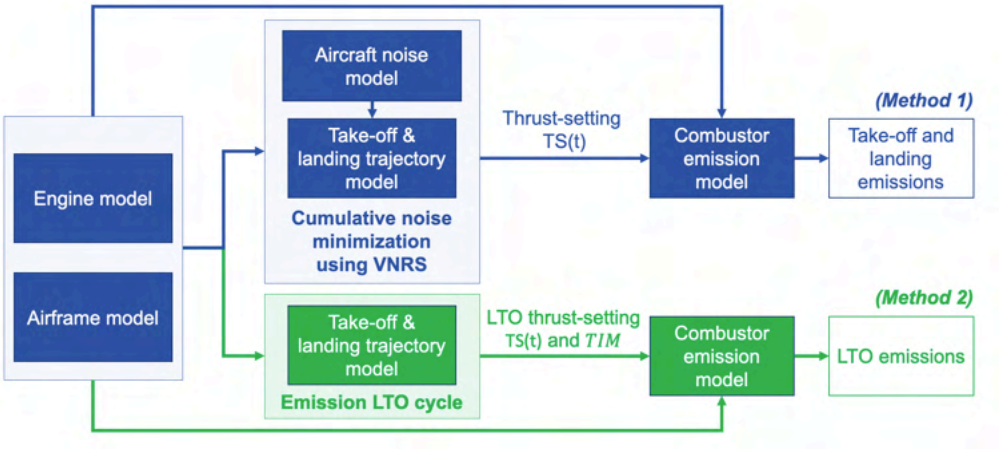

Figure 11. Flow chart of the approach to estimate the effect of variable noise reduction systems (VNRS) on take-off emissions of engines for supersonic transport.

LTO engine emissions certification cycles

The current subsonic and supersonic LTO emissions cycles indicating thrust setting and time in mode for the different phases are shown in Table 7 and Table 8, respectively (ICAO, 2008).

Table 7. Subsonic landing and take-off (LTO) engine emissions certification cycle.

Subsonic operating mode	Subsonic engine power (percentage of standard day sea-level static thrust, F_{00})	Subsonic time in mode
Idle (taxi)	7%	26.0 min
Take-off	100%	0.7 min
Climb-out	85%	2.2 min
Approach	30%	4.0 min

Table 8. Supersonic landing and take-off (LTO) engine emission certification cycle.

Supersonic operating mode	Supersonic engine power (percentage of standard day sea-level static thrust, F_{00})	Supersonic time in mode
Idle (taxi)	5.8%	26.0 min
Take-off	100%	1.2 min
Climb-out	65%	2.0 min
Descent	15%	1.2 min
Approach	34%	2.3 min

Modeling take-off trajectories

The reference take-off trajectory is composed of five phases, summarized in Table 9. During the ground roll phase, the aircraft accelerates until it reaches rotation speed, $V_{\text{rot}} = k_{\text{rot}} V_{\text{stall}}$ (with $k_{\text{rot}} = 1.3$). In the rotation phase, the aircraft pitches up, increasing its angle of attack, α, with a constant rate ($d\alpha/dt = 3.5$ deg/s) until its net upward force is zero. In the climb phase, the aircraft climbs until it reaches the obstacle height, z_{obstacle}, after which the programmed thrust cutback, TS_{PTCB}, as well as pilot-initiated cutback, TS_{cb}, is applied in the PTCB and cutback phases, respectively. The trajectory stops when the aircraft reaches an altitude $z_{\text{end}} = 1500\,\text{m}$. The first three phases of the take-off trajectory are performed using a take-off thrust setting $TS_{TO} = 100\%$. The angle of attack, α, serves as control parameter in the climb, PTCB, and cutback phases and its schedule is determined by optimizing the trajectory for the minimum time to climb to $z_{\text{end}} = 1500\,\text{m}$.

Table 9. Definition of take-off trajectory model.

Phase	Boundary constraint	Path constraint	Control parameters	
			α	TS
Ground roll	$V_{\text{start}} = 0\,\text{m/s} \rightarrow v_{\text{end}} = v_{\text{rot}}$		$\alpha = \alpha_0$	TS=100%
Rotation	$\alpha_{\text{start}} = \alpha_0 \rightarrow \alpha_{\text{end}}\ \text{s.t.}\ F_{\text{up,end}} = 0$		$\frac{d\alpha}{dt} = \text{const}$	TS=100%
Climb	$z_{\text{start}} = 0 \rightarrow z_{\text{end}} = z_{\text{obstacle}}$	$\gamma > 4\%$* $v_{\text{eas}} < 250$ kts	$\alpha = \alpha(t)$	TS=100%
PTCB	$z_{\text{start}} = z_{\text{obstacle}} \rightarrow z_{\text{end}} = z_{\text{cb}}$	$\gamma > 4\%$* $v_{\text{eas}} < 250$ kts	$\alpha = \alpha(t)$	TS=TS_{ptcb}
Cutback	$z_{\text{start}} = z_{\text{cb}} \rightarrow z_{\text{end}} = 1500\,\text{m}$	$\gamma > 4\%$* $v_{\text{eas}} < 250$ kts	$\alpha = \alpha(t)$	TS=TS_{cb}

* This path constraint can be replaced by the one-engine-inoperative condition.

The allowable level of PTCB for the reference trajectory is governed by noise certification regulations and airworthiness standards: the thrust shall not be reduced below that required to maintain a minimum climb gradient of 4% or steady-level flight with one engine inoperative (for multi-engine airplanes), whichever thrust is greater (ICAO, Annex 16 Volume I: Aircraft Noise, 2017). The aircraft shall not have an indicated airspeed of more than 250 kts at altitudes below 10,000 feet MSL (14 CFR §91.117 Aircraft speed., 2021). These limits are applied as path constraints of the reference take-off trajectory in Table 9.

Aircraft and engine modeling
In this task, two supersonic vehicles are analyzed that span 8 to 55 passengers and low supersonic (Mach 1.4) to high supersonic (Mach 2.2). The NASA STCA (Berton et al., 2020) is an 8-passenger supersonic business jet with cruise Mach number 1.4 (hereafter referred to as the NASA STCA). A larger 55-passenger supersonic airliner with cruise Mach number 2.2 designed by Georgia Institute of Technology (hereafter referred to as the M2.2 medium SST) is also analyzed. The engine used in the analysis of the effects of PTCB for the STCA aircraft is a derivative engine, based on the CFM56-5B core, whereas the engine used for the M2.2 medium SST is a clean-sheet engine (Voet et al., 2021).

Estimating NO_x emissions
The P_3-T_3 method (DuBois & Paynter, 2006) is used to estimate the engine NO_x emissions. The P_3-T_3 method uses a polynomial regression to model the NO_x emissions from the combustor as a function of the combustor inlet pressure, P_{t3}, and temperature, T_{t3}. We used publicly available data on the NO_x emissions of the CFM56 family of engines from the ICAO Emissions Databank, EDB (ICAO, 2020) to determine the coefficients needed in our P_3-T_3 method. It is assumed that the emissions index of NO_x scales with $P_{t3}^{0.4}$ as shown in the following equation:

$$\frac{EI(NO_x)}{P_{t3}^{0.4}} = 6.26 \cdot 10^{-8} T_{t3}^3 - 1.17 \cdot 10^{-4} T_{t3}^2 + 0.074 T_{t3} - 15.04.$$

Since the production of NO_x in a RQL combustor is primarily controlled by the flame temperature and the mixing of the primary zone gas, it is assumed that the above P_3-T_3 correlation is representative of the emissions we expect from a derivative engine that uses the CFM56 core.

The clean-sheet engine designed for the M2.2 medium SST is assumed to have the same combustor technology as in the STCA engine as well as the CFM56-5B3. This allows us to use the same P_3-T_3 model to estimate emissions of NO_x from the combustor and facilitates a comparison between the two aircraft-engine pairs while holding the combustor technology fixed.

Modeling take-off noise
The take-off certification noise levels, in terms of the lateral and flyover EPNL, are computed using the aircraft noise estimation model, developed as part of Task 3. The sideline (lateral) and flyover noise metrics, defined by ICAO Annex 16 (ICAO, 2017), are computed for each of the take-off trajectories in the design space. The flyover microphone is located 6500 m downstream of break release; the location of the lateral microphone is located 450 m away from the runway center line at the position of maximum sideline noise.

Milestone
The difference in NO_x pollutant emissions of engines for supersonic transport aircraft flying a range of trajectories and varying VNRS was estimated for two different aircraft configurations.

Major Accomplishments

Estimate of PTCB range based on trajectory simulations
The possible range of PTCB for the two supersonic vehicles is estimated using take-off trajectory simulations. A single pilot-initiated cutback maneuver is analyzed for the STCA and M2.2 medium SST. The cutback procedure is described by two parameters; namely, a cutback altitude, z_{cb}, and a cutback thrust setting, TS_{cb}. The design space of the single-cutback PTCB is explored by varying both parameters: $z_{cb} \in [25, 750]\text{m}$ and $TS_{cb} \in [50, 100]\%$ for the STCA and $TS_{cb} \in [60, 100]\%$ for the M2.2 medium SST. Thrust settings outside these ranges fail to meet the noise certification and airworthiness requirements for the respective vehicles. As stated in previously, a take-off thrust setting $TS_{TO} = 100\%$ is employed. Sample trajectories with and without cutback are shown for the STCA and M2.2 medium SST in Figure 12.

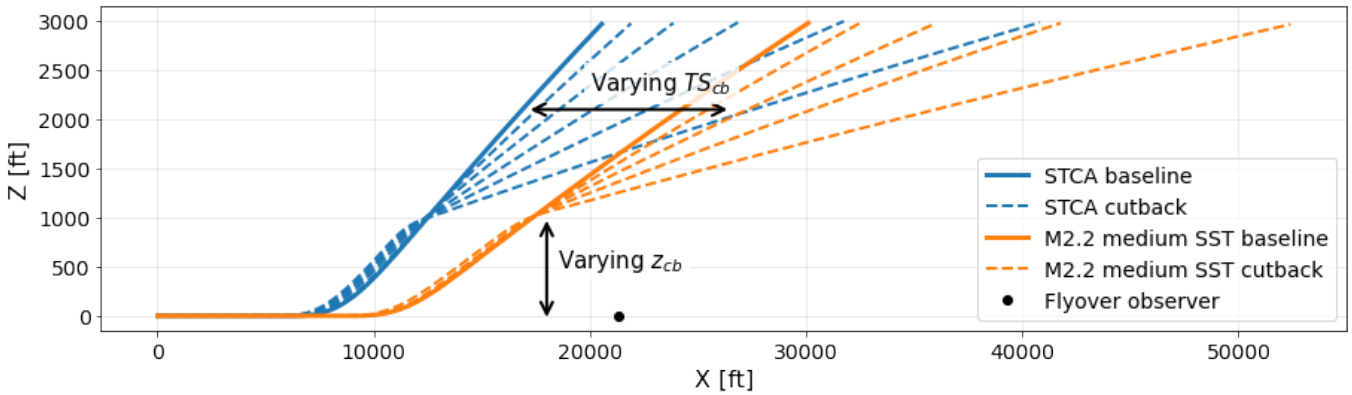

Figure 12. Example of single thrust cutback trajectories for STCA and M2.2 medium SST for **cutback altitude z_{cb}**=1000 ft and cutback thrust setting $\boldsymbol{TS_{cb}} \in [\mathbf{50}, \mathbf{100}]$% (for STCA) and $\boldsymbol{TS_{cb}} \in [\mathbf{60}, \mathbf{100}]$% (for M2.2 medium SST). The baseline trajectory has a constant thrust setting TS=100%.

The lateral, flyover, and cumulative EPNL as a function of TS_{cb} and z_{cb} is plotted for the single thrust cutback of the STCA and the M2.2 medium SST in Figure 13 and Figure 14, respectively.

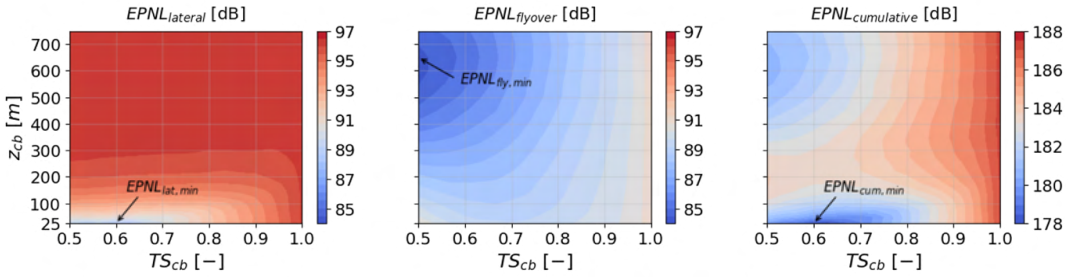

Figure 13. Lateral, flyover, and cumulative noise reduction for single-cutback trajectories of the STCA. EPNL = effective perceived noise level; TS_{cb} = cutback thrust setting; z_{cb} = cutback altitude.

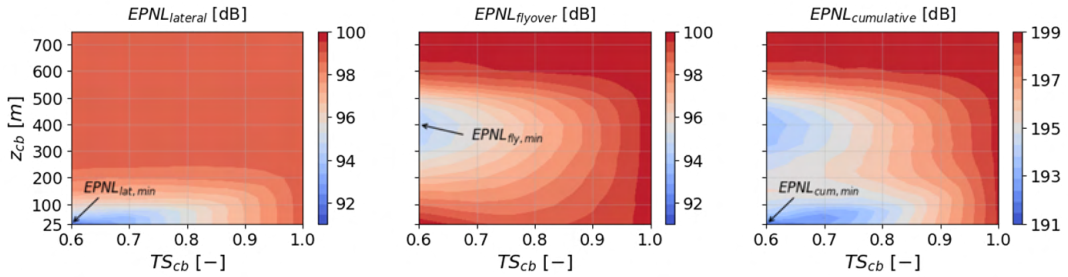

Figure 14. Lateral, flyover, and cumulative noise reduction for single-cutback trajectories of the M2.2 medium SST. EPNL = effective perceived noise level; TS_{cb} = cutback thrust setting; z_{cb} = cutback altitude.

In Figure 13 and Figure 14, a cutback at low altitudes monotonically decreases the lateral EPNL for both vehicles. A cutback at altitudes z_{cb} > 200 m does not result in further improvement in lateral noise, as the aircraft is already past the region of influence of the lateral microphone. For the flyover microphone, a local minimum exists at z_{cb} = 650 m for the STCA and at z_{cb} = 400 m for the M2.2 medium SST: cutting back later results in more source noise at the flyover microphone; cutting back earlier results in a smaller distance between the aircraft and the flyover microphone, increasing noise. For both vehicles, the

lateral noise reduction dominates the cumulative noise reduction. Therefore, the point in the feasible design space that results in the minimum cumulative noise occurs at ($TS_{cb} = 60\%, z_{cb} = 25$ m) for both vehicles.

The single-cutback minimum noise trajectory is considered a lower bound on the thrust setting during climb-out, whereas a trajectory without any cutback is considered an upper bound. Two additional trajectories—a standard and advanced trajectory based on the NASA STCA noise assessment (Berton et al., 2018)—are also considered with thrust cutbacks in between these bounds. The definitions of these four reference trajectories are shown in Table 10 and their thrust-setting schedules are illustrated in Figure 15.

Table 10. Comparison of reference trajectories.

Name	TS_{TO}	PTCB		Pilot-initiated cutback	
		h_{cb}	TS_{cb}	h_{cb}	TS_{cb}
No cutback	100%	-	-	-	-
Standard	100%	-	-	584.7m	65%
Advanced	100%	15.3m	85%	544.1m	65%
Single CB min. noise	100%	25 m (M 1.4, 8 pax) 25 m (M2.2, 55 pax)	60% (M 1.4, 8 pax) 65% (M 2.2, 55 pax)	-	-

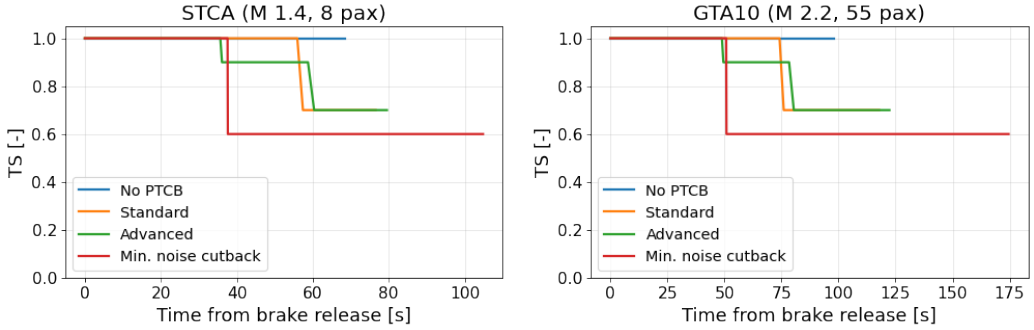

Figure 15. Thrust-setting (TS) schedules for trajectories in Table 10 for STCA and M2.2 medium SST.

Instantaneous engine conditions at various PTCB levels during climb-out

The thermodynamic conditions at the inlet to the combustor, T_{t3} and P_{t3}, are shown by the shaded region in Figure 16 at various climb thrust settings for the STCA. The flight Mach number is varied from 0.2 to 0.48 (typical Mach numbers between the aircraft stall speed and $v_{\text{eas}} = 250$ kts) and the flight altitude from 500 to 3000 ft (LTO is considered to consist only of flight phases below 3000 ft altitude). The thermodynamic conditions are normalized by the ICAO LTO conditions for a climb-out thrust setting; that is, 85% of the sea-level static thrust, F_{00}. The thermodynamic conditions for the three cutback trajectories are shown in Figure 16.

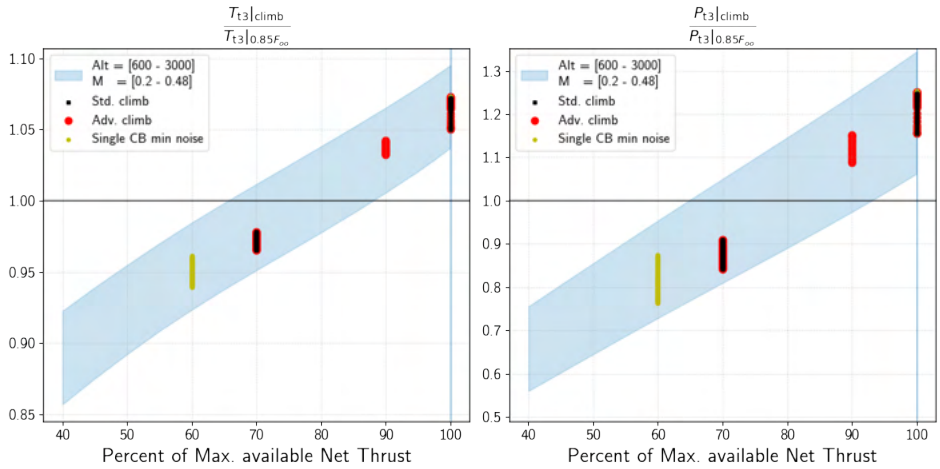

Figure 16. Combustor inlet conditions (P_{t3}, T_{t3}) for flight Mach numbers M ∈ [0.2, 0.48] and altitudes Alt ∈ [500, 3000] ft for the NASA STCA. The black marker and horizontal line indicate the sea-level static (SLS) conditions at the corresponding thrust setting (TS). The SLS value at 85% F_{oo} corresponds to the ICAO LTO climb-out thrust level.

Figure 16 shows that, for the possible range of PTCB identified, the temperature at the inlet to the combustor for the STCA can vary between ~7% below and ~8% above that at the ICAO LTO climb-out thrust setting. The pressure at the combustor inlet can vary between ~30% below and 25% above that of ICAO LTO climb-out thrust setting.

The instantaneous EI(NO_x) for the four trajectories listed in Table 10 are shown in Figure 17. The take-off and climb-out phases of the subsonic certification and supersonic certification LTO cycle are also indicated for reference.

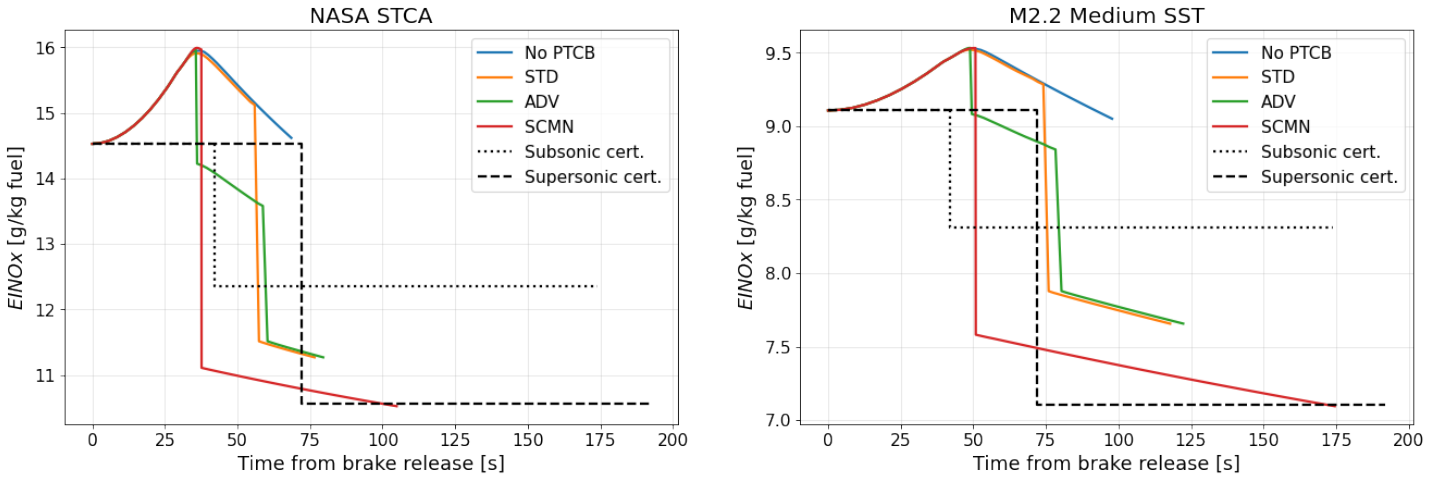

Figure 17. Trajectory instantaneous emissions index of NO_x, EI(NO_x), compared to the subsonic and supersonic certification.

The emissions index of NO_x, EI(NO_x), during the climb phase relative to the EI at the 85% F_{oo} LTO value, is shown in Figure 18. We show the trends of the EI(NO_x) values for various PTCB cutback levels for the STCA and the M2.2 medium SST.

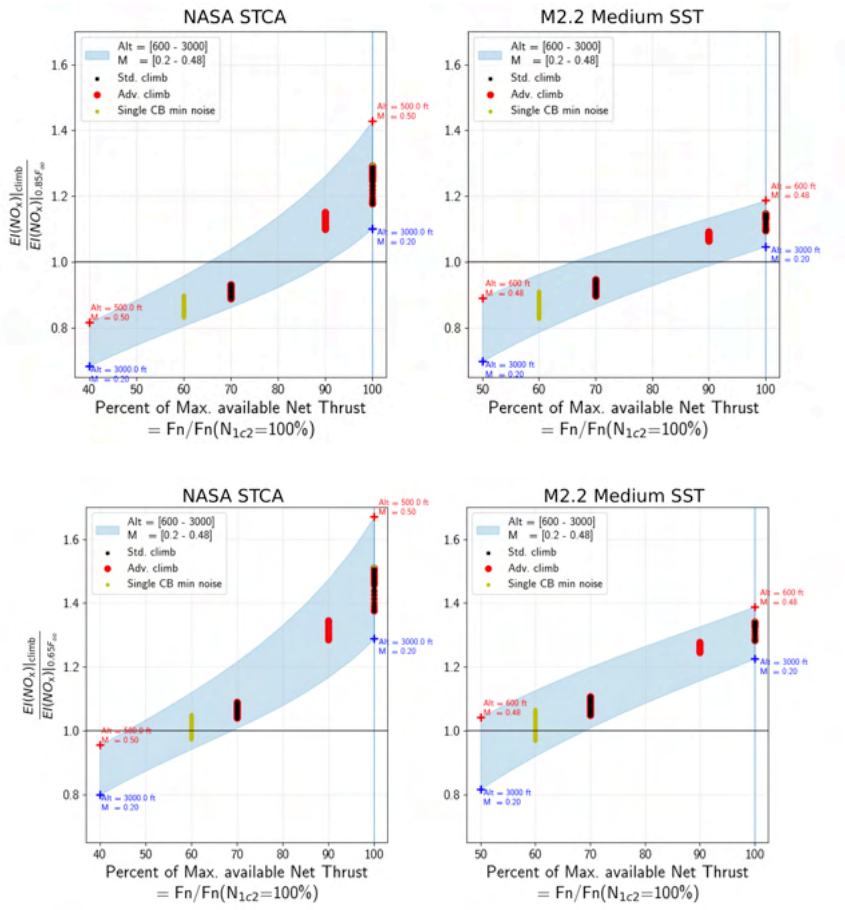

Figure 18. NO_x emissions relative to the 85% (top row) and 65% (bottom row) LTO thrust setting for various flight conditions for two example SST: the 8-passenger M1.4 NASA STCA and the 55-passenger M2.2 Medium SST. The black markers indicate the sea-level static conditions at the corresponding thrust setting.

The overall compressor pressure rise (inlet of fan root to combustor inlet) is limited by the maximum allowable T_{t3} based on the materials used in the engine. As the cruise Mach number increases—from M=1.4 for the STCA to M=2.2 for the M2.2 medium SST—the ram compression increases the inlet temperature and, therefore, the allowable compressor pressure ratio reduces. The lower design pressure ratio for the M2.2 medium SST implies a lower T_{t3} in the LTO cycle relative to the STCA. Therefore, the combustor inlet temperatures (and consequently NO_x emissions) are driven by the compressor pressure ratio.

Figure 18 shows that the trend of $EI(NO_x)$ varies for the different aircraft. The STCA climb profile shows that at a 65% thrust setting, the $EI(NO_x)$ is approximately 7% to 12% lower than the LTO value. However, at a thrust setting of 50% (determined by the minimum noise trajectory for a single FADEC-controlled cutback event), the $EI(NO_x)$ is 12% to 20% lower than the LTO value. If the available thrust during climb is higher than the required thrust, the PTCB level can be higher, leading to lower TS and, therefore, even lower $EI(NO_x)$ relative to the LTO 85% value. On the other hand, if the required thrust is close to the available thrust, then the PTCB level will be lower, resulting in $EI(NO_x)$ values greater than the 85% LTO value. For the M2.2 medium SST at a 65% thrust setting, we observed an $EI(NO_x)$ ~10% lower than the LTO value. These variations are due in part to the lower required compressor pressure ratios as the cruise Mach number increases. This indicates that the deviation from the LTO 85% value is dependent on the aircraft-engine combination. The variation in the trends of $EI(NO_x)$ at various flight conditions is observed in the difference between the shaded regions for the two aircraft under consideration.

We observe that the spread of the normalized $EI(NO_x)$ for the STCA is larger at the 100% thrust setting relative to the 50% thrust setting, whereas the spread at the 100% thrust setting is smaller than that at the 50% thrust setting for the M2.2

aircraft. This is due to the sensitivity of EI(NO_x) predicted by the P_3-T_3 model to T_{t3}. The slope of the EI(NO_x) vs T_{t3} is higher at lower temperatures of ~500-550 K than that at temperatures of 600-650 K. Therefore, for similar variation in T_{t3}, the variation in EI(NO_x) is larger for the M2.2 aircraft than the STCA at lower thrust settings.

Estimate of difference in integrated emissions between reference trajectories and LTO certification cycles during climb-out

The cumulative mass of NO_x emitted from 35 ft to 3000 ft for the four trajectories is shown in Figure 19 and Figure 20 for the NASA STCA and M2.2 Medium SST, respectively. The comparison of the final cumulative mass of NO_x with the subsonic and supersonic certification LTO cycle, i.e., $m_{NO_x,35<h<3000ft}/m_{NO_x,cert.}$, is shown in Table 11. Note that for the certification mass of NO_x emitted, $m_{NO_x,cert.}$, only the climb-out phase is used.

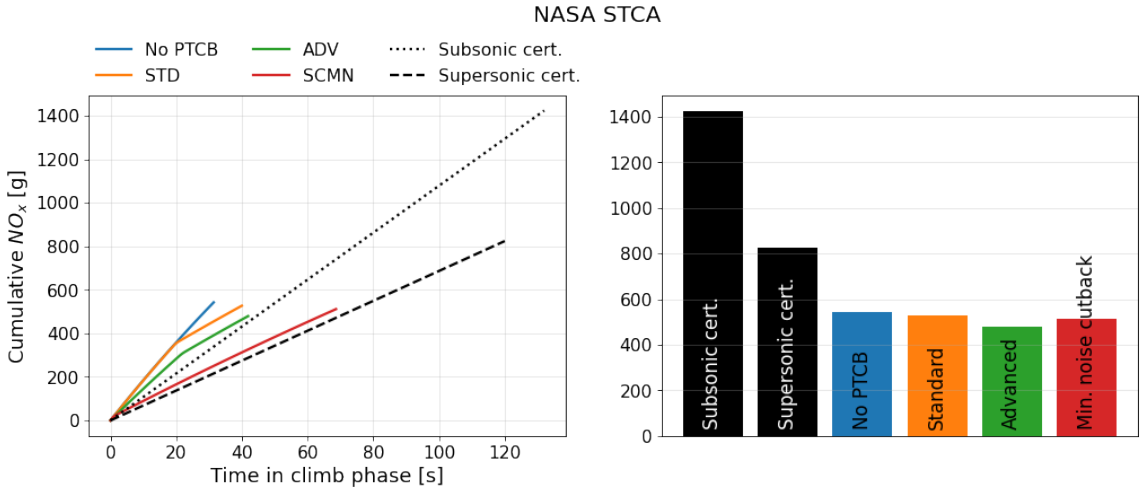

Figure 19. Integrated emissions comparison to subsonic and supersonic certification standards for M1.4 NASA STCA.

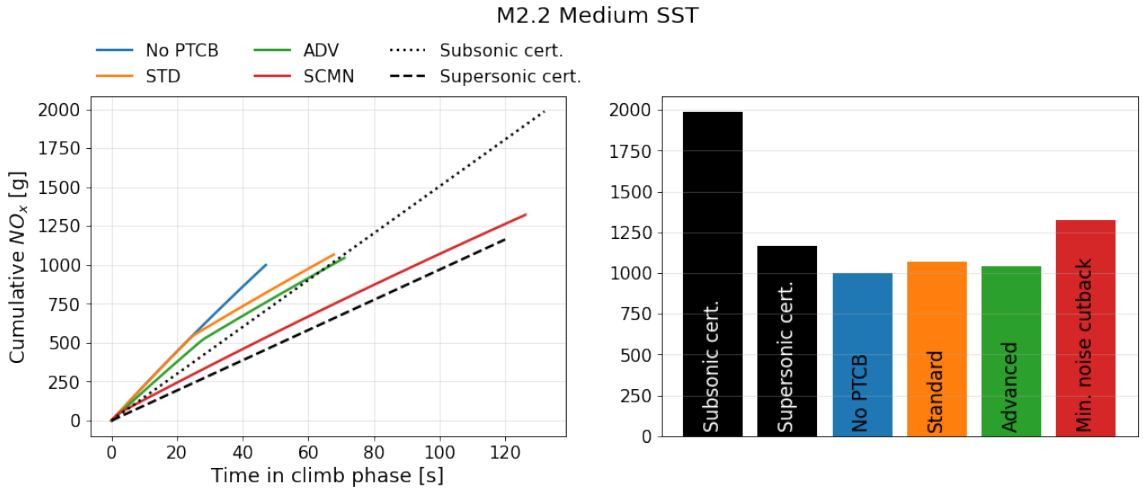

Figure 20. Integrated emissions comparison to subsonic and supersonic certification standards for M2.2 medium SST.

A comparison of the integrated emissions has been made on a D_p/F_{oo} basis, where only the take-off and climb phases are considered (hereafter referred to as m_{NO_x}/F_{oo}). The difference in m_{NO_x}/F_{oo} between the four trajectories and the subsonic and supersonic certification LTO cycle are shown in Table 11.

Table 11. Comparison of the climb-out m_{NO_x}/F_{oo} ($35 < h < 3000$ ft) for NASA STCA and M2.2 medium SST with subsonic and supersonic certification LTO cycles (+ means certification cycle is overestimating).

Trajectory name	NASA STCA			M2.2 medium SST		
	$\frac{m_{NO_x}}{F_{oo}}\left[\frac{g}{kN}\right]$	$\Delta_{subsonic}$ [%]	$\Delta_{supersonic}$ [%]	$\frac{m_{NO_x}}{F_{oo}}\left[\frac{g}{kN}\right]$	$\Delta_{subsonic}$ [%]	$\Delta_{supersonic}$ [%]
Subsonic certification	17.8	-	-	14.6	-	-
Supersonic certification	10.3	-	-	8.5	-	-
No cutback	6.8	+61.9	+34.2	7.3	+49.7	+14.1
Standard	6.6	+63.0	+36.1	7.8	+46.3	+8.3
Advanced	6.0	+66.3	+41.8	7.7	+47.4	+10.2
Single CB min. noise	6.4	+64.1	+37.9	9.7	+33.5	−13.6

Table 11 shows that for the STCA aircraft, the subsonic certification climb-out time in mode and thrust setting overestimates the mass of NO_x emissions per unit thrust (m_{NO_x}/F_{oo}) of real trajectories by 64% (for the single-cutback minimum noise trajectory) to 62% (for no cutback). The supersonic certification time in mode and thrust setting also overestimates m_{NO_x}/F_{oo}, but by smaller margins: 38% to 34% (for the single-cutback minimum noise trajectory and no cutback trajectory, respectively). For the M2.2 medium SST, the subsonic certification climb-out time in mode and thrust setting overestimates m_{NO_x}/F_{oo} by 33.5% to 50%. Although the supersonic certification climb-out time in mode and thrust setting underestimates m_{NO_x}/F_{oo} of real single-cutback minimum noise trajectory by −13.6% and overestimates m_{NO_x}/F_{oo} for the no cutback trajectory by 14%, the margin is smaller than for the subsonic rules. This suggests that the thrust setting prescribed by the current supersonic certification LTO climb-out mode (i.e., 65% F_{oo}) is more representative of the real trajectories of the M1.4 STCA and M2.2 Medium SST than the subsonic certification thrust setting of 85% F_{oo}.

Publications

Mr. Laurens Voet presented an Information Paper titled “Investigation of the effects of VNRS on LTO emissions of engines for supersonic transport aircraft” at the CAEP/12-WG3/5-ESTG meeting on November 3, 2020.

A Working Paper titled “Accounting for Climb-Out Emissions in the Supersonic LTO Emissions Cycle” was submitted to the CAEP/12-WG3/6-ESTG meeting on April 12-20, 2021, in collaboration with ASCENT Project 10.

A Working Paper titled “Accounting for Climb-Out Emissions in the Supersonic LTO Emissions Cycle” was submitted to the CAEP/12-WG3/7-ESTG meeting on September 20-24, 2021, in collaboration with ASCENT Project 10.

Outreach Efforts

Mr. Laurens Voet gave a presentation titled “Development of optimal control framework to design VNRS for take-off operations of civil supersonic transport” at NASA Glenn Research Center on July 22, 2021.

Mr. Laurens Voet gave a presentation titled “Design of variable noise reduction systems for civil supersonic transport certification noise reduction” at the NASA Acoustics Technical Working Group Meeting Fall 2021 on October 19, 2021.

Awards

None.

Student Involvement

This task was conducted primarily by graduate research assistant Laurens Voet, working under the supervision of Dr. Jayant Sabnis, Dr. Raymond Speth, and Dr. Choon Tan.

Plans for Next Period

We plan to apply this analysis to engines with different emissions characteristics to understand whether the emissions LTO cycle is relevant to real-world operations.

References

J. J. Berton, K. Geiselhart (2019). NASA 55-tonne Supersonic Transport Concept Aeroplane (STCA) release package. NASA GRC/NASA LaRC.

D. DuBois and G. C. Paynter (2006), Fuel Flow Method2 for Estimating Aircraft Emissions, *SAE Transactions,* pp. 1-14.

ICAO (2020). Aircraft Engine Emission Databank, EASA.

ICAO (2017). Annex 16 Volume I: Aircraft Noise, ICAO.

ICAO (2008). Annex 16 to the Convention on International Civil Aviation Environmental Protection Volume 2: Aircraft Engine Emissions (Edition 3). Technical report, ICAO.

L. Voet, P. Prakash, R. Speth, J. Sabnis, C. Tan and S. Barrett (2021). The impact of design space constraints on the noise and emissions from derivative engines for civil supersonic aircraft., *AIAA Scitech 2021 Forum,* p. 1272.

Project 048 Analysis to Support the Development of an Engine nvPM Emissions Standard

Massachusetts Institute of Technology

Project Lead Investigator

Steven Barrett
Associate Professor
Department of Aeronautics & Astronautics
Massachusetts Institute of Technology
77 Massachusetts Ave
Building 33-316
Cambridge, MA 02139
617-452-2550
sbarrett@mit.edu

University Participants

Massachusetts Institute of Technology

- PI: Professor Steven Barrett
- Co-PI: Dr. Raymond Speth
- FAA Award Number: 13-C-AJFE-MIT, Amendment Nos. 027, 036, 045, 054, 065, 069, 083, and 087
- Period of Performance: July 8, 2016 to November 30, 2022 (reporting here with the exception of funding level and cost share only for the period October 1, 2020 to September 30, 2021)
- Tasks:
    1. Developing a no-change criterion for engine re-measurement
    2. Extending the non-volatile particulate matter (nvPM) fuel correction method for blended fuels
    3. Analyze emissions data collected for the Committee on Aviation Environmental Protection (CAEP)/10 nvPM standard
    4. Evaluating cruise emissions based on ground-based measurements

Project Funding Level

The funding included $950,000 FAA funding and $950,000 matching funds. The matching funds comprised approximately $214,000 from MIT, plus third-party in-kind contributions of $87,000 from University College London, $158,000 from Oliver Wyman Group, $156,000 from Byogy Renewables, Inc., $153,000 from NuFuels LLC, and $182,000 from Savion Aerospace Corp.

Investigation Team

- Professor Steven Barrett (MIT) serves as PI for the A48 project as head of the Laboratory for Aviation and the Environment. Professor Barrett coordinates internal research efforts and maintains communication among investigators in the various MIT research teams.
- Dr. Raymond Speth (MIT) serves as co-PI for the A48 project. Dr. Speth directly advises student research in the Laboratory for Aviation and the Environment focused on assessment of fuel and propulsion system technologies targeting reduction of aviation's environmental impacts. Dr. Speth also coordinates communication with FAA counterparts.
- Dr. Jayant Sabnis (MIT) serves as co-investigator for the A48 project. Dr. Sabnis co-advises student research in the Laboratory for Aviation and the Environment. His research interests include turbomachinery, propulsion systems, gas turbine engines, and propulsion system–airframe integration.

- Akshat Agarwal (MIT) was a graduate student in the Laboratory for Aviation and the Environment. Until graduating in 2021, he was responsible for conducting the cost–benefit analysis of the nvPM emissions standard and developing methods for estimating nvPM emissions based on smoke number measurements.
- Dr. Bang-Shiuh Chen (MIT) is a postdoctoral associate in the Laboratory for Aviation and the Environment. He is primarily responsible for evaluating and improving models for estimating full-flight emissions from certification measurements.

Project Overview

The FAA's Office of Environment and Energy (FAA-AEE) is working with the international community to implement an international aircraft engine nvPM standard for engines with rated thrust greater than 26.7 kN. The proposed nvPM standard will influence the development of future engine technologies, thus resulting in the reduction of nvPM emissions from aircraft engines, and consequently leading to improved human health and climate impacts of aviation. During the CAEP/11 cycle, the FAA, alongside other national aviation authorities, developed an nvPM emissions standard for the mass and particle number emitted by aircraft engines. During the current cycle (CAEP/12), the FAA requires support to provide a technical basis for the implementation of the nvPM emissions standards.

Task 1 - Developing a No-change Criterion for Engine Re-measurement

Massachusetts Institute of Technology

Objective

The objective of this task was to identify when an engine, after small changes are made to it, needs its emissions remeasured.

Research Approach

The landing and takeoff (LTO) nvPM mass and number standards were developed and agreed upon during CAEP/11. This process identified the total emissions per unit rated thrust that an engine can emit during the LTO procedure as the quantity to be evaluated. For gaseous emissions and the CAEP/10 maximum mass concentration standard, allowances are made for small changes to the engine design, which do not require emissions re-certification. In this task, we developed no-change criteria for the CAEP/11 LTO nvPM mass and number standards, on the basis of the uncertainty of the nvPM mass and number measurement system. If an engine's nvPM mass or number metric value (MV = D_p/F_{00}) is estimated to change by more than the combined uncertainty of the underlying measurements, then an engine should be retested because there is statistical certainty that the emissions of the engine have changed.

To quantify the uncertainty of an MV, we first introduce the approach to estimate it. It is calculated as:

$$\mathrm{MV} = \frac{D_p}{F_{00}} = \frac{\sum_{i=1}^{4} \mathrm{EI}_i \dot{m}_{f,i}}{F_{00}}$$

where D_p is the total LTO emissions, F_{00} is the engine rated thrust, EI_i is the emissions index in International Civil Aviation Organization (ICAO) mode of operation i, and $\dot{m}_f$ is the fuel flow rate. To calculate each EI_i, we use:

$$\mathrm{EI}_m \left[\frac{\mathrm{mg}}{\mathrm{kg_f}}\right] = \frac{22.4 \times 10^{-3}\ \mathrm{nvPM}_m\ k_t k_f}{\left([\mathrm{CO_2}]_{\mathrm{dil}} + \frac{1}{\mathrm{DF}_1}([\mathrm{CO}] - [\mathrm{CO_2}]_{\mathrm{b}} + [\mathrm{HC}])\right)(M_C + \alpha M_H)}$$

where nvPM_m is the mass concentration, k_t is the thermophoretic correction, k_f is the fuel correction, $[X]$ is the diluted mass concentration of species X, DF_1 is dilution factor 1, $M_C = 12.0$ g/mol, $M_H = 1.0$ g/mol, and α is the ratio of moles of hydrogen to moles of carbon in the fuel. The subscripts b and dil represent the background and post-dilution concentrations of a species. The derivation of this equation can be found in AIR6241 (2013). A similar form of the equation is used for number emissions.

To calculate the uncertainty in the MV, we must combine the uncertainties of each EI measurement. For this task, we assume that $\dot{m}_{f,i}$ and F_{00} have negligible uncertainty. The uncertainty in each value required for estimating the EI is defined by the SAE E31 team, and the key values are included in Table 1.

Table 1. Uncertainty of each component of the nvPM mass and number measurement system (reproduced from CAEP/12-WG3-ECTG/6-WP/08)

	Mass	**Number**
Instrument $\left(\frac{u(\mathrm{nvPM}_m)}{\mathrm{nvPM}_m}\right)$	30 μg/m^3 + 13%	6×10^4/cm^3 + 7%
Dilution factor 1 $\left(\frac{u(\mathrm{DF}_1)}{\mathrm{DF}_1}\right)$	4%	4%
CO_2 concentrations $\left(\frac{u([\mathrm{CO_2}]_{\mathrm{dil}})}{[\mathrm{CO_2}]_{\mathrm{dil}}}, \left(\frac{u([\mathrm{CO_2}]_{\mathrm{b}})}{[\mathrm{CO_2}]_{\mathrm{b}}}\right)\right)$	4%	4%
Dilution factor 2 $\left(\frac{u(\mathrm{DF}_2)}{\mathrm{DF}_2}\right)$		10%
Thermophoretic losses $\left(\frac{u(k_t)}{k_t}\right)$	2%	2%
Fuel correction $\left(\frac{u(k_f)}{k_f}\right)$	12%	12%
Instrument drift	2%	5%
Year-to-year line loss variability	2%	5%
Year-to-year CPC response change	–	5%
VPR penetration	–	10%

We assume that all uncertain components follow a Gaussian distribution and are statistically independent. This allows us to combine uncertainties in quadrature. To calculate the relative uncertainties of each emissions index, $u_{r,c}(\mathrm{EI})$, quadrature is performed as follows:

$$u_{r,c}(\mathrm{EI}) = \frac{1}{\mathrm{EI}} \sqrt{\begin{array}{c} \left(\frac{\partial \mathrm{EI}}{\partial \mathrm{nvPM}_m} u_r(\mathrm{nvPM})\right)^2 + \left(\frac{\partial \mathrm{EI}}{\partial k_t} u_r(k_t)\right)^2 + \left(\frac{\partial \mathrm{EI}}{\partial k_f} u_r(k_f)\right)^2 + \\ \left(\frac{\partial \mathrm{EI}}{\partial [\mathrm{CO_2}]_{\mathrm{dil}}} u_r([\mathrm{CO_2}]_{\mathrm{dil}})\right)^2 + \left(\frac{\partial \mathrm{EI}}{\partial \mathrm{DF}_1} u_r(\mathrm{DF}_1)\right)^2 + \left(\frac{\partial \mathrm{EI}}{\partial [\mathrm{CO_2}]_{\mathrm{b}}} u_r([\mathrm{CO_2}]_{\mathrm{b}})\right)^2 \end{array}}$$

where $u_r(X)$ is the relative uncertainty of component X as defined in Table 1. Finally, to obtain the uncertainty in the MV, we again use quadrature, assuming that the uncertainty at each mode of operation is independent and follows a Gaussian distribution.

To identify potential options for the no-change criteria, we estimate the uncertainty of EIs and MVs for engines with reported data. Emissions are converted to concentrations by estimating the volumetric flow rate through the engine. The approach for this is described in detail in Agarwal et al. (2019). We can then propagate uncertainties using the previous set of equations. This process is conducted for all engines with reported data.

Figures 1 and 2 show the relative uncertainty in nvPM mass and particle number EI, respectively, for all engines in the ICAO Engine Emissions Databank (EDB). In both cases, the uncertainty increases as emissions decrease, because of the instrument limit of detection of 30 μg/m^3 and 6 × 10^4 particles/cm^3. Both figures are colored according to the mode of operation. The difference by mode is driven by the conversion from concentration to EI, thus leading to a dependence on thrust setting in the relationship between EI and relative uncertainty.

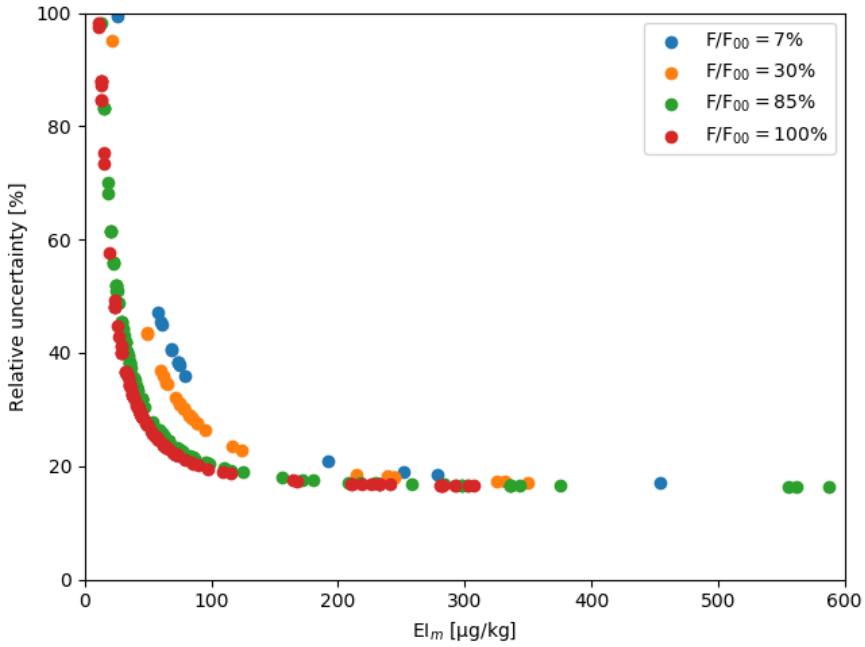

Figure 1. Relative uncertainty in mass emissions index as a function of mass emissions index.

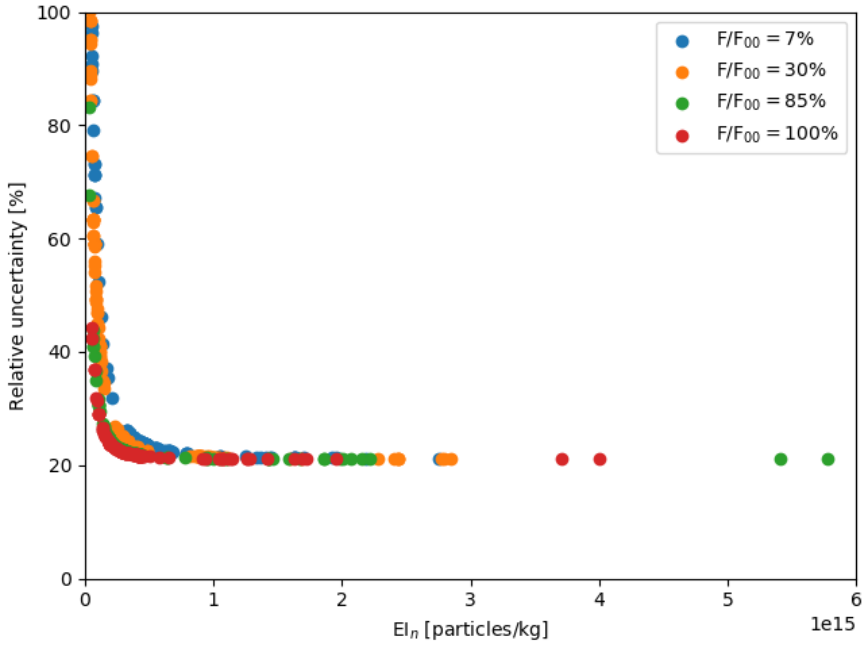

Figure 2. Relative uncertainty in number emissions index as a function of number emissions index.

Figures 3 and 4 show the relative uncertainty in nvPM mass and number MV ($D_{\mathrm{p}}/F_{\mathrm{oo}}$). As with the emissions index, the uncertainty in the metric value increases as the metric value decreases. This relationship can be modeled using an inverse proportional function, as shown in each figure. The relationship shows substantial scatter caused by the differing contributions of each mode of operation to the overall D_p value. The relationships show that the uncertainty tends toward 12.5% for mass and 9.9% for number.

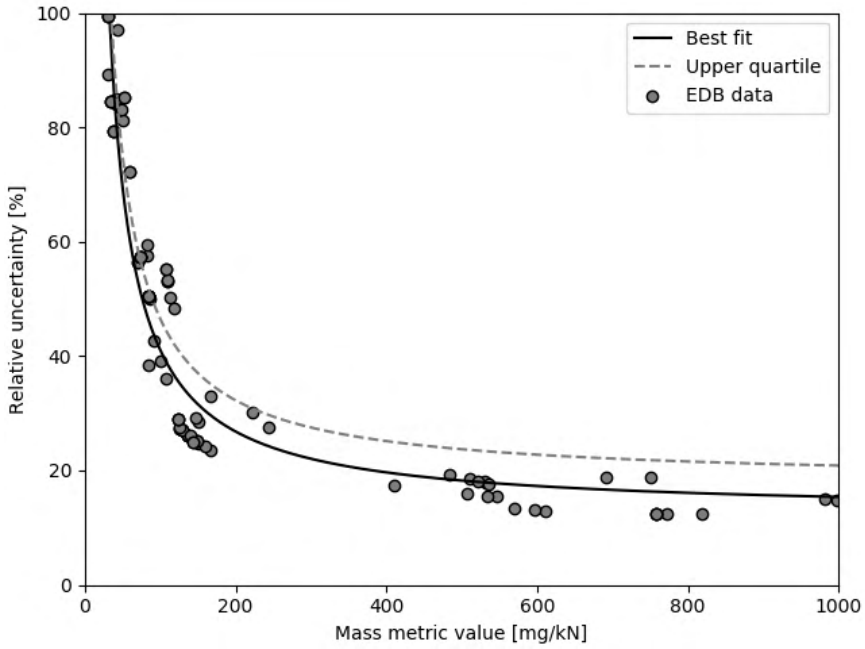

Figure 3. Relative uncertainty in mass metric value as a function of the mass metric value, with best fit curve and upper quartile.

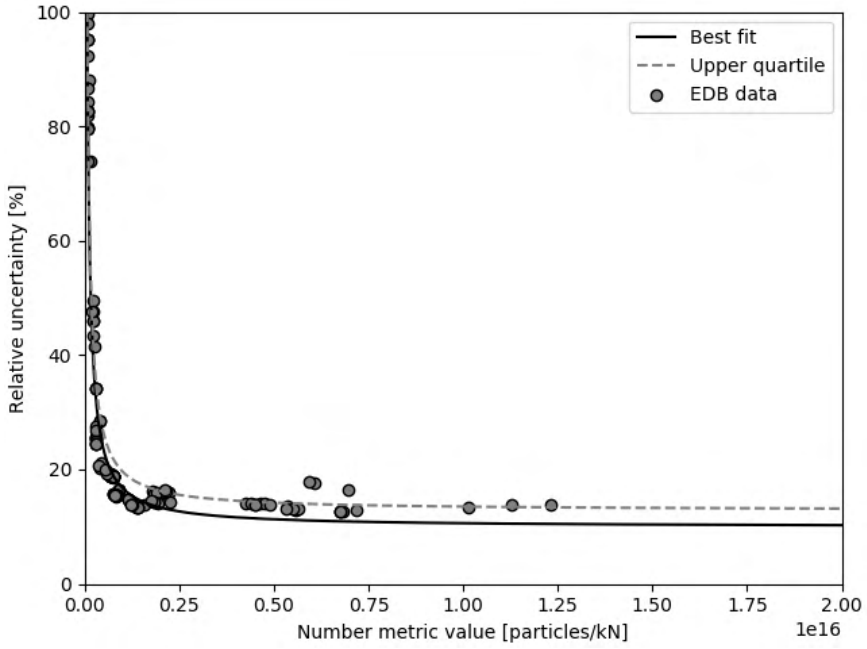

Figure 4. Relative uncertainty in the number metric value as a function of the number metric value, with best fit curve and upper quartile.

We define the no-change criteria as a piecewise continuous function. Below a threshold metric value, we use the absolute uncertainty to determine the no-change criteria. Above this threshold, we use the relative uncertainty. To define the values of the absolute and relative uncertainties in each region, we use two approaches. The first approach starts with the upper quartile of the best-fit relationships found in Figures 3 and 4. We select the threshold metric value and identify the relative uncertainty according to the upper quartile of the best-fit relationships. This also defines the absolute uncertainty, which is calculated by multiplying the relative uncertainty with the metric value. This is used to determine the no-change criteria below the threshold metric value. The second approach is to freely define both the threshold metric value and the relative uncertainty. The absolute uncertainty is defined the same way as in the first approach.

Six sample no-change criteria for mass emissions are shown in Figure 5, and four sample no-change criteria for number emissions are shown in Figure 6. Two options (blue and orange lines) use the upper quartiles of the best-fit relationship. The green lines show a rounded version of the blue no-change criteria. Finally, additional options are provided in red for mass and number, and purple and brown for only mass, wherein the threshold value and relative uncertainty are set separately. These can maintain a similar absolute uncertainty to the blue and green lines but have lower relative uncertainty for emissions above their respective thresholds. A range of options is provided to showcase this balancing effect.

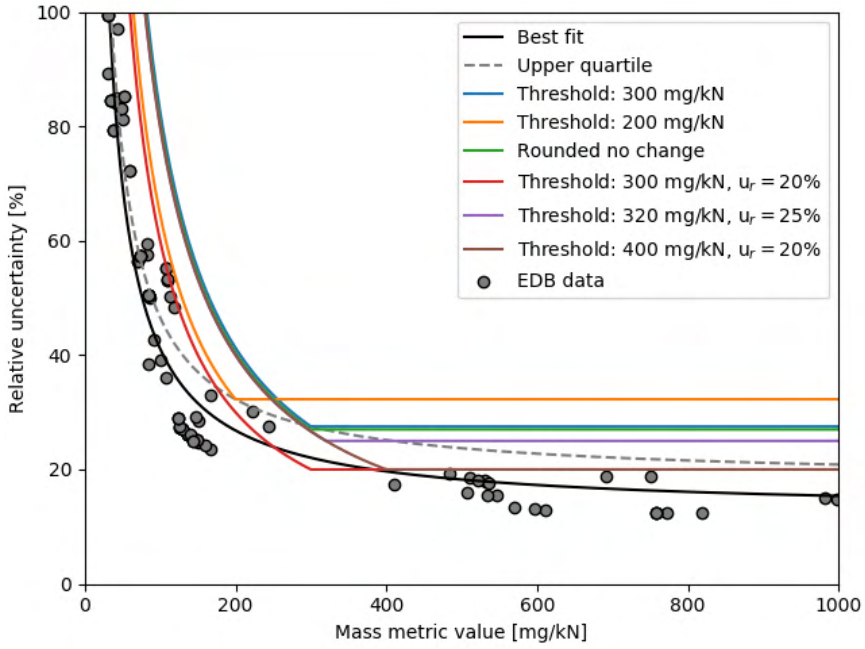

Figure 3. As in Figure 3, but including six options for the mass no-change criterion.

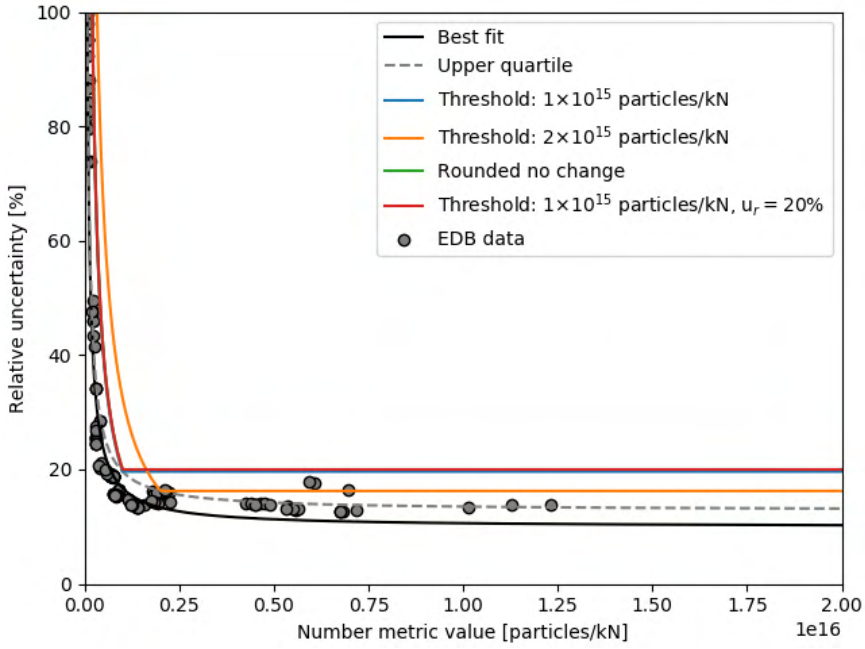

Figure 4. As in Figure 4, but including four options for the number no-change criterion.

The potential no-change criteria indicate a balance between increasing the uncertainty for low emissions and the constant uncertainty at higher emissions. The blue, green, and purple options are considered to balance both of these levels, providing sufficient spacing above the best-fit line and the scatter of the uncertainty values calculated from the EDB.

Milestone
The complete analysis was presented to the FAA and in a working paper for CAEP/12-WG3-ECTG/6.

Major Accomplishments
This work was presented to CAEP/12-WG3-ECTG/6 and used to help the group reach consensus on a no-emissions-change criterion for nvPM mass and number emissions.

Publications
None

Outreach Efforts
Our results have been communicated to the FAA and CAEP-WG3 in a detailed report and presentation.

Awards
None

Student Involvement
Graduate student Akshat Agarwal conducted the analyses and presented the work.

Plans for Next Period
This task is complete.

References
E-31P Particulate Matter Committee. (2013). Procedure for the continuous sampling and measurement of non-volatile particle emissions from aircraft turbine engines (Report No. SAE AIR 6241). SAE International.

Agarwal, A., Speth, R. L., Fritz, T. M., Jacob, S. D., Rindlisbacher, T., Iovinelli, R., Owen, B., Miake-Lye, R. C., Sabnis, J. S., & Barrett, S. R. H. (2019). SCOPE11 method for estimating aircraft black carbon mass and particle number emissions. Environmental Science and Technology, *53*(3), 1364–1373. https://doi.org/10.1021/acs.est.8b04060

Task 2 - Extending the nvPM Fuel Correction Method for Blended Fuels
Massachusetts Institute of Technology

Objective
This task aimed to identify the accuracy for the nvPM fuel correction method for blended fuels and compare it to other formulations.

Research Approach
Current fuel standards allow aircraft engines to use conventional fuels that are blended with up to 50% by volume of biofuels. Biofuels tend to have higher hydrogen content than conventional jet fuels; therefore, blended fuels also have higher hydrogen content than conventional jet fuels. Increasing the hydrogen content of a fuel is expected to decrease nvPM emissions (Moore et al., 2017; Speth et al., 2015). To assess the reduction in emissions, the modeling and database group (MDG) requested WG3 to provide an approach to estimate the decrease in emissions associated with using blended fuels. In this task, we first assessed the accuracy of using the current certification fuel correction approach developed during CAEP/11. In addition, we developed a different formulation that assumes a quadratic relationship between the change in emissions and hydrogen content.

To test the performance and fit coefficients of all model, we combine several engine measurement datasets that comprise six different engines for mass emissions and two additional engines for number emission (Bulzan et al. 2010; Beyersdorf et al. 2014; Timko et al. 2011; 2010; Corporan et al. 2013; 2011; Cain et al. 2013; Corporan et al. 2010; Brem et al. 2015). In addition, we included auxiliary-power-unit (APU) emissions data provided by Prem Lobo (personal communication). Two forms of fits were tested on these datasets. The first follows an exponential trend in hydrogen content (*H*) and thrust setting (F/F_{00}) as:

$$\hat{E} = \exp\big((k_1 + k_2 F/F_{00})(H_0 - H)\big)$$

where $\hat{E}$ is the relative change in emissions, $H_0 = 13.8\%$ is the reference-fuel hydrogen content, and k_1 and k_2 are coefficients to be fitted. The second form assumes a quadratic relationship in the hydrogen content as:

$$\hat{E} = \big(1 - \tilde{H}\big)\big[\big(k_1 + k_2 \hat{F}\big)\tilde{H} + 1\big]$$

where $\tilde{H} = \frac{H - H_0}{H_\infty - H_0}$, and H_∞, k_1, and k_2 are coefficients to be fitted. Both forms are fitted to the entire dataset, and the coefficients are shown in Table 2 below. This table also includes the coefficients used for the certification fuel correction approach.

Table 2. Fitted coefficient values for all models tested

	Certification		Exponential refitted		Quadratic	
	Mass	Number	Mass	Number	Mass	Number
k_1	1.12	1.05	1.33	1.11	−1.25	−1.30
k_2	−0.95	−0.99	−0.79	−0.69	1.54	1.98
H_∞					15.92	15.93

The performance of the certification, exponential refitted, and quadratic approaches is shown in Figures 7-9. The certification approach (Figure 7) exhibits low error for relative mass and number emissions above 1.0. This result is expected because the model was fitted to this set of CFM56-7 data. Below this range, the performance degrades, and the approach tends to find a bias of −0.10 for mass and −0.09 for number. After refitting the coefficients in the certification approach for all available data (Figure 8), the overall performance improves, with the mean absolute error reducing by 20% for mass and 12.5% for number, and the mean error reducing by a factor of 3.2 and 6.0 for mass and number, respectively. The main region where the approach improves for biofuel prediction is for relative emissions below 1.0, which shows lower variance away from the parity line. Above relative emissions of 1.0, the approach does not perform as well as the certification approach, and high bias is present in the results. Finally, the results of the quadratic approach (Figure 9) show the lowest bias, by a factor of 1.9 for mass and factor of 12.5 for number, as compared with the refitted exponential approach. This approach balances the performance at all relative emissions levels (above and below 1.0) better than the exponential form.

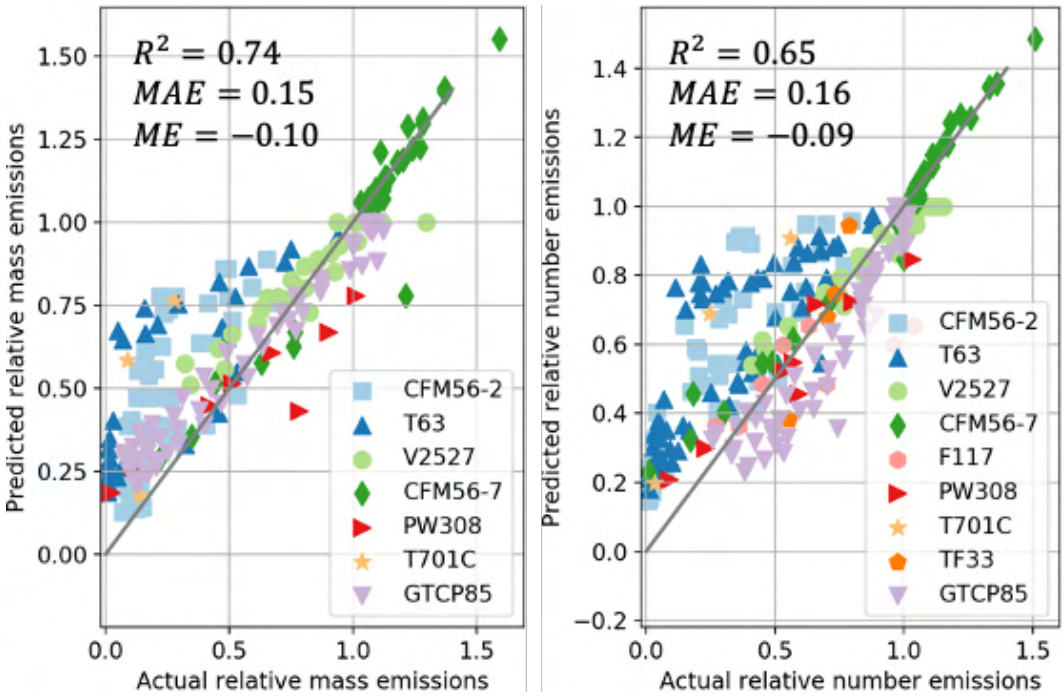

Figure 5. Actual/measured versus predicted relative mass emissions (left) and number emissions (right) using the certification fuel approach.

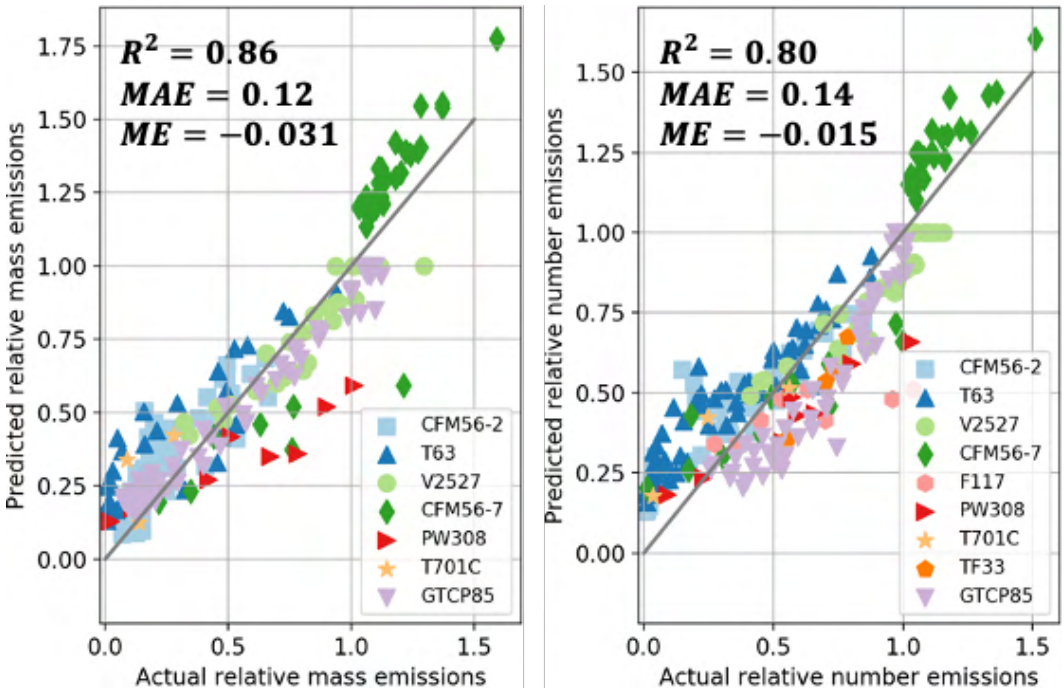

Figure 6. Actual/measured versus predicted relative mass emissions (left) and number emissions (right) using the exponential refitted approach.

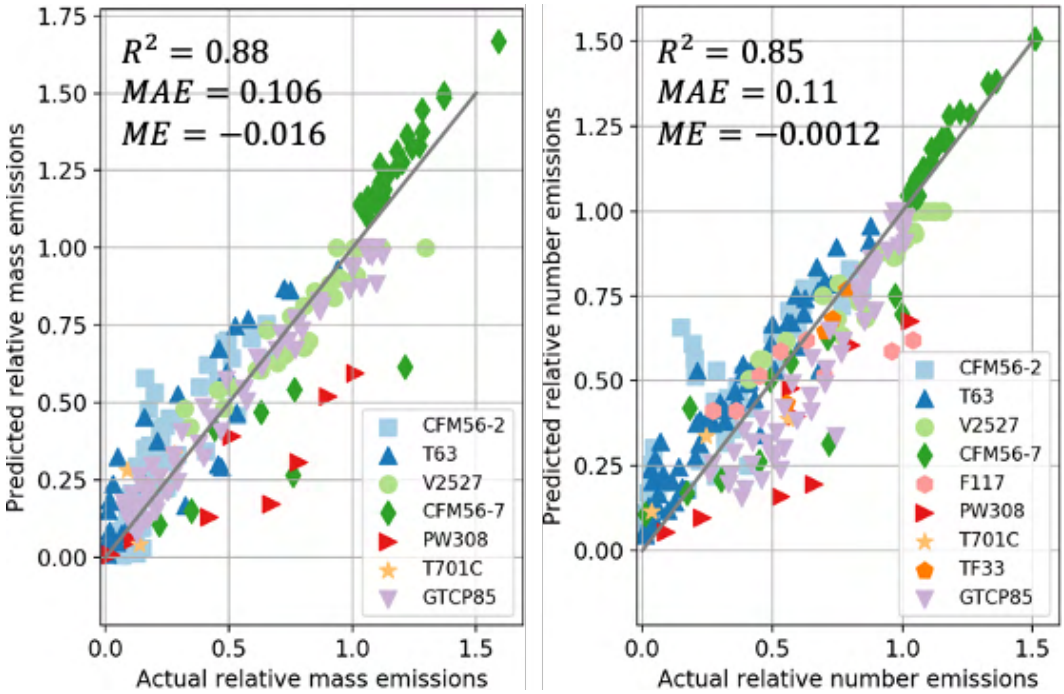

Figure 7. Actual/measured versus predicted relative mass emissions (left) and number emissions (right) using the quadratic approach.

To further understand the differences between these methods arising from the different fuel sources and measurement systems used in the different data sets, the error metrics (R^2, MAE, and ME) were evaluated for each of these different subsets, as shown in Figures 10–12 respectively.

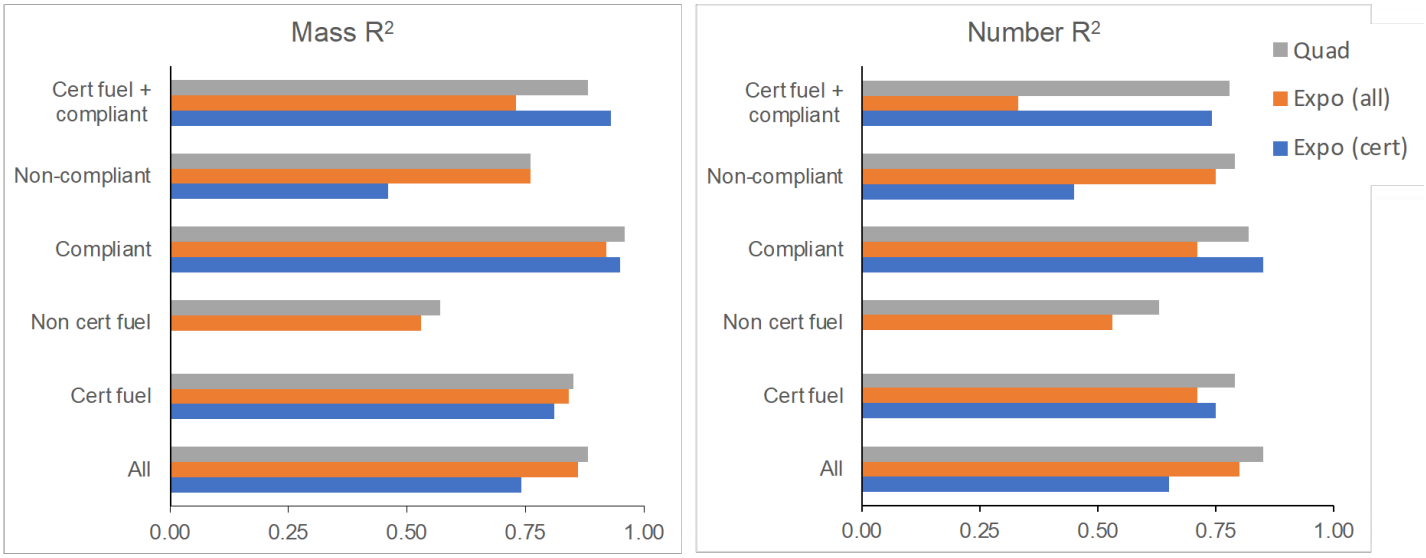

Figure 10. R^2 of each fuel correction formula for mass and number emissions, evaluated for different data subsets.

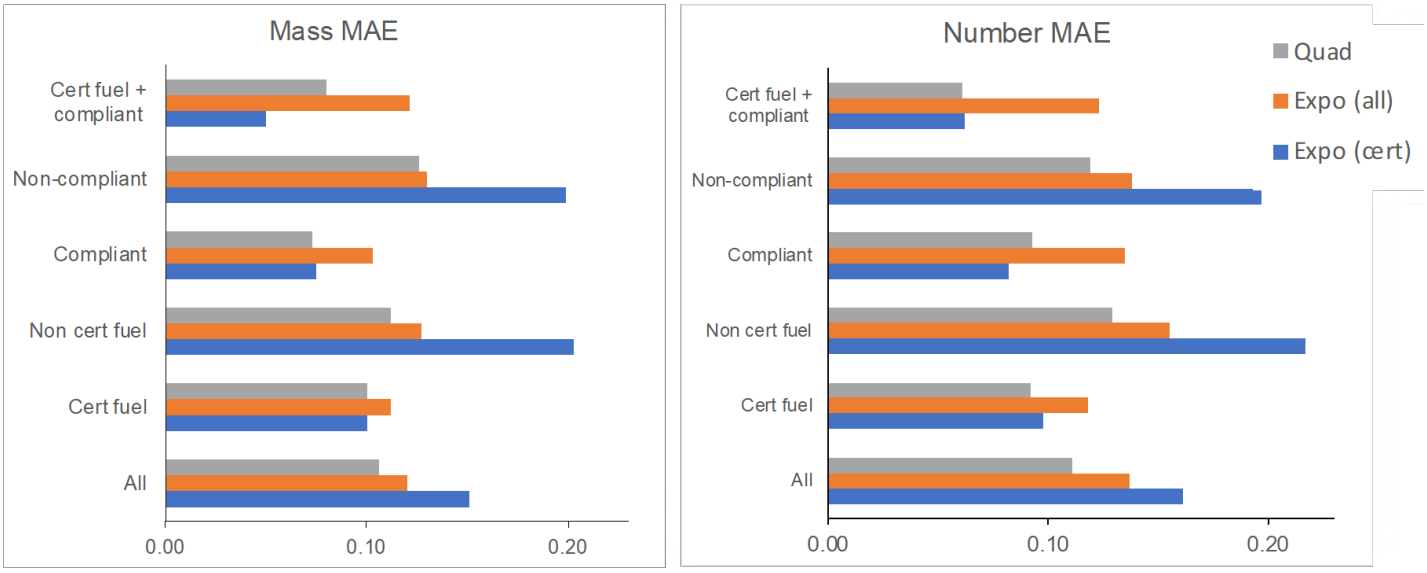

Figure 11. Mean absolute error of each fuel correction formula for mass and number emissions, evaluated for different data subsets.

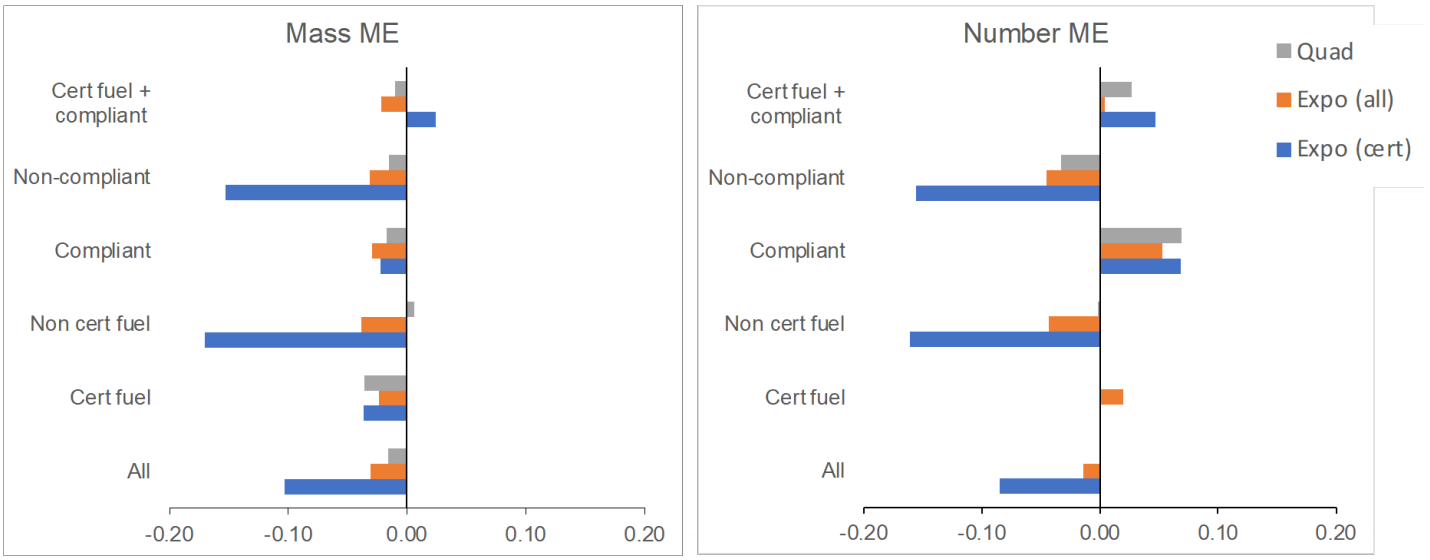

Figure 12. Mean error of each fuel correction formula for mass and number emissions, evaluated for different data subsets.

For the R^2 metric (Figure 10), in which values closer to 1 indicate better performance, the certification method performs best. This finding is expected because this data set was used to develop this correction. In all other cases, the quadratic approach tends to perform best, but the extent to which it outperforms the other methods varies with different data subsets. With this metric, very little difference is found between the quadratic approach and the refitted exponential relationship.

For the mean absolute error (Figure 11), the certification method again performs the best on the smaller data set that was used to fit its parameters. For all other combinations of datasets, the quadratic approach yields the best results. The effect of refitting the exponential relationship has varying effects depending on the target dataset.

Finally, the mean error (Figure 12) shows that the quadratic approach has the lowest bias, except when only measurements taken with certification-compliant fuels and measurement systems are considered, in which case the two methods perform similarly. However, for other data subsets, the bias of the quadratic approach is much smaller than the bias of the exponential approach.

Milestone

The results of this analysis were presented to FAA project managers and to members of the ECTG group under WG3 at the 7th meeting of CAEP/12-WG3.

Major Accomplishments

None

Publications

None

Outreach Efforts

Our results have been communicated to the FAA and ICAO-CAEP in a detailed report and presentation.

Awards

None

Student Involvement

Graduate student Akshat Agarwal conducted the analysis.

Plans for Next Period

This task is complete.

References

Beyersdorf, A. J., M. T. Timko, L. D. Ziemba, D. Bulzan, E. Corporan, S. C. Herndon, R. Howard, et al. 2014. "Reductions in Aircraft Particulate Emissions Due to the Use of Fischer–Tropsch Fuels." *Atmospheric Chemistry and Physics* 14 (1): 11–23. https://doi.org/10.5194/acp-14-11-2014.

Brem, Benjamin T., Lukas Durdina, Frithjof Siegerist, Peter Beyerle, Kevin Bruderer, Theo Rindlisbacher, Sara Rocci-Denis, et al. 2015. "Effects of Fuel Aromatic Content on Nonvolatile Particulate Emissions of an In-Production Aircraft Gas Turbine." *Environmental Science and Technology*, October. https://doi.org/10.1021/acs.est.5b04167.

Bulzan, Dan, Bruce Anderson, Changlie Wey, Robert Howard, Edward Winstead, Andreas Beyersdorf, Edwin Corporan, et al. 2010. "Gaseous and Particulate Emissions Results of the NASA Alternative Aviation Fuel Experiment (AAFEX)," October, 1195–1207. https://doi.org/10.1115/GT2010-23524.

Cain, Jeremy, Matthew J. DeWitt, David Blunck, Edwin Corporan, Richard Striebich, David Anneken, Christopher Klingshirn, W. M. Roquemore, and Randy Vander Wal. 2013. "Characterization of Gaseous and Particulate Emissions From a Turboshaft Engine Burning Conventional, Alternative, and Surrogate Fuels." *Energy & Fuels* 27 (4): 2290–2302. https://doi.org/10.1021/ef400009c.

Corporan, Edwin, Matthew J. DeWitt, Christopher D. Klingshirn, David Anneken, Linda Shafer, and Richard Streibich. 2013. "Comparisons of Emissions Characteristics of Several Turbine Engines Burning Fischer-Tropsch and Hydroprocessed Esters and Fatty Acids Alternative Jet Fuels." In , 425–36. American Society of Mechanical Engineers Digital Collection. https://doi.org/10.1115/GT2012-68656.

Corporan, Edwin, Matthew J. DeWitt, Christopher D. Klingshirn, Richard Striebich, and Meng-Dawn Cheng. 2010. "Emissions Characteristics of Military Helicopter Engines with JP-8 and Fischer-Tropsch Fuels." *Journal of Propulsion and Power* 26 (2): 317–24. https://doi.org/10.2514/1.43928.

Corporan, Edwin, Tim Edwards, Linda Shafer, Matthew J. DeWitt, Christopher Klingshirn, Steven Zabarnick, Zachary West, Richard Striebich, John Graham, and Jim Klein. 2011. "Chemical, Thermal Stability, Seal Swell, and Emissions Studies of Alternative Jet Fuels." *Energy & Fuels* 25 (3): 955–66. https://doi.org/10.1021/ef101520v.

Moore, Richard H., Kenneth L. Thornhill, Bernadett Weinzierl, Daniel Sauer, Eugenio D'Ascoli, Jin Kim, Michael Lichtenstern, et al. 2017. "Biofuel Blending Reduces Particle Emissions from Aircraft Engines at Cruise Conditions." *Nature* 543 (7645): 411–15. https://doi.org/10.1038/nature21420.

Speth, Raymond L., Carolina Rojo, Robert Malina, and Steven R. H. Barrett. 2015. "Black Carbon Emissions Reductions from Combustion of Alternative Jet Fuels." *Atmospheric Environment* 105 (Supplement C): 37–42. https://doi.org/10.1016/j.atmosenv.2015.01.040.

Timko, M. T., Scott C. Herndon, Elena de la Rosa Blanco, Ezra C. Wood, Zhenhong Yu, Richard C. Miake-Lye, W. Berk Knighton, Linda Shafer, Matthew J. DeWitt, and Edwin Corporan. 2011. "Combustion Products of Petroleum Jet Fuel, a Fischer–Tropsch Synthetic Fuel, and a Biomass Fatty Acid Methyl Ester Fuel for a Gas Turbine Engine." *Combustion Science and Technology* 183 (10): 1039–68. https://doi.org/10.1080/00102202.2011.581717.

Timko, M. T., Z. Yu, T. B. Onasch, H.-W. Wong, R. C. Miake-Lye, A. J. Beyersdorf, B. E. Anderson, et al. 2010. "Particulate Emissions of Gas Turbine Engine Combustion of a Fischer–Tropsch Synthetic Fuel." *Energy & Fuels* 24 (11): 5883–96. https://doi.org/10.1021/ef100727t.

Task 3 - Analyze Emissions Data Collected for the CAEP/10 nvPM Standard

Massachusetts Institute of Technology

Objective

The objective of this task was to conduct an analysis of emissions data provided by engine manufacturers to satisfy the requirements of the CAEP/10 nvPM standard.

Research Approach

The CAEP/10 nvPM standard includes reporting requirements for nvPM mass and number emissions measurements at the thrust settings used in the ICAO LTO cycle. For this task, we used this information to evaluate each engine and compare the results with the CAEP/11 nvPM mass and number standards for in-production and new type engines. This analysis provides information needed to understand possible industry responses to the CAEP/11 standards.

Figure 13 shows the nvPM and NO_x emissions as a percentage of the new-type nvPM and NO_x standards, for in-production engines for which nvPM emissions data were added to the ICAO Emissions Databank (EDB). Although all of these engines meet the applicable certification standards according to their date of type certification, some of these engines would not pass the CAEP/8 NO_x standard if they were certified today, and some would not pass the CAEP/11 nvPM standard if they were certified after that standard becomes applicable on January 1, 2023. Specifically, five engines in three families would not pass the nvPM mass standard, whereas six other engine families include engines within 10% of the nvPM mass limit. Four in-production engines in two families would not pass the nvPM number standard, whereas two other engine families include engines within 10% of the limit.

The distribution of margins to the relevant limits differs among engine families. Whereas the margins to the CAEP/8 NO_x limit vary between 10% and 55% (that is, no engine is below 45% of the CAEP/8 limit), the margins to the CAEP/11 nvPM standard are effectively as high 100% for some engines.

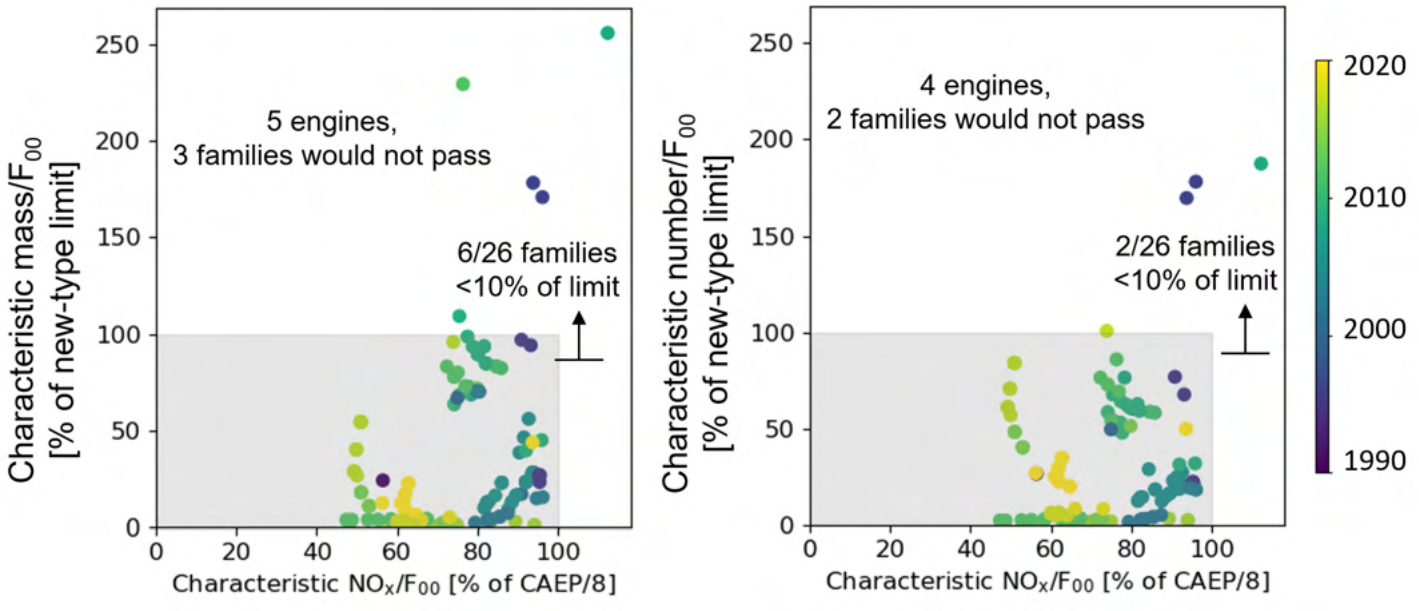

Figure 13. Performance of in-production engines relative to the CAEP/11 new-type limits for nvPM mass (left) and number (right) emissions (vertical axis) and to the CAEP/8 NO_x regulation (horizontal axis).

Emissions data reported for an engine that has been recertified after a change to the combustor can provide insight into potential interdependencies between NO_x and nvPM emissions. Figure 14 shows data for one such example using data from the EDB. Although the reasons for recertification are not reported in the EDB, the emissions results for this combustor show

that NO_x emissions increased by 5%–15% depending on the thrust condition, and nvPM mass emissions decreased by 20%–80%.

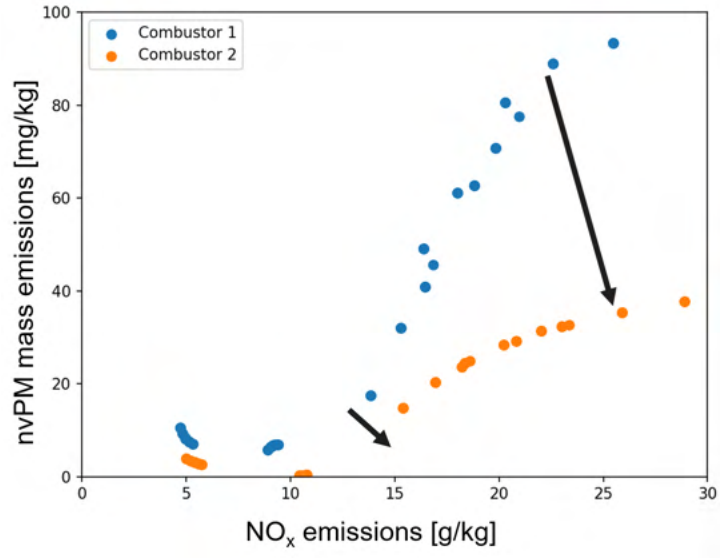

Figure 14. Changes in NO_x and nvPM mass emissions after a combustor revision.

Milestone
The complete analysis was presented to the FAA and the ECTG Emissions Data Analysis ad hoc group.

Major Accomplishments
This work has been presented during CAEP/12-WG3-ECTG/7.

Publications
None

Outreach Efforts
Our results have been communicated to the FAA and CAEP/WG3 in a detailed report and presentation.

Awards
None

Student Involvement
Graduate student Akshat Agarwal conducted the analyses and presented the work.

Plans for Next Period
This task is complete.

Task 4 - Evaluating Cruise Emissions Based on Ground Measurements

Massachusetts Institute of Technology

Objective

The objective of this task is to develop a modeling-based approach for estimating nvPM emissions at cruise and to use this approach to evaluate cruise emissions of different combustor technologies.

Research Approach

Because of the lack of cruise emission data, cruise emission estimation methods such as P_3T_3 and fuel flow methods (Dubois & Paynter, 2006; Schaefer & Bartosch, 2013) are used to calculate the emissions profiles of aircraft operations. P_3T_3 and fuel flow methods were developed for conventional rich burn, quick-mix, lean burn (RQL)-style combustors (Samuelsen, 2006) and have not been rigorously evaluated for newer technologies such as lean, staged combustors (Foust et al, 2012). The LTO emission measurements available from certification tests do not cover the range of middle power percentage (30%–85%) in which the switching to lean combustion occurs for such combustors. Moreover, the prediction of nvPM emissions in these estimation methods is not included.

For this task, we will calibrate a reactor network model of a gas turbine combustor by using ground-based emissions measurements from the EDB. The primary zone of the combustor is split into several zero-dimensional reactors with different volumes and equivalent ratios. Such reactor network models have been successfully used to predict combustor emissions (Allaire, 2006; Moniruzzaman & Yu, 2012). Using an engine cycle deck developed in the Numerical Propulsion System Simulation (Claus et all, 1991) and matched to that engine's performance, we will calculate the combustor inlet conditions at cruise, and use the combustor model to evaluate the resulting nvPM mass and number emissions. We will apply this approach to an engine with an RQL combustor and to an engine with a lean, staged combustion system.

Milestone

Validate the engine model by comparing it with EDB data and the conventional emission estimation methods.

Major Accomplishments

None

Publications

None

Outreach Efforts

None

Awards

None

Student Involvement

None

Plans for Next Period

After development of the model is completed, it will be validated against combustor rig test data which provides a surrogate for cruise-relevant conditions. The model will then be used to evaluate existing methods for predicting cruise emissions and to determine modifications that enhance the accuracy of those methods.

References

Claus, R. W., Evans, A. L., Lylte, J. K., & Nichols, L. D. (1991). Numerical propulsion system simulation. Computing Systems in Engineering, *2*(4), 357-364.DuBois, D., & Paynter, G. C. (2006). Fuel Flow Method 2 for Estimating Aircraft Emissions. *SAE Transactions*, 1-14.

Schaefer, M., & Bartosch, S. (2013). Overview on fuel flow correlation methods for the calculation of NOx, CO and HC emissions and their implementation into aircraft performance software. *Institut für Antriebstechnik, Köln*.

Samuelsen, S. (2006). Rich burn, quick-mix, lean burn (RQL) combustor. *The Gas Turbine Handbook*, 227-233.
Foust, M., Thomsen, D., Stickles, R., Cooper, C., & Dodds, W. (2012). Development of the GE aviation low emissions TAPS combustor for next generation aircraft engines. In *50th AIAA aerospace sciences meeting including the new horizons forum and aerospace exposition* (p. 936).
Claus, R. W., Evans, A. L., Lylte, J. K., & Nichols, L. D. (1991). Numerical propulsion system simulation. *Computing Systems in Engineering*, *2*(4), 357-364.
Allaire, D. L. (2006). A physics-based emissions model for aircraft gas turbine combustors (Doctoral dissertation, Massachusetts Institute of Technology).
Moniruzzaman, C. G., & Yu, F. (2012). A 0D aircraft engine emission model with detailed chemistry and soot microphysics. Combustion and Flame, 159(4), 1670-1686.

Project 049 Urban Air Mobility Noise Reduction Modeling

The Pennsylvania State University and Continuum Dynamics Inc.

Project Lead Investigator

Kenneth S. Brentner
Professor of Aerospace Engineering
Department of Aerospace Engineering
The Pennsylvania State University
233 Hammond Building, University Park, PA
(814) 865-6433
ksbrentner@psu.edu

University Participants

The Pennsylvania State University

- PI: Kenneth S. Brentner, Professor of Aerospace Engineering
- FAA Award Number: 13-C-AJFE-PSU-049, Amendment No. 66
- Period of Performance: October 1, 2020, to September 30, 2021
- Tasks:
  6. Complete coupling of DEPSim flight simulation software with Comprehensive Hierarchical Aeromechanics Rotorcraft Model (CHARM) and PSU-WOPWOP noise prediction code
  7. Validate the new flight simulation/noise prediction system
  8. Develop several notional urban air mobility (UAM)/electric vertical takeoff and landing (eVTOL) aircraft models for noise testing
  9. Develop and test trim strategies for notional UAM/eVTOL vehicles
  10. Begin compilation of noise predictions for notional UAM and eVTOL vehicles during various stages of operation
  11. Evaluate the computational algorithm for efficient processing of many rotors and noise-generating bodies

Project Funding Level

FAA provided $280,000 in funding. The Pennsylvania State University (PSU) provided $148,213 faculty academic year cost-sharing and $110,000 equipment cost-sharing.[1]

Investigation Team

- Kenneth S. Brentner, PI, The Pennsylvania State University; acoustic prediction lead on all tasks.
- Eric Greenwood, co-PI, The Pennsylvania State University; acoustics prediction/analysis supporting acoustic tasks.
- Joseph F. Horn, co-PI, The Pennsylvania State University; flight simulation lead supporting flight simulation tasks
- Daniel A. Wachspress and Mrunali Botre, co-PIs, Continuum Dynamics Inc. (CDI); responsible for rotor loads, wake integration, and CHARM coupling
- Ze Feng (Ted) Gan, graduate research assistant, The Pennsylvania State University; primarily responsible for developing PSU-WOPWOP noise prediction software and performing acoustic predictions (Tasks 6, 7, 11)
- Bhaskar Mukherjee, graduate research assistant, The Pennsylvania State University; primarily responsible for software coupling, establishing new aircraft models, developing simulations for new aircraft types, performing acoustic predictions, and developing flight abatement procedures (Tasks 6–10)

[1] The cost sharing is less than 100% for Project 49 because the cost sharing for Project 38 is greater than needed. When combined, the total cost share for Projects 38 and 49 is 100%, matching the government funds. This was done so CDI did not need to report the cost sharing as multiple parts for the two projects.

Project Overview

A wide variety of unconventional configurations for urban air mobility (UAM)/electric vertical takeoff and landing (eVTOL) aircraft, with many electrically driven propellers and lifting rotors, have been proposed and are currently under development by companies worldwide. These novel configurations make up a new category of aircraft that will need to be certified, especially for acceptable noise levels, given their urban operations. Furthermore, the noise of UAM and eVTOL vehicles is expected to be one of the determining factors for community and passenger acceptance. Therefore, first-principles noise predictions of these aircraft will be important for providing information that is independent from manufacturers for the FAA, and before manufacturer flight test or certification noise data are available.

In ASCENT Project 38, the helicopter noise prediction system initially developed in ASCENT Project 6 was successful in accurately predicting the noise of six helicopters (usually within 1-3 dB of the sound exposure level [SEL]), when comparing the predictions to flight test results from an FAA/NASA rotorcraft noise abatement flight test that was carried out in August and October 2017. The SEL contours from the flight tests were compared with predictions for several flight procedures. This noise prediction system developed in Project 38 consisted of the PSUHeloSim flight dynamics simulation code coupled to the CHARM aeromechanics modeling software and the PSU-WOPWOP noise prediction code. This coupling with the flight simulation code was shown to be important for noise predictions, which improved noticeably when the simulation was modified to track the time-dependent aircraft position, velocity, and attitude flown in the individual run, rather than the nominal flight path.

To build upon the success of ASCENT Project 38, an analogous approach of coupling a flight simulation code with CHARM and PSU-WOPWOP is taken in this ASCENT Project 49. In this project, the PSUHeloSim flight simulation component of the noise prediction system used in Project 38 is replaced with DEPSim, a flight simulation code designed for many electrically driven rotors and the unique control strategies to fly such vehicles effectively. Coupling of DEPSim with CHARM was done in work outside of ASCENT, but the DEPSim-CHARM coupling with PSU-WOPWOP will be performed in this project.

In previous work for ASCENT Project 38, the initial capability to analyze the noise from UAM and eVTOL vehicles with unique configurations under any flight condition was initiated. This will enable the FAA, manufacturers, and related entities to investigate how this new class of vehicles—and their noise—might be integrated into the national airspace. Emphasis was placed on modeling the unique features of UAM and eVTOL configurations not commonly seen in conventional rotorcraft, such as variable rotation speed rotors and complex unsteady aerodynamic interactions between the many rotors and airframe. UAM vehicles will likely have lower tip speeds to achieve acceptable noise levels, so broadband noise is expected to become the dominant rotor noise source; therefore, fast, accurate modeling of rotor broadband noise was undertaken. Another goal of this project is to use the noise prediction system developed to provide guidance on how to fly these vehicles quietly through flight operations. As the analysis and computations are based on fundamental physics, noise abatement procedures for novel new vehicles can be developed.

The objective of this continuing project is to proceed toward the extension of the flight simulation/noise prediction system developed in ASCENT Project 6, “Rotorcraft Noise Abatement Operating Conditions Modeling,” and refined in ASCENT Project 38, “Rotorcraft Noise Abatement Procedures Development.” The new flight simulation software DEPSim (Distributed Electric Propulsion Simulation) is similar in structure to the PSUHeloSim code used in the previous ASCENT Project 6 and Project 38 efforts, but DEPSim is capable of modeling multiple interacting rotors driven by variable-speed electric motors along with their interactions with lifting surfaces. Completion of this change in flight simulation elements and coupling with PSU-WOPWOP will require testing and validation to provide confidence in the enhanced system. The trim strategies and control allocation schemes for DEP configurations are also different from those for helicopters and may be nonunique, and the new sim code can analyze these alternative control strategies. Testing and evaluation of the flight simulation system been initiated but more will be required.

Task 6 - Complete Coupling of PSUDEPSim Flight Simulation Software with CHARM and PSU-WOPWOP

The Pennsylvania State University

Objectives

The goal of this task is to couple the new flight simulation PSUDEPSim (flight simulator) with both the CHARM rotor module (higher fidelity airloads) and PSU-WOPWOP (noise prediction) as was done in ASCENT Project 6 for helicopter noise prediction

(PSUHeloSim/CHARM/PSU-WOPWOP). The UAM/eVTOL flight simulation/noise prediction tool must also consider the noise generated by unsteady airloads on the airframe, typically caused by aerodynamic interactions with propellers or rotors. These interactions will change with flight condition. This task will complete the work begun in the first year of Project 49.

Research Approach

Analogous to the PSUHeloSim system, the PSUDEPSim flight simulator has been coupled with the CHARM rotor module (Theron, Horn, & Wachspress, 2020). This enables the flight simulator to capture necessary interactional effects between several moving components reasonably. Using DEPSim, a variety of control schemes will be explored to study the trim envelope. Based on experience from noise abatement strategies developed in ASCENT Project 38, control schemes with potential for noise reduction will be studied further. The impact of variable revolution per minute (RPM) and variable collective pitch control schemes is expected to be an important factor. Real-time flight unsteadiness, such as gust (Theron, Horn, Wachspress, & Enciu, 2020), will also be included to study its impact on noise.

Milestones

Milestones achieved for this task are (1) making the noise prediction system more robust for higher speed maneuvers; and (2) robust coupling for new configurations: new configurations do not require external modifications to set up the coupling.

Major Accomplishments

The code from Task 1 was updated to be more robust. The PSUDEPSim flight controller was updated to handle a wider range of aggressive maneuvers. The coupling was also updated to process new configurations without any modifications in the source code required. A series of pilot commands along a time vector is used to fly the DEP aircraft. The generic eVTOL configuration (Figure 1a) was flown by giving a $-20°$ roll angle pilot command to simulate a 50 knots turn maneuver (Figure 2).

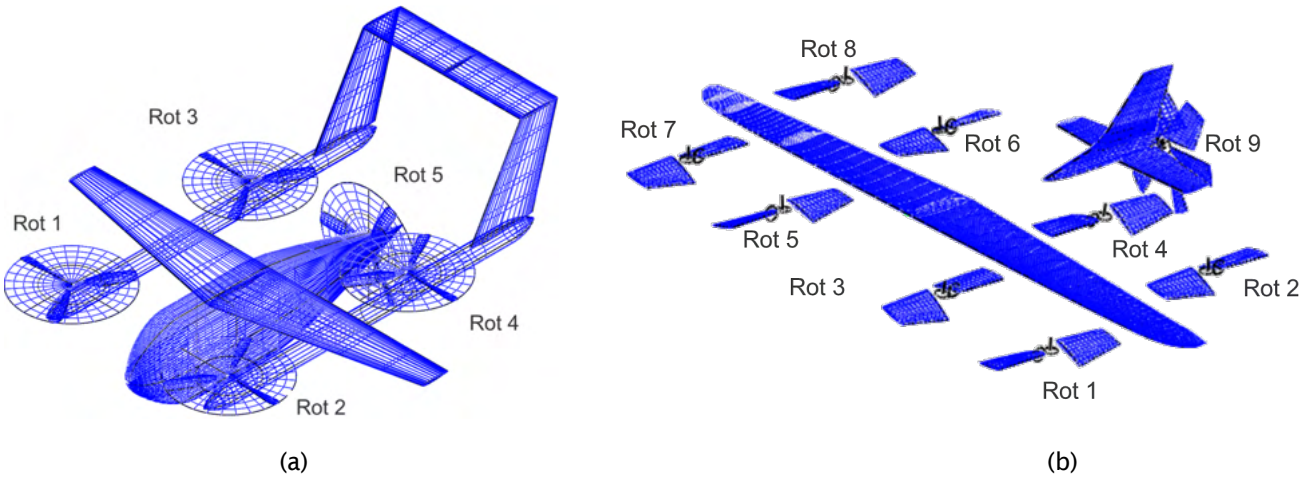

Figure 1. Urban air mobility (UAM)/electric vertical takeoff and landing (eVTOL) aircraft models currently available for noise simulation. (a) Generic eVTOL configuration; (b) NASA Lift + Cruise.

An aircraft pitch command was used to override the default actions of the trim scheduler. This provides control of the distribution of aircraft weight between the generation of rotor thrust and wing lift (Figure 3b). As a compound eVTOL aircraft, this is just one of the possible choices to achieve trimmed flight. Two rotor thrust control schemes are used to control the hover rotors: (1) variable angular speed, constant collective pitch (varrpm) and (2) variable pitch, constant angular speed (varpitch). The impact of rotor thrust control scheme can be first seen in the rotor thrust generation (Figure 4), and the

resultant deterministic noise from the five rotors (Figure 1a) throughout the maneuver is shown in Figure 5. While the DEPSim-PSUWOPWOP system provides data for broadband noise (BPM), the results have not been investigated yet.

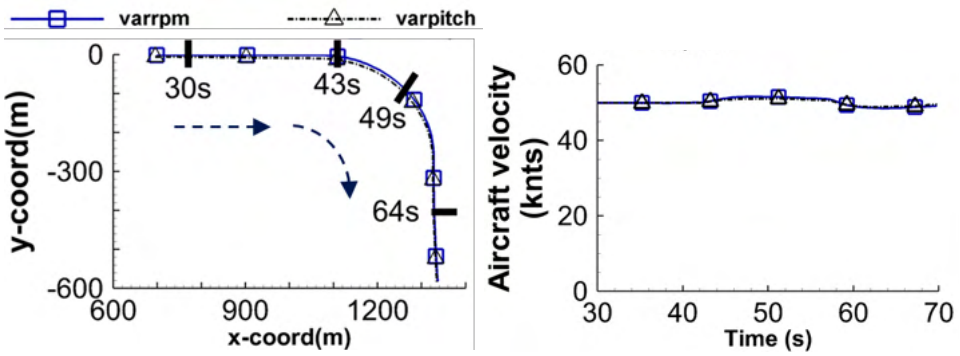

Figure 2. Fifty knots turn maneuver with generic electric vertical takeoff and landing (eVTOL): Trajectory (left), aircraft velocity magnitude (right). varrpm = variable angular speed, constant collective pitch; varpitch = variable pitch, constant angular speed.

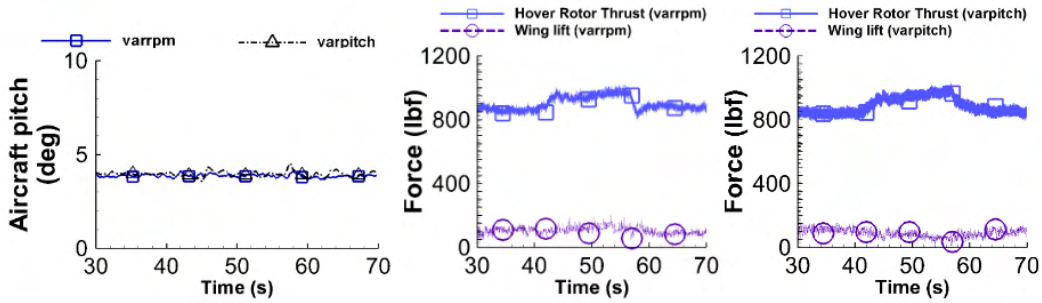

Figure 3. Fifty knots turn maneuver: Aircraft pitch (left), combined hover rotor thrust and wing lift (variable rpm, center:; variable pitch, right).

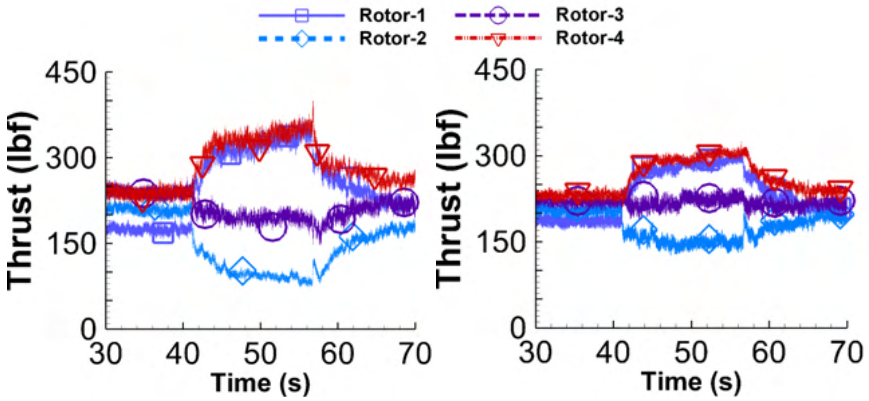

Figure 4. Fifty knots turn maneuver: Rotor thrust: variable RPM (left), variable pitch (right).

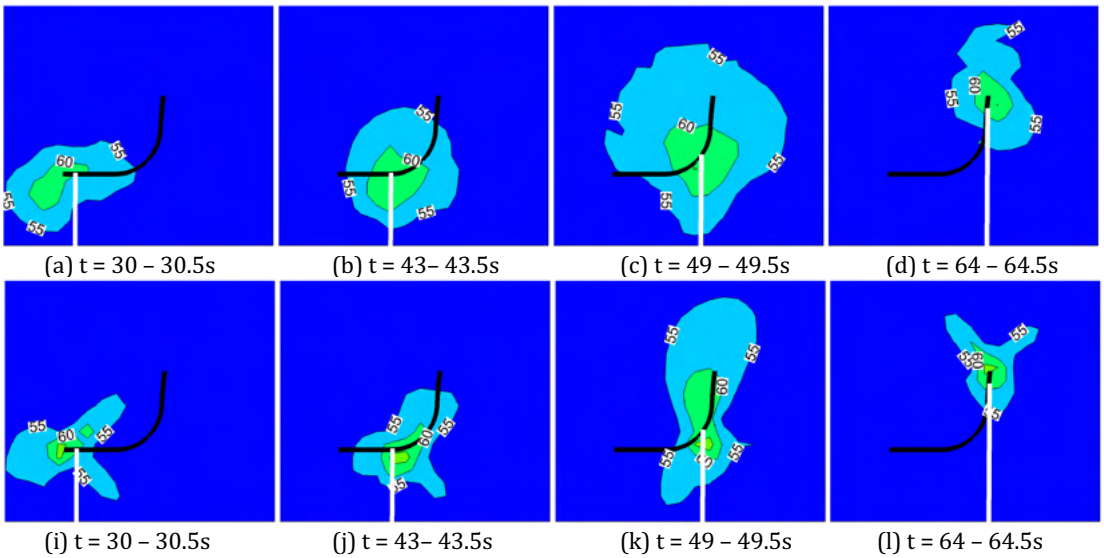

Figure 5. Fifty knots turn maneuver: Overall sound pressure level from variable RPM (top), and variable pitch (bottom).

Aperiodic time-varying broadband noise prediction capabilities of PSU-WOPWOP are currently being developed and coupled to the noise prediction system. This is because the time variation of broadband noise within a rotor period has been found to be relevant for noise levels (from the previous year's work for Project 49) and human perception (Christian et al., 2019).

The physical mechanisms responsible for this time variation of broadband noise within a rotor period were investigated for a single 4-bladed, model-scale rotor operating in hover with a tip Mach number of 0.6, with only the outermost 20% blade span considered. Figure 6a shows the full broadband noise spectrogram; retarded-time effects and convective amplification are individually removed in Figures 6b and 6c, respectively. Figure 6 demonstrates that, for this specific case, convective amplification increases the amplitude of the broadband noise but does not have as much impact on the modulation as retarded-time effects.

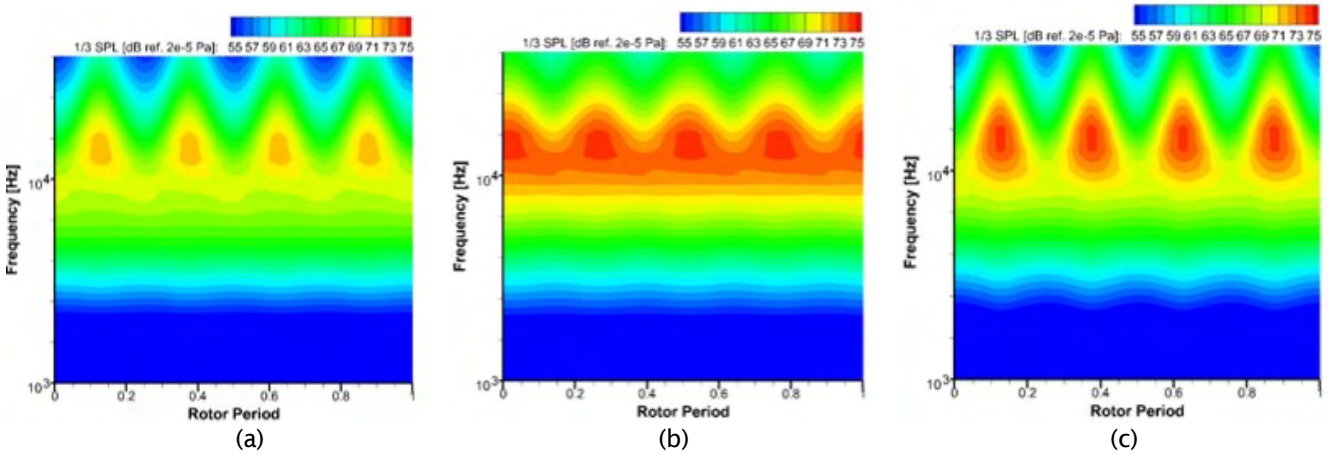

Figure 6. Spectrograms demonstrating effects of isolating physical mechanisms contributing to amplitude modulation. (a) Total baseline noise; (b) retarded-time effects removed; (c) convective amplification removed.

Publications

Published conference proceedings

Gan, Z. F. T., Brentner, K. S., & Greenwood, E. (2021, January 26-28). Time variation of rotor broadband noise [Presentation]. Vertical Flight Society 8th Annual Electric VTOL Symposium.

Mukherjee, B., Gan, Z. F. T., Theron, J.-P., Botre, M., Brentner, K. S., Greenwood, E., & Horn, J. F. (2021, May 11-13). A new distributed electric propulsion aircraft simulation tool for coupled flight dynamics, free wake, and acoustic predictions [Presentation]. Vertical Flight Society 77th Annual Forum & Technology Display.

Outreach Efforts

None.

Awards

None.

Student Involvement

Bhaskar Mukherjee, a graduate assistant starting his PhD at PSU, is working on coupling DEPSim with PSU-WOPWOP and developing a robust release version for usage in Project 49 and other FAA projects.

Ze Feng (Ted) Gan, a graduate assistant who recently completed his master's degree and started his PhD program at PSU, is working on broadband noise and its time variation.

Plans for Next Period

Using the data currently provided from the DEPSim-PSUWOPWOP noise production system, contribution of nonrotary components, such as wing and vertical and horizontal tail, will be integrated into current noise calculations from rotors. Aperiodic time-varying broadband noise prediction capabilities of PSU-WOPWOP will continue to be developed and coupled into the noise prediction system. The time variation of rotor broadband noise for realistic UAM aircraft will be simulated and analyzed. The physical mechanisms causing the modulation (e.g., relative contributions of convective amplification and retarded-time effects) will be analyzed for a wider variety of cases.

New broadband noise models may be integrated into the noise prediction system: presently, only airfoil self-noise is modeled, whereas ingestion and blade-wake interaction (BWI) noise are not. However, to justify the integration of models for additional broadband noise sources, the importance of these noise sources to the total vehicle broadband noise and its time variation must first be explored. This study on the relevance of different time-varying broadband noise sources is a high-priority, immediate next step that has recently been initiated. Presently, the Bell 206 helicopter flight test noise measurements (Schmitz et al., 2007) are being analyzed for their time-varying broadband noise characteristics. Studying the time variation of broadband noise of helicopter rotors will provide insight into the time variation of broadband noise of UAM rotors, which are expected to experience greater aerodynamic interactions due to the geometric configurations of proposed UAM aircraft.

References

Christian, A., Caston, J., Greenwood, E., & Branch, A. (2019, May 13-16). Regarding the perceptual significance and characterization of broadband components of helicopter source noise [Presentation]. Vertical Flight Society 75th Annual Forum & Technology Display, Philadelphia, PA.

Schmitz, F. H., Greenwood, E., Sickenberger, R. D., Gopalan, G., Sim, B. W.-C., Conner, D. A., Moralez, E., & Decker, W. (2007, May 1-3). Measurement and characterization of helicopter noise in steady-state and maneuvering flight [Presentation]. American Helicopter Society 63rd Annual Forum, Virginia Beach, VA.

Theron, J.-P., Horn, J. F., & Wachspress, D. (2020, January). An integrated simulation tool for e-VTOL aeromechanics and flight control analysis [Presentation]. 2020 VFS Aeromechanics for Advanced Vertical Flight Technical Meeting, San Jose, CA.

Theron, J.-P., Horn, J. F., Wachspress, D., & Enciu, J. (2020, October). Nonlinear dynamic inversion control for urban air mobility aircraft with distributed electric propulsion [Presentation]. Vertical Flight Society 76th Annual Forum & Technology Display, Virginia Beach, VA.

Task 7 - Validate the New Flight Simulation/Noise Prediction System

The Pennsylvania State University

Objective

The objective of this task is to validate the new flight simulation/noise prediction system with reference measured data. This will provide confidence in the predictions and may point to areas where improvements are needed.

Research Approach

In this task, the new DEPSim-based noise prediction system will be used to model helicopters that were flown in the 2017 and 2019 FAA/NASA noise abatement flight tests. Comparisons will be made both with the previously developed PSUHelosim-based noise prediction system and the flight test data. The new DEPSim-based noise prediction system will also be used to model a hovering multirotor unmanned aerial system (UAS), and the predictions validated against measured data collected at PSU.

Currently, the DEPSim system is not capable of modeling a traditional helicopter because it does not include modeling of the traditional turboshaft engine system. This is something that needs to be explored to see whether the DEPSIM system can be enhanced. PSU is collecting acoustic data for UAS vehicles in ASCENT Project 77, but the data were not ready for use during this year's effort.

Milestone

We achieved strong qualitative agreement between the time-varying broadband noise predictions of PSU-WOPWOP and processed helicopter flight test noise measurements.

Major Accomplishments

To determine the extent to which the time-varying broadband noise predictions of PSU-WOPWOP are realistic, the Bell 206 flight test case studied in Christian et al. (2019) was simulated in PSU-WOPWOP, with input files from the HeloSim system developed and validated in ASCENT Project 38 (Botre et al., 2019). Details of the original flight test can be found in Schmitz et al. (2017). Only the main rotor was studied, as the data processing method of Christian et al. (2019) involves synchronous averaging of main rotor blade passages, which averages out the tail rotor noise.

The overall noise levels of the PSU-WOPWOP predictions (Figure 7b) are lower than those of the processed flight test data (Figure 7a) by up to approximately 5-10 dB across all frequencies; this might be expected because the PSU-WOPWOP predictions only include blade self-noise, whereas the flight test data include other noise sources, such as tones from blade passage frequency harmonics and engine noise, turbulence ingestion noise, and wind over the microphone. Despite these differences, Figures 1 and 8 share a similar modulation trend/shape, and an amplitude modulation of about 15 dB. In summary, the overall trends/shape and range of amplitude modulation observed in the time-varying spectrum predictions match with experimental data, supporting that the predictions are realistic.

Noise due to variable rotor speed was studied analytically and numerically. Analytical manipulation of the governing equation for rotor thickness noise (the thickness noise component of Farassat's Formulation 1A) found that for realistic angular accelerations (limited by rotor inertia and motor torque) expected of UAM aircraft, thickness noise due to variable rotor speed can be thought of as "quasi-steady": at any instant in time, the noise of a rotor undergoing angular acceleration is equivalent to the same rotor with constant rotor speed equal to the instantaneous rotor speed (i.e., angular acceleration contributes little thickness noise at any instant in time). These findings were confirmed in computational predictions using PSU-WOPWOP for a notional UAM rotor undergoing realistic sinusoidal variations in rotor angular speed observed in DEPSim flight simulations (see Figure 8). Validation of these findings would be useful and is planned for future work.

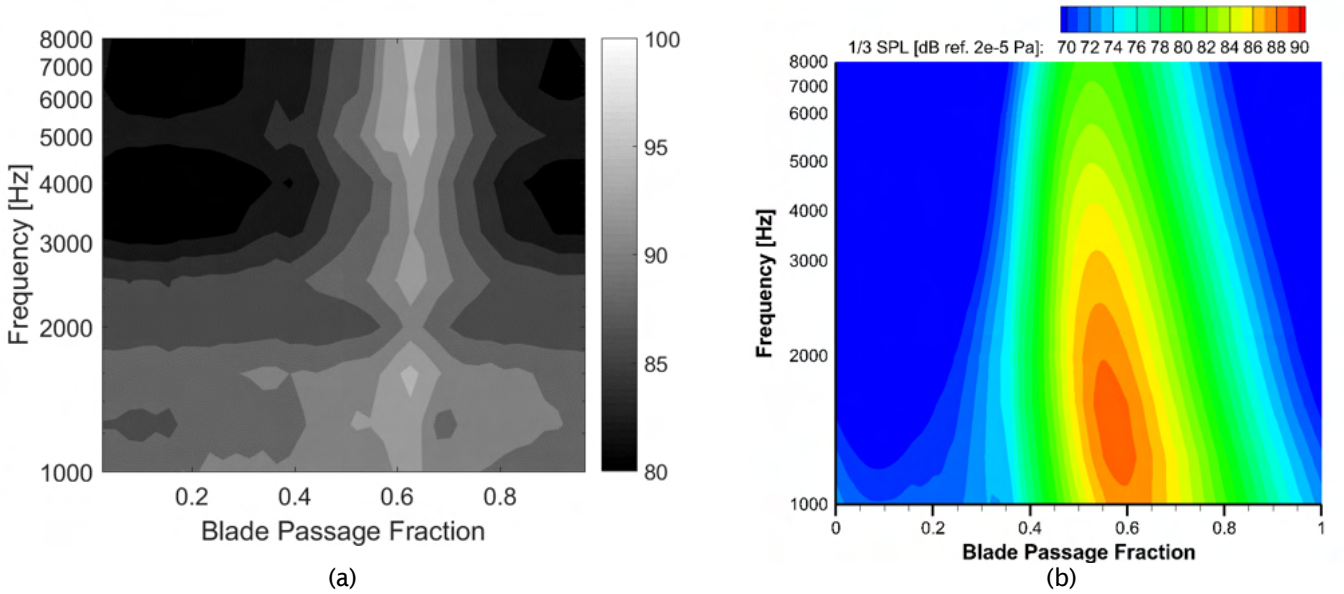

(a) (b)

Figure 7. Broadband noise spectrogram for Bell 206 helicopter in 60 knots level forward flight. (a) Processed flight test data (Christian et al., 2019); (b) PSU-WOPWOP prediction.

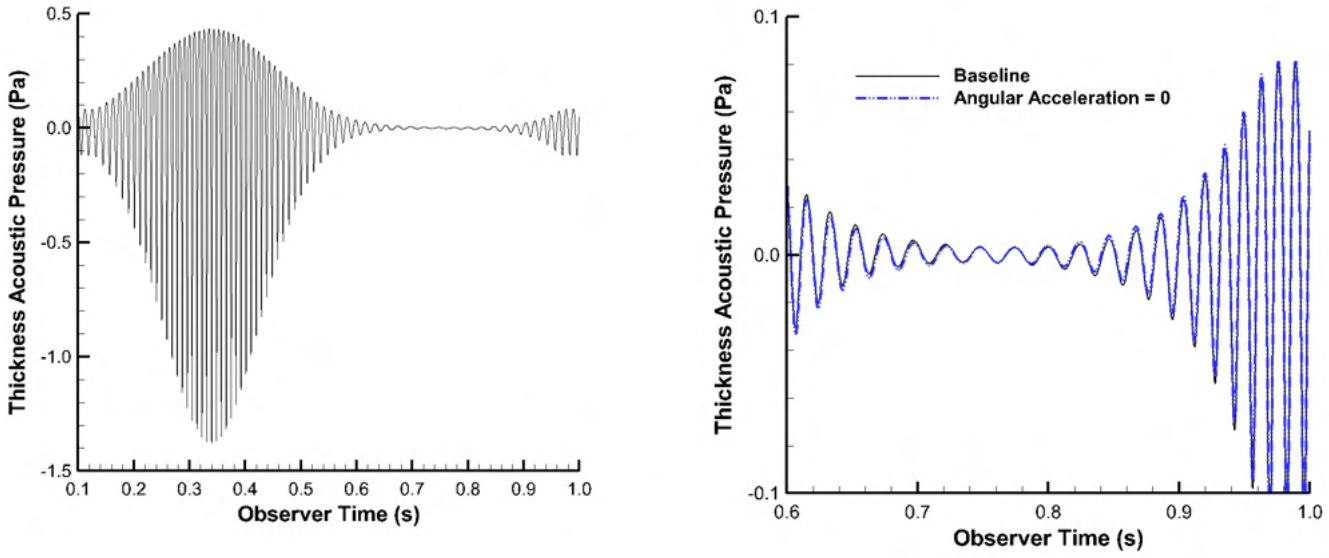

(a) (b)

Figure 8. Thickness noise for isolated hovering rotor with sinusoidal rotor speed variation. (a) Total baseline thickness noise; (b) thickness noise calculations neglecting angular acceleration.

Publications

Published conference proceedings

Gan, Z. F. T., Brentner, K. S., & Greenwood, E. (2021, January 26-28). Time variation of rotor broadband noise [Presentation]. Vertical Flight Society 8th Annual Electric VTOL Symposium.

Mukherjee, B., Gan, Z. F. T., Theron, J.-P., Botre, M., Brentner, K. S., Greenwood, E., & Horn, J. F. (2021, May 11-13). A new distributed electric propulsion aircraft simulation tool for coupled flight dynamics, free wake, and acoustic predictions [Presentation] Vertical Flight Society 77th Annual Forum & Technology Display.

Outreach Efforts

None.

Awards

None.

Student Involvement

Bhaskar Mukherjee, a graduate assistant starting his PhD at PSU, is working on coupling DEPSim with PSU-WOPWOP and developing a robust release version for usage in Project 49 and other FAA projects.

Ze Feng (Ted) Gan, a graduate assistant who recently completed his master's degree and started his PhD program at PSU, worked on time-varying broadband noise and thickness noise due to variable speed for this task.

Plans for Next Period

Further comparison of time-varying broadband noise predictions with noise measurements will be performed. Presently, Bell 206 helicopter flight test noise measurements (Schmitz et al., 2007) are being analyzed for their time-varying broadband noise characteristics. If their data are available (e.g., from ASCENT Project 77), flight test noise measurements from small UAS and/or UAM aircraft may serve as useful cases for validating the time-varying broadband noise predictions of the noise prediction system.

The analysis and computational predictions of noise due to variable rotor speed will be validated using data from higher fidelity simulations (e.g., CHARM) and/or experimental noise measurements.

References

Botre, M., Brentner, K. S., Horn, J. F., & Wachspress, D. (2019, May 13-16). Validation of helicopter noise prediction system with flight data [Presentation]. Vertical Flight Society 75th Annual Forum & Technology Display, Philadelphia, PA.

Christian, A., Caston, J., Greenwood, E., & Branch, A. (2019, May 13-16). Regarding the perceptual significance and characterization of broadband components of helicopter source noise [Presentation]. Vertical Flight Society 75th Annual Forum & Technology Display, Philadelphia, PA.

Schmitz, F. H., Greenwood, E., Sickenberger, R. D., Gopalan, G., Sim, B. W.-C., Conner, D. A., Moralez, E., & Decker, W. (2007, May 1-3). Measurement and characterization of helicopter noise in steady-state and maneuvering flight [Presentation]. American Helicopter Society 63rd Annual Forum, Virginia Beach, VA.

Task 8 - Develop Several Notional UAM/eVTOL Aircraft Models for Noise Testing

The Pennsylvania State University

Objective

In this task, several notional UAM/eVTOL vehicle models will be developed and tested. For expediency, nominal configurations used in related work, used by CDI, and those proposed by NASA will be potential sources of example cases. The vehicle models will be tested, and the initial/baseline trim and noise levels will be determined for hover, transition to forward flight, and level cruise.

Research Approach

As new aircraft are studied, they will be developed into new UAM/eVTOL aircraft. Extension of the flight control system in PSUDEPSim will require development of new flight controllers in many cases.

Milestone

Integrating a new aircraft with DEPSim-WOPWOP system.

Major Accomplishments

Two DEP aircraft are currently available to be simulated by the DEPSim-PSUWOPWOP noise predictions system: a generic eVTOL and NASA Lift + Cruise configuration (Figure 9). Both configurations are compound aircraft, with hover rotors controlled by variable angular speed-constant pitch (varrpm) and variable pitch-constant angular speed (varpitch). Relevant properties of the aircrafts are provided in Table 1.

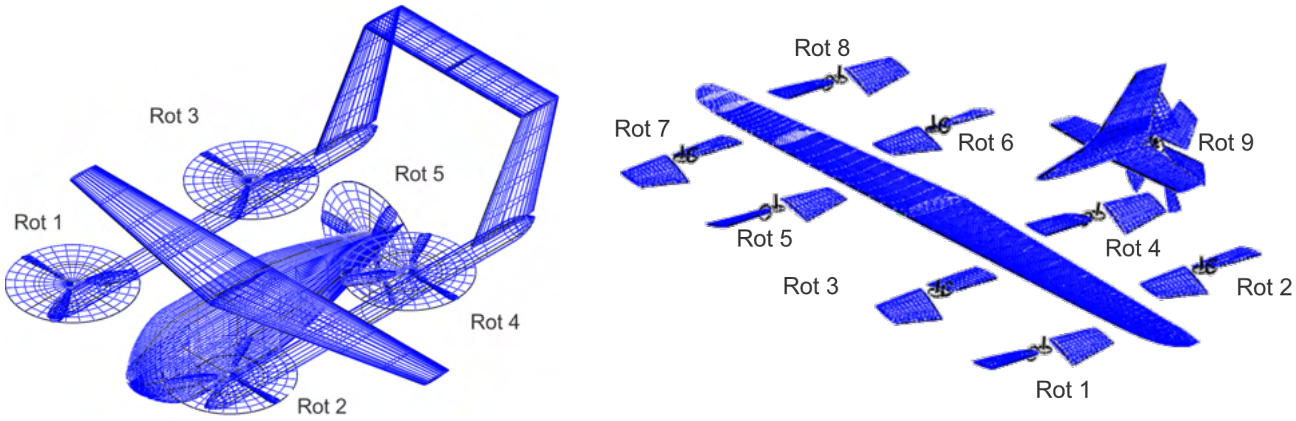

Figure 9. Urban air mobility (UAM)/electric vertical takeoff and landing (eVTOL) aircraft models currently available for noise simulation.

Table 1. Properties of configurations currently compatible with DEPSim-PSUWOPWOP system.

Parameter	Generic eVTOL	NASA Lift + Cruise
Number of lift rotors	4	8
Number of pusher propeller	1	1
Gross weight	1000 lbs	7270 lbs
Lift rotor radius	2.82 ft	0.42 ft
Pusher prop radius	2.82 ft	0.375 ft

Publications
Published conference proceedings

Outreach Efforts
None.

Awards
None.

Student Involvement
Bhaskar Mukherjee, a graduate assistant starting his PhD at PSU, is working on coupling DEPSim with PSU-WOPWOP and developing a robust release version for usage in Project 49 and other FAA projects.

Plans for Next Period
The DEPSim-PSUWOPWOP system is currently robust enough to integrate new vehicles without any external interference. More aircraft designs will be integrated subject to the design of aircraft flight controllers robust enough to fly a range of maneuvers.

Task 9 - Develop and Test Trim Strategies for Notional UAM/eVTOL Vehicles
The Pennsylvania State University

Objectives
UAM/eVTOL vehicles have significant control redundancy inherent in their design. This includes not only multiple propellers and rotors, but also lifting surfaces, such as wings and tail surfaces. As a result, the trim of the vehicle is not unique; hence, some strategies to determine an “optimal” trim will be required. In this task, alternative trim approaches will be developed and demonstrated. Baseline performance-oriented trim strategies will be compared with trim for maximum noise reduction. These trim strategies and their use in anticipated flight operations will be evaluated in the Penn State flight simulation facility to test feasibility for practical UAM operations.

Research Approach
The past year was spent studying trim strategies for the generic eVTOL aircraft. This compound aircraft has three primary ways to control trim: hover rotor thrust, aircraft pitch attitude, and cruise propeller thrust. The forward flight speed of the aircraft is primarily controlled by controlling the cruise propeller thrust. Keeping the forward flight speed constant, the aircraft is then controlled by varying the aircraft pitch attitude and hover rotor thrust. At any instant, trimmed aircraft flight requires vertical force generated by hover rotors and wing to balance the aircraft weight. This allows the required vertical thrust to be divided between the hover rotors and wing, resulting in an under-prescribed system with an infinite range of trim solutions. This task explores different strategies in controlling hover rotor thrust and aircraft pitch attitude.

Milestones
Explored the following trim strategies: (1) hover rotor thrust control schemes: variable RPM, variable pitch, *mixed variable RPM and pitch scheme*; (2) hover rotor controller bias, (3) aircraft-specific trim strategies: impact of variation of aircraft pitch attitude on noise.

Major Accomplishments
Impact of hover rotor thrust control scheme on noise

At any instant, the thrust of hover rotors in the generic eVTOL aircraft (Figure 1) can be controlled by varying their angular velocity (varrpm) or varying their blade collective pitch (varpitch). The method of control substantially determines the nature of noise. The control strategy influence on rotor thrust levels and rotor kinematic state variables varies with scheme. Figure 10 shows the thrust levels generated by hover rotors in 50 knots level cruise. The combined hover rotor thrust levels (Figure 10b) show that the variable RPM thrust levels are nominally the same as the variable pitch scheme. The greater degree of fluctuations observed for the variable pitch scheme can be explained by the hover rotors being in phase. Individual hover

rotor thrust levels for the variable RPM scheme (rotor 3,4) are found to have slightly higher thrust levels than those in the variable pitch scheme.

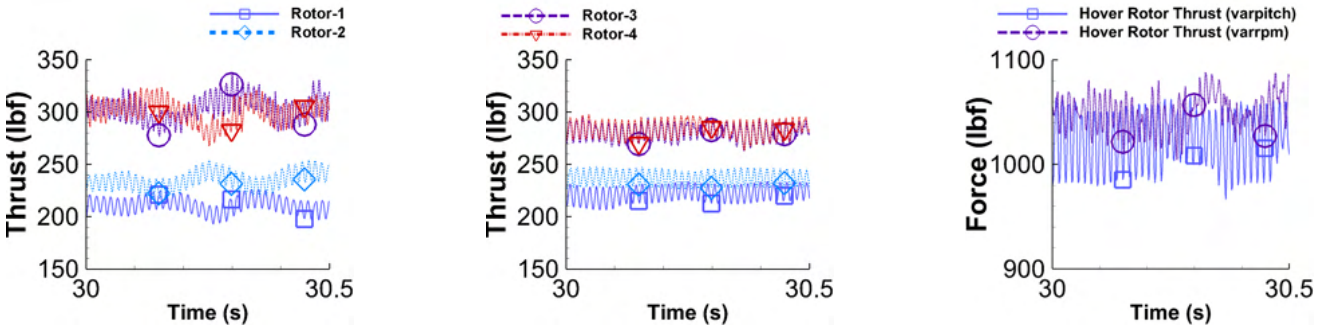

Figure 10. Fifty knots turn maneuver (aircraft pitch 0°). (a) Individual hover rotor thrust; (b) combined hover rotor thrust vs wing lift.

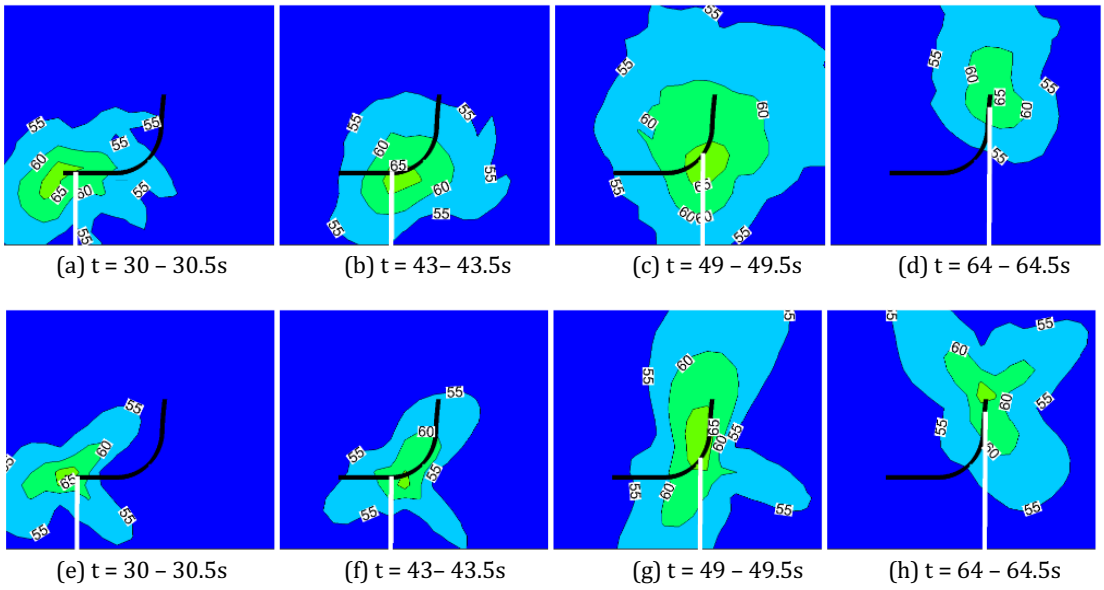

Figure 11. Fifty knots turn maneuver (aircraft pitch 0°): Effect of hover rotor thrust control scheme. (a–d) Variable RPM scheme; (e–h) variable pitch scheme.

Figure 11(a–d) shows that the variable RPM scheme has larger area noise contours than the variable pitch scheme (Figure 11(e–h)). A closer examination of individual rotor noise levels in level cruise (30–30.5 s) is shown in Figure 12. The variable pitch scheme can be observed to have higher constructive interference due to the constant rotor phase, while the variable RPM scheme has more of an incoherent interference pattern (i.e., it lacks the “lobes” seen in the variable pitch (constant RPM) case.

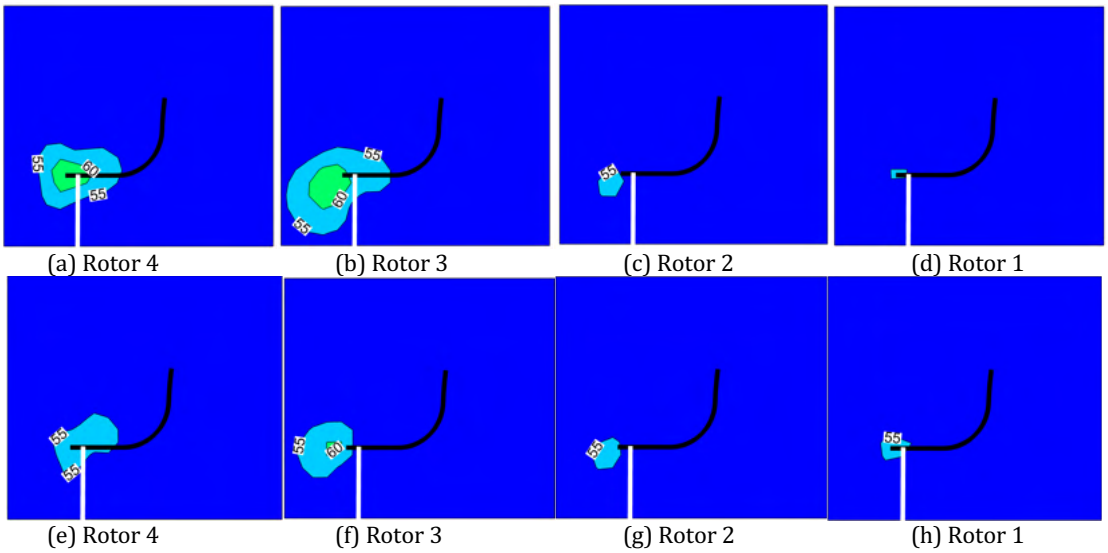

Figure 12. Fifty knots turn maneuver (aircraft pitch 0°): Individual hover rotor thrust levels. (a–d) Variable RPM scheme; (e–h) variable pitch scheme.

Impact of hover control bias on noise

Another approach to controlling the noise from hover rotors is shifting the hover rotor bias. The variable RPM and variable pitch control schemes have an inherent bias: a blade trim parameter that stays constant throughout the simulation. The variable RPM scheme has a constant blade pitch, while the variable pitch scheme has a constant rotor RPM. Figure 13 shows the impact of shifting hover control bias for the variable RPM scheme, where the rotors have blade pitch angles of 5˚ (Figure 13 a, c) and 7˚ (Figure 13 b, d). Increasing the blade pitch enables the controller to generate the same thrust from a hover rotor with lower angular velocity. This uniquely results in slightly lower peak thrust levels of rotors 3 and 4. The decrease in rotor angular velocity and lowering of peak rotor thrust levels lowers noise levels (Figure 13), with the impact more visible in individual rotor noise levels (Figure 14).

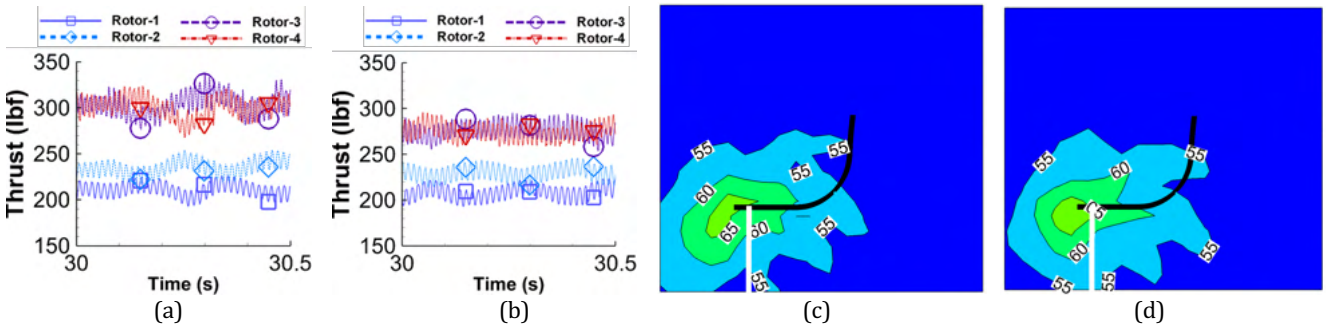

Figure 13. Fifty knots turn maneuver (aircraft pitch 0°): Effect of shifted controller bias (a, c) Variable RPM scheme: 5° blade pitch; (b, d) variable RPM scheme: 7° blade pitch.

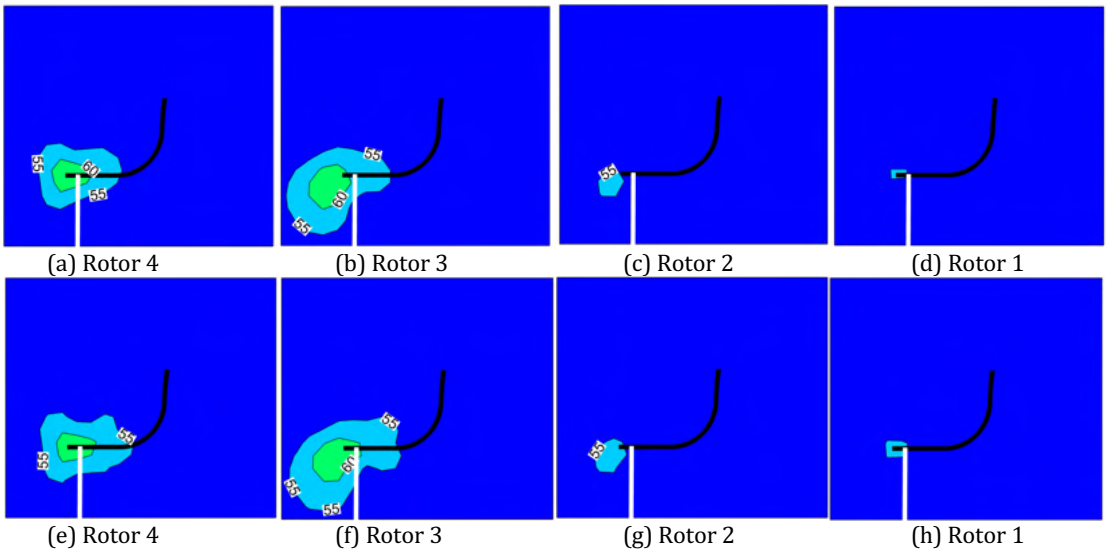

Figure 14. Fifty knots turn maneuver (aircraft pitch 0°): Effect of shifted controller bias. (a–d) Variable RPM scheme: 5° blade pitch; (e–h) variable RPM scheme: 7° blade pitch.

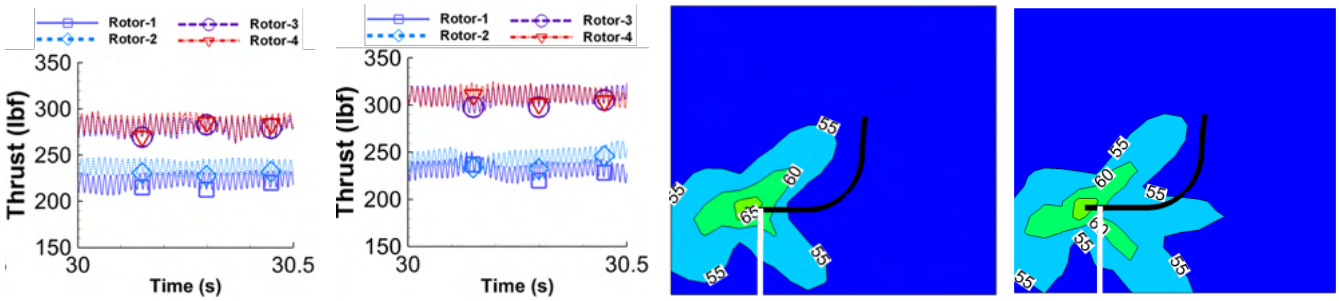

Figure 15. Fifty knots turn maneuver (aircraft pitch 0°): Effect of shifted controller bias. (a, c) Variable pitch scheme: $\omega = 155$ rad/s; (b, d) variable pitch scheme: $\omega = 170$ rad/s. ω = base rotor angular velocity.

Like the variable RPM scheme, shifting the hover bias in the variable pitch scheme has a significant impact on noise. Figure 15 shows that increasing the base rotor angular velocity (ω) results in higher noise levels, correlating with the increased rotor thrust levels (and higher tip-Mach numbers).

Impact of aircraft pitch attitude on noise

As described earlier, the compound configuration of the generic eVTOL aircraft results in an under-prescribed system with an infinite range of trim solutions. One of the major drivers is the distribution of vertical thrust requirement between the hover rotors and wing. Figures 10-15 show the noise levels from hover rotors when the aircraft is pitched at 0°. This results in hover rotors having to generate most of the thrust required to balance the aircraft weight. Alternatively, the aircraft can be pitched such that the wings generate more lift, relieving the hover rotors to generate lower thrust levels. Figure 16 shows two such conditions, where the wing generates lower lift (Figure 16a) with the aircraft pitched at $\approx 3.85°$ and the wing generates higher lift (Figure 16b) with the aircraft pitched at $\approx 7.48°$. The near doubling of pitch results in increased wing lift resulting in lowered rotor thrust levels. The impact of this can be directly observed in significantly lowered noise levels and areas of Figures 17 and 18 compared to Figure 11, where the same 50 knots turn maneuver is executed by keeping the

aircraft pitch 0°. The control of hover rotor thrust levels is reduced by exploiting the compound nature of the aircraft providing another promising path forward, where the nonunique trim of the aircraft can be exploited in a maneuver to control noise levels. It should be noted that the wing noise contributions have not yet been accounted for.

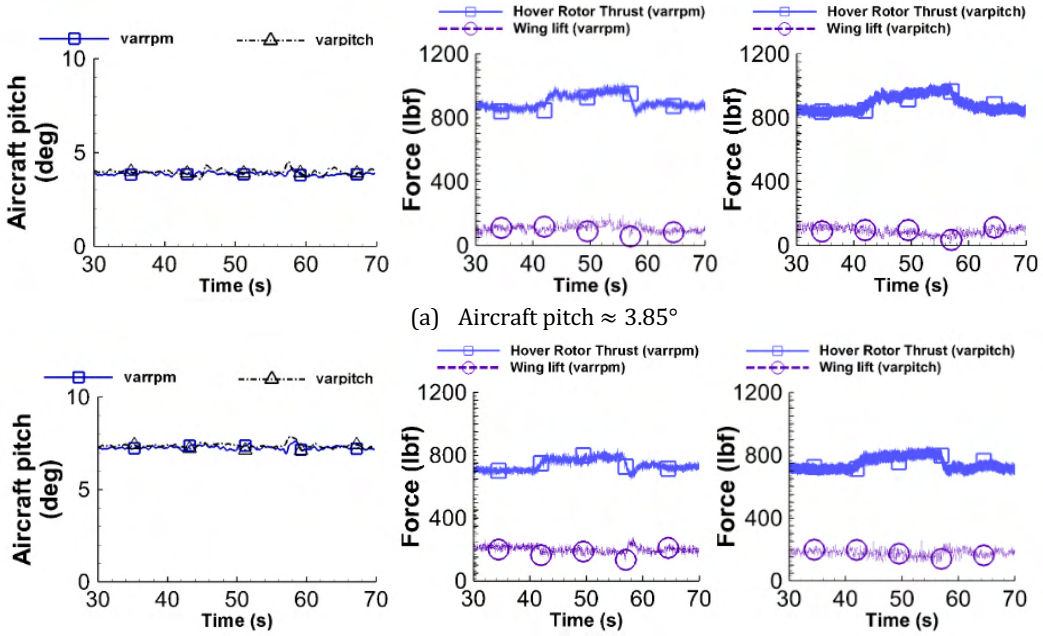

(a) Aircraft pitch ≈ 3.85°

(b) Aircraft pitch ≈ 7.48°

Figure 16. Combined hover rotor thrust and wing lift levels.

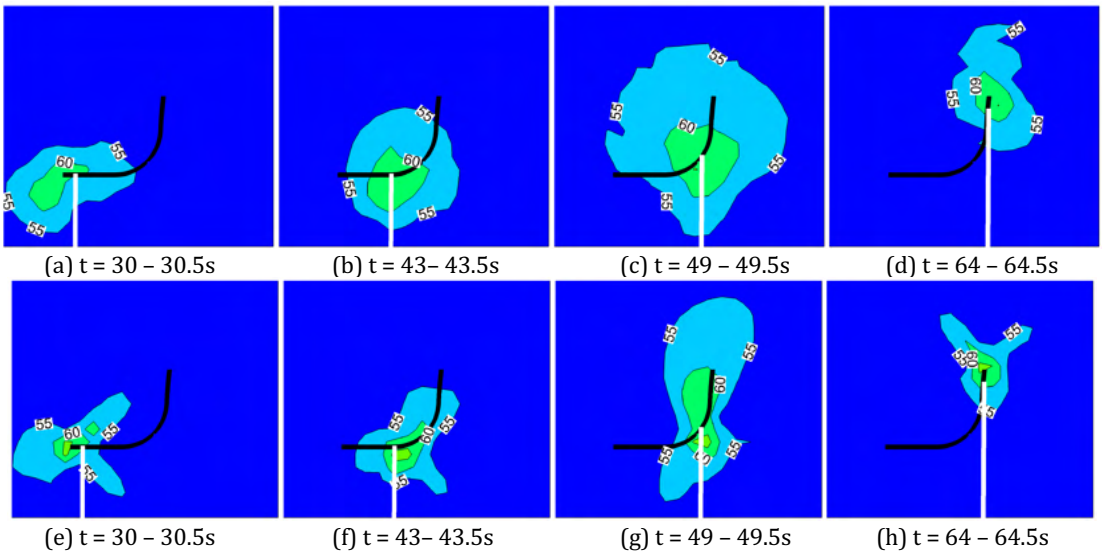

Figure 17. Fifty knots turn maneuver (aircraft pitch 3.85°): Effect of hover rotor thrust control scheme. (a–d) Variable RPM scheme; (e–h) variable pitch scheme.

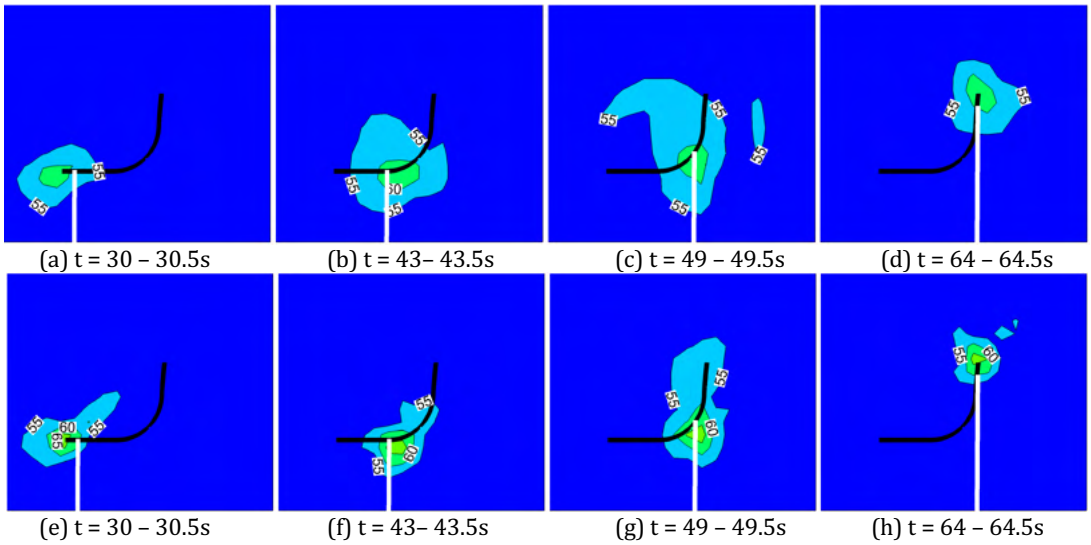

Figure 18. Fifty knots turn maneuver (aircraft pitch 7.48°): Effect of hover rotor thrust control scheme. (a–d) Variable RPM scheme; (e–h) variable pitch scheme.

Publications
None.

Outreach Efforts
None.

Awards
None.

Student Involvement
Bhaskar Mukherjee, a graduate assistant starting his PhD at PSU, is working on coupling DEPSim with PSU-WOPWOP and developing a robust release version for usage in Project 49 and other FAA projects.

Plans for Next Period
The differences in acoustic interference of noise signals from different rotors arising due to rotor thrust control scheme will serve as an important basis for development of noise-aware trim strategies. The nonunique trim of the aircraft also allows another degree of control over noise levels. However, further work needs to be done by including wing noise and broadband noise levels emitted from both components.

Task 10 - Begin Compilation of Noise Predictions for Notional UAM and eVTOL Vehicles During the Various Stages of Operation
The Pennsylvania State University

Objective
The goal of this task is to begin building a database of predictions that are performed throughout this work, which can be used to provide basic configuration, operation, and noise details to inform the users of the database what to expect from eVTOL noise.

Research Approach
In this task, the data generated in Tasks 7 and 9 will be compiled into a database of vehicle models and noise predictions for various aircraft. Documentation of the “database,” its contents, and how to add more vehicle data to the database will be developed. It is envisioned that this database will be sufficient to make comparisons between vehicle concepts and operating conditions and could be used to as part of a model of the community noise impacts of UAM operations.

Milestones
None.

Major Accomplishments
The noise predictions to date do not include broadband noise; therefore, none of the predictions are suitable for a database yet. Broadband noise is important because it is likely a dominant, if not the dominant, noise source for civil operations.

Publications
None.

Outreach Efforts
None.

Awards
None.

Student Involvement
Bhaskar Mukherjee, a graduate assistant starting his PhD at PSU, is working on coupling DEPSim with PSU-WOPWOP and developing a robust release version for usage in Project 49 and other FAA projects.

Plans for Next Period
As noise predictions begin to include broadband noise, wing noise, interaction noise, and so on, a noise database will be established. The format and location of the database will be decided and updated as experience is gained. The full computational model will be available to users, along with the simulation system predictions.

Task 11 - Computational Algorithm Evaluation for Efficient Processing of Many Rotors and Noise-Generating Bodies

The Pennsylvania State University

Objective

This task will evaluate the effectiveness of the computational algorithm, especially for many rotors and airframe noise-generating bodies used in the noise prediction system. In particular, during a PSU-WOPWOP noise prediction, as the number of rotors and noise-generating airframe components increases, the computational demands can increase significantly. Furthermore, aerodynamic interactions between components can also increase computational requirements, and calculating the noise-optimal trim condition of the vehicle may require many iterations of the acoustic prediction method. This task will evaluate the potential for modeling approximations to ensure that the computations do not become too long for practical application and that any approximations made still capture the key physics.

Research Approach

The research approach taken will be to first use a code profiler to identify which parts of the computational algorithm serve as bottlenecks for noise prediction of UAM and eVTOL aircraft. These computational bottlenecks will be the focus of efforts to make the code more efficient, including techniques to make the code parallel. The eVTOL aircraft design attributes will also be considered as part of the study on the computational algorithm, with the goal of using appropriate knowledge of the number of noise-producing components (rotors, wings, etc.), as part of the algorithm design of the noise prediction system in order to reduce computational bottlenecks.

Computational efficiency is especially important for implementing the data structures and algorithms needed to predict and store time-varying broadband noise, which is currently being coupled into the noise prediction system as part of Task 6. These data structures and algorithms pertaining to time-varying broadband noise must be compatible with data structure changes made for Project 38, and compatible with possible future expansion to include additional broadband noise sources, such as turbulence ingestion noise. In particular, object-oriented programming practices are being considered. Candidate data structures and algorithms must be evaluated for their accuracy and speed using unit tests, which are currently being developed.

Milestones

Evaluating data structures and algorithms pertaining to time-varying broadband noise predictions in PSU-WOPWOP is a work in progress.

Aside from that work, this task has not yet been started. The milestones for this task will be to (1) investigate where any bottlenecks appear in the noise predictions system, both for configurations with a low number of rotors and eVTOL configurations with up to 10 rotors, and other noise-generating surfaces; (2) review the configuration components and assess whether the computational algorithms can be improved by taking the aircraft configuration into account, especially in developing parallel processing strategies.

Major Accomplishments

None.

Publications

None.

Outreach Efforts

None.

Awards

None.

Student Involvement

Ze Feng (Ted) Gan, a graduate assistant who recently completed his master's degree and started his PhD program at PSU, is working on evaluating computational efficiency for time-varying broadband noise data structures and algorithms. Ted will also perform the remainder of this task.

Plans for Next Period

The computational efficiency of time-varying broadband noise data structures and algorithms will continue to be evaluated. The remainder of task will be initiated after completion of Task 6, using the planned research approach.